# Small Molecule Activation Facilitated by Main Group Elements

By

Blake Stanley Norman Huchenski

Submitted in partial fulfillment of the requirements

for the degree of Doctor of Philosophy

at

Dalhousie University

Halifax, Nova Scotia

August 2021

"*Don't overthink things too much and trust yourself more often*"

- Blake Huchenski

# Table of Contents

# List of Tables

# List of Figures

# List of Schemes

# Abstract

Main group containing systems are emerging as an alternative to transition metal catalysts, often showing complementary reactivity. Transition metal complexes have provided the basis for fascinating catalytic reactions such as the reduction of unsaturated bonds, as well as the formation of new carbon-carbon and carbon-pnictogen bonds. The cost of many second and third row late transition metals, precious metals commonly used in catalysis, is high, and fluctuates, so discovery of alternative methods is important. Two paths have been taken to create alternative, more affordable systems. The first is harnessing the power of less expensive first row, or early transition metals and the second is using organic and main group containing catalysts to facilitate similar transformations, which is a focus of this thesis.

Within this thesis, main group complexes containing boron or phosphorus are explored in bond activation chemistry. While the groundwork for hydrogenation via boron cations and neutral boranes has been reported, this thesis explores the application of bis(amino)cyclopropenylidene (BAC) carbenes in borane complexation through synthesis of new BAC borane adducts and carbenes. These adducts are explored in hydrogenation and hydrosilylation reactions with imines and some enamines to form amines including pharmaceutically relevant ones.

The latter portion of this thesis explores the application of diazaphospholenes in bond activations. Recently diazaphospholenes have emerged as potent reductants in a variety of transformations as polar hydride donors. Diazaphospholenes have been made catalytic in these polar (two electron) transformations, and are readily synthesized from abundant materials. This thesis shows development of distinct radical (single electron) chemistry using diazaphospholenes, including phosphorus-carbon bond formation reactions, and radical cyclization reactions. The single-electron chemistry of diazaphospholenes was applied to the challenging problem of sulfur hexafluoride reduction. Sulfur hexafluoride is a highly potent greenhouse gas, which is used in the power industry with a global warming potential of approximately 23,500 times that of carbon dioxide. This thesis explores three new methods of the decomposition of this highly potent greenhouse gas. Reactions using stoichiometric phosphides or catalytic phosphines are shown, and finally a new route to sulfur hexafluoride reduction with magnesium (0) discovered during this work is shown.

# List of Abbreviations and Symbols

| | |
|---|---|
| 9-BBN | 9-borabicyclo[3.3.1]nonane |
| α | alpha (carbon position) |
| β | beta (carbon position) |
| γ | gamma |
| δ | chemical shift |
| λ | wavelength |
| Å | angstrom |
| Ad | adamantyl |
| AIBN | azobisisobutyronitrile |
| anh. | anhydrous |
| APCI | atmospheric pressure chemical ionization |
| Ar | aryl |
| BAC | bis(amino)cyclopropenylidene |
| $BAr^{F}{}_{20/24}$ | tetrakis(pentafluorophenyl)borate /tetrakis((3,5trifluoromethyl)phenyl)borate |
| $BAr^{Cl}{}_{8}$ | tetrakis(3,5-dichlorophenyl)borate |
| BINOL | 1,1'-bi-2-naphthol |
| Binap | 2,2′-Bis(diphenylphosphino)-1,1′-binaphthalene |
| Bn | benzyl |
| Boc | *tert*-butyloxycarbonyl |
| br | broad |
| Bu | butyl |
| CAAC | cyclic alkyl amino carbene |
| Cage phos | 2,4,6-Trioxa-1,3,5,7-tetramethyl-8-phosphaadamantane |
| calc'd | calculated |
| cat. | catalytic or catalyst |
| CBS | Corey-Bakshi-Shibata |
| CDC | carbodicarbene |
| cod | 1,5-cyclooctadiene |
| conv. | conversion |
| cy | cyclohexyl |
| d | doublet(s) |
| *d* | deuterium |
| DABCO | 1,4-diazabicyclo[2.2.2]octane |
| 1,2-DFB | 1,2-difluorobenzene |
| DCM | dichloromethane |
| *d.r.* | diasteromeric ratio |
| dd | doublet of doublets |
| Dipp | 2,6-diisopropylphenyl |
| DMAP | 4-(dimethylamino)pyridine |
| *e.e.* | enantiomeric excess |
| equiv. | equivalent(s) |

| | |
|---|---|
| *e.r.* | enantiomeric ratio |
| Et | ethyl |
| ESI | electrospray ionization |
| FLP | Frustrated Lewis Pair |
| h | hour |
| HRMS | high-resolution mass spectrometry |
| HPLC | high performance liquid chromatography |
| ipc | isocamphenyl |
| *i*Pr | isopropyl |
| *J* | coupling constant(s) |
| KHMDS | potassium hexamethyldisilazide |
| LED | light-emitting diode |
| m | multiplet(s) |
| M | molar (concentration) or molecule |
| m/z | mass-to-charge ratio |
| *m*-CPBA | meta-chloroperoxybenzoic acid |
| MeCN | acetonitrile |
| Mes | mesityl or 2,4,6-trimethylphenyl |
| Me | methyl |
| MIC | mesoionic carbene |
| min | minute |
| MTBE | methyl-*tert*-butylether |
| NHC | *N*-heterocyclic carbene |
| NHP | N-heterocyclic phosphine |
| NMR | nuclear magnetic resonance |
| *o* | ortho |
| OBn | benzyloxy |
| *o*-DCB | 1,2-dichlorobenzene |
| OMe | methoxy |
| *o*-tolyl | ortho tolyl |
| *p* | para |
| PCP | pentachlorocyclopropane |
| Ph | phenyl |
| pin | pinacol |
| pip | piperidyl |
| PMB | para-methoxybenzyl |
| PMP | para-methoxyphenyl |
| ppm | parts per million |
| PTFE | polytetrafluoroethylene |
| q | quartet(s) |
| qd | quartet of doublets |
| Quin | *N*-benzyl-quinolinium |
| R | generic group |

| | |
|---|---|
| RT | room temperature |
| s | singlet(s) or second(s) |
| sat'd | saturated |
| solv. | Solvent |
| SSRI | selective serotine reuptake inhibitor |
| t | triplet(s) |
| TBAT | tetrabutylammonium difluorotriphenylsilicate |
| *t*Bu | *tert*-butyl |
| TCP | tetrachlorocyclopropene |
| TEMPO | 2,2,6,6-Tetramethylpiperidine 1-oxyl |
| Tf | trifluoromethanesulfonyl |
| TFT | α,α,α-trifluorotoluene |
| Thexyl | 2,3-dimethyl-2-butyl |
| THF | tetrahydrofuran |
| TMINO | 1,1,3-trimethylisoindole *N*-oxide |
| TMS | trimethylsilyl |
| TOF | turn-over frequency |
| TON | turn-over number |
| Trityl | triphenylmethyl |
| X | generic anionic group |

## Acknowledgements

First of all, I would like to thank my family, because without them I technically wouldn't exist. In all seriousness, I would not know who I would be today without them. I hope to live life with kindness and care that they have taught me. This includes Helia Hollenhorst, and all her family as well, who have been here to support me through this journey. I know I have not been able to see everyone since we are all so scattered, but your all always in my heart.

I would like to thank my supervisor Dr. Alex Speed for taking me in to become his inaugural PhD student. It has been an amazing journey to watch the lab grow and become what it is today. I have learned much more than I would have ever expected about chemistry and life skills I will never forget. I have loved the dynamic in the lab, which has allowed me to explore and grow into the chemist that I am today. Thank you to my group members, Matt, Tien, and Erin for making this journey fun and exciting.

I would also like to thank the members of my supervisory committee Dr. Laura Turculet, Dr. Mark Stradiotto, and Dr. Saurabh Chitnis for your guidance throughout my degree. Additionally, I would like to thank my external examiner Dr. Chris Caputo for taking the time to evaluate my thesis work.

Thank you to all those who have helped me with my research such as Dr. Mike Lumsden (NMR), Xiao Feng (Mass Spectrometry), Dr. Robert McDonald (X-ray), Dr. Mike Ferguson (X-ray), Dr. Katherine Robertson (X-ray), Dr. Mita Dasog (SEM), and Maxine Kirshenbaum (SEM).

My time at Dalhousie has been adventurous to say the least. From the late-night study sessions in the resource centre to the amazing times at Chem Beer will never be forgotten. University has changed me in many ways for the better, changing both my outlook on life and my view of the world around us.

# Chapter 1: Introduction

## 1.1 Introduction

From stoichiometric to catalytic reactions, main group elements have shaped the synthetic chemistry that we all use or receive benefits from. In a world where the importance of pharmaceuticals and materials is ever-growing, as a pandemic has reshaped our society, the need for new synthetic tools has only become more prominent. In this regard, main group elements have been crucial in the synthesis of pharmaceuticals. From reagents in cross-coupling reactions,[1] to the ligands that facilitate catalysis,[2] main group elements are found in all stages of synthesis, including in some end-stage pharmaceuticals.[3] In recent years, main group complexes have emerged as complementary form of catalysis to the ever-expanding field of transition metal catalysis. Where main group elements were once used as components in other chemical transformations, these elements are now being featured as the centerpoint in their own catalytic transformations. While main group catalysts have existed throughout the years, only recently, with the emergence of Frustrated Lewis Pairs (FLP) has this field undergone an explosive growth.[4–6] These findings gave also sparked the exploration of main group elements in a variety of bond activation reactions.[6] The first part of this introductory chapter provides an overview of boron/borocation chemistry relevant to the first part of this thesis, while the second part of this introductory chapter provides and overview of the phosphorus/diazaphospholene chemistry relevant to the second part of this thesis.

## 1.2 Lewis Acids, Bases and Frustrated Pairs

### 1.2.1 Introduction

The concept of Lewis acids and bases in synthetic transformations has existed for many years. A Lewis acid acts as electron pair acceptor and a Lewis base as electron pair

donor. This idea of electron donors and acceptors was put forth by Gilbert Lewis in 1923.[7] The theory describes the interaction between the Lewis acids and bases where the resulting products have properties that differ from the original components. The product of a Lewis acid and base combination is defined as an adduct. An early example of this is the combination of ammonia and borane where the lone pair of ammonia donates to the empty p-orbital of the borane, resulting in ammonia-borane, a product with vastly differing properties and reactivity.[8] The difference in reactivity arises from the increase in electron density within the Lewis acid and the decrease in electron density within the Lewis base component of the adduct, and also the quenching of available lone-pairs or vacant orbitals. Lewis acids and bases have been utilized in catalytic transformations independently as well as synergistically.

### 1.2.2 Lewis Acids in Catalysis

The primary application of a Lewis acid in catalysis or as a stoichiometric reagent is to enhance the electrophilicity of a substrate via coordination, resulting in polarization of the adduct. A notable example of this reactivity is in a rearrangement reaction such as an oxime to a lactam that proceeds at -40 °C in the presence of a Lewis acid such as $AlCl_3$ (**Scheme 1.1**).[9] Brønsted acids in this application often afforded product in low yields of 20% while Lewis acids in this reaction yield around 90% yield of product.[9] One of the most prominent uses of Lewis acids in elementary organic reactions are in Friedel-Crafts alkylation or acylation reactions.[9] The common Lewis acid for this transformation is once again $AlCl_3$, which allows for the formation of an electrophilic carbocation or acylium intermediate. Other Lewis acids such as $TiCl_4$, $GaCl_3$, $SnCl_4$, $ZnCl_2$, and $FeCl_3$ have also been used in Friedel-Crafts reactions (**Scheme 1.1**).[9]

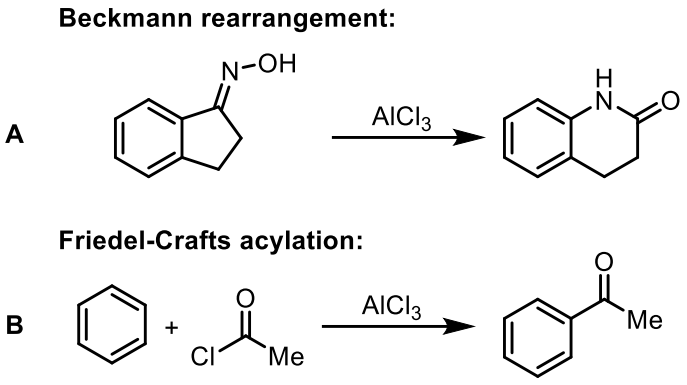


**Scheme 1.1** Aluminum-catalyzed Beckmann rearrangement (**A**) and Friedel-Crafts acylation (**B**).

Further developments of Lewis acid-catalyzed transformations can be highlighted in the Mukaiyama aldol reaction (**Scheme 1.2**).[9] This reaction involves the use of a Lewis acid to enhance the electrophilicity of a carbonyl, allowing for greater reactivity with the silyl enol ether, which is of relatively low nucleophilicity. The addition of a chiral ligand to this reaction allows for an asymmetric process to occur with moderate to high enantioinduction.[10] Another example that highlights the power of Lewis acids in asymmetric processes is in the Sharpless asymmetric epoxidation reaction,[11] a reaction featured in the 2001 Nobel prize in chemistry. The key feature of the Lewis acid/base chemistry in this transformation is the coordination of the substrate to the chiral titanium complex.

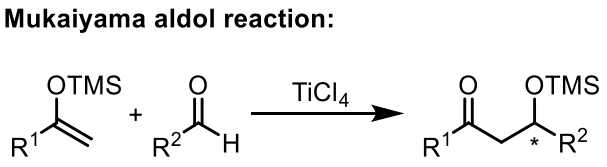


**Scheme 1.2** Mukaiyama aldol reaction with a titanium tetrachloride catalyst.

Finally, boron containing compounds are amongst the most prominent modern Lewis acids used within catalysis. An early example of great importance of boron as a Lewis acid is the Corey-Bakshi-Shibata reduction (**Scheme 1.3**).[12] This reaction features a

chiral oxazaborolidine, which catalyzes the asymmetric reduction of carbonyl compounds. Boron Lewis acids have been featured in many chemical transformations which are detailed later within this chapter.

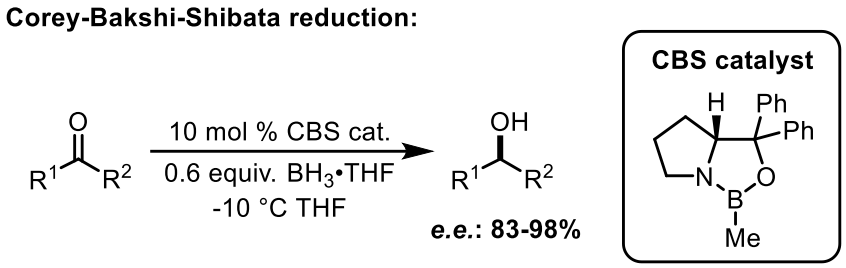


**Scheme 1.3** Corey-Bakshi-Shibata reduction of ketones with a chiral oxazaborolidine catalyst.

### 1.2.3 Lewis Bases in Catalysis

A Lewis base catalyzes a reaction by enhancing the nucleophilicity of the substrate but also it may enhance the electrophilicity of the acceptor itself. An early example of a Lewis base catalyzed reaction was disclosed by Kirichenko in 1967 (**Scheme 1.4**).[13] This acylation reaction is catalyzed by *N*,*N*-dimethylamino pyridine (DMAP), which reacts with the acid chloride, enhancing its electrophilicity for the subsequent attack by the aniline reactant. Fu later reported that chiral derivatives of this catalyst are capable of kinetic resolution of alcohols with high enantiomeric selectivity.[14]

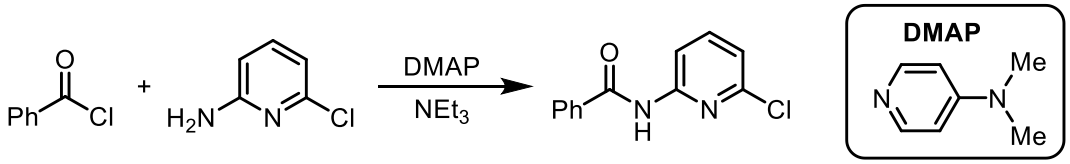


**Scheme 1.4** First Lewis base catalyzed acylation which used DMAP as the catalyst.

Furthermore, Denmark reported that chiral derivatives of hexamethylphosphoramide can facilitate asymmetric allylation reactions.[15] These compounds were also applied in an alternative pathway for asymmetric catalysis of silyl

enol ether aldol reactions through a Lewis base.[15] Lewis bases are also capable of facilitating the reduction of imines and carbonyls, involving boranes or silanes as the reductants.[16]

### 1.2.4 Frustrated Lewis Pairs

The combination of a Lewis acid and base under most conditions will form an adduct, resulting in the quenching, or at least attenuation of Lewis reactivity from either component. However, as early as 1942, H. C. Brown reported the first example that not all Lewis acids and bases are capable of forming adducts.[17] In this example, lutidine was found to form a stable adduct with $BF_3$ while the more sterically demanding $BMe_3$ did not. More than 15 years later, Wittig reported a second example of this phenomenon involving the addition of triphenylphosphine and triphenylborane to benzyne.[18] Following this example, Tochterman reported that the reaction of a trityl anion and triphenylborane with butadiene produced a zwitterionic species.[19] In both of these cases, the nucleophile and electrophile reacted with a third partner, rather than self-quenching.

Approximately 30 years passed until the first example of a fluorinated triarylborane as a component of a Frustrated Lewis Pair was reported by Piers.[20] This example involved the use of the highly acidic tris(pentafluorophenyl)borane ($B(C_6F_5)_3$) in hydrosilylation. The Lewis acid can activate a Si–H bond followed by subsequent attack from a ketone, which acts as the Lewis base. While the term FLP was not utilized, this finding would become the first of many to show the cooperative nature of a frustrated donor and acceptor in catalysis and bond activation.[5] In 2006, Stephan and co-workers reported the first example of metal free reversible activation of hydrogen (**Scheme 1.5**), bringing about the beginning of a massive field of study on the reactivity and nature of FLPs, and presenting an overarching definition of the field.[21] From this point forward, the term FLP has become

known as a system, that due to steric or geometric restraints cannot form a classical adduct upon mixture.[22] However, this rule is not to be taken as though adduct formation is not at all possible, with many examples displaying more of an adduct equilibria.[5] Thus, a FLP is a system that does not form a highly stable adduct and exists in equilibria with the free Lewis acid and base.[5]

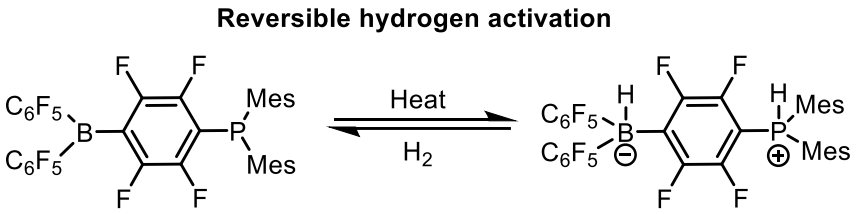


**Scheme 1.5** First example of reversible hydrogen activation with a main group complex.

Over the past 10 years, the development of FLP catalysts has grown exponentially, with over 2000 reports of FLP catalysts in many bond activation systems and reviews on the topic.[6] One such reaction of importance is the hydrogenation of nitrogen containing species. With approximately 75% of pharmaceuticals containing a nitrogen heterocycle,[23] the need for new synthetic methods involving the formation of amines is of great importance. Following the development of the first metal-free compound capable of reversible hydrogen activation,[21] this species was found to facilitate hydrogenation reactions on imines and aziridines.[24] Since this seminal publication, many FLP hydrogenation catalysts have been developed involving either P,B or N,B systems.[4,6,25] Tris(pentafluorophenyl)borane and derivatives thereof were found to facilitate hydrogenation reactions in the absence of a strong Lewis base, with the imine substrate acting as the base in the reaction (**Scheme 1.6**).[26] This result shows how the hydrosilylation reaction by Piers foreshadowed the application of this borane in hydrogenation chemistry

as well as the importance of the pentafluorophenyl group, which is featured in the majority of these systems.

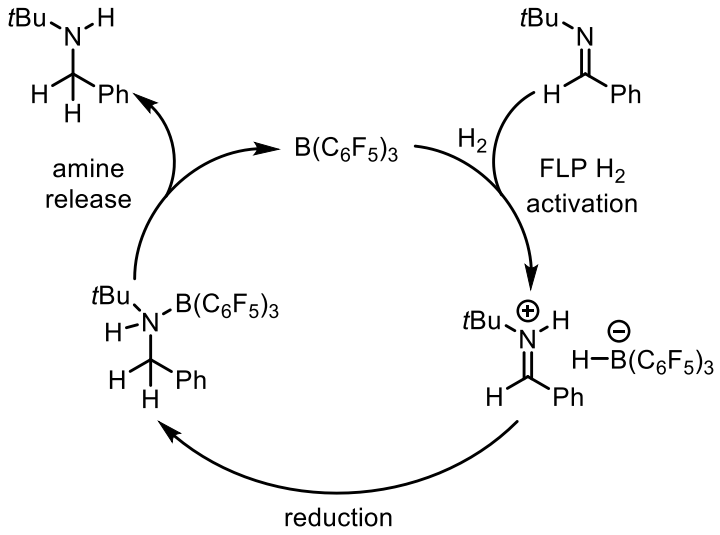


**Scheme 1.6** Proposed catalytic cycle for imine hydrogenation via a Lewis acidic borane.

The largest advancement in FLP reductive chemistry occurred with the emergence of chiral catalysts (**Figure 1.1**). In 2008 a pinene derivative of Piers borane allowed for the realization of enantioselective hydrogenation of imines via FLP systems. However, the largest enantiomeric excess (*e.e.*) found was only 13%.[27] It was not until the report by Klankermayer, which featured a chiral camphor borane, that an *e.e.* of up to 83% was achieved.[28] Following this result, many chiral catalysts have been developed from a chiral organic scaffold, with the best catalysts being derived from binaphthyl scaffolds, as reported by various groups.[29] The highest enantioselectivity achieved thus far in hydrogenation with these systems was reported by Pápai and Repo in 2015.[30] While the enantioselectivity in imine reduction was modest, when enamines were examined as substrates, an enantiomeric excess of up to 99% was observed. These chiral catalysts have been extended into other nitrogen containing substrates with varying levels of enantioinduction. Overall, the main limitation of these catalysts is the requirement of the

bis-pentafluorophenylborane moiety, which is relatively challenging to prepare[31] along with the lengthy chiral ligand synthesis itself.[30]

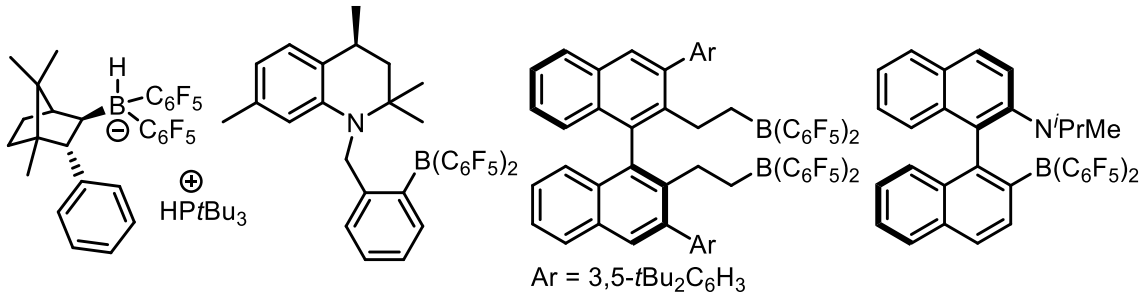


**Figure 1.1** Enantioselective neutral borane catalysts in the hydrogenation of imines and enamines.

## 1.3 Borocations in Catalysis

### 1.3.1 Introduction

The development and discovery of FLPs has brought a renaissance within main group chemistry and catalysis as a whole. The discovery that nonmetals can facilitate bond activation of a variety of small molecules and then facilitate subsequent reactions in both stoichiometric and catalytic manifolds has prompted the investigation of main group complexes to undergo explosive growth. Of particular interest is boron, as this element represents a multitude of reactivity modes and is featured in countless reactions. Boron containing compounds are held in high regard for their multitude of uses within chemistry such as a Lewis acid catalyst, a hydride donor in reductions, and ability of organoboranes to act as a transmetallating agents in reactions such as cross-coupling.[32] Reactions such as olefin hydroboration, cross-coupling, reductions and protecting group chemistry rely on boron and its reactivity.[32] Many modern synthetic protocols within the literature would not exists without the discoveries within boron chemistry.

Boron species can exist in a variety of coordination states which greatly affect their reactivity. The most used boron species within synthesis and catalysis are tricoordinate boron and tetracoordinate boron. The tricoordinate boron species are referred to as boranes, which have Lewis acidic properties, as well as hydridic properties if a hydrogen is bound to the boron. The Lewis acidity arises from the vacant p-orbital allowing for bonding from a donor. The strength of the Lewis acid is highly dependant on the substituents attached to the boron, and examples such as tris(pentafluorophenyl)borane are amongst the strongest of the species.[33] Boranes are also often featured as reducing agents within synthesis, often as a mono, di or trihydride. These boron hydrides with a vacant p-orbital allow for unique bonding by allowing both substrate coordination/activation as well as hydride delivery. Coordination of a Lewis base to the borane may enhance its hydricity allowing it to become a stronger hydride donor.[34] Tetracoordinate boron species are referred to a borates. These anionic species are often used as counterions in catalysis. The stability of aryl borate anions has allowed for their application as weakly coordination anions, with examples such as $BAr^{F}_{24}$ and $BAr^{F}_{20}$ being amongst the most prominent.[35] Borates are also featured as hydride donors, with exceptional hydricity, serving as strong reducing agents. Sodium borohydride is one of the most common reducing agents used in synthesis, because of its ease of synthesis and low cost.[34] Triethylborohydride salts, also known as superhydride reagents, are very strong reducing agents[34] used to effectively reduce compounds, as well as being used as hydride transfer reagents for the generation of metal hydrides.

### 1.3.2 Boron Cation Synthesis

The less readily accessible but most reactive coordination state of boron are known as borocations. Borocations are highly reactive species which are usually bound by at least one donor to decrease the electron deficiency at the boron centre. The nomenclature of a

boron cation depends on the number of donors coordinating to boron (**Figure 1.1**).[32] With no donor ligands, a linear disubstituted boron cation is known as a borinium. Isolation and characterization of these borinium compounds is quite challenging due to their high reactivity.[36] A single donor coordinated to the otherwise disubstituted boron results in a trigonal complex called a borenium ion, and these structures are the most catalytically active with one vacant p-orbital accessible for reactivity.[32] These compounds are of great interest for their catalytic application and are detailed later. A coordinatively saturated borocation with two X-type substituents and two dative L donors adopts a tetrahedral geometry and is called a boronium ion. These compounds are also catalytically active and are sometimes in equilibria with a borenium ion through the loss of an L donor.[32,37] While the synthesis and study of borinium, borenium, and boronium complexes are of great interest, the catalytic activity of borenium complexes is most often considered.

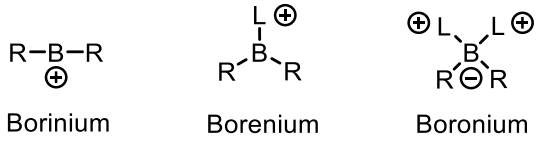


**Figure 1.2** The three coordination states of a boron cation.

The isolation of an observable borenium complex had remained elusive for many years. In 1970, Ryschkewitsch and Wiggins reported the first borenium complex that was isolated and subsequently characterized.[38] Since then, a variety of methods have been developed to generate borenium complexes.[32,36,37,39] One method to generate a borenium complex is through halide abstraction.[32] This method may be used when the borane contains at least one boron-halide bond, and can be conducted via abstraction with a Lewis acid or by metathesis with a weakly coordinating anion. Such examples include the synthesis of the first carbene-supported borenium complex.[40] Boron complexes containing

hydrides can be converted into borenium ions via hydride abstraction with a Lewis acid such as tris(pentafluorophenyl)borane or more commonly, a trityl salt.[32] Additionally, a borenium complex can be generated through elimination of hydrogen with a Brønsted acid, if enough steric bulk or stability from the L donor is present.[32] Boranes containing a sufficient leaving group can also be transformed into borenium complex when a L donor with sufficient nucleophilicity to displace the leaving group is added to the solution.[32] Finally, boron compounds containing B–N bonds can be converted into a borenium complex though protonation or coordination of a Lewis acid.[32]

### 1.3.3 Borocation Catalysis

While the synthesis of borenium complexes has been established, only recently have catalytic applications been reported. The recent discoveries with FLP complexes have shown that highly Lewis acidic boron complexes can facilitate hydrogenation reactions.[6] One of the most important set of borenium complexes have been carbene-supported borenium complexes.[32] The unique properties of carbenes have allowed for impressive stability as borane adducts, which has made a variety of transformations feasible.

#### 1.3.3.1 Hydrogenation with Borenium Complexes

Curran and co-workers reported that a NHC borane adduct was capable of radical hydride reduction of xanthanates.[41] Following this work, Lindsay reported that a chiral NHC 9-BBN complex was capable of stoichiometric reduction of ketones with enantioinduction.[42] Hydrogen activation was then observed with a NHC borenium complex and tributylphosphine in a report by Stephan and co-workers.[43] This discovery provided the grounds that the highly Lewis acidic borenium complexes may be capable of hydrogenation, like the FLP complexes reported previously. In this report, the first borenium catalyzed hydrogenation was conducted with impressive loadings as low as 1

mol % with most substrates reduced at 5 mol %.[43] The scope of substrates for this reaction were imines and enamines, which would set the precedent for the remainder of borenium hydrogenation.

The next generation of catalyst reported by the Stephan group involved smaller and more electron withdrawing carbenes, which was found to increase the catalytic activity of these complexes and subsequently allow lower loadings, reaction time or both (**Figure 1.3**).[44] Within the same timeframe, Crudden and co-workers reported that meso-ionic carbene (MIC) borenium complexes were also able to catalyze hydrogenation reactions (**Figure 1.3**).[45] The hydrogenations of imines with this catalyst were conducted under milder conditions than the NHC borenium catalyzed reductions, with the reactions operating at atmospheric pressure, albeit with higher loadings and longer reaction times than the NHC borenium complexes.[45] These complexes were found to be more robust than previously reported systems and did not require purification of the hydrogen gas. The reasoning for higher stability from MIC borenium complexes can be rationalized by the increase in basicity of the carbene, which results from only singular heteroatom donation to the carbene.[37] The resulting effect is an increase in hydricity of the borane, and an included stability of the borenium complex.

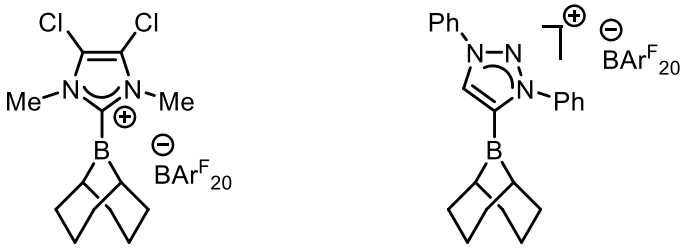


**Figure 1.3** Current best achiral borenium catalysts for the hydrogenation of imines and enamines.

The mechanism for borenium hydrogenation is thought to be analogous to tris(pentafluorophenyl)borane mediated hydrogenation (**Scheme 1.7**).[32] The highly Lewis acidic borenium complex and the Lewis basic imine heterolytically split hydrogen to form a carbene-coordinated borane and iminium complex. The borane then reduces the imine complex generating an amine as well as regeneration of the borenium catalyst. In these reactions, it can be expected that full frustration of the Lewis acid and base does not occur, as the imine borenium adduct has been detected by $^{11}B$ NMR during hydrogenation reactions.[45] This supports the idea that frustrated Lewis pairs can exist in equilibria of the adduct and the free acid/base pair.[45] The carbene borane adducts have a lower hydride affinity, while maintaining a comparable Lewis acidity compared to tris(pentafluorophenyl)borane, which allows for the observed reactivity.[45]

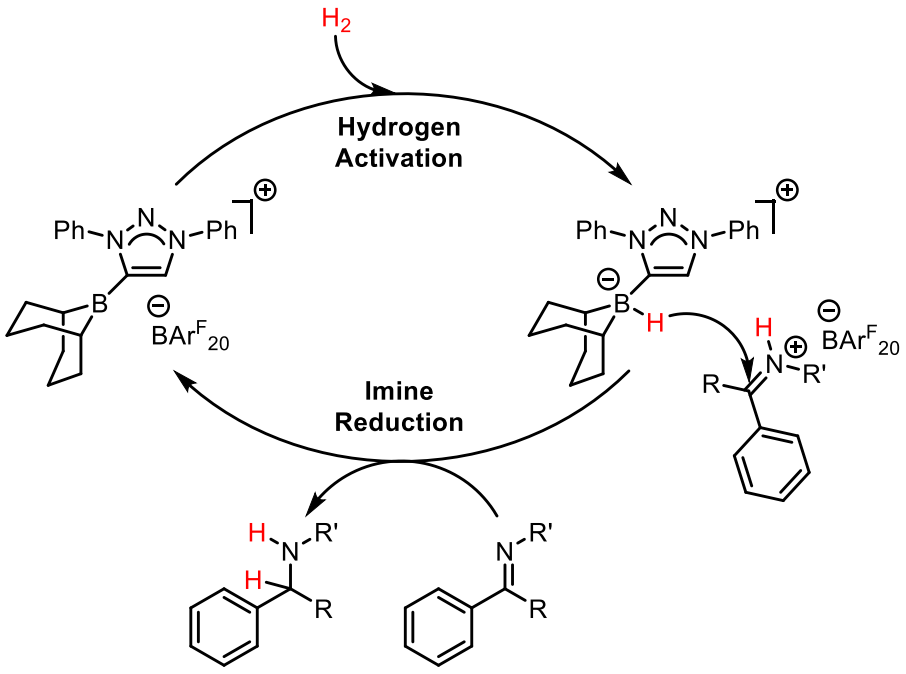


**Scheme 1.7** Proposed mechanism for imine hydrogenation via a carbene supported borenium complex.[45]

Following the initial hydrogenation investigations, Stephan, Crudden and Melen collaborated to investigate asymmetric hydrogenation of imines with borenium complexes (**Figure 1.4**).[46] In this report, many complexes were assessed, however the highest enantiomeric excess observed was 13% *e.e.* at room temperature and 20% *e.e.* at -30 °C with chiral boranes. When chiral carbenes were examined, the highest enantioselectivity observed was 12% *e.e.* which decreased with increasing reaction time. In 2019, Fuchter reported that the same borenium complex substituted with a triflimide anion in place of $BAr^F_{24}$ increased the enantioselectivity of the reaction to 18%.[47] Gratifyingly, when a broader substrate scope was examined by Fuchter, the same catalyst was able to facilitate highly enantioselective reductions (78-80% *e.e.*) in moderate yields when the substrates were *N*-cycloalkyl imines.[47] However, in all hydrogenation reactions reported within the literature prior to this thesis, *N*-benzyl imines were not suitable substrates for borenium hydrogenation, providing only trace amounts of conversion under conditions tested.[44–47]

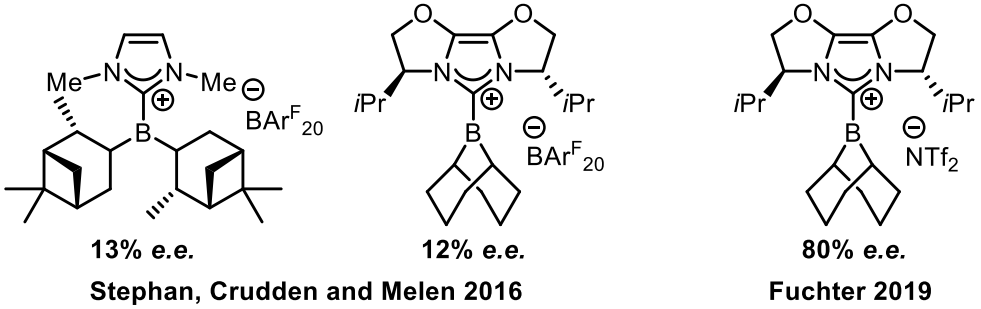


**Figure 1.4** Current best enantioselective borenium complexes in imine and enamine hydrogenation.[46,47]

### 1.3.3.2 Hydrosilylation with Borenium Complexes

Hydrosilylation has been an important transformation in organic synthesis for many years. Between 1990 and the early 2000s, Piers reported that tris(pentafluorophenyl)borane was capable of hydrosilylating ketones and imines.[20,48] These results showed that highly

Lewis acidic boron species are capable of catalytic hydrosilylation. In 2013, Denmark and Ueki reported that a lutidine supported 9-BBN borenium complex was capable of catalytically hydrosilylating ketones in a 10 mol % loading (**Scheme 1.8**).[49] The mechanism proposed within describes that the borenium pathway outcompetes a silylium mediated reduction. With this mechanism the borohydride would be the stereodefining step of the reaction, allowing for potential enantioselective catalytic activity. Jäkle reported the synthesis and subsequent catalytic reactivity of a planar chiral ferrocenyl-borenium complex that at cold temperatures was able to give 20% *e.e.* in the reduction of acetophenone.[50] A 2017 report by Ryu found that an oxazaborolidine scaffold was able to facilitate highly enantioselective borenium hydrosilylation of ketones, however the borenium in this reaction participated as a Lewis acid and not the hydride donor.[51]

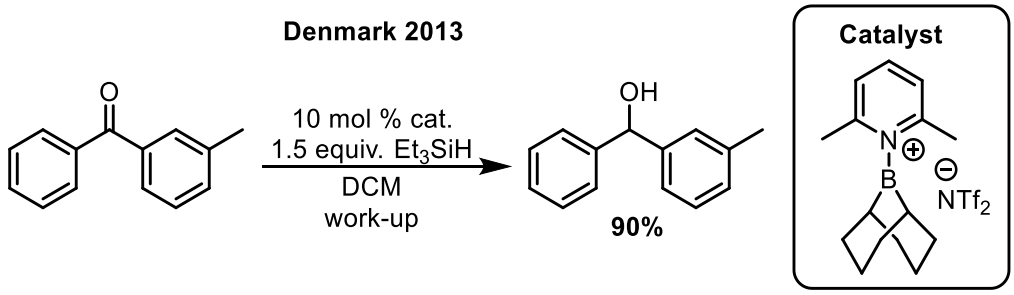


**Scheme 1.8** Early example of borenium catalyzed hydrosilylation.[49]

In the same seminal paper reported by Fuchter in 2019 that disclosed the asymmetric borenium hydrogenation, it was also reported that this catalyst could perform highly enantioselective hydrosilylations of imines.[47] This report was the first example of highly asymmetric borenium catalyzed hydrosilylation of imines with the highest enantiomeric excess observed was 86%. with a sterically demanding substrate. Overall, borenium hydrosilylation is less developed compared to its hydrogenation counterpart.

### 1.3.4 Other Reactions with Borocation Complexes

Over recent years borenium complexes have been reported in a variety of reactions. Borocations have been utilized in both the catalytic hydroboration of imines as well as N-heterocycles. NHC borane complexes have also been applied as stoichiometric reagents in the hydroboration of alkenes which proceeds through a cationic boron mechanism.[32] An activator such as triflimide or iodine is required for this reaction to generate the borenium complex. Similarly, boron cations have been shown to insert into C–H bonds via intramolecular addition.[32] This reaction proceeds via borenium generation with triflimide followed by loss of hydrogen. This insertion step can proceed at room temperature and when catalytic amounts of triflimide are used, elevated reaction temperatures are required. Asymmetric cyanation and allylation reactions have also been reported using chiral oxazaborolidinium complexes.[32] Both silicon and tin reagents have been utilized in these transformations. Borocations have also been featured in a variety of other carbon addition reactions as well as cycloaddition transformations which are detailed in reviews.[32,37]

## 1.4 Bis(amino)cyclopropenylidene (BAC) Carbenes

The cyclopropene moiety has been of great interest for over the past 55 years, with many derivatives and functional groups containing this core structure. While tris and bis amino cyclopropenium complexes have been prepared for many years, isolation of the free cyclopropenylidene carbene remained elusive for many years.[52,53] The radio-astronomical detection of cyclopropenylidenes was first reported in 1985 and this carbene motif is considered the most abundant cyclic hydrocarbon in interstellar space.[53] In 2006, Bertrand reported the synthesis and characterization of the free carbene.[53] This carbene can only be isolated in moderate to low yields and exhibits low stability with moisture and air. Interestingly, the free carbene was first thought to have been isolated by Weiss and Yoshida

independently.[54] However, the compound isolated was determined to be lithium adduct of the carbene. Generation of the lithium adduct in solution has been used to prepare a variety of BAC complexes. However, it was not until Bertrand reported the synthesis and isolation of the lithium adduct as a fluoroborate salt was this structure fully confirmed (**Scheme 1.9**).[54] The reagent was aptly named the Weiss-Yoshida reagent.

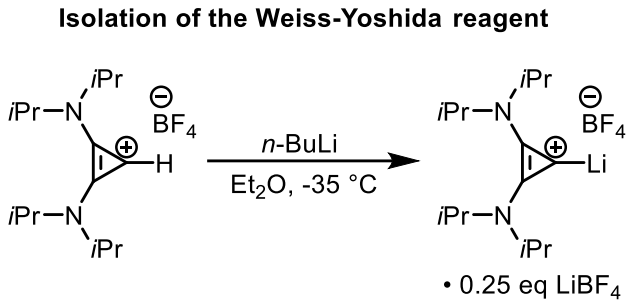


**Scheme 1.9** Formation of the Weiss-Yoshida reagent.[54]

Transition metal complexes with BAC carbenes have been prepared with metals such as rhodium,[55] iridium,[55] palladium,[55,56] platinum,[56] nickel,[57] as well as coinage metal complexes.[55,58] A nickel BAC carbene complex reported by Montgomery and co-workers was found to catalyze a reductive vinylation reaction with high regioselectivity.[57] Coinage metal complexes of BAC carbenes such as copper complexes have been utilized in click chemistry and act as transfer reagents to other transition metals.[55] The formation of BAC carbene adducts with main group elements have been reported prior to the isolation of the free carbene. Main group element-complexes involving phosphorus,[59] tin,[60] arsenic,[61] lead,[60] and germanium[60] have all been prepared as BAC adducts (**Figure 1.5**). Phosphorus and arsenic containing BAC complexes have been utilized as ligands for transition metal catalysis in cyclization reactions.[61,62] Prior to this thesis work, the only BAC carbene adduct with a boron containing species was reported by Bertrand and co-workers, involving a bis(carbene)borylene complex (**Figure 1.5**).[63]

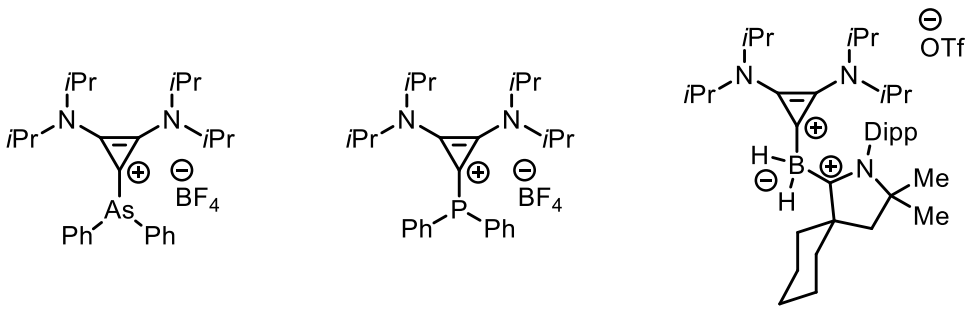


**Figure 1.5** Main group complexes with BAC carbenes.

BAC carbenes have been featured as catalysts in organic transformations such as Stetter and Benzoin reactions.[64–66] Initial asymmetric variants of these reactions only gave low enantioselectivity however the pyrrolidine scaffold has allowed for a chiral BAC carbene that facilitates enantioselective Stetter transformations with a maximum *e.e.* of 92% (**Scheme 1.10**).[64] BAC carbenes were also found to react with electrophiles such as carbon dioxide, carbon disulfide, and carbodiimides.[67] Comparatively, BAC carbenes are relatively underexplored in comparison to widely used NHCs.

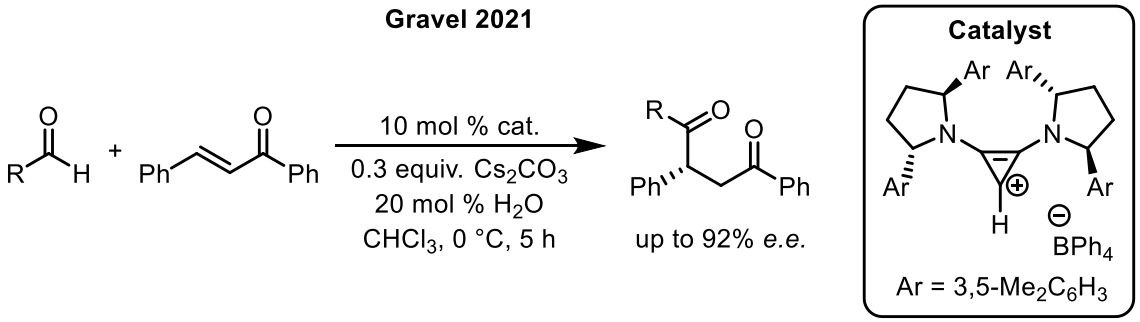


**Scheme 1.10** Enantioselective Stetter reaction catalyzed via a chiral BAC carbene.

## 1.5 Diazaphospholenes

### 1.5.1 Introduction

Diazaphospholenes are a class of compounds that consist of a five membered ring containing two carbons, two nitrogen atoms and one phosphorus.[68,69] While other five

member compounds containing these atoms may be possible, the isomer of diazaphospholenes of greatest importance in synthesis and catalysis are 1,3,2-diazaphospholenes.[68] These compounds are normally unsaturated in the backbone with a trivalent phosphorus atom. While the first diazaphospholenes were isolated in the early 1980s,[70,71] a greater focus on these compounds was acquired after the boom in NHC chemistry following the initial isolation of persistent carbenes.[72] The reasoning for the coinciding boom of interest in diazaphospholenes in conjunction with NHCs results from the structure of the phosphenium cation being valence isoelectronic to that of an NHC.[73] Diazaphospholenes are often the precursors to these phosphenium cations (**Scheme 1.11**). Over many years, the synthesis and applications of diazaphospholenes in a variety of transformations has been explored, and they have even been used as ligands in transition metal catalysis.[68,69,74] The greatest discovery of interesting reactivity in these diazaphospholene complexes is the umpolung of the P–H bond, where it behaves as a hydride.[69] While this discovery was noted in the early 2000s,[75] only recently have diazaphospholenes been used in reductive catalysis.[69]

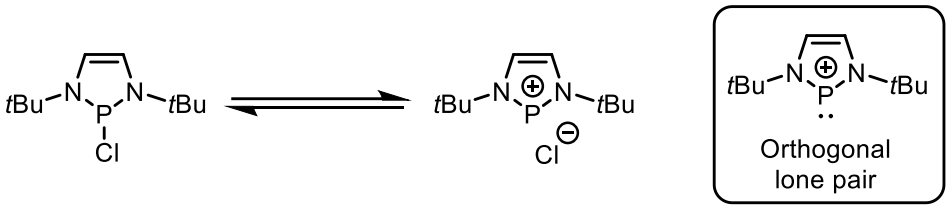


**Scheme 1.11** Dissociation of the chloride anion is stabilized by the formation of an aromatic compound.[69]

### 1.5.2 Synthesis of Diazaphospholenes and Derivatives

Diazaphospholene complexes have been prepared with a variety of functional groups on the nitrogen substituents and the backbone of the ring. While benzo-fused complexes have been prepared, catalytically relevant diazaphospholenes are mainly

hydrogen substituted on the backbone or in rare instances, contain alkyl groups.[69] Bearing structural resemblance to NHCs, diazaphospholenes can be synthesized from 1,4-diazadienes (**Scheme 1.12**). Initial synthetic routes to prepare diazaphospholenes involved the reduction of the 1,4-diazadiene to a dianion with a metal such as lithium or sodium (**Scheme 1.12**).[68] Following reduction, the dianion can be quenched with phosphorus trichloride to produce a diazaphospholene chloride (**Scheme 1.12**). Alternatively, the dianion can be quenched with tetrachlorosilane to produce a silole and then subsequently allowed to react with phosphorus trichloride to produce the diazaphospholene chloride, with loss of $SiCl_4$ (**Scheme 1.12**).[69] Quenching the dianion with triethylammonium hydrochloride produces an isolable aminoaldimine, which can be cyclized into the diazaphospholene chloride in higher yield than the one pot method (**Scheme 1.12**).[68] The dianion exists as the *Z* and *E* isomers, and only the *Z* isomer reacts with the phosphorus trichloride.[69] The aminoaldimine produced from protonation of both isomers reacts with the phosphorus trichloride in the presence of triethylamine (**Scheme 1.12**). The aminoaldimine allows for equilibration to the reactive *Z* geometry.[69] The mildest and most cost-effective route to prepare diazaphospholenes was reported by Macdonald and co-workers,[76] and involves treatment of an aryl 1,4-diazadiene with phosphorus tribromide and cyclohexene (**Scheme 1.13**). The side product from this reaction, *trans*-dibromocyclohexane is readily separated from the product, allowing for facile isolation through filtration. This method has been applied by the Speed group to prepare a variety of highly active diazaphospholene catalysts, including chiral examples.[69]

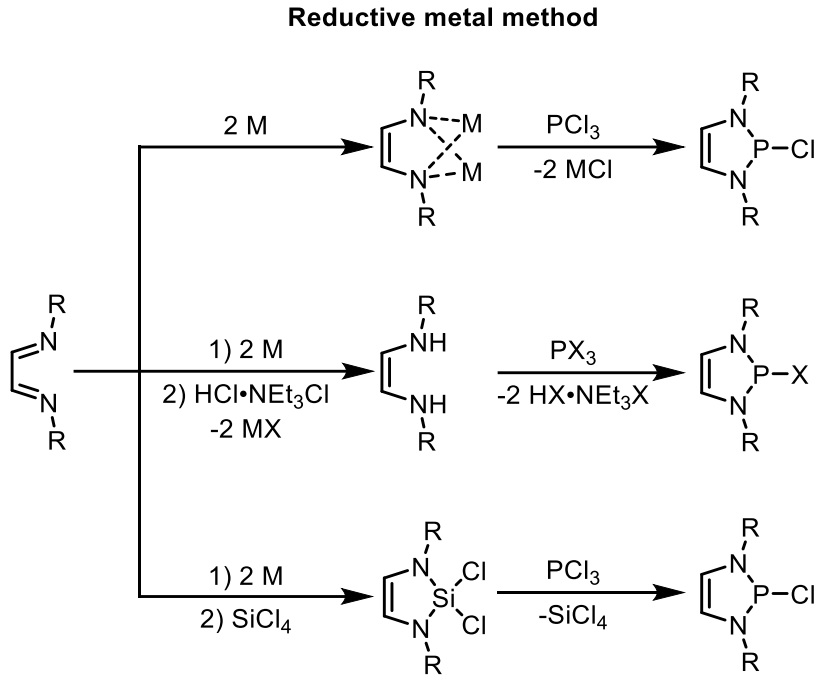


**Scheme 1.12** Diazaphospholene synthesis using a metal reductant.

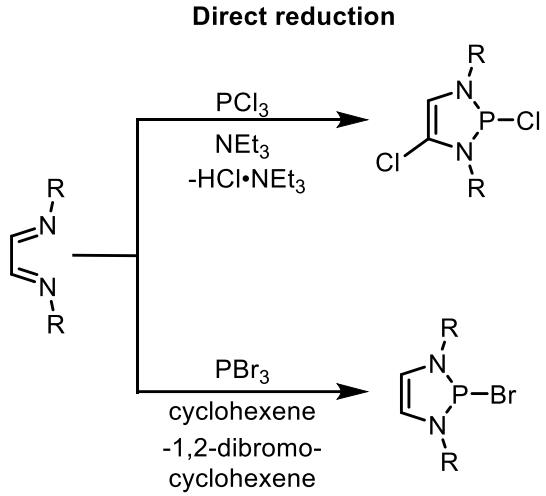


**Scheme 1.13** Diazaphospholene synthesis directly from a phosphorus trihalide.

Diazaphospholene halides are the general synthetic precursor for a variety of catalysts.[69] The unique reactivity of diazaphospholenes arises from the highly polarized exocyclic bond from phosphorus (**Scheme 1.11**). Conjugation of the electrons in the backbone and the nitrogen atoms allows for an aromatic system of 6 pi electrons, since the lone pair on phosphorus is orthogonal to the ring system and does not count toward this

Hückel number. This conjugation allows development of aromaticity to be a driving force leading to polarization of this compound. The effect of this polarization has been observed by various researchers, and the properties extensively reviewed.[72] Substitution of the *P*-substituents can be harnessed to synthesize a variety of diazaphospholene derivatives for applications in catalysis and functionalization (**Scheme 1.14**).[69] Reacting a diazaphospholene halide with hydrides such as Red-Al or $LiAlH_4$ results in the formation of a diazaphospholene hydride, a highly reducing species (**Scheme 1.14**).[69] Treatment with silver triflate or TMS triflate affords the phosphenium triflate ion pair, a catalyst in reductive chemistry (**Scheme 1.14**).[69] Additionally, treatment of a diazaphospholene halide with an alcohol and base, or alkoxide results in the formation of a *P*-alkoxy diazaphospholene (**Scheme 1.14**).[69] These complexes were shown by the Speed group to act as a stable precatalyst for reduction chemistry.[77,78] Hydrolysis of many diazaphospholene derivatives results in the formation of a diazaphospholene oxide, which acts as an air-stable precatalyst in reduction chemistry.[79]

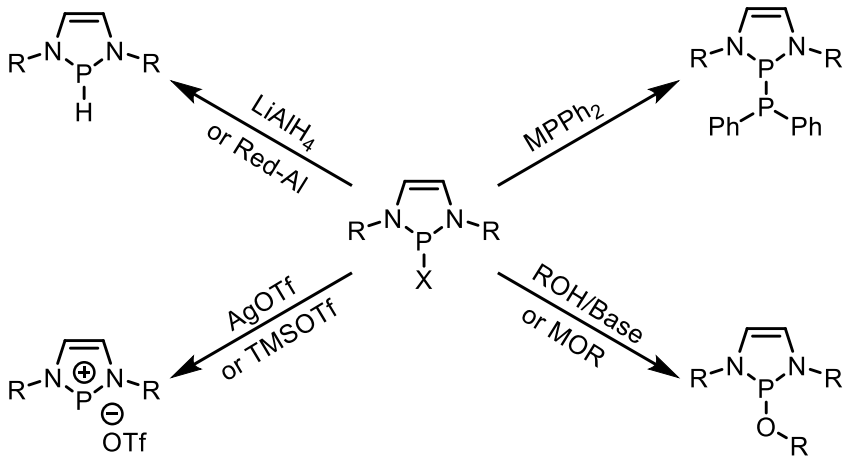


**Scheme 1.14** Derivatization of diazaphospholene halides.

Bisphosphane compounds can also be prepared from diazaphospholenes (**Scheme 1.15**).[68] Gudat reported that addition of trimethylstannyl diphenylphosphide to a

diazaphospholene halide results in a diazaphospholene-diphenylphosphide complex as well as trimethylstannyl chloride.[80] A diazaphospholene dimer can be prepared through reductive coupling methods, such as treatment of a diazaphospholene halide with magnesium or though photolysis of a diazaphospholene hydride with concomitant loss of hydrogen gas (**Scheme 1.15**).[68] The synthesis and reactivity of diazaphospholene dimers is less explored in comparison to other diazaphospholene derivatives.[68,81]

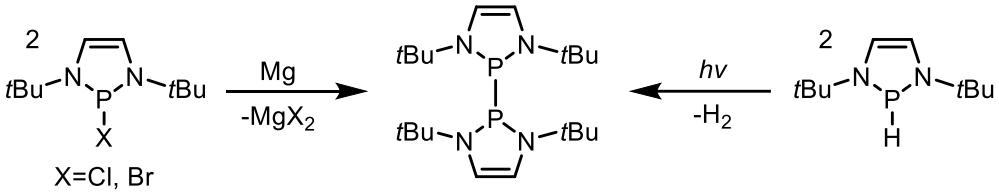


**Scheme 1.15** Formation of diazaphospholene dimers via two methods.

### 1.5.3 Reactivity of Diazaphospholenes

The catalytic application of diazaphospholenes had been limited since the first reports of diazaphospholene hydrides in the early 2000s.[75] Only in the past 7 years have diazaphospholene hydrides been greatly investigated as reductive catalysts.[69] The discovery that diazaphospholenes bearing a hydrogen are hydric was disclosed by Gudat and co-workers in the early 2000s.[75] These compounds exhibit hydridic properties rather than being weakly acidic like a traditional P–H bond. The same rationale of aromatic stabilization that accounts for the stability of the phosphenium cations can be used to understand the umpolung properties of this bond. More recently, Yang and Cheng have quantified that diazaphospholenes are stronger hydride donors than common neutral boranes and silanes.[82] The hydricity of a diazaphospholene is dependent on its substituents, with *N*-alkyl being more reactive than *N*-aryl, and unsaturation of the backbone greatly increasing the hydricity (**Figure 1.6**).

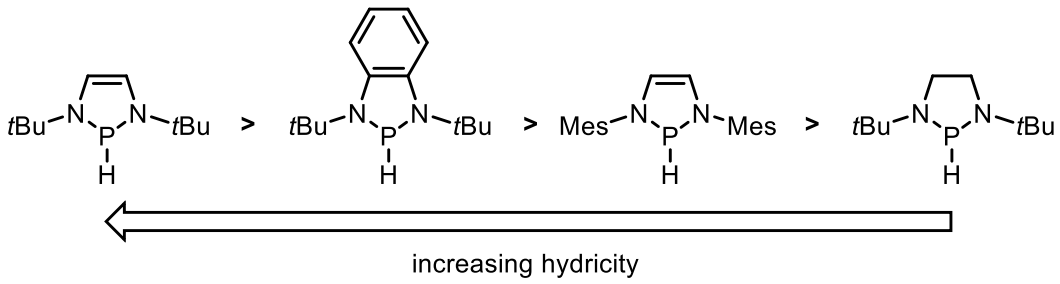


**Figure 1.6** Hydricity scale of diazaphospholene hydrides.

Seminal work by Gudat showed that diazaphospholene hydrides can react with aldehydes and conjugate acceptors (**Scheme 1.16**).[75] The result of these reactions were hydrophosphinations resulting in a P-O-bound diazaphospholene product. The reduction of conjugate acceptors with diazaphospholenes was found to be 1,4-selective.[83] Kinjo, Hirao and co-workers then disclosed that the diazaphospholenes can be used in catalytic amounts with ammonia borane as the terminal reductant in the reduction of azo compounds.[84] This same team then showed that the stoichiometric reduction of carbonyls reported by Gudat could be made catalytic with pinacolborane to regenerate the catalyst.[85] The mechanism for regeneration of the catalyst was determined to be sigma bond metathesis. Following these initial investigations, Kinjo reported that carbon dioxide can be reduced with a diazaphospholene catalyst and diphenylsilane as the reductant.[86] The Speed group and Cramer group then reported that the *P*-alkoxy diazaphospholene compounds could act as entry points in catalysis (**Scheme 1.16**).[77,87] These intermediates are more stable and readily isolable than the extremely moisture and oxygen-sensitive diazaphospholene hydride. The Speed group then disclosed the catalytic reduction of imines as well as the asymmetric reduction of imines.[77,78] Since these reports, a variety of diazaphospholene precatalysts have been prepared investigating the reduction of a variety of unsaturated substrates.[69] The attractive feature of diazaphospholenes in catalysis relies on the variety of available entry

points into catalysis and the diversity of available reductants that function with these catalysts.[69]

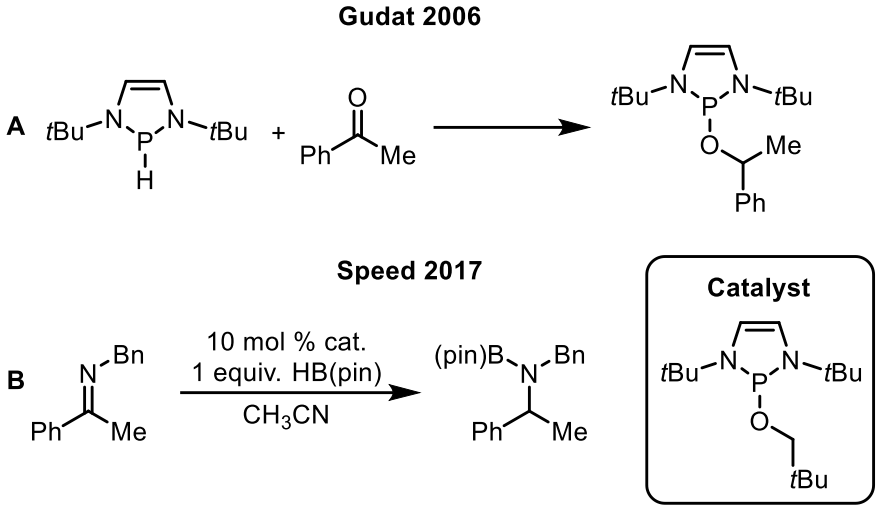


**Scheme 1.16** (**A**) hydrophosphination of a ketone forms an alkoxy diazaphospholene. (**B**) An alkoxy diazaphospholene can be used as a more stable precatalyst in the reduction of imines.

While the majority of diazaphospholene catalysis has investigated the polar reactivity of diazaphospholenes, these compounds are capable of radical reactions as well. The radical properties of a diazaphospholene were recognised by Gudat and Wright though the formation and scission of diazaphospholene dimers.[88–90] It was found that monomeric diazaphospholene radicals were only observed upon an increase in temperature with a *N*-*tert*-butyl diazaphospholene dimer.[89] Sterically demanding dimers were found to exhibit an increased radical behavior. Only recently, Yang, Cheng, and co-workers have reported that diazaphospholenes are able to facilitate radical transformations (**Scheme 1.17**).[91,92] Their work required the use of AIBN to initiate the radical behavior of the diazaphospholenes, and elevated temperatures. Within Chapters 6 and 7 is a continued look into the radical behavior of diazaphospholenes.

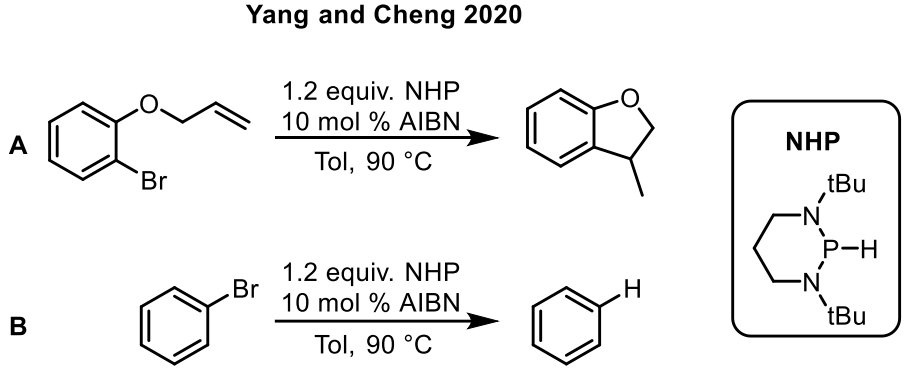


**Scheme 1.17** (**A**) Radical cyclization and (**B**) dehalogenation facilitated by a *N*-heterocyclic phosphine hydride.

Bisphosphane compounds have also been applied in stoichiometric and catalytic transformations.[68] Early work by Gudat shown that a diazaphospholene-diphenylphosphide complex can react stoichiometrically with alkyl halides and a variety of other electrophilic substrates in substitution reactions (**Scheme 1.18**).[80,93–95] Alkynes and alkenes were also found to react with these complexes, resulting in addition across the unsaturated bond. The reactivity with alkyl halides to produce diphenylphosphine-substituted alkanes was rendered catalytic with use of trimethylsilyl diphenylphosphide to regenerate the catalyst.[93] Diazaphospholene dimers have also been studied in their reactivity (**Scheme 1.19**).[95] These compounds were reported by Gudat to undergo a variety of reactions with electrophilic substrates. Such examples include the addition across alkynes, like the work conducted with diazaphospholene-diphenylphosphide.[95] These dimers were found to cleave metal halide bonds to produce dimeric metal complexes and diazaphospholene halides.[96] In a similar manner, diazaphospholene dimers were found to react with triethylammonium hydrochloride to produce a diazaphospholene hydride and chloride as products from the reaction.[90] Lastly, Masuda and co-workers reported that saturated diazaphospholene dimers were able to react with heteroallenes (**Scheme 1.20**).[97] The continued exploration of diazaphospholene dimers in functionalization reactions is explored in chapter 7.

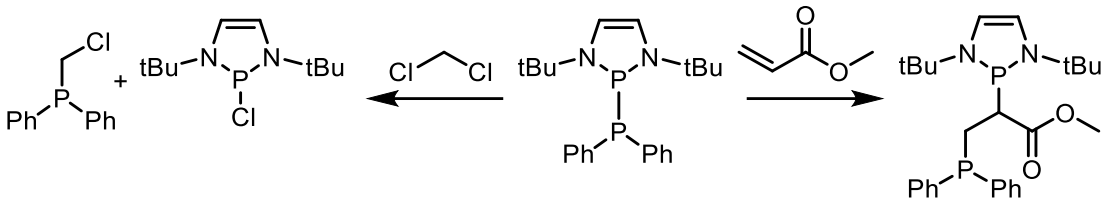

**Scheme 1.18** Functionalization of electrophiles facilitated by a bisphosphine.

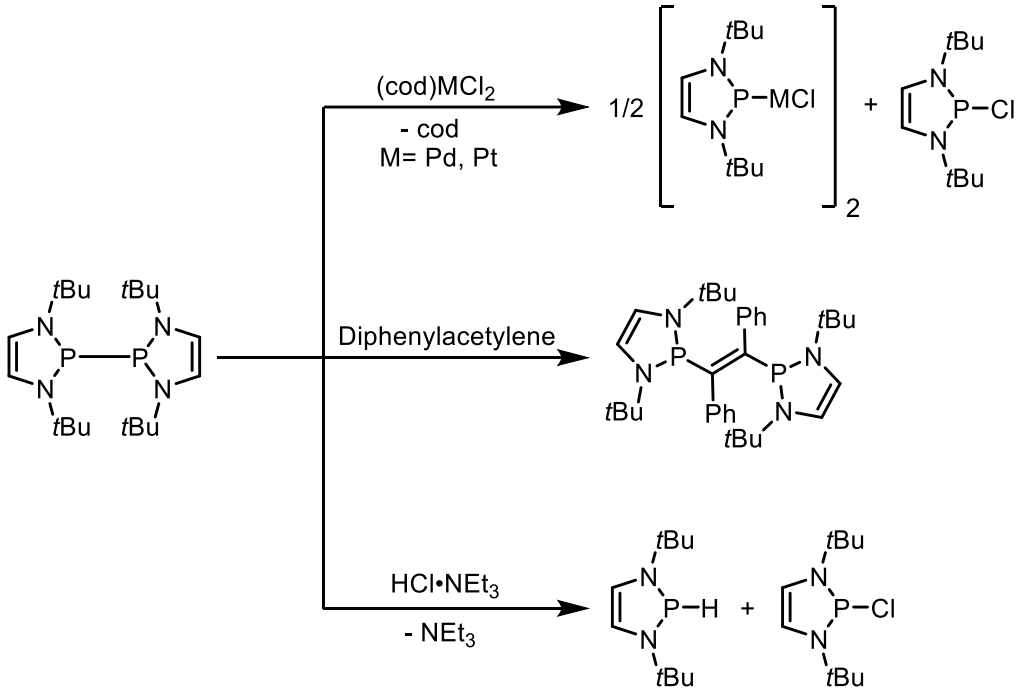

**Scheme 1.19** Examples of diazaphospholene dimer reactivity.

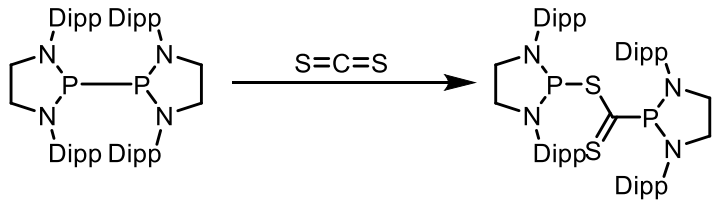

**Scheme 1.20** Saturated diazaphospholene dimer reactivity.

# Chapter 2: Synthesis and Catalytic Reactivity of Bis(amino)cyclopropenylidene Carbene-Borane Adducts

Reprinted with permission from **B. S. N. Huchenski**, M. R. Adams, R. McDonald, M. J. Ferguson, A. W. H. Speed, *Organometallics*, **2016**, 35, 3101. Copyright 2021 American Chemical Society. The manuscript has been reformatted to match the global thesis format, and references and compounds have renumbered where appropriate. Sub-section headers have been added.

Contributions to manuscript: All synthetic work in this chapter was carried out by B. S. N. Huchenski, except the synthesis of BAC carbene precursors **2-8a, 2-8b, 2-10,** and **2-11**, and $NaBAr^{F}_{24}$ which were prepared by Dr. A. W. H. Speed. Imines **2-21**, **2-23**, and **2-25** were prepared collaboratively between B. S. N Huchenski and M. R. Adams. The X-ray crystallography was conducted by Dr. R. McDonald, and Dr. M. J. Ferguson. Mass spectrometric data were acquired by Mr. Xiao Feng (Mass Spectrometry Laboratory, Dalhousie University). The manuscript was written by B. S. N. Huchenski and Dr. A. W. H. Speed. In addition, the structure of compound **2-7**, in **Figure 2.2** was obtained by Dr. Katherine N. Robertson, and was not contained in the original manuscript.

## 2.1 Introduction

Adducts of carbenes and boranes have recently emerged as powerful reducing reagents. The most common type of adduct employs *N*-heterocyclic carbenes (NHCs), for example adduct **2-1** (**Figure 2.1**).[41,98,99] These neutral adducts are remarkably stable stoichiometric reductants,[100] frequently being stable to silica gel chromatography,[101] despite their capacity to reduce carbonyl and imine compounds and hydroborate olefins in the presence of activating reagents. Not all carbenes can form stable adducts with borane; for example, while cyclic amino alkyl carbene (CAAC) boron trifluoride adduct **2-2a** could

be isolated, the corresponding borane adduct **2-2b** was not isolable.[100] Notwithstanding the above difficulties, changing the identity of the carbene has allowed development of enhanced reactivity; mesoionic carbene (MIC) borane adducts such as **2-3** have been shown to be more potent reducing reagents than the corresponding NHC adducts.[102] In addition to stoichiometric reactivity, carbene borane adducts have recently been used to generate borenium cations that serve as the Lewis acid component in frustrated Lewis pair based hydrogenation catalysts.[43] As an example, NHC supported borenium cation **2-4** represents the most active NHC-borane based hydrogenation catalyst, capable of reducing *tert*-butyl or phenyl ketimines, and hindered enamines at 5 mol % loading under 102 atmospheres of $H_2$.[44] In a further demonstration of the importance exploring different carbene motifs, MIC supported borenium cation **2-5** represents the most active borenium based hydrogenation catalyst reported to date, capable of hydrogenating *tert*-butyl or phenyl imines, and sterically encumbered nitrogen containing heterocycles at pressures of hydrogen varying from one to 102 atmospheres at 10 mol % loading.[45]

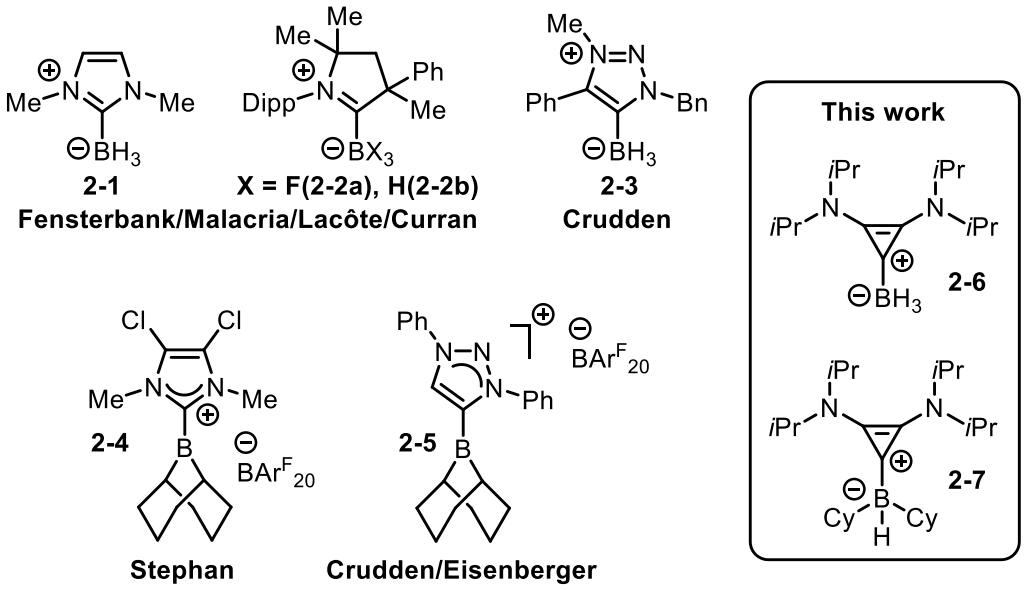


**Figure 2.1** Various Adducts of Boron and Carbenoids (Dipp = 2,6-diisopropylphenyl).

Bis(amino)cyclopropenylidene carbenes (BAC carbenes) represent an alternative and emerging carbene architecture. The first example of an isolated BAC carbene was disclosed by Bertrand and co-workers in 2006 as a highly air and moisture sensitive crystalline solid.[53] Since that time, catalysts based on BAC carbenes have been used to promote Stetter and benzoin reactions,[65,66,103] and have been used as ligands in a nickel catalyzed reductive vinylation.[57] The abovementioned work in nickel catalyzed reactions has shown that BAC carbenes possess reactivity characteristic of having a smaller steric profile than *N*-heterocyclic carbenes.[57] We anticipated that this decreased steric demand would enhanced reactivity in stoichiometric and catalytic reactions employing BAC carbene-borane adducts. Also, BAC carbene precursors are readily and inexpensively synthesized, being accessible from commercially available pentachlorocyclopropane in a single pot operation on multigram scale, unlike current lengthier routes to MIC precursors.[102,104] This present work discloses the synthesis, stoichiometric carbonyl reduction, and catalytic imine reduction with BAC carbene borane adducts **2-6** and **2-7**.

Disclosure of BAC carbenes adducts with main group elements preceded the isolation of the parent BAC carbene, and examples including tin, germanium, and lead,[60] phosphorus[59] and arsenic[61] adducts have been synthesized. Additional complexes of BAC carbenes and metals include copper, silver, rhodium, iridium and palladium.[55,105] To the best of our knowledge, BAC carbenes have not been employed in the formation of adducts with neutral boranes.[63]

**2.2 Results and Discussion**

Our initial attempt to synthesize adduct **2-6** involved heating BAC carbene precursor **2-8a** at reflux in toluene for 20 h with sodium borohydride (**Scheme 2.1**). While we undertook this operation with the hope of directly synthesizing target BAC borane

adduct **2-6** with concomitant loss of hydrogen and sodium tetraphenylborate, in analogy to known chemistry with imidazolium iodides,[106] we instead observed clean formation of a crystalline, air stable product exhibiting a broad singlet at -9.4 ppm in the proton-coupled $^{11}B$ NMR spectrum. Integration of the phenyl and isopropyl signals in the $^{1}H$ NMR spectrum suggested the formation of **2-9**, which was verified on the basis of a single crystal X-ray crystallography experiment (**Scheme 2.1**). Compound **2-9** features a boron to carbon interatomic distance of 1.6394(15) Å. This is similar to the 1.666(3) Å boron to carbon interatomic distance reported by Ong and co-workers for an NHC triphenylboron adduct.[107] The presence of an ionic additive proved necessary for the formation of **2-9**, as **2-8a** was stable for 24 h in refluxing toluene without any additional additive. Sodium tetrafluoroborate also promoted the formation of **2-9** from **2-8a**.

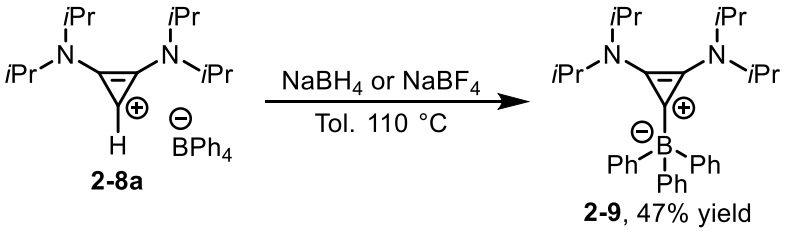


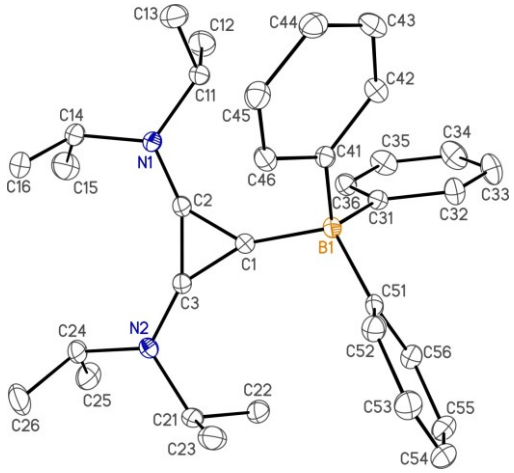


**Scheme 2.1** Synthesis and structure of BAC carbene triphenylborane adduct **2-9**. The thermal ellipsoids are scaled at the 30% probability level. Hydrogen atoms are omitted for clarity. Selected interatomic distances (Å); C1–B1 1.6394(15), C1–C3 1.3871(15), C2–C3 1.3892(14), N1–C2 1.3267(14).

In an attempt to develop a more general synthesis of BAC carbene borane adducts, we added crystalline BAC carbene **2-10** to borane dimethyl sulfide or 9-BBN in ethereal solvents or toluene (**Scheme 2.2**). Each of these trials resulted in the formation of intractable tacky red mixtures exhibiting complex $^{1}H$ and $^{11}B$ NMR spectra. Despite these initial setbacks, our attention turned to the use of a BAC carbene lithium tetrafluoroborate adduct **2-11** (the Weiss-Yoshida reagent).[54]

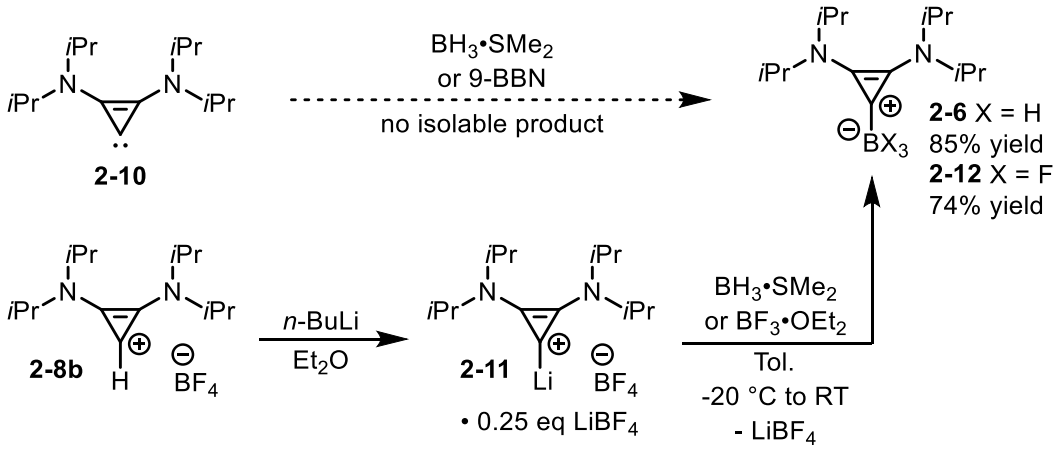


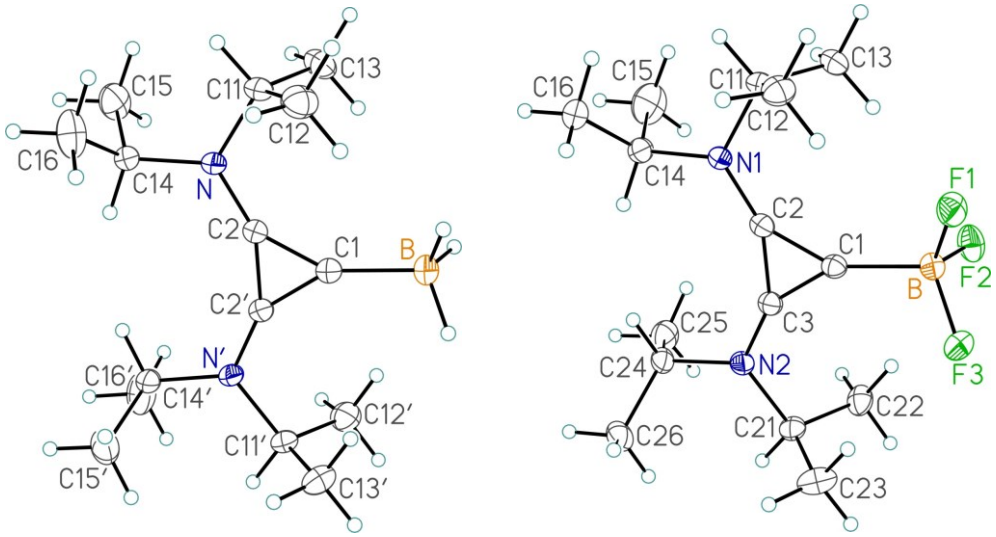


**Scheme 2.2** Synthesis and structures of BAC Carbene $BH_3$ **2-6** (left) and $BF_3$ **2-12** (right) adducts. The thermal ellipsoids are scaled at the 30% probability level. Selected interatomic distances (Å): **2-6** C1–B1 1.608(5); **2-12**, C1–B1 1.641(3).

This reagent was crystallized and characterized by Bertrand and co-workers as a polymeric material consisting of a BAC carbene lithium adduct with a 5:4 lithium tetrafluoroborate to BAC carbenenoid stoichiometry. In our hands, deprotonation of **2-8b** with butyllithium in diethyl ether, in the presence of 0.25 equivalents of lithium tetrafluoroborate, followed by concentration and pentane trituration under a dry nitrogen atmosphere gives a 93% yield of a free-flowing white powder (**2-11**) that was used in subsequent reactions without additional purification. Mixture of this reagent with borane dimethyl sulfide or boron trifluoride etherate complexes in toluene, followed by evaporation and extraction of the resulting residue with dichloromethane resulted in clean formation of the desired adducts **2-6** and **2-12**. Adducts **2-6** and **2-12** can be stored indefinitely under air without decomposition (> 4 months), however some decomposition of **2-6** is noted with silica gel chromatography.

The structures of **2-6** and **2-12** were confirmed on the basis of NMR spectroscopy and single crystal X-ray diffraction data. Compound **2-6** features a C–B interatomic distance of 1.608(5) Å, while compound **2-12** features a C–B interatomic distance of 1.641(3) Å. A quartet is observed at -35.1 ppm with $^{1}J_{B,H}$ = 86 Hz in the $^{11}$B NMR spectrum of **2-6** and a quartet is also observed in the $^{11}$B NMR spectrum of **2-12** at -0.4 ppm, with $^{1}J_{B,F}$ = 34 Hz. These metrics are comparable to previously reported carbene borane adducts.[102,108]

The ability of adduct **2-6** to serve as a source of hydride was investigated (**Scheme 2.3**). While no reaction occurred when 0.5 equivalents of **2-6** were mixed with 4-cyanobenzaldehyde (**2-13a**), addition of silica gel, a precedented activator for carbonyl reduction by NHC-boranes,[100] resulted in clean reduction to alcohol **2-14a** in only 1 h.

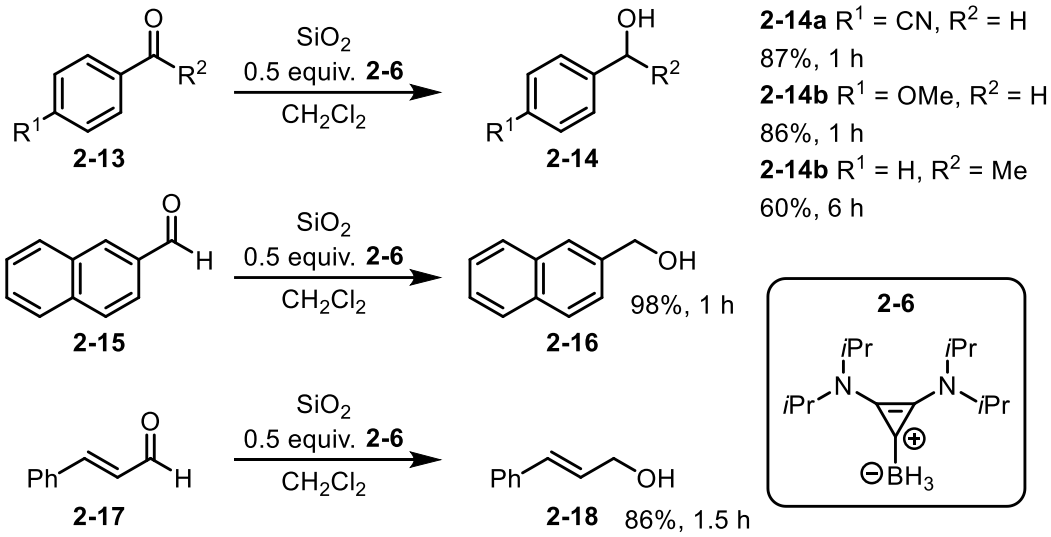


**Scheme 2.3** Reduction of carbonyl compounds using 0.5 equivalents of **2-6** in the presence of silica gel.

Electron rich anisaldehyde (**2-13b**) and 2-naphthaldehyde (**2-15**) were also reduced under the same conditions. A slightly higher yield of 2-napthylmethanol (**2-16**) was attributed to decreased product volatility. Acetophenone (**2-13c**), proved a more challenging substrate, with only 60% conversion observed after 6 h. Cinnamaldehyde (**2-17**) was cleanly reduced in a 1,2 fashion, with cinnamyl alcohol (**2-18**) as the only product; no 1,4-addition product was observed. These reaction times are faster than those reported for NHC-boranes,[100] and comparable to those observed for MIC-borane **2-3**.[102]

Our methodology was extended to a borane bearing both a hydride and alkyl groups. Addition of dicyclohexylborane to reagent **2-11** in diethyl ether gave adduct **2-7** in 84% yield as an air stable beige solid that is unstable to silica gel chromatography.[109] A single crystal suitable for X-ray analysis grown from evaporation in benzene, NMR, and MS data corroborate the structure of **2-7** depicted in **Scheme 2.4** and **Figure 2.1**. As a diagnostic feature, a doublet is observed at -12.1 ppm with $^{1}J_{B,H}$ = 71 Hz in the $^{11}$B NMR spectrum of **2-7**.

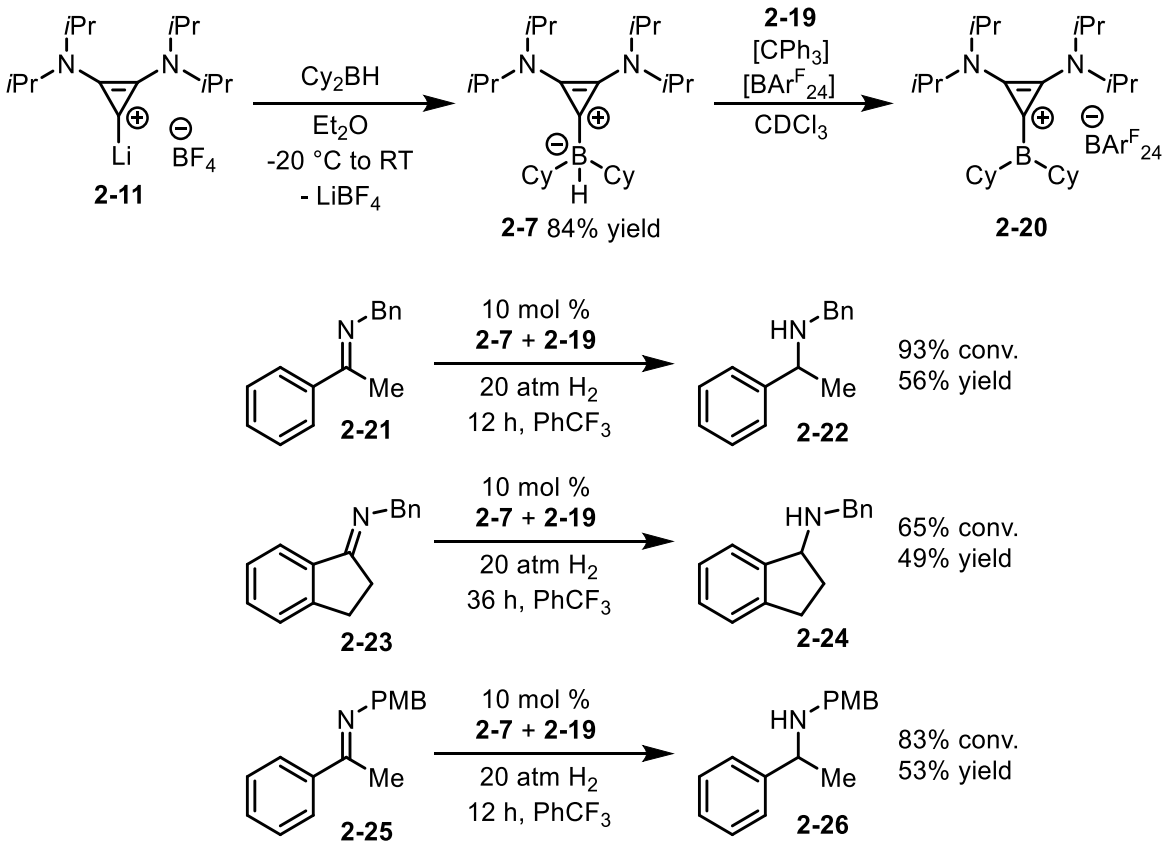


**Scheme 2.4** Hydrogenations of benzyl imines catalyzed by borenium cation **2-20**.

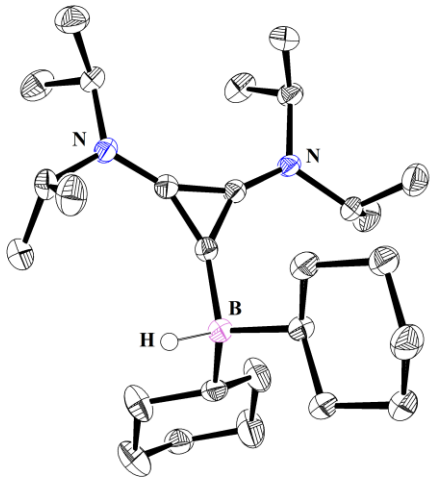


**Figure 2.2** The structure of **2-7**. Thermal ellipsoids have been drawn at the 50% probability level. Hydrogen atoms have not been labelled except for the borane.

Combination of adduct **2-7** with trityl tetrakis[3,5-(trifluoromethyl)phenyl]borate **2-19** in dry $CDCl_3$ resulted in hydride transfer, and formation of putative borenium cation

**2-20**, identified by the disappearance of the doublet at -12.1 ppm, and appearance of a broad signal at 81.0 ppm in the $^{11}$B NMR spectrum (a range comparable to adduct **2-4**, 82.9 ppm).[44] One equivalent of triphenylmethane also appeared in the $^{1}$H spectrum of the reaction. Since borenium cations **2-4** and **2-5** are hydrogenation catalysts, we explored the application of **2-7** to catalytic hydrogenation. A 10 mol % combination of **2-7** and **2-19** in trifluorotoluene was able to effect the hydrogenation of benzyl imines **2-21**, **2-23**, and paramethoxybenzyl (PMB) imine **2-25** to the corresponding amines with high conversion under 20 atmospheres of $H_2$ at ambient temperature. The hydrogenation was conducted in a Parr bomb, with 99.999% purity grade hydrogen, which was otherwise used as received.[110] Importantly, benzyl imines are not substrates for previously reported borenium based hydrogenation catalysts.[111] Catalysts **2-4** and **2-5** cannot hydrogenate substrate **2-21** (0% conversion reported at 102 atmospheres $H_2$ pressure for **2-4**, and "trace" conversion reported at 102 atmospheres $H_2$ for **2-5**).[44,45] Since the benzyl and PMB groups are one of the most commonly used protecting group for amines, the work disclosed herein represents an advance in borenium catalyzed hydrogenation reactions, enabled by the use of BAC carbene borane complexes.

## 2.3 Conclusion

In conclusion, we have developed a reliable and high yielding synthesis of crystallographically characterized BAC carbene borane adducts, where success was dependent on the use of lithium tetrafluoroborate adducts of BAC carbenes rather than the free carbene. We have shown BAC carbene borane adducts are capable of stoichiometric reduction of carbonyl compounds, and catalytic reductions of benzyl imines, a challenging class of substrate for catalytic reduction by borenium catalysts. Preparation of additional

BAC carbene borane adducts to increase reaction efficiency, expand substrate scope, and effect asymmetric imine hydrogenations is underway and will be reported in due course.

## 2.4 Experimental

### 2.4.1 General Considerations

Isolation of the Weiss-Yoshida reagent (**2-11** *i*PrBAC-$LiBF_4$ adduct) and addition to boranes was carried out under a $N_2$ atmosphere in a 2001 issue IT Glovebox ($O_2$ levels typically 7 ppm, $H_2O$ levels typically 15 ppm) or oven dried Schlenk glassware. Hydrogenation reactions were carried out in scintillation vials equipped with magnetic stir bars inside a Parr bomb. The reactions were loaded into the Parr bomb, and the bomb was assembled inside the IT Glovebox. The reactor removed from the box and was purged by pressurizing to 300 psi with $H_2$, and venting two times, before the final pressure was established. All other work-ups and reactions were carried out under ambient atmosphere in undried glassware. $^{1}H$, $^{13}C$, $^{11}B$, and $^{19}F$ NMR data were collected at 300K on Bruker AV-500 or AV-300 NMR spectrometers. Chemical shifts are reported in parts per million downfield of $BF_3$•$Et_2O$ (for $^{11}B$ NMR) and $CFCl_3$ (for $^{19}F$ NMR). $^{1}H$ NMR spectra are referenced to residual non deuterated NMR solvent ($CHCl_3$ = 7.26 ppm). $^{13}C$ NMR spectra are referenced to the central $CDCl_3$ peak (77.16 ppm). Two $^{13}C$ resonances in compound **2-7** were not observed, despite prolonged acquisition time. Melting points were acquired using an Electrothermal® apparatus and are uncorrected. Mass spectrometric data were acquired by Mr. Xiao Feng (Mass Spectrometry Laboratory, Dalhousie University). IR Spectra were acquired on a Bruker Tensor 27 FTIR, on NaCl plates.

### 2.4.2 Solvent Purification

**Pentane** for purification (ACS grade) was purchased from Fisher and used as received. **Toluene and pentane** for reactions were deoxygenated and dried by sparging with

dinitrogen gas, followed by passage through a double-column solvent purification system purchased from mBraun Inc. The solvents were stored over dry 3 Å molecular sieves in the glovebox.

**Diethyl ether** for purification (ACS grade) was purchased from Fisher and used as received.

**Diethyl ether** for reactions was further distilled from a purple solution of benzophenone/sodium ketyl and stored over dry 3 Å molecular sieves in the glovebox.

**Dichloromethane** (ACS grade) was purchased from Fisher and used as received.

**Deuterochloroform** (Cambridge Isotopes) was stored over dry 3 Å molecular sieves, but otherwise used as received.

**Trifluorotoluene** (Anhydrous >99%) was purchased in a Sure/Seal™ container from Aldrich and cannula transferred onto dry 3 Å molecular sieves for storage in the glovebox, but otherwise used as received.

### 2.4.3 Reagents for Synthesis

**3 Å Molecular Sieves** were purchased from Aldrich and dried at 200 °C at approximately 0.5 torr for 12 h prior to use.

***i*PrBAC Carbene Precursors 2-8a** and **2-8b** were prepared according to literature procedures and purified by recrystallization from dichloromethane/diethyl ether.[53,54]

**Borane-Dimethyl Sulfide Complex** was purchased from Aldrich and used as received.

**Boron Trifluoride Etherate** was purchased from Fisher and distilled under a nitrogen atmosphere into a storage bomb prior to use.

***n*-Butyllithium** was purchased from Aldrich as a 2.5 M solution in pentane and the concentration was verified by titration with 1,10-phenanthroline/butanol prior to use.

**Celite® S** was purchased from Aldrich and used as received.

**Hydrogen** was purchased from Praxair as UHP (99.999%) grade and used as received.

**Silica Gel** (40-63 μm, Silaflash, P60) was purchased from Silicycle, and used as received.

**Sodium Borohydride** was purchased from Aldrich and used as received.

**Trityl $BAr^F_{24}$** was prepared according to literature procedures.[112,113]

**Reduction Substrates:** Acetophenone, anisaldehyde, cinnamaldehyde, 4-cyanobenzaldehyde, and 2-naphthaldehyde were purchased from Aldrich, and used as received after purity was verified by $^1$H NMR. Imines **2-21**, **2-23** and **2-25** were prepared by a 1:1 combination of the appropriate ketone and benzylamine in dichloromethane, in the presence of 1 equivalent of titanium ethoxide for 24 h. The reactions were quenched by addition of aqueous KOH (15 %), filtered onto $Na_2SO_4$, refiltered and concentrated. Purification was accomplished by taking up the obtained solids in warm pentane, and cooling the resulting clear pentane solutions of the imine to -15 °C. The resulting crystals were collected by suction filtration and were dried for 12 h in a vacuum desiccator at approximately 30 torr over $P_2O_5$ before being brought into the IT glovebox. Yields of imines were typically > 60% by this method.

### 2.4.4 Synthetic Procedures

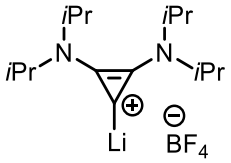


**Weiss-Yoshida Reagent** (**2-11**)**.** Two routes to **2-11** are presented below. Added lithium tetrafluoroborate in the deprotonation of **2-8b** enhances the amount of material isolated. Compound **2-11** prepared by either route was found to give the same yield in replicate reactions with borane dimethyl sulfide complex for the formation of **2-6**.

**Preparation of 2-11 without $LiBF_4$ addition:** Compound **2-8b** (375 mg, 1.16 mmol, 1 equiv.) was added to an oven dried 4 dram vial equipped with a magnetic stir bar and suspended in diethyl ether (9 mL). The slurry was cooled to -25 ℃ and a solution of *n*-BuLi in pentane (2.5 M, 0.46 mL, 1.2 mmol) was added drop-wise with stirring. The reaction turned orange, briefly clarified, and then became turbid again with a beige colour. After 20 min, volatiles were removed *in vacuo* and the residue was triturated with pentane (1 mL). The resulting solid was then washed on a frit with pentane (3 x 4 mL) and dried *in vacuo* to obtain *i*PrBAC-$LiBF_4$ (**2-11**) as a white powder, (310 mg, 0.87 mmol, based on Bertrand's composition:[54] 353.5825 g/mol BAC complex, 1 BAC: 1.25 $LiBF_4$, 75% yield, maximum theoretical yield is 80%). This white solid was stored at -25 °C and used without further purification.

**Preparation of 2-11 with $LiBF_4$ addition:** Compound **2-8b** (1.00 g, 3.08 mmol, 1 equiv.) was placed in a dry 50 mL Schlenk flask equipped with a magnetic stir bar. To the flask was added lithium tetrafluoroborate (72 mg, 0.77 mmol, 0.25 equiv.), then 17 mL diethyl ether. The slurry was cooled to -25 °C and a solution of *n*-BuLi in pentane (2.5 M, 1.23 mL, 3.08 mmol, 1 equiv.) was added dropwise with stirring. The reaction turned light orange, briefly clarified, and then became turbid again. After 25 min, volatiles were removed *in vacuo* and the residue was triturated with pentane (5 mL). The resulting solid was then washed on a frit with pentane (3 x 10 mL) and dried *in vacuo* to obtain *i*PrBAC-$LiBF_4$ as a white powder, (1.01 g, 2.86 mmol, based on Bertrand's composition:[54] 353.5825 g/mol BAC complex, 1 *i*PrBAC: 1.25 $LiBF_4$, 93% yield). This white solid was stored at -25 °C and used without further purification.

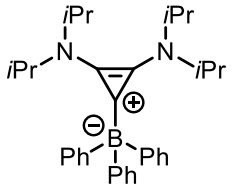

***i*PrBAC-BPh$_3$ (2-9).** Compound **2-8a** (300 mg, 0.539 mmol) was placed in a 10 mL round bottom flask equipped with a magnetic stir bar and suspended in toluene (4 mL) under nitrogen. To this suspension was added $NaBH_4$ (20 mg, 0.539 mmol, 1 equiv.), and the suspension was then allowed to heat at reflux for 17 h. The mixture was allowed to cool, then was filtered over celite® which was washed with toluene (3 x 5 mL). The volatiles were then removed from the washings and filtrate *in vacuo* to yield pure title compound **2-9** as a colourless solid (121 mg, 47%). Crystals suitable for X-ray analysis were grown by slow diffusion of pentane into a concentrated solution of **2-9** in toluene.

**MP:** 172-175 °C

**IR (neat):** 3128 (m), 2933 (m), 1857 (s), 1492 (s), 1208 (m), 1148 (m), 704 (s).

**$^1$H** (500 MHz, $CDCl_3$): δ 7.31 (t, 6H), 7.19 (t, 6H), 7.07 (t, 3H), 3.87 (br s, 4H, CH), 1.08 (br s, 24H, $CH_3$).

**$^{13}$C** {$^1$H} (125.8 MHz, $CDCl_3$): δ 141.6, 135.3, 126.5, 123.7, 51.6, 21.7.

**$^{11}$B** (160.5 MHz, $CDCl_3$): δ -9.4 (br s).

**HRMS(APCI):** calc'd for $C_{33}H_{44}BN_2$ $[M + H]^+$ 479.3592; Found: 479.3604.

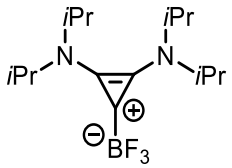

***i*PrBAC-BF$_3$ (2-12).** Compound **2-11** (53 mg, 0.15 mmol) was placed in an oven dried Schlenk tube equipped with a magnetic stir bar and dissolved in ether (3 mL), then removed from the glove box. Under nitrogen, $BF_3$•$OEt_2$ (0.020 mL, 0.16 mmol, 1.1 equiv.) was

added in one portion to the mixture. After 30 min the solution was transferred in air to a 25 mL round bottom flask, rinsing with dichloromethane (5 mL). The volatiles were removed *in vacuo*. The residue was dissolved in dichloromethane (5 mL) and filtered over celite®, which was washed with dichloromethane (2 x 2 mL). Removal of volatiles from the combined washings and filtrate *in vacuo* yielded title compound **2-12** as a colourless solid (34 mg, 0.11 mmol, 74%). Crystals suitable for X-ray analysis were grown by slow diffusion of pentane into a concentrated solution of **2-12** in dichloromethane.

**MP:** Colour turns from colourless to brown from 188-190 °C, melts at 200-206 °C

**IR (neat):** 2976 (m), 1871 (m), 1518 (s), 1347(m), 1072 (m), 973 (m)

**$^{1}$H** (300 MHz, $CDCl_3$): δ 3.89 (ap sept, 4H, CH), 1.43 (d, $J$ = 6.8 Hz, 12H, $CH_3$), 1.29 (d, $J$ = 6.8Hz, 12H, $CH_3$).

**$^{13}$C** {$^{1}$H} (75.5 MHz, $CDCl_3$): δ 138.6, 54.2, 49.4, 21.3, 20.5.

**$^{19}$F** (282.4 MHz, $CDCl_3$): δ -138.5 (q, $J$ = 34 Hz).

**$^{11}$B** (96.3 MHz, $CDCl_3$): δ -0.4 (q, $J$ = 34 Hz).

**HRMS (ESI):** calc'd for $C_{15}H_{28}BF_3N_2Na$ $[M + Na]^+$ 327.2190; Found: 327.2185.

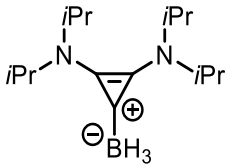


***i*PrBAC-BH$_3$ (2-6).** Compound **2-11** (532 mg, 1.50 mmol) was placed in an oven dried 4 dram vial equipped with a magnetic stir bar and suspended in toluene (10 mL). The solution was first cooled to -25 °C and then $BH_3$•$SMe_2$ (1M in toluene, 1.61 mL, 1.61 mmol, 1.07 equiv.) was added dropwise to the suspension. After 30 min the solution was filtered over celite® and the celite® was washed with dichloromethane (3 x 5 mL). Volatiles were removed from the combined filtrate and washings *in vacuo* resulting in the title compound

**2-6** as a beige solid (322 mg, 1.28 mmol, 85%). Colourless crystals suitable for X-ray analysis were grown by slow diffusion of diethyl ether into a concentrated solution of **2-6** in benzene.

**MP:** Turns brown at 202 °C, decomposes to liquid at 205-209 °C

**IR (neat):** 3440 (br), 2976 (m), 2850 (w), 2286 (w), 1766 (m), 1493 (m), 1328 (m), 1158 (m).

**$^{1}$H** (500 MHz, $CDCl_3$): δ 3.77 (br s, 4H, CH), 1.34 (br s, 24H, $CH_3$), 1.65-0.80 (m, 3H, $BH_3$, partially obscured by signal at 1.34).

**$^{13}$C** {$^{1}$H} (125.8 MHz, $CDCl_3$): δ 141.1, 54.7, 47.9, 22.0, 21.6.

**$^{11}$B** (160.5 MHz, $CDCl_3$): δ -35.1 (q, $J$ = 86 Hz).

**HRMS (APCI):** calc'd for $C_{15}H_{32}BN_2$ $[M + H]^+$ 251.2653; Found: 251.2662.

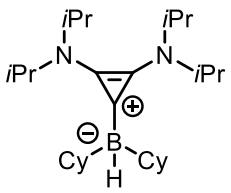


***i*PrBAC-BCy$_2$H (2-7).** Compound **2-11** (375 mg, 1.06 mmol) was placed in an oven dried 4 dram vial equipped with a magnetic stir bar and dissolved in ether (8 mL). The solution was first cooled to -25 °C and then dicyclohexylborane (188 mg, 1.06 mmol) was added in one portion to the resulting suspension and stirred for 1 h. Ether was then removed *in vacuo* and the residue was taken up in dichloromethane (4 mL) and filtered on a fine frit. The collected solids were washed with dichloromethane (3 x 3mL) and volatiles removed *in vacuo* resulting in the title compound **2-7** as a beige solid (370 mg 0.893 mmol, 84%).

**MP:** Turns orange at 102 °C, decomposes to liquid at 104 °C

**$^{1}$H** (300 MHz, $CDCl_3$): δ 4.02 (br s, 4H, CH), 1.79 (m), 1.62 (m), 1.32 (d, $J$ = 6.8 Hz, 24H, $CH_3$), 1.14 (m), 0.83 (m), 0.45 (br t, 2H).

**$^{13}$C {$^{1}$H}** (125.8 MHz, $CDCl_3$): δ 142.5, 50.5, 35.6, 34.9, 32.1-32.5 (br), 29.8, 29.6, 28.3, 21.5.

**$^{11}$B** (96.3 MHz, $CDCl_3$): δ -12.1 (d, $J$ = 71 Hz).

**HRMS (APCI):** calc'd for $C_{27}H_{52}BN_2$ $[M + H]^+$ 415.4218; Found: 415.4234.

### 2.4.5 Borenium Ion Generation

In a glovebox, compound **2-7** (15 mg 0.036 mmol) and trityl $Bar^F{}_{24}$ **2-19** (40 mg, 0.036 mmol) were placed in an oven dried 1 dram vial equipped with a magnetic stir bar. To the solids was added 0.6 mL of $CDCl_3$. The solution was stirred for 20 min, then placed in a standard NMR tube. The cap was secured with Teflon tape, the tube was removed from the glovebox, and NMR spectra were acquired.

**Diagnostic NMR Data:**

**$^{1}$H** (300 MHz, $CDCl_3$): δ 7.69 (s, 8H, $BAr^F{}_{24}$), 7.52 (s, 4H, $BAr^F{}_{24}$), 7.11-7.30 (m, 15H, $Ph_3CH$), 5.55 (s, 1H, $Ph_3CH$), 4.07-3.91 (m, 2H, CH), 3.76-3.62 (m, 2H, CH), 1.81-1.706 (m), 1.34-1.12 (m), 1.32 (d, $J$ = 6.6 Hz, 24H, $CH_3$).

**$^{11}$B** (96.3 MHz, $CDCl_3$): δ 81 ($B^+$), -6.6 ($BAr^F{}_{24}$).

### 2.4.6 General Reduction Procedures

**General procedure for reduction with 2-6 in presence of $SiO_2$ (GPA):** Under air, compound **2-6** (63 mg, 0.25 mmol) was placed in a 4 dram vial equipped with magnetic stir bar and silica gel (901 mg). To the solids was added an aldehyde or ketone (0.5 mmol, 2 equiv.) and dichloromethane (2.5 mL (0.2M) or 1.6 mL (0.3M)). Reaction progress was followed by TLC. The reaction was allowed to stir for the allotted time and then filtered through a porous frit. The silica was then washed with dichloromethane (20 mL) and

volatiles were removed from the combined filtrates *in vacuo*. The resulting residue was taken up in $Et_2O$ (2 mL) and filtered through a cotton plug, which was then washed with $Et_2O$ (2 x 2 mL). The $Et_2O$ was then removed *in vacuo* and an NMR spectrum was recorded in $CDCl_3$. If impurities of aldehyde or ketone were remaining the resulting sample may be passed through a small plug of silica and eluted with ethyl acetate/ hexanes (1:5) to obtain product with $^1H$ NMR spectra corresponding to the reduced product.

**General Hydrogenation Procedure (GPB):** *i*PrBAC-$BCy_2H$ **2-7** (10 mg, 0.024 mmol, 10 mol %) and trityl $BAr^F_{24}$ **2-19** (27 mg, 0.24 mmol, 10 mol %) were placed in an oven dried 1 dram vial equipped with a magnetic stir bar. To this vial was added trifluorotoluene (0.6 mL) and the solution stirred for 5 min. Then the substrate was added as a solid, and the vial equipped with a septum and 16 gauge needle. This was placed into a Parr-bomb which was then assembled and removed from the glove box. In a fume hood, the bomb was placed on a stir plate, and purged twice by pressurizing to 20 atm of $H_2$ followed by careful release. The bomb was subsequently pressurized to 20 atm. After the allotted time, the bomb was carefully depressurized, disassembled, and the vials were removed. Solvent was removed *in vacuo*, conversion was ascertained by $^1H$ NMR (comparison of starting material and product, or triphenyl methane and product give values that agree). The amines were then subject to appropriate purification.

### 2.4.7 Reduced Products

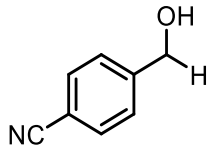


**4-cyanobenzyl alcohol** (**2-14a**)**.** Following the general procedure (**GPA**) the reaction was completed after 1 h using a 0.2 M solution and monitoring by TLC (ethyl acetate/ hexane 1:5) to afford the alcohol (58 mg, 87%).

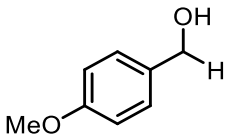


**4-methoxybenzyl alcohol** (**2-16b**)**.** Following the general procedure (**GPA**) the reaction was completed after 1 h using a 0.2 M solution and monitoring by TLC (ethyl acetate/ hexane 1:5) to afford the alcohol (59 mg, 86%).

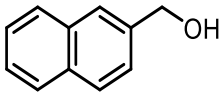


**2-napthalenemethanol** (**2-16**)**.** Following the general procedure (**GPA**) the reaction was completed after 1 h using a 0.2 M solution and monitoring by TLC (ethyl acetate/ hexane 3:7) to afford the alcohol (78 mg, 99%).

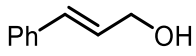


**Cinnamyl alcohol** (**2-18**)**.** Following the general procedure (**GPA**) the reaction was completed after 1.5 h using a 0.3 M solution and monitoring by TLC (ethyl acetate/ hexane 1:5) to afford the alcohol (56 mg, 86%) after purification with a small silica plug.

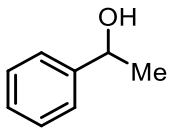


**2-phenyl ethanol** (**2-14c**)**.** Following the general procedure (**GPA**) the reaction was halted after 6 h using a 0.2 M solution and monitoring by TLC (ethyl acetate/ hexane 1:5) to afford the alcohol in a 1.5:1 ratio with the starting material as observed by NMR integration.

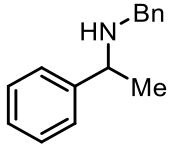


***N*-Benzyl-(1-phenylethyl)amine** (**2-22**)**.** Following the general procedure (**GPB**), acetophenone benzylimine (50 mg, 0.241 mmol) was added and stirred for 12 h. Crude NMR indicated a 93% conversion. The reaction mixture was purified by column chromatography on basic alumina (ether-hexanes 15:85 then ethyl acetate-hexanes 1:1) to afford the title compound (28 mg, 56% isolated yield).

**$^1$H** (300 MHz, $CDCl_3$): δ 7.36-7.20 (m, 10H), 3.81 (q, *J* = 6.8 Hz, 1H), 3.66 (AB d, *J* = 13.7 Hz, 1H), 3.59 (AB d, *J*= 13.6 Hz, 1H) 1.61 (br. s, 1H), 1.36 (d, *J* = 6.6 Hz).

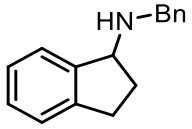


***N*-benzyl-1-aminoindan** (**2-24**)**.** Following the general procedure (**GPB**) indanone benzylimine (53 mg, 0.241 mmol) was added and stirred for 36 h. Crude NMR indicated a 65% conversion. The reaction mixture was purified by column chromatography on silica gel (dichloromethane to elute unreacted imine, followed by 5% MeOH/DCM to elute product), affording the title compound (26 mg, 49 % isolated yield).

**$^1$H** (300 MHz, $CDCl_3$): δ 7.41-7.36 (m, 3H), 7.32 (t, *J* = 6.3 Hz, 2H), 7.26-7.17 (m, 4H), 4.29 (t, *J* = 6.5 Hz, 1H), 3.93 (AB d, *J* = 13.1 Hz, 1H), 3.89 (AB d, *J* = 13.1 Hz, 1H), 3.09-2.98 (m, 1H), 2.84-2.78 (m, 1H), 2.46-2.40 (m, 1H), 1.92-1.86 (m, 1H), 1.61 (br. s, 1H).

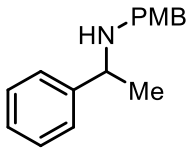


***N*-4-methoxybenzyl-(1-phenethyl)amine** (**2-26**)**.** Following the general procedure (**GPB**), acetophenone 4-methoxybenzylimine (58 mg, 0.241 mmol) was added and stirred for 12 h. Crude NMR indicated a 83% conversion. The reaction mixture was purified by dissolving in diethyl ether, adding 3 drops of concentrated sulfuric acid, extracting the ether with water, making the combined aqueous extracts basic, and extracting the amine with diethyl ether. Concentration *in vacuo* afforded the title compound (31 mg, 53 % isolated yield)

**$^1$H** (300 MHz, $CDCl_3$): 7.36-7.32 (m, 5H), 7.19, (ap. d, *J* = 8.6 Hz, 2H), 6.84 (ap. d, *J* = 8.6 Hz, 2H), 3.81-3.79 (m, 1H), 3.79 (s, 3H), 3.59 (AB d, *J* = 12.9 Hz, 1H), 3.53 (AB d, *J* = 12.9 Hz, 1H) 1.58 (br s, 1H), 1.36 (d, *J* = 6.6 Hz, 3H).

# Chapter 3: Bis(amino)cyclopropenylidene Carbene Borane Catalyzed Imine Hydrogenation

Reprinted with permission from **B. S. N. Huchenski**, C. J. Christopherson, K. N. Robertson and A. W. H. Speed, *Org. Biomol. Chem.,* **2019**, 17, 6158.  The manuscript has been reformatted to match the thesis format, and references and compounds have renumbered where appropriate. Sub-sections headers have been added.

Contributions to manuscript: All synthetic work in this chapter was carried out by B. S. N. Huchenski, with the following exceptions: boron fluorides **3-19**, **3-20**, and **3-21** were originally prepared by Cheyenne J. Christopherson, and subsequently scaled up by B. S. N. Huchenski and reactions **D**, **E**, and **F** of **Scheme 3.1** were conducted by Dr. A.W.H. Speed along with scale-up of starting materials **3-9** and **3-8a**. The X-ray crystallography was conducted by Dr. Katherine N. Robertson. Mass spectrometric data were acquired by Mr. Xiao Feng (Mass Spectrometry Laboratory, Dalhousie University). The manuscript was written by B. S. N. Huchenski and Dr. A. W. H. Speed.

## 3.1 Introduction

Adducts between carbenes and boranes have emerged as valuable tools in synthesis over the past two decades.[101] These adducts have been employed as radical precursors,[114] and as hydroborating reagents for arynes.[115] Carbene borane adducts also serve as precursors for stabilized Lewis-Acidic borenium cations.[39] Borenium cations can function as the Lewis acid component in frustrated Lewis pairs,[43] and have been employed as catalysts to hydrogenate imines.[32] Many borenium cations have been explored in this context. Cation **3-1** (**Figure 3.1**), reported by Stephan and co-workers has particular high activity in hydrogenation reactions.[44] Cation **3-2**, reported by Crudden, Eisenberger, and

co-workers is active for hydrogenation of imines and quinolines at hydrogen pressures of one atmosphere.[45] A series of chiral carbene borane adducts were investigated by Melen, Crudden, Stephan, and co-workers,[46] where combinations included an achiral carbene combined with a chiral borane such as **3-3** or a chiral carbene combined with an achiral borane such as **3-4**. While observed enantiomeric excesses did not exceed 20 % for imine reductions using these systems, this work provided an important benchmark for further research in the field. Very recently, Fuchter and co-workers reported the use of **3-4** for highly enantioselective imine hydrogenations and hydrosilylations of cyclohexyl and cyclopentyl imines.[42,47]

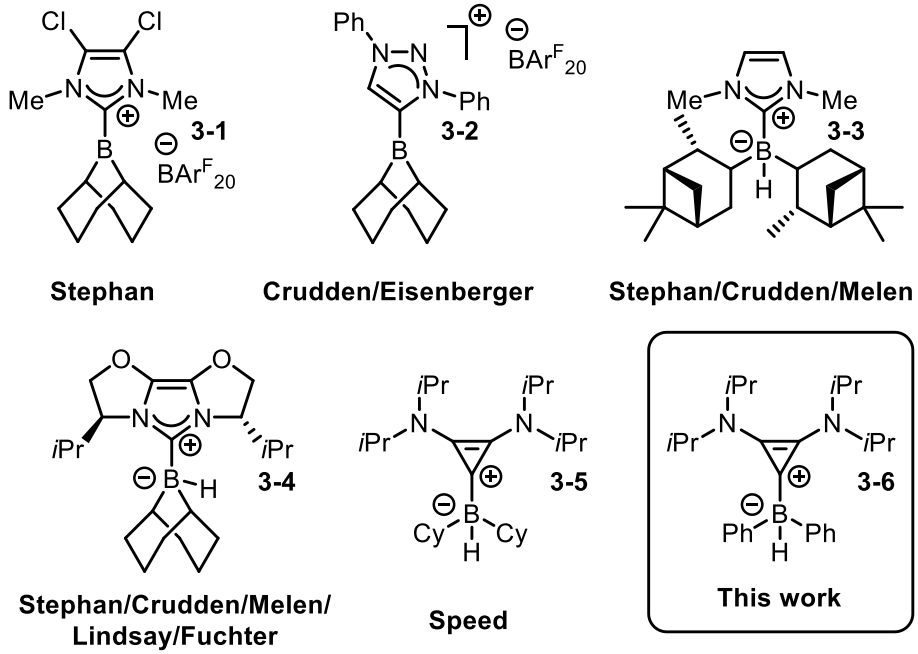


**Figure 3.1** Selected examples of borocations and carbene borane adducts used in imine hydrogenation.

Bis(amino)cyclopropenylidene (BAC) carbenes were first isolated by Bertrand and co-workers,[53] building on a rich history of work on precursor compounds, most predominantly by the groups of Weiss and Yoshida.[116,117] BAC carbenes are emerging as organocatalysts in work pioneered by Gravel and co-workers, and subsequently by Anand

and co-workers.[65,66,118,119] Despite BAC carbenes being a distinct class of carbene,[57] they have remained relatively underexplored as supporting ligands for boranes. Bertrand and co-workers reported a heteroleptic borocation, where one of the supporting ligands was a BAC carbene.[63] Schneider and co-worker reported an adduct between a BAC carbene and triethylborane.[120] Dudding and co-workers reported an adduct between a BAC carbene and boron trifluoride.[121] Our group reported adducts of BAC carbenes with borane, boron trifluoride, and dicyclohexylborane (**3-5**, **Figure 3.1**).[122] Initial attempts to form a BAC carbene adduct with 9-BBN resulted in decomposition, so dicyclohexylborane was chosen for the practical reason that it led to a complex that did not decompose. Abstraction of the hydride led to a borenium cation that was able to hydrogenate imines, however surprisingly a different selectivity was noted than that exhibited by previous borenium cation-catalyzed hydrogenations. System **3-5** was able to hydrogenate imines generated from benzylamine, which are not hydrogenated by prior borenium cations. This paper discloses further efforts to understand the origin of this different reactivity by exploring the substitution of other groups on boron. We were especially interested in diarylboranes as close surrogates of the cyclohexyl group, and these efforts culminated in the synthesis of compound **3-6** (**Figure 3.1**).

## 3.2 Results and Discussion

In order to further our investigations of the chemistry of **3-5** we first developed a more efficient route to the requisite starting materials. Tetrachlorocyclopropene **3-7** is commonly used for the synthesis of BAC carbene precursors **3-8a** and **3-8b** (**Equation A**, **Scheme 3.1**).

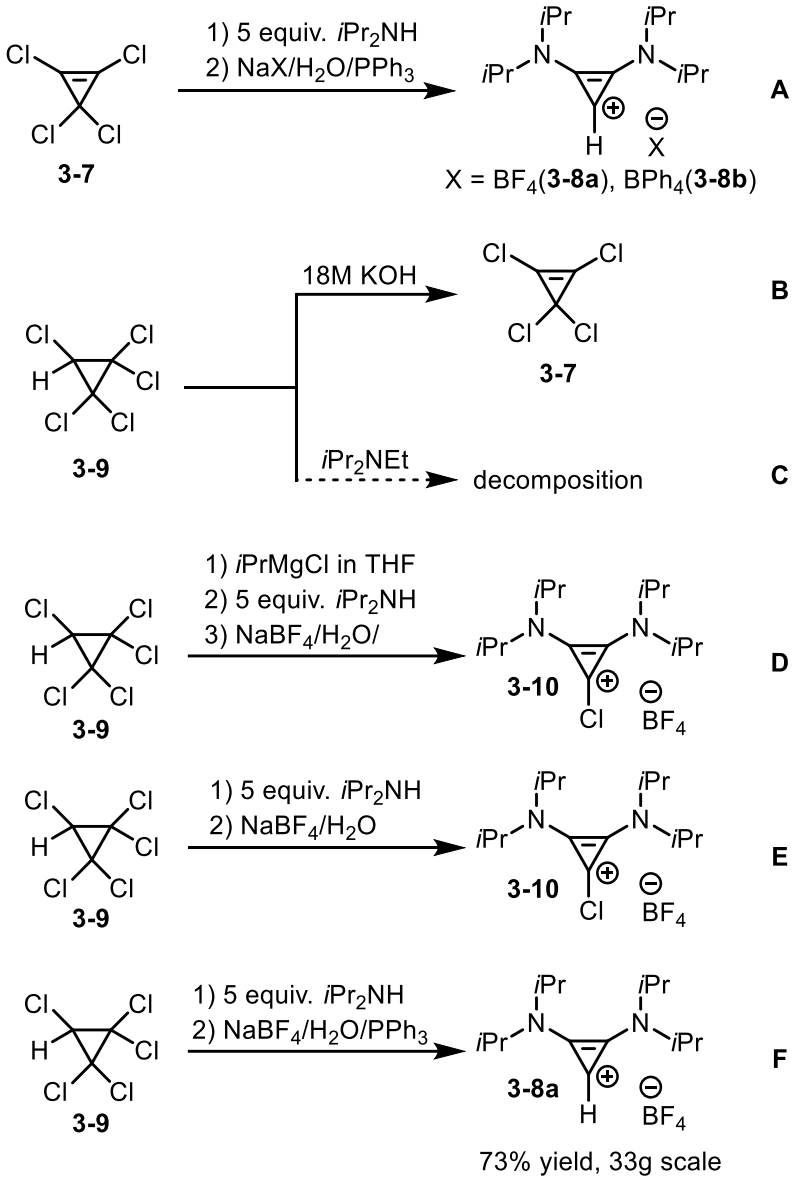


**Scheme 3.1** Improved synthesis of a BAC carbene precursor.

Tetrachlorocyclopropene **3-7** is in turn prepared from pentachlorocyclopropane **3-9**, which is prepared from sodium trichloroacetate and trichloroethylene.[123] The conversion of **3-9** to **3-7** is effected by a hot aqueous solution of KOH (**Equation B**, **Scheme 3.1**), and in our hands this reaction has proven to be capricious, with yields varying dramatically over different scales and batches. We hypothesized that the elimination of pentachlorocyclopropane **3-9** to pentachlorocyclopropene **3-7** might be carried out using a

milder base, possibly even in the same reaction vessel as the addition of the amine to form compound **3-8a**. Addition of Hünig's base to a solution of pentachlorocyclopropane **3-9** in dichloromethane resulted in rapid discolouration and decomposition (**Equation C**, **Scheme 3.1**). Use of the Grignard reagent isopropylmagnesium chloride in THF was also attempted (**Equation D**, **Scheme 3.1**). We anticipated that the Grignard reagent could either behave as a base to form **3-7** or might conduct magnesium halogen exchange to reduce the pentachlorocyclopropane to trichlorocyclopropene. Attempts to isolate **3-7** from treatment of **3-9** with 1 equivalent of Grignard reagent were unsuccessful, however following the Grignard addition with addition of diisopropylamine and aqueous sodium tetrafluoroborate resulted in the isolation of **3-10** (**Equation D**, **Scheme 3.1**). Taylor and co-workers have shown substitutions can occur directly on **3-9** rather than **3-7**,[124] and Lambert and co-workers have shown that chloride **3-10** can be directly prepared from the combination of pentachlorocyclopropane **3-9** and an excess of diisopropylamine (**Equation E**, **Scheme 3.1**).[125] We accordingly attempted the direct replacement of tetrachlorocyclopropene with pentachlorocyclopropane in the formation of **3-8a**. Cautious addition of 5 equivalents of diisopropylamine to a solution of pentachlorocyclopropane **3-9** in dichloromethane revealed a delayed exotherm, however the reaction remained relatively colourless in contrast to the attempted elimination of **3-9** to **3-7** with Hünig's base. Subsequent addition of water, 1 equivalent of triphenylphosphine, and 1 equivalent of sodium tetrafluoroborate allowed the isolation of **3-8a** in 73% yield on a 33-gram scale, revealing that a separate elimination step to form tetrachlorocyclopropene is unnecessary for the formation of **3-8a**. Several other counterions can be introduced by replacing $NaBF_4$ with the corresponding salts ($NaPF_6$, $NaBPh_4$, $NaBAr^F{}_{20}$), however in our hands only the $NaBF_4$ salt can be deprotonated with butyllithium without decomposition.

Compound **3-5** can be prepared as in our previously reported work, by combination of the Weiss-Yoshida reagent **3-11**,[54] and dicyclohexylborane in diethyl ether.[122] A modified route to **3-5** was also developed. Chloride **3-8c** can be obtained from tetrafluoroborate **3-8a** by treatment with an ion exchange resin.[55] Direct formation of chloride **3-8c** by omitting sodium tetrafluoroborate from the reaction to form **3-8a** was complicated by the high water solubility of chloride **3-8c** precluding an extractive isolation. Treatment of chloride **3-8c** with *n*-butyllithium afforded a white solid that was not soluble in pentane.[60] While this solid was not characterized, combination with dicyclohexylborane also yielded **3-8c**, which is distinct from the reactivity of the free carbene with dicyclohexylborane.[122] This route does not have any advantage over the aforementioned route, however we include it since this alternate carbene transfer protocol to boron may be of use to other exploring different carbene variants.

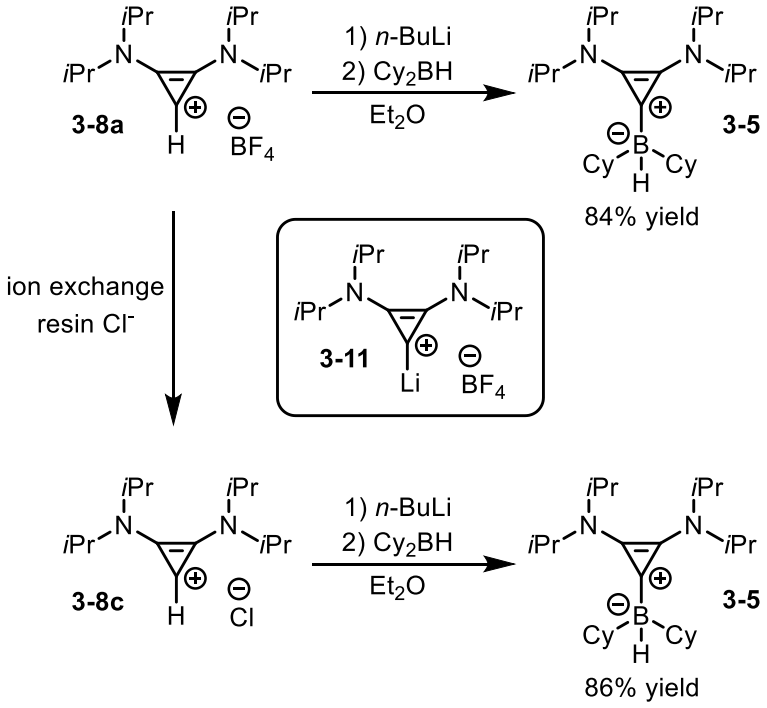


**Scheme 3.2** Synthesis of complex **3-5**.

With reliable route to BAC carbene precursor **3-8a** and dicyclohexyl complex **3-5**, we initially sought to determine if the ability of complex **3-5** to hydrogenate benzylamine derived imines stemmed from the BAC carbene, the use of dicyclohexylborane, or an interplay between both substituents.

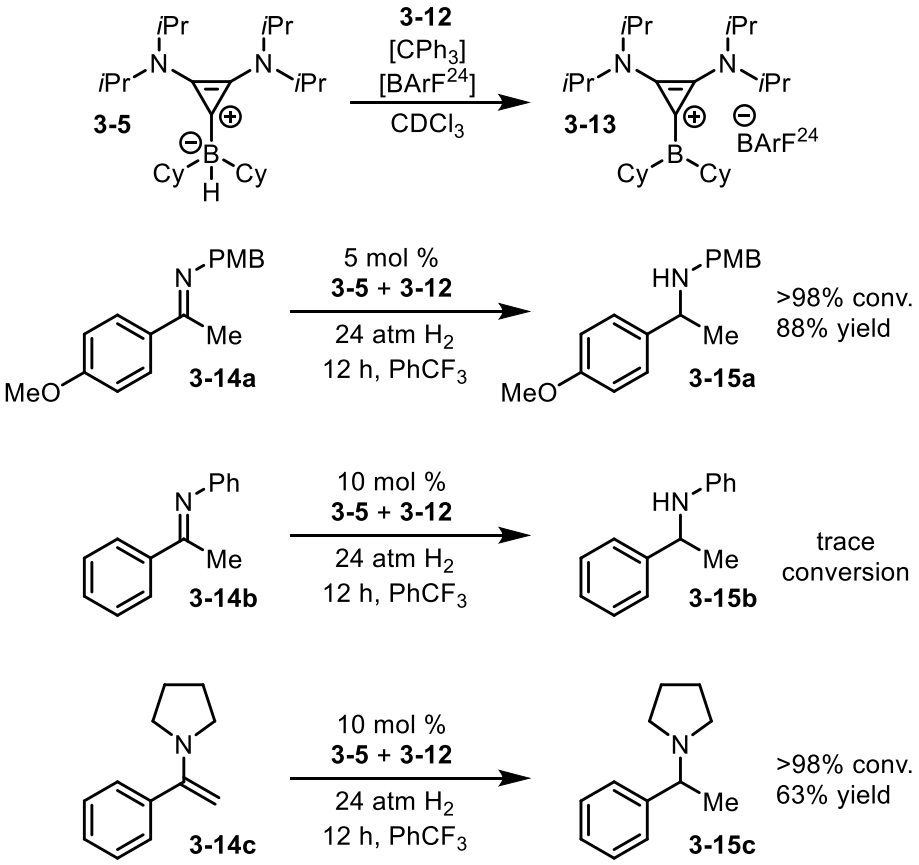


**Scheme 3.3** Hydrogenation reactions with **3-5**.

In our initial report, we only showed the activity of **3-5** in the hydrogenation of benzyl imines employing 10 mol % loading of adduct **3-5**, with an equal amount of trityl $BAr^{F}_{24}$ **3-12** as a hydride abstraction agent to generate borenium cation **3-13** *in situ*.[112] For substrate **3-14a**, loading could be dropped to 5 mol % maintaining complete conversion to amine **3-15a**. Hydrogenation of aniline-derived imine **3-14b** was attempted with **3-13**, however only trace conversion was observed, demonstrating that the aniline-derived imine

is a poorer substrate for this catalytic system. In addition, **3-13** was able to hydrogenate enamine **3-14c** with high conversion at 10 mol % loading. These three substrates of different character would be used as points of comparison for subsequent catalysts that were developed.

We subsequently turned our attention to the generation of a 9-BBN adduct of a BAC carbene. We had previously reported that 9-BBN adducts of BAC carbenes underwent decomposition upon isolation. After subsequent experimentation, we found that 9-BBN adduct **3-16** could be generated upon the combination of **3-11** and 9-BBN dimer in toluene at room temperature for 1 h, followed by filtration and concentration (**Scheme 3.4**). Compound **3-16** persisted in a solution of benzene-$d_6$ or chloroform-*d* for several hours, but gradually decomposed to an unidentified product, however **3-16** is stable for months as a solid at -35 °C under an atmosphere of dry nitrogen.

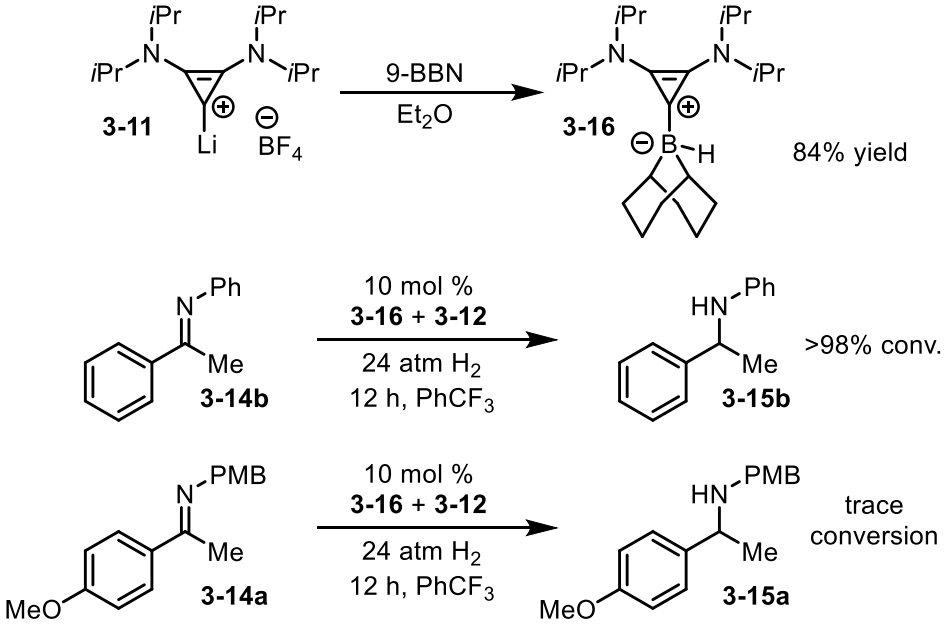


**Scheme 3.4** Generation of 9-BBN BAC carbene adduct **3-16**.

Adduct **3-16** combined with trityl salt **3-12** was able to hydrogenate aniline derived imine **3-14b**, but not para-methoxybenzyl amine **3-14a**, strongly implying that the unique

ability of **3-5** to hydrogenate benzyl imines originated from the presence of the cyclohexyl groups on boron. As a further experiment, we prepared an analogue of Stephan's boron complex **3-1**, an adduct between dicyclohexylborane and the corresponding dichlorocarbene (**3-17**, **Figure 3.2**).[44] This adduct was not active in the hydrogenation of benzylamine derived imine **3-14a**, imine **3-14b**, or enamine **3-14c**. These results suggest that the unique activity of **3-5** stems from an interplay between the dicyclohexylborane and the BAC carbene. We hypothesize that the relatively large steric bulk of the cyclohexyl groups prevents catalyst inhibition by the benzylamine products. The relatively small size of the BAC carbene allows catalytic activity to be maintained. Use of the larger carbene in complex **3-17** suppresses reactivity with the cyclohexylborane under the same pressure of hydrogen. These observations suggested that variation of the R groups on boron may uncover other changes in reactivity, so we subsequently explored addition to other boranes. Thexylborane was combined with Weiss-Yoshida reagent generating adduct **3-18a** This proved to be inactive in a hydrogenation of **3-14a** with either 1 or 2 equivalents of trityl salt **3-12**. In the same vein, use of diisocamphenylborane and Weiss-Yoshida reagent provided adduct **3-18b**, however this was also inactive in the hydrogenation reaction of imine **3-14a** or enamine **3-14c** upon mixture with trityl $BAr^{F}{}_{24}$ **3-12**. This contrasts with work of Melen, Crudden, Stephan, and co-workers, where an adduct of a carbene and diisocamphenylborane (**3-3**) was catalytically active, albeit with low enantioinduction.[46]

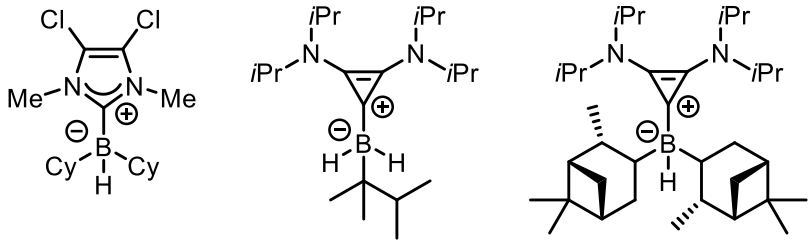


**3-17** **3-18a** **3-18b**

**Figure 3.2** Inactive boranes for the hydrogenation of **3-14a**.

At this point, our attention turned to the use aryl substituents on the boron. Work by the Stephan group showed an adduct of a carbene and Piers borane underwent an intramolecular C-H activation,[44] but this compound was not explored in a hydrogenation. In another example from Stephan and co-workers, an intramolecular cyclization of a carbene-borane led to a planar carbene diarylborane adduct.[126] Catalytic activity of this complex was not disclosed in that communication.

We anticipated an adduct of a BAC carbene and diphenylborane would have the closest steric profile to the dicyclohexylboron adducts we had previously prepared, while introducing an electronic difference. Unfortunately, the preparation of uncomplexed diphenylborane is not well documented,[127] which complicated an envisioned preparation of the desired BAC carbene-borane adduct through combination of the borane and Weiss-Yoshida reagent **3-11**. We sought an alternate route to access this scaffold that would not require use of the free borane. Gabbaï and co-workers pioneered a formation of carbene supported borenium cations through combination of a carbene and dimesitylboron fluoride. Rather than use hindered dimesitylboron fluoride,[40] we sought to perform a complexation with diphenylboron fluoride **3-19** to maintain a similar steric profile to the dicyclohexylborane we had previously used.[122]

The preparation of diphenylboron fluoride by direct addition of an organometallic to boron trifluoride-diethyl etherate complex is not a reliable transformation.[128] We decided to investigate the use of diphenylborinic acid **3-20** as a precursor to diphenylboron fluoride, reminiscent of Wagner and co-workers' approach to diarylhaloboranes (**Scheme 3.5**).[129] We anticipated conversion to the known potassium difluoroborate salt **3-21**, followed by fluoride abstraction may provide a convenient route to diphenylboron fluoride **3-19**. Ito and co-workers' previously reported procedure of addition of 2 equivalents of phenylmagnesium bromide to triisopropylborate followed by hydrolysis provided diphenylborinic acid **3-20**. Conversion of this to a potassium difluoroborate was readily achieved by treatment with potassium bifluoride. Compound **3-21** has been previously reported and is a non-hygroscopic air-stable white solid.[130]

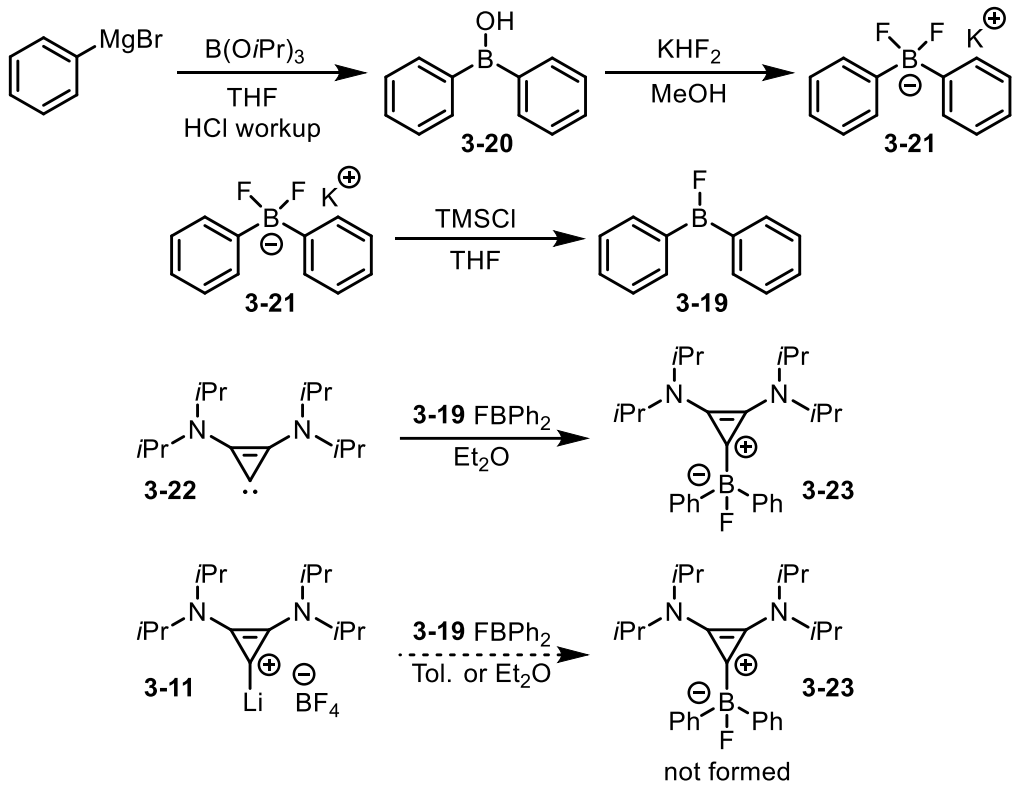


**Scheme 3.5** Synthesis of diphenylboron fluoride and initial complexation studies with a BAC carbene.

Upon exposure to TMSCl in THF solvent, formation of diethyl ether soluble diphenylfluoroborane **3-19** was observed in 77% yield. $^{19}F$ and $^{11}B$ NMR spectroscopy corroborated the formation of this compound. Upon mixture of compound **3-19** with free carbene **3-22**, we observed formation of a new product, adduct **3-23** by NMR spectroscopy. This reaction was conducted on a milligram scale, and a yield was not measured. On a small scale, the preparation of free carbene **3-22** consistently gave low yields relative to the formation of Weiss-Yoshida reagent **3-11**, so we wished to ascertain if the overall efficiency of the synthetic sequence could be improved by using **3-11** rather than free carbene **3-22**. Exposure of diphenylfluoroborane **3-19** to **3-11** resulted in formation of a complex mixture. After these somewhat discouraging results, we explored the direct reaction of **3-11** with potassium fluoroborinate **3-21** in the anticipation that elimination of a metal fluoride and metal tetrafluoroborate could allow formation of complex **3-23**. Soós, Pápai and co-workers have previously demonstrated addition of aryl Grignard reagents to trifluoroborate salts to form carbon boron bonds.[131] Gratifyingly, mixture of these two compounds resulted in formation of adduct **3-23** (**Scheme 3.6**).

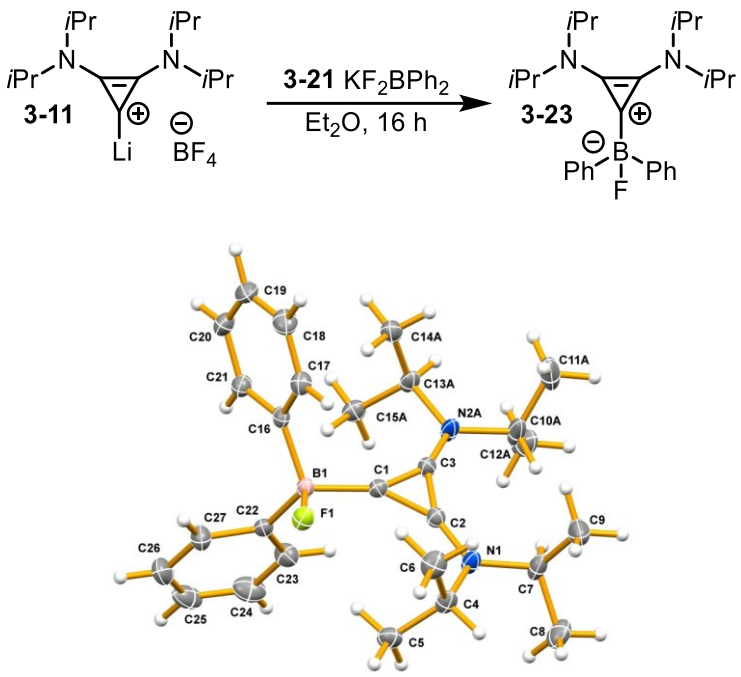


**Scheme 3.6** Formation of BAC complex directly from potassium difluoroborinate, and X-ray crystal structure of **3-23.**

A crystal of compound **3-23** was grown from cold toluene. An X-ray diffraction study of this crystal confirmed the structure of **3-23**. We investigated the substitution chemistry of the fluoride in adduct **3-23** (**Scheme 3.7**). Treatment with dimethylchlorosilane resulted in the predominant formation of hydride **3-6**.[132] Trituration allowed the purification of hydride **3-6**. $^{1}$H NMR spectra confirm the presence of a B–H bond. A block shaped crystal of **3-6** was grown from cold toluene, and X-ray analysis confirmed the structure of hydride **3-6**. In addition, a small plate shaped crystal was noted in one of the batches. This crystal was also able to diffract, and was revealed to be chloride **3-24**, the alternate substitution product from treatment with dimethylchlorosilane. Treatment of **3-23** with 2 separate doses of dimethylchlorosilane with removal of volatiles in between the additions suppresses formation of this product. Chloride **3-24** could be deliberately prepared in essentially quantitative yield by treatment of fluoride **3-23** with

chlorotrimethylsilane. The use of triethylsilane or diphenylsilane to conduct the metathesis of fluoride **3-23** to hydride **3-6** and avoid the formation of **3-24** was unsuccessful, however the more expensive triphenylsilane was able to effect this transformation.

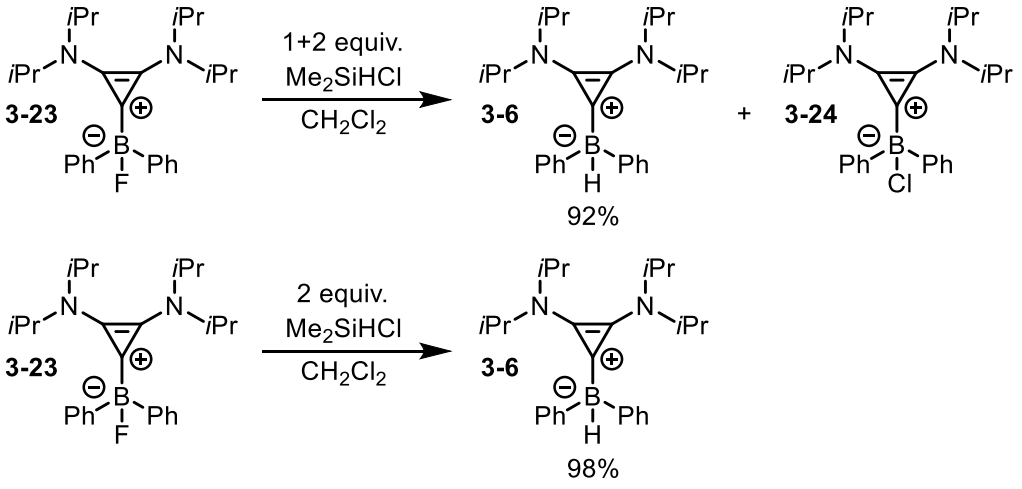


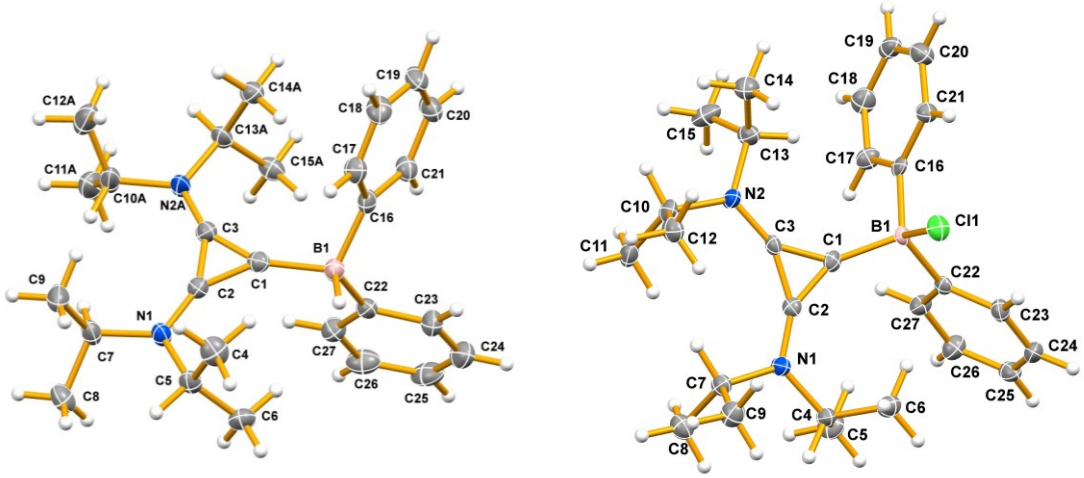


**Scheme 3.7** Transformation of adduct **3-23**.

With hydride **3-6** in hand, we investigated its use in hydrogenation. Combination of adduct **3-6** and trityl $BAr^{F}{}_{24}$ **3-12** in dry chloroform-*d* resulted in changes in the $^{1}H$ and $^{11}B$ NMR spectra characteristic of the formation of a borenium cation **3-25** (**Scheme 3.8**). The observed chemical shift of +64.5 ppm agrees well with Gabbaï's observed chemical shift of +65.9 ppm for diaryl borenium cation **3-26**.[40]

Exposure of a mixture of borenium salt **3-26** and tricyclohexyl phosphine to hydrogen gas in trifluorotoluene resulted in the reformation of boron hydride **3-6** and formation of the protonated phosphine, showing that complex **3-25** was able to activate hydrogen.[43] Unfortunately, a combination of **3-6** and trityl $BAr^{F}_{24}$ **3-12** in trifluorotoluene was unable to effect the hydrogenation of imine **3-14a**, imine **3-14b**, or enamine **3-14c**, with only trace conversion observed under the standard reaction conditions. Based on these results, compound **3-24** is not an effective hydrogenation catalyst under the conditions screened. A summary of the reactivity of activated boranes **3-5**, **3-16**, and **3-6** with the three substrate classes explored in this study is included in **Scheme 3.8**. We hypothesize that the reduced steric demand of the phenyl groups increases the catalyst's susceptibility to poisoning by Lewis bases such as the substrates, or amine reduction products. Supporting this hypothesis, cation **3-25** was generated and mixed with imine **3-14a** in chloroform-d (Scheme **3.9**). The $^{1}$H NMR spectrum revealed perturbations in the chemical shifts of the imine (and possible formation of Z and E isomers), and appearance of a broad signal at -1.77 ppm in the $^{11}$B NMR spectrum. This provides evidence for the formation of an adduct. Conversely, mixture of cation **3-13** and imine **3-14a** resulted in minimal perturbations of the $^{1}$H NMR spectrum, indicating this Lewis pair remained frustrated in chloroform-*d*.

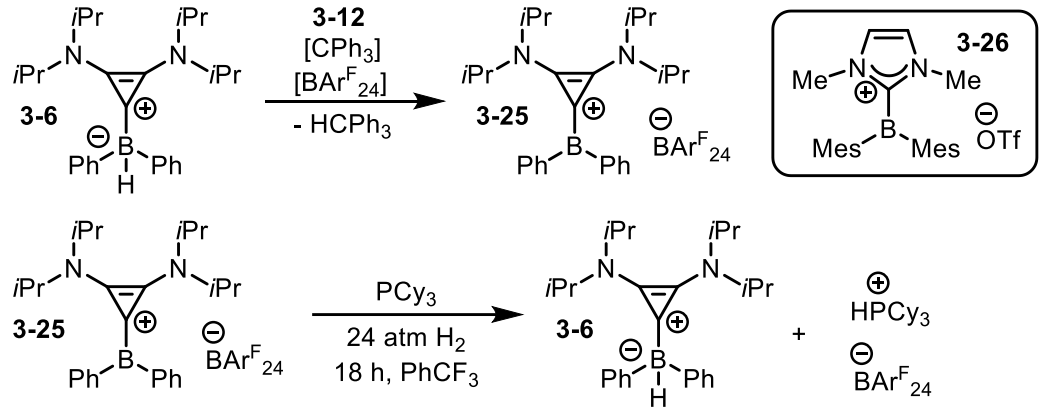


**Summary of Observed Reactivity in Hydrogenations**
(Y= observed hydrogenation, N= no or trace hydrogenation)

| | Borane adduct | | |
|---|---|---|---|
| | **3-5** | **3-16** | **3-6** |
| **Substrate** | | | |
| **3-14a** (PMB) | Y | N | N |
| **3-14b** (Ph) | N | Y | N |
| **3-14c** (enamine) | Y | N | N |

**Scheme 3.8** Borenium cation formation, and hydrogen activation.

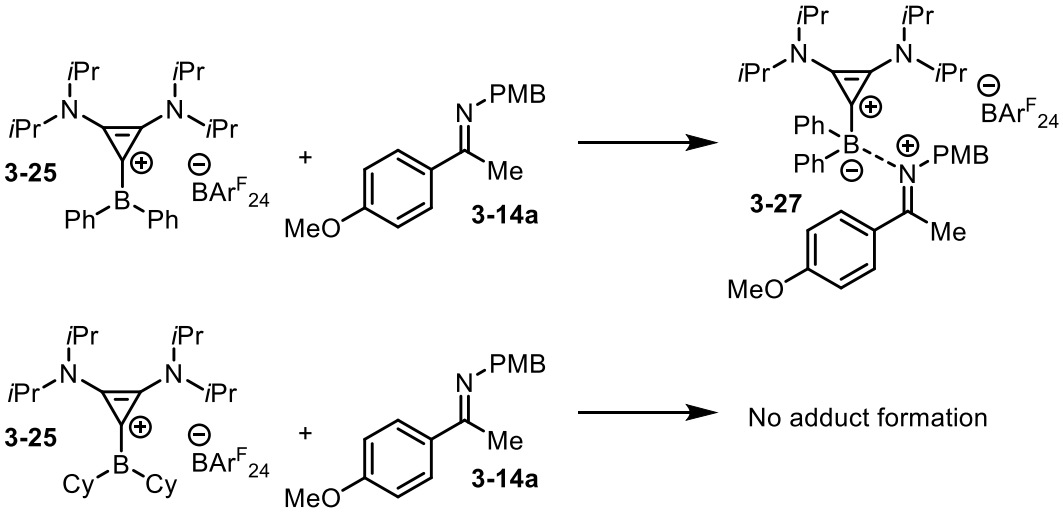


**Scheme 3.9** Adduct formation with imine and borocation **3-26**.

Given the poor performance of complex **3-26** in comparison with both the dicyclohexylborane adduct **3-5** and 9-BBN adduct **3-16**, we did not explore other aryl variants with this catalyst in this investigation.

The prospects for borenium-based hydrogenation catalysts must be tempered by consideration of competing technologies. Precious metal and base-metal catalysts generally function at far lower loadings, which obviate any cost savings posed by not using precious metals in the boron-based catalysts. A number of new chiral boranes have proven to be highly efficient and enantioselective hydrogenation catalysts as FLP components.[29,133] In addition, earth abundant systems for asymmetric imine hydroboration, including asymmetric examples, avoid the use of pressurized equipment altogether for small-scale reduction reactions.[78,87]

### 3.3 Conclusion

We have provided evidence that the unique activity of BAC carbene dicyclohexylborane adducts in hydrogenation reactions stems specifically from the combination of cyclohexylborane and the BAC carbene. We further developed a preparative route to make diphenylborane adducts of a BAC carbene via the fluoride, and showed that a borenium cation derived from this entity shows poor reactivity as a hydrogenation catalyst for imines. While borenium-catalyzed imine hydrogenations are not currently competitive with existing technologies for hydrogenation, the work presented in this manuscript provides new avenues for the synthesis of BAC carbene supported diarylboron compounds. In addition, we present a practical improvement in the synthesis of the precursor to the most commonly used BAC carbene, which will be of use to synthetic chemists working in this area.

## 3.4 Experimental

### 3.4.1 General Considerations

Boron compounds, carbene complexes, imines, trityl salts and solvents were dispensed in a 2001 issue IT Glovebox ($H_2O$ levels are approximately 30 ppm on average). Carbene complexes and precursors were prepared in oven dried 4 dram scintillation vials equipped with magnetic stir bars and green Qorpak® PTFElined caps. Hydrogenations were carried out in 1 dram scintillation vials equipped with a magnetic stir bar and septa caps pierced with a needle were screwed on. All reactions were conducted at ambient temperature unless otherwise stated. $^{1}H$, $^{11}B$, $^{19}F$ and $^{13}C$ NMR data were collected at 300K on either a Bruker AV-300 or AV-500 spectrometer. $^{1}H$ NMR spectra are referenced to residual non-deuterated NMR solvent from the sample ($C_6H_6$ = 7.16 ppm, $CHCl_3$ = 7.26 ppm, $CH_3CN$ = 1.94 ppm). $^{13}C$ NMR spectra are referenced to deuterated NMR solvent from the sample ($C_6D_6$ = 128.06 ppm, $CDCl_3$ = 77.16 ppm, $CD_3CN$ = 1.32 ppm or 118.26 ppm). Mass spectrometric data were acquired by Mr. Xiao Feng (Mass Spectrometry Laboratory, Dalhousie University).

### 3.4.2 Solvent Purification

**Ether** was purchased as anhydrous >99% ACS grade from Sigma Aldrich and stored over 3Å molecular sieves under nitrogen.

**Trifluorotoluene** was purchased as anhydrous >99% ACS grade from Sigma Aldrich and dried over 3Å molecular sieves under nitrogen.

**Pentane** was purchased in a drum as ACS grade from Fisher, sparged with N2 and stored over 3Å molecular sieves under nitrogen.

**Dichloromethane** was distilled from calcium hydride under nitrogen.

**Tetrahydrofuran** was distilled from a purple sodium benzophenone mixture under nitrogen. The solvent was stored over 3Å molecular sieves under nitrogen.

### 3.4.3 Reagents for Synthesis

**Imines** were prepared according to literature procedures.[122]

**Dimethylchorosilane** was purchased from Sigma Aldrich and used as received.

**Chlorotrimethylsilane** was purchased from Sigma Aldrich and distilled before use.

**Pentachlorocyclopropane** was prepared according to a literature procedure.[125]

**[$Ph_3C$][$BAr^F_{24}$] (3-12)** was prepared according to literature procedures.[112]

***i*PrBAC-$BCy_2H$ (3-5)** was prepared according to previously reported methods.[122]

***i*PrBAC-$LiBF_4$ (3-11)** was prepared according to previously reported methods.[54]

***i*PrBAC-HCl (3-8c)** was prepared according to previously reported methods.[55]

**Tricyclohexylphosphine** was purchased from Oakwood Chemical and stored under nitrogen.

**Boranes** were prepared according to literature procedures.[134–136]

### 3.4.4 Synthetic Procedures

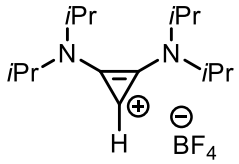


***i*PrBAC-$HBF_4$ (3-8a).** Caution: the following reaction is exothermic and undergoes a delayed exotherm. Use of oversized glassware and a condenser is recommended. This is the largest scale upon which we have conducted the reaction: In a 3-neck 2 L flask equipped with a reflux condenser, pentachlorocyclopropane (30 g, 0.14 mol) is dissolved in 400 mL dichloromethane, under ambient atmosphere. The mixture is cooled in an ice bath, and diisopropylamine (98 mL, 0.70 mol, 5 equiv.) is added over 5 min with stirring. A copious

precipitate formed, and the reaction turned a pale yellow colour. Heating of the reaction mixture to reflux was observed around the end of the addition of base, despite the use of an ice bath. The reflux subsided after several minutes. The cooling bath was allowed to decay naturally, and the reaction was stirred for 16 h. After this time, the reaction was an amber colour. To the reaction was added 100 mL deionized water, then triphenylphosphine (36.7 g, 0.140 mmol, 1 equiv.). Solid sodium tetrafluoroborate (15.4 g, 0.14 mmol, 1 equiv.) was added, and the biphasic reaction was stirred vigorously for 12 h. The aqueous layer is colourless and cloudy in appearance. After the completion of 12 h of stirring, the layers were separated. The organic layer was washed with 100 mL of deionized water containing 12 grams of sodium tetrafluoroborate. The amber organic layer was dried over $Na_2SO_4$, filtered, and concentrated to give a brown oil. To this residue was added 100 mL of diethyl ether, which caused it to solidify. The diethyl ether was removed *in vacuo*. The residue was slurried in 30 mL of a 2:1 mixture of diethyl ether and isopropanol, and filtered. The solid filter cake was washed with 2 x 100 mL cold diethyl ether, then dried *in vacuo* to afford 33g (0.10 mol, 73% yield) of compound *i*PrBAC-$HBF_4$ **(3-8a)** as an off-white solid. Spectral data were in agreement with literature values.[54]

**$^1$H** (500 MHz, $CDCl_3$): δ 7.42 (s, 1H), 4.02 (sept, $J$ = 6.6 Hz, 2H), 3.85 (s, $J$ = 6.6 Hz, 2H), 1.4 (d, $J$ = 6.6 Hz, 12H), 1.37 (d, 12H, $J$ = 6.6 Hz, 12H).

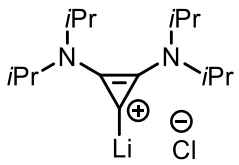


***i*PrBAC-LiCl.** *i*PrBAC-HCl (412 mg, 1.509 mmol, 1 equiv.) was added to an oven dried 4 dram vial equipped with a magnetic stir bar. *i*PrBAC-HCl was suspended in diethyl ether (8 mL) and the slurry was cooled to -35 °C. A solution of *n*-BuLi in pentane (2.5 M, 0.6

mL, 1.5 mmol) was added drop-wise with stirring. The reaction briefly clarified, and then became turbid again with a beige colour over a 10-min period. After 20 min, volatiles were removed *in vacuo*. The resulting solid was then washed on a frit with pentane (3 x 5 mL) and dried *in vacuo* to obtain *i*PrBAC-LiCl as a white powder, (363 mg, 1.3 mmol, 86%).

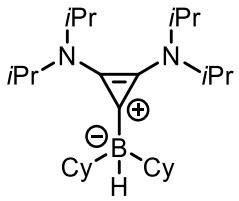


***i*PrBAC-BCy$_2$H (3-5).** *i*PrBAC-LiCl (55 mg, 0.197mmol) was placed in an oven dried 4 dram vial equipped with a magnetic stir bar. *i*PrBAC-LiCl was then suspended in ether (3 mL) and the solution was cooled to -35 °C. Then dicyclohexylborane (35 mg, 0.197 mmol) was added in one portion to the resulting suspension and stirred for 1 h. The solution was filtered with a 3-micron syringe filter and ether rinse (2 x 1 mL). Volatiles were removed *in vacuo* resulting in the title compound *i*PrBAC-BCy$_2$H **(3-5)** as a beige solid (70 mg, 0.169 mmol, 86%). Spectral data was in accordance with previously reported data.[122]

**$^1$H** (500 MHz, $CDCl_3$): δ 4.01 (br s, 4H), 1.78 (d, $J$ = 13 Hz, 2H), 1.60 (m, 6H), 1.31 (d, $J$ = 6.5 Hz, 24H), 1.17 (m, 8H), 0.83 (m, 4H), 0.44 (t, $J$ = 10 Hz, 2H).

**$^{11}$B** (160.5 MHz, $CDCl_3$): δ -12.11 (d, $J$ = 74 Hz).

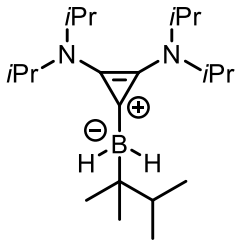


***i*PrBAC-BH$_2$Thex (3-18a).** *i*PrBAC-LiBF$_4$ **3-11** (212 mg, 0.6 mmol) was weighed in an oven dried 4 dram vial equipped with a magnetic stir bar. Toluene (5 mL) was then added

and the slurry was cooled to -35 °C. Thexylborane (0.6 mL, 0.6 mmol, 1 M toluene) was added slowly to the slurry and a white precipitate formed after 3 min. The slurry stirred for 1 h and then volatiles were removed *in vacuo*. Dichloromethane (3 mL) was then added to the crude material and the mixture was filtered on a fine porous frit containing celite and the celite was washed further with dichloromethane (3 x 3 mL). Dichloromethane was then removed *in vacuo* resulting in the title compound *i*PrBAC-$BH_2$Thex **3-18a** as a beige solid (166 mg, 0.496 mmol, 83%).

**$^1$H** (500 MHz, $CDCl_3$): δ 4.07 (br s, 4H), 1.42 (m, 1H), 1.32 (d, $J$ = 6.7 Hz, 24H), 0.88 (d, $J$ = 6.6 Hz, 6H), 0.74 (s, 6H).

**$^{13}$C** {$^1$H} (125.8 MHz, $C_6D_6$): δ 142, 50.2, 39.6, 28.9, 21.8, 19.1.

**$^{11}$B** (160.5 MHz, $CDCl_3$): δ -21.3 (t, $J$ = 82 Hz).

**HRMS (APCI):** calc'd for $C_{21}H_{43}BN_2Na$ $[M + Na]^+$ 357.3412; Found: 357.3403.

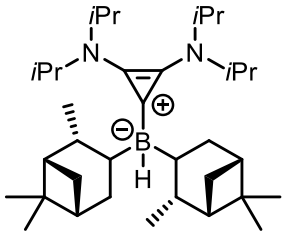


***i*PrBAC-Bipc$_2$H (3-18b).** *i*PrBAC-$LiBF_4$ **3-11** (327 mg, 0.925mmol) was placed in an oven dried 4 dram vial equipped with a magnetic stir bar. *i*PrBAC-$LiBF_4$ **3-11** was dissolved in ether (5 mL) and the solution was cooled to -35 °C. Then diisocamphenylborane (264 mg, 0.925 mmol) was added in one portion to the resulting suspension and stirred for 1 h. Ether was then removed *in vacuo* and the residue was taken up in benzene (4 mL) and filtered on a fine frit. The collected solids were washed with benzene (3 x 3mL) and volatiles removed *in vacuo* resulting in the title *i*PrBAC-Bipc$_2$H **3-18b** as a beige solid (415 mg 0.794 mmol, 86%).

**$^1$H** (500 MHz, $CDCl_3$): δ 4.04 (br s, 4H), 2.09 (m, 4H), 2.01 (m, 2H), 1.87 (m, 4H), 1.76 (m, 4H), 1.58 (m, 4H), 1.33 (m, 24H), 1.13 (s, 3H), 1.1 (s, 3H), 1.10 (s, 3H), 1.09 (s, 3H), 1.0 (d, $J$ = 7.1 Hz, 3H), 0.75 (d, $J$ = 7.1 Hz, 3H).

**$^{13}$C** {$^1$H} (125.8 MHz, $CDCl_3$): δ 143, 50.7, 49.5, 44.3, 43.4, 43.0, 42.5, 39.6, 35.0, 34.2, 33.6, 33, 28.7, 24.5, 23.1, 22.8, 21.7.

**$^{11}$B** (160.5 MHz, $CDCl_3$): δ -9.7 (d, $J$ = 73 Hz).

**HRMS (APCI):** calc'd for $C_{35}H_{64}BN_2$ $[M + H]^+$ 523.5157; Found: 523.5156.

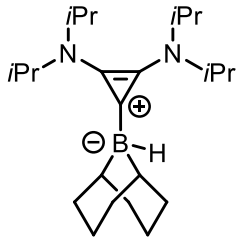


***i*PrBAC-(9-BBN) (3-16).** *i*PrBAC-$LiBF_4$ **3-11** (200 mg, 0.566 mmol) was weighed in an oven dried 4 dram vial equipped with a magnetic stir bar followed by 9-BBN (69 mg, 0.566 mmol. Toluene (3 mL) was added in one portion to the solids and the slurry stirred for 1 h. The slurry was the filtered on a fine porous fit and the solid was washed further with toluene (5 x 1 mL). Toluene was then removed *in vacuo* and the residue was triturated with pentane until a solid beige powder formed. The resulting solid was washed with pentane by decanting (2 x 1 mL) and then remaining volatiles were removed *in vacuo* resulting in the title compound *i*PrBAC-(9-BBN) **3-16** as a white solid (118 mg, 0.329 mmol, 58%).

**$^1$H** (500 MHz, $CDCl_3$): δ 4.06 (br s, 4H), 1.87 (m, 4H), 1.7 (m, 4H), 1.7 (m, 2H), 1.6 (m, 6H), 1.31 (d, $J$ = 6.9 Hz, 24H), 1.15 (m, 2H).

**$^{13}$C** {$^1$H} (125.8 MHz, $C_6D_6$): δ 143, 50.4, 37.0, 33.7, 26.8, 26.2, 24.6 (br), 21.5.

**$^{11}$B** (160.5 MHz, $CDCl_3$): δ -16.3 (d, $J$ = 75 Hz).

**HRMS (APCI):** calc'd for $C_{23}H_{44}BN_2$ $[M + H]^+$ 359.3592; Found: 359.3587.

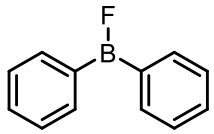


**Boron diphenylfluoride (3-19).** Under a nitrogen atmosphere, potassium diphenyldifluoroborate **3-21** (0.967 g, 3.99 mmol) was dissolved in THF (10 mL). TMS-Cl (0.5 mL, 3.99 mmol) was added dropwise. The reaction was stirred at room temperature for 2 h, and the solvent was removed under reduced pressure. In the glovebox, the product was extracted with ether, filtered, and the filtrate was concentrated to afford diphenylboron fluoride **3-19** as an off-white solid (0.565 g, 3.07 mmol, 77% yield).

**$^{11}$B** (96.6 MHz, $CDCl_3$): δ 43.8 (s).

**$^{19}$F** (282.4 MHz, $CDCl_3$): δ -73.6 (s).

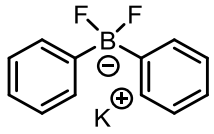


**$KF_2BPh_2$ (3-21).** A 1.47 M solution of phenylmagnesium bromide in tetrahydrofuran (37.4 mL, 55 mmol, 1 equiv) was cooled to 0 °C, and triisopropyl borate (6.34 mL, 27.5 mmol, 0.5 equiv.) was added over 30 min. A light-yellow precipitate formed. The solution was stirred at ambient temperature for 16 h, after which time 55 mL of 1N aqueous HCl was added. The layers were separated, and the organic layer extracted with diethyl ether. The combined organic layers were dried over $Na_2SO_4$, concentrated, and the oily colourless residue was used directly in the next reaction. The residue was dissolved in 80 mL methanol, cooled to 0 °C, and $KHF_2$ (8.6 g, 110 mmol, 2 equiv.) was added. The cloudy solution was stirred for 1 h, then volatiles were removed. The residue was taken up in 100 mL of acetone and filtered. The filtrate was concentrated, and the residue was slurried in

50 mL diethyl ether and collected by suction filtration affording the title compound **3-21** as a white powder (10.2 g, 42 mmol, 76% yield over 2 steps).

**$^{1}$H** (300 MHz, $CD_3CN$): δ 7.42 (m, 4H), 7.12 (t, 4H), 7.02 (m, 2H).

**$^{13}$C** {$^{1}$H} (75.5 MHz, $CD_3CN$): δ 132 (t, $J$ = 3.8 Hz), 127, 125.

**$^{19}$F** (282.4 MHz, $CD_3CN$): δ -159.

**$^{11}$B** (96.3 MHz, $CD_3CN$): δ 7.29 (t, $J$ = 66 Hz).

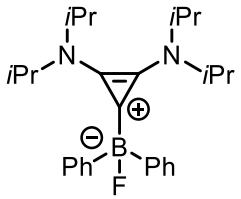


***i*PrBAC-BPh$_2$F (3-23).** *i*PrBAC-LiBF$_4$ **3-11** (300 mg, 0.848 mmol) and potassium difluorodiphenylborate (205 mg, 0.848 mmol) were weighed into an oven dried 4 dram vial equipped with a magnetic stir bar. Ether was added to the solids and the slurry was stirred overnight. Solvent was removed *in vacuo* and the product was taken up in toluene (3 mL). The slurry was then filtered through a fine porous frit filled with celite. The celite was washed with toluene (4 x 3 mL) and the resulting toluene was removed *in vacuo* to obtain the title compound *i*PrBAC-BPh$_2$F **3-23** as a beige solid (307 mg, 0.730 mmol, 86 %).

**$^{1}$H** (300 MHz, $CDCl_3$): δ 7.38 (m, 4H), 7.22 (m, 4H), 7.12 (m, 2H), 3.88 (br s, 4H), 1.24 (br s, 24H).

**$^{13}$C** {$^{1}$H} (75.5 MHz, $CDCl_3$): δ 139 (d, $J$ = 5 Hz), 133 (d, $J$ = 3 Hz), 127, 125, 51.1, 21.0.

**$^{19}$F** (282.4 MHz, $CDCl_3$): δ -192.

**$^{11}$B** (96.3 MHz, $CDCl_3$): δ 2.6 (br s).

**HRMS (ESI):** calc'd for $C_{27}H_{38}BFN_2Na$ $[M + Na]^+$ 443.3004; Found: 443.3011.

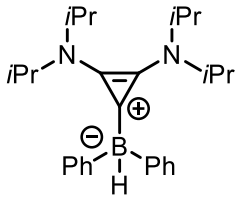

***i*PrBAC-BPh$_2$H (3-6).** *i*PrBAC-BPh$_2$F **3-23** (464 mg, 1.10 mmol) was placed in an oven dried 4 dram vial equipped with a magnetic stir bar and then dissolved in dichloromethane (5 mL). Chlorodimethylsilane (0.12 mL, 1.10 mmol) was added to the suspension and stirred overnight. Volatiles were removed *in vacuo* and the product was taken up in dichloromethane (5 mL) and chlorodimethylsilane was added once more (0.24 mL, 2.20 mmol, 2 equiv.) to stir overnight. Volatiles were removed *in vacuo* and the residue was triturated with pentane to obtain a beige solid as the title compound *i*PrBAC-BPh$_2$H **3-6** (409 mg, 1.01 mmol, 92%)

**$^1$H** (300 MHz, $CDCl_3$): δ 7.26 (m, 4H), 7.16 (m, 4H), 7.03 (m, 2H), 3.87 (br s, 4H), 3.67 (br q, BH) 1.24 (br s, 24H).

**$^1$H** (500 MHz, $C_6D_6$): δ 7.78 (d, 4H), 7.41 (t, 4H), 7.24 (t, 2H), 4.39 (br q, BH), 3.45 (br s, 4H), 0.88 (br s, 24H).

**$^{13}$C** {$^1$H} (75.5 MHz, $CDCl_3$): δ 140, 134, 127, 124, 50.7, 21.4.

**$^{11}$B** (96.3 MHz, $CDCl_3$): δ -14.7 (d, $J$ = 81 Hz).

**HRMS (ESI):** calc'd for $C_{27}H_{39}BN_2Na$ $[M + Na]^+$ 425.3099; Found: 425.3109.

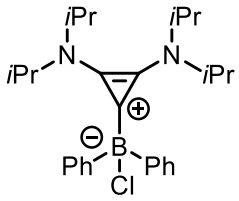

***i*PrBAC-BPh$_2$Cl (3-24).** *i*PrBAC-BPh$_2$F **3-23** (100 mg, 0.238 mmol) was placed in an oven dried 4 dram vial equipped with a magnetic stir bar and dissolved in dichloromethane (3

mL). Trimethylchlorosilane (0.06 mL, 0.476 mmol, 2 equiv.) was added to the solution and stirred overnight. Volatiles were removed *in vacuo* and the product was triturated with pentane to obtain a beige solid as the title compound *i*PrBAC-$BPh_2Cl$ **3-24** (102 mg, 0.233 mmol, 98%)

**$^{1}$H** (300 MHz, $CDCl_3$): δ 7.40 (m, 4H), 7.18 (m, 4H), 7.08 (m, 2H), 3.92 (br s, 4H), 1.15 (br s, 24H).

**$^{13}$C** {$^{1}$H} (75.5 MHz, $CDCl_3$): δ 139, 134, 127, 125, 51.1, 21.4.

**$^{11}$B** (96.3 MHz, $CDCl_3$): δ -1.28 (br s).

**HRMS (ESI):** calc'd for $C_{27}H_{38}BN_2$ $[M - Cl]^+$ 401.3123; Found: 401.3127.

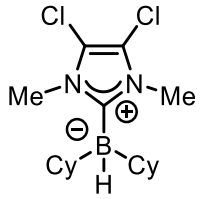


**Cl-NHC-$BCy_2H$ (3-17).** Dichlorodimethylimidazolium iodide (151 mg, 0.515 mmol) was weighed into an oven dried 4 dram vial equipped with a magnetic stir bar. Potassium hexamethyldisilazide (108 mg, 0.541 mmol, 1.05 equiv.) and dicyclohexylborane (151 mg, 0.515 mmol) were then added to the vial and cooled to -35 °C and a separate vial containing tetrahydrofuran (5 mL) was also cooled to -35 °C. The tetrahydrofuran was added in one portion to the vial containing the solids and the reaction was left to stir overnight. Volatiles were removed *in vacuo* and the resulting solid was taken up in pentane (3 mL) and filtered over celite. The resulting celite was washed with pentane (4 x 3 mL) and the pentane was removed *in vacuo*. The resulting solid was triturated with pentane to afford the product Cl-NHC-$BCy_2H$ **3-17** (148 mg, 0.431 mmol, 84%)

**$^{1}$H** (500 MHz, $CDCl_3$): δ 3.82 (s, 3H), 3.72 (s, 3H), 1.84 (d, *J* = 13 Hz, 2H), 1.63 (m, 6H), 1.17 (m, 8H), 0.77 (m, 4H), 0.64 (m, 2H).

**$^{13}$C** {$^{1}$H} (125.8 MHz, $CDCl_3$): δ 116, 115, 35.8, 36.8, 34.4, 31.5, 29.3, 29.2, 27.9.

**$^{11}$B** (160.5 MHz, $CDCl_3$): δ -12.6 (d, *J* = 79 Hz).

### 3.4.5 Borenium Ion Generation, Hydrogen Activation and Coordination Studies

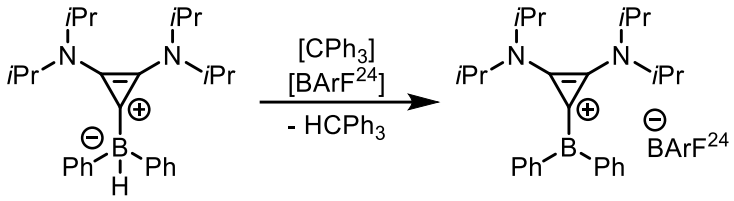


**Formation of Borenium Cation [*i*PrBAC-BPh$_2$][BAr$^{F}_{24}$] 3-25 in situ from trityl BAr$^{F}_{24}$.** In a glovebox, *i*PrBAC-BPh$_2$H **3-5** (15 mg 0.037 mmol) and trityl BAr$^{F}_{24}$ **3-12** (41 mg, 0.037 mmol) were placed in an oven dried 1 dram vial. The solids were dissolved in $CDCl_3$ (approx. 1 mL) and the solution was transferred to a standard NMR tube and NMR spectra were acquired after 15 min.

**Diagnostic NMR Data:**

**$^{1}$H** (500 MHz, $CDCl_3$): δ 5.56 (s, 1H, $Ph_3CH$), 3.99 (sept, *J* = 6.7 Hz, 2H), 3.68 (s, *J* = 6.7 Hz, 2H), 1.30 (d, *J* = 6.7 Hz, 12H), 1.00 (d, *J* = 6.7 Hz, 12H).

**$^{11}$B** (160.5 MHz, $CDCl_3$): δ 64.5 ($B^+$), -6.6 (BAr$^{F}_{24}$).

***i*PrBACBH$_2$Thex pyridine trityl addition:** In the glove-box, *i*PrBAC-BH$_2$Thex **3-18a** (12.5 mg, 0.0373 mmol) was weighed into a 1 dram vial and the solid dissolved in chloroform (1 mL). Pyridine was added (3 drops) followed by trityl BAr$^{F}_{24}$ **3-12** (41 mg, 0.0373 mmol). The use of pyridine was necessary to maintain homogeneity in this solvent. The sample was then transferred to an NMR tube, which was sealed with a standard cap and Teflon tape. The mixture analyzed using $^{1}$H and $^{11}$B NMR spectroscopy. The solution

was then transferred back into the 1 dram vial and another equivalent of trityl $BAr^F_{24}$ **3-12** (41mg, 0.0373 mmol) was added. The sample was then transferred to an NMR tube once more and analyzed using $^1H$ and $^{11}B$ NMR spectroscopy. No change in the key chemical shifts was observed, indicating a second hydride abstraction did not occur under these conditions. In addition, no increase in the amount of triphenylmethane was observed, as further evidence a second hydride abstraction did not occur.

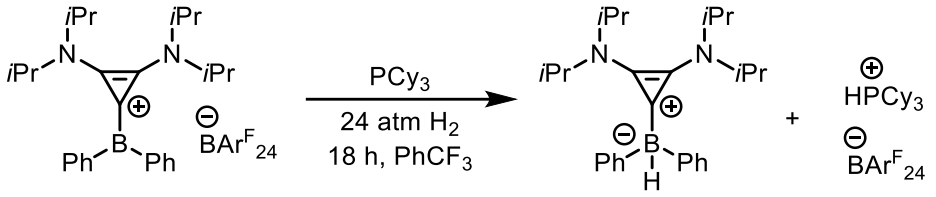


**Hydrogen activation with [*i*PrBAC-BPh$_2$][BAr$^F_{24}$] 3-25 and PCy$_3$:** In a glovebox, *i*PrBAC-BPh$_2$H **3-6** (15 mg 0.037 mmol) and trityl $BAr^F_{24}$ **3-12** (41 mg, 0.037 mmol) were weighed into an oven dried 1 dram vial. In a separate vial, tricyclohexylphosphine (10.5 mg, 0.037 mmol was weighed and equipped with a magnetic stir bar. The solids in the vial containing *i*PrBAC-BPh$_2$H **3-6** and trityl $BAr^F_{24}$ **3-12** were dissolved trifluorotoluene (approx. 0.3 mL). The solution was transferred to the vial containing $PCy_3$ and the previous vial was washed with trifluorotoluene (0.4 mL). The vial was closed with a septa cap pierced with a needle. The vial was then paced in a parr bomb and pressurized with 10 atm of $H_2$. The mixture was stirred for 18 h and was then brought back into the glove box and 11 drops of deuterated benzene were added. The solution was transferred to a standard NMR tube and NMR spectra were acquired.

**Diagnostic NMR Data:**

**$^1$H** (500 MHz, $C_6D_6$): δ 5.37 (s, 1H, $Ph_3CH$), 3.61 (br s, 4H), 0.98 (br s, 24H).

**$^{11}$B** (160.4 MHz, $C_6D_6$): δ -6.1 ($BAr^F_{24}$), -14.2 (d, $J$ = 74 Hz).

**$^{31}$P** (202.5 MHz, $C_6D_6$): δ 31 (d, $J$ = 450 Hz).

**Imine complexation reactions.** *i*PrBAC-B$Cy_2$H **3-5** (15.5 mg, 0.0373 mmol) or *i*PrBAC-B$Ph_2$H **3-6** (15 mg, 0.0373 mmol) was weighed into a 1 dram vial along with trityl B$Ar^F{}_{24}$ **3-12** (41 mg, 0.0373 mmol). Approximately 1 mL of chloroform-*d* was used to dissolve the solids and the solutions were left for 2 min. Imine **3-14a** (10 mg, 0.0373 mmol) was then added in one portion and the resulting solution was transferred to an NMR tube and analyzed using $^{11}$B and $^{1}$H NMR spectroscopy.

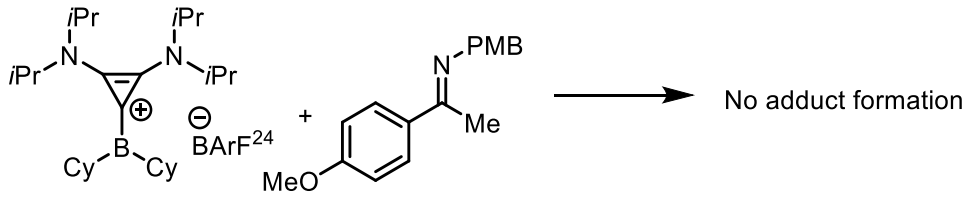


For dicyclohexylboron adduct **2-5**, minimal perturbations in the spectra were observed upon imine addition. While the borenium peak is not well defined in the $^{11}$B NMR, the inequivalent signals of the methane signals of the isopropyl peaks on the BAC scaffold, which are consistent with borenium **3-13** persist. (See chapter 2 for data of **3-13**).

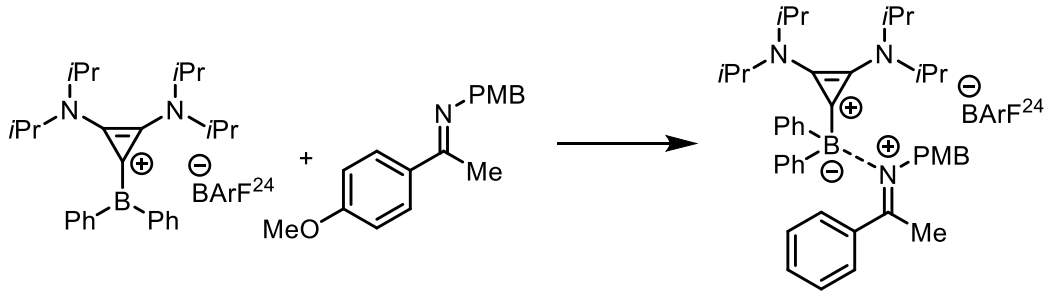


With **3-12**, significant perturbations in the $^{1}$H and $^{11}$B spectra are observed, which we take as evidence of formation of a Lewis adduct.

### 3.4.6 General Hydrogenation Procedure and Reduced products

*i*PrBAC-B$R_2$H (0.02 mmol, 10 mol %) and trityl B$Ar^F{}_{24}$ **3-12** (22 mg, 0.02 mmol, 10 mol %) were placed in an oven dried 1 dram vial equipped with a magnetic stir bar. To this vial

trifluorotoluene (0.2 mL) was added and the solution stirred for 2 min. Then substrate was added (0.2 mmol) as a solid and then the solution was diluted with trifluorotoluene (0.1 mL) or a solution of the substrate (0.1 mL, 2M) was added, and the vial equipped with a septum cap and 16-gauge needle. Vials were placed into a Parr-bomb which was then assembled and removed from the glove box. In a fume hood, the bomb was placed on a stir plate, and purged seven times by pressurizing to 20 atm of $H_2$ followed by careful release. The bomb was subsequently pressurized to 24 atm. The parr bomb was left on the stir plate over night and then was carefully depressurized, disassembled, and the vials were removed. $CDCl_3$ (approx. 0.5 mL) was added and conversion was ascertained by $^1H$ NMR (comparison of starting material and product, or triphenyl methane and product give values that agree). The solvents were then removed *in vacuo* and the crude material was then subjected to column chromatography with a gradient of 2.5% to 100% ether to hexanes as needed. $^1H$ NMR data was then acquired of the amine products.

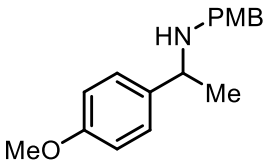


***N*-(4-methoxybenzyl)-(1-(4-methoxyphenyl)ethyl)amine (3-15a).** 48mg, 0.177mmol, 88%

**$^1$H** (300 MHz, $CDCl_3$): δ 7.25 (m, 2H), 7.18 (m, 2H), 6.87 (m, 2H), 6.83 (m, 2H), 3.79 (s, 3H), 3.77 (s, 3H). 3.74 (q, *J* = 6.6 Hz, 1H), 3.55 (ab q, 2H), 1.53 (s, 1H), 1.32 (d, *J* = 6.6 Hz, 3H).

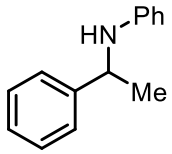


***N*-Phenyl-(1-phenethyl)amine (3-15b).** 0.172 mmol as determined by ferrocene internal standard = 85% yield.

**$^1$H** (300 MHz, $CDCl_3$): δ 7.34 (m, 2H), 7.29 (m, 2H), 7.20 (m, 1H), 7.07 (m, 2H), 6.6 (t, 1H), 6.50 (d, 2H). 4.47 (q, *J* = 6.7 Hz, 1H), 3.99 (s, 1H), 1.49 (d, *J* = 6.7 Hz, 3H).

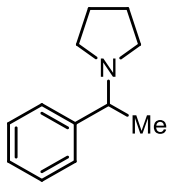


**1-(1-Phenylethyl)pyrrolidine (3-15c).** 22mg, 0.123 mmol, isolated yield 63%

**$^1$H** (300 MHz, $CDCl_3$): δ 7.31 (m, 5H), 3.17 (q, *J* = 6.6 Hz, 1H), 2.53 (m, 2H), 2.37 (m, 2H), 1.75 (m, 4H), 1.39 (d, *J* = 6.6 Hz, 3H). Several impurities were noted in this compound, which were not readily removed by column chromatography. This product was also somewhat volatile complicating isolation. In a separate procedure, 0.5 mL of a 0.1 molar solution of ferrocene was added directly to the reaction mixture without removal of the trifluorotoluene. Since there are 0.5 mmol of ferrocene, and the integral for the ferrocene is set to 10.00, the integral of 4.02 for the benzylic proton indicates 0.2 mmol of amine product are present, which essentially indicates quantitative conversion and NMR yield for this reaction.

# Chapter 4: Borenium Generation via Quinolinium Salts

Contributions to manuscript: All synthetic work in this chapter was carried out by B. S. N. Huchenski, with the following exceptions: Imines were prepared collaboratively between B. S. N Huchenski, M. R. Adams and C.-H. Tien. $NaBAr^{F}_{24}$ was prepared by Dr. A. W. H. Speed and $NaBar^{Cl}_{8}$ was prepared by M. R. Adams. The X-ray crystallography was conducted by Dr. R. McDonald, Dr. M. J. Ferguson, and Yuqiao Zhou. Mass spectrometric data were acquired by Mr. Xiao Feng (Mass Spectrometry Laboratory, Dalhousie University). The manuscript was written by B. S. N. Huchenski.

## 4.1 Introduction

Within borenium catalysis, the borenium ion is often generated through hydride abstraction with trityl $BAr^{F}$ (**Scheme 4.1)**.[44,45,122,137] This reagent while effective, is limited to handling and storage under an inert atmosphere. In addition, this reagent suffers from instability in certain ethereal solvents.[112] The precursor to a borenium ion, the carbene borane adduct (**4-1)**, is air and moisture stable, allowing for preparation and handling under less rigorous conditions.[122,137] If a hydride abstraction reagent can be prepared that is also moisture-stable and tolerant to more solvents, then precursors to borenium catalysis can be handed without the need of specialized equipment. The overall gain from generating the borenium ion *in situ* rather than pre-isolation is in the inherent greater stability of the precursor reagents.

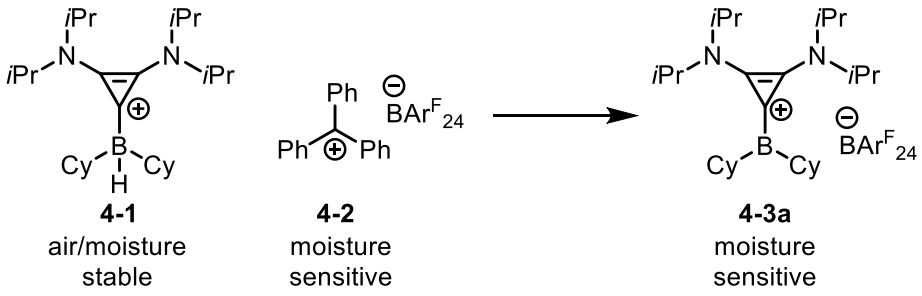


**Scheme 4.1** Borenium ion generation via trityl salts.

To develop a new method of hydride abstraction for borenium catalysis, an understanding of the catalytic cycle may yield critical information. In 2015 Crudden and co-workers proposed a catalytic cycle for borenium hydrogenation (**Scheme 1.7**),[45] in which the boron cation and imine act as a frustrated Lewis pair to split hydrogen. The subsequent step involves the reduction of an imine, producing an amine product as well as regenerating the borenium cation. During this critical turnover step, it is the transfer of a hydride to an iminium ion that forms the borenium ion. Therefore, an abstraction reagent that can mimic the activated imine in reduction may be suitable. While the preparation of an iminium salt as the hydride abstraction reagent may seem viable, the hydroscopic nature of the smaller iminium salts results in their poor long-term stability and inappropriateness as a stable benchtop reagent. In addition, the smaller imine structure, and amine reduction products pose potential catalyst poisons which could inhibit or slow down catalytic activity through competitive coordination or lysis of the carbene borane bond.

While an iminium salt is not viable for hydride abstraction, a similar set of compounds such as heterocyclic ammonium salts have been reported as hydride abstraction reagents.[138,139] These compounds (**4-4a**) have been reported by Ingleson to undergo hydrogen activation in the presence of a base such as lutidine, effectively forming a FLP system (**Scheme 4.2**).[138] Furthermore, hydrogen activation with an imine was possible,

however only 25% abstraction was observed at 100 °C over 72 h. Hydride abstraction was also observed from boron hydrogen bonds as well as hydrosilanes, which allowed for these complexes to be applied in catalytic hydrosilylation reactions. While these complexes were effective in hydrosilylation reactions, the substrates examined were limited to aldimines, which required heating between 60 to 100 °C. Following this initial report, Ingleson disclosed that smaller *N*-methyl-benzothiazolium complexes were also capable of hydride abstraction.[139] Imine reduction was also possible with these complexes albeit at 100 °C. Room temperature reduction was also possible with these complexes but is limited to ketone reduction. Overall, the ability of heterocyclic ammonium complexes to activate hydrogen and abstract hydrides provides a potential use in borenium catalysis.

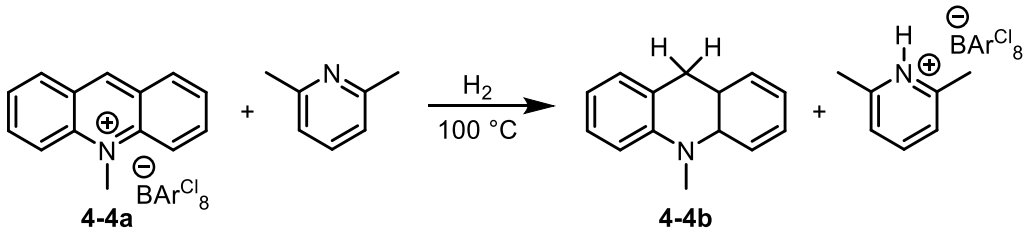


**Scheme 4.2** Hydrogen activation via a cyclic iminium salt and lutidine.

## 4.2 Synthesis of Cyclic Iminium Salts

The investigation of *N*-methyl acridinium (**4-4a**) and *N*-methyl-benzothiazolium complexes provided the foundation that heterocyclic ammonium salts are capable of hydrogen activation/abstraction.[138,139] These complexes closely resemble the acyclic iminium salts, which are reduced in a borenium catalyzed hydrogenation.[45] The hydride affinity for these cyclic iminium complexes is between that of trityl salts and tris(pentafluorophenyl)borane[138] and therefore should be capable of hydride abstraction from carbene borane adducts. While acridinium **4-4a** shown exceptional hydride affinity,

the large steric bulk of this iminium complex could provide challenges in hydride abstraction.

To obtain a mixture of sufficient hydride affinity and steric bulk, acridine was substituted for quinoline. In replacing the acridine with a quinoline moiety, the carbon on which hydride transfer will occur is now more open to attack from the sterically demanding carbene borane adduct. The methyl was also substituted for a benzyl group, to closer resemble successful substrates with BAC borane hydrogenation as seen in chapters 2 and 3. The synthesis of *N*-benzyl-quinolinium bromide **4-5** (**Scheme 4.3**) can be conducted as a neat reaction with a 1:1 combination of quinoline and benzyl bromide which is easily purified from unreacted materials through washing with dichloromethane. While some iminium ions and pyridinium ions are hygroscopic,[140] this compound remains a free-flowing powder with no signs of degradation by water. The next step is the preparation of a $BAr^F_{24}$ salt **4-6**, due the requirement of a weakly coordinating cation for borenium catalyzed hydrogenation.[32] Benzyl quinolinium complex **4-5** was then treated with sodium $BAr^F_{24}$ to generate the quinolinium salt **4-6**. This $BAr^F_{24}$ salt (**4-6**) was found to be air stable and non-hygroscopic allowing for a potential reagent for hydride abstraction as a bench stable reagent.

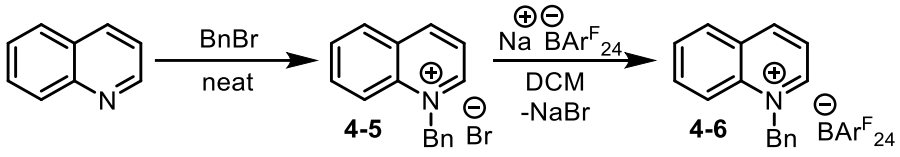


**Scheme 4.3** Synthesis of *N*-benzyl quinolinium $BAr^F_{24}$ **4-5**.

With the quinolinium complex **4-6** in hand, hydride abstraction of BAC borane complexes was then examined. Hydride abstraction studies are important for determining if clean borenium generation will occur and if the subsequent amine will coordinate with

the borenium ion, which may indicate potential catalyst poisoning or slower reaction times. In a comparable manner to the generation of borenium complex **4-3a** with trityl $BAr^F_{24}$ **4-2**, quinolinium complex **4-6** was combined with BAC borane **4-1** in $CDCl_3$ (**Scheme 4.4**). Within a 10-min span, complete formation of borenium ion **4-3a** was observed. The $^{11}B$ NMR chemical shift did not change between hydride abstraction methods, indicating that coordination of the amine product from this abstraction was not present. Hydride abstraction was also examined with *i*PrBAC-$BPh_2H$ **4-8**, and it was found that hydride abstraction occurred. Successful formation of borenium complex **4-3a** without interference from the by-product of hydride abstraction provided evidence that this reagent may be viable in borenium catalysis.

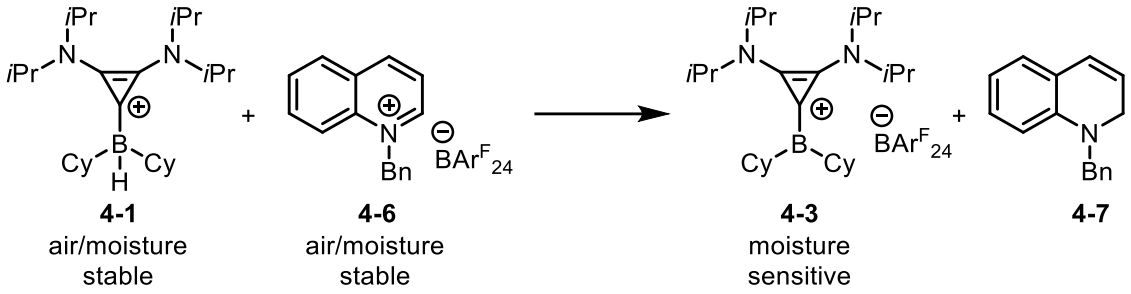


**Scheme 4.4** Hydrogen activation via *N*-benzyl quinolinium $BAr^F_{24}$.

### 4.3 Hydrogenation via Quinolinium Activation

Initial examination of borenium generation with quinolinium salts resulted in clean formation of a borenium ion identical to that of a trityl-generated borenium ion **4-3a**. Hydrogenation of imines were then investigated with this new iminium salt activator. Similar to previous hydrogenation reactions, *N*-benzyl imines were chosen as substrates. Using a 10 mol % loading of the BAC complex **4-1** and quinolinium salt **4-6**, *N*-benzyl imines shown in **Scheme 4.5** were successfully reduced. These results further supported

that the amine **4-7** produced from borenium generation did not affect the catalytic ability of the complex.

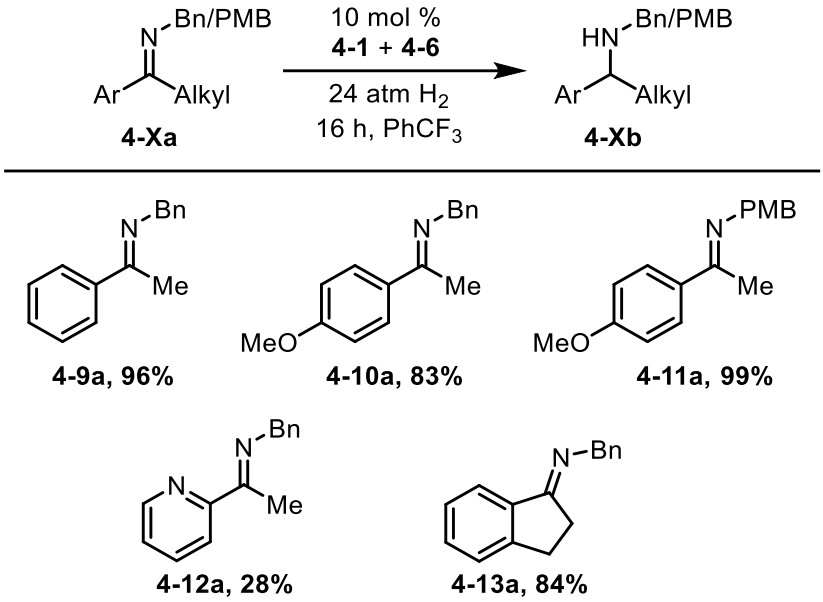


**Scheme 4.5** Hydrogenation scope with *N*-benzyl quinolinium $BAr^{F}_{24}$ **4-6** as the hydride abstraction reagent. Percent yields were calculated based on relative proportions of the starting material versus product in $^{1}H$ NMR.

Successful hydrogenation of *N*-benzyl imines with the new hydride abstraction reagent **4-6** led to a broader investigation of viable substrates for this hydrogenation system. While the current best borenium hydrogenation catalysts are limited to imines derived from sterically demanding amines,[44,45,47] BAC carbene complexes can hydrogenate *N*-benzyl imines with high conversions as seen in chapter 2 and 3. A more challenging substrate for borenium hydrogenation would be an imine with even less steric bulk around the nitrogen centre. Imines with a low steric bulk around the nitrogen centre pose a two-fold problem. The first of which is if the imine has a low steric bulk around the nitrogen, the coordination to the boron cation may be too strong, prohibiting a frustrated pair and acting as a relatively inert adduct. The second challenge is in inhibition by the product of hydrogenation. If the

amine product itself is too small, lysis of the carbene borane adduct may occur or an adduct may form from with the amine product.

A *N*-propargyl imine (**4-14a)** was examined for the purpose of a low steric demand around nitrogen, in addition to having an alkyne group. The alkyne functional group may allow for potential further functional modification to the reduced product post-hydrogenation. In addition, this substrate will determine if alkynes poison the borenium complex, inhibiting hydrogenation or become reduced to the subsequent alkene. Imine **4-14a** was treated with a 10 mol % loading of BAC complex **4-1** and quinolinium salt **4-6** under similar conditions to previous hydrogenation reactions (**Scheme 4.6**). It was found that imine **4-14a** was reduced to approximately 29% conversion to the corresponding amine **4-14b**. While the conversion of this substrate to the amine was less than the *N*-benzylamine derivatives, no reduction of the alkyne was observed. This indicated that the BAC carbene complexes can tolerate even less sterically demanding substrates as well as alkyne functional groups.

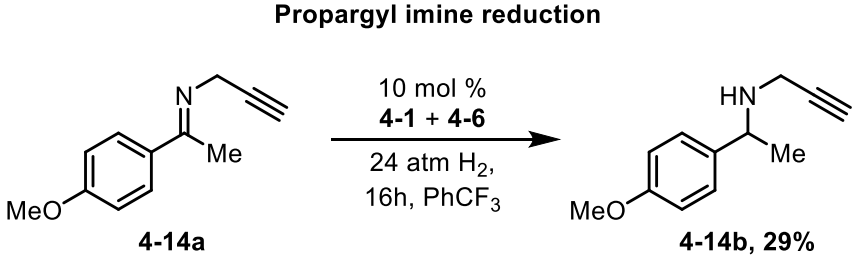


**Scheme 4.6** Hydrogenation of a *N*-propargyl imine **4-14a**. Percent yields were calculated based on relative proportions of the starting material versus product in $^{1}$H NMR.

### 4.4 Improving BAC Borenium Catalysis

The synthesis and application of quinolinium complexes in borenium catalysis has allowed for the air stable preparation of a hydride abstraction reagent. The facile synthesis of this activator allows for the investigation of other suitable anions for borenium catalyzed

hydrogenation. In this investigation of borenium hydrogenation, as well as a variety of other reports, fluoroaryl borates also known as $BAr^F$ salts have been the standard.[44–46,122,137] The application of $BAr^F$ salts in catalysis has been used for its stability and high solubility compared to other anions. In addition, while some anions such as $PF_6$ and $BF_4$ are non-innocent under certain reactions, $BAr^F$ salts are known to be more resilient to decomposition.[35] However, the cost of $BAr^F$ salts is much greater than other achiral anions and the synthesis of $BAr^F{}_{20}$ salt (**Figure 4.1**) is challenging because of the explosive nature of the intermediate through lithiation and the corresponding Grignard not reliably engaging in addition to boron[141]. Additionally, trifluoromethyl containing anions are known to exhibit more disorder in their structure, which adds increased difficulty in the accurate determination of the structure by single-crystal X-ray crystallography.[35] While the fluoroborate salts are the most commonly used weakly coordination anions, a variety of other anions could be applied to this chemistry. The synthesis of a more cost effective and facile anion for borenium catalysis would allow this chemistry to be more accessible in research applications.

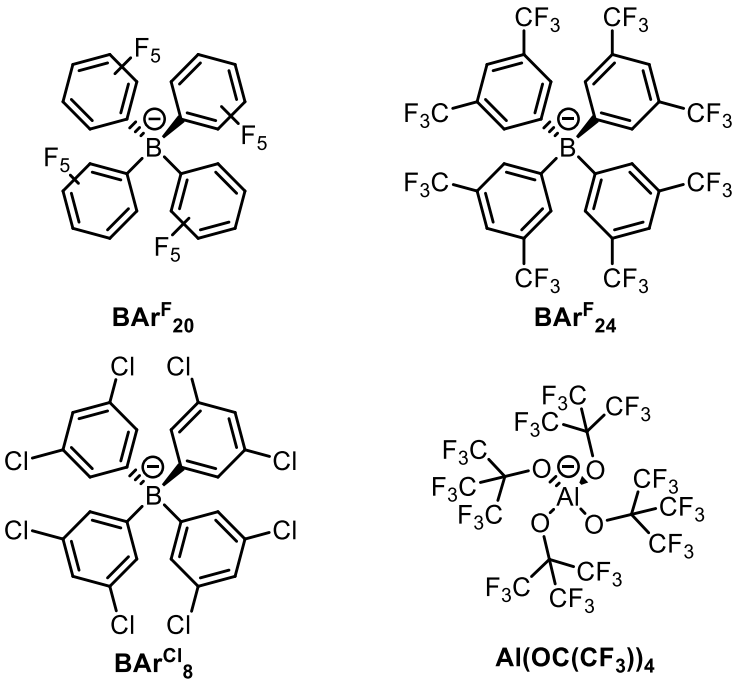


**Figure 4.1** Weakly coordinating anions used in catalysis.

An alternative weakly coordinating anion, the $Bar^{Cl}_8$ anion, capable of stabilizing borenium ions, was reported by Vidović in 2013.[142] While this anion was not stable for the majority of carbene borane complexes synthesized, one borenium complex was able to be prepared, and is a stable complex at room temperature.[142] Following this initial report, Vidović disclosed an additional borenium complex stabilized by the $Bar^{Cl}_8$ anion.[143] The 3,5-dichlorotetraphenylborate anion closely resembles the 3,5-trifufloromethyltetraphenylborate which has been a viable anion for BAC borenium catalysis.[122,137] Ingleson has also disclosed the synthesis of acridinium and benzoimidazolium salts stabilized by $Bar^{Cl}_8$ anions, which were also active in hydrosilylation and hydride abstraction.[138,139]

The 3,5-dichlorotetraphenylborate anion can be readily prepared via Grignard addition to $NaBF_4$ to produce the corresponding borate salt.[141] In a similar manner to the *N*-benzyl quinolinium $BAr^F_{24}$ salt **4-6**, combination of the sodium $Bar^{Cl}_8$ and *N*-benzyl

quinolinium bromide **4-5** in DCM afforded the *N*-benzyl quinolinium $Bar^{Cl}_8$ salt **4-15**. When examined in hydride abstraction, *N*-benzyl quinolinium $Bar^{Cl}_8$ salt **4-15** generated the borenium ion **4-3b** with no observed degradation. Hydrogenation was then examined using *N*-benzyl quinolinium $Bar^{Cl}_8$ salt **4-15** as the hydride abstraction reagent. This was tested with successful substrates used with *N*-benzyl quinolinium $BAr^{F}_{24}$ salt **4-6** as the hydride abstraction reagent. *N*-benzyl quinolinium $Bar^{Cl}_8$ salt **4-15** preformed in an essentially identical manner to the $BAr^{F}_{24}$ analog, providing a suitable alternative, and non-fluorinated anion for borenium hydrogenation (**Scheme 4.8**).

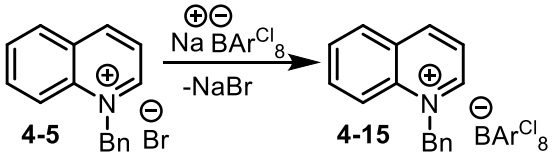


**Scheme 4.7** Synthesis of *N*-benzyl quinolinium $Bar^{Cl}_8$ **4-15**.

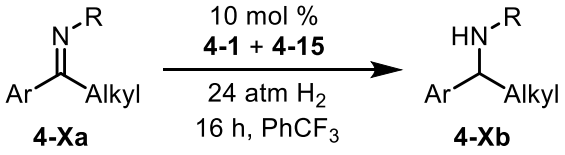


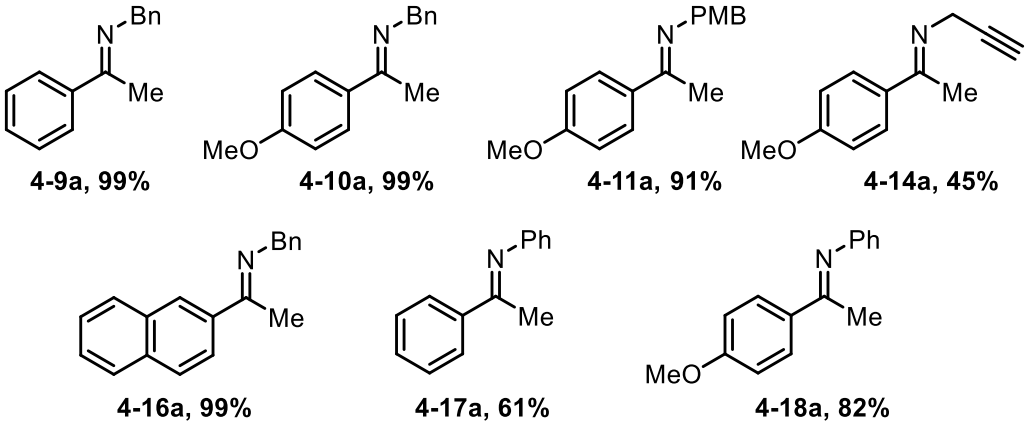


**Scheme 4.8** Hydrogenation scope with *N*-benzyl quinolinium $Bar^{Cl}_8$ **4-15** as the hydride abstraction reagent. Percent yields were calculated based on relative proportions of the starting material versus product in $^1$H NMR.

A variety of pharmaceuticals can be produced from the reduction of imines.[144] The potential for the BAC complexes in the synthesis of pharmaceuticals is possible with the current results suggesting the tolerance for benzyl and propargyl groups. This method of hydrogenation is more accessible than other methods that require metals or specialized equipment for the preparation of the catalyst and can have use in preparation of pharmaceutical intermediates. Sertaline, an SSRI, can be produced in few synthetic steps, with the final step being an imine reduction.[144] The precursor imine to this pharmaceutical, was treated with a 10 mol % loading of BAC complex **4-1** and quinolinium salt **4-15** under the standard hydrogenation conditions (**Scheme 4.9**). The Sertaline precursor **4-20a** was not reduced under these conditions so a derivative of this imine with a N-benzyl amine was prepared. This substrate was also not viable with BAC borenium hydrogenation. Rasagiline, a monoamine oxidase inhibititor[145] can also be produced via imine reduction of substrate **4-19a**.[77] Previously the *N*-benzyl imine derivative of the precursor imine **4-13a** was a viable substrate for hydrogenation with the BAC system. In addition, *N*-propargyl imine **4-14a** was a viable substrate for imine hydrogenation. However, the imine precursor of Rasagiline **4-19a** which resembles a combination of the previously mentioned substrates, was not a viable substrate with BAC borenium hydrogenation (**Scheme 4.7**). Fendiline, a calcium channel blocker[146] that can be made through the reduction of imine **4-21a** may be challenging for the majority of borenium complexes in hydrogenation due to the low steric bulk surrounding nitrogen. This imine (**4-21a**) when tested with 10 mol% of the carbene borane adduct **4-1** and activator **4-15** was found to be nearly fully reduced in the standard reaction times and conditions (**Scheme 4.9**). This result indicated that other non-sterically demanding imines are suitable for this catalyst system, which can be applied to real world applications such as pharmaceutical synthesis, and selective hydrogenations.

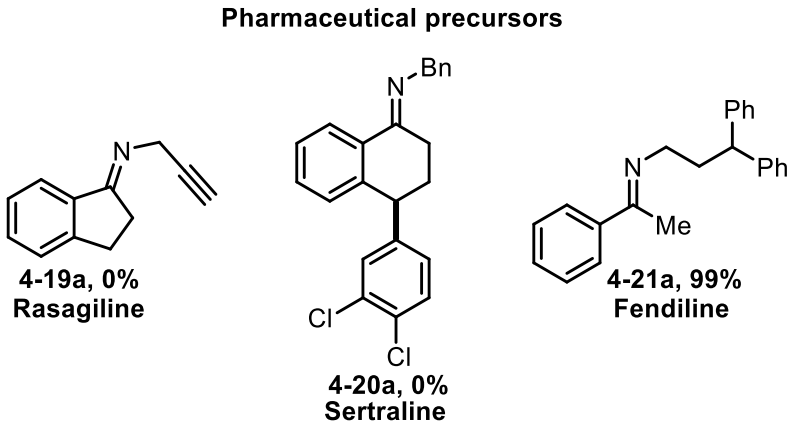


**Scheme 4.9** Pharmaceutical precursor imines examined though borenium hydrogenation. Imines were examined with a 10 mol % loading of **4-1** and either **4-6** or **4-15** as the activator under standard reaction conditions. Percent yields were calculated based on relative proportions of the starting material versus product in $^{1}$H NMR.

### 4.5 Hydrosilylation with $Bar^{Cl}{}_{8}$ and $BAr^{F}{}_{24}$.

Borenium catalyzed hydrogenation is attractive for its atom economy. However, the specialized equipment required for these reactions would restrict its wide application in research. In addition, borenium hydrogenation reactions are highly sensitive to minor impurities and moisture, which can result in loss of conversion or complete shutdown of reactivity. This results in rigorous purification requirements and higher loadings for high conversion processes.[44] Conversely, while reduction processes which use reductants such as hydroboranes or hydrosilanes have less atom economical reagents, but often require less harsh conditions and are more robust towards impurities, which ultimately can make them more practical.[47]

The application of boranes in the hydrosilylation of imines has been an active field of research for numerous years. Early examples include BCF hydrosilylation of imines which can reduce both ketimines and aldimines.[48] Subsequent developments have involved a variety of chiral boranes that are able to facilitate asymmetric reductions of imines.[29] Borocations have also been applied in hydrosilylation reactions, namely in the reduction of

ketones.[32] A primary example of this process was disclosed by Denmark in 2013 (**Scheme 4.10**).[49] This reaction is facilitated by a lutidine supported borocation **4-23** that can reduce ketones at a 10 mol % loading at room temperature. While the report of borocations in ketone and aldehyde reduction is investigated thoroughly, the application of imine reductions with borocations is sparse.[32,37] An important example for borenium catalyzed asymmetric reduction of imines and the only example published of carbene supported borenium (**4-24**) reduction of imines was reported in 2019 (**Scheme 4.10**).[47] This example featured loadings as low as 4 mol % of **4-23**, supporting the reduction of both aryl and alkyl imines. However, all borane methods reported thus far are highly sensitive catalysts, prohibiting their handing in a benchtop setting. Advancements in air stable precatalysts could allow for these processes to reach a wider application.

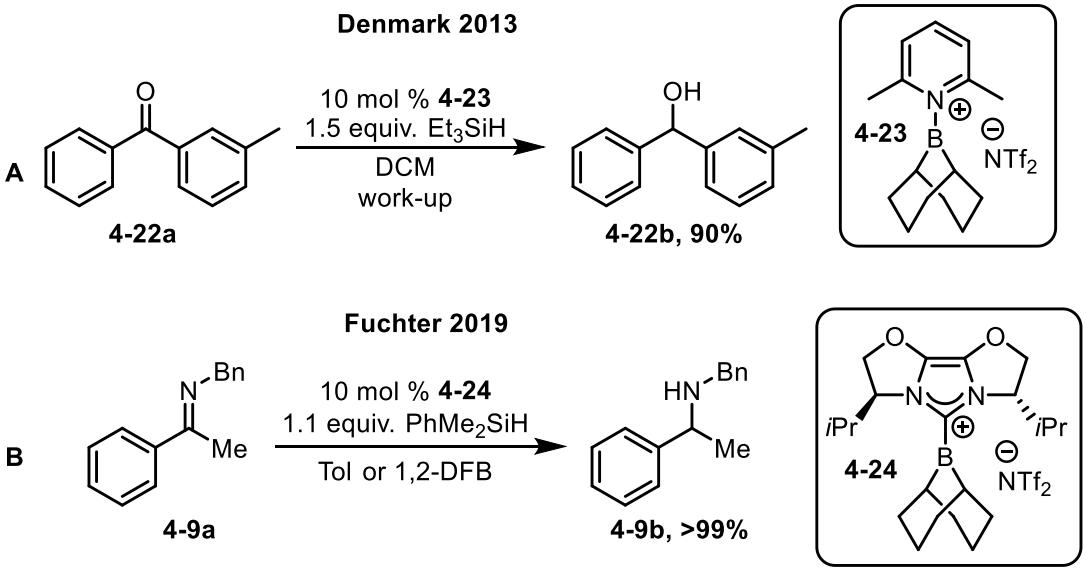


**Scheme 4.10** Early example of borenium-catalyzed hydrosilylation (**A**) versus current best asymmetric borenium hydrosilylation (**B**).

The development of the quinolinium hydride abstraction reagents in section 4.3-4.4 show that hydrogenation of imine substrates can be facilitated by a borenium ion which is generated from air stable precursors. In an effort to apply this air-stable system to more

reductive chemistry, these complexes were investigated in hydrosilylation reactions. The advantage of the air stable precatalyst not only allows for better handling of the complexes but it also allows for the *in situ* generation of the catalyst. A potential complication within borenium catalysis involving hydrosilylation reactions, namely asymmetric reactions, is in the generation of the borenium ion. Hydride abstraction reagents such as trityl $BAr^F_{24}$ have been reported to facilitate chain reaction hydrosilylations of substrates.[147,148] Ingleson has also reported that compounds similar to the quinolinium $BAr^F_{24}$ and $Bar^{Cl}_8$ complexes have facilitated the hydrosilylation of ketones and imines (**Scheme 4.11**).[138,139] However, only aldimines have been reduced by these complexes, which required heating to facilitate the reduction.

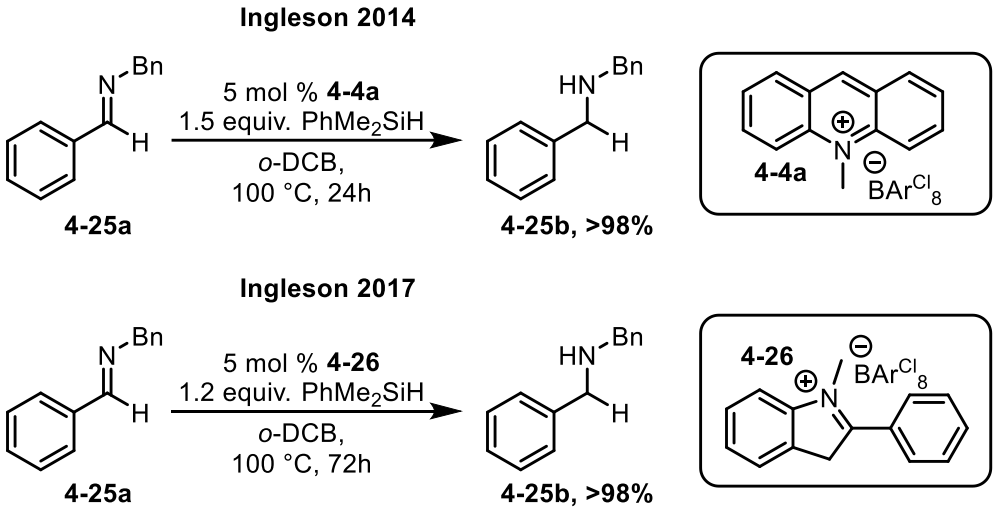


**Scheme 4.11** Hydrosilylation facilitated by cyclic iminium salts.

An initial exploratory reaction was conducted with a 12 mol % loading of BAC borane **4-1** and quinolinium $BAr^F_{24}$ **4-6** with imine **4-10a**. Full conversion to a mixture of amine and silylamine were observed in the $^1$H NMR spectrum. This initial reaction was conducted in TFT to closely resemble the hydrogenation conditions reported in section 4.3-4, however solvent variation may yield increased conversion or lower loadings as seen in

other published hydrosilylations.[47] A solvent screen was then conducted with imine **4-9a** and found that both TFT and MTBE gave comparable levels of conversion, while DCM gave the lowest conversion of approximately 66% in the same timeframe. MTBE was selected as the primary solvent for subsequent reactions because of its lower environmental impact. Following the initial solvent screen, imine **4-10a** was re-examined with a 5 mol% loading of the precatalyst components (**4-1** and **4-6)**. Full consumption of the imine starting material was observed once again. A substrate scope was then conducted with a 5 mol% loading of the precatalyst components detailed in scheme (**Scheme 4.12**).

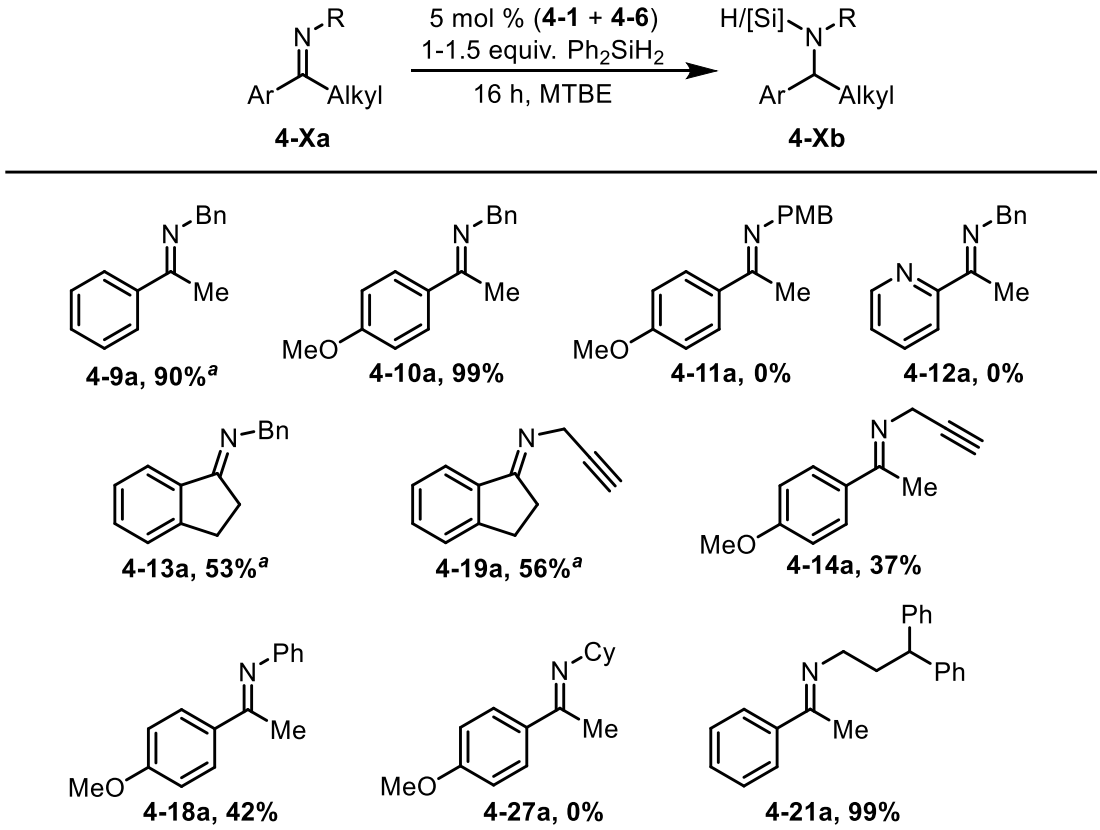


**Scheme 4.12** Hydrosilylation facilitated by *i*PrBAC borenium complex **4-3a** generated from combination of **4-1** and **4-6** *in situ*. Percent yields were calculated based on relative proportions of the starting material versus product in $^{1}$H NMR. [a]Reactions conducted with 10 mol % of **4-1** and **4-6**.

In this initial scope of substrates, a similar pattern of suitable substrates was observed when compared to the hydrogenation scope. Benzyl imines **4-9a** and **4-10a** were found to be reduced with high levels of conversion at either 5 or 10 mol % loading of the catalyst. Indanone derived imine **4-13a** was reduced in a lower conversion comparatively to the hydrogenation conditions. Surprisingly the indanone derived imine **4-19a**, the precursor to Rasagiline was reduced with a 56% conversion which was not possible under hydrogenation conditions. This indicates that the silylamine formed may inhibit some of the catalyst poisoning. Fendiline precursor **4-21a** was fully reduced in a 5 mol% loading under these conditions allowing for the preparation of this pharmaceutical under mild conditions. Imine **4-27a** was also investigated as a comparative substrate to the work by Fuchter but no conversion was observed indicating that steric bulk of the cyclohexyl group may be prohibiting reduction.[47] In contrast to the hydrogenation results, imine **4-11a** displayed no consumption of the imine under the standard conditions. When the solvent was substituted for TFT, reduction was once again observed albeit in an approximately 77% conversion. Imines **4-10a** and **4-14a** were also examined in TFT and were found to have decreased conversions. These results indicate that solvent plays an important role in the reduction of these substrates.

To confirm catalyst importance, a set of control reactions were conducted Quinolinium salts **4-5** and **4-6** and sodium $BAr^{F}_{24}$ were examined in a 12 mol% loading with imine **4-10a** and diphenylsilane. Reduction was not observed under these conditions, indicating that this activator is not autocatalytic and cannot facilitate the reduction of imines. The process was repeated then with *i*PrBAC complex **4-1** and quinolinium salt **4-5** in a 12 mol % loading. The imine was not reduced as indicated in the $^{1}$H NMR spectrum, which indicates a free borenium cation is needed for reduction to occur. While some

substrates were reduced with high conversion, similar substrates showed little to no conversion under the same conditions such as imine **4-12a**. To determine if imine purity may play a factor in the low conversion of some substrates, reduction of imine **4-10a** was repeated but with 20% fluorenone present to represent a ketone impurity. The reduction proceeded to full conversion with the ketone present. This result indicates that impurities may not be the cause for low conversion but rather the steric and electronics of the imine and silylamine may be affecting the reaction. In addition, the low conversion of some substrates may result from the stability of the silylamine in particular solvents.

In the hydrogenation studies, it was found that the $Bar^{Cl}_8$ anion performed similarly to the $BAr^{F}_{24}$ supported borenium complex. The largest difference between these anions was observed in the hydrogenation of *N*-Ph imines, a substrate that could not be reduced with a $BAr^{F}_{24}$ supported borenium complex. This led to the investigation of hydrosilylation of imines using a $Bar^{Cl}_8$ supported borenium complex. An initial reaction with imine **4-9a** was conducted with a 5 mol % loading of catalyst to compare against the $BAr^{F}_{24}$ supported reactions. Imine **4-9a** was fully reduced with these conditions providing evidence that the $Bar^{Cl}_8$ anion can support borenium complexes in hydrosilylation. The reduction was then repeated with both the $BAr^{F}_{24}$ (**4-6)** and $Bar^{Cl}_8$ (**4-15)** quinolinium complexes in DCM, to understand if the borenium stabilized with $Bar^{Cl}_8$ results in higher conversion to the amine. DCM was chosen as this solvent resulted in the lowest conversion when previously examined. Surprisingly the $Bar^{Cl}_8$ supported complex performed the reduction of **4-9a** with much higher conversion, at approximately 92% to the silyamine while the $BAr^{F}_{24}$ supported complex only provided approximately 63% conversion, similar to the previously test at 10 mol % loading.

A substrate scope was then conducted with the selected imines varying in steric and electronic properties. Gratifyingly all imines examined displayed high levels of reduction as shown in **Scheme 4.13**. Challenging substrates such as *N*-Ph imine **4-18a** which only displayed modest levels of reduction with the $BAr^{F}_{24}$ anion now went to near full conversion. Propargyl derived imine **4-14a** also displayed high levels of conversion with an increase from 37% to near 50% conversion making the reduction similar to the 10 mol % hydrogenation conditions. However, Ingleson reported that in some borane and borate synthesis, the impure materials were able to facilitate hydrosilylation reactions and reductive aminations.[149] In addition sodium $Bar^{Cl}_{8}$ was able to facilitate reductive amination reactions as well. To test if a side reaction was the result for the increased conversion, a control reaction using imine **4-10a** with only quinolinium $Bar^{Cl}_{8}$ **4-15** was conducted in a 5 mol % loading. The reaction conditions provided no indication of imine reduction which supports the importance of the borocation.

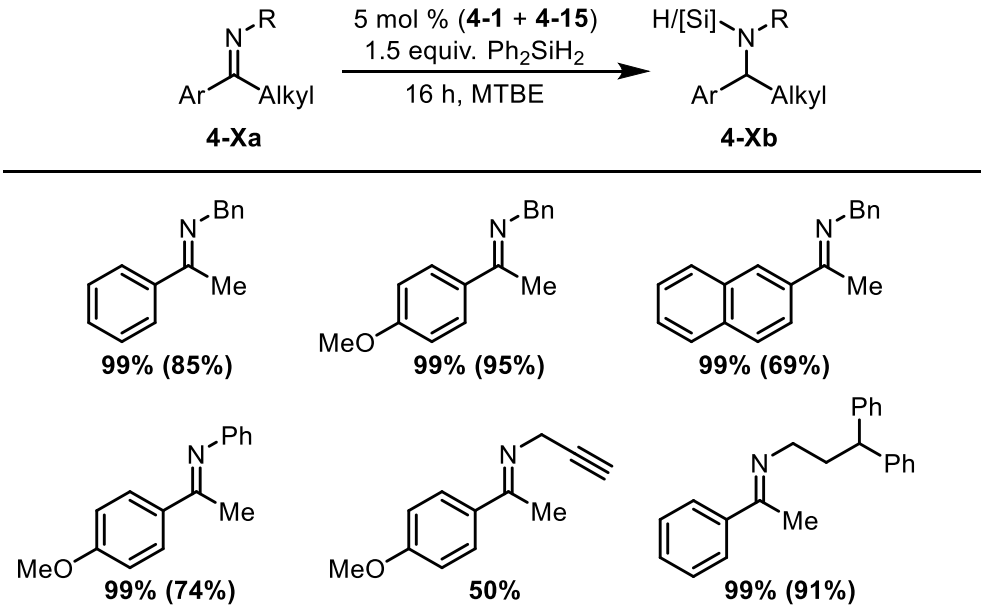


**Scheme 4.13** Hydrosilylation facilitated by *i*PrBAC borenium complex **4-3b** generated from combination of **4-1** and **4-15** *in situ*. Percent yields were calculated based on relative

proportions of the starting material versus product in $^{1}H$ NMR. Percentages in parentheses are isolated yields.

Current results show that the quinolinium complexes are viable hydride abstraction reagents for borenium generation in the application of hydrogenation and hydrosilylation. While this current catalytic system provides a more accessible method for these transformations, the loadings and substrate scope are not optimal. However, the results by Fuchter show that asymmetric hydrogenations and hydrosilylations are possible with borenium catalysis and this system could be modified to attempt asymmetric reductions of imines.[47]

### 4.6 Asymmetric Reduction of Imines

The development of alternative methods for the synthesis of chiral amines is of great importance with applications in pharmaceuticals.[144] Previously, boranes have been reported to achieved high enantioselectivity in the reduction of imines. Such examples include FLP complexes prepared by Repo et al.[30] and binaphthyl complexes reported by Du et al.[29] These chiral boranes can be used in hydrogenation, hydrosilylation, or transfer hydrogenation chemistry allowing for numerous reduction conditions for amine preparation from imines and enamines.[29] Early examples involving the collaboration by Stephan, Crudden and Melen in carbene-borenium catalysis displayed low enantioinduction with only *N*-Ph imines examined.[46] In 2019 Fuchter reported that asymmetric imine hydrogenation and hydrosilylation is possible with *N*-alkyl imine substrates.[47] This system utilized a chiral carbene to facilitate the asymmetric reduction. While asymmetric reductions were possible with this catalyst, the asymmetric hydrogenation of *N*-Bn remains a challenge.[44–47] Only BAC borane catalysts prepared

within this thesis can reduce *N*-Bn imines in high yield through hydrogenation reactions.[122,137]

To achieve enantioinduction in asymmetric hydrogenation within carbene borenium catalysis, 3 points of catalyst modification can be examined (**Figure 4.8**). The first point of modification is introducing chirality into the boron component of the catalyst. The boron centre is the location of hydride transfer and therefore in closest proximity to the imine, allowing for the highest chance of enantioinduction. The second type of modification is by altering the carbene to contain chiral components. While modification of some carbenes is facile, with a wide library of structures,[150] this can be challenging for other carbenes, often requiring multiple step syntheses. The third type of modification is altering the anion that supports the borenium ion. Introducing a chiral anion could allow for enatioinduction because the iminium ion, in close proximity to the anion, is the intermediate that is reduced in the catalytic cycle. Currently, only the introduction of a chiral carbene has allowed for enantioselectivity in hydrogenation and hydrosilylation reactions but this is only a singular example within the field.[47]

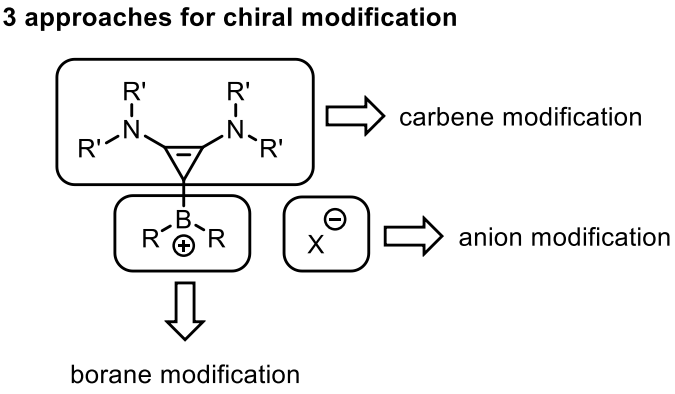


**Figure 4.2** Various methods of chiral modifications to carbene borane adducts.

### 4.6.1 Borane Modification

While previously borane modification has not yielded any enantioinduction, the singular publication by Stephan, Crudden and Melen only investigated 3 imines with only an in-depth look into *N*-Ph derived imines (**Scheme 4.14**).[46] The chiral borane investigated within this publication was $Ipc_2BH$, a borane derived from a natural chiral source α-pinene.[151] This borane is the predominantly used chiral borane within the literature because of its facile preparation and ease of isolation.[151] While this borane is widely used, the enantioinduction of this borane in reactions varies greatly. Another chiral borane within the literature with reported high levels of enantioinduction is Masamunae borane.[152] However, this borane is synthetically challenging and often avoided in catalysis for this reason. While previous results with carbene-$Ipc_2BH$ were unsuccessful within the literature[46] and seen in chapter 3,[137] the potential for the quinolinium activated complexes stabilized by either $BAr^F{}_{24}$ or $Bar^{Cl}{}_8$ anions may still yield results.

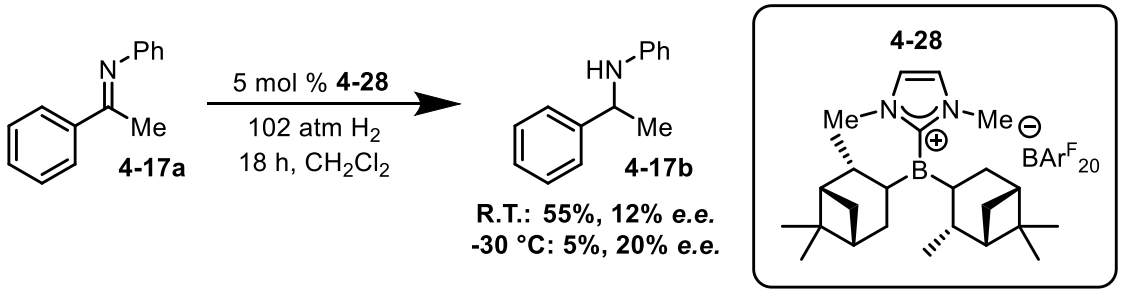


**Scheme 4.14** Hydrogenation facilitated by NHC-borenium complex **4-28**.

Previously in chapter 3, *i*PrBAC-$BIpc_2H$ **4-29** was prepared and examined in hydrogenation reactions and found little to no reactivity. However, the borenium was generated with trityl $BAr^F{}_{24}$ **4-2**. While $BAr^F{}_{24}$ ions have been effective in borenium stabilization, previously in section 4.4-5 it was found that $Bar^{Cl}{}_8$ ions can offer equal and or greater conversions in catalysis. *i*PrBAC-$BIpc_2H$ **4-29** was examined first in

hydrogenation reactions with both quinolinium $BAr^{F}_{24}$ **4-6** and $Bar^{Cl}_{8}$ **4-15** as the hydride abstraction reagent. In all tests, either no reduction or trace reduction was observed. While the initial hydrogenation reactions were unsuccessful, hydrosilylation reactions facilitated by borenium complexes have been found to reduce a wider scope of substrates. The increased scope of substrates can be expected from the silylamine produced which blocks potential poisoning of the catalyst by the protic N–H bond. *i*PrBAC-Ipc$_2$BH **4-29** was then examined in the hydrosilylation of a variety of imines. Varying levels of conversion were observed (**Scheme 4.15**), with the highest conversion observed from imine **4-17a** which contains an *N*-Ph. Enantioselectivity was measured using HLPC analysis and found that in all instances tested, the reaction was racemic. Investigation of chiral boranes in borenium catalysis was not further pursued.

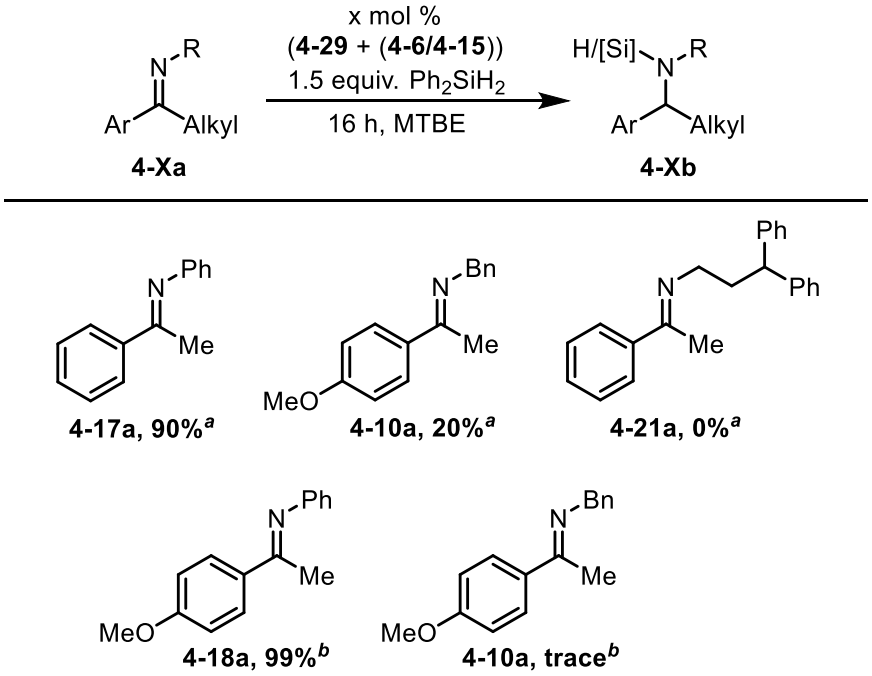


**Scheme 4.15** Hydrosilylation facilitated by a chiral *i*PrBAC borenium complex generated from combination of **4-29** and **4-6/15** *in situ*. Percent yields were calculated based on relative proportions of the starting material versus product in $^{1}$H NMR. [a]Reaction conducted with 10 mol % **4-29** and **4-6**. [b]Reaction conducted with 5 mol % **4-29** and **4-15**.

### 4.6.2 Carbene Modification

Attempts at asymmetric reduction through boron modification of the borenium catalyst were unsuccessful. This result was expected based on the previous reports within the literature. The next method investigated for enantioinduction within borenium catalysis involves carbene modification. While the preparation of chiral NHCs and triazole derivatives are well known,[150] the preparation of chiral BAC carbene complexes is challenging with only few examples of chiral and achiral carbene precursors in the literature.[64–66] The challenge with synthesizing a BAC carbene precursor arises in the amine substitution onto the cyclopropane ring.[52]

Tamm et al reported the synthesis of a chiral BAC carbene precursor[58] **4-30a** (**Figure 4.3**) which can be prepared as the free carbene **4-30b** or a bis-carbene silver complex. The carbene was examined in asymmetric benzoin condensations however the largest chiral induction resulted in 18% *e.e.*. Nevertheless, the free carbene was prepared and a carbene borane adduct was generated via the general synthetic methods. Formation of the carbene borane adduct **4-34** (**Figure 4.4**) was determined though $^{11}B$ NMR analysis, indicative by a signal at -12 ppm. The crude material was examined in the hydrogenation of imines, however no reactivity was observed.

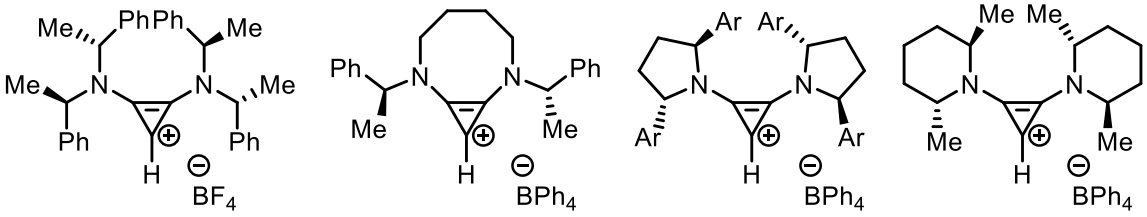


**Figure 4.3** Examples of chiral BAC carbene precursors.

Gravel et al have reported the synthesis of two types of chiral BAC carbene precursors. The first of which contained a tethered diamine **4-31** (**Figure 4.3**).[65] This carbene is reported to exhibit enantioinduction in Stetter reactions, with the highest selectivity being 36% *e.e.*. In an aza-benzion condensation, the catalyst was found to be racemic.[66] Following this work, a chiral BAC carbene was developed with chiral pyrrolidine **4-32** and piperidyl **4-33** groups (**Figure 4.3**).[64] These BAC carbenes were reported to exhibit high enantioinduction up to 92% *e.e.* in Stetter reactions (**Scheme 1.10**). The first carbene type involving a tethered backbone was investigated with some modifications to the structure to potentially enhance enantioselectivity. In the original BAC carbene precursor developed by Gravel, **4-31**, the amines contained an amine with a phenylethyl moiety. In the development of asymmetric diazaphospholene catalysis within the Speed group, it was found that substitution of the phenyl with naphthyl resulted in a larger enantioinduction.[78] The synthetic route to prepare the tethered amine reported by Gravel is lengthy and was therefore modified through a simpler synthesis.[65] While synthesis of the carbene precursor **4-35** was successful (**Figure 4.4**), attempts to produce the carbene borane adduct though the formation of the lithium adduct or via the free carbene generated *in situ* were not successful.

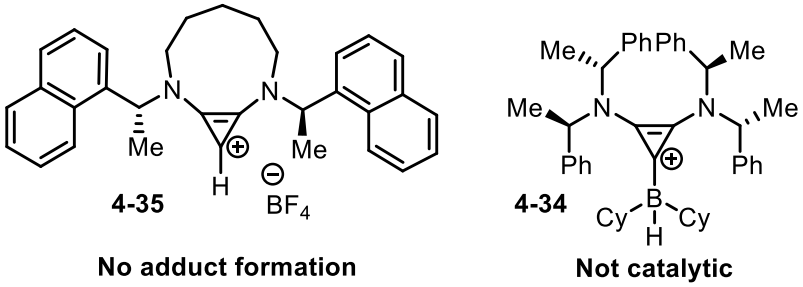


**Figure 4.4** Attempted formation of chiral BAC carbene complexes with boranes.

The chiral pool of amino acids has been applied in numerous asymmetric reactions. Proline and piperidine derivatives have displayed high enantioinduction in a variety of organic reactions.[64,153] In asymmetric boron mediated reactions, the CBS catalyst, derived from diphenylprolinol is widely used in the asymmetric reduction of carbonyls[12] and stoichiometric reduction of imines.[154] In addition, this scaffold is used in borocation catalysis and was found to facilitate asymmetric reactions.[39] Diphenylprolinol was treated with PCP **4-36a** in an attempt to form BAC carbene precursor **4-38**. The product isolated from the reaction was examined using $^{1}$H NMR analysis and found to contain a peak at 5.7 ppm. A crystal was grown from evaporation with dichloromethane and was analyzed using X-ray crystallography and found to have formed a carbodicarbene precursor **4-37** instead of the chloro BAC complex **4-38** (**Figure 4.5**). The formation of a carbodicarbene from PCP **4-36a** has been reported previously in the attempted formation of cyclopropenium ions.[155] Treatment of the carbodicarbene complex **4-37** with various bases and boranes did not yield a borane adduct.

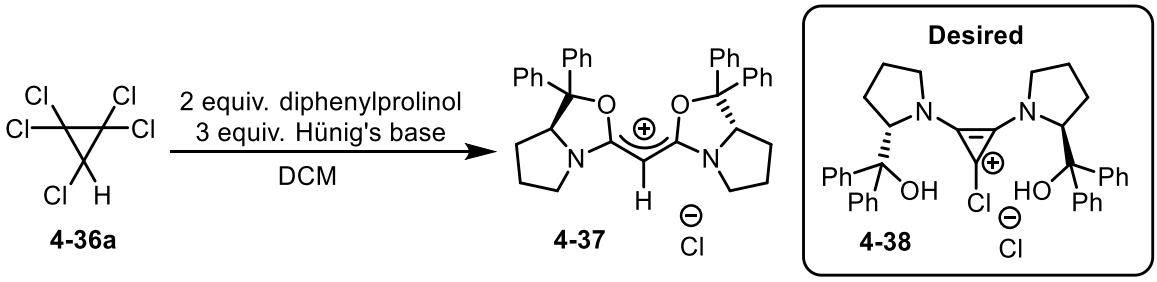


**Scheme 4.16** Attempted formation of BAC complex **4-38**.

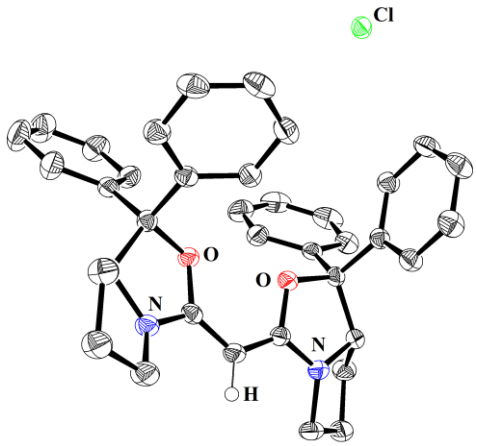


**Figure 4.5** The structure of **4-37**. Thermal ellipsoids have been drawn at the 50% probability level. Most hydrogen atoms have been removed for clarity. This structure has not been fully refined.

To prevent the formation of carbodicarbene **4-37**, the methylation of diphenylprolinol was examined. Formation of the *N*-boc protected amine was successful, producing compound **4-39** (**Scheme 4.17**). Treatment of **4-39** with sodium hydride and methyl iodide resulted in the undesired formation of compound **4-40** (**Scheme 4.17**). While the formation of compound **4-40** was initially undesired, the product can be modified to produce compound **4-41** through palladium reduction.[156] Overall, the new amine produced still resulted in the desired removal of the hydroxyl moiety which caused the formation of carbodicarbene **4-37**, albeit by reduction, rather than ether formation. Treatment of amine **4-41** with TCP **4-36b** at room temperature resulted in the formation of a tris amino cyclopropenium product. The previous synthesis of chiral BAC complexes required cooling the during addition of the amine to -78 ˚C. Treatment of TCP **4-36b** with amine **4-41** at -78 ˚C resulted in the formation of a new solid upon isolation. Analysis of the product in $CDCl_3$ indicated the presence of 3 compounds. However, analysis in $CD_3CN$ indicated that the apparent 3 compounds were rotamers of a singular compound **4-42**, which was

confirmed using mass spectrometry. This compound was not investigated further to prioritize other methods.

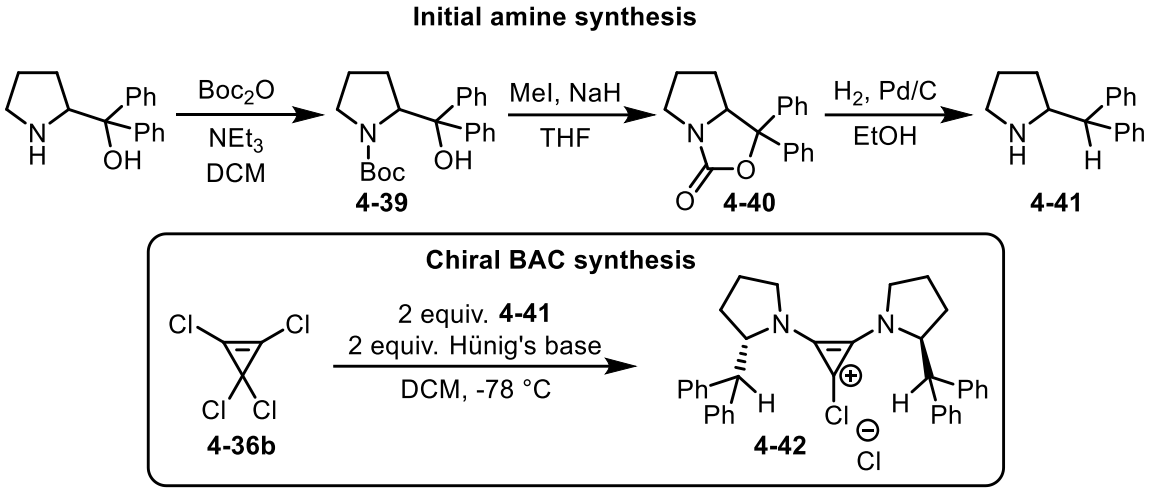


**Scheme 4.17** Attempted formation of BAC complex **4-42**.

### 4.6.3 Anion Modification

Chiral anion mediated catalysis is a relatively underdeveloped field of asymmetric catalysis because most efforts have focused on the development of chiral ligands.[157] The majority of chiral anions within catalysis are derived from the conjugate base of a Brønsted acid such as chiral phosphates (**4-43, Figure 4.6**).[158] The synthesis of a chiral borate **4-45** and non-phosphoric acid derived phosphates **4-44** is often lengthy or challenging.[159] More recently, there have been new developments in the application or synthesis of chiral borates as either spiroborates or a chiral binaphthylborate.[160–168]

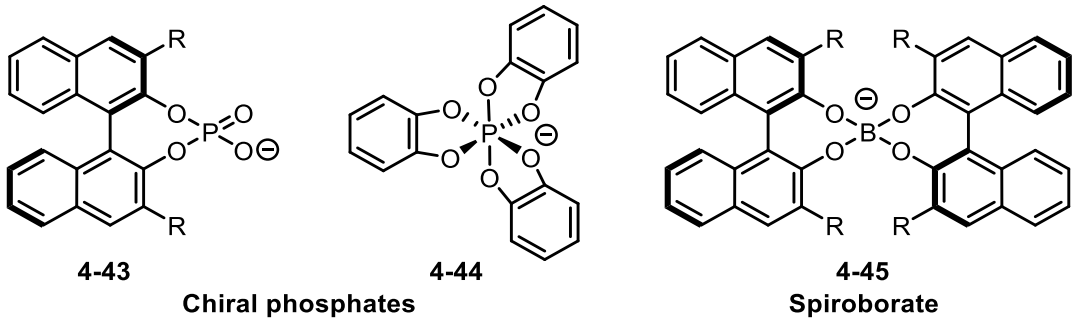


**Figure 4.6** Examples of chiral anions.

Spiroborates are a class of chiral borate which contain axial chirality though two bidentate interactions with the boron centre. A common spiroborate anion is derived from BINOL which has been used in transition metal catalysis.[163,164] An early example of spiroborate mediated asymmetric catalysis is a copper aziridination reported by Arndtsen which only an *e.e.* of up to 28% was observed.[163] However, an example of asymmetric hydrogenation by Leitner and Klankermayer involving a rhodium complex with a spiroborate anion was able to achieve an *e.e.* up to 57% (**Scheme 4.18**).[164] More recently an example by Wulff and Vetticatt reported that spiroborates with a larger steric bulk and greater substitution gave higher enantioselectivity with an enantiomeric excess up to 78%.[168]

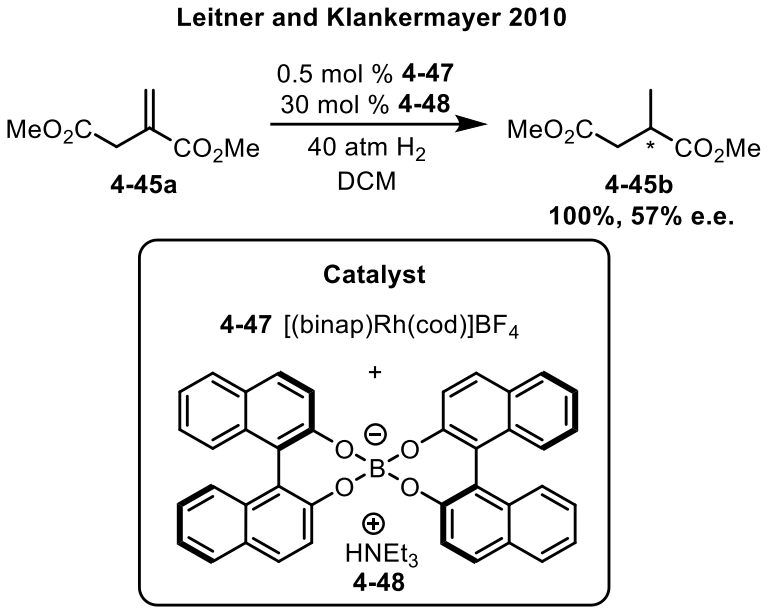


**Scheme 4.18** Asymmetric hydrogenation facilitated by a rhodium complex with a chiral spiro borate.

The recent success of spiroborates in asymmetric catalysis including the support of an iminium in chiral reactions led to the investigation of this chemistry in borenium catalysis. The quinolinium ion method developed in this chapter for borenium generation may allow for facile preparation of a spiroborate salt capable of generating and the subsequently stabilizing the borenium ion. The spiroborate was prepared as the potassium salt **4-49** from literature known triethylammonium salt[164] **4-48** via deprotonation using KHMDS. The potassium salt was then combined with quinolinium bromide to form the quinolinium spiroborate **4-50** (**Scheme 4.19**). An X-ray crystal structure was obtained of **4-50** through crystallization with acetonitrile and dichloromethane, thereby confirming the assignment (**Figure 4.7**).

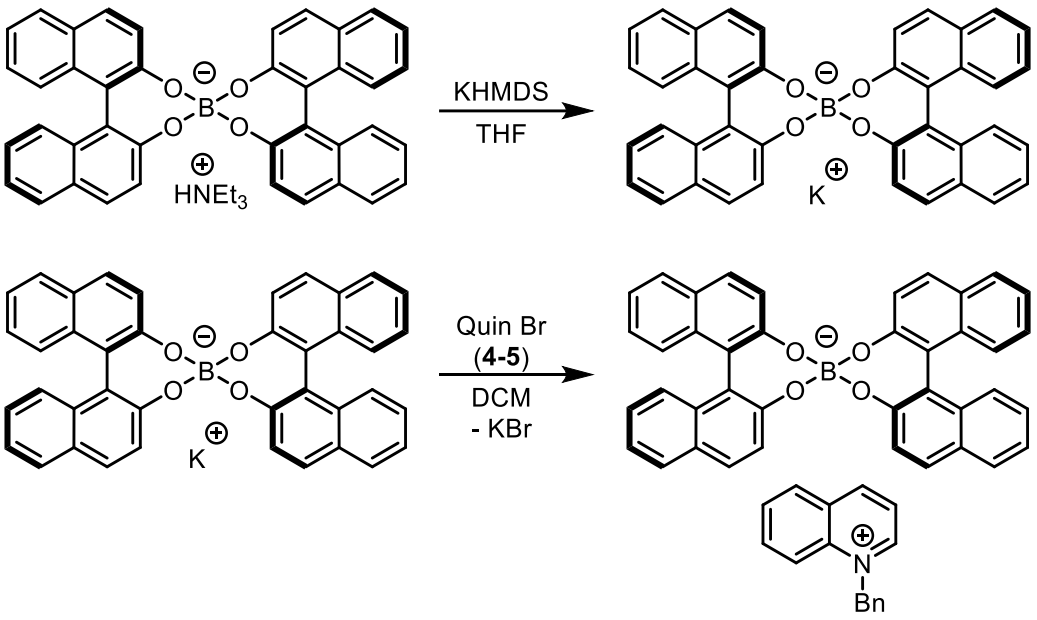


**Scheme 4.19** Synthesis of *N*-Bn Quinolinium B(R-BINOL)$_2$ **4-50**.

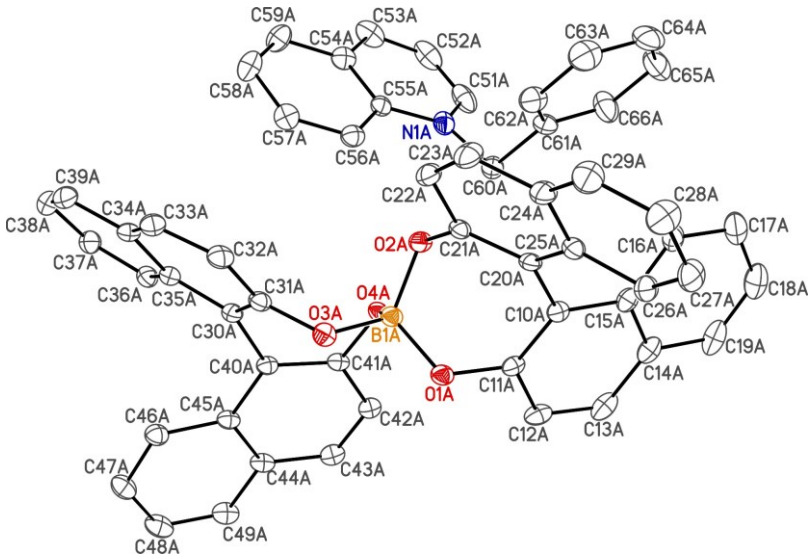


**Figure 4.7** The structure of **4-50**. Thermal ellipsoids have been drawn at the 50% probability level. Hydrogen atoms have been removed for clarity.

Newly formed quinolinium salt **4-50** was then examined in catalysis with BAC complex **4-1**. Hydrosilylation of imine **4-10a** was tested with a 10 mol % loading of the catalyst components (**4-1** and **4-50)**. No reduction was observed under these reaction conditions. Hydrogenation was then examined with a selection of substrates (**Scheme 4.20**). Smaller *N*-Bn imines **4-10a** and **4-11a** were not able to be reduced by this complex,

with no conversion observed by $^{1}$H NMR analysis. However, larger substrates such as *N*-Bn imine **4-16a** and *N*-Ph imines **4-17a**and **4-18a** were reduced, albeit in lower conversion than with other anions. Crude HPLC analysis of the amine product from the reduction of imine **4-16a** was found to have an enantiomeric excess of 22%. While the enantioinduction of this reaction was low, this result provides evidence that chiral anions in borenium catalysis may yield higher selectivity with more research.

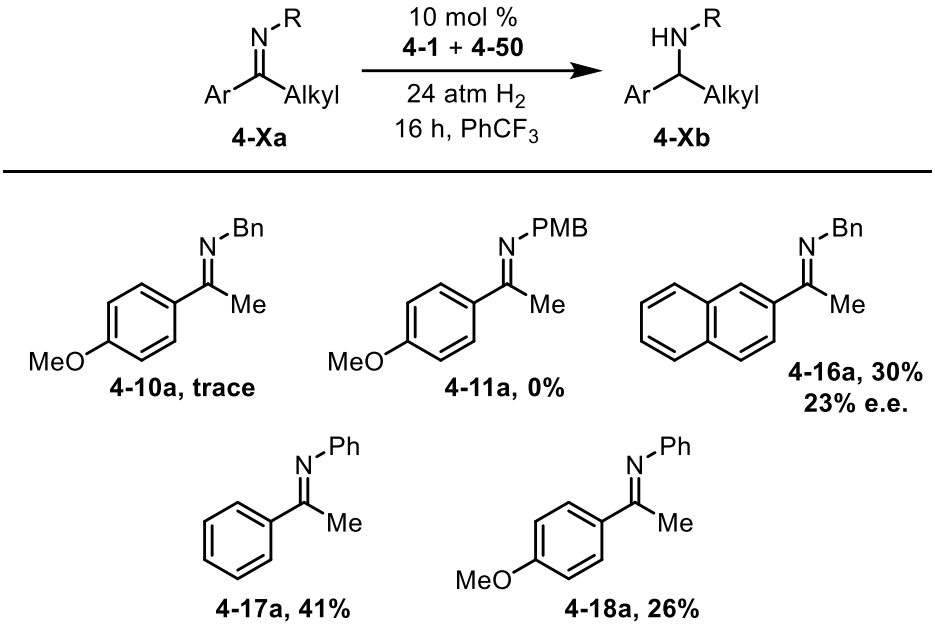


**Scheme 4.20** Hydrogenation facilitated by *i*PrBAC borenium complex **4-3c** generated from combination of **4-1** and **4-50** *in situ*.

The lower conversion from these reactions may be a result of greater separation between the larger anion and the boron centre, which may destabilize the borenium ion. Another reason for this observed reactivity may be a result of spiroborate decomposition by the amine product or from a reaction with the borenium centre. The amine produced in the reaction may cleave the spiroborate B–O bond. Alternatively, the highly Lewis acidic borenium ion can potentially open the spiroborate ring. This can be seen as the opposite effect to the $Bar^{Cl}{}_{8}$ anion which is slightly smaller and gives higher conversion than the

$BAr^{F}_{24}$ anion. Overall, the stability of the spiroborate derivatives will have to be assessed to improve the conversion of this catalytic system or other chiral anions will have be explored in borenium catalysis.

## 4.7 Conclusion

The results thus far have indicated that quinolinium complexes provide a suitable reagent for hydride abstraction, which is air and moisture stable. The synthesis of these complexes is facile with the first step requiring no solvent. Current results show that these complexes are capable generating borenium complexes without the by-product interfering in the hydrogenation reactions. These quinolinium salts allowed for the *in situ* generation of a borenium complex in hydrosilylation reactions allowing for overall lower loadings of the catalyst at the cost of using a reductant such as diphenysilane. The application of $Bar^{Cl}_{8}$ as the anion has allowed for higher levels of conversion compared to $BAr^{F}_{24}$ stabilized borenium complexes, potentially resulting from increased catalyst stability.

## 4.8 Experimental

### 4.8.1 General Considerations

Boron compounds, carbene complexes, imines, quinolinium salts, and solvents were dispensed in a 2001 issue IT Glovebox ($H_2O$ levels are approximately 30 ppm on average). Carbene complexes and precursors were prepared in oven dried 4 dram scintillation vials equipped with magnetic stir bars and green Qorpak® PTFE lined caps unless otherwise stated. Hydrogenations were carried out in 1 dram scintillation vials equipped with a magnetic stir bar and septa caps pierced with a needle were screwed on. Hydrosilyation reactions were carried out in oven dried 1 dram scintillation vials equipped with magnetic stir bars and green Qorpak® PTFE lined caps. All reactions were conducted at ambient temperature unless otherwise stated. $^{1}H$, $^{11}B$, $^{19}F$, $^{31}P$ and $^{13}C$ NMR data were collected at

300K on either a Bruker AV-300 or AV-500 spectrometer. $^{1}H$ NMR spectra are referenced to residual non-deuterated NMR solvent from the sample ($C_6H_6$ = 7.16 ppm, $CHCl_3$ = 7.26 ppm, $(CH_3)_2SO$ = 2.50 ppm). $^{13}C$ NMR spectra are referenced to NMR solvent from the sample ($C_6D_6$ = 128.06 ppm, $CDCl_3$ = 77.16 ppm, $(CD_3)_2SO$ = 39.52 ppm). HPLC data were acquired on a Varian Prostar instrument, equipped with detection at 254 nm, using a CHIRALPAK® AD-H. A 99:1 hexanes/isopropanol solvent mixture was used as the eluent, with a flow rate of 0.5 mL/min. Melting points were acquired using an Electrothermal® apparatus and are uncorrected. Mass spectrometric data were acquired by Mr. Xiao Feng (Mass Spectrometry Laboratory, Dalhousie University).

### 4.8.2 Solvents

**Pentane** for reactions were deoxygenated and dried by sparging with dinitrogen gas, followed by passage through a double-column solvent purification system purchased from mBraun Inc. The solvents were stored over dry 3 Å molecular sieves in the glovebox.

**Diethyl ether** for purification (ACS grade) was purchased from Fisher and used as received. Diethyl ether for reactions was further distilled from a purple solution of benzophenone/sodium ketyl and stored over dry 3 Å molecular sieves in the glovebox.

**Methyl *tert*-butyl ether** for reactions was purchased from Aldrich and distilled from a purple solution of benzophenone/sodium ketyl and stored over dry 3 Å molecular sieves in the glovebox.

**Trifluorotoluene** (Anhydrous >99%) was purchased in a Sure/Seal™ container from Aldrich and cannula transferred onto dry 3 Å molecular sieves for storage in the glovebox, but otherwise used as received.

**Acetonitrile** for reactions was purchased from Fisher used as received.

**Hexanes** for purification was purchased from Fisher and used as received.

**Dichloromethane** (ACS grade) was purchased from Fisher and used as received.

**Deuterochloroform** (Cambridge Isotopes) was stored over dry 3 Å molecular sieves, but otherwise used as received.

**Dimethylsulfoxide-$d_6$** was purchased in ampoules from Aldrich and used as received.

### 4.8.3 Reagents

All ketones and amines employed in imine preparation were purchased from Aldrich and used as received after purity was verified by $^1$H NMR. Imines were prepared by a 1:1 combination of the appropriate ketone/aldehyde and amine in dichloromethane, in the presence of 1 equivalent of titanium ethoxide for 24 h. The reactions were quenched by addition of aqueous KOH (15 %), filtered onto $Na_2SO_4$, re-filtered and concentrated. Purification of solid imines was accomplished by taking up the obtained solids in warm pentane, and cooling the resulting clear pentane solutions of the imine to -15 °C. The resulting crystals were collected in air by suction filtration and were dried for 12 h in a vacuum desiccator at approximately 30 torr over $P_2O_5$ before being brought into the glovebox. Liquid imines were dried by azeotropic distillation with benzene before use. Yields of imines were typically > 60% by this method.

**Quinoline** was purchased from Sigma Aldrich and used as received.

**Benzyl bromide** was purchased from Sigma Aldrich and used as received.

**Diphenylsilane** was purchased from Oakwood chemicals and used as received.

**(S)-Diphenyprolinol** was purchased from Oakwood chemicals and used as received.

**(S)-(-)-2-(Diphenylmethyl)pyyrolidine** was prepared according to literature known methods.[156]

**Pentachlorocyclopropane 4-36a** was prepared according to literature known methods.[125]

**Tetrachlorocyclopropene 4-36b** was prepared according to literature known methods.[125]

**(Me,Ph)BAC 4-30b** was prepared according to literature known methods.[58]

**[HNEt$_3$][B(R-BINOL)$_2$] 4-48** was prepared according to literature known methods.[164]

**Hünig's base** was purchased from Sigma Aldrich and used as received.

**NaBAr$^F_{24}$** was prepared according to literature known methods.[113]

**NaBAr$^{Cl}_8$** was prepared according to literature known methods.[141]

**NaBF$_4$** was purchased from Sigma Aldrich and used as received.

**Glutaryl chloride** was purchased from Sigma Aldrich and used as received.

**(R)-(+)-1-(2-Naphthyl)ethylamine** was purchased from Oakwood chemicals and used as received.

**KHMDS** was purchased from Sigma Aldrich and used as received.

**Triethylamine** was purchased from Sigma Aldrich and used as received.

**LiAlH$_4$** was purchased from Sigma Aldrich and used as received.

**Triphenylphosphine** was purchased from Sigma Aldrich and used as received.

### 4.8.4 Synthetic Procedures

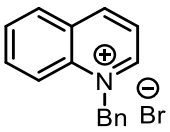


***N*-Bn Quinolinium bromide (4-5).** Quinoline (1 mL, 8.46 mmol) is added to an Erlenmeyer flask (50 mL) equipped with a magnetic stir bar, followed by benzyl bromide (1 mL, 8.46 mmol). The mixture was left to stir in open air overnight. The solid residue was then broken into a fine powder and rinsed with dichloromethane (3 x 5mL) to afford the title compound **4-5** (1.8g, 5.99 mmol, 71% yield).

**$^1$H** (300 MHz, $CDCl_3$): δ 9.83, 9.40 (d, 1H), 8.53 (d, 2H), 8.31 (m, 1H), 8.21 (m, 1H), 8.02 (m, 1H), 7.37 (m, 5H), 6.42 (s, 1H).

**$^{13}$C** {$^{1}$H} (125.8 MHz, $CDCl_3$): δ 150.4, 148.1, 137.5, 135.7, 133.8, 130.8, 129.9, 129.8, 128.7, 122.4, 119.2, 59.8.

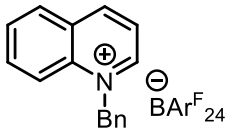


***N*-Bn Quinolinium BAr$^{F}_{24}$ (4-6).** *N*-Bn Quinolinium bromide **4-5** (339 mg, 1.13 mmol) and NaBAr$^{F}_{24}$ (1 g, 1.13 mmol) were placed in a 50 mL flask under nitrogen. Ether (9 mL) was added and the slurry was stirred overnight. Ether was removed *in vacuo* and the residue was taken up in 10mL dichloromethane and filtered over celite. The celite was then washed with dichloromethane (2 x 5mL) and all dichloromethane was removed *in vacuo* to afford the title compound **4-6** (1.02g, 0.941 mmol, 83%).

**MP:** 132-134 °C

**$^{1}$H** (500 MHz, $CDCl_3$): δ 8.74 (d, $J$ = 8.2 Hz, 1H), 8.58 (dd, $J$ = 5.9 Hz, 1H), 8.18 (ap doublet, 1H) 8.10 (m, 2H with overlap), 7.90 (ap t, 1H), 7.69 (m, 9H with overlap), 7.44 (m, 7H with overlap), 7.11 (ap d, 2H), 5.88 (s, 2H).

**$^{13}$C** {$^{1}$H} (125.8 MHz, $CDCl_3$): δ 161.8 (q, $J_{C,B}$ = 49 Hz), 148.7, 146.3, 138.5, 137.9, 134.9, 131.6, 131.3, 131.2, 130.6, 130.4, 129.3, 129.1 (q, $J_{C,F}$ = 30 Hz), 127.9 (two peaks), 125.7, 123.5, 121.3, 117.9, 117.7, 61.8.

**$^{11}$B** (160.4 MHz, $CDCl_3$): δ -6.6 (s).

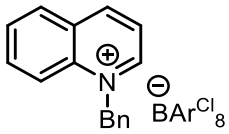


***N*-Bn Quinolinium BAr$^{Cl}_{8}$ (4-15).** *N*-Bn Quinolinium bromide **4-5** (243 mg, 0.809 mmol) and NaBAr$^{Cl}_{8}$ (500 mg, 0.809 mmol) were placed in a 4 dram vial equipped with a magnetic stir bar. Dichloromethane (7 mL) was added and the solution was stirred overnight. The

dichloromethane solution was filtered over celite and the celite was then washed with dichloromethane (2 x 5mL). The filtrate was concentrated *in vacuo* to afford the title compound **4-15** (581g, 0.712 mmol, 95%).

**$^{1}$H** (500 MHz, $CDCl_3$): δ 8.60 (d, $J$ = 8.4 Hz, 1H), 8.14 (ap d, 1H), 8.07 (d, 1H), 8.02 (m, 1H), 7.95 (ap d, 1H), 7.90 (m, 1H), 7.42 (m, 5H), 7.06 (m, 8H), 7.02 (m, 2H), 6.75 (m, 4H), 5.55 (s, 2H).

**$^{13}$C** {$^{1}$H} (125.8 MHz, $CDCl_3$): δ 164.9 (q, $J_{C,B}$ = 49 Hz), 148.1, 146.9, 138.2, 137.2, 133.2 (overlapping peaks), 131.2, 130.6, 130.3, 130.2, 127.8, 123.3, 121.4, 118.1, 61.5.

**$^{11}$B** (160.4 MHz, $CDCl_3$): δ -6.9 (s).

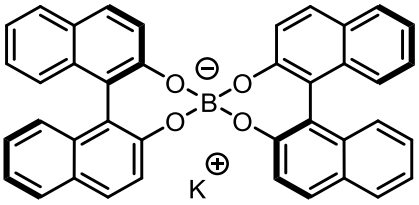


**KB(R-BINOL)$_2$ (4-49).** This product was generated from deprotonation of **[**$HNEt_3$**][**B(R-BINOL)$_2$] **4-48** with KHMDS in THF. Volatiles were removed *in vacuo* to afford the potassium salt **4-49**, which was used as-is.

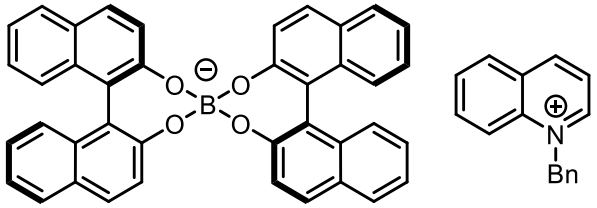


***N*-Bn Quinolinium B(R-BINOL)$_2$ (4-50).** *N*-Bn Quinolinium bromide **4-6** (432 mg, 1.44 mmol) and KB(R-BINOL)$_2$ (890 mg, 1.44 mmol) were placed in a 4 dram vial equipped with a magnetic stir bar. Dichloromethane (7 mL) was added and the solution was stirred overnight. The dichloromethane solution was filtered over celite and the celite was then

washed with dichloromethane (2 x 5mL). The filtrate was concentrated *in vacuo* to afford the title compound **4-50** (869 mg, 1.08 mmol, 76%).

**$^{1}$H** (500 MHz, $(CD_3)_2SO$): δ 9.56 (ap d, 1H), 9.17 (ap d, 1H), 8.35 (ap t, 2H), 8.09 (m, 2H), 7.97 (m, 4H), 7.91 (m, 5H), 7.37 (m, 4H), 7.31-7.24 (m, 9H), 7.12 (m, 8H), 6.22 (s, 2H).

**$^{13}$C** {$^{1}$H} (125.8 MHz, $(CD_3)_2SO$): δ 156, 150, 147.8, 137.3, 135.5, 133.7, 132.7, 130.7, 129.7, 129.6, 128.9, 128.8, 128.7, 128.2, 127.9, 127.2, 125.7, 127.7, 124.5, 122.3, 122.1, 121.8, 118.9, 59.7.

**$^{11}$B** (160.4 MHz, $(CD_3)_2SO$): δ 9.13 (s).

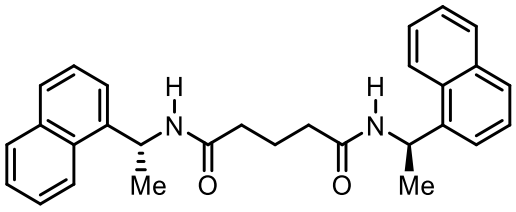


***N,N*-bis[(1-(R)-napthylethyl]pentanediamide.** (R)-(+)-1-(2-Naphthyl)ethylamine (5.03 mL, 31.3 mmol, 2 equiv.) was dissolved in DCM (25 mL) and cooled to -15 °C. Triethylamine (4.80 mL, 34.5 mmol, 2.2 equiv.) was then added followed by dropwise addition of glutaryl chloride (2 mL, 15 mmol, 1 equiv.) and the solution was maintained at -15 °C for 40 min. the solution was then warmed to room temperature and stirred for an additional 20 min. Volatiles were removed *in vacuo* and the resulting solid was washed with $H_2O$ (3 x 50 mL), acetone (30 mL) and hexane (30 mL). The resulting solid was placed in a desiccator for 2 days to afford the desired product **4-20** (6 g, 14.61 mmol, 93% yield).

**$^{1}$H** (500 MHz, DMSO-$d_6$): δ 8.37 (d, 2H), 8.09 (d, 2H), 7.93 (d, 2H), 7.81 (d, 2H), 7.51 (m, 8H), 5.70 (m, 2H), 2.13 (t, $J$ = 8 Hz, 4H), 1.73 (m, 2H), 1.47 (d, $J$ = 7 Hz, 6H).

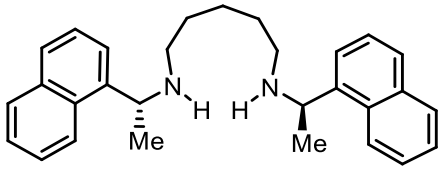


***N,N*-bis[(1-(R)-napthylethyl]pentanediamine.** In a dry 2 neck 250 mL flask equipped with a condenser placed under a $N_2$ atmosphere, THF (40 mL) was added followed by *N,N*-bis[(1-(R)-napthylethyl]pentanediamide (4g, 9.12 mmol). $LiAlH_4$ (1.38g, 36.48 mmol) was then added in one portion and the resulting slurry was heated to reflux for 2 days. Once cooled, the reaction was quenched with NaOH (35 mL, 1M) and then DCM (50 mL) was added and left to stir for 15 min. The solution was poured into a separatory funnel and the process repeated. The organic layer was then separated and washed with a sat'd sodium bicarbonate solution (30 mL). The organic layer was then dried with anh. Sodium sulfate and the solvents were removed *in vacuo* to afford the title compound (3.4 g, 8.28 mmol, 91% yield).

**$^1$H** (500 MHz, $CDCl_3$): δ 8.21 (d, 2H), 7.89 (d, 2H), 7.76 (d, 2H), 7.66 (d, 2H), 7.50 (m, 7H), 4.63 (q, $J$ = 7 Hz, 2H), 2.57 (m, 4H), 1.5 (d, $J$ = 6.7 Hz, overlapping m, 10H), 1.35 (m, 2H).

**$^{13}$C** {$^1$H} (125.8 MHz, $CDCl_3$): δ 141.5, 134.1, 131.4, 129.1, 127.2, 125.8, 125.3, 123, 122.7, 48.1, 30.5, 25.3, 23.7.

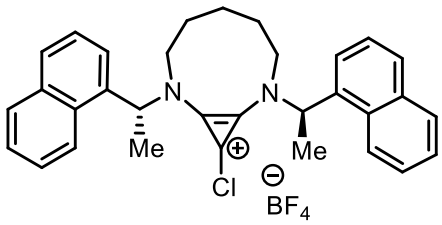


**[(*N,N*-bis[(1-(R)-napthylethyl]pentanediamine)cycloprop-2-en-1-ylidene]chloro tetrafluoroborate.** In a 50 mL round bottom flask tetrachlorocyclopropene **4-36b** (0.15

mL, 1.27 mmol) was added and diluted with DCM (25 mL). The solution was cooled to -78 °C and *N,N*-bis[(1-(R)-napthylethyl]pentanediamine was added as a solution in DCM (5 mL) dropwise. Hünig's base was then added and the reaction was warmed to room temperature over 2 h and then stirred overnight. The organic solution was washed with $H_2O$ (30 mL), followed by sat'd $NaBF_4$. The organic layer was then dried with anhydrous sodium sulfate and volatiles were removed *in vacuo*. The crude solid was taken up in DCM (1 mL) and precipitated with $Et_2O$ (30 mL). The product was then filtered to obtain the title compound (624 mg, 1.10 mmol, 86% yield).

**$^1$H** (500 MHz, $CDCl_3$): δ 7.94 (d, 2H), 7.88 (m, 4H), 7.65 (d, 2H), 7.55 (m, 2H), 5.57 (q, 2H), 3.75 (m, 4H), 1.97 (d, 6H), 1.5 (d, 2H), 1.3 (d, 2H), 1.2 (d, 2H)

**$^{11}$B** (160.5 MHz, $CDCl_3$): δ -0.89 (br s).

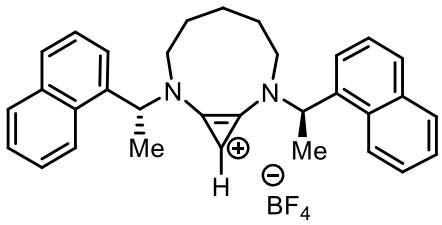


**[(N,N-bis[(1-(R)-napthylethyl]pentanediamine)cycloprop-2-en-1-ylidene] tetrafluoroborate (4-35).** [(*N,N*-bis[(1-(R)-napthylethyl]pentanediamine)cycloprop-2-en-1-ylidene]chloro tetrafluoroborate (460 mg, 0.811 mmol) was dissolved in DCM (7 mL) and cooled to -15 °C. Triphenylphosphine (213 mg, 0.811 mmol, 1 equiv.) was added and the reaction was left to stir overnight. The organic solution was washed with $H_2O$ (20 mL) and sat'd $NaBF_4$ (10 mL) and then dried with anh. sodium sulfate. Volatiles were removed *in vacuo* to afford a crude solid. The solid was then dissolved in DCM (1 mL) and precipitated with $Et_2O$ (20 mL) which was then filtered to afford the title compound **4-35** (338 mg, 0.634 mmol, 78% yield)

**$^1$H** (500 MHz, $CDCl_3$): δ 7.94 (d, 2H), 7.92 (m, 2H), 7.81 (d, 2H), 7.66 (d, 2H), 7.55 (m, 7H), 6.2 (s, 1H), 5.61 (q, *J* = 7 Hz, 2H), 3.61 (m, 4H), 1.95 (d, 6H), 1.55 (d, *J* = 7 Hz, 2H), 1.26 (m, 2H), 1.13 (m, 2H)

**$^{11}$B** (160.5 MHz, $CDCl_3$): δ -0.89 (br s)

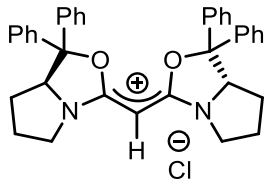


**BOXCDC** (**4-37**)**.** Pentachlorocyclopropane **4-36a** (0.5 mL, 3.892 mmol) was dissolved in DCM (15 mL) in a 100 mL round bottom flask. The solution was cooled to -15 °C and then diphenyl prolinol (1.97 g, 7.78 mmol, 2 equiv.) was added followed by Hünig's base (3.39 mL, 19.455 mmol, 5 equiv.). The reaction was left to stir overnight, and the resulting mixture was diluted with DCM (15 mL) and washed with $H_2O$ (2 x 30 mL). The organic layer was then dried with anh. Sodium sulfate and the DCM was removed *in vacuo*. The crude material was dissolved in minimal amount of DCM followed by precipitation with $Et_2O$ to afford an off-white solid **4-37** (2.2g, $Et_2O$ could not be fully removed from the solid material).

**$^1$H** (500 MHz, $CDCl_3$): δ 7.49 (m, 5H), 7.41 (m, 5H), 7.28 (m, 5H), 7.22 (m, 5H), 5.05 (dd, *J* = 5.8, 10 Hz, 2H), 5.04 (s, 1H), 4.02 (m, 2H), 3.84 (m, 2H), 2.48 (m, 2H), 2.16 (m, 2H), 1.97 (qd, 2H), 1.16 (m, 2H)

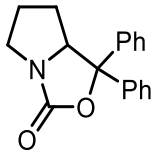


**Diphenylprolinol carbamate** (**4-40**)**.** *N*-boc Diphenylprolinol **4-39** (2g, 5.65 mmol) was weighed into a 25 mL round bottom flask and dissolved THF (12 mL). Sodium hydride

(203 mg, 8.48 mmol, 1.5 equiv.) was then added along with a stir bar and the reaction was stirred for 3h. Carefully, a saturated ammonium chloride solution (10 mL) was added and then the mixture was extracted with DCM (30 mL) and ammonium chloride solution, (30mL). The aqueous solution was then washed with an additional amount of DCM (20 mL). The combined organic solutions were then washed with brine (20 mL). The organic solution was then dried with sodium sulfate and then subsequently filtered and volatiles removed *in vacuo* to afford a solid (1.48g) containing the title compound and impurities. *Tert*-butanol and other impurities wer present but the title compound was identified in the NMR spectrum in accordance with literature values[169] and used without futher purification. **$^1$H** (300 MHz, $CDCl_3$): δ 7.54 (m, 2H), 7.36 (m, 8H), 7.28 (m, 5H), 4.56 (m, 1H), 3.74 (m, 1H), 3.26 (m, 1H), 1.93 (m, 1H), 1.73 (m, 2H), 1.14 (m, 2H).

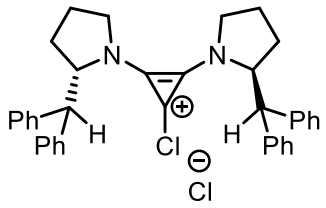


**Attempted preparation of BAC complex (4-42).** Tetrachlorocyclopropene **4-36b** (0.05 mL, 0.407 mmol) was weighed into a 25 mL Schlenk tube equipped with a magnetic stir bar. DCM (6 mL) was added and the solution was cooled to -78 °C. A solution of amine **4-41** (193 mg, 0.815 mmol, 2 equiv.) in DCM (2 mL) was slowly added to the reaction followed by Hünig's base (0.15 mL, 0.856 mmol, 2.1 equiv.) which was added in one portion. Reaction temperature was maintained at -78 °C for 2 h and then allowed to gradually warm to room temperature. The crude product was obtained via a similar workup to previously reported methods. The product contained multiple impurities but was identified in the mixture through mass spectrometry analysis.

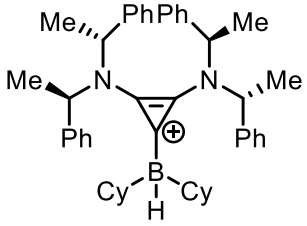


**Formation of Me,PhBAC-BCy$_2$H (4-34).** (Me,Ph)BAC **4-30b** (21 mg, 0.043 mmol) was weighed into a 1 dram vial along with dicyclohexylborane (7.6 mg, 0.043 mmol). Diethyl ether (1 mL) was then added to the solids along with a mechanical stir bar and the solution was mixed. Volatiles were then removed *in vacuo* and the solution was analyzed using NMR analysis in benzene-$d_6$. The product was used in reactions without further purification.

**$^{11}$B** (160.5 MHz, $C_6D_6$): δ -12.

### 4.8.5 Borenium Ion Generation

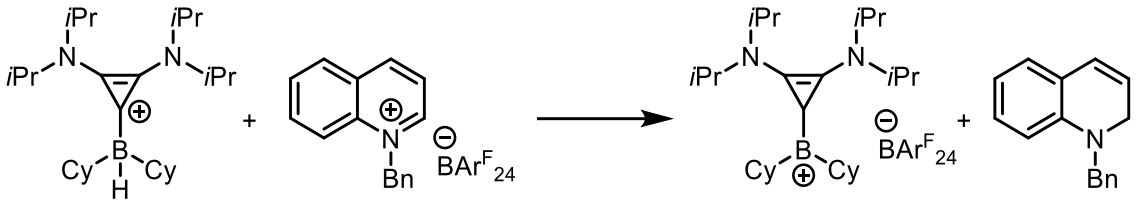


**4-1** air/moisture stable

**4-6** air/moisture stable

**4-3** moisture sensitive

**4-7**

**Formation of Borenium Cation [*i*PrBAC-BCy$_2$][BAr$^F_{24}$] 4-3a *in situ* from *N*-Bn Quinolinium BAr$^F_{24}$ (4-6).** In a glovebox, *i*PrBAC-BCy$_2$H **4-1** (15 mg 0.037 mmol) and *N*-Bn quinolinium BAr$^F_{24}$ **4-6** (41 mg, 0.037 mmol) were placed in an oven dried 1 dram vial. The solids were dissolved in $CDCl_3$ (approx. 1 mL) and the solution was transferred to a standard NMR tube and NMR spectra were acquired after 15 min.

**Diagnostic NMR Data:**

**$^{1}$H** (500 MHz, $CDCl_3$): δ 7.69 (m, 8H), 7.52 (s, 4H), 3.96 (m, 2H), 3.67 (m, 2H), 1.74 (m, 10H), 1.58 (m, 2H), 1.30 (d with overlapping signals, $J$ = 6.4 Hz, 28H), 1.16 (m, 6H).

**$^{11}$B** (160.5 MHz, $CDCl_3$): δ 82 ($B^+$), -6.6 ($BAr^F_{24}$).

### 4.8.6 General Reduction Procedures and Scope

**General hydrogenation procedure.** *i*PrBAC-$BR_2H$ (5-10 mol %) and a quinolinium salt (5-10 mol %) were placed in an oven dried 1 dram vial equipped with a magnetic stir bar. To this vial trifluorotoluene (0.2 mL) was added and the solution stirred for 2 min. Then substrate was added (0.18 mmol) as a solid and then the solution was diluted with trifluorotoluene (0.1 mL) and the vial equipped with a septum cap and 16-gauge needle. Vials were placed into a Parr-bomb which was then assembled and removed from the glove box. In a fume hood, the bomb was placed on a stir plate, and purged seven times by pressurizing to 20 atm of $H_2$ followed by careful release. The bomb was subsequently pressurized to 24 atm. The Parr bomb was left on the stir plate over night and then was carefully depressurized, disassembled, and the vials were removed. Volatiles were removed *in vacuo* and $CDCl_3$ (approx. 0.7 mL) was added and conversion was ascertained by $^{1}$H NMR analysis (comparison of starting material and product).

**General hydrosilylation prodecure.** *i*PrBAC-$BR_2H$ (2.5-10 mol %) and a quinolinium salt (2.5-10 mol %) were placed in an oven dried 1 dram vial equipped with a magnetic stir bar. Imine (approx. 0.18 mmol) was then added to the vial followed by either TFT or MTBE (approx. 0.7mL). Diphenylsilane was then added (approx. 1-1.5 equiv. in relation to substrate). Reactions were left to stir overnight. Volatiles were removed *in vacuo* and $CDCl_3$ (approx. 0.7 mL) was added and conversion was ascertained by $^{1}$H NMR analysis (comparison of starting material and product).

**Hydrosilylation procedure with isolated yields.** *i*PrBAC-BCy$_2$H **4-1** (4 mg, 0.009 mmol, 5 mol %) and *N*-Bn quinolinium Bar$^{Cl}{}_8$ **4-15** (7.5 mg, 0.009 mmol, 5 mol %) were placed in an oven dried 1 dram vial equipped with a magnetic stir bar. Imine (0.0184 mmol) was then added to the vial followed by MTBE (approx. 0.7mL). Diphenylsilane (0.05 mL, 0.276 mmol, 1.5 equiv.) and reactions were left to stir overnight. Volatiles were removed *in vacuo* and $CDCl_3$ (approx. 0.7 mL) was added and conversion was ascertained by $^1$H NMR analysis (comparison of starting material and product). The solvent was then removed *in vacuo* and the crude material was then subjected to column chromatography with a gradient of 2.5% to 100% ether in hexanes as needed. $^1$H NMR data was then acquired of the amine products.

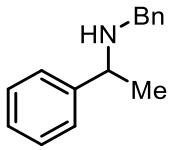


***N*-Benzyl-(1-phenylethyl)amine (4-9b).**

**Yield:** 33mg, 0.156 mmol, 85%

**$^1$H** (300 MHz, $CDCl_3$): δ 7.28 (m, 10H), 3.8 (q, *J* = 6.6 Hz, 1H), 3.62 (AB q, 2H), 1.87 (s, 1H), 1.36 (d, *J* = 6.6 Hz, 3H).

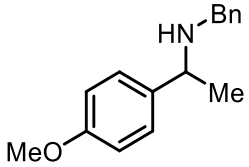


***N*-Benzyl-(1-(4-methoxyphenyl)ethyl)amine (4-10b).**

**Yield:** 42mg, 0.174 mmol, 95%

**$^1$H** (300 MHz, $CDCl_3$): δ 7.26 (m, 7H), 6.87 (m, 2H), 3.79 (s, 3H), 3.76 (q, *J* = 6.6 Hz, 1H), 3.61 (AB q, 2H), 1.64 (s, 1H), 1.33 (d, *J* = 6.6 Hz, 3H).

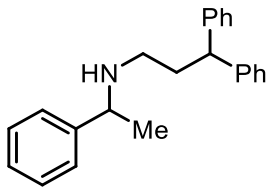


***N*-(3,3-Diphenylpropyl)-(1-phenylethyl)amine (4-21b).**

**Yield:** 53mg, 0.168 mmol, 91%

**$^1$H** (300 MHz, $CDCl_3$): δ 7.20 (m, 15H), 3.95 (t, *J* = 7.8 Hz, 1H), 3.55 (q, *J* = 6.6 Hz, 1H), 2.42 (m, 2H), 2.19 (m, 2H), 1.52 (s, 1H), 1.27 (d, *J* = 6.6 Hz, 3H).

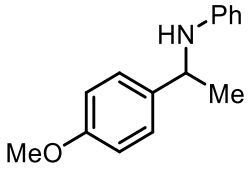


***N*-Phenyl-(1-(4-methoxyphenyl)ethyl)amine (4-18b).**

**Yield:** 31mg, 0.136 mmol, 74%

**$^1$H** (500 MHz, $CDCl_3$): δ 7.27 (ap d, 2H), 7.08 (ap t, 2H), 6.84 (ap d, 2H), 6.63 (ap t, 2H), 6.50 (ap d, 2H), 4.43 (q, *J* = 6.7 Hz, 1H), 3.95 (s, 1H), 3.76 (s, 3H), 1.48 (d, *J* = 6.6 Hz, 3H).

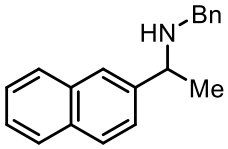


***N*-Benzyl-(1-naphthylethyl)amine (4-16b).**

**Yield:** 33mg, 0.126 mmol, 69%

**$^1$H** (500 MHz, $CDCl_3$): δ 7.82 (ap t, 3H), 7.76 (s, 1H), 7.52 (ap d, 1H), 7.44 (m, 2H), 7.29 (m, 4H), 7.22 (m, 1H) 3.97 (q, *J* = 6.6 Hz, 1H), 3.64 (ab q, 2H), 1.88 (s, 1H), 1.43 (d, *J* = 6.6 Hz, 3H).

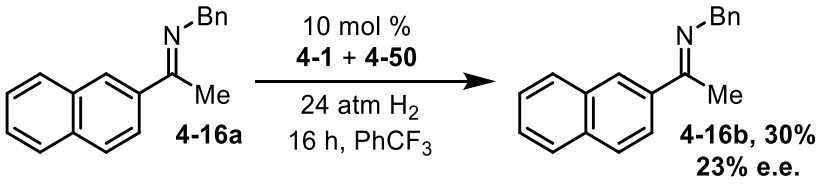


**Asymmetric hydrogenation procedure.** *i*PrBAC-BCy$_2$H **4-1** (7.6 mg, 0.018 mmol, 10 mol %) *N*-Bn Quinolinium B(R-BINOL)$_2$ **4-50** (15 mg, 0.018 mmol, 10 mol %) were placed in an oven dried 1 dram vial equipped with a magnetic stir bar. To this vial, trifluorotoluene (0.75 mL) was added and the solution stirred for 2 min. 2-acetonaphthone-*N*-(benzyl)imine **4-16a** was added (48 mg, 0.18 mmol) and the vial equipped with a septum cap and 16-gauge needle. The vial was placed into a Parr-bomb which was then assembled and removed from the glove box. In a fume hood, the bomb was placed on a stir plate, and purged seven times by pressurizing to 20 atm of $H_2$ followed by careful release. The bomb was subsequently pressurized to 24 atm. The Parr bomb was left on the stir plate overnight and then was carefully depressurized, disassembled, and the vial was removed. Volatiles were removed *in vacuo* and $CDCl_3$ (approx. 0.7 mL) was added and a 30% reduction to the amine was ascertained by $^1$H NMR analysis (comparison of starting material and product). Volatiles were once again removed *in vacuo* and the crude material was subjected to HPLC analysis through a pentane extraction of the crude material. Crude HPLC data indicated an *e.e.* of 23%.

# Chapter 5: Protic Additives or Impurities Promote Imine Reduction with Pinacolborane

Reprinted with permission from **B. S. N. Huchenski** and A. W. H. Speed, *Org. Biomol. Chem.*, **2019**, 17, 1999.  The manuscript has been reformatted to match the thesis format, and references and compounds have renumbered where appropriate. Sub-sections headers have been added.

Contributions to manuscript: All synthetic work in this chapter was carried out by B. S. N. Huchenski, with the following exceptions: The reactions shown in **Scheme 5.2** and **Scheme 5.6** were conducted by Dr. A. W. H. Speed. Imine **5-10** was prepared by T. M. Hynes and all other imines were prepared collaboratively between B. S. N Huchenski, M. R. Adams and C.-H. Tien. Mass spectrometric data were acquired by Mr. Xiao Feng (Mass Spectrometry Laboratory, Dalhousie University). The manuscript was written by B. S. N. Huchenski and Dr. A. W. H. Speed.

## 5.1 Introduction

The use of pinacolborane as a reductant for carbonyl and imine compounds has undergone extensive growth in recent years.[170] A variety of protocols and catalysts have been disclosed for carbonyl reduction with pinacolborane. Frequently, Lewis-base activation of the borane is an integral part of the reduction mechanism.[171] Alkoxides, and recently butyllithium have been used as Lewis-bases in the reduction of carbonyls.[172,173] Under neat conditions, it has been shown that the hydride transfer can proceed from pinacolborane to aldehydes or benzophenone imine in an uncatalyzed manner.[174]

Imine reduction by neutral boranes such as pinacolborane has undergone many relatively recent developments **(Figure 5.1)**.

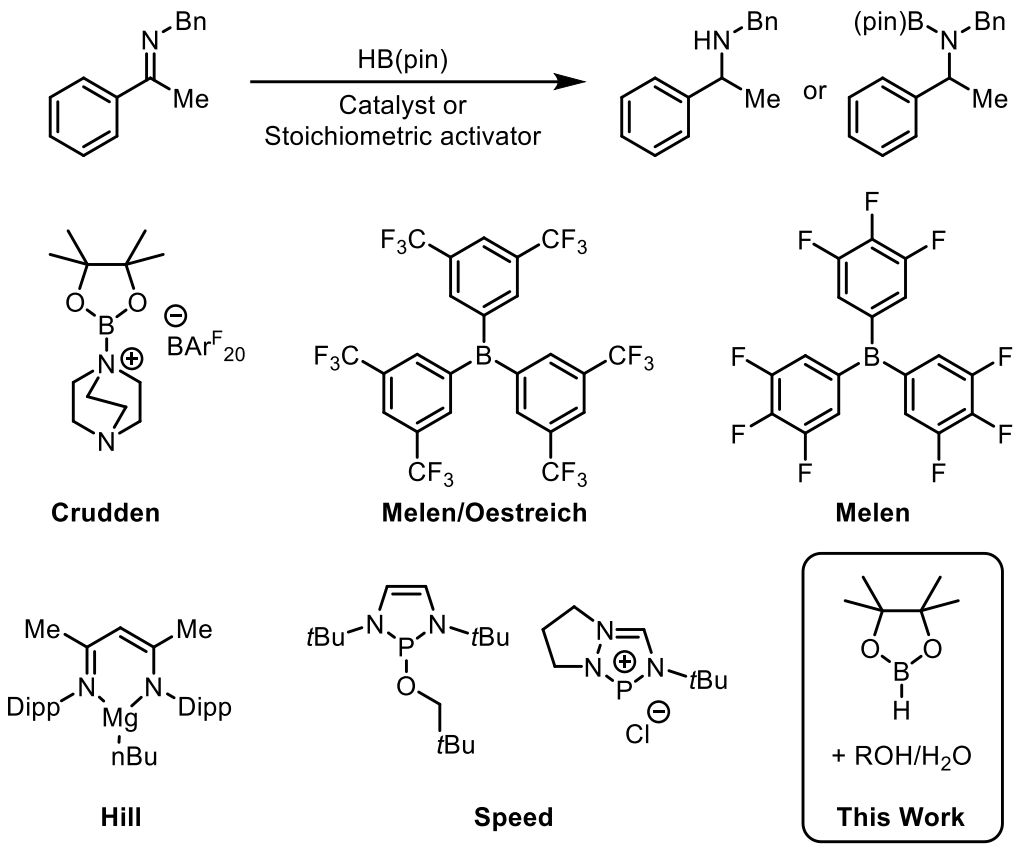


**Figure 5.1** Selected existing systems for imine reduction with pinacolborane.

In contrast to Lewis-base mediated ketone and aldehyde hydroborations with pinacolborane, Lewis or Brønsted acid mechanisms appear to be more prevalent in imine hydroboration. Seminal reports on imine hydroboration with catecholborane showed that coinage metal complexes could catalyse imine hydroboration.[175] Catecholborane slowly reacts with imines in the absence of catalysis, however Brønsted acid catalysed imine reductions with catecholborane employing chiral phosphoric acids did allow significant enantioinduction, demonstrating the merit of exploring catalysed processes even when a background reaction exists.[176,177] Despite the initial use of coinage metal complexes in imine hydroboration with catecholborane, main-group element-based catalytic systems have grown to occupy a pre-eminent position in imine hydroboration reactions with pinacolborane, which is considered to be less reactive than catecholborane.[178] In 2012,

Crudden and co-workers reported borenium catalysed imine hydroboration with pinacolborane, which did not undergo a non-catalyzed background reaction with imines.[179] The proposed mechanism for this reaction involves hydride delivery from a borane-imine complex to an imine activated by complexation to a borenium cation. After this report, a number of protocols for imine hydroboration with pinacolborane have been reported, involving several different mechanistic proposals.[180,181] Neutral boron-based Lewis acids have been shown to catalyse imine hydroboration, with a proposed mechanism involving imine activation by the Lewis acid, rather than a borenium-catalyzed reaction.[182,183] Magnesium centres have also proven competent at imine hydroboration, via the intermediacy of magnesium hydrides which are regenerated through pinacolborane.[184,185] Most recently, the use of diazaphospholene-based phosphorus hydride complexes for imine hydroboration has recently been reported by our group and others.[77,78,186,187] Diazaphospholene hydrides effect reduction through delivery of a phosphorus hydride to an imine, and represent one of the least Lewis-acidic catalyst systems for imine reduction. Finally, several transition metal based catalysts, including ruthenium, rhenium, and cobalt-based catalysts have been employed in imine hydroboration.[188–191] These reductions are typically proposed to occur through the intermediacy of metal-hydride bonds

During the course explorations of catalysed imine hydroboration reactions, we explored the use of methanol to rapidly quench reactions. We observed that with the use of methanol as a quenching agent, even control reactions without added catalyst showed high conversions to the amine product. Since previous reports of imine hydroboration had not reported background reactions between pinacolborane and imines, this result suggested that methanol was promoting the observed reduction reaction. In addition, we conducted experiments verifying no background reaction between pinacolborane and the imines under

question in the absence of methanol, suggesting that other contaminants in our solvents or substrates were not promoting this observed background reaction.

## 5.2 Results and Discussion

It has been reported that reduction of carbonyl functionality with pinacolborane occurs in some cases in the absence of solvent, while addition of solvent supresses the reduction reaction.[174] Verifying the absence of a background reaction for imine reduction at room temperature under neat conditions, mixing imine **5-1** with pinacolborane **5-2** for 3 h, followed by dissolution in chloroform-*d* showed no reduction reaction. Upon addition of 10 equiv. of methanol as a 2 M solution in chloroform-*d* to a mixture of **5-1** and **5-2** we observed conversion to the amine by NMR spectroscopy (**Equation B, Scheme 5.1**).

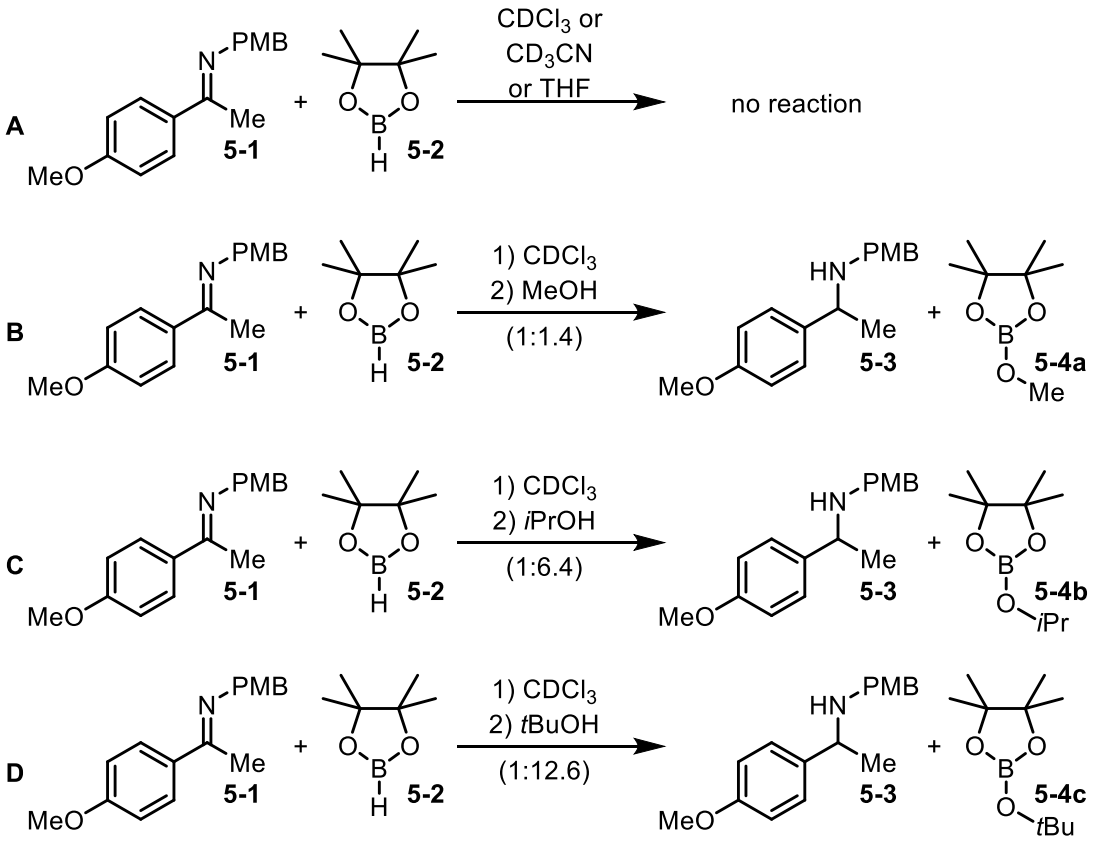


**Scheme 5.1** Investigation of primary, secondary, and tertiary alcohols as reduction promoters. Amine reduction (**5-3**) was measured as a ratio relative to imine **5-1** using $^{1}$H NMR analysis written in parentheses under reaction arrows.

Spectra were obtained within 10 min of mixing, with the time limitation being transport of the sample to the spectrometer, and subsequent pre-acquisition steps of sample insertion, locking, and shimming. No additional conversion was observed after further reaction time. Supporting this lack of further reactivity, unreacted boron hydride was not observed in the $^{11}$B NMR spectra during acquisition of the initial spectra in these experiments. Conversion was measured by measuring ratios of starting material to product as determined by integration of the $^{1}$H NMR spectra of the reaction mixtures. The ratios are shown under the corresponding equation arrows in **Scheme 5.1**. The reduction reactions were relatively clean, generally only showing starting material and product as the only nitrogen containing compounds, supporting the use of this measurement method. Use of ferrocene as an internal standard in some cases to calculate NMR yield gave good agreement with the ratios of starting material to product determined by NMR spectroscopy. Switching to isopropyl alcohol or tert-butyl alcohol resulted in higher conversions **(Equations C** and **D, Scheme 5.1)**. Use of isopropyl alcohol allowed determination of the fate of the B(pin) moiety. The boron was transferred to the isopropyl alcohol with concomitant loss of the proton, as revealed by comparison of spectral data of the reaction mixture with an authentic sample of *i*PrOB(pin) **5-4b** in chloroform-*d*.

Despite the use of excess pinacolborane **5-2** relative to imine, some imine starting material remained, despite complete consumption of the pinacolborane, indicating that dehydrocoupling of the alcohol and pinacolborane is a competitive process. Non-catalyzed dehydrocoupling of HB(pin) **5-2** and alcohols, amines, and thiols with concomitant loss of hydrogen gas has been reported by Bertrand and co-workers.[192]

In these dehydrocoupling reactions, simple mixing of the pinacolborane **5-2**, with the protic substrates in the presence or absence of solvent results in loss of hydrogen, and

formation of a boron-heteroatom bond. In our reactions, gas bubbles, presumed to be hydrogen, were observed during the mixing process. In conjunction with the formation of *i*PrOB(pin) **5-4b**, these results show a dehydrocoupling process is also active under our reported reaction conditions. We attribute the higher conversions for imine reduction with the bulkier alcohols isopropyl alcohol and *tert*-butyl alcohol to a slower rate of dehydrocoupling relative to imine reduction.

Given the ability of alcohols to promote reduction of imines by pinacolborane **5-2**, we decided to explore the ability of water to promote this reaction. While pinacolborane **5-2** rapidly reacts with water and is therefore intrinsically dry, water would be expected to be the most common protic contaminant in solvents or imines that have not been adequately dried. If water can promote imine reduction in a fashion analogous to alcohols, this would represent an important source of non-catalyzed reactivity of the reactions of imines with pinacolborane **5-2**. This could lead to unexpected outcomes, or erosion of stereoselectivity in reactions conducted with chiral catalysts. We prepared a 0.25 M solution of water in either THF or acetonitrile. These water-miscible and hygroscopic solvents are commonly used in imine reduction chemistry.[184,185] While addition of 1.25 equivalents of water in either acetonitrile (**Equation A, Scheme 5.2**) or tetrahydrofuran (**Equation B, Scheme 5.2**) to neat mixtures of pinacolborane **5-2** and imine **5-1** resulted in rapid gas release indicating significant reaction of pinacolborane **5-2** with water, concentration of the resulting mixture and analysis by NMR spectroscopy in chloroform-*d* showed approximately 80% conversion to the amine, indicating water is also an effective promoter of this reduction reaction. The gas release was observed only for the first couple of seconds of mixing, implying that reaction of pinacolborane **5-2** with water is rapid. For the observed levels of reduction of the imine to have occurred, the imine reduction must also be rapid. These

results indicate the importance of ensuring the dryness of solvent and substrate in the exploration of catalytic hydroboration reactions, especially asymmetric ones, since a rapid and uncatalyzed water-mediated background reaction would erode catalyst-mediated selectivity.

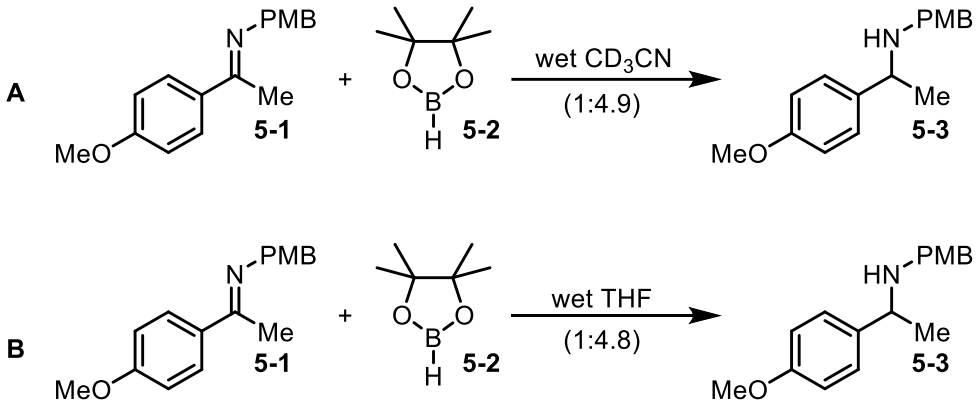


**Scheme 5.2** Water as a reduction promoter. Amine reduction (**5-3**) was measured as a ratio relative to imine (**5-1**) using $^{1}$H NMR analysis written in parentheses under reaction arrows.

We explored several other reducible substrates, including electron rich and poor aniline derived imines **5-5** and **5-6**, chalcone **5-7**, ketone **5-8**, pyridine **5-9**, and cyclic imine **5-10**, which is a precursor to the pharmaceutical candidate SIB-1508Y (**Figure 5.2**).[193] In the case of aniline derived imines **5-5**, and **5-6**, only trace conversion to the product amines was observed, in contrast to the relatively high conversion observed with **5-1**. Chalcone **5-7**, ketone **5-8**, pyridine **5-9**, and imine **5-10** did not undergo reduction reactions, with dehydrocoupling of the pinacolborane being the only observed reaction.

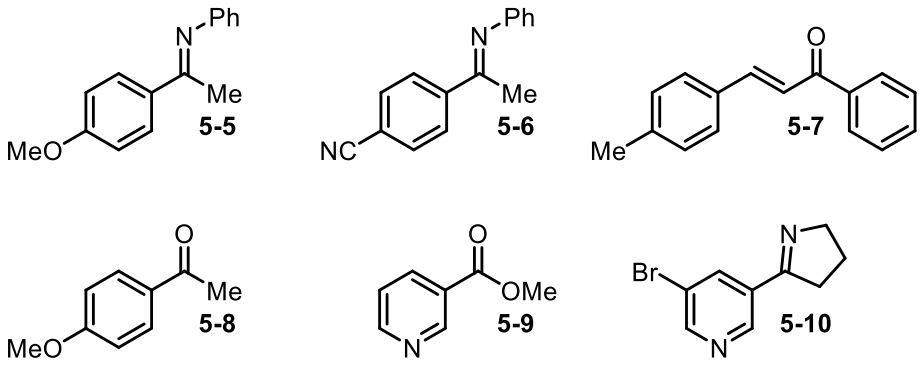


**Figure 5.2** Substrates that were not efficiently reduced with pinacolborane/alcohol mixtures.

Aniline derived imines have lower Lewis-basicity than alkyl imines. The above results suggest that a relatively basic alkyl imine is important for high conversion, and that addition of alcohol or water is necessary for reduction to take place. A mechanism involving a six membered transition state is proposed for the reduction reaction (**Scheme 5.3**).

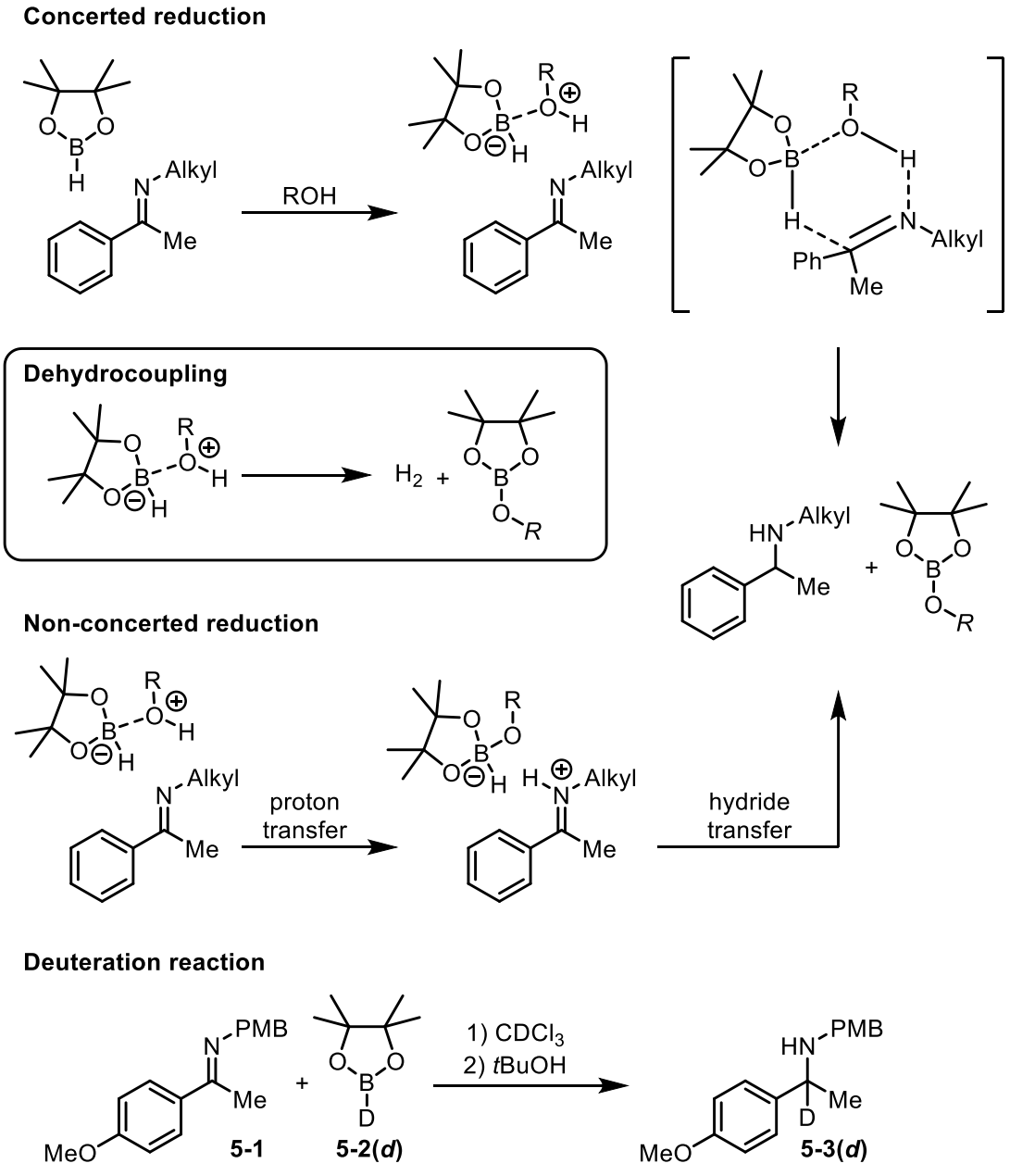


**Scheme 5.3** Proposed mechanism for imine reduction.

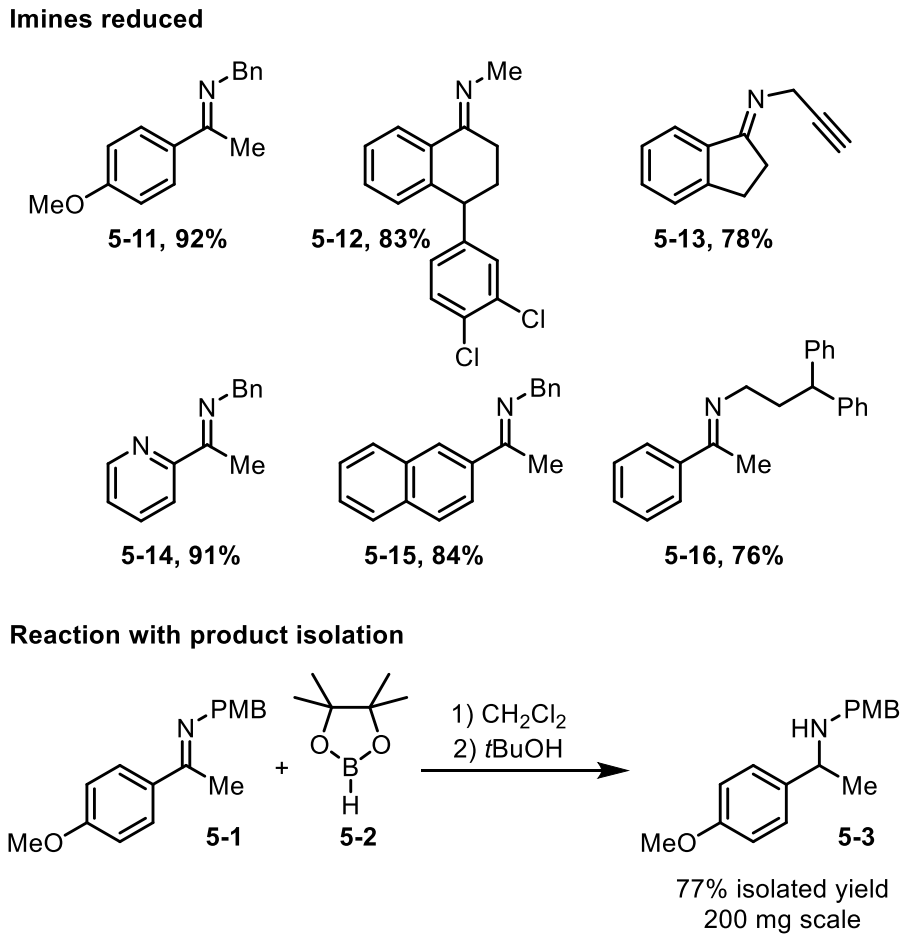


**Scheme 5.4** Imines reduced with tert-butyl alcohol/pinacolborane (NMR yields from integration with ferrocene internal standard)

Association of the HB(pin) **5-2** and alcohol would be expected to increase both the acidity of the alcohol, and hydricity of the boron hydride.[188–191] In the absence of an imine, hydrodecoupling and release of hydrogen would occur. In the presence of a reducible imine, the hydride and hydrogen could be delivered to the imine via the cyclic six-membered transition state. The current data does not rule out an open transition state or non-concerted proton/hydride transfer for this reaction and this scenario is also shown in **Scheme 5.3**. The use of deuterated pinacolborane **5-2(*d*)** as a reductant resulted in delivery of the deuterium to the imine carbon, which is consistent with the mechanistic proposals presented in **Scheme 5.3**.[194] The results of the small substrate screen shown in **Figure 5.2** suggest that

having a relatively basic substrate is important. We postulate that the reduced basicity of the aniline derived imines reduces the extent of intermolecular interaction with the HB(pin) **5-2**/ alcohol complex, either by hydrogen bonding, or a full deprotonation, increasing the relative proportion of dehydrocoupling within the complex. The other unreactive substrates shown in **Figure 5.2** can be considered in this context: Carbonyl-based substrates **5-7** and **5-8** are also less basic than alkyl imines, corroborating the need for a relatively basic substrate. The failure of pyridine **5-9** to undergo reduction may be a consequence of the added energetic penalty of pyridine dearomatization making the rate of reduction uncompetitive with dehydrocoupling. The failure of imine **5-10** to undergo reduction was slightly more unexpected, since it is an alkyl imine. In this case, the basicity of the pyridine may interfere with imine reduction by changing the site of protonation on the molecule.

We subsequently explored a small scope of alkyl imines. The imines shown in **Scheme 5.4** were reduced with varying conversions. The yields reported under substrates **5-11–16** were obtained by integration of NMR spectra with addition of 0.050 mmol of ferrocene as an internal standard. These numbers were in good agreement with observed ratios of starting material to product, showing that the reactions were relatively clean. Substitution of the 4-methoxybenzyl (PMB) group for a benzyl group (**5-11**) did not perturb the reaction. The precursor to the antidepressant sertraline (**5-12**) was reduced, however an essentially 1:1 mixture of diastereomers was obtained.[195] An alkyne in the precursor to rasagiline (**5-13**) did not interfere with the reaction. A pyridyl imine (**5-14**) was reduced, in contrast to imine **5-10**. In this substrate, the imine in the 2 position of the pyridyl ring may attenuate the pyridine basicity by withdrawing electrons through conjugation, reducing its interference in proton transfer, as compared with imine **5-10**. It is also possible that even if the pyridine is protonated, the close proximity of the imine nitrogen would allow rapid

proton transfer, and subsequent imine reduction. Imines **5-15** and **5-16** were reduced uneventfully. Imine **5-16** is the precursor to fendiline, which is a pharmaceutical molecule. A reduction of imine **5-1** on 200 mg scale was also conducted using *tert*-butyl alcohol. The product was isolated and purified, affording amine **5-3** in 77% isolated yield. These reaction conditions are convenient, however imine reductions employing alternative reagents such as sodium borohydride or catecholborane can reach higher conversions, which means this reported method does not have added preparative value.

Since alcohols promote the observed reduction, we decided to investigate if the use of chiral non-racemic alcohols could result in chirality transfer. Solutions of the alcohols in chloroform-*d* were added to mixtures of **5-1** and pinacolborane (**5-2**). The use of the alcohols cedrenol (**5-17**), (1S,2R,5S)-(+)-menthol (**5-18**), 1(S)-and endo-(-)-borneol (**5-19**) did provide varying levels of conversion, however the amines obtained were essentially racemic. Use of (R)-(+)-1,1'-bi-2-naphthol **5-20** resulted in modest induction (63:37 R to S). The sense of induction was determined HPLC on a chiral stationary phase, and by comparing the order of elution a previous report of analysis of amine **5-3** of known configuration under the same HPLC conditions.[184,185] Finally, we investigated the use of Ellman's (S)-(-)-*tert*-butylsulfinimide (**5-21**), to examine if this protic functionality could also promote hydroboration. Meng and Du have reported catalytic reductions of imines employing an adduct of Piers' borane and Ellman's sulfinimide.[196] While addition of **5-21** to a mixture of imine **5-1** and pinacolborane (**5-2**) did promote reduction, but in our case, no asymmetric reduction was observed (**Scheme 5.5**).

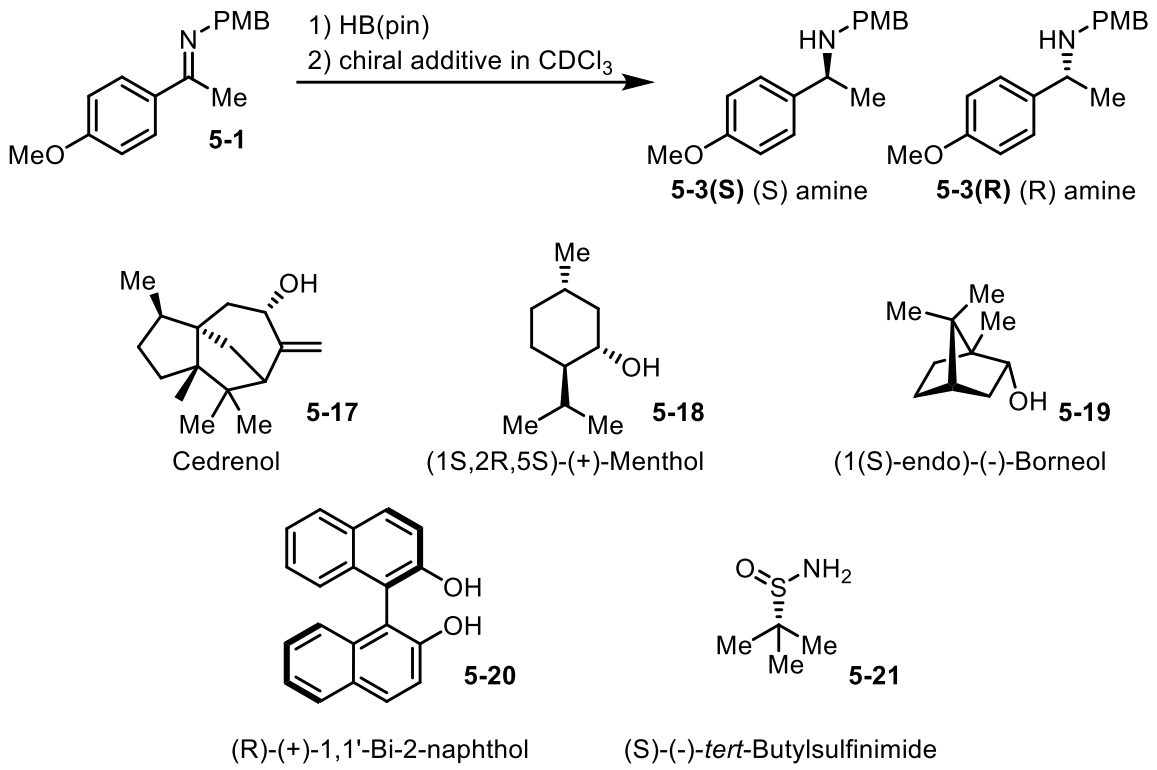


**Scheme 5.5** Investigation of chiral additives.

The observation that nitrogen containing compound **5-21** promoted reduction raised the possibility that other nitrogen-containing compounds may promote the reaction. Of special interest as promoters are alkyl amines, since these are the products of the reduction reaction of imines, raising the possibility that imine reduction by pinacolborane could occur via an autocatalytic reaction. Since imines are typically made from the condensation of an amine and carbonyl compound, excess amine is a likely impurity in imines, representing another potentially confounding factor in amine reduction.

To test for autocatalysis, two substrates were examined. Imines **5-1** and **5-13** were separately mixed with pinacolborane in chloroform-*d*, in the presence of ferrocene as an internal standard (**Scheme 5.6**). Amine **5-3** was added to each sample. NMR spectra were obtained for each reaction after approximately 30 min, then again after 24 h. In both cases, approximately 30% consumption of starting imine was observed in the 30 min NMR

spectra. Neither reaction went to completion in the 24 h timeframe but there was an increase in conversion to approximately 60% consumption of starting material for each reaction in the 24 h measurement. The spectra were complicated compared to those obtained from the use of stoichiometric protic additives because of the presence of a mixture of borylated and non-borylated amines, so rather than measuring product formation, decrease of peak area corresponding to imine starting material were used to ascertain starting material consumption. The observation of continued conversion over several hours, in contrast to results with the water and alcohol mediated reactions suggests that autocatalysis is occurring, however the reaction is slow relative to the reduction observed in the presence of alcohols or water. Dehydrocoupling of amine with pinacolborane **5-2** and loss of hydrogen would terminate the autocatalytic process by removing free amine without producing more amine to continue the catalytic cycle. The structure (steric environment) of the imine and amine is probably a factor in the extent of autocatalysis, and some substrates may prove to be more susceptible to autocatalysis than others. Because of the lack of high conversion for the substrates tested, and slow progression, amine autocatalysis is probably not a significant factor in ketimine reductions with pinacolborane **5-2**, but ensuring imine substrates are free of amines would ensure absence of this possible background reaction in future catalytic investigations.

**Autocatalysis scenario**

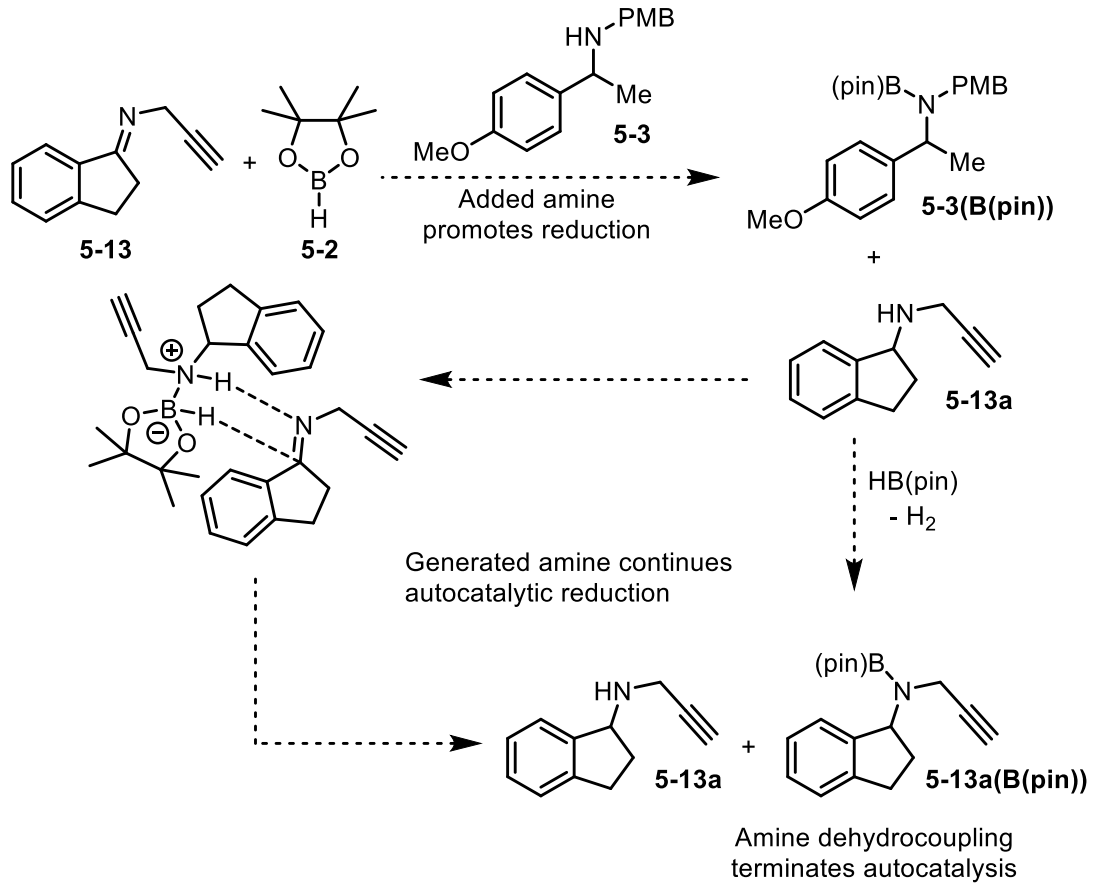


**Autocatalysis experiment**

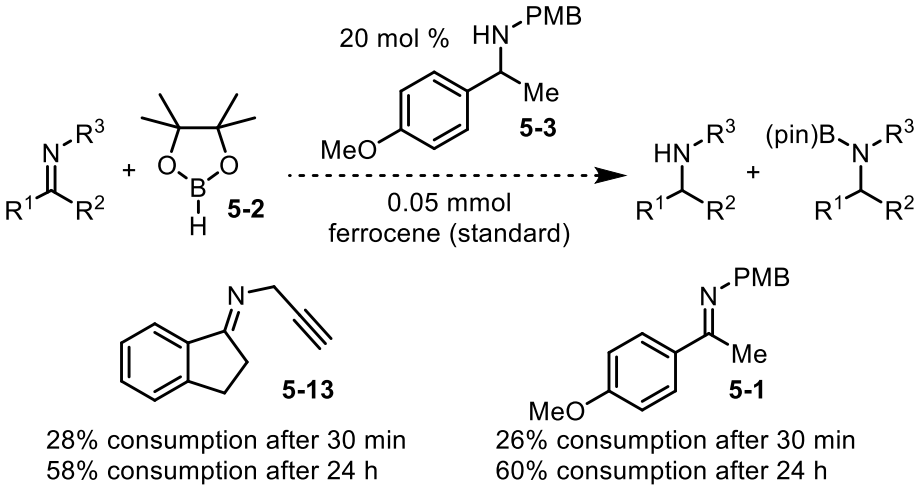


**Scheme 5.6** Investigation of amine autocatalysis.

## 5.3 Conclusion

We have demonstrated that a combination of pinacolborane **5-2** and alcohol or water results in the reduction of alkyl imines. Imines that are electron deficient are not reduced under these conditions. The use of chiral alcohols in chloroform-*d* did not result in chirality transfer except for BINOL **5-20**, which afforded modest selectivity. This transformation is operationally simple and rapid, however the preparative value is limited by incomplete conversion of imine to amine because of competitive dehydrocoupling of the pinacolborane **5-2** with the protic additive. The most important consideration arising from this work is that the promotion of imine reduction with pinacolborane **5-2** by protic contaminants represents an important potential background reaction that must be considered in future studies of catalysed reductions of imines, since this reactivity could erode intended selectivity of catalytic systems.

## 5.4 Experimental

### 5.4.1 General Considerations

Imines, pinacolborane **5-2**, chiral additives, and solvents were dispensed in a 2001 issue IT Glovebox ($H_2O$ levels typically 20-70 ppm). Reduction reactions were carried out in 4 dram oven dried scintillation vials equipped with magnetic stir bars and green Qorpak® PTFE lined caps. Substrates, reagents, and solvents were loaded into vials inside the IT Glovebox. Reactions at ambient temperature were stirred within the glovebox. $^{1}H$ and $^{11}B$ NMR data were collected at 300K on a Bruker AV-500 NMR spectrometer. Standard NMR tubes and caps were used. $^{1}H$ NMR spectra are referenced to residual non-deuterated NMR solvent ($CHCl_3$ =7.26 ppm, $CH_3CN$ = 1.94 ppm). HPLC data were acquired on a Varian Prostar instrument, equipped with detection at 254 nm, using a Astec Cellulose DMP column. A 99:1 hexanes/isopropanol solvent mixture was used as the eluent, with a flow rate of 0.5

mL/min. Configuration of the reduction product was determined by comparison with a known sample. Conversion ratios were measured by integration of the benzylic signals of the starting material and product, unless a signal was obscured, in which case the methyl group was instead integrated. A 0.10 M solution of ferrocene in $CDCl_3$ was also employed as an internal standard. 0.50 mL of this solution was dispensed to deliver 0.050 mmol of ferrocene to reactions. The ferrocene signal was integrated as 10, and molar quantities of substrates/products were accordingly calculated by multiplying obtained integral value by amount of ferrocene (0.050 mmol) divided by number of protons the signal represented (since ferrocene was normalized to 10). Mass spectrometric data were acquired by Mr. Xiao Feng (Mass Spectrometry Laboratory, Dalhousie University).

### 5.4.2 Solvent Purification

**Acetonitrile** was purchased from VWR in a 1L EMD Drisolv® bottle. This bottle was taken into the glovebox and activated 3 Å molecular sieves were added. A 0.25 M solution of water in acetonitrile was prepared by adding water to dry acetonitrile outside of the glovebox.

**Tetrahydrofuran** was purchased from Fisher, distilled from a purple solution of benzophenone/sodium ketyl and stored in the glovebox over activated 3 Å molecular sieves were added. A 0.25 M solution of water in THF was prepared by adding water to dry THF outside of the glovebox.

**Deuterochloroform** (Cambridge Isotopes) was stored over activated 3 Å molecular sieves, but otherwise used as received.

### 5.4.3 Reagents

**Chiral Additives** were purchased from Oakwood Chemical (BINOL and sulfinimide) or Aldrich.

**Imines** were prepared according to literature procedures. Imine **5-10** was prepared by Mr. Toren Hynes.[77,78,193,195]

**Isopropyl alcohol and methanol** were obtained from Dalhousie University chemical stockroom (Fisher Drums, absolute grade), and used as received.

**Pinacolborane** 5-2 was purchased from Oakwood Chemical, stored at ambient temperature in the glovebox, and used as received.

**Pinacolborane-*d*** was prepared by Dr. Casper Macaulay from $B_2Pin_2$, using the procedure of Hartwig and Hall.[194]

***Tert*-Butyl alcohol** was purchased from Sigma and used as received.

### 5.4.4 General Reduction Procedures and Results

All product amines are known compounds, and match previously reported spectra data.[77,78,193,195]

**Control experiment.** Compound **5-1** (50 mg, 0.186 mmol) was weighed into a 4 dram vial and equipped with a magnetic stir bar. Pinacol borane **5-2** (0.02 mL, 0.278 mmol, 1.5 equiv.) was added to the vial and the mixture was left to stir for 3 h. Deuterated chloroform (1 mL) was then added, and the solution left to stir for 10 min. NMR spectra were acquired after a further 15 min and 1.5 h after chloroform-d addition with no observable reduction.

**Deuterated methanol studies.** Compound **5-1** (50 mg, 0.186 mmol) was weighed into a 4 dram vial. Pinacol borane **5-2** was added to the vial followed by deuterated chloroform containing methanol-$d_4$ in the amounts detailed in the table below. The vial was then shaken and transferred to an NMR tube and NMR spectrum were acquired.

**Table 5.1** Effect of methanol-$d_4$ added to induce reduction of imine **5-1** to amine **5-3**. Percent yields were calculated based on relative proportions of the starting material versus product in $^1$H NMR.

| Entry | Pinacol Borane | Methanol-$d_4$ | Chloroform-*d* | **5-1**:**5-3** |
|---|---|---|---|---|
| 1 | 0.04 mL | 0.02 mL | 1 mL | 1:6.6 |
| | **(1.5 equiv.)** | **(2.6 equiv.)** | | |
| 2 | 0.04 mL | 0.04 mL | 1 mL | 1:10.9 |
| | **(1.5 equiv.)** | **(5.3 equiv.)** | | |
| 3 | 0.04 mL | 0.08 mL | 1 mL | 1:22.1 |
| | **(1.5 equiv.)** | **(10.6 equiv.)** | | |
| 4 | 0.04 mL | 0.04 mL | 0.5 mL | 1:12.6 |
| | **(1.5 equiv.)** | **(5.3 equiv.)** | | |

**Primary, secondary, and tertiary alcohol study.** Compound **5-1** (50 mg, 0.186 mmol) was weighed into a 4 dram vial. Pinacol borane **5-2** (0.04 mL, 0.278 mmol, 1.5 equiv.) was added to the vial followed by a solution of the respective alcohol in deuterated chloroform (0.93 mL, 10 equiv., 2M in deuterated chloroform). The vial was then shaken and transferred to an NMR tube and NMR spectrum were acquired.

**Table 5.2** Steric effect of alcohol added on the reduction of imine **5-1**. Percent yields were calculated based on relative proportions of the starting material versus product in $^1$H NMR.

| Entry | Alcohol | **5-1**:**5-3** |
|---|---|---|
| 1 | Methanol | 1:1.4 |
| 2 | Isopropyl alcohol | 1:6.4 |
| 3 | *Tert*-butyl alcohol | 1:12.6 |

***Tert*-butyl alcohol optimization study.** Compound **5-1** (50 mg, 0.186 mmol) was weighed into a 4 dram vial. Pinacol borane **5-2** was added to the vial and then dissolved in deuterated

chloroform. *Tert*-butanol was added in amounts detailed in the table below. The vial was then shaken and transferred to an NMR tube and NMR spectrum were acquired.

**Table 5.3** Optimization of amount of *tert*-butyl alcohol added to maximize the reduction of imine **5-1**.

| Entry | Pinacol Borane | *tert*-butyl alcohol | Chloroform-*d* | **5-1**:**5-3** |
|---|---|---|---|---|
| 1 | 0.04 mL **(1.5 equiv.)** | 26 µL **(3 equiv.)** | 1 mL | 1:3.1 |
| 2 | 0.04 mL **(1.5 equiv.)** | 26 µL **(3 equiv.)** | 0.5 mL | 1:3.8 |
| 3 | 0.04 mL **(1.5 equiv.)** | 53 µL **(6 equiv.)** | 0.5 mL | 1:6.6 |
| 4 | 0.05 mL **(1.8 equiv.)** | 53 µL **(6 equiv.)** | 0.5 mL | 1:7.8 |
| 5 | 0.06 mL **(2.2 equiv.)** | 53 µL **(6 equiv.)** | 0.5 mL | 1:12.6 |

**General procedure for imine reduction.** A substrate (0.186 mmol) was weighed into a 4 dram vial. Pinacol borane **5-2** (0.06 mL, 0.408 mmol, 2.2 equiv.) was added to the vial and then dissolved in deuterated chloroform (0.5 mL). Tert-butyl alcohol (53 µL, 0.556 mmol, 3 equiv.) was then added to the solution. The vial was then shaken and transferred to an NMR tube and NMR spectrum were acquired. Results of starting material to product integrations are detailed in the table below.

**Table 5.4** Scope of imines reduced with *tert*-butyl alcohol. Percent yields were calculated based on relative proportions of the starting material versus product in $^{1}H$ NMR.

| Compound # | Starting material: product |
|---|---|
| **5-1** | 1:13.8 |
| **5-5** | 1: trace |
| **5-6** | 1:0 |
| **5-7** | 1:0 |
| **5-8** | 1:0 |
| **5-9** | 1:0 |
| **5-10** | 1:0 |
| **5-11** | 1:13.1 |
| **5-12** | 1:3.7 |
| **5-13** | 1:4.2 |
| **5-14** | 1:8.5 |
| **5-15** | 1:8.6 |
| **5-16** | 1:3.7 |

**Procedure for reduction with an internal standard.** An imine (0.1856 mmol) was weighed into a 1 dram vial. HB(pin) **5-2** (0.06 mL, 0.4135 mmol, approx. 2.2 equiv.) was then added to the vial followed by ferrocene (0.50 mL of a 0.10M solution in $CDCl_3$). The contents were then shaken in the vial and then tert-butyl alcohol (53 μL, 0.5568 mmol, 3 equiv.) was added and the mixture was shaken for 5s. The solution was transferred to an NMR tube and NMR spectra were acquired after 10 min. Calculations and yields with internal standards are shown on the NMR spectra (appendix).

**Chiral alcohol studies.** Compound **5-1** (50 mg, 0.186 mmol) was weighed into a 4 dram vial. Pinacol borane **5-2** (0.04 mL, 0.278 mmol, 1.5 equiv.) was added to the vial. A chiral alcohol (0.278 mmol, 1.5 equiv.) dissolved in deuterated chloroform (0.75 mL) was then added to the vial and shaken. BINOL **5-20** was added as a solid after chloroform addition

due to incomplete solubility in the chloroform. The vial was then shaken and the contents were transferred to an NMR tube and NMR spectrum were acquired. Samples were subsequently acidified with 2N HCl, the organic layer was discarded, and the aqueous layer was made basic, then extracted with dichloromethane, dried over sodium sulfate, concentrated, and analyzed by HPLC.

**Table 5.5** Effect of chiral alcohol or amine added on the reduction of imine **5-1**. Percent yields were calculated based on relative proportions of the starting material versus product in $^1$H NMR.

| Alcohol | **5-1**:**5-3** | *e.r.* (% *e.e.*) |
|---|---|---|
| (1(S)-endo(-))-Borneol **5-19** | 1:8.4 | racemic |
| (R)-(+)-1,1'-Bi-2-napthol **5-20** | / | 63.5:36.5 (27 %) |
| (1S,2R,5S)-(+)-Menthol **5-18** | 1:7.7 | racemic |
| Cedrenol **5-17** | 1:5.9 | racemic |
| (S)-(-)-*tert*-Butylsulfinamide **5-21** | 1:4.8 | racemic |

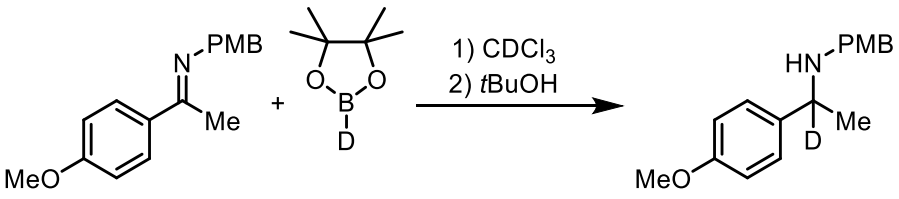


**Deuteration study.** 4-methoxyacetophenone-*N*-(4-methoxybenzyl)imine **5-1** (50 mg, 0.186 mmol) was weighed into a 1 dram vial. DB(pin) **5-2(*d*)** (0.06 mL, 0.4135 mmol, approx. 2.2 equiv.) was then added to the vial followed by ferrocene (0.5mL, 0.1M in $CDCl_3$). The contents were then shaken in the vial and then *tert*-butyl alcohol (53 µL, 0.5568 mmol, 3 equiv.) was added and the mixture was shaken for 5 s. The solution was transferred to an NMR tube and an NMR spectrum was acquired after 10 min. The solvent was then removed *in vacuo*. Ether (2 mL) was then added followed by HCl (1 mL, 2M in

$Et_2O$). Solvent was removed *in vacuo* and the residue was washed with pentane (3 x 5mL) by decanting the pentane. NaOH (10 mL, 2M) was then added as well as DCM (10 mL) which was then transferred to a separatory funnel. The aqueous layer was washed with DCM (3 x 7 mL) and the combined organic layers were dried with anh. sodium sulfate. Solvent was removed *in vacuo* and the resulting residue was purified by column chromatography with a gradient of 9:1 (hexanes : ether) to ether (100%), resulting in the pure amine **5-3(*d*)** (38mg, 0.14 mmol, 75% yield).

**$^1$H** (500 MHz, $CDCl_3$): δ 7.26 (m, 2H), 7.18 (m, 2H), 6.88 (m, 2H), 8.84 (m, 2H), 3.80 (s, 3H), 3.78 (s, 3H), 3.55 (ab q, 2H), 1.50 (s, 1H), 1.32 (s, 3H).

**$^{13}$C** {$^1$H} (500 MHz, $CDCl_3$): δ 158.7, 137.8, 133.0, 129.4, 127.8, 113.9, 113.8, 56.3 (t), 55.4, 51.0, 24.5.

**HRMS (APCI):** calc'd for $C_{17}H_{21}DNO_2$ [M+H$^+$] 273.1708, found: 273.1715.

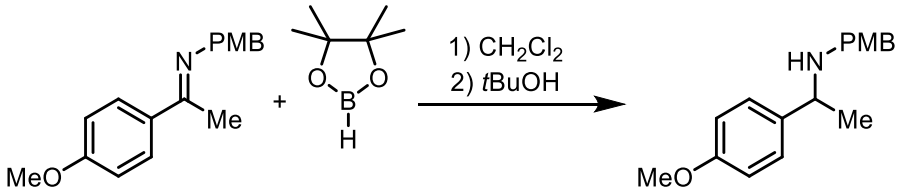


**200 mg scale reaction and product (5-3) isolation.** 4-methoxyacetophenone-*N*-(4-methoxybenzyl)imine **5-1** (200 mg, 0.7426 mmol) was weighed into a 4 dram vial equipped with a magnetic stir bar. HB(pin) **5-2** (0.24 mL, 1.633 mmol, approx. 2.2 equiv.) was then added to the vial followed by DCM (2 mL). The contents were then stirred in the vial and then *tert*-butyl alcohol (0.21 mL, 2.227 mmol, 3 equiv.) was added and the mixture was stirred for 30 min. An aliquot was taken, and an NMR spectrum was acquired. Solvent was then removed *in vacuo* and the residue was dissolved in ether (15 mL) and the amine was extracted with HCl (2 x 15 mL, 2M). The aqueous layer was then basified with NaOH (2M)

and the product extracted with ether (3 x 20 mL). The organic extracts were then dried with anhydrous sodium sulfate and the filtered. Solvent was removed *in vacuo* and the resulting residue was purified by column chromatography with a gradient of 9:1 (hexanes : ether) to ether (100%), resulting in the amine **5-3**, which was then purified again with the same acid base wash mentioned above to remove a small amount of remaining pinacol, which afforded the amine **5-3** (153 mg, 0.565 mmol, 77% yield).

**$^1$H** (500 MHz, $CDCl_3$): δ 7.26 (m, 2H), 7.18 (m, 2H), 6.88 (m, 2H), 8.84 (m, 2H), 3.80 (s, 3H), 3.79 (s, 3H), 3.75(q, *J* = 6.6 Hz, 1H), 3.55 (ab q, 2H), 1.50 (s, 1H), 1.33 (d, *J* = 6.6 Hz, 3H).

**Procedure for autocatalytic reactions.** *N*-(4-methoxybenzyl)-(1-(4-methoxyphenyl)ethyl)amine **5-1** (50 mg, 0.1856 mmol) was weighed into a 1 dram vial. HB(pin) **5-2** (0.06 mL, 0.4135 mmol, approx. 2.2 equiv.) was then added to the vial followed by ferrocene (0.5 mL, 0.1M in CDCl3). The contents were then shaken in the vial and then *N*-(4-methoxybenzyl)-(1-(4-methoxyphenyl)ethyl)amine **5-3** (10 mg, 0.03712 mmol, 0.2 equiv.) was added as a solution in $CDCl_3$ (0.25 mL) and the mixture was shaken for 5s. The solution was transferred to an NMR tube after 10 min and NMR spectrum were acquired at 30 min and then at 24 h.

# Chapter 6: $SF_6$ Decomposition

Section **6.2** and **6.5** contains information from the following manuscript:

**B. S. N. Huchenski** and A. W. H. Speed, *Chem. Commun.,* **2021**, Advance Article. Reprinted with permission from the Royal Society of Chemistry, copyright 2021. The manuscript has been rewrttien for section **6.**2 and references and compounds have renumbered where appropriate. Section **6.5** is reprinted directly from the manuscript and references and compounds have renumbered where appropriate. Sub-sections headers have been added. The orignal manuscript was written by B. S. N. Huchenski and Dr. A. W. H. Speed.

Contributions to manuscript: All synthetic work in this chapter was carried out by B. S. N. Huchenski, with the following exceptions: Compounds **6-19**, **6-51**, **6-61**, and **6-62** were prepared by Dr. A. W. H. Speed and **6-63** was prepared by Mostafa Hagar. The X-ray crystallography was conducted by Dr. Katherine N. Robertson. Mass spectrometric data were acquired by Mr. Xiao Feng (Mass Spectrometry Laboratory, Dalhousie University). The manuscript was written by B. S. N. Huchenski. The SEM images were acquired by Maxine Kirschenbaum and Dr. Mita Dasog.

## 6.1 Introduction

Sulfur hexafluoride is a robust gaseous molecule which is colorless, odorless, non-combustible, and highly thermally stable.[197,198] Two French chemists Moissan and Lebau, known for their important developments in fluorine chemistry, discovered[199] and prepared[200] sulfur hexafluoride in the early 1900s. The predominantly inert nature of this gas has made it attractive in the electric power industry, as well as a variety of other applications such as metal smelting, insulation for tires and windows, and as an etching agent.[198] The stability of sulfur hexafluoride under electrical currents arises from its high

dielectric constant.[197] Sulfur hexafluoride will quench electrical arcs that would otherwise damage equipment by behaving as an electron trapper in the circuit breaker, with a fascinating ability to "self heal" during the process (**Scheme 6.1**).[201] In addition, the insulation capability of sulfur hexafluoride is three times greater than air,[202] allowing for more compact devices. Another benefit is the increased density of the gas allows for less leakage. The electrical industry accounts for about 80% of the sulfur hexafluoride usage in the world today and in many countries such as India, China, and Brazil, the amount of sulfur hexafluoride used is increasing every year.[197] The release of sulfur hexafluoride into the atmosphere occurs in all stages of the electrical power industry from manufacturing to maintenance to testing.[197]

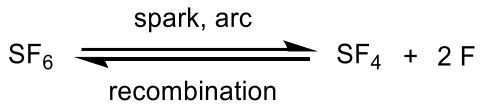


**Scheme 6.1**"Self Healing" of $SF_6$ in an electric arc.

From an initial viewpoint, sulfur hexafluoride is the optimal gas for the electrical power industry. However, sulfur hexafluoride is a highly potent greenhouse gas, which cannot be overlooked in assessing its value. According to the UN Kyoto protocol and Paris agreement,[202] sulfur hexafluoride is among the six greenhouse gasses that should be restricted. Although the concentration of sulfur hexafluoride in the atmosphere relative to $CO_2$ is low, the global warming potential of sulfur hexafluoride is approximately 23,500 times greater than $CO_2$.[202] The atmospheric lifetime of sulfur hexafluoride is over 3200 years making reduction of usage of great importance.[202] While some countries like the United States and Canada have seen a steady decline in sulfur hexafluoride emissions, and increased monitoring, the global increase of sulfur hexafluoride is expected to reach 64 Mt $CO_2$ equiv. by 2030, mainly resulting from developing countries.[203] Approximately 24% of

these emissions arise from the disposal and maintenance of electric power systems.[203] New alternatives are being developed to replace sulfur hexafluoride but with the current global production and usage of sulfur hexafluoride remaining quite large, methods to destroy surplus sulfur hexafluoride are currently an important area of research.[197]

### 6.1.1 Thermal Decomposition

Currently, there are a variety of methods to destroy unwanted sulfur hexafluoride, such as using thermal, photochemical, catalytic or plasma generation. Early methods to decompose $SF_6$ utilized thermal degradation techniques.[197] To decompose $SF_6$ thermally requires extremely high temperatures because of the high stability of this gaseous molecule.[198] A report in 1997 details the degradation of $SF_6$ by blowing the exhaust into a >1000˚C furnace containing $CaCO_3$ to convert $SF_6$ into $CaSO_4$ and $CaF_2$. However, this method requires a large excess of $CaCO_3$ to ensure no HF remains.[197] This method is highly undesirable because of the large energy requirements of the furnace, yet is currently one of the most widely used abatement systems in operation. A major downfall to this method arises from the high temperatures, which also allow for other reactions to occur such as $NO_x$ formation. Oxides of nitrogen are also greenhouse gases, and contribute to acid rain.[197]

### 6.1.2 Metal Reactivity with $SF_6$

Metals have also been reported to react with $SF_6$. The first example of an alkali metal reacting with $SF_6$ was reported by Cowen in 1953.[204] In this system, sodium metal was coated onto a tube and it was found that at 250 °C a reaction with $SF_6$ occurred, as evidenced by a pressure drop in the system. The next lowest temperature reaction with $SF_6$ gas and a metal species was disclosed by Nyman and Case in 1962,[205] which involved the use of a Lewis acid, namely aluminum trichloride, which was heated to 180–200 °C in the

presence of $SF_6$. Reactivity of $SF_6$ with lithium aluminum hydride was also examined at room temperature, but was found to only consume approximately 28% of the material after 1 week. Following Cowen's initial example, MacDiarmid reported that the reaction temperature can be greatly lowered when sodium metal was dissolved in either ammonia or a diphenyl-ethylene glycol dimethyl ether mixture.[206] With sodium, this reaction occurs at -64 °C and in the ethereal solution at -10 °C. Cesium metal was later also found to react in a similar manner as described by King et al in 1970.[207] A detailed investigation of metals in liquid ammonia reacting with $SF_6$ to produce metal fluorides and sulfides is described by Kraus in 2017.[208]

### 6.1.3 Catalytic Decomposition

An improvement to the previously mentioned thermal decomposition methods involves the use of catalysts to decrease operating temperatures. The catalysts used to remove sulfur hexafluoride are supported metal catalysts, zeolites and metal oxides, phosphates, and transition metal complexes. Two important pathways for heterogeneous degradation of sulfur hexafluoride are hydrolysis and oxidation reactions.[197] While catalysts offered minor improvements, recent advances have greatly reduced operating temperatures.

Metal phosphates are a common catalyst for the degradation of $SF_6$ and in 2009 Takita examined the efficiency of a variety of these metal phosphates.[209] From their findings, the most active phosphates were $AlPO_4$, $CePO_4$, $YPO_4$ and $Zr_3(PO_4)_4$ when conducted between 526–726 °C.[209] In a follow up study, it was found that $CePO_4$ was greatly more active than the other phosphates examined.[210] In 2012 Lee reported the application of $AlPO_4/\gamma\text{-}Al_2O_3$ as a catalyst for the degradation of $SF_6$.[211] This was an improvement on their previously reported system using only $\gamma\text{-}Al_2O_3$ which would be

deactivated by the HF produced. The preparation of this catalyst requires drying for 24 h followed by calcination for 4 h at 750 °C. After exploring a variety of operating conditions by varying temperature and phosphoric acid content. The most optimal conditions after rigorous testing were concluded to be 4.8 wt % of phosphoric acid at 750 °C.[211]

In a related manner, metal oxides can be used to decompose $SF_6$. In 2013 Qian reported the use of electroplating sludge for $SF_6$ removal which contains a mixture of metal oxides, hydroxides, sulfates, silicates, and phosphates.[212] Electroplating sludge is a waste product which often needs to be disposed of carefully but now can be recycled as an $SF_6$ decomposition catalyst. The optimal operating temperature for this system was 600 °C, 150 °C lower than the $AlPO_4/\gamma\text{-}Al_2O_3$ catalyst.[212] Another waste product kirschsteinite-dominant stainless-steel slag was reported to also decompose $SF_6$ at 600 °C.[213] The slag contains predominantly CaO, FeO and $SiO_2$ and when reacted with $SF_6$ was found to contain metal fluorides on the surface. The advantage to using slag is that there was minimal HF detected from the reactions with the major products being $SO_2$ and $SiF_4$.[213] However, these methods along with many other phosphate and metal oxide catalysts reported all require very high temperatures and often specialized equipment. A recent advancement in metal oxide catalysis was reported in 2020 by Gutiérrez et al.[214] which utilizes Mg/MgO with plasmonics to remove $SF_6$. This advancement displays the potential for a simple system to remove $SF_6$ compared to the complex mixtures used in the past which are often done with harsh conditions.

To decrease operating temperatures and produce more mild products of $SF_6$ decomposition, a variety of transition metal complexes have been explored for use in $SF_6$ decomposition or fluorination purposes (**Figure 6.1**). Early examples by Ernst displayed that transition metals outfitted with cyclopentadienyl ligands **6-1**(**a-e**) can react with

$SF_6$.[215,216] Limberg later reported a nickel complex **6-2** which generated nickel fluorides and sulfides from $SF_6$.[217] Braun reported a rhodium complex **6-3** which can react with $SF_6$ and $SF_5$ derivatives and generate $H_2S$ as well as the original complex, leading to potential catalytic use.[218]

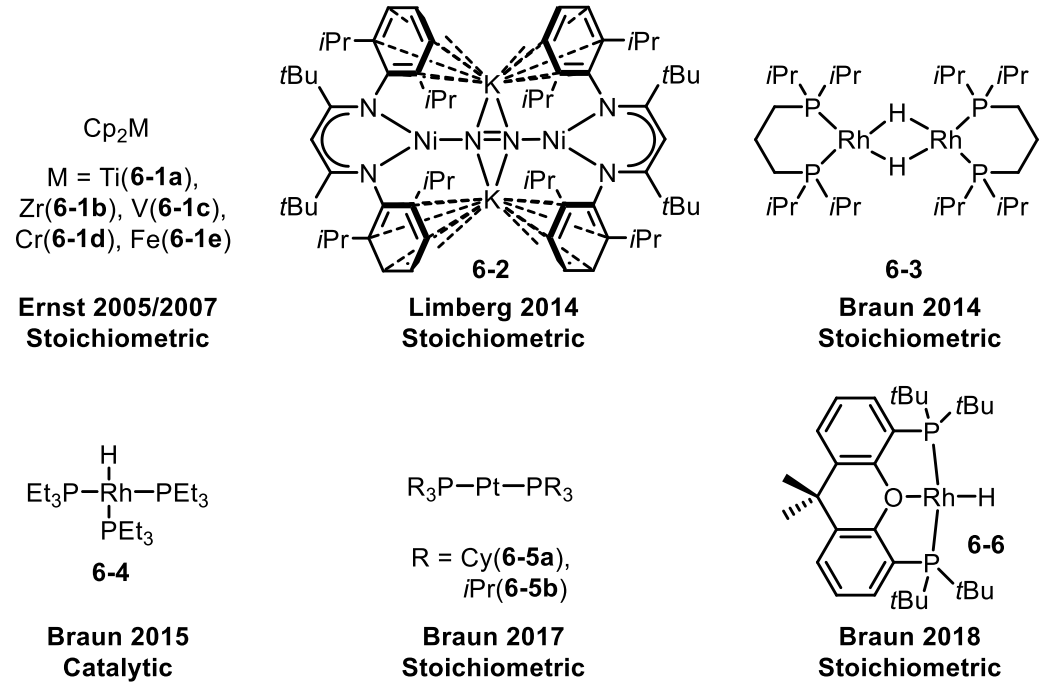


**Figure 6.1** Transition metal complexes capable of reaction with $SF_6$.

Braun later reported a rhodium catalyzed **6-4** $SF_6$ decomposition,[219] with the use of silanes and a trialkyl or aryl phosphine as a sulfur trapping reagent. Progress was monitored by the conversion of the phosphine to the phosphine sulfide. This method is more favorable compared to previous methods because the products formed are less toxic or less volatile. Most methods reported produce products that are volatile and are toxic, such as HF, or common greenhouse gasses.[197,201] However, the maximum conversion to the phosphine sulfide was 36% at 80 °C over 16 h, leaving much room for improvement. In 2017, Braun reported a platinum complex **6-5a/b** which was utilized in deoxyfluorination of ketones and alcohols,[220] but loadings were high, and conversions were low. Following the platinum

paper, Braun reported another rhodium complex **6-6** capable of reacting with $SF_6$, but no catalytic activity was reported.[221] In 2016, Jamison reported the use of an iridium photocatalyst, in the deoxyfluorination of allylic alcohols with $SF_6$ as the fluorine source.[222] A significant advancement in transition metal catalysis with $SF_6$ gas was reported in 2018 by Wagenknecht which utilizes a copper and phenothiazine-based photoredox catalytic system.[223] This was able to pentafluorosulfanylate α-methyl and α-phenyl styrene with modest conversions, but was notable as the first degradation method that left the $SF_5$ group intact. Overall, the advancements in transition metal catalyzed $SF_6$ decomposition indicate that milder reaction conditions are possible and that these reactions can be used to produce materials which may be of synthetic use.

### 6.1.4 Organic Reagents Capable of Reacting with $SF_6$

There are a variety of modes in which a reagent can react with sulfur hexafluoride. As described by Beier,[224] these modes vary from electron transfer, radical generation, photochemical excitation and Lewis acid/base chemistry. While the bond dissociation energy of the S–F bond in $SF_6$ is quite large, being around 380 kJ/mol,[224] a variety of methods have been reported utilizing organic molecules which can react with $SF_6$ through reductive processes.

Reactive molecules generated by photolysis or plasma are reported react with $SF_6$. Some common reductive agents that have been studied are acetone, styrene, and propene.[197] This process generates strong electron donors such as in the instance of acetone, where radicals such as $CH_3$, $CH_2$, and H form under 184.9 nm.[225] The most efficient system found was using propene for 180 min at 184.9 nm and 253.7 nm with a destruction removal efficiency of 75%.[226] This method is desirable because of low power consumption but the production of undesirable absorbing by-products can affect transmittance.[197]

An early example of mild $SF_6$ activation was patented by Kirsch et al in 2003 and involved two electron transfer using UV light with tetrakis(dimethylamino) ethylene **6-7** (**Figure 6.2**).[227] This method was improved upon by Rueping in 2017,[228] with the stronger organic reductant of a DMAP derived reagent **6-8** originally reported by Murphy, which can react with $SF_6$ without requiring UV light. This method also demonstrated an early example of the entrapment of a $SF_5$ anion with an organic cation. Following these results, Braun reported that NHCs **6-10a/b** can undergo single electron transfer to $SF_6$ upon irradiation with light,[229] producing difluoroimidazolines, and in some instances thioureas, both of which represent NHCs trapping $SF_6$. When an alcohol or carboxylic acid is present, the products of this reaction were found to undergo deoxyfluorination with the alcohols. Another example of radical functionalization with $SF_6$ involves the lithium salt of the TEMPO anion **6-9**,[224] which was found to reduce $SF_6$ and transfer a pentafluorosulfanyl group to alkenes in the process. However, this reaction is very low yielding, providing only 2% yield by $^{19}F$ NMR with 2 equivalents of TEMPO per 4-phenylbut-1-ene and 3.5% if 4 equivalents of the alternate nitroxyl TMINO were used. Wagenknecht's method originally involving phenothiazine photocatalyst and copper[223] was improved further with the removal of copper from the system, and addition of triethylborane as a radical mediator to conduct an α-pentafluorosulfanylation of similar substrates.[230] These results indicate that metal-free pentafluorosulfanylation is possible and can potentially be accessed in higher yields through different radical systems. More recently, Nagorny and co-workers have reported that simple photocatalysts such as 4,4'-dimethoxybenzophenone **6-11** are capable of deoxyfluorinating the anomeric centre of carbohydrates in the presence of $SF_6$ and ultraviolet light.[231]

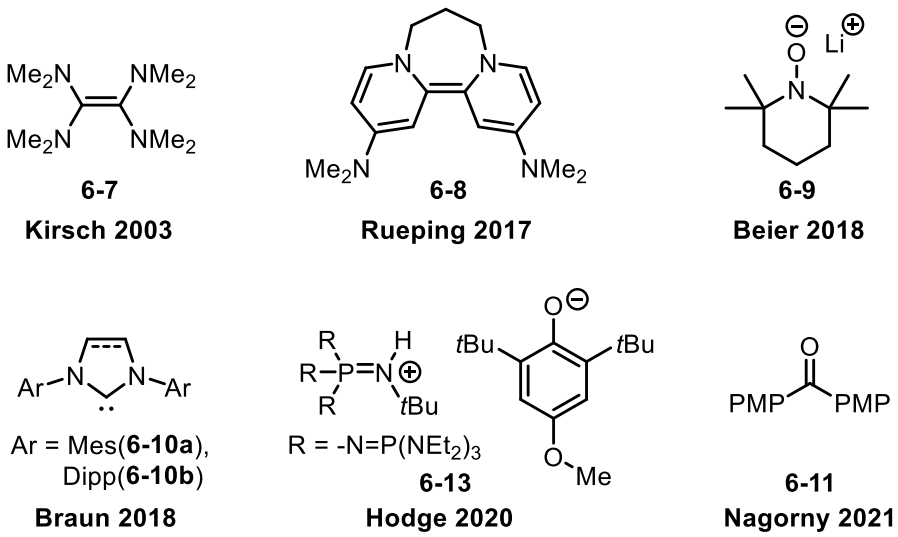


**Figure 6.2** Radical reagents capable of reacting with $SF_6$.

A unique example of reactivity with $SF_6$ was reported in a patent by Shigeyoshi in 2013, which uses simple alkyllithium reagents such as *tert*-butyl lithium, which was found to react with $SF_6$ at cold temperatures.[232] This represented the first example of nucleophilic $SF_6$ degradation, however few details were provided in the patent. The most significant advance in controlled organic reactivity with $SF_6$ was reported by Dielmann in 2018,[233] where superbasic phosphines were shown to react through a nucleophilic mechanism with $SF_6$ (**Scheme 6.2**). Prior to this work there were no reports of phosphines reacting with $SF_6$. Phosphine **6-12** was found to selectivity form a fluorophosphonium and pentafluorosulfanyl anion **6-18** when treated with $SF_6$ at low temperatures. This provided one of the few examples in which an $SF_5$ anion can be isolated and the first example of formation of the $SF_5$ anion from $SF_6$. The $SF_5$ anion produced from this reaction was bench stable and crystalline, providing a non-volatile product from $SF_6$ decomposition. Following this work, Hoge and co-workers reported that phenolate salts of phosphazene superbases **6-13** can react with $SF_6$ to undergo a two-electron transfer,[234] forming a salt complex with a pentafluorosulfanyl anion and fluoride anion. Overall, these results suggest simple

organic containing compounds can react with $SF_6$. However, all the various organic entities shown here require multistep synthesis, and in most cases, it is not apparent how the oxidized products could be reduced to close a catalytic cycle. Accordingly, searching for simpler or catalytic metal-free methods for $SF_6$ reduction remains a worthy goal.

## 6.2 Phosphide Mediated $SF_6$ Decomposition

### 6.2.1 Introduction

In the initial report by Dielmann et al.,[233] a variety of phosphines were examined for their reactivity with $SF_6$ (**Scheme 6.2**). This search involved highly basic trialkylphosphines. Trialkyl phosphines P(*n*-Bu)$_3$ **6-14** and P(*t*Bu)$_3$ **6-15** were examined, and no reactivity with $SF_6$ was observed, even at 150 °C for 21 h. When one of the alkyl groups was substituted with an imidazolin-2-imine group **6-16** under similar conditions of 150 °C for 29 h, quantitative consumption of the phosphine was observed with a 1:3 ratio of phosphine sulfide and difluorophosphorane products, reflecting the stoichiometry of $SF_6$.[233] The increase in donor ability and basicity of a phosphine by the addition of a strong imino donor was reported earlier by Dielmann et al in the context of $CO_2$ functionalization, allowing the phosphine to exhibit superbasic properties.[235] Organic superbases are described as compounds with a greater than or comparable basicity to a proton sponge, such as DMAN,[236] It is important to note that in this work, the basicity as well as the steric environment were vital to the selectivity observed in their optimal results.

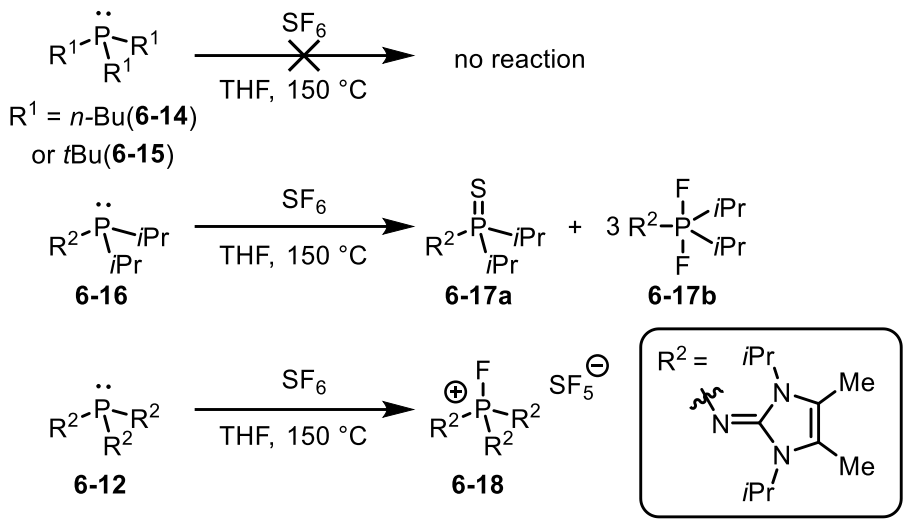


**Scheme 6.2** Superbasic phosphine reactivity with $SF_6$.

As described by Dielmann,[233] if a sufficient basicity threshold is reached, $SF_6$ reactivity can occur. This is evidenced by the reactivity of alkyl lithium reagents and superbasic phosphines. Diazaphospholenes **6-19** have been reported to exhibit strong hydridic and radical properties in a variety of transformations.[68,69,82,91,92] We hypothesized a diazaphospholene phosphide **6-20** might exhibit strong donor properties similar-to Dielmann's superbases as the protic form of these complexes are already highly nucleophilic. In some instances, diazaphospholenes have formed stable metal complexes, which initially appear to resemble phosphides[73] but instead electronically resemble phosphenium complexes coordinated to a metal. In an effort to prepare a highly basic diazaphosphophide, we sought to deprotonate a diazaphospholene hydride.

### 6.2.2 Results and Discussion

In an initial experiment, treatment of diazaphospholene **6-19** with benzyl potassium rapidly turned the solution dark (**Scheme 6.3**). When examined by $^{31}P$ NMR the solution contained new phosphorus signals at 94.8, 79.8 (**6-21**), and -95 ppm. Treatment of this solution with $SF_6$ at room temperature resulted in the formation of new compounds by $^{31}P$

NMR, of which the fluorodiazaphospholene **6-22** was present. In an effort to prepare a single phosphide product, diazaphospholene **6-19** was treated with *n*-butyllithium in pentane and was also exposed to $SF_6$ gas and found to react, producing a multitude of compounds. Isolation of potassium phosphide **6-20** was attempted but the crude solid was found to be an energetic material, undergoing a vigorous/explosive decomposition on a filter frit in the glovebox. Accordingly, this compound was not further investigated.

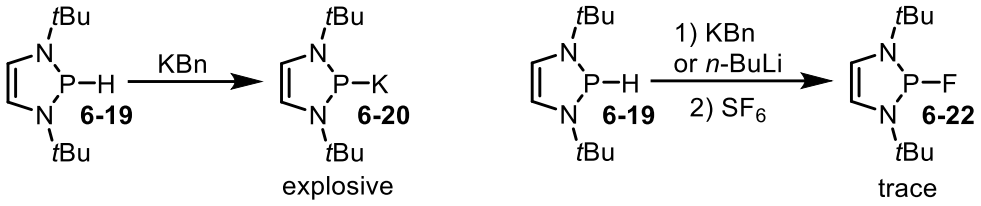


**Scheme 6.3** Generation of diazaphosphophide **6-20** and subsequent reactivity with $SF_6$.

To tame the reactivity of these phosphides, the borane adduct **6-23** of diazaphospholene was then explored in this chemistry. The purpose of the borane adduct is to reduce the basicity and increase the steric bulk to potentially allow a cleaner defluorination process. In, addition some of the side products from the initial reactions may be from multiple deprotonations or ring opening. The borane adduct will increase the acidity of the phosphine potentially allowing for more selective deprotonation. Upon treatment of diazaphospholene **6-19** with a borane dimethylsulfide solution, a new borane-adduct **6-23** formed as indicated in the $^{31}P$ and $^{11}B$ NMR data. Treatment of this solution with *n*-butyllithium produced a singular product **6-24** at 143 ppm. Treatment of this solution with $SF_6$ resulted in multiple peaks in $^{31}P$ NMR spectrum. Among the products, the diazaphospholene dimer **6-21** was observed. Given the difficulties in deprotonating the diazaphospholene, we did not investigate anions of this system further. However, this work hinted that simple basic phosphines in the form of phosphides may react with $SF_6$.

In an effort to find simpler reagents for $SF_6$ degradation, and to explore the reaction space of phosphorus containing species with $SF_6$ gas further, we investigated the application of simple disubstituted phosphides, bearing carbon substituents rather than nitrogen (**Scheme 6.4**). Potassium diphenylphosphide **6-25** is a commercially available reagent which can be purchased as a 0.5 M solution in THF. This reagent exhibits a strong orange/red color in solution, which serves as a good indicator for the presence of this compound. Recently Stephan et al have reported that phosphides can activate small molecules such as hydrogen gas.[237] When $SF_6$ gas was bubbled through a dilute solution of this phosphide **6-25**, the solution rapidly turned from orange to a clear/yellow color. A major product formed at -15.6 ppm in the $^{31}P$ NMR spectrum, which is consistent with the presence of tetraphenyldiphosphine **6-26**.[238] This result indicated that a reaction occurred with $SF_6$. We hypothesized that a nucleophilic mechanism might be occurring in which fluorodiphenylphosphine **6-27** is generated and then an additional equivalence of phosphide **6-25** rapidly reacts with this product to form the dimer. Alternatively, the fluorodiphenylphosphine **6-27** can react with itself to from the dimer **6-26** as well as fluorophosphorane **6-28**.[239] Since the fluorophosphorane **6-28** was not observed in the $^{31}P$ NMR analysis it can be speculated that the first mechanism is likely occurring, but further investigation will be required. Alternatively, phosphinyl radicals could be abstracting a fluorine which would generate the same end products in the reaction.[240,241]

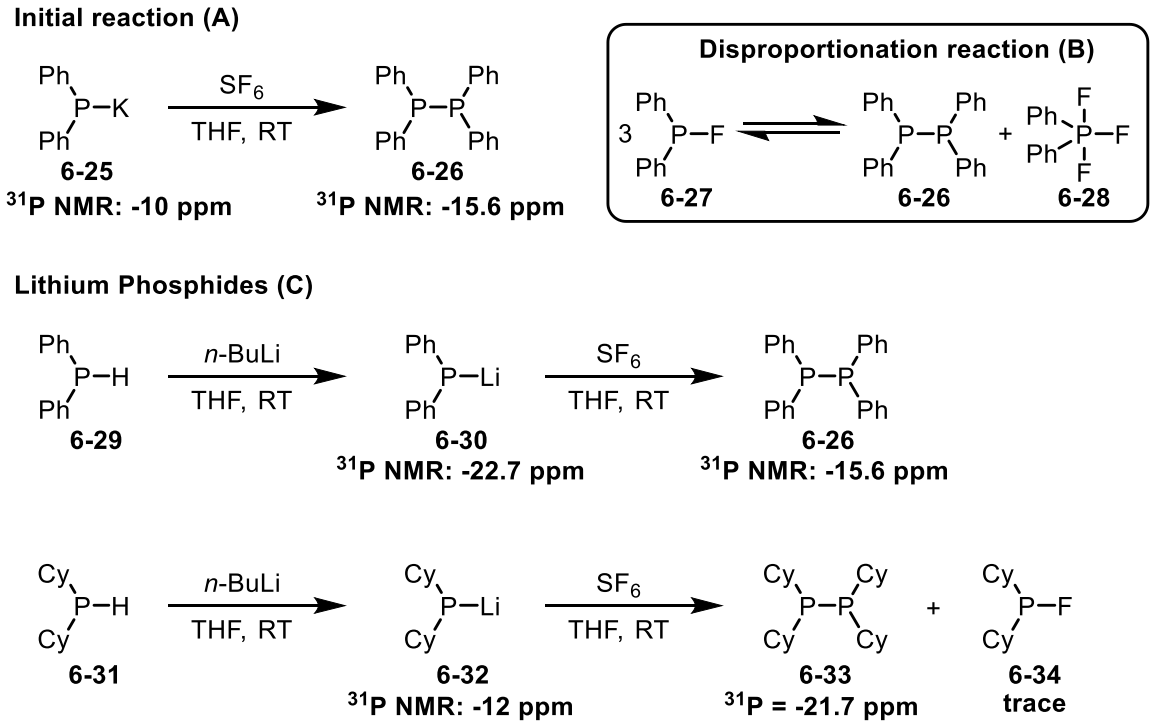


**Scheme 6.4** (**A**) Initial reaction of potassium diphenylphosphide and $SF_6$. (**B**) Potential disproportionation reaction of fluorodiphenylphosphine. (**C**) Reaction of lithium diphenylphosphides with $SF_6$.

In an analogous manner to the deprotonation of diazaphospholenes, *n*-butyllithium was used as base to determine if lithium phosphides exhibit similar reactivity (**Scheme 6.4**). Treatment of diphenylphosphine **6-29** with *n*-butyllithium at room temperature produced a single product **6-30** at -22.7 ppm in the $^{31}$P NMR spectrum. This solution was then bubbled with $SF_6$ gas and found to decolorize in a similar manner to the potassium salt. Analysis of the $^{31}$P NMR spectrum indicated that once again tetraphenyldiphosphine **6-26** formed relatively cleanly.[238] These results indicate that the reactivity between potassium and lithium phosphides is similar, allowing for the generation of phosphides *in situ* from secondary phosphines using *n*-butyllithium. Minor impurities were noted in these reactions and found to be a mixture of phosphine sulfides.[242,243]

Alkyl substituted phosphides were then investigated in their reactivity with $SF_6$ gas (**Scheme 6.4**). Lithium dicyclohexylphosphide **6-32** was generated with *n*-butylithium and treated with $SF_6$ gas. The reaction once again produced a dimeric phosphorus species **6-33** as the main product[238] with a variety of impurities present in trace amounts in the $^{31}P$ NMR spectrum. One of the impurities was found to contain fluorine **6-34** which would support the nucleophilic mechanism. Cooling the reaction to -15 °C did not improve the yield of this product.

To determine the fate of fluorine and sulfur, the reaction of **6-25** and **6-30** was scaled up to 0.25 mmol and the residue was separated with a mixture of DCM and water. Analysis of the aqueous solution $^{19}F$ NMR spectrum indicated the presence of fluoride salts. The presence of sulfides were determined with a methylene blue test.[244] This chemical test will form the common dye methylene blue if sulfide is present. The aqueous solution was treated with a solution of *N*,*N*-dimethylphenylenediamine and a separate solution of ferric chloride both in 6M HCl. The vibrant blue of methylene blue was observed from an aqueous extract of both a potassium and lithium phosphide after approximately 1 h.

While we hypothesized the intermediacy of fluorophosphines, it was unclear from the current results if this intermediate was forming, thus other phosphides with potentially larger steric bulk may be required to stabilize such an intermediate. This was also observed in Dielmann's report with superbasic phosphines where steric bulk allowed for a more selective reaction.[233] In addition, sterically demanding fluorophosphines such a di-*tert*-butylfluorophosphine **6-35**, fluorophosphaadamantane **6-36** and fluorophobanes have been reported to not disproportionate as readily compared to other, smaller, reported fluorophosphines.[245] Deprotonation was attempted with di-*tert*-butylphosphine **6-38** but was unsuccessful at room temperature. Cooling of the reaction mixture prior to

deprotonation allowed for clean deprotonation of the phosphine **6-38** to form **6-39** in 1 h.[246] When treated with $SF_6$ gas three distinct products formed, which were observed in the $^{31}P$ NMR spectrum (**Scheme 6.5**). These products were determined to be the fluoroditertbutylphosphine **6-35**,[245] diphosphanylsulfane **6-40**,[247] and the dimer **6-41**.[238] The presence of both the fluorophosphine **6-35** and diphosphanylsulfane **6-40** support the phosphide mediated decomposition of $SF_6$ and intermediacy of fluorophosphines. The presence of the diphosphanylsulfane **6-40** further supports the complete decomposition of $SF_6$ with reduction of sulfur to the -2 oxidation state.

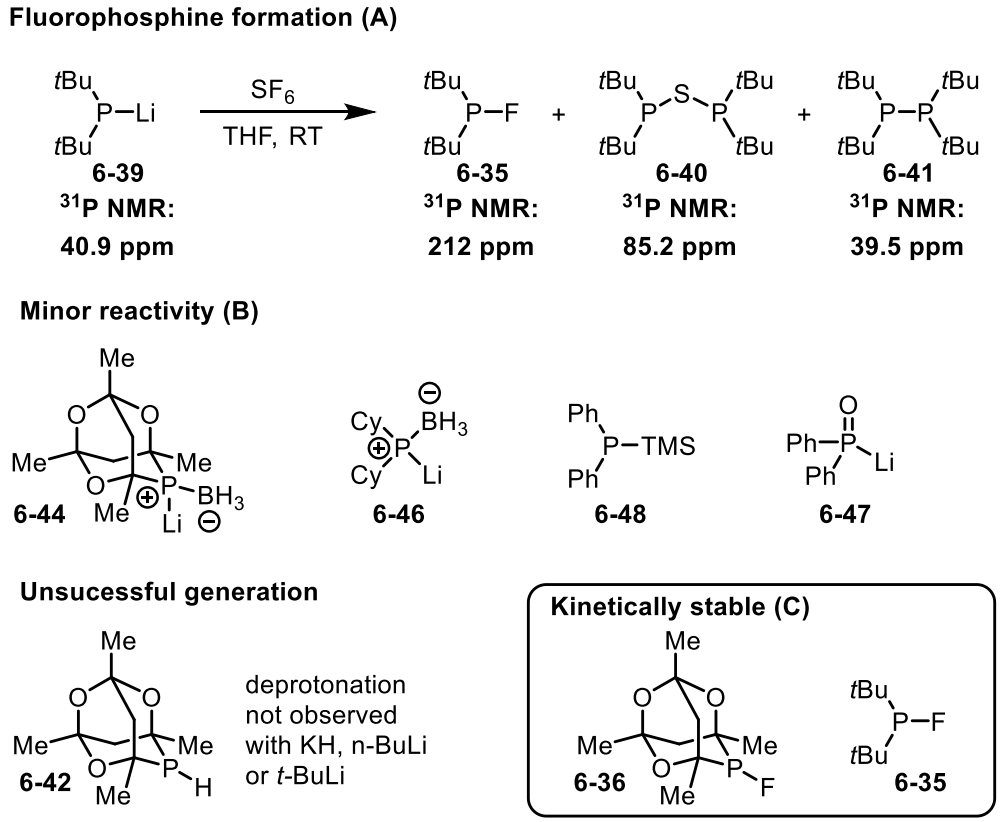


**Scheme 6.5** (**A**) Sterically demanding di-*tert*-butylphosphide reaction with $SF_6$. (**B**) Phosphides with little to no reactivity with $SF_6$. (**C**) Stable fluorophosphines.

Successful formation of a fluorophosphine when using a more sterically demanding phosphine prompted the investigation of cage phos **6-42** in $SF_6$ reactivity (**Scheme 6.5**).

Deprotonation of phosphine **6-42** was attempted using a variety of bases, shown in scheme **Scheme 6.5**. In some instances, such as the treatment of phosphine **6-42** with KH resulted in a precipitate which formed slowly over time. However, this product did not react with $SF_6$ even when stirred overnight. Deprotonating of phosphine **6-42** has only been reported as the borane adduct **6-43**,[248] so this phosphine was treated with a solution of borane dimethylsulfide, which produced a doublet at 0.36 ppm in the $^{31}P$ NMR spectrum. Treatment of this solution with *n*-butyllithium produced a new product **6-44** at -32.6 ppm in the $^{31}P$ NMR spectrum which was compared with literature data. Bubbling of $SF_6$ gas through the reaction mixture did not result in any significant change in the NMR spectrum. To determine if the lack of reactivity was due to the unique structure of **6-42**, or attenuation of the reactivity by the borane, dicyclohexylphosphine was treated using the same strategy of borane addition and deprotonation. While the uncomplexed phosphide reacted with $SF_6$, the borane adduct **6-45** showed no reactivity with $SF_6$ once deprotonated to the phosphide borane adduct **6-46**, indicating that significant electron density on the phosphorus may be important to the reactivity of the phosphides. This was supported further by the deprotonation of diphenyl phosphine oxide with either *n*-butyllithium or KH, producing an anion **6-47** which did not react with $SF_6$ gas.

Preparation of $SF_5$ salts is challenging, with most methods requiring the reaction of fluorides with highly toxic $SF_4$ gas and use of elaborate countercations to stabilize the anion.[249] The rapid reactivity of these phosphides and the indication of a nucleophilic mechanism may allow for the facile preparation of an $SF_5$ anion salt. A stable complex of $SF_5^-$ was prepared recently as the cesium salt with glyme coordinated to the cesium for stabilization.[249] In the reactions conducted thus far in this chapter, only lithium and potassium salts have been investigated. To first investigate the reactivity of cesium

phosphides, trimethylsilyl diphenylphosphine **6-48** was examined. This reagent was found to have no reactivity with $SF_6$ gas and therefore if the cesium salt formed would be able to be tested for reactivity. Treatment of this phosphine **6-48** with cesium fluoride resulted in only the formation of the dimer **6-26** and selective phosphide formation was not observed. In another attempt to generate a cesium complex, potassium diphenylphosphide **6-25** was stirred with cesium carbonate, which formed a new peak at -7.5 ppm in the $^{31}P$ NMR spectrum. When treated with $SF_6$ gas, the cesium complex **6-49** was found to display similar reactivity to the lithium and potassium salts, and no $SF_5$ anion was observed.

The reactivity of lithium Di-*tert*-butylphosphide **6-39** was found to be more selective in comparison to the other phosphides examined, so we hypothesized it may be the better reagent to obtain the fragile $SF_5$ anion. Therefore, this phosphide **6-39** was also explored to determine if $SF_5$ anions could be generated using this method. The lithium phosphide **6-39** was first generated and then this solution was treated with cesium fluoride, which produced a new compound **6-50** at 70.6 ppm in the $^{31}P$ NMR. This solution was then bubbled with $SF_6$ gas, but was found to exhibit similar reactivity to the lithium salt **6-39**. The process was then repeated with the addition of glyme to the solution, before $SF_6$ addition. While the glyme greatly shifted the signal of the phosphide as indicated in the $^{31}P$ NMR spectrum, the reactivity of this solution was not greatly changed. The only difference between the reaction with and without glyme was the absence of the signal for the di-*tert*-butylfluorophosphine **6-35** in the $^{31}P$ NMR spectrum. The absence of this signal is potentially due to the trace presence of water which is supported by a new chemical shift at 165 ppm in the $^{31}P$ NMR spectrum. In addition, no amount of $SF_5$ anion was observed in the $^{19}F$ NMR spectrum from these reactions. With no indication for the capture of an $SF_5$ anion, reactivity with cesium salts was not investigated further.

### 6.2.3 Conclusion

The reactivity of phosphides with $SF_6$ represents a facile method using commercially available reagents to decompose $SF_6$ in a stoichiometric fashion. The ability of these reagents to react at room temperature within seconds and without the need of light provides a milder method compared to previously reported examples. Previous examples involving phosphorus mediated decomposition of $SF_6$ have required lengthy syntheses[233] or harsh conditions while this method requires little to no preparatory work and is tolerant of both aryl and alkyl substituents. The reactivity of these compounds also further explores and clarifies the requirements for reactivity with $SF_6$. While these compounds were not suitable for the preparation of pentafluorosulfanyl anions, further investigation into these reactions could be explored. Overall, these findings prompted the exploration for other potential phosphine reagents that may be capable of reacting with $SF_6$.

## 6.3 Diazaphospholene Mediated $SF_6$ Decomposition

### 6.3.1 Introduction

Diazaphospholenes have recently emerged as highly active reduction catalysts. As stated in Chapter 1, their ability to act as a strong hydride donors in a variety of systems is enabled by the strong resonance contribution of formation of an aromatic system in cationic form.[75] In a similar set of compounds, diazaphospholene dimers display radical character,[89,91,92] and have been reported to undergo radical additions to compounds such as diphenylacetylene.[95] While current studies suggest the dissociation of these dimers to radicals is low under standard conditions, the potential for radical reactivity is possible as evidenced by the reduction of group 10 metals.[96] In addition, Masuda recently reported the radical reactivity of saturated diphosphines with heteroallenes.[97] Currently, the mildest methods of $SF_6$ decomposition rely on the reaction of single or two electron donors, such

as Rueping's work.[228] With the potential for radical based reactivity in diazaphospholenes, we sought to investigate the application of diazaphospholene dimers and other diazaphospholene species to $SF_6$ reactivity.

### 6.3.2 Diazaphospholene Dimer Reactivity

Previously, diazaphospholene dimers **6-21** have been prepared from the corresponding diazaphospholene chlorides through a magnesium reduction.[81] It was found that treatment of the diazaphospholene bromide **6-51** with magnesium turnings can also afford the diazaphospholene dimer **6-21** in approximately 4 h on a large scale.[250] In an initial test, diazaphospholene dimer **6-21** was dissolved in either THF or Benzene-$d_6$ and $SF_6$ was bubbled through in a similar manner to the phosphide experiments in **6.2.2**. Three main products were generated from the addition of $SF_6$ and two were identified as the diazaphospholene fluoride **6-22** and oxide **6-52**, which the latter presumably formed from moisture entering during the addition of the gas (**Scheme 6.6**). To confirm the presence of diazaphospholene fluoride **6-22**, an authentic sample of this compound was separately prepared. Diazaphospholene fluoride **6-22** was initially synthesized by Gudat involving a multi-day metathesis process with silver fluoride,[251] which is poorly soluble in solvents such as THF or acetonitrile. It was found that highly-soluble tetramethylammonium fluoride allows for clean formation of the diazaphospholene fluoride **6-22** in a few minutes. The additional product formed form the $SF_6$ reaction at 64 ppm in the $^{31}P$ NMR spectrum was identified as the diazaphospholene fluorosulfide **6-53**. This compound was confirmed by the addition of the sulfur-transfer reagent S-42 to a sample of diazaphospholene fluoride **6-22** (**Scheme 6.6**), and observed through NMR analysis and X-ray crystallography (**Figure 6.3**). The formation of this product **6-53** indicates that $SF_6$ is reduced to a -2 oxidation state from its original +6 oxidation state.

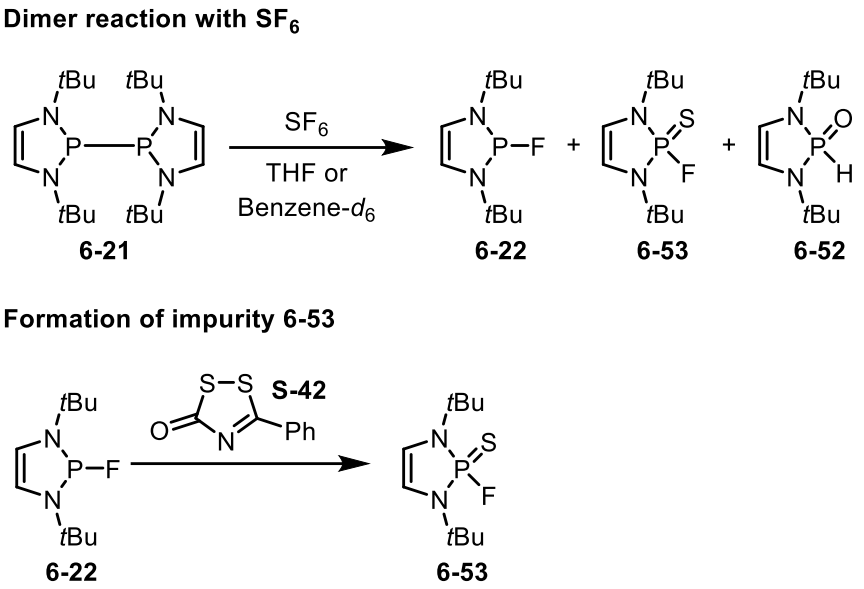


**Scheme 6.6** Diazaphospholene dimer reactivity with $SF_6$ and formation of impurity **6-53**.

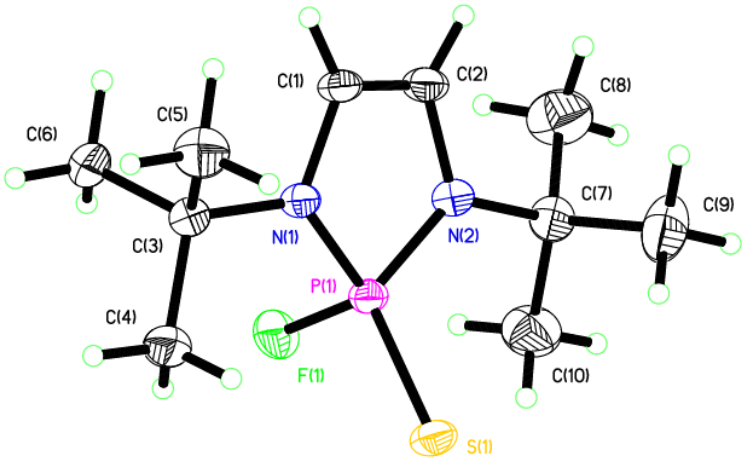


**Figure 6.3** The structure of **6-53**. Thermal ellipsoids have been drawn at the 50% probability level. Hydrogen atoms have not been labelled.

The useage light iradiation to alter the reactivity in diazaphospholene chemistry is highlighted in a report by Gudat on dehydrocoupling of diazaphospholene hydrides.[90] It was found that irradiation of the dimer in either THF or Benzene-$d_6$ allowed for full consumption of the dimer **6-21** and a formation of similar product distribution to the ambient conditions. The formation of product **6-53** in both the ambient and light accelerated reactions pose a two-fold challenge. The first of which is that this is a potentially toxic

compound as it bears resemblance to cholinesterase inhibitors. Secondly, if this reaction is to be made catalytic, the entrapment of sulfur on the diazaphospholene will eventually consume all of the diazaphospholene, preventing potential regeneration of the dimer **6-21**. Braun reported in 2018 that sulfur entrapment in $SF_6$ reductions can be facilitated by trialkylphosphines (**Scheme 6.7**).[219] To this end, tricyclohexylphosphine **6-54** and triphenylphosphine **6-55** were added in a 2:1 ratio in relation to the dimer **6-21**. Samples were irradiated for 30 min and then analyzed (**Scheme 6.7**). Sulfur capture was low in both instances with a 1:2.5 sulfide **6-56** to phosphine **6-54** ratio for tricyclohexylphosphine and a 1:4 ratio for triphenylphosphine sulfide **6-58** to triphenylphosphine **6-55**. The apparent low rate of capture of sulfur in both tests indicates the reaction is too fast for complete sulfur capture, which was also evidenced by the formation of fluorosulfide **6-53**. This also indicates that the reaction is not selective for the trisubstituted phosphines due to the rapid reactivity.

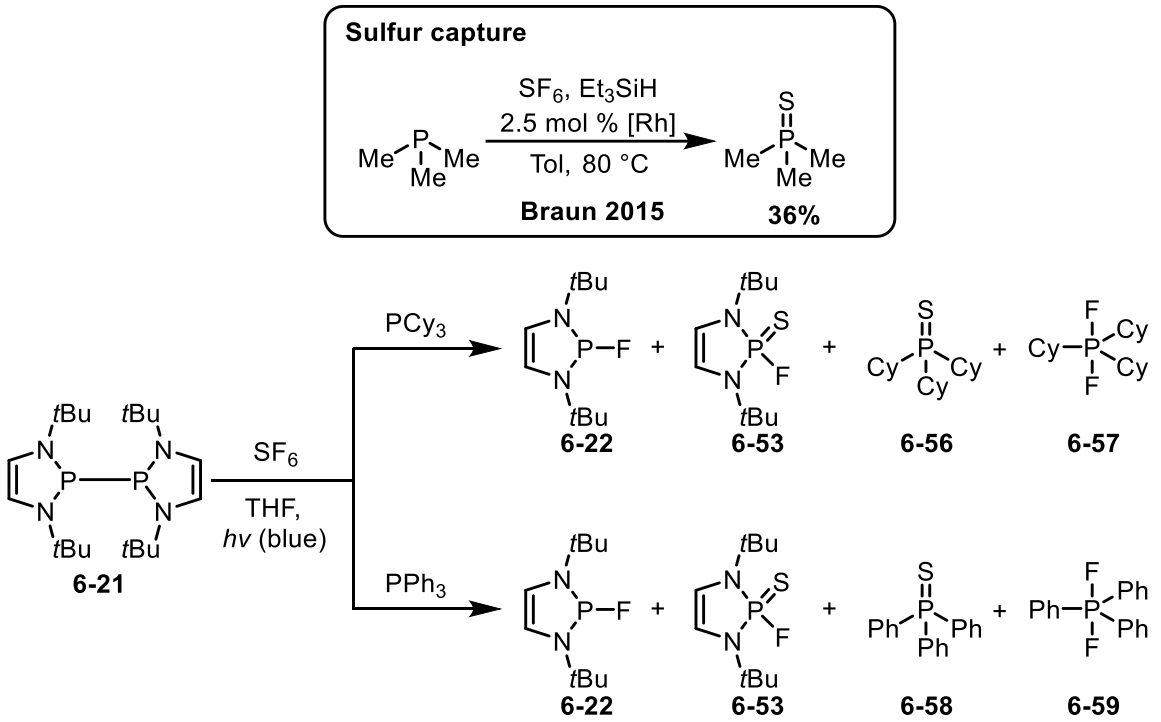


**Scheme 6.7** Sulfur capture attempts during dimer **6-21** reaction with $SF_6$.

While sulfur capture was modest in the initial tests, the potential for catalytic turnover is possible, as the majority of diazaphospholene fluoride **6-22** was still present. Regeneration of the dimer **6-21** from the diazaphospholene fluoride **6-22** was attempted using magnesium, similarly to the methods of diazaphospholene dimer **6-21** formation involving reduction of a diazaphospholene chloride or bromide. Formation of the dimer **6-21** was not observed, indicating that the diazaphospholene fluoride **6-22** has different reactivity, and is not viable for turnover in this method. To allow for formation of the dimer **6-21**, it was found that treatment of the fluoride **6-22** with dimethylchlorosilane generated the diazaphospholene chloride **6-60** *in situ*. This then reacted with the magnesium to form dimer **6-21** (**Scheme 6.8**). A reaction was then conducted at a 10 mol % loading of dimer **6-21** gave a conversion of approximately 2:1 sulfide **6-56** to product **6-54** by $^{31}P$ NMR. The reaction was further optimized using the diazaphospholene bromide **6-51** as the pre-

catalyst, which will become the dimer **6-21** upon addition of magnesium. The optimal conditions were found to be a 2.5 mol % loading of **6-51** when left overnight (**Scheme 6.9**). This afforded the sulfide **6-56** as the major product with only trace impurities in $^{31}$P NMR spectrum. However, during the course of this reaction optimization, a control reaction with removal of the diazaphospholene **6-51** showed full conversion to the sulfide **6-56** (**Scheme 6.9**). This revealed the catalyst was not necessary in the magnesium reaction, despite clear evidence the diazaphospholene was engaging with $SF_6$. Reactivity of $SF_6$ with magnesium in this capacity at room temperature has not been reported and is further investigated in section 6.4. Meanwhile, the investigation of the diazaphospholene reactivity with $SF_6$ was continued.

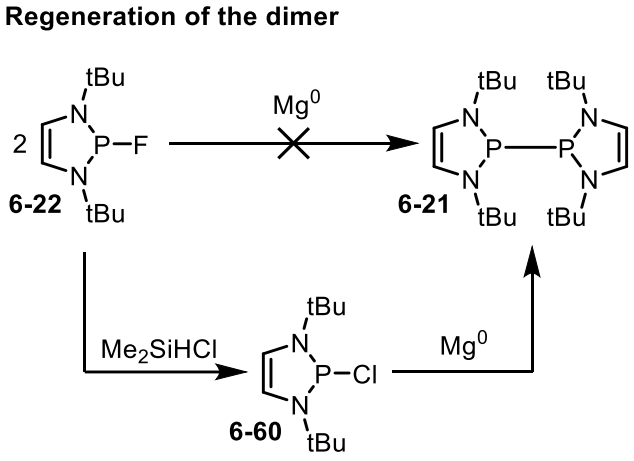


**Scheme 6.8** Formation of the dimer **6-21** via the addition of dimethylchlorosilane to magnesium metal.

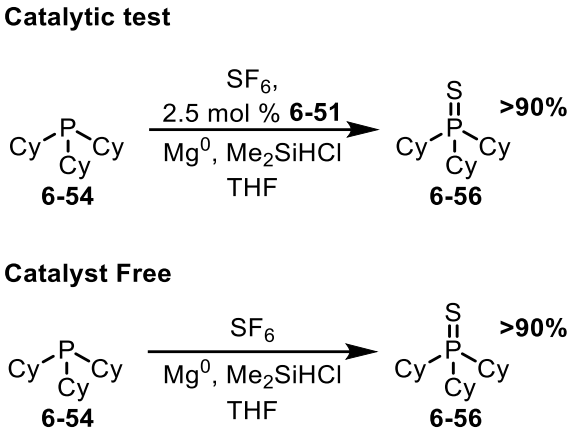


**Scheme 6.9** Catalytic reduction of $SF_6$ with **6-51** and magnesium metal as well as a control reaction.

### 6.3.3 Diazaphospholene Hydride Reactivity

The lack of available methods for regeneration of the diazaphospholene dimer **6-21** from the reaction products, as well as the inability to stop the formation of fluorosulfide **6-53** complicates use of the dimer **6-21** in catalysis. What we initially presumed to be catalysis was actually due to the magnesium reacting with $SF_6$. Notwithstanding this result, the isolated dimer **6-21** did exhibit reactivity with $SF_6$ in the absence of magnesium. However, diazaphospholene hydrides **6-19** are also capable of exhibiting radical reactivity as described in chapter 7, as well as other reports described in the literature.[91,92] Accordingly, it was decided to investigate the reactivity of the diazaphospholene hydride **6-19** with $SF_6$. Initial reactions involving the addition of $SF_6$ to diazaphospholene hydride **6-19** showed no reactivity when conducted in aromatic solvents. When THF was examined as the solvent, trace amount of diazaphospholene fluoride **6-22** was observed over several hours. This sample was exposed to direct sunlight and precipitates rapidly formed along with full consumption of the diazaphospholene hydride **6-19**, with the major product as the diazaphospholene fluoride **6-22**. Irradiation of the sample proved to greatly affect the reactivity of the diazaphospholene with $SF_6$.

**Table 6.1** Comparison of dark vs light reactivity of diazaphospholene **6-19** with $SF_6$. Percent conversion was measured as a relative proportion of hydride **6-19** to fluoride **6-22**.

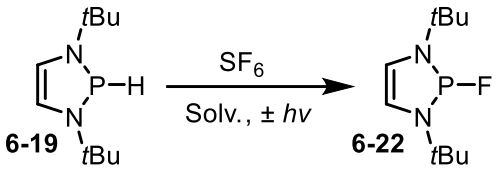


| Entry | Solvent | Time | No Light | Light |
|---|---|---|---|---|
| 1 | Benzene | 30 min | 0% | 7.4% |
| 2 | THF | 30 min | 3.6% | 7.9% |
| 3 | THF | 1h | N/A | 26% |
| 4 | Acetonitrile | 30 min | 100% | 100% |

To understand the effect of light and solvent on this reaction, 3 solvents (**Table 6.1**) were chosen, and samples were left in the absence of light or exposed to a Kessil tuna blue LED (463 nm). Astonishingly, acetonitrile showed full conversion to diazaphospholene fluoride **6-22** in the absence of light while THF and benzene provided similar levels of conversion to one another in the presence of light and THF displayed trace conversion in the absence of light. While light irradiation is required for the hydride **6-19**, unlike the diazaphospholene dimer **6-21**, proceeding through a hydride-based mechanism is attractive, given the ability to regenerate the hydride **6-19** from the fluoride **6-22** through multiple methods. To this end, a variety of hydride sources were screened. Treatment of the diazaphospholene fluoride with the hydride sources is detailed in figure (**Scheme 6.10**). Phenylsilane and pinacolborane proved to be the most effective at generating the hydride.

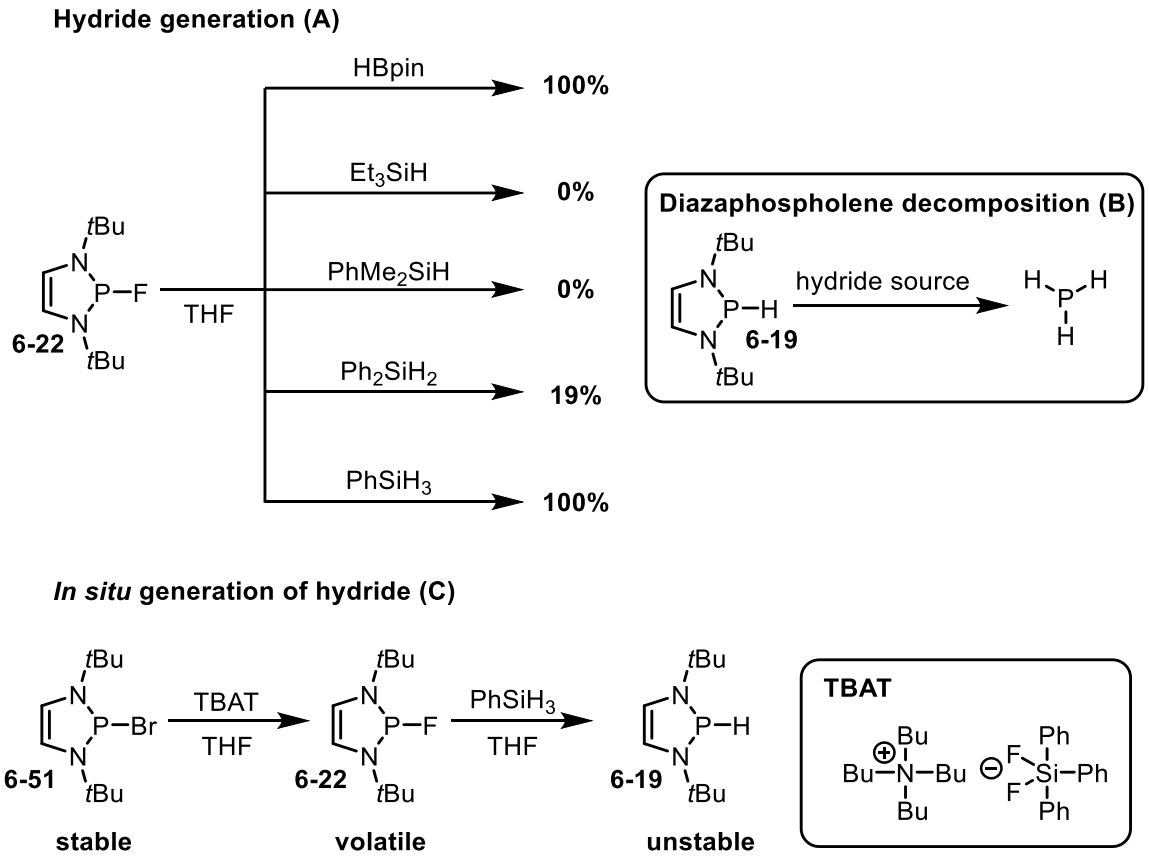


**Scheme 6.10** (**A**) Generation of the diazaphospholene hydride from multiple sources and the subsequently measured formation of hydride after 15 min by $^{31}$P NMR. (**B**) Potential decomposition product from hydride addition. (**C**) *In situ* generation of the hydride from **6-51**.

Preparation and isolation of the diazaphospholene hydride **6-19** is typically accomplished through reduction of a diazaphospholene halide with an aluminum hydride,[75,83] and isolation is challenging and low yielding due to the volatility and sensitivity of the hydride. Because of the difficulty of accessing pure hydride **6-19**, a precatalyst strategy is often used in diazaphospholene catalysis. Ideally a precatalyst is more stable and isolable than the parent hydride **6-19** but, can be converted into the hydride **6-19** *in situ*. In this instance the diazaphospholene fluoride **6-22** would be suitable, as this compound is a stable solid. However, the yield for the preparation of the isolated fluoride **6-22** is not optimal and the crude product must be sublimed in order to remove oxide **6-52**

impurities. To avoid the low yields and unstable reagents it was found that treatment of the diazaphospholene bromide **6-51** with TBAT allowed for rapid generation of the fluoride **6-22** *in situ*. Following the addition of TBAT, treatment of the solution with a hydride source such as phenylsilane or pinacolborane provided clean generation of the hydride **6-19**. The overall benefit of this system is that the diazaphospholene bromide **6-51** is highly stable under a dry atmosphere, and can be prepared in two steps in high yield and purity on a multi-gram scale.

The slower reactivity of the diazaphospholene hydride **6-19** compared to the dimer **6-21** may allow for a more selective reaction, allowing for the trisubstituted phosphine to capture sulfur. Treatment of the diazaphospholene hydride **6-19** with tricyclohexylphosphine **6-54** was conducted. In a 1:1 reaction of hydride **6-19** to phosphine **6-54,** approximately 10% of the phosphine was converted to the sulfide **6-56**. The fluorosulfide **6-53** was only observed when the amount of hydride **6-19** was increased to a 6:1 ratio, which will only be present near the end of a catalytic reaction. The ability for selective sulfur capture and the use of hydride sources for regeneration of the catalyst allows this system to potentially operate under catalytic conditions. An initial reaction involving a 1:6 ratio of hydride **6-19** to phosphine **6-54** was conducted in an NMR tube exposed to blue light. Only 5% conversion to **6-54** was observed during this time frame. This was initially confusing, since each step of the putative catalytic cycle had been separately validated. To understand the low conversion to **6-54** in this reaction, the role of the products of the $SF_6$ reduction must be considered, as these compounds could be interfering with the catalysis. During this transformation, the hydride of the diazaphospholene **6-19** presumably forms HF during the reaction. While HF is not observed directly, it could be consuming the catalyst or silane or inhibiting the reaction in some way.

To determine if HF is generated from this reaction, Fluolead, a trifluorosulfur reagent, was treated with 2 equivalences of diazaphospholene **6-19**. HF was not observed in the $^{19}F$ NMR spectrum. The process was repeated with 10 equivalents of triethylamine and a sharp peak was observed at -156 ppm in the $^{19}F$ NMR spectrum (**Scheme 6.11**). The chemical shift of this peak is similar to that of triethylamine trihydrofluoride complex (TREAT-HF) which was confirmed by adding additional TREAT-HF to the sample, resulting in an increase in signal intensity. The conformation of formation of HF from the reaction of a fluorosulfur species and a diazaphospholene further supports that HF may be the cause of low conversion. The catalytic transformation was then repeated with the addition of approximately 9 equivalents of triethylamine. Gratifyingly a 28% conversion to **6-56** was observed in the same timeframe as the reaction without triethylamine. Differing reaction times and light sources were screened as highlighted in **Table 6.2**. In all instances tricyclohexylphosphine was not fully consumed since the amount of $SF_6$ in the NMR tube had become the limiting reagent.

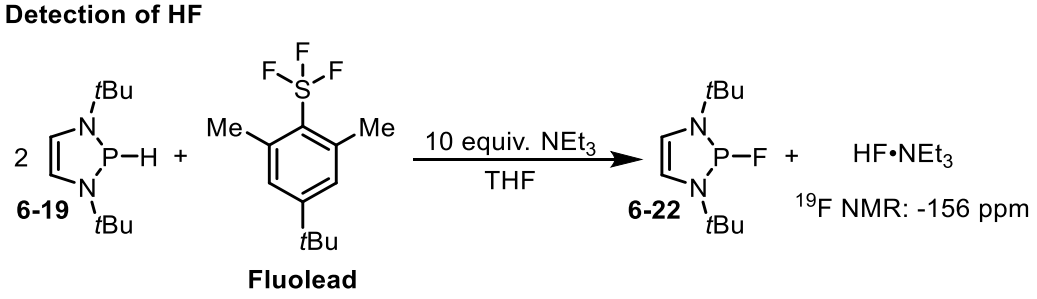


**Scheme 6.11** Detection of HF from the addition of Fluolead to diazaphospholene **6-19**.

**Table 6.2** NMR scale catalytic tests. Amounts of **6-54** and **6-56** determined by $^{31}$P NMR. Entry 1 was conducted without the addition of triethylamine. All other reactions contained approximately 9 equivalents of triethylamine.

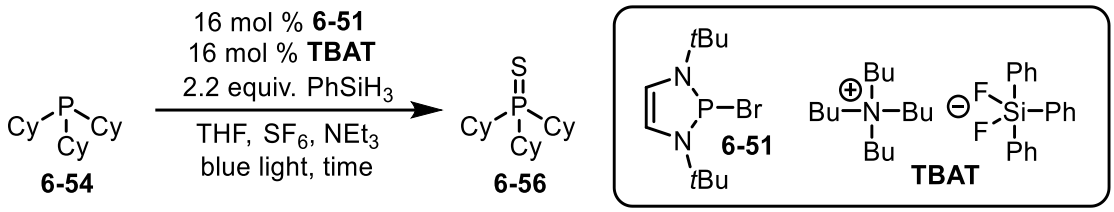


| Entry | Light | Time | **6-54** | **6-56** |
|---|---|---|---|---|
| 1* | Blue | 4h | 20 | 1 |
| 2 | Blue | 4h | 2.6 | 1 |
| 3 | Blue | 6h | 1.7 | 1 |
| 4 | UV | 4h | 1.5 | 1 |
| 5 | UV | 2h | 2.8 | 1 |

In the initial catalytic screening, the NMR tubes used for the reactions did not allow for enough $SF_6$ to be present for complete consumption of the phosphine. In addition, the borosilicate glass may limit the light permeating the glass depending on the frequency of light source. Thus 45 mL quartz tubes were selected for their UV transmission and larger volume for $SF_6$ gas. The effect of amine concentration was first determined before further optimization of the reaction conditions (**Table 6.3**). With a loading of 5 mol% of diazaphospholene **6-51**, it was found that the optimal amount of triethylamine was 30 equivalents on this scale (**Entry 2, Table 6.3**), providing high conversion to the phosphine sulfide **6-56**. Additionally, it was found that the triethylamine also served to activate the catalyst directly from the bromide **6-51**. The addition of a hydride source to a diazaphospholene bromide **6-51** does not generate any detectible amount of diazaphospholene hydride **6-19** in 1 h. However, the addition of triethylamine to these conditions resulted in hydride **6-19** formation when multiple hydride sources were

examined. A reaction was then conducted at 5 mol % diazaphospholene **6-51** loading without triethylamine or TBAT was found to produce only 10% conversion to the sulfide **6-56** (**Entry 6, Table 6.3**). The reaction was then repeated with 30 equivalents of triethylamine and the reaction once again went to high conversion to **6-56** (**Entry 5, Table 6.3**). This finding allowed for the removal of TBAT from the reaction mixture, reducing the overall complexity of the reaction mixture, as well as eliminating an expensive reagent.

**Table 6.3** Determination of the optimal amount of triethylamine. Amounts of **6-54** and **6-56** determined by $^{31}$P NMR.

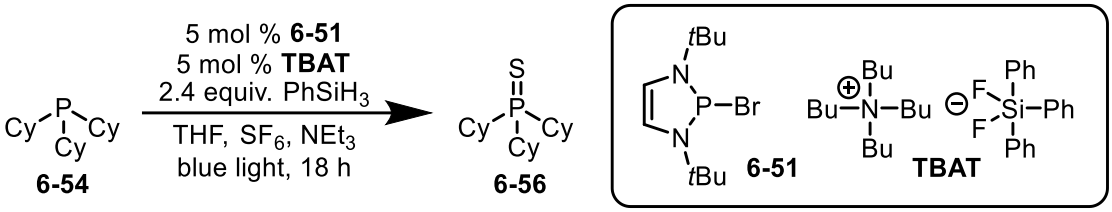


| Entry | TBAT | Equiv. $NEt_3$ | **6-54** | **6-56** |
|---|---|---|---|---|
| 1 | Y | 60 | 0 | 1 |
| 2 | Y | 30 | 0.03 | 1 |
| 3 | Y | 20 | 0.1 | 1 |
| 4 | Y | 8.6 | 0.98 | 1 |
| 5 | N | 30 | 0 | 1 |
| 6 | N | 0 | 7.85 | 1 |

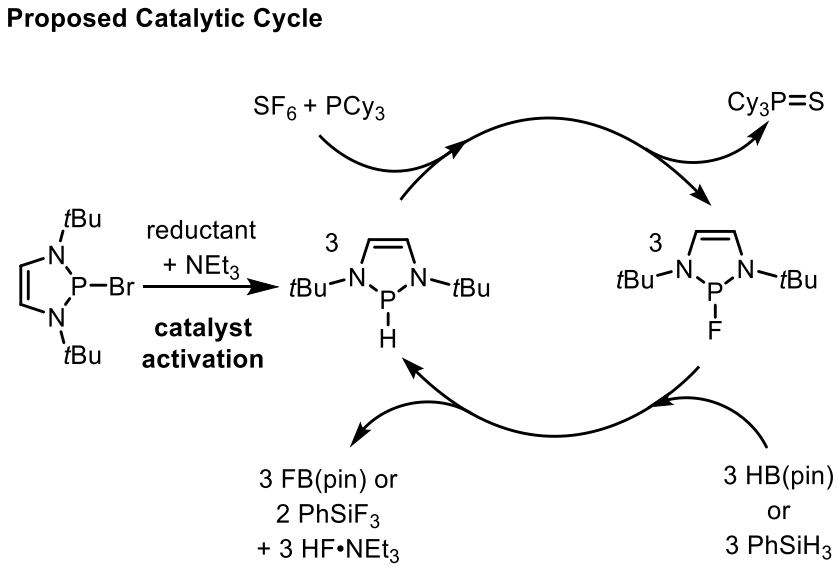


**Scheme 6.12** Proposed catalytic cycle for the diazaphospholene-mediated reduction of SF6.

As seen in **Scheme 6.12** if a diazaphospholene hydride is present the reduction should occur. All reactions conducted thus far have involved the use of diazaphospholene bromide **6-51**. To explore the electronic and steric effects of the diazaphospholene on the reaction, a variety of diazaphospholene derivatives were screened (**Table 6.4**). Increasing the steric bulk of the catalyst with adamantyl groups provided little to no change in the reactivity (**Entry 2, Table 6.4**), indicating that the reactive site is not being constrained in this system. Substitution of the alkylamino groups with mesityl greatly decreased the reaction rate as the overall conversion was reduced to only trace formation of the sulfide **6-56** (**Entry 3, Table 6.4**). Removal of the unsaturation from the backbone of the diazaphospholene also shut down reactivity (**Entry 4, Table 6.4**). The lack of substantial reactivity with the saturated catalyst **6-63** was expected, as the aromaticity of the system may play a large role in radical stability.[89] In addition, the hydride donor strength of the of the *N*-aryl diazaphospholenes and saturated diazaphospholenes is lower than

diazaphospholene **6-19**. Moving forward diazaphospholene **6-51** was only screened for further optimization.

**Table 6.4** Exploration of the electronic and steric affects in $SF_6$ decomposition. Amounts of **6-54** and **6-56** determined by $^{31}P$ NMR.

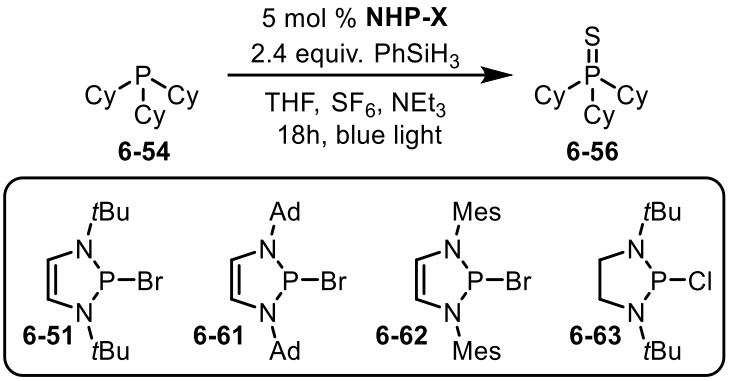


| Entry | Catalyst | TBAT | **6-54** | **6-56** |
|---|---|---|---|---|
| 1 | **6-51** | N | 0 | 1 |
| 2 | **6-61** | N | 0.03 | 1 |
| 3 | **6-62** | Y | 473 | 1 |
| 4 | **6-63** | Y | 278 | 1 |

Phenylsilane was chosen as the initial hydride source for the catalytic optimization but the amount of hydride source and the type of hydride source in a catalytic setting have not been thoroughly investigated. Pinacolborane and diphenylsilane were both examined in place of phenylsilane (**Table 6.5**). As expected from the hydride generation tests (see **Table 6.15**) diphenyl silane was much slower in catalysis only providing 6% conversion to **6-56** in the same time frame (**Entry 3, Table 6.5**). It is presumed that catalyst decomposition is faster than the regeneration of the hydride **6-19** in this instance. When pinacolborane was examined, the reaction went to 64% conversion to **6-56** due to catalyst degradation (**Entry 4, Table 6.5**). Pinacolborane mixed with diazaphospholene hydride **6-19** will eventually form phosphine ($PH_3$). Pinacolborane is an effective hydride

regeneration source from the diazaphospholene fluoride **6-22**, but it is also able to degrade the diazaphospholene **6-19** faster than the silane, as observed with this reaction as well as a few small NMR scale tests. The amount of phenylsilane was decreased to 72 hydride equivalents from the initial 144 (**Entry 1, Table 6.5**). While the reaction went to high conversion, a large amount of difluorotricyclohexylphosphorane **6-57** was observed. The large presence of this material indicates that an excess of the phenylsilane is required to remove the phosphorane **6-57**.

**Table 6.5** Examination of hydride sources in the catalytic transformation. Equivalence of phosphines were measured in the $^{31}$P NMR spectrum relative to **6-56**.

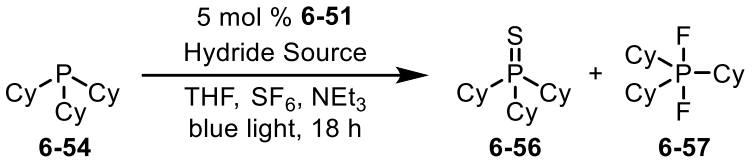


| Entry | Hydride | Hydride Equiv. added | **6-54** | **6-56** | **6-57** |
|---|---|---|---|---|---|
| 1 | $PhSiH_3$ | 144 | 0 | 1 | 0 |
| 2 | $PhSiH_3$ | 72 | 0.07 | 1 | 0.16 |
| 3 | $Ph_2SiH_2$ | 144 | 14.74 | 1 | 0 |
| 4 | HBpin | 144 | 0.56 | 1 | 0 |

Tricyclohexylphosphine **6-54** was the only sulfur capture reagent examined to this point. Phosphines such as tri-*n*-butylphosphine **6-14** and triphenylphosphine **6-55** were examined to determine how sulfur capture may be affect and if cheaper phosphines may be used in this chemistry (**Table 6.6**). On a 5 mol % scale, the cheaper tri-*n*-butylphosphine **6-14** performed similarly (**Entry 2, Table 6.6**) to tricyclohexylphosphine **6-54** while triphenylphosphine **6-55** was found to produce a larger quantity of difluorotriphenylphosphorane **6-59** (**Entry 3, Table 6.6**). Substitution of toluene for THF

resulted in similar conversion however catalyst solubility was lower (**Entry 4, Table 6.6**). Tri-*n*-butylphosphine **6-14** and triphenylphosphine **6-55** were examined in acetonitrile and gave only 20% and 29% conversion to the phosphine sulfides respectively (**Entry 5 and 6, Table 6.6**). During initial hydride reactivity studies, acetonitrile was the solvent which allowed for the most reactivity. However, it was found that this solvent results in faster diazaphospholene **6-19** breakdown under catalytic conditions, preventing the reaction from going to completion.

**Table 6.6** Examination of phosphine and solvent effects. Equivalence of phosphines were measured in the $^{31}$P NMR spectrum relative to phosphine sulfide.

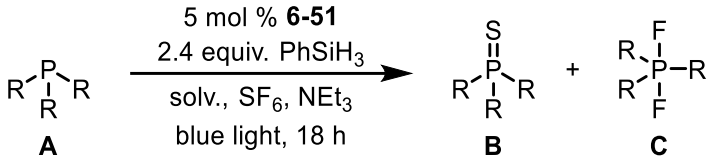


| Entry | Phosphine | Solvent | **A** | **B** | **C** |
|---|---|---|---|---|---|
| 1 | **6-54** | THF | 0 | 1 | 0 |
| 2 | **6-14** | THF | 0 | 1 | 0 |
| 3 | **6-55** | THF | 0.03 | 1 | 0.34 |
| 4 | **6-54** | Tol | 0.01 | 1 | 0.07 |
| 5 | **6-14** | $CH_3CN$ | 3.93 | 1 | 0 |
| 6 | **6-55** | $CH_3CN$ | 2.39 | 1 | 0 |

Loadings of diazaphospholene precatlyst, as well as light sources were further optimized in **Table 6.7**. Blue light was found to be the optimal light source for this reaction and as a result the requirement for quartz glass could be removed. The reaction was repeated at 5 mol % in a round bottom flask made of borosilicate glass and found to produce similar conversion at the same light distance (**Entry 5, Table 6.7**). Moving the reaction closer to the blue light source allowed for a lower catalyst loading of 2.5 mol % with a conversion

to 93% sulfide **6-56** (**Entry 6, Table 6.7**). Upon lowering the loading further (1 mol %), incomplete conversion to **6-56** was observed, even when the reaction was left for 48h (**Entry 7 and 8, Table 6.7**). This is speculated to result from catalyst degradation outcompeting $SF_6$ reactivity. The products of reaction conducted at 2.5 mol % were purified by column chromatography and the structure of the tricyclohexylphosphine product **6-56** was confirmed through NMR analysis and X-ray crystallography (**Figure 6.4**). Two control reactions were conducted to fully determine the importance of the catalyst and light (**Entry 9 and 10, Table 6.7**). A reaction wrapped in foil was left under standard reaction conditions and only trace amounts of product was observed. A final control reaction was conducted with the optimal conditions in a quartz tube with no diazaphospholene present. The formation of sulfide **6-56** was not observed in this reaction confirming the requirement of the diazaphospholene as a catalyst in this reaction.

**Table 6.7** Final reaction optimization for the light mediated decomposition of $SF_6$ catalyzed by diazaphospholene hydride **6-19**. Equivalence of phosphines were measured in the $^{31}P$ NMR spectrum relative to **6-56**.

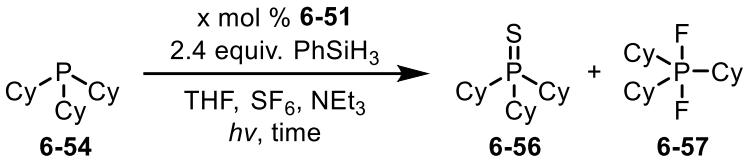


| Entry | Loading | Light | Time | Glass | **6-54** | **6-56** | **6-57** |
|---|---|---|---|---|---|---|---|
| 1 | 5% | Blue | 18h | Quartz | 0 | 1 | 0 |
| 2 | 5% | UV | 4h | Quartz | 0.1 | 1 | 0 |
| 3 | 2.5% | UV | 4h | Quartz | 0.78 | 1 | 0 |
| 4 | 2.5% | Blue | 18h | Quartz | 0.11 | 1 | 0 |
| 5 | 5% | Blue | 18h | Borosilicate | 0.14 | 1 | 0 |
| 6 | 2.5% | Blue | 18h | Borosilicate | 0.05 | 1 | 0.02 |
| 7 | 1% | Blue | 18h | Borosilicate | 1.36 | 1 | 0.05 |
| 8 | 1% | Blue | 48h | Borosilicate | 0.86 | 1 | 0.02 |
| 9 | 5% | none | 18h | Quartz | 238 | 1 | 0 |
| 10 | 0 | Blue | 18h | Quartz | 1 | 0 | 0 |

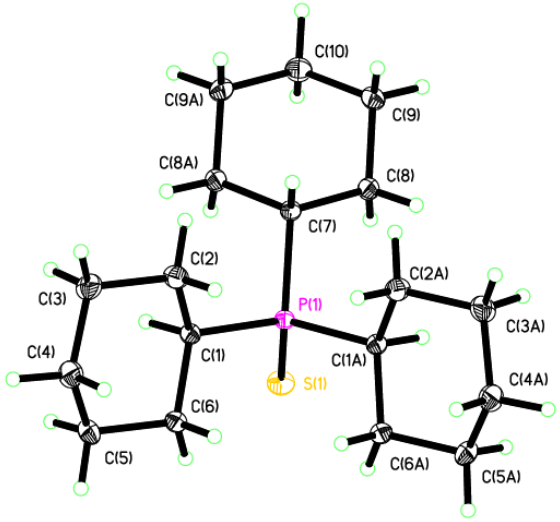


**Figure 6.4** Structure of **6-56**. Thermal ellipsoids have been drawn at 50% probability. Hydrogen atoms have not been labelled.

The optimization of this reaction has allowed for a catalytic decomposition of $SF_6$ gas that is better than the previous best published results (**Scheme 6.13**). The current best catalyst as described in section 6.1.3 by Braun et al only provides a maximum TON of 12 in the same time frame,[219] while requiring the heating to 80 °C. Not only does the current diazaphospholene reaction provide a higher TON of 37 but no heating is required. In addition, diazaphospholene precatalyst **6-51** can be prepared in two steps and has been prepared in our lab on up to a 45 gram scale. The reagents are low cost, in contrast to rhodium-based catalysts. However, the mechanism for this reaction remains elusive as the whole process is presumably a net 8 electron reduction, and accounting for the multiple species that must be present over the course of this reaction would be a complex endeavour. With a variety of reductive species present in the reaction mixture, determination of the mechanistic steps may be challenging.

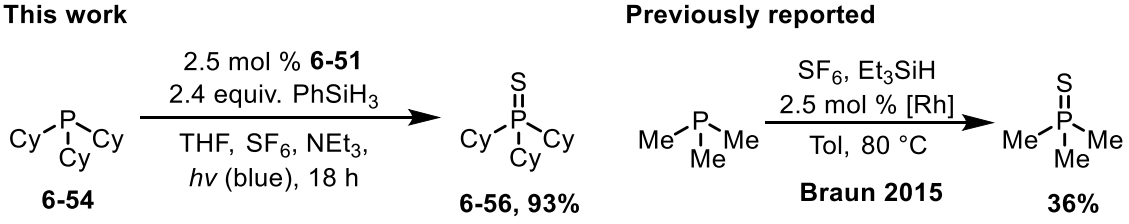


**Scheme 6.13** Comparison of this catalytic decomposition of $SF_6$ to the current best comparable method.

Despite the potential complexity of this reaction, certain reactions may provide an indication of the key steps or reagents in the process. As shown in **Scheme 6.12** it is postulated that the first step of the reaction is the removal of a fluoride from $SF_6$ and the hydride from the diazaphospholene **6-19**. The reactivity of a diazaphospholene dimers **6-21** and hydrides **6-19** with alkyl and aryl halides was observed to operate under radical chemistry and is detailed in chapter 7. Yang and Cheng have also reported

diazaphospholenes undergoing single electron chemistry.[91,92] Similarly, Beier,[224] and Wagenknecht[223,230] showed that single electron reactions of $SF_6$ can be utilized to trap $SF_5$ radicals, albeit in low yields. Treatment of known radical acceptor **6-65a**[223] with diazaphospholene in the presence of $SF_6$ revealed the trace presence of a pentafluorosulfanylated product in the $^{19}F$ NMR spectrum. In an effort to optimize the yield of this transformation, the acceptor, solvent and ratio of substrate to diazaphospholene were altered (**Scheme 6.14**). In all instances the yield of pentafluorosulfanylated product was observed in trace amounts, much like the reaction with TEMPOLi and $SF_6$ Beier reported previously.[224] The highest conversion observed qualitatively which was the use of 1-octene **6-65d** as the acceptor. The product was initially thought to be a pentafluorosulfanyl alkane, however mass spectrometry analysis indicated the presence of both a pentafluorosulfanyl group as well as an alkene. This would indicate that radical addition occurs but instead of quenching the radical hydrocarbon with a fluorine or hydrogen, elimination is occurring. While reaction yields could not be improved, the evidence of pentafluorosulfanylation through multiple substrates provides support for a radical based mechanism within this chemistry.

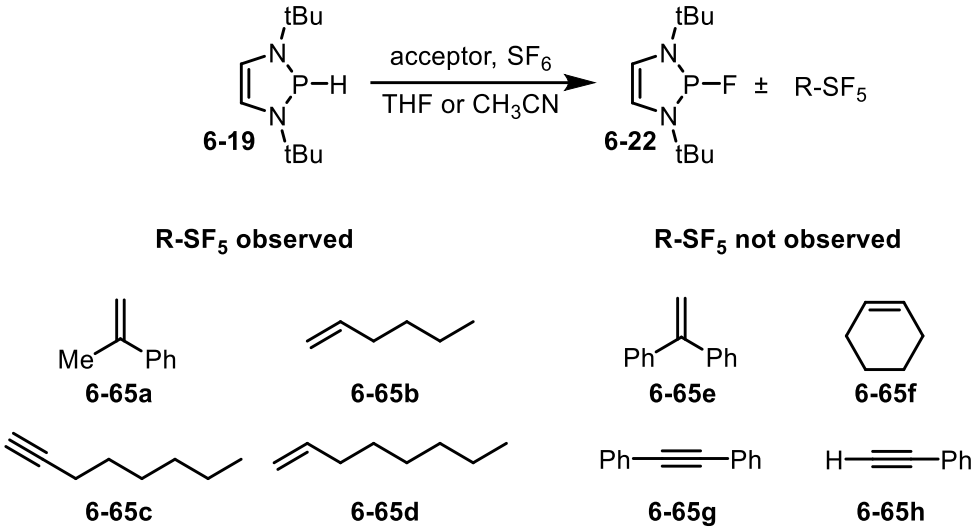


**Scheme 6.14** Attempted formation of pentafluorosulfanyl alkanes or alkenes.

In some instances, substrates such as α-methylstyrene **6-65a** and 1,1-diphenylethylene **6-65e** underwent alternative reactions. α-Methylstyrene **6-65a** underwent predominately a dimerization reaction. This result has been observed during the radical $SF_6$ chemistry reported by Wagenknecht.[223] In the instance of 1,1-diphenylethylene **6-65e**, hydrophosphination of the alkene was observed, as evidenced by a new phosphorus signal at 101.8 ppm in $^{31}P$ NMR spectrum, corresponding to substituted diazaphospholenes.[250] This was confirmed in a stoichiometric reaction of the two reagents in benzene. Alkynes substituted with aryl groups were not able to trap a $SF_5$ radical and instead decomposed or underwent no reaction. Overall, these results indicate that diazaphospholenes can undergo a variety of radical transformations which could further be investigated in detail as the basis of future projects.

Subsequent steps of the reaction mechanism remain unclear as lower valent sulfur compounds were not observed in the reaction mixture. The lack of lower valent sulfur products in the mixture may suggest that the reactivity of the diazaphospholenes or silane reagents is rapid. This is supported by the reaction reported earlier with Fluolead and

diazaphospholene, in which this S(IV) compound rapidly reacts with diazaphospholene **6-19** without needing light (**Scheme 6.15**). Treatment of the dimer **6-21** with Fluolead also resulted in complete reaction in seconds affording fluorodiazaphospholene **6-22** as well as a compound presumed to be a diazaphospholene thiophenylate **6-66a**, of which a derivative is isolated in chapter 7. While the reaction of diazaphospholenes and trifluorosulfur compounds such as Fluolead are rapid, pentafluorosulfanyl derivatives were not. Combination of the diazaphospholene dimer **6-21** with pentafluorosulfanyl benzene only gave trace amounts of reactivity. When irradiated, the reaction was accelerated but did not go to completion in the same time frame as a reaction with $SF_6$. Acetonitrile allows for the reactivity of diazaphospholenes and $SF_6$ to occur in the absence of a light source. Thus, pentafluorosulfanyl benzene was treated with diazaphospholene **6-19** in acetonitrile. After 20 h only trace amount of diazaphospholene fluoride **6-22** was observed in the $^{31}P$ NMR spectrum. These results indicate that aryl pentafluorosulfanyl derivatives might be more stable than $SF_6$ itself. These results clearly indicate that lower-valent sulfur-fluorides are more reactive with diazaphospholenes than higher-valent sulfur fluorides. However, it cannot be ruled out that alkyl pentaflurosulfanyl derivatives exhibit the same reactivity order. Further studies will be required to understand the reactivity of diazaphospholenes with fluorosulfur derivatives.

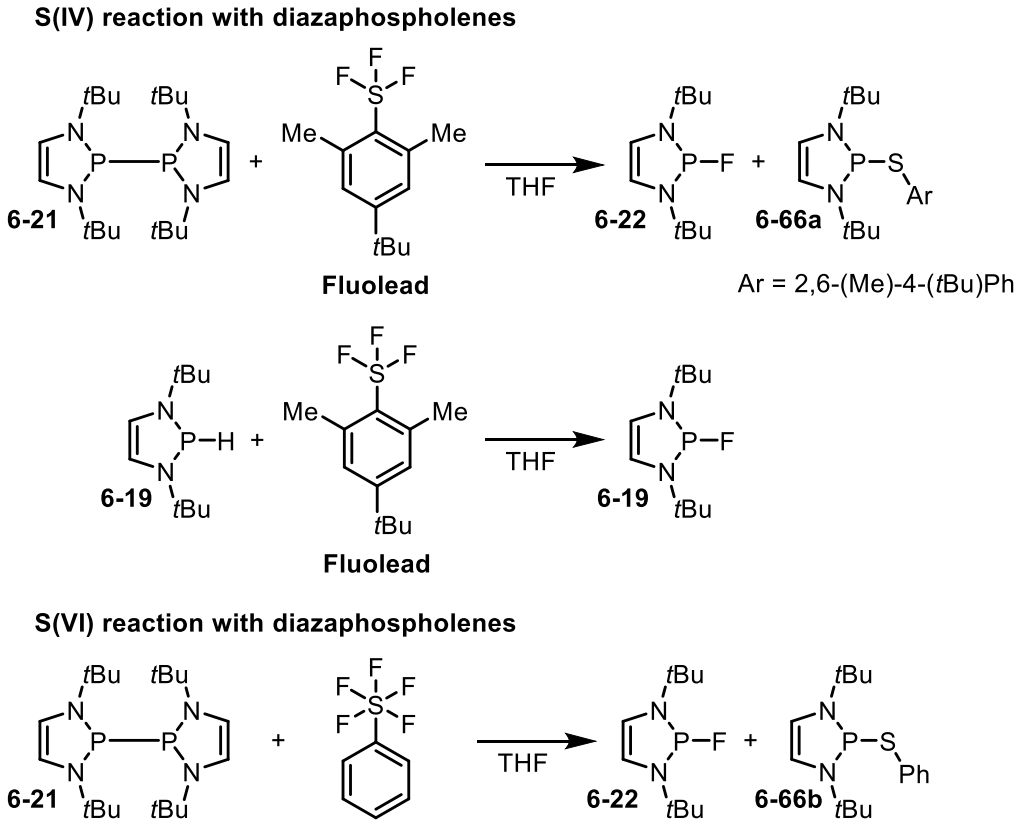


**Scheme 6.15** Fluorosulfur derivative reactivity with diazaphospholene derivatives.

The next point of confusion arose from the relative reaction rates of the stoichiometric reactions in comparison to the catalytic reactions. While 1 h of reaction time of the diazaphospholene hydride **6-19** with $SF_6$ gave only 26% conversion to **6-22** in a stoichiometric reaction, it was observed that a 2.5 mol % reaction went completion in 18 h. These results suggest that some component of the reaction mixture is accelerating this reaction. Since the phosphine and triethylamine are present in some stoichiometric reactions without acceleration, these reagents can be ruled out. This leaves the reductant as a potential source of reaction acceleration. In the hydride generations studies, phenyldimethylsilane did not react with the fluorodiazaphospholene **6-22** and therefore could be used as substitute for phenylsilane. When phenyldimethylsilane was present in a reaction of diazaphospholene **6-19** and $SF_6$ the reaction went to completion in 40 min. This

suggests that arylsilanes may be assisting in acceleration the reaction, potentially through a charge transfer mechanism. Reagents such as 1,1-diphenylethene **6-65e** were also found to also accelerate the reaction even though hydrophosphination was also occurring.

The final reaction that must be considered is the formation of the dimer **6-21** from the hydride **6-19**, which Gudat has shown occurs in the presence of light.[90] The dimers **6-21** are known to be more reactive than the hydride **6-19** species which would explain the rapid rate of reaction in the catalytic studies. Irradiation of the hydride **6-19** in the presence of silane or other reagents, without $SF_6$ only displayed trace amounts of dimer **6-21** even during long reaction times. Another possible route dimer **6-21** formation is in an elimination reaction. Diazaphospholene fluoride **6-22** in the presence of diazaphospholene hydride **6-19** and triethylamine could theoretically eliminate HF resulting in dimer **6-21** formation. However, this would contradict results established by Gudat that described the reverse reaction being favorable.[90] Nevertheless, diazaphospholene fluoride **6-22** and hydride **6-19** were combined and irradiated with and without phenyl dimethylsilane or triethylamine. Negligible amount of dimer **6-21** was formed in these reactions. The trace amount of dimer **6-21** formed can be attributed to the hydride **6-19** as the proportion of fluoride remained the major signal in the $^{31}P$ NMR spectrum. These combined results indicate that the dimer **6-21** is likely not a major reductant in the catalysis, supporting the hydride **6-19** as the primary reductant for $SF_6$.

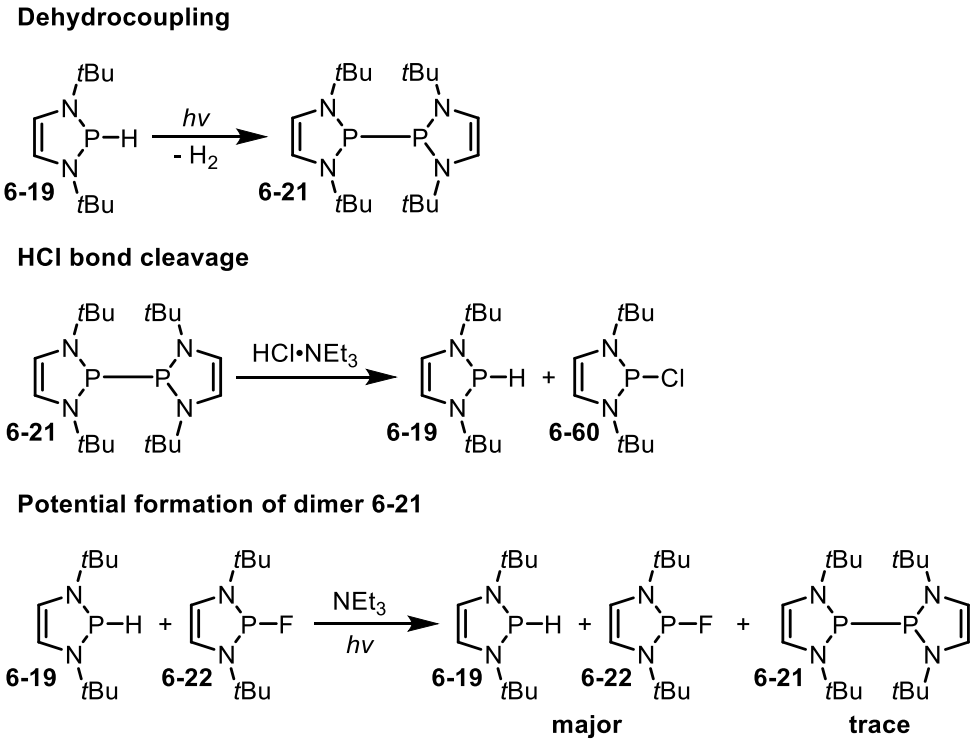


**Scheme 6.16** Potential formation of the dimer **6-21** during catalysis.

### 6.3.4 Conclusion

The results of this study provides the first catalytic main group reduction of $SF_6$ and the highest conversion to phosphine sulfide **6-56** observed in this process. The optimized conditions are of equal loading to that of the best literature example reported during this time,[219] while being milder $SF_6$ degradation conditions. Within this study it was found that addition of triethylamine was essential to ensure the stability of the reaction and that the reductant, phenylsilane may play an additional role to being the hydride source in accelerating the reaction. Similarly to Braun's investigation,[219] trialkylphosphines proved to be good reagents for sulfur scavenging in the hydride **6-19** reductions, but not in the dimer **6-21** reactions with $SF_6$. Current mechanistic results indicate that the reactivity of fluorosulfur (IV) is faster than that of fluorosulfur (VI), which the latter requires light for accelerated reactivity. The ability to generate a diazaphospholene hydride **6-19** directly

from the bromide can be applied into other applications within diazaphospholene catalysis. Generating a reductive species from the bromide reduces the number of synthetic steps to make a viable precatalyst. Overall, this work displays another application of the reductive power of diazaphospholenes.[69] This is also the first use of a diazaphospholene in a photocatalytic reaction other than dehydrocoupling,[90] which could be extended to other photocatalytic processes later.

## 6.4 Magnesium Mediated $SF_6$ Decomposition

### 6.4.1 Introduction

As previously stated in section 6.3, initial experiments indicated that magnesium dust in the absence of a diazaphospholene was able to facilitate $SF_6$ decomposition. This result is significant, as previous reports of $SF_6$ reduction with metals required highly reactive alkali metals, under either high temperatures, or dissolving-metal conditions requiring liquid ammonia. In fact, the reduction of $SF_6$ with magnesium seems counterintuitive, as $SF_6$ is used in the metallurgical industry to passivate the surface of molten magnesium. Section 6.1 further describes how alkali metals have been reported to react with $SF_6$ however these reactions were often conducted at cold temperatures in liquid ammonia.[208] A recent report has been disclosed with a magnesium/ magnesium oxide nanoparticle system using plasmons to decompose $SF_6$,[214] however, this method still requires specialized equipment and carefully prepared nano-structured materials, complicating its large-scale application. In comparison the magnesium-mediated reduction method found within this project, if optimized, could afford the mildest and most cost-effective method to decompose $SF_6$.

### 6.4.2 Results and Discussion

Before reaction optimization can be conducted, the required components for reactivity to occur must be identified. The importance of phosphine, silane and metal were examined along with their respective ratios to one another. In the initial control experiment from section 6.3, the $^{31}P$ NMR data showed the formation of two major products. The largest component was tricyclohexylphosphine sulfide **6-56** which was identified previously in section 6.3, and the other was an unidentified product at 59 ppm. To understand how the reaction is taking place, identification of the impurities may yield critical information. Under this initial reaction condition, the reaction is expected to produce the sulfide **6-56**, as well as a magnesium halide salt. Other expected impurities may be unreacted materials such as silane or phosphine oxide **6-67**, which can form from the addition of $SF_6$. To this end, a set of experiments were conducted with differing combinations of the starting materials, products and impurities without the addition of $SF_6$ (**Scheme 6.7**). It was found that the combination of tricyclohexylphosphine oxide **6-67** with magnesium chloride exclusively produced a product **6-68** with a chemical shift in the $^{31}P$ NMR spectrum at 59 ppm. While this specific adduct of a phosphine oxide **6-67** and magnesium halide is not reported, similar complexes have been observed and isolated.[252,253] In addition to the formation of the oxide adduct, another impurity was observed as a doublet at 22 ppm in the $^{31}P$ NMR spectrum. This was determined to be a hydrophosphonium salt[254] **6-69**, which was confirmed with treatment of tricyclohexylphosphine **6-54** with HCl etherate.

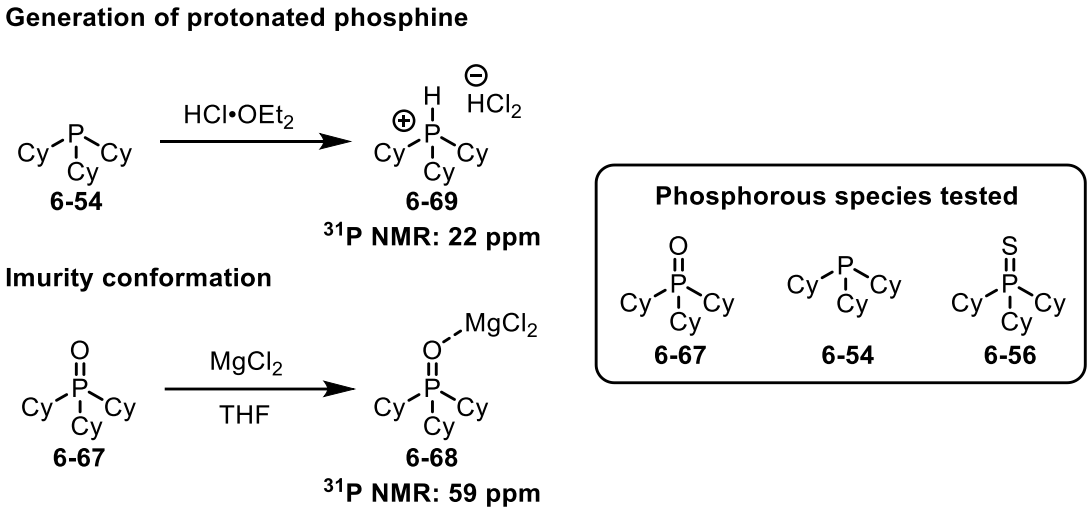


**Scheme 6.17** Formation of major impurities during the magnesium mediated decomposition of $SF_6$.

With an understanding of the identity of the minor impurities in the reaction, the goal was then shifted to the minimization of these impurities through modifying reaction stoichiometry. It is presumed that the phosphonium salt **6-69** forms as moisture from the balloon or magnesium turnings reacting with the dimethylchlorosilane. The $SF_6$ gas is transferred via balloon and therefore subject to moisture and air from the surrounding area and cannot easily be avoided besides purging the balloon before addition. However, an increase in the added equivalents of silane could resolve this issue, because the silane that is consumed by moisture cannot react with the other reagents. Increasing the equivalence of silane from 5 to 15 with respect to the phosphine **6-54** greatly changed the product distribution (**Entry 2, Table 6.8**). Gratifyingly, the amount of oxide adduct **6-68** as well as phosphonium **6-69** were greatly decreased from the change.

**Table 6.8** Modification of reagent equivalence and effect on product distribution. [a]Reactions were conducted with magnesium dust. Equivalence of phosphines were measured in the $^{31}$P NMR spectrum relative to **6-56**.

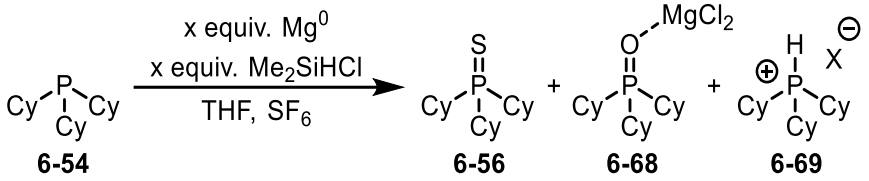


| Entry | Mg (Equiv.) | Silane (Equiv.) | $SPCy_3$ **6-56** | $MgCl_2$•$(OPCy_3)_2$ **6-68** | $HPCy_3^+$ **6-69** | $PCy_3$ **6-54** |
|---|---|---|---|---|---|---|
| 1[a] | 5 | 5 | 1 | 0.6 | 0 | 0 |
| 2[a] | 5 | 15 | 1 | 0.09 | 0 | 0 |
| 3 | 5 | 15 | 1 | 0.2 | 0.12 | 0 |
| 4 | 15 | 5 | 1 | 0.7 | 0 | 0 |
| 5 | 15 | 15 | 1 | 0.09 | 0 | 0 |
| 6 | 10 | 20 | 1 | 0.11 | 0 | 0 |

In the initial discovery of this reaction, magnesium dust was used. However, magnesium turnings are a more stable and cost-effective form of magnesium. If magnesium turnings can be applied in this chemistry, the formation of unwanted products may be possible with less surface area. Five equivalents of magnesium turnings were treated with approximately 15 equivalents of dimethylchlorosilane with respect to tricyclohexylphosphine (**Entry 3, Table 6.8**). Magnesium turnings were found to successfully reduce $SF_6$ however with a larger number of impurities formed. While 5 equivalents of magnesium dust can cleanly produce the sulfide in the presence of 15 equivalence of silane, the same proportion of magnesium turnings did not. Larger amounts of oxide adduct **6-68** and phosphonium **6-69** were present in this reaction mixture as evidenced in the $^{31}$P NMR data. This is likely due to the smaller surface area of the turnings comparatively to the magnesium dust. Increasing the equivalents of magnesium turnings to

15 allowed for a product distribution comparable to magnesium dust (**Entry 5, Table 6.8**). Starving the reaction of silane also increased the amount of oxide **6-68** formed, supporting the requirement for an excess of this reagent (**Entry 4, Table 6.8**).

While the effect of the relative proportions of each reagent is better understood after the above experiments, the structure-activity properties of the silane remain unclear. Dimethylchlorosilane contains both a chlorine and hydride in its structure, and while it is expected that the chlorosilane component is facilitating this process, the function of the hydride may also play a role. Thus, trimethylchlorosilane was utilized in this reaction in place of dimethylchlorosilane (**Entry 2, Table 6.9**). The reaction performed similarly to dimethylchlorosilane, albeit with more oxide **6-68** present in the product distribution. The success of this reaction indicates that the hydride in dimethylchlorosilane is not required for this process but, the increase in impurities may indicate that a steric effect might be a factor in this reaction. To determine the effect of steric bulk of the silane on this reaction, triethylchlorosilane was examined (**Entry 3, Table 6.9**). This silane was found to produce even more of the oxide impurity **6-68**, indicating that increased steric bulk may indeed play a role in this reaction. The results of silane substitution on this process indicates that steric bulk of the silane must be considered in this chemistry. The postulated reason for this effect may be that the smaller silanes are able to react with the surface of the magnesium more effectively. As the magnesium surface reacts with $SF_6$, magnesium fluoride is expected to be produced and would likely alter the surface morphology of this metal (**Scheme 6.18**). The smaller silanes may be able to more closely approach the magnesium surface, producing a cleaner surface for faster reactivity.

**Table 6.9** Determination of steric effect of silane on the reaction conditions. Equivalence of phosphines were measured in the $^{31}P$ NMR spectrum relative to **6-56**.

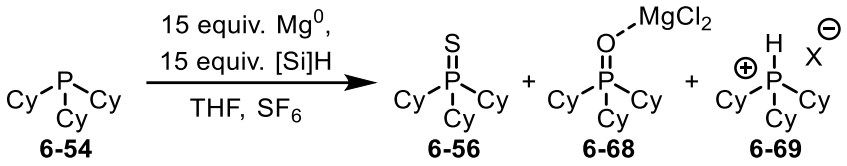


| Entry | Silane | $SPCy_3$ **6-56** | $MgCl_2•(OPCy_3)_2$ **6-68** | $HPCy_3^+$ **6-69** | $PCy_3$ **6-54** |
|---|---|---|---|---|---|
| 1 | $Me_2SiHCl$ | 1 | 0.6 | 0 | 0 |
| 2 | $Me_3SiCl$ | 1 | 0.09 | 0 | 0 |
| 3 | $Et_3SiCl$ | 1 | 0.2 | 0.12 | 0 |
| 4 | PolySiH | 0 | 0.7 | 0 | 0 |

To understand the surface chemistry of the magnesium turnings, a collaboration with the Dasog group was conducted to acquire SEM images of the surface. These images will allow for a visual representation of the surface as different aspects of the reaction are examined. Accordingly, a variety of experiments were set up to visualize everything from mechanical stirring to full reaction conditions of this system. Figure 6.5 displays samples of these results and the corresponding tests. Image (**A**) of Figure 6.5 displays a fresh magnesium turning before any reactivity or solvation. A set of magnesium turnings was left to stir overnight and found while some abrasion had occurred (**Image B, Figure 6.4**), the turnings remained relative unchanged. This indicates that while the mechanical actions of stirring may have some effect on the roughening of the surface the change to morphology is not major. This process was repeated with $SF_6$ in solution, and it was found the turnings were relatively unchanged (**Image C, Figure 6.4**). Little to no fluoride was detected on the surface. This is expected as the initial surface of the turnings is often covered in a layer of oxide which the chlorosilane is presumed to remove. The largest change to the surface of

the magnesium was in the addition of silane, which caused a roughening of the surface when left overnight (**Image E, Figure 6.4**). When this process was repeated with silane and $SF_6$, the magnesium turnings was greatly degraded (**Image F, Figure 6.4**). These results provide support of a hypothesis where the silane cleans the surface, which allows for $SF_6$ reactivity followed by further removal of magnesium fluoride by the silane (**Scheme 6.18**).

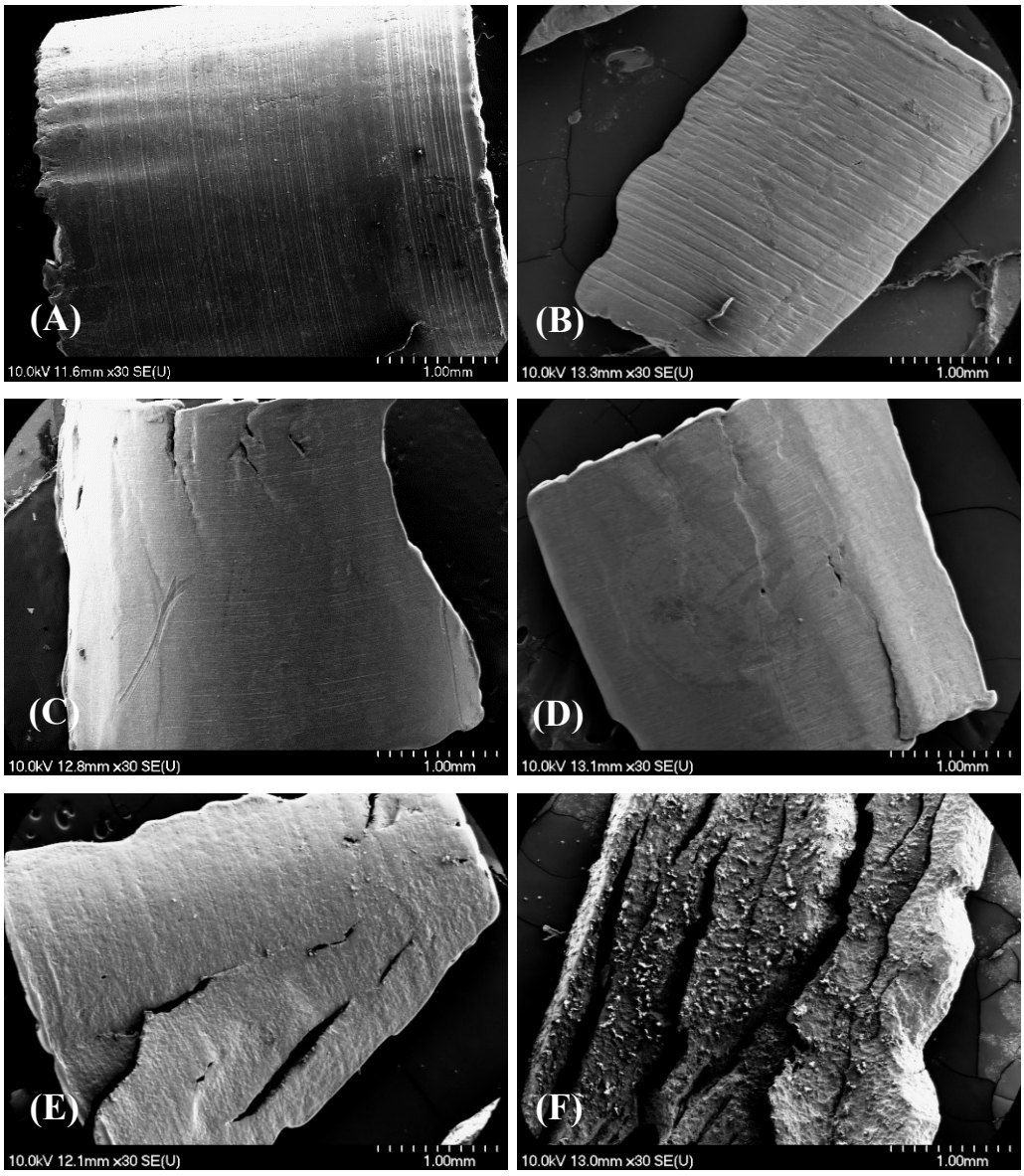


**Figure 6.5** SEM images acquired of magnesium turnings (smooth side). Image (**A**) contains a magnesium turning as received. Image (**B**) contains a magnesium turning after

mechanical stirring for 18 h. Image (**C**) contains a magnesium turning mechanically stirred and exposed to an atmosphere of $SF_6$ for 18 h. Image (**D**) contains a magnesium turning mechanically stirred, exposed to $SF_6$ and tricyclohexylphosphine **6-54** for 18 h. Image (**E**) contains a magnesium turning exposed to dimethylchlorosilane and mechanically stirred for 18h. Image (**F**) contains a magnesium turning exposed to dimethylchlorosilane, $SF_6$, and mechanically stirred for 18 h.

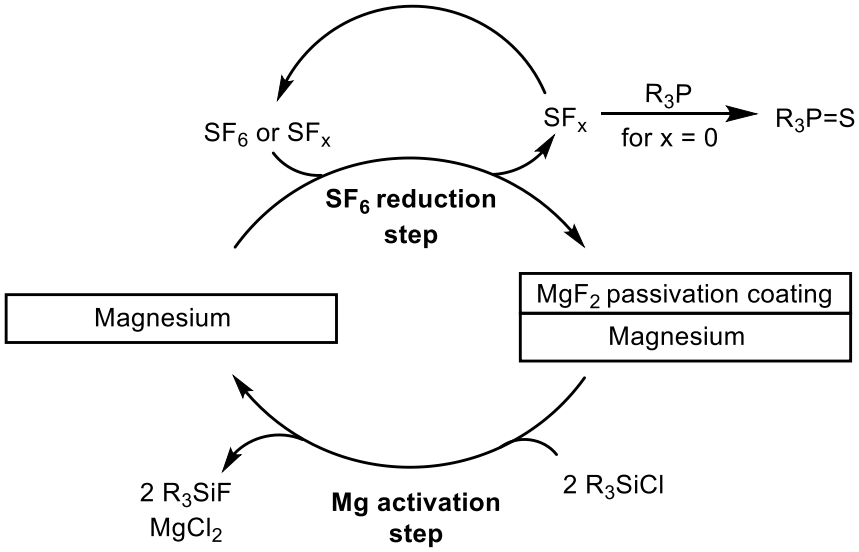


**Scheme 6.18** Postulated mechanism for the magnesium reduction of $SF_6$.

The SEM images indicated that the process does not require the phosphine which is also supported by the presence of fluorosilane in the $^{19}F$ NMR data. However, the scavenging of sulfur with the phosphine **6-54** may protect against the formation of magnesium sulfide or lower valent sulfur-fluoride gases which can be toxic, or highly malodorous silyl sulfides. Since it is presumed that the phosphine **6-54** only plays a role in scavenging the sulfur, this reagent may be altered for optimal sulfur capture through the modification of steric and electronic effects. In a report by Braun,[219] a variety of phosphines were examined for sulfur capture. Phosphines with the least steric bulk such as *n*-butyl **6-14** and methyl exhibited a higher conversion and turnover number in comparison to phosphines with large steric environment such as *tert*-butyl and *iso*-propyl. However, trimethylphosphine is extremely malodorous and is expensive, so is not an attractive reagent. Thus, *n*-butyl phosphine **6-14** was examined for its low cost and lower volatility

in comparison to other phosphines. Treatment of tri-*n*-butylphosphine **6-14** with 15 equivalents of magnesium turnings and dimethylchlorosilane resulted in the formation of the sulfide **6-64** and the tentatively assigned oxide/magnesium salt adduct **6-70**. This adduct **6-70** was the major product formed, in a 1.5:1 ratio with the sulfide **6-64** and was therefore not examined further. Triphenylphosphine **6-55** was then treated with 15 equivalents of magnesium turnings and dimethylchlorosilane (**Entry 3, Table 6.10**). The sulfide **6-58** formed as the predominant product with only a trace amount of oxide **6-71** as the only other product. These results indicate that triphenylphosphine **6-55** was highly effective in the capture of sulfur from $SF_6$ decomposition. Surprisingly, these results differ from the catalysis reported in section 6.3 where tricyclohexylphosphine **6-54** was more effective than triphenylphosphine **6-55**. The low cost and air stability of triphenylphosphine **6-55** makes it an attractive reagent for the capture of sulfur from $SF_6$ along with lower volatility and toxicity for large scale use.

**Table 6.10** Exploration of other phosphines for sulfur capture. Equivalence of phosphines were measured in the $^{31}P$ NMR spectrum relative to the phosphine sulfide.

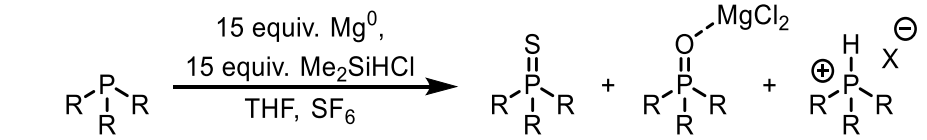


| Entry | Phosphine | $SPR_3$ | $MgCl_2•(OPR_3)_2$ | $HPR_3^+$ | $PR_3$ |
|---|---|---|---|---|---|
| 1 | $PCy_3$ **6-54** | 1 | 0.09 | 0 | 0 |
| 2 | $PPh_3$ **6-55** | 1 | 0.06 | 0 | 0 |
| 3 | $P(n\text{-Bu})_3$ **6-14** | 1 | 0.2 | 0 | 0 |

Magnesium was found to decompose $SF_6$ in the presence of silanes, but it is uncertain if other reducing metals could facilitate this transformation under similar

conditions. Calcium and zinc were explored in this chemistry (**Table 6.11**). Tricyclohexylphosphine **6-54** or triphenylphosphine **6-55** were treated with 15 equivalents of calcium chips and dimethylchlorosilane (**Entry 2, Table 6.11**). Calcium was successful in facilitating $SF_6$ decomposition, however the oxide adduct was produced in higher quantities with a ratio to the tricyclohexylphosphine sulfide **6-56** of 1:0.4. Triphenylphosphine **6-55** performed worse than tricyclohexylphosphine **6-54** in sulfide trapping with a ratio of sulfide **6-58** to oxide adduct of 1:1. Calcium being a stronger reducing agent than magnesium was not able to facilitate a clean reduction of $SF_6$ as monitored by the phosphine products. Zinc was then examined with tricyclohexylphosphine **6-54** under similar conditions to the calcium experiment (**Entry 3, Table 6.11**). It was found that zinc was not an effective reagent for the decomposition of $SF_6$ due to the detection of only a small amount of sulfide **6-56** in the presence of multiple other phosphine products. This results overall indicated that the reduction potential of magnesium is critical to the selectivity observed in this reaction and that zinc is not a strong enough reducing agent.

**Table 6.11** Exploration of other metals in the reduction of $SF_6$. Equivalence of phosphines were measured in the $^{31}P$ NMR spectrum relative to **6-56**.

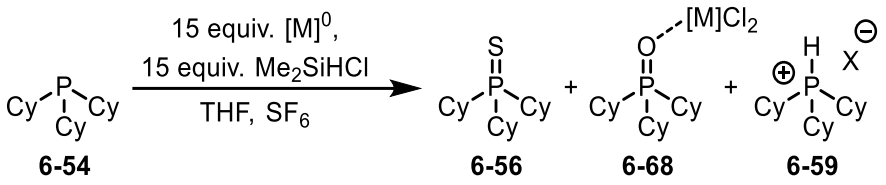


| Entry | Metal | $SPCy_3$ **6-56** | $[M]Cl_2•(OPCy_3)_2$ | $HPCy_3^+$ **6-69** | $PCy_3$ **6-54** |
|---|---|---|---|---|---|
| 1 | Mg | 1 | 0.09 | 0 | 0 |
| 2 | Ca | 1 | 0.4 | 0 | 0 |
| 3 | Zn | 1 | 0 | 7.6 | 9 |

Under these conditions the reduction of sulfur hexafluoride can proceed to completion. Previously in our investigation of the reduction other perfluorosulfur derivatives it was found that while sulfur (IV) derivatives were easily reduced, compounds such as pentafluorosulfanylbenzene (VI) were more challenging. However, treatment of pentafluorosulfanylbenzene under the standard conditions for this reaction were found to fully consume the pentafluorosulfanylbenzene which was no longer detectable in the $^{19}F$ NMR spectrum. Acidification and extraction of this reaction solution yielded thiophenol **6-72**, which was observed through $^{1}H$ NMR analysis.

Current reactions reported thus far were conducted on a small scale of 0.25 mmol of phosphine. While these experiments have been informative, larger scale testing will need to be examined to fully understand if the chemistry is scalable and how the stoichiometry may change (**Table 6.12**). Increasing the scale to 0.5 mmol resulted in similar product distribution (**Entry 2, Table 6.12**). A five-fold increase in scale from the original reaction was then examined with only 7 equivalents of magnesium turnings and dimethylchlorosilane. When conducted in a 25 mL flask, this reaction produced a large

portion of phosphonium salt **6-69** detected in the crude mixture (**Entry 3 and 4, Table 6.12**). It was determined that the lack of a larger excess of $SF_6$ was the cause, as increase the flask volume to 50 mL resulted in a better product distribution (**Entry 5, Table 6.12**). Triphenylphosphine **6-55** was then examined on this scale and found to give excellent performance, with less than 8% oxide impurities **6-71** (**Entry 6, Table 6.12**). Triphenylphosphine **6-55** was exclusively used for further optimization as it is more oxidatively stable and cost effective then tricyclohexylphosphine **6-54**. Trimethylchlorosilane was then examined at this scale and found to effectively reduce $SF_6$ albeit with more impurities than dimethylchlorosilane (**Entry 7, Table 6.12**). One of these impurities, a doublet at 101 ppm in the $^{31}P$ NMR likely arises from a fluorophosphonium salt, similar to a literature prepared derivative. A final set of optimal conditions was found at a 2.5 mmol scale with 5 equivalents of magnesium and 7 equivalents of dimethylchlorosilane (**Entry 10, Table 6.12**). At this ratio, the reactants are near their minimum stoichiometric values of 3 equivalents of magnesium and six equivalents of silane.

**Table 6.12** Reaction optimization for the reduction of $SF_6$ facilitated by magnesium metal. [a]Reaction conducted with trimethylchlorosilane. [b]Reaction conducted in an open-air setup before the addition of $SF_6$. Equivalence of phosphines were measured in the $^{31}P$ NMR spectrum relative to **6-56** or **6-58**.

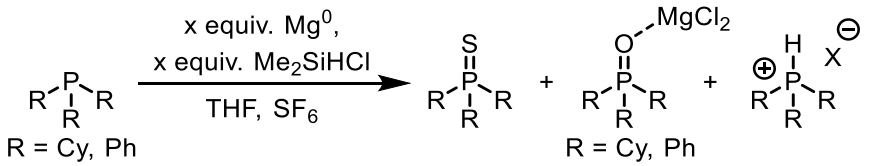


| Entry | $PR_3$ (mmol) | Mg/[Si] Equiv. | Flask Vol. mL | $SPR_3$ | $MgCl_2•(OPR_3)_2$ | $HPR_3^+$ | $PR_3$ |
|---|---|---|---|---|---|---|---|
| 1 | $PCy_3$ (0.25) | 15/15 | 10 | 1 | 0.09 | 0 | 0 |
| 2 | $PCy_3$ (0.5) | 15/15 | 10 | 1 | 0.1 | 0 | 0 |
| 3 | $PCy_3$ (1.25) | 5/5 | 25 | 1 | 0.16 | 0.05 | 0 |
| 4 | $PCy_3$ (1.25) | 7/7 | 25 | 1 | 0.09 | 0.15 | 0 |
| 5 | $PCy_3$ (1.25) | 7/7 | 50 | 1 | 0.07 | 0 | 0 |
| 6 | $PPh_3$ (1.25) | 7/7 | 50 | 1 | 0.06 | 0 | 0 |
| 7[a] | $PPh_3$ (1.25) | 7/7 | 50 | 1 | 0.1 | 0 | 0 |
| 8 | $PPh_3$ (1.25) | 5/7 | 50 | 1 | 0.06 | 0 | 0 |
| 9 | $PPh_3$ (1.25) | 3/7 | 50 | 1 | 0.7 | 0 | 0.24 |
| 10 | $PPh_3$ (2.5) | 5/7 | 100 | 1 | 0.06 | 0 | 0 |
| 11[b] | $PPh_3$ (1.25) | 5/7 | 50 | 1 | 0.1 | 0 | 0 |
| 12[a,b] | $PPh_3$ (1.25) | 5/7 | 50 | 1 | 0.15 | 0 | 0 |

If this method is to be used as a removal technique for waste $SF_6$, the reaction will have to perform under wet conditions with gas that is contaminated with air. All reactions conducted so far have been under highly dried conditions with the only exposure to air occurring during $SF_6$ addition via balloon. To test the robustness of this reaction, the triphenylphosphine **6-55** and magnesium were added to a flask in open air and THF was used without any additional drying. A septum was added and the gas sparged through the

system. Silane was then added to the reaction and left according for the reaction time. The product distribution of this reaction remained the same as dryer conditions, indicating that the reaction can perform under relatively wet and oxygenated conditions (**Entry 11, Table 6.12**). Trimethylchlorosilane was also examined and found to perform with a similar product distribution to a completely anhydrous setting (**Entry 12, Table 6.12**). The stability of this system under wet conditions is possible due to the stability of triphenylphosphine **6-55** in air and magnesium turnings having low surface area, protecting the metal from extensive oxidation. In addition, a slight excess of silane, can scavenge any moisture from the reaction mixture. Altogether these results indicate a highly scalable method for the decomposition of $SF_6$ gas.

### 6.4.3 Conclusion

Magnesium turnings, a common and versatile reagent, was found to be effective in the decomposition of $SF_6$ gas. Most other methods reported thus far have required specialized equipment, high energy costs in heating or cooling or expensive materials to facilitate this process. With minimal reagents required and the low cost/ high stability of each component makes this an attractive method for $SF_6$ decomposition. Low cost and accessibility are critical if a method for $SF_6$ decomposition is going to be applied on an industrial scale. Overall, magnesium metal is unique in its reductive capability of $SF_6$, and this room temperature reaction represents a state of the art development in chemical $SF_6$ decomposition at ambient temperature.

## 6.5 Experimental for section 6.2

### 6.5.1 General Considerations

All reagents and solvents were dispensed in a 2001 issue IT Glovebox ($H_2O$ levels vary between 2-6 ppm) unless otherwise stated. All reactions were conducted at ambient

temperature unless otherwise stated. $^{1}H$, $^{31}P$, $^{19}F$, $^{11}B$ and $^{13}C$ NMR data were collected at 300K on either a Bruker AV-300 or AV-500 spectrometer, and hetereonuclei were referenced to external standards. Benzene-$d_6$ was added to samples to enable autosampler use/automated locking on the Bruker instruments. $^{1}H$ NMR spectra are referenced to residual non-deuterated NMR solvent from the sample ($C_6H_6$ = 7.16 ppm). $^{13}C$ NMR spectra are referenced to NMR solvent from the sample ($C_6D_6$ = 128.06 ppm). Sulfur hexafluoride was dispensed from a "Prextex" 12 inch "party balloon" latex balloon, purchased from Amazon. The balloon was taped with electrical tape to a cut 6 mL syringe equipped with a Luer lock. Mass spectrometric data were acquired by Mr. Xiao Feng (Mass Spectrometry Laboratory, Dalhousie University).

### 6.5.2 Solvents

**Tetrahydrofuran** was purchased as anhydrous >99% ACS grade from Sigma Aldrich and stored over 3Å molecular sieves under nitrogen.

**Toluene** was purchased in a drum, ACS grade from Fisher and was passed through a double column purification system (activated alumina and activated Q-5) from MBraun Inc. and stored over 3Å molecular sieves under nitrogen.

**Ether** was purchased as anhydrous >99% ACS grade from Sigma Aldrich and stored over 3Å molecular sieves under nitrogen.

**Dichloromethane** (ACS grade) was purchased from Fisher and used as received.

### 6.5.3 Reagents

**Borane dimethyl sulfide** was purchased from Sigma Aldrich and used as received.

***n*-butyllithium** and ***tert*-butyllithium** were purchased from Sigma Aldrich and used as received.

**Di-*tert*-butylphosphine 6-38**, **Diphenyl(trimethylsilyl)phosphine 6-48** and **diphenylphosphine oxide** were purchased from Sigma Aldrich and used as received.

**Diphenylphosphine 6-29**, **dicyclohexylphosphine 6-31** and **1,3,5,7-Tetramethyl-2,4,6-trioxaphosphaadamantane 6-42** (35 wt % in xylenes) were obtained from Cytec/Solvay and diluted to 0.5 M solutions in THF before use.

**Potassium diphenylphosphide solution 6-25** (0.5M in THF) was purchased from Sigma Aldrich and used as received.

**Sulfur Hexafluoride** was purchased from Air-Liquide in an F-Cylinder as "Chemically Pure, 7, grade, CGA-590.".

### 6.5.4 Synthetic Procedures

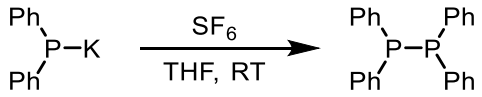


**Reaction of potassium diphenylphosphide 6-25 and $SF_6$ gas.** Potassium diphenylphosphide **6-25** (0.2 mL, 0.1 mmol, 0.5M in THF) was dispensed into a 1 dram vial. The solution was diluted with additional solvent (0.55 mL THF and 0.05 mL benzene-$d_6$). The solution was then transferred to an NMR tube and the sample was capped with a septum. An $SF_6$ gas filled balloon equipped with a needle was used to bubble $SF_6$ through the solution for 15s. The solution went from an orange to clear/yellow colour during this period in which the needle and septum were removed and replaced with a standard NMR cap (**Figure 6.6**). The solution was then analyzed using NMR spectroscopy.

**NMR spectrum of $KPPh_2$ 6-25 solution:**

**$^{31}P$** (202.5 MHz, THF, $C_6D_6$ (lock)): δ -10.0 (s).

**NMR spectra after $SF_6$ addition:**

**$^{31}P$** (202.5 MHz, THF, $C_6D_6$ (lock)): δ -15.6 (s).

**$^{19}$F (0 center point)** (470.6 MHz, THF, $C_6D_6$ (lock)): δ 57.4 (s, $SF_6$).

**$^{19}$F (-200 center point)** (470.6 MHz, THF, $C_6D_6$ (lock)): δ -132 (br, s).

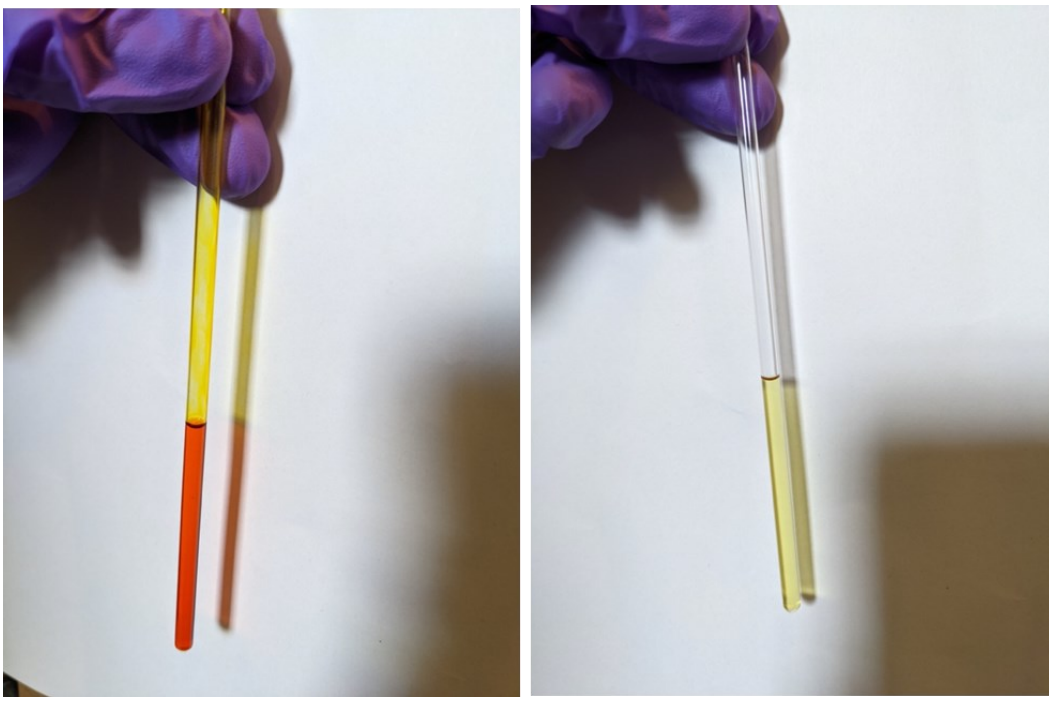

**Figure 6.6** $KPPh_2$ **6-25** solution before $SF_6$ addition (left), and after $SF_6$ addition (right). The images are described as follows: The tube on the left contains a bright orange liquid, the tube on the right contains a pale yellow liquid.

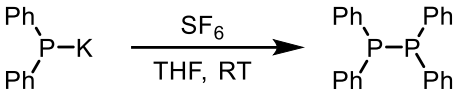


**Scale up and isolation of tetraphenyldiphosphine** (**6-26**)**.** Potassium diphenylphosphide **6-25** (2 mL, 1 mmol, 0.5M in THF) was dispensed into a 10 mL round bottom flask equipped with a septum. The solution was diluted with additional solvent (2 mL THF). An $SF_6$ gas filled balloon equipped with a needle was used to bubble $SF_6$ through the solution until all orange color dissipated and then the bubbling was continued for an additional 15s. The solution was then analyzed using NMR spectroscopy to confirm reaction completion. Volatiles were then removed *in vacuo* and ether was added (10 mL). The slurry was filtered over a fine porous frit and then washed with additional ether (2 x 5mL). The ether was then

removed *in vacuo* and the solid taken up in toluene (3 mL). The solution was filtered through a fine porous syringe filter and the toluene was then removed *in vacuo*. The crude solid obtained (177 mg) was then characterized without further purification.

**$^{1}$H** (500 MHz, $C_6D_6$): δ 7.55 (8H, m), 6.96 (12H, m).

**$^{31}$P** (202.5 MHz, $C_6D_6$): δ -15.6 (s).

**NMR analysis of the crude solution in $D_2O$:**

A portion of the solid remaining from filtration was taken up in $D_2O$, and a fluorine NMR spectrum was acquired. Analysis of the NMR spectrum indicated the presence of potassium fluoride.

**$^{19}$F (-100 center point)** (470.6 MHz, $D_2O$): δ -122 (s).

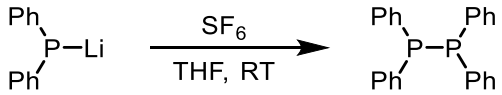


**Reaction of lithium diphenylphosphide 6-30 and $SF_6$ gas.** Diphenylphosphine **6-29** (0.2 mL, 0.1 mmol, 0.5 M in THF) was dispensed into a 1 dram vial. The solution was diluted with additional solvent (0.55 mL THF and 0.05 mL benzene-$d_6$). *n*-Butyllithium (0.04 mL, 0.1 mmol, 2.5M) was then added and the solution turned orange. The solution was then transferred to an NMR tube and the sample was capped with a septum. An $SF_6$ gas filled balloon equipped with a needle was used to bubble $SF_6$ through the solution for 15s. The solution went from orange to clear/yellow colour during this period in which the needle and septum were removed and replaced with a standard NMR cap. The solution was then analyzed using NMR spectroscopy.

**NMR spectrum of $LiPPh_2$ 6-30 before $SF_6$ addition:**

**$^{31}$P** (121.5 MHz, THF, $C_6D_6$ (lock)): δ -22.6 (s).

**NMR spectrum after $SF_6$ addition:**

**$^{31}$P** (121.5 MHz, THF, $C_6D_6$ (lock)): δ -15.7 (s).

**Sulfide test.** To determine the presence of potassium sulfide, reaction of sulfide with lead (II) acetate was initially tested, but inconclusive. An expected black precipitate did not form, however a white precipitate did form. Exposure of lead (II) acetate to solutions of KF also resulted in white precipitates, so presumably the presence of fluoride interferes with this test. A qualitative test with *N,N*-dimethyl-phenylenediamine and iron (III) chloride was successful in detecting sulfide. Residual phosphine appeared to interfere with the test reaction, by slowing formation of the blue colour, possibly through reduction of the methylene blue that was formed, so removal of the phosphine by extraction with dichloromethane was conducted as described. The test solutions were prepared as follows:

*N,N*-dimethyl-phenylenediamine (20 mg) was dissolved in 10 mL of 6M HCl.

$FeCl_3$ (30 mg) was dissolved in 10 mL of 6M HCl.

**Scale up of $LiPPh_2$ 6-30 and $KPPh_2$ 6-25 for testing for sulfides.** Diphenylphosphine **6-29** (0.5 mL, 0.25 mmol, 0.5 M THF) was dispensed into a 1 dram vial. This solution was further diluted with THF (0.5 mL). A base was then added either as *n*-butylithium (0.1 ml, 0.25 mmol, 2.5M) or potassium hydride (10 mg, 0.25 mmol). The solution was then stirred at room temperature for 30 min and then analyzed using NMR spectroscopy to show the presence of the phosphides. Sulfur hexafluoride was then added as per the previous procedures, then the solutions were again analyzed using NMR spectroscopy. The sample was then transferred to a flask and the volatiles removed *in vacuo*. Deionized water was then added (approx. 5-7 mL) followed by DCM (5 mL) and the mixture shaken. The aqueous layer was then removed and filtered through a fine porous syringe filter to remove small amounts of insoluble materials. An aliquot of this solution was then added to a standard culture tube and diluted. A solution of *N,N*-dimethyl-*p*-phenylenediamine

(approx. 0.3-0.5 mL) was added, followed by a solution of iron trichloride (approx. 0.3-0.5 mL). The solution was left for approximately 1h in which time the pink color became a deep blue. A control was conducted with KF (25 mg) in water (4mL) under the same conditions which remained pink (**Figure 6.7**).

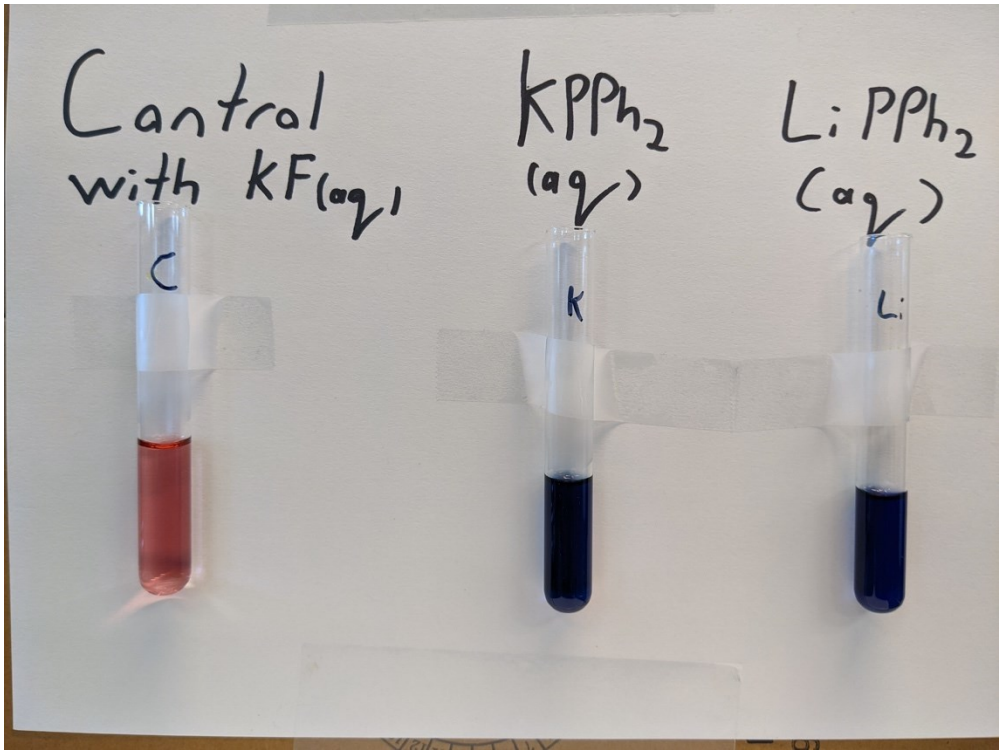


**Figure 6.7** Sulfide test reactions. Control (KF) solution on left, reaction with residue from $KPPh_2$ **6-25** reaction in middle, reaction with residue from $LiPPh_2$ **6-30** reaction on right. Description of images: three vials taped to a labelled card, the vial on the left is half-filled with a pink liquid, and the two other vials are half-filled with dark blue liquid.

**NMR spectra for samples used in sulfide test:**

**NMR spectrum of lithium diphenylphosphide 6-30 in THF:**

$^{31}$**P** (202.5 MHz, THF, no lock): δ -22.3 (s).

**NMR spectra of lithium diphenylphosphide 6-30 after $SF_6$ addition:**

$^{31}$**P** (202.5 MHz, THF, no lock): δ -15.4 (s).

$^{19}$**F (0 center point)** (470.6 MHz, THF, no lock): δ 57.4 (s, $SF_6$).

**$^{19}$F (-200 center point)** (470.6 MHz, THF, no lock): sharp peak due to fluoride ions not observed.

**NMR spectrum of potassium diphenylphosphide 6-25 prepared from KH and $HPPh_2$ in THF:**

**$^{31}$P** (202.5 MHz, THF, no lock): δ -9.7 (s).

**NMR spectra of potassium diphenylphosphide 6-25 after $SF_6$ addition:**

**$^{31}$P** (202.5 MHz, THF, no lock): δ -9.9 (s).

**$^{19}$F (0 center point)** (470.6 MHz, THF, no lock): δ 57.4 (s, $SF_6$).

**$^{19}$F (-200 center point)** (470.6 MHz, THF, no lock): δ -133.

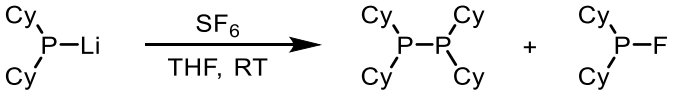


**Reaction of lithium dicyclohexylphosphide 6-32 and $SF_6$ gas.** Dicyclohexylphosphine **6-31** (0.2 mL, 0.1 mmol, 0.5M in THF) was dispensed into a 1 dram vial. The solution was diluted with additional solvent (0.55 mL THF and 0.05 mL benzene-$d_6$). *n*-Butyllithium (0.04 mL, 0.1 mmol, 2.5M) was then added and the solution turned orange. The solution was then transferred to an NMR tube and the sample was capped with a septum. An $SF_6$ gas filled balloon equipped with a needle was then inserted into the solution and bubbled through for 15s. The solution went from orange to clear/yellow colour during this period in which the needle and septum were removed and replaced with a standard NMR cap. The solution was then analyzed using NMR spectroscopy.

**NMR spectrum of $LiPCy_2$ 6-32 before $SF_6$ addition:**

**$^{31}$P** (202.5 MHz, THF, $C_6D_6$ (lock)): δ -12 (s).

**NMR spectrum after $SF_6$ addition:**

**$^{31}$P** (202.5 MHz, THF, $C_6D_6$ (lock)): δ -21.6 (s).

**$^{19}$F (0 center point)** (470.6 MHz, THF, $C_6D_6$ (lock)): δ 57.3 (s, $SF_6$).

**$^{19}$F (-200 center point)** (470.6 MHz, THF, $C_6D_6$ (lock)): δ -106 (d, $^1J_{P,F}$ = 1027 Hz), -202 (s).

**The reaction was repeated at -15 °C, but $^{31}$P NMR did not show any significant change in purity.** Dicyclohexylphosphine **6-31** (0.2 mL, 0.1 mmol, 0.5M in THF) was dispensed into a 1 dram vial. The solution was diluted with additional solvent (0.55 mL THF and 0.05 mL benzene-$d_6$). *n*-Butyllithium (0.04 mL, 0.1 mmol, 2.5M) was then added and the solution turned orange. The solution was then transferred to an NMR tube and the sample was capped with a septum. The sample was cooled to –15 °C in an ice/acetone bath. An $SF_6$ gas filled balloon equipped with a needle was then inserted into the solution and bubbled through for 15s. The solution went from orange to clear/yellow colour during this period in which the needle and septum were removed and replaced with a standard NMR cap. The solution was then analyzed using NMR spectroscopy.

**$^{31}$P** (202.5 MHz, THF, $C_6D_6$ (lock)): δ -21.6 (s).

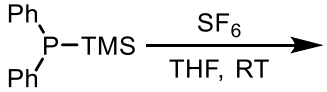


**Reaction of (trimethylsilyl)diphenylphosphine 6-48 and $SF_6$ gas.** (Trimethylsilyl)diphenylphosphine **6-48** (25.8 mg, 0.1 mmol) was weighed into a 1 dram vial. The solution was diluted with additional solvent (0.75 mL THF and 0.05 mL benzene-$d_6$). The solution was then transferred to an NMR tube and analyzed. The sample was capped with a septum and an $SF_6$ gas filled balloon equipped with a needle was then inserted into the solution and bubbled through for 15s. The septum was removed and replaced with a standard NMR cap. The solution was then analyzed using NMR spectroscopy.

**NMR spectrum of 6-48 in THF before addition of $SF_6$.**

**$^{31}$P** (202.5 MHz, THF, $C_6D_6$ (lock)): δ -57.1 (s).

**NMR spectrum of 6-48 in THF after addition of $SF_6$.**

**$^{31}$P** (202.5 MHz, THF, $C_6D_6$ (lock)): δ -57.1 (s).

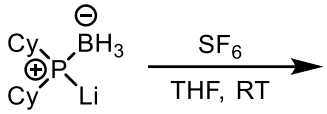


**Reaction of lithium dicyclohexylphosphide borane adduct 6-46 and $SF_6$ gas.** Dicyclohexylphosphine **6-31** (0.2 mL, 0.1 mmol, 0.5M in THF) was dispensed into a 1 dram vial. The solution was diluted with additional solvent (0.55 mL THF and 0.05 mL benzene-$d_6$). Borane dimethylsulfide (0.1 mL, 0.1 mmol, 1M toluene) was added to the vial, solution was then transferred to an NMR tube and an NMR spectrum was acquired. *n*-Butyllithium (0.04 mL, 0.1 mmol, 2.5M) was then added and the solution turned a yellow colour. The sample cap was then replaced with a septum. An $SF_6$ gas filled balloon equipped with a needle was then inserted into the solution and bubbled through for 15s. The solution went from orange to clear/yellow colour during this period in which the needle and septum were removed and replaced with a standard NMR cap. The solution was then analyzed using NMR spectroscopy.

**NMR spectrum of mixture of $HPCy_2$ and $BH_3$ in THF (6-45)**:

**$^{31}$P** (202.5 MHz, THF, $C_6D_6$ (lock)): δ 18 (d, $^1J_{P,H}$ = 350 Hz).

**NMR spectrum of *n*-BuLi deprotonation of $HPCy_2$ and $BH_3$ adduct (6-46):**

**$^{31}$P** (202.5 MHz, THF, $C_6D_6$ (lock)): δ -36 (m).

**NMR spectrum after addition of $SF_6$:**

**$^{31}$P** (202.5 MHz, THF, $C_6D_6$ (lock)): δ -36 (m).

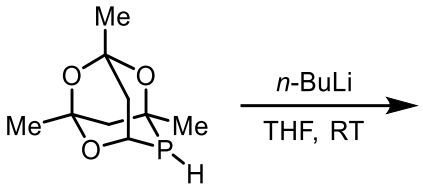


**Cage Phos 6-42 deprotonation attempt 1.** Cage Phos **6-42** (67 mg, 0.1 mmol, ~32% w/w in xylene) was dispensed into a 1 dram vial. The solution was diluted with additional solvent (0.75 mL THF and 0.05 mL benzene-$d_6$). *n*-Butyllithium (0.04 mL, 0.1 mmol, 2.5M) was then added and the solution turned orange. The solution was then transferred to an NMR tube and the sample was capped with a septum. The sample was analyzed and found no change in the $^{31}$P NMR spectrum. An $SF_6$ gas filled balloon equipped with a needle was then inserted into the solution and bubbled through for 15s. The solution went from an orange to clear/yellow colour during this period in which the needle and septum were removed and replaced with a standard NMR cap. The solution was then analyzed using NMR spectroscopy, however no formation of soluble, NMR active, new phosphorus containing products were observed.

**NMR spectrum of 6-42 before addition of *n*-BuLi:**

**$^{31}$P** (121.5 MHz, THF, $C_6D_6$ (lock)): δ -50.6 (d, $^1J_{P,H}$ = 187 Hz).

**NMR spectrum of 6-42 after addition of *n*-BuLi:**

**$^{31}$P** (121.5 MHz, THF, $C_6D_6$ (lock)): δ -50.6 (d, $^1J_{P,H}$ = 187 Hz ).

**NMR spectrum of 6-42 and *n*-BuLi, after addition of $SF_6$:**

**$^{31}$P** (121.5 MHz, THF, $C_6D_6$ (lock)): δ -50.6 (d, $^1J_{P,H}$ = 187 Hz ).

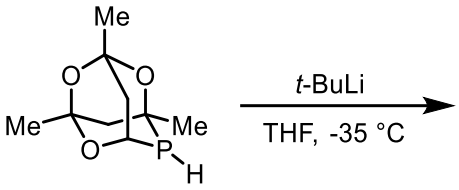


**Cage Phos 6-42 deprotonation attempt 2.** Cage Phos **6-42** (67 mg, 0.1 mmol, ~32% w/w in xylene) was dispensed into a 1 dram vial. The solution was diluted with additional solvent (0.75 mL THF and 0.05 mL benzene-$d_6$) The solution was then cooled to -35 °C. *Tert*-butyllithium (0.06 mL, 0.1 mmol, 1.7 M) was then added and the solution turned orange. The solution was stirred for 1 h and then analyzed by NMR analysis and found no change in the spectrum.

**NMR spectrum of 6-42 after addition of *tert*-BuLi:**

**$^{31}$P** (202.5 MHz, THF, $C_6D_6$ (lock)): δ -50.5 (d, $^1J_{P,H}$ = 187 Hz).

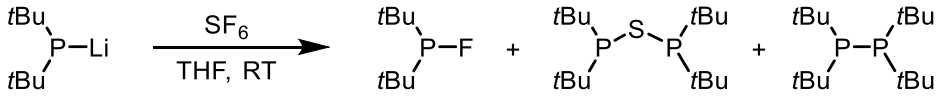


**Reaction of lithium ditertbutylphosphide 6-39 and $SF_6$ gas.** Di-*tert*-butylphosphine **6-38** (0.2 mL, 0.1 mmol, 0.5M in THF) was dispensed into a 1 dram vial. The solution was diluted with additional solvent (0.55 mL THF and 0.05 mL benzene-$d_6$). *n*-Butyllithium (0.04 mL, 0.1 mmol, 2.5M) was then added and the solution turned orange. The solution was then transferred to an NMR tube and the sample was capped with a septum. An $SF_6$ gas filled balloon equipped with a needle was then inserted into the solution and bubbled through for 15s. The solution went from orange to clear/yellow colour during this period in which the needle and septum were removed and replaced with a standard NMR cap. The solution was then analyzed using NMR spectroscopy. Mass spectrometry identified the presence of dimer **6-41**, but fragments corresponding to the other components observed by NMR were not observed by mass spectrometry.

**NMR spectrum of 6-39 formed from mixing 6-38 and *n*-BuLi in THF:**

**$^{31}$P** (121.5 MHz, THF, $C_6D_6$ (lock)): δ 40.8 (s).

**NMR spectra of addition of $SF_6$ to 6-39 in THF:**

**$^{31}$P** (121.5 MHz, THF, $C_6D_6$ (lock)): δ 212 (d, $^1J_{P,F}$ = 870 Hz), 85.2 (s), 39.5 (s).

**$^{19}$F (0 center point)** (282.4 MHz, THF, $C_6D_6$ (lock)): δ 57.3 (s, $SF_6$).

**$^{19}$F (-200 center point)** (282.4 MHz, THF, $C_6D_6$ (lock)): δ -203 (s), - 217 (d, $^1J_{P,F}$ = 870 Hz).

**HRMS (ESI):** calc'd for $C_{16}H_{37}P_2$ [M + H+] 291.2365; Found: 291.2363.

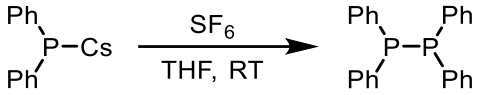


**Reaction of cesium diphenylphosphide 6-49 and $SF_6$ gas.** Cesium carbonate (17 mg, 0.052 mmol) was weighed into a 1 dram vial equipped with a magnetic stir bar. A solution of THF and benzene-$d_6$ was added (0.55 mL THF and 0.05 mL benzene-$d_6$) followed by potassium diphenylphosphide **6-25** (0.2 mL, 0.1 mmol, 0.5M in THF). The reaction was stirred for 2 h. The solution went from orange to red during this period and then the solution was then transferred to an NMR tube and the sample was analyzed using NMR spectroscopy. The sample cap was then replaced with a septum. An $SF_6$ gas filled balloon equipped with a needle was then inserted into the solution and bubbled through for 15s. The solution went from orange to clear/yellow colour during this period in which the needle and septum were removed and replaced with a standard NMR cap. The solution was then analyzed using NMR spectroscopy.

**NMR spectrum after addition of cesium carbonate:**

**$^{31}$P** (202.5 MHz, THF, $C_6D_6$ (lock)): δ -7.5 (s).

**NMR spectra of addition of $SF_6$ to 6-49 in THF:**

**$^{31}$P** (121.5 MHz, THF, $C_6D_6$ (lock)): δ -15.6 (s).

**$^{19}$F (0 center point)** (282.4 MHz, THF, $C_6D_6$ (lock)): δ 57.3 (s). $SF_6$.

**$^{19}$F (-200 center point)** (282.4 MHz, THF, $C_6D_6$ (lock)): δ -132 (s).

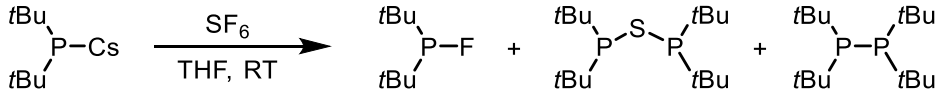


**Reaction of Cesium ditertbutylphosphide 6-50 and $SF_6$ gas.** Di-*tert*-butylphosphine **6-38** (0.2 mL, 0.1 mmol, 0.5M in THF) was dispensed into a 1 dram vial. The solution was diluted with additional solvent (0.55 mL THF and 0.05 mL benzene-$d_6$). *n*-Butyllithium (0.04 mL, 0.1 mmol, 2.5M) was then added and the solution turned orange/yellow and was stirred for 1 h. Cesium fluoride (15 mg, 0.1 mmol) was added to the solution and stirred for 1h. The solution was then transferred to an NMR tube and the sample was analyzed using NMR spectroscopy. The sample cap was then replaced with a septum. An $SF_6$ gas filled balloon equipped with a needle was then inserted into the solution and bubbled through for 15s. The solution went from orange to clear/yellow colour during this period in which the needle and septum were removed and replaced with a standard NMR cap. The solution was then analyzed using NMR spectroscopy.

**NMR spectrum after addition of cesium fluoride:**

**$^{31}$P** (202.5 MHz, THF, $C_6D_6$ (lock)): δ 70.6 (s).

**NMR spectra of addition of $SF_6$ to 6-50 in THF:**

**$^{31}$P** (202.5 MHz, THF, $C_6D_6$ (lock)): δ 212 (d, $^1J_{P,F}$ = 870 Hz), 85.4 (s), 39.8 (s).

**$^{19}$F (0 center point)** (470.6 MHz, THF, $C_6D_6$ (lock)): δ 57.3 (s, $SF_6$).

**$^{19}$F (-200 center point)** (470.6 MHz, THF, $C_6D_6$ (lock)): δ - 217 (d, $^1J_{P,F}$ = 870 Hz).

## 6.6 Experimental for section 6.3

### 6.6.1 General Considerations

All reagents and solvents were dispensed in a 2001 issue IT Glovebox ($H_2O$ levels vary between 2-6 ppm) unless otherwise stated. Diazaphospholenes were prepared in either a Schlenk flask under a nitrogen atmosphere or in oven dried 4 dram scintillation vials equipped with magnetic stir bars and green Qorpak® PTFE lined caps unless otherwise stated. All reactions were conducted at ambient temperature unless otherwise stated. $^{1}H$, $^{31}P$, $^{19}F$, and $^{13}C$ NMR data were collected at 300K on either a Bruker AV-300 or AV-500 spectrometer. $^{1}H$ NMR spectra are referenced to residual non-deuterated NMR solvent from the sample ($C_6H_6$ = 7.16 ppm, $CHCl_3$ = 7.26 ppm). $^{13}C$ NMR spectra are referenced to NMR solvent from the sample ($C_6D_6$ = 128.06 ppm, $CDCl_3$ = 77.16 ppm). LED irradiation was conducted using a Kessil H150-Blue lamp. The maximum emission wavelength of this lamp is centered around 465 nm. The lamp also produces a secondary emission peak approximately 30% the intensity of the primary peak, centered around 417 nm. UV irradiation was conducted using a Luzchem LZC-4V photobox with 350 nm bulbs. Blue (450-460 nm) and green bulbs (510-530 nm) were also used in this photobox. Mass spectrometric data were acquired by Mr. Xiao Feng (Mass Spectrometry Laboratory, Dalhousie University). Melting points were acquired using an Electrothermal® apparatus and are uncorrected.

### 6.6.2 Solvents

**Toluene** was purchased in a drum ACS grade from Fisher and was passed through a double column purification system (activated alumina and activated Q-5) from MBraun Inc. and stored over 3Å molecular sieves under nitrogen.

**Pentane** was purchased in a drum as ACS grade from Fisher, sparged with nitrogen and stored over 3Å molecular sieves under nitrogen.

**Tetrahydrofuran** was purchased as anhydrous >99% ACS grade from Sigma Aldrich and stored over 3Å molecular sieves under nitrogen.

**Acetonitrile** was purchased as anhydrous >99% ACS grade from Sigma Aldrich and used without further purification.

**Hexanes** was purchased in a drum ACS grade from Fisher and used as is.

### 6.6.3 Reagents

**Tricyclohexylphosphine 6-54** was purchased from oakwood and either used as received or crystallized from ethanol under a nitrogen atmosphere.

**Triphenylphosphine 6-55** was purchased from Sigma Aldrich and used as received.

**Tri-*n*-butylphosphine 6-14** was purchased from Sigma Aldrich and used as received.

**Tricyclohexylphosphine sulfide 6-56** was prepared according to literature procedure.

**Diazaphospholene dimer 6-21** was prepared according to literature procedure.[250]

**Diazaphospholene bromide 6-51** was prepared according to literature procedure.[77]

**Phenylsilane** was purchased from Sigma Aldrich and used as received.

**Triethylsilane** was purchased from Sigma Aldrich and used as received.

**Dimethylphenylsilane** was purchased from Sigma Aldrich and used as received.

**Diphenylsilane** was purchased from Oakwood Chemicals and used as received.

**Pinacol borane** was purchased from Oakwood Chemicals and used as received.

**Triethylamine (anhydrous)** was purchased from Sigma Aldrich and used as received.

**Tetrabutylammonium difluorotriphenylsilicate (TBAT)** was purchased from Sigma Aldrich and used as received.

**Tetramethylammonium fluoride (TMAF)** was purchased from Sigma Aldrich and used as received.

**Sulfur 42** was purchased from Sigma Aldrich and used as received.

**Pentafluorosulfanyl benzene** was purchased from Oakwood Chemicals and used as received.

**Fluolead** was purchased from TCI chemicals and used as received.

All alkenes or alkynes were purchased from Sigma Aldrich or Oakwood Chemicals and used as received.

### 6.6.4 Synthetic Procedures

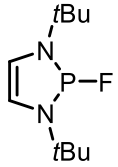


**Diazaphospholene fluoride** (**6-22**)**.** Diazaphospholene bromide **6-51** (558mg, 2 mmol) was weighed into a 4 dram vial containing a magnetic stir bar. Tetramethylammonium fluoride (186, 2 mmol) was then added to the vial followed by the addition of dichloromethane (5 mL). The reaction was left to stir overnight, followed by the removal volatiles *in vacuo*. Pentane (10 mL) was added to the crude solid and the subsequent mixture was filtered over a fine porous frit. The remaining solid was washed with pentane (2 x 10mL) and the pentane extracts were evaporated to dryness affording the product **6-22**. Diazaphospholene oxide **6-52** is present in the sample and was not further purified.

**$^{1}$H** (300 MHz, $C_6D_6$): δ 6.03 (d, $^{3}J_{H,P}$ = 1.8 Hz, 2H), 1.32 (d, $^{4}J_{H,P}$ = 1.5 Hz, 18H).

**$^{13}$C** {$^{1}$H} (75.5 MHz, $C_6D_6$): δ 112 (d, $^{2}J_{C,P}$ = 9 Hz), 53.3 (d, $^{2}J_{C,P}$ = 13 Hz), 31.3 (d, $^{3}J_{C,P}$ = 11 Hz).

**$^{31}$P** (121.5 MHz, $C_6D_6$): δ 110 (d, $^{1}J_{P,F}$ = 1067 Hz).

**$^{19}$F** (282.4 MHz, $C_6D_6$): δ -33.4 (d, $^{1}J_{F,P}$ = 1067 Hz).

**HRMS (APCI):** calc'd for $C_{10}H_{20}FN_2P$ [M +] 218.1343; Found: 218.1352.

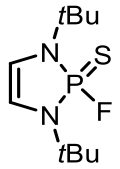


**Diazaphospholene fluorosulfide (6-53).** Diazaphospholene fluoride **6-22** (33 mg, 0.15 mmol) was weighed into a 1 dram vial and dissolved with tetrahydrofuran (1.5 mL) and triethylamine (0.1 mL, 0.75 mmol, 5 equiv.). Sulfur 42 (29 mg, 0.15 mmol) was weighed into a 4 dram vial equipped with a magnetic stir bar. The solution containing diazaphospholene fluoride was added to the 4 dram vial with sulfur 42 and the reaction was stirred for 1.5 h. Volatiles were removed *in vacuo* and pentane was added to the crude solid. The pentane was filtered through a syringe filter and the process was repeated with pentane (5 mL) twice more. The pentane was evaporated to dryness affording the product (33 mg). This product contained impurities and was not purified further due to potential toxcicity.

**$^{1}$H** (500 MHz, $C_6D_6$): δ 5.71 (dd, $^{3}J_{H,P}$ = 21.6 Hz, $^{4}J_{H,F}$ = 1 Hz, 2H), 1.35 (s, 18H).

**$^{13}$C** {$^{1}$H} (125.7 MHz, $C_6D_6$): δ 110 (dd, $^{2}J_{C,P}$ = 14.2 Hz, $^{3}J_{C,F}$ = 2.2 Hz), 55.6 (d, $^{2}J_{C,P}$ = 4.0 Hz), 29.7 (s)

**$^{31}$P** (202.5 MHz, $C_6D_6$): δ 64.2 (dt, $^{1}J_{P,F}$ = 1147 Hz, $^{3}J_{P,H}$ = 14.2 Hz).

**$^{19}$F** (470.6 MHz, $C_6D_6$): δ 11.8 (d, $^{1}J_{F,P}$ = 1147 Hz)

**HRMS (APCI):** calc'd for $C_{10}H_{21}FN_2PS$ [M + H+] 251.1142; Found: 251.1135.

### 6.6.5 Reactivity Studies

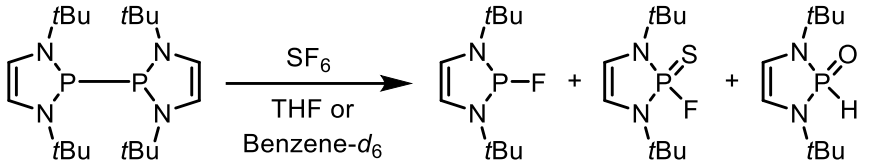


**Diazaphospholene dimer 6-21 reactivity with $SF_6$.** Diazaphospholene dimer **6-21** (20mg, 0.05 mmol) was weighed into a 1 dram vial and dissolved in either benzene-$d_6$ (0.7 mL) or a mixture of tetrahydrofuran (0.65 mL) and benzene-$d_6$ (0.05 mL). The solution was transferred to a standard NMR tube. The NMR tube was capped with a septum and $SF_6$ was bubbled through the NMR tube for approximately 11s using a balloon filled with $SF_6$ equipped with a needle. The septum was quickly replaced with a standard NMR cap and wrapped with Teflon tape. The NMR tubes were either irradiated with blue light or enclosed in a dark confinement for 30 min. Samples were then analyzed using NMR spectroscopy. The products were reported in relative proportion to diazaphospholene fluoride.

**Table 6.13** Diazaphospholene dimer **7-1** reacted with $SF_6$ in a standard NMR tube for 30 min before NMR acquisition. Equivalence of phosphines were measured in the $^{31}P$ NMR spectrum relative to **6-22**.

| Conditions | NHP-F (**6-22**) | $NHP_2$ (**6-21**) | NHP(S)-F (**6-53**) | NHP(O)-H (**6-52**) |
|---|---|---|---|---|
| 30 min, benzene-$d_6$, no light | 1 | 0.16 | 0.07 | 0.09 |
| 30 min, benzene-$d_6$, blue LED *hv* | 1 | 0 | 0.07 | 0.11 |
| 30 min, THF, no light | 1 | 0.01 | 0.02 | 0.05 |
| 30 min, THF, blue LED *hv* | 1 | 0 | 0.04 | 0.06 |

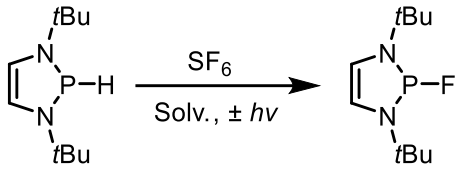


**Diazaphospholene hydride 6-19 reactivity.** Diazaphospholene hydride **6-19** (10mg, 0.05 mmol) was weighed into a 1 dram vial and dissolved in either benzene-$d_6$ (0.7 mL), a mixture of tetrahydrofuran (0.65 mL) and benzene-$d_6$ (0.05 mL) or a mixture of acetonitrile (0.65 mL) and benzene-$d_6$ (0.05 mL). The solution was transferred to a standard NMR tube. The NMR tube was capped with a septum and $SF_6$ was bubbled through the NMR tube for approximately 11s using a balloon filled with $SF_6$ equipped with a needle. The septum was quickly replaced with a standard NMR cap and wrapped with Teflon tape. The NMR tubes were either irradiated with a light source or enclosed in a dark confinement for the reported time. Samples were then analyzed using NMR spectroscopy. The products were reported in relative proportion to diazaphospholene fluoride.

**Table 6.14** Diazaphospholene hydride **6-19** reacting with $SF_6$ for the indicated time before NMR acquisition. Equivalence of phosphines were measured in the $^{31}P$ NMR spectrum relative to **6-22**.

| Conditions | NHP-F (**6-22**) | NHP-H (**6-19**) | NHP(S)-F (**6-53**) | NHP(O)-H (**6-52**) |
|---|---|---|---|---|
| 30 min, THF, blue LED *hv* | 1 | 11.57 | 0 | 1.15 |
| 30 min, benzene-$d_6$, blue LED *hv* | 1 | 12.49 | 0 | 1.43 |
| 30 min, $CH_3CN$, blue LED *hv* | 1 | 0 | 0 | 0.10 |
| 1 h, THF, blue LED *hv* | 1 | 2.8 | 0 | 0.95 |
| 1 h, THF, blue photobox *hv* | 1 | 2.86 | 0 | 0.60 |
| 1 h, THF, green photobox *hv* | 1 | 19.62 | 0 | 1.88 |
| 30 min, THF, UV photobox *hv* | 1 | 5.04 | 0 | 0.41 |
| 1 h, THF[a], blue LED *hv* | 1 | 6.05 | 0 | 0.66 |
| 1 h, THF[b], UV photobox *hv* | 1 | 0 | 0 | 1.59 |
| 6 h, THF, blue LED *hv* | 1 | 0 | 0.01 | 0.37 |
| 30 min, THF, no light | 1 | 29.8 | 0 | 1.7 |
| 30 min, benzene-$d_6$, no light | 0 | 1 | 0 | 0.07 |
| 30 min, $CH_3CN$, no light | 1 | 0 | 0 | 0.15 |

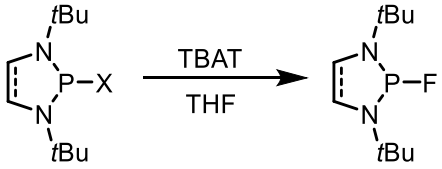


**Diazaphospholene fluoride 6-22 generation *in situ*.** A Diazaphospholene halide (7 mg, 0.025 mmol) was weighed into a 1 dram vial followed by the addition of tetrabutylammonium difluorotriphenylsilicate (13.5 mg, 0.025 mmol, 1 equiv.). The solids were dissolved with tetrahydrofuran (0.65 mL) and benzene-$d_6$ (0.05 mL) and the solution was transferred to a standard NMR tube. The solution was analyzed using NMR spectroscopy.

**Diazaphospholene bromide 6-51 to fluoride 6-22:**

**$^{31}$P** (121.5 MHz, $C_6D_6$): δ 110 (d, $^{1}J_{P,F}$ = 1065 Hz).

**$^{19}$F** (282.4 MHz, $C_6D_6$): δ -33.8 (d, $^{1}J_{F,P}$ = 1065 Hz) , -170 (s, $Ph_3SiF$).

**Saturated diazaphospholene chloride 6-63 to fluoride:**

**$^{31}$P** (121.5 MHz, $C_6D_6$): δ 130 (d, $^{1}J_{P,F}$ = 1037 Hz).

**$^{19}$F** (282.4 MHz, $C_6D_6$): δ -55.3 (dt, $^{1}J_{P,F}$ = 1037 Hz, $^{3}J_{P,H}$ = 5.6 Hz), -170 (s, $Ph_3SiF$).

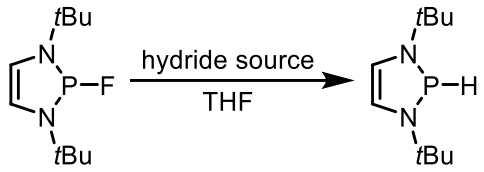


**Diazaphospholene hydride 6-19 formation from fluoride 6-22.** Diazaphospholene bromide **6-51** (7 mg, 0.025 mmol) was weighed into a 1 dram vial followed by the addition of tetrabutylammonium difluorotriphenylsilicate (13.5 mg, 0.025 mmol, 1 equiv.). The solids were dissolved with tetrahydrofuran (0.65 mL) and benzene-$d_6$ (0.05 mL). A silane or borane was then added (approx. 8-11 hydride equivalence) and the solution was transferred to a standard NMR tube. After 15 min, the solution was analyzed using NMR spectroscopy and if complete conversion or no reactivity was observed, the reaction was then analyzed after the specified time. The products were reported in relative proportion to diazaphospholene fluoride **6-22**.

**Table 6.15** Diazaphospholene hydride **6-19** formation from fluoride **6-22** with NMR acquisition after 15 min. Amounts of **6-19** and **6-22** determined by $^{31}$P NMR.

| Silane or borane | NHP-F (**6-22**) | NHP-H (**6-19**) |
|---|---|---|
| HB(Pin) | 0 | 1 |
| $PhSiH_3$ | 0 | 1 |
| $Ph_2SiH_2$ | 1 | 0.24 |
| $PhMe_2SiH$ | 1 | 0 |
| $Et_3SiH$ | 1 | 0 |

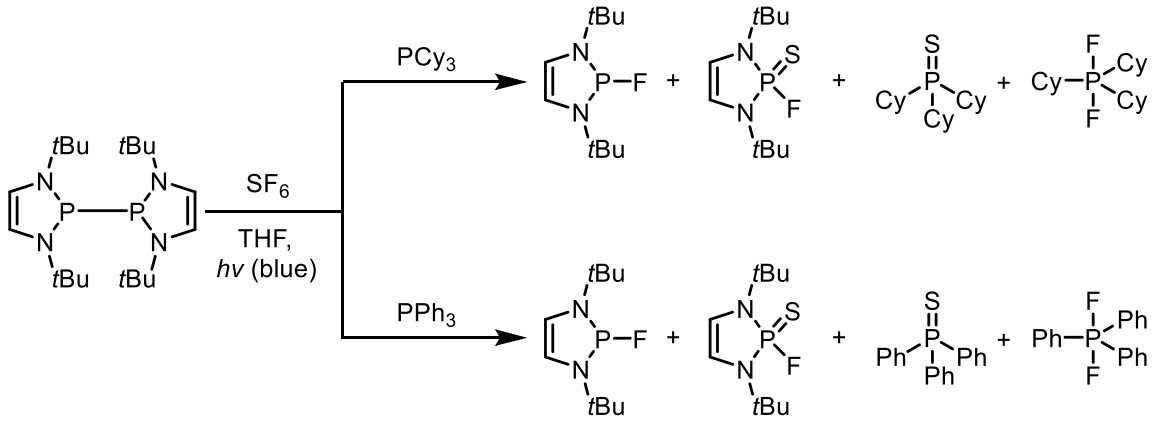


**Sulfur capture with phosphines in the presence of diazaphospholene 6-21.** Diazaphospholene dimer **6-21** (0.05-0.3 mmol) and a phosphine (0.1 mmol) was weighed into a 1 dram vial and dissolved in a mixture of tetrahydrofuran (0.65 mL) and benzene-$d_6$ (0.05 mL). The solution was transferred to a standard NMR tube. The NMR tube was capped with a septum and $SF_6$ was bubbled through the NMR tube for approximately 11s using a balloon filled with $SF_6$ equipped with a needle. The septum was quickly replaced with a standard NMR cap and wrapped with Teflon tape. The NMR tubes were irradiated with blue light for the allotted time. Samples were then analyzed using NMR spectroscopy.

**Table 6.16** Sulfur capture with phosphines **6-54** or **6-55** in the presence of diazaphospholene **6-21**. [a]Reaction conducted in a quartz tube with double the specified volume of solvent. Equivalence of phosphines were measured in the $^{31}P$ NMR spectrum relative to phosphine sulfide.

| Conditions | $SPR_3$ | $PR_3$ | NHP(S)-F **6-53** | $F_2PR_3$ |
|---|---|---|---|---|
| $NHP_2$ **6-21**, $PCy_3$ **6-54**, 1:1 ratio, 30 min | 1 | 2.86 | 0.08 | 0.7 |
| $NHP_2$ **6-21**, $PPh_3$ **6-55**, 1:1 ratio, 30 min | 1 | 4 | 0 | 0.2 |
| NHP-H **6-19**, $PCy_3$ **6-54**, 1:1 ratio, 6 h | 1 | 9.1 | 0 | 0.1 |
| NHP-H **6-19**, $PCy_3$ **6-54**, 6:1 ratio, 6 h[a] | 1 | 1.5 | 0.19 | 0.19 |

**Early catalytic test reactions.** Diazaphospholene bromide **6-51** (7 mg, 0.025 mmol) was weighed into a 1 dram vial followed by the addition of tetrabutylammonium difluorotriphenylsilicate (13.5 mg, 0.025 mmol, 1 equiv.). Tricyclohexylphosphine **6-54** was then added to the vial (42 mg, 0.15 mmol, 6 equiv.). The solids were dissolved in a mixture of tetrahydrofuran (0.65 mL) and benzene-$d_6$ (0.05 mL) and then followed by the addition of phenylsilane (0.04 mL, 0.32 mmol, 2.2 equiv.) and triethylamine (0.03 mL, 0.225 mmol, 9 equiv.). The solution was transferred to a standard NMR tube. The NMR tube was capped with a septum and $SF_6$ was bubbled through the NMR tube for approximately 11s using a balloon filled with $SF_6$ equipped with a needle. The septum was quickly replaced with a standard NMR cap and wrapped with Teflon tape. The NMR tube was irradiated with a light source for the specified time. The sample was then analyzed using NMR spectroscopy.

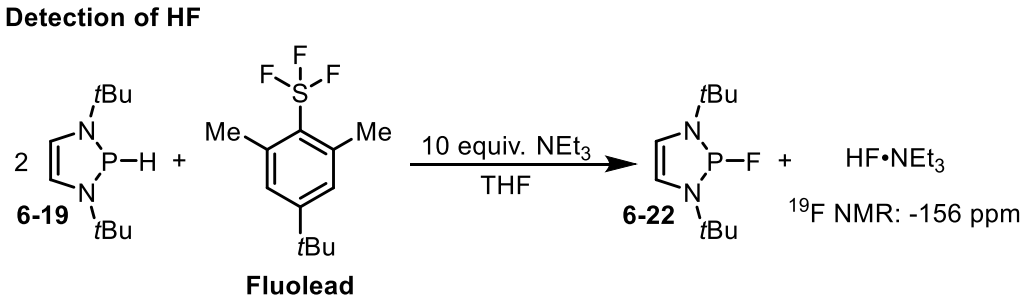


**Detection of HF.** Diazaphospholene hydride **6-19** (16mg, 0.08 mmol, 2 equiv.) was weighed into a 1 dram vial and dissolved in tetrahydrofuran (0.65 mL) and benzene-$d_6$ (0.05 mL). Triethylamine (0.06 mL, 0.4 mmol, approx. 10 equiv.) was then added followed by Fluolead (10mg, 0.04 mmol) The solution was transferred to a standard NMR tube. The sample was then analyzed using NMR spectroscopy.

**General Procedure for the catalytic reduction of $SF_6$.** Diazaphospholene halide was weighed into a 1 dram vial. In some instances, this was followed by the addition of tetrabutylammonium difluorotriphenylsilicate (13.5 mg, 0.025 mmol, 1 equiv.). A phosphine was then weighed into a separate vial. The phosphine was dissolved with 1 mL of the specified solvent followed by the addition of the hydride source (144 hydride equivalence) and triethylamine. The solution was added to the vial containing the diazaphospholene bromide. The solution was then transferred to a 45 mL quartz tube or flask of specified volume equipped with magnetic stir bar and the vial rinsed with an additional solvent up to the specified amount, which was added to the tube/flask. The glass vessel was capped with a septum and sealed with electrical tape. $SF_6$ was bubbled through the solution with a full balloon. The septum was then fully sealed with electrical tape and the reaction was stirred under a light source for the allotted time.

**Procedure for optimized conditions.** Diazaphospholene bromide **6-51** (7 mg, 0.025 mmol) was weighed into a 1 dram vial. Tricylclohexylphosphine **6-54** (280 mg, 1 mmol)

was then weighed into a separate vial. The phosphine was dissolved in THF (1 mL) followed by the addition of phenylsilane (0.3 mL, approx. 2.4 mmol) and triethylamine (0.21 mL, 1.43 mmol). The solution containing the phosphine was added to the vial containing the diazaphospholene bromide. The solution was then transferred to a 50 mL round bottom flask equipped with magnetic stir bar and the vial rinsed with an additional solvent (2 mL), which was added to the flask. The flask was capped with a septum and sealed with electrical tape. $SF_6$ was bubbled through the solution with a full balloon. The septum was then fully sealed with electrical tape and the reaction was stirred under blue light for 18 h. An aliquot was then taken from the reaction and analyzed using NMR spectroscopy. The sample was then recombined with the reaction mixture and all volatiles were removed *in vacuo*. The sample was dry loaded onto a column and purified using an eluent gradient of 0 to 10% ether in hexanes to afford the product **6-56** (256 mg, 0.819 mmol, 82%).

**$^{1}$H** (500 MHz, $C_6D_6$): δ 1.98 (m, 6H), 1.8 (m, 3H), 1.65 (m, 6H), 1.53 (m, 3H), 1.42 (m, 6H), 1.05 (m, 9H).

**$^{13}$C** {$^{1}$H} (125.8 MHz, $C_6D_6$): δ 37.6 (d, $^{1}J_{C,P}$ = 45.4 Hz), 27.6 (d, $^{3}J_{C,P}$ = 2.4 Hz), 27.3 (d, $^{2}J_{C,P}$ = 12.1 Hz), 26.4 (s).

**$^{31}$P** (202.5 MHz, $C_6D_6$): δ 61.1.

**MP:** 185-188 °C

HRMS (ESI): calc'd for $C_{18}H_{33}PSNa$ [M + Na +] 335.1933; Found: 335.1930.

**General procedure for Pentafluorosulfanylation.** Diazaphospholene **6-19** (40 mg, 0.2 mmol) was weighed into a 1 dram vial equipped with a magnetic stir bar. Benzene-$d_6$, tetrahydrofuran (0.65 mL) or acetonitrile (0.65 mL) were added to the vial followed by an amount of acceptor for a total volume of 0.7 mL. The solution was transferred to a standard

NMR tube. The NMR tube was capped with a septum and $SF_6$ was bubbled through the NMR tube for approximately 11s using a balloon filled with $SF_6$ equipped with a needle. The septum was quickly replaced with a standard NMR cap and wrapped with Teflon tape. The sample was then analyzed using NMR spectroscopy between 1-2 h.

**Preparation of Pentafluorosulfanyloctene.** Diazaphospholene **6-19** (40 mg, 0.2 mmol) was weighed into a 1 dram vial equipped with a magnetic stir bar. Acetonitrile (0.35 mL) and 1-octene **6-65d** (0.35 mL) were added to the vial. The vial was fitted with a septum and sparged with $SF_6$ gas. The reaction was left to stir for 2 h and the two layers of the reaction were then separated, benzene-$d_6$ (approx. 0.3 mL) added and analyzed with NMR spectroscopy. Both layers were found to contain pentafluorosulfanyloctene and were recombined and the solution was concentrated to approximately 0.3 mL. The solution was then diluted with pentane (2 mL) and passed through a silica plug with an additional amount of pentane (5 mL. The pentane fractions were then combined, and the solution concentrated to an oil. $CDCl_3$ was then added to the sample and the solution was analyzed with NMR and MS to determine the product as pentafluorosulfanyloctene.

**$^{19}$F** (470.6 MHz, $CDCl_3$): δ 85.3 (p, $^1J_{F,F}$ = 145 Hz), 63.6 (dt, $^1J_{F,F}$ = 145 Hz, $^3J_{F,H}$ = 8.0 Hz).

HRMS (ESI): calc'd for $C_8H_{16}F_5S$ [M +] 239.0887; Found: 239.0894.

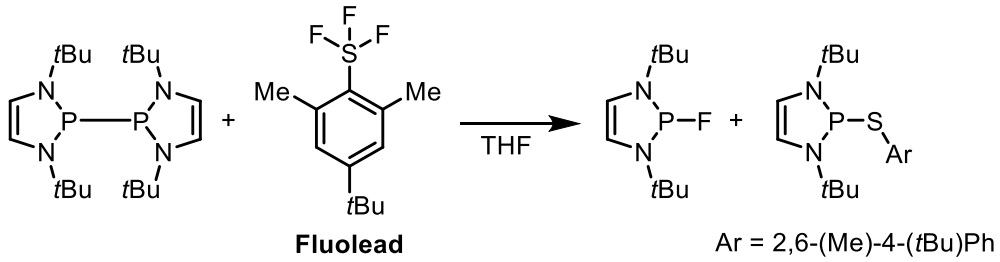


**Reaction of diazaphospholene dimer 6-21 with Fluolead.** Diazaphospholene dimer **6-21** (32 mg, 0.08 mmol, 2 equiv.) was weighed into a 1 dram vial and then dissolved in THF (0.75 mL). This solution was then transferred into a vial with Fluolead (10mg, 0.04 mmol). The solution was transferred to a standard NMR tube. The sample was then analyzed using NMR spectroscopy.

**$^{31}$P** (202.5 MHz, $C_6D_6$): δ 133 (s, P-SAr), 110 (d, $^{1}J_{P,F}$ = 1065 Hz, P-F).

**$^{19}$F** (282.4 MHz, $C_6D_6$): δ -34.8 (d, $^{1}J_{F,P}$ = 1065 Hz) ,

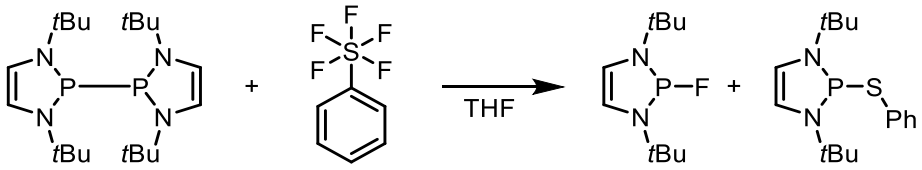


**Reaction of diazaphospholene dimer 6-21 with $PhSF_5$.** Diazaphospholene dimer **6-21** (32 mg, 0.12 mmol, 3 equiv.) was weighed into a 1 dram vial and then dissolved in THF (0.75 mL). This solution was then transferred into a vial with $PhSF_5$ (8 mg, 0.04 mmol). The solution was transferred to a standard NMR tube. The sample was then analyzed using NMR spectroscopy after 1h. The solution was then irradiated for 30 min with a blue LED and was then analyzed using NMR spectroscopy. Only trace amount of diazaphospholene fluoride was present in the reaction.

## 6.7 Experimental for section 6.4

### 6.7.1 General Considerations

All reagents and solvents were dispensed in a 2001 issue IT Glovebox ($H_2O$ levels vary between 2-6 ppm) unless otherwise stated. All reactions were conducted at ambient temperature unless otherwise stated. $^{1}H$, $^{31}P$, $^{19}F$, and $^{13}C$ NMR data were collected at 300K on either a Bruker AV-300 or AV-500 spectrometer, and hetereonuclei were referenced to external standards. Benzene $d_6$ was added to samples to enable autosampler use/automated locking on the Bruker instruments. $^{1}H$ NMR spectra are referenced to residual non-deuterated NMR solvent from the sample ($C_6H_6$ = 7.16 ppm, $CHCl_3$ = 7.26 ppm). $^{13}C$ NMR spectra are referenced to NMR solvent from the sample ($C_6D_6$ = 128.06 ppm, $CDCl_3$ = 77.16 ppm). Sulfur hexafluoride was dispensed from a "Prextex" 12 inch "party balloon" latex balloon, purchased from Amazon. The balloon was taped with electrical tape to a cut 6 mL syringe equipped with a Luer lock. The SEM images were acquired by Maxine Kirschenbaum and Dr. Mita Dasog on a Hitachi S-4700 electron microscope (either used in secondary electron or backscattered electron mode).

### 6.7.2 Solvents

**Toluene** was purchased in a drum ACS grade from Fisher and was passed through a double column purification system (activated alumina and activated Q-5) from MBraun Inc. and stored over 3Å molecular sieves under nitrogen.

**Pentane** was purchased in a drum as ACS grade from Fisher, sparged with nitrogen and stored over 3Å molecular sieves under nitrogen.

**Dichloromethane** was purchased in a drum as ACS grade from Fisher, distilled over calcium hydride and stored over 3Å molecular sieves under nitrogen.

**Tetrahydrofuran** was purchased as anhydrous >99% ACS grade from Sigma Aldrich and stored over 3Å molecular sieves under nitrogen.

**Hexanes** was purchased in a drum ACS grade from Fisher and used as is.

**Ether** was purchased as anhydrous >99% ACS grade from Sigma Aldrich and stored over 3Å molecular sieves under nitrogen.

**Ethnaol** (100%) was purchased in a drum ACS grade from Fisher and used as is.

### 6.7.3 Reagents

**Chlorodimethylsilane** was purchased from Sigma Aldrich and used as received.

**Trimethylchlorosilane** was purchased from Sigma Aldrich and distilled using a short path distillation.

**Triethylchlorosilane** was purchased from Sigma Aldrich and used as received.

**Magnesium turnings** 98% were purchased from Sigma Aldrich and used as received.

**Magnesium dust** <0.1 nm was purchased from EM Science <0.1 nm and used as received.

**Tricyclohexylphosphine 6-54** was purchased from oakwood chemicals and used as received

**Triphenyphosphine 6-55** was purchased from Sigma Aldrich and used as received.

**Tri-*n*-butylphosphine 6-14** was purchased from Sigma Aldrich and used as received.

**Sulfur** USP sublimed was purchased from Fisher and used as received.

**Hydrogen peroxide** 30% ACS grade was purchased from Fisher and used as received.

**HCl•$Et_2O$ (1M in $Et_2O$)** was purchased from Sigma Aldrich and used as received.

### 6.7.4 Synthetic Procedures for Products and Impurities

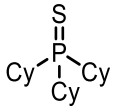

**SPCy$_3$ (6-56).** The following procedure is a modified version of a literature reported procedure.[255] Tricyclohexylphosphine **6-54** (594 mg, 2.12 mmol) was weighed into an oven dried 4 dram vial equipped with a magnetic stir bar under a nitrogen atmosphere. Sulfur (68 mg, 2.12 mmol, 1 equiv.) was added to the vial followed by toluene (3 mL). The reaction was left to stir overnight. Ether (15 mL) was added to the vial and the precipitate was collected via suction filtration under air. The solid was washed with ether (5 x 5 mL) and the solid was further dried under vacuum to afford the desired sulfide **6-56** (395 mg, 1.26 mmol, 60% yield).

**$^1$H** (500 MHz, $C_6D_6$): δ 1.98 (d, $J_{H,H}$ = 12 Hz, 6H), 1.8 (qt, $J_{H,H}$ = 12, 3 Hz, 3H), 1.65 (m, 6H), 1.53 (m, 3H), 1.43 (m, 6H), 1.05 (m, 9H).

**$^{13}$C** {$^1$H} (125.8 MHz, $C_6D_6$): δ 37.6 (d, $J_{C,P}$ = 45 Hz), 27.6 (d, $J_{C,P}$ = 2 Hz), 27.3 (d, $J_{C,P}$ = 12 Hz), 26.4 (s).

**$^{31}$P** (202.5 MHz, $C_6D_6$): δ 61.1.

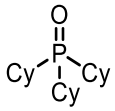

**OPCy$_3$ (6-67).** The following procedure is a modified version of a literature reported procedure.[256] Tricyclohexylphosphine **6-54** (1.07 g, 3.81 mmol) was weighed into a 50 mL pear-shaped flask equipped with a magnetic stir bar under nitrogen. The phosphine was dissolved in a mixture of ethanol (10 mL) and toluene (5 mL) and was then exposed to air. The solution was cooled to 0 °C and hydrogen peroxide (0.5 mL, 30% w/w soln) was added slowly. The solution was left to warm to room temperature overnight. The solution was

then cooled again to 0 °C and sodium sulfite (0.5 g) was added and left to stir for 1 h. Sodium sulfate was then added, and the solution filtered over a fine porous frit. Volatiles were removed *in vacuo* and the product was dried with a toluene azeotrope (3 x 5 mL) to afford the desired product tricyclohexylphosphine oxide **6-67** (1.07 g, 3.6 mmol, 95 % yield).

**$^{1}$H** (500 MHz, $C_6D_6$): δ 1.92 (m, 6H), 1.75 (qt, $J_{H,H}$ = 12, $J_{H,H}$ = 3 Hz, 3H), 1.67 (m, 6H), 1.55 (br s, 3H), 1.42 (m, 6H), 1.08 (m, 9H).

**$^{31}$P** (202.5 MHz, $C_6D_6$): δ 46.4

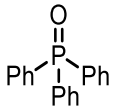


**OPPh$_3$.** The following procedure is a modified version of a literature reported procedure.[256] Triphenylphosphine **6-55** (1 g, 3.81 mmol) was weighed into a 50 mL pear-shaped flask equipped with a magnetic stir bar under nitrogen. The phosphine was dissolved in a mixture of ethanol (10 mL) and toluene (5 mL) and was then exposed to air. The solution was cooled to 0 °C and hydrogen peroxide (0.5 mL, 30% w/w soln.) was added slowly. The solution was left to warm to room temperature overnight. The solution was then cooled again to 0 °C and sodium sulfite (0.5 g) was added and left to stir for 1 h. Sodium sulfate was then added, and the solution filtered over a fine porous frit. Volatiles were removed *in vacuo* and the crude product was dissolved in dichloromethane (25 mL) and washed with sodium hydroxide (2 x 25 mL). The organic layer was dried with sodium sulfate and filtered over a fine porous frit. The product was dried via an azeotrope with toluene (3 x 5 mL) to afford the desired product triphenylphosphine oxide (886 mg, 3.18 mmol, 84 % yield).

**$^{1}$H** (500 MHz, $C_6D_6$): δ 7.75 (m, 6H), 7.04 (m, 3H), 7.00 (m, 6H).

**$^{31}$P** (202.5 MHz, $C_6D_6$): δ 24.9.

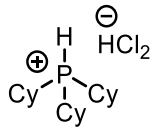


**$HCl_2$•$HPCy_3$ (6-69).** Tricyclohexylphosphine **6-54** (500 mg, 1.78 mmol) was weighed into a 4 dram vial equipped with a magnetic stir bar and a septa cap. HCl (2.7 mL, 5.35 mmol, 2M in $Et_2O$, 3 equiv.) was added cautiously to the mixture and the reaction was left to stir for 3h. The reaction was filtered over a fine porous frit and the solid was washed with pentane (3 x 3 mL) an the dried further *in vacuo* to afford the desired product **6-69** (585 mg, 1.66 mmol, 93% yield).

**$^{1}$H** (500 MHz, $CDCl_3$): δ 11.39 (s, 1H), 7.11 (d, $J_{H,P}$ = 479 Hz, 1H), 2.53 (m, 3H), 2.07 (br s, 6H), 1.89 (m, 6H), 1.76 (m, 3H), 1.62 (m, 6H), 1.39 (m, 6H), 1.31 (m, 3H).

**$^{13}$C** {$^{1}$H} (125.8 MHz, $CDCl_3$): δ 28.5 (d, $J_{C,P}$ = 39 Hz), 28.1 (d, $J_{C,P}$ = 3 Hz), 26.4 (d, $J_{C,P}$ = 13 Hz), 25.2 (s).

**$^{31}$P** (202.5 MHz, $CDCl_3$): δ 23.7 (d, $J_{P,P}$ = 479 Hz).

### 6.8.5 Reactivity Studies

**Determination of impurity 6-68 at 58ppm in the $^{31}$P NMR spectrum.** Tricyclohexylphosphine oxide **6-67** (150 mg, 0.506 mmol, 2 equiv.) and magnesium chloride (24 mg, 0.253 mmol) were dissolved in tetrahydrofuran (1 mL) a 4 dram vial equipped with a magnetic stir bar. The solution was left to sir for 1 h and then volatiles were removed *in vacuo*. The resulting solids were triturated with pentane (3 x 4 mL). The solid was dissolved in benzene-$d_6$ and NMR spectrum were acquired. The resulting solid contained THF, from potential complexation with the magnesium adduct.

**$^1$H** (500 MHz, $C_6D_6$): δ 1.95 (m, 3H), 1.88 (m, 6H), 1.67 (m, 6H), 1.54 (m, 3H), 1.49 (m, 6H), 1.13 (m, 9H).

**$^{31}$P** (202.5 MHz, $C_6D_6$): δ 58.7.

**General procedure for the decomposition of $SF_6$ with metal reductants.** To an oven dried 10 mL flask, an alkyl or aryl trisubstituted phosphine was added followed by magnesium turnings (5-20 equiv. with deviation of +1-4 mg) and a magnetic stir bar. In some instances, magnesium metal was substituted for calcium chips or zinc shavings. Tetrahydrofuran was added to the flask followed by silane (5-15 equiv.). The flask was sealed with a red septum and electrical tape and taken out of the glove box. A balloon was then filled with $SF_6$ and the gas was purged into the flask with an additional output needle in the septum. The holes in the septa were sealed with electrical tape and the flask left to stir overnight. The solution was diluted with tetrahydrofuran and an aliquot taken for NMR analysis.

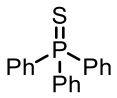


**General procedure for the decomposition of $SF_6$ with metal reductants (open air setup).** To an oven dried 50 mL flask, triphenylphosphine **6-55** (328 mg, 1.25 mmol) was added followed by magnesium turnings (152 mg, 6.25 mmol, 5 equiv. with deviation of +1-4 mg) and a magnetic stir bar. Tetrahydrofuran (5 mL, anhydrous from Sigma Aldrich) was added to the flask and the flask was sealed with a red septum. A balloon was then filled with $SF_6$ and the gas was purged into the flask with an additional output needle in the septum. Dimethylchlorosilane or trimethylchlorosilane (8.75 mmol, 7 equiv.) was then added to the flask and the holes sealed with electrical tape. The flask was left to stir overnight. The solution was diluted with tetrahydrofuran and an aliquot taken for NMR

analysis. The reactions were then removed of volatiles *in vacuo* and then dry loaded onto a column. Reactions were purified with silica gel using an ether-hexanes gradient (0-100%) and removed of all volatiles *in vacuo* to afford triphenylphosphine sulfide **6-58**.

**Dimethylchlorosilane reaction:**

**Yield:** 357 mg, 97%.

**$^{1}$H** (500 MHz, $CDCl_3$): δ 7.72 (m, 6H), 7.50 (m, 3H), 7.44 (m, 6H).

**$^{13}$C** {$^{1}$H} (125.8 MHz, $CDCl_3$): δ 133 (d, $J_{C,P}$ = 85 Hz), 132 (d, $J_{C,P}$ = 11 Hz), 131 (d, $J_{C,P}$ = 3 Hz), 128 (d, $J_{C,P}$ = 13 Hz).

**$^{31}$P** (202.5 MHz, $CDCl_3$): δ 43.3.

**Trimethylchlorosilane reaction:**

**Yield:** 168 mg, 46%.

**$^{1}$H** (500 MHz, $CDCl_3$): δ 7.72 (m, 6H), 7.50 (m, 3H), 7.44 (m, 6H).

**$^{13}$C** {$^{1}$H} (125.8 MHz, $CDCl_3$): δ 133 (d, $J_{C,P}$ = 85 Hz), 132 (d, $J_{C,P}$ = 11 Hz), 131 (d, $J_{C,P}$ = 3 Hz), 128 (d, $J_{C,P}$ = 13 Hz).

**$^{31}$P** (202.5 MHz, $CDCl_3$): δ 43.3.

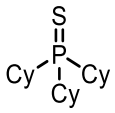


**Scale up and isolation of tricyclohexylphosphine sulfide (6-56).** To an oven dried 50 mL flask, tricyclohexylphosphine **6-54** (350 mg, 1.25 mmol) was added followed by magnesium turnings (216 mg, 9 mmol, 7.2 equiv.) and a magnetic stir bar. Tetrahydrofuran (5 mL) followed by dimethylchlorosilane (0.97 mL, 8.75 mmol, 7 equiv.) was added to the flask and the flask was sealed with a red septum. A balloon was then filled with $SF_6$ and the gas was purged into the flask with an additional output needle in the septum and the

holes sealed with electrical tape. The flask was left to stir overnight. The solution was diluted with tetrahydrofuran and an aliquot taken for NMR analysis. The reactions were then removed of volatiles *in vacuo* and then dry loaded onto a frit with silica gel attached to a suction flask. The silica gel was washed with hexane (150 mL) which was discarded. The silica was then washed with dichloromethane (150mL) which was then removed of all volatiles *in vacuo* to afford tricyclohexylphosphine sulfide **6-56** (285 mg, 0.912 mmol, 73%).

**$^{1}$H** (500 MHz, $CDCl_3$): δ 1.98 (m, 6H), 1.9 (m, 3H), 1.84 (m, 6H), 1.72 (m, 3H), 1.43 (m, 6H), 1.24 (m, 9H).

**$^{31}$P** (202.5 MHz, $CDCl_3$): δ 62.0.

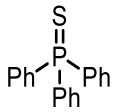


**Scale up and isolation of triphenylphosphine sulfide (6-58).** To an oven dried 100 mL flask, triphenylphosphine **6-55** (656 mg, 2.5 mmol) was added followed by magnesium turnings (305mg, 12.5 mmol, 5 equiv.) and a magnetic stir bar. Tetrahydrofuran (11 mL) followed by dimethylchlorosilane (1.94 mL, 17.5 mmol, 7 equiv.) was added to the flask and the flask was sealed with a red septum. A balloon was then filled with $SF_6$ and the gas was purged into the flask with an additional output needle in the septum and the holes sealed with electrical tape. The flask was left to stir overnight. The solution was diluted with tetrahydrofuran and an aliquot taken for NMR analysis. The reactions were then removed of volatiles *in vacuo* and then dry loaded onto a column. Reactions were purified with silica gel using an ether-hexanes gradient (0-100%) and removed of all volatiles *in vacuo* to afford triphenylphosphine sulfide **6-58**.

**Yield:** 694 mg, 94%.

**$^{1}$H** (500 MHz, $CDCl_3$): δ 7.72 (m, 6H), 7.50 (m, 3H), 7.44 (m, 6H).

**$^{13}$C** {$^{1}$H} (125.8 MHz, $CDCl_3$): δ 133 (d, $J_{C,P}$ = 85 Hz), 132 (d, $J_{C,P}$ = 11 Hz), 131 (d, $J_{C,P}$ = 3 Hz), 128 (d, $J_{C,P}$ = 13 Hz).

**$^{31}$P** (202.5 MHz, $CDCl_3$): δ 43.3.

**Reduction of $PhSF_5$ with magnesium turnings.** $PhSF_5$ (51 mg, 0.25 mmol) was weighed into a 4 dram vial equipped with a magnetic stir bar followed by tetrahydrofuran (2 mL). Magnesium turnings (93 mg, 3.87 mmol, 15.5 equiv.) were then added followed by dimethylchlorosilane (0.42 mL, 3.75 mmol, 15 equiv.). HCl (3 mL, 2M) was carefully added to the vial followed by brine (7 mL). The solution was transferred to a separatory funnel followed by rinsing the vial with hexane (10 mL) which was also transferred to the separatory funnel. The hexane layer was separated, and the aqueous layer was washed with an additional amount of hexane (10 mL). The combined hexanes extracts were washed with brine (10 mL) followed by water (10 mL). The organic solution was then dried with sodium sulfate and then filtered. The solution was removed of hexanes on a rotary evaporator to afford a crude oil (8 mg). This product was then analyzed using NMR analysis.

# Chapter 7: Diazaphospholene Dimer Reactivity with Electrophiles and Other Polarized Species

The chapter contains contains information from the following manuscript:

**B. S. N. Huchenski**, K. N. Robertson, and A. W. H. Speed. *Eur. J. Org. Chem.,* **2020**, 5140-5144. Reprinted with permission from John Wiley and Sons, copyright 2021. The manuscript has been rewrttien and references and compounds have renumbered where appropriate. Sub-sections headers have been added. The orignal manuscript was written by B. S. N. Huchenski and Dr. A. W. H. Speed.

Contributions to manuscript: All synthetic work in this chapter was carried out by B. S. N. Huchenski, with the following exceptions: Compounds **7-5**, **7-21**, and **7-30**, were prepared by Dr. A. W. H. Speed and **7-14** was originally prepared by Michael Charlton, and subsequently repeated by B. S. N. Huchenski. The reactions of **7-1** with diboranes were originally conduectd by Kristen Giffen and repeated by B. S. N. Huchenski. The X-ray crystallography was conducted by Dr. Katherine N. Robertson. Mass spectrometric data were acquired by Mr. Xiao Feng (Mass Spectrometry Laboratory, Dalhousie University). The manuscript was written by B. S. N. Huchenski.

## 7.1 Introduction

Previously, as explained in chapter 1 and 6, diazaphospholene dimers have been explored in bond activation chemistry. Such examples include the cleavage of metal halide bonds[96] and reactivity with hydrochloride salts to form diazaphospholene *P*-halides and diazaphospholene hydrides.[90] Diazaphospholene and diazaphospholidine dimers are also reported to add into or across multiple bonds such as diphenylacetylene[95] and heteroallenes.[97] Overall, the reactivity of diazaphospholene dimers is relatively underexplored. Unsymmetrical bisphosphines have been reported by Gudat in phosphine

transfer reactions.[93] These compounds consist of a diazaphospholene with a diphenylphosphine bound to the phosphorus.[80] These compounds were found to transfer the diphenylphosphine moiety to a variety of electrophilic substrates as well as add both the diphenylphosphine and diazaphospholene across an unsaturated bond.[80] The reactivity of these compounds can be attributed to the polarized nature of the P–P bond that allows for nucleophilic attack. However, the overall resulting products from this reaction either contain only the diphenylphosphine component or both components from the reaction, which does not allow for selective diazaphospholene functionalization of carbon-halide bonds or other electrophilic species. Recently, functionalized diazaphospholenes have been used as ligands in high impact catalysis (**Figure 7.1**),[257–259] so the exploration of new methods for diazaphospholene functionalization is of great importance.

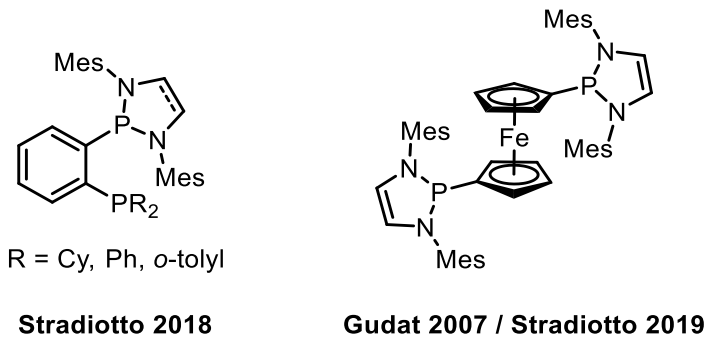


**Figure 7.1** Ligands derived from diazaphospholenes.

## 7.2 Aryl Functionalization of Diazaphospholenes

As stated in section 7.1, substituted diazaphospholenes have been reported to act as ligands in catalysis, with performance comparable to other bulky phosphine ligands in certain cases. Previous results within the literature indicated that diazaphospholenes can react with polarized bonds.[68] The results from chapter 6 indicated that diazaphospholene dimers **7-1** are capable of reacting with sulfur fluoride bonds. The synthesis of aryl

phosphines is of great importance in catalysis due to the high prevalence of these compounds within ligands.[260] We sought to investigate if symmetrical diazaphospholene dimers **7-1** could react with appropriate carbon electrophiles to produce diazaphospholene-functionalized compounds.

Diphenyliodonium hexafluorophosphate, an iodine-(III)-based arylating agent, was treated with diazaphospholene dimer **7-1** in benzene (**Scheme 7.1**). A $^{31}$P NMR spectrum was acquired and after 10 min a new product **7-3** was observed at 74.5 ppm. The reaction was repeated over 1 h and complete consumption of the dimer was observed. An additional product was observed at 185 ppm in the $^{31}$P NMR spectrum which was presumed to be diazaphospholenium salt **7-2**, with a chemical shift comparable to literature values.[261] The reaction was increased in scale to isolate the precipitate was well as the new product at 74.5 ppm. Upon increasing the scale of the reaction, a new predominant peak at 78 ppm that was observed in the filtrate, alongside the originally observed peak at 74.5 ppm. The insoluble material was confirmed to contain diazaphospholenium hexafluorophosphate **7-2**. *Para*-bromophenyldiazonium tetrafluoroborate was also examined as a different electrophile and found to produce multiple products in the $^{31}$P NMR spectrum. The source of additional products from these reactions could arise from the highly reactive arylating reagents reacting with the products, by either arylating the phosphorus to form a phosphonium salt or substituting onto the diazaphospholene ring.

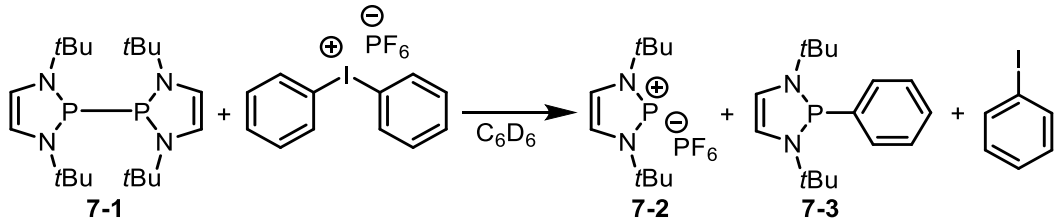


**Scheme 7.1** Initial reactivity of diazaphospholene dimer **7-1** with an iodonium salt.

Treatment of the diazaphospholene dimer **7-1** with diphenyliodonium hexafluorophosphate results in the potential formation of iodobenzene as a side product. This product could potentially also have reacted with the dimer **7-1**, resulting in the multiple products observed. Aryl iodides are highly polarized and have been reported to react with bisphosphines.[262] To test this hypothesis, diazaphospholene dimer **7-1** was treated with an excess of iodobenzene in benzene and found to produce a single product **7-3** at 74.5 ppm in the $^{31}$P NMR spectrum when left overnight (**Scheme 7.2**). A precipitate formed from this reaction which is presumed to be diazaphospholene iodide **7-4** which was observed as a small broad peak at 186 in the $^{31}$P NMR spectrum. The formation of the product **7-3** at 74.5 ppm indicates a common product formed between both iodobenezne and diphenyliodonium hexafluorophosphate, which is striking, since one compound was an iodine (I) compound, and the other is an iodine (III) compound. To determine if the product **7-3** formed at 74.5 ppm is *P*-phenyl diazaphospholene **7-3**, diazaphospholene bromide **7-5** was treated with phenylmagnesium bromide, to synthesize **7-3** by an alternate route (**Scheme 7.2**). The pentane extraction yielded a single product determined to be *P*-phenyl diazaphospholene **7-3** at 74.5 ppm in the $^{31}$P NMR spectrum. Once again, the reaction was increased in scale from 0.05 mmol to 0.38 mmol in toluene and left overnight. The reaction produced additional products upon increase in scale, similar to previous reactions. A predominant product was observed at 87 ppm in the $^{31}$P NMR data with the desired product **7-3** at 74 ppm in a 1:1.4 ratio.

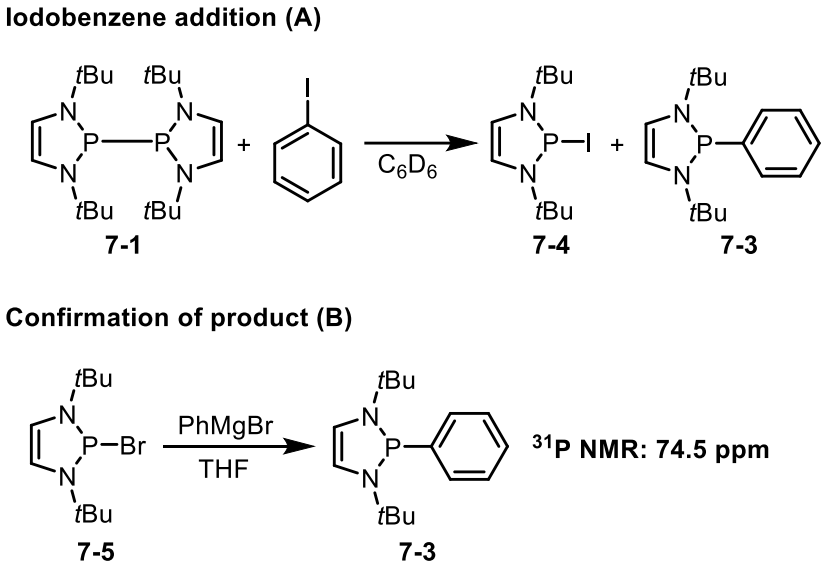


**Scheme 7.2** (**A**) Reaction of iodobenzene with diazaphospholene dimer **7-1**. (**B**) Reaction of diazaphospholene bromide **7-5** with phenyl magnesium bromide to form product **7-3**.

The formation of additional products upon an increase in reaction scale with iodobenzene in toluene prohibited the isolation of the desired *P*-phenyl diazaphospholene **7-3** product. Solvent variation was then assessed to determine if product selectivity could be increased. Irradiation may also affect the reactions, as Gudat reported that irradiation of diazaphospholene hydrides resulted in radical dehydrocoupling to form diazaphospholene dimer **7-1**.[90] Furthermore, irradiation of tetraphenyldiphosphine allowed for reactivity with perfluoroalkylhalides.[263] Diazaphospholene dimer **7-1** was dissolved in toluene and treated with iodobenzene, with one sample exposed to blue light. Light was found to increase the rate of the reaction resulting in exclusive formation of the product **7-3** at 74.5 ppm in 15 min. Once again, the reaction was increased in scale to 0.3 mmol and the reaction irradiated for 30 min. The reaction once extracted with pentane, revealed the presence of a product at 87 ppm, the diazaphospholene dimer **7-1** at 80 ppm and the desired product **7-3** at 74.5 ppm in a ratio of 1:1:2.5. THF was then examined, and the reaction was left to stir for 1 h. The formation of *P*-phenyl diazaphospholene **7-3**, and a peak at 73.8 ppm was observed in a

ratio of 1:1.3, with an additional product at 87 ppm as a minor species. Diazaphospholene iodide **7-4** was observed once again at 186 ppm. The reaction was repeated once again in 15 min timescale with one sample being exposed to blue light. The reaction exposed to blue light displayed full consumption of the diazaphospholene dimer **7-1** and the formation of the *P*-phenyl diazaphospholene **7-3** and product at 73.8 ppm in a ratio of 1:1.5. The reaction in the absence of blue light did not go to completion and resulted in a similar product distribution. Diethyl ether was examined and found to not be selective for the formation of *P*-phenyl diazaphospholene **7-3**. Acetonitrile was examined in the presence and absence of blue light and found that even in the absence of light, full and selective formation of *P*-phenyl diazaphospholene **7-3** was observed along with the formation of diazaphospholenium iodide **7-5**. Upon increasing scale to 0.3 mmol the reaction retained selectivity for *P*-phenyl diazaphospholene which was isolated with a pentane filtration after removal of the acetonitrile, extraction of the residue with pentane, and evaporation to recover pentane soluble product. Diazaphospholene iodide **7-4** was isolated as the insoluble powder from the filtration of the reaction.

These findings are an improvement to currently reported methods involving tetraphenyldiphosphine functionalization of aryl iodides, which requires heat and $(TMS)_3SiH$,[262] while this method operates at ambient temperature with no additives. Iodobenzene was found to be a suitable substrate for C–X bond cleavage facilitated by diazaphospholene dimers. To investigate if less polarized halocarbon bonds can be cleaved by diazaphospholene dimers **7-1**, bromobenzene was examined. Treatment of diazaphospholene dimer **7-1** with bromobenzene in benzene resulted in no reactivity. Exposure to blue light for 1 h resulted in minimal but selective formation of *P*-phenyl diazaphospholene **7-3**. When exposed to blue light for 3 h, diazaphospholene dimer **7-1**

was converted into *P*-phenyl diazaphospholene **7-3** in a 1:0.32 ratio as observed in the $^{31}P$ NMR data. Similar to iodobenzene, when the diazaphospholene dimer **7-1** was treated with bromobenzene in THF and irradiated with blue light multiple products were observed. Bromobenzene was re-examined in acetonitrile and left for 6 h under blue irradiation. Formation of *P*-phenyl diazaphospholene **7-3** was observed however diazaphospholene dimer remained **7-1** in a 1:7 ratio with the desired product. Blue light irradiation for 8 h led to the complete consumption of the diazaphospholene dimer **7-1** into *P*-phenyl diazaphospholene **7-3** and diazaphospholenium bromide **7-5** which were both isolated from the reaction mixture in a similar manner to the iodobenzene reaction (**Scheme 7.3**).

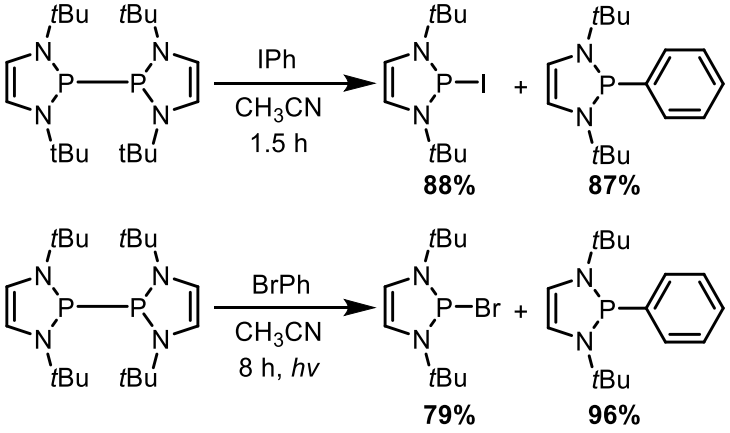


**Scheme 7.3** Comparison of reaction times between iodobenzene and bromobenzene with diazaphospholene dimer **7-1**.

Successful substitution of bromobenzene to form *P*-phenyl diazaphospholene **7-3** led to the investigation of other aryl bromides detailed in **Scheme 7.4**. Interestingly, a variety of electron poor aryl bromides were able to undergo C–X bond cleavage in the absence of light. Substrates such as pentaflurophenylbromobenzene formed *P*-aryl diazaphospholene **7-6** faster than iodobenzene. This can be expected due to its highly electrophilic nature. The reaction formed an orange product in 15 min with isolation after 30 min on a larger scale. Pyridyl substrates were also highly reactive with

diazaphospholene dimers to from *P*-pyridyl diazaphospholenes (**Scheme 7.4**) in 2 h. Pyridyl substrates such as 2-bromonicotinate **7-9** are challenging to prepare through organometallic metalation of the pyridine ring,[264] since metalated pyridines have low thermal stability. This diazaphospholene dimer **7-1** method provides an alternative synthesis to introduce phosphines to pyridine substrates. Reactions with more electron-rich substrates such as 3-bromobenzothiophene **7-10** and 2-bromonaphthalene **7-11** required light to form the products in an appreciable amount of time but were still shorter reaction times than bromobenzene.

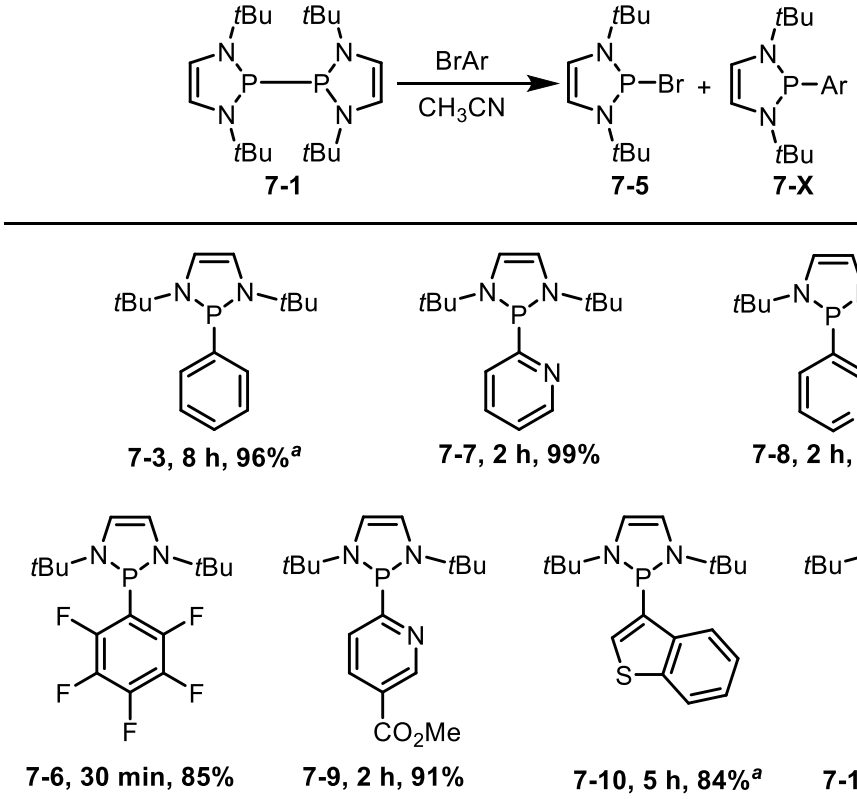


**Scheme 7.4** Scope of aryl bromides investigated for reactivity with diazaphospholene dimer **7-1** and their respective products are shown. [a]Reactions were conducted with blue light irradiation.

The results thus far have shown that aryl iodides react faster than their bromide counterparts. 2-bromo-iodobenzene was examined to test this apparent reactivity difference

with the diazaphospholene dimer **7-1**. The product isolated from the reaction with 2-bromo-iodobenzene was *P*-(2-bromo-phenyl) diazaphospholene **7-12** supporting the greater preference for C–I bonds (**Scheme 7.5**). This halo-selectivity allows for selective diazaphosphination of aryl rings for the preparation of ligands or the general introduction of a phosphine in a metal-free synthesis.

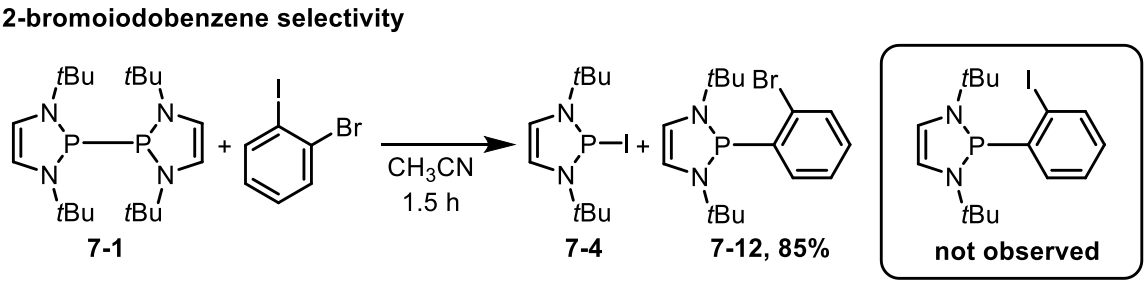


**Scheme 7.5** Reaction to examine the selectivity of diazaphospholene dimer **7-1** with aryl bromides and iodides.

Ferrocenyl ligands containing phosphines are amongst the foremost class of privileged ligands in catalysis.[265] Previously *P*-ferrocenyl diazaphospholenes have been utilized in catalysis and were synthesized through organometallic metalation of the ferrocene, followed by addition to the bromophosphine. Bromoferrocene was treated with diazaphospholene dimer **7-1** in acetonitrile and found to form a *P*-ferrocenyl diazaphospholene **7-13** albeit in low conversion after 4 h of irradiation with additional products observed. Iodoferrocene was prepared and treated with diazaphospholene dimer and found to selectively form *P*-ferrocenyl diazaphospholene **7-13** in 2.5 h, in acetonitrile with no irradiation (**Scheme 7.6**). The product formed was crystalized from pentane, and single crystal X-ray crystallography confirmed the structure of the compound. This method allows for the addition of a phosphine to the ferrocene ring without the need for harsh alkylating conditions which may interfere with other functional groups on the ligand or may exhibit polymetalation.

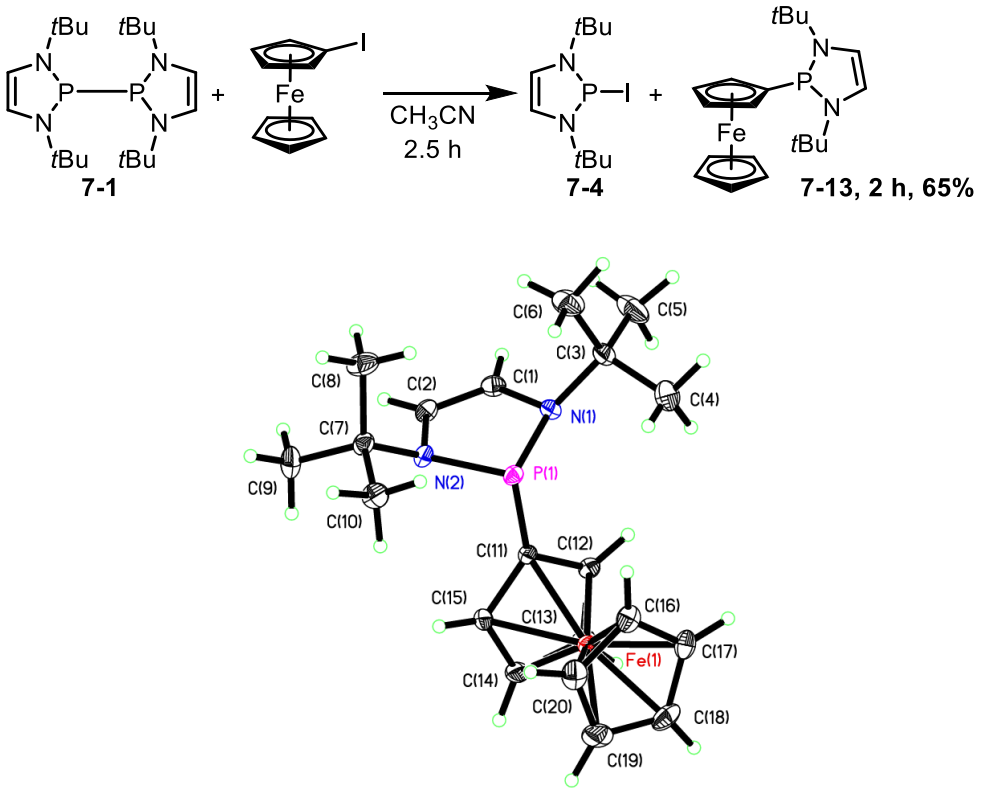


**Scheme 7.6** Reaction of iodoferrocene with diazaphospholene dimer **7-1**. Structure of compound **7-13**. Thermal ellipsoids have been drawn at the 50% probability level. Hydrogen atoms have not been labelled.

### 7.3 Alkyl Functionalization of Diazaphospholenes

Alkyl diazaphospholenes have the potential to be utilized as ligands in catalysis or for further bond forming reactions. Ogawa and co-workers have reported that tetraphenyldiphosphine irradiation in the presence of perfluoroalkylhalides allowed for substitution of a diphenylphoshine through C–X bond cleavage.[263] Previously an honors student Michael Charlton treated iodoperfluorohexane with diazaphospholene dimer **7-1** which selectively formed *P*-$C_6F_{13}$ diazaphospholene **7-14**, confirming similar reactivity with the diazaphospholene dimer **7-1**. The procedure was repeated with in the standard conditions done for *P*-aryl diazaphospholenes to confirm the reactivity. Gudat reported the alkylation of less reactive alkyl halides with the highly polarized bisphosphines.[93]

However, it remains unknown if less reactive alkyl bromides would react with diazaphospholene dimers. In addition, it is unclear if Gudat's results represent a polar or radical process. Tertiary alkyl halides are unreactive in $S_N2$ reactions, yet tertiary radicals are more stable than their less substituted counterparts, therefore bromo adamantane was selected as a substrate. Adamantyl phosphines are also known as suitable ligands in catalysis. Bromoadamantane was combined with diazaphospholene dimer **7-1** in benzene and irradiated with blue light. It was found that diazaphospholene dimer **7-1** was fully consumed in 2 h and resulted in exclusive formation of *P*-adamantyl diazaphospholene **7-15** (**Figure 7.2**). The reaction was found to proceed in the absence of blue light, however it is greatly accelerated upon irradiation. Acetonitrile was also examined and found to be a suitable solvent for this substrate.

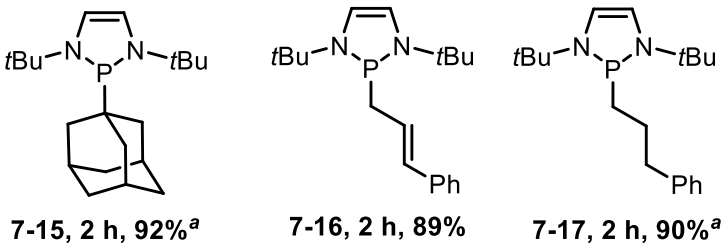


**Figure 7.2** Reaction of alkyl bromides with diazaphospholene dimer **7-1**. Reactions were conducted with a 1:1 combination of diazaphospholene dimer **7-1** and alkyl bromide in toluene (**7-15**) or $CH_3CN$ (**7-16**/**17**). [a]Reactions were conducted with blue light irradiation.

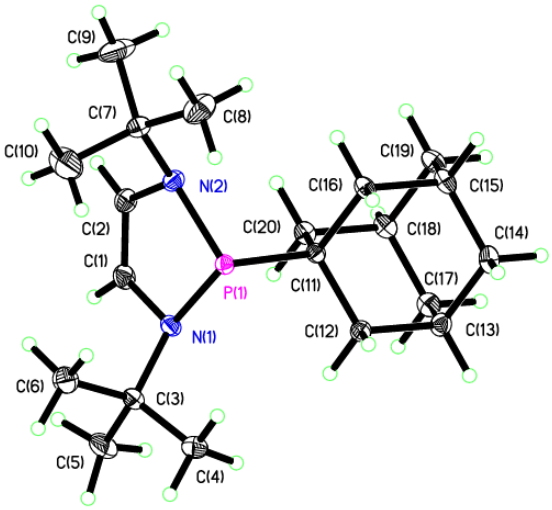


**Figure 7.3** Structure of compound **7-15**. Thermal ellipsoids have been drawn at the 50% probability level. Hydrogen atoms have not been labelled. Only one molecule of the two unique molecules in the asymmetric unit is shown.

Cinnamyl-bromide was then examined to determine if reactivity would occur and what regioselectivity would be observed, whether by $S_N2$, $S_N2'$ or a radical rearrangement. Clean formation of *P*-cinnamyl diazaphospholene **7-16** was observed as the only alkyl phosphine product (**Figure 7.2**). However, the product was found to decompose in solution forming multiple products overnight. To determine if unsaturation is required, hydrocinammyl bromide was examined and with blue light irradiation. Complete formation of *P*-(3-phenyl-1-propyl) diazaphospholene **7-17** was observed in 2 h (**Figure 7.2**). It was noted this product was much more stable than the cinnamyl diazaphospholene.

### 7.4 Mechanism Investigation

The mechanism for the reaction of carbon halide bonds and diazaphospholene dimers can be postulated as being radical, nucleophilic, or a mixture of both, varying by substrate. Wright has reported the radical character of symmetrical diazaphospholene dimers[89] however the radical species exists in low quantities at room temperature. More recently Yang and Cheng have reported diazaphospholenes displaying radical behavior in

a variety of reactions.[91,92] Conversely, the non symmetrical P–P substitution reactions reported by Gudat involve highly polarized phosphorus species, and potentially undergo a nucleophilic mechanism.[93] To investigate the reactive nature of diazaphospholene dimers further, a radical clock reagent,[266] 3-bromomethylcyclopropane was treated with diazaphospholene dimer **7-1** in toluene under blue light. The toluene and blue light irradiation were selected to represent the reactions with irradiation. The exclusive product was determined to be the ring opened 1-*P*-3-butenyl diazaphospholene **7-18** (**Scheme 7.7**). This demonstrates a radical mechanism occurs for blue light irradiated samples at some point in the reaction. The ring opened species will form from this reaction if a radical has a lifetime long enough for rearrangement. The reaction was then repeated in acetonitrile with no blue light irradiation, similar to the conditions that were most successful for the electron poor arylbromides and iodides, which could participate in $S_NAr$ reactions. Interestingly, the reaction produced two compounds, one being the ring opened radical produced product **7-18**, while the other was the $S_N2$ derived product **7-19** (**Scheme 7.7**). These results demonstrate competing reaction pathways that are both viable and present in the diazaphospholene dimer C–X bond cleavage reactions.

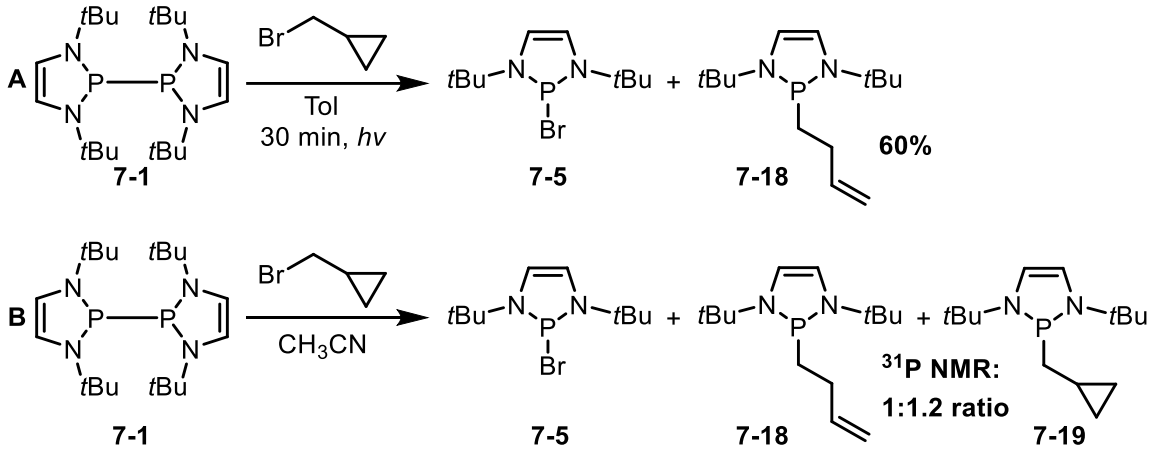


**Scheme 7.7** (**A**) Treatment of dimer **7-1** with cyclopropyl methyl bromide in toluene with blue light irradiation. (**B**) Treatment of dimer **7-1** with cyclopropyl methyl bromide in acetonitrile without blue light irradiation.

The radical nature of diazaphospholene dimers were investigated further by the treatment of 1-(2-Iodophenoxy)-3-methyl-2-butene with diazaphospholene dimer **7-1** (**Scheme 7.8**). If the aryl radical has a long enough lifetime, cyclization can occur before phosphine addition. The mixture of compound 1-(2-Iodophenoxy)-3-methyl-2-butene and diazaphospholene dimer **7-1** resulted in selective formation of the cyclized product **7-20**. This demonstrates that aryl radicals are likely forming in some of the reactions with more electron-rich aryl halides. In this case, the diazaphospholene dimer **7-1** would reduce or abstract the halide to form an aryl radical, followed by aryl radical addition to the diazaphospholene radical. In this instance the aryl radical lifetime is long enough that intramolecular cyclization can occur before aryl addition to the diazaphospholene radical. With this in mind, radical hydrides can result in cyclization reactions, and Gudat has shown that diazaphospholene hydrides participate in radical chemistry.[80] In addition, chapter 6 explores the reduction of $SF_6$ with diazaphospholene hydrides which may be operating under a radical mechanism.

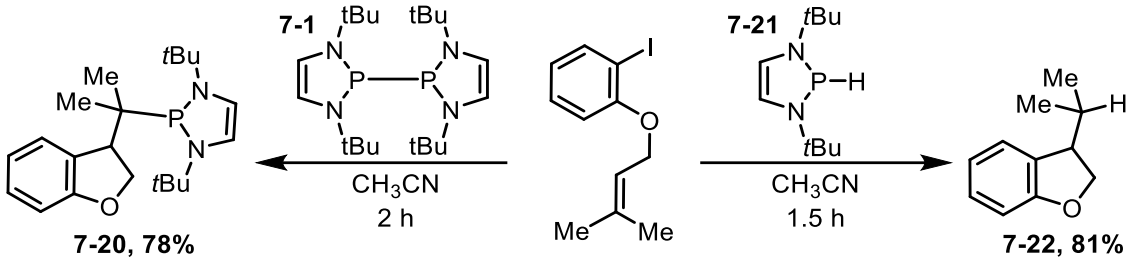


**Scheme 7.8** Treatment of 1-(2-Iodophenoxy)-3-methyl-2-butene with diazaphospholene **7-1** or **7-21**. Percentages are isolated yields.

Thus, diazaphospholene hydride **7-21** was treated with 1-(2-Iodophenoxy)-3-methyl-2-butene in acetonitrile and found to fully consume the hydride in the absence of light. To allow for reaction completion, a large excess of diazaphospholene hydride **7-21** was required. The requirement for a large excess of diazaphospholene hydride **7-21** may possibly be due to the instability of the hydride **7-21** under the reaction conditions in which the diazaphospholene hydride might be decomposing into phosphine as seen in Chapter 6. The major product of the reaction was the cyclized product **7-22** in 81% isolated yield (**Scheme 7.8**). The reports by Yang and Cheng,[91,92] which appeared as our work was nearing completion, showed that NHP hydrides also exhibit radical properties under similar conditions (**Scheme 1.17**). In these reactions AIBN and heat were required for radical initiation, for the cyclization to occur rather than light initiation with the diazaphospholene examined within this chapter. Our results are not able to differentiate between chain reactions, and single electron transfer, followed by radical-radical recombination, however given the absence of a need for a radical initiator in our chemistry, the latter option is a strong possibility.

### 7.5 Reactivity with Dimeric Compounds

In Chapter 6 it was found that the diazaphospholene dimer **7-1** readily reacts with sulfur hexafluoride to form diazaphospholene fluoride. When diazaphospholene dimer **7-1**

was treated with Fluolead, the resulting $^{31}$P NMR indicated the presence of another species, with a similar chemical shift range of diazaphospholene derivatives containing a heteroatom, which we determined was the P–S bond. To exclusively produce this product diphenyldisulfide was examined for reactivity with diazaphospholene dimer **7-1**. The diazaphospholene dimer **7-1** and diphenyldisulfide were combined in benzene, and a single product **7-23** was observed in the $^{31}$P NMR spectrum. The process was scaled up in acetonitrile and found to remain selective for the single product formation (**Scheme 7.9**). Proton NMR data of the isolated product further supported the formation of a diazaphospholene *P*-thiophenylate compound **7-23**. This product was examined in diazaphospholene hydride formation, similar to the oxy-diazaphospholenes used as precatalysts.[77,78] Formation of the diazaphospholene hydride **7-21** was slow upon treatment with HBpin indicating that the P–S bond may not be as reactive as P–O bonds. Successful reactivity with diphenyldisulfide prompted the investigation into other dimeric compounds such as diboranes (**Scheme 7.9**). Both $B_2Pin_2$ and $B_2Cat_2$ were examined in benzene and but no reactivity was observed with the diazaphospholene dimer **7-1**. The results indicated that while the diazaphospholene dimer **7-1** can reduce a disulfide bond, it does not have suitable reactivity to react with diboranes, possibly due to the high barrier required to form a boryl radical or boryl anion.

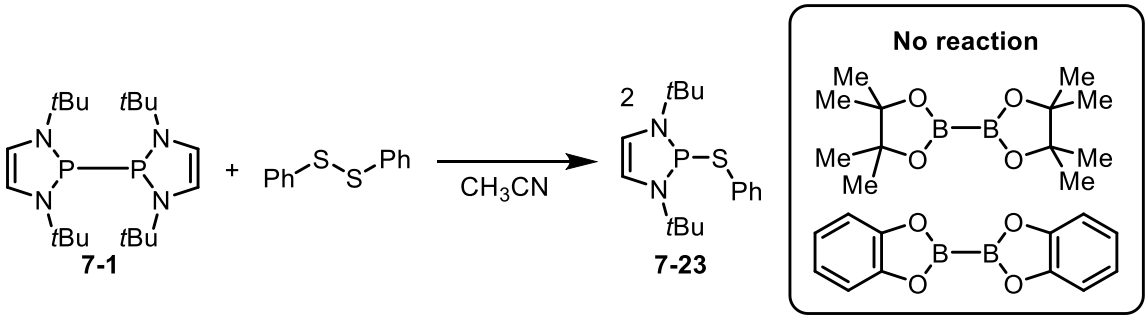


**Scheme 7.9** Reaction of diazaphospholene dimer **7-1** with diphenyldisulfide or diboranes.

## 7.6 Functionalization Facilitated by Diazaphospholenes

When the products of diazaphospholene addition were examined by mass spectrometry, a common observation was the formation of diazaphospholene radical cations as the base peak. The observation of these diazaphospholene radicals indicates a potential formation of these compounds, potentially accessible via a photochemically excited state, indicating at further reactivity. *P*-pentafluorophenyl diazaphospholene **7-6** was treated with neopentyl alcohol and irradiated with blue light. When left for 3 h, complete consumption of *P*-pentafluorophenyl diazaphospholene **7-6** was observed. The major products isolated were the *P*-alkoxydiazaphospholene **7-24** and pentafluorobenzene as observed by the $^{1}H$ and $^{19}F$ NMR data (**Scheme 7.10**). This implied anionic character on the pentafluorophenyl ring, rather than electrophilic character, which might have resulted in the formation of a neopentyl pentafluorophenyl ether. To determine if blue light was required, the reaction was repeated without blue light and found to produce the products in the same purity. Other substituted diazaphospholenes were examined for similar reactivity such as *P*-adamantyl **7-15**, nicotinate **7-9** and napthyl **7-11**, however no reaction between these diazaphospholenes and neopentyl alcohol was observed (**Scheme 7.10**).

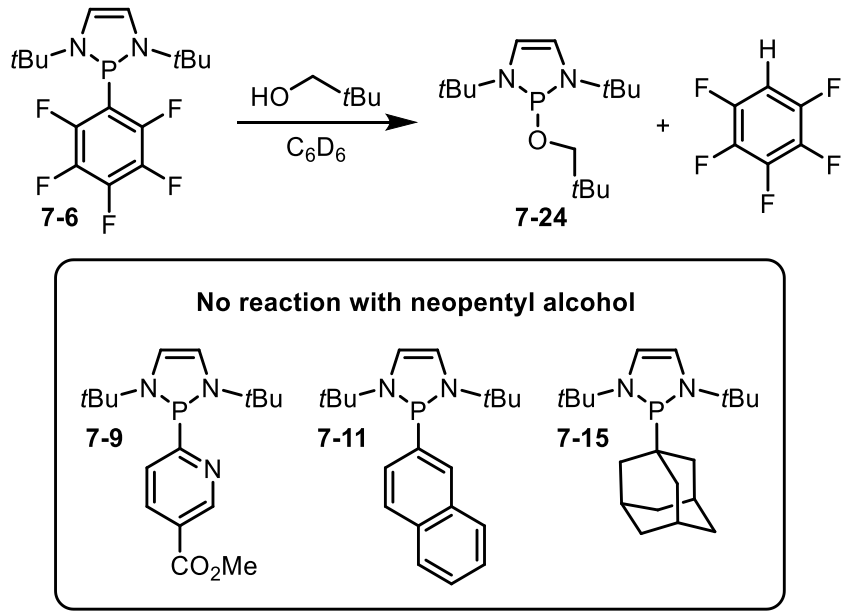


**Scheme 7.10** Reaction of *P*-aryl diazaphospholenes with neopentyl alcohol.

Amines were then investigated to determine if C–P cleavage can be facilitated. Dibenzylamine was then mixed with *P*-pentafluorophenyl diazaphospholene **7-6** and irradiated for 3 h. $^{31}$P NMR data indicated the formation of an aminodiazaphospholene albeit in small quantities. Isopropylamine also indicated the formation of a P–N bond after 2 h of irradiation in low quantities. The results indicate a large reactivity difference between hydroxyl and amino bonds.

The potential for aryl transfer was highlighted by the cleavage of the C–P bond and the O–H bond. *N*-benzyl quinolinium bromide was then examined because these compounds have been utilized as highly electrophilic acceptors of hydrides as seen in chapter 4. When *P*-pentafluorophenyl diazaphospholene **7-6** was combined with *N*-benzyl quinolinium bromide in acetonitrile, complete consumption of the *P*-pentafluorophenyl diazaphospholene **7-6** and the formation of diazaphospholenium bromide **7-5** was observed (**Scheme 7.11**). Analysis of the $^{19}$F NMR spectrum indicated the formation of a single new product. Isolation of this product **7-25** indicated a selective arylation of the *N*-benzyl

quinolinium bromide, and the diastereotopic splitting of the benzylic hydrogens showed a new stereocentre had formed. This represents the first carbon-carbon bond formation via carbon-transfer from a diazaphospholene. The compound **7-25** was crystalized and analysis by X-ray crystallography determined the substitution of the product arose from a 1,2 addition to the quinolinium, rather than a 1,4 addition.

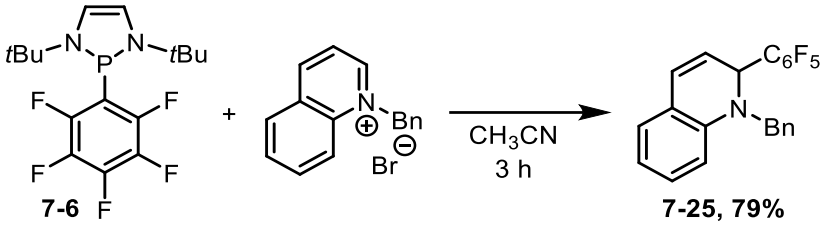


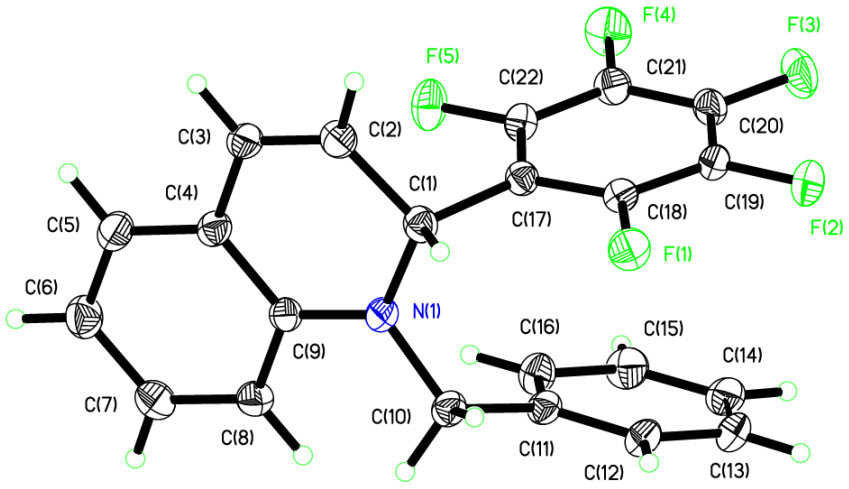


**Scheme 7.11** Reaction of *P*-pentafluorophenyl diazaphospholene **7-6** with *N*-benzyl quinolinium bromide. Structure of compound **7-25**. Thermal ellipsoids have been drawn at the 50% probability level. Hydrogen atoms have not been labelled.

*P*-pentafluorophenyl diazaphospholene **7-6** was suitable for the transfer of pentafluorophenyl to quinonlinium ion. However, it is unknown if other substrates that are less electrophilic will are able to function in this reaction. Aldehydes are suitable substrates for diazaphospholene reduction with diazaphospholene hydrides, so naphthaldehyde was examined as an arylation substrate. Naphthaldehyde was treated with *P*-pentafluorophenyl

diazaphospholene **7-6**, and after 4 h no reactivity was observed. Alternative *P*-aryl diazaphospholenes were investigated to determine if the reactivity of *P*-pentafluorophenyl diazaphospholene was unique to the pentafluoro group. *P*-phenyl diazaphospholene **7-3** was treated with quinolinium bromide and left overnight. No reactivity was observed as indicated by the absence of any new phosphorus compounds and the intact signal for *P*-phenyl diazaphospholene **7-3**.

To streamline potential reactivity in carbon transfer reactions, *P*-pentafluorophenyl diazaphospholene **7-6** was generated *in situ* followed by *N*-benzyl quinolinium bromide addition, without isolation of the diazaphospholene intermediate. The desired product **7-25** was generated with the same selectivity. *P*-cinnamyl diazaphospholene **7-16** was found to decompose in solution, potentially indicating a reactive alkyl phosphine bond is present. Diazaphospholene dimer **7-1** was combined with cinnamyl bromide to generate *P*-cinnamyl diazaphospholene **7-16** *in situ*. *N*-benzyl quinolinium bromide was then added and stirred for 5 h. Consumption of *P*-cinnamyl diazaphospholene **7-16** was observed along with the formation of diazaphospholenium bromide **7-5**, indicating a reaction occurred instead of complete decomposition. Filtration through silica and analysis of the product by $^{1}$H NMR indicated multiple products present. The sample was analyzed by mass spectrometry and found to contain the alkylated quinolinium product. However, the complex NMR spectrum indicates multiple isomers from a non-selective reaction, therefore the reaction was not investigated further. In this case, allylic alkylation could have led to diastereomeric compounds.

Trifluoromethylation of organic compounds is a highly sought-after reaction for its application in pharmaceutical synthesis.[267] Trifluoromethyl groups are bioisosteres within pharmaceuticals, and derivatization allows for alteration of the solubility properties of a

pharmaceutical, while also altering electronic properties and metabolism. While there are many methods to trifluoromethylate compounds, new methods, especially mild or metal free methods are of great importance. Rupert's reagent is common source of trifluoromethyl used in trifluoromethylation[268] reactions but was found to have no reactivity with the diazaphospholene dimer **7-1**. Umemoto's reagent,[269] an electrophilic trifluoromethyl source was then investigated with the diazaphospholene dimer **7-1** and upon combination of these reagents a new product **7-26** formed at 68 ppm in the $^{31}$P NMR spectrum and a peak at 204 ppm which represents the formation of diazaphospholenium triflate **7-27**[83] (**Scheme 7.12**). Attempted scale up and isolation of the putative *P*-$CF_3$ product **7-26** was unsuccessful due to its volatility. Diazaphospholene hydride **7-21** was treated with Umemoto's reagent and rapid bubbling occurred. Analysis of the resulting solution indicated the formation of multiple products including the trifluoromethyl product **7-26** which formed from the combination of diazaphospholene dimer **7-1** and Umemoto's reagent. Fluoroform was also detected in the $^{19}$F NMR spectrum. Formation of *P*-trifluoromethyl diazaphospholene **7-26** was not investigated further due to low isolation yields from volatility.

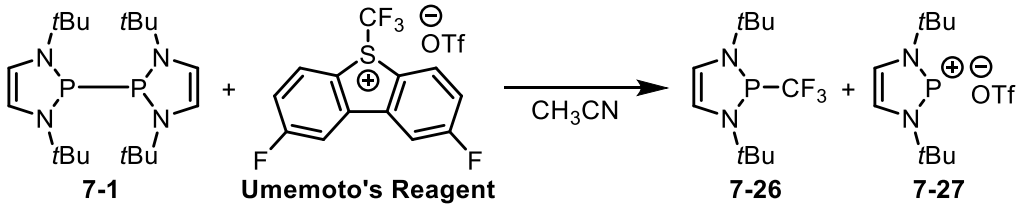


**Scheme 7.12** Reaction of diazaphospholene dimer **7-1** with Umemoto's reagent.

Transfer of the pentafluorophenyl from a diazaphospholene to a quinolinium substrate prompted an investigation into an asymmetric variant of this transformation. Chiral diazaphospholenes display great enantioinduction in the reduction of imine

substrates.[69] Since this transformation is a diazaphospholene mediated transfer of a pentafluorophenyl group rather than a hydride, it was speculated that this process may be facilitated with enantioinduction from the diazaphospholene. Chiral diazaphospholene dimer **7-28** was generated in a similar manner to the achiral variant with a product chemical shift at 88.7 ppm in the $^{31}$P NMR spectrum. This dimer **7-28** was treated with pentafluorobromobenzene for 30 min in acetonitrile. Formation of a substituted diazaphospholene **7-29** as well as the parent diazaphospholene bromide **7-30** were observed in the $^{31}$P NMR spectrum. *N*-benzyl quinolinium bromide was then added to the reaction and left overnight. NMR analysis of the reaction mixture indicated transfer of the pentafluorophenyl functional group, however HPLC analysis of the product **7-26** indicated a racemic reaction occurred (**Scheme 7.13**). This made us speculate the process may involve either a dissociation of pentafluorophenyl group as an anion before addition, or a radical process, or the facial preference (steric differentiation) for the quinoline may not be specific enough. However, purely racemic products are unusual in chiral diazaphospholene catalysis, even with poorly sterically differentiated substrates. Overall, the lack of enantioinduction in this attempt resulted in us moving on to other chemistry, though a solvent screen may be warranted for future work.

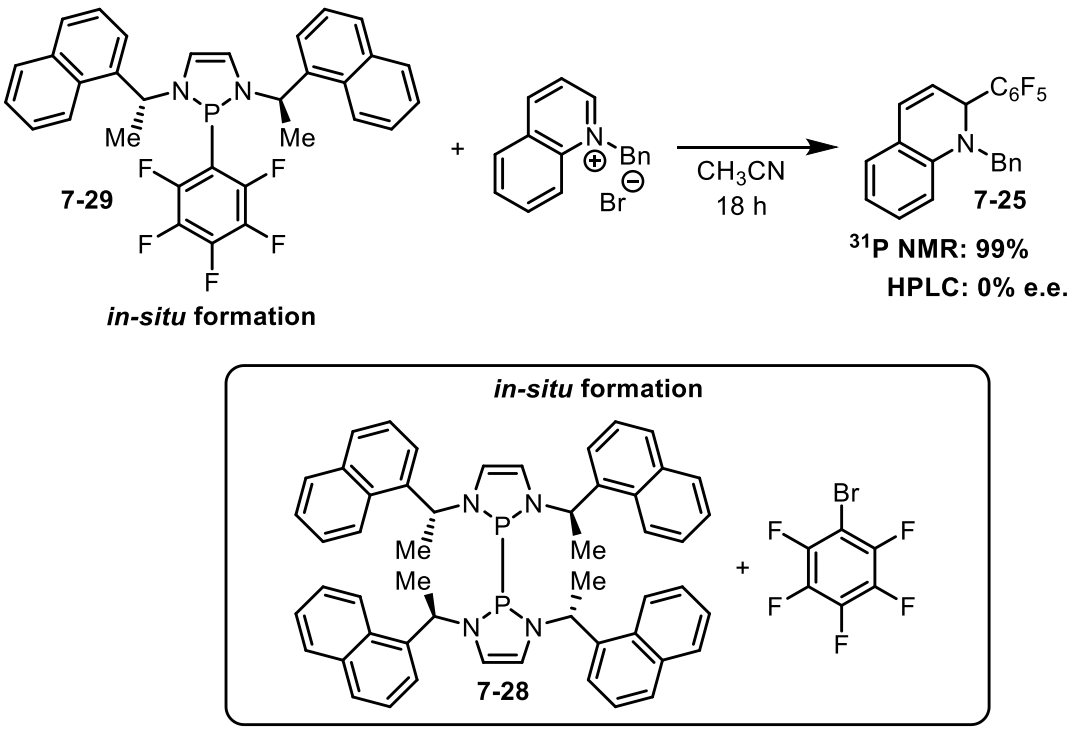


**Scheme 7.13** Reaction of *P*-pentafluorophenyl *N*-(R)-napthylmethyl-diazaphospholene **7-29** (*in situ* generation) with *N*-benzyl quinolinium bromide.

A potential derivatization of *P*-aryl diazaphospholenes is through borylation of the C–P bond, allowing for the preparation of singular substituted boranes. Boron trihalides are known to facilitate borylation on electron-rich substrates, such as in TMS-aryl cleavage reactions. Boron tribromide was examined in reaction with aryl diazaphospholenes, as this boron source is the most common for substitution reactions. Electron-rich *P*-(p-methoxyphenyl) diazaphospholene **7-31** (generated via Grignard addition to **7-5**) was initially examined in a variety of solvents. The $^{11}$B NMR data indicated formation of an aryl boron product, however demethylation was also prominent in these reactions, which is a common application of boron tribromide. Toluene and dichloromethane produced the desired product in the largest quantities therefore would be the solvents tested in in later reactions. Boron trichloride was then examined with *P*-(p-methoxyphenyl) diazaphospholene **7-31** in toluene at room temperature and -15 °C. The cold reaction

formed a clean product in the $^{31}P$ NMR data as a boron coupled phosphorus. Boron NMR data also indicated the presence of a phosphine coordinated boron with a doublet in the $^{11}B$ spectrum at 3.2 ppm. A minor peak was observed in the $^{11}B$ NMR spectrum at 54 ppm, indicating some aryl borane formation. The reaction conducted at room temperature formed an almost identical spectrum with a minor amount of aryl boron formation.

The propensity for *P*-(p-methoxyphenyl) diazaphospholene **7-31** to undergo demethylation indicated that this substrate was not suitable for borylation reactions. To avoid the demethylation reaction, *P*-phenyl diazaphospholene **7-3** was examined in borylation. To ensure complete consumption of the diazaphospholene **7-3**, 2 equivalents of boron tribromide were added to *P*-phenyl diazaphospholene **7-3** in toluene or dichloromethane. The reactions were first cooled followed by boron addition, which were analyzed after 1 h. The $^{11}B$ NMR data indicated that the formation of an aryl boron species, when dichloromethane was used however both reactions were not selective in the formation of the desired product.

The reactions were repeated at room temperature with both 1 and 2 equivalents of boron tribromide in both toluene and dichloromethane. Interestingly, addition of one equivalent of boron tribromide in either toluene or dichloromethane resulted in the formation of a boron-phosphine adduct. When two equivalents of boron tribromide was added, the formation of the desired aryl boron product **7-32** was observed with dichloromethane providing a larger proportion of the desired product. Boron trichloride was also examined with 3 equivalents added in dichloromethane, however the exclusive product was a boron adduct and was not investigated further. Dichloromethane was found to be the most suitable solvent for borylation of the aryl group. The reaction was scaled up and the boron product **7-32** was isolated from pentane extraction. The precipitate from the

reaction was assumed to contain diazaphospholenium tetrabromoborate **7-33** due to the similarities in the $^{31}$P NMR chemical shift with the tetrafluoroborate derivative.[251] The results indicate that an excess of the boron tribromide is needed because the diazaphospholene bromide **7-5** captures an equivalent of the boron. The reaction was repeated but before isolation, pinacol and triethylamine were added,[270] and the reaction was stirred for an additional amount of time. The product isolated was phenyl-Bpin **7-34**, albeit in low yields. The low yield for both aryl boron products can be attributed to potential side reactions found in the preliminary reactions, and the presence of excess boron. While these reactions display that derivatization is possible with these compounds and is the first example of transfer of a substituent from a diazaphospholene to boron, there is no advantage over other synthetic methods, which give higher yields of aryl boron compounds from simpler substrates.

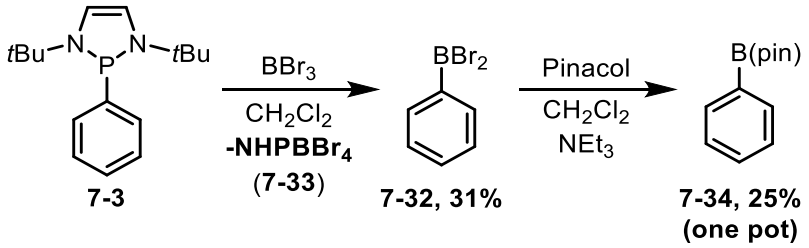


**Scheme 7.14** Transfer of aryl group from phosphorus to boron.

## 7.7 Conclusion

Diazaphospholene dimers were relatively underexplored in their reactivity, with only limited examples within the literature. Within this chapter diazaphospholene dimers have been shown to react with a variety of aryl bromides and iodides allowing for aryl functionalization of the diazaphospholene. This finding is important as it allows for a new method to prepare ligand synthons. In addition, pyridyl functionalization is challenging though metallation routes and this method allows for the phosphination of these substrates.

Alkylation was also successful in this reactivity with the formation of new diazaphospholene complexes. The reactions described within this chapter may be operating under either radical, polar or a combination of both depending on the nature of the solvent, absence or presence of light, and substrate. The radical nature of these reactions can be exploited to facilitate radical cyclizations which were shown within this chapter, as well as by other groups during the contemporary period. Unique reactivity was observed with *P*-pentafluorophenyl diazaphospholene **7-6**, in which the combination of this reagent and an electrophile resulted in the first carbon-carbon bond formation facilitated by transfer from a diazaphospholene, however this reactivity did not appear generalizable to other diazaphospholenes. Overall, this work expands the scope of diazaphospholene chemistry allowing for new applications of this highly versatile compound.

## 7.8 Experimental

### 7.8.1 General Considerations

All reagents and solvents were dispensed in a 2001 issue IT Glovebox ($H_2O$ levels vary between 2-6 ppm) unless otherwise stated. The diazaphospholene dimer **7-1** and corresponding products from reactions with the diazaphospholene dimer **7-1** were prepared in oven dried 4 dram scintillation vials equipped with magnetic stir bars and green Qorpak® PTFE lined caps. All reactions were conducted at ambient temperature unless otherwise stated. The material selected to prepare NMR samples gave visually homogenous solutions unless otherwise noted. $^{1}H$, $^{31}P$, $^{19}F$, $^{11}B$ and $^{13}C$ NMR data were collected at 300K on either a Bruker AV-300 or AV-500 spectrometer. $^{1}H$ NMR spectra are referenced to residual non-deuterated NMR solvent from the sample ($C_6H_6$ = 7.16 ppm, $CHCl_3$ = 7.26 ppm, $CH_3CN$ = 1.94 ppm). $^{13}C$ NMR spectra are referenced to NMR solvent from the sample ($C_6D_6$ = 128.06 ppm, $CDCl_3$ = 77.16 ppm, $CD_3CN$ = 1.32 ppm or 118.26 ppm). LED irradiation

was conducted using a Kessil H150-Blue lamp. The maximum emission wavelength of this lamp is centered around 465 nm. The lamp also produces a secondary emission peak approximately 30% the intensity of the primary peak, centered around 417 nm. HPLC data were acquired on a Varian Prostar instrument, equipped with detection at 254 nm, using a Astec Cellulose DMP column. A 99:1 hexanes/isopropanol solvent mixture was used as the eluent, with a flow rate of 0.5 mL/min. Mass spectrometric data were acquired by Mr. Xiao Feng (Mass Spectrometry Laboratory, Dalhousie University).

### 7.8.2 Solvent Purification

**Toluene** was purchased in a drum ACS grade from Fisher and was passed through a double column purification system (activated alumina and activated Q-5) from MBraun Inc. and stored over 3Å molecular sieves under nitrogen.

**Pentane** was purchased in a drum as ACS grade from Fisher, sparged with nitrogen and stored over 3Å molecular sieves under nitrogen.

**Tetrahydrofuran** was purchased as anhydrous >99% ACS grade from Sigma Aldrich and stored over 3Å molecular sieves under nitrogen.

**Acetonitrile** was purchased as anhydrous >99% ACS grade from Sigma Aldrich and used without further purification.

**Diethyl ether** was purchased in a drum ACS grade from Fisher and used as is.

**Hexanes** was purchased in a drum ACS grade from Fisher and used as is.

**Dimethylformamide anhydrous** was purchased from Sigma Aldrich and used as received.

### 7.8.3 Reagents

Iodobenzene, 1-bromoadamantane, 3-bromopyridine, 2-bromopyridine, 3-bromobenzothiophene, 1-bromo-3-phenylpropane, cinnamyl bromide, 3,3-dimethylallyl bromide, diphenyl disulphide, neopentyl alcohol, phenylmagensium bromide, boron

tribromide, triethylamine, pinacol, iodine, and tert-butyllithium were purchased from Sigma Aldrich and used as received.

Pentafluorobromobenzene, 2-bromoiodobenzene, (bromomethyl)cyclopropane, 2-bromonaphthalene, methyl 6-bromonicotinate, and 2-iodophenol were purchased from Oakwood chemicals and used as received.

**Ferrocene** was a sample that had been purchased from Eastman.

**Bromobenzene** was purchased from Fisher and used as received.

**Magnesium turnings** 98% were purchased from Sigma Aldrich and used as received.

**Potassium carbonate** was purchased from ACP and used as received.

**Iodoferrocene** was prepared according to literature procedures.[271] In some runs, further purification was necessary, which was accomplished by washing with aqueous $FeCl_3$.[272]

**Diazaphospholene bromide 7-5** was prepared according to literature procedures.[77]

**Diazaphospholene bromide 7-30** was prepared according to literature procedures.[78]

**Quinolinium bromide** was prepared in section **4.8.4**.

**Umemoto's reagent** was purchased from TCI and used as received.

### 7.8.4 Synthetic Procedures an Initial Experiments

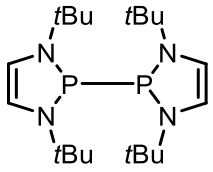


**Synthesis of the diazaphospholene dimer (7-1).** Compound **7-1** was prepared according to a modified procedure using magnesium turnings in place of magnesium dust.[89] *Tert*-butyl diazaphospholene bromide **7-5** (2.00 g, 7.16 mmol) was weighed into a 50 mL flask equipped with a magnetic stir bar. Magnesium turnings (528 mg, 21.7 mmol, 3 equiv.) was added to the flask and THF (12 mL) was then added to the solids creating a suspension.

Iodine (188 mg, 0.74 mmol, 0.1 equiv.) was then added to the slurry and the reaction was stirred for 4 h. Volatiles were then removed from the reaction mixture and pentane (15 mL) was added to the crude material to dissolve the product. The slurry was filtered over a fine frit packed with celite and the flask was rinsed with pentane (2 x 15 mL) which was subsequently filtered as well. Pentane was removed *in vacuo* to afford the desired product **7-1** (1.1g, 2.84 mmol, 79% yield). NMR spectral data were in accordance with literature values.[89]

**$^{1}$H** (500 MHz, $C_6D_6$): δ 5.94 (apparent t, $^{3}J_{H,P}$ = 2 Hz, 4H), 1.25 (s, 36H).

**$^{13}$C** {$^{1}$H} (125.7 MHz, $C_6D_6$): δ 121, 54.2 (apparent t, $^{2}J_{C,P}$ = 7.6 Hz), 30.3 (apparent t, $^{3}J_{C,P}$ = 3.4 Hz).

**$^{31}$P** (202.5 MHz, $C_6D_6$): δ 80.

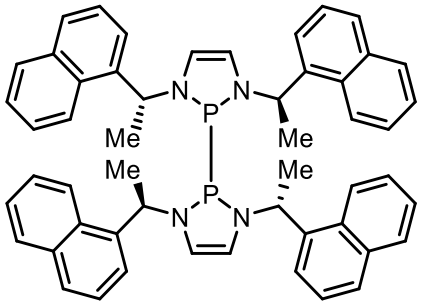


**Synthesis of the bis-*N*-(R)-napthylmethyl-diazaphospholene.** Compound **7-28** was prepared according to a modified procedure using magnesium turnings in place of magnesium dust.[89] *N*-(R)-napthylmethyl-diazaphospholene bromide **7-30** (500 mg, 1.05 mmol) was weighed into a 4 dram vial equipped with a magnetic stir bar. Magnesium turnings (76 mg, 3.15 mmol, 3 equiv.) were added to the vial and THF (4 mL) was then added to the solids creating a suspension and the reaction was stirred for 4 h. Volatiles were then removed from the reaction mixture and a pentane toluene mixture (50/50) was added to the crude material to dissolve the product. The slurry was filtered over a fine frit packed

with celite and the flask was rinsed with toluene (2 x 15 mL) which was subsequently filtered as well. Volatiles were removed *in vacuo* to afford the desired product **7-30** (1.1g, 2.84 mmol, 79% yield).

**$^{31}$P** (202.5 MHz, $C_6D_6$): δ 89.

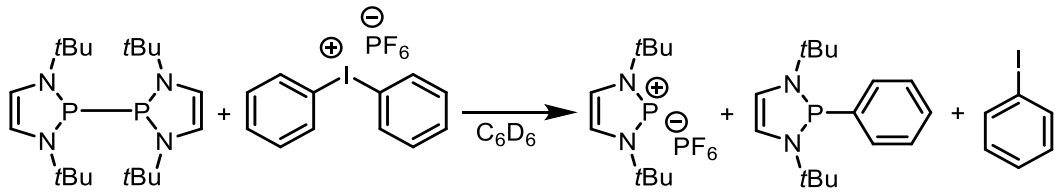


**Initial reaction of diazaphospholene dimer 7-1 with $Ph_2IPF_6$.** An initial reaction was conducted with **7-1** and diphenyl iodonium hexafluorophosphate. Diazaphospholene dimer **7-1** (15 mg, 0.037 mmol) was weighed into a 1 dram vial and dissolved in benzene-$d_6$ (approx. 0.7 mL). Diphenyl iodonium hexafluorophosphate (16 mg, 0.037 mmol) was added to the vial and the reaction was stirred for either 10 min or 4 h. A precipitate was observed during both reaction times and the slurries were transferred to an NMR tube and were then analyzed using NMR spectroscopy. Since the reactions were not homogenous, only $^{31}$P NMR spectra were recorded, and integral values should not be taken as quantification of the product formation, since not all material was in solution. While it may be assumed that the precipitate is primarily the phosphenium hexafluorophosphate **7-2**, the iodobenzene that was released under the reaction conditions can react with compound **7-1** as well. The solid could be a mixture of **7-2** and **7-4**, however further analysis would be necessary. The primary purpose of this experiment was to demonstrate diphenyl iodonium salts could arylate **7-1**, however after the discovery that cheaper and more readily available aryl iodides and bromides could serve as arylating agents, exploration of reactivity of less

accessible iodonium salts was terminated. These results are included to note that at least one diaryl iodonium is also capable of the arylation reaction.

**Spectrum after 10 min:**

**$^{31}$P** (202.5 MHz, $C_6D_6$): δ 80 (diazaphospholene dimer **7-1**), 74.5 (new compound, **7-3**) in a ratio approximately 1:0.14.

**Spectrum after 4h:**

**$^{31}$P** (121.5 MHz, $C_6D_6$): δ 184 (trace amount of a putative diazaphospholenium salt **7-2**), 74.5 (new compound, **7-3**)

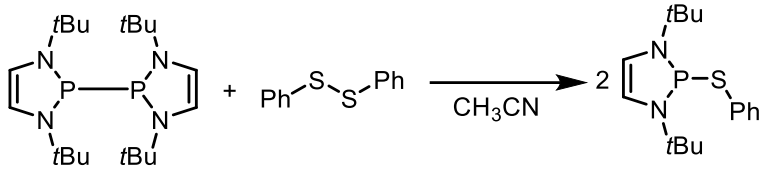


**Reaction of diazaphospholene dimer 7-1 with diphenyldisulfide.** Diazaphospholene dimer **7-1** (119 mg, 0.3 mmol, 1 equiv.) was weighed into a 4 dram vial equipped with a magnetic stir bar and dissolved in acetonitrile (1 mL). Diphenyldisulfide 6 (65.5 mg, 0.3 mmol, 1 equiv.) was added and the sides rinsed with acetonitrile (0.3 mL). The resulting solution was left to stir for 30 min. Volatiles were removed, and the crude material triturated with pentane (3 x 1 mL) to afford the product which was characterized without further purification. Mass spectrometry was attempted but did not yield a hit for the molecular ion, presumably due to facile fragmentation.

**Yield:** 176mg, 95% yield.

**$^{1}$H** (500 MHz, $C_6D_6$): δ 7.70 (apparent d, 2H), 7.16 (apparent t, 2H), 7.01 (apparent t, 1H), 6.06 (s, 2H), 1.29 (d, $^{4}J_{H,P}$ = 1.7 Hz, 18H).

**$^{13}$C** {$^{1}$H} (125.8 MHz, $C_6D_6$): δ 138, 134, 128, 125, 116 (d, $^{2}J_{C,P}$ = 9.9 Hz), 54.1 (d, $^{2}J_{C,P}$ = 8.3 Hz), 30.3 (d, $^{3}J_{C,P}$ = 10.7 Hz).

**$^{31}$P** (202.5 MHz, $C_6D_6$): δ 144.8.

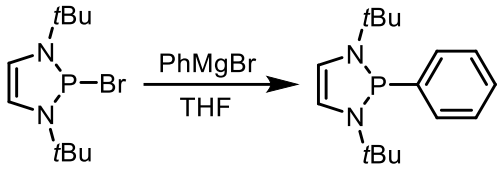


***P*-phenyl diazaphospholene 7-3 from Grignard Reagent.** A sample of **7-1** was independently prepared by the reaction of **7-5** and phenylmagnesium bromide, and was used for spectral comparisons in initial experiments. Diazaphospholene bromide **7-5** (1.00 g, 3.58 mmol) was weighed into a 4 dram vial equipped with a magnetic stir bar. Tetrahydrofuran (5 mL) was added to the vial followed by carful addition of phenyl magnesium bromide (1.19 mL, 3.58 mmol, 3M in ether) with stirring. The solution was stirred for 3 h followed by removal of volatiles *in vacuo*. Pentane (10 mL) was added to the vial and the crude slurry was filtered over a fine porous frit with celite. The frit was washed with additional pentane (4 x 10 mL) and the combined filtrated were removed of all volatiles *in vacuo* to afford the pure product (712 mg, 2.57 mmol, 72% yield). NMR analysis of the product was identical to the product obtained by reaction with iodobenzene and the diazaphospholene dimer **7-1**.

**$^{1}$H** (500 MHz, $CDCl_3$): δ 7.71 (apparent t, 2H), 7.24 (m, 2H), 7.12 (apparent t, 1H), 5.72 (d, $^{3}J_{H,P}$ = 4.4 Hz, 2H), 1.24 (s, 18H).

**$^{31}$P** (202.5 MHz, $C_6D_6$): δ 74.5.

### 7.8.5 General Procedure and Products for the Reaction of Diazaphospholene Dimer 7-1 and Aryl/Alkyl Halides

Diazaphospholene dimer **7-1** (119 mg, 0.3 mmol, 1 equiv.) was weighed into a 4 dram vial equipped with a magnetic stir bar and dissolved in toluene or acetonitrile (1 mL). The alkyl/aryl halide was added as a solution (0.3 mL, 1M toluene) if the reagent is liquid or

added directly if the reagent is solid and the sides rinsed with toluene (0.3 mL) to quantitative transfer. The resulting solution was left to stir for the allotted time with or without the presence of blue light. Irradiation was accomplished with a Kessil H150 Blue LED lamp clamped between 4-10 cm from the vial or NMR tube. Thermocouple measurements showed the reaction temperature remained under 25 °C during the course of the reaction under these conditions. Solvents were removed *in vacuo*. The crude material was suspended in pentane (7 mL) and filtered over a fine porous frit and washed with pentane (4 x 3 mL) to collect the diazaphospholene bromide or iodide as a white to off white solid. If the diazaphospholene halide is not to be isolated, celite was added to make the filtration faster. The filtrate was removed of all volatiles to provide the diazaphospholene alkyl or aryl product. The crude material triturated with pentane (3 x 1 mL) to afford the alkyl or aryl diazaphospholene which was characterized as-is or crystalized from pentane.

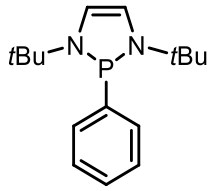


***P*-phenyl diazaphospholene 7-3 from Iodobenzene.** Prepared from **7-1** and iodobenzene according to the general procedure without blue light irradiation. The reaction time was 1.5 h. In this case, both product **7-3** and diazaphospholene iodide **7-4** were isolated and characterized.

**Diazaphospholene iodide (7-4).**

**Yield:** 86 mg, 88% yield.

**$^1$H** (500 MHz, $CDCl_3$): δ 7.33 (s, 2H), 1.74 (d, $^4J_{H,P}$ = 1.9 Hz, 18H).

**$^{13}$C** {$^{1}$H} (125.8 MHz, $CDCl_3$): δ 125 (d, $^{2}J_{C,P}$ = 6.3 Hz), 60.0 (d, $^{2}J_{C,P}$ = 7.1 Hz), 29.8 (d, $^{3}J_{C,P}$ = 9.7 Hz).

**$^{31}$P** (202.5 MHz, $CDCl_3$): δ 194.

***P*-phenyl diazaphospholene (7-3).**

**Yield:** 72 mg, 87% yield.

**$^{1}$H** (300 MHz, $C_6D_6$): δ 7.71 (m, 2H), 7.24 (m, 2H), 7.12 (m, 1H), 5.72 (d, $^{3}J_{H,P}$ = 4.4 Hz, 2H), 1.24 (s, 18H).

**$^{13}$C** {$^{1}$H} (75.5 MHz, $C_6D_6$): δ 147 (d, $^{1}J_{C,P}$ = 19.9 Hz), 129 (d, $^{2}J_{C,P}$ = 19.7 Hz), 128-127 (2 peaks overlap with $C_6D_6$), 118 (d, $^{2}J_{C,P}$ = 5.3 Hz), 54.2 (d, $^{2}J_{C,P}$ = 16.6 Hz), 30.1 (d, $^{3}J_{C,P}$ = 8.6 Hz).

**$^{31}$P** (121.5 MHz, $C_6D_6$): δ 74.5.

**HRMS (ESI):** calc'd for $C_{16}H_{26}N_2P$ $[M + H]^+$ 277.1828; Found: 277.1818 (3.6 ppm difference)

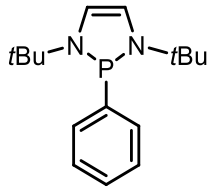


***P*-phenyl diazaphospholene 7-3 from bromobenzene.** Prepared from **7-1** and bromobenzene according to the general procedure with blue light irradiation. The reaction time was 8 h. In this case, both product **7-3** and diazaphospholene bromide **7-5** were isolated and characterized.

**Diazaphospholene bromide (7-5).**

**Yield:** 66 mg, 79% yield.

**$^{1}$H** (300 MHz, $CDCl_3$): δ 7.25 (s, 2H), 1.7 (d, $^{4}J_{H,P}$ = 1.9 Hz, 18H).

**$^{13}$C** {$^{1}$H} (75.5 MHz, $CDCl_3$): δ 124 (d, $^{2}J_{C,P}$ = 6.8 Hz), 59.4 (d, $^{2}J_{C,P}$ = 7.4 Hz), 30.2 (d, $^{3}J_{C,P}$ = 10.1 Hz).

**$^{31}$P** (121.5 MHz, $CDCl_3$): δ 186.

***P*-phenyl diazaphospholene (7-3).**

**Yield:** 80 mg, 96% yield.

**$^{1}$H** (300 MHz, $C_6D_6$): δ 7.71 (m, 2H), 7.24 (m, 2H), 7.12 (m, 1H), 5.72 (d, $^{3}J_{H,P}$ = 4.4 Hz, 2H), 1.24 (s, 18H).

**$^{13}$C** {$^{1}$H} (75.5 MHz, $C_6D_6$): δ 147 (d, $^{1}J_{C,P}$ = 19.9 Hz), 129 (d, $^{2}J_{C,P}$ = 19.7 Hz), 128-127 (2 peaks overlap with $C_6D_6$), 118 (d, $^{2}J_{C,P}$ = 5.3 Hz), 54.2 (d, $^{2}J_{C,P}$ = 16.6 Hz), 30.1 (d, $^{3}J_{C,P}$ = 8.6 Hz).

**$^{31}$P** (121.5 MHz, $C_6D_6$): δ 74.5.

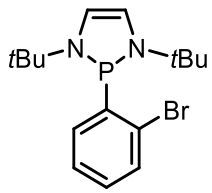


***P*-(2-bromo-phenyl) diazaphospholene (7-12).** Prepared according to the general procedure from 2-bromoiodobenzene in $CH_3CN$ without blue light irradiation, reaction time 1.5 h.

**Yield:** 91 mg, 85% yield.

**$^{1}$H** (300 MHz, $C_6D_6$): δ 7.83 (dt, $^{3}J_{H,H}$ = 7.6 Hz, $J$ = 1.9 Hz, 1H), 7.34 (ddd, $^{3}J_{H,H}$ = 8.0 Hz, $J$ = 3.3 Hz, $J$ = 0.98 Hz, 1H), 7.03 (td,$^{3}J_{H,H}$ = 7.6 Hz, $J$ = 0.98 Hz, 1H), 6.73 (td, $^{3}J_{H,H}$ = 7.6 Hz, $J$ = 1.8 Hz, 1H), 5.74 (d, $^{3}J_{H,P}$ = 4.1 Hz, 2H), 1.24 (s, 18H).

**$^{13}$C** {$^{1}$H} (75.5 MHz, $C_6D_6$): δ 144 (d, $^{1}J_{C,P}$ = 33.9 Hz), 133 (d, $^{2}J_{C,P}$ = 37.4 Hz), 130, 128 (signal overlap with $C_6D_6$) 127, 125 (d, $^{2}J_{C,P}$ = 36.9 Hz), 118 (d, $^{2}J_{C,P}$ = 5.5 Hz), 55.0 (d, $^{2}J_{C,P}$ = 20.3 Hz), 30.1 (d, $^{3}J_{C,P}$ = 8.4 Hz).

**$^{31}$P** (121.5 MHz, $C_6D_6$): δ 77.5.

**HRMS (ESI):** calc'd for $C_{16}H_{25}BrN_2P$ $[M + H]^+$ 355.0933; Found: 355.0919. (3.9 ppm difference).

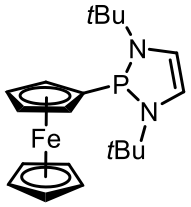


***P*-ferrocenyl diazaphospholene (7-13).** Prepared according to the general procedure from iodoferrocene in $CH_3CN$ without blue light irradiation, reaction time 2.5 h. Additional purification required where the sample must be dissolved in pentane and cooled to -35 °C. The residual solution is then decanted from the pure product. Crystals suitable for X-ray diffraction were grown using this method.

**Yield:** 75 mg, 65% yield.

**$^{1}$H** (500 MHz, $C_6D_6$): δ 5.70 (d, $^{3}J_{H,P}$ = 4.2 Hz, 2H), 4.30 (apparent q, 2H), 4.17 (s, 5H), 4.06 (apparent t, 2H), 1.26 (s, 18H).

**$^{13}$C** {$^{1}$H} (125.8 MHz, $C_6D_6$): δ 118 (d, $^{2}J_{C,P}$ = 5.4 Hz), 87.1 (d, $^{1}J_{C,P}$ = 16 Hz), 69.6 (d, $^{2}J_{C,P}$ = 13 Hz), 69.4 (d, $^{3}J_{C,P}$ = 2.4 Hz), 68.9, 54.2 (d, $^{2}J_{C,P}$ = 17 Hz), 30.1 (d, $^{3}J_{C,P}$ = 8.7 Hz).

**$^{31}$P** (202.5 MHz, $C_6D_6$): δ 74.2.

**HRMS (ESI):** calc'd for $C_{20}H_{29}N_2P$ $[M + H]^+$ 385.1496; Found: 385.1472. (6.2 ppm difference).

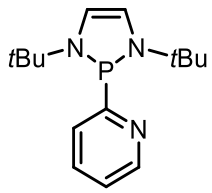


***P*-(2-pyridyl) diazaphospholene** (**7-7**). Prepared according to the general procedure from 2-bromopyridine in $CH_3CN$ without blue light irradiation, reaction time 2 h. Mass-spectral data was inadvertently not acquired for this compound before shutdown of research due to the COVID-19 crisis, however spectral properties are similar to **7-8**.

**Yield:** 82 mg, 99% yield.

**$^1$H** (500 MHz, $C_6D_6$): δ 8.62 (dt, $^3J_{H,H}$ = 4.6 Hz, $J$ = 1.0 Hz, 1H), 7.63 (dt,$^3J_{H,H}$ = 7.63 Hz, $J$ = 1.0 Hz, 1H), 7.13 (tt, $^3J_{H,H}$ = 7.6 Hz, $J$ = 1.7 Hz, 1H), 6.59 (dd, $^3J_{H,H}$ = 7.6 Hz, $J$ = 4.6 Hz, 1H), 5.74 (d, $^3J_{H,P}$ = 4.1 Hz, 2H), 1.34 (s, 18 H).

**$^{13}$C** {$^1$H} (125.8 MHz, $C_6D_6$): δ 170 (d, $^1J_{C,P}$ = 4.6 Hz), 150 (d, $^3J_{C,P}$ = 13 Hz), 134, 123 (d, $^2J_{C,P}$ = 12 Hz), 122, 118 (d, $^2J_{C,P}$ = 5.7 Hz), 54 (d, $^2J_{C,P}$ = 18 Hz), 30 (d, $^3J_{C,P}$ = 8.3 Hz).

**$^{31}$P** (202.5 MHz, $C_6D_6$): δ 65.6.

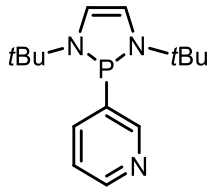


***P*-(3-pyridyl) diazaphospholene** (**7-8**). Prepared according to the general procedure from 3-bromopyridine in $CH_3CN$ without blue light irradiation, reaction time 2 h.

**Yield:** 54 mg, 65% yield.

**$^1$H** (300 MHz, $C_6D_6$): δ 9.06 (tt, $J$ = 2.2 Hz, $J$ = 1.0 Hz, 1H), 8.53 (dd, $^3J_{H,H}$ = 4.8 Hz, $J$ = 1.4 Hz, 1H), 7.7 (dt, $^3J_{H,H}$ = 6.0 Hz, $J$ = 2.0 Hz, 1H), 6.8 (dt, $^3J_{H,H}$ = 7.8 Hz, $J$ = 1.0 Hz, 1H), 5.63 (d, $^3J_{H,P}$ = 4.5 Hz, 2H), 1.16 (s, 18H).

**$^{13}$C** {$^{1}$H} (75.5 MHz, $C_6D_6$): δ 151 (d, $^{2}J_{C,P}$ = 20.9 Hz), 150, 141 (d, $^{1}J_{C,P}$ = 24.6 Hz), 136 (d, $^{2}J_{C,P}$ = 17.7 Hz), 122 (d, $^{3}J_{C,P}$ = 2.9 Hz), 118 (d, $^{2}J_{C,P}$ = 5.2 Hz), 54.3 (d, $^{2}J_{C,P}$ = 17.6 Hz), 30.0 (d, $^{3}J_{C,P}$ = 8.6 Hz).

**$^{31}$P** (121.5 MHz, $C_6D_6$): δ 71.8.

**HRMS (ESI):** calc'd for $C_{15}H_{25}N_3P$ $[M + H]^+$ 278.1781; Found: 278.1770. (3.9 ppm difference).

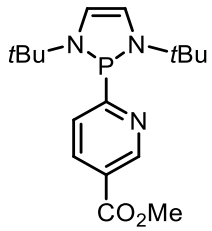


***P*-(2-(6-methyl-nicotinyl)) diazaphospholene (7-9).** 2,3-dihydro-1,3-tert-butyl-2-(6-methyl-nicotinyl)-1H-1,3,2-Diazaphosphole. Prepared according to the general procedure from 6-bromomethylnicotinate in $CH_3CN$ without blue light irradiation, reaction time 1.5 h.

**Yield:** 91 mg, 91% yield.

**$^{1}$H** (500 MHz, $C_6D_6$): δ 9.46 (s, 1H), 8.06 (d, $^{3}J_{H,H}$ = 7.9 Hz, 1H), 7.63 (d, $^{3}J_{H,H}$ = 7.9 Hz, 1H), 5.71 (d, $^{3}J_{H,P}$ = 4.2 Hz, 2H), 3.36 (s, 3H), 1.32 (s, 18H).

**$^{13}$C** {$^{1}$H} (125.8 MHz, $C_6D_6$): δ 176 (d, $^{1}J_{C,P}$ = 9.1 Hz), 165, 151 (d, $^{3}J_{C,P}$ = 12.8 Hz), 135, 124, 122 (d, $^{2}J_{C,P}$ = 12.0 Hz), 118 (d, $^{2}J_{C,P}$ = 5.5 Hz), 54.3 (d, $^{2}J_{C,P}$ = 17.5 Hz), 51.5, 30.2 (d, $^{3}J_{C,P}$ = 8.3 Hz).

**$^{31}$P** (202.5 MHz, $C_6D_6$): δ 65.8.

**HRMS (ESI):** calc'd for $C_{17}H_{27}N_3OP$ $[M + H]^+$ 336.1835; Found: 336.1830. (1.5 ppm difference).

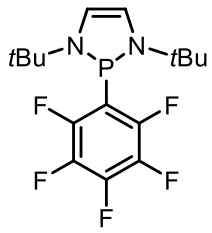


***P*-pentafluorophenyl diazaphospholene (7-6).** Prepared according to the general procedure from 1-bromopentafluorobenzene in $CH_3CN$ without blue light irradiation, reaction time 30 min.

**Yield:** 93 mg, 85% yield.

**$^{1}$H** (500 MHz, $C_6D_6$): δ 5.9 (d, $^{3}J_{H,P}$ = 3.3 Hz, 2H), 1.13 (s, 18H).

**$^{13}$C** {$^{1}$H} (125.8 MHz, $C_6D_6$): δ 147, 141, 137, 117 (d, $^{2}J_{C,P}$ = 8.2 Hz), 54.3 (d, $^{2}J_{C,P}$ = 18.1 Hz), 29.8 (d, $^{3}J_{C,P}$ = 10.1 Hz). Peaks missing due to low intensity of signals from C bound to F and P.

**$^{31}$P** (202.5 MHz, $C_6D_6$): δ 68.9.

**$^{19}$F** {$^{1}$H} (470.6 MHz, $C_6D_6$): δ -133, -154, -161.

**HRMS (APPI):** calc'd for $C_{16}H_{20}F_5N_2P$ $[M]^{\bullet+}$ 366.1279; Found: 366.1280. (0.27 ppm difference).

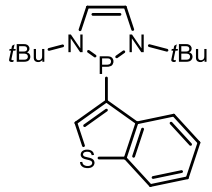


***P*-(3-benzothienyl) diazaphospholene (7-10).** Prepared according to the general procedure from 3-bromobenzothiophene in $CH_3CN$ with blue light irradiation, reaction time 5 h.

**Yield:** 84 mg, 84% yield.

**$^1$H** (500 MHz, $C_6D_6$): δ 8.48 (d, $^3J_{H,H}$ = 8.1 Hz, 1H), 7.68 (d, $^3J_{H,P}$ = 3.7 Hz, 1H), 7.59 (d, $^3J_{H,H}$ = 8.1 Hz, 1H), 7.27 (apparent t, 1H), 7.07 (apparent t, 1H), 5.79 (d, $^3J_{H,P}$ = 4.4 Hz, 2H), 1.20 (s, 18 H).

**$^{13}$C** {$^1$H} (125.8 MHz, $C_6D_6$): δ 142 (d, $^1J_{C,P}$ = 2.7 Hz), 141 (d, $^2J_{C,P}$ = 39.2 Hz), 140 (d, $^3J_{C,P}$ = 21.6 Hz), 131 (d, $J_{C,P}$ = 11.7 Hz), 124.2 (d, $J_{C,P}$ = 25.0 Hz), 124.1 (d, $J_{C,P}$ = 6.9 Hz), 123, 121, 118 (d, $^2J_{C,P}$ = 5.8 Hz), 55 (d, $^2J_{C,P}$ = 18 Hz), 30 (d, $^3J_{C,P}$ = 8.7 Hz).

**$^{31}$P** (202.5 MHz, $C_6D_6$): δ 66.6.

**HRMS (ESI):** calc'd for $C_{18}H_{25}N_2PS$ $[M]^{\bullet+}$ 332.1470; Found: 332.1472. (0.60 ppm difference).

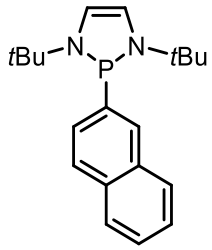


***P*-(2-naphthyl) diazaphospholene (7-11).** Prepared according to the general procedure from 2-bromonaphthalene in $CH_3CN$ with blue light irradiation, reaction time 4 h.

**Yield:** 87 mg, 89% yield.

**$^1$H** (300 MHz, $C_6D_6$): δ 8.16 (d, $^3J_{H,H}$ = 7.8 Hz, 1H), 7.86 (dd, $^3J_{H,H}$ = 8.7 Hz, $J$ =1.4 Hz, 1H), 7.71 (m, 2H), 7.60 (m, 1H), 7.23 (m, 2H), 5.77 (d, $^3J_{H,P}$ = 4.4 Hz, 2H), 1.29 (s, 18H).

**$^{13}$C** {$^1$H} (75.5 MHz, $C_6D_6$): δ 144 (d, $^1J_{C,P}$ = 21.5 Hz), 134, 133 (d, $^3J_{C,P}$ = 6.6 Hz), 129 (d, $J_{C,P}$ = 22.2 Hz), 128-127 (2 peaks overlap with $C_6D_6$), 126.8 (d, $J_{C,P}$ = 18.9 Hz), 126.1 (d, $J_{C,P}$ = 11.6 Hz), 118 (d, $^2J_{C,P}$ = 5.34 Hz), 54.3 (d, $^2J_{C,P}$ = 17.3 Hz), 30.1 (d, $^3J_{C,P}$ = 8.6 Hz).

**$^{31}$P** (121.5 MHz, $C_6D_6$): δ 75.4.

**HRMS (ESI):** calc'd for $C_{20}H_{27}N_2P$ $[M]^{\bullet+}$ 326.1906; Found: 326.1892. (4.3 ppm difference).

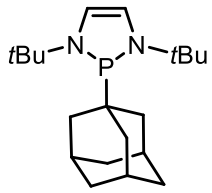


***P*-adamantyl diazaphospholene (7-15).** Prepared according to the general procedure from 1-bromoadamantane in toluene with blue light irradiation, reaction time 2 h.

**Yield:** 92 mg, 92% yield.

**$^1$H** (500 MHz, $C_6D_6$): δ 5.71 (d, $^3J_{H,P}$ = 4.5 Hz, 2H). 1.96 (m, 3H), 1.7 (m, 12H), 1.21 (s, 18H).

**$^{13}$C** {$^1$H} (125.8 MHz, $C_6D_6$): δ 120 (d, $^2J_{C,P}$ = 4.9 Hz), 54.1 (d, $^2J_{C,P}$ = 14.6 Hz), 38.7 (d, $^1J_{C,P}$ = 16.4 Hz), 37.8, 35.9 (d, $^2J_{C,P}$ = 13.2 Hz), 30 (d, $^3J_{C,P}$ = 7.9 Hz), 28.7 (d, $^3J_{C,P}$ = 9.2 Hz).

**$^{31}$P** (202.5 MHz, $C_6D_6$): δ 95.5.

**HRMS (ESI):** calc'd for $C_{20}H_{36}N_2P$ $[M + H]^+$ 335.2611; Found: 335.2609. (0.60 ppm difference).

Diazaphospholene bromide **7-5** was also isolated from this reaction, and its identity was confirmed by NMR spectroscopy.

**Yield:** 67 mg, 80% yield.

**$^1$H** (300 MHz, $CDCl_3$): δ 7.28 (s, 2H), 1.7 (s, 18H).

**$^{13}$C** {$^1$H} (75.5 MHz, $CDCl_3$): δ 124 (d, $^2J_{C,P}$ = 6.8 Hz), 59.4 (d, $^2J_{C,P}$ = 7.4 Hz), 30.2 (d, $^3J_{C,P}$ = 10.1 Hz).

**$^{31}$P** (121.5 MHz, $CDCl_3$): δ 186.

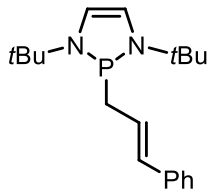


***P*-cinnamyl diazaphospholene (7-16).** Prepared according to the general procedure from cinnamyl bromide in acetonitrile without blue light irradiation, reaction time 2 h. During characterization, instability was noted in $C_6D_6$, so NMR spectra were also acquired in $CD_3CN$ in which compound **7-16** appeared to be more stable.

**Yield:** 85 mg, 89% yield.

**$^1$H** (500 MHz, $C_6D_6$): δ 7.32 (apparent d, 2H), 7.14 (apparent d, 2H, overlap with $C_6D_6$), 7.02 (apparent t., 1H), 6.36 (dd, $J$ = 15.8, 3.4 Hz, 1H), 6.24 (m, 1H), 5.75 (d, $^3J_{H,P}$ = 3.9 Hz, 2H), 2.30 (dd, 2H, $J$ = 7.9, 4.2 Hz). 1.17 (s, 18H).

**$^{13}$C** {$^1$H} (125.8 MHz, $C_6D_6$): Sample decomposed while in queue for overnight carbon NMR.

**$^{31}$P** (202.5 MHz, $C_6D_6$): δ 85.4

**$^1$H** (500 MHz, $CD_3CN$): δ 7.33 (apparent d, 2H), 7.28 (apparent t, 2H), 7.17 (apparent t, 1H), 6.25 (dd, $^3J_{H,H}$ = 15.8 Hz, $J$ = 3.4 Hz, 1H), 6.14 (m, 1H), 5.84 (d, $^3J_{H,P}$ = 3.9 Hz, 2H), 2.08 (ddd, $^3J_{H,H}$ = 7.9 Hz, $J$ = 4.0 Hz, $J$ = 0.9 Hz, 2H). 1.18 (s, 18H).

**$^{13}$C** {$^1$H} (125.8 MHz, $CD_3CN$): 139 (d, $^4J_{C,P}$ = 2.1 Hz), 132 (d, $^3J_{C,P}$ = 8.5 Hz), 129, 127, 126, 125 (d, $^2J_{C,P}$ = 5.3 Hz), 117 (d, $^2J_{C,P}$ = 5.9 Hz), 54.6 (d, $^2J_{C,P}$ = 15.9 Hz), 42.1 (d, $^1J_{C,P}$ = 24.4 Hz), 30.1 (d, $^3J_{C,P}$ = 8.5 Hz).

**$^{31}$P** (202.5 MHz, $CD_3CN$): δ 85.4

**HRMS (APCI):** calc'd for $C_{19}H_{30}N_2P$ $[M + H]^+$ 317.2141; Found: 317.2132. (2.8 ppm difference).

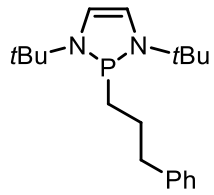


***P*-(3-phenyl-1-propyl) diazaphospholene** (**7-17**)**.** Prepared according to the general procedure from 1-bromo-3-phenylpropane in acetonitrile with blue light irradiation, reaction time 2 h. Unlike cinnamyl compound **7-16** compound **7-17** appeared highly stable in $C_6D_6$.

**Yield:** 86 mg, 90% yield.

**$^1$H** (500 MHz, $C_6D_6$): δ 7.14 (apparent d, 2H), 7.10 (apparent d, 2H), 7.04 (apparent t, 1H), 5.72 (d, $^3J_{H,P}$ = 4.3 Hz, 2H), 2.61 (t, $^3J_{H,H}$ = 7.7 Hz, 2H), 1.77 (m, 2H), 1.38 (m, 2H), 1.17 (s, 18H).

**$^{13}$C** {$^1$H} (125.8 MHz, $C_6D_6$): δ 142, 128, 126, 117 (d, $^2J_{C,P}$ = 5.3 Hz), 53.9 (d, $^2J_{C,P}$ = 16 Hz), 37.6 (d, $^3J_{C,P}$ = 11 Hz), 35.7 (d, $^1J_{C,P}$ = 17 Hz), 30 (d, $^3J_{C,P}$ = 8.5 Hz), 24.7 (d, $^2J_{C,P}$ = 14 Hz).

**$^{31}$P** (202.5 MHz, $C_6D_6$): δ 86.9.

**HRMS (ESI):** calc'd for $C_{19}H_{32}N_2P$ [M + H+] 319.2298; Found: 319.2287. (3.4 ppm difference).

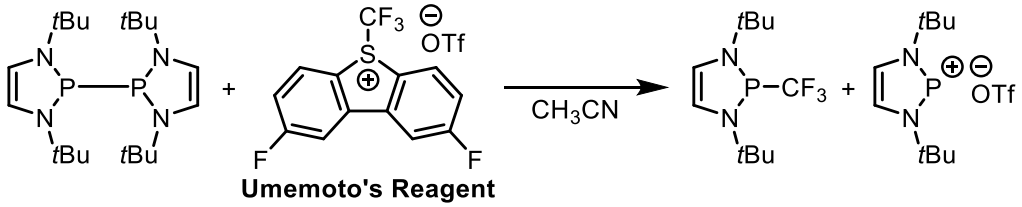


**Reaction of diazaphospholene dimer 7-1 with Umemoto's reagent.** Umemoto's reagent (23 mg, 0.052 mmol) was weighed into a 1 dram vial equipped with a magnetic stir bar and dissolved in acetonitrile (0.7 mL). Diazaphospholene dimer **7-1** (20 mg, 0.05 mmol) was

added to the vial and the solution stirred for 5 min. The solution was then transferred to a standard NMR tube an analyzed using NMR analysis. The solution displayed diazaphospholene triflate **7-27** as well as a new product **7-26** in the $^{31}$P NMR spectrum and the $^{19}$F NMR spectra revealed the presence of a singular new product.

**$^{31}$P** (202.5 MHz, $C_6D_6$): δ 204 ppm (s, NHP-OTf), 68 ppm (qt, $^{2}J_{P,F}$ = 63 Hz, NHP-$CF_3$)

**$^{19}$F** {$^{1}$H} (470.6 MHz, $C_6D_6$): δ -76.55 ($^{2}J_{F,P}$ = 63 Hz, NHP-$CF_3$).

### 7.8.6 Radical Clock Test and Radical Cyclized Products

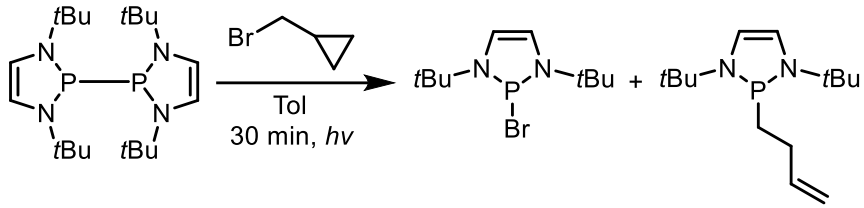


**Treatment of dimer 7-1 with cyclopropyl methyl bromide in toluene with blue light irradiation. *P*-(3-butenyl) diazaphospholene (7-18).** Prepared according to the general procedure from cyclopropylmethylbromide in toluene with blue light irradiation, reaction time 30 min. Unlike cinnamyl compound **7-16** compound **7-18** appeared highly stable in $C_6D_6$.

**Yield:** 46 mg, 60% yield.

**$^{1}$H** (500 MHz, $C_6D_6$): δ 5.89 (m, 1H), 5.71 (d, $^{3}J_{H,P}$ = 4.3 Hz, 2H), 5.07 (dq, $^{3}J_{H,H}$ = 17.3 Hz, $J$ = 1.7 Hz, 1H), 4.95 (d, $^{3}J_{H,H}$ = 10.2 Hz, 1H), 2.21 (m, 2H), 1.45 (m, 2H), 1.17 (s, 18H).

**$^{13}$C** {$^{1}$H} (125.8 MHz, $C_6D_6$): δ 140 (d, $^{3}J_{C,P}$ = 12.2 Hz), 117 (d, $^{2}J_{C,P}$ = 5.3 Hz), 113, 53.9 (d, $^{2}J_{C,P}$ = 15.8 Hz), 35.3 (d, $^{1}J_{C,P}$ = 18.3 Hz), 29.8 (d, $^{3}J_{C,P}$ = 8.6 Hz), 27.0 (d, $^{2}J_{C,P}$ = 14.9 Hz).

**$^{31}$P** (202.5 MHz, $C_6D_6$): δ 86.8.

**HRMS (ESI):** calc'd for $C_{14}H_{28}N_2P$ $[M + H]^+$ 255.1985; Found: 255.1985. (0 ppm difference).

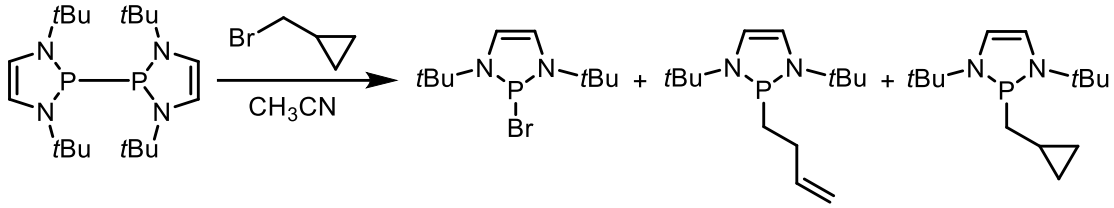


**Treatment of dimer 7-1 with cyclopropyl methyl bromide in acetonitrile without blue light irradiation. *P*-(3-butenyl) diazaphospholene (7-18). / *P*-(cyclopropylmethyl) diazaphospholene (7-19).** Prepared according to the general procedure from cyclopropyl methylbromide in acetonitrile without blue light irradiation, reaction time 30 min. The ratio of **7-18/7-19** was comparable in both the $^1$H and $^{31}$P NMR spectra. The ratio did not appear to change over time. The reaction products were not isolated. Mass-spectrometry data was not acquired for the unpurified reaction mixture.

***P*-(3-butenyl) diazaphospholene (7-18).**

**$^1$H** (500 MHz, $C_6D_6$): δ 5.89 (m, 1H), 5.71 (d, $^3J_{H,P}$ = 4.3 Hz, 2H), 5.07 (dq, $^3J_{H,H}$ = 17.3 Hz, $J$ = 1.7 Hz, 1H), 4.95 (d, $^3J_{H,H}$ = 10.2 Hz, 1H), 2.20 (m, 2H), 1.44 (m, 2H), 1.17 (s, 18H).

**$^{31}$P** (202.5 MHz, $C_6D_6$): δ 86.8.

***P*-(cyclopropylmethyl) diazaphospholene (7-19).**

**$^1$H** (500 MHz, $C_6D_6$): δ 5.73 (d, $^3J_{H,P}$ = 4.2 Hz, 2H), 1.29 (dd, $^3J_{H,H}$ = 7.2 Hz, $J$ = 3.5 Hz, 2H), 1.21 (s, 18H), 0.76 (m, 1H), 0.43 (m, 2H), 0.16 (m, 2H).

**$^{31}$P** (202.5 MHz, $C_6D_6$): δ 84.8.

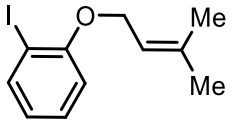


**Preparation of 1-(2-Iodophenoxy)-3-methyl-2-butene.** In a 50 mL round-bottom flask was weighed 2-iodophenol (1 g, 4.54 mmol), equipped with a magnetic stir bar which was placed under nitrogen. Potassium carbonate (1.88 g, 13.6 mmol, 3 equiv.) was added to the flask followed by DMF (7 mL). To the flask was added 3,3-dimethylallyl bromide (0.62 mL, 5 mmol, 1.1 equiv.) and the reaction was stirred overnight. The solution was diluted with water (10 mL) and the transferred to a separatory funnel. A solution of sodium hydroxide (30 mL, 2M) was then added and the product was extracted with hexanes (50 mL). The aqueous layer was then extracted once more with hexanes (20 mL) and the organic extracts were combined. The combined organic layers were washed with sodium thiosulfate (30 mL) followed by brine (30 mL) and then the organic extract was dried with sodium sulfate and filtered. Volatiles were removed *in vacuo* to afford the product (1.07g, 3.71 mmol, 82% yield). NMR spectra were in accordance with literature values.[273]

**$^{1}$H** (500 MHz, $CDCl_3$): δ 7.77 (dd, $^{3}J_{H,H}$ = 7.8, $J$ = 1.6 Hz, 1H), 7.27 (ddd, $^{3}J_{H,H}$ = 8.8 Hz, $J$ = 7.0 Hz, $J$ = 1.6 Hz, 1H), 6.83 (dd, $^{3}J_{H,H}$ = 8.2 Hz, $J$ = 1.1 Hz, 1H), 6.69 (td, $^{3}J_{H,H}$ = 7.6 Hz, $J$ = 1.3 Hz, 1H), 5.52 (m, 1H), 4.56 (d, $^{3}J_{H,H}$ = 6.5 Hz, 2H), 1.8 (s, 3H), 1.75 (s, 3H).

**$^{13}$C** {$^{1}$H} (125.8 MHz, $CDCl_3$): δ 157, 139, 138, 129, 122, 119, 112, 87.1, 66.4, 25.9, 18.5.

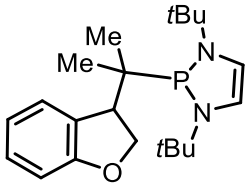


**Compound (7-20).** Prepared according to the general procedure from 1-(2-Iodophenoxy)-3-methyl-2-butene in acetonitrile without blue light irradiation, reaction time 2 h.

**Yield:** 84mg, 78% yield.

**$^{1}$H** (500 MHz, $C_6D_6$): δ 7.28 (d, $^{3}J_{H,H}$ = 7.4 Hz, 1H), 7.04 (t, $^{3}J_{H,H}$ = 7.8 Hz, 1H), 6.92 (d, $^{3}J_{H,H}$ = 6.92 Hz, 1H), 6.79 (td, $^{3}J_{H,H}$ = 7.5 Hz, $J$ = 1.0 Hz, 1H), 5.61 (m, 2H), 5.07 (ddd, $^{3}J_{H,H}$ = 9.2 Hz, 3.7 Hz, 1.8 Hz, 1H), 4.32 (t, $^{3}J_{H,H}$ = 8.9 Hz, 1H), 3.50 (td, $^{3}J_{H,H}$ = 8.5 Hz, 3.5 Hz, 1H), 1.12 (s, 9H), 1.09 (s, 9H), 1.01 (d, $^{3}J_{H,P}$ = 11 Hz, 3H), 0.82 (d, $^{3}J_{H,P}$ = 14 Hz, 3H).

**$^{13}$C** {$^{1}$H} (125.8 MHz, $C_6D_6$): δ 162, 128.5, 128.4 (d, $J_{C,P}$ = 6.5 Hz), 127.6 (d, $J_{C,P}$ = 3.1 Hz), 120 (d, $^{2}J_{C,P}$ = 5.2 Hz), 119 (two signals, doublet and singlet), 109, 73.7 (d, $^{3}J_{C,P}$ = 14 Hz), 54.6 (d, $^{2}J_{C,P}$ = 9.7 Hz), 54.5 (d, $^{2}J_{C,P}$ = 9.7 Hz), 45.2 (d, $^{2}J_{C,P}$ = 12 Hz), 41.5 (d, $^{1}J_{C,P}$ = 24 Hz), 30.0 (d, $^{3}J_{C,P}$ = 7.8 Hz), 29.8 (d, $^{3}J_{C,P}$ = 8.0 Hz), 20.6 (d, $^{2}J_{C,P}$ = 12 Hz), 16.2 (d, $^{2}J_{C,P}$ = 19 Hz).

**$^{31}$P** (202.5 MHz, $C_6D_6$): δ 100.

**HRMS (ESI):** calc'd for $C_{21}H_{33}N_2P$ $[M]^{\bullet+}$ 360.2325; Found: 360.2323. (0.60 ppm difference).

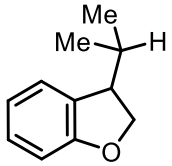


**Reductive cyclization of 1-(2-Iodophenoxy)-3-methyl-2-butene with diazaphospholene hydride (7-21).** 1-(2-Iodophenoxy)-3-methyl-2-butene (57 mg, 0.2 mmol) was weighed into a 1 dram vial equipped with a magnetic stir bar. Diazaphospholene **7-21** (80 mg, 0.4 mmol, 2 equiv.) was weighed into another 1 dram vial and dissolved in acetonitrile (0.5 mL). The solution containing **7-21** was transferred to the 1 dram vial containing 1-(2-Iodophenoxy)-3-methyl-2-butene. The vial was rinsed with acetonitrile (0.2 mL) which was added to the reaction vial. The reaction was stirred for 1.5 h and then

was diluted with ether (3 mL). The solution was filtered through a cotton plug into a round bottom flask 10 mL and the vial rinsed with ether (2 x 2 mL) through the cotton plug as well. The solution was concentrated to an oil and then passed through a silica plug with ether in hexanes (10% soln., approx. 25 mL total) to afford the product **7-22**. NMR data were in accordance with literature values.[274]

**Yield:** 26 mg, 81% yield.

**$^{1}$H** (300 MHz, $CDCl_3$): δ 7.19 (d, $^{3}J_{H,H}$ = 7.1 Hz, 1H), 7.13 (t, $^{3}J_{H,H}$ = 7.7 Hz, 1H), 6.85 (t, $^{3}J_{H,H}$ = 7.4 Hz, 1H), 6.78 (d, $^{3}J_{H,H}$ = 7.9 Hz, 1H), 4.52 (t, $^{3}J_{H,H}$ = 9.1 Hz, 1H), 4.38 (dd, $^{3}J_{H,H}$ = 9.1, $J$ = 5.1 Hz, 1H), 3.33 (m, 1H), 1.97 (m, 1H), 0.96 (d, $^{3}J_{H,H}$ = 6.8 Hz, 3H), 0.88 (d, $^{3}J_{H,H}$ = 6.8 Hz, 3H).

**$^{13}$C** {$^{1}$H} (75.5 MHz, $CDCl_3$): δ 160, 129, 125, 120, 109, 73.9, 48.3, 31.8, 19.9, 18.6.

### 7.8.7 Functionalization Reactions of Aryl Diazaphospholenes

**Transfer of aryl group from phosphorus to boron:**

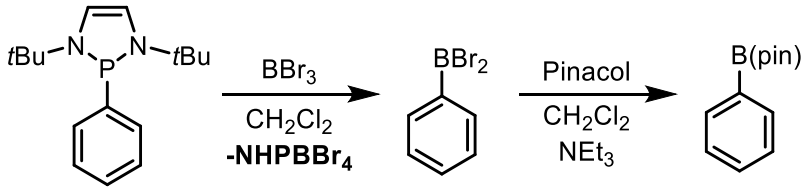


Phenyl diazaphospholene **7-3** (138 mg, 0.5 mmol) was weighed into a 4 dram vial equipped with a magnetic stir bar. Dichloromethane (2 mL) was added to dissolve the diazaphospholene derivative. A septa vial cap was used to seal the vial and secured with electrical tape. Boron tribromide (0.11 mL, 1.15 mmol, 2.3 equiv.) was added to the solution with vigorous stirring. The solution was stirred for 4h and then a solution of triethylamine (1.05 mL, 7.5 mmol, 15 equiv.) and pinacol (177 mg, 1.5 mmol, 3 equiv.) in dichloromethane (2 mL) was added in one portion and stirred for 1 h. Volatiles were

removed *in vacuo* and the crude material was purified via short silica column with an ether-hexanes gradient to afford phenyl-Bpin **7-34** (26 mg, 0.127 mmol, 25% yield). NMR data were in accordance with literature values.[275]

**$^{1}$H** (300 MHz, $CDCl_3$): δ 7.82 (apparent d, 2H), 7.47 (apparent t, 1H), 7.37 (apparent t, 2H), 1.35 (s, 12H).

**$^{13}$C** {$^{1}$H} (75.5 MHz, $CDCl_3$): δ 134, 131, 127, 83.9, 25.0.

**$^{11}$B** (96.3 MHz, $CDCl_3$): δ 30.9.

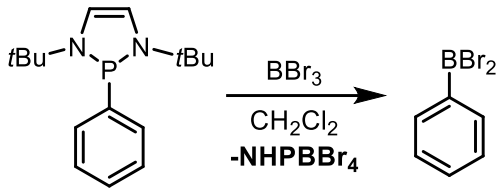


Phenyl diazaphospholene **7-3** (138 mg, 0.5 mmol) was weighed into a 4 dram vial equipped with a magnetic stir bar. Dichloromethane (2 mL) was added to dissolve the diazaphospholene derivative. A septa vial cap was used to seal the vial and secured with electrical tape. Boron tribromide (0.11 mL, 1.15 mmol, 2.3 equiv.) was added to the solution with vigorous stirring. Volatiles were removed *in vacuo* and the crude material was extracted with pentane (4 x 4 mL) to afford phenyl-$BBr_2$ **7-32** (38 mg, 0.153 mmol, 31% yield). NMR data were in accordance with literature values.[275]

**$^{1}$H** (500 MHz, $C_6D_6$): δ 8.05 (apparent d, 2H), 7.13 (apparent t, 1H), 6.97 (apparent t, 2H).

**$^{11}$B** (160.4 MHz, $C_6D_6$): δ 57.3.

Analysis of the solid recovered from filtration: data consistent with a phosphenium tetrabromoborate.

**$^{1}$H** (500 MHz, $CDCl_3$): δ 8.16 (s, 2H), 1.84 (d, $^{4}J_{H,P}$ = 1.6 Hz, 18H).

**$^{31}$P** (202.5 MHz, $CDCl_3$): δ 200.

**$^{11}$B** (160.4 MHz, $CDCl_3$): δ -24.0.

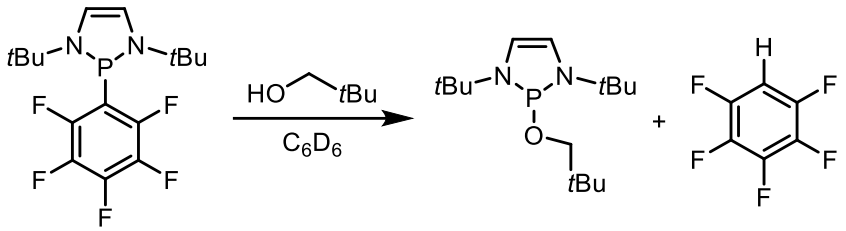


**Reaction of *P*-pentafluorophenyl diazaphospholene 7-6 with neopentyl alcohol.** Neopentyl alcohol (9 mg, 0.1 mmol) was weighed into a 1 dram vial and diluted with benzene-$d_6$ (0.2 mL). A solution of *P*-pentafluorophenyl diazaphospholene **7-6** (0.4 mL, 0.1 mmol, 0.25 M) in benzene-$d_6$ was added to the vial and the solution was transferred to a standard NMR tube. The contents of the tube were allowed to react for 3h. The sample was then analyzed using NMR spectroscopy with spectra shown below. The products were not isolated, however the spectra were in accordance with literature values for the products.[77]

**Signals corresponding to (7-24).**

**$^{1}$H** (500 MHz, $C_6D_6$): δ 5.96 (d, $^{3}J_{H,P}$ = 1.6 Hz, 2H), 3.00 (d, $^{3}J_{H,P}$ = 4.0 Hz, 2H), 1.35 (d, $^{4}J_{H,P}$ = 1.1 Hz, 18H), 0.96 (s, 9H).

**$^{31}$P** (202.5 MHz, $C_6D_6$): δ 92.5.

**Fluorobenzene:**

**$^{1}$H** (500 MHz, $C_6D_6$): δ 5.86 (m, 1H, in an approximate ratio of 1:2 with the diazaphospholene product)

**$^{19}$F** (470.6 MHz, $C_6D_6$): δ -139, -154, -162.

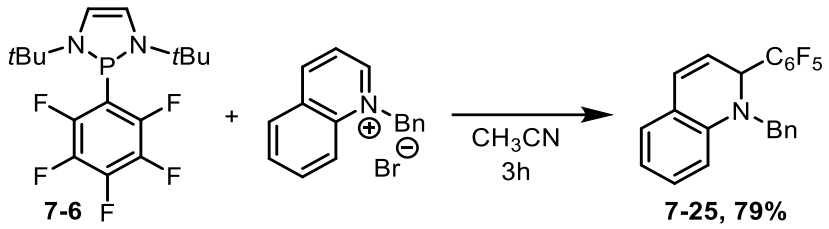


**Reaction of *P*-pentafluorophenyl diazaphospholene 7-6 with *N*-benzyl quinolinium bromide.** *N*-benzyl quinolinium bromide (45 mg, 0.15 mmol) was weighed into a 1 dram vial equipped with a magnetic stir bar and dissolved in acetonitrile (0.7 mL). A solution of *P*-pentafluorophenyl diazaphospholene **7-6** (0.6 mL, 0.15 mmol, 0.25 M) in benzene-$d_6$ was added to the vial and the reaction was stirred for 3 h. The reaction was then diluted with ether (2 mL) and filtered through a cotton plug into a round bottom flask 10 mL and the vial was rinsed with ether (2 x 2 mL) through the cotton plug as well. The solution was concentrated to an oil and then passed through a silica plug with ether in hexanes (10% soln., approx. 20 mL total) to afford the product **7-25**. Crystals suitable for X-ray diffraction were grown in pentane at 0 °C.

**Yield:** 46mg, 79% yield.

**$^1$H** (300 MHz, $CDCl_3$): δ 7.21 (m, 5H), 7.04 (t, $^3J_{H,H}$ = 7.8 Hz, 1H), 6.96 (dd, $^3J_{H,H}$ = 7.6 Hz, $J$ = 1.4 Hz, 1H), 6.65 (t, $^3J_{H,H}$ = 7.3 Hz, 1H), 6.50 (apparent t, 2H), 5.93 (d, $^3J_{H,H}$ = 4.7 Hz, 1H), 5.47 (dd, $^3J_{H,H}$ = 9.8, $J$ = 5.0 Hz, 1H), 4.36 (ab q, 2H).

**$^{13}$C** {$^1$H} (75.5 MHz, $CDCl_3$): δ 143, 137, 129, 128, 127.7, 127.5, 127.4, 126, 120, 119, 117, 110, 55.1, 53.2.

**$^{19}$F** {$^1$H} (282.4 MHz, $CDCl_3$): δ -143, -155, -161.

**HRMS (APCI):** calc'd for $C_{22}H_{15}F_5N_1$ $[M + H]^+$ 388.1119; Found: 388.1114. (1.3 ppm difference).

**Reaction of *P*-pentafluorophenyl diazaphospholene 7-6 (*in situ* generation) with *N*-benzyl quinolinium bromide.** Diazaphospholene dimer **7-1** (20 mg, 0.05 mmol) was weighed into a 1 dram vial equipped with a magnetic stir bar and dissolved in acetonitrile (0.7 mL). A solution of pentaflurophenylbromobenzene (0.05 mL, 1M) was added to the vial and the solution stirred for 30 min in which the solution became orange. *N*-benzyl quinolinium bromide (15 mg, 0.05 mmol) was added to the vial and the reaction was stirred for 30 min. The solution was then transferred to a standard NMR tube an analyzed using NMR analysis. The solution displayed only diazaphospholene bromide in the $^{31}$P NMR spectrum and the $^{19}$F NMR spectra revealed the presence of product **7-25**.

**$^{31}$P** (121.5 MHz, $C_6D_6$): δ 186.

**$^{19}$F** {$^1$H} (282.4 MHz, $C_6D_6$): δ -144, -158, -164.

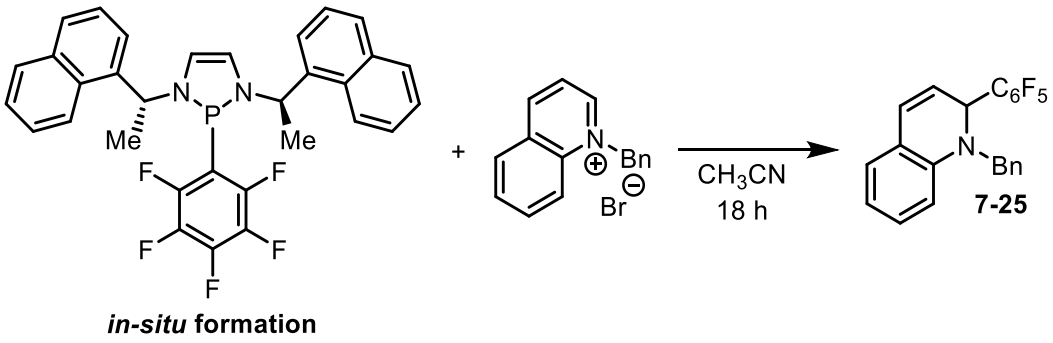


**Reaction of pentafluorophenyl *N*-(R)-napthylmethyl-diazaphospholene 7-29 (*in situ* generation) with *N*-benzyl quinolinium bromide.** Bis-(R)-napthylmethyl-diazaphospholene **7-28** (39.5 mg, 0.05 mmol) was weighed into a 1 dram vial equipped with a magnetic stir bar and dissolved in acetonitrile (0.7 mL). A solution of pentaflurophenylbromobenzene (0.05 mL, 1M) was added to the vial and the solution stirred for 30 min in which the solution became orange. *N*-benzyl quinolinium bromide (15 mg, 0.05 mmol) was added to the vial and the reaction was stirred for 24 h. The solution

was then transferred to a standard NMR tube an analyzed using NMR analysis. The solution displayed only *N*-(R)-napthylmethyl-diazaphospholene bromide **7-30** in the $^{31}P$ NMR spectrum and the $^{19}F$ NMR spectra revealed the presence of product **7-25**. Volatiles were removed *in vacuo* and the crude product extracted with ether. The solution was concentrated to an oil and then passed through a silica plug with ether in hexanes (10% soln.) to afford the product **7-25**.

**$^{31}P$** (121.5 MHz, $C_6D_6$): δ 186.

**$^{19}F$** $\{^1H\}$ (282.4 MHz, $C_6D_6$): δ -144, -158, -164.

# Chapter 8: Conclusions and Future Work

## 8.1 Summary and Conclusions for Chapters 2, 3, and 4

Borenium catalysis has undergone explosive growth in recent years. Early examples of borenium catalysis involved amine supported borenium cations, as highlighted by Denmark's application of boreniums for hydrosilylation[49], and the borenium catalyzed hydroboration by Crudden.[179] Following these examples, it was found that carbenes could stabilize boron cations to form isolable borenium complexes,[40] which resulted in an large advancement in borenium catalysis. These complexes were found to facilitate the hydrogenation of a variety of substrates including, imines, enamines and pyridine derivatives.[43–46] More recently, carbene supported borenium complexes have been found to facilitate the asymmetric hydrogenation of select imines.[47] However, in all instances, *N*-benzyl imines could not be reduced. Prior to this thesis work, only NHC and MIC carbenes have been explored in borenium hydrogenation catalysis.

The BAC carbene is a relatively underexplored carbene with only minimal publications investigating its applications. The lack of research into this carbene can be postulated as a consequence of the lack of derivatives and difficulty in isolation of the free carbene.[53,54] The carbene precursor is highly stable and has been applied in a variety of Stetter and benzoin condensation reactions.[64–66] We sought to investigate BAC carbenes in borenium catalysis as we anticipated their unique geometry might allow finding new substrate selectivity or lowering overall catalyst loading compared to previously reported systems. In our initial investigations it was found that the free carbene was not effective for the formation of BAC carbene borane adducts due to additional reactivity, and the overall low yield from this method, in-part resulting from the low isolation yield of the free carbene. The Weiss-Yoshida reagent, a $LiBF_4$ adduct of the carbene, was found to be a

more effective carbene transfer reagent. This reagent can be generated in near-quantitative yields from the carbene precursor. The initial attempts to form a 9-BBN adduct with the BAC carbene were unsuccessful (Chapter 2), so dicyclohexyl borane was chosen. The application of dicyclohexyl borane as the boron source allowed for the discovery of a BAC carbene borane adduct capable of hydrogenating a variety of *N*-benzyl imines.

Following this initial investigation, an investigation into the selectivity of this hydrogenation reaction was conducted. While all current systems of carbene supported borenium ions reported could hydrogenate aniline derived imines,[44–47] but not tolerate *N*-alkyl imines, this BAC carbene system was found to have opposite selectivity. The reasoning for this selectivity could be postulated to be a consequence of two factors, the BAC carbene or the dicyclohexyl borane. To determine to effect of the boron moiety, the 9-BBN adduct would need to be prepared, however previous attempts were not successful using the method established for all other BAC borane adducts. It was found that substitution of the ethereal solvent for toluene and reduction of reaction time allowed for the isolation of the *i*PrBAC-(9-BBN) complex. When examined in hydrogenation, *i*PrBAC-(9-BBN) was found to hydrogenate only *N*-Ph imines, displaying similar reactivity to previously reported borenium catalyst examples. When examined with *N*-benzyl imines, only trace reactivity was observed, indicating potential catalyst poisoning. To further investigate this selectivity, a dicyclohexylboron derivative of the highly active NHC borane complex reported by Stephen and co-workers was prepared. Stephan's version was a 9-BBN adduct.[44] If the dicyclohexyl boron is the controlling factor in *N*-benzyl imine selectivity, this catalyst should be able to hydrogenate *N*-benzyl imines much like the BAC borane complexes investigated (Chapters 2, 3, and 4). However, when investigated in the hydrogenation of *N*-benzyl imines, it was found that little to no reactivity in hydrogenation

reactions occurred, indicating that the success of our catalyst resulted from an interplay of the dicyclohexyl boron and the BAC carbene.

All current borenium catalysts prepared within the literature are derived from alkyl boranes. While aryl boron cations have been prepared,[40,126] there are no examples of hydrogenation or hydrosilylation catalysis with these complexes. The main challenge in the preparation of diaryl borane complexes is in the limited and challenging synthetic methods available for the parent diaryl borane. It was found that a synthetic pathway though a fluoroborane provided the BAC borane adduct in high yield. While this complex was found to activate hydrogen, it was not viable in hydrogenation reactions, potentially due to the higher Lewis acidity. This was observed by adduct formation with the imines in an NMR study.

The most common hydride abstraction reagents used with borenium catalysis to generate the borenium ions are trityl salts. Trityl reagents are effective for hydride abstraction but are highly sensitive to ethereal solvents[112] and moisture which limits their application. It was found that *N*-benzyl quinolinium $BAr^F_{24}$ was capable of hydride abstraction to generate a borenium complex capable of hydrogenating imines, without interference of the amine generated from the hydride abstraction/ concomitant reduction of the quinolinium. This system was further improved by the substitution of the $BAr^F_{24}$ anion with the $Bar^{Cl}_8$ anion which allowed for the hydrogenation of *N*-Ph imines, which were previously not suitable substrates for the BAC dicyclohexyl borane adducts in imine hydrogenation. The application of *N*-benzyl quinolinium salts also allowed the investigation of these carbene borane adducts in hydrosilylation reactions. These borenium ions could be generated from two air stable components, while all other previous systems required isolation of the borenium ion due to autocatalysis which can occur from trityl salt.

The application of the BAC borenium complexes in hydrosilylation yielded the reduction of substrates which were not tolerable under hydrogenation conditions. In addition, overall lower loadings were possible under hydrosilylation conditions.

Within borenium catalysis there is only one example of a carbene borenium complex capable of high enantioinduction in hydrogenation or hydrosilylation reactions.[47] Within chapter 4, a variety of methods for the preparation of a chiral catalyst were investigated. However, none of the methods were fruitful in the preparation of a system that could either hydrogenate imines in high conversion or achieve high enantioinduction. Chiral anions have not been previously investigated in borenium catalysis, and during the course of this thesis it was found that the application of a chiral anion in borenium hydrogenation yielded an observable but low conversion and enatioinduction in hydrogenation reactions.

In conclusion BAC borane adducts were prepared and the adducts with dicyclohexylborane and 9-BBN were found to be viable in the formation of a stable borenium complex capable of hydrogenating imines. While BAC carbene borane adducts did not offer the lowest pressure of hydrogen required for hydrogenation, or have the lowest loading, these complexes were found to hydrogenate a set of substrates which cannot be reduced in hydrogenation reactions by any other reported borenium complexes within the literature.

**8.2 Summary and Conclusions for Chapter 5**

Within the literature, a variety of main group and metal catalysts utilize pinacolborane to reduce imines.[170] More recently it has been reported that this reducing agent can reduce aldehydes without the requirement of a catalyst at higher temperatures.[174] Following the reduction of an imine with pinacolborane, the excess borane is often

quenched with an alcohol or water. However, it was found that protic additives can cause the reduction of the imine if it is an *N*-alkyl imine. When examined with chiral alcohols, enantioinduction was observed with one case, albeit with a very low *e.e.*. This finding is important as often imines can contain water or other protic impurities which may result in partial reduction of the imine. This previously unrecognized background reaction is likely to result in lower observed enantiomer ratios in asymmetric reduction of impurity-containing substrates.

### 8.3 Summary and Conclusions for Chapter 6

Sulfur hexafluoride is a highly potent greenhouse gas with a global warming potential of approximately 23,500 times that of carbon dioxide.[202] Previous methods to remove this potent greenhouse gas have involve extreme high temperatures with heterogenous catalysts to remove this potent gas.[197] More recently, there have been developments in the application of transition metals in the destruction of sulfur hexafluoride, however only modest conversions were observed.[219] The majority of organic reagents capable of reacting with $SF_6$ operate under a radical mechanism and have been shown to function catalytically in the pentafluorosulfanylation of select substrates.[223]

Dielmann reported that superbasic phosphines reacted with $SF_6$ and in some instances formed stable $SF_5$ anion complexes.[233] Following this result, chapter 6 explored the reactivity of phosphides with $SF_6$. Phosphides can be purchased and used directly, or prepared from deprotonation of the corresponding phosphine with *n*-butyl lithium. It was found that phosphides react with $SF_6$ and form bisphosphines as the predominant product. When a more sterically demanding *tert*-butyl phosphine was examined, a fluorophosphine was observed which gave an indication as to the mechanism of this reaction. However, it could not be determined if this reaction is operating by a nucleophilic or radical mechanism.

Overall, this method provided a cheap and facile method of destroying $SF_6$ which can operate at room temperature.

Diazaphospholenes were then investigated for reactivity with $SF_6$. Initial examination of the reactivity of diazaphospholene dimers with $SF_6$ resulted in rapid degradation of $SF_6$ and the formation of diazaphospholene fluoride. Light was found to accelerate this reaction but did not greatly change the distribution of products. A variety of methods were attempted to regenerate the dimer from the diazaphospholene fluoride however this compound would not react with magnesium. Formation of a diazaphospholene chloride *in situ* using a chlorosilane allowed for dimer formation when magnesium was present however it was later found that magnesium is able to facilitate the reduction of $SF_6$ in the presence of chlorosilane without the diazaphospholene being present.

Diazaphospholene hydrides were then examined for reactivity with $SF_6$. It was found that little to no reaction occurred with $SF_6$ in the absence of light, with the exception of acetonitrile as the solvent. The addition of blue light to the reaction allowed for moderate reactivity with $SF_6$. The reaction was examined under a catalytic loading of the diazaphospholene hydride and was found to catalytically reduce $SF_6$. Loadings as low as 2.5 mol % were achieved with conversion of a phosphine to a phosphine sulfide as the metric for conversion. Unlike the magnesium reaction, diazaphospholene was essential for catalysis. The conversion observed from this reaction was approximately 93% with an isolated yield of the phosphine sulfide of 82%. This method resulted in higher conversion than previously reported methods, which used a rhodium-based catalyst which required heating to 80 °C.[219] This current method developed in this thesis is the mildest catalytic method for the destruction of $SF_6$, with the only external energy requirement being a blue

light source rather than heating. In addition, the removal of an expensive transition metal, and replacement with a main group catalyst, which can be prepared in two synthetic steps offers a more cost-effective method overall. Diazaphospholene hydrides were also examined in pentafluorosulfanylation of a variety of radical-acceptor substrates, but were found to result in poor conversion to the pentafluorosulfanylated products.

During the exploration of diazaphospholenes in $SF_6$ decompostion, it was found that magnesium could reduce $SF_6$ in the presence of silanes. This method, once optimized, resulted in the mildest method of decomposing $SF_6$ reported in the literature to date. The reagents used within this reaction are all highly abundant, and the magnesium as well as triphenylphosphine used are both air stable. This allowed for the reaction to be conducted with benchtop anhydrous solvent and to be set up under less rigorous conditions. Upon increase in scale, the stoichiometry of materials required were able to be reduced to near their stochiometric amounts. In comparison to all other methods, this method requires no heating or light and only requires mechanical stirring of the magnesium turnings to facilitate the destruction of $SF_6$.

Overall, within this thesis, three new methods have been developed to remove the potent greenhouse gas $SF_6$. All methods developed function under mild conditions and utilize cost effective materials. Most importantly the finding that magnesium can decompose $SF_6$ under extremely mild conditions may allow for the industrial application of this method as the materials are readily abundant, and could be used on large scale.

### 8.4 Summary and Conclusions for Chapter 7

Diazaphospholenes have recently undergone explosive growth in exploration for stoichiometric and catalytic reactivity.[68,69] While diazaphospholene hydrides have been studied in great detail and found applications in reductive catalysis,[69] diazaphospholene

dimers are underexplored.[68] Previous reports on diazaphospholene dimer reactivity have shown that cleavage of bonds is possible.[96] In chapter 6 it was found that diazaphospholene dimers can cleave S–F bonds. Functionalized diazaphospholenes have applications as ligands in catalysis,[257–259] and therefore the reactivity with polarized bonds was explored. It was found that diazaphospholenes can react with aryl iodides and bromides, as well as alkyl bromides, with some substrates requiring irradiation by light. The mechanism of this transformation was investigated however it was determined that both a radical and polar mechanism may be operating for this transformation, depending on substrate and reaction conditions. The observation of a radical based mechanism allowed for the reductive cyclization of iodo-allyl ethers. In addition, it was found that the pentafluorophenyl group could be transferred from a diazaphospholene to an iminium salt, resulting in the first carbon-carbon bond formation facilitated by group-transfer from a diazaphospholene. Overall, the results found in this chapter indicate that further exploration into the radical chemistry of diazaphospholenes should be done.

### 8.5 Future Work for Chapters 2, 3, and 4

Within chapters 2, 3, and 4 it was found that BAC carbenes can form stable borane adducts and generate borenium complexes capable of hydrogenating imines and enamines. However, an in-depth investigation into asymmetric hydrogenations facilitated by BAC borane complexes has not been explored. The results by Fuchter showed that asymmetric hydrogenation is possible with borenium catalysis with a very limited substrate scope.[47] In an effort to further develop the field of asymmetric borenium hydrogenation, chiral BAC carbene complexes could be prepared and investigated as either the dicyclohexylborane or 9-BBN adduct of the carbene. During the course of the work disclosed in this thesis, Gravel and co-workers reported the synthesis of two new chiral BAC carbene precursors which

could be prepared and investigated in borane adduct formation (**Figure 8.1**).[64] In addition, the results from section **4.6.2** indicate that the synthesis of the chiral BAC carbene derived from diphenylprolinol can be prepared with further investigation. The analysis of these complexes in borenium hydrogenation and hydrosilylation can be assessed and a wider substrate scope examined.

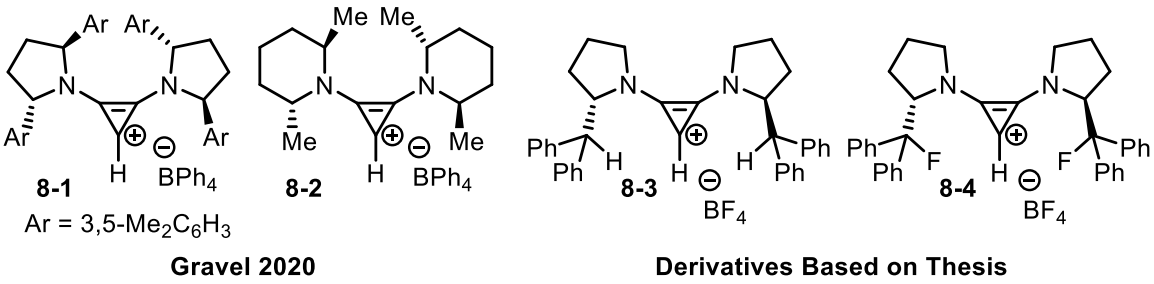


**Figure 8.1** Potential chiral BAC carbenes for complexation with boranes.

Another method of chiral modification that shown promising results is in the synthesis of derivatives of the *N*-Bn Quinolinium spiroborate complex shown in section **4.6.3**. In the report by Wulff and Vetticatt, it was found that substitution onto the binapthyl rings resulted in a great increase in enantioselectivity of the reaction (**Figure 8.2**).[168] When unsubstituted BINOL was used in their chemistry it was found that only a 13% *e.e.* was obtained and adding bromine substitution on the 3 and 3' position allowed for an increase in *e.e.* to 55%. Further substitution to a phenyl allowed for the greatest increase to an *e.e.* of 76-78%. Larger aryl ring substitution did not result in a further increase in enantioselectivity, and in some instances resulted in a decrease in selectivity.[168] Therefore, the bromo and phenyl derivatives could be investigated in spiroborate formation followed by application in borenium catalysis.

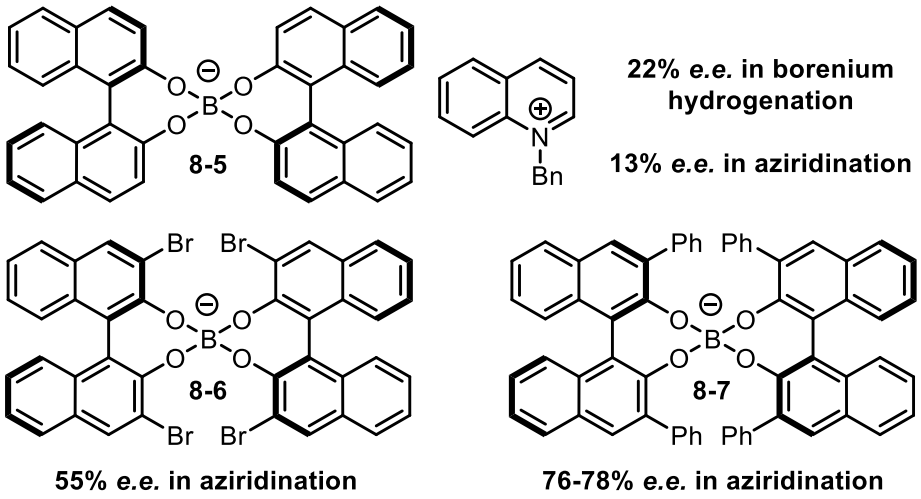


**Figure 8.2** Selectivity achived in this thesis in hydrogenation reactions, and enantiomeric excess in aziridination reactions with different chiral spiroborates derived from BINOL.[168]

Finally, while the diarylborenium BAC complexes prepared in chapter 3 were not able to facilitate hydrogenation reactions, these highly Lewis acidic complexes may be applicable in hydrosilylation reactions. The higher Lewis acidity may allow for lower loadings or faster reaction times overall improving current hydrosilylation methods. If viable, chiral derivatives can be prepared and assessed in asymmetric hydrosilylation. The current best results reported in chapter 4 required loadings of 5 mol % while the current best methods reported 4 mol % loading.[47] Further optimization of solvent and catalyst may yield a lower loading or reaction time. While there are many avenues for further investigation, these proposals should be tempered by context that asymmetric hydrogenation mediated by metal-complexes is a relatively mature field. While borenium complexes have shown interesting reactivity, work from our group and others has failed to uncover applications where they show clear superiority to existing transition-metal catalysts.

## 8.6 Future Work for Chapter 6

The methods developed in chapter 6 resulted in the mildest methods of $SF_6$ decomposition to date. While both the diazaphospholene and magnesium mediated $SF_6$ decomposition has been optimized, further investigation into the phosphide reactivity may yield more results. The current exploration of trapping a $SF_5$ anion with with phosphide reductants were not fruitful. This may be a result of a radical based mechanism, or the consequence of the breakdown of the $SF_5$ anion under the current reaction conditions. Colder reaction temperatures and crown ethers to stabilize the product may allow for the formation of a $SF_5$ complex.[249] This would be of value, since current methods to access the $SF_5$ anion require lengthy synthesis, or use of the toxic gas $SF_4$, severely limiting investigations into the chemistry and possible functionalization of the $SF_5$ anion.

In section **6.3.3** it was found that pentafluorosulfanylation mediated by diazaphospholene hydrides was possible, albeit in trace conversion. Preliminary attempts at optimizing this reaction by varying solvent or substrate did not yield a large increase in product. A possible reason for the observed low conversion may be due to the product of this reaction being reduced by the diazaphospholene hydride. The application of a weaker (less hydridic) hydride in this chemistry may yield an increase in the conversion to the pentafluorosulfanylated product.[82] Such hydrides may include saturated diazaphospholene or the mesityl diazaphospholene (**Figure 8.3**), which have been shown by others to be less reducing than the unsaturated *tert*-butyl diazaphospholene. These hydrides might be able to react with $SF_6$, but not with the pentafluorosulfanylated product. This effect can be examined with treatment of these hydrides with pentafluorosulfanyl benzene to determine if any reactivity will occur. In addition, a wider substrate scope of more optimal radical acceptors may be investigated.

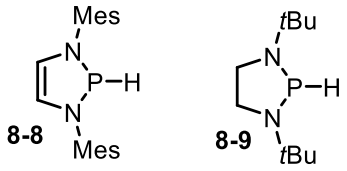


**Figure 8.3** Potential diazaphospholenes to be explored in $SF_6$ chemsitry.

## 8.7 Future Work for Chapter 7

In section **7.8.6** it was found that both diazaphospholene dimers and hydrides are able to facilitate the radical cyclization of 1-(2-Iodophenoxy)-3-methyl-2-butene. This reaction was conducted stoichiometrically and only few substrates were examined. An in-depth substrate scope may be examined for this chemistry to determine the types of substrates that may be viable for this radical cyclization. In addition, this process may be rendered catalytic similar to the catalytic decomposition of $SF_6$, which is potentially operating under a radical mechanism and can operate under loadings as low as 2.5 mol %. The work presented in this thesis provides the grounds for an exploration into making the radical chemistry of diazaphospholenes catalytic, which recently has been reported by other groups as well.

Furthermore, it was found in section **7.8.7** that transfer of a pentafluorophenyl group was possible to *N*-benzyl quinolinium bromide. However few electrophiles were investigated in this chemistry and a wider scope of iminium ions could be investigated to see if the pentafluorophenyl transfer is general (**Scheme 8.1**). The addition of a Lewis acid may also yield pentafluorophenyl transfer to imines, by increasing the electrophilicity of these substrates as long as sufficient steric bulk of the Lewis acid prevents formation of a diazaphospholene borane adduct. The *P*-trifluoromethyl diazaphospholene was able to be generated *in situ,* however could not be isolated due to volatility. This compound could be investigated in the trifluoromethylation of *N*-benzyl quinolinium bromide as well as any

other electrophiles that may be found in the pentafluorophenyl transfer scope. Alternatively, other fluorophenyl derivatives with less fluoride substitution may be investigated in this chemistry. Trifluoromethylation is important for the derivatization of pharmaceuticals.[267] Extending the transfer chemistry to trifluoromethyl may enable the formation of trifluoromethylated amines, which may be useful synthons in pharmaceutical chemistry.

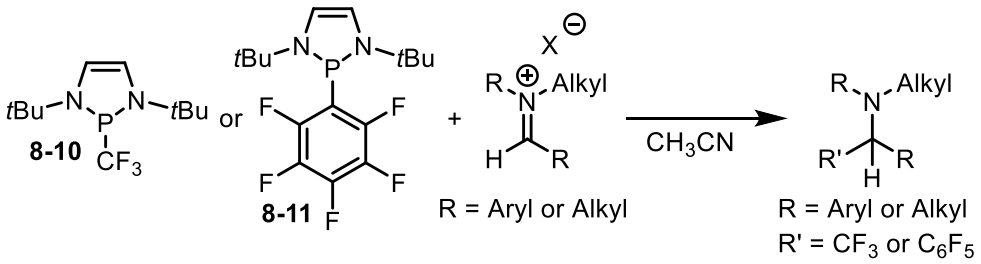


**Scheme 8.1** Futher exploration in functionalization reactions via diazaphospholenes.

### 8.8 Conclusion for Thesis

Main group chemistry has undergone rapid development in recent years with many advancements in catalysis and bond reactivity. The work of this thesis primarily focused on reductive processes, initially involving BAC carbene borane complexes, and moving to phosphorus complexes. In the first part of this thesis, it was shown that BAC carbene borane adducts are capable of facilitating the hydrogenation and hydrosilylation of imines and enamines, while filling a gap within previously reported substrate scopes, namely the ability to hydrogenate *N*-benzyl imines. Turning attention to reductive phosphorus chemistry, diazaphospholene dimers were found to cleave carbon halide bonds, have applications in radical chemistry, and show promise in carbon-carbon bond formation reactions. Diazaphospholene dimers and hydrides were also applied to the decomposition of $SF_6$, with the hydrides being applied in catalytic $SF_6$ decomposition. Phosphides and

magnesium turnings were also found to decompose $SF_6$ with magnesium turnings allowing for the mildest and most cost-effective method of $SF_6$ decomposition to date.

## References


(1) Lennox, A. J. J.; Lloyd-Jones, G. C. Selection of Boron Reagents for Suzuki–Miyaura Coupling. *Chem. Soc. Rev.* **2014**, *43* (1), 412–443.

(2) Goettel, J. T.; Braunschweig, H. Recent Advances in Boron-Centered Ligands and Their Transition Metal Complexes. *Coord. Chem. Rev.* **2019**, *380*, 184–200.

(3) Fernandes, G. F. S.; Denny, W. A.; Dos Santos, J. L. Boron in Drug Design: Recent Advances in the Development of New Therapeutic Agents. *Eur. J. Med. Chem.* **2019**, *179*, 791–804.

(4) Stephan, D. W.; Erker, G. Frustrated Lewis Pair Chemistry: Development and Perspectives. *Angew. Chem. Int. Ed.* **2015**, *54* (22), 6400–6441.

(5) Fontaine, F.-G.; Stephan, D. W. On the Concept of Frustrated Lewis Pairs. *Phil. Trans. R. Soc. A.* **2017**, *375*.

(6) Li, N.; Zhang, W.-X. Frustrated Lewis Pairs: Discovery and Overviews in Catalysis. *Chin. J. Chem.* **2020**, *38* (11), 1360–1370.

(7) Lewis, G. N. *Valence and the Structure of Atoms and Molecules, Chemical Catalogue Company*; The Chemical Catalog Company: New York, 1923.

(8) Shore, S. G.; Parry, R. W. THE CRYSTALLINE COMPOUND AMMONIA-BORANE,[1] $H_3NBH_3$. *J. Am. Chem. Soc.* **1955**, *77* (22), 6084–6085.

(9) Corma, A.; García, H. Lewis Acids: From Conventional Homogeneous to Green Homogeneous and Heterogeneous Catalysis. *Chem. Rev.* **2003**, *103* (11), 4307–4365.

(10) Yamashita, Y.; Yasukawa, T.; Yoo, W.-J.; Kitanosono, T.; Kobayashi, S. Catalytic Enantioselective Aldol Reactions. *Chem. Soc. Rev.* **2018**, *47* (12), 4388–4480.

(11) Katsuki, T.; Sharpless, B. K. The First Practical Method for Asymmetric Epoxidation. *J. Am. Chem. Soc.* **1980**, *102* (18), 5974–5976.

(12) Corey, E. J.; Bakshi, R. K.; Shibata, S.; Chen, C.-P.; Singh, V. K. A Stable and Easily Prepared Catalyst for the Enantioselective Reduction of Ketones. Applications to Multistep Syntheses. *J. Am. Chem. Soc.* **1987**, *109* (25), 7925–7926.

(13) Litvinenko, L. M.; Kirichenko, A. I. Basicity and Stereospecificity in Nucleophile Catalysis by Tertiary Amines. *Dokl. Akad. Nauk. SSSR Ser. Chem.* **1967**, *176*, 97–100.

(14) Ruble, J. C.; Latham, H. A.; Fu, G. C. Effective Kinetic Resolution of Secondary Alcohols with a Planar–Chiral Analogue of 4-(Dimethylamino)Pyridine. Use of the Fe($C_5Ph_5$) Group in Asymmetric Catalysis. *J. Am. Chem. Soc.* **1997**, *119* (8), 1492–1493.

(15) Denmark, S. E.; Beutner, G. L. Lewis Base Catalysis in Organic Synthesis. *Angew. Chem. Int. Ed.* **2008**, *47* (9), 1560–1638.

(16) Kočovský, P.; Malkov, A. V. Lewis Bases as Catalysts in the Reduction of Imines and Ketones with Silanes (n?→?σ*). *Lewis Base Catalysis in Organic Synthesis*; John Wiley & Sons, Ltd, 2016; pp 1077–1112. DOI:10.1002/9783527675142.

(17) Brown, H. C.; Schlesinger, H. I.; Cardon, S. Z. Studies in Stereochemistry. I. Steric Strains as a Factor in the Relative Stability of Some Coördination Compounds of Boron. *J. Am. Chem. Soc.* **1942**, *64* (2), 325–329.

(18) Wittig, G.; Benz, E. Über Das Verhalten von Dehydrobenzol Gegenüber Nucleophilen Und Elektrophilen Reagenzien. *Chem. Ber.* **1959**, *92* (9), 1999–2013.

(19) Tochtermann, W. Structures and Reactions of Organic Ate-Complexes. *Angew. Chem. Int. Ed.* **1966**, *5* (4), 351–371.

(20) Parks, D. J.; Piers, W. E. Tris(Pentafluorophenyl)Boron-Catalyzed Hydrosilation of Aromatic Aldehydes, Ketones, and Esters. *J. Am. Chem. Soc.* **1996**, *118* (39), 9440–9441.

(21) Welch, G. C.; San Juan, R. R.; Masuda, J. D.; Stephan, D. W. Reversible, Metal-Free Hydrogen Activation. *Science.* **2006**, *314* (5802), 1124–1126.

(22) McCahill, J. S. J.; Welch, G. C.; Stephan, D. W. Reactivity of "Frustrated Lewis Pairs": Three-Component Reactions of Phosphines, a Borane, and Olefins. *Angew. Chem. Int. Ed.* **2007**, *46* (26), 4968–4971.

(23) Kerru, N.; Gummidi, L.; Maddila, S.; Gangu, K. K.; Jonnalagadda, S. B. A Review on Recent Advances in Nitrogen-Containing Molecules and Their Biological Applications. *Molecules.* **2020**, *25* (8), 1909.

(24) Chase, P. A.; Welch, G. C.; Jurca, T.; Stephan, D. W. Metal-Free Catalytic Hydrogenation. *Angew. Chem. Int. Ed.* **2007**, *46* (42), 8050–8053.

(25) Lam, J.; Szkop, K. M.; Mosaferi, E.; Stephan, D. W. FLP Catalysis: Main Group Hydrogenations of Organic Unsaturated Substrates. *Chem. Soc. Rev.* **2019**, *48* (13), 3592–3612.

(26) Chase, P. A.; Jurca, T.; Stephan, D. W. Lewis Acid-Catalyzed Hydrogenation: $B(C_6F_5)_3$-Mediated Reduction of Imines and Nitriles with $H_2$. *Chem. Commun.* **2008**, *2* (14), 1701–1703.

(27) Chen, D.; Klankermayer, J. Metal-Free Catalytic Hydrogenation of Imines with Tris(Perfluorophenyl) Borane. *Chem. Commun.* **2008**, (18), 2130–2131.

(28) Chen, D.; Wang, Y.; Klankermayer, J. Enantioselective Hydrogenation with Chiral Frustrated Lewis Pairs. *Angew. Chem. Int. Ed.* **2010**, *49* (49), 9475–9478.

(29) Meng, W.; Feng, X.; Du, H. Frustrated Lewis Pairs Catalyzed Asymmetric Metal-Free Hydrogenations and Hydrosilylations. *Acc. Chem. Res.* **2018**, *51* (1), 191–201.

(30) Lindqvist, M.; Borre, K.; Axenov, K.; Kótai, B.; Nieger, M.; Leskelä, M.; Pápai, I.; Repo, T. Chiral Molecular Tweezers: Synthesis and Reactivity in Asymmetric Hydrogenation. *J. Am. Chem. Soc.* **2015**, *137* (12), 4038–4041.

(31) Schnurr, A.; Samigullin, K.; Breunig, J. M.; Bolte, M.; Lerner, H.-W.; Wagner, M. One-Pot Synthesis of $[(C_6F_5)_2BH_2]^-$ from $C_6F_5MgBr/BH_3{\bullet}SMe_2$ and Its in Situ Transformation to Piers' Borane. *Organometallics.* **2011**, *30*, 2838–2843.

(32) Eisenberger, P.; Crudden, C. M. Borocation Catalysis. *Dalton Trans.* **2017**, *46* (15), 4874–4887.

(33) Sivaev, I. B.; Bregadze, V. I. Lewis Acidity of Boron Compounds. *Coord. Chem. Rev.* **2014**, *270–271* (1), 75–88.

(34) Heiden, Z. M.; Lathem, A. P. Establishing the Hydride Donor Abilities of Main Group Hydrides. *Organometallics.* **2015**, *34* (10), 1818–1827.

(35) Chaplin, A. B.; Weller, A. S. $[B(3,5\text{-}C_6H_3Cl_2)_4]^-$ as a Useful Anion for Organometallic Chemistry. *Eur. J. Inorg. Chem.* **2010**, *2010* (32), 5124–5128.

(36) Piers, W. E.; Bourke, S. C.; Conroy, K. D. Borinium, Borenium, and Boronium Ions: Synthesis, Reactivity, and Applications. *Angew. Chem. Int. Ed.* **2005**, *44* (32), 5016–5036.

(37) Stefkova, K.; Gierlichs, L.; Willcox, D.; Melen, R. L. *Borocations in Catalysis*; Encyclopedia of Inorganic and Bioinorganic Chemistry, John Wiley & Sons, Ltd., 2020. DOI: 10.1002/9781119951438.eibc2641.

(38) Ryschkewitsch, G. E.; Wiggins, J. W. Trigonal Boron Cation. *J. Am. Chem. Soc.* **1970**, *92* (6), 1790–1791.

(39) De Vries, T. S.; Prokofjevs, A.; Vedejs, E. Cationic Tricoordinate Boron Intermediates: Borenium Chemistry from the Organic Perspective. *Chem. Rev.* **2012**, *112* (7), 4246–4282.

(40) Matsumoto, T.; Gabbaï, F. P. A Borenium Cation Stabilized by an N-Heterocyclic Carbene Ligand. *Organometallics.* **2009**, *28* (15), 4252–4253.

(41) Ueng, S.-H.; Brahmi, M. M.; Derat, É.; Fensterbank, L.; Lacôte, E.; Malacria, M.; Curran, D. P. Complexes of Borane and N-Heterocyclic Carbenes: A New Class of Radical Hydrogen Atom Donor. *J. Am. Chem. Soc.* **2008**, *130* (31), 10082–10083.

(42) Lindsay, D. M.; McArthur, D. The Synthesis of Chiral N-Heterocyclic Carbene–Borane and –Diorganoborane Complexes and Their Use in the Asymmetric Reduction of Ketones. *Chem. Commun.* **2010**, *46* (14), 2474–2476.

(43) Farrell, J. M.; Hatnean, J. A.; Stephan, D. W. Activation of Hydrogen and Hydrogenation Catalysis by a Borenium Cation. *J. Am. Chem. Soc.* **2012**, *134* (38), 15728–15731.

(44) Farrell, J. M.; Posaratnanathan, R. T.; Stephan, D. W. A Family of N-Heterocyclic Carbene-Stabilized Borenium Ions for Metal-Free Imine Hydrogenation Catalysis. *Chem. Sci.* **2015**, *6* (3), 2010–2015.

(45) Eisenberger, P.; Bestvater, B. P.; Keske, E. C.; Crudden, C. M. Hydrogenations at Room Temperature and Atmospheric Pressure with Mesoionic Carbene-Stabilized Borenium Catalysts. *Angew. Chem. Int. Ed.* **2015**, *54* (8), 2467–2471.

(46) Lam, J.; Günther, B. A. R.; Farrell, J. M.; Eisenberger, P.; Bestvater, B. P.; Newman, P. D.; Melen, R. L.; Crudden, C. M.; Stephan, D. W. Chiral Carbene–Borane Adducts: Precursors for Borenium Catalysts for Asymmetric FLP Hydrogenations. *Dalton Trans.* **2016**, *45* (39), 15303–15316.

(47) Mercea, D. M.; Howlett, M. G.; Piascik, A. D.; Scott, D. J.; Steven, A.; Ashley, A. E.; Fuchter, M. J. Enantioselective Reduction of: N-Alkyl Ketimines with Frustrated Lewis Pair Catalysis Using Chiral Borenium Ions. *Chem. Commun.* **2019**, *55* (49), 7077–7080.

(48) Blackwell, J. M.; Sonmor, E. R.; Scoccitti, T.; Piers, W. E. $B(C_6F_5)_3$-Catalyzed Hydrosilation of Imines via Silyliminium Intermediates. *Org. Lett.* **2000**, *2* (24), 3921–3923.

(49) Denmark, S. E.; Ueki, Y. Lewis Base Activation of Lewis Acids: Group 13. In Situ Generation and Reaction of Borenium Ions. *Organometallics.* **2013**, *32* (22), 6631–6634.

(50) Chen, J.; Lalancette, R. A.; Jäkle, F. Synthesis and Lewis Acid Properties of a Ferrocene-Based Planar-Chiral Borenium Cation. *Chem. Commun.* **2013**, *49* (43), 4893–4895.

(51) Kang, B. C.; Shin, S. H.; Yun, J.; Ryu, D. H. Highly Enantioselective Hydrosilylation of Ketones Catalyzed by a Chiral Oxazaborolidinium Ion. *Org. Lett.* **2017**, *19* (23), 6316–6319.

(52) Bandar, J.; Lambert, T. H. Aminocyclopropenium Ions: Synthesis, Properties, and Applications. *Synthesis.* **2013**, *45* (18), 2485–2498.

(53) Lavallo, V.; Canac, Y.; Donnadieu, B.; Schoeller, W. W.; Bertrand, G. Cyclopropenylidenes: From Interstellar Space to an Isolated Derivative in the Laboratory. *Science.* **2006**, *312* (5774), 722–724.

(54) Lavallo, V.; Ishida, Y.; Donnadieu, B.; Bertrand, G. Isolation of Cyclopropenylidene–Lithium Adducts: The Weiss–Yoshida Reagent. *Angew. Chem. Int. Ed.* **2006**, *45* (40), 6652–6655.

(55) Bidal, Y. D.; Lesieur, M.; Melaimi, M.; Cordes, D. B.; Slawin, A. M. Z.; Bertrand, G.; Cazin, C. S. J. A Simple Access to Transition Metal Cyclopropenylidene Complexes. *Chem. Commun.* **2015**, *51* (23), 4778–4781.

(56) Konishi, H.; Matsumoto, S.; Kamitori, Y.; Ogoshi, H.; Yoshida, Z. SYNTHESIS AND PROPERTIES OF DIAMINOCYCLOPROPENYLIDENE TRANSITION METAL COMPLEXES. *Chem. Lett.* **1978**, *7* (3), 241–244.

(57) Malik, H. A.; Sormunen, G. J.; Montgomery, J. A General Strategy for Regiocontrol in Nickel-Catalyzed Reductive Couplings of Aldehydes and Alkynes. *J. Am. Chem. Soc.* **2010**, *132* (18), 6304–6305.

(58) Holschumacher, D.; Hrib, C. G.; Jones, P. G.; Tamm, M. A Stable Chiral Diaminocyclopropenylidene. *Chem. Commun.* **2007**, (35), 3661–3663.

(59) Petuškova, J.; Bruns, H.; Alcarazo, M. Cyclopropenylylidene-Stabilized Diaryl and Dialkyl Phosphenium Cations: Applications in Homogeneous Gold Catalysis. *Angew. Chem. Int. Ed.* **2011**, *50* (16), 3799–3802.

(60) Schumann, H.; Glanz, M.; Girgsdies, F.; Hahn, F. E.; Tamm, M.; Grzegorzewski, A. Cyclopropenylidene Adducts of Divalent Germanium, Tin, and Lead. *Angew. Chem. Int. Ed.* **1997**, *36* (20), 2232–2234.

(61) Dube, J. W.; Zheng, Y.; Thiel, W.; Alcarazo, M. α-Cationic Arsines: Synthesis, Structure, Reactivity, and Applications. *J. Am. Chem. Soc.* **2016**, *138* (21), 6869–6877.

(62) Mehler, G.; Linowski, P.; Carreras, J.; Zanardi, A.; Dube, J. W.; Alcarazo, M. Bis(Cyclopropenium)Phosphines: Synthesis, Reactivity, and Applications. *Chem. Eur. J.* **2016**, *22* (43), 15320–15327.

(63) Ruiz, D. A.; Melaimi, M.; Bertrand, G. An Efficient Synthetic Route to Stable Bis(Carbene)Borylenes [$(L_1)(L_2)$BH]. *Chem. Commun.* **2014**, *50* (58), 7837–7839.

(64) Khalkhali, M. R.; Wilde, M. M. D.; Gravel, M. Enantioselective Stetter Reactions Catalyzed by Bis(Amino)Cyclopropenylidenes: Important Role for Water as an Additive. *Org. Lett.* **2021**, *23* (1), 155–159.

(65) Wilde, M. M. D.; Gravel, M. Bis(Amino)Cyclopropenylidenes as Organocatalysts for Acyl Anion and Extended Umpolung Reactions. *Angew. Chem. Int. Ed.* **2013**, *52* (48), 12651–12654.

(66) Wilde, M. M. D.; Gravel, M. Bis(Amino)Cyclopropenylidene (BAC) Catalyzed Aza-Benzoin Reaction. *Org. Lett.* **2014**, *16* (20), 5308–5311.

(67) Kuchenbeiser, G.; Soleilhavoup, M.; Donnadieu, B.; Bertrand, G. Reactivity of Cyclic (Alkyl)(Amino)Carbenes (CAACs) and Bis(Amino)Cyclopropenylidenes (BACs) with Heteroallenes: Comparisons with Their N-Heterocyclic Carbene (NHCs) Counterparts. *Chem. Asian J.* **2009**, *4* (11), 1745–1750.

(68) Gudat, D. Diazaphospholene Chemistry. *EIBC.* **2018**, 1–23.

(69) Speed, A. W. H. Applications of Diazaphospholene Hydrides in Chemical Catalysis. *Chem. Soc. Rev.* **2020**, *49* (22), 8335–8353.

(70) Schmidpeter, A.; Karaghiosoff, K. 4,5-Dicyano-1,3,2 $\lambda^3$-Diazaphospholate – an Anionic 1,3,2-Diazaphosphole, Stable as a Monomer. *Z. Naturforsch.* **1981**, *36b*, 1273–1276.

(71) Karaghiosoff, K.; Majoral, J. P.; Meriem, A.; Navech, J.; Schmidpeter, A. 1,3,2-Diazaphosphole Derivatives from the Reaction of $PCl_n$ $(NR_2)_{3-n}$ with Diaminomaleonitrile. *Tetrahedron Lett.* **1983**, *24* (21), 2137–2140.

(72) Gudat, D. Diazaphospholenes: N-Heterocyclic Phosphines between Molecules and Lewis Pairs. *Acc. Chem. Res.* **2010**, *43* (10), 1307–1316.

(73) Gudat, D. A Very Peculiar Family of N-Heterocyclic Phosphines: Unusual Structures and the Unique Reactivity of 1,3,2-Diazaphospholenes. *Dalton Trans.* **2016**, *45* (14), 5896–5907.

(74) Ould, D. M. C.; Melen, R. L. Diazaphospholene and Diazaarsolene Derived Homogeneous Catalysis. *Chem. Eur. J.* **2020**, *26* (44), 9835–9845.

(75) Gudat, D.; Haghverdi, A.; Nieger, M. Umpolung of P-H Bonds. *Angew. Chem. Int. Ed.* **2000**, *39* (17), 3084–3086.

(76) Dube, J. W.; Farrar, G. J.; Norton, E. L.; Szekely, K. L. S.; Cooper, B. F. T.; Macdonald, C. L. B. A Convenient Method for the Preparation of N-Heterocyclic Bromophosphines: Excellent Precursors to the Corresponding N-Heterocyclic Phosphenium Salts. *Organometallics.* **2009**, *28* (15), 4377–4384.

(77) Adams, M. R.; Tien, C.-H.; Huchenski, B. S. N.; Ferguson, M. J.; Speed, A. W. H. Diazaphospholene Precatalysts for Imine and Conjugate Reductions. *Angew. Chem. Int. Ed.* **2017**, *56* (22), 6268–6271.

(78) Adams, M. R.; Tien, C.-H.; McDonald, R.; Speed, A. W. H. Asymmetric Imine Hydroboration Catalyzed by Chiral Diazaphospholenes. *Angew. Chem. Int. Ed.* **2017**, *56* (52), 16660–16663.

(79) Lundrigan, T.; Tien, C.-H.; Robertson, K. N.; Speed, A. W. H. Air and Water Stable Secondary Phosphine Oxides as Diazaphospholene Precatalysts. *Chem. Commun.* **2020**, *56* (58), 8027–8030.

(80) Burck, S.; Gudat, D.; Nieger, M. Diphosphanes with Polarized and Highly Reactive P–P Bonds. *Angew. Chem. Int. Ed.* **2004**, *43* (36), 4801–4804.

(81) Puntigam, O.; Förster, D.; Giffin, N. A.; Burck, S.; Bender, J.; Ehret, F.; Hendsbee, A. D.; Nieger, M.; Masuda, J. D.; Gudat, D. Rational Synthesis and Mutual Conversion of Bis-N-Heterocyclic Diphosphanes and Secondary N-Heterocyclic Phosphanes. *Eur. J. Inorg. Chem.* **2013**, *4* (12), 2041–2050.

(82) Zhang, J.; Yang, J.-D.; Cheng, J.-P. A Nucleophilicity Scale for the Reactivity of Diazaphospholenium Hydrides: Structural Insights and Synthetic Applications. *Angew. Chem. Int. Ed.* **2019**, *58* (18), 5983–5987.

(83) Burck, S.; Gudat, D.; Nieger, M.; Du Mont, W.-W. P-Hydrogen-Substituted 1,3,2-Diazaphospholenes: Molecular Hydrides. *J. Am. Chem. Soc.* **2006**, *128* (12), 3946–3955.

(84) Chong, C. C.; Hirao, H.; Kinjo, R. A Concerted Transfer Hydrogenolysis: 1,3,2-Diazaphospholene-Catalyzed Hydrogenation of N=N Bond with Ammonia–Borane. *Angew. Chem. Int. Ed.* **2014**, *53* (13), 3342–3346.

(85) Chong, C. C.; Hirao, H.; Kinjo, R. Metal-Free σ-Bond Metathesis in 1,3,2-Diazaphospholene-Catalyzed Hydroboration of Carbonyl Compounds. *Angew. Chem. Int. Ed.* **2015**, *54* (1), 190–194.

(86) Chong, C. C.; Kinjo, R. Hydrophosphination of $CO_2$ and Subsequent Formate Transfer in the 1,3,2-Diazaphospholene-Catalyzed N-Formylation of Amines. *Angew. Chem. Int. Ed.* **2015**, *54* (41), 12116–12120.

(87) Miaskiewicz, S.; Reed, J. H.; Donets, P. A.; Oliveira, C. C.; Cramer, N. Chiral 1,3,2-Diazaphospholenes as Catalytic Molecular Hydrides for Enantioselective Conjugate Reductions. *Angew. Chem. Int. Ed.* **2018**, *57* (15), 4039–4042.

(88) Gudat, D.; Haghverdi, A.; Gans-Eichler, T.; Nieger, M. High Stability of a Phosphenium Ion Allows Umpolung of P-H Bonds. *Phosphorus, Sulfur Silicon Relat. Elem.* **2002**, *177* (6–7), 1637–1640.

(89) Edge, R.; Less, R. J.; McInnes, E. J. L.; Müther, K.; Naseri, V.; Rawson, J. M.; Wright, D. S. Formation of a New Class of 7π Radicals via Sterically Induced P–P Bond Cleavage of the Dimers $[(CH)_2(NR)_2P]_2$. *Chem. Commun.* **2009**, *2* (13), 1691–1693.

(90) Puntigam, O.; Könczöl, L.; Nyulászi, L.; Gudat, D. Specific Photochemical Dehydrocoupling of N-Heterocyclic Phosphanes and Their Use in the Photocatalytic Generation of Dihydrogen. *Angew. Chem. Int. Ed.* **2015**, *54* (39), 11567–11571.

(91) Zhang, J.; Yang, J.-D.; Cheng, J.-P. Exploiting the Radical Reactivity of Diazaphosphinanes in Hydrodehalogenations and Cascade Cyclizations. *Chem. Sci.* **2020**, *11* (18), 4786–4790.

(92) Zhang, J.; Yang, J.-D.; Cheng, J.-P. Diazaphosphinanes as Hydride, Hydrogen Atom, Proton or Electron Donors under Transition-Metal-Free Conditions: Thermodynamics, Kinetics, and Synthetic Applications. *Chem. Sci.* **2020**, *11* (14), 3672–3679.

(93) Burck, S.; Förster, D.; Gudat, D. Phosphorus-Carbon Bond Formation Catalysed by Electrophilic N-Heterocyclic Phosphines. *Chem. Commun.* **2006**, (26), 2810–2812.

(94) Hajdók, I.; Lissner, F.; Nieger, M.; Strobel, S.; Gudat, D. Diphosphination of Electron Poor Alkenes. *Organometallics.* **2009**, *28* (6), 1644–1651.

(95) Förster, D.; Dilger, H.; Ehret, F.; Nieger, M.; Gudat, D. An Insight into the Reversible Dissociation and Chemical Reactivity of a Sterically Encumbered Diphosphane. *Eur. J. Inorg. Chem.* **2012**, *2012* (25), 3989–3994.

(96) Förster, D.; Nickolaus, J.; Nieger, M.; Benko, Z.; Ehlers, A. W.; Gudat, D. Donor-Free Phosphenium–Metal(0)–Halides with Unsymmetrically Bridging Phosphenium Ligands. *Inorg. Chem.* **2013**, *52* (13), 7699–7708.

(97) Giffin, N. A.; Hendsbee, A. D.; Masuda, J. D. Reactions of a Persistent Phosphinyl Radical/Diphosphine with Heteroallenes. *Dalton Trans.* **2016**, *45* (32), 12636–12638.

(98) Ueng, S.-H.; Fensterbank, L.; Lacôte, E.; Malacria, M.; Curran, D. P. Radical Deoxygenation of Xanthates and Related Functional Groups with New Minimalist N-Heterocyclic Carbene Boranes. *Org. Lett.* **2010**, *12* (13), 3002–3005.

(99) Monot, J.; Fensterbank, L.; Malacria, M.; Lacôte, E.; Geib, S. J.; Curran, D. P. CAAC Boranes. Synthesis and Characterization of Cyclic (Alkyl) (Amino) Carbene Borane Complexes from $BF_3$ and $BH_3$. *Beilstein J. Org. Chem.* **2010**, *6*, 709–712.

(100) Taniguchi, T.; Curran, D. P. Silica Gel Promotes Reductions of Aldehydes and Ketones by N-Heterocyclic Carbene Boranes. *Org. Lett.* **2012**, *14* (17), 4540–4543.

(101) Curran, D. P.; Solovyev, A.; Brahmi, M. M.; Fensterbank, L.; Malacria, M.; Lacôte, E. Synthesis and Reactions of N-Heterocyclic Carbene Boranes. *Angew. Chem. Int. Ed.* **2011**, *50* (44), 10294–10317.

(102) De Oliveira Freitas, L. B.; Eisenberger, P.; Crudden, C. M. Mesoionic Carbene-Boranes. *Organometallics.* **2013**, *32* (22), 6635–6638.

(103) Ramanjaneyulu, B. T.; Mahesh, S.; Anand, R. V. Bis(Amino)Cyclopropenylidene-Catalyzed 1,6-Conjugate Addition of Aromatic Aldehydes to Para-Quinone Methides: Expedient Access to α,α′-Diarylated Ketones. *Org. Lett.* **2015**, *17* (16), 3952–3955.

(104) Current routes to mesoionic carbenes require the use of expensive ($307 USD for 50 mL of a 0.5 M solution of $PhN_3$, $12.28/mmol, Aldrich), unstable, and potentially explosive aryl azides and hypervalent iodine reagents. BAC carbene precursors are prepared in a one-pot procedure from commercially available pentachlorocyclopropene ($38 USD for 5 g, $1.52/mmol, Aldrich). Pentachlorocyclopropene can also be easily and inexpensively prepared on a 100 g scale.

(105) Kuchenbeiser, G.; Donnadieu, B.; Bertrand, G. Stable Bis(Diisopropylamino)Cyclopropenylidene (BAC) as Ligand for Transition Metal Complexes. *J. Organomet. Chem.* **2008**, *693* (5), 899–904.

(106) Gardner, S.; Kawamoto, T.; Curran, D. P. Synthesis of 1,3-Dialkylimidazol-2-Ylidene Boranes from 1,3-Dialkylimidazolium Iodides and Sodium Borohydride. *J. Org. Chem.* **2015**, *80* (19), 9794–9797.

(107) Tai, C.-C.; Chang, Y.-T.; Tsai, J.-H.; Jurca, T.; Yap, G. P. A.; Ong, T.-G. Subtle Reactivities of Boron and Aluminum Complexes with Amino-Linked N-Heterocyclic Carbene Ligation. *Organometallics.* **2012**, *31* (2), 637–643.

(108) Arduengo, A. J.; Davidson, F.; Krafczyk, R.; Marshall, W. J.; Schmutzler, R. Carbene Complexes of Pnictogen Pentafluorides and Boron Trifluoride. *Monatsh. Chem.* **2000**, *131* (3), 251–265.

(109) Attempts to form an adduct with 9-BBN resulted in formation of a putative product ($^{11}B$ chemical shift of -16.1 ppm in $Et_2O$), that was unstable to concentration or isolation and was not otherwise characterized.

(110) The Equipment we had access to was limited to a maximum pressure of 20 atmospheres. Higher pressures of hydrogen gas will be explored in due course. Trifluorotoluene was an optimal solvent in reference 45. Dichloromethane provides inferior conversions in our chemistry (34 % for **2-21**).

(111) A Single Example of hydrogenation of the benzyl imine of benzophenone, employing a MIC carbene supported borenium cation, with 99% conversion at 102 atm was reported in the supporting information of reference 45. Presumably the steric bulk of this substrate prevents product inhibition, as the same catalyst provided only trace hydrogenation of less bulky **2-21** under the same conditions.

(112) Bahr, S. R.; Boudjouk, P. Trityl Tetrakis[3,5-Bis(Trifluoromethyl)Phenyl]Borate: A New Hydride Abstraction Reagent. *J. Org. Chem.* **1992**, *57* (20), 5545–5547.

(113) Yakelis, N. A.; Bergman, R. G. Safe Preparation and Purification of Sodium Tetrakis[(3,5-Trifluoromethyl)Phenyl]Borate ($NaBArF_{24}$): Reliable and Sensitive Analysis of Water in Solutions of Fluorinated Tetraarylborates. *Organometallics.* **2005**, *24* (14), 3579–3581.

(114) Silva Valverde, M. F.; Schweyen, P.; Gisinger, D.; Bannenberg, T.; Freytag, M.; Kleeberg, C.; Tamm, M. N-Heterocyclic Carbene Stabilized Boryl Radicals. *Angew. Chem. Int. Ed.* **2017**, *56* (4), 1135–1140.

(115) Taniguchi, T.; Curran, D. P. Hydroboration of Arynes with N-Heterocyclic Carbene Boranes. *Angew. Chem. Int. Ed.* **2014**, *53* (48), 13150–13154.

(116) Yoshida, Z. NOVEL PI SYSTEMS POSSESSING CYCLOPROPENYLIDENE MOIETY. *Pure Appl. Chem.* **1982**, *54* (5), 1059–1074.

(117) Weiss, R.; Priesner, C.; Wolf, H. Structure and Formation of Triorganylphosphoniocyclopropenylium Ions. *Angew. Chem. Int. Ed.* **1979**, *18* (6), 472–473.

(118) Singh, G.; Goswami, P.; Anand, R. V. Exploring Bis-(Amino)Cyclopropenylidene as a Non-Covalent Brønsted Base Catalyst in Conjugate Addition Reactions. *Org. Biomol. Chem.* **2018**, *16* (3), 384–388.

(119) Goswami, P.; Sharma, S.; Singh, G.; Anand, R. V. Bis(Amino)Cyclopropenylidene Catalyzed Rauhut–Currier Reaction between α,β-Unsaturated Carbonyl Compounds and Para-Quinone Methides. *J. Org. Chem.* **2018**, *83* (7), 4213–4220.

(120) Lu, X.; Schneider, U. Aza-Morita–Baylis–Hillman Reactions Catalyzed by a Cyclopropenylidene. *Chem. Commun.* **2016**, *52* (88), 12980–12983.

(121) Mir, R.; Dudding, T. Bis(Amino)Cyclopropenium Trifluoroborates: Synthesis, Hydrolytic Stability Studies, and DFT Insights. *J. Org. Chem.* **2018**, *83* (8), 4384–4388.

(122) Huchenski, B. S. N.; Adams, M. R.; McDonald, R.; Ferguson, M. J.; Speed, A. W. H. Synthesis and Catalytic Reactivity of Bis(Amino)Cyclopropenylidene Carbene–Borane Adducts. *Organometallics.* **2016**, *35* (18), 3101–3104.

(123) Tobey, S. W.; West, R. Tetrachlorocyclopropene, Tetrabromocyclopropene, and Some Fluorinated Cyclopropenes and Cyclopropanes. *J. Am. Chem. Soc.* **1966**, *88* (11), 2481–2488.

(124) Taylor, M. J.; Surman, P. W. J.; Clark, G. R. Allyl, Amidinium and Cyclopropenyl Cations from the Reactions of Primary and Secondary Amines with Pentachlorocyclopropane. *Chem. Commun.* **1994**, (21), 2517–2518.

(125) Nacsa, E. D.; Lambert, T. H. Higher-Order Cyclopropenimine Superbases: Direct Neutral Brønsted Base Catalyzed Michael Reactions with α-Aryl Esters. *J. Am. Chem. Soc.* **2015**, *137* (32), 10246–10253.

(126) Farrell, J. M.; Stephan, D. W. Planar N-Heterocyclic Carbene Diarylborenium Ions: Synthesis by Cationic Borylation and Reactivity with Lewis Bases. *Angew. Chem. Int. Ed.* **2015**, *54* (17), 5214–5217.

(127) Jacob, P. Diphenylborane. A New Hydroborating Agent. Synthesis of Alkyldiphenylboranes and Their Application to the Conjugate Addition Reaction of Organoboranes. *J. Organomet. Chem.* **1978**, *156* (1), 101–110.

(128) Farooq, O. A Convenient High-Yield Preparation of Phenylfluoroboranes. *J. Fluor. Chem.* **1995**, *70* (2), 225–227.

(129) Samigullin, K.; Bolte, M.; Lerner, H.-W.; Wagner, M. Facile Synthesis of (3,5-$(CF_3)_2C_6H_3)_2BX$ (X = H, OMe, F, Cl, Br): Reagents for the Introduction of a Strong Boryl Acceptor Unit. *Organometallics.* **2014**, *33* (13), 3564–3569.

(130) Ito, T.; Iwai, T.; Mizuno, T.; Ishino, Y. Palladium-Catalyzed Cross-Coupling Reaction of Potassium Diaryldifluoroborates with Aryl Halides. *Synlett.* **2003**, (10), 1435–1438.

(131) Dorkó, É.; Kótai, B.; Földes, T.; Gyömöre, Á.; Pápai, I.; Soós, T. Correlating Electronic and Catalytic Properties of Frustrated Lewis Pairs for Imine Hydrogenation. *J. Organomet. Chem.* **2017**, *847*, 258–262.

(132) Welch, G. C.; Cabrera, L.; Chase, P. A.; Hollink, E.; Masuda, J. D.; Wei, P.; Stephan, D. W. Tuning Lewis Acidity Using the Reactivity of "Frustrated Lewis Pairs": Facile Formation of Phosphine-Boranes and Cationic Phosphonium-Boranes. *Dalton Trans.* **2006**, *9226* (31), 3407–3414.

(133) Li, X.; Tian, J.-J.; Liu, N.; Tu, X.-S.; Zeng, N.-N.; Wang, X.-C. Spiro-Bicyclic Bisborane Catalysts for Metal-Free Chemoselective and Enantioselective Hydrogenation of Quinolines. *Angew. Chem. Int. Ed.* **2019**, *58* (14), 4664–4668.

(134) Soderquist, J. A.; Negron, A. 9-BORABICYCLO[3.3.1]NONANE DIMER. *Org. Synth.* **1992**, *70*, 169.

(135) Abiko, A. DICYCLOHEXYLBORON TRIFLUOROMETHANESULFONATE. *Org. Synth.* **2002**, *79*, 103.

(136) Walton, J. C.; Brahmi, M. M.; Monot, J.; Fensterbank, L.; Malacria, M.; Curran, D. P.; Lacôte, E. Electron Paramagnetic Resonance and Computational Studies of Radicals Derived from Boron-Substituted N-Heterocyclic Carbene Boranes. *J. Am. Chem. Soc.* **2011**, *133* (26), 10312–10321.

(137) Huchenski, B. S. N.; Christopherson, C. J.; Robertson, K. N.; Speed, A. W. H. Bis-Aminocyclopropenylidene Carbene Borane Catalyzed Imine Hydrogenation. *Org. Biomol. Chem.* **2019**, *17* (25), 6158–6164.

(138) Clark, E. R.; Ingleson, M. J. N-Methylacridinium Salts: Carbon Lewis Acids in Frustrated Lewis Pairs for σ-Bond Activation and Catalytic Reductions. *Angew. Chem. Int. Ed.* **2014**, *53* (42), 11306–11309.

(139) Fasano, V.; Radcliffe, J. E.; Curless, L. D.; Ingleson, M. J. N-Methyl-Benzothiazolium Salts as Carbon Lewis Acids for Si−H σ-Bond Activation and Catalytic (De)Hydrosilylation. *Chem. Eur. J.* **2017**, *23* (1), 187–193.

(140) Keim, M.; Kratzer, P.; Derksen, H.; Isakov, D.; Maas, G. Terminal Acetylenic Iminium Salts – Synthesis and Reactivity. *Eur. J. Org. Chem.* **2019**, *2019* (4), 826–844.

(141) Anulewicz-Ostrowska, R.; Kliś, T.; Krajewski, D.; Lewandowski, B.; Serwatowski, J. Synthesis of Some Halogenated Tetraarylborates. *Tetrahedron Lett.* **2003**, *44* (39), 7329–7331.

(142) Muthaiah, S.; Do, D. C. H.; Ganguly, R.; Vidović, D. Counterion Dependence on the Synthetic Viability of NHC-Stabilized Dichloroborenium Cations. *Organometallics.* **2013**, *32* (22), 6718–6724.

(143) Do, D. C. H.; Muthaiah, S.; Ganguly, R.; Vidović, D. Synthesis of N-Heterocyclic Carbene Stabilized Catecholatoborenium Cations by Ligand Substitution. *Organometallics.* **2014**, *33* (16), 4165–4168.

(144) Afanasyev, O. I.; Kuchuk, E.; Usanov, D. L.; Chusov, D. Reductive Amination in the Synthesis of Pharmaceuticals. *Chem. Rev.* **2019**, *119* (23), 11857–11911.

(145) Youdim, M. B. H.; Gross, A.; Finberg, J. P. M. Rasagiline [N-Propargyl-1R(+)-Aminoindan], a Selective and Potent Inhibitor of Mitochondrial Monoamine Oxidase B. *Br. J. Pharmacol.* **2001**, *132* (2), 500–506.

(146) van der Hoeven, D.; Cho, K. -j.; Ma, X.; Chigurupati, S.; Parton, R. G.; Hancock, J. F. Fendiline Inhibits K-Ras Plasma Membrane Localization and Blocks K-Ras Signal Transmission. *Mol. Cell. Biol.* **2013**, *33* (2), 237–251.

(147) Xu, T.; Chen, E. Y.-X. Silylium Dual Catalysis in Living Polymerization of Methacrylates via In Situ Hydrosilylation of Monomer. *J. Polym. Sci. Part A Polym. Chem.* **2015**, *53* (16), 1895–1903.

(148) Müther, K.; Oestreich, M. Self-Regeneration of a Silylium Ion Catalyst in Carbonyl Reduction. *Chem. Commun.* **2011**, *47* (1), 334–336.

(149) Fasano, V.; Ingleson, M. J. Expanding Water/Base Tolerant Frustrated Lewis Pair Chemistry to Alkylamines Enables Broad Scope Reductive Aminations. *Chem. Eur. J.* **2017**, *23* (9), 2217–2224.

(150) Flanigan, D. M.; Romanov-Michailidis, F.; White, N. A.; Rovis, T. Organocatalytic Reactions Enabled by N-Heterocyclic Carbenes. *Chem. Rev.* **2015**, *115* (17), 9307–9387.

(151) Abbott, J. R.; Allais, C.; Roush, W. R. Preparation of Crystalline (Diisopinocampheyl)Borane. *Org. Synth.* **2015**, *92*, 26–37.

(152) Masamune, S.; Kim, B. M.; Petersen, J. S.; Sato, T.; Veenstra, S. J.; Imai, T. Organoboron Compounds in Organic Synthesis. 1. Asymmetric Hydroboration. *J. Am. Chem. Soc.* **1985**, *107* (15), 4549–4551.

(153) Liu, X.; Dong, S.; Lin, L.; Feng, X. Chiral Amino Acids-Derived Catalysts and Ligands. *Chin. J. Chem.* **2018**, *36* (9), 791–797.

(154) Cho, B. T.; Chun, Y. S. Asymmetric Reduction of N-Substituted Ketimines with the Reagent Prepared from Borane and (S)-(–)-2-Amino-3-Methyl-1,1-Diphenylbutan-1-ol (Itsuno's Reagent): Enantioselective Synthesis of Optically Active Secondary Amines. *J. Chem. Soc. Perkin Trans. 1.* **1990**, (11), 3200–3201.

(155) Clark, G. R.; Rickard, C. E. F.; Surman, P. W. J.; Taylor, M. J. Structural and Spectroscopic Investigations of 1,1,3,3-Tetrakis(Alkylamino)Allyl Cations, Methylene-Bis(N,N′-Dialkylformamidinium) Dications and Related Formamidine Derivatives. *J. Chem. Soc., Faraday Trans.* **1997**, *93* (15), 2503–2507.

(156) Kobayashi, S.; Kinoshita, T.; Uehara, H.; Sudo, T.; Ryu, L. Organocatalytic Enantioselective Synthesis of Nitrogen-Substituted Dihydropyran-2-ones, a Key Synthetic Intermediate of 1β-Methylcarbapenems. *Org. Lett.* **2009**, *11* (17), 3934–3937.

(157) Hamilton, G. L.; Kang, E. J.; Mba, M.; Toste, F. D. A Powerful Chiral Counterion Strategy for Asymmetric Transition Metal Catalysis. *Science.* **2007**, *317* (5837), 496 496–499.

(158) Phipps, R. J.; Hamilton, G. L.; Toste, F. D. The Progression of Chiral Anions from Concepts to Applications in Asymmetric Catalysis. *Nat. Chem.* **2012**, *4* (8), 603–614.

(159) Lacour, J.; Hebbe-Viton, V. Recent Developments in Chiral Anion Mediated Asymmetric Chemistry. *Chem. Soc. Rev.* **2003**, *32* (6), 373–382.

(160) Raskatov, J. A.; Brown, J. M.; Thompson, A. L. Chiral Selection in the Formation of Borates from Racemic Binaphthols and Related Diols. *CrystEngComm.* **2011**, *13* (8), 2923–2929.

(161) Raskatov, J. A.; Thompson, A. L.; Cowley, A. R.; Claridge, T. D. W.; Brown, J. M. Chiral Recognition in Contact Ion-Pairs; Observation, Characterization and Analysis. *Chem. Sci.* **2013**, *4* (8), 3140–3147.

(162) Pommerening, P.; Mohr, J.; Friebel, J.; Oestreich, M. Synthesis of a Chiral Borate Counteranion, Its Trityl Salt, and Application Thereof in Lewis-Acid Catalysis. *Eur. J. Org. Chem.* **2017**, *2017* (16), 2312–2316.

(163) Llewellyn, D. B.; Adamson, D.; Arndtsen, B. A. A Novel Example of Chiral Counteranion Induced Enantioselective Metal Catalysis: The Importance of Ion-Pairing in Copper-Catalyzed Olefin Aziridination and Cyclopropanation. *Org. Lett.* **2000**, *2* (26), 4165–4168.

(164) Chen, D.; Sundararaju, B.; Krause, R.; Klankermayer, J.; Dixneuf, P. H.; Leitner, W. Asymmetric Induction by Chiral Borate Anions in Enantioselective Hydrogenation Using a Racemic Rh–Binap Catalyst. *ChemCatChem.* **2010**, *2* (1), 55–57.

(165) Ueda, M.; Yagyu, Y.; Ryu, I. Ammonium Chiral Borate Salt Catalyzed Asymmetric Friedel-Crafts Alkylation of Indoles with α,β-Disubstituted Enals. *Tetrahedron Asymmetry.* **2017**, *28* (8), 1070–1077.

(166) Wong, L. W.-Y.; Kan, J. W.-H.; Nguyen, T.; Sung, H. H.-Y.; Li, D.; Au-Yeung, A. S.-F.; Sharma, R.; Lin, Z.; Williams, I. D. Bis(Mandelato)Borate: An Effective, Inexpensive Spiroborate Anion for Chiral Resolution. *Chem. Commun.* **2015**, *51* (87), 15760–15763.

(167) Wong, L. W.-Y.; Au-Yeung, A. S.-F.; Tam, G. S.-S.; Kan, J. W.-H.; Sung, H. H.-Y.; Sheong, F. K.; Lin, Z.; Williams, I. D. Isolation and Enantiostability of the B-Chiral Bis(Salicylato)Borate Anions [BR(Sal)$_2$] and [BS(Sal)$_2$]. *RSC Adv.* **2018**, *8* (3), 1451–1460.

(168) Hu, G.; Gupta, A. K.; Huang, L.; Zhao, W.; Yin, X.; Osminski, W. E. G.; Huang, R. H.; Wulff, W. D.; Izzo, J. A.; Vetticatt, M. J. Pyro-Borates, Spiro-Borates, and Boroxinates of BINOL–Assembly, Structures, and Reactivity. *J. Am. Chem. Soc.* **2017**, *139* (30), 10267–10285.

(169) Delaunay, D.; Le Corre, M. A New Route to Oxazolidinones. *J. Chem. Soc. Perkin Trans. 1* **1994**, (20), 3041–3042.

(170) Chong, C. C.; Kinjo, R. Catalytic Hydroboration of Carbonyl Derivatives, Imines, and Carbon Dioxide. *Adv. Synth. Catal.* **2015**, *5* (6), 3238–3259.

(171) Schömberg, F.; Zi, Y.; Vilotijevic, I. Lewis-Base-Catalysed Selective Reductions of Ynones with a Mild Hydride Donor. *Chem. Commun.* **2018**, *54* (26), 3266–3269.

(172) Query, I. P.; Squier, P. A.; Larson, E. M.; Isley, N. A.; Clark, T. B. Alkoxide-Catalyzed Reduction of Ketones with Pinacolborane. *J. Org. Chem.* **2011**, *76* (15), 6452–6456.

(173) Zhu, Z.; Wu, X.; Xu, X.; Wu, Z.; Xue, M.; Yao, Y.; Shen, Q.; Bao, X. *n*-Butyllithium Catalyzed Selective Hydroboration of Aldehydes and Ketones. *J. Org. Chem.* **2018**, *83* (17), 10677–10683.

(174) Stachowiak, H.; Kaźmierczak, J.; Kuciński, K.; Hreczycho, G. Catalyst-Free and Solvent-Free Hydroboration of Aldehydes. *Green Chem.* **2018**, *20* (8), 1738–1742.

(175) Baker, R. T.; Calabrese, J. C.; Westcott, S. A. Coinage Metal-Catalyzed Hydroboration of Imines. *J. Organomet. Chem.* **1995**, *498* (2), 109–117.

(176) Enders, D.; Rembiak, A.; Stöckel, B. A. Chemo- and Enantioselective Brønsted Acid-Catalyzed Reduction of α-Imino Esters with Catecholborane. *Adv. Synth. Catal.* **2013**, *355* (10), 1937–1942.

(177) Enders, D.; Rembiak, A.; Seppelt, M. Asymmetric Organocatalytic Reduction of Ketimines with Catecholborane Employing a N-Triflyl Phosphoramide Brønsted Acid as Catalyst. *Tetrahedron Lett.* **2013**, *54* (6), 470–473.

(178) Tucker, C. E.; Davidson, J.; Knochel, P. Mild and Stereoselective Hydroborations of Functionalized Alkynes and Alkenes Using Pinacolborane. *J. Org. Chem.* **1992**, *57* (12), 3482–3485.

(179) Eisenberger, P.; Bailey, A. M.; Crudden, C. M. Taking the F out of FLP: Simple Lewis Acid–Base Pairs for Mild Reductions with Neutral Boranes via Borenium Ion Catalysis. *J. Am. Chem. Soc.* **2012**, *134* (42), 17384–17387.

(180) Bisai, M. K.; Pahar, S.; Das, T.; Vanka, K.; Sen, S. S. Transition Metal Free Catalytic Hydroboration of Aldehydes and Aldimines by Amidinato Silane. *Dalton Trans.* **2017**, *46* (8), 2420–2424.

(181) Pollard, V. A.; Fuentes, M. Á.; Kennedy, A. R.; McLellan, R.; Mulvey, R. E. Comparing Neutral (Monometallic) and Anionic (Bimetallic) Aluminum Complexes in Hydroboration Catalysis: Influences of Lithium Cooperation and Ligand Set. *Angew. Chem. Int. Ed.* **2018**, *57* (33), 10651–10655.

(182) Yin, Q.; Soltani, Y.; Melen, R. L.; Oestreich, M. $BArF_3$-Catalyzed Imine Hydroboration with Pinacolborane Not Requiring the Assistance of an Additional Lewis Base. *Organometallics.* **2017**, *36* (13), 2381–2384.

(183) Lawson, J. R.; Wilkins, L. C.; Melen, R. L. Tris(2,4,6-Trifluorophenyl)Borane: An Efficient Hydroboration Catalyst. *Chem. Eur. J.* **2017**, *23* (46), 10997–11000.

(184) Arrowsmith, M.; Hill, M. S.; Kociok-Köhn, G. Magnesium Catalysis of Imine Hydroboration. *Chem. Eur. J.* **2013**, *19* (8), 2776–2783.

(185) Manna, K.; Ji, P.; Greene, F. X.; Lin, W. Metal-Organic Framework Nodes Support Single-Site Magnesium-Alkyl Catalysts for Hydroboration and Hydroamination Reactions. *J. Am. Chem. Soc.* **2016**, *138* (24), 7488–7491.

(186) Lin, Y.-C.; Hatzakis, E.; McCarthy, S. M.; Reichl, K. D.; Lai, T.-Y.; Yennawar, H. P.; Radosevich, A. T. P–N Cooperative Borane Activation and Catalytic Hydroboration by a Distorted Phosphorous Triamide Platform. *J. Am. Chem. Soc.* **2017**, *139* (16), 6008–6016.

(187) Tien, C.-H.; Adams, M. R.; Ferguson, M. J.; Johnson, E. R.; Speed, A. W. H. Hydroboration Catalyzed by 1,2,4,3-Triazaphospholenes. *Org. Lett.* **2017**, *19* (20), 5565–5568.

(188) Koren-Selfridge, L.; Londino, H. N.; Vellucci, J. K.; Simmons, B. J.; Casey, H. P.; Clark, T. B. A Boron-Substituted Analogue of the Shvo Hydrogenation Catalyst: Catalytic Hydroboration of Aldehydes, Imines, and Ketones. *Organometallics.* **2009**, *28* (7), 2085–2090.

(189) Kaithal, A.; Chatterjee, B.; Gunanathan, C. Ruthenium-Catalyzed Selective Hydroboration of Nitriles and Imines. *J. Org. Chem.* **2016**, *81* (22), 11153–11163.

(190) Arévalo, R.; Vogels, C. M.; Macneil, G. A.; Riera, L.; Pérez, J.; Westcott, S. A. Rhenium-Catalysed Hydroboration of Aldehydes and Aldimines. *Dalton Trans.* **2017**, *46* (24), 7750–7757.

(191) Wu, J.; Zeng, H.; Cheng, J.; Zheng, S.; Golen, J. A.; Manke, D. R.; Zhang, G. Cobalt(II) Coordination Polymer as a Precatalyst for Selective Hydroboration of Aldehydes, Ketones, and Imines. *J. Org. Chem.* **2018**, *83* (16), 9442–9448.

(192) Romero, E. A.; Peltier, J. L.; Jazzar, R.; Bertrand, G. Catalyst-Free Dehydrocoupling of Amines, Alcohols, and Thiols with Pinacol Borane and 9-Borabicyclononane (9-BBN). *Chem. Commun.* **2016**, *52* (69), 10563–10565.

(193) Bleicher, L. S.; Cosford, N. D. P.; Herbaut, A.; Stuart McCallum, J.; McDonald, I. A. A Practical and Efficient Synthesis of the Selective Neuronal Acetylcholine-Gated Ion Channel Agonist (S)-(-)-5-Ethynyl-3-(1-methyl-2-pyrrolidinyl)pyridine Maleate (SIB-1508Y). *J. Org. Chem.* **1998**, *63* (4), 1109–1118.

(194) Wei, C. S.; Jiménez-Hoyos, C. A.; Videa, M. F.; Hartwig, J. F.; Hall, M. B. Origins of the Selectivity for Borylation of Primary over Secondary C–H Bonds Catalyzed by Cp-Rhodium Complexes. *J. Am. Chem. Soc.* **2010**, *132* (9), 3078–3091.

(195) Vukics, K.; Fodor, T.; Fischer, J.; Fellegvári, I.; Lévai, S. Improved Industrial Synthesis of Antidepressant Sertraline. *Org. Process Res. Dev.* **2002**, *6* (1), 82–85.

(196) Li, S.; Li, G.; Meng, W.; Du, H. A Frustrated Lewis Pair Catalyzed Asymmetric Transfer Hydrogenation of Imines Using Ammonia Borane. *J. Am. Chem. Soc.* **2016**, *138* (39), 12956–12962.

(197) Zhang, X.; Xiao, H.; Tang, J.; Cui, Z.; Zhang, Y. Recent Advances in Decomposition of the Most Potent Greenhouse Gas SF6. *Crit. Rev. Environ. Sci. Technol.* **2017**, *47* (18), 1763–1782.

(198) Zhuang, Q.; Clements, B.; Mcfarlan, A.; Fasoyinu, Y. Decomposition of the Most Potent Greenhouse Gas (GHG) Sulphur Hexafluoride ($SF_6$) Using a Dielectric Barrier Discharge (DBD) Plasma. *Can. J. Chem. Eng.* **2014**, *92* (1), 32–35.

(199) Lebeau, P.; Moissan, H. Sur Un Nouveau Corps Gazeux: Le Perfluorure de Soufre $SF_6$. *C. R. Acad. Sci.* **1900**, 865–871.

(200) Lebeau, P.; Moissan, H. ÉTUDE DES FLUORURES ET OXYFLUORURES DE SOUFRE. *Ann. Chim. Phys.* **1902**, 145–177.

(201) Tsai, W.-T. The Decomposition Products of Sulfur Hexafluoride ($SF_6$): Reviews of Environmental and Health Risk Analysis. *J. Fluor. Chem.* **2007**, *128* (11), 1345–1352.

(202) Widger, P.; Haddad, A. Evaluation of $SF_6$ Leakage from Gas Insulated Equipment on Electricity Networks in Great Britain. *Energies.* **2018**, *11* (8), 1–14.

(203) Petrusa, J.; Ragnauth, S.; Alsalam, J.; Godwin, D.; Creason, J.; Li, J.; Beach, R. *Global Mitigation of Non-$CO_2$ Greenhouse Gases: 2010-2030*; Washington, DC, 2013.

(204) Cowen, H. C.; Riding, F.; Warhurst, E. The Reaction of Sulphur Hexafluoride with Sodium. *J. Chem. Soc.* **1983**, 4168–4169.

(205) Case, J. R.; Nyman, F. Some Chemical Reactions of Sulphur Hexafluoride. *Nature.* **1962**, *193* (4814), 473.

(206) Demitras, G. C.; MacDiarmid, A. G. The Low Temperature Reaction of Sulfur Hexafluoride with Solutions of Sodium. *Inorg. Chem.* **1964**, *3* (8), 1198–1199.

(207) Brewer, L.; Chang, C. A.; King, B. A. Sulfur Hexafluoride. Its Reaction with Ammoniated Electrons and Its Use as a Matrix for Isolated Gold, Silver, and Copper Atoms. *Inorg. Chem.* **1970**, *9* (4), 814–816.

(208) Deubner, H. L.; Kraus, F. The Decomposition Products of Sulfur Hexafluoride ($SF_6$) with Metals Dissolved in Liquid Ammonia. *Inorganics.* **2017**, *5* (4), 1–7.

(209) Kashiwagi, D.; Takai, A.; Takubo, T.; Nagaoka, K.; Inoue, T.; Takita, Y. Metal Phosphate Catalysts Effective for Degradation of Sulfur Hexafluoride. *Ind. Eng. Chem. Res.* **2009**, *48* (2), 632–640.

(210) Kashiwagi, D.; Takai, A.; Takubo, T.; Yamada, H.; Inoue, T.; Nagaoka, K.; Takita, Y. Catalytic Activity of Rare Earth Phosphates for $SF_6$ Decomposition and Promotion Effects of Rare Earths Added into AlPO4. *J. Colloid Interface Sci.* **2009**, *332* (1), 136–144.

(211) Park, N.-K.; Park, H.-G.; Lee, T. J.; Chang, W.-C.; Kwon, W.-T. Hydrolysis and Oxidation on Supported Phosphate Catalyst for Decomposition of $SF_6$. *Catal. Today.* **2012**, *185* (1), 247–252.

(212) Zhang, J.; Zhou, J. Z.; Liu, Q.; Qian, G.; Xu, Z. P. Efficient Removal of Sulfur Hexafluoride ($SF_6$) Through Reacting with Recycled Electroplating Sludge. *Environ. Sci. Technol.* **2013**, *47* (12), 6493–6499.

(213) Zhang, J.; Zhou, J. Z.; Xu, Z. P.; Li, Y.; Cao, T.; Zhao, J.; Ruan, X.; Liu, Q.; Qian, G. Decomposition of Potent Greenhouse Gas Sulfur Hexafluoride ($SF_6$) by Kirschsteinite-Dominant Stainless Steel Slag. *Environ. Sci. Technol.* **2014**, *48* (1), 599–606.

(214) Gutiérrez, Y.; Giangregorio, M. M.; Palumbo, F.; González, F.; Brown, A. S.; Moreno, F.; Losurdo, M. Sustainable and Tunable Mg/MgO Plasmon-Catalytic Platform for the Grand Challenge of $SF_6$ Environmental Remediation. *Nano Lett.* **2020**, *20* (5), 3352–3360.

(215) Basta, R.; Harvey, B. G.; Arif, A. M.; Ernst, R. D. Reactions of SF6 with Organotitanium and Organozirconium Complexes: The "Inert" $SF_6$ as a Reactive Fluorinating Agent. *J. Am. Chem. Soc.* **2005**, *127* (34), 11924–11925.

(216) Harvey, B. G.; Arif, A. M.; Glöckner, A.; Ernst, R. D. $SF_6$ as a Selective and Reactive Fluorinating Agent for Low-Valent Transition Metal Complexes. *Organometallics.* **2007**, *26* (11), 2872–2879.

(217) Holze, P.; Horn, B.; Limberg, C.; Matlachowski, C.; Mebs, S. The Activation of Sulfur Hexafluoride at Highly Reduced Low-Coordinate Nickel Dinitrogen Complexes. *Angew. Chem. Int. Ed.* **2014**, *53* (10), 2750–2753.

(218) Zámostná, L.; Braun, T.; Braun, B. S–F and S–C Activation of $SF_6$ and $SF_5$ Derivatives at Rhodium: Conversion of $SF_6$ into $H_2S$. *Angew. Chem. Int. Ed.* **2014**, *53* (10), 2745–2749.

(219) Zámostná, L.; Braun, T. Catalytic Degradation of Sulfur Hexafluoride by Rhodium Complexes. *Angew. Chem. Int. Ed.* **2015**, *54* (36), 10652–10656.

(220) Berg, C.; Braun, T.; Ahrens, M.; Wittwer, P.; Herrmann, R. Activation of $SF_6$ at Platinum Complexes: Formation of $SF_3$ Derivatives and Their Application in Deoxyfluorination Reactions. *Angew. Chem. Int. Ed.* **2017**, *56* (15), 4300–4304.

(221) Wozniak, M.; Braun, T.; Ahrens, M.; Braun-Cula, B.; Wittwer, P.; Herrmann, R.; Laubenstein, R. Activation of $SF_6$ at a Xantphos-Type Rhodium Complex. *Organometallics.* **2018**, *37* (5), 821–828.

(222) McTeague, T. A.; Jamison, T. F. Photoredox Activation of $SF_6$ for Fluorination. *Angew. Chem. Int. Ed.* **2016**, *55* (48), 15072–15075.

(223) Rombach, D.; Wagenknecht, H.-A. Photoredox Catalytic Activation of Sulfur Hexafluoride for Pentafluorosulfanylation of α-Methyl- and α-Phenyl Styrene. *ChemCatChem.* **2018**, *10* (14), 2955–2961.

(224) Iakobson, G.; Pošta, M.; Beier, P. Reductive Activation of Sulfur Hexafluoride with TEMPOLi: Addition of the Pentafluorosulfanyl Group and TEMPO to Terminal Alkenes. *J. Fluor. Chem.* **2018**, *213*, 51–55.

(225) Huang, L.; Dong, W.; Zhang, R.; Hou, H. Investigation of a New Approach to Decompose Two Potent Greenhouse Gases: Photoreduction of $SF_6$ and $SF_5CF_3$ in the Presence of Acetone. *Chemosphere.* **2007**, *66* (5), 833–840.

(226) Huang, L.; Shen, Y.; Dong, W.; Zhang, R.; Zhang, J.; Hou, H. A Novel Method to Decompose Two Potent Greenhouse Gases: Photoreduction of $SF_6$ and $SF_5CF_3$ in the Presence of Propene. *J. Hazard. Mater.* **2008**, *151* (2–3), 323–330.

(227) Sevenard, D.; Kirsch, P.; Kolomeitsev, A.; Röschenthaler, G.-V. Verfahren Zur Fluorierung Organischer Verbindungen. DE 10220901A1, 2003.

(228) Rueping, M.; Nikolaienko, P.; Lebedev, Y.; Adams, A. Metal-Free Reduction of the Greenhouse Gas Sulfur Hexafluoride, Formation of $SF_5$ Containing Ion Pairs and the Application in Fluorinations. *Green Chem.* **2017**, *19* (11), 2571–2575.

(229) Tomar, P.; Braun, T.; Kemnitz, E. Photochemical Activation of $SF_6$ by N-Heterocyclic Carbenes to Provide a Deoxyfluorinating Reagent. *Chem. Commun.* **2018**, *54* (70), 9753–9756.

(230) Rombach, D.; Wagenknecht, H.-A. Photoredox Catalytic α-Alkoxypentafluorosulfanylation of α-Methyl- and α-Phenylstyrene Using $SF_6$. *Angew. Chem. Int. Ed.* **2020**, *59* (1), 300–303.

(231) Kim, S.; Khomutnyk, Y.; Bannykh, A.; Nagorny, P. Synthesis of Glycosyl Fluorides by Photochemical Fluorination with Sulfur(VI) Hexafluoride. *Org. Lett.* **2021**, *23* (1), 190–194.

(232) Shigeyoshi, N.; Hideyoshi, S. Method for Producing Fluorinated Organic Compound. JP2009292749A, 2008.

(233) Buß, F.; Mück-Lichtenfeld, C.; Mehlmann, P.; Dielmann, F. Nucleophilic Activation of Sulfur Hexafluoride: Metal-Free, Selective Degradation by Phosphines. *Angew. Chem. Int. Ed.* **2018**, *57* (18), 4951–4955.

(234) Weitkamp, R. F.; Neumann, B.; Stammler, H.-G.; Hoge, B. Non-Coordinated Phenolate Anions and Their Application in $SF_6$ Activation. *Chem. Eur. J.* **2021**, *27* (21), 6460–6464.

(235) Wünsche, M. A.; Mehlmann, P.; Witteler, T.; Buß, F.; Rathmann, P.; Dielmann, F. Imidazolin-2-ylidenaminophosphines as Highly Electron-Rich Ligands for Transition-Metal Catalysts. *Angew. Chem. Int. Ed.* **2015**, *54* (40), 11857–11860.

(236) Ishikawa, T. General Aspects of Organosuperbases. *Superbases for Organic Synthesis*; John Wiley & Sons, Ltd, 2009; pp 1–7. DOI:10.1002/9780470740859.

(237) Xu, M.; Jupp, A. R.; Qu, Z.-W.; Stephan, D. W. Alkali Metal Species in the Reversible Activation of $H_2$. *Angew. Chem. Int. Ed.* **2018**, *57* (34), 11050-11054.

(238) Dodds, D. L.; Haddow, M. F.; Orpen, A. G.; Pringle, P. G.; Woodward, G. Stereospecific Diphosphination of Activated Acetylenes: A General Route to Backbone-Functionalized, Chelating 1,2-Diphosphinoethenes. *Organometallics.* **2006**, *25* (25), 5937–5945.

(239) Seel, F.; Rudolph, K.; Gombler, W. Dimethylfluorophosphine. *Angew. Chem. Int. Ed.* **1967**, *6* (8), 708.

(240) Sueishi, Y.; Nishihara, Y. Spin Trapping Chemistry of the Diphenylphosphinyl Radical. *J. Chem. Research (S).* **2001**, No. 2, 84–86.

(241) Fischbach, U.; Trincado, M.; Grützmacher, H. Oxidative Formation of Phosphinyl Radicals from a Trigonal Pyramidal Terminal Phosphide Rh(I) Complex, with an Unusually Long Rh–P Bond. *Dalton Trans.* **2017**, *46* (11), 3443–3448.

(242) Gruber, M.; Jones, P. G.; Schmutzler, R. Eine Neue Bildungsweise Der Phosphor–Phosphor-Bindung. Kristallstrukturanalyse von Tetramethyldiphosphanmonosulfid. *Chem. Ber.* **1990**, *123* (6), 1313–1317.

(243) Sato, Y.; Nishimura, M.; Kawaguchi, S.; Nomoto, A.; Ogawa, A. Reductive Rearrangement of Tetraphenyldiphosphine Disulfide To Trigger the Bisthiophosphinylation of Alkenes and Alkynes. *Chem. Eur. J.* **2019**, *25* (27), 6797–6806.

(244) Cline, J. D. SPECTROPHOTOMETRIC DETERMINATION OF HYDROGEN SULFIDE IN NATURAL WATERS. *Limnol. Oceanogr.* **1969**, *14*, 454.

(245) Fey, N.; Garland, M.; Hopewell, J. P.; McMullin, C. L.; Mastroianni, S.; Orpen, A. G.; Pringle, P. G. Stable Fluorophosphines: Predicted and Realized Ligands for Catalysis. *Angew. Chem. Int. Ed.* **2012**, *51* (1), 118–122.

(246) Jones, R. A.; Stuart, A. L.; Wright, T. C. Isolation and X-Ray Structure of $[Li_2(\mu_3\text{-}t\text{-}Bu_2P)(\mu_2\text{-}t\text{-}Bu_2P)(C_4H_8O)]_2$ Containing a Staggered, Planar $Li_4$ Unit. The First Structurally Characterized Alkali Metal Diorganophosphide. *J. Am. Chem. Soc.* **1983**, *105* (25), 7459–7460.

(247) Yogendra, S.; Chitnis, S. S.; Hennersdorf, F.; Bodensteiner, M.; Fischer, R.; Burford, N.; Weigand, J. J. Condensation Reactions of Chlorophosphanes with Chalcogenides. *Inorg. Chem.* **2016**, *55* (4), 1854–1860.

(248) Dodds, D. L.; Floure, J.; Garland, M.; Haddow, M. F.; Leonard, T. R.; McMullin, C. L.; Orpen, A. G.; Pringle, P. G. Diphosphanes Derived from Phobane and Phosphatrioxa-Adamantane: Similarities, Differences and Anomalies. *Dalton Trans.* **2011**, *40* (27), 7137–7146.

(249) Matsumoto, K.; Haruki, Y.; Sawada, S.; Yamada, S.; Konno, T.; Hagiwara, R. Stabilization of $SF_5^-$ with Glyme-Coordinated Alkali Metal Cations. *Inorg. Chem.* **2018**, *57* (23), 14882–14889.

(250) Huchenski, B. S. N.; Robertson, K. N.; Speed, A. W. H. Functionalization of Bis-Diazaphospholene P–P Bonds with Diverse Electrophiles. *Eur. J. Org. Chem.* **2020**, *2020* (32), 5140–5144.

(251) Gudat, D.; Haghverdi, A.; Hupfer, H.; Nieger, M. Stability and Electrophilicity of Phosphorus Analogues of Arduengo Carbenes–An Experimental and Computational Study. *Chem. Eur. J.* **2000**, *6* (18), 3414–3425.

(252) Frazer, M. J.; Gerrard, W.; Twaits, R. Triphenylphosphine Oxide Complexes of Non-Transition Metal Halides. *J. Inorg. Nucl. Chem.* **1963**, *25* (6), 637–640.

(253) Batesky, D. C.; Goldfogel, M. J.; Weix, D. J. Removal of Triphenylphosphine Oxide by Precipitation with Zinc Chloride in Polar Solvents. *J. Org. Chem.* **2017**, *82* (19), 9931–9936.

(254) Tan, K. L.; Vasudevan, A.; Bergman, R. G.; Ellman, J. A.; Souers, A. J. Microwave-Assisted C-H Bond Activation: A Rapid Entry into Functionalized Heterocycles. *Org. Lett.* **2003**, *5* (12), 2131–2134.

(255) McDonough, J. E.; Mendiratta, A.; Curley, J. J.; Fortman, G. C.; Fantasia, S.; Cummins, C. C.; Rybak-Akimova, E. V.; Nolan, S. P.; Hoff, C. D. Thermodynamic, Kinetic, and Computational Study of Heavier Chalcogen (S, Se, and Te) Terminal Multiple Bonds to Molybdenum, Carbon, and Phosphorus. *Inorg. Chem.* **2008**, *47* (6), 2133–2141.

(256) Hilliard, C. R.; Bhuvanesh, N.; Gladysz, J. A.; Blümel, J. Synthesis, Purification, and Characterization of Phosphine Oxides and Their Hydrogen Peroxide Adducts. *Dalton Trans.* **2012**, *41* (6), 1742–1754.

(257) Gatien, A. V.; Lavoie, C. M.; Bennett, R. N.; Ferguson, M. J.; McDonald, R.; Johnson, E. R.; Speed, A. W. H.; Stradiotto, M. Application of Diazaphospholidine/Diazaphospholene-Based Bisphosphines in Room-Temperature Nickel-Catalyzed C($Sp^2$)–N Cross-Couplings of Primary Alkylamines with (Hetero)Aryl Chlorides and Bromides. *Adv. Synth. Catal.* **2018**, *8* (6), 5328–5339.

(258) Lavoie, C. M.; Stradiotto, M. Bisphosphines: A Prominent Ancillary Ligand Class for Application in Nickel-Catalyzed C–N Cross-Coupling. *Adv. Synth. Catal.* **2018**, *8* (8), 7228–7250.

(259) McGuire, R. T.; Clark, J. S. K.; Gatien, A. V.; Shen, M. Y.; Ferguson, M. J.; Stradiotto, M. Bulky 1,1′-Ferrocenyl Ligands Featuring Diazaphospholene or Dioxaphosphepine Donor Fragments: Catalytic Screening in Nickel-Catalyzed C-N Cross-Coupling. *Eur. J. Inorg. Chem.* **2019**, *2019* (38), 4112–4116.

(260) Musina, E. I.; Balueva, A. S.; Karasik, A. A. Phosphines: Preparation, Reactivity and Applications. *Organophosphorus Chemistry: Volume 48*; The Royal Society of Chemistry, 2019; Vol. 48, pp 1–63. DOI: 10.1039/9781788013055-00001.

(261) Denk, M. K.; Gupta, S.; Lough, A. J. Aromatic Phosphenium Cations. *Eur. J. Inorg. Chem.* **1999**, *1999* (1), 41–49.

(262) Sato, A.; Yorimitsu, H.; Oshima, K. Radical Phosphination of Organic Halides and Alkyl Imidazole-1-Carbothioates. *J. Am. Chem. Soc.* **2006**, *128* (13), 4240–4241.

(263) Kawaguchi, S.; Minamida, Y.; Ohe, T.; Nomoto, A.; Sonoda, M.; Ogawa, A. Synthesis and Properties of Perfluoroalkyl Phosphine Ligands: Photoinduced Reaction of Diphosphines with Perfluoroalkyl Iodides. *Angew. Chem. Int. Ed.* **2013**, *52* (6), 1748–1752.

(264) Khartabil, H. K.; Gros, P. C.; Fort, Y.; Ruiz-López, M. F. Metalation of Pyridines with *n*Buli–Li–Aminoalkoxide Mixed Aggregates: The Origin of Chemoselectivity. *J. Am. Chem. Soc.* **2010**, *132* (7), 2410–2416.

(265) Cunningham, L.; Benson, A.; Guiry, P. J. Recent Developments in the Synthesis and Applications of Chiral Ferrocene Ligands and Organocatalysts in Asymmetric Catalysis. *Org. Biomol. Chem.* **2020**, *18* (46), 9329–9370.

(266) Bowry, V. W.; Lusztyk, J.; Ingold, K. U. Calibration of the Bicyclo[2.1.0]pent-2-yl Radical Ring Opening and an Oxygen Rebound Rate Constant for Cytochrome P-450. *J. Am. Chem. Soc.* **1989**, *111* (5), 1927–1928.

(267) Wang, J.; Sánchez-Roselló, M.; Aceña, J. L.; Del Pozo, C.; Sorochinsky, A. E.; Fustero, S.; Soloshonok, V. A.; Liu, H. Fluorine in Pharmaceutical Industry: Fluorine-Containing Drugs Introduced to the Market in the Last Decade (2001-2011). *Chem. Rev.* **2014**, *114* (4), 2432–2506.

(268) Liu, X.; Xu, C.; Wang, M.; Liu, Q. Trifluoromethyltrimethylsilane: Nucleophilic Trifluoromethylation and Beyond. *Chem. Rev.* **2015**, *115* (2), 683–730.

(269) Umemoto, T.; Zhang, B.; Zhu, T.; Zhou, X.; Zhang, P.; Hu, S.; Li, Y. Powerful, Thermally Stable, One-Pot-Preparable, and Recyclable Electrophilic Trifluoromethylating Agents: 2,8-Difluoro- and 2,3,7,8-Tetrafluoro-S-(Trifluoromethyl)Dibenzothiophenium Salts. *J. Org. Chem.* **2017**, *82* (15), 7708–7719.

(270) Iqbal, S. A.; Cid, J.; Procter, R. J.; Uzelac, M.; Yuan, K.; Ingleson, M. J. Acyl-Directed Ortho-Borylation of Anilines and C7 Borylation of Indoles Using Just $BBr_3$. *Angew. Chem. Int. Ed.* **2019**, *58* (43), 15381–15385.

(271) Roemer, M.; Nijhuis, C. A. Syntheses and Purification of the Versatile Synthons Iodoferrocene and 1,1′-Diiodoferrocene. *Dalton Trans.* **2014**, *43* (31), 11815–11818.

(272) Goeltz, J. C.; Kubiak, C. P. Facile Purification of Iodoferrocene. *Organometallics.* **2011**, *30* (14), 3908–3910.

(273) Kurono, N.; Honda, E.; Komatsu, F.; Orito, K.; Tokuda, M. Regioselective Synthesis of Substituted 1-Indanols, 2,3-Dihydrobenzofurans and 2,3-Dihydroindoles by Electrochemical Radical Cyclization Using an Arene Mediator. *Tetrahedron.* **2004**, *60* (8), 1791–1801.

(274) Liang, K.; Li, N.; Zhang, Y.; Li, T.; Xia, C. Transition-Metal-Free α-Arylation of Oxindoles via Visible-Light-Promoted Electron Transfer. *Chem. Sci.* **2019**, *10* (10), 3049–3053.

(275) Clary, J. W.; Rettenmaier, T. J.; Snelling, R.; Bryks, W.; Banwell, J.; Wipke, W. T.; Singaram, B. Hydride as a Leaving Group in the Reaction of Pinacolborane with Halides under Ambient Grignard and Barbier Conditions. One-Pot Synthesis of Alkyl, Aryl, Heteroaryl, Vinyl, and Allyl Pinacolboronic Esters. *J. Org. Chem.* **2011**, *76* (23), 9602–9610.

## Appendix A: Appendix for Chapter 2

### A1: Crystallographic Solution and Refinement Details

Crystallographic data for **2-6** and **2-9** were obtained at -100 °C on a Bruker D8/Apex II CCD diffractometer using microfocus source Cu Kα (λ=1.54178 Å) radiation, employing samples that were mounted in inert oil and transferred to a cold gas stream on the diffractometer. Crystallographic data for **2-12** were obtained at -80 °C on a Bruker PLATFORM/Apex II CCD diffractometer using graphite-monochromated Mo Kα (λ=0.71073 Å) radiation, employing a sample that was mounted in inert oil and transferred to a cold gas stream on the diffractometer. Programs for diffractometer operation, data collection, data reduction and absorption correction were supplied by Bruker. Gaussian integration (face-indexed) was employed as the absorption correction method for **2-6**, **2-9** and **2-12**. The structures of **2-6** and **2-9** were solved by use of intrinsic phasing methods, while **2-12** was solved by use of direct methods/ dual space procedures; all were refined by use of full-matrix least-squares procedures (on $F^2$) with $R_1$ based on $F_o^2 \geq 2\sigma(F_o^2)$. In the case of **2-9**, two crystallographically independent molecules with similar metrics were observed. Data for one is selected in the text.

Crystallographic data for **2-7.** The crystal chosen was attached to the tip of a MicroLoop with paratone-N oil. Measurements were made on a Bruker APEXII CCD equipped diffractometer (30 mA, 50 kV) using monochromated Mo Kα radiation (λ = 0.71073 Å) at 125 K [1]. The initial orientation and unit cell were indexed using a least-squares analysis of a random set of reflections collected from three series of 0.5° ω-scans, 10 seconds per frame and 12 frames per series, that were well distributed in reciprocal space. For data collection, four ω-scan frame series were collected with 0.5° wide scans, 45 second frames and 366 frames per series at varying φ angles (φ = 0°, 90°, 180° and 270°). The crystal to

detector distance was set to 6 cm and a complete sphere of data was collected. Cell refinement and data reduction were performed with the Bruker SAINT [2] software, which corrects for beam inhomogeneity, possible crystal decay, Lorentz and polarisation effects. A multi-scan absorption correction was applied (SADABS [3]). The structure was solved using SHELXT-2014 [4] and was refined using a full-matrix least-squares method on $F^2$ with SHELXL-2018 [4]. The initial refinement was unremarkable. The non-hydrogen atoms were refined anisotropically. The hydrogen atoms bonded to carbon were included at geometrically idealized positions and were not refined. The isotropic thermal parameters of these hydrogen atoms were fixed at $1.2U_{eq}$ of the parent carbon atom or $1.5U_{eq}$ for methyl hydrogens. The hydrogen atoms bonded to boron were located in a near final Fourier difference map. Their positions were refined, while their isotropic thermal parameters were fixed at 1.5 times that of the boron atoms to which they were bonded.

Five reflections were partially obscured by the beam stop during the data collection and were removed from the refinement (1 1 0; 1 1 1; 1 1 -1; 0 3 0; 2 1 1).

There are two complete molecules in the asymmetric unit. An overlay of the two molecules shows that they have slightly different conformations in the crystal. The Add Sym routine in the program Platon [5] did not detect any additional or missed symmetry in the lattice.

With no heavier atoms in the crystal, the absolute structure was not well determined, the Flack parameter having an unreasonable final value of 0.4(10). Values were calculated for the related Hooft and Parson's parameters using the program Platon [5]. These values came out to -0.4(7) and -0.5(8), respectively. Both of these values lie closer to zero than do the same parameters calculated for the inverted structure, suggesting that this is the more correct packing arrangement to use.

1) APEX II (Bruker, 2008) Bruker AXS Inc., Madison, Wisconsin, USA.

2) SAINT (Bruker, 2008) Bruker AXS Inc., Madison, Wisconsin, USA.

3) SADABS (Bruker, 2009) Bruker AXS Inc., Madison, Wisconsin, USA.

4) Sheldrick, G.M. (2008) Acta Cryst., A64, 112-122; Sheldrick, G.M. (2015) Acta Cryst.,A71, 3-8; Sheldrick, G.M. (2015) Acta Cryst., C71, 3-8.

5) Spek, A. L. (2003). J. Appl. Cryst. 36, 7-13.

**Table A1.** Crystallographic Experimental Details for **2-9**

*A. Crystal Data*

| | |
|---|---|
| formula | $C_{33}H_{43}BN_2$ |
| formula weight | 478.50 |
| crystal dimensions (mm) | 0.34 × 0.09 × 0.07 |
| crystal system | triclinic |
| space group | $P\bar{1}$ (No. 2) |
| unit cell parameters[a] | |
| $a$ (Å) | 10.79160 (10) |
| $b$ (Å) | 15.6476 (2) |
| $c$ (Å) | 19.1459 (3) |
| $\alpha$ (deg) | 113.9745 (6) |
| $\beta$ (deg) | 90.0092 (7) |
| $\gamma$ (deg) | 93.4348 (7) |
| $V$ (Å$^3$) | 2947.73 (7) |
| $Z$ | 4 |
| $\rho_{calcd}$ (g cm$^{-3}$) | 1.078 |
| $\mu$ (mm$^{-1}$) | 0.459 |

*B. Data Collection and Refinement Conditions*

| | |
|---|---|
| diffractometer | Bruker D8/APEX II CCD[b] |
| radiation ($\lambda$ [Å]) | Cu K$\alpha$ (1.54178) (microfocus source) |
| temperature (°C) | –100 |
| scan type | $\omega$ and $\phi$ scans (1.0°) (5 s exposures) |
| data collection $2\theta$ limit (deg) | 144.42 |
| total data collected | 20770 (-10 ≤ $h$ ≤ 12, -19 ≤ $k$ ≤ 19, -23 ≤ $l$ ≤ 23) |
| independent reflections | 11229 ($R_{int}$ = 0.0158) |
| number of observed reflections (*NO*) | 9699 [$F_o^2 \geq 2\sigma(F_o^2)$] |
| structure solution method | intrinsic phasing (*SHELXT-2014*[c]) |
| refinement method | full-matrix least-squares on $F^2$ (*SHELXL–2014*[d]) |

| | |
|---|---|
| absorption correction method | Gaussian integration (face-indexed) |
| range of transmission factors | 0.9333–0.8233 |
| data/restraints/parameters | 11229 / 0 / 649 |
| goodness-of-fit ($S$)[e] [all data] | 1.041 |
| final $R$ indices[f] | |
| $R_1$ [$F_o^2 \geq 2\sigma(F_o^2)$] | 0.0382 |
| $wR_2$ [all data] | 0.1037 |
| largest difference peak and hole | 0.244 and –0.176 e Å$^{-3}$ |

[a]Obtained from least-squares refinement of 9917 reflections with $6.20° < 2\theta < 144.32°$.

[b]Programs for diffractometer operation, data collection, data reduction and absorption correction were those supplied by Bruker.

[c]Sheldrick, G. M. *Acta Crystallogr.* **2015**, *A71*, 3–8. (*SHELXT-2014*)

[d]Sheldrick, G. M. *Acta Crystallogr.* **2015**, *C71*, 3–8. (*SHELXL-2014*)

[e]$S = [\Sigma w(F_o^2 - F_c^2)^2/(n-p)]^{1/2}$ ($n$ = number of data; $p$ = number of parameters varied; $w = [\sigma^2(F_o^2) + (0.0507P)^2 + 0.6030P]^{-1}$ where $P = [\text{Max}(F_o^2, 0) + 2F_c^2]/3$).

[f]$R_1 = \Sigma||F_o| - |F_c||/\Sigma|F_o|$; $wR_2 = [\Sigma w(F_o^2 - F_c^2)^2/\Sigma w(F_o^4)]^{1/2}$.

**Table A2.** Crystallographic Experimental Details for **2-12**

*A. Crystal Data*

| | |
|---|---|
| formula | $C_{15}H_{28}BF_3N_2$ |
| formula weight | 304.20 |
| crystal dimensions (mm) | 0.32 × 0.19 × 0.16 |
| crystal system | orthorhombic |
| space group | *Pna*2$_1$ (No. 33) |
| unit cell parameters[a] | |
| $a$ (Å) | 12.6370 (5) |
| $b$ (Å) | 13.9619 (5) |
| $c$ (Å) | 9.6818 (4) |
| $V$ (Å$^3$) | 1708.22 (12) |
| $Z$ | 4 |
| $\rho_{calcd}$ (g cm$^{-3}$) | 1.183 |
| $\mu$ (mm$^{-1}$) | 0.091 |

*B. Data Collection and Refinement Conditions*

| | |
|---|---|
| diffractometer | Bruker PLATFORM/APEX II CCD[b] |
| radiation ($\lambda$ [Å]) | graphite-monochromated Mo K$\alpha$ (0.71073) |
| temperature (°C) | –80 |
| scan type | $\omega$ scans (0.3°) (15 s exposures) |
| data collection $2\theta$ limit (deg) | 56.66 |
| total data collected | 15632 (-16 ≤ $h$ ≤ 16, -18 ≤ $k$ ≤ 18, -12 ≤ $l$ ≤ 12) |

| | |
|---|---|
| independent reflections | 4229 ($R_{int}$ = 0.0272) |
| number of observed reflections (*NO*) | 3739 [$F_o^2 \geq 2\sigma(F_o^2)$] |
| structure solution method | direct methods/dual space (*SHELXD*[c]) |
| refinement method | full-matrix least-squares on $F^2$ (*SHELXL–2014*[d]) |
| absorption correction method | Gaussian integration (face-indexed) |
| range of transmission factors | 1.0000–0.9200 |
| data/restraints/parameters | 4229 / 0 / 191 |
| Flack absolute structure parameter[e] | 0.3(7) |
| goodness-of-fit (*S*)[f] [all data] | 1.057 |
| final *R* indices[g] | |
| $R_1$ [$F_o^2 \geq 2\sigma(F_o^2)$] | 0.0355 |
| $wR_2$ [all data] | 0.0938 |
| largest difference peak and hole | 0.151 and –0.144 e Å$^{-3}$ |

[a]Obtained from least-squares refinement of 7364 reflections with 4.34° < 2$\theta$ < 45.04°.

[b]Programs for diffractometer operation, data collection, data reduction and absorption correction were those supplied by Bruker.

[c]Schneider, T. R.; Sheldrick, G. M. *Acta Crystallogr.* **2002**, *D58*, 1772-1779.

[d]Sheldrick, G. M. *Acta Crystallogr.* **2015**, *C71*, 3–8.

[e]Flack, H. D. *Acta Crystallogr.* **1983**, *A39*, 876–881; Flack, H. D.; Bernardinelli, G. *Acta Crystallogr.* **1999**, *A55*, 908–915; Flack, H. D.; Bernardinelli, G. *J. Appl. Cryst.* **2000**, *33*, 1143–1148. The Flack parameter will refine to a value near zero if the structure is in the correct configuration and will refine to a value near one for the inverted configuration. The low anomalous scattering power of the atoms in this structure (none heavier than oxygen) implies that the data cannot be used for absolute structure assignment, thus the Flack parameter is provided for informational purposes only.

w=1/[\s^2^(Fo^2^)+(0.0462P)^2^+0.1799P]

[f]$S = [\Sigma w(F_o^2 - F_c^2)^2/(n-p)]^{1/2}$ ($n$ = number of data; $p$ = number of parameters varied; $w = [\sigma^2(F_o^2) + (0.0462P)^2 + 0.1799P]^{-1}$ where $P = [\mathrm{Max}(F_o^2, 0) + 2F_c^2]/3$).

[g]$R_1 = \Sigma||F_o| - |F_c||/\Sigma|F_o|$; $wR_2 = [\Sigma w(F_o^2 - F_c^2)^2/\Sigma w(F_o^4)]^{1/2}$.

**Table A3.** Crystallographic Experimental Details for **2-6**

*A. Crystal Data*

| | |
|---|---|
| formula | $C_{15}H_{31}BN_2$ |
| formula weight | 250.23 |
| crystal dimensions (mm) | 0.28 × 0.14 × 0.07 |
| crystal system | orthorhombic |
| space group | *Fdd*2 (No. 43) |
| unit cell parameters[a] | |
| *a* (Å) | 19.1093 (9) |
| *b* (Å) | 21.6601 (10) |

| | |
|---|---|
| $c$ (Å) | 8.1721 (4) |
| $V$ (Å$^3$) | 3382.5 (3) |
| $Z$ | 8 |
| $\rho_{calcd}$ (g cm$^{-3}$) | 0.983 |
| $\mu$ (mm$^{-1}$) | 0.415 |

*B. Data Collection and Refinement Conditions*

| | |
|---|---|
| diffractometer | Bruker D8/APEX II CCD[b] |
| radiation ($\lambda$ [Å]) | Cu K$\alpha$ (1.54178) (microfocus source) |
| temperature (°C) | –100 |
| scan type | $\omega$ and $\phi$ scans (1.0°) (5 s exposures) |
| data collection 2$\theta$ limit (deg) | 148.24 |
| total data collected | 5811 (-18 ≤ $h$ ≤ 22, -26 ≤ $k$ ≤ 26, -10 ≤ $l$ ≤ 10) |
| independent reflections | 1661 ($R_{int}$ = 0.0803) |
| number of observed reflections (*NO*) | 1416 [$F_o^2 \geq 2\sigma(F_o^2)$] |
| structure solution method | intrinsic phasing (*SHELXT-2014*[c]) |
| refinement method | full-matrix least-squares on $F^2$ (*SHELXL–2014*[d]) |
| absorption correction method | Gaussian integration (face-indexed) |
| range of transmission factors | 1.0000–0.7478 |
| data/restraints/parameters | 1661 / 0 / 86 |
| extinction coefficient ($x$)[e] | 0.0011(3) |
| Flack absolute structure parameter[f] | 0.3(10) |
| goodness-of-fit ($S$)[g] [all data] | 1.036 |
| final $R$ indices[h] | |
| $R_1$ [$F_o^2 \geq 2\sigma(F_o^2)$] | 0.0528 |
| $wR_2$ [all data] | 0.1381 |
| largest difference peak and hole | 0.275 and –0.170 e Å$^{-3}$ |

[a]Obtained from least-squares refinement of 6923 reflections with 12.34° < 2$\theta$ < 147.02°.

[b]Programs for diffractometer operation, data collection, data reduction and absorption correction were those supplied by Bruker.

[c]Sheldrick, G. M. *Acta Crystallogr.* **2015**, *A71*, 3–8.

[d]Sheldrick, G. M. *Acta Crystallogr.* **2015**, *C71*, 3–8.

[e]$F_c^* = kF_c[1 + x\{0.001F_c^2\lambda^3/\sin(2\theta)\}]^{-1/4}$ where $k$ is the overall scale factor.

[f]Flack, H. D. *Acta Crystallogr.* **1983**, *A39*, 876–881; Flack, H. D.; Bernardinelli, G. *Acta Crystallogr.* **1999**, *A55*, 908–915; Flack, H. D.; Bernardinelli, G. *J. Appl. Cryst.* **2000**, *33*, 1143–1148. The Flack parameter will refine to a value near zero if the structure is in the correct configuration and will refine to a value near one for the inverted configuration. The low anomalous scattering power of the atoms in this structure (none heavier than nitrogen) implies that the data cannot be used for absolute structure assignment, thus the Flack parameter is provided for informational purposes only.

[g] $S = [\Sigma w(F_o^2 - F_c^2)^2/(n-p)]^{1/2}$ ($n$ = number of data; $p$ = number of parameters varied; $w = [\sigma^2(F_o^2) + (0.0823P)^2]^{-1}$ where $P = [\mathrm{Max}(F_o^2, 0) + 2F_c^2]/3$).

[h] $R_1 = \Sigma||F_o| - |F_c||/\Sigma|F_o|$; $wR_2 = [\Sigma w(F_o^2 - F_c^2)^2/\Sigma w(F_o^4)]^{1/2}$.

**Table A4.** Crystal data and structure refinement for **2-7**.

| | | |
|---|---|---|
| Empirical formula | $C_{27}H_{51}BN_2$ | |
| Formula weight | 414.50 | |
| Temperature | 125(2) K | |
| Wavelength | 0.71073 Å | |
| Crystal system | Orthorhombic | |
| Space group | $Pca2_1$ | |
| Unit cell dimensions | $a$ = 15.4035(17) Å | $\alpha$ = 90° |
| | $b$ = 29.345(3) Å | $\beta$ = 90° |
| | $c$ = 11.9961(13) Å | $\gamma$ = 90° |
| Volume | 5422.4(10) $Å^3$ | |
| $Z$ | 8 | |
| Density (calculated) | 1.015 $Mg/m^3$ | |
| Absorption coefficient | 0.057 $mm^{-1}$ | |
| F(000) | 1856 | |
| Crystal size | 0.420 x 0.320 x 0.200 $mm^3$ | |
| Theta range for data collection | 1.388 to 28.934° | |
| Index ranges | -20<=h<=20, -39<=k<=39, -16<=l<=15 | |
| Reflections collected | 64427 | |
| Independent reflections | 13523 [R(int) = 0.0503] | |
| Completeness to theta = 25.242° | 99.9 % | |
| Absorption correction | Semi-empirical from equivalents | |
| Max. and min. transmission | 0.7458 and 0.6216 | |
| Refinement method | Full-matrix least-squares on $F^2$ | |
| Data / restraints / parameters | 13523 / 1 / 563 | |
| Goodness-of-fit on $F^2$ | 1.011 | |
| Final R indices [I>2sigma(I)] | R1 = 0.0480, wR2 = 0.1076 | |
| R indices (all data) | R1 = 0.0740, wR2 = 0.1208 | |
| Absolute structure parameter | -0.9(8) | |
| Extinction coefficient | n/a | |
| Largest diff. peak and hole | 0.272 and -0.169 e.$Å^{-3}$ | |

## A2: NMR Spectra for Chapter 2

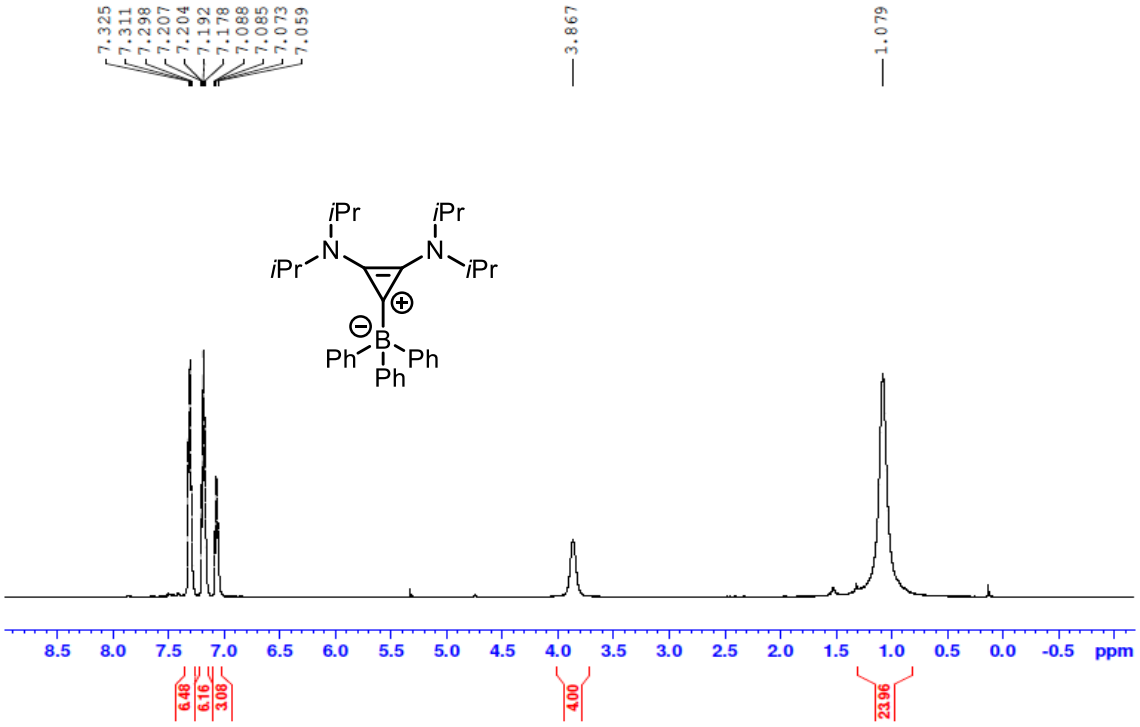


**Figure A1:** $^{1}$H NMR (500 MHz, $CDCl_3$) spectrum of *i*PrBAC-$BPh_3$ **2-9**.

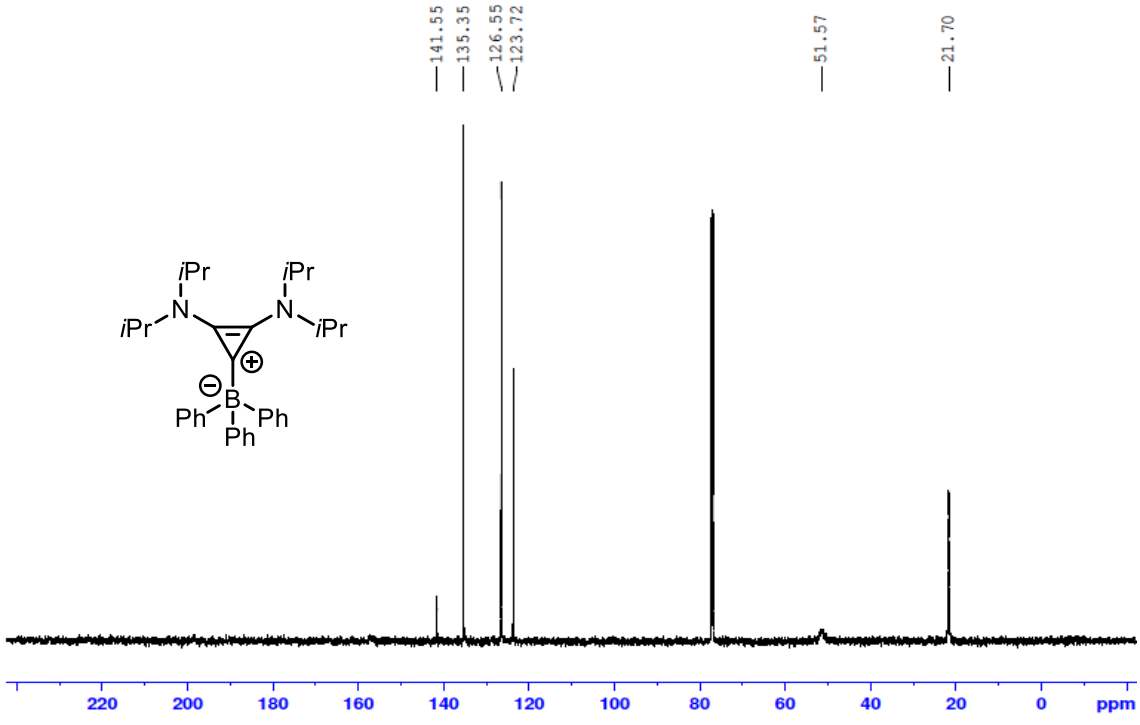


**Figure A2:** $^{13}$C {$^{1}$H} NMR (125.8 MHz, $CDCl_3$) spectrum of *i*PrBAC-$BPh_3$ **2-9**.

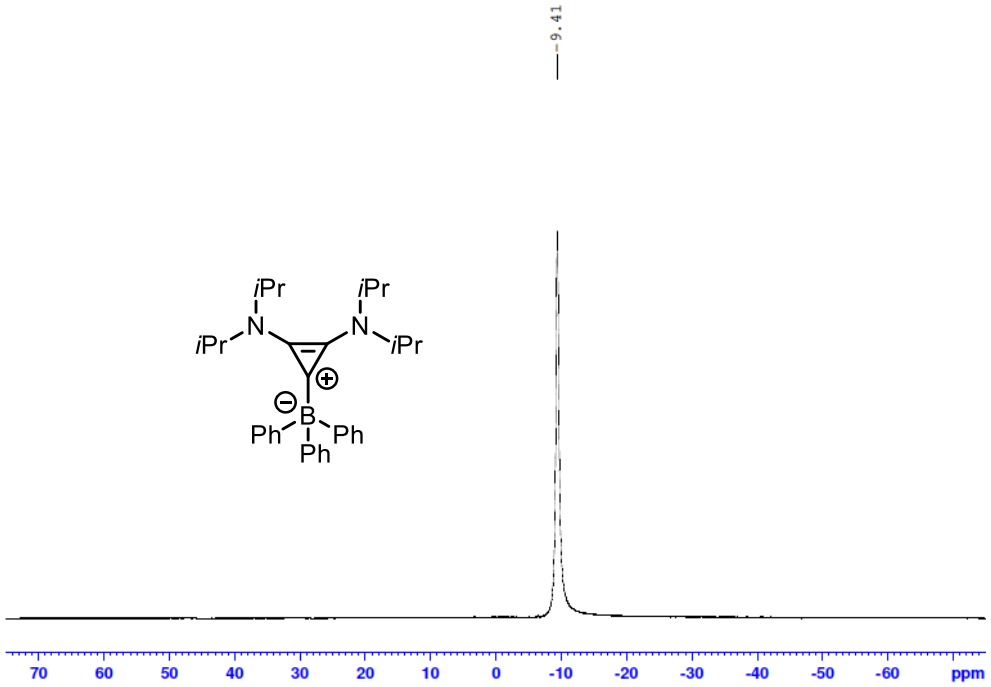


**Figure A3:** $^{11}$B NMR (160.5 MHz, $CDCl_3$) spectrum of *i*PrBAC-$BPh_3$ **2-9**.

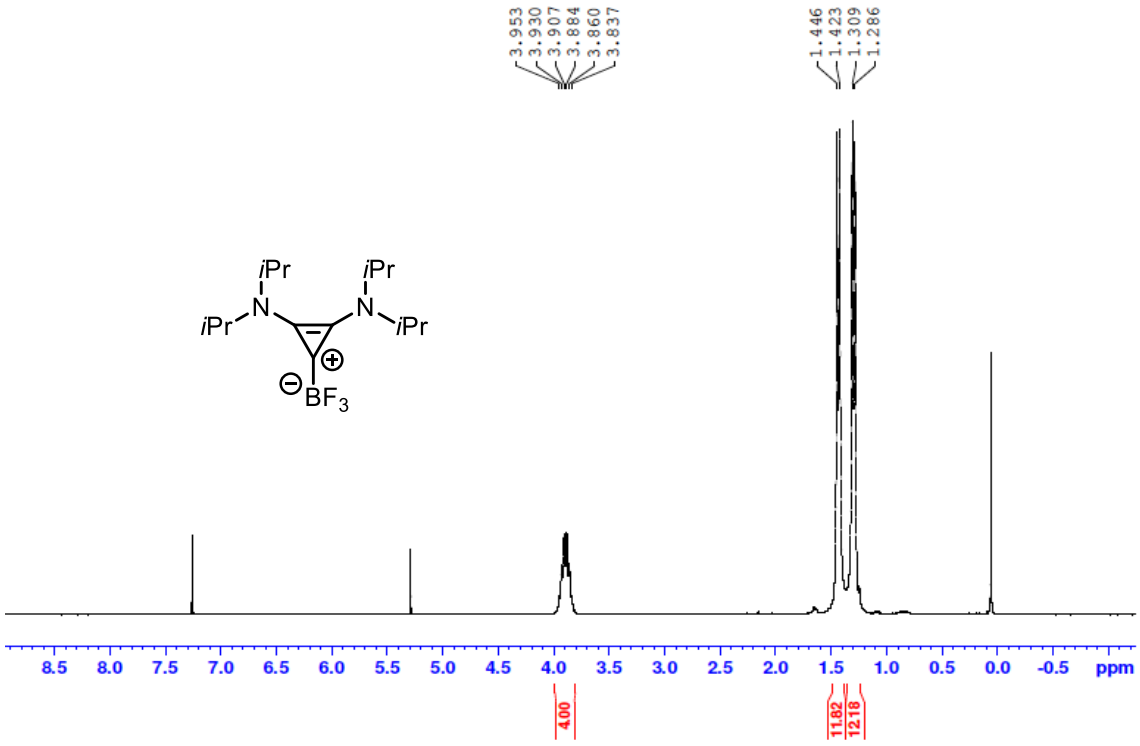


**Figure A4:** $^{1}$H NMR (300 MHz, $CDCl_3$) spectrum of *i*PrBAC-$BF_3$ **2-12**.

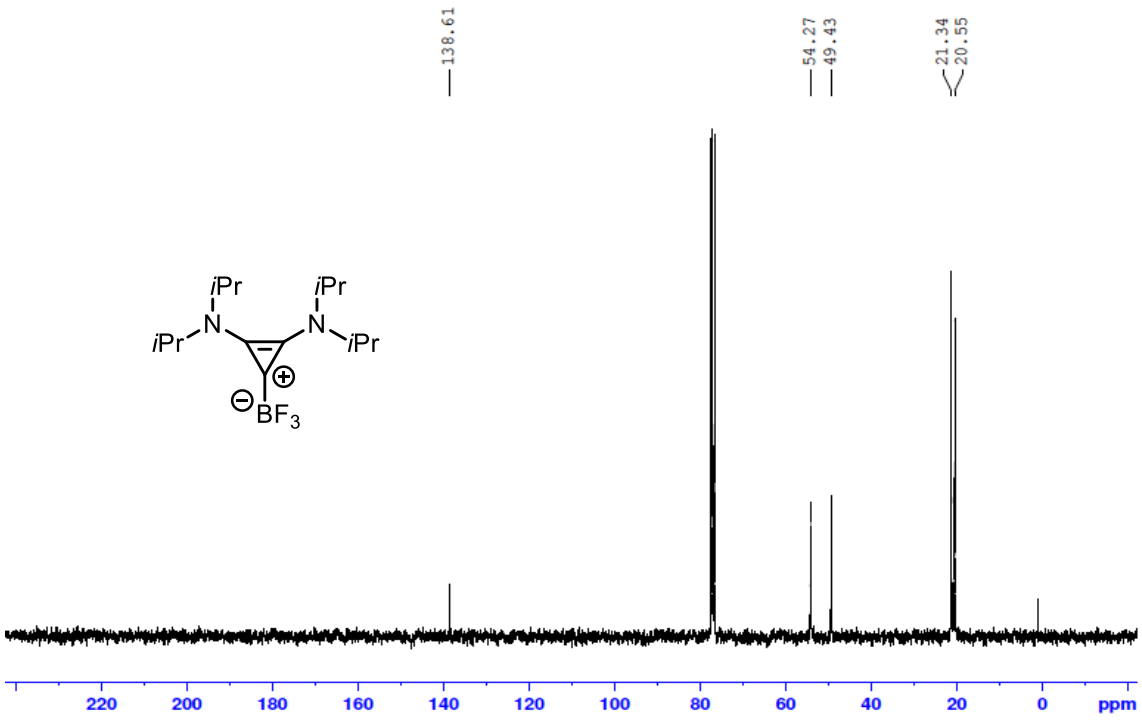


**Figure A5:** $^{13}C$ {$^{1}H$} NMR (75.5 MHz, $CDCl_3$) spectrum of *i*PrBAC-$BF_3$ **2-12**.

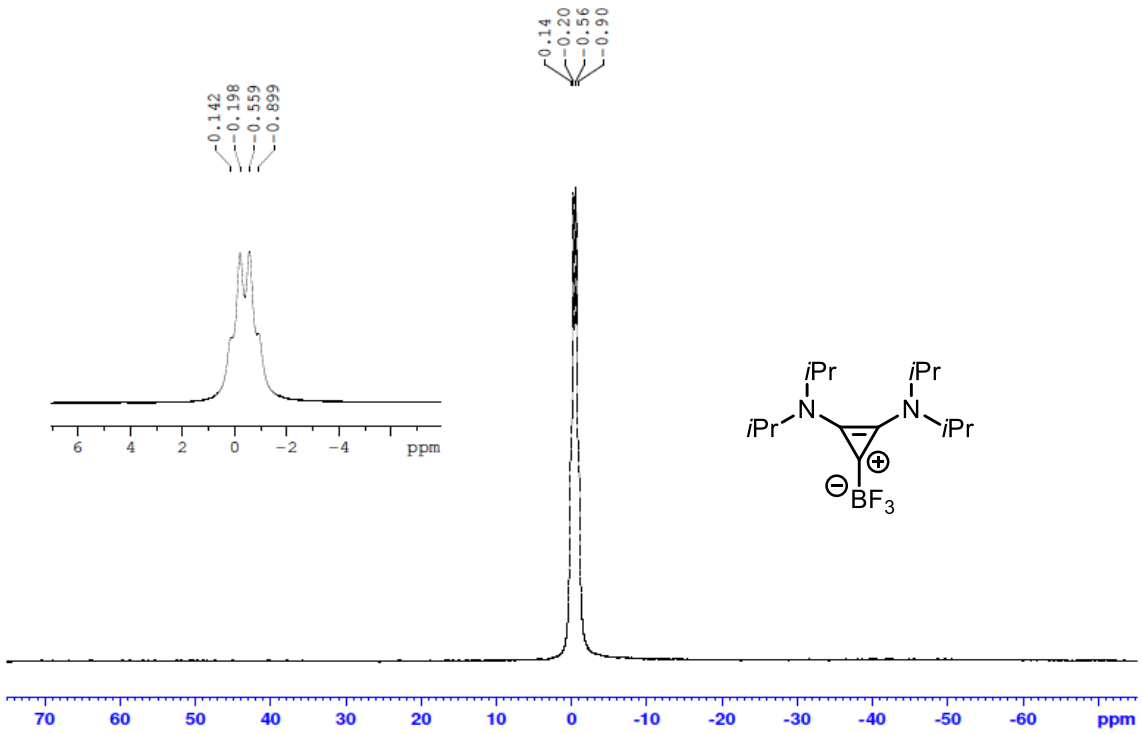


**Figure A6:** $^{11}B$ NMR (96.3 MHz, $CDCl_3$) spectrum of *i*PrBAC-$BF_3$ **2-12**.

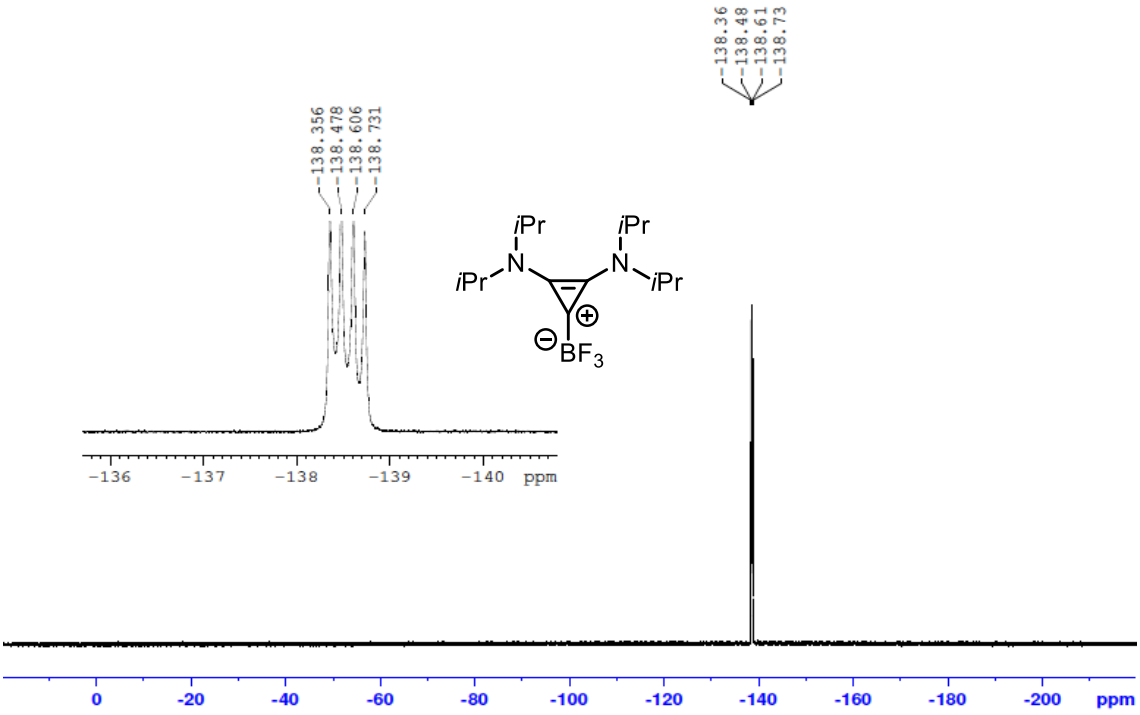


**Figure A7:** $^{19}$F NMR (282.4 MHz, $CDCl_3$) spectrum of *i*PrBAC-$BF_3$ **2-12**.

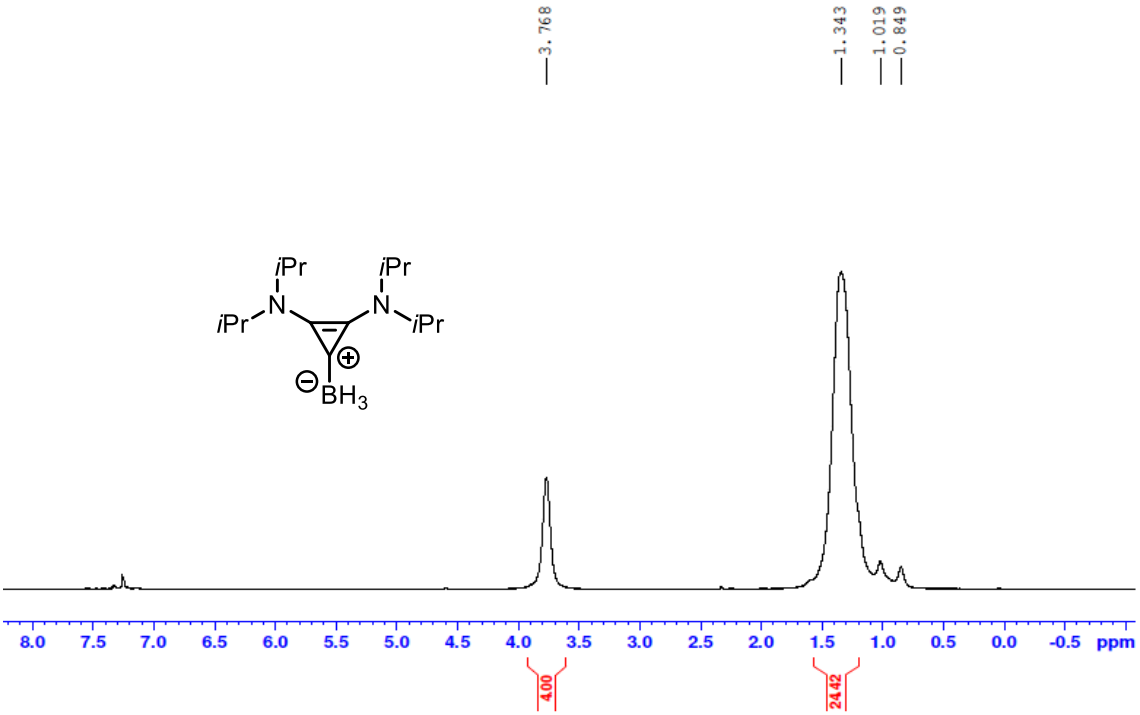


**Figure A8:** $^{1}$H NMR (500 MHz, $CDCl_3$) spectrum of *i*PrBAC-$BH_3$ **2-6**.

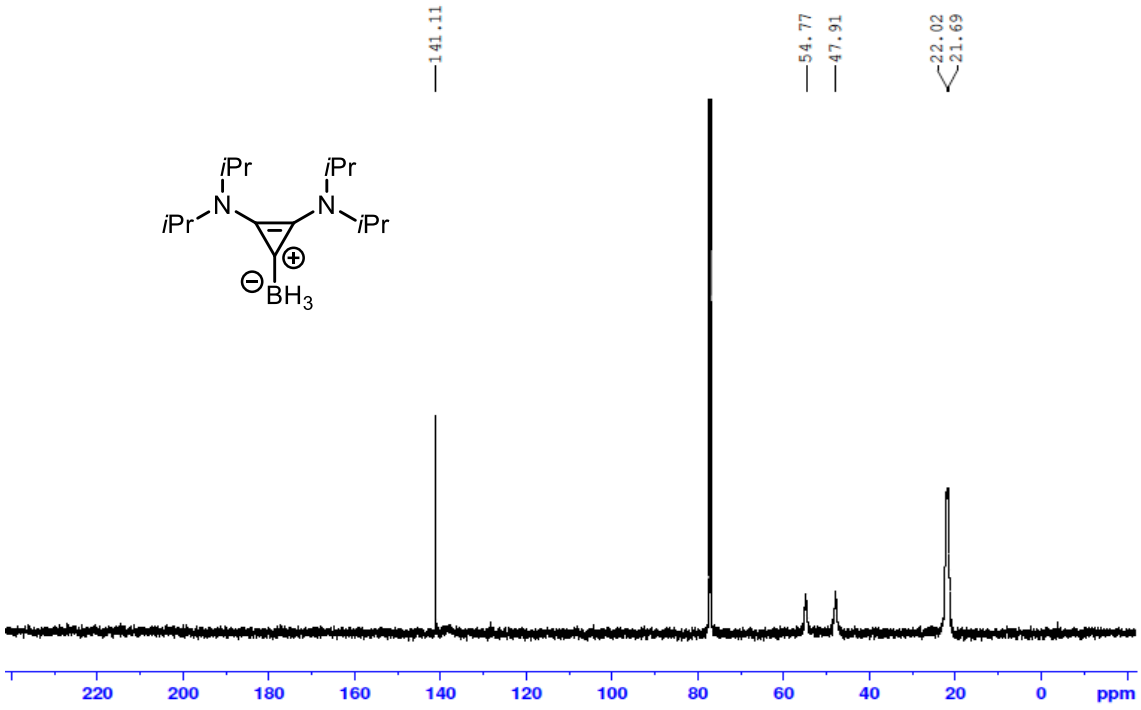


**Figure A9:** $^{13}C$ {$^{1}H$} NMR (125.8 MHz, $CDCl_3$) spectrum of *i*PrBAC-$BH_3$ **2-6**.

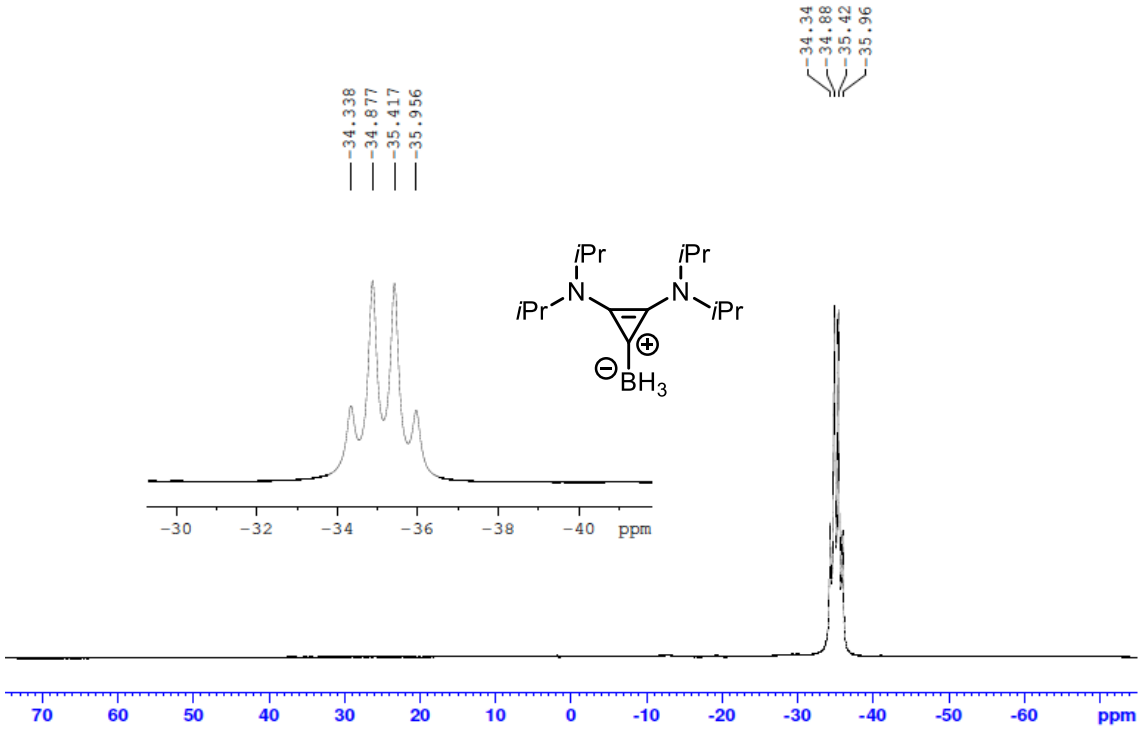


**Figure A10:** $^{11}B$ NMR (160.5 MHz, $CDCl_3$) spectrum of *i*PrBAC-$BH_3$ **2-6**

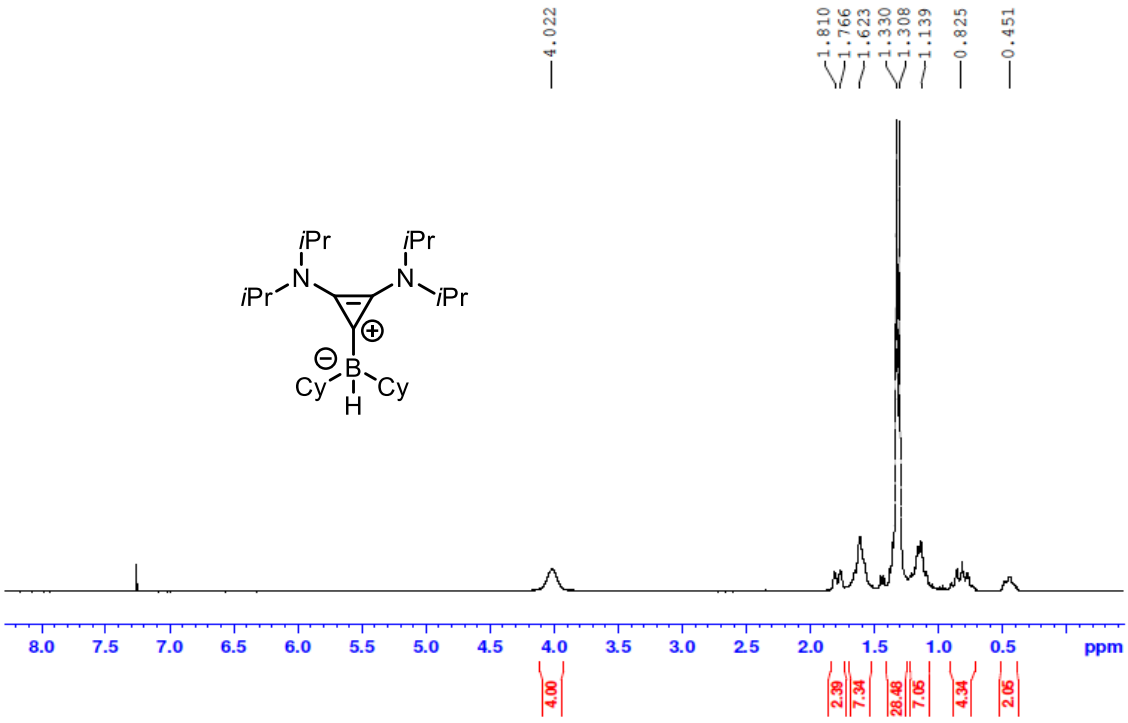


**Figure A11:** $^{1}$H NMR (300 MHz, $CDCl_3$) spectrum of *i*PrBAC-BCy$_2$H **2-7**.

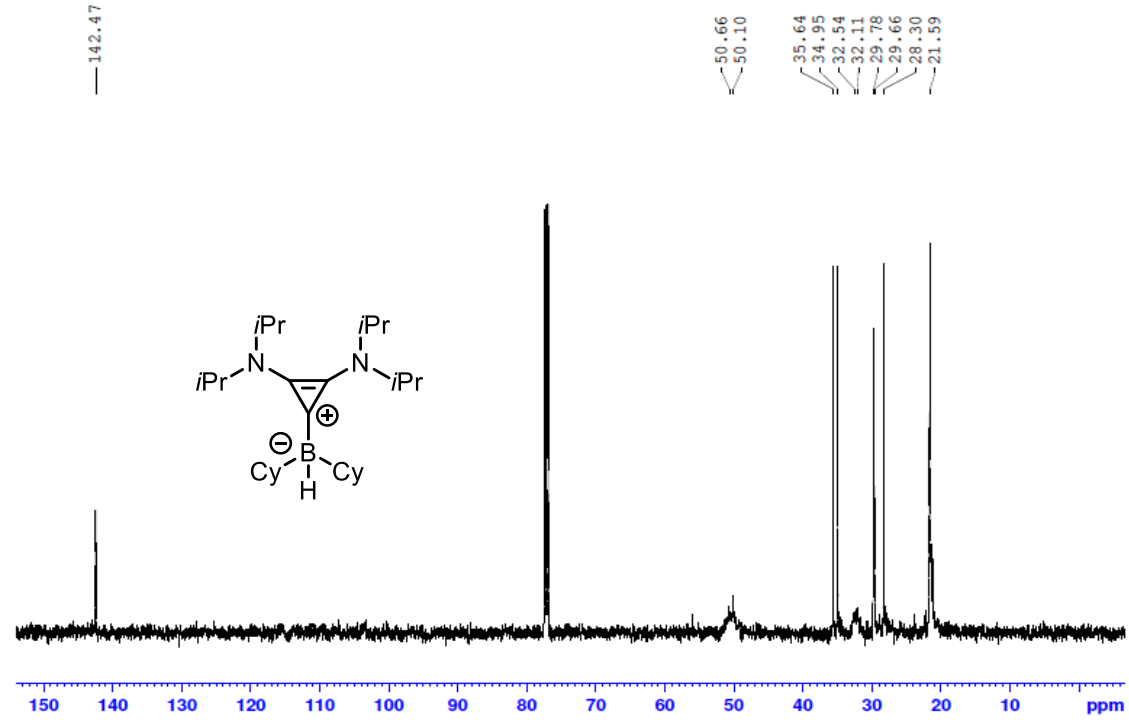


**Figure A12:** $^{13}$C {$^{1}$H} NMR (125.8 MHz, $CDCl_3$) spectrum of *i*PrBAC-BCy$_2$H **2-7**.

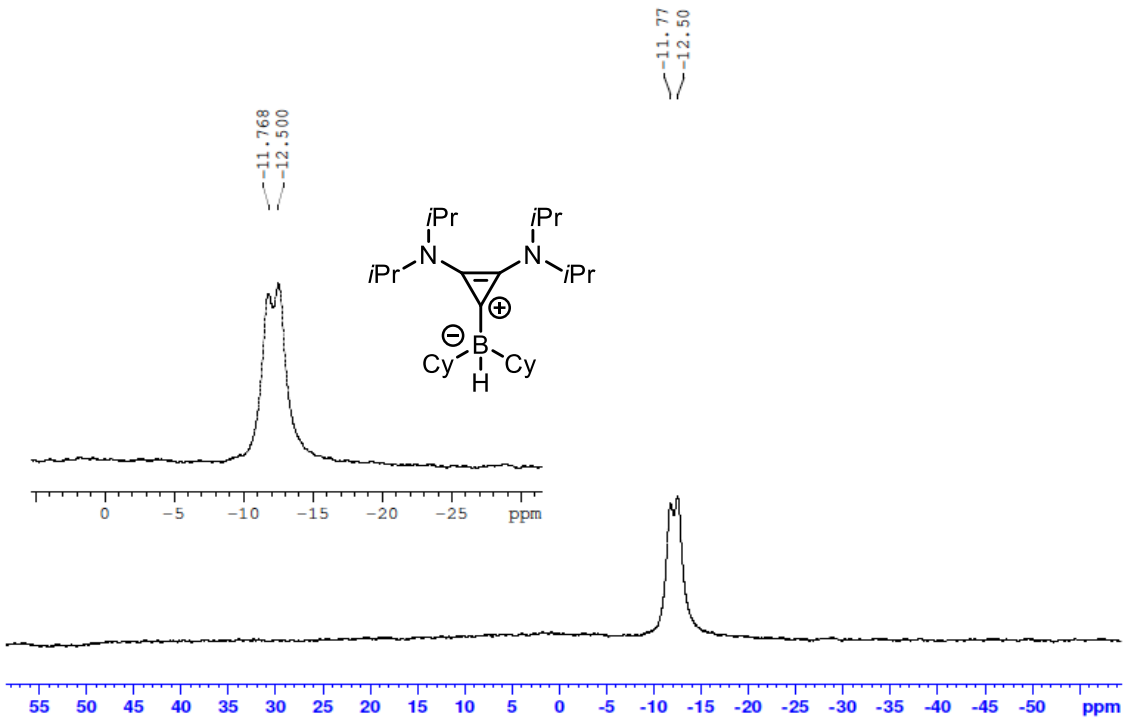


**Figure A13:** $^{11}$B NMR (96.3 MHz, $CDCl_3$) spectrum of *i*PrBAC-BCy$_2$H **2-7**.

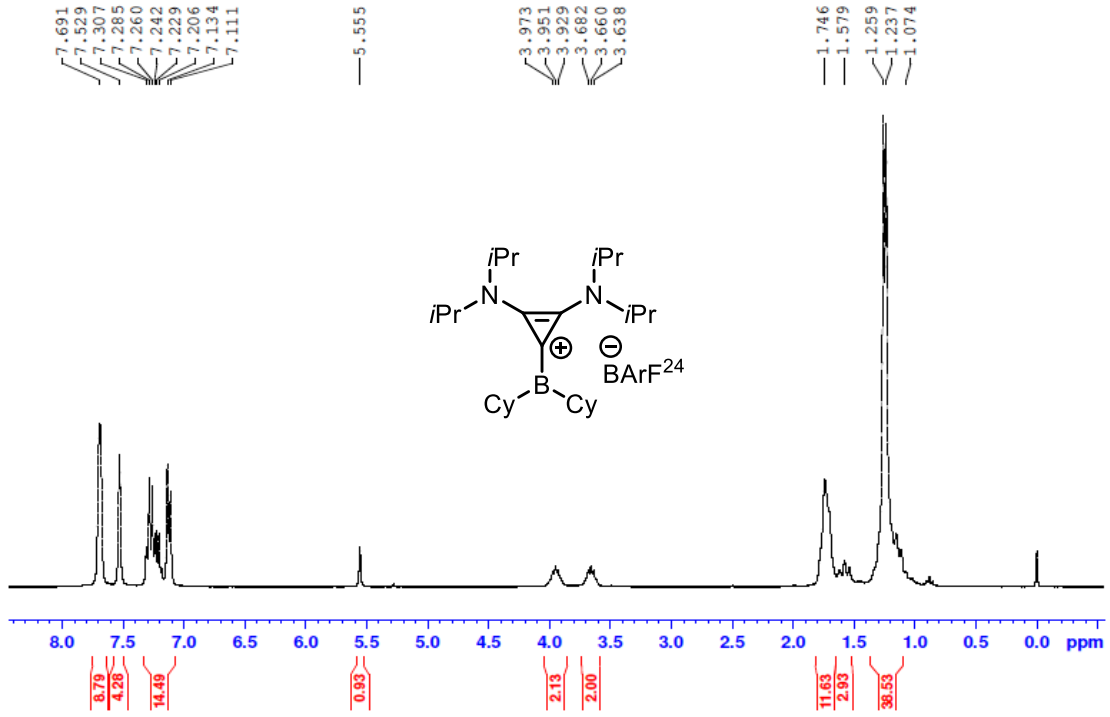


**Figure A14:** $^{1}$H NMR (300 MHz, $CDCl_3$) spectrum borenium ion *i*PrBAC-BCy$_2$H **2-20** generated from **2-7** and **2-19**.

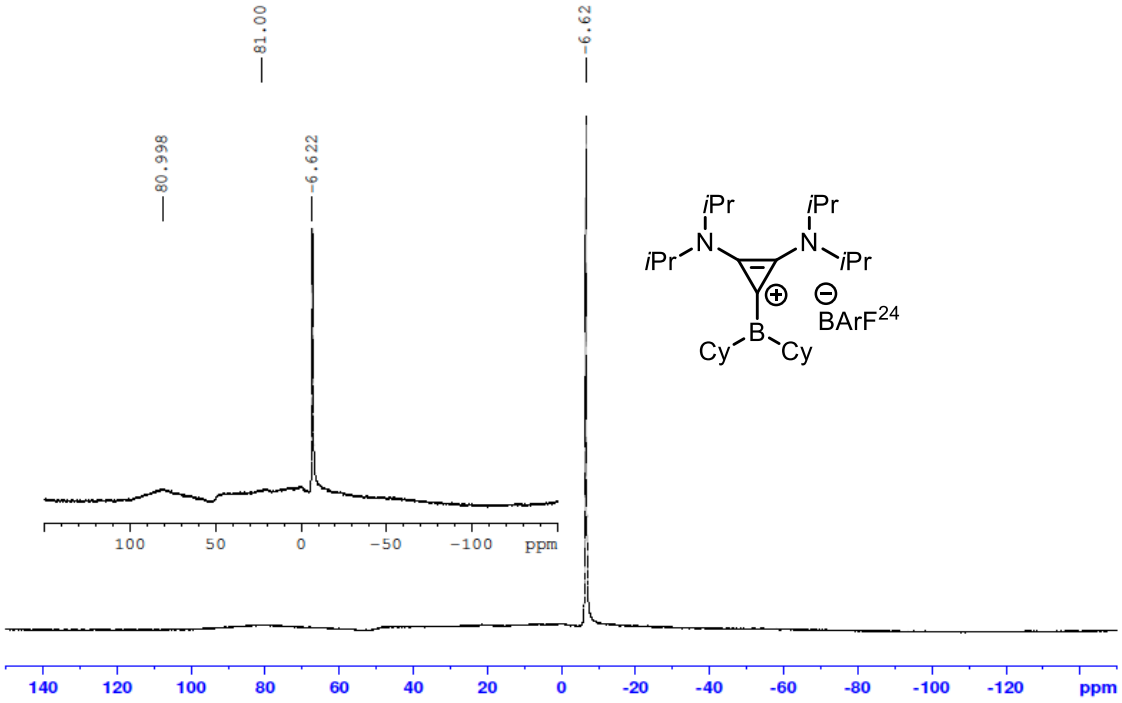


**Figure A15:** $^{11}$B NMR (96.3 MHz, $CDCl_3$) spectrum borenium ion *i*PrBAC-B$Cy_2$H **2-20** generated from **2-7** and **2-19**.

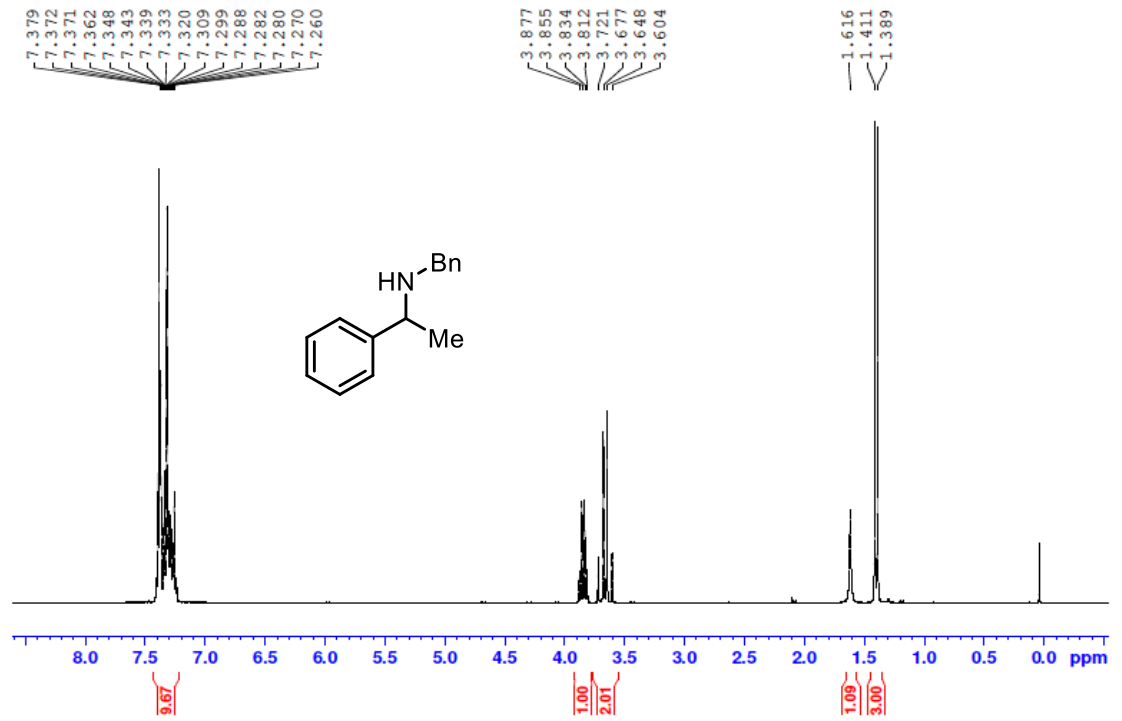


**Figure A16:** $^{1}$H NMR (300 MHz, $CDCl_3$) spectrum of *N*-Benzyl(1-phenethyl)amine **2-22**

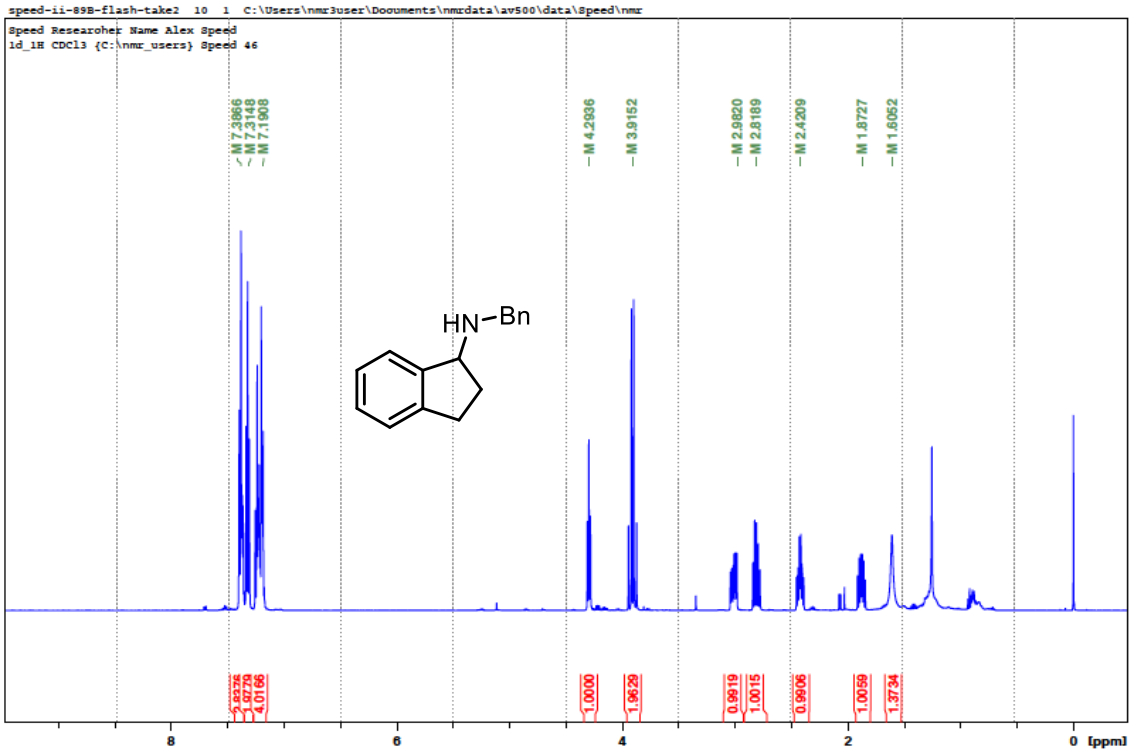


**Figure A17:** $^{1}$H NMR (300 MHz, $CDCl_3$) spectrum of *N*-benzyl-1-aminoindan **2-24**.

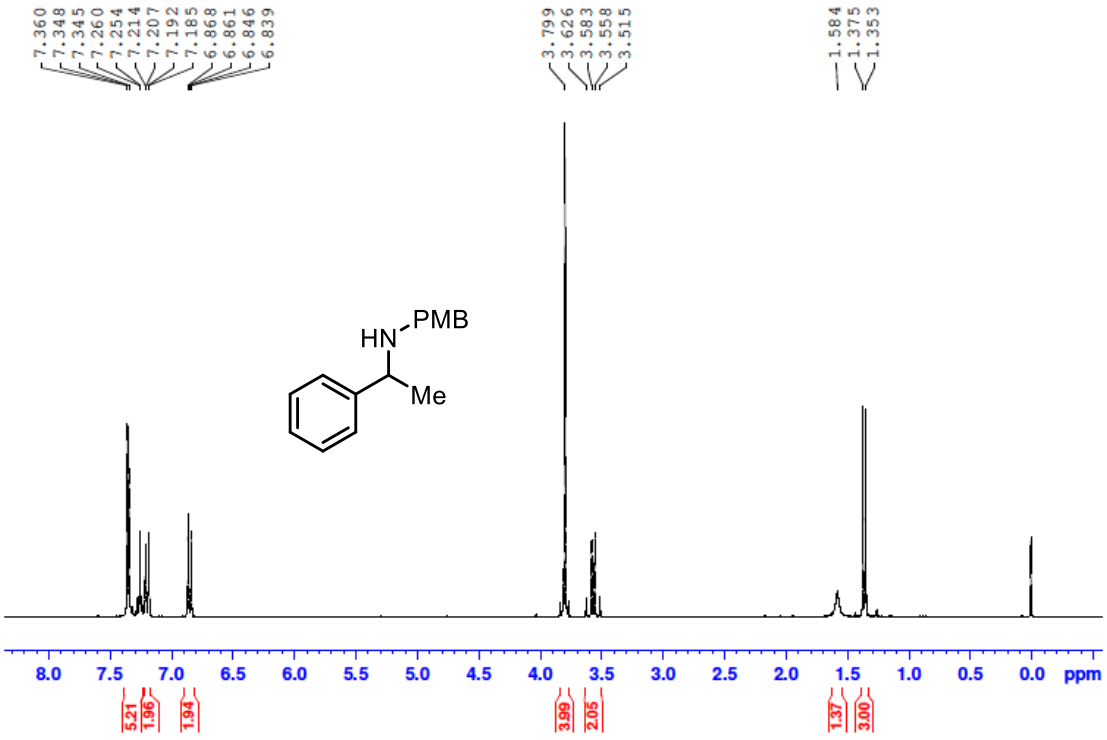


**Figure A18:** $^{1}$H NMR (300 MHz, $CDCl_3$) spectrum of *N*-4-methoxybenzyl(1-phenethyl)amine **2-26**.

## Appendix B: Appendix for Chapter 3

### B1: Crystallographic Solution and Refinement Details

Crystallographic data for **3-23.** The crystal chosen was attached to the tip of a MicroLoop with paratone-N oil. Measurements were made on a Bruker APEXII CCD equipped diffractometer (30 mA, 50 kV) using monochromated Mo Kα radiation (λ = 0.71073 Å) at 125 K [1]. The initial orientation and unit cell were indexed using a least-squares analysis of a random set of reflections collected from three series of 0.5° ω-scans, 10 seconds per frame and 12 frames per series, that were well distributed in reciprocal space. For data collection, four ω-scan frame series were collected with 0.5° wide scans, 30 second frames and 366 frames per series at varying φ angles (φ = 0°, 90°, 180° and 270°). The crystal to detector distance was set to 6 cm and a complete sphere of data was collected. Cell refinement and data reduction were performed with the Bruker SAINT [2] software, which corrects for beam inhomogeneity, possible crystal decay, Lorentz and polarisation effects. A multi-scan absorption correction was applied (SADABS [3]). The structure was solved using SHELXT-2014 [4] and was refined using a full-matrix least-squares method on $F^2$ with SHELXL-2018 [4]. The initial refinement was unremarkable. The non-hydrogen atoms were refined anisotropically. The hydrogen atoms bonded to carbon were included at geometrically idealized positions and were not refined. The isotropic thermal parameters of these hydrogen atoms were fixed at $1.2U_{eq}$ of the parent carbon atom or $1.5U_{eq}$ for methyl hydrogens.

There was some minor disorder in the structure, involving one of the N(*i*Pr)$_2$ groups. The heavy atoms involved were each split over two positions with the occupancies of the two parts refined (to a total of 100%). A SAME instruction was used in Shelxl to add restraints to keep the geometries of the two parts similar. The disordered heavy atoms were all

restrained to have similar thermal parameters. The C-C bonds in the disordered group were restrained to 1.51 (0.015) Å, while the bond lengths N2A-C3 and N2B-C3 were restrained to be similar. In addition, RIGU was used on the disordered group to add enhanced rigid bond restraints to the atomic displacement parameters for 1,2- and 1,3- heavy atom pairs. The occupancies of the disordered group refined to 88.1(4)/11.9% for part 1 and part 2, respectively.

Using a disordered model for the structure resulted in a checkcif file with several more warnings (and of higher level) than had been obtained with the original unsplit results (these are available if you want to use them). Of primary concern is the level B warning that is obtained with the split model:

Short Intermolecular Interaction H27…H15E = 1.91 Ang.

This interaction arises between a phenyl ring of the main molecule and one of the methyl protons in the second (minor) part of the disordered group on a second molecule. Since this methyl position is occupied only a small fraction of the time, it is unlikely to be of serious concern in the overall stability of the system. Overall, the split model is to be preferred as it results in better statistical parameters than the unsplit refinement.

The Flack parameter refined to a final value of 0.25(14). This result was supported by values calculated for the Hooft and Parson's parameters using the program Platon [5]. These values came out to 0.20(13) and 0.23(14), respectively. The result is likely slightly unreliable (owing to the lack of heavier atoms in the structure) and likely not an indication of racemic twinning being present in the crystal.

Crystallographic data for **3-6.** The crystal chosen was attached to the tip of a MicroLoop with paratone-N oil. Measurements were made on a Bruker APEXII CCD equipped diffractometer (30 mA, 50 kV) using monochromated Mo Kα radiation (λ = 0.71073 Å) at

125 K [1]. The initial orientation and unit cell were indexed using a least-squares analysis of a random set of reflections collected from three series of 0.5° ω-scans, 10 seconds per frame and 12 frames per series, that were well distributed in reciprocal space. For data collection, four ω-scan frame series were collected with 0.5° wide scans, 30 second frames and 366 frames per series at varying φ angles (φ = 0°, 90°, 180° and 270°). The crystal to detector distance was set to 6 cm and a complete sphere of data was collected. Cell refinement and data reduction were performed with the Bruker SAINT [2] software, which corrects for beam inhomogeneity, possible crystal decay, Lorentz and polarisation effects. A multi-scan absorption correction was applied (SADABS [3]). The structure was solved using SHELXT-2014 [4] and was refined using a full-matrix least-squares method on $F^2$ with SHELXL-2018 [4]. The initial refinement was unremarkable. The non-hydrogen atoms were refined anisotropically. The hydrogen atoms bonded to carbon were included at geometrically idealized positions and were not refined. The isotropic thermal parameters of these hydrogen atoms were fixed at $1.2U_{eq}$ of the parent carbon atom or $1.5U_{eq}$ for methyl hydrogens. The hydrogen atom bonded to boron was located in a near final Fourier difference map. Its position was refined, while its isotropic thermal parameter was fixed at 1.5 times that of the boron atom to which it was bonded.

There was some minor disorder in the structure, involving one of the N(*i*Pr)$_2$ groups. The heavy atoms involved were each split over two positions with the occupancies of the two parts refined (to a total of 100%). A SAME instruction was used in Shelxl to add restraints to keep the geometries of the two parts similar. The carbon atoms of the ring were restrained to have similar thermal parameters, as were N2A and N2B. The C-C bonds in the disordered group were restrained to 1.51 (0.015) Å, while the bond lengths N2A-C3 and N2B-C3 were restrained to be similar. In addition, RIGU was used on the disordered group to add

enhanced rigid bond restraints to the atomic displacement parameters for 1,2- and 1,3-heavy atom pairs. The occupancies of the disordered group refined to 87.4(6)/12.6% for part 1 and part 2, respectively.

Using a disordered model for the structure resulted in a checkcif file with several more warnings (and of higher level) than had been obtained with the original unsplit results (these are available if you want to use them). Of primary concern is the level B warning that is obtained with the split model:

Short Intermolecular Interaction H23 ..H15F = 1.95 Ang.

This interaction arises between a phenyl ring of the main molecule and one of the methyl protons in the second (minor) part of the disordered group on a second molecule. Since this methyl position is occupied only a small fraction of the time, it is unlikely to be of serious concern in the overall stability of the system. Overall, the split model is to be preferred as it results in better statistical parameters than the unsplit refinement.

The absolute structure could not be reliably determined, the Flack parameter having a final value of -2.0(10). This result was supported by values calculated for the Hooft and Parson's parameters using the program Platon [5]. These values came out to -1.0(7) and -1.8(12), respectively. The lack of heavier atoms in the structure and the use of Mo radiation made calculations based on the anomalous scattering in the crystal ambiguous.

Crystallographic data for **3-24**. The crystal chosen was attached to the tip of a MicroLoop with paratone-N oil. Measurements were made on a Bruker APEXII CCD equipped diffractometer (30 mA, 50 kV) using monochromated Mo Kα radiation (λ = 0.71073 Å) at 125 K [1]. The initial orientation and unit cell were indexed using a least-squares analysis of a random set of reflections collected from three series of 0.5° ω-scans, 10 seconds per frame and 12 frames per series, that were well distributed in reciprocal space. For data

collection, four ω-scan frame series were collected with 0.5° wide scans, 45 second frames and 366 frames per series at varying φ angles (φ = 0°, 90°, 180° and 270°). The crystal to detector distance was set to 6 cm and a complete sphere of data was collected. Cell refinement and data reduction were performed with the Bruker SAINT [2] software, which corrects for beam inhomogeneity, possible crystal decay, Lorentz and polarisation effects. A multi-scan absorption correction was applied (SADABS [3]). The structure was solved using SHELXT-2014 [4] and was refined using a full-matrix least-squares method on $F^2$ with SHELXL-2018 [4]. The initial refinement was unremarkable. The non-hydrogen atoms were refined anisotropically. The hydrogen atoms bonded to carbon were included at geometrically idealized positions and were not refined. The isotropic thermal parameters of these hydrogen atoms were fixed at $1.2U_{eq}$ of the parent carbon atom or $1.5U_{eq}$ for methyl hydrogens.

One reflection (0 0 -1) was found to have been partially obscured by the beam stop during the data collection and was removed from the refinement.

This compound crystallized in the space group P1 with two complete molecules in the asymmetric unit. Because of low coverage the absolute structure was not well determined, the Flack parameter having a final value of 0.04(4). This result was supported by values calculated for the Hooft and Parson's parameters using the program Platon [5]. These values came out to 0.03(4) and 0.04(4), respectively. That all of the values lie close to zero does suggest that the absolute structure is correct as given in these results.


1) APEX II (Bruker, 2008) Bruker AXS Inc., Madison, Wisconsin, USA.
2) SAINT (Bruker, 2008) Bruker AXS Inc., Madison, Wisconsin, USA.
3) SADABS (Bruker, 2009) Bruker AXS Inc., Madison, Wisconsin, USA.

4) Sheldrick, G.M. (2008) *Acta Cryst*., A64, 112-122; Sheldrick, G.M. (2015) *Acta Cryst*., A71, 3-8; Sheldrick, G.M. (2015) *Acta Cryst*., C71, 3-8.

5) Spek, A. L. (2003). J. Appl. Cryst. 36, 7-13.

**Table A5.** Crystal data and structure refinement for **3-23**.

| | | |
|---|---|---|
| Empirical formula | $C_{27}H_{38}BFN_2$ | |
| Formula weight | 420.40 | |
| Temperature | 125(2) K | |
| Wavelength | 0.71073 Å | |
| Crystal system | Orthorhombic | |
| Space group | $Pna2_1$ | |
| Unit cell dimensions | $a$ = 17.3954(17) Å | $\alpha$ = 90° |
| | $b$ = 9.9115(10) Å | $\beta$ = 90° |
| | $c$ = 14.4462(14) Å | $\gamma$ = 90° |
| Volume | 2490.7(4) $Å^3$ | |
| $Z$ | 4 | |
| Density (calculated) | 1.121 $Mg/m^3$ | |
| Absorption coefficient | 0.069 $mm^{-1}$ | |
| F(000) | 912 | |
| Crystal size | 0.520 x 0.450 x 0.350 $mm^3$ | |
| Theta range for data collection | 2.342 to 28.960° | |
| Index ranges | -23<=h<=22, -13<=k<=12, -19<=l<=19 | |
| Reflections collected | 28896 | |
| Independent reflections | 6214 [R(int) = 0.0192] | |
| Completeness to theta = 25.242° | 100.0 % | |
| Absorption correction | Semi-empirical from equivalents | |
| Max. and min. transmission | 0.7458 and 0.7074 | |
| Refinement method | Full-matrix least-squares on $F^2$ | |
| Data / restraints / parameters | 6214 / 250 / 352 | |
| Goodness-of-fit on $F^2$ | 1.041 | |
| Final R indices [I>2sigma(I)] | R1 = 0.0324, wR2 = 0.0835 | |
| R indices (all data) | R1 = 0.0354, wR2 = 0.0857 | |
| Absolute structure parameter | 0.25(14) | |
| Extinction coefficient | n/a | |
| Largest diff. peak and hole | 0.245 and -0.156 e.$Å^{-3}$ | |

**Table A6.** Crystal data and structure refinement for **3-6**.

| | | |
|---|---|---|
| Empirical formula | $C_{27}H_{39}BN_2$ | |
| Formula weight | 402.41 | |
| Temperature | 125(2) K | |
| Wavelength | 0.71073 Å | |
| Crystal system | Orthorhombic | |
| Space group | $Pna2_1$ | |
| Unit cell dimensions | $a$ = 17.467(4) Å | $\alpha$ = 90° |
| | $b$ = 9.736(2) Å | $\beta$ = 90° |
| | $c$ = 14.482(3) Å | $\gamma$ = 90° |
| Volume | 2462.9(10) $Å^3$ | |
| $Z$ | 4 | |
| Density (calculated) | 1.085 $Mg/m^3$ | |
| Absorption coefficient | 0.062 $mm^{-1}$ | |
| F(000) | 880 | |
| Crystal size | 0.350 x 0.250 x 0.200 $mm^3$ | |
| Theta range for data collection | 2.332 to 28.951° | |
| Index ranges | -23<=h<=23, -12<=k<=13, -19<=l<=19 | |
| Reflections collected | 28757 | |
| Independent reflections | 6169 [R(int) = 0.0532] | |
| Completeness to theta = 25.242° | 100.0 % | |
| Absorption correction | Semi-empirical from equivalents | |
| Max. and min. transmission | 0.7458 and 0.6979 | |
| Refinement method | Full-matrix least-squares on $F^2$ | |
| Data / restraints / parameters | 6169 / 202 / 350 | |
| Goodness-of-fit on $F^2$ | 1.029 | |
| Final R indices [I>2sigma(I)] | R1 = 0.0440, wR2 = 0.0817 | |
| R indices (all data) | R1 = 0.0681, wR2 = 0.0914 | |
| Absolute structure parameter | -2.0(10) | |
| Extinction coefficient | n/a | |
| Largest diff. peak and hole | 0.174 and -0.152 e.$Å^{-3}$ | |

**Table A7.** Crystal data and structure refinement for **3-24**.

| | |
|---|---|
| Empirical formula | $C_{27}H_{38}BClN_2$ |
| Formula weight | 436.85 |

| | | |
|---|---|---|
| Temperature | 125(2) K | |
| Wavelength | 0.71073 Å | |
| Crystal system | Triclinic | |
| Space group | *P*1 | |
| Unit cell dimensions | $a$ = 6.2971(15) Å | $\alpha$ = 92.240(3)° |
| | $b$ = 10.739(3) Å | $\beta$ = 91.774(3)° |
| | $c$ = 18.714(5) Å | $\gamma$ = 94.792(3)° |
| Volume | 1259.4(5) $Å^3$ | |
| $Z$ | 2 | |
| Density (calculated) | 1.152 $Mg/m^3$ | |
| Absorption coefficient | 0.168 $mm^{-1}$ | |
| F(000) | 472 | |
| Crystal size | 0.450 x 0.200 x 0.150 $mm^3$ | |
| Theta range for data collection | 1.905 to 29.028° | |
| Index ranges | -8<=h<=8, -13<=k<=14, -25<=l<=25 | |
| Reflections collected | 15446 | |
| Independent reflections | 11562 [R(int) = 0.0351] | |
| Completeness to theta = 25.242° | 99.8 % | |
| Absorption correction | Semi-empirical from equivalents | |
| Max. and min. transmission | 0.7458 and 0.6760 | |
| Refinement method | Full-matrix least-squares on $F^2$ | |
| Data / restraints / parameters | 11562 / 3 / 575 | |
| Goodness-of-fit on $F^2$ | 0.993 | |
| Final R indices [I>2sigma(I)] | R1 = 0.0643, wR2 = 0.1190 | |
| R indices (all data) | R1 = 0.1083, wR2 = 0.1392 | |
| Absolute structure parameter | 0.04(4) | |
| Extinction coefficient | n/a | |
| Largest diff. peak and hole | 0.460 and -0.294 $e.Å^{-3}$ | |

## B2: NMR Spectra for Chapter 3

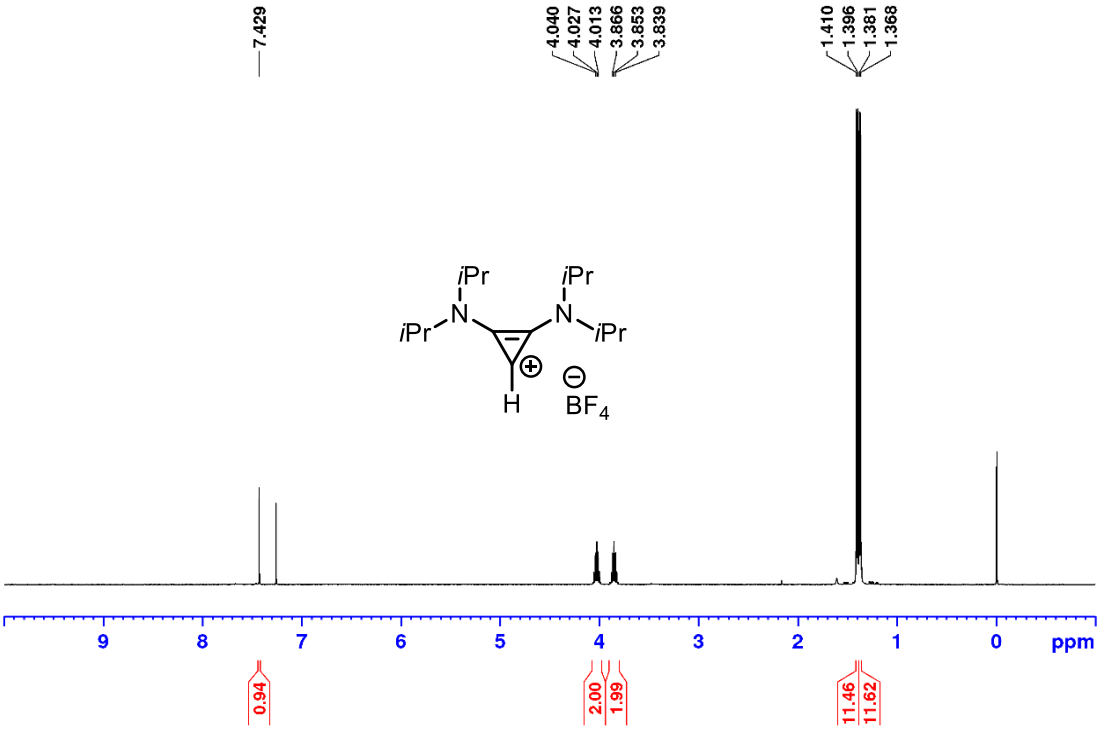


**Figure A19:** $^{1}$H NMR (500 MHz, $CDCl_3$) spectrum of *i*PrBAC-$HBF_4$ **3-8a**.

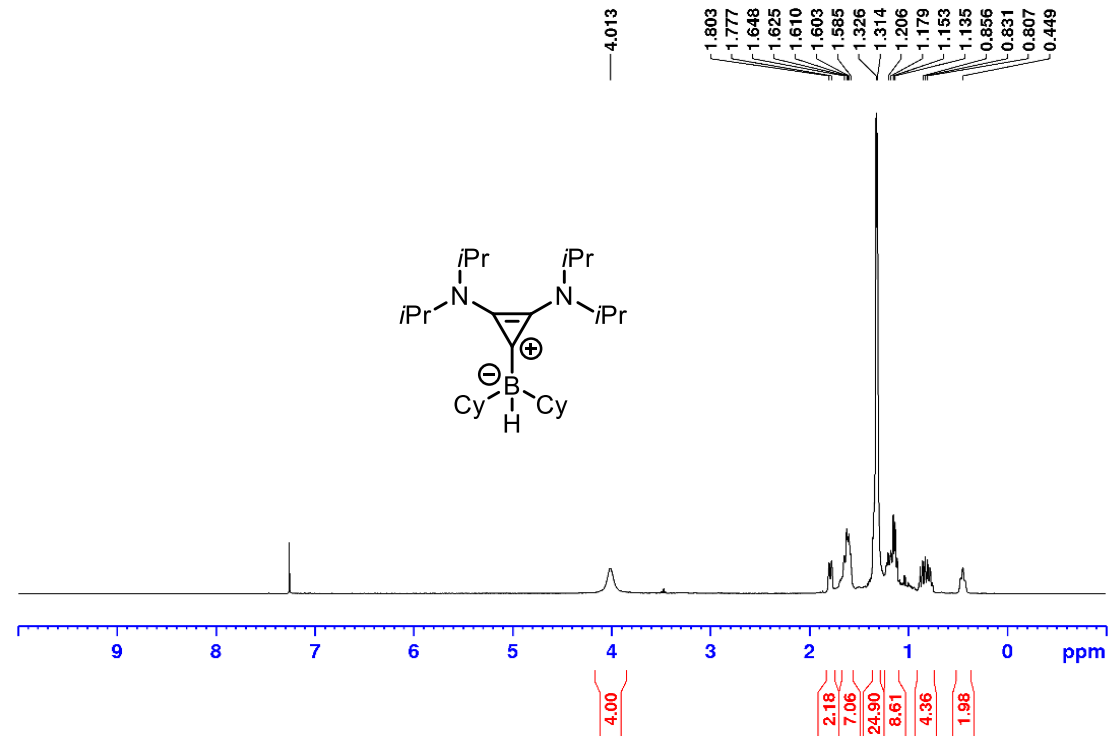


**Figure A20:** $^{1}$H NMR (500 MHz, $CDCl_3$) spectrum of *i*PrBAC-$BCy_2H$ **3-5**.

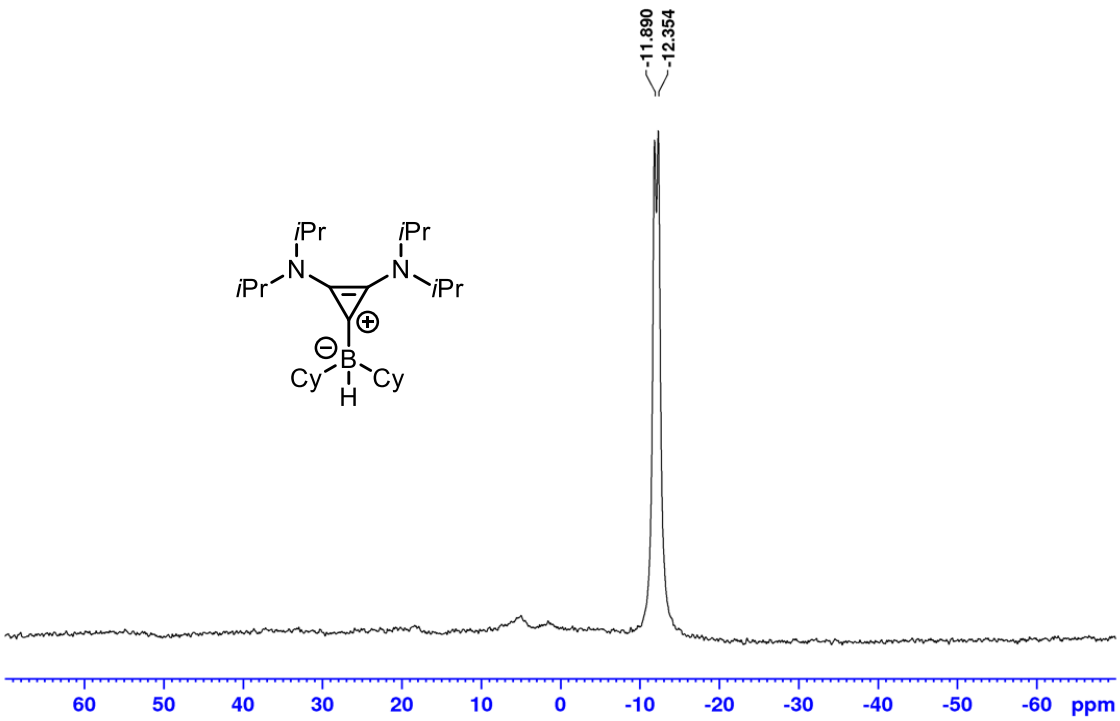


**Figure A21:** $^{11}$B NMR (160.5 MHz, $CDCl_3$) spectrum of *i*PrBAC-$BCy_2H$ **3-5**.

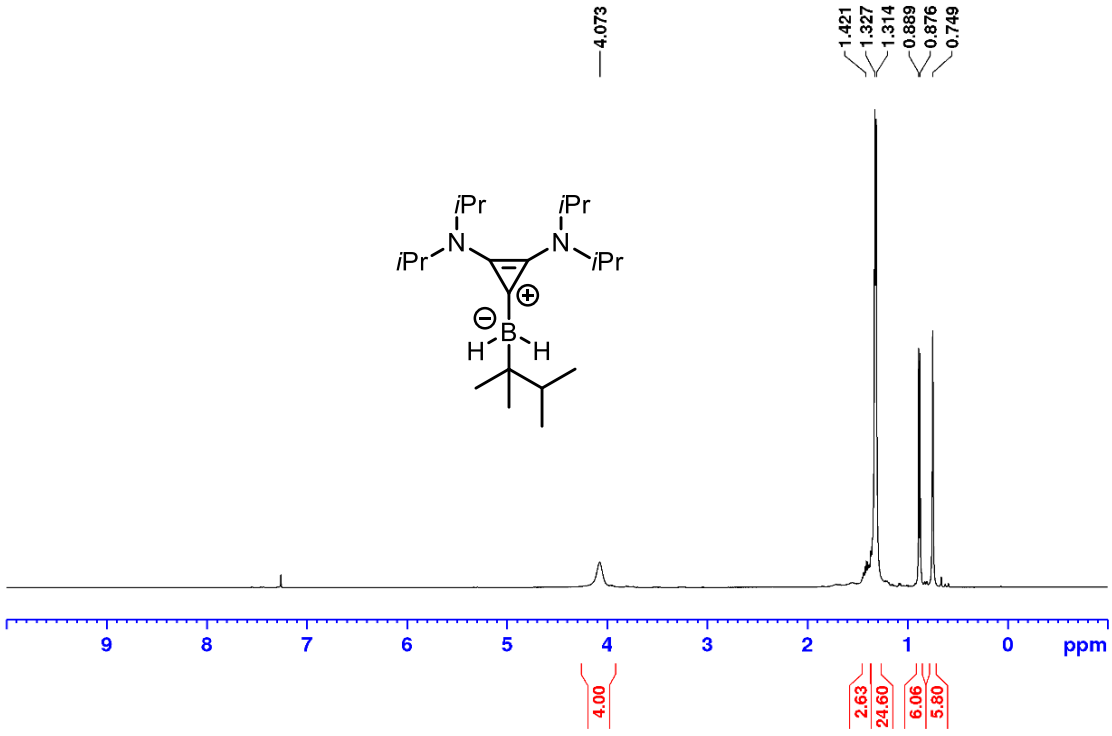


**Figure A22:** $^{1}$H NMR (500 MHz, $CDCl_3$) spectrum of *i*PrBAC-$BH_2$Thex **3-18a**.

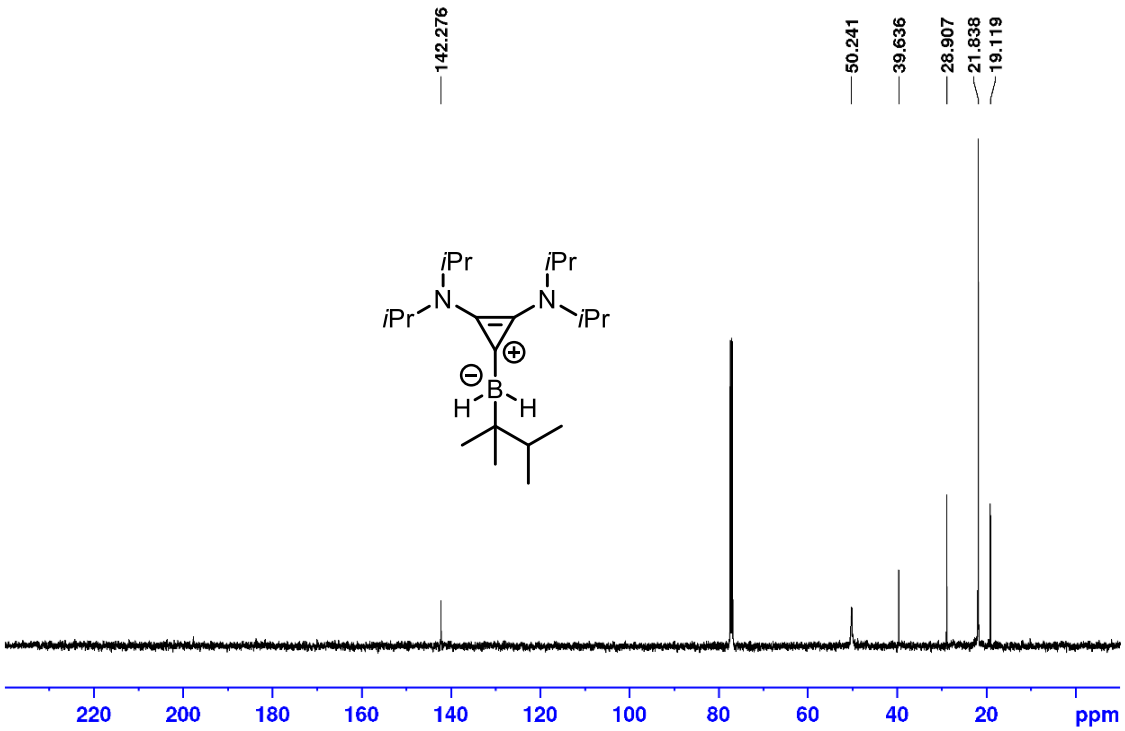


**Figure A23:** $^{13}C$ {$^{1}H$} NMR (125.8 MHz, $C_6D_6$) spectrum of *i*PrBAC-$BH_2$Thex **3-18a**.

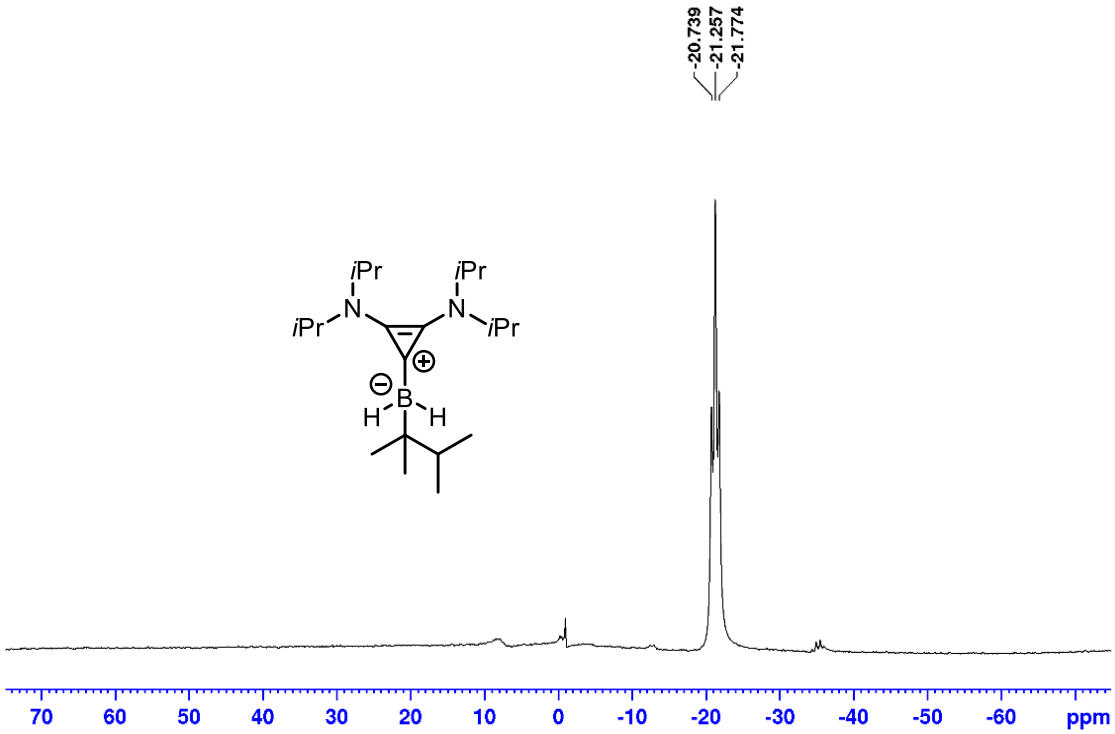


**Figure A24:** $^{11}B$ NMR (160.5 MHz, $CDCl_3$) spectrum of *i*PrBAC-$BH_2$Thex **3-18a**.

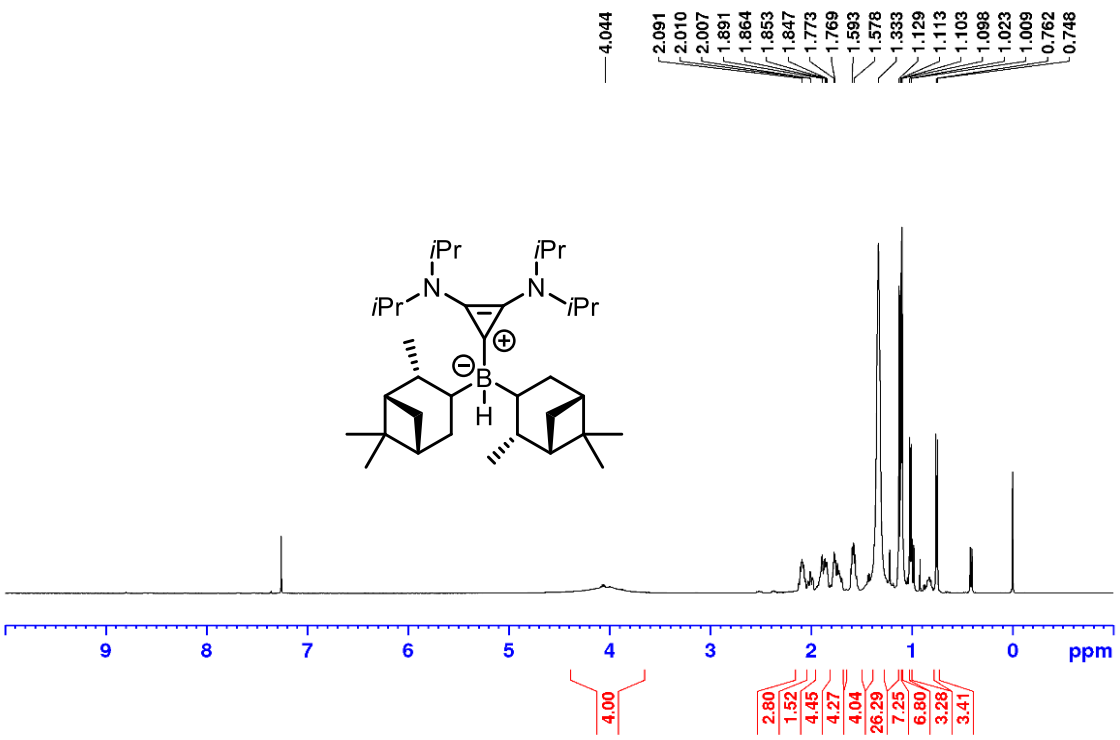


**Figure A25:** $^{1}$H NMR (500 MHz, $CDCl_3$) spectrum of *i*PrBAC-Bipc$_2$H **3-18b**.

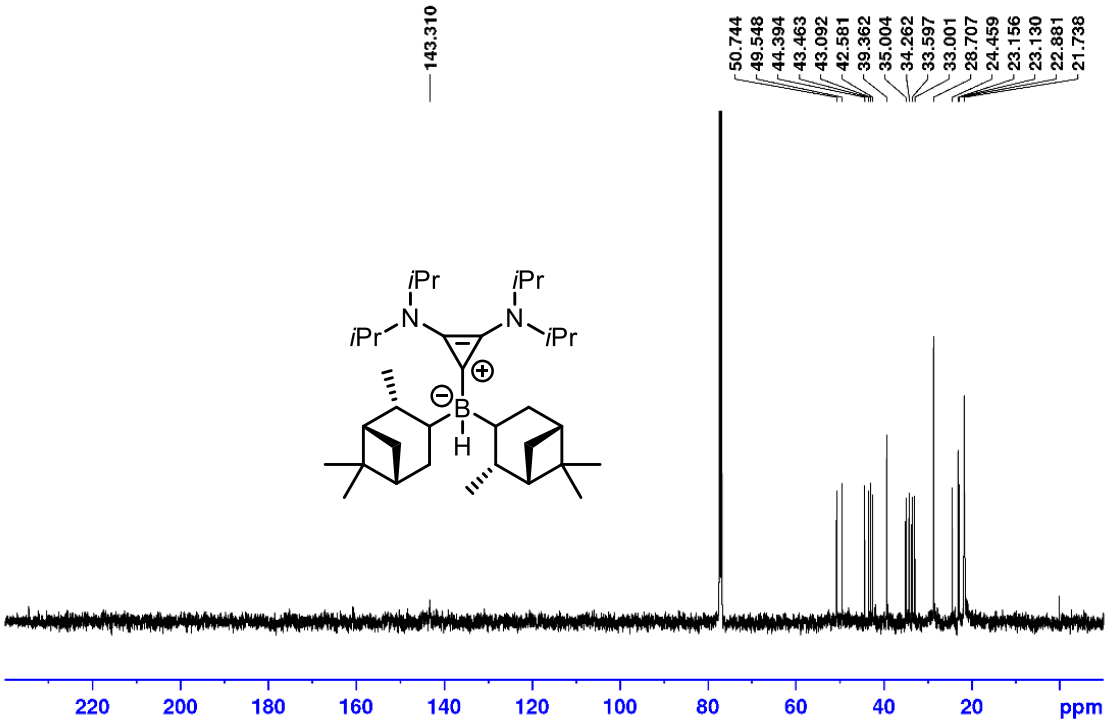


**Figure A26:** $^{13}$C {$^{1}$H} NMR (125.8 MHz, $CDCl_3$) spectrum of *i*PrBAC-Bipc$_2$H **3-18b**.

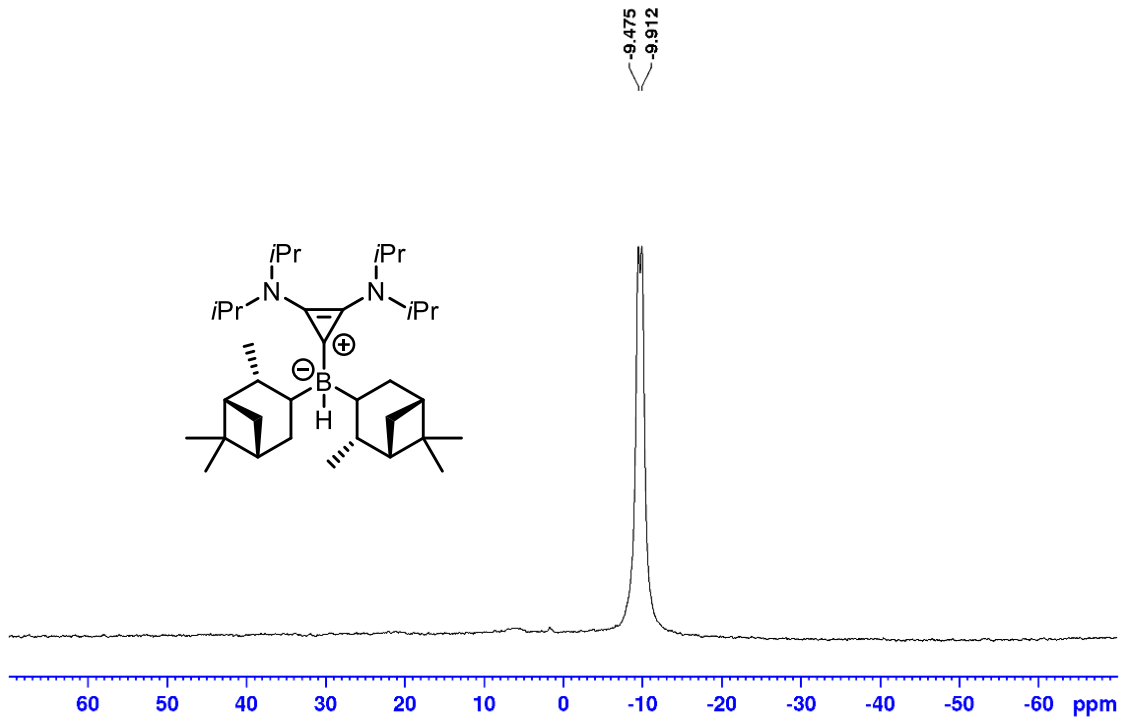


**Figure A27:** $^{11}$B NMR (160.5 MHz, $CDCl_3$) spectrum of *i*PrBAC-Bipc$_2$H **3-18b**.

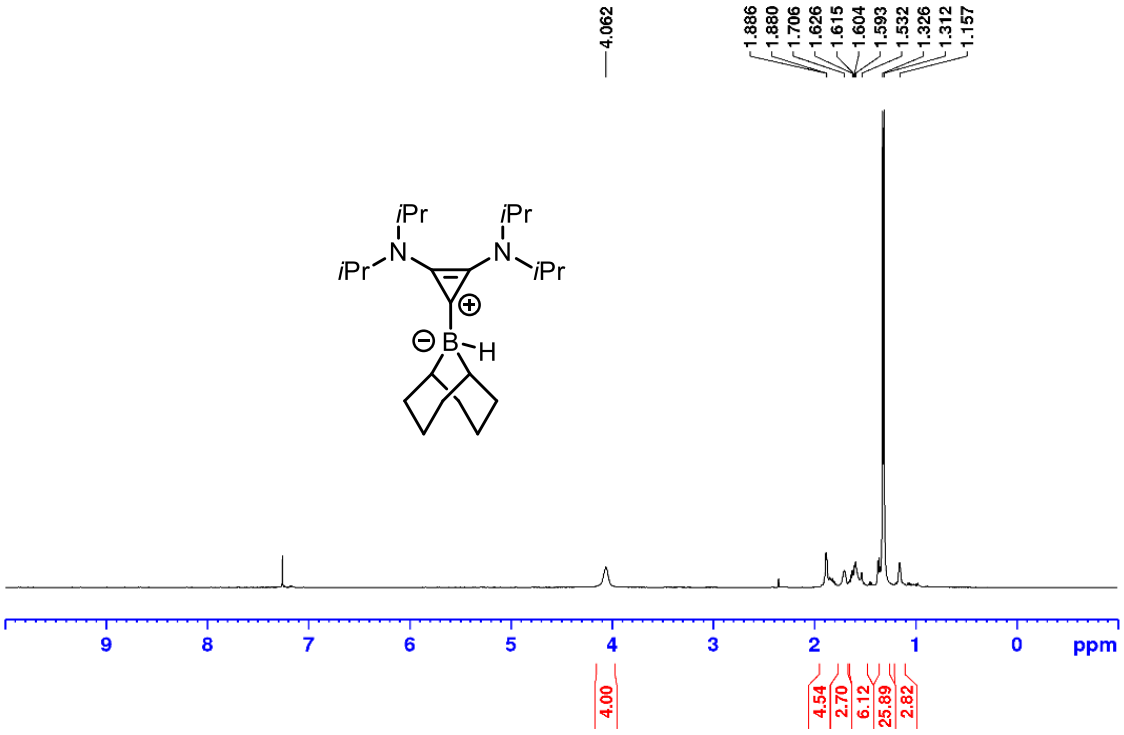


**Figure A28:** $^{1}$H NMR (500 MHz, $CDCl_3$) spectrum of *i*PrBAC-9BBNH **3-16**.

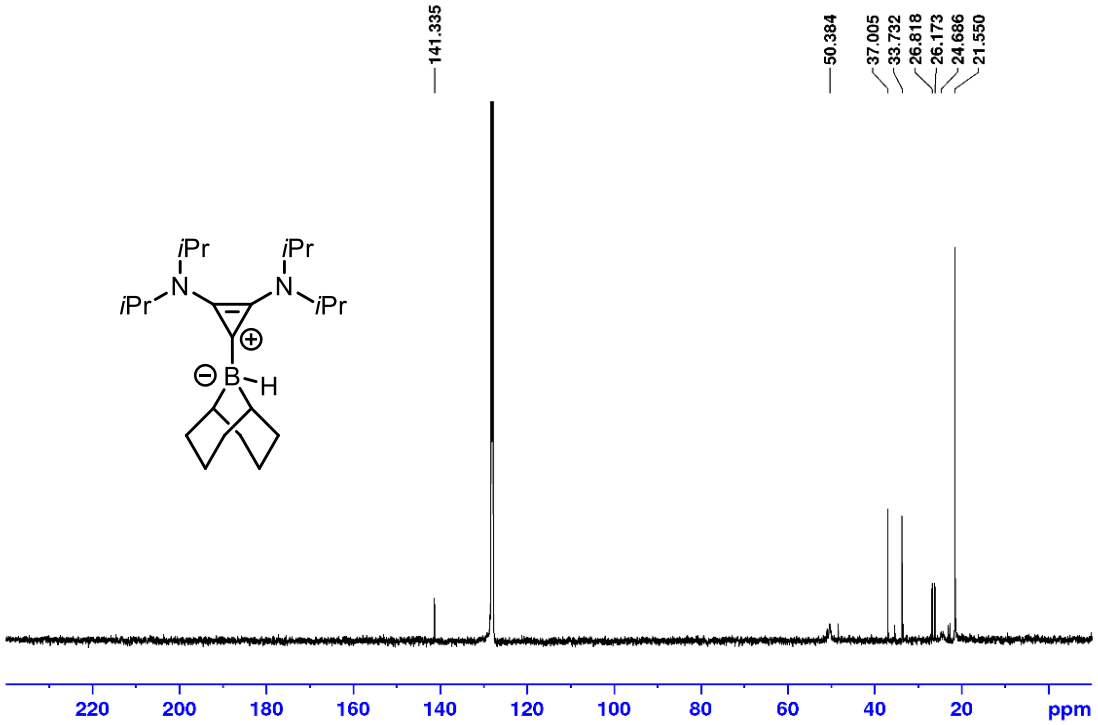


**Figure A29:** $^{13}C$ {$^{1}H$} NMR (125.8 MHz, $C_6D_6$) spectrum of *i*PrBAC-9BBNH **3-16**.

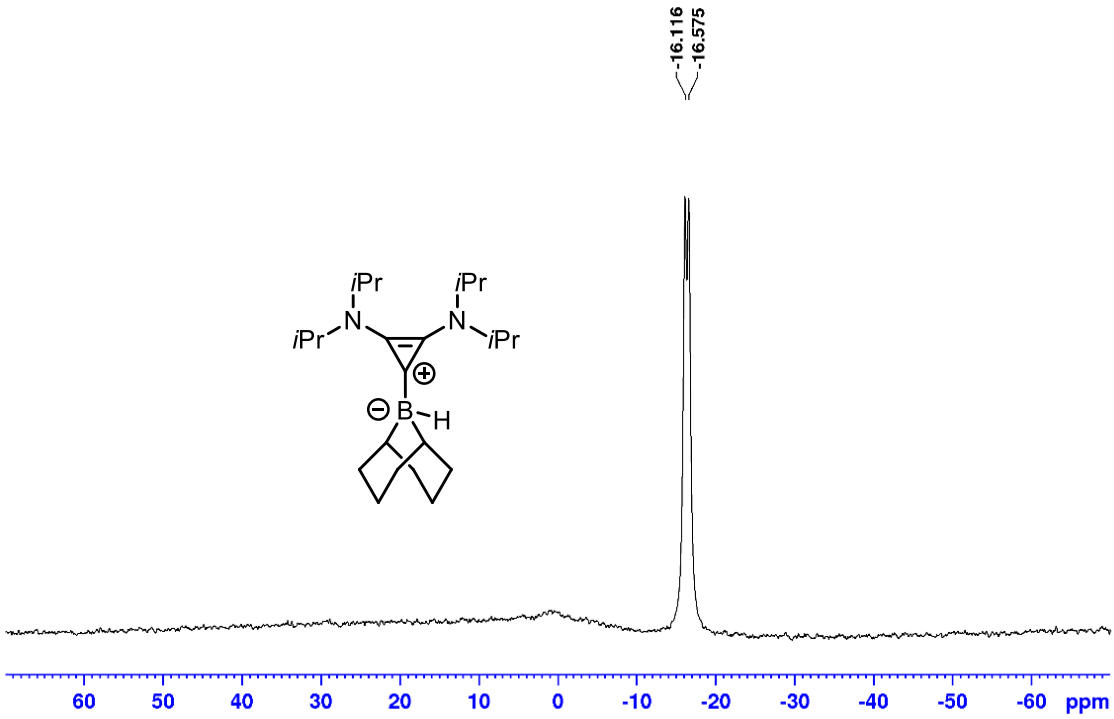


**Figure A30:** $^{11}B$ NMR (160.5 MHz, $CDCl_3$) spectrum of *i*PrBAC-9BBNH **3-16**.

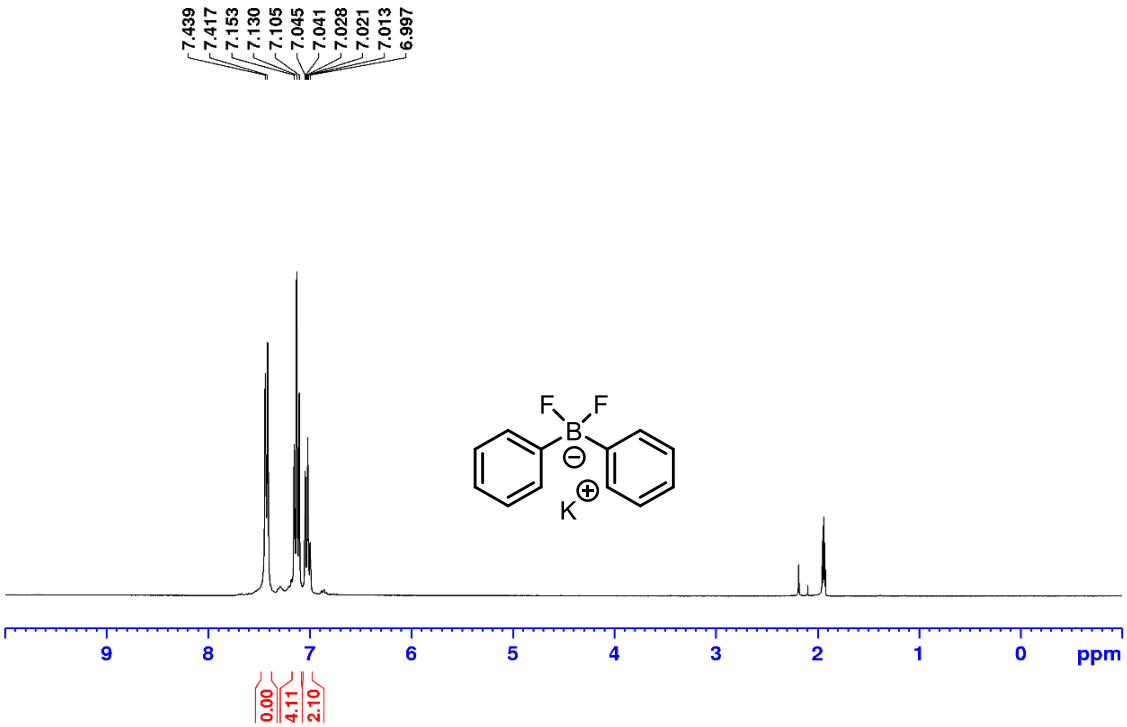


**Figure A31:** $^{1}H$ NMR (300 MHz, $CD_3CN$) spectrum of $KF_2BPh_2$ **3-21**.

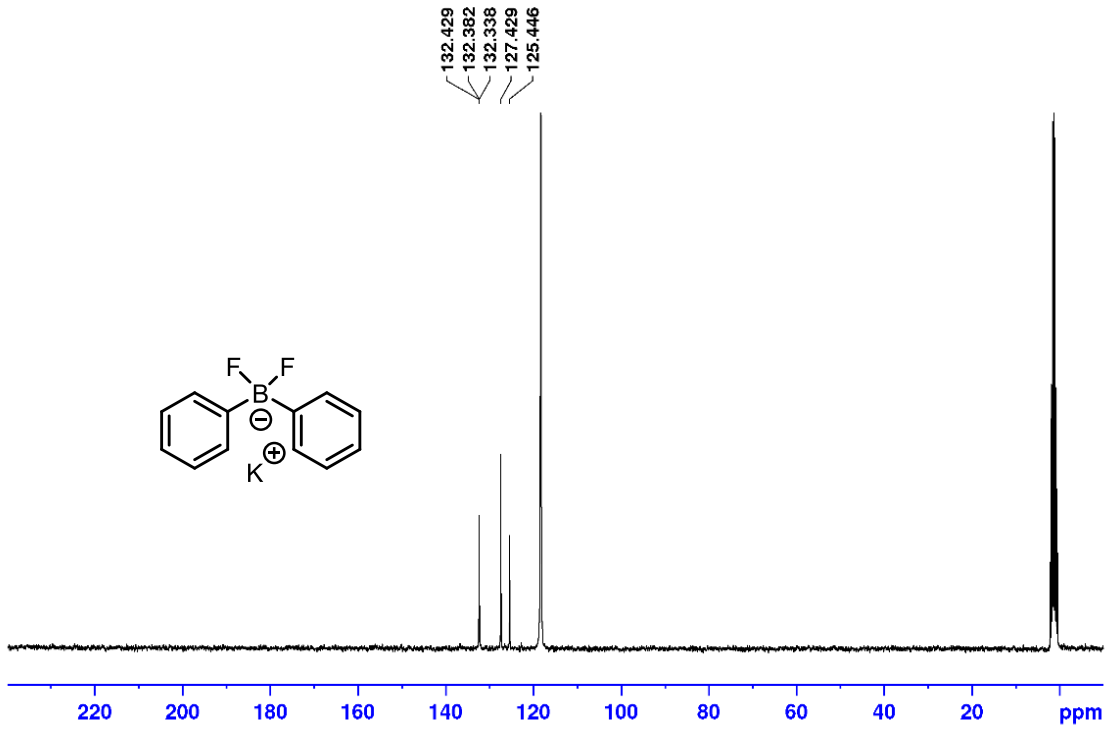


**Figure A32:** $^{13}C$ $\{^{1}H\}$ (75.5 MHz, $CD_3CN$) spectrum of $KF_2BPh_2$ **3-21**.

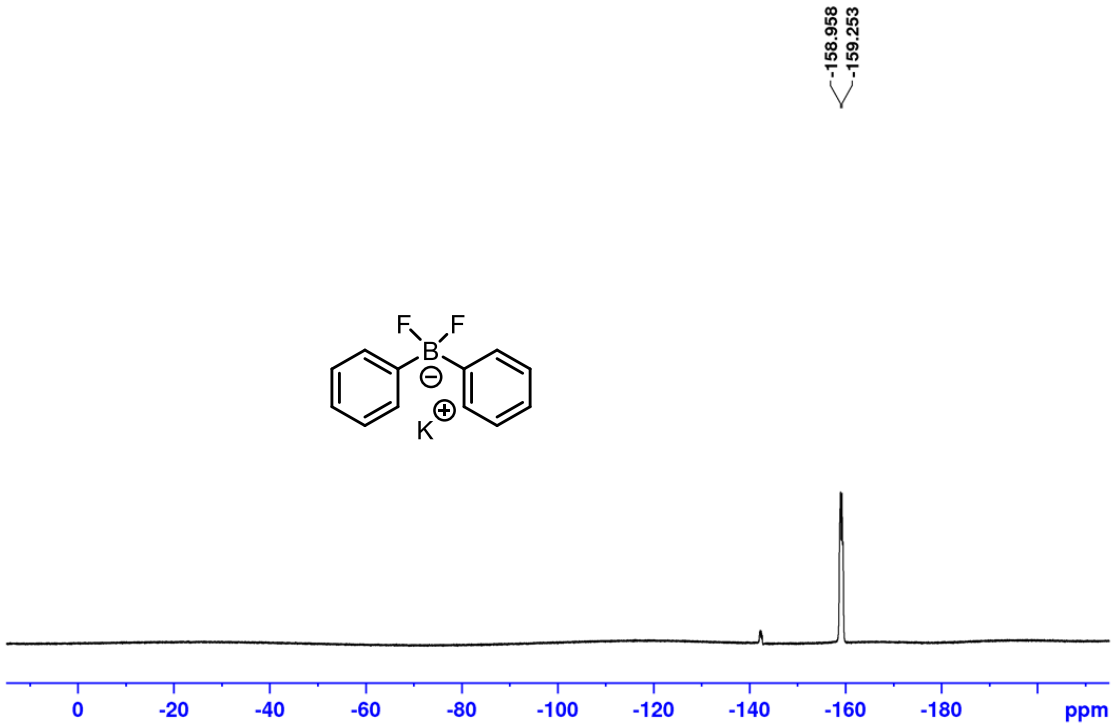


**Figure A33:** $^{19}F$ NMR (282.4 MHz, $CD_3CN$) spectrum of $KF_2BPh_2$ **3-21**.

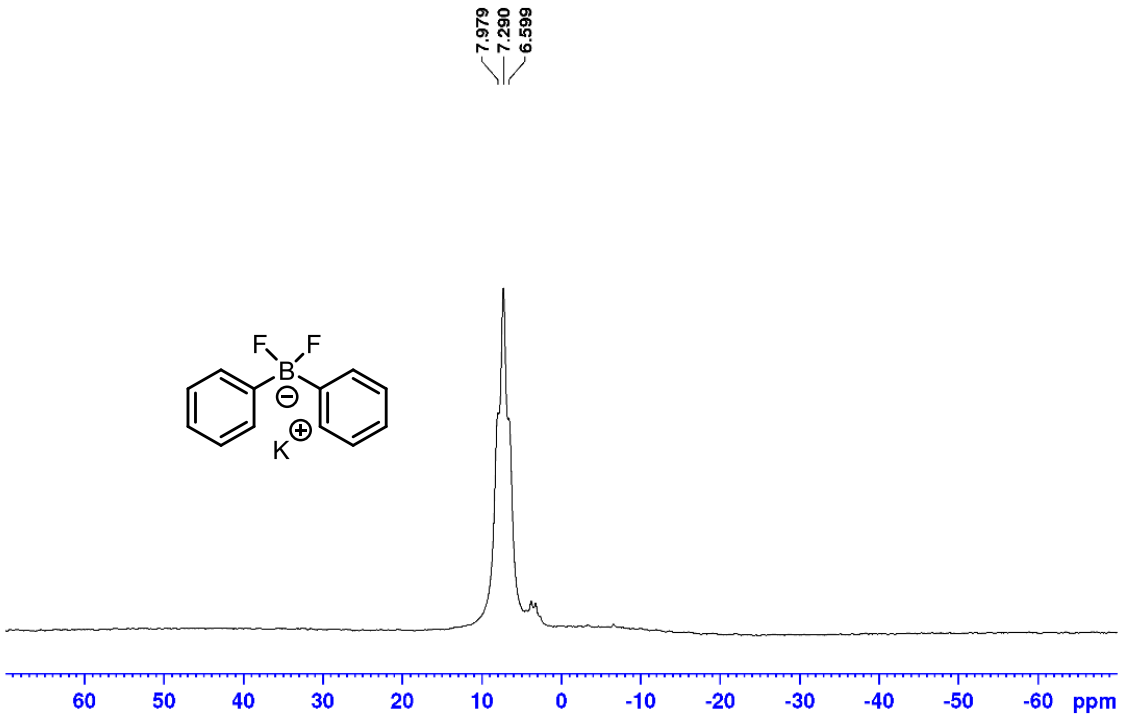


**Figure A34:** $^{11}B$ NMR (96.3 MHz, $CD_3CN$) spectrum of $KF_2BPh_2$ **3-21**.

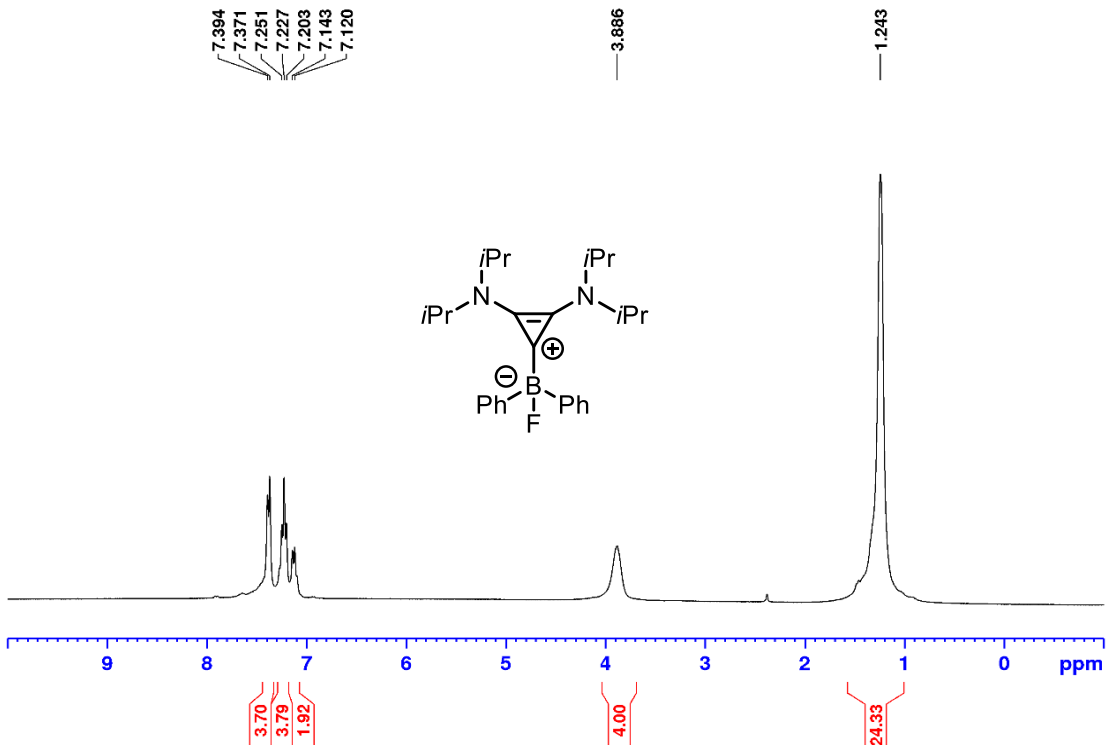


**Figure A35:** $^{1}$H NMR (300 MHz, $CDCl_3$) spectrum of *i*PrBAC-$BPh_2F$ **3-23**.

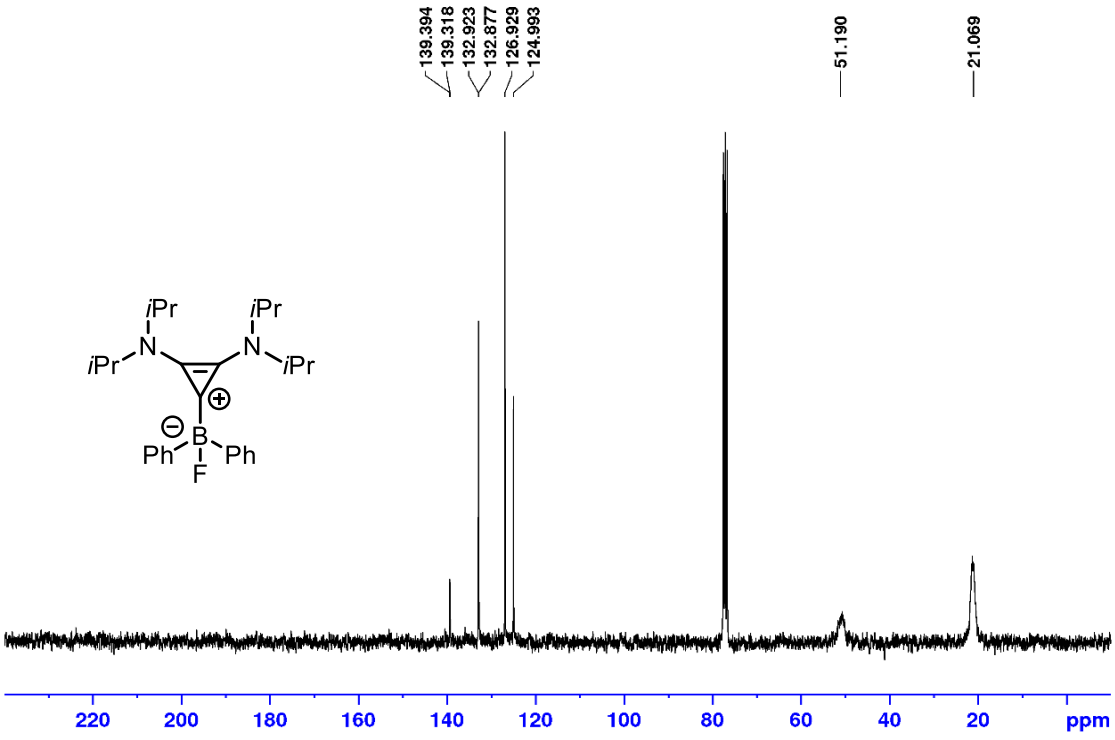


**Figure A36:** $^{13}$C {$^{1}$H} NMR (75.5 MHz, $CDCl_3$) spectrum of *i*PrBAC-$BPh_2F$ **3-23**.

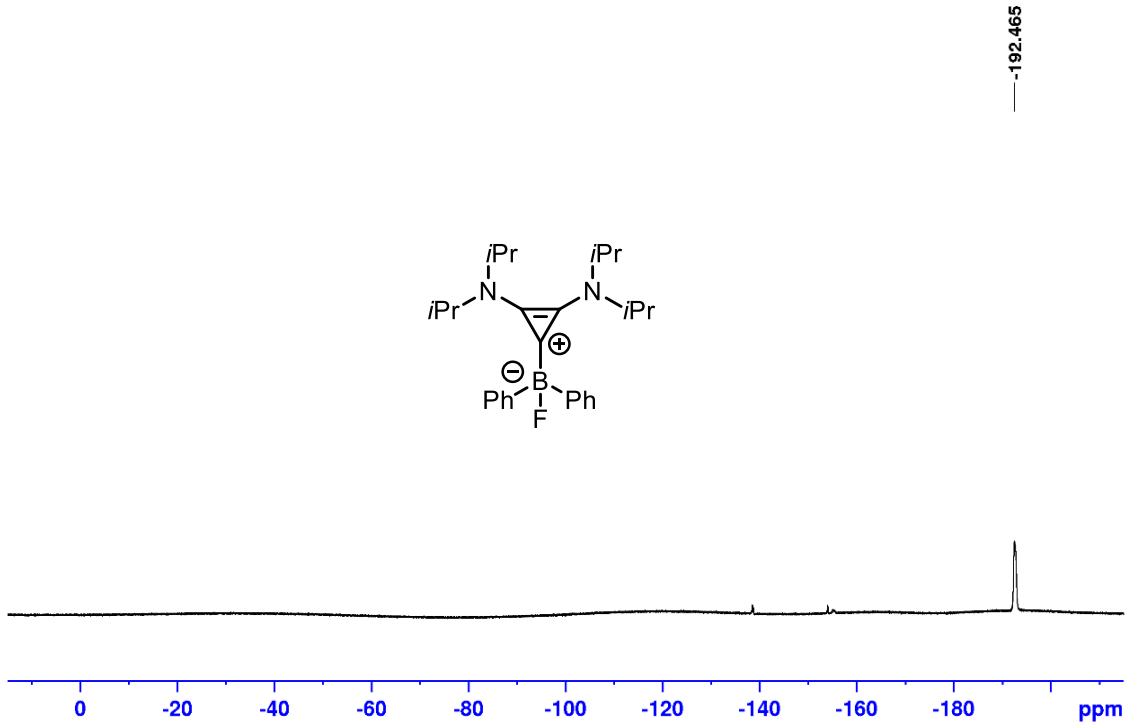


**Figure A37:** $^{19}$F NMR (282.4 MHz, $CDCl_3$) spectrum of *i*PrBAC-$BPh_2F$ **3-23**.

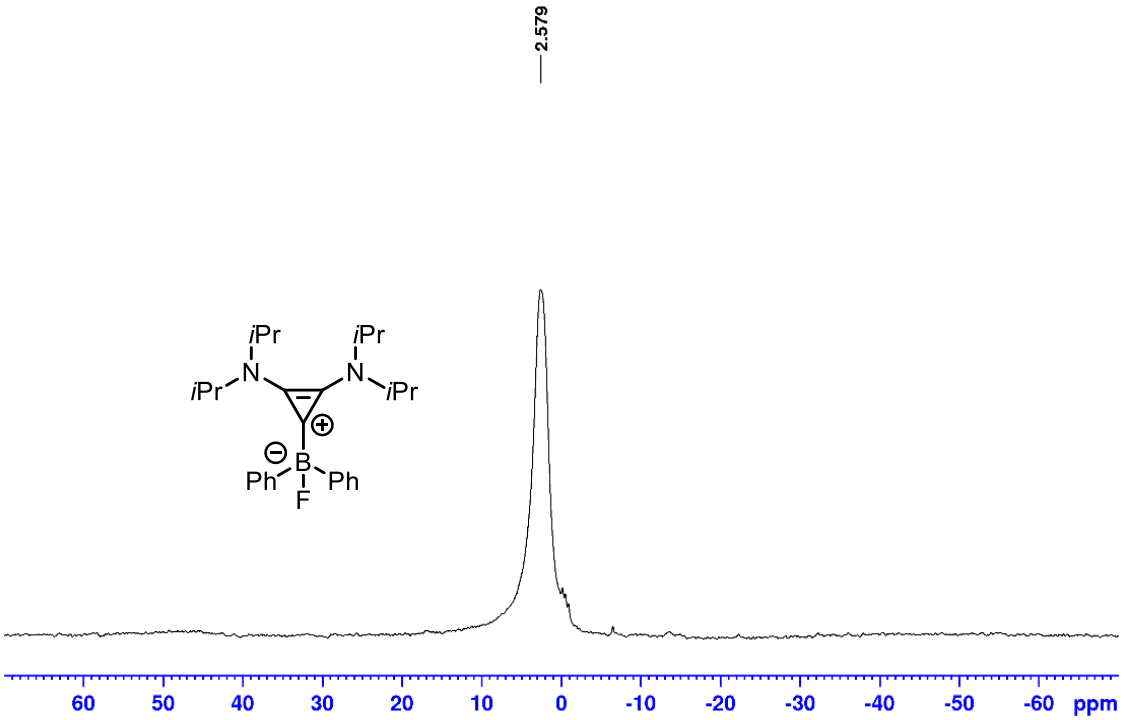


**Figure A38:** $^{11}$B NMR (96.3 MHz, $CDCl_3$) spectrum of *i*PrBAC-$BPh_2F$ **3-23**.

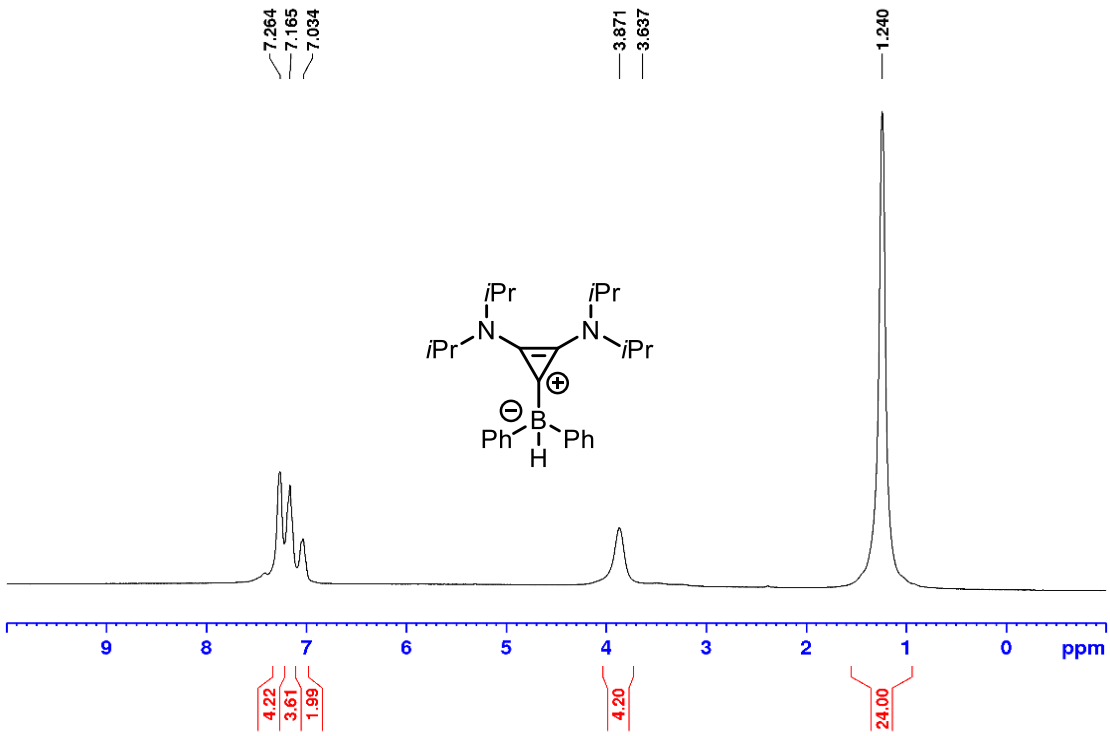


**Figure A39:** $^{1}$H NMR (300 MHz, $CDCl_3$) spectrum of iPrBAC-$BPh_2H$ **3-6**.

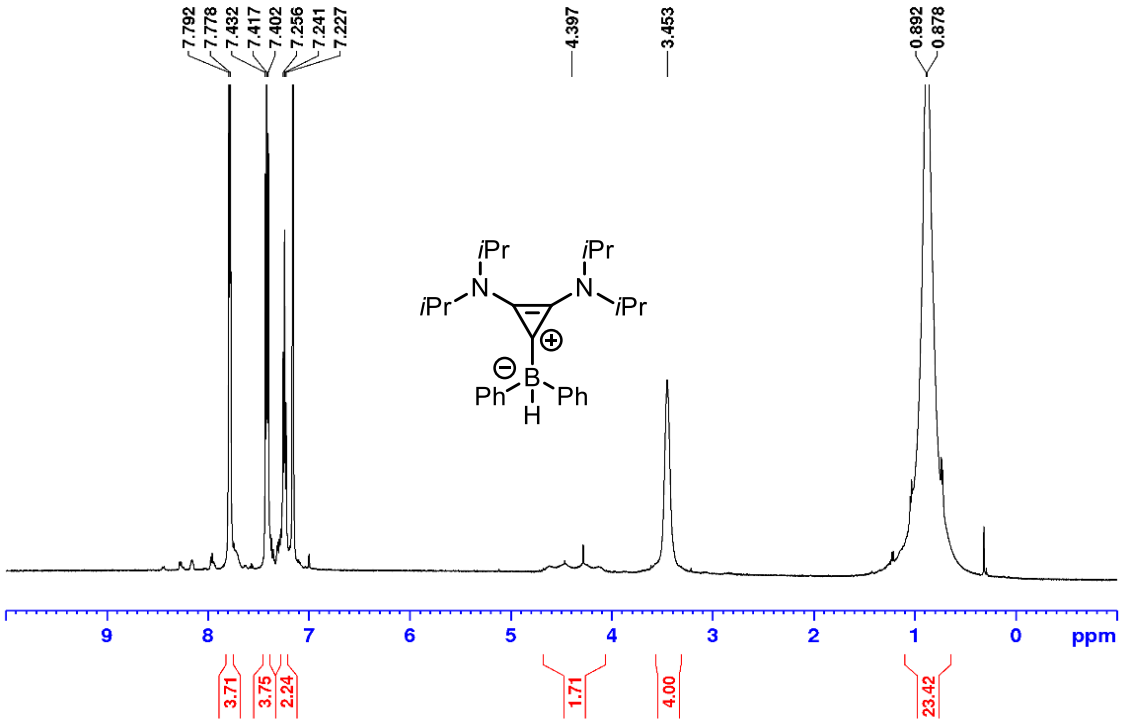


**Figure A40:** $^{1}$H NMR (500 MHz, $C_6D_6$) spectrum of iPrBAC-$BPh_2H$ **3-6**.

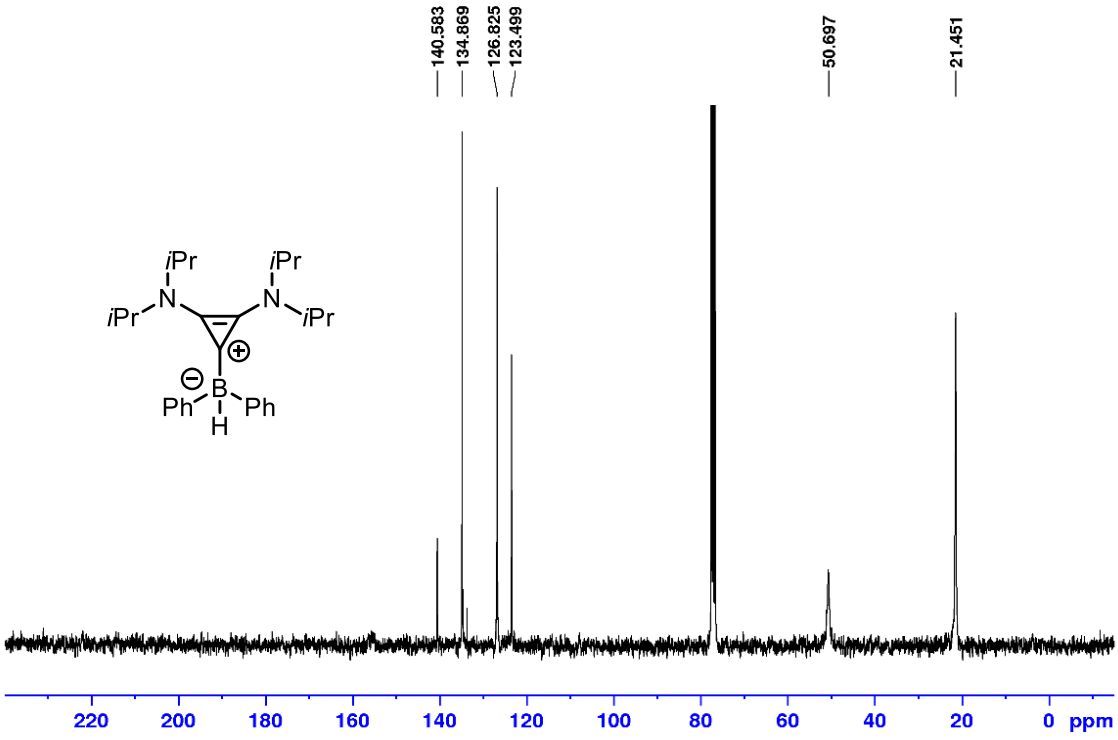


**Figure A41:** $^{13}C$ {$^{1}H$} NMR (75.5 MHz, $CDCl_3$) spectrum of iPrBAC-$BPh_2H$ **3-6**.

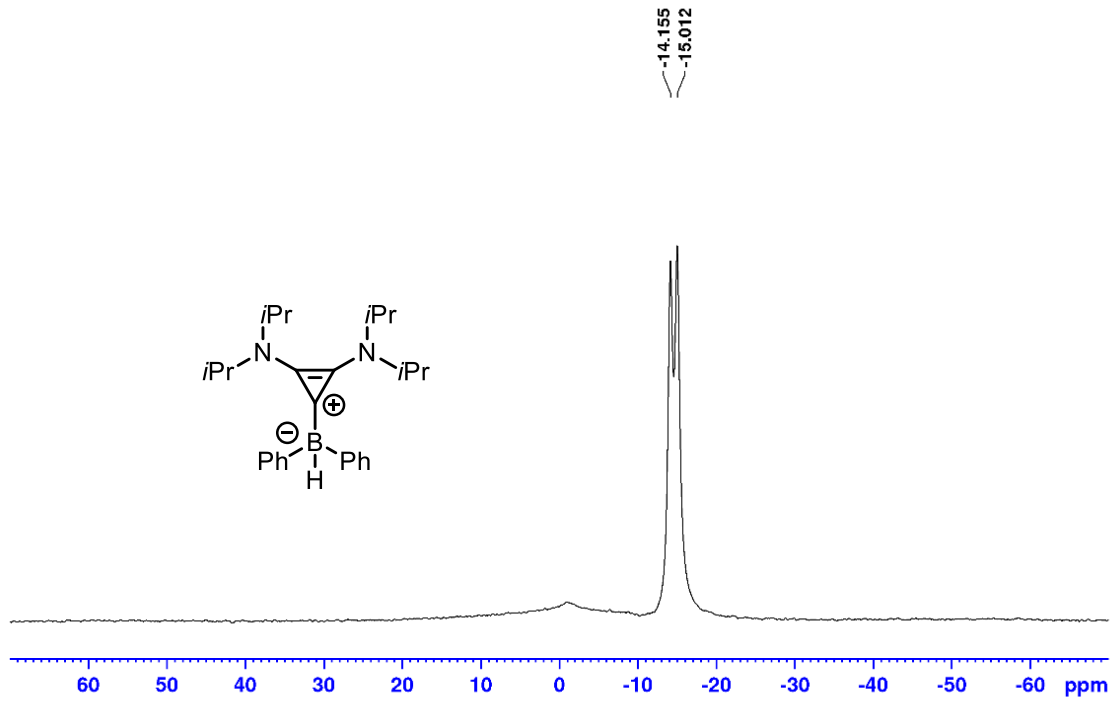


**Figure A42:** $^{11}B$ NMR (96.3 MHz, $CDCl_3$) spectrum of iPrBAC-$BPh_2H$ **3-6**.

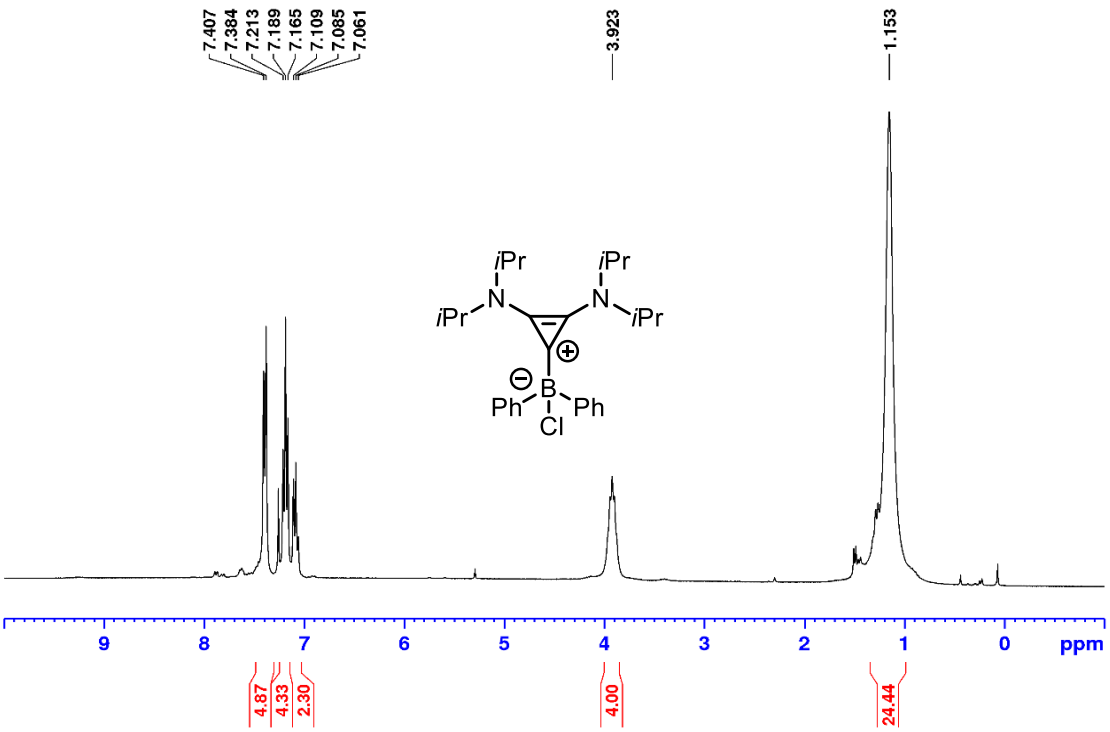


**Figure A43:** $^{1}$H NMR (300 MHz, $CDCl_3$) spectrum of *i*PrBAC-$BPh_2Cl$ **3-24**.

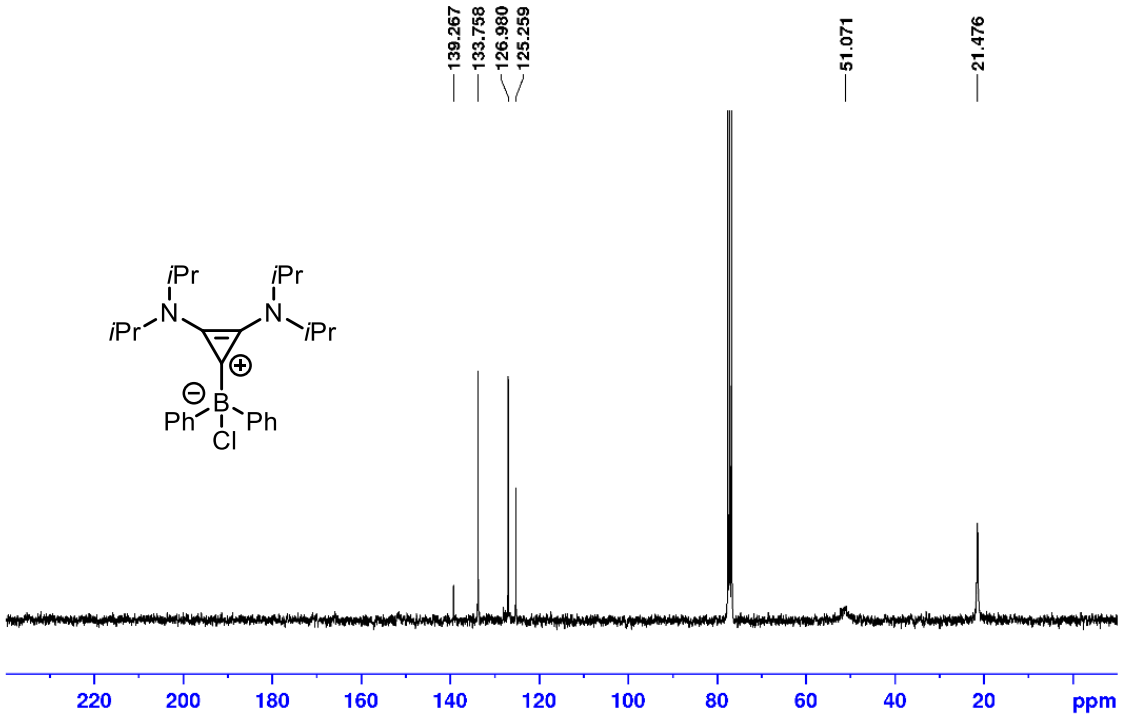


**Figure A44:** $^{13}$C {$^{1}$H} NMR (75.5 MHz, $CDCl_3$) spectrum of *i*PrBAC-$BPh_2Cl$ **3-24**.

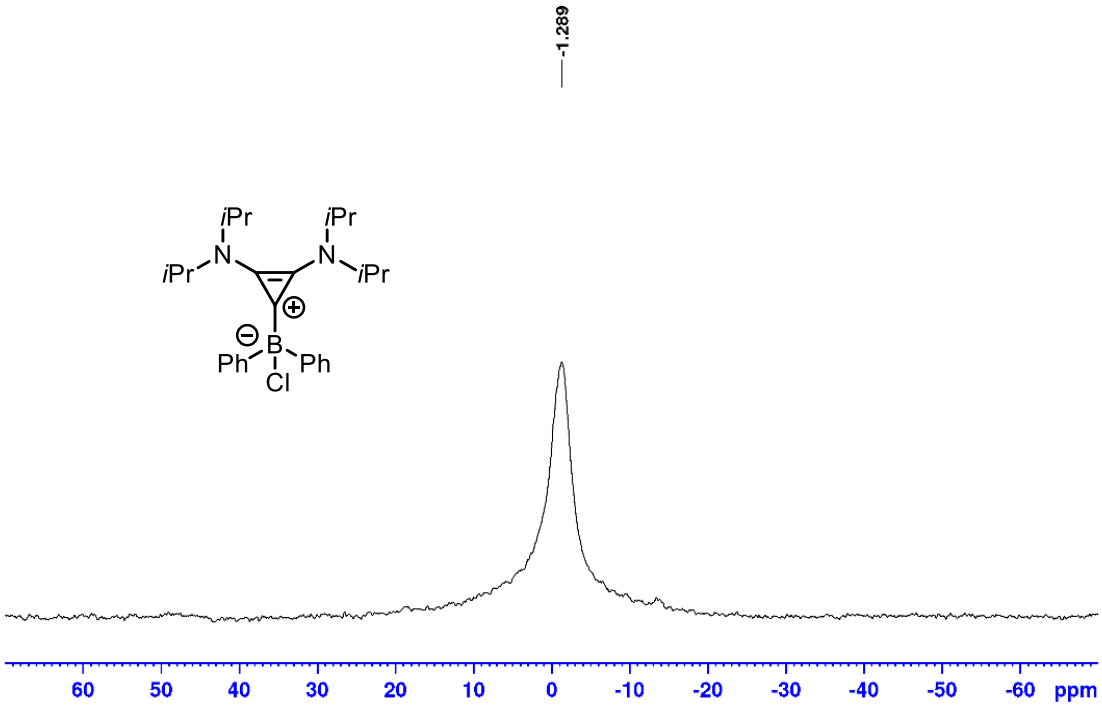


**Figure A45:** $^{11}$B NMR (96.3 MHz, $CDCl_3$) spectrum of *i*PrBAC-$BPh_2Cl$ **3-24**.

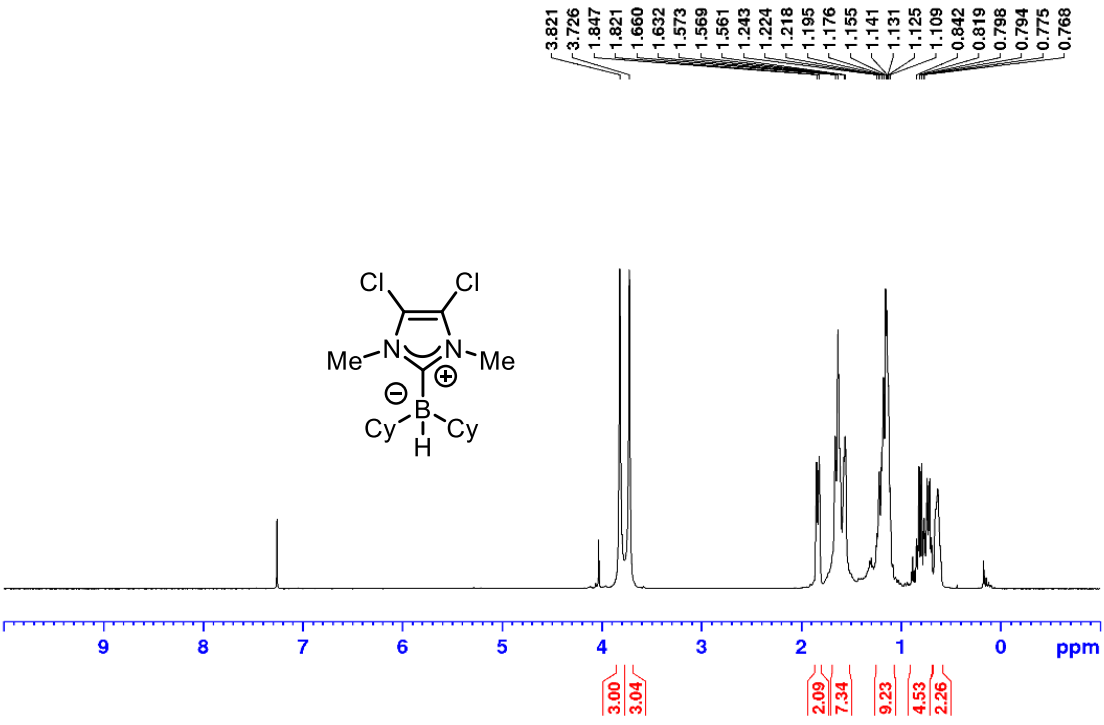


**Figure A46:** $^{1}$H NMR (500 MHz, $CDCl_3$) spectrum of Cl-NHC-$BCy_2H$ **3-17**.

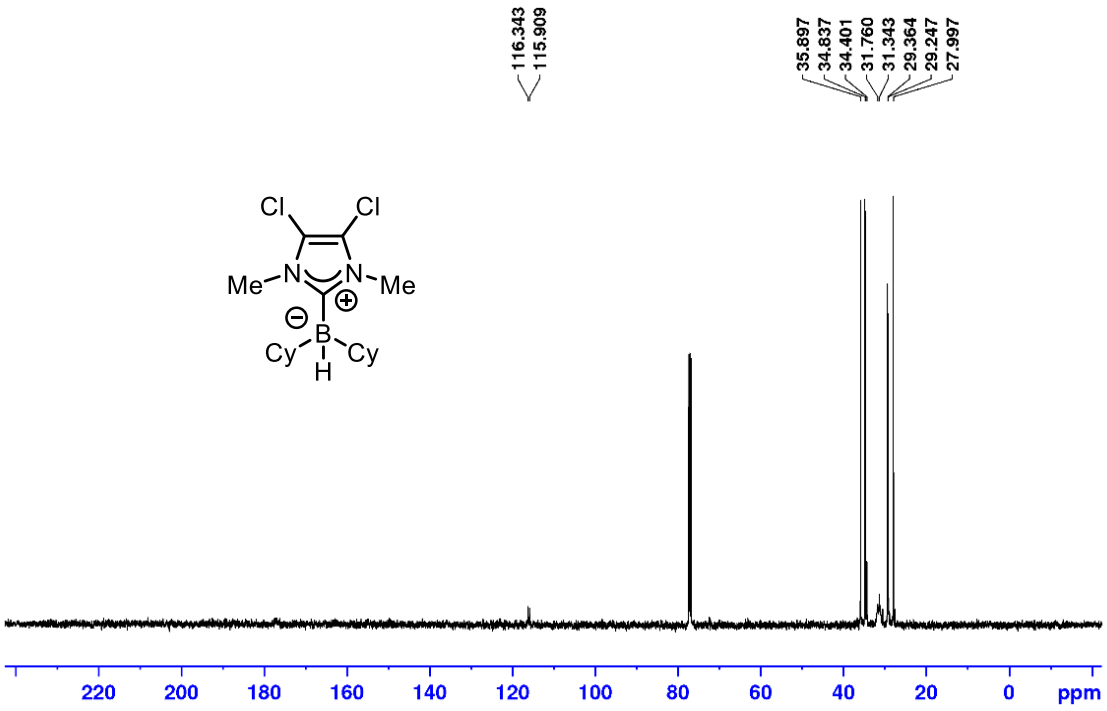


**Figure A47:** $^{13}C$ {$^{1}H$} NMR (125.8 MHz, $CDCl_3$) spectrum of Cl-NHC-$BCy_2H$ **3-17**.

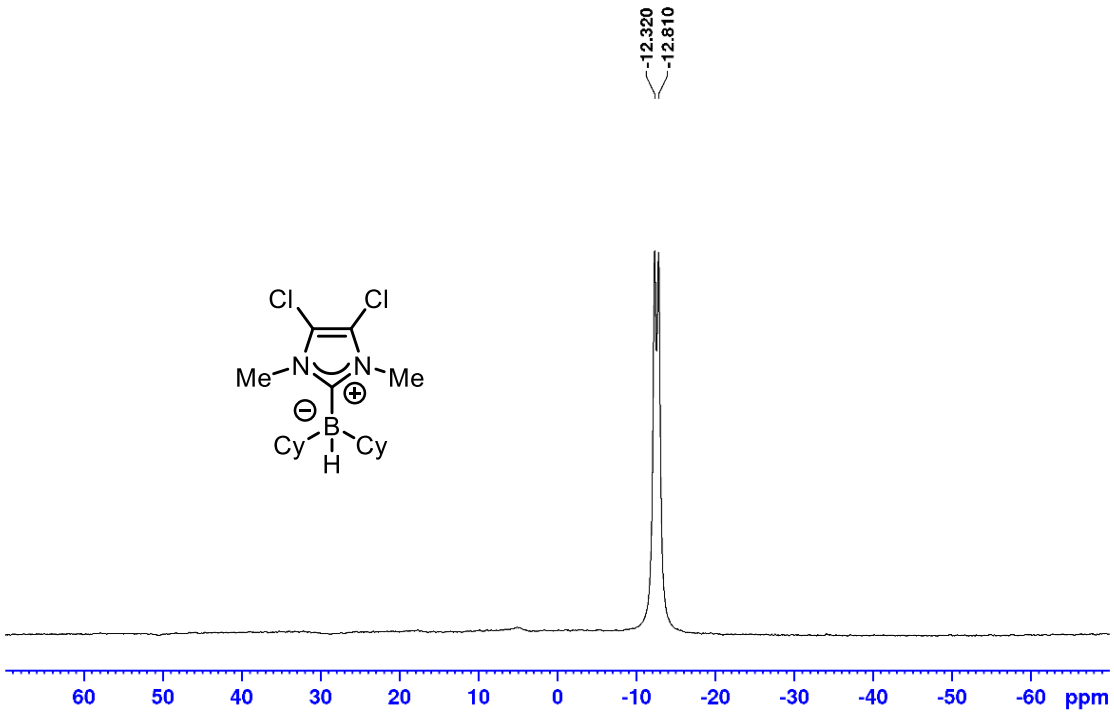


**Figure A48:** $^{11}B$ NMR (160.5 MHz, $CDCl_3$) spectrum of Cl-NHC-$BCy_2H$ **3-17**.

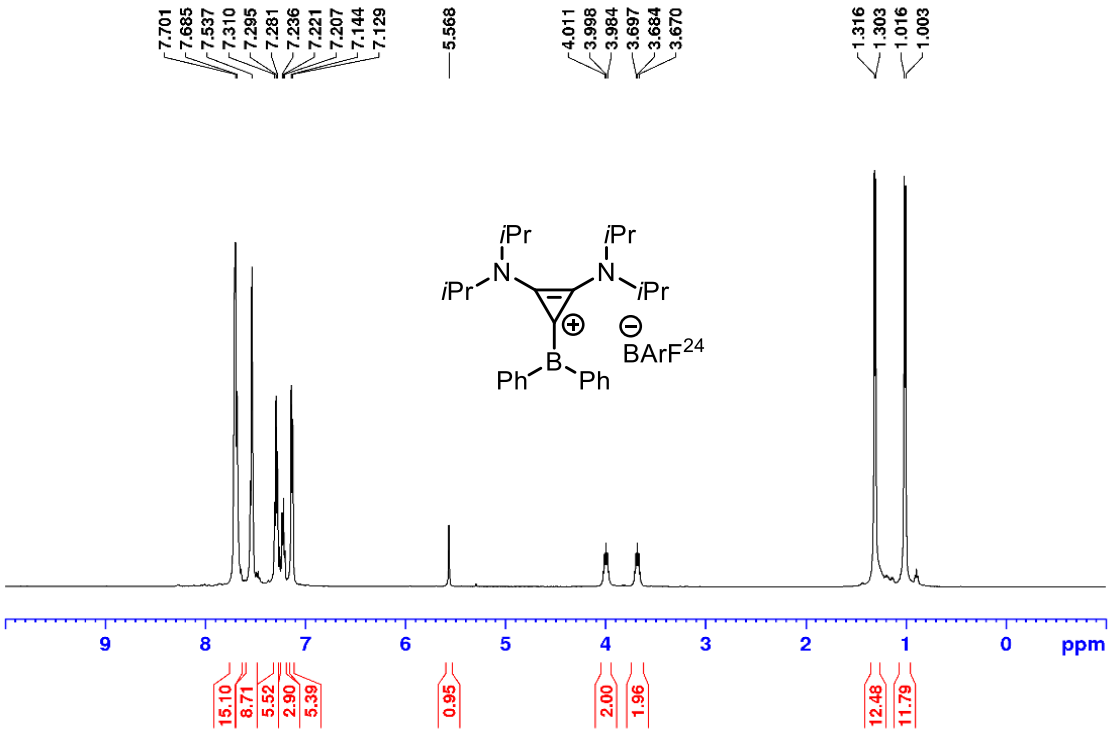


**Figure A49:** $^{1}$H NMR (500 MHz, $CDCl_3$) spectrum of formation of borenium cation [*i*PrBAC-$BPh_2$][$BAr^F{}_{24}$] **3-25** *in situ* from trityl $BAr^F{}_{24}$.

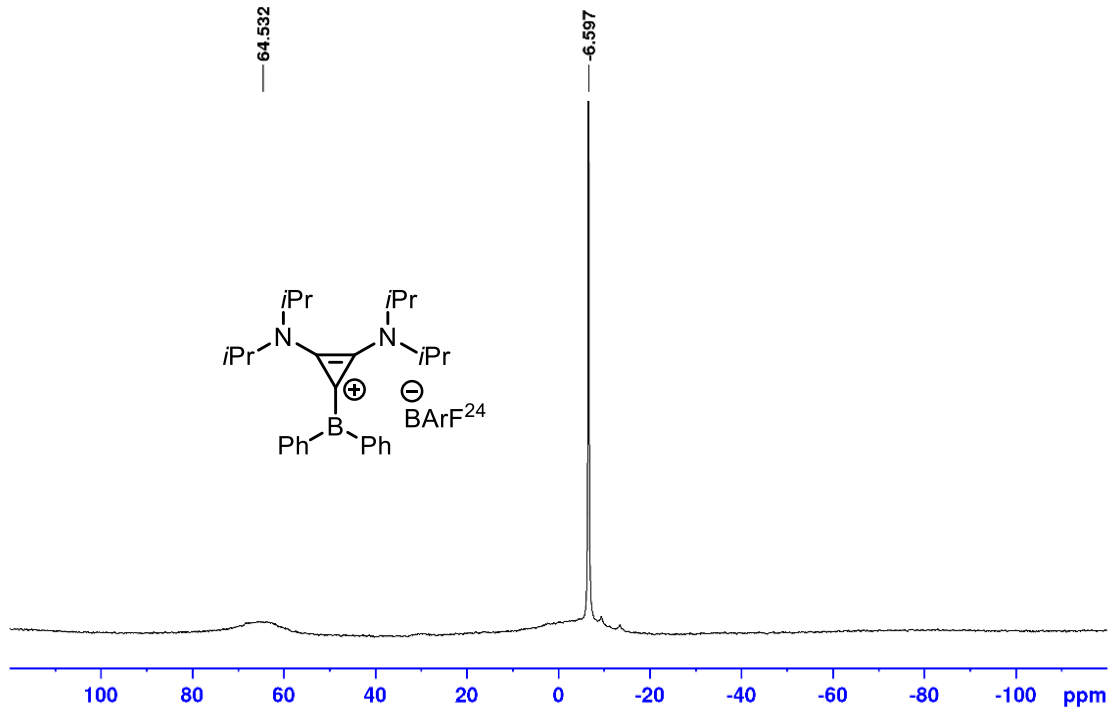


**Figure A50:** $^{11}$B NMR (160.4 MHz, $CDCl_3$) spectrum of formation of borenium cation [*i*PrBAC-$BPh_2$][$BAr^F{}_{24}$] **3-25** *in situ* from trityl $BAr^F{}_{24}$

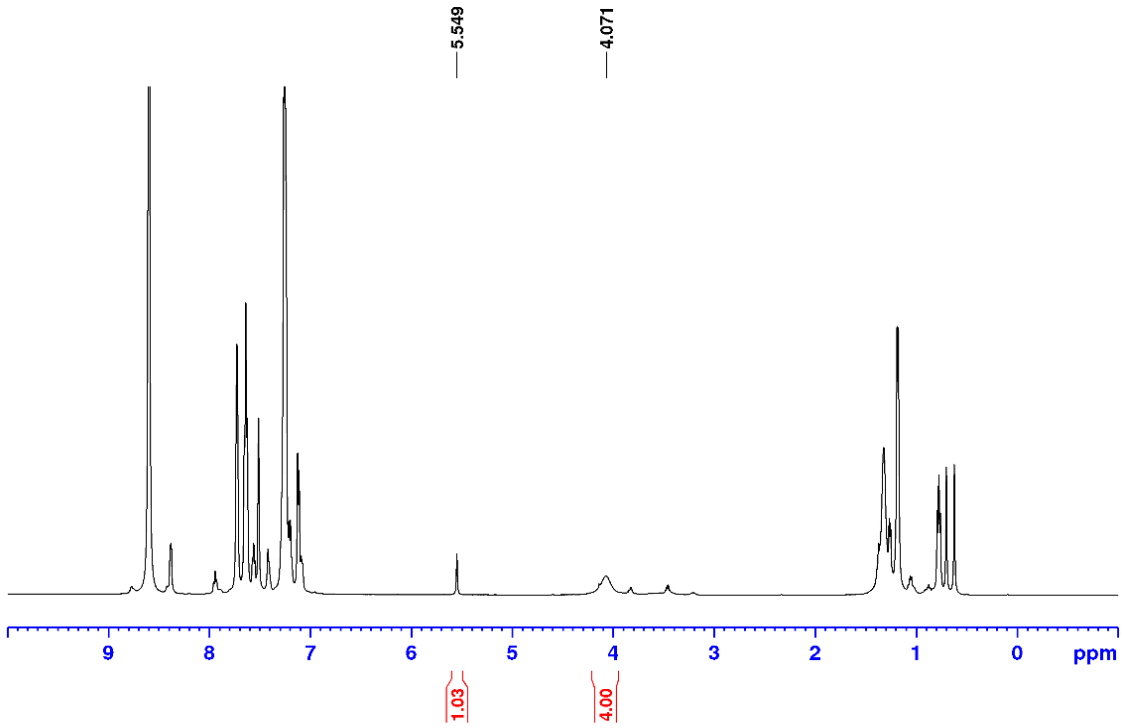


**Figure A51:** $^{1}$H NMR ($CDCl_3$) spectrum of *i*PrBAC-$BH_2$Thex **3-18a** pyridine trityl addition, with 1 equiv. of pyridine.

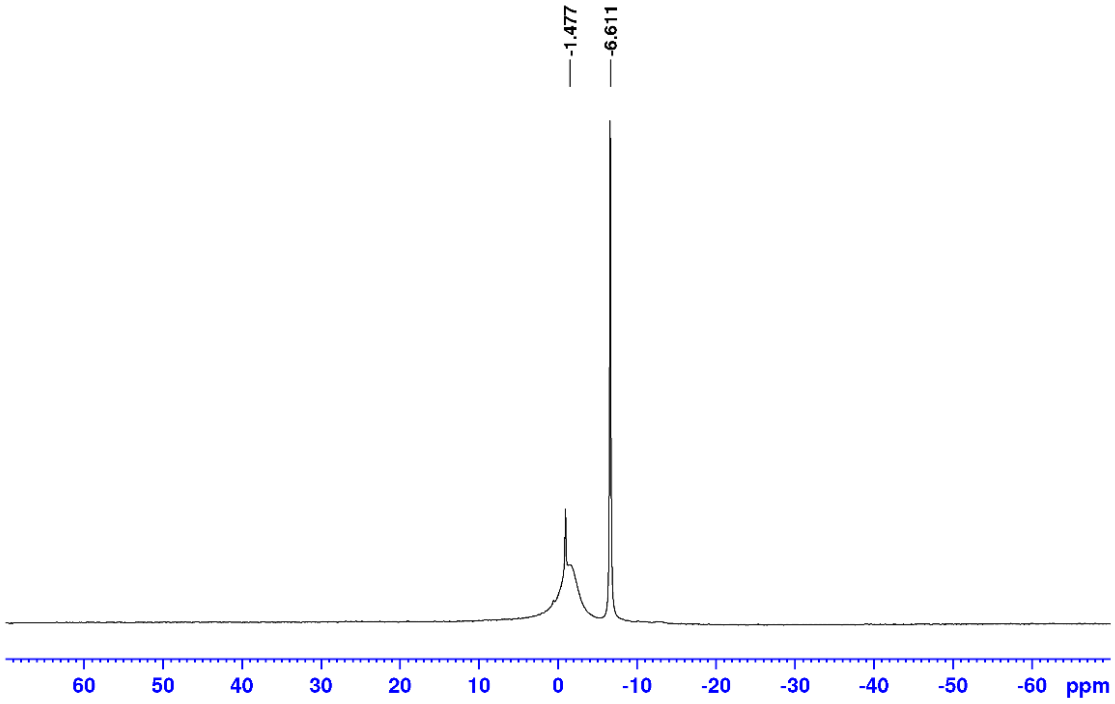


**Figure A52:** $^{11}$B NMR ($CDCl_3$) spectrum of *i*PrBAC-$BH_2$Thex **3-18a** pyridine trityl addition, with 1 equiv. of pyridine.

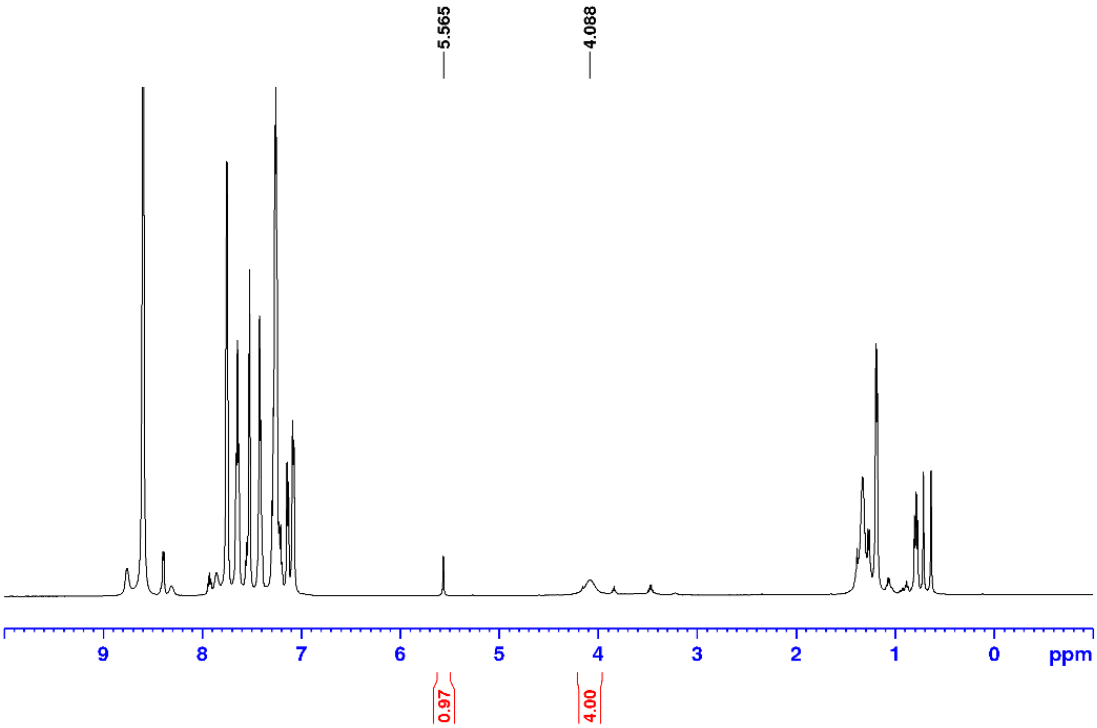


**Figure A53:** $^{1}$H NMR ($CDCl_3$) spectrum of *i*PrBAC-$BH_2$Thex **3-18a** pyridine trityl addition, with 2 equiv. of pyridine.

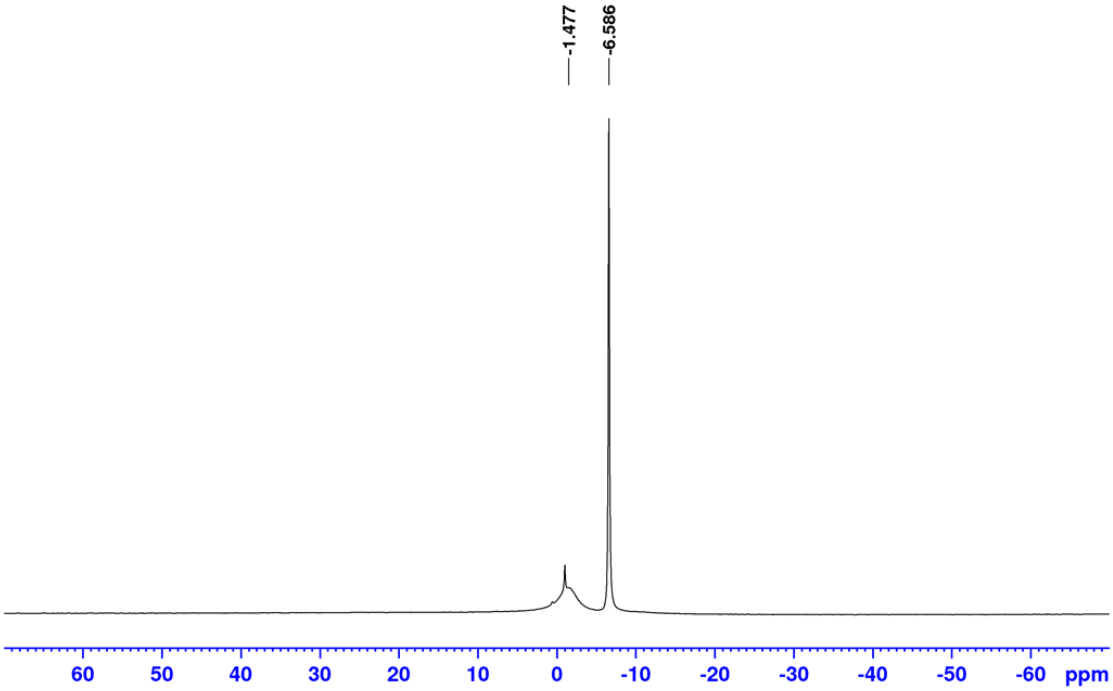


**Figure A 54:** $^{11}$B NMR ($CDCl_3$) spectrum of *i*PrBAC-$BH_2$Thex **3-18a** pyridine trityl addition, with 2 equiv. of pyridine.

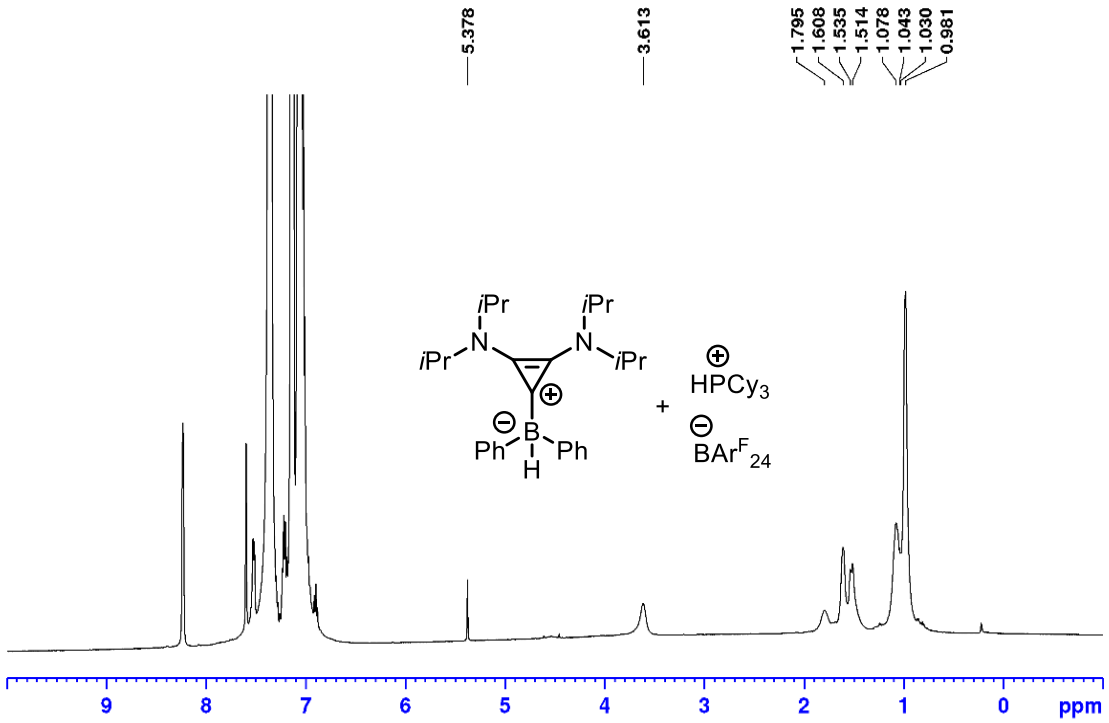


**Figure A55:** $^{1}$H NMR (500 MHz, $C_6D_6$) spectrum of Hydrogen activation with [*i*PrBAC-$BPh_2$][$BAr^F_{24}$] **3-25** and $PCy_3$.

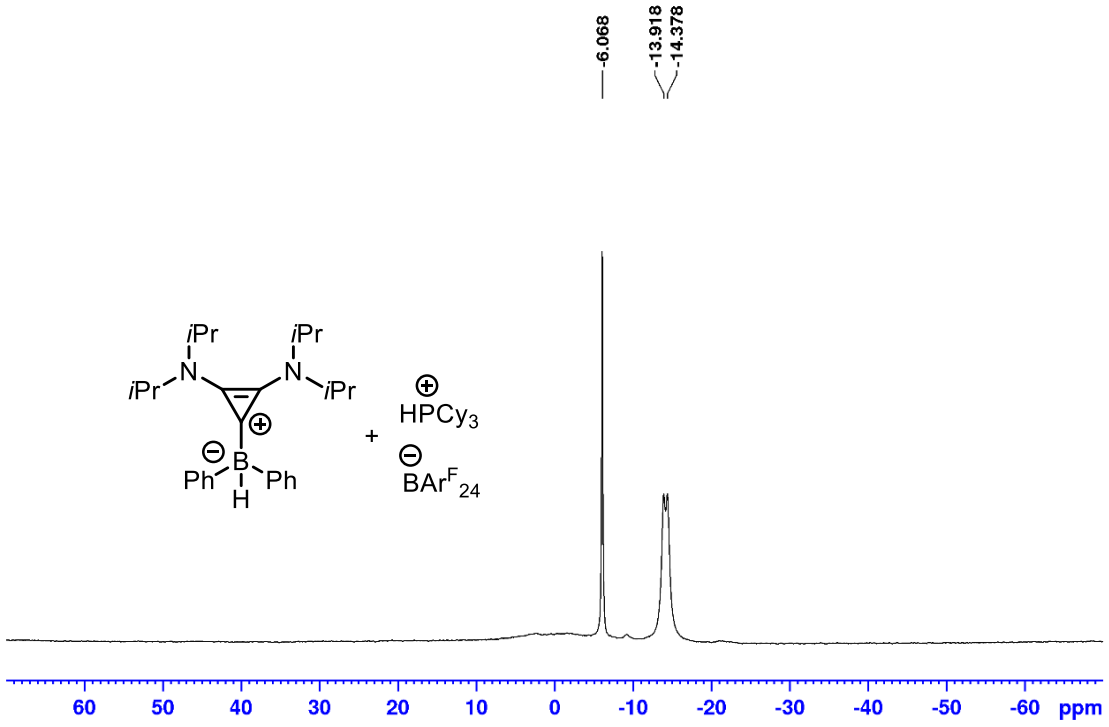


**Figure A 56:** $^{11}$B NMR (500 MHz, $C_6D_6$) spectrum of Hydrogen activation with [*i*PrBAC-$BPh_2$][$BAr^F_{24}$] **3-25** and $PCy_3$.

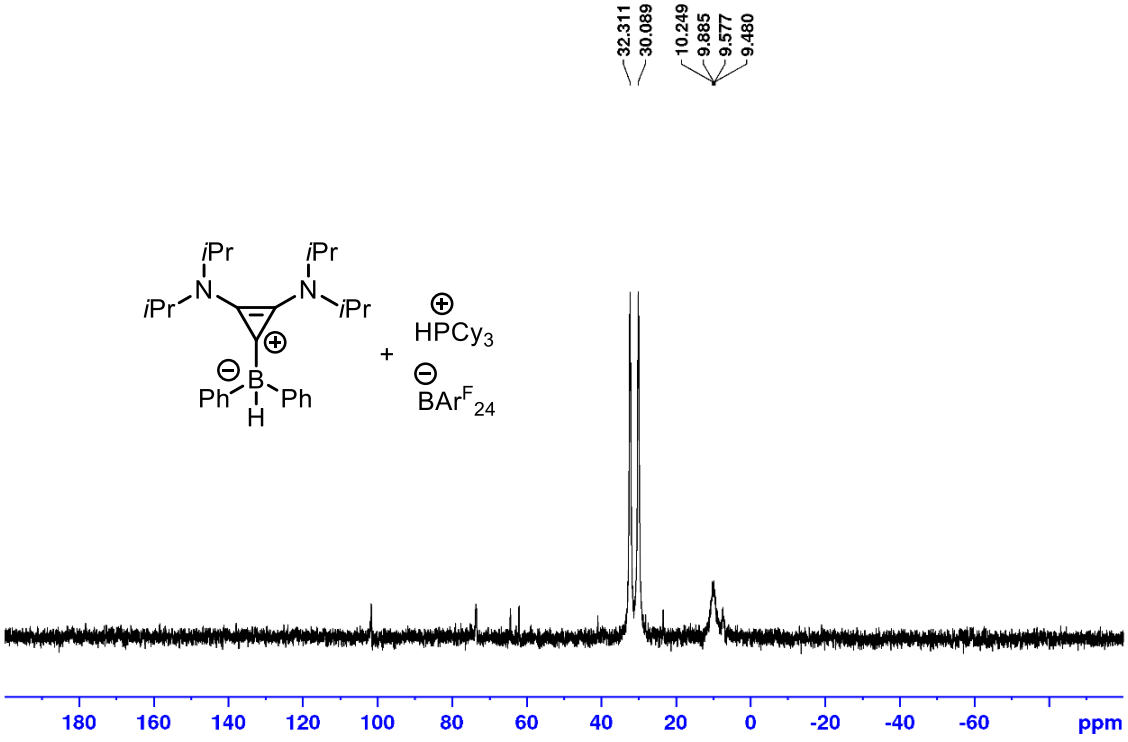


**Figure A57:** $^{31}$P NMR (500 MHz, $C_6D_6$) spectrum of Hydrogen activation with [*i*PrBAC-$BPh_2$][$BAr^F{}_{24}$] **3-25** and $PCy_3$.

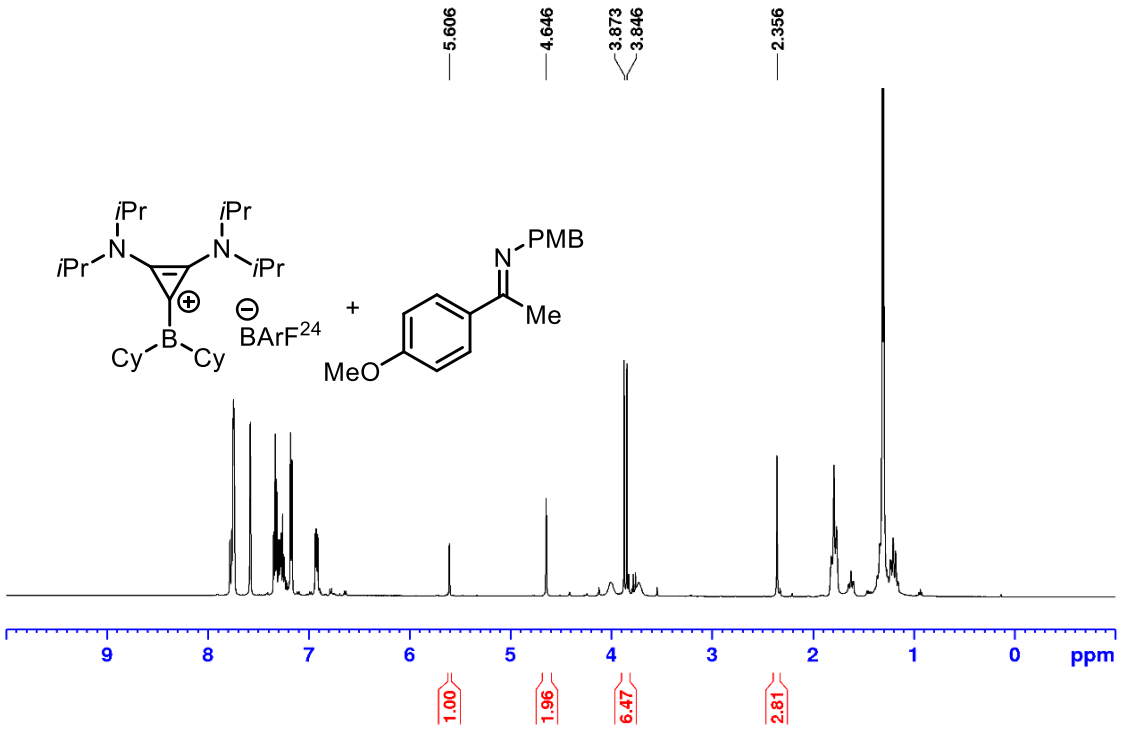


**Figure A58:** $^1$H NMR ($CDCl_3$) spectrum of imine complexation reaction with borenium **3-13** and imine **3-14a**.

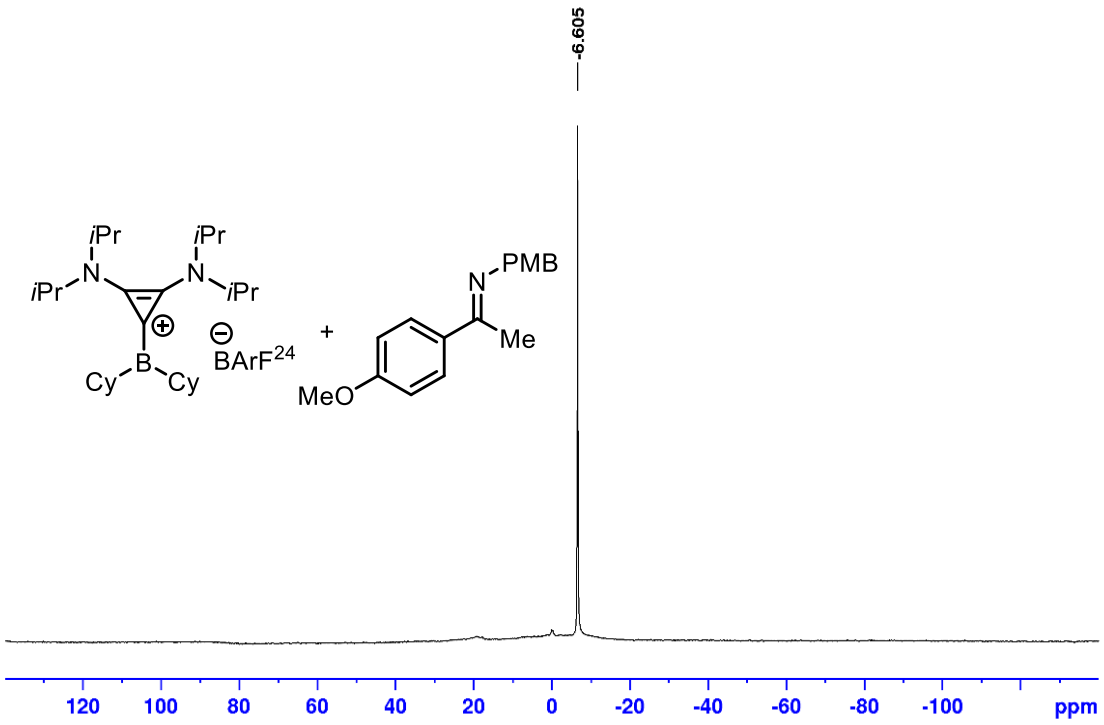


**Figure A59:** $^{11}B$ NMR ($CDCl_3$) spectrum of imine complexation reaction with borenium **3-13** and imine **3-14a**.

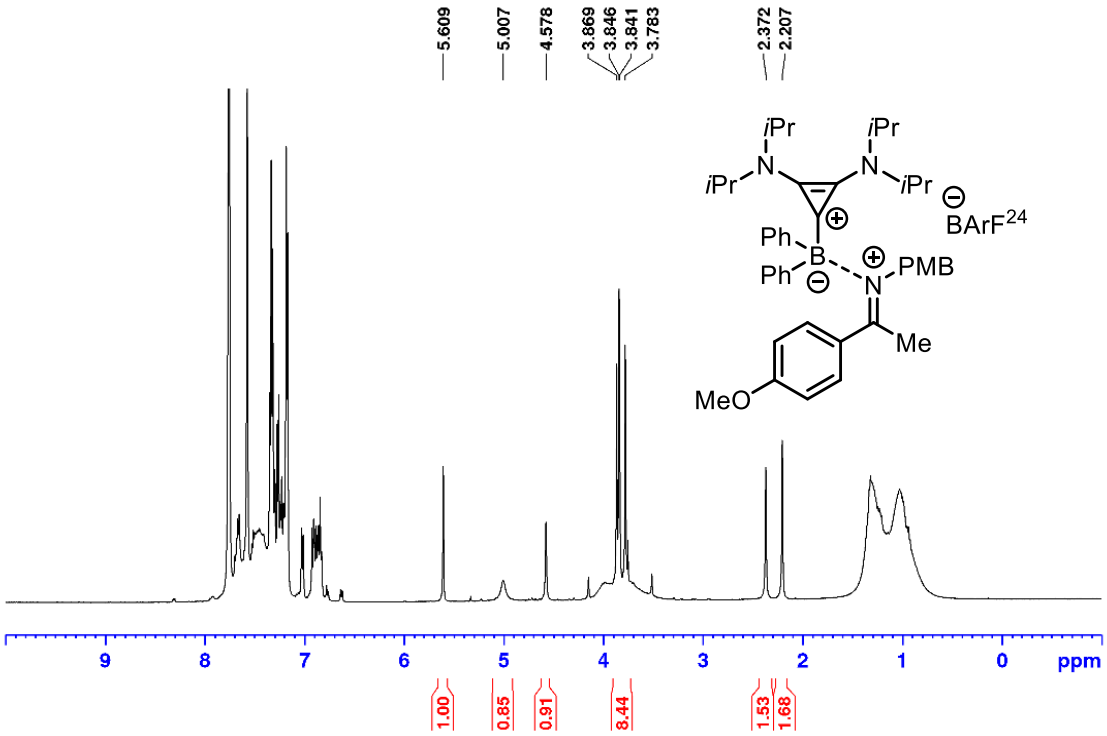


**Figure A60:** $^{1}H$ NMR ($CDCl_3$) spectrum of imine complexation reaction with borenium **3-25** and imine **3-14a**.

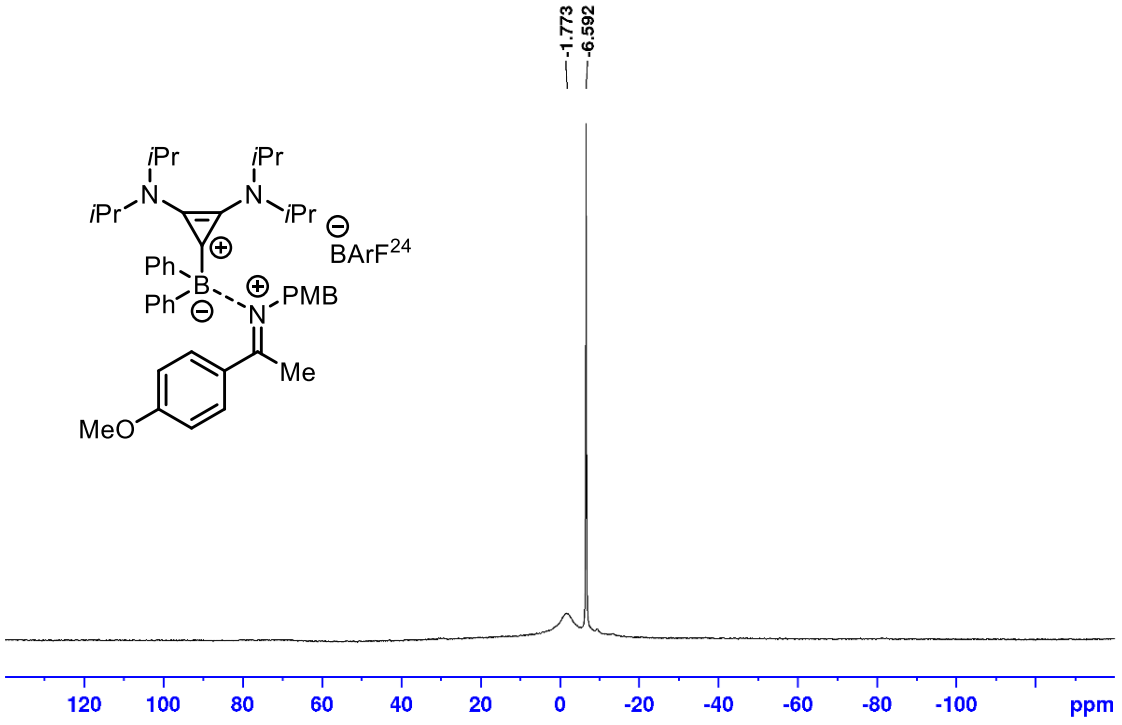


**Figure A61:** $^{11}$B NMR ($CDCl_3$) spectrum of imine complexation reaction with borenium **3-25** and imine **3-14a**.

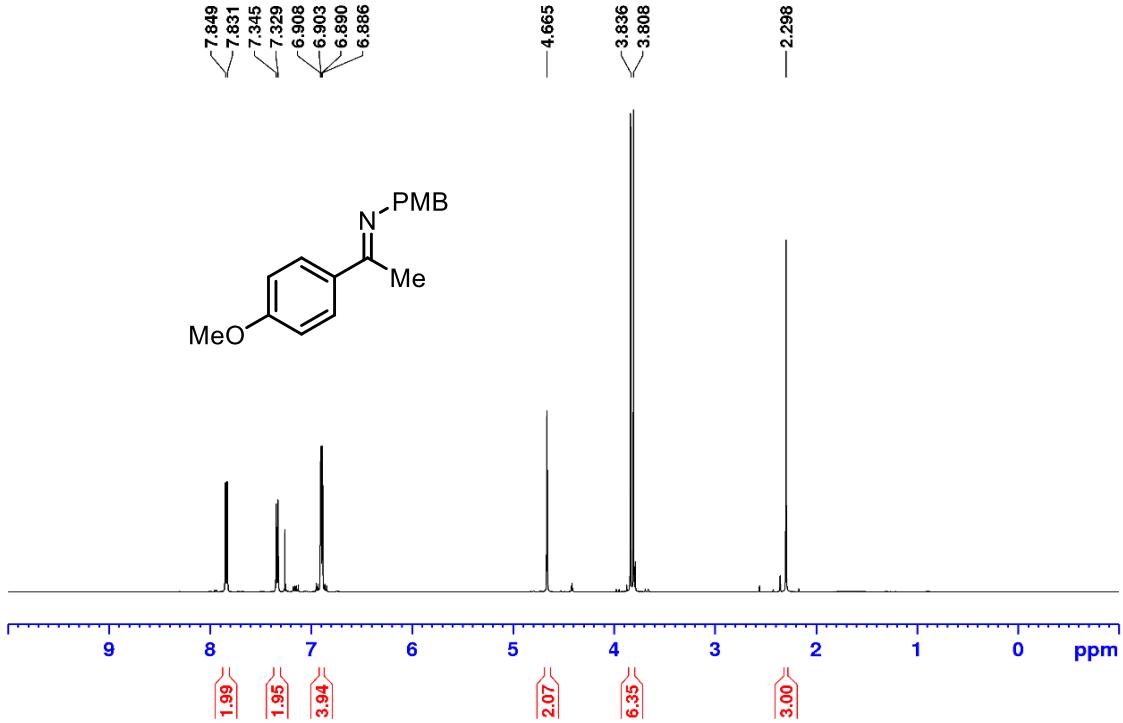


**Figure A62:** $^{1}$H NMR (300 MHz, $CDCl_3$) spectrum of imine **3-14a**.

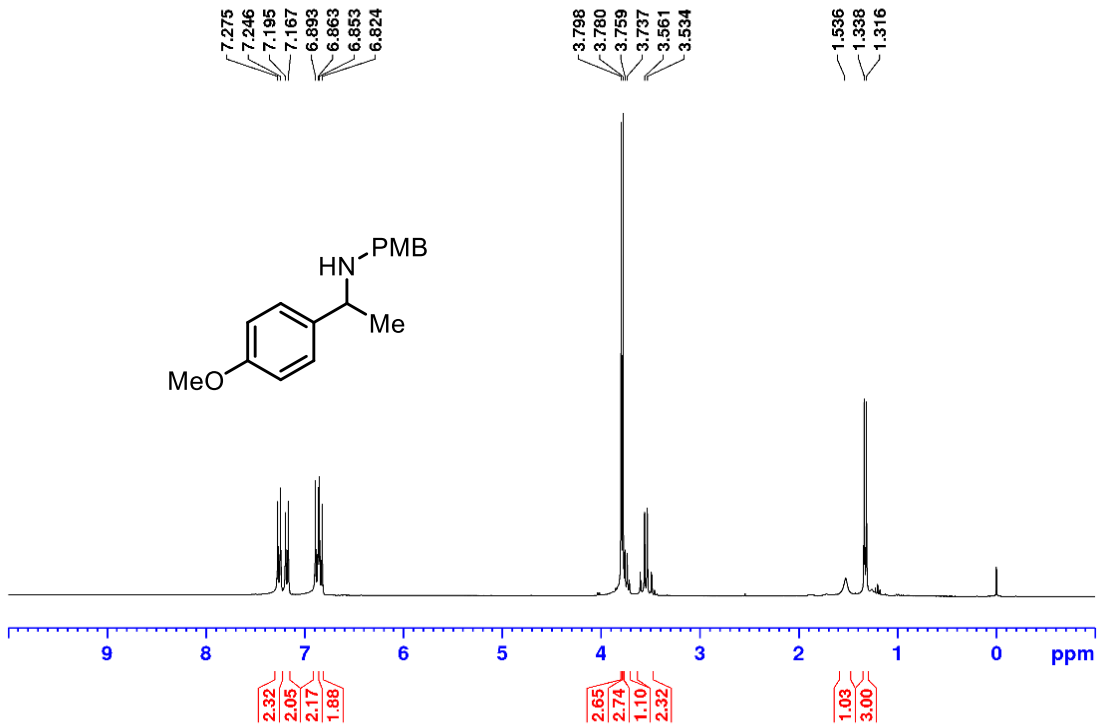


**Figure A63:** $^{1}$H NMR (300 MHz, $CDCl_3$) spectrum of amine **3-15a**.

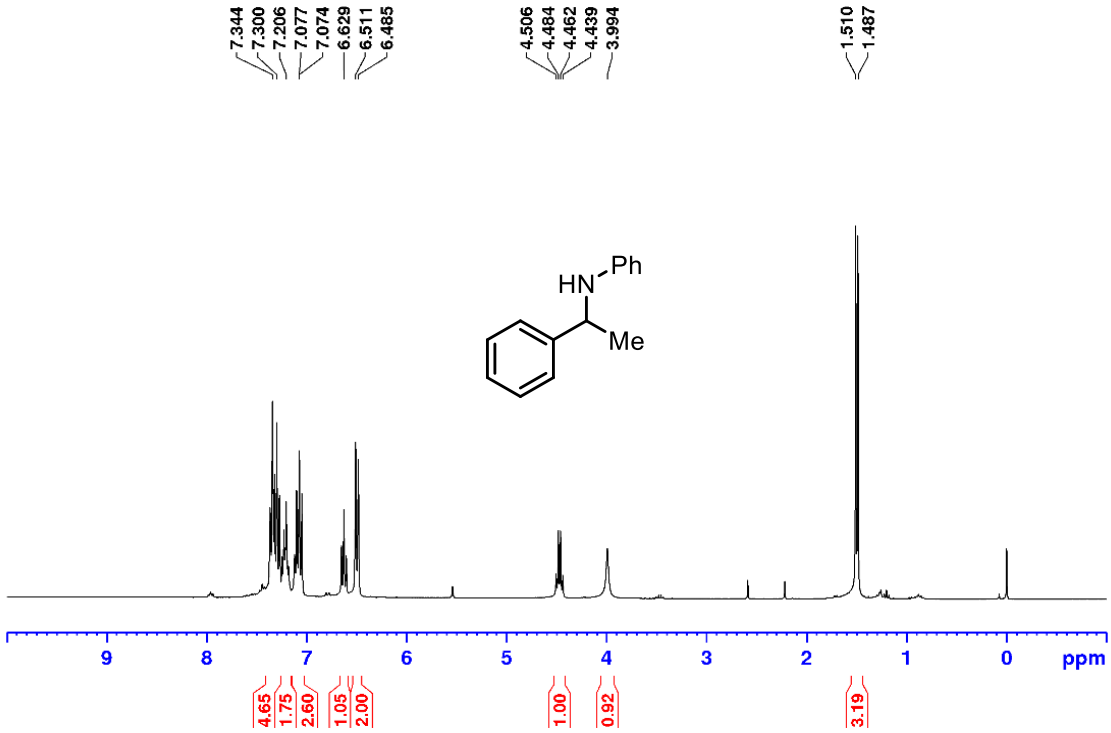


**Figure A64:** $^{1}$H NMR (300 MHz, $CDCl_3$) spectrum of amine **3-15b**.

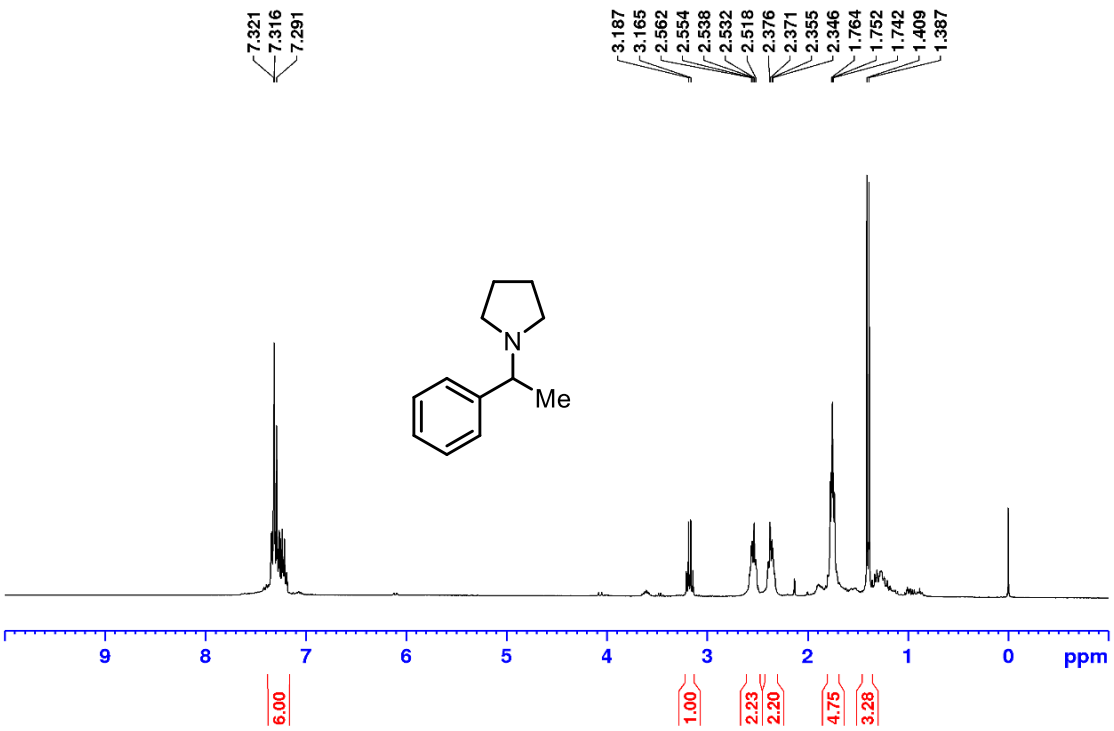


**Figure A65:** $^{1}$H NMR (300 MHz, $CDCl_3$) spectrum of amine **3-15c**.

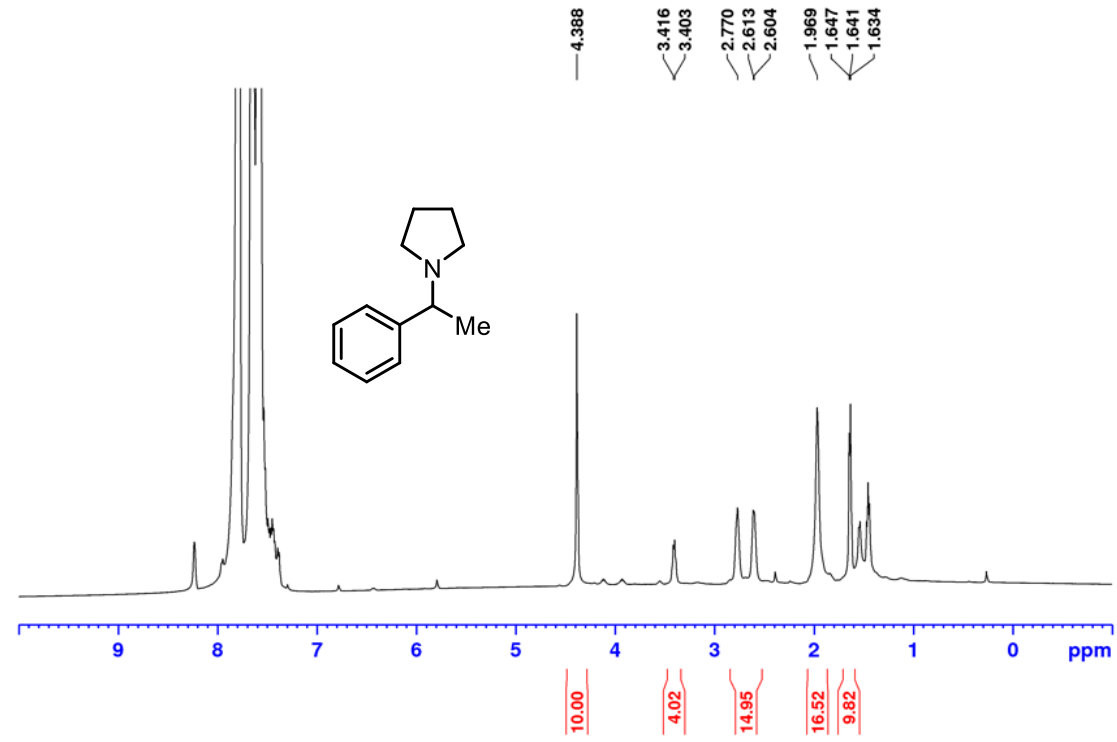


**Figure A66:** $^{1}$H NMR (300 MHz, $CDCl_3$) spectrum of amine **3-15c** *in situ* with 0.5 mmol of ferrocene.

## Appendix C: Appendix for Chapter 4

### C1: Crystallographic Solution and Refinement Details

**Table A8.** Crystallographic Experimental Details for **4-50**

| | |
|---|---|
| *A. Crystal Data* | |
| formula | $C_{58}H_{41.5}BCl_2N_{1.50}O_4$ |
| formula weight | 905.13 |
| crystal dimensions (mm) | 0.74 × 0.34 × 0.33 |
| crystal system | monoclinic |
| space group | $P2_1$ (No. 4) |
| unit cell parameters[a] | |
| $a$ (Å) | 14.7951(7) |
| $b$ (Å) | 19.1577(9) |
| $c$ (Å) | 16.1613(8) |
| $\alpha$ (deg) | 90.000 |
| $\beta$ (deg) | 94.160(3) |
| $\gamma$ (deg) | 90.000 |
| $V$ (Å$^3$) | 4568.7(4) |
| $Z$ | 4 |
| $\rho_{calcd}$ (g cm$^{-3}$) | 1.316 |
| $\mu$ (mm$^{-1}$) | 1.684 |
| *B. Data Collection and Refinement Conditions* | |
| diffractometer | Bruker D8[b] |
| radiation ($\lambda$ [Å]) | Cu K$\alpha$ (1.54178) (microfocus source) |
| temperature (°C) | –100 |
| scan type | $\omega$ and $\phi$ scans (1.0°) (5-5-10 s exposures)[c] |
| data collection $2\theta$ limit (deg) | 149.29 |
| total data collected | 90684 (-18 ≤ $h$ ≤ 18, -23 ≤ $k$ ≤ 21, -20 ≤ $l$ ≤ 20) |
| independent reflections | 17061 ($R_{int}$ = 0.0892) |
| number of observed reflections (*NO*) | 14723 [$F_o^2 \geq 2\sigma(F_o^2)$] |
| structure solution method | intrinsic phasing (*SHELXT-2014*[d]) |
| refinement method | full-matrix least-squares on $F^2$ (*SHELXL–2016*[e]) |
| absorption correction method | multi-scan (*SADABS*) |
| range of transmission factors | 1.0000–0.5400 |
| data/restraints/parameters | 17061 / 2[f] / 1177 |
| extinction coefficient ($x$)[g] | 0.0020(3) |
| Flack absolute structure parameter[h] | 0.13(4) |
| goodness-of-fit ($S$)[i] [all data] | 1.061 |
| final $R$ indices[j] | |
| $R_1$ [$F_o^2 \geq 2\sigma(F_o^2)$] | 0.0736 |
| $wR_2$ [all data] | 0.2104 |

largest difference peak and hole 0.700 and –0.704 e $Å^{-3}$

[a]Obtained from least-squares refinement of 9779 reflections with $5.48° < 2\theta < 147.58°$.

[b]Programs for diffractometer operation, data collection, data reduction and absorption correction were those supplied by Bruker.

[c]Data were collected with the detector set at three different positions. Low-angle (detector $2\theta = –33^{o}$) data frames were collected using a scan time of 5 s, medium-angle (detector $2\theta = 75^{o}$) frames using a scan time of 5 s, and high-angle (detector $2\theta = 117^{o}$) frames using a scan time of 10 s.

[d]Sheldrick, G. M. *Acta Crystallogr.* **2015**, *A71*, 3–8. (*SHELXT-2014*)

[e]Sheldrick, G. M. *Acta Crystallogr.* **2015**, *C71*, 3–8. (*SHELXL-2016*)

[f]The bond length of Cl1S–C1S, Cl2S–C1S was restrained by the *SHELXL* instruction *SADI* to maintain suitable distances of these solvent atoms.

[g]$F_c^* = kF_c[1 + x\{0.001F_c^2\lambda^3/\sin(2\theta)\}]^{-1/4}$ where $k$ is the overall scale factor.

[h]Flack, H. D. *Acta Crystallogr.* **1983**, *A39*, 876–881; Flack, H. D.; Bernardinelli, G. *Acta Crystallogr.* **1999**, *A55*, 908–915; Flack, H. D.; Bernardinelli, G. *J. Appl. Cryst.* **2000**, *33*, 1143–1148. The Flack parameter will refine to a value near zero if the structure is in the correct configuration and will refine to a value near one for the inverted configuration. The value indicated herein is indicative of a small degree of racemic twinning.

[i]$S = [\Sigma w(F_o^2 - F_c^2)^2/(n - p)]^{1/2}$ ($n$ = number of data; $p$ = number of parameters varied; $w = [\sigma^2(F_o^2) + (0.1322P)^2 + 1.7399P]^{-1}$ where $P = [\mathrm{Max}(F_o^2, 0) + 2F_c^2]/3$).

[j]$R_1 = \Sigma||F_o| - |F_c||/\Sigma|F_o|$; $wR_2 = [\Sigma w(F_o^2 - F_c^2)^2/\Sigma w(F_o^4)]^{1/2}$.

## C2: NMR Spectra for Chapter 4

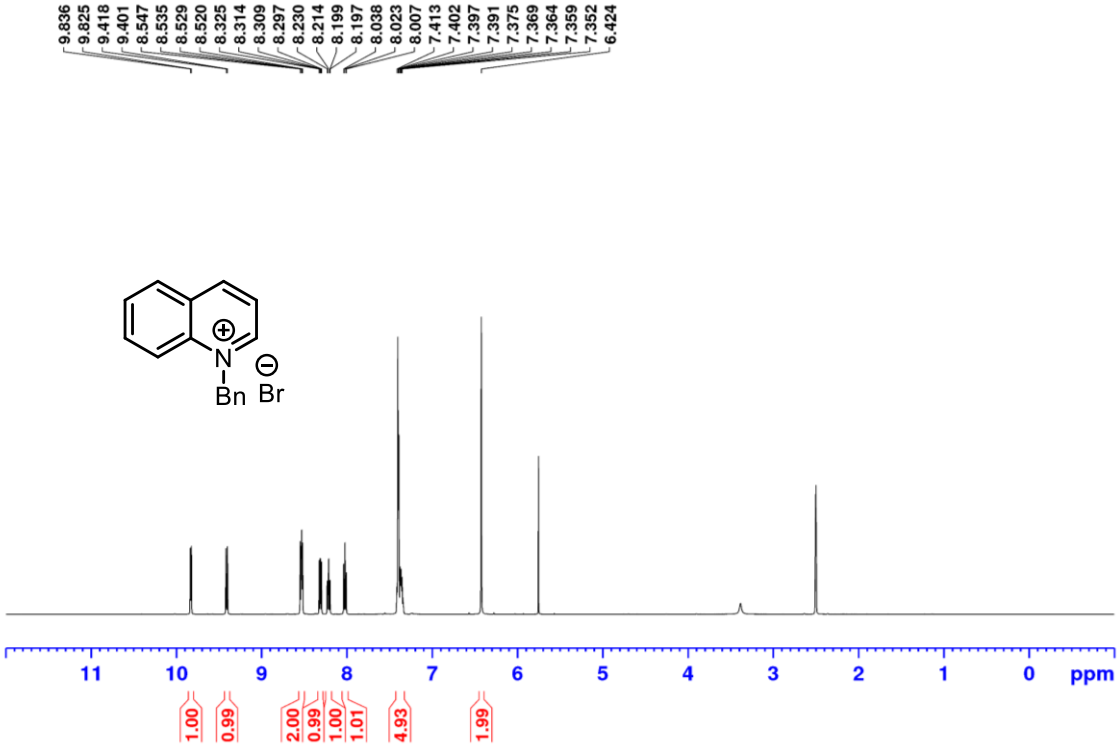


**Figure A67:** $^{1}$H NMR (500 MHz, $CDCl_3$) spectrum of *N*-Bn Quinolinium bromide **4-5**.

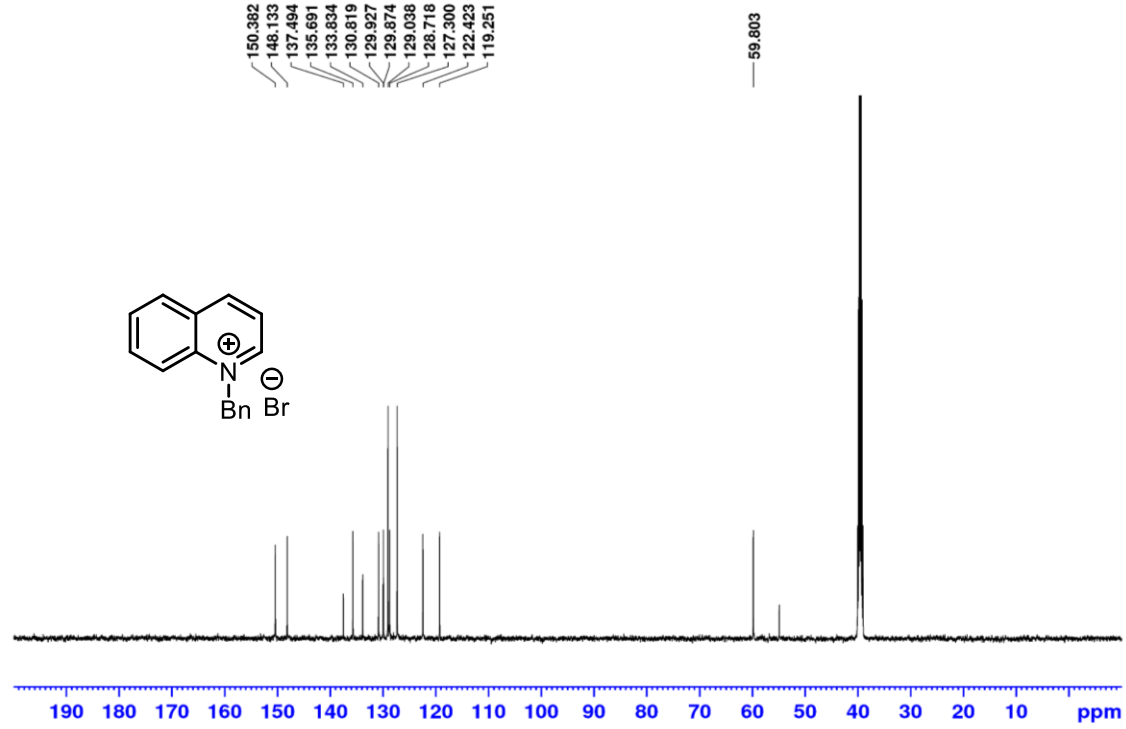


**Figure A68:** $^{13}$C {$^{1}$H} NMR (125.8 MHz, $CDCl_3$) spectrum of *N*-Bn Quinolinium bromide **4-5**.

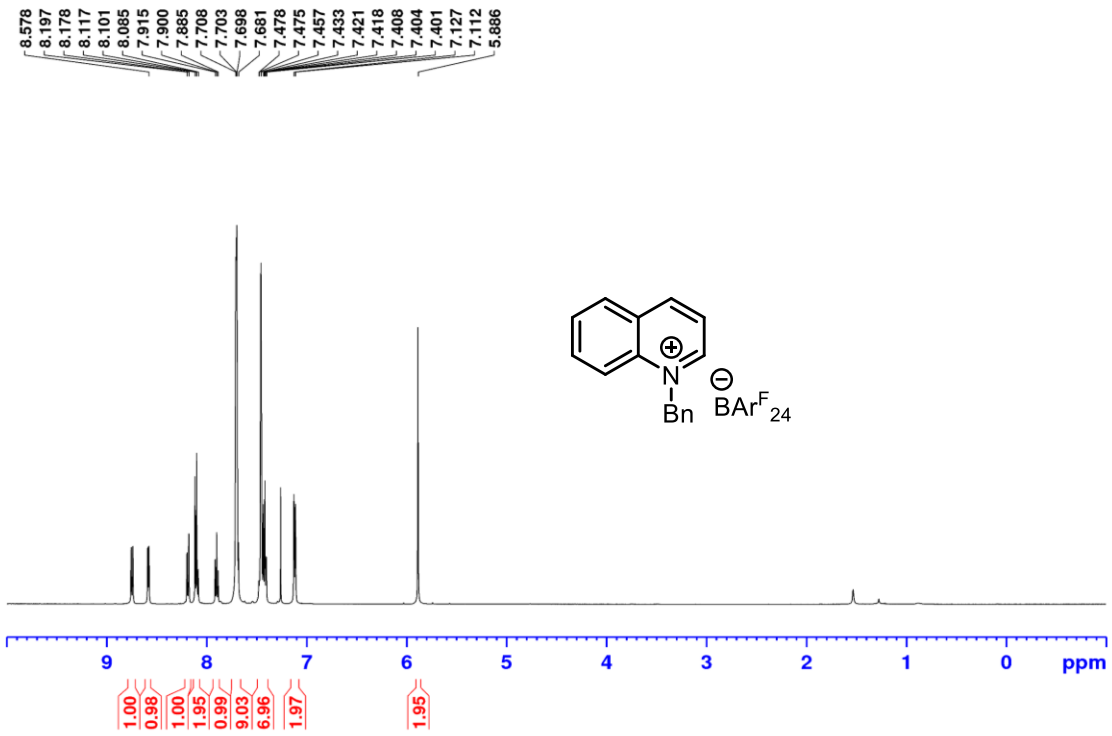


**Figure A69:** $^{1}$H NMR (500 MHz, $CDCl_3$) spectrum of *N*-Bn Quinolinium $BAr^{F}_{24}$ **4-6**.

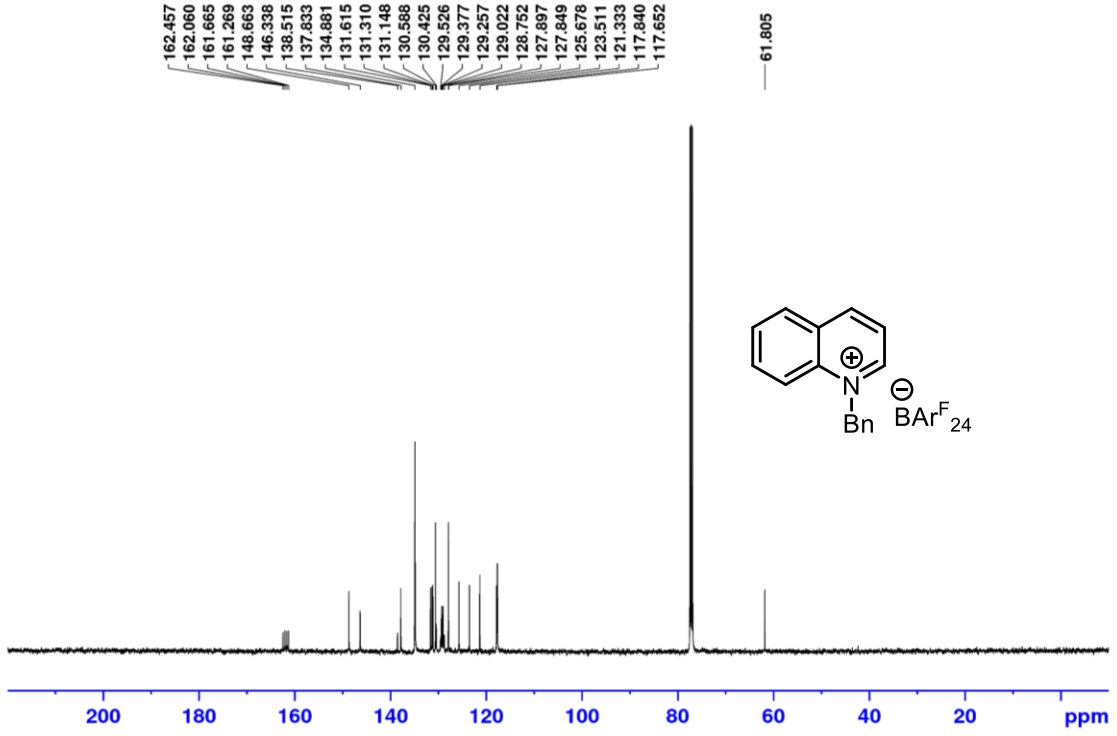


**Figure A70:** $^{13}$C {$^{1}$H} NMR (125.8 MHz, $CDCl_3$) spectrum of *N*-Bn Quinolinium $BAr^{F}_{24}$ **4-6**.

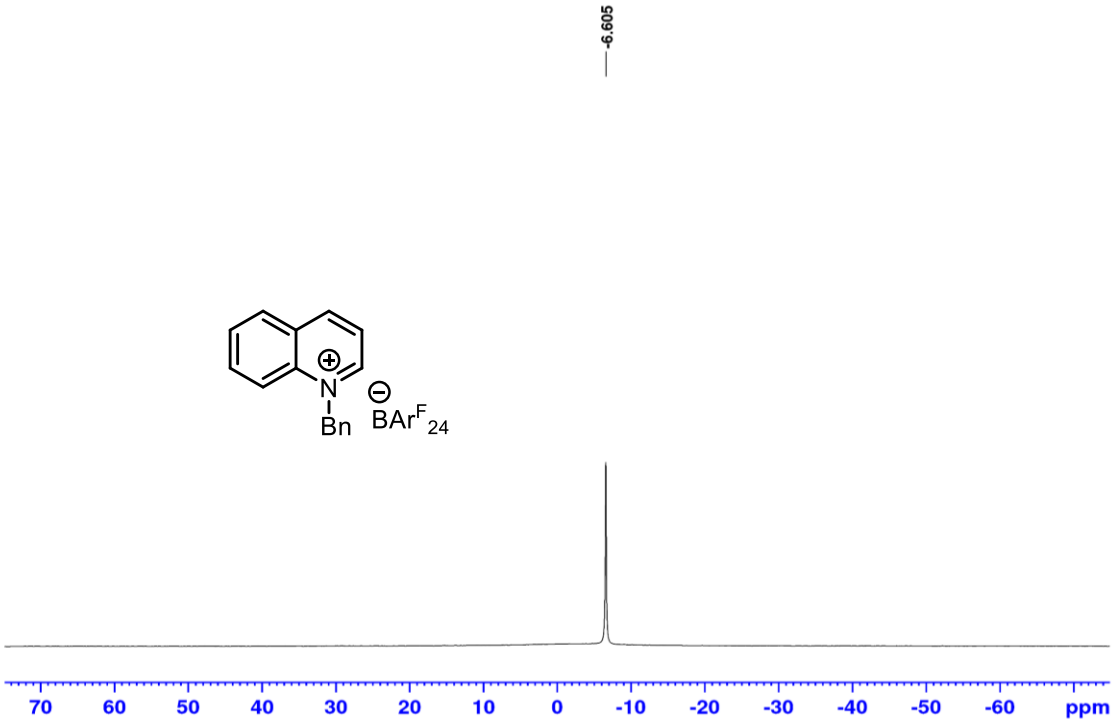


**Figure A71:** $^{11}$B NMR (160.5 MHz, $CDCl_3$) spectrum of *N*-Bn Quinolinium BAr$^{F}_{24}$ **4-6**.

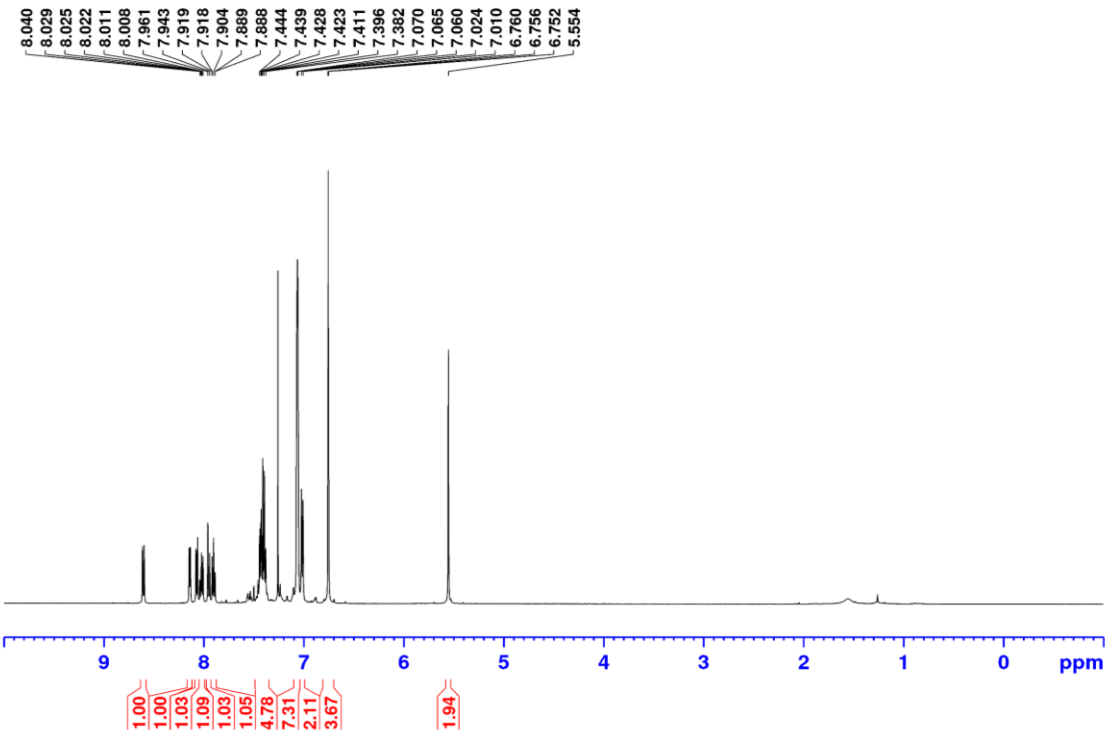


**Figure A72:** $^{1}$H NMR (500 MHz, $CDCl_3$) spectrum of *N*-Bn Quinolinium BAr$^{Cl}_{8}$ **4-15**.

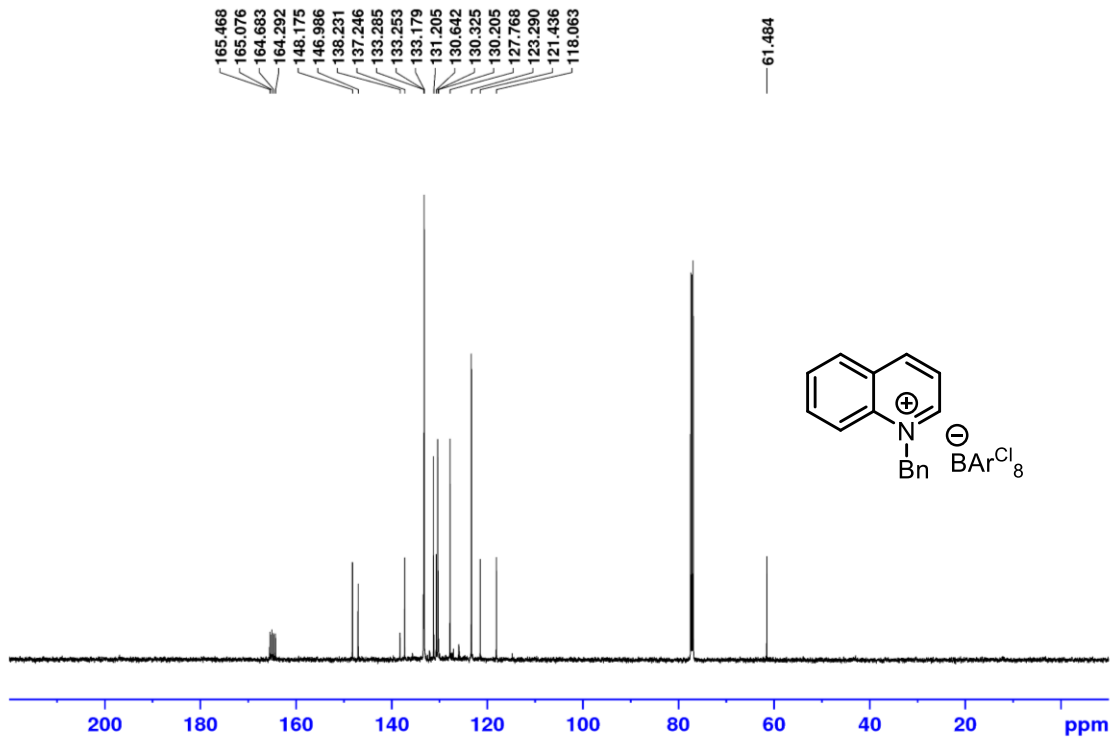


**Figure A73:** $^{13}C$ {$^{1}H$} NMR (125.8 MHz, $CDCl_3$) spectrum of *N*-Bn Quinolinium $BAr^{Cl}_8$ **4-15**.

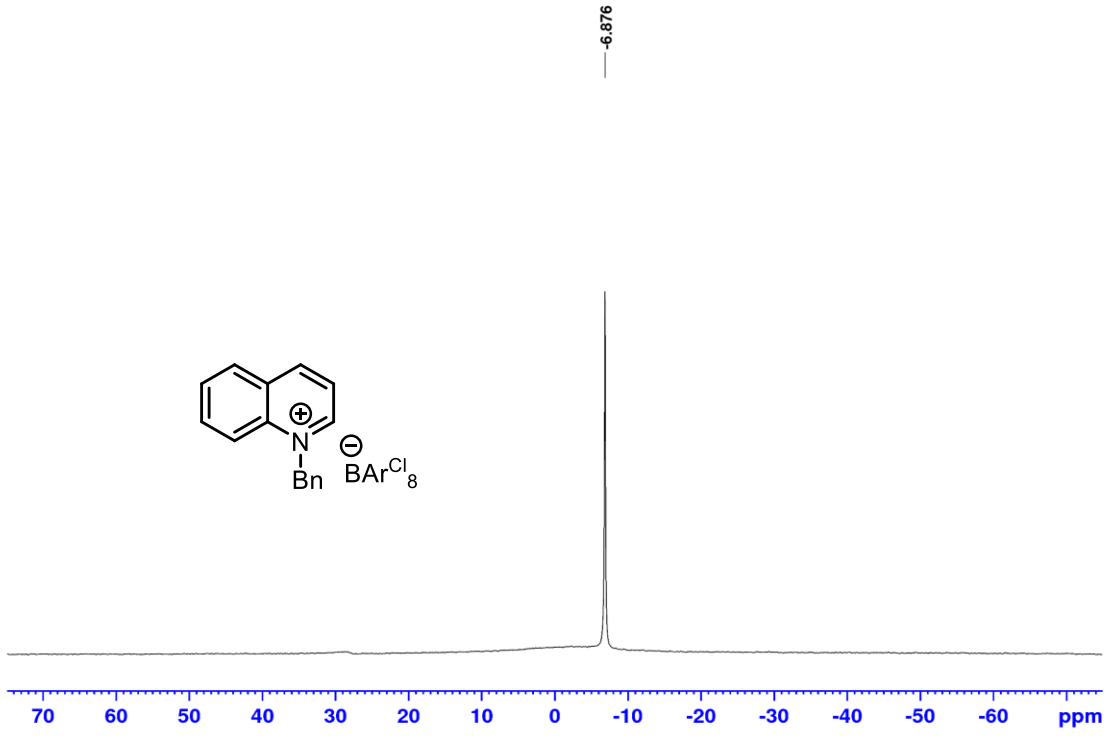


**Figure A74:** $^{11}B$ NMR (160.5 MHz, $CDCl_3$) spectrum of *N*-Bn Quinolinium $BAr^{Cl}_8$ **4-15**.

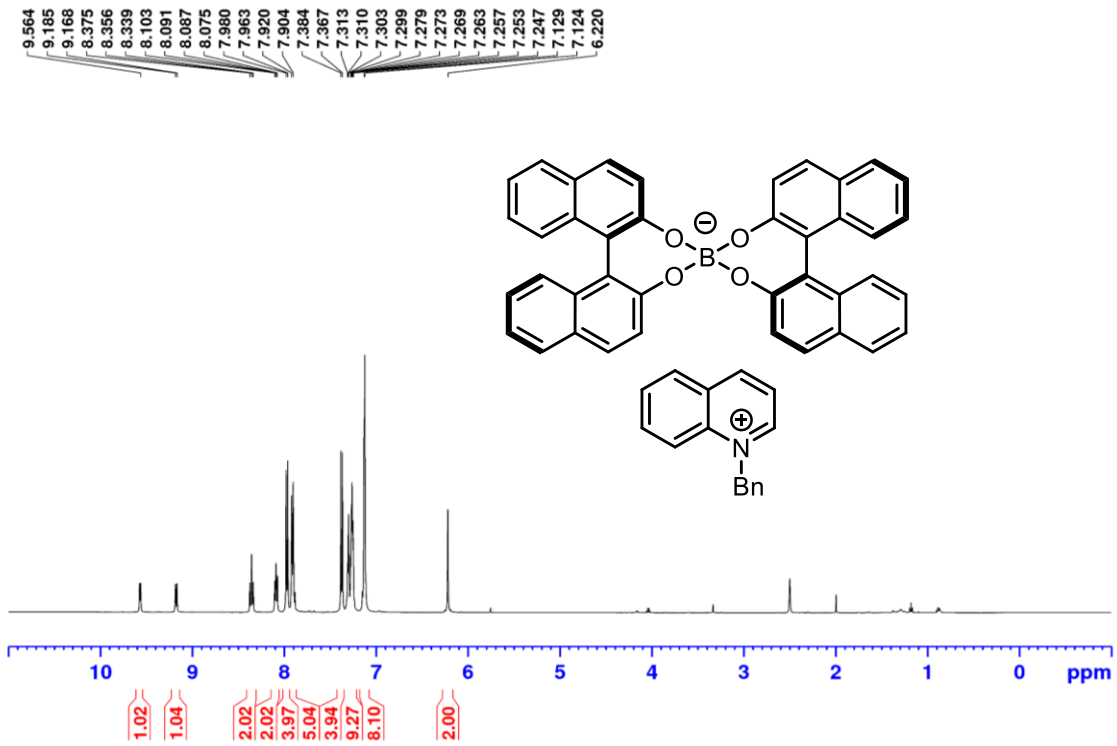


**Figure A75:** $^{1}$H NMR (500 MHz, $(CD_3)_2SO$) spectrum of *N*-Bn Quinolinium B(R-BINOL)$_2$ **4-50**.

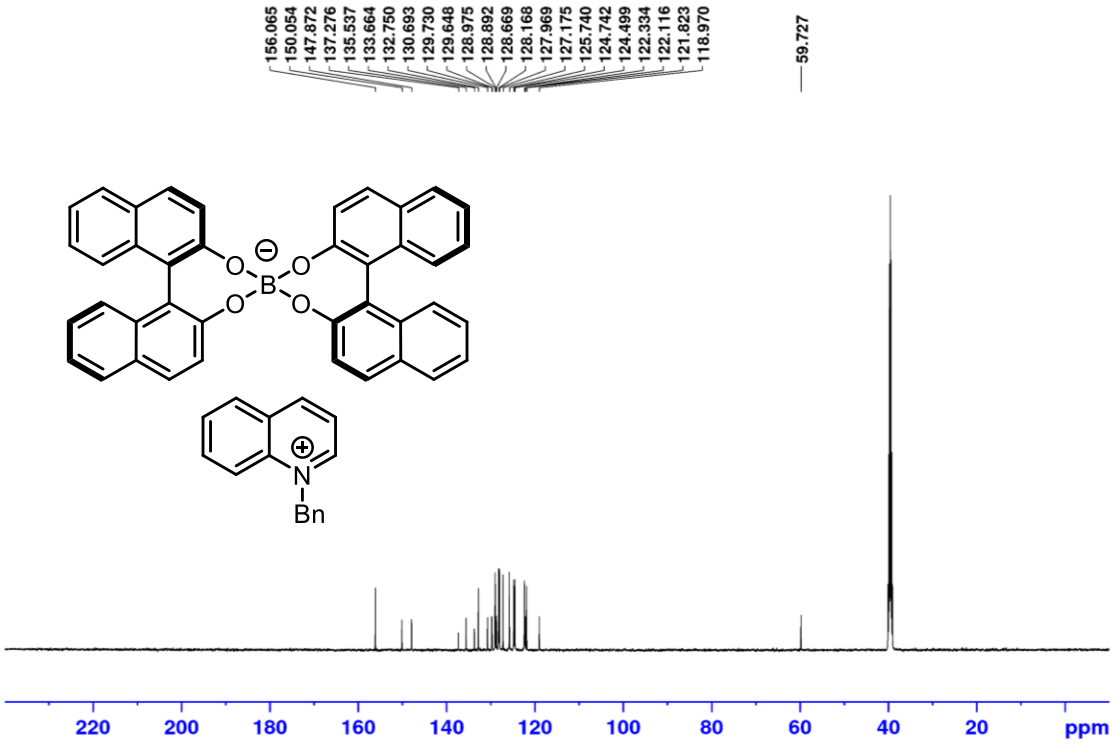


**Figure A76**: $^{13}$C {$^{1}$H} NMR (125.8 MHz, $(CD_3)_2SO$) spectrum of *N*-Bn Quinolinium B(R-BINOL)$_2$ **4-50**.

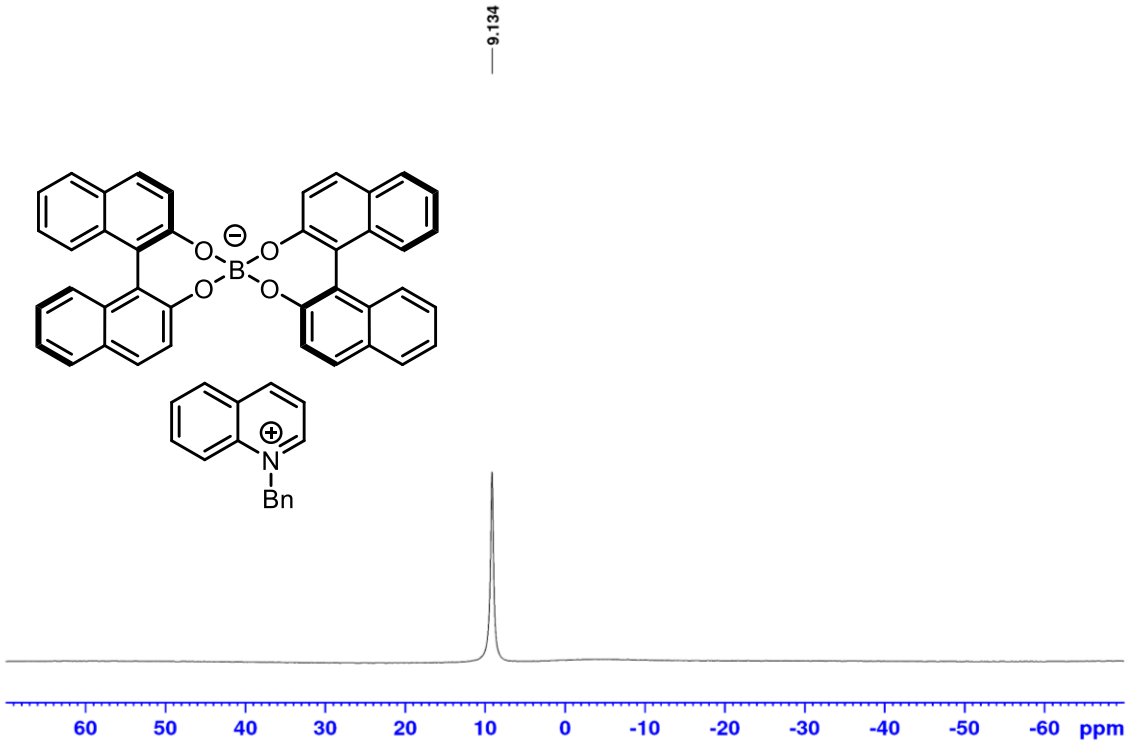


**Figure A77:** $^{11}$B NMR (160.5 MHz, $(CD_3)_2SO$) spectrum of *N*-Bn Quinolinium B(R-BINOL)$_2$ **4-50**.

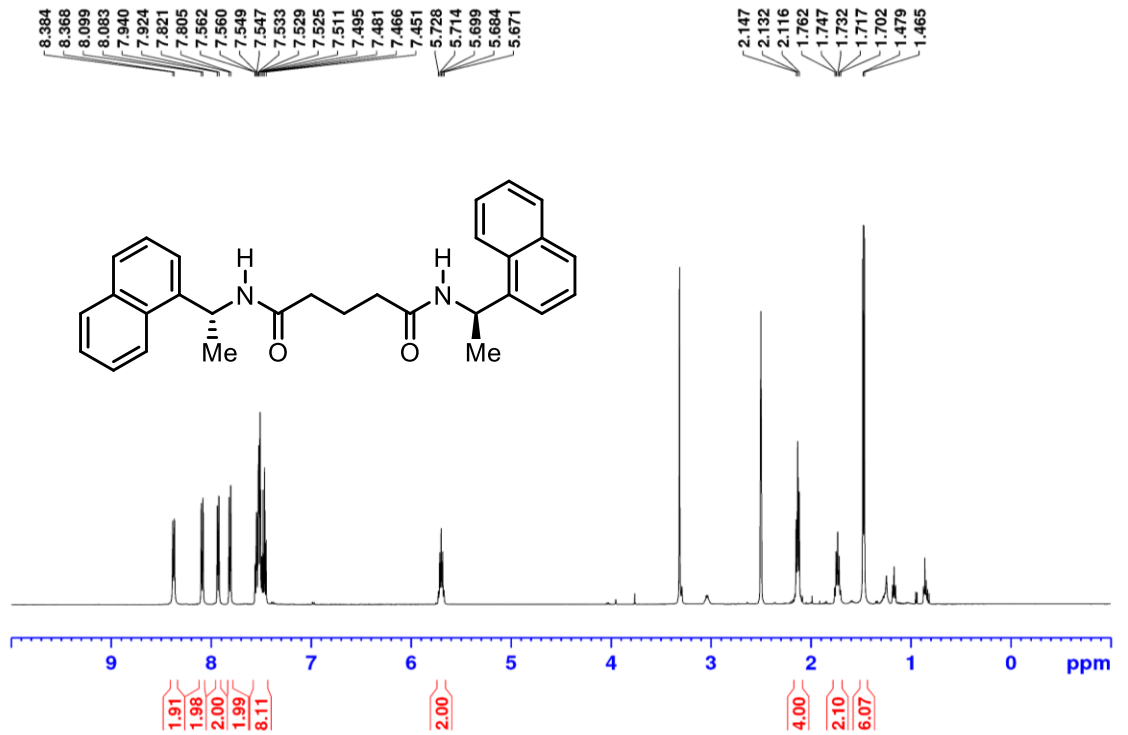


**Figure A78:** $^{1}$H NMR (500 MHz, $(CD_3)_2SO$) spectrum of *N,N*-bis[(1-(R)-napthylethyl]pentanediamide.

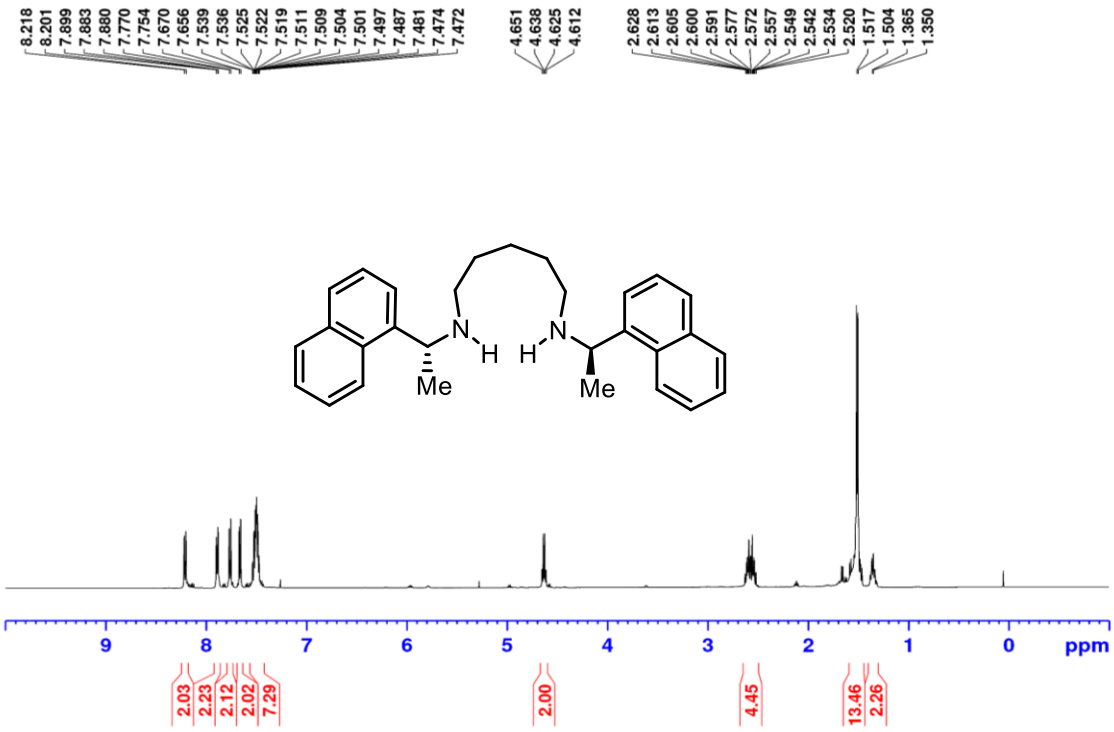


**Figure A79:** $^{1}H$ NMR (500 MHz, $CDCl_3$) spectrum of *N,N*-bis[(1-(R)-napthylethyl]pentanediamine.

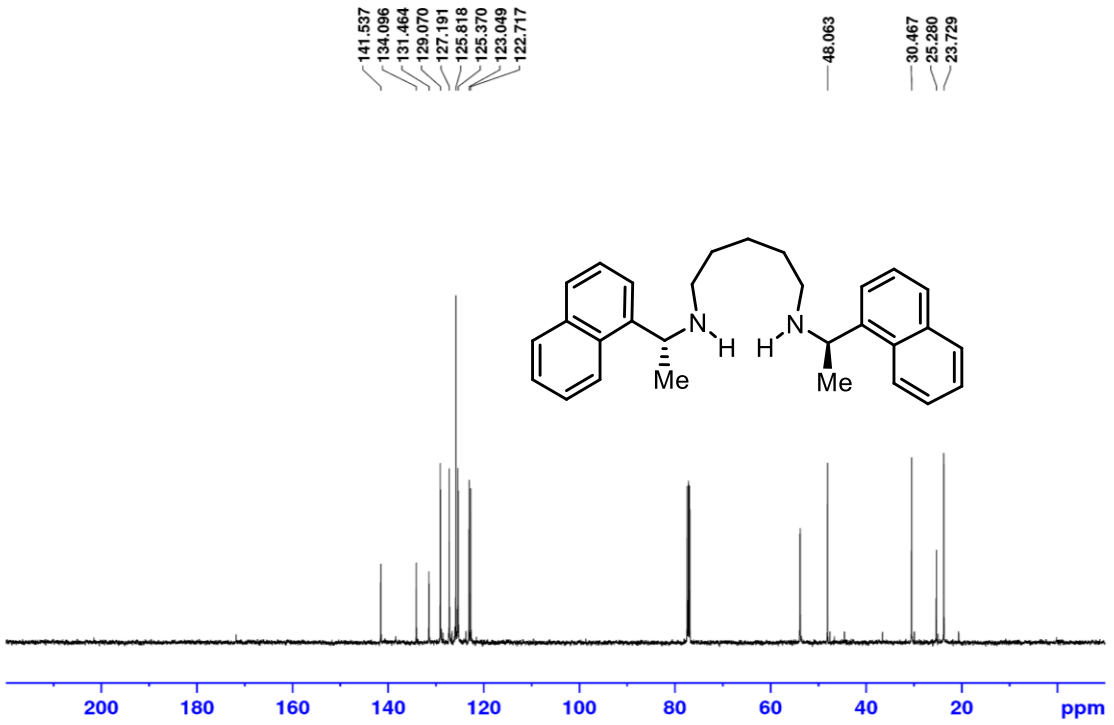


**Figure A80:** $^{13}C$ {$^{1}H$} NMR (125.8 MHz, $CDCl_3$) spectrum of *N,N*-bis[(1-(R)-napthylethyl]pentanediamine.

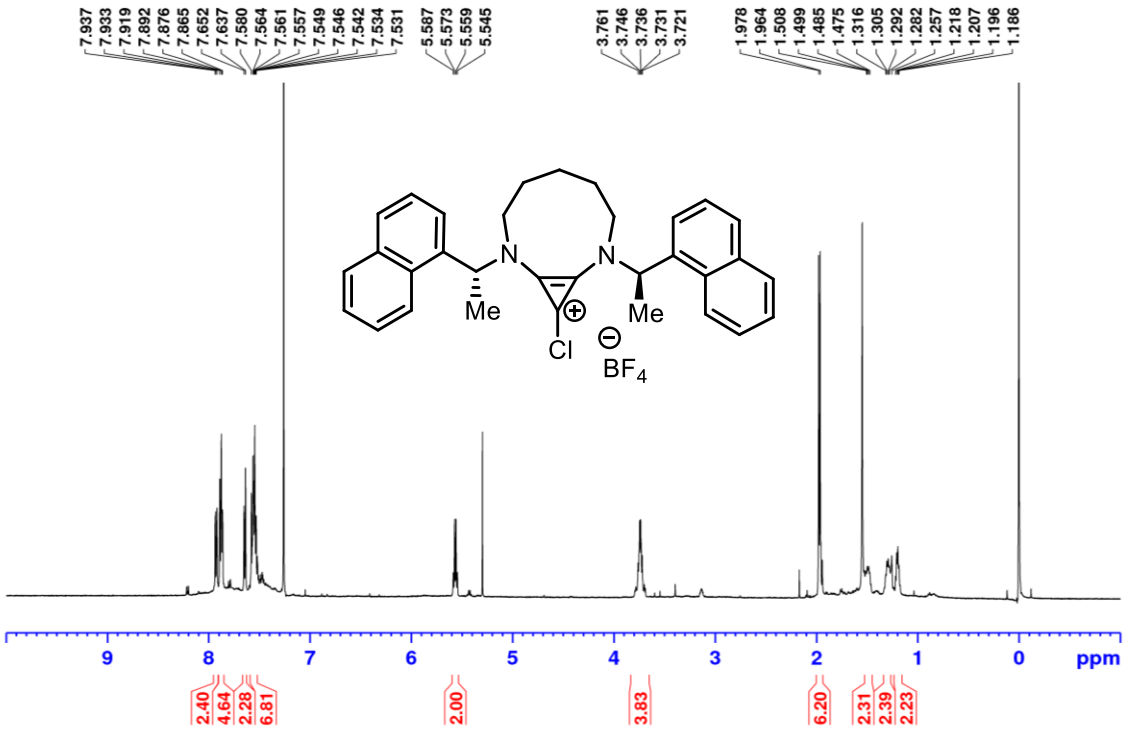


**Figure A81:** $^{1}$H NMR (500 MHz, $CDCl_3$) spectrum of [(*N,N*-bis[(1-(R)-napthylethyl]pentanediamine)cycloprop-2-en-1-ylidene]chloro tetrafluoroborate.

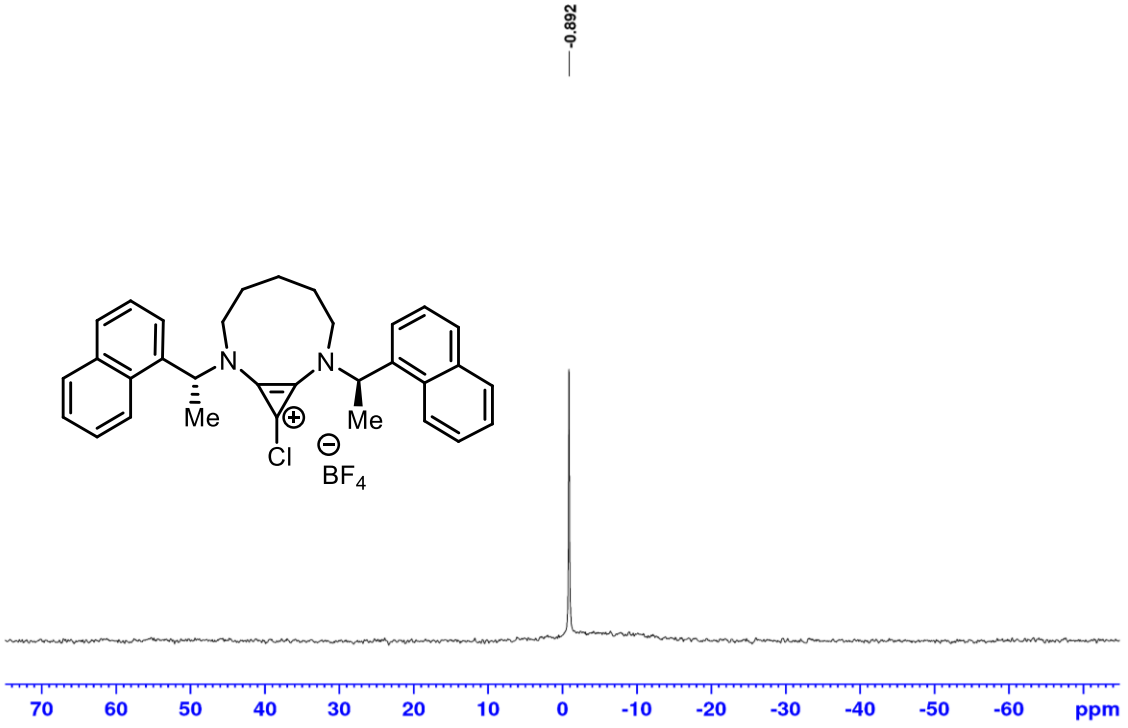


**Figure A82:** $^{11}$B NMR (160.5 MHz, $CDCl_3$) spectrum of [(*N,N*-bis[(1-(R)-napthylethyl]pentanediamine)cycloprop-2-en-1-ylidene]chloro tetrafluoroborate.

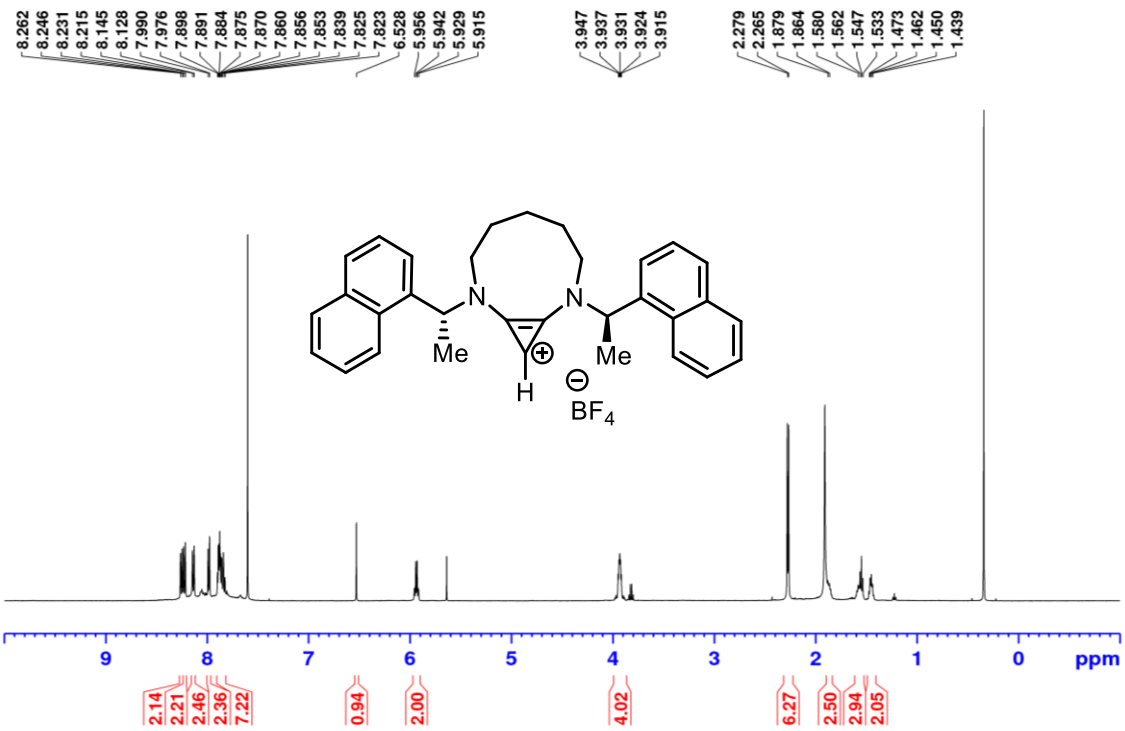


**Figure A83:** $^{1}$H NMR (500 MHz, $CDCl_3$) spectrum of [(N,N-bis[(1-(R)-napthylethyl]pentanediamine)cycloprop-2-en-1-ylidene] tetrafluoroborate **4-35**.

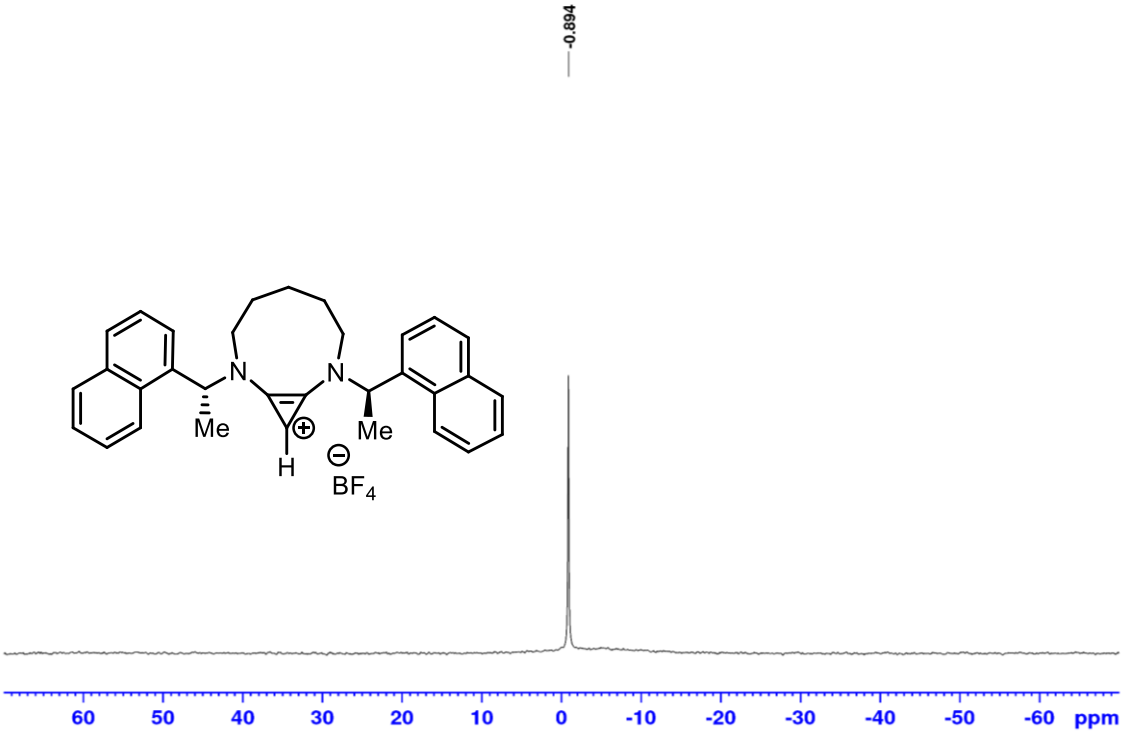


**Figure A84:** $^{11}$B NMR (160.5 MHz, $CDCl_3$) spectrum of [(N,N-bis[(1-(R)-napthylethyl]pentanediamine)cycloprop-2-en-1-ylidene] tetrafluoroborate **4-35**.

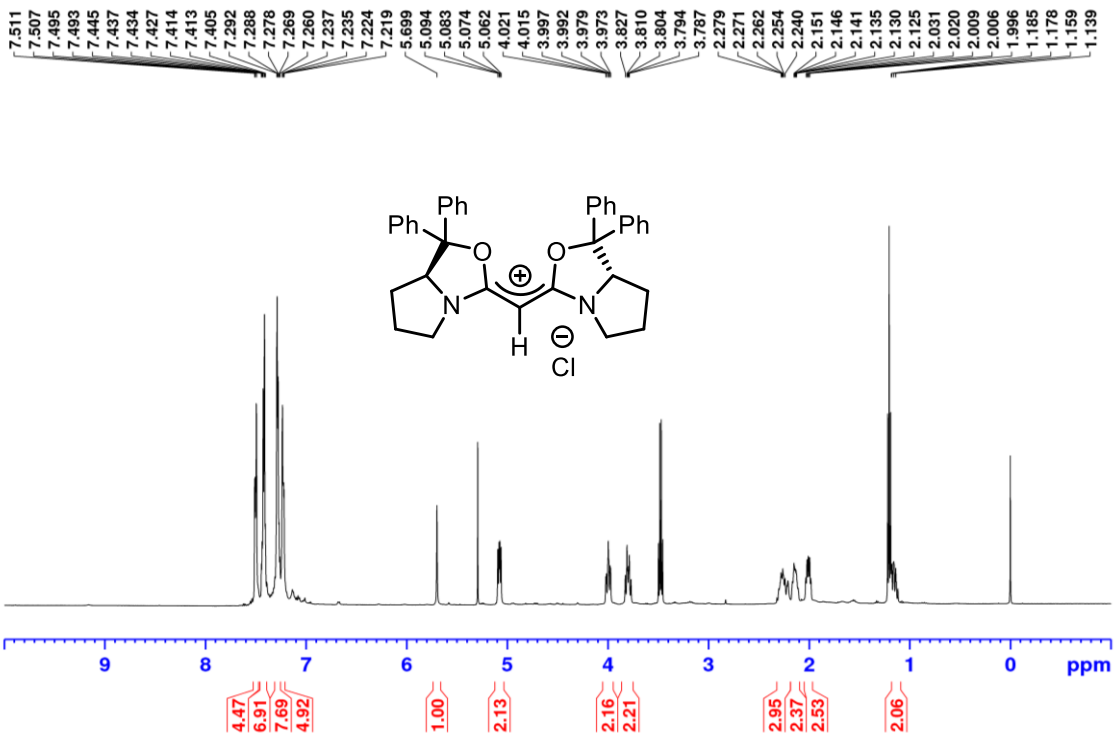


**Figure A85:** $^{1}$H NMR (500 MHz, $CDCl_3$) spectrum of BOXCDC **4-37**.

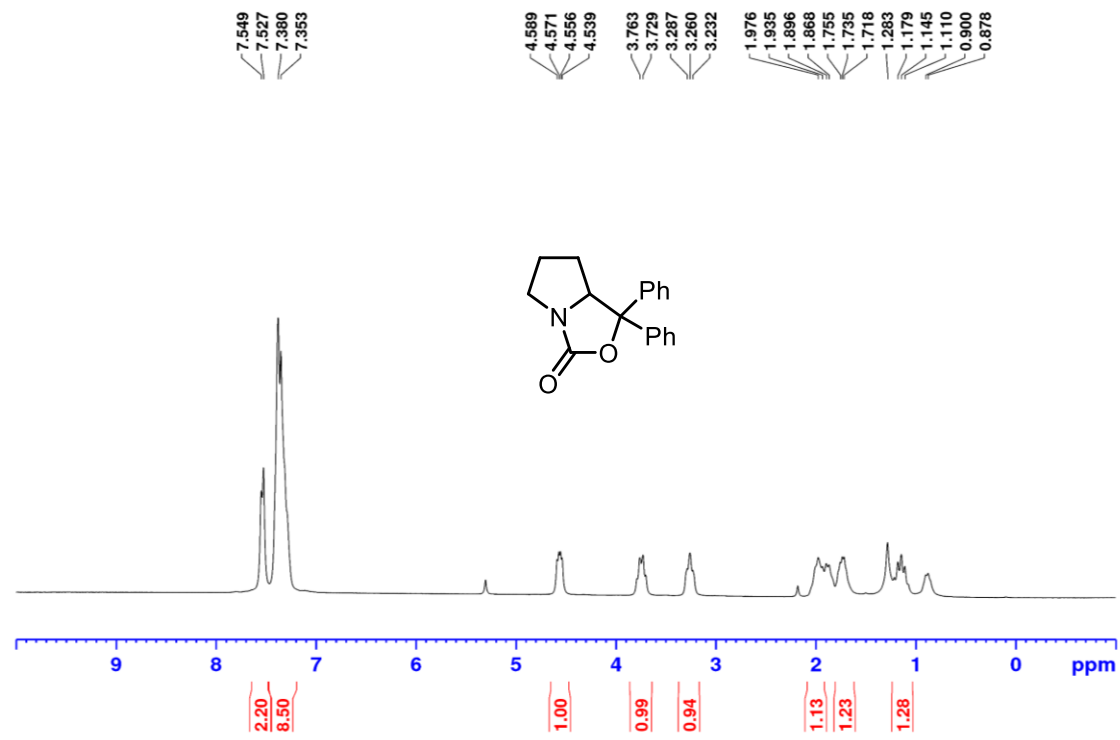


**Figure A86:** $^{1}$H NMR (300 MHz, $CDCl_3$) spectrum of diphenylprolinol carbamate **4-40**.

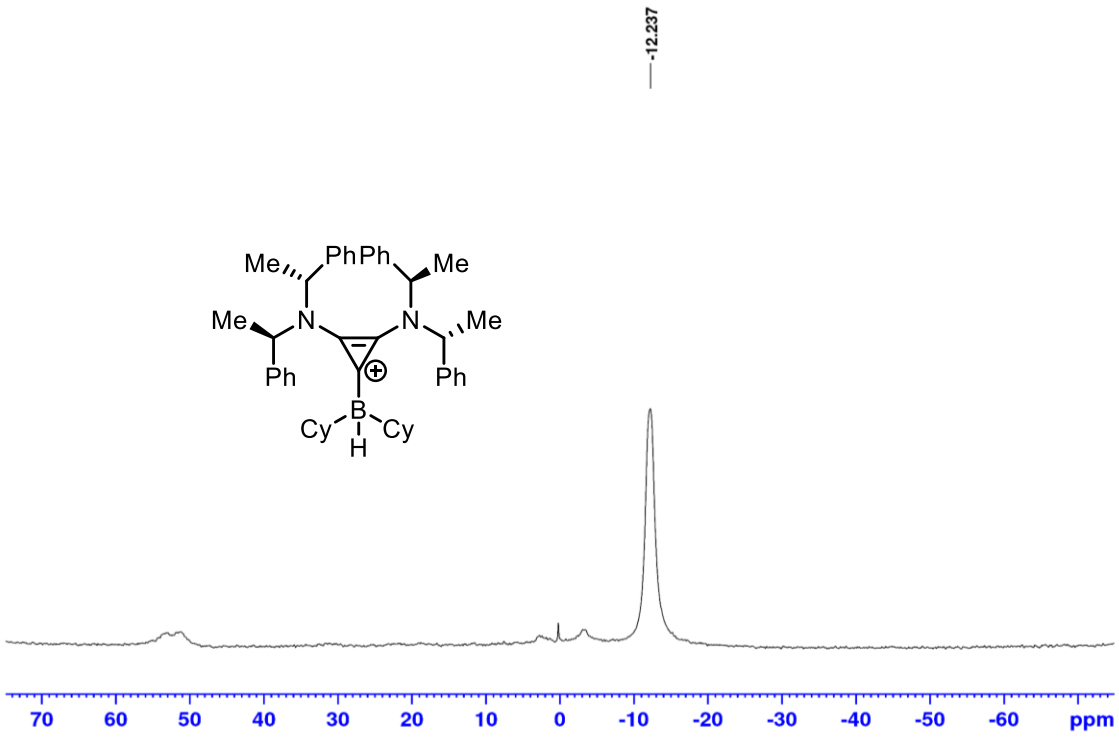


**Figure A87**: $^{11}$B NMR (160.5 MHz, $C_6D_6$) spectrum of formation of Me,PhBAC-BCy$_2$H **4-34** *in situ*.

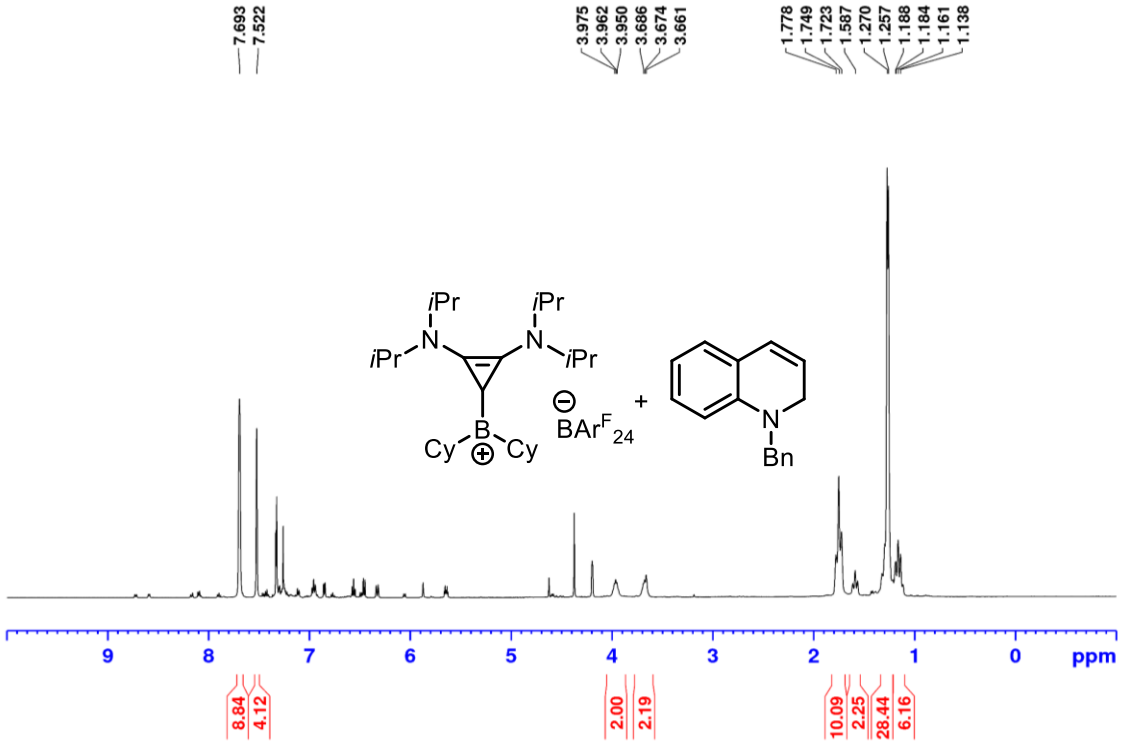


**Figure A88:** $^1$H NMR (500 MHz, $CDCl_3$) spectrum of formation of borenium cation [*i*PrBAC-BCy$_2$][BAr$^F$$_{24}$] **4-3a** *in situ* from *N*-Bn Quinolinium BAr$^F$$_{24}$ **4-6**.

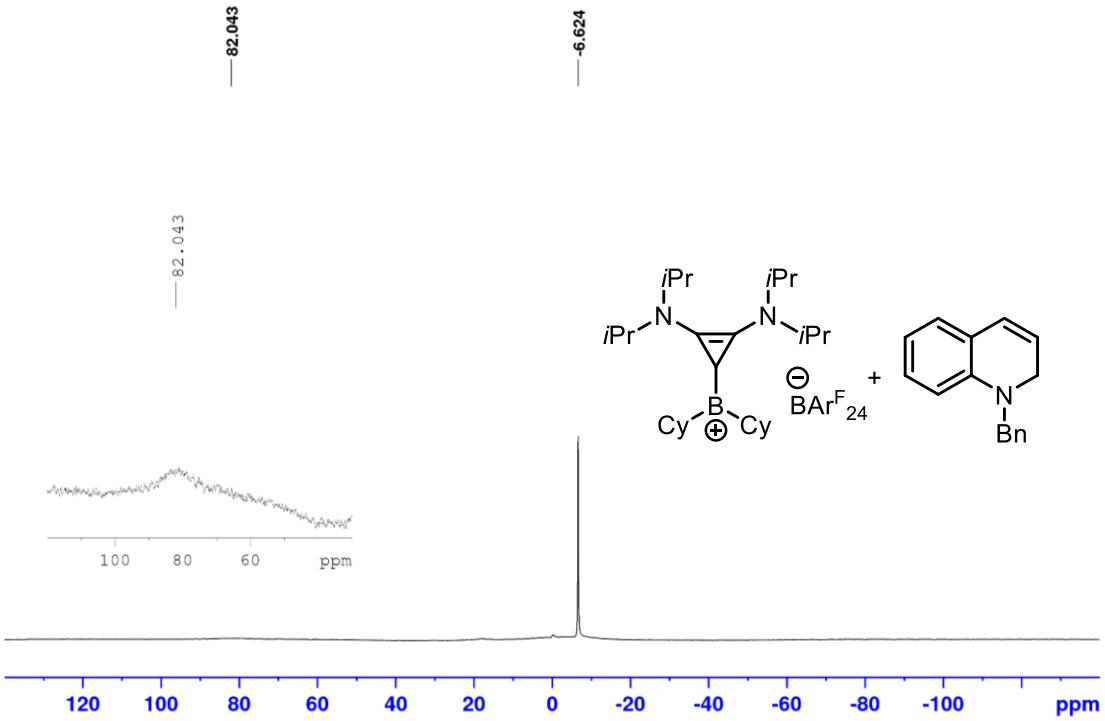


**Figure A89:** $^{11}$B NMR (160.5 MHz, $CDCl_3$) spectrum of spectrum of formation of borenium cation [*i*PrBAC-BCy$_2$][BAr$^F_{24}$] **4-3a** *in situ* from *N*-Bn Quinolinium BAr$^F_{24}$ **4-6**.

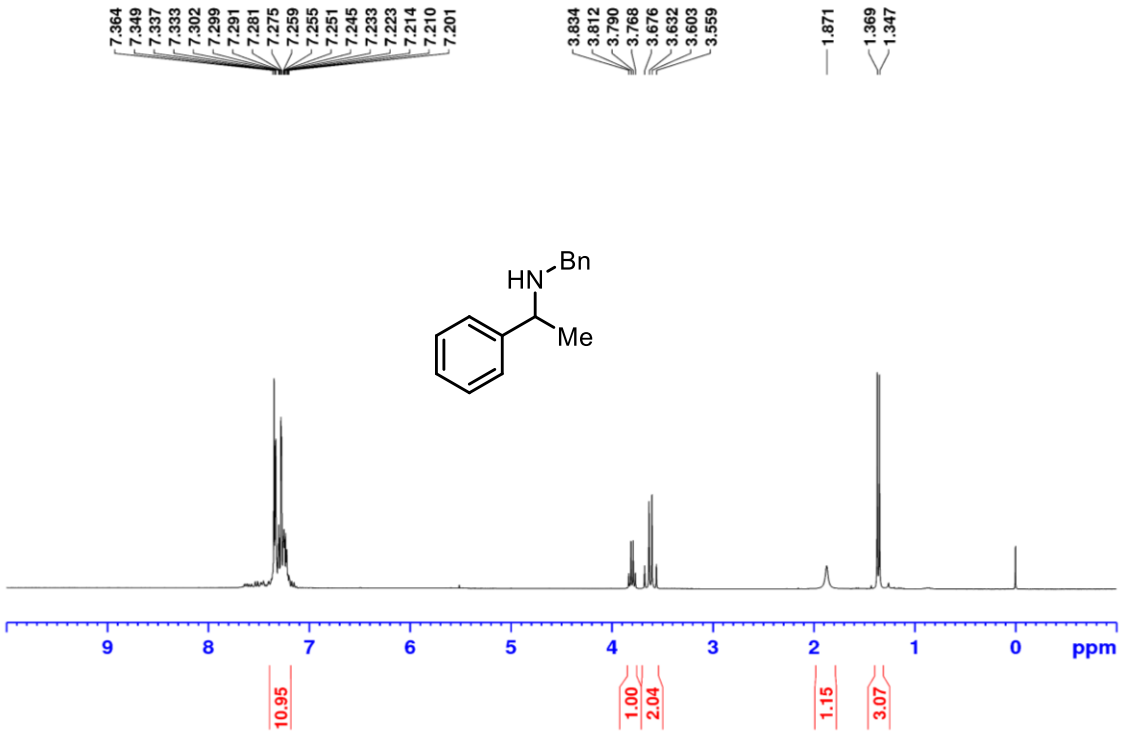


**Figure A90:** $^1$H NMR (300 MHz, $CDCl_3$) spectrum of acetophenone-*N*-(benzyl)imine **4-9a**.

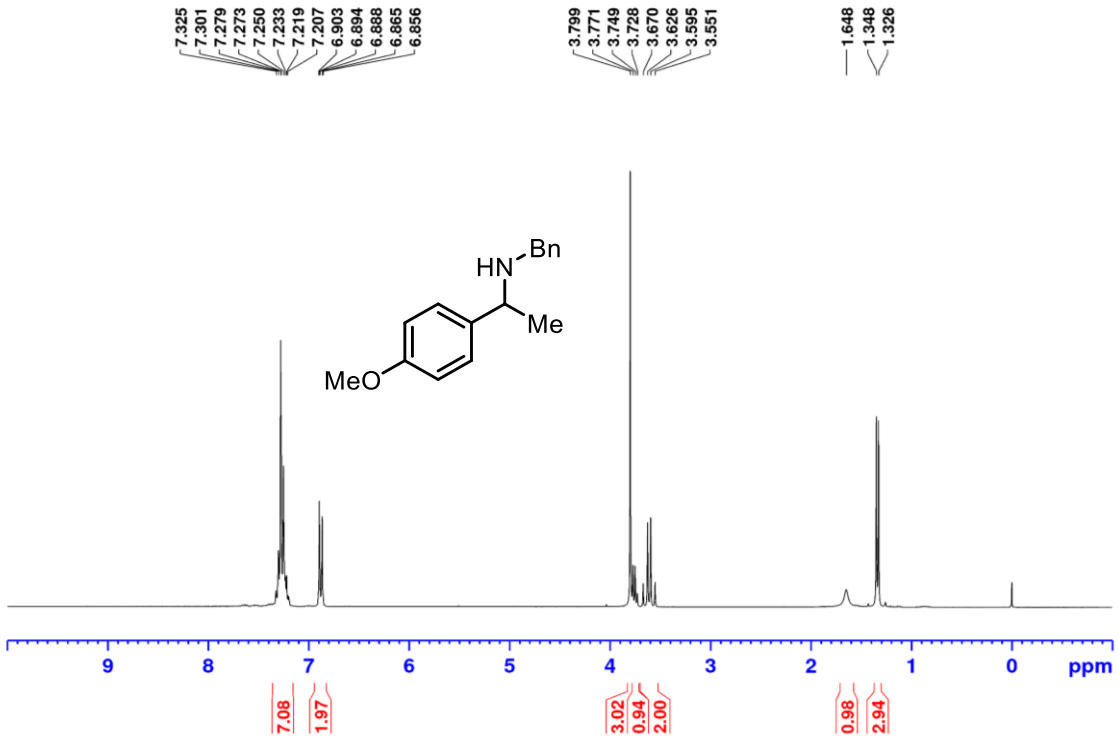


**Figure A91:** $^{1}$H NMR (300 MHz, $CDCl_3$) spectrum of 4-methoxyacetophenone-*N*-(benzyl)imine **4-10a**.

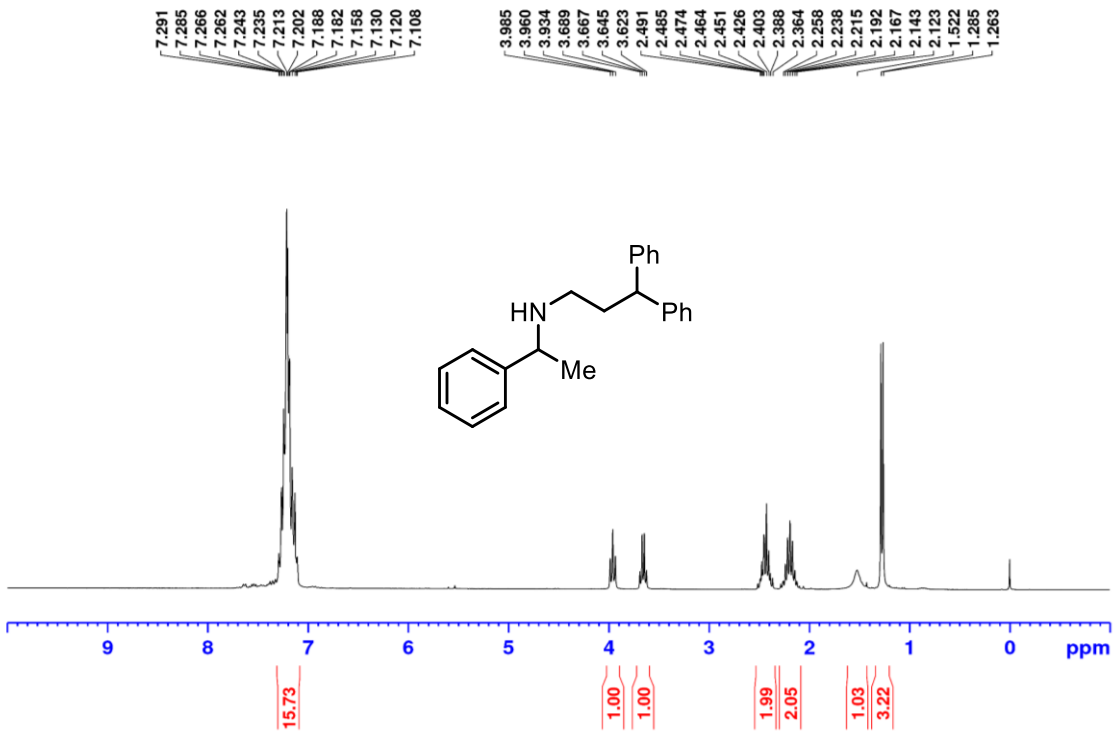


**Figure A92:** $^{1}$H NMR (300 MHz, $CDCl_3$) spectrum of acetophenone-*N*-(2-Diphenylethane)imine **4-21a**.

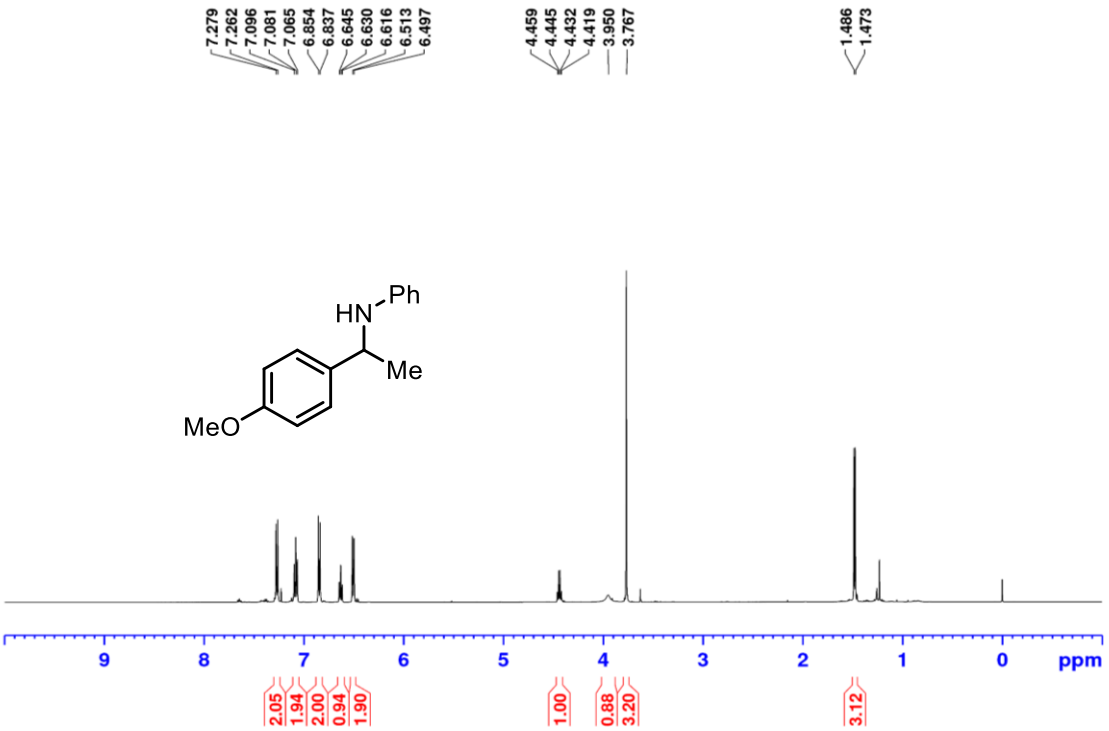


**Figure A93:** $^{1}$H NMR (500 MHz, $CDCl_3$) spectrum of 4-methoxyacetophenone-*N*-(Ph)imine **4-18a**.

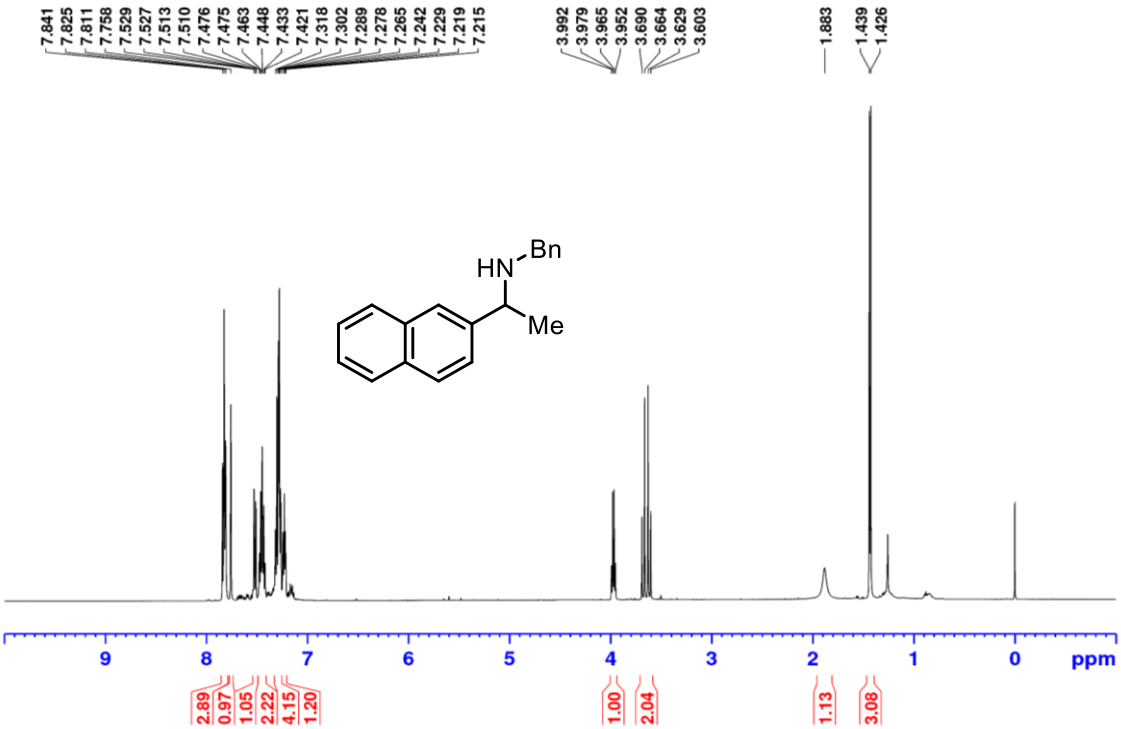


**Figure A94:** $^{1}$H NMR (500 MHz, $CDCl_3$) spectrum of 2-acetonaphthone-*N*-(benzyl)imine **4-16a**.

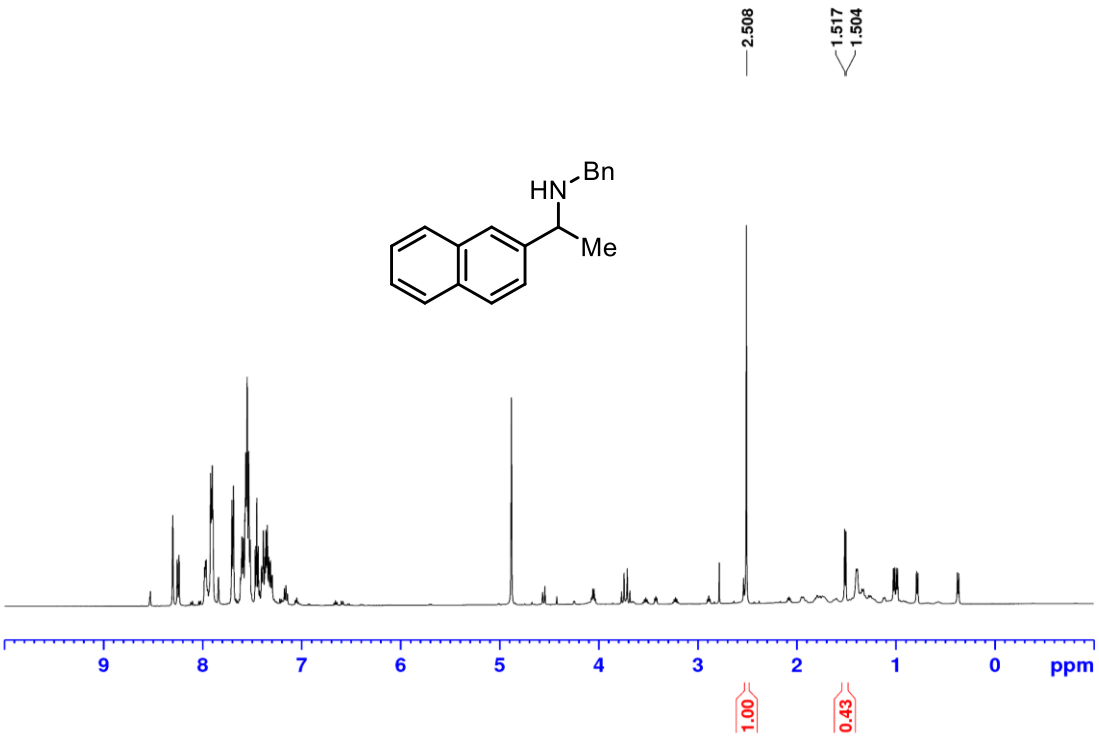


**Figure A95:** $^{1}$H NMR (500 MHz, $CDCl_3$) spectrum of 2-acetonaphthone-*N*-(benzyl)imine **4-16a** *in situ* for HPLC with *N*-Bn Quinolinium B(R-BINOL)$_2$ **4-50** as the hyride abstraction reagent.

## C3: HPLC Data for Chapter 4

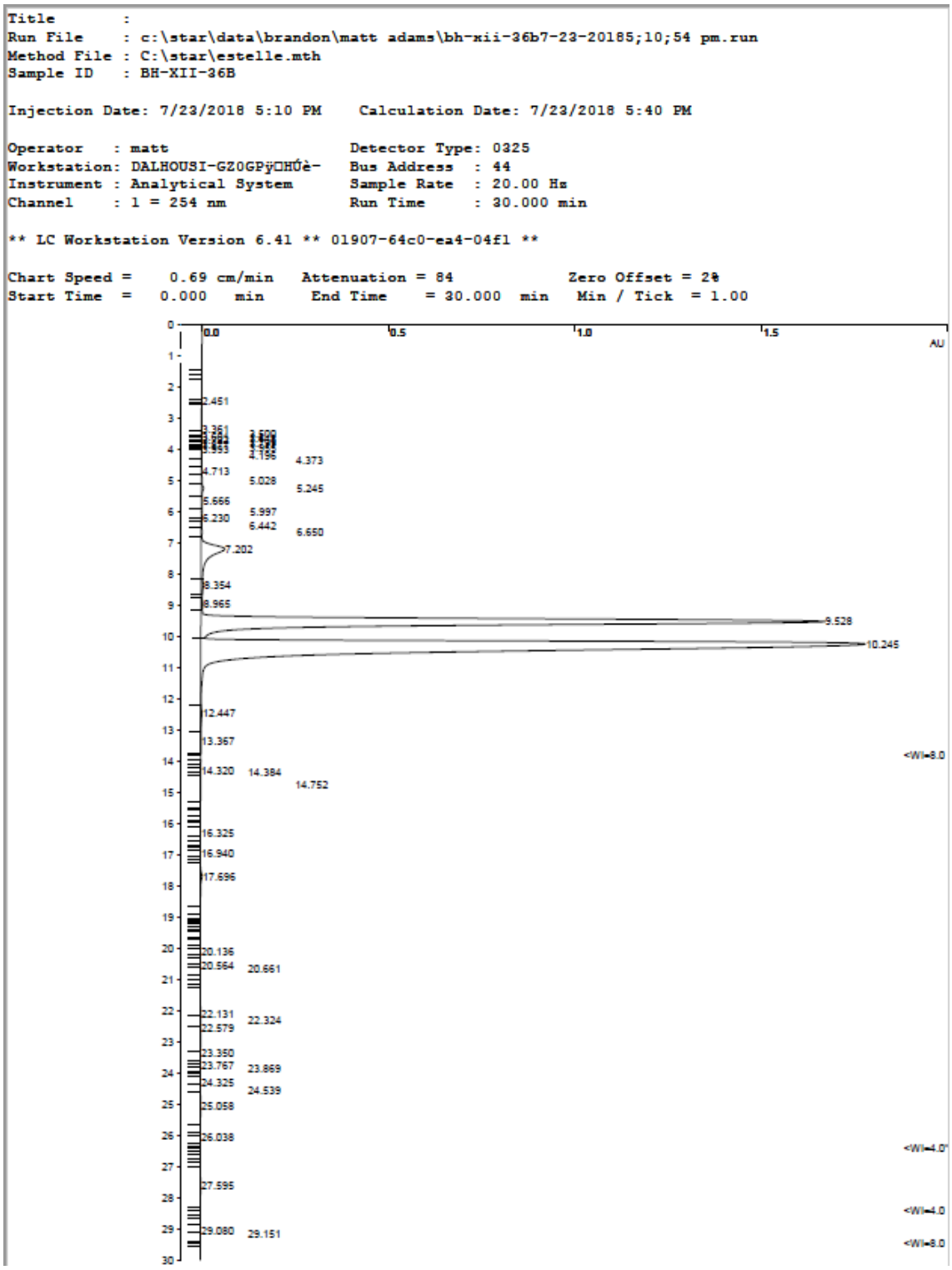


**Figure A96:** HPLC trace from the reduction of imine **4-16a** when **4-50** was used as the activator and **4-1** as the catalyst.

Print Date: Mon Jul 23 17:44:10 2018 Page 1 of 2

Title :
Run File : c:\star\data\brandon\matt adams\bh-xii-36b7-23-20185;10;54 pm.run
Method File : C:\star\estelle.mth
Sample ID : BH-XII-36B

Injection Date: 7/23/2018 5:10 PM Calculation Date: 7/23/2018 5:40 PM

Operator : matt Detector Type: 0325
Workstation: DALHOUSI-GZ0GPV□HÚè- Bus Address : 44
Instrument : Analytical System Sample Rate : 20.00 Hz
Channel : 1 = 254 nm Run Time : 30.000 min

** LC Workstation Version 6.41 ** 01907-64c0-ea4-04f1 **

Run Mode : Analysis
Peak Measurement: Peak Area
Calculation Type: Percent

| Peak No. | Peak Name | Result () | Ret. Time (min) | Time Offset (min) | Area (counts) | Sep. Code | Width 1/2 (sec) | Status Codes |
|---|---|---|---|---|---|---|---|---|
| 1 | | 0.0004 | 2.451 | 0.000 | 2288 | BV | 2.8 | |
| 2 | | 0.0249 | 3.361 | 0.000 | 151467 | VV | 0.0 | |
| 3 | | 0.0087 | 3.500 | 0.000 | 53034 | VV | 0.0 | |
| 4 | | 0.0051 | 3.601 | 0.000 | 30983 | VV | 0.0 | |
| 5 | | 0.0045 | 3.648 | 0.000 | 27494 | VV | 0.0 | |
| 6 | | 0.0035 | 3.722 | 0.000 | 21085 | VV | 0.0 | |
| 7 | | 0.0068 | 3.799 | 0.000 | 41546 | VV | 0.0 | |
| 8 | | 0.0031 | 3.877 | 0.000 | 18969 | VV | 0.0 | |
| 9 | | 0.0047 | 3.955 | 0.000 | 28455 | VV | 0.0 | |
| 10 | | 0.0042 | 3.993 | 0.000 | 25807 | VV | 0.0 | |
| 11 | | 0.0263 | 4.196 | 0.000 | 160209 | VV | 11.7 | |
| 12 | | 0.0317 | 4.373 | 0.000 | 193197 | VV | 0.0 | |
| 13 | | 0.0369 | 4.713 | 0.000 | 224891 | VV | 15.4 | |
| 14 | | 0.0480 | 5.028 | 0.000 | 292700 | VV | 0.0 | |
| 15 | | 0.1474 | 5.245 | 0.000 | 898187 | VV | 10.8 | |
| 16 | | 0.0959 | 5.666 | 0.000 | 584410 | VV | 18.9 | |
| 17 | | 0.0524 | 5.997 | 0.000 | 319257 | VV | 0.0 | |
| 18 | | 0.0227 | 6.230 | 0.000 | 138331 | VV | 0.0 | |
| 19 | | 0.0304 | 6.442 | 0.000 | 185159 | VV | 0.0 | |
| 20 | | 0.0625 | 6.650 | 0.000 | 380591 | VV | 0.0 | |
| 21 | | 3.0262 | 7.202 | 0.000 | 18434336 | VV | 19.6 | |
| 22 | | 0.0549 | 8.354 | 0.000 | 334333 | TS | 0.0 | |
| 23 | | 0.0252 | 8.965 | 0.000 | 153209 | TS | 0.0 | |
| 24 | | 36.7690 | 9.528 | 0.000 | 223981328 | VV | 12.2 | |
| 25 | | 59.1152 | 10.245 | 0.000 | 360104896 | VB | 18.8 | |
| 26 | | 0.1118 | 12.447 | 0.000 | 681075 | TS | 0.0 | |
| 27 | | 0.0178 | 13.367 | 0.000 | 108455 | TS | 0.0 | |
| 28 | | 0.0005 | 14.320 | 0.000 | 2777 | VV | 14.9 | |
| 29 | | 0.0004 | 14.384 | 0.000 | 2420 | VV | 0.0 | |
| 30 | | 0.0190 | 14.752 | 0.000 | 115508 | VB | 15.8 | |
| 31 | | 0.0022 | 16.325 | 0.000 | 13309 | VV | 3.0 | |
| 32 | | 0.0015 | 16.940 | 0.000 | 9243 | VP | 3.8 | |
| 33 | | 0.1364 | 17.696 | 0.000 | 830748 | PP | 17.5 | |
| 34 | | 0.0004 | 20.136 | 0.000 | 2625 | VV | 0.0 | |
| 35 | | 0.0004 | 20.564 | 0.000 | 2176 | VV | 0.0 | |
| 36 | | 0.0005 | 20.661 | 0.000 | 2956 | VP | 0.0 | |
| 37 | | 0.0107 | 22.131 | 0.000 | 65141 | PV | 0.0 | |
| 38 | | 0.0129 | 22.324 | 0.000 | 78627 | VV | 0.0 | |
| 39 | | 0.0180 | 22.579 | 0.000 | 109471 | VV | 0.0 | |
| 40 | | 0.0019 | 23.350 | 0.000 | 11291 | VV | 0.0 | |
| 41 | | 0.0004 | 23.767 | 0.000 | 2728 | VV | 0.0 | |
| 42 | | 0.0004 | 23.869 | 0.000 | 2341 | VV | 0.0 | |
| 43 | | 0.0010 | 24.325 | 0.000 | 6037 | VV | 0.0 | |
| 44 | | 0.0016 | 24.539 | 0.000 | 9802 | VV | 0.0 | |
| 45 | | 0.0159 | 25.058 | 0.000 | 96734 | VB | 0.0 | |
| 46 | | 0.0004 | 26.038 | 0.000 | 2596 | VP | 2.6 | |
| 47 | | 0.0337 | 27.595 | 0.000 | 205510 | VB | 29.2 | |
| 48 | | 0.0007 | 29.080 | 0.000 | 4091 | BV | 14.2 | |
| 49 | | 0.0011 | 29.151 | 0.000 | 6467 | VB | 15.2 | |
| | Totals: | 100.0002 | | 0.000 | 609158290 | | | |

Total Unidentified Counts : 609158272 counts

Detected Peaks: 91 Rejected Peaks: 42 Identified Peaks: 0

Multiplier: 1 Divisor: 1 Unidentified Peak Factor: 0

Baseline Offset: 0 microAU LSB: 0.1 microAU

**Figure A97:** HPLC chart from the reduction of imine **4-16a** when **4-50** was used as the activator and **4-1** as the catalyst.

## Appendix D: Appendix for Chapter 5

### D1: NMR Spectra for Chapter 5

Full data is available at https://doi.org/10.1039/C8OB02330A

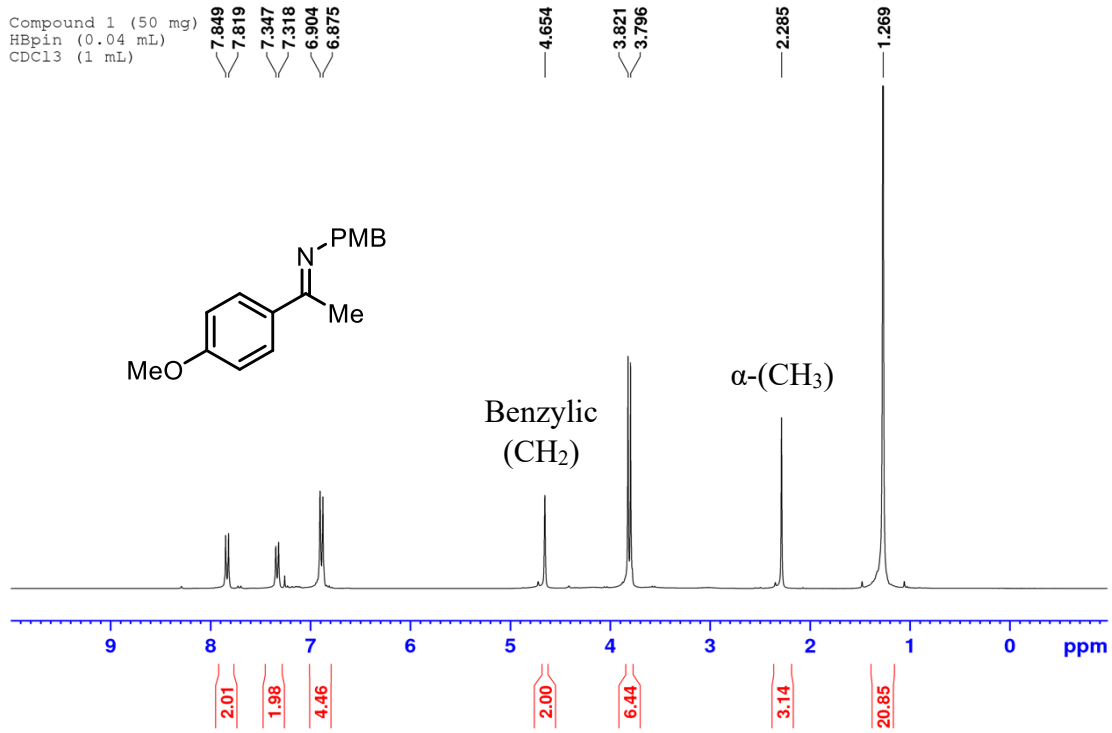


**Figure A98:** $^{1}$H NMR ($CDCl_3$) spectrum of control reaction. Mixture of imine **5-1** and HB(pin) **5-2** in $CDCl_3$.

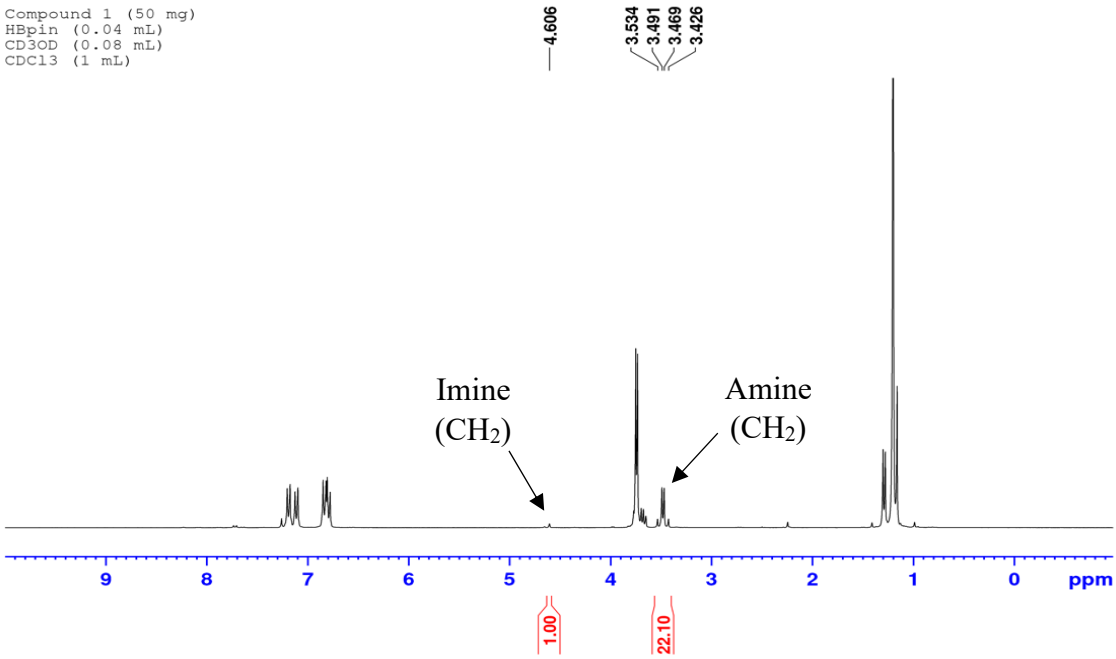


**Figure A99:** $^{1}$H NMR ($CDCl_3$) spectrum of methanol-$d_4$ addition **Entry 3, Table 5.1**.

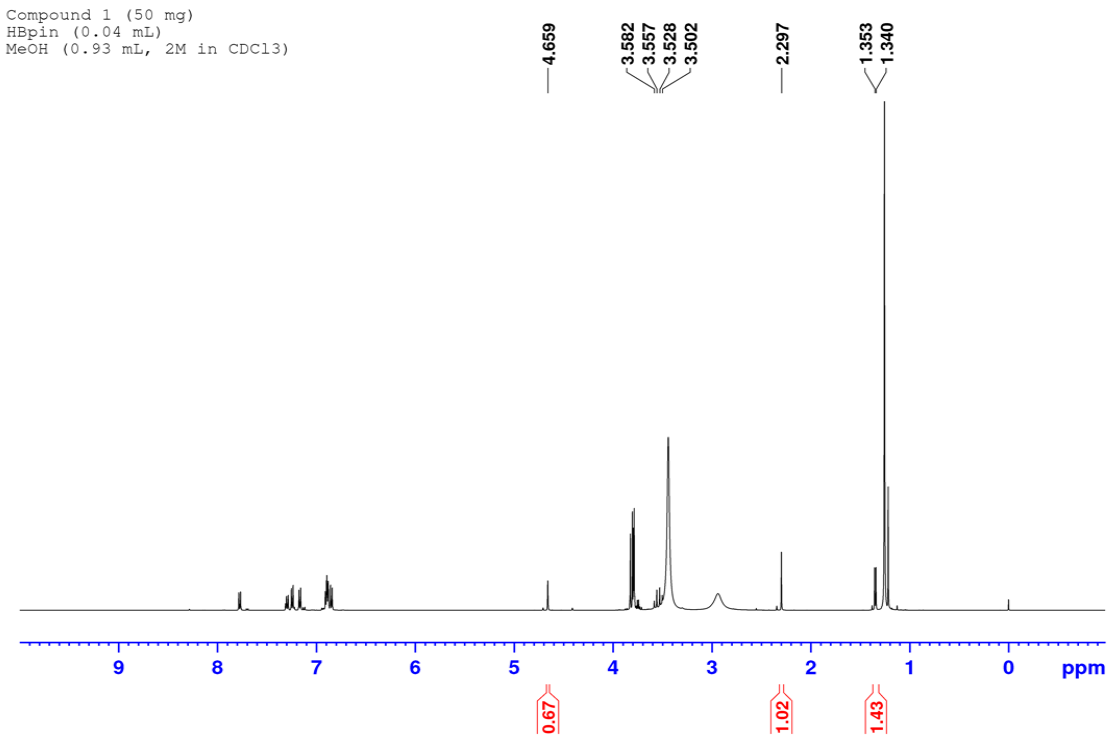


**Figure A100:** $^{1}$H NMR ($CDCl_3$) spectrum of methanol addition **Table 5.2**.

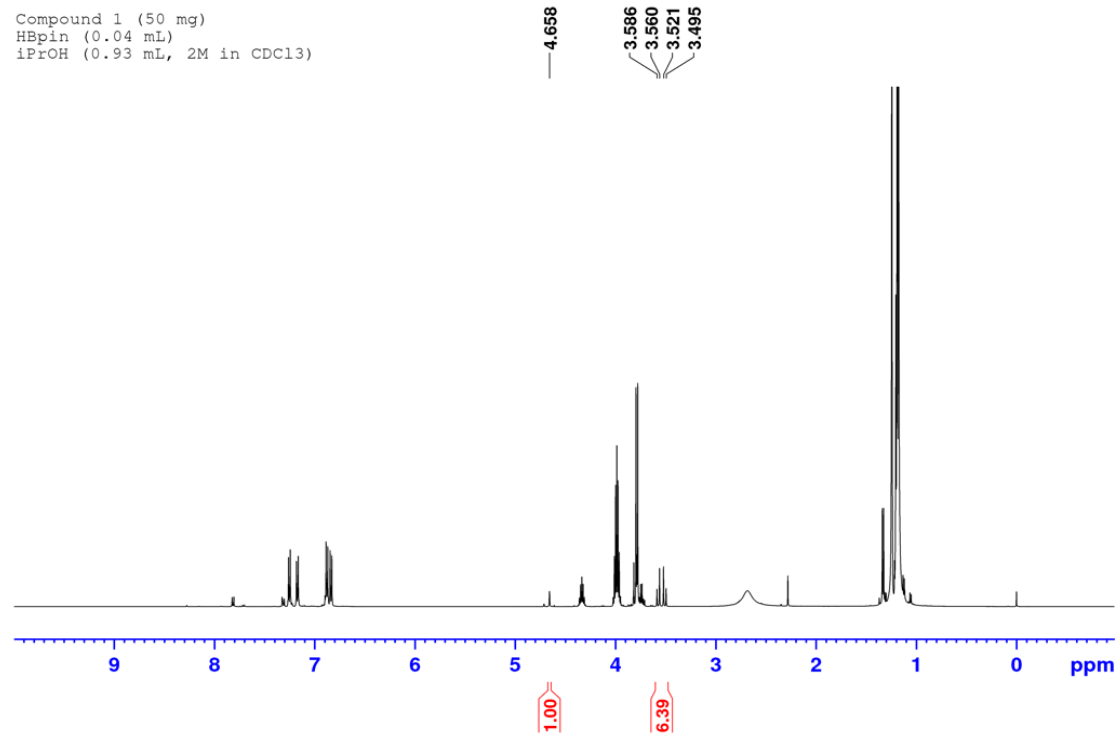


**Figure A101:** $^{1}$H NMR ($CDCl_3$) spectrum of isopropyl alcohol addition **Table 5.2**.

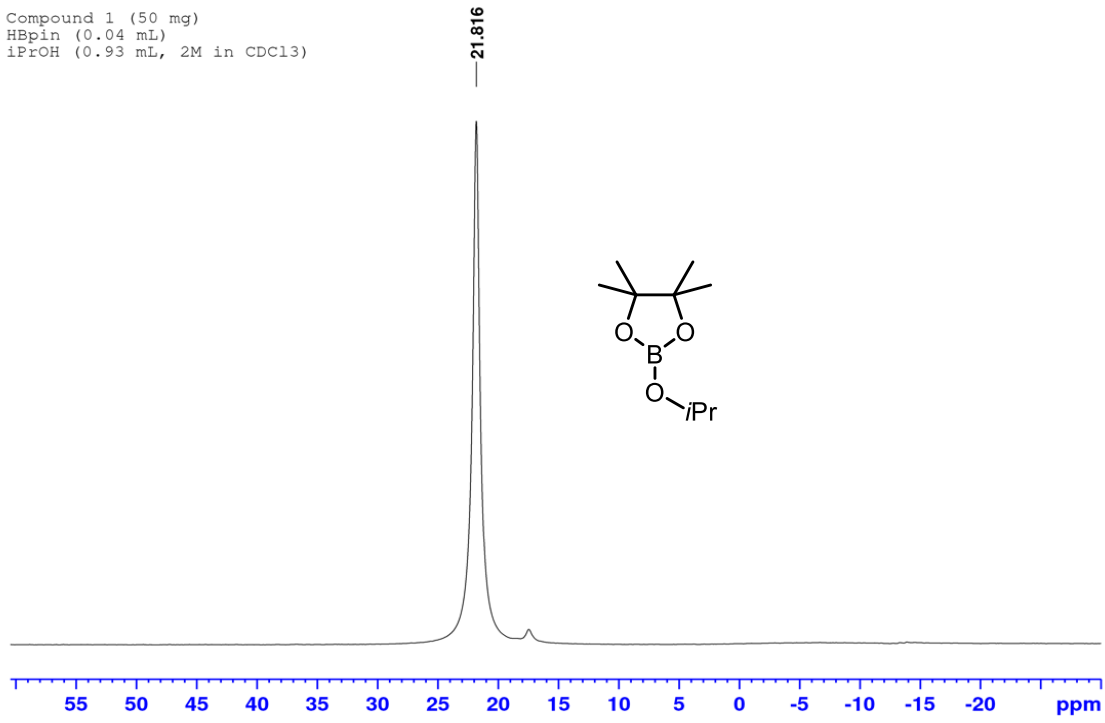


**Figure A102:** $^{11}$B NMR ($CDCl_3$) spectrum of isopropyl alcohol addition **Table 5.2**.

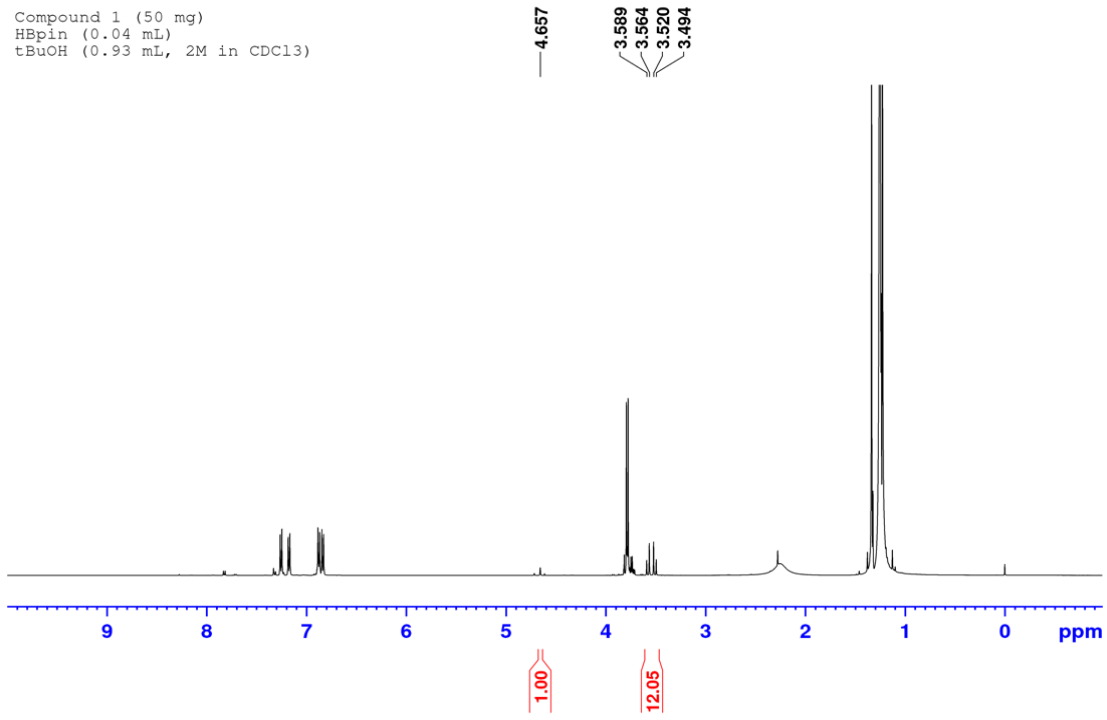


**Figure A103:** $^{1}$H NMR ($CDCl_3$) spectrum of *tert*-butyl alcohol addition **Table 5.2**.

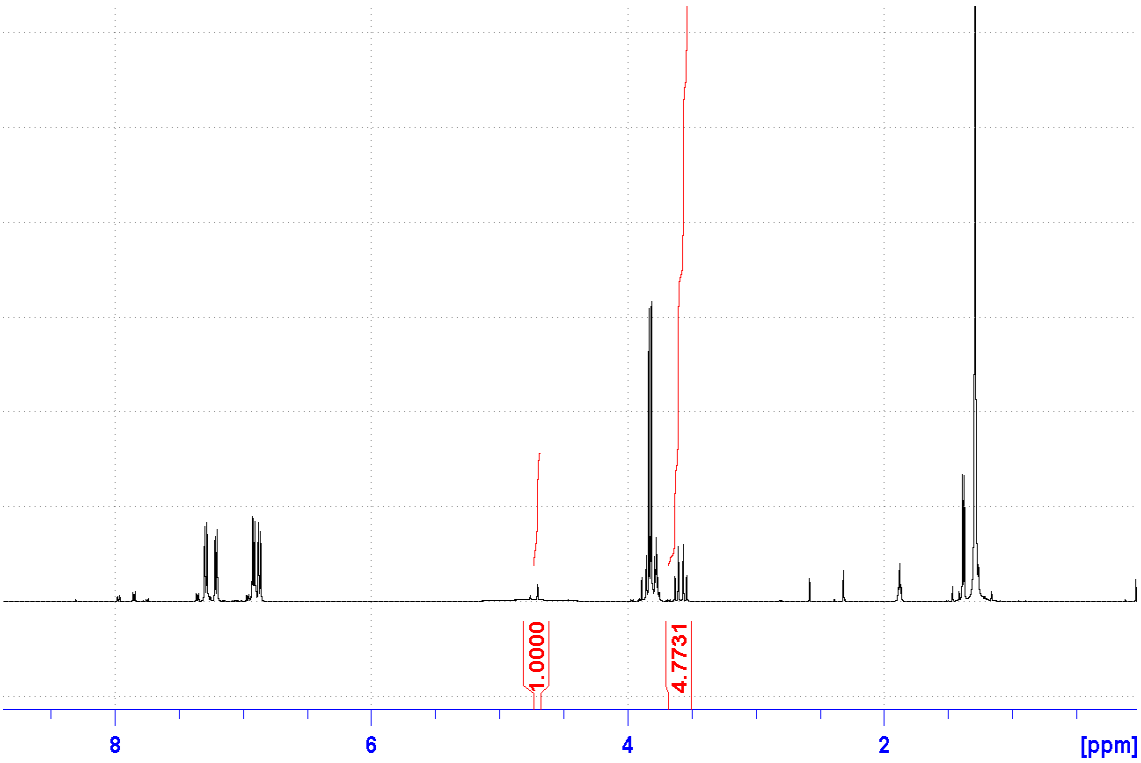


**Figure A104:** $^{1}$H NMR spectrum from addition of 0.25 M solutions of water in THF to mixture of imine **5-1** and pinacolborane **5-2**.

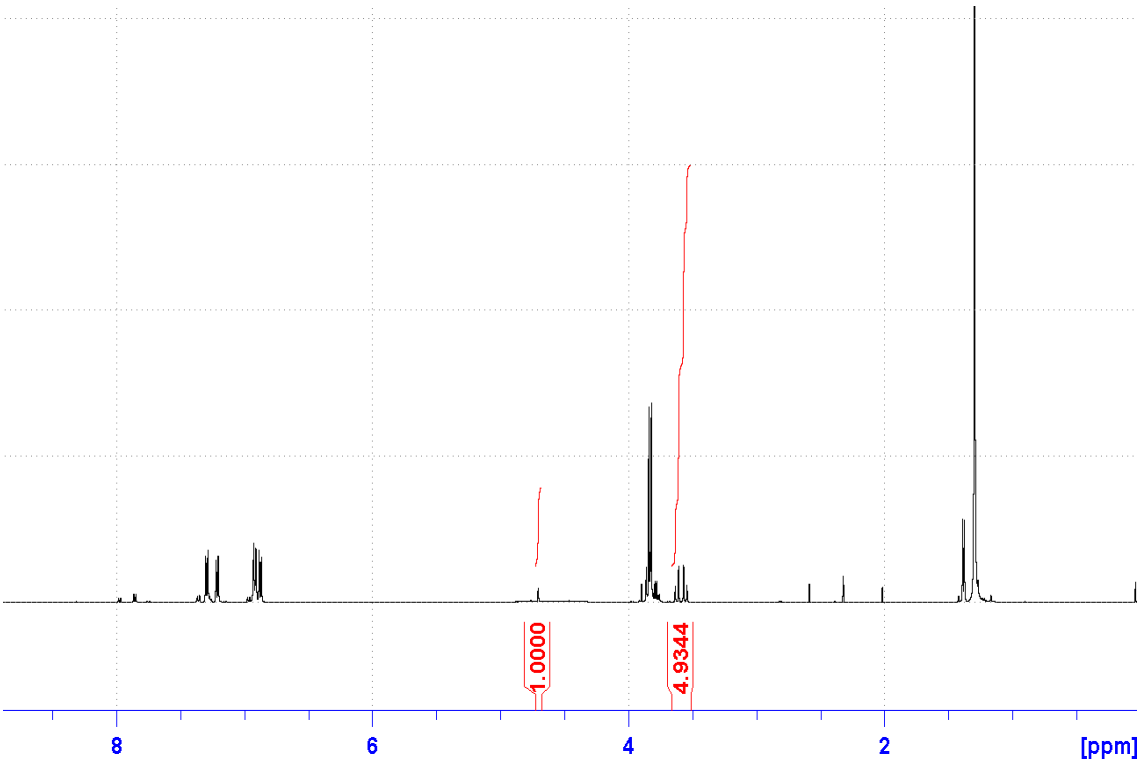


**Figure A105:** $^{1}$H NMR spectrum from addition of 0.25 M solutions of water in Acetonitrile to mixture of imine **5-1** and pinacolborane **5-2**.

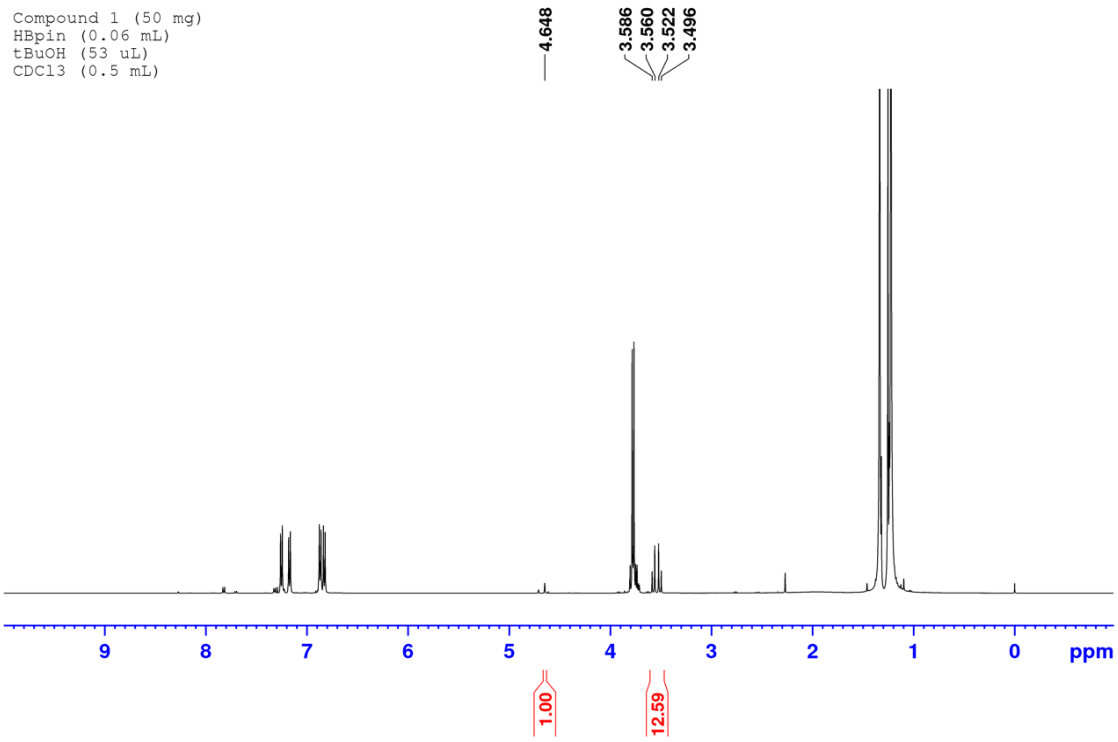


**Figure A106:** $^{1}$H NMR ($CDCl_3$) spectrum of optimized of amount of *tert*-butyl alcohol added to maximize the reduction of imine **5-1**. **Entry 5, Table 5.3**.

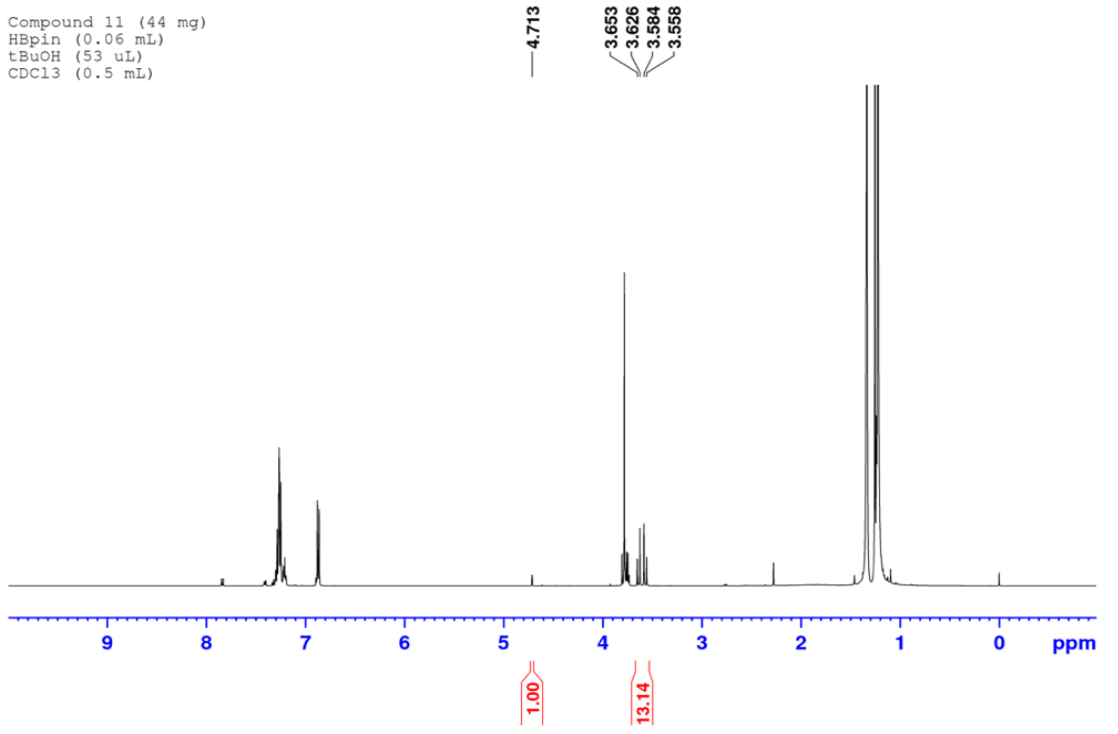


**Figure A107:** $^{1}$H NMR ($CDCl_3$) spectrum of the reduction of imine **5-11** without internal standard.

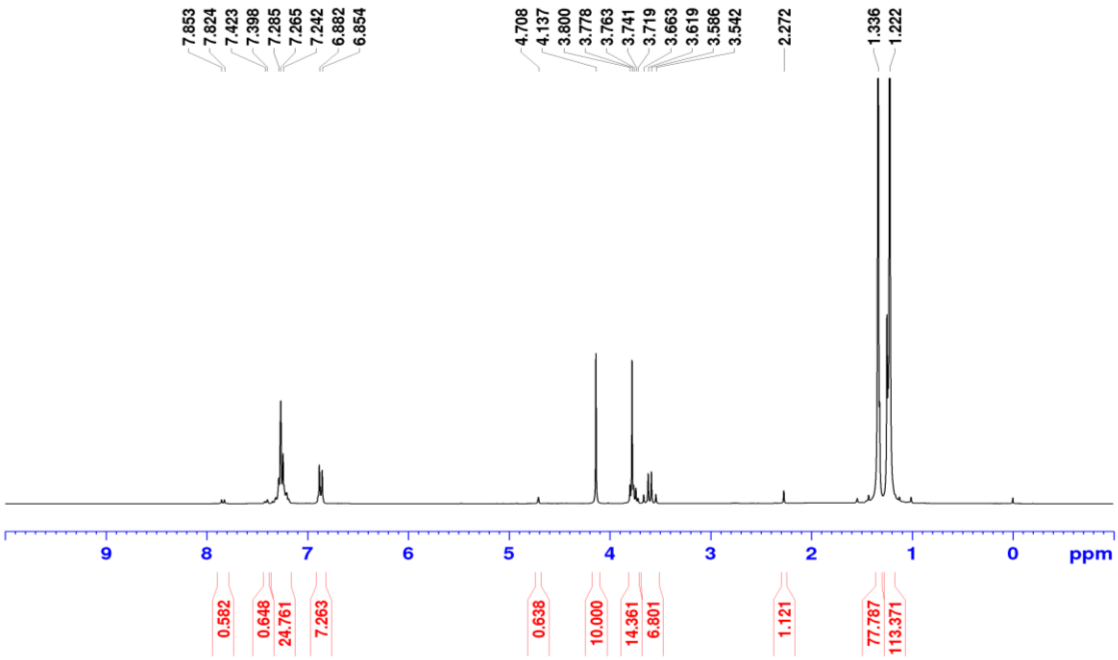


**Figure A108:** $^{1}$H NMR ($CDCl_3$) spectrum of the reduction of imine **5-11** with 0.05 mmol ferrocene internal standard. Calculation: 6.801*0.05/2 = 0.1700 mmol pdt, 0.186 mmol sm added = 91% NMR Yield.

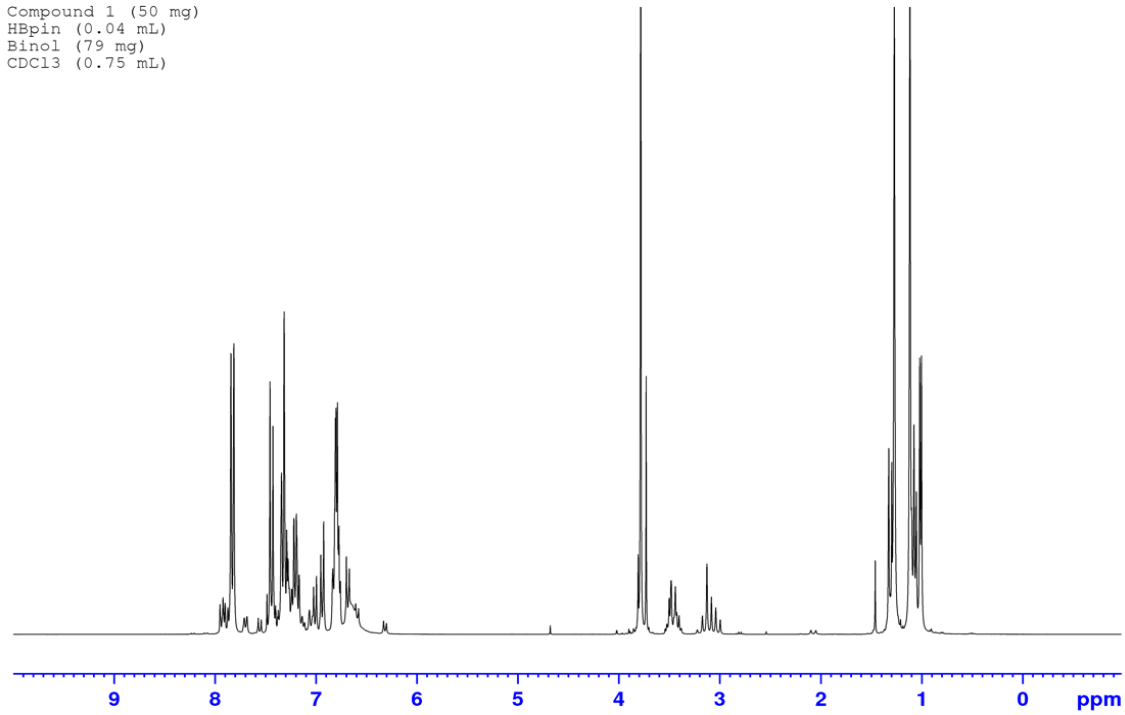


**Figure A109:** $^{1}$H NMR ($CDCl_3$) spectrum of the reduction of imine **5-1** with (R)-(+)-1,1'-Bi-2-napthol **5-20**.

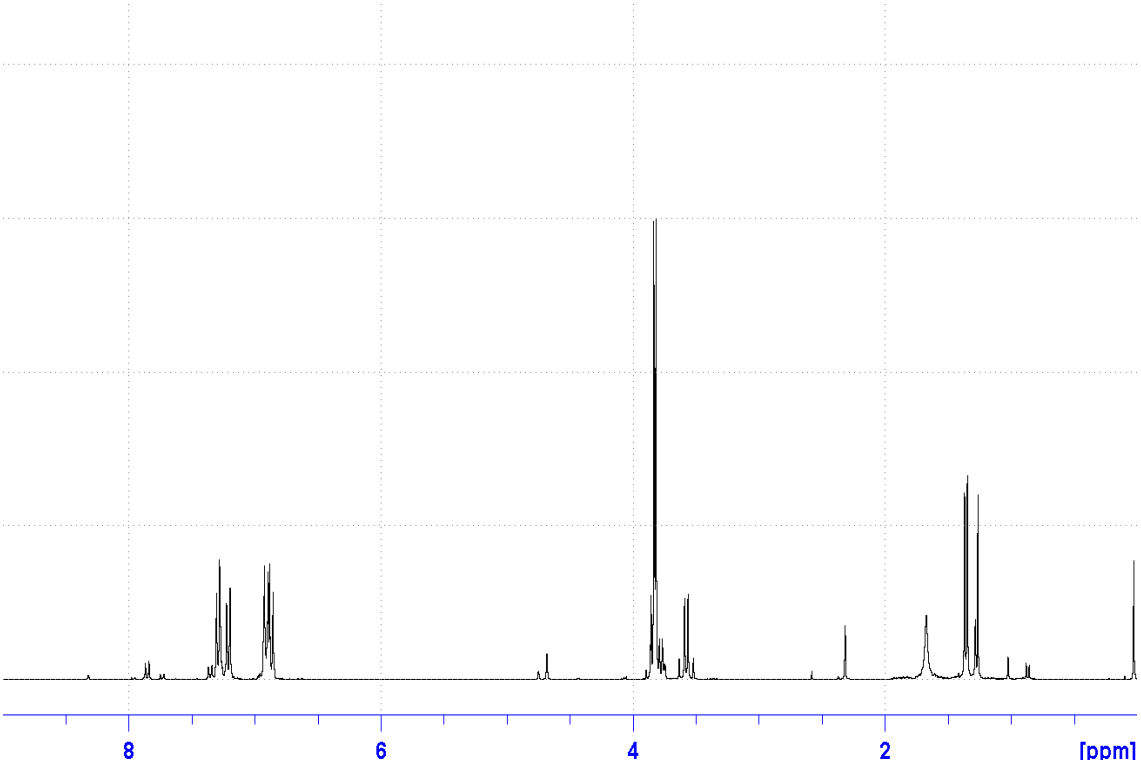


**Figure A110:** $^{1}$H NMR ($CDCl_3$) spectrum of the reduction of imine **5-1** with (R)-(+)-1,1'-Bi-2-napthol **5-20** after acid base wash.

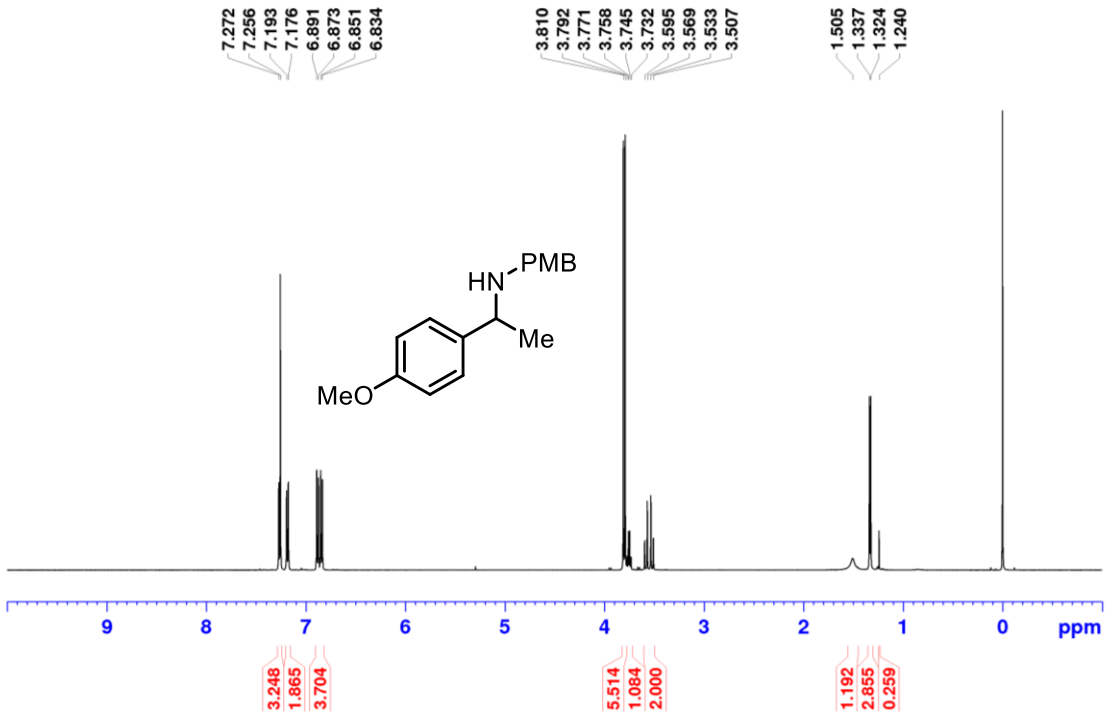


**Figure A111:** $^{1}$H NMR (500 MHz, $CDCl_3$) spectrum of isolated product from the reduction of imine **5-1** on a 200 mg scale.

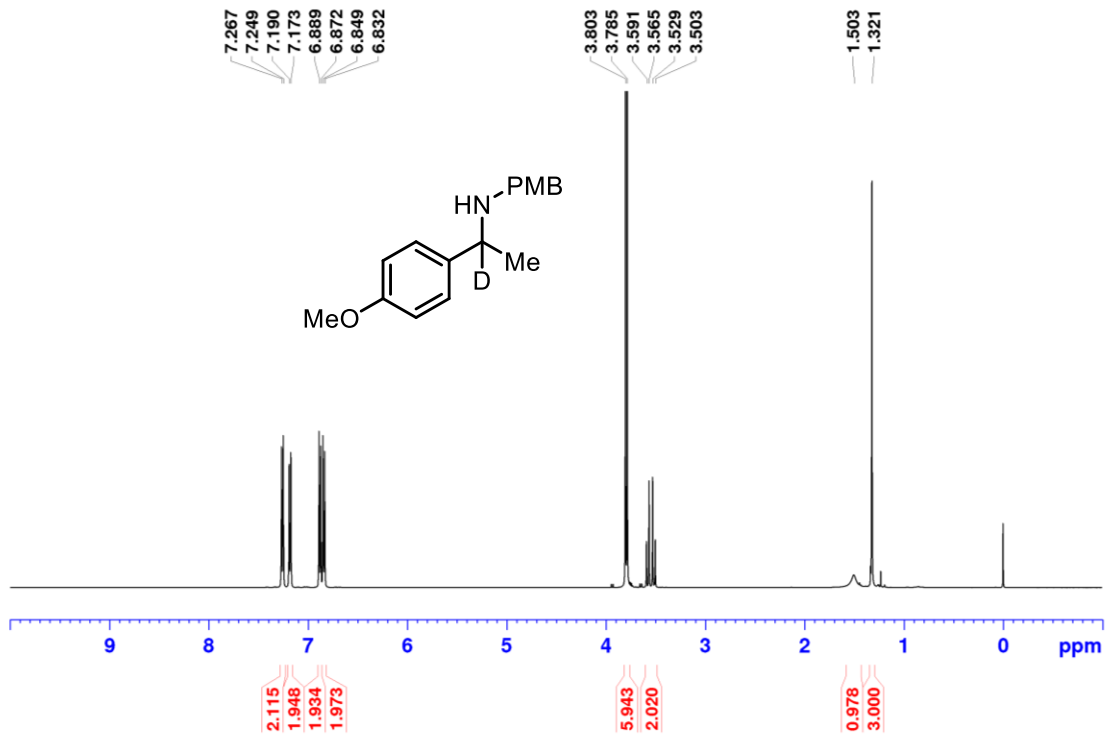


**Figure A112:** $^{1}$H NMR (500 MHz, $CDCl_3$) spectrum of amine **5-3(*d*)**.

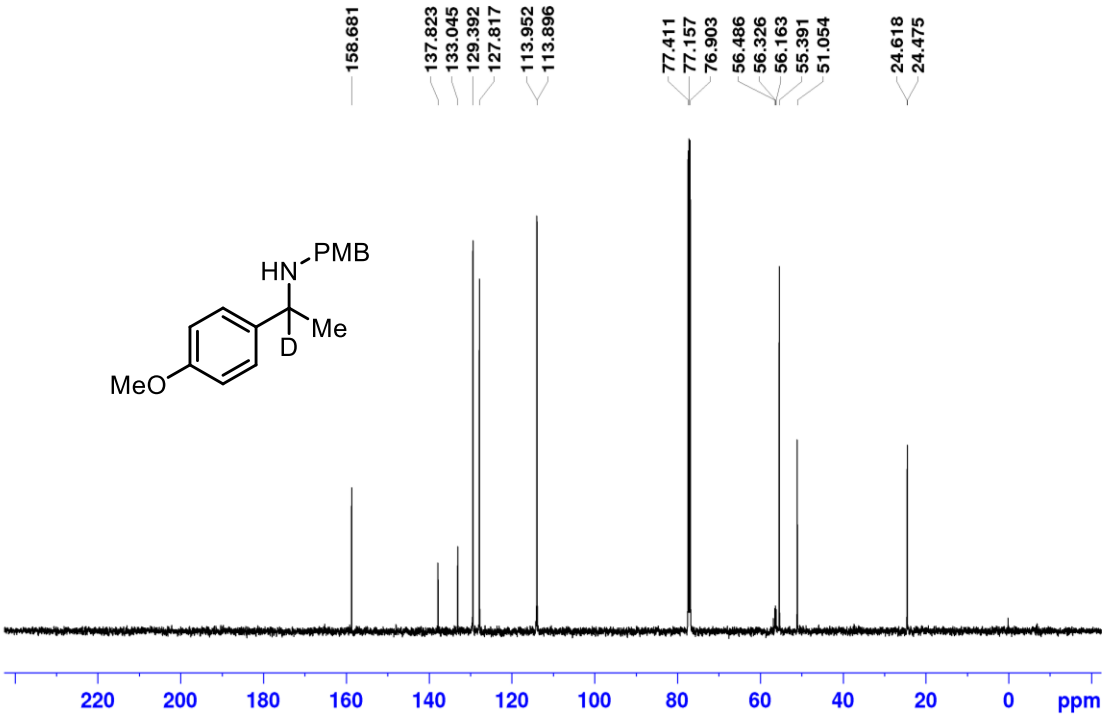


**Figure A113:** $^{13}C\{^{1}H\}$ (125.8 MHz, $CDCl_3$) spectrum of amine **5-3(*d*)**.

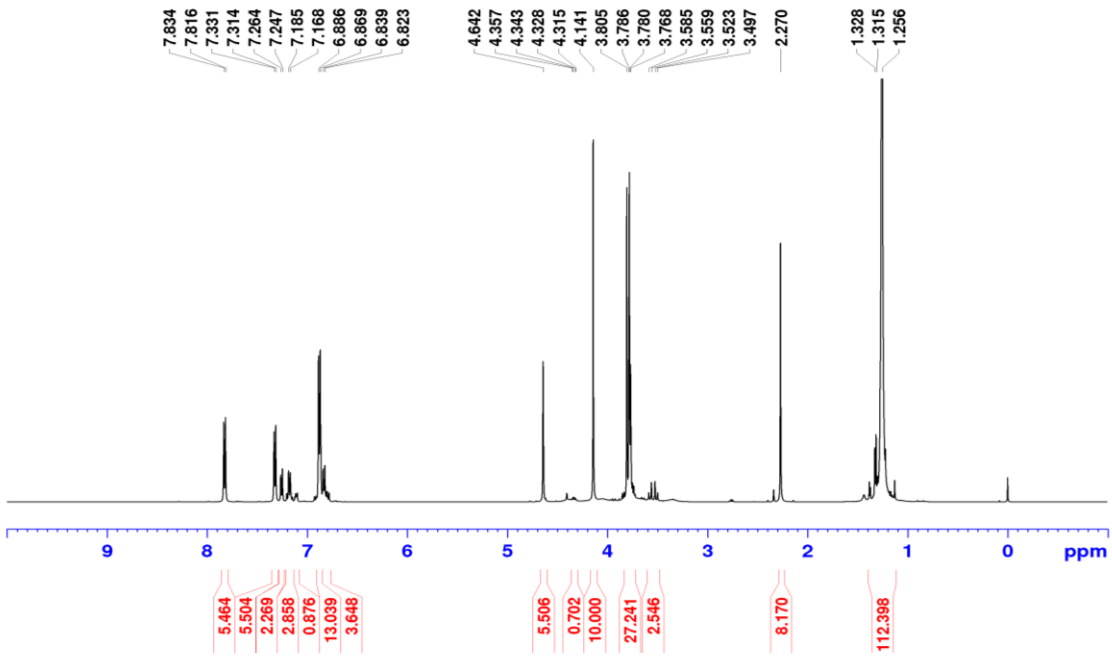


**Figure A114:** $^{1}$H NMR ($CDCl_3$) spectrum for autocatalytic reaction for imine **5-1** after 30 min, 0.05 mmol ferrocene internal standard added. 5.506*0.05/2 = 0.1376 mmol imine remain, 0.186 mmol imine were added 74% of imine remains, 26% was converted.

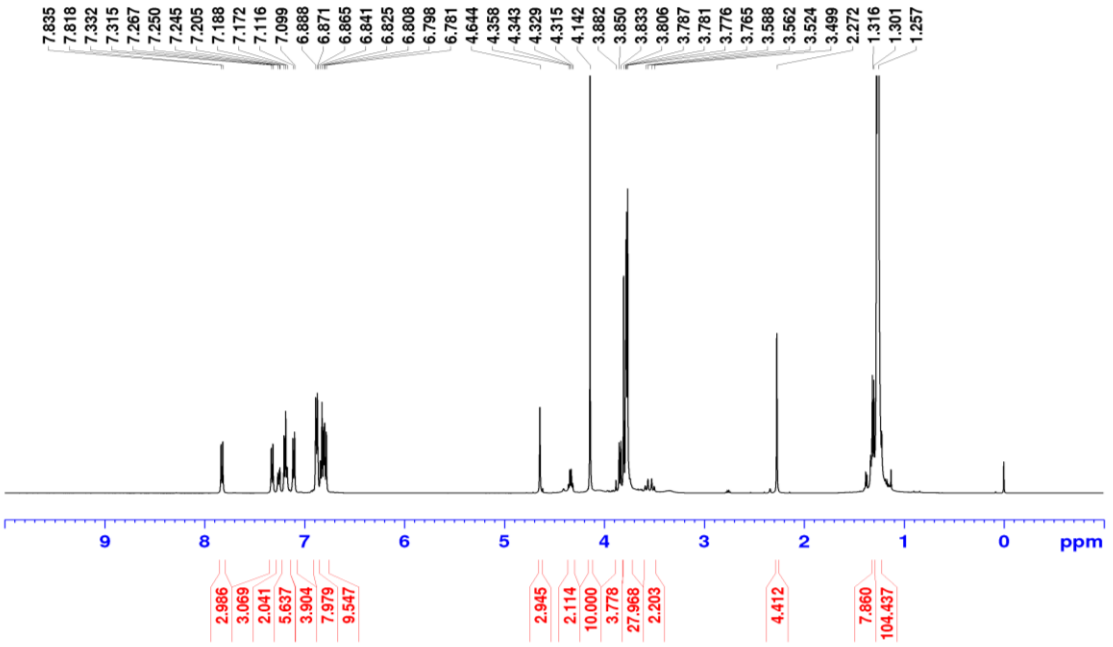


**Figure A115:** $^{1}$H NMR ($CDCl_3$) spectrum for autocatalytic reaction for imine **5-1** after 24 h, 0.05 mmol ferrocene internal standard added. 5.506*0.05/2 = 0.1376 mmol imine remain, 0.186 mmol imine were added 74% of imine remains, 26% was converted.

## D2: HPLC Data for Chapter 5

```
Title       :
Run File    : c:\star\data\brandon\matt adams\bh-xii-74b9-18-20185;31;25 pm.run
Method File : C:\star\estelle.mth
Sample ID   : bh-xii-74b

Injection Date: 9/18/2018 5:31 PM    Calculation Date: 9/18/2018 6:06 PM

Operator   : matt                    Detector Type: 0325
Workstation: DALHOUSI-GZ0GPÿ HÚè-    Bus Address  : 44
Instrument : Analytical System       Sample Rate  : 20.00 Hz
Channel    : 1 = 254 nm              Run Time     : 35.000 min

** LC Workstation Version 6.41 ** 01907-64c0-ea4-04f1 **

Chart Speed =    0.59 cm/min   Attenuation = 3             Zero Offset = 4%
Start Time  =   0.000   min     End Time    = 35.000  min   Min / Tick  = 1.00
```

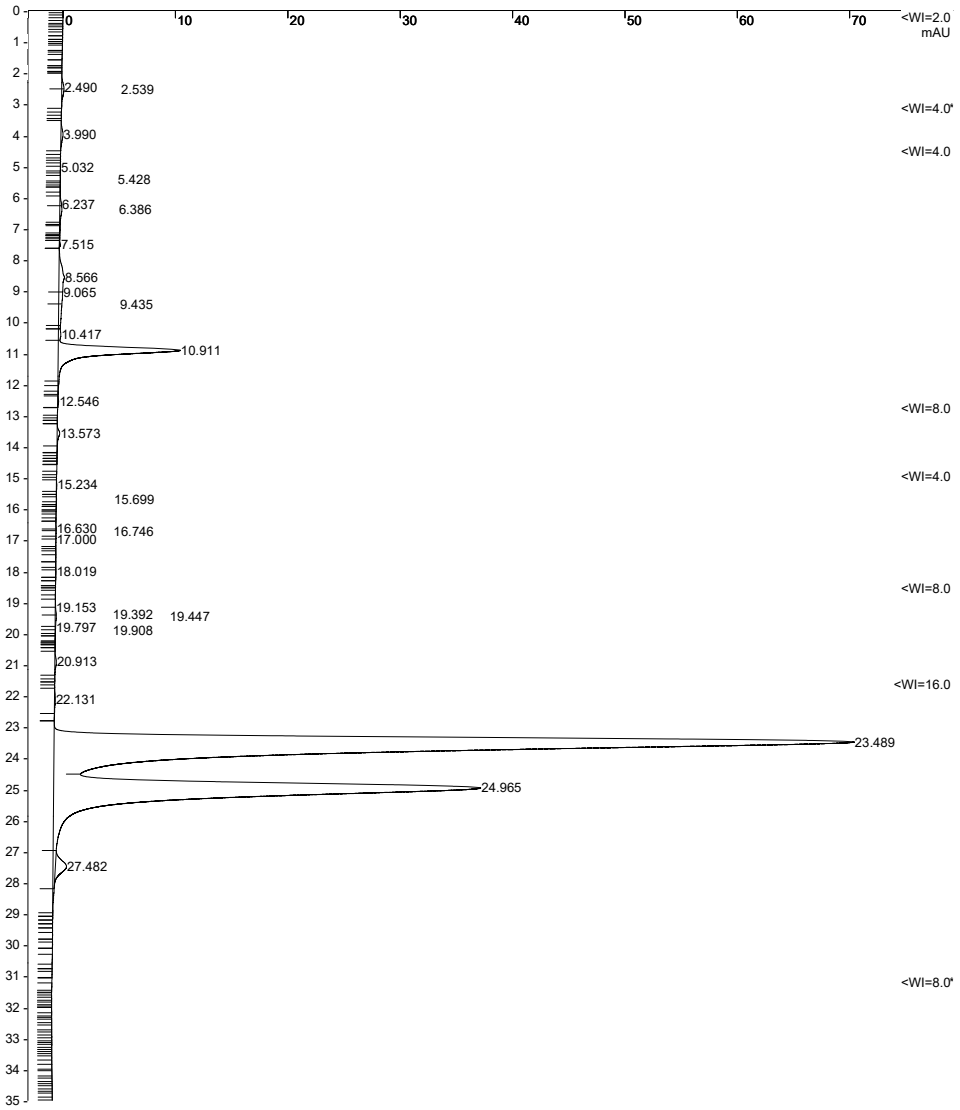


**Figure A116:** HPLC Trace from the reduction of imine **5-1** with (R)-(+)-1,1'-Bi-2-napthol **5-20** after acid base wash.

Print Date: Tue Sep 18 18:07:19 2018 Page 1 of 1

Title :
Run File : c:\star\data\brandon\matt adams\bh-xii-74b9-18-20185;31;25 pm.run
Method File : C:\star\estelle.mth
Sample ID : bh-xii-74b

Injection Date: 9/18/2018 5:31 PM Calculation Date: 9/18/2018 6:06 PM

Operator : matt Detector Type: 0325
Workstation: DALHOUSI-GZ0GPý HÚè- Bus Address : 44
Instrument : Analytical System Sample Rate : 20.00 Hz
Channel : 1 = 254 nm Run Time : 35.000 min

** LC Workstation Version 6.41 ** 01907-64c0-ea4-04f1 **

Run Mode : Analysis
Peak Measurement: Peak Area
Calculation Type: Percent

| Peak No. | Peak Name | Result () | Ret. Time (min) | Time Offset (min) | Area (counts) | Sep. Code | Width 1/2 (sec) | Status Codes |
|---|---|---|---|---|---|---|---|---|
| 1 | | 0.0730 | 2.490 | 0.000 | 26347 | PV | 0.0 | |
| 2 | | 0.0906 | 2.539 | 0.000 | 32693 | VB | 27.8 | |
| 3 | | 0.1361 | 3.990 | 0.000 | 49086 | BB | 25.9 | |
| 4 | | 0.0077 | 5.032 | 0.000 | 2775 | VV | 2.8 | |
| 5 | | 0.0285 | 5.428 | 0.000 | 10279 | VV | 0.8 | |
| 6 | | 0.0517 | 6.237 | 0.000 | 18664 | VV | 12.7 | |
| 7 | | 0.1656 | 6.386 | 0.000 | 59746 | VP | 22.5 | |
| 8 | | 0.0175 | 7.515 | 0.000 | 6306 | TS | 0.0 | |
| 9 | | 0.5978 | 8.566 | 0.000 | 215623 | PV | 0.0 | |
| 10 | | 0.2032 | 9.065 | 0.000 | 73295 | VV | 0.0 | |
| 11 | | 0.2944 | 9.435 | 0.000 | 106196 | VV | 41.4 | |
| 12 | | 0.1125 | 10.417 | 0.000 | 40562 | VV | 7.2 | |
| 13 | | 5.1533 | 10.911 | 0.000 | 1858862 | VB | 14.0 | |
| 14 | | 0.0198 | 12.546 | 0.000 | 7125 | TS | 0.0 | |
| 15 | | 0.1234 | 13.573 | 0.000 | 44525 | VB | 14.3 | |
| 16 | | 0.0162 | 15.234 | 0.000 | 5855 | VV | 11.3 | |
| 17 | | 0.0113 | 15.699 | 0.000 | 4079 | VB | 3.2 | |
| 18 | | 0.0074 | 16.630 | 0.000 | 2667 | PV | 7.9 | |
| 19 | | 0.0100 | 16.746 | 0.000 | 3606 | VV | 21.3 | |
| 20 | | 0.0158 | 17.000 | 0.000 | 5710 | VP | 1.3 | |
| 21 | | 0.0069 | 18.019 | 0.000 | 2497 | TF | 0.0 | |
| 22 | | 0.0090 | 19.153 | 0.000 | 3237 | VV | 8.7 | |
| 23 | | 0.0273 | 19.392 | 0.000 | 9861 | VV | 15.1 | |
| 24 | | 0.0443 | 19.447 | 0.000 | 15973 | VV | 27.6 | |
| 25 | | 0.0069 | 19.797 | 0.000 | 2476 | VV | 6.3 | |
| 26 | | 0.0232 | 19.908 | 0.000 | 8356 | VV | 0.0 | |
| 27 | | 0.0822 | 20.913 | 0.000 | 29648 | VP | 15.3 | |
| 28 | | 0.0553 | 22.131 | 0.000 | 19940 | VP | 20.8 | |
| 29 | | 58.5499 | 23.489 | 0.000 | 21119578 | PV | 25.9 | |
| 30 | | 33.3011 | 24.965 | 0.000 | 12012069 | VP | 26.1 | |
| 31 | | 0.7580 | 27.482 | 0.000 | 273416 | TS | 0.0 | |
| | Totals: | 99.9999 | | 0.000 | 36071052 | | | |

Total Unidentified Counts : 36071052 counts

Detected Peaks: 162 Rejected Peaks: 131 Identified Peaks: 0

Multiplier: 1 Divisor: 1 Unidentified Peak Factor: 0

Baseline Offset: 0 microAU LSB: 0.1 microAU

Noise (used): 0 microAU - monitored before this run

Vial: 2 Injection Number: 1 Partial Loopfill Volume: 10 ul

**********

**Figure A117:** HPLC chart from the reduction of imine **5-1** with (R)-(+)-1,1'-Bi-2-napthol **5-20** after acid base wash.

```
Title       :
Run File    : c:\star\data\brandon\matt adams\bh-xii-75d real9-18-20187;55;14 pm.run
Method File : C:\star\estelle.mth
Sample ID   : bh-xii-75d real

Injection Date: 9/18/2018 7:55 PM    Calculation Date: 9/18/2018 8:25 PM

Operator   : matt                   Detector Type: 0325
Workstation: DALHOUSI-GZ0GPÿ HÚè-   Bus Address  : 44
Instrument : Analytical System      Sample Rate  : 20.00 Hz
Channel    : 1 = 254 nm             Run Time     : 30.000 min

** LC Workstation Version 6.41 ** 01907-64c0-ea4-04f1 **

Chart Speed =    0.69 cm/min   Attenuation = 9             Zero Offset = 5%
Start Time  =   0.000   min     End Time    = 30.000  min   Min / Tick  = 1.00
```

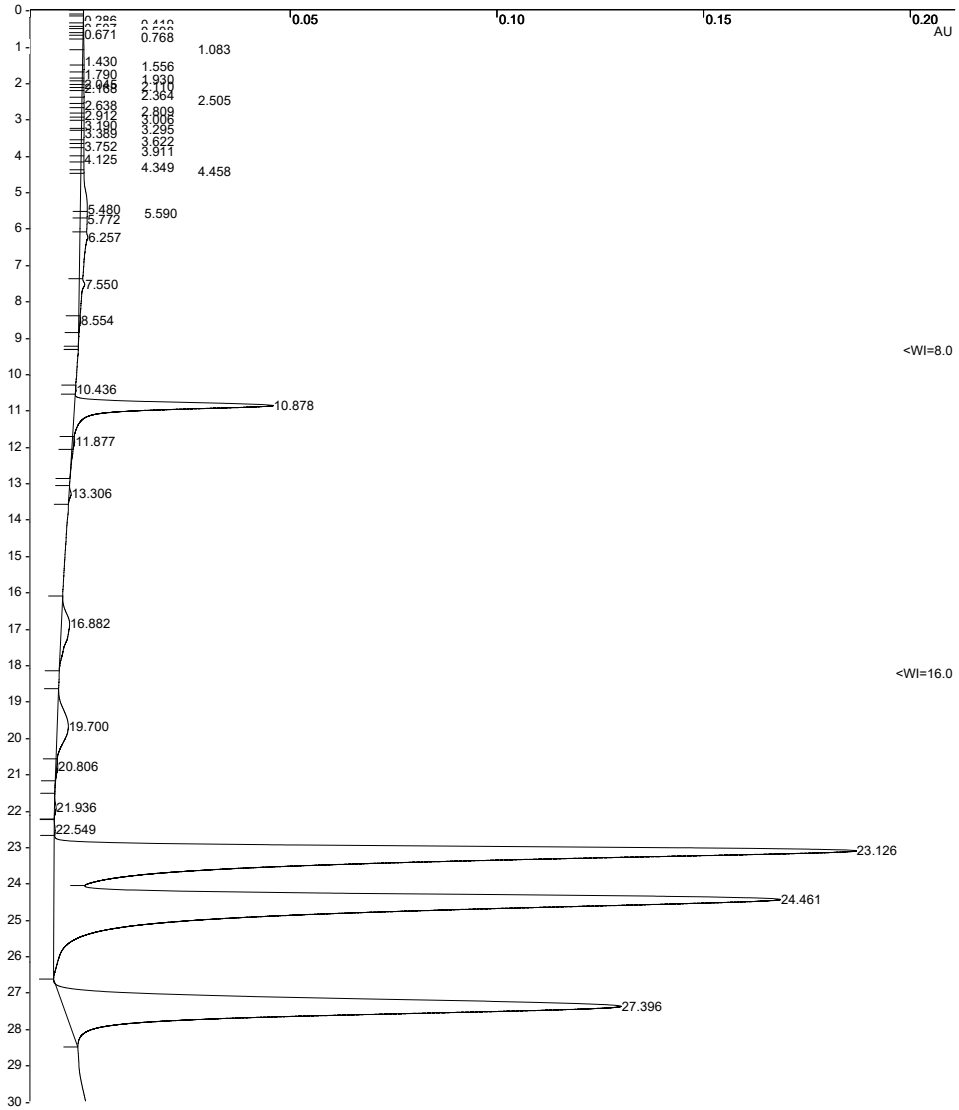


**Figure A118:** HPLC Trace from the racemate of the reduction of imine **5-1**.

## Appendix E: Appendix for Chapter 6

### E1: Crystallographic Solution and Refinement Details

Crystallographic data for **6-53**. The crystal chosen was attached to the tip of a MicroLoop with Paratone-N oil. Measurements were made on a Bruker D8 VENTURE diffractometer equipped with a PHOTON III CMOS detector using monochromated Mo Kα radiation (λ = 0.71073 Å) from an Incoatec micro-focus sealed tube at 125 K [1]. The initial orientation and unit cell were indexed using a least-squares analysis of the reflections collected from a 180° phi-scan, 2 seconds per frame and 1° per frame. For data collection, a strategy was calculated to maximize data completeness and multiplicity, in a reasonable amount of time, and then implemented using the Bruker Apex 3 software suite [1]. The crystal to detector distance was set to 4.0 cm. Cell refinement and data reduction were performed with the Bruker SAINT [2] software, which corrects for beam inhomogeneity, possible crystal decay, Lorentz and polarisation effects. A multi-scan absorption correction was applied (SADABS [3]). The structure was solved using SHELXT-2014 [4] and was refined using a full-matrix least-squares method on $F^2$ with SHELXL-2018 [4]. The non-hydrogen atoms were refined anisotropically. The hydrogen atoms bonded to carbon were included at geometrically idealized positions and were not refined. The isotropic thermal parameters of these hydrogen atoms were fixed at $1.2U_{eq}$ of the parent carbon atom or $1.5U_{eq}$ for methyl hydrogens.

The data was cut off at a resolution of 0.72Å using a SHEL instruction during the refinement. Above this value the reflections were mostly noise, $I/\sigma(I) < 2$.

Crystallographic data for **6-56**. The crystal chosen was attached to the tip of a MicroLoop with Paratone-N oil. Measurements were made on a Bruker D8 VENTURE diffractometer equipped with a PHOTON III CMOS detector using monochromated Mo Kα radiation (λ

= 0.71073 Å) from an Incoatec micro-focus sealed tube at 125 K [1]. The initial orientation and unit cell were indexed using a least-squares analysis of the reflections collected from a 180° phi-scan, 2 seconds per frame and 1° per frame. For data collection, a strategy was calculated to maximize data completeness and multiplicity, in a reasonable amount of time, and then implemented using the Bruker Apex 3 software suite [1]. The crystal to detector distance was set to 4.0 cm. Cell refinement and data reduction were performed with the Bruker SAINT [2] software, which corrects for beam inhomogeneity, possible crystal decay, Lorentz and polarisation effects. A multi-scan absorption correction was applied (SADABS [3]). The structure was solved using SHELXT-2014 [4] and was refined using a full-matrix least-squares method on $F^2$ with SHELXL-2018 [4]. The non-hydrogen atoms were refined anisotropically. The hydrogen atoms bonded to carbon were included at geometrically idealized positions and were not refined. The isotropic thermal parameters of these hydrogen atoms were fixed at $1.2U_{eq}$ of the parent carbon atom or $1.5U_{eq}$ for methyl hydrogens.

The molecule was found to lie on a mirror plane, passing through the heavy atoms P1, S1, C7 and C10. These atoms have occupancies of only 0.5 and only one and a half of the atoms in the cyclohexyl rings are unique. The other half of the molecule is generated using the symmetry operator (+x, -y+1/2, +z).

The only “traditional” hydrogen bond acceptor in the molecule is the sulfur atom. It accepts a pair of symmetry related, intermolecular contacts, C6-H6B…S1, from equivalent rings on either side of the mirror plane in a single neighbouring molecule.

1) APEX 3 (Bruker, 2018) Bruker AXS Inc., Madison, Wisconsin, USA.

2) SAINT (Bruker, 2016) Bruker AXS Inc., Madison, Wisconsin, USA.

3) SADABS (Bruker, 2016) Bruker AXS Inc., Madison, Wisconsin, USA.

4) Sheldrick, G.M. (2015) *Acta Cryst*., A71, 3-8; Sheldrick, G.M. (2015) *Acta Cryst*., C71, 3-8.

5) Spek, A.L. (2009) *Acta Cryst*., D65, 148-155.

**Table A9.** Crystal data and structure refinement for **6-53**.

| | | |
|---|---|---|
| Empirical formula | $C_{10}H_{20}FN_2PS$ | |
| Formula weight | 250.31 | |
| Temperature | 125(2) K | |
| Wavelength | 0.71073 Å | |
| Crystal system | Monoclinic | |
| Space group | $P2_1/n$ | |
| Unit cell dimensions | $a$ = 11.1474(10) Å | α = 90°. |
| | $b$ = 9.6074(8) Å | β = 112.922(3)° |
| | $c$ = 13.5790(11) Å | γ = 90° |
| Volume | 1339.4(2) $Å^3$ | |
| $Z$ | 4 | |
| Density (calculated) | 1.241 $Mg/m^3$ | |
| Absorption coefficient | 0.346 $mm^{-1}$ | |
| F(000) | 536 | |
| Crystal size | 0.200 x 0.150 x 0.140 $mm^3$ | |
| Theta range for data collection | 2.017 to 29.575° | |
| Index ranges | -15<=h<=15, -13<=k<=13, -18<=l<=18 | |
| Reflections collected | 20694 | |
| Independent reflections | 3757 [R(int) = 0.0493] | |
| Completeness to theta = 25.242° | 100.0 % | |
| Absorption correction | Semi-empirical from equivalents | |
| Max. and min. transmission | 0.7471 and 0.5728 | |
| Refinement method | Full-matrix least-squares on $F^2$ | |
| Data / restraints / parameters | 3757 / 0 / 142 | |
| Goodness-of-fit on $F^2$ | 1.039 | |
| Final R indices [I>2sigma(I)] | R1 = 0.0440, wR2 = 0.1119 | |

| | |
|---|---|
| R indices (all data) | R1 = 0.0615, wR2 = 0.1247 |
| Extinction coefficient | n/a |
| Largest diff. peak and hole | 0.622 and -0.345 e.Å$^{-3}$ |

**Table A10.** Crystal data and structure refinement for **6-56**.

| | | |
|---|---|---|
| Empirical formula | $C_{18}H_{33}PS$ | |
| Formula weight | 312.47 | |
| Temperature | 125(2) K | |
| Wavelength | 0.71073 Å | |
| Crystal system | Orthorhombic | |
| Space group | *Pnma* | |
| Unit cell dimensions | a = 10.7291(2) Å | α = 90° |
| | b = 15.7263(3) Å | β = 90° |
| | c = 10.3163(3) Å | γ = 90° |
| Volume | 1740.66(7) Å$^3$ | |
| Z | 4 | |
| Density (calculated) | 1.192 Mg/m$^3$ | |
| Absorption coefficient | 0.269 mm$^{-1}$ | |
| F(000) | 688 | |
| Crystal size | 0.148 x 0.101 x 0.065 mm$^3$ | |
| Theta range for data collection | 2.361 to 39.826° | |
| Index ranges | -19<=h<=19, -28<=k<=28, -18<=l<=17 | |
| Reflections collected | 74281 | |
| Independent reflections | 5331 [R(int) = 0.0378] | |
| Completeness to theta = 25.242° | 99.8 % | |
| Absorption correction | Semi-empirical from equivalents | |
| Max. and min. transmission | 0.7478 and 0.6552 | |
| Refinement method | Full-matrix least-squares on F$^2$ | |
| Data / restraints / parameters | 5331 / 0 / 97 | |
| Goodness-of-fit on F$^2$ | 1.039 | |
| Final R indices [I>2sigma(I)] | R1 = 0.0273, wR2 = 0.0739 | |
| R indices (all data) | R1 = 0.0358, wR2 = 0.0787 | |
| Extinction coefficient | n/a | |
| Largest diff. peak and hole | 0.400 and -0.346 e.Å$^{-3}$ | |

**E2: NMR Spectra for Section 6.2**

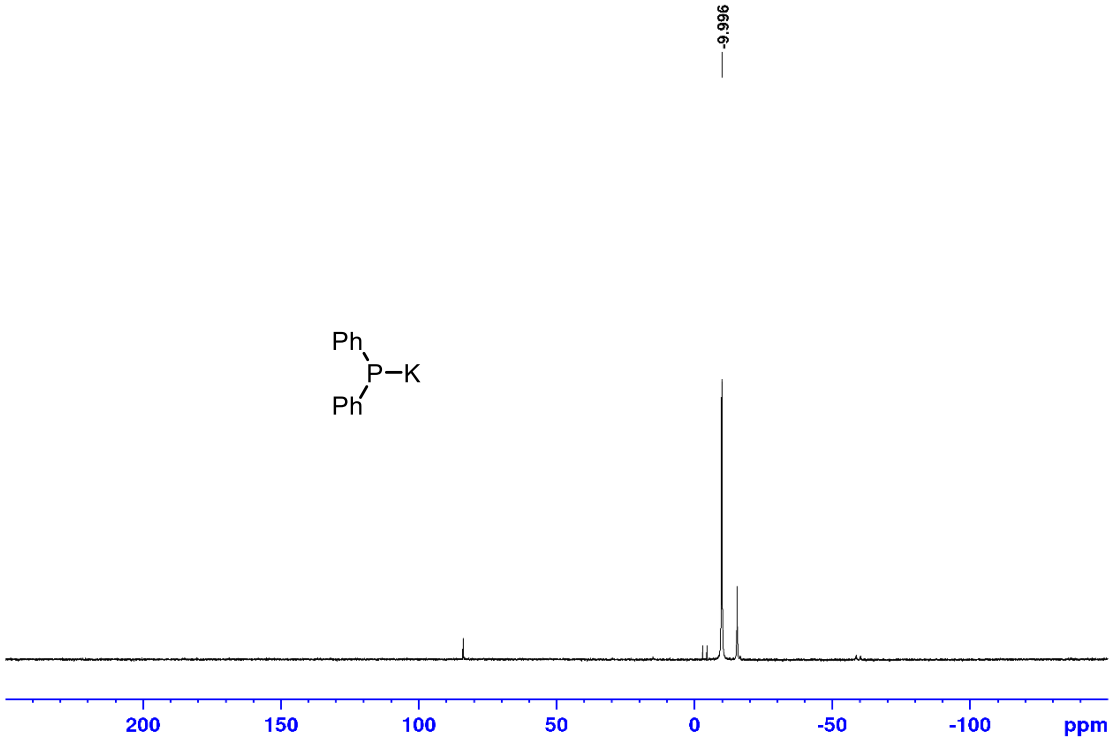


**Figure A119:** $^{31}$P NMR spectrum (202.5 MHz, THF, $C_6D_6$ (lock)) of **6-25** pre $SF_6$.

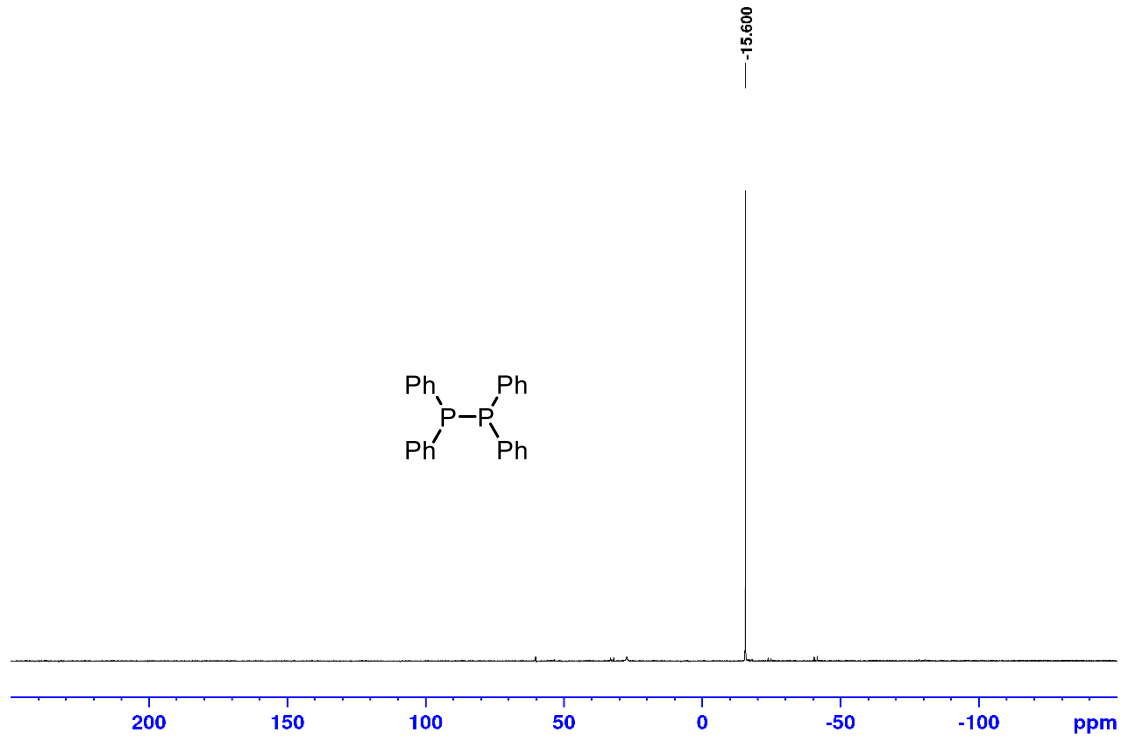


**Figure A120:** $^{31}$P NMR spectrum (202.5 MHz, THF, $C_6D_6$ (lock)) of **6-25** after $SF_6$ addition.

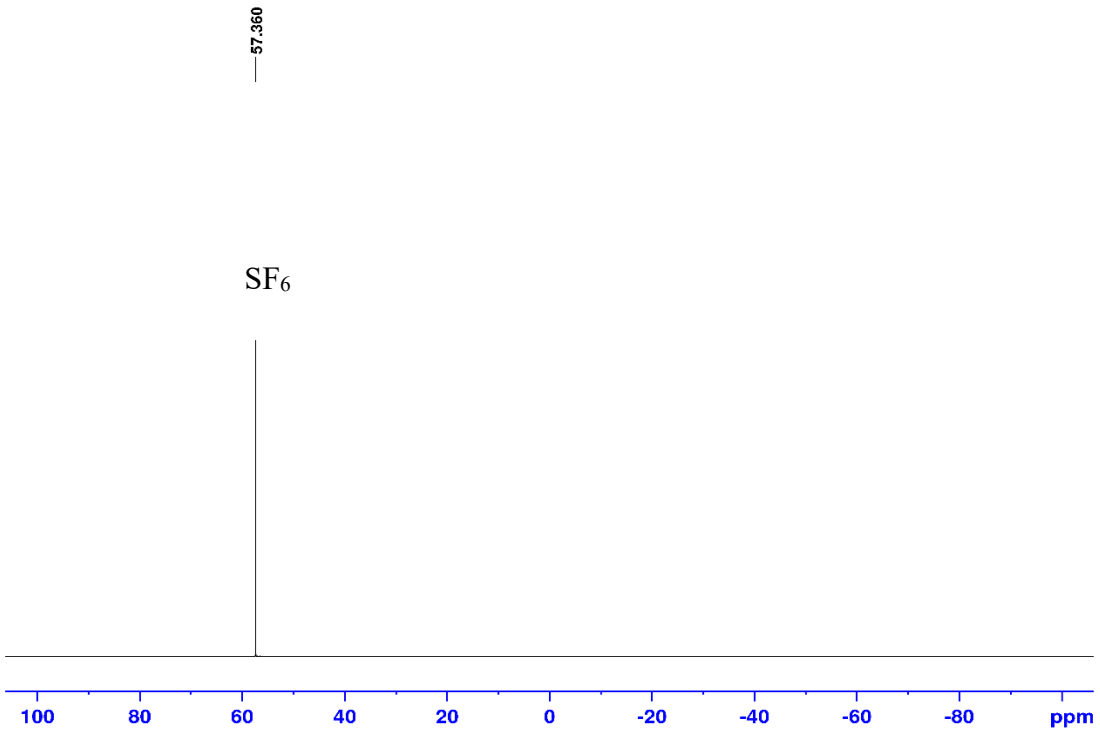


**Figure A121:** $^{19}F$ NMR spectrum (0 center point) (470.6 MHz, THF, $C_6D_6$ (lock)) of **6-25** after $SF_6$ addition.

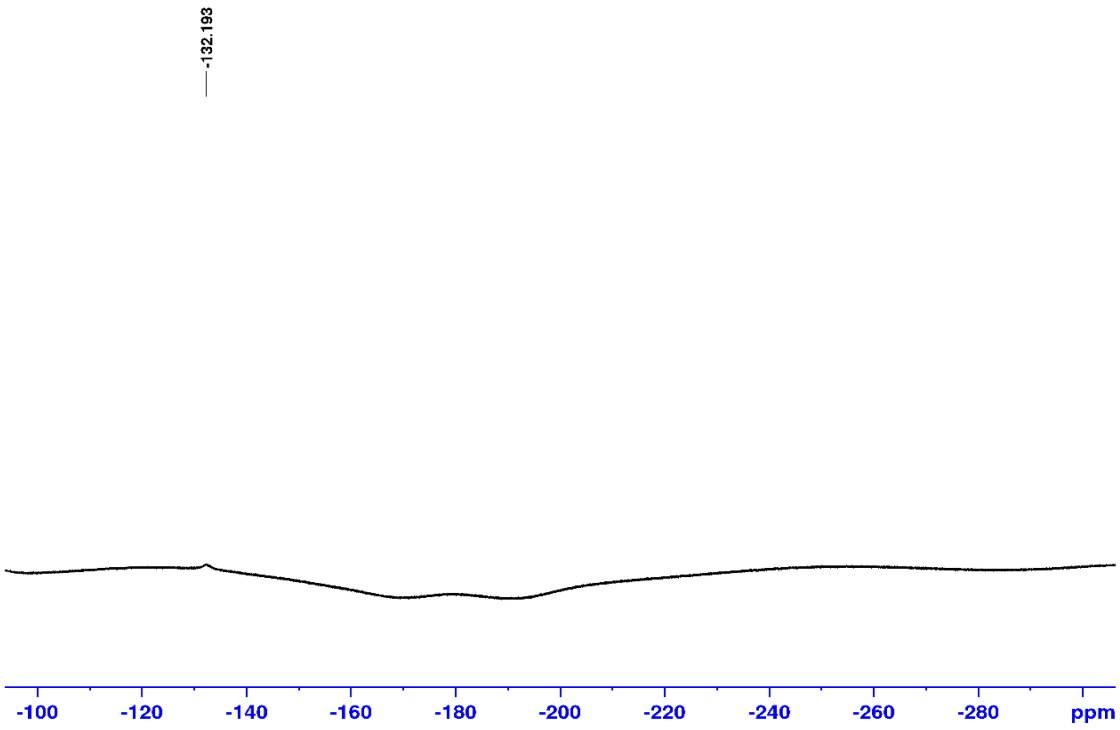


**Figure A122**: $^{19}F$ NMR spectrum (-200 center point) (470.6 MHz, THF, $C_6D_6$ (lock)) of **6-25** after $SF_6$ addition.

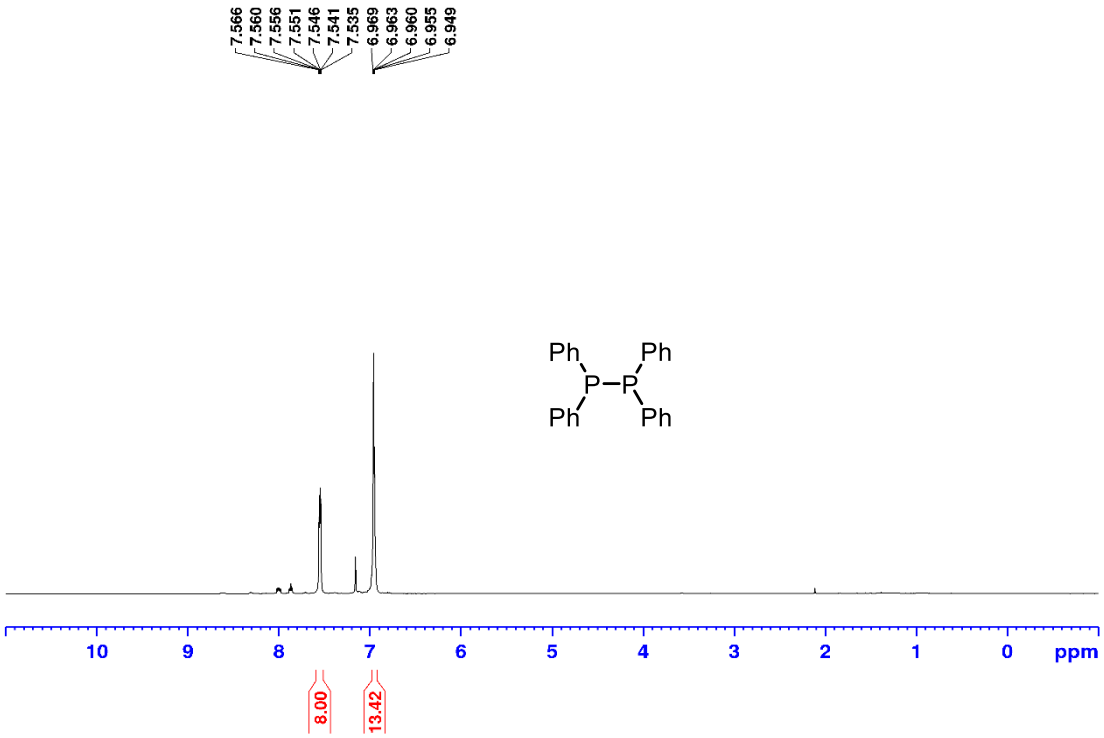


**Figure A123:** $^{1}$H NMR spectrum (500 MHz, $C_6D_6$) scale up and isolation of tetraphenyldiphosphine **6-26**.

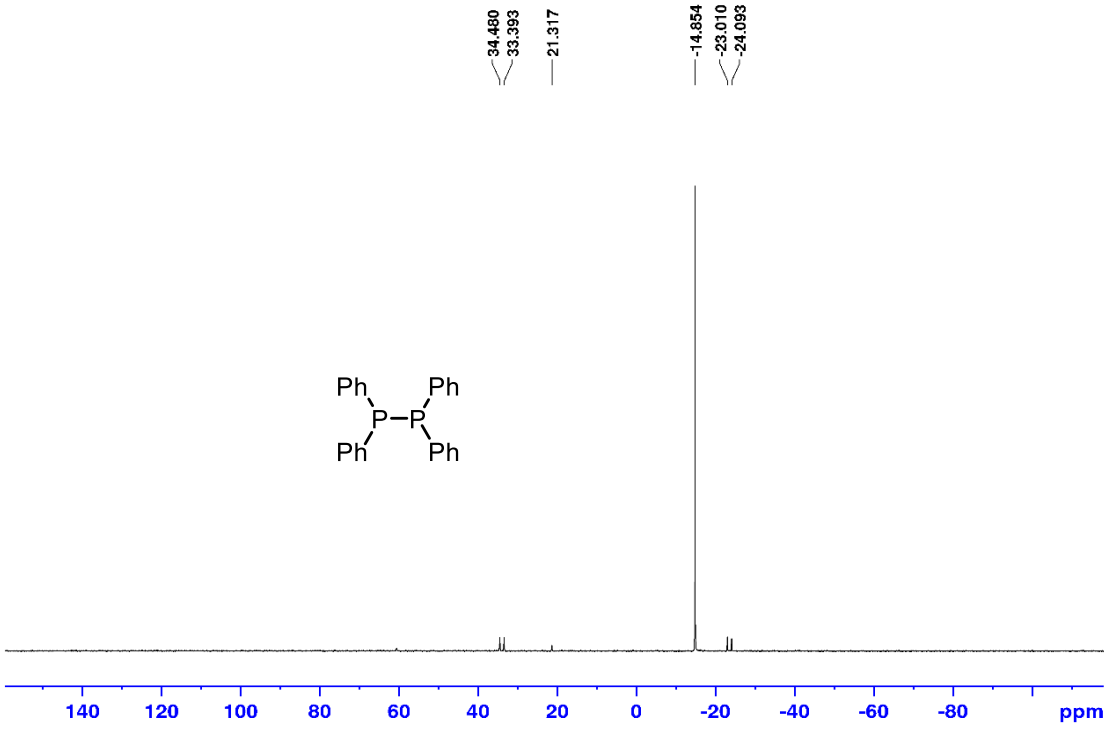


**Figure A124:** $^{31}$P NMR spectrum (202.5 MHz, $C_6D_6$) scale up and isolation of tetraphenyldiphosphine **6-26**.

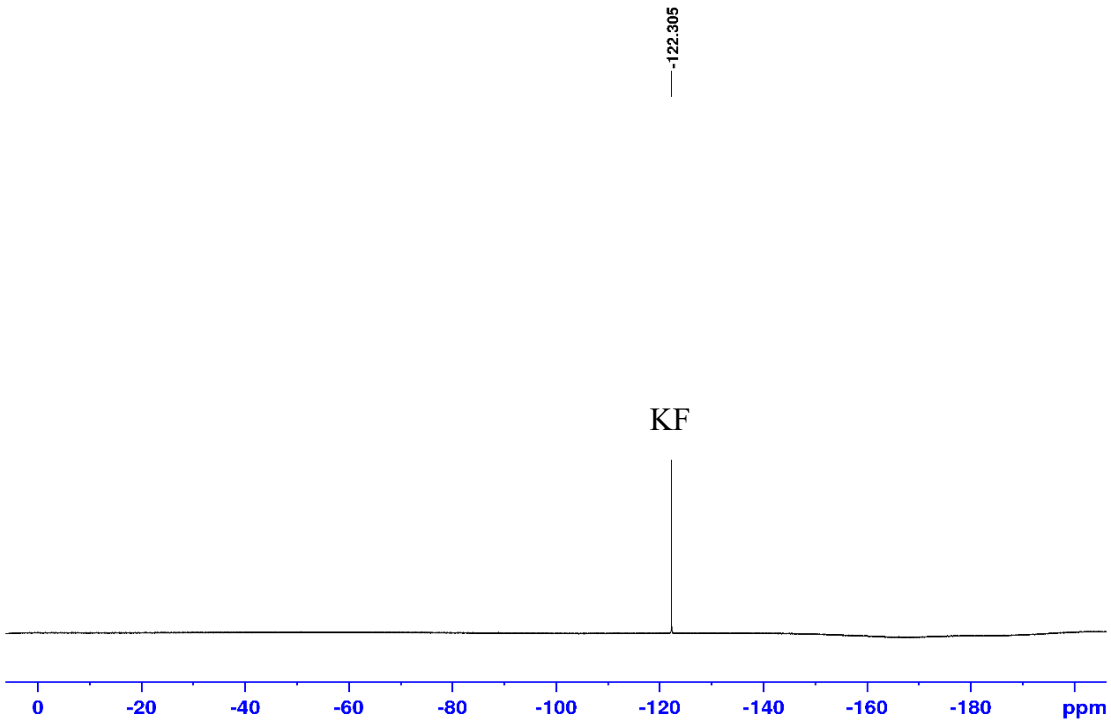


**Figure A125:** $^{19}F$ NMR spectrum (-100 center point) (470.6 MHz, $D_2O$) NMR analysis of the crude solution in $D_2O$.

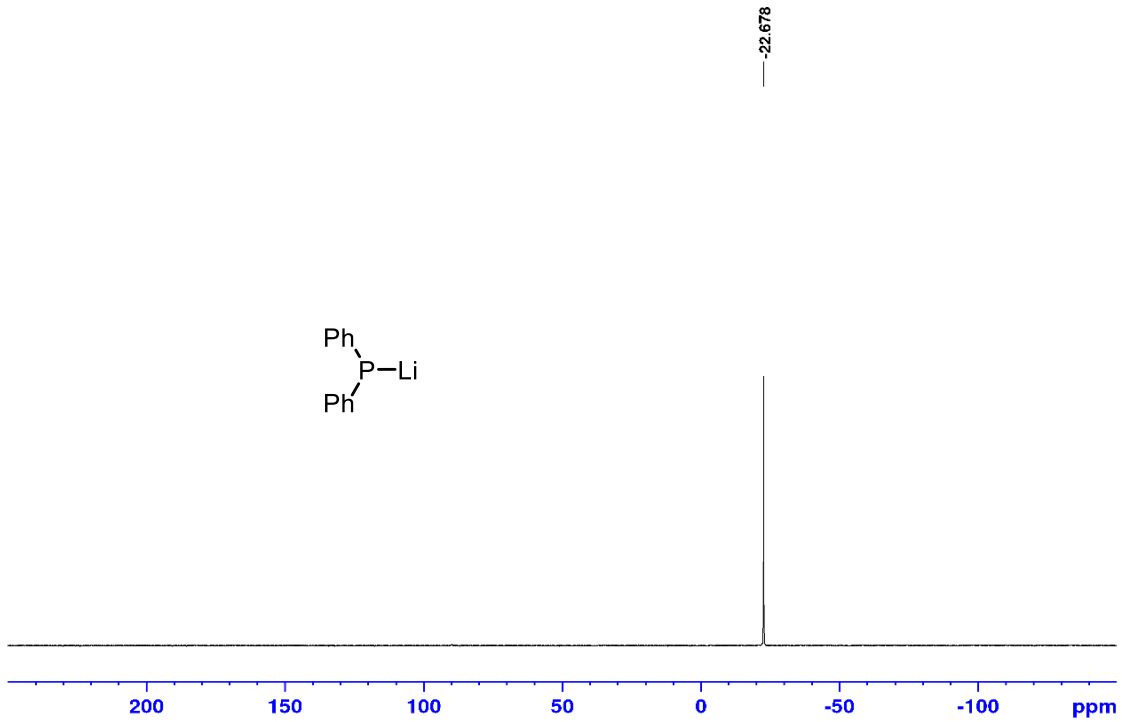


**Figure A126:** $^{31}P$ NMR spectrum (202.5 MHz, THF, $C_6D_6$ (lock)) of **6-30** pre $SF_6$.

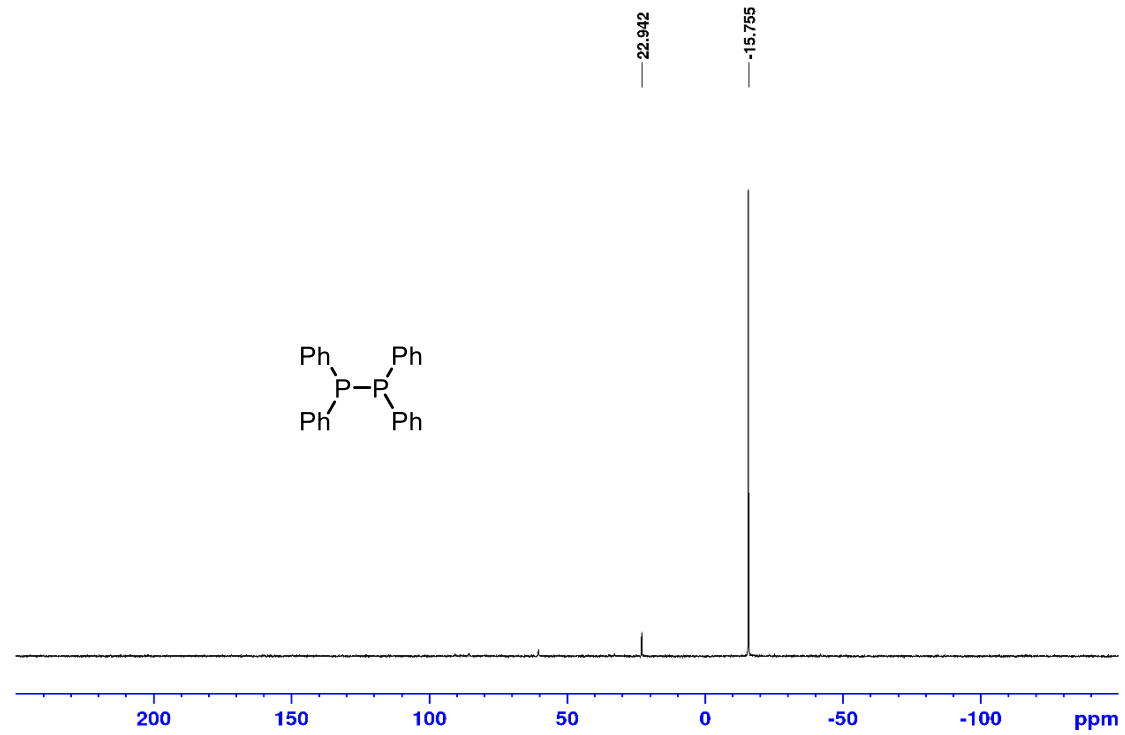


**Figure A127:** $^{31}$P NMR spectrum (202.5 MHz, THF, $C_6D_6$ (lock)) of **6-30** after $SF_6$ addition.

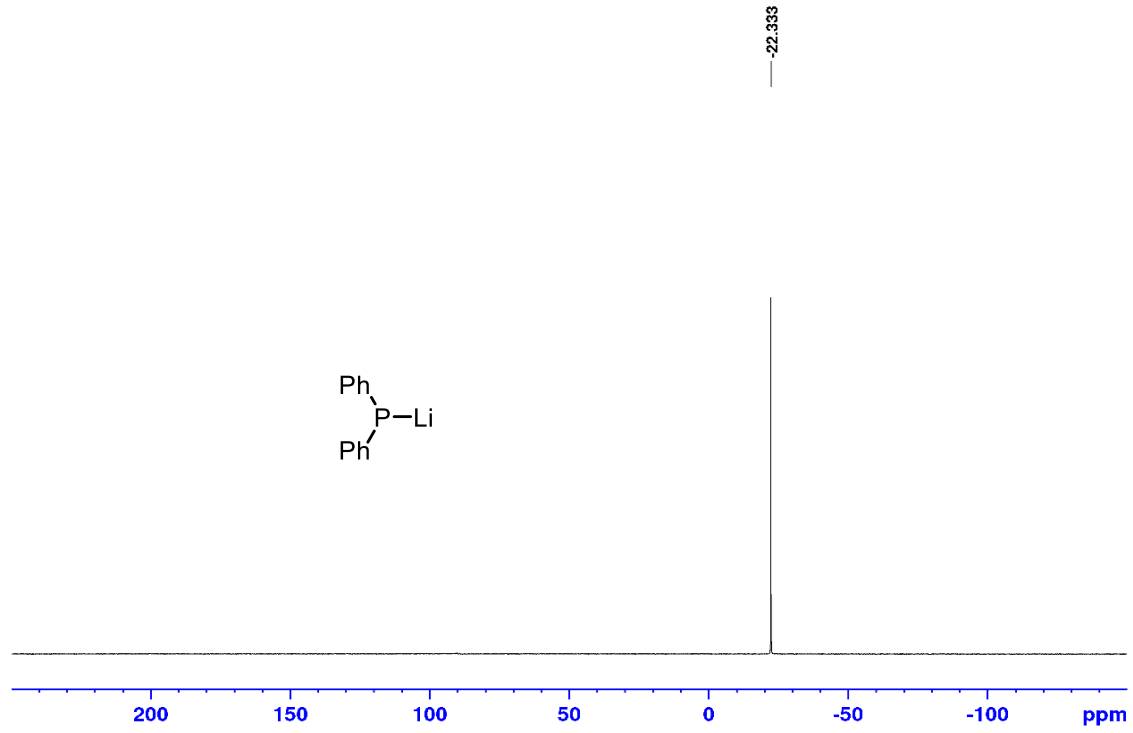


**Figure A128:** $^{31}$P NMR spectrum (202.5 MHz, THF, $C_6D_6$ (lock)) of **6-30** pre $SF_6$ for sulfide test.

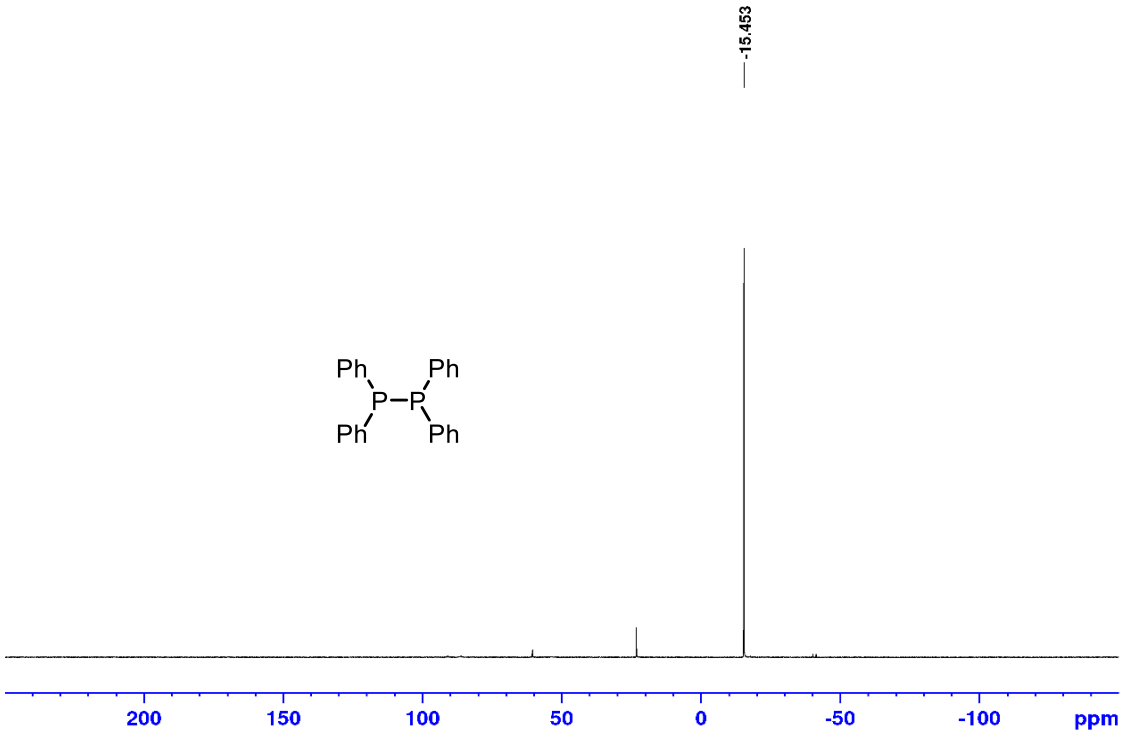


**Figure A129:** $^{31}P$ NMR spectrum (202.5 MHz, THF, $C_6D_6$ (lock)) of **6-30** after $SF_6$ addition for sulfide test.

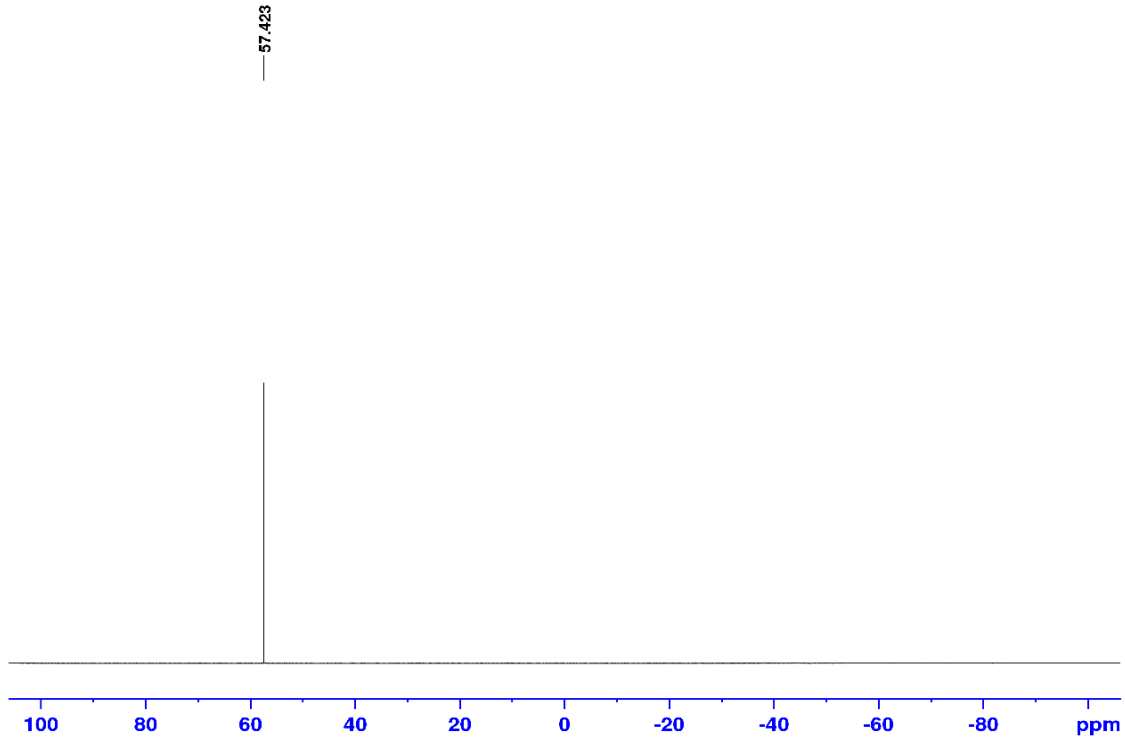


**Figure A130:** $^{19}F$ NMR spectrum (0 center point) (470.6 MHz, THF, $C_6D_6$ (lock)) of **6-30** after $SF_6$ addition for sulfide test.

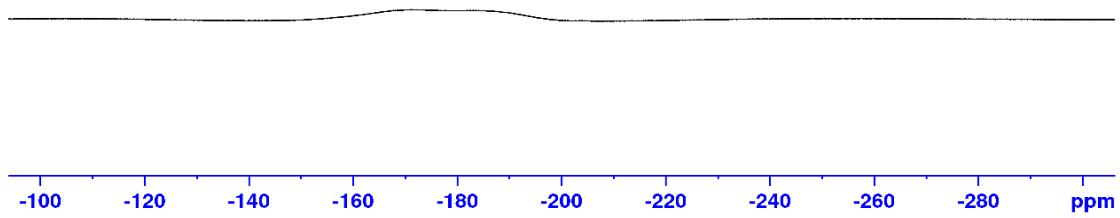


**Figure A131:** $^{19}F$ NMR spectrum (-200 center point) (470.6 MHz, THF, $C_6D_6$ (lock)) of **6-30** after $SF_6$ addition for sulfide test.

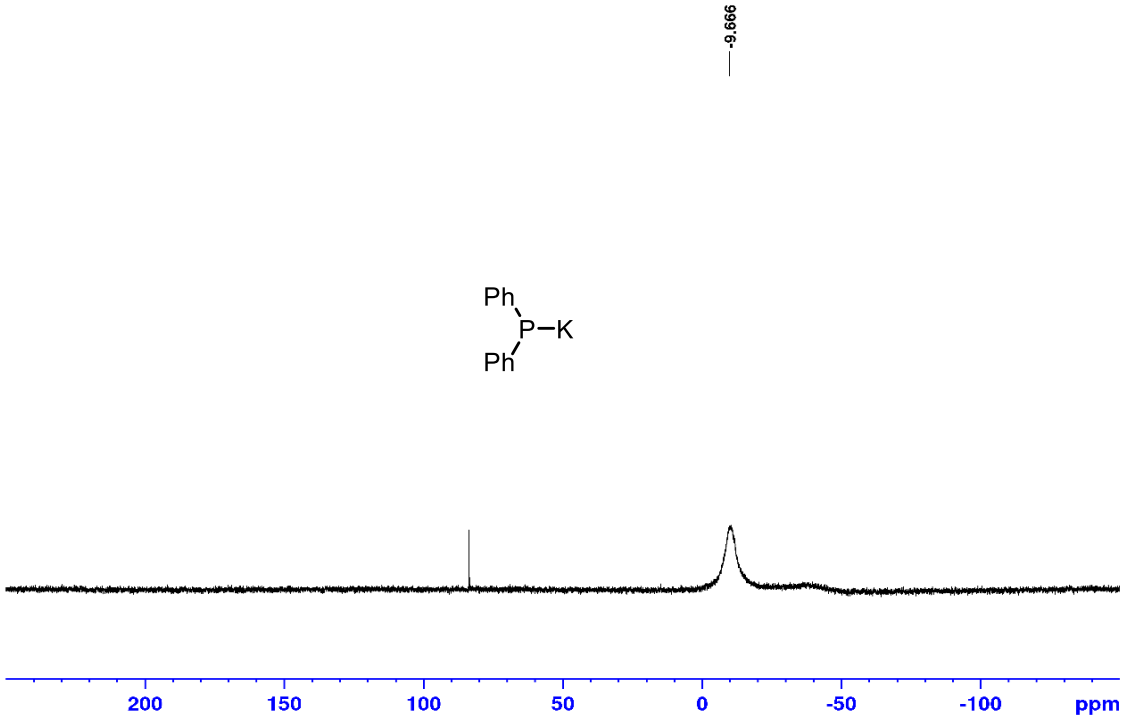


**Figure A132:** $^{31}P$ NMR spectrum (202.5 MHz, THF, $C_6D_6$ (lock)) of **6-25** (*in situ*) pre $SF_6$ for sulfide test.

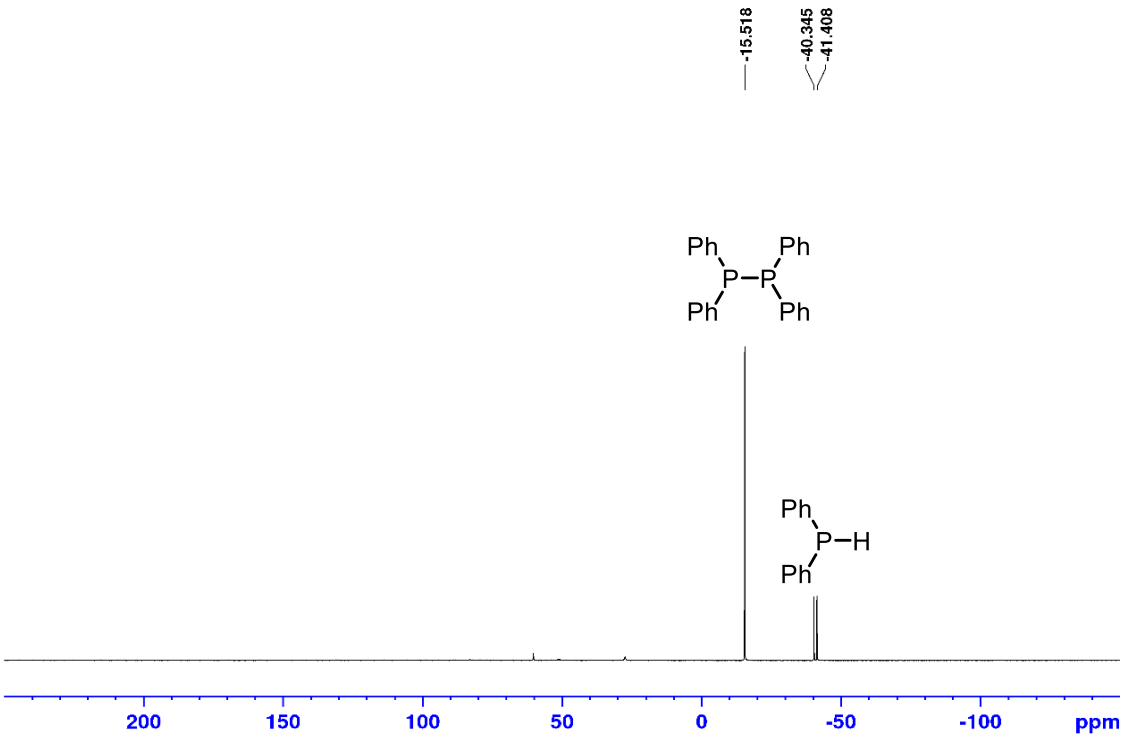


**Figure A133:** $^{31}P$ NMR spectrum (202.5 MHz, THF, $C_6D_6$ (lock)) of **6-25** (*in situ*) after $SF_6$ addition for sulfide test.

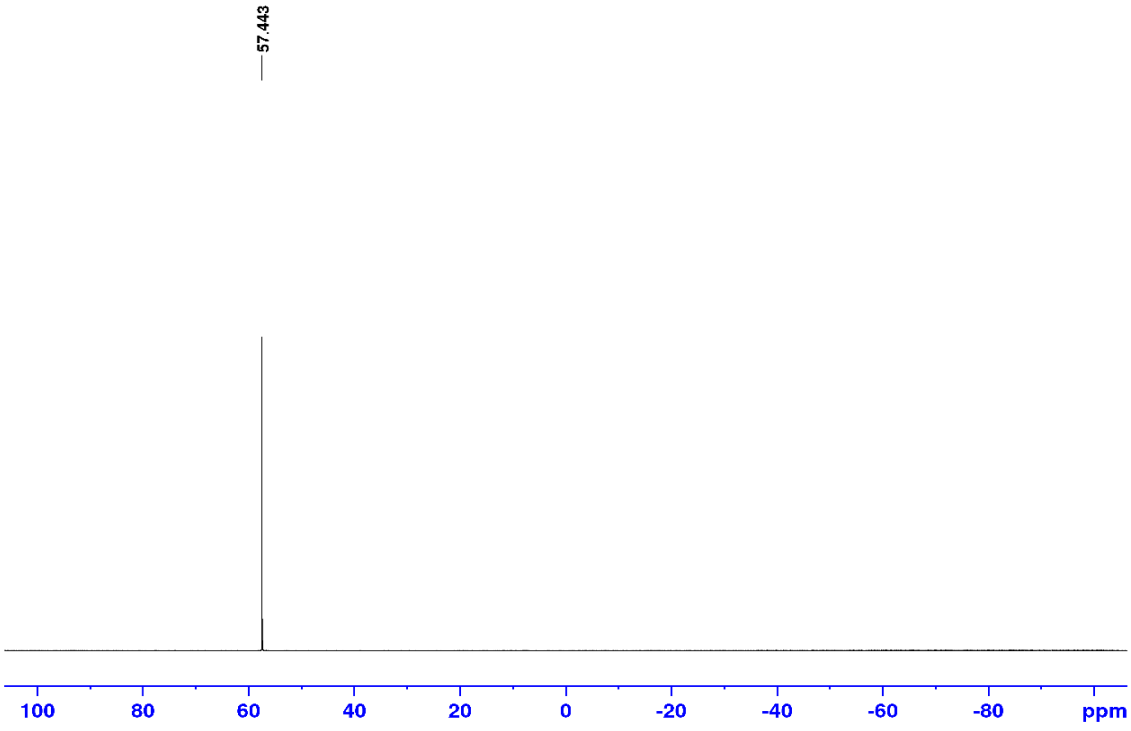


**Figure A134:** $^{19}F$ NMR spectrum (0 center point) (470.6 MHz, THF, $C_6D_6$ (lock)) of **6-25** (*in situ*) after $SF_6$ addition for sulfide test.

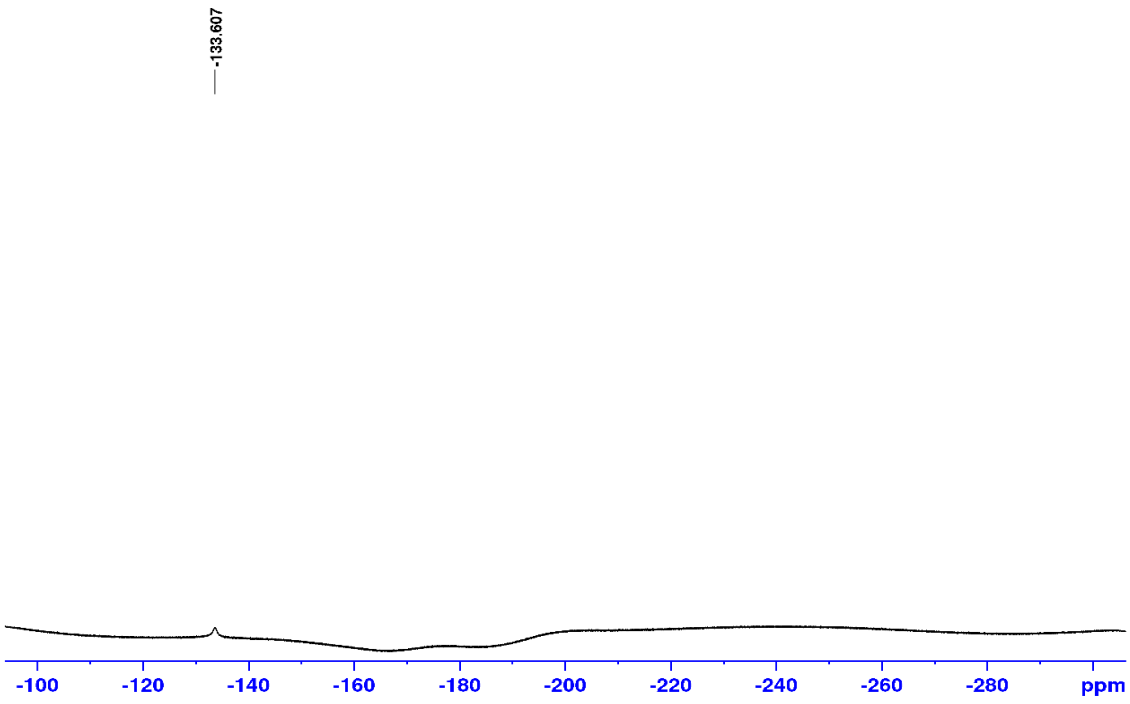


**Figure A135:** $^{19}F$ NMR spectrum (-200 center point) (470.6 MHz, THF, $C_6D_6$ (lock)) of **6-25** (*in situ*) after $SF_6$ addition for sulfide test.

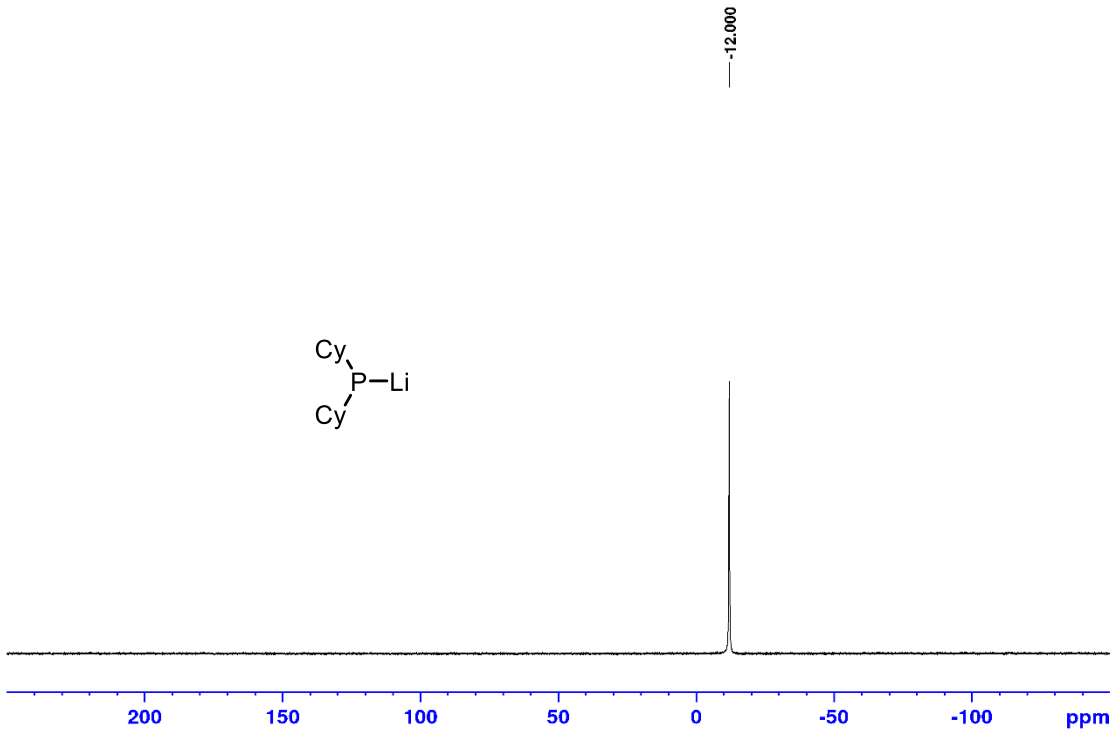


**Figure A136:** $^{31}P$ NMR spectrum (202.5 MHz, THF, $C_6D_6$ (lock)) of **6-32** pre $SF_6$.

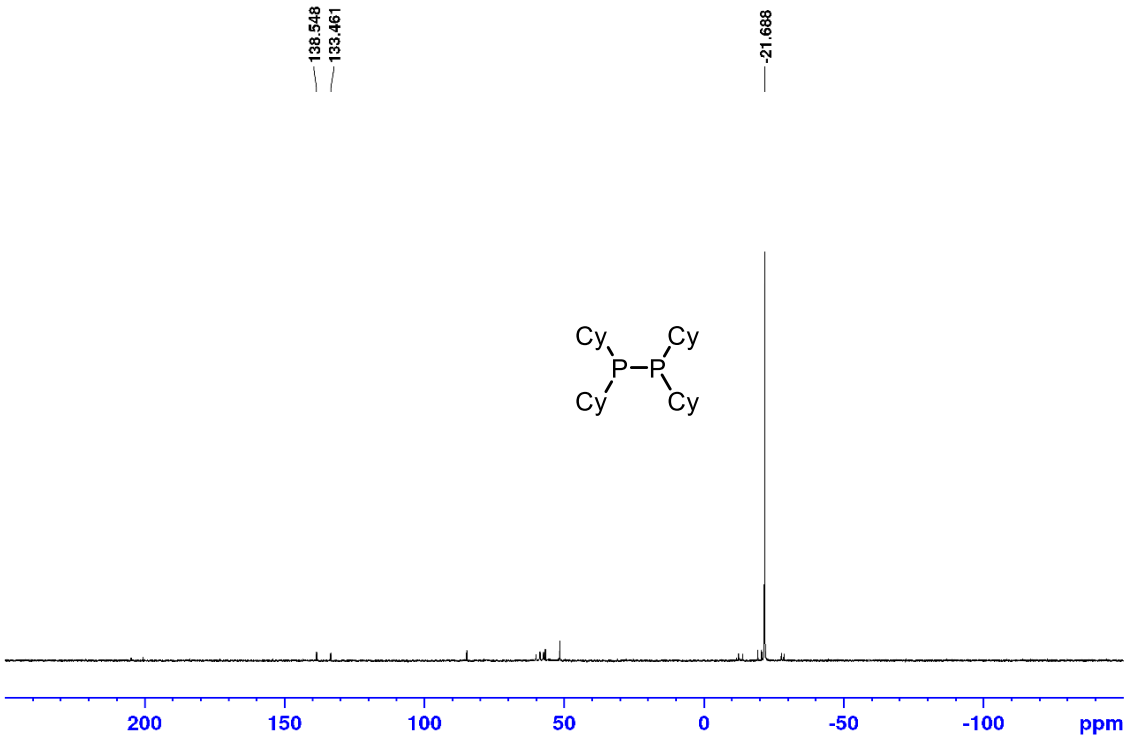


**Figure A137:** $^{31}P$ NMR spectrum (202.5 MHz, THF, $C_6D_6$ (lock)) of **6-32** after $SF_6$ addition.

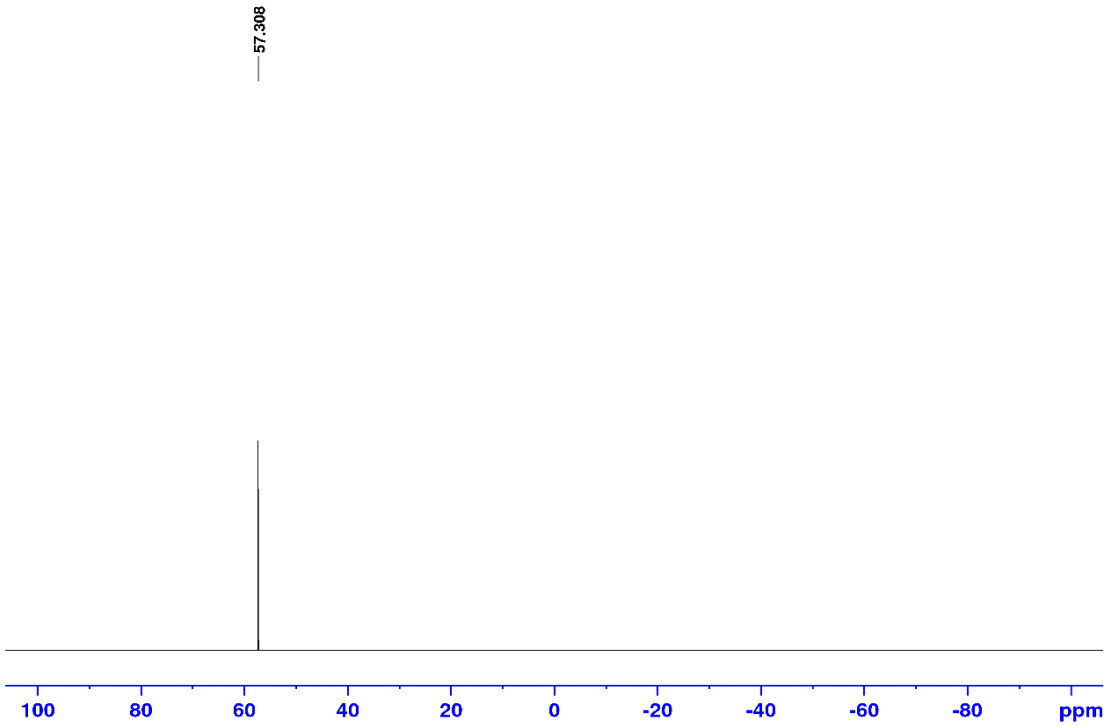


**Figure A138:** $^{19}F$ NMR spectrum (0 center point) (470.6 MHz, THF, $C_6D_6$ (lock)) of **6-32** after $SF_6$ addition.

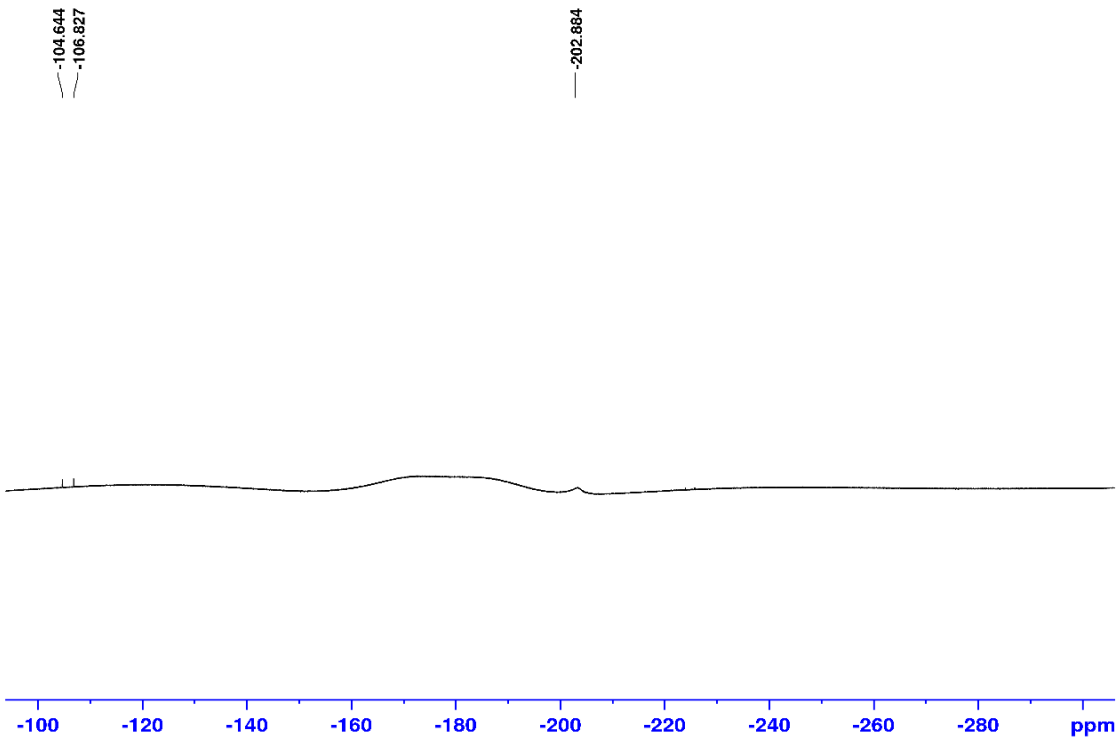


**Figure A139:** $^{19}F$ NMR spectrum (-200 center point) (470.6 MHz, THF, $C_6D_6$ (lock)) of **6-32** after $SF_6$ addition.

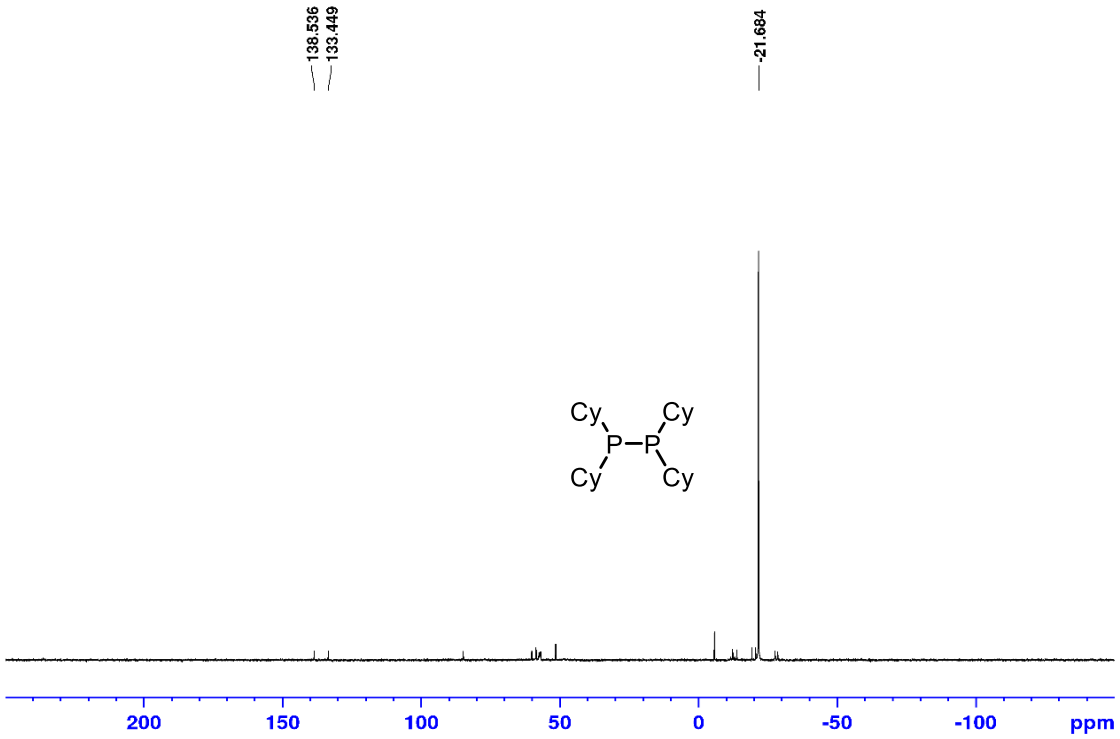


**Figure A140:** $^{31}P$ NMR spectrum (202.5 MHz, THF, $C_6D_6$ (lock)) of **6-32** after $SF_6$ addition at -15 °C.

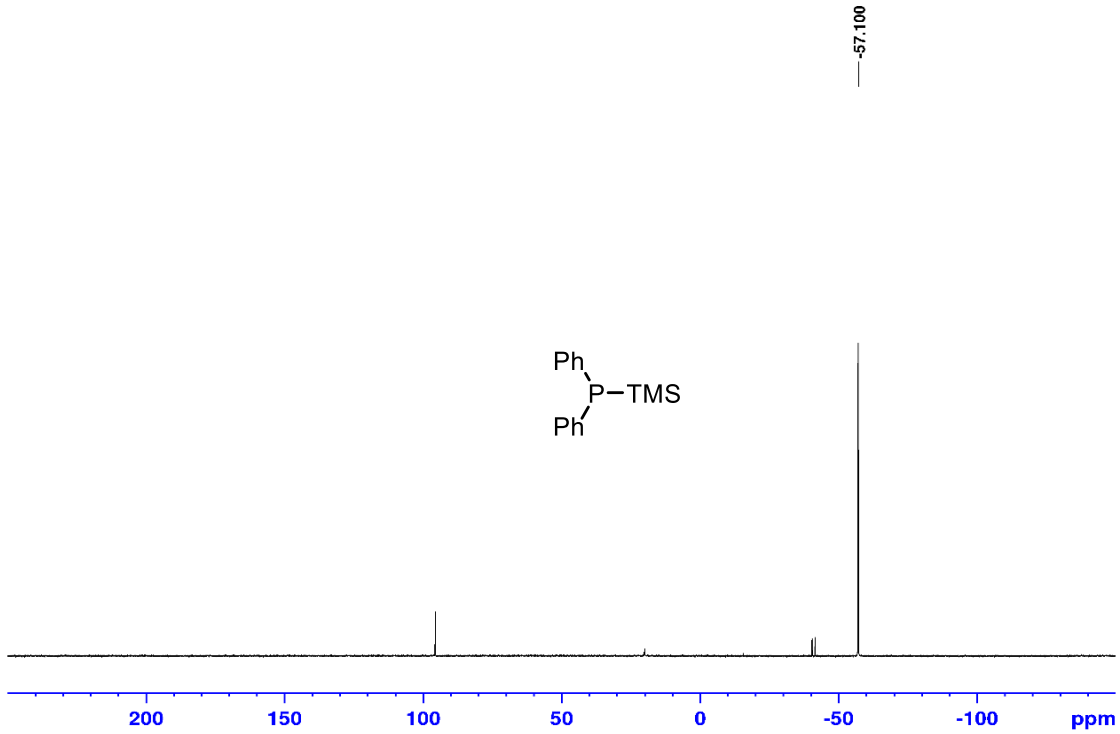


**Figure A141:** $^{31}P$ NMR spectrum (202 MHz, THF, $C_6D_6$ (lock)) of **6-48** pre $SF_6$.

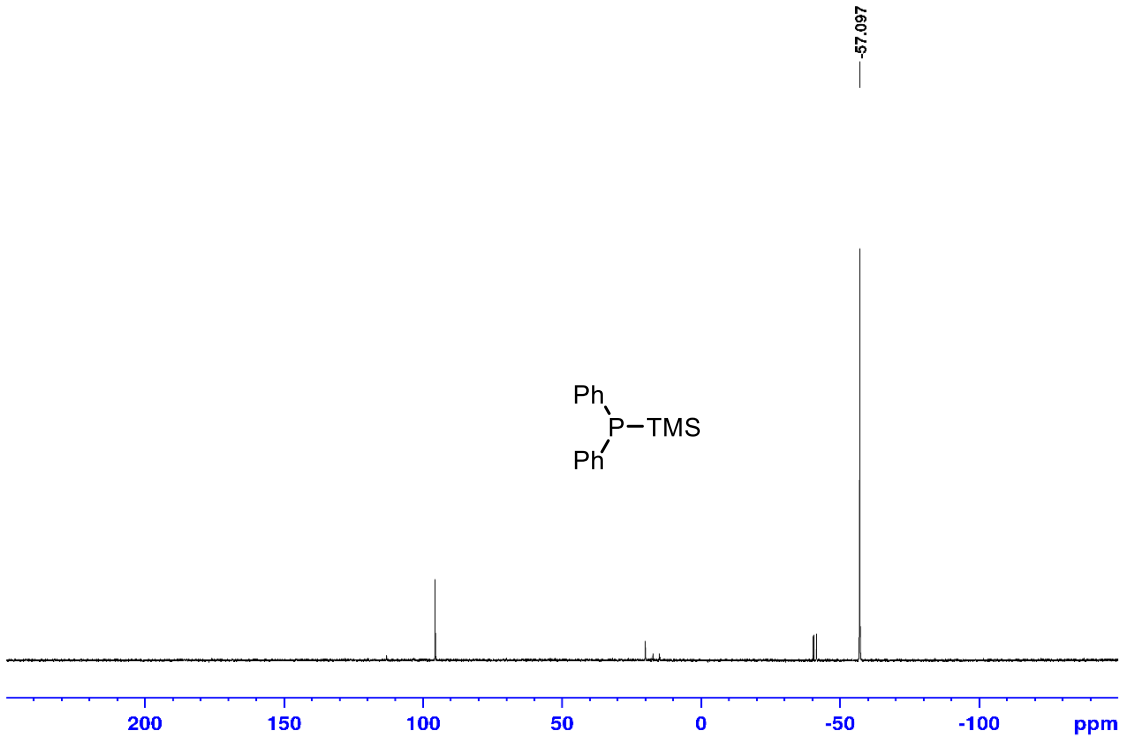


**Figure A142:** $^{31}P$ NMR spectrum (202.5 MHz, THF, $C_6D_6$ (lock)) of **6-48** after $SF_6$ addition.

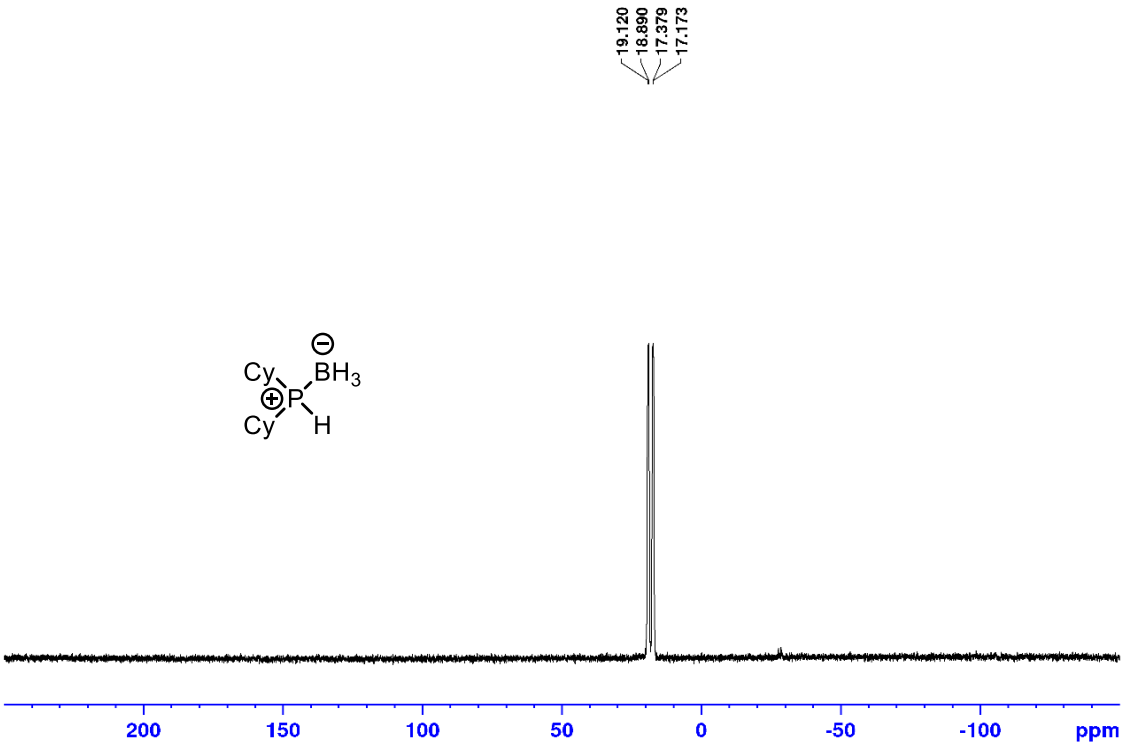


**Figure A143:** $^{31}$P NMR spectrum (202.5 MHz, THF, $C_6D_6$ (lock)) of **6-45**.

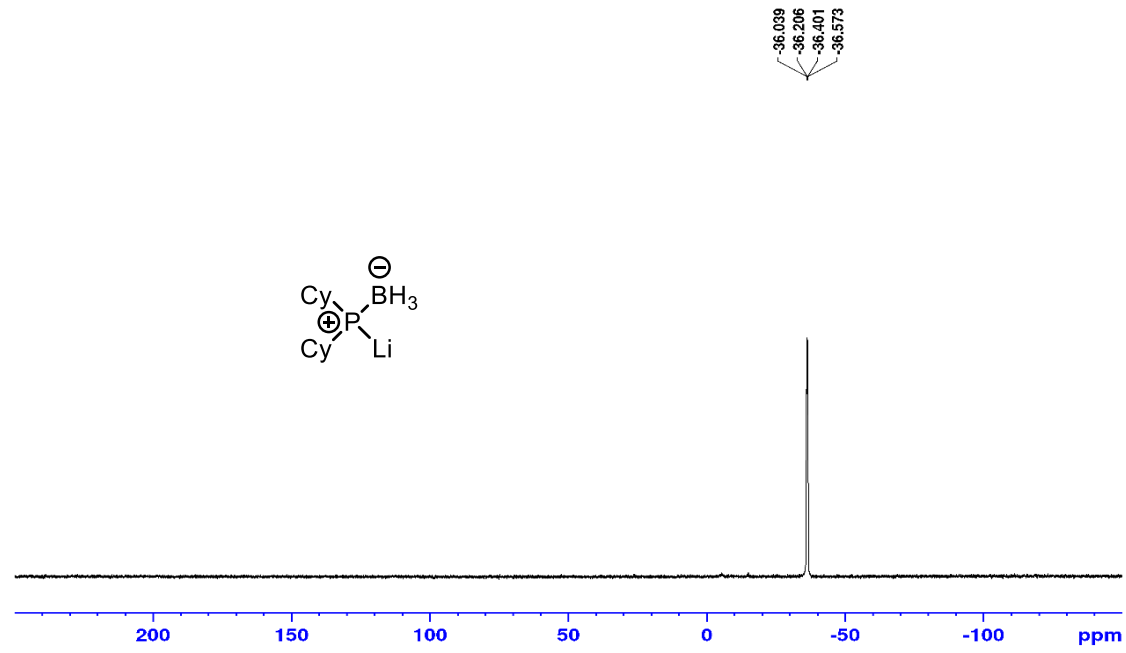


**Figure A144:** $^{31}$P NMR spectrum (202.5 MHz, THF, $C_6D_6$ (lock)) of **6-46** pre $SF_6$.

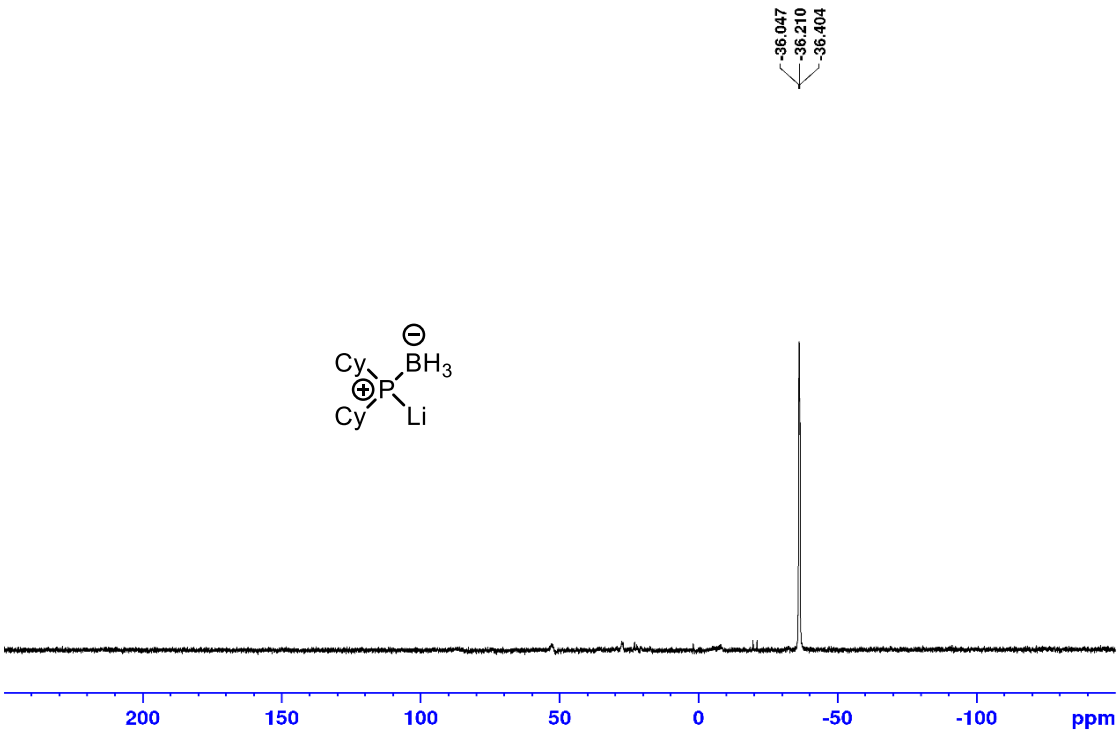


**Figure A145:** $^{31}$P NMR spectrum (202.5 MHz, THF, $C_6D_6$ (lock)) of **6-46** after $SF_6$ addition.

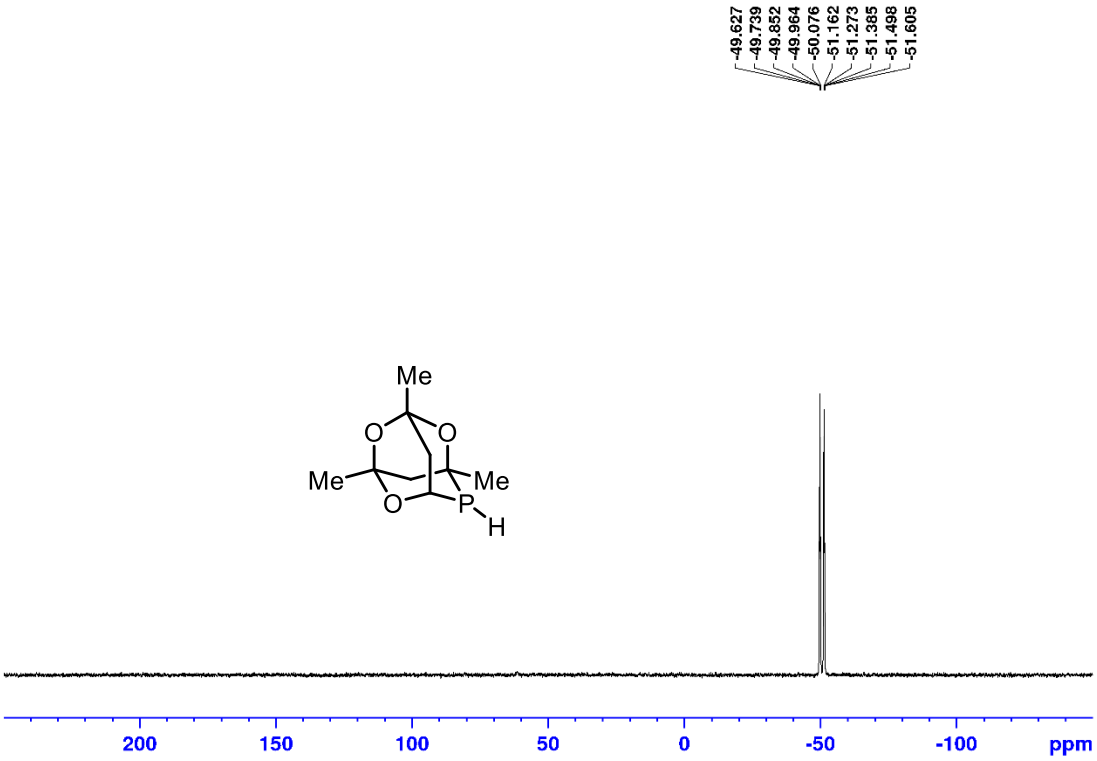


**Figure A146:** $^{31}$P NMR spectrum (202.5 MHz, THF, $C_6D_6$ (lock)) of Cage Phos.

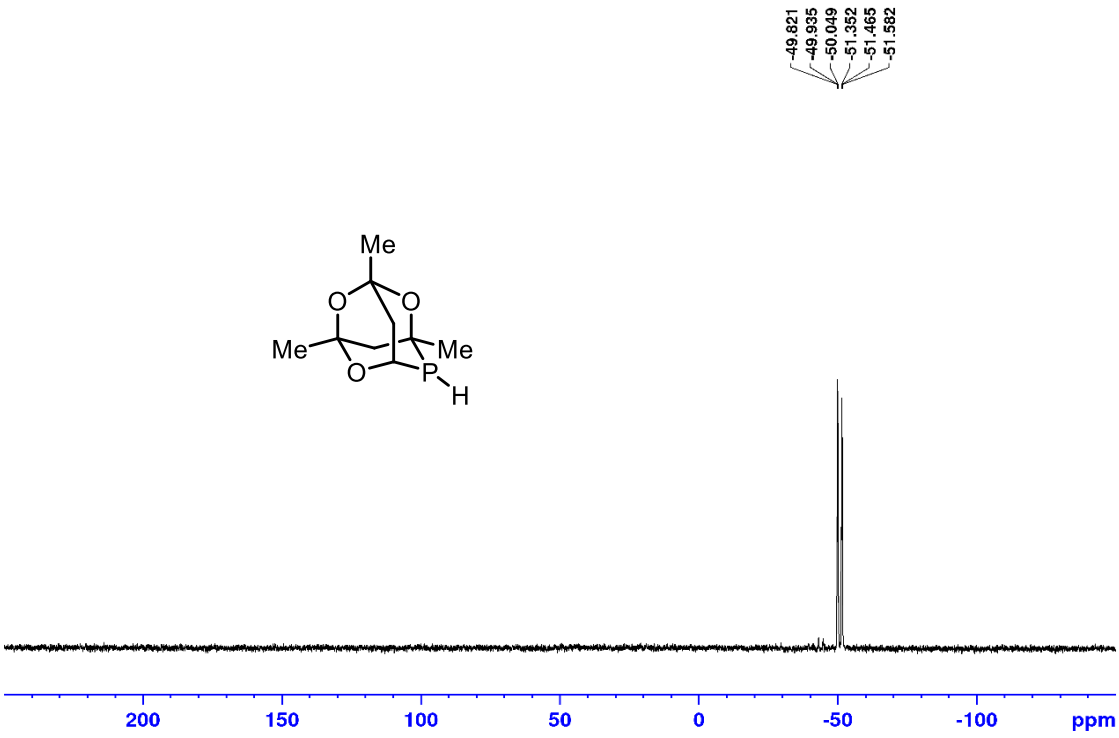


**Figure A147:** $^{31}$P NMR spectrum (202.5 MHz, THF, $C_6D_6$ (lock)) of Cage Phos after addition of *n*-BuLi.

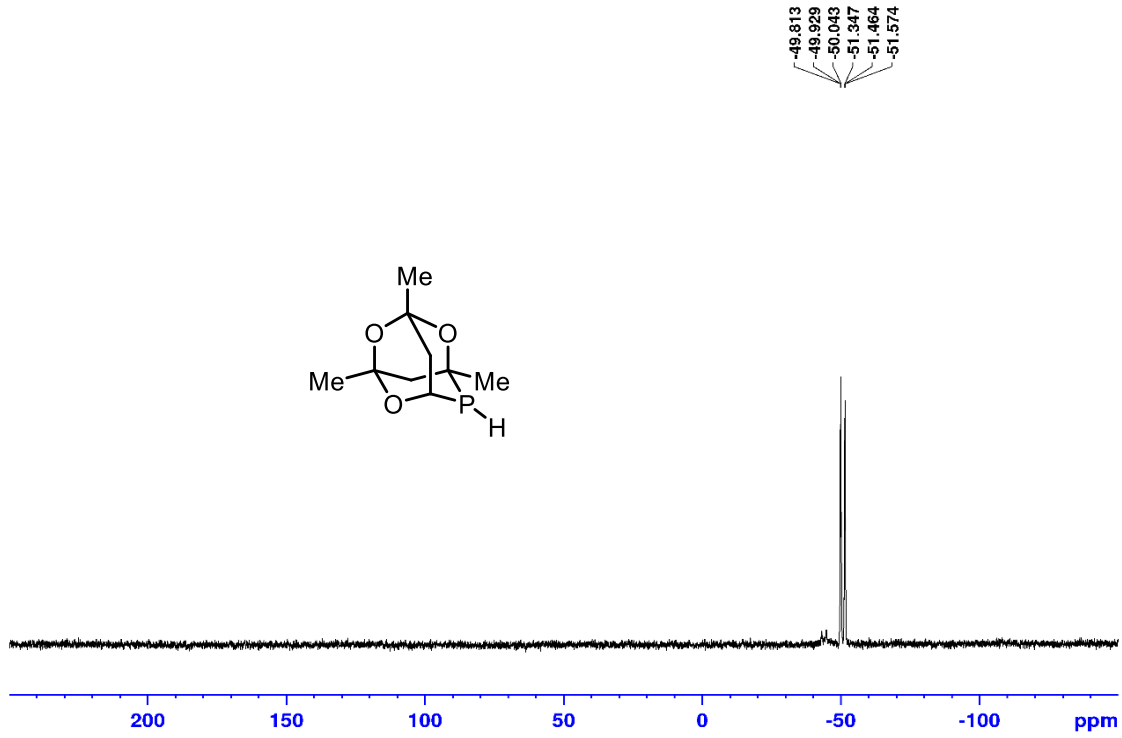


**Figure A148:** $^{31}$P NMR spectrum (202.5 MHz, THF, $C_6D_6$ (lock)) of Cage Phos and *n*-BuLi, after addition of $SF_6$.

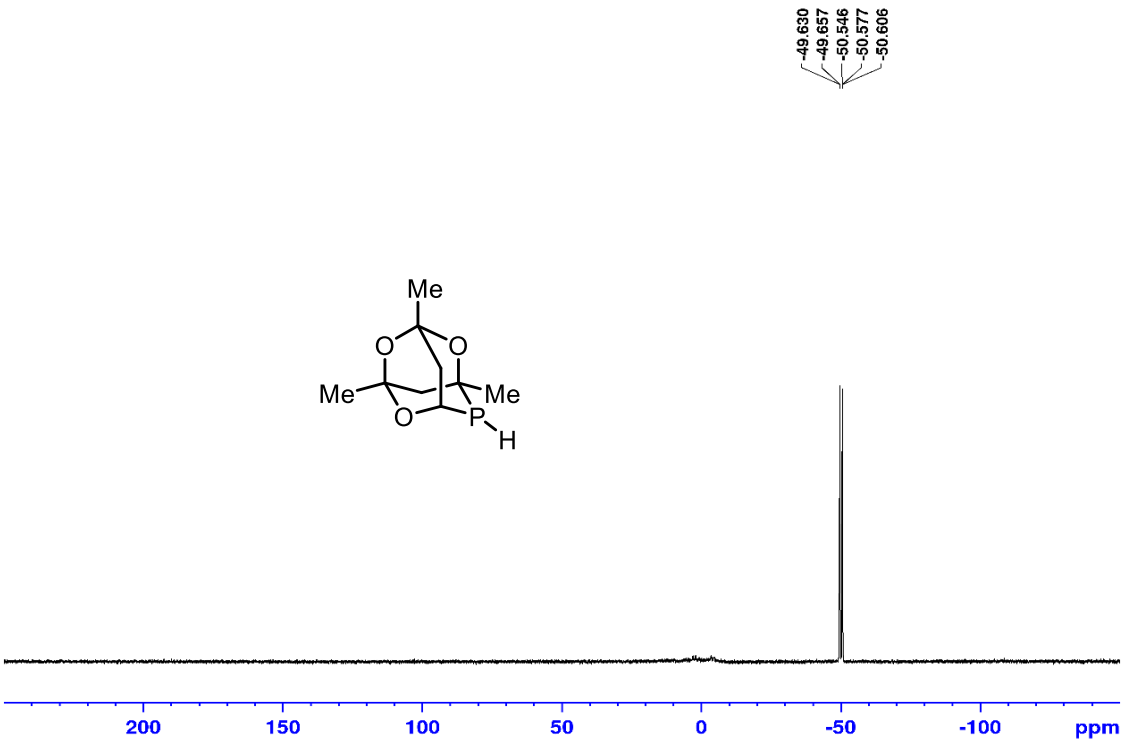


**Figure A149:** $^{31}$P NMR spectrum (202.5 MHz, THF, $C_6D_6$ (lock)) of Cage Phos after addition of *tert*-BuLi.

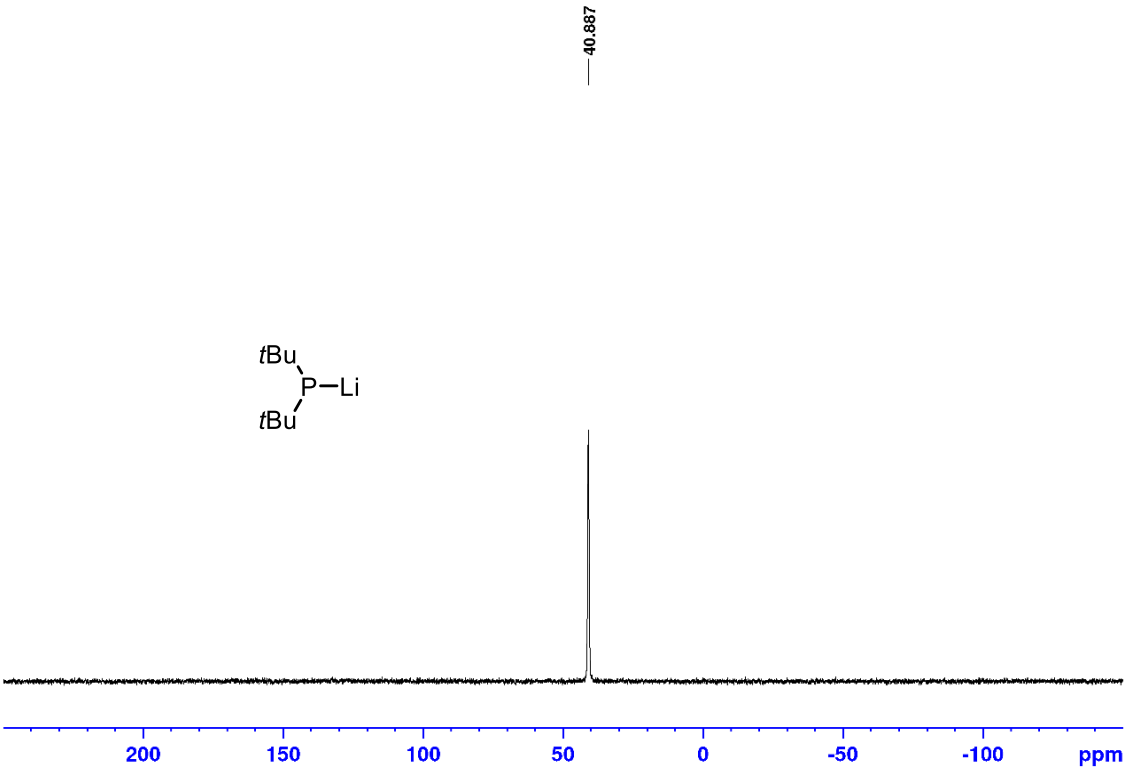


**Figure A150:** $^{31}$P NMR spectrum (202.5 MHz, THF, $C_6D_6$ (lock)) of **6-39** formed from mixing **6-38** and *n*-BuLi in THF.

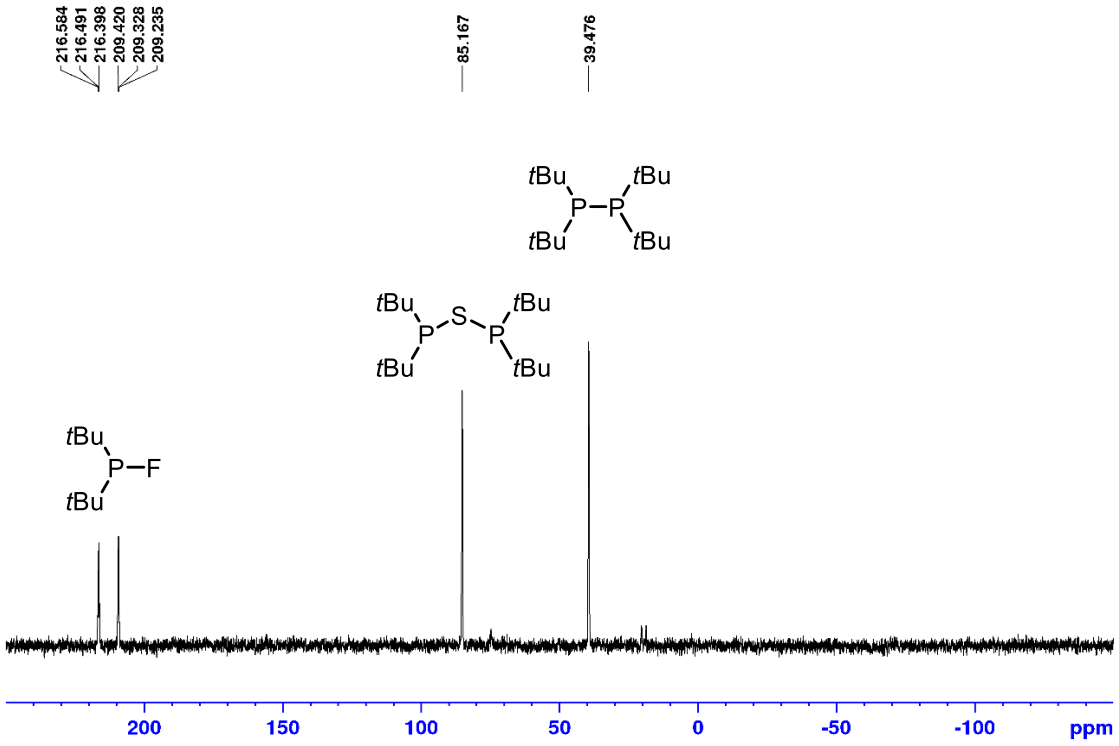


**Figure A151:** $^{31}$P NMR spectrum (202.5 MHz, THF, $C_6D_6$ (lock)) of addition of $SF_6$ to **6-39** in THF.

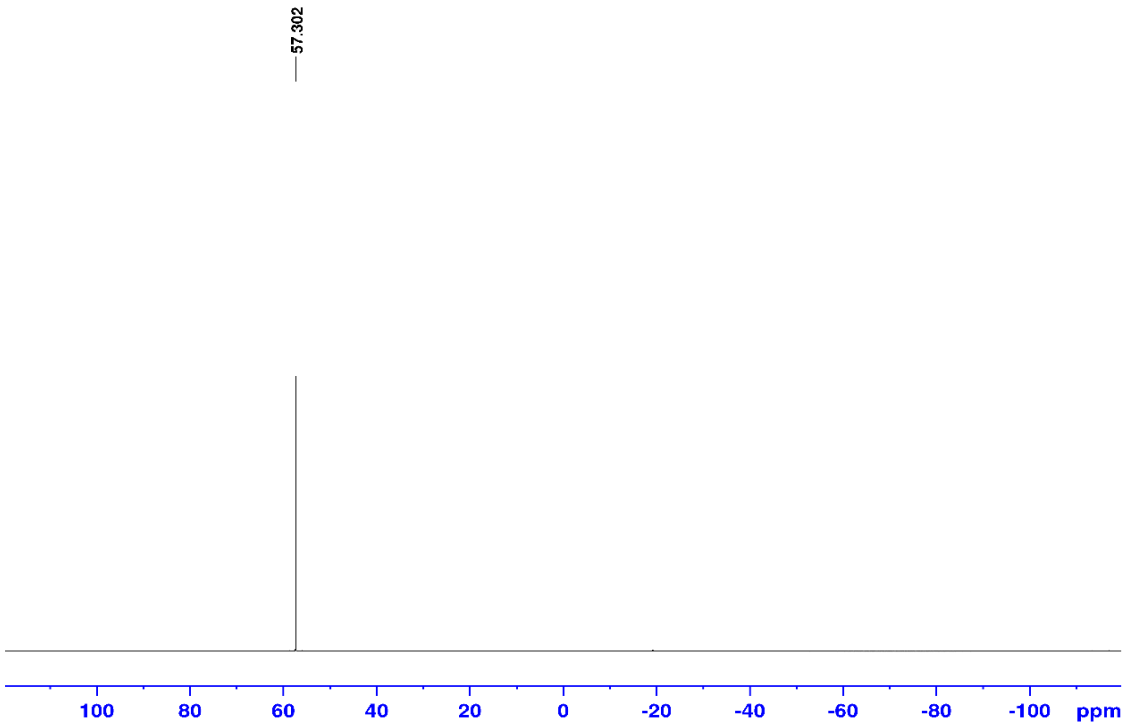


**Figure A152:** $^{19}$F NMR spectrum (0 center point) (470.6 MHz, THF, $C_6D_6$ (lock)) of addition of $SF_6$ to **6-39** in THF.

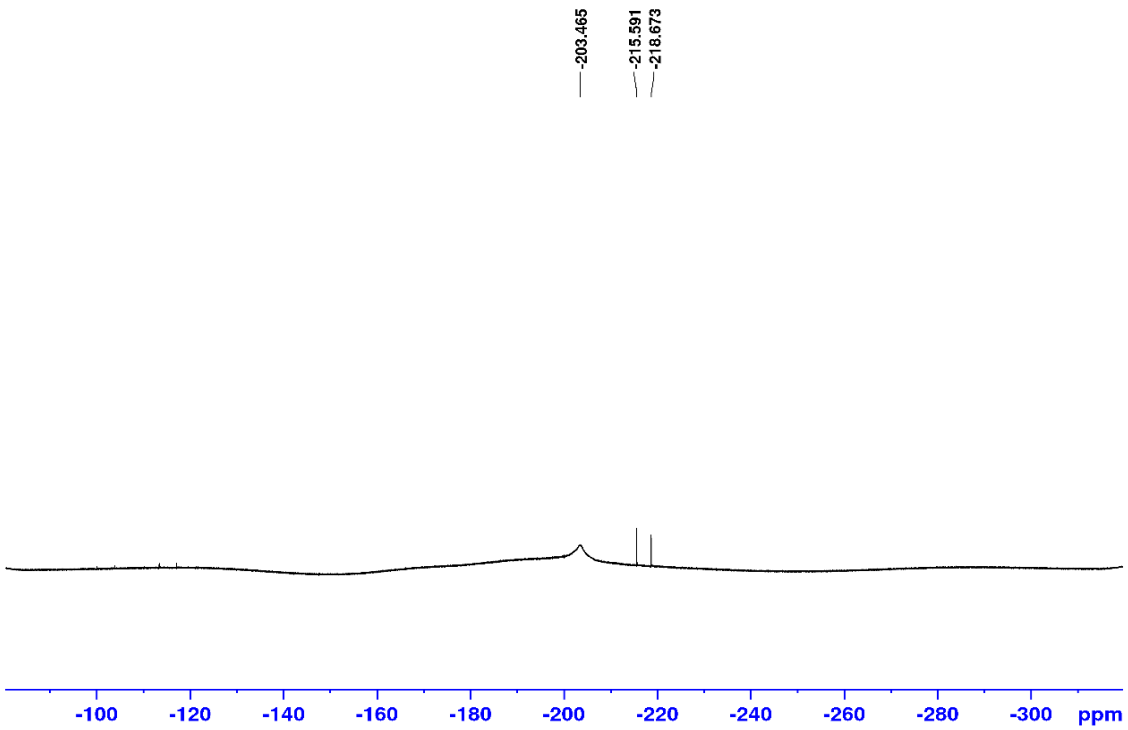


**Figure A153:** $^{19}F$ NMR spectrum (-200 center point) (470.6 MHz, THF, $C_6D_6$ (lock)) of addition of $SF_6$ to **6-39** in THF.

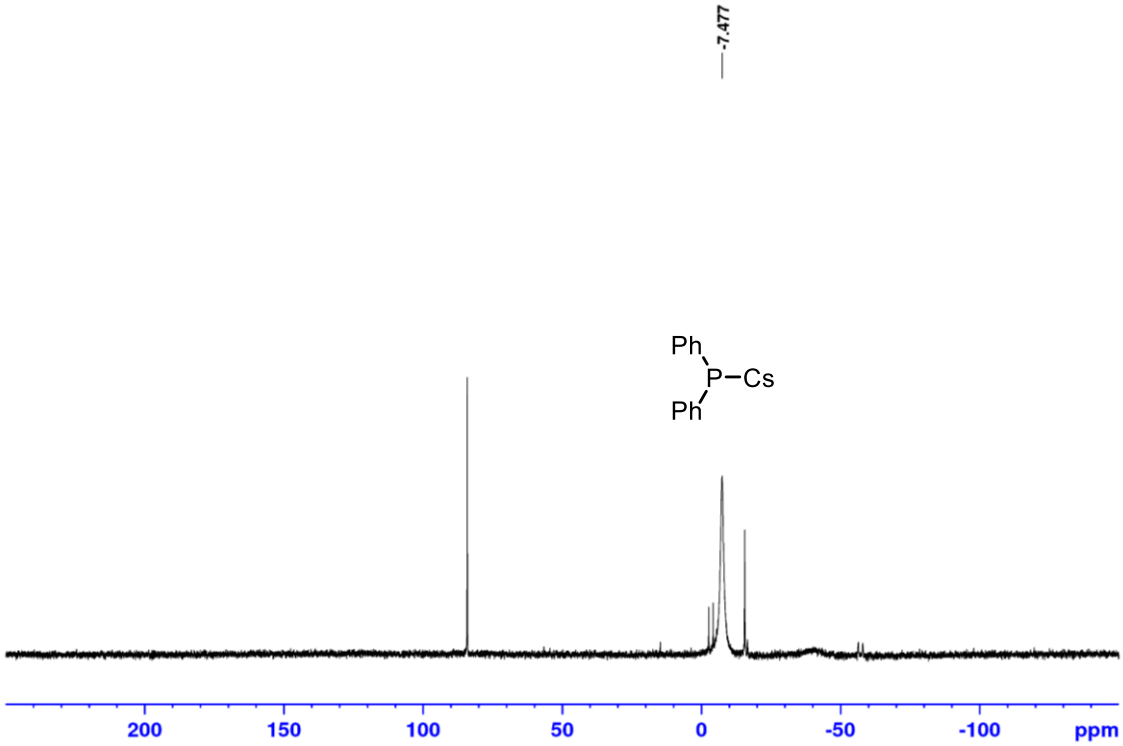


**Figure A154:** $^{31}P$ NMR spectrum (202.5 MHz, THF, $C_6D_6$ (lock)) of **6-49** formed from mixing **6-25** and cesium carbonate in THF.

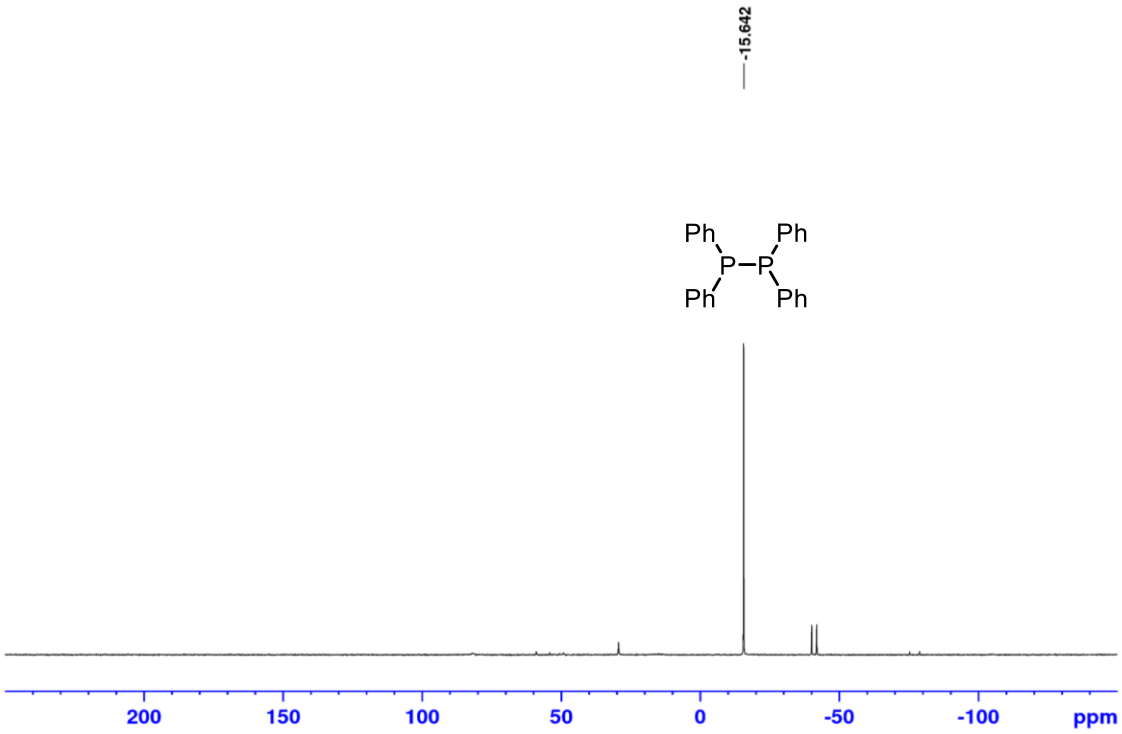


**Figure A155:** $^{31}$P NMR spectrum (202.5 MHz, THF, $C_6D_6$ (lock)) of addition of $SF_6$ to **6-49** in THF.

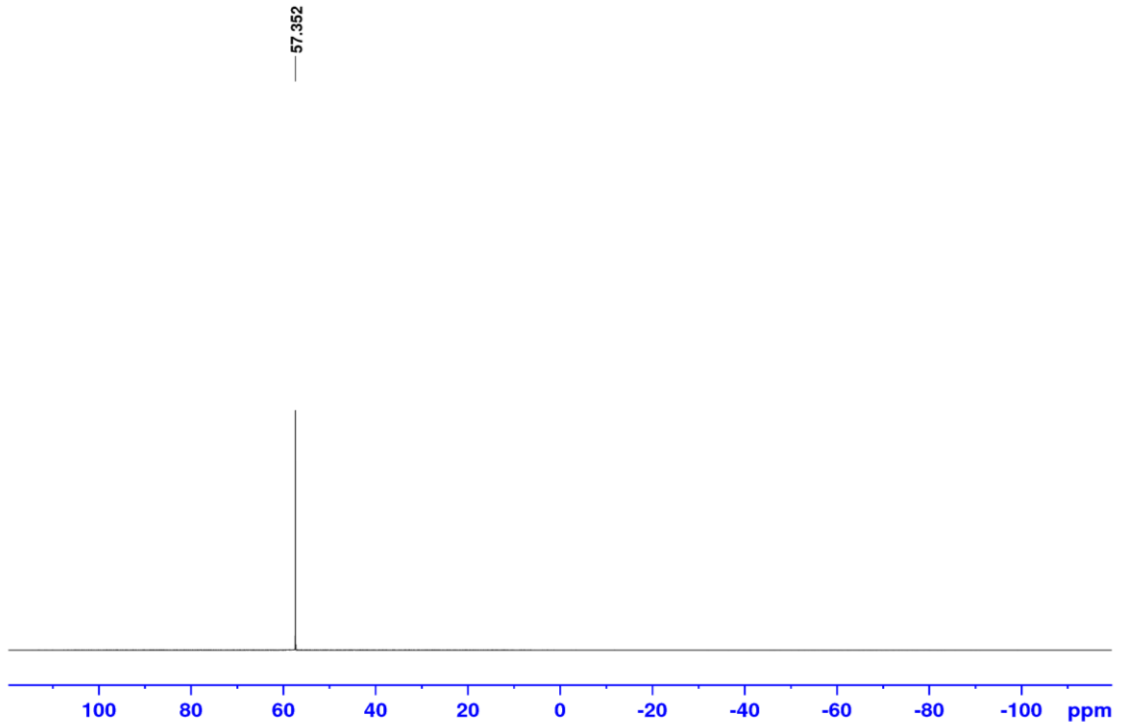


**Figure A156:** $^{19}$F NMR spectrum (0 center point) (470.6 MHz, THF, $C_6D_6$ (lock)) of addition of $SF_6$ to **6-49** in THF.

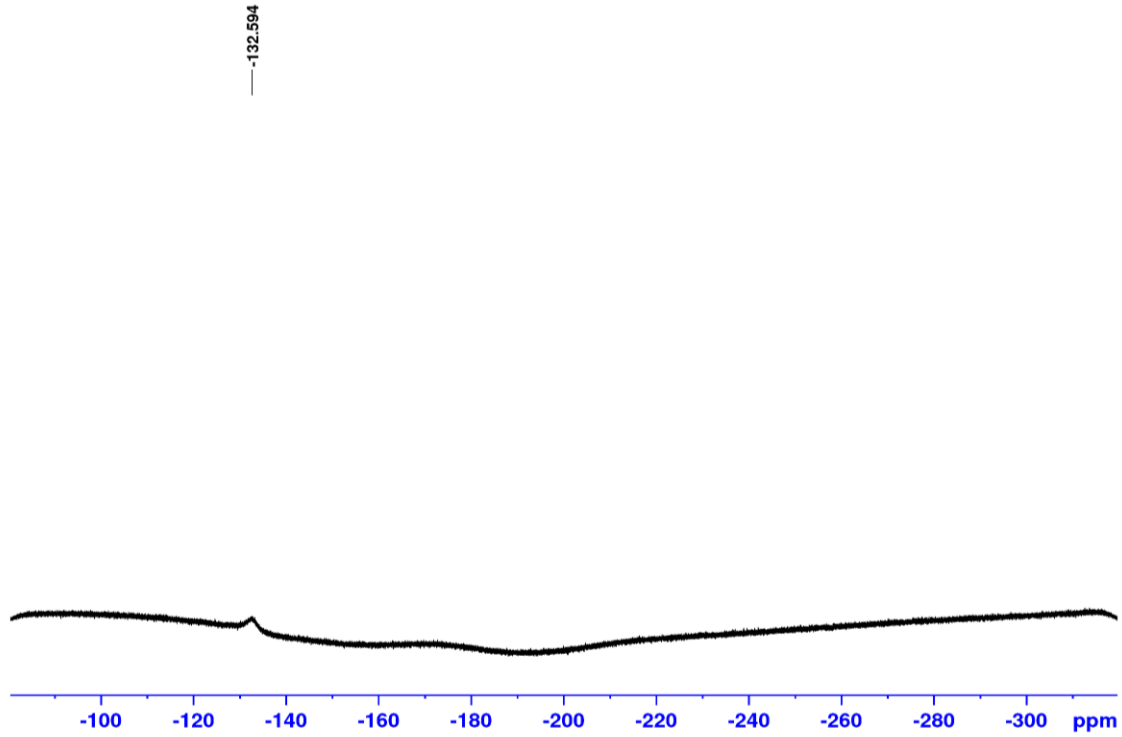


**Figure A157:** $^{19}F$ NMR spectrum (-200 center point) (470 MHz, THF, $C_6D_6$ (lock)) of addition of $SF_6$ to **6-49** in THF.

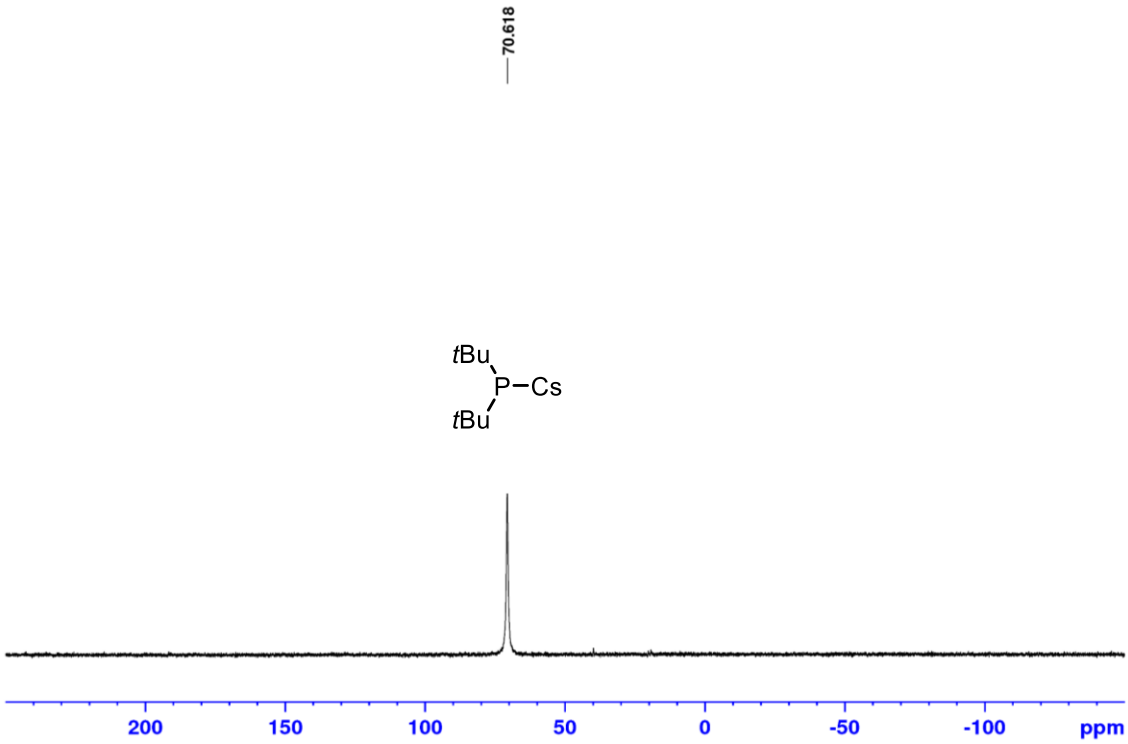


**Figure A158:** $^{31}P$ NMR spectrum (202.5 MHz, THF, $C_6D_6$ (lock)) of **6-50** formed from mixing **6-38** and cesium fluoride in THF.

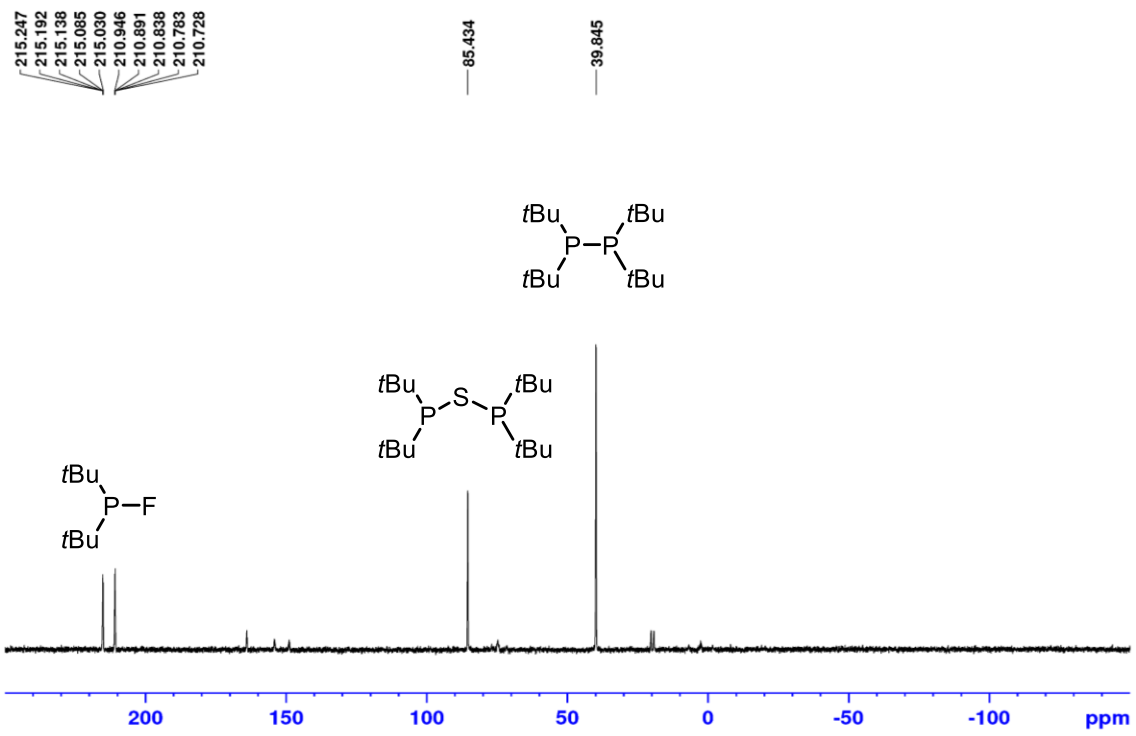


**Figure A159:** $^{31}$P NMR spectrum (202.5 MHz, THF, $C_6D_6$ (lock)) of addition of $SF_6$ to **6-50** in THF.

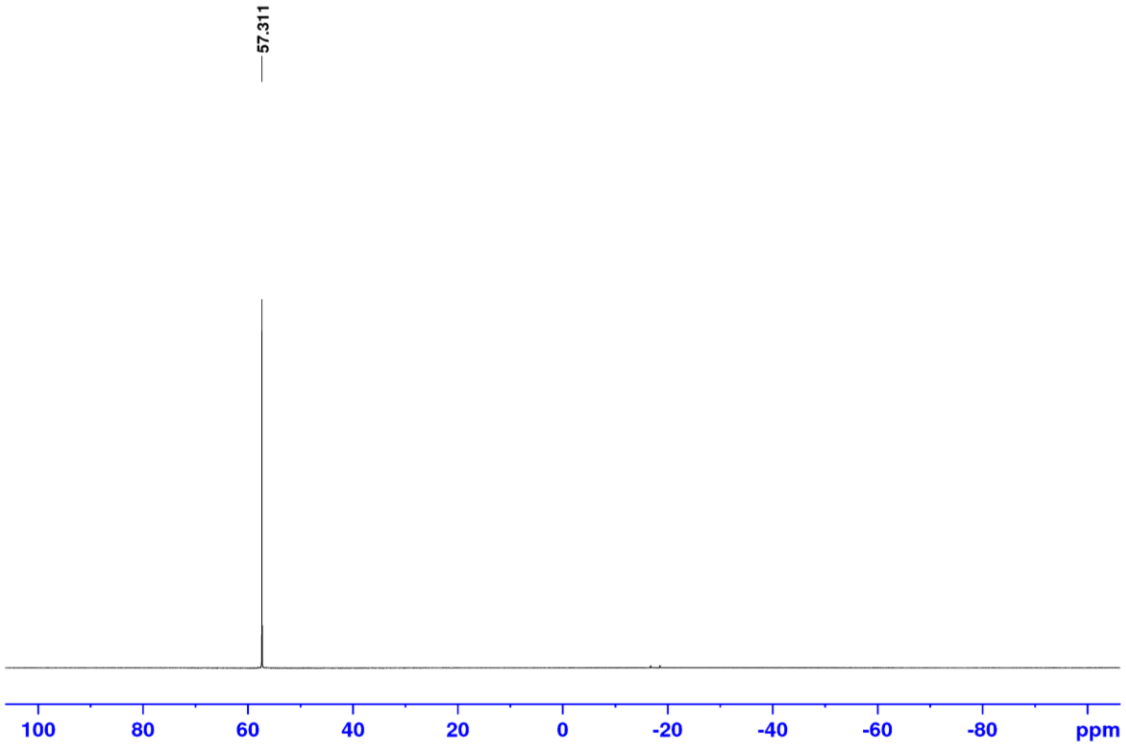


**Figure A160:** $^{19}$F NMR spectrum (0 center point) (470.6 MHz, THF, $C_6D_6$ (lock)) of addition of $SF_6$ to **6-50** in THF.

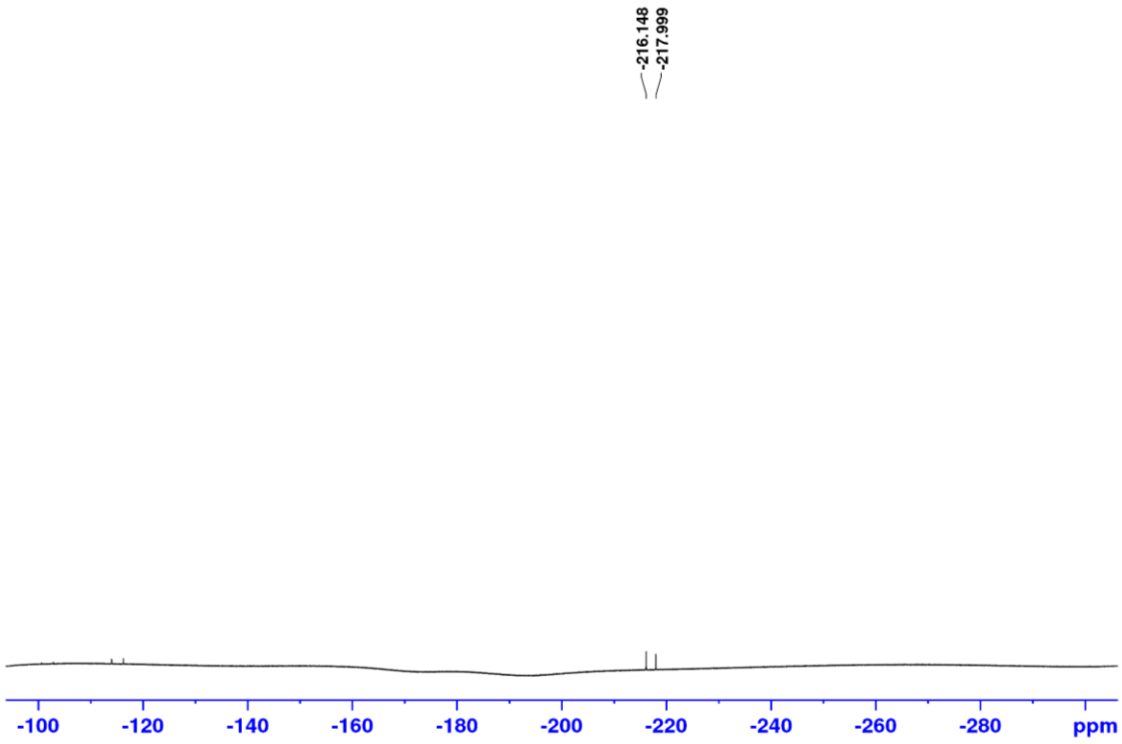


**Figure A161:** $^{19}F$ NMR spectrum (-200 center point) (470.6 MHz, THF, $C_6D_6$ (lock)) of addition of $SF_6$ to **6-50** in THF.

## E3: NMR Spectra for Section 6.3

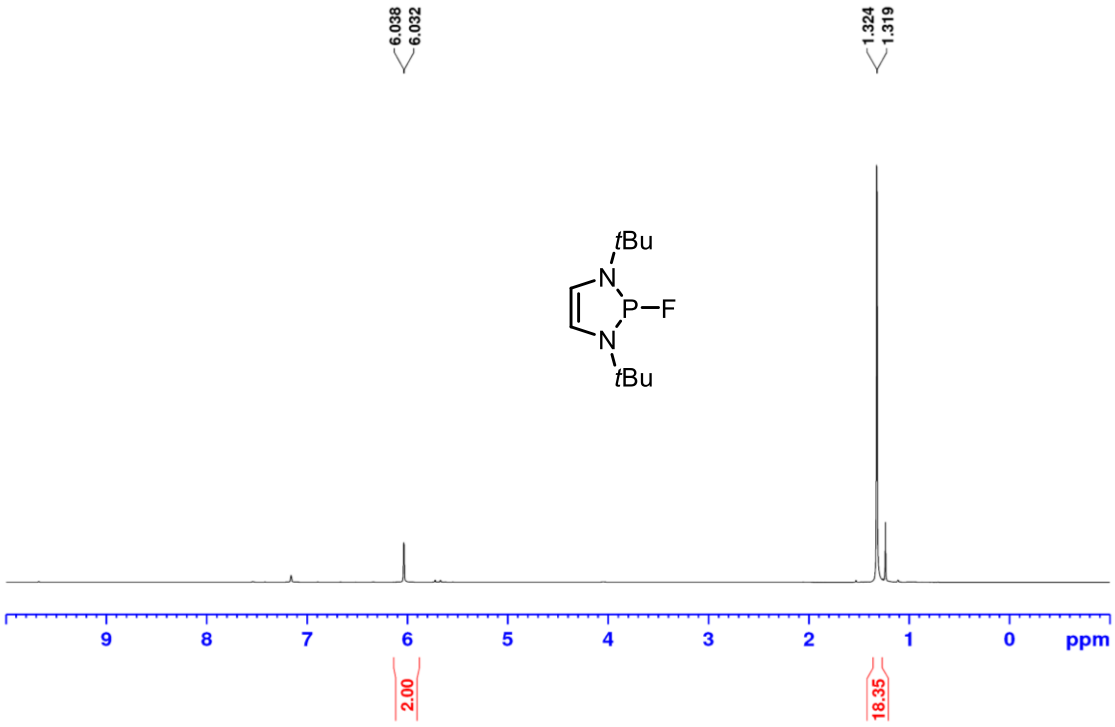


**Figure A162:** $^{1}$H NMR spectrum (300 MHz, $C_6D_6$) of diazaphospholene fluoride **6-22**.

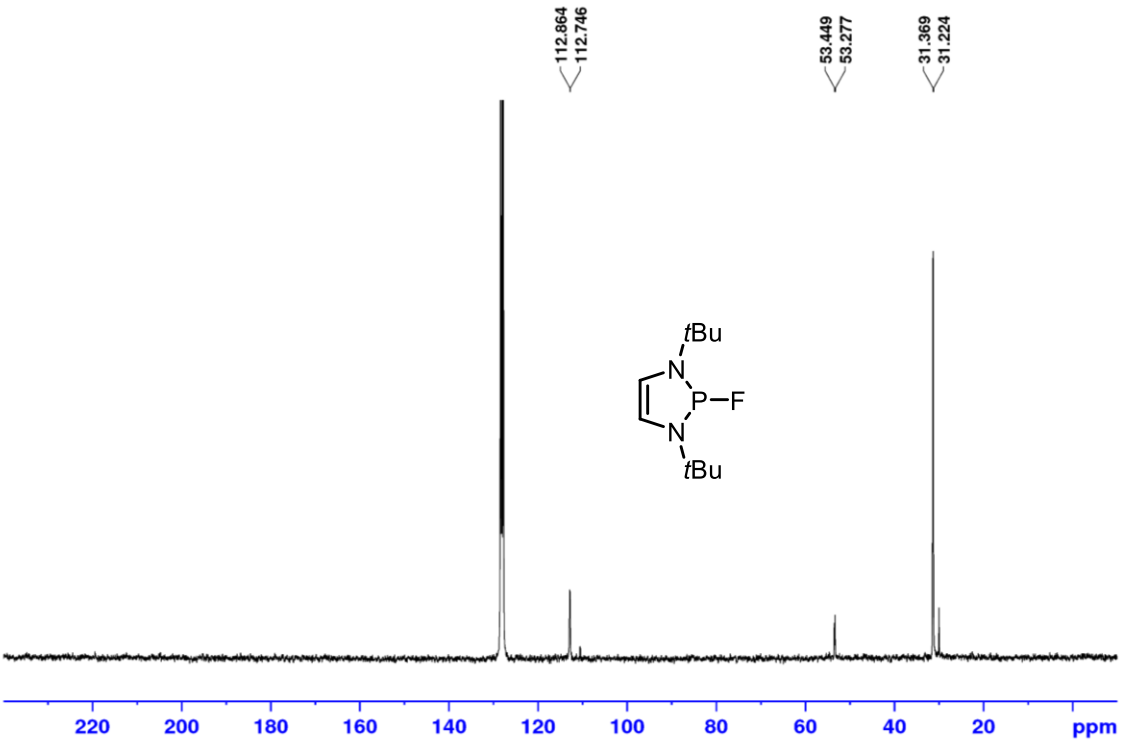


**Figure A163:** $^{13}$C NMR spectrum {$^{1}$H} (75.5 MHz, $C_6D_6$) of diazaphospholene fluoride **6-22**

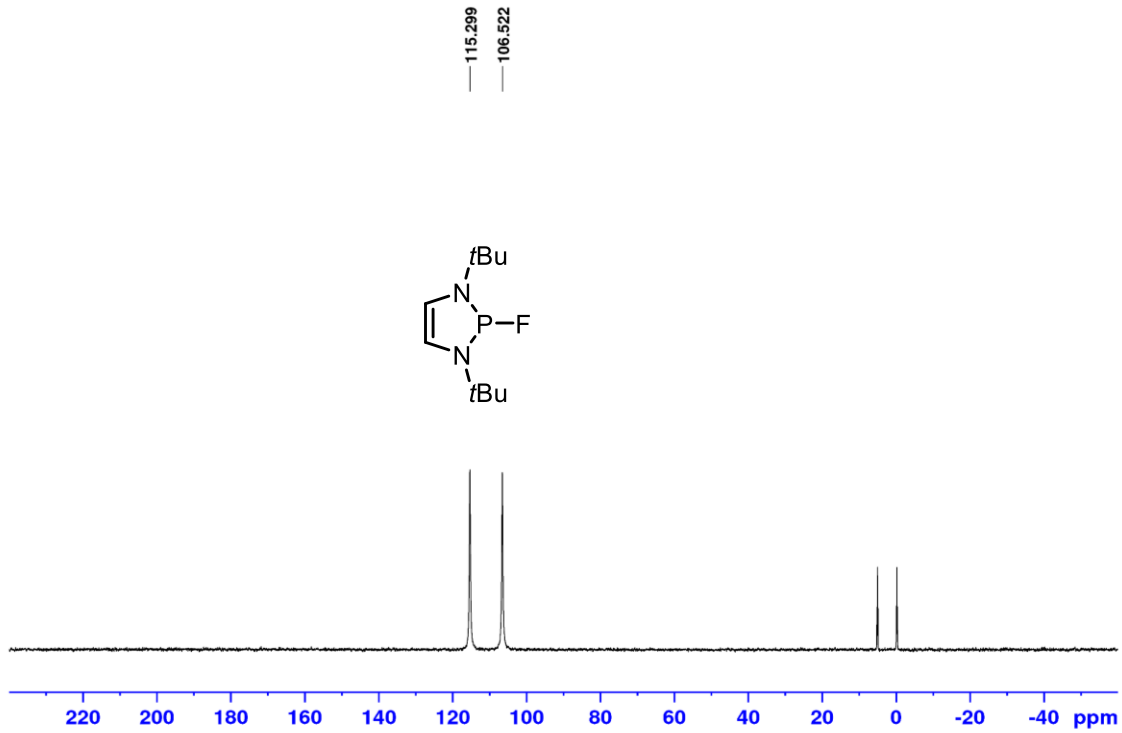


**Figure A164:** $^{31}P$ NMR spectrum (121.5 MHz, $C_6D_6$) of diazaphospholene fluoride **6-22**.

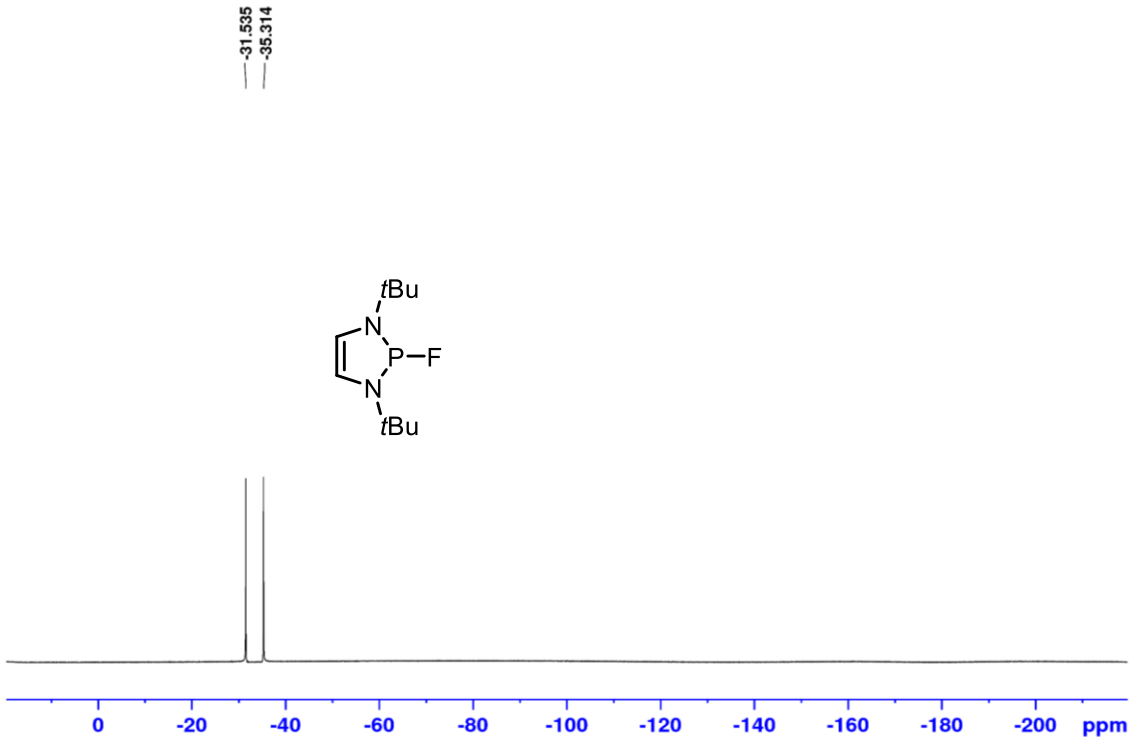


**Figure A165:** $^{19}F$ NMR spectrum (282.4 MHz, $C_6D_6$) of diazaphospholene fluoride **6-22**.

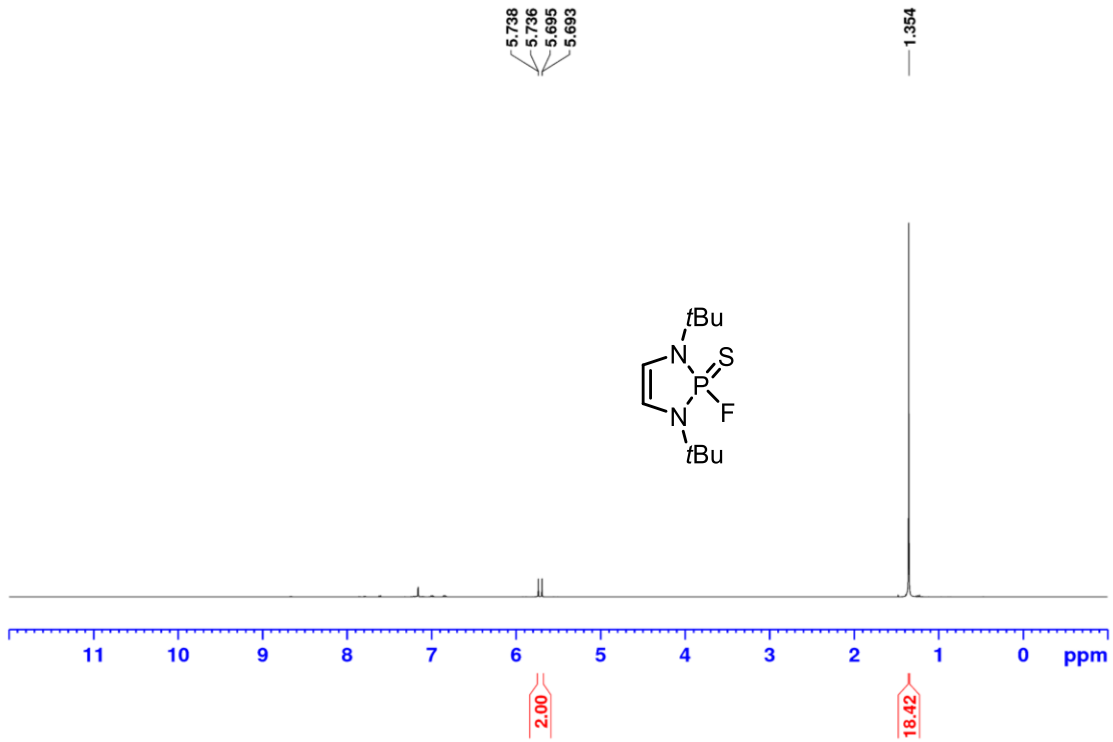


**Figure A166:** $^{1}$H NMR spectrum (500 MHz, $C_6D_6$) of diazaphospholene fluorosulfide **6-53**.

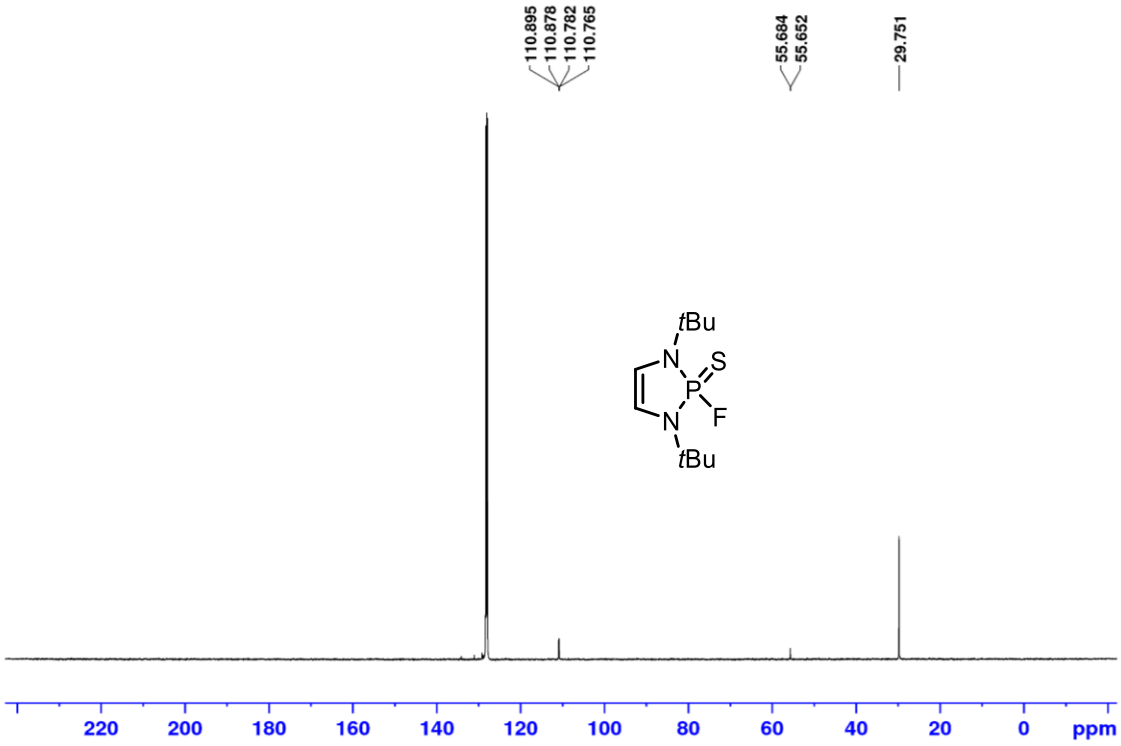


**Figure A167:** $^{13}$C NMR spectrum {$^{1}$H} (125.8 MHz, $C_6D_6$) of diazaphospholene fluorosulfide **6-53**.

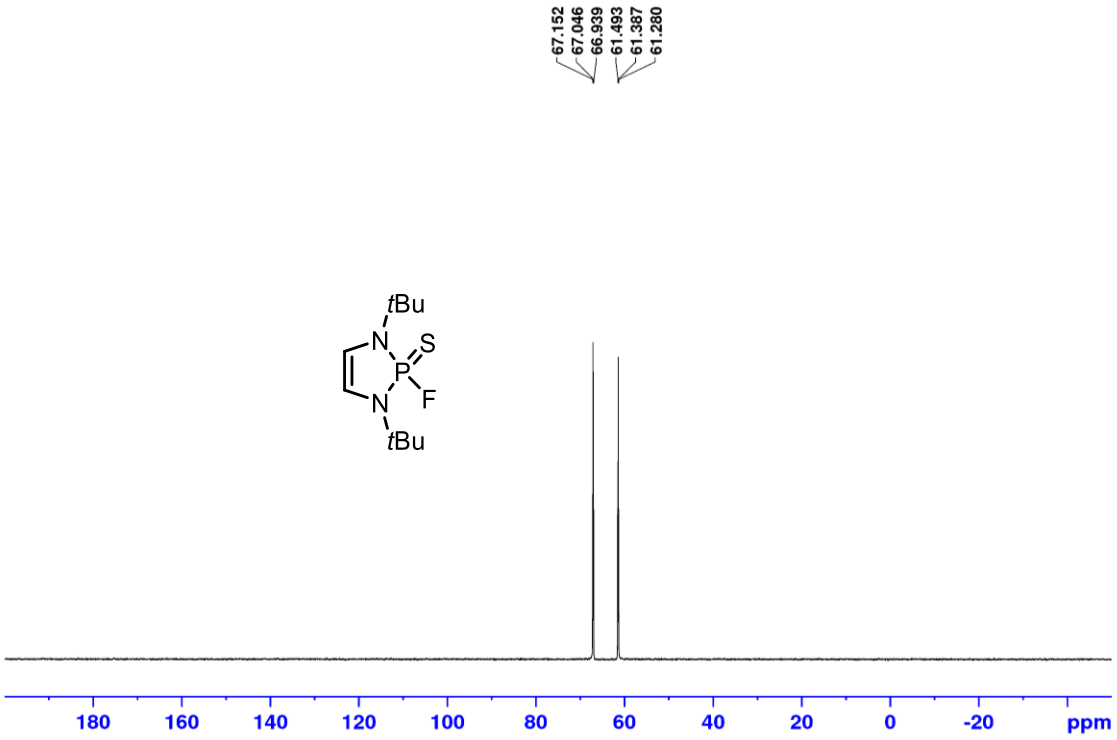


**Figure A168:** $^{31}$P NMR spectrum (202.5 MHz, $C_6D_6$) of diazaphospholene fluorosulfide **6-53**.

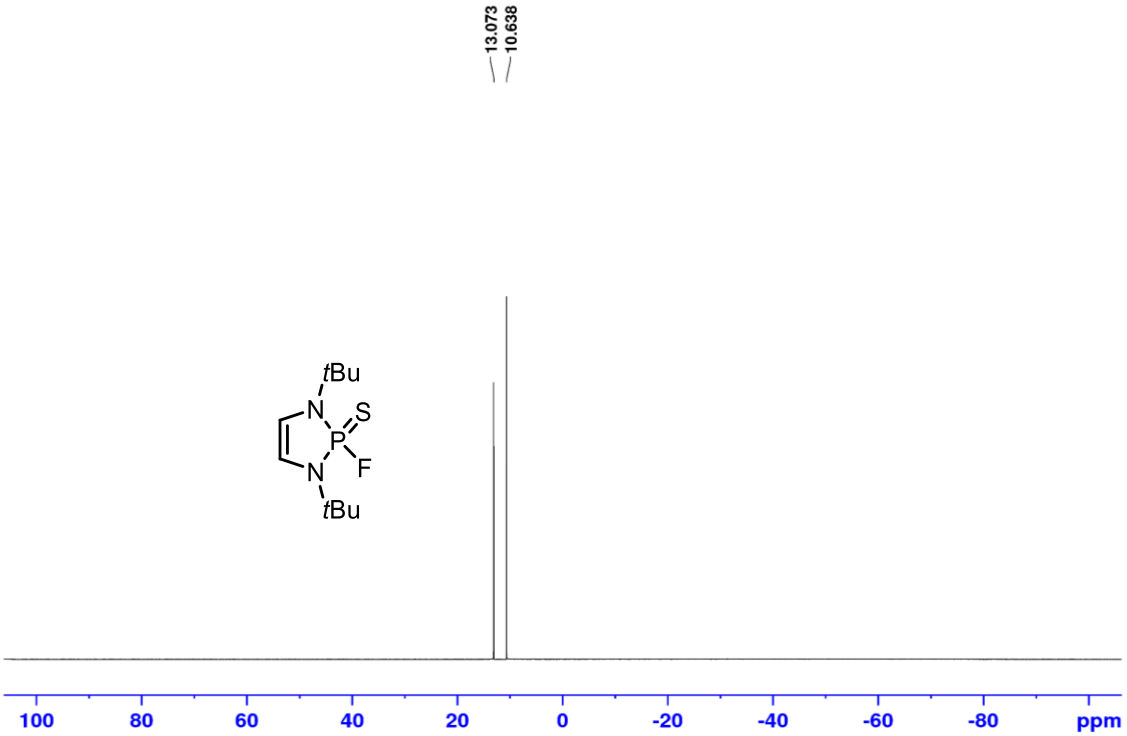


**Figure A169:** $^{19}$F NMR spectrum (470.6 MHz, $C_6D_6$) of diazaphospholene fluorosulfide **6-53**.

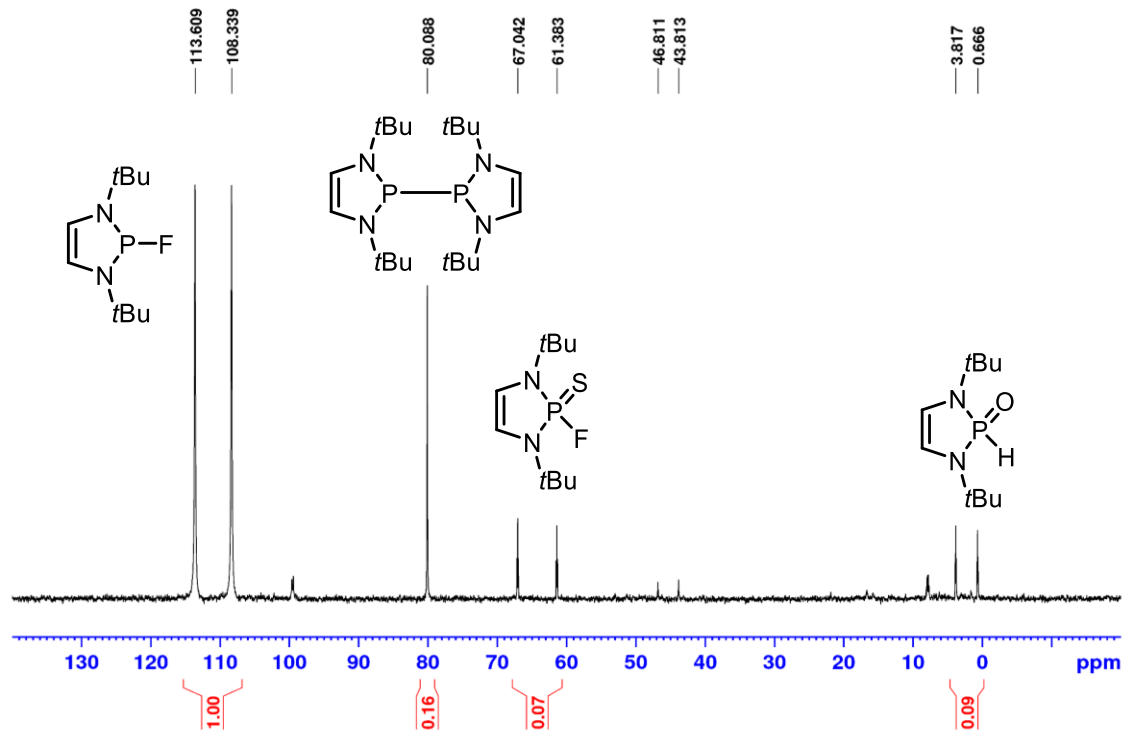


**Figure A170:** $^{31}$P NMR spectrum (202.5 MHz, $C_6D_6$) of diazaphospholene dimer **6-21** reactivity with $SF_6$. 30 min, benzene-$d_6$, no light.

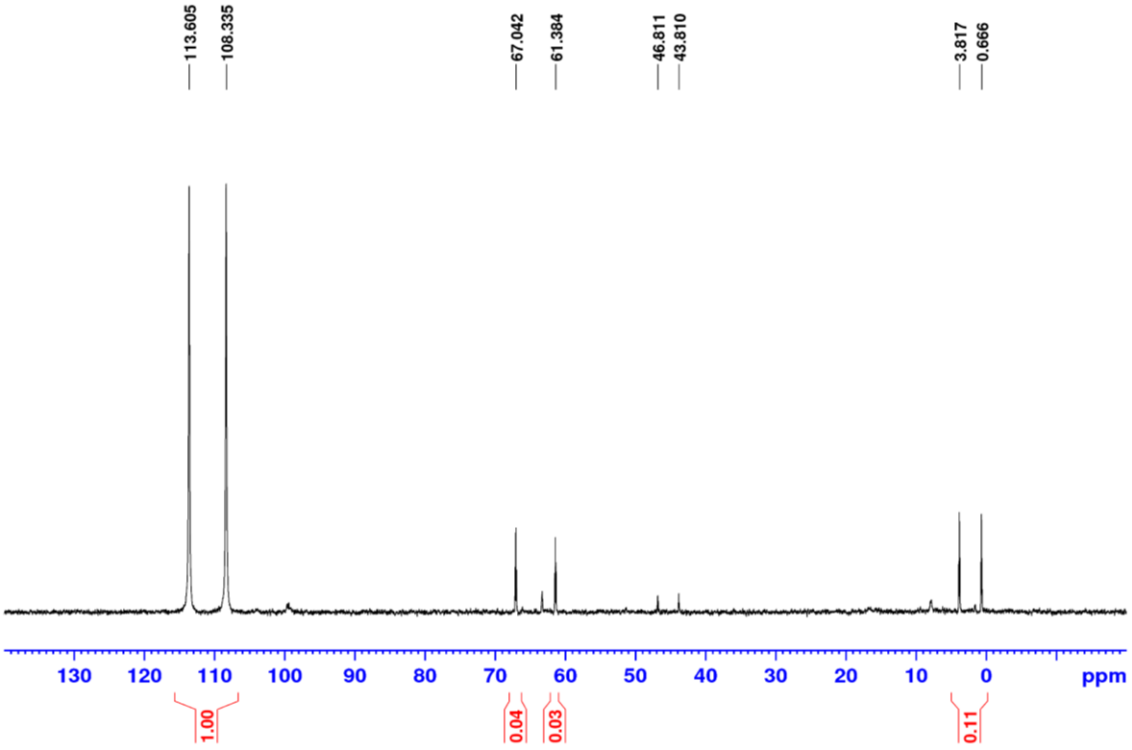


**Figure A171:** $^{31}$P NMR spectrum (202.5 MHz, $C_6D_6$) of diazaphospholene dimer **6-21** reactivity with $SF_6$. 30 min, benzene-$d_6$, blue LED *hv*.

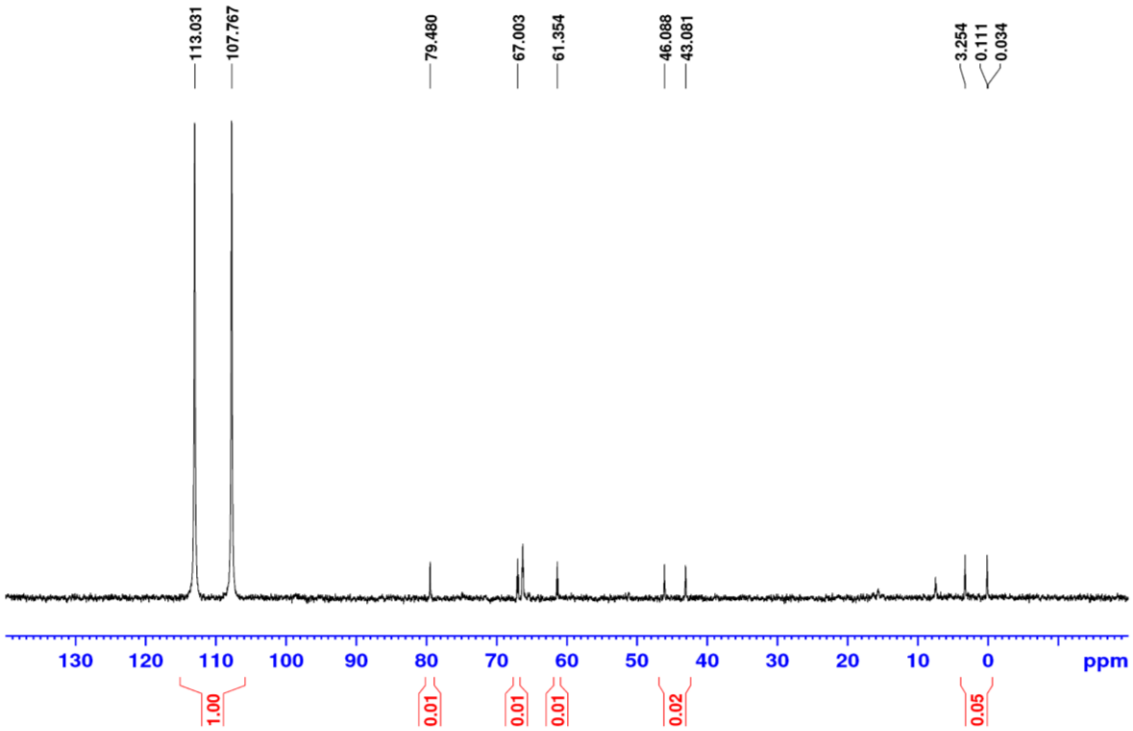


**Figure A172:** $^{31}$P NMR spectrum (202.5 MHz, THF/$C_6D_6$) of diazaphospholene dimer **6-21** reactivity with $SF_6$. 30 min, THF, no light.

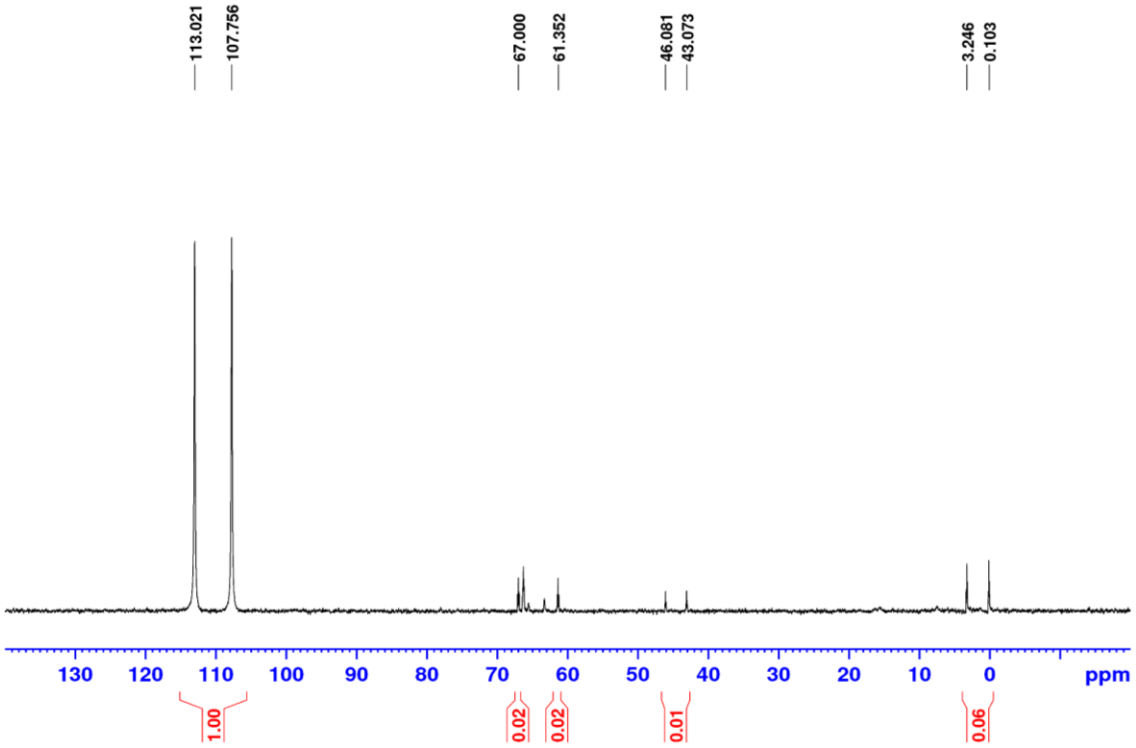


**Figure A173:** $^{31}$P NMR spectrum (202.5 MHz, THF/$C_6D_6$) of diazaphospholene dimer **6-21** reactivity with $SF_6$. 30 min, THF, blue LED *hv*.

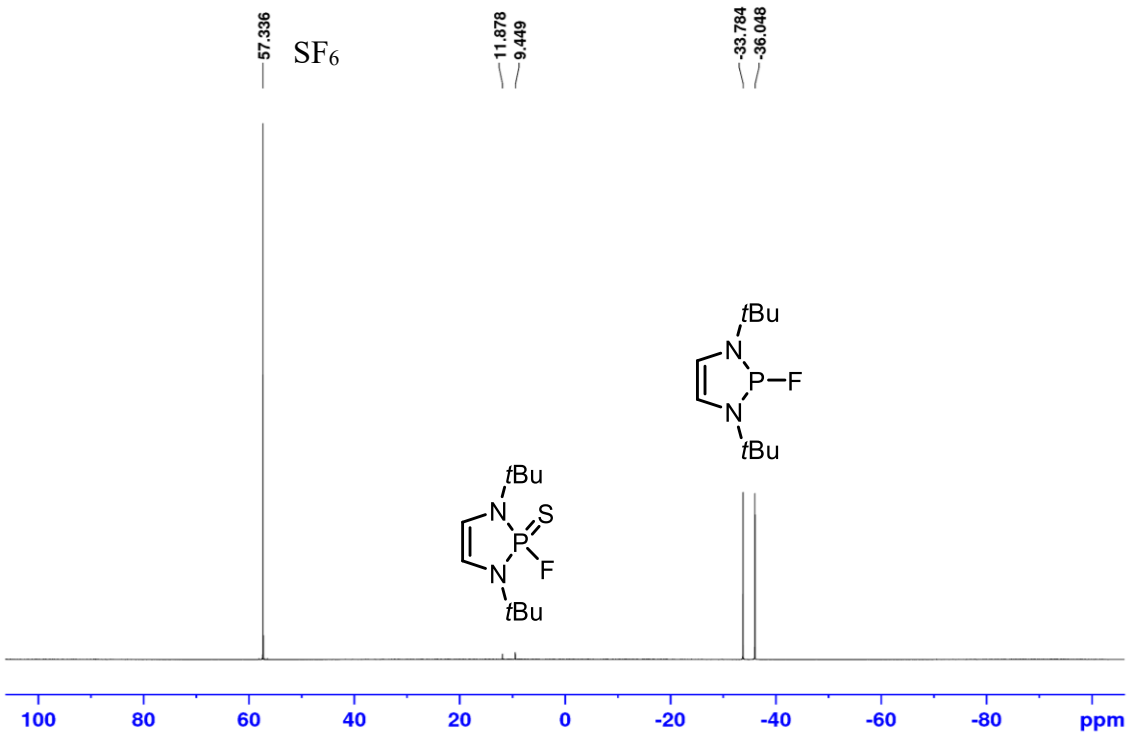


**Figure A174:** $^{19}F$ NMR spectrum (0 center point) (470.6 MHz, THF/$C_6D_6$) of diazaphospholene dimer **6-21** reactivity with $SF_6$. 30 min, THF, blue LED *hv*.

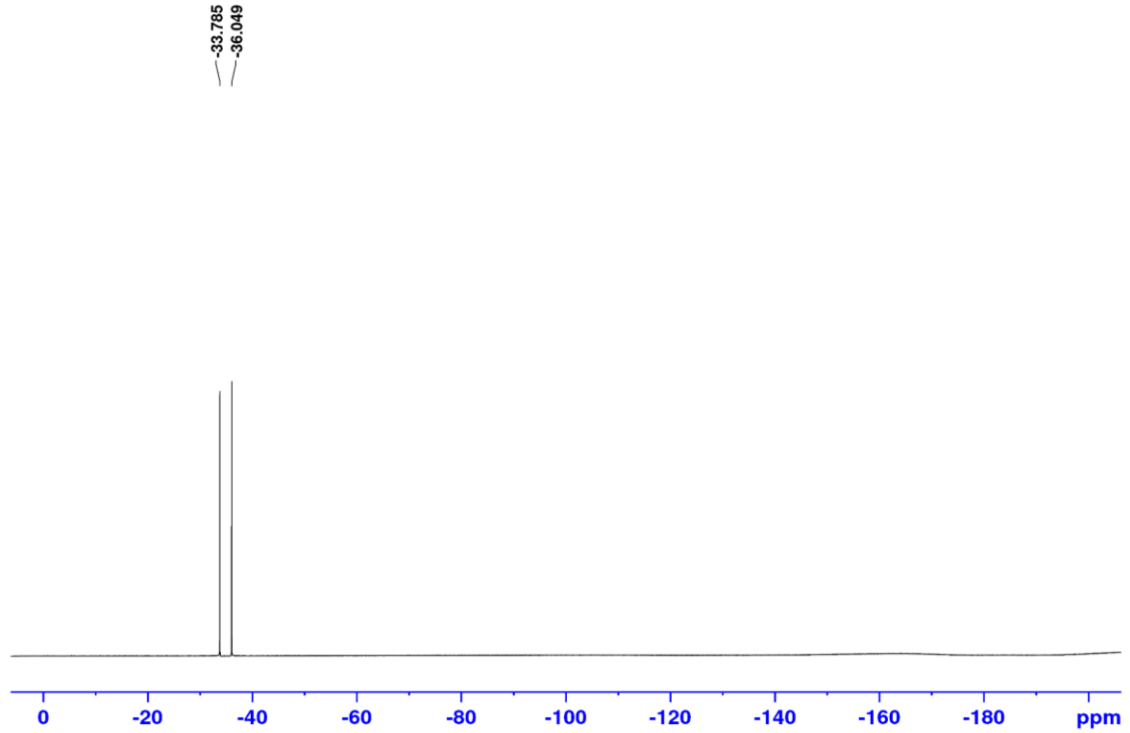


**Figure A175:** $^{19}F$ NMR spectrum (-200 center point) (470.6 MHz, THF/$C_6D_6$) of diazaphospholene dimer **6-21** reactivity with $SF_6$. 30 min, THF, blue LED *hv*.

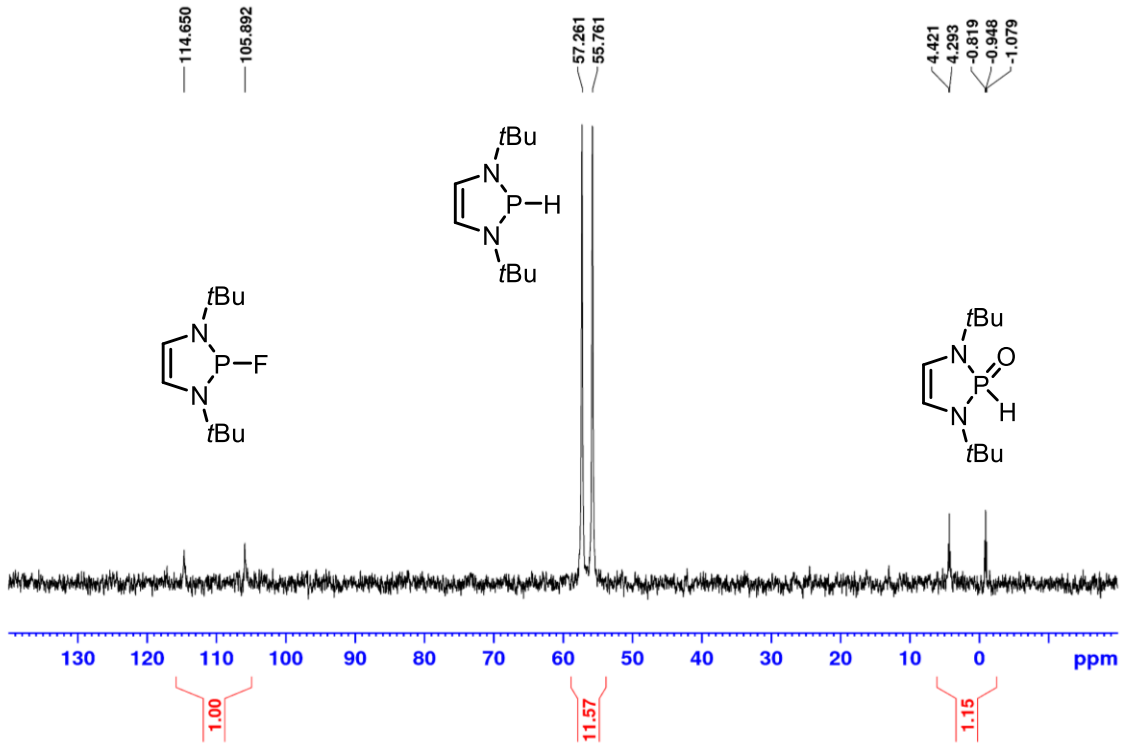


**Figure A176:** $^{31}$P NMR spectrum (121.5 MHz, THF/$C_6D_6$) of diazaphospholene hydride **6-19** reactivity with $SF_6$. 30 min, THF, blue LED *hv*. **Entry 1, Table 6.14**.

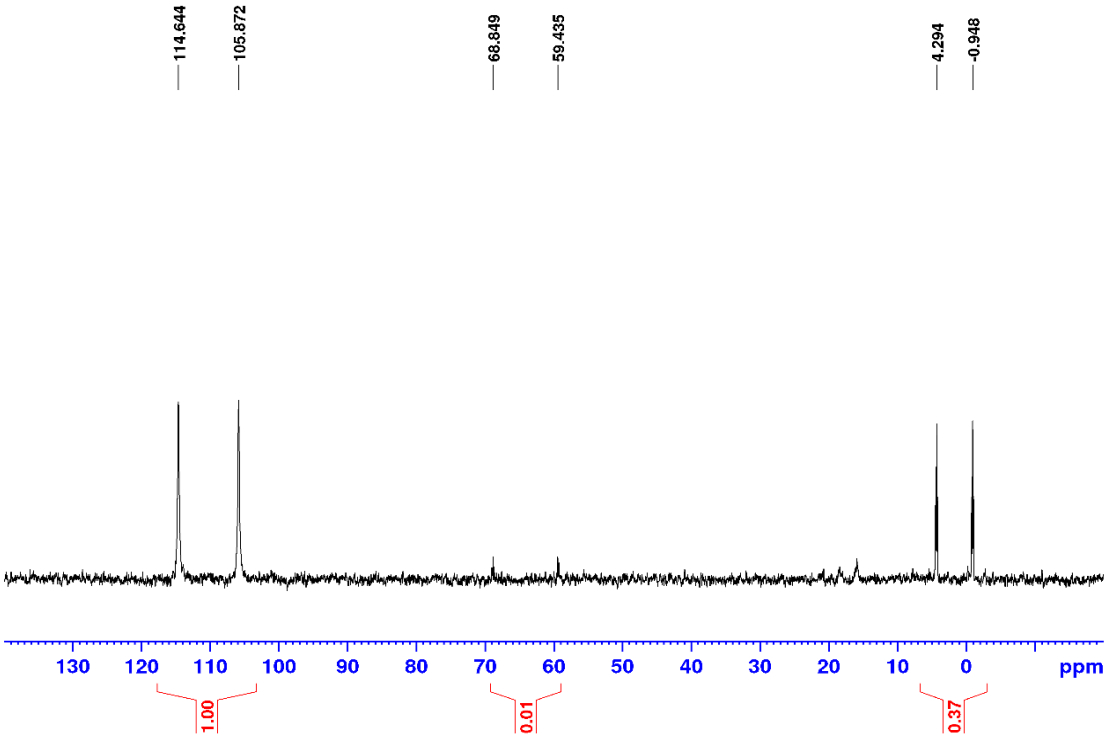


**Figure A177:** $^{31}$P NMR spectrum (121.5 MHz, THF/$C_6D_6$) of diazaphospholene hydride **6-19** reactivity with $SF_6$. 6 h, THF, blue LED *hv*. **Entry 10, Table 6.14**.

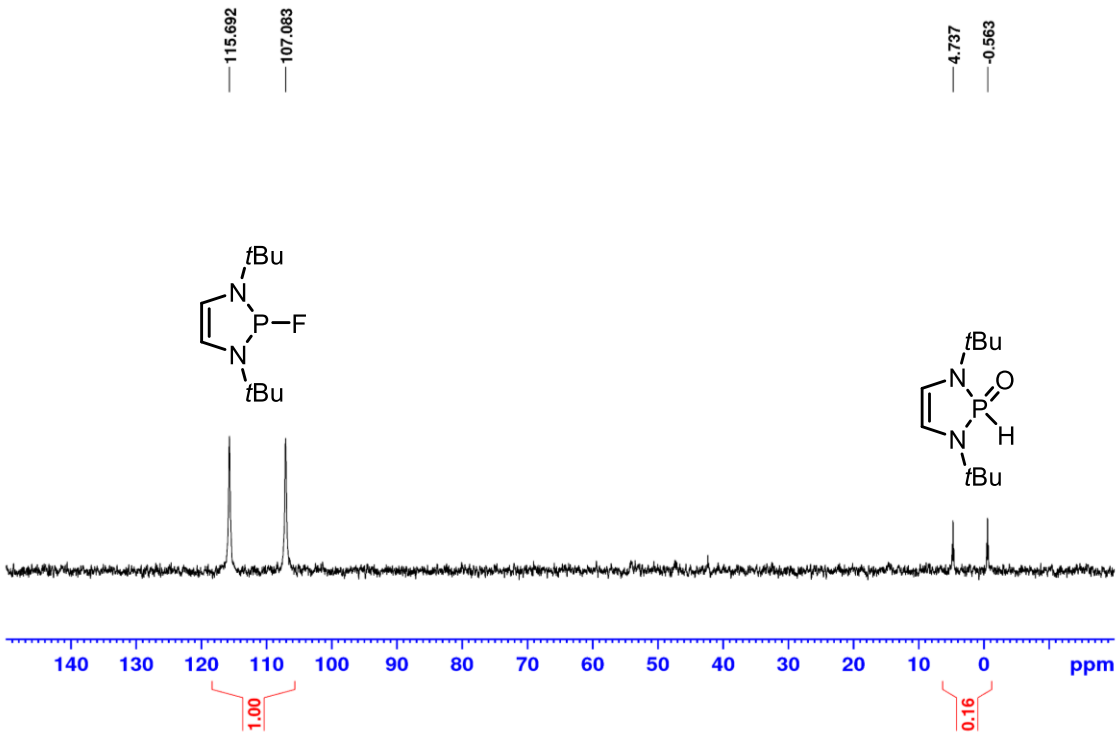


**Figure A178:** $^{31}$P NMR spectrum (121.5 MHz, THF/$C_6D_6$) of diazaphospholene hydride **6-19** reactivity with $SF_6$. 30 min, $CH_3CN$, no light. **Entry 13, Table 6.14**.

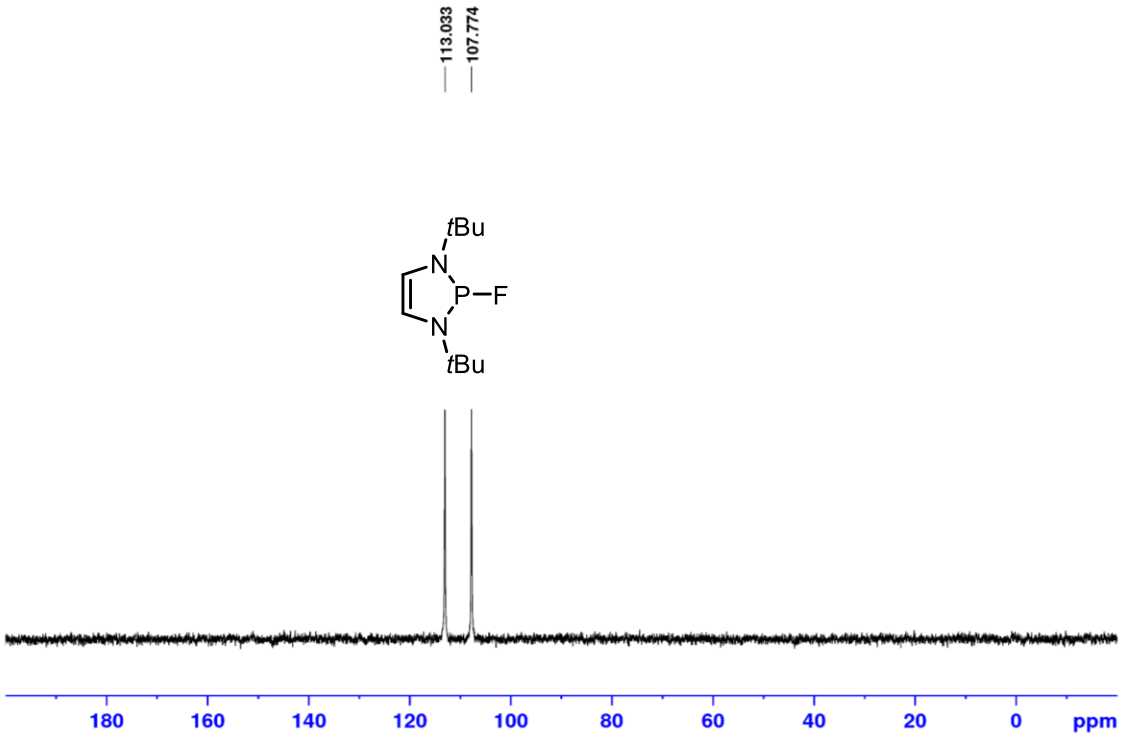


**Figure A179:** $^{31}$P NMR spectrum (121.5 MHz, THF/$C_6D_6$) of diazaphospholene fluoride **6-22** generation *in situ* from diazaphospholene bromide **6-51**.

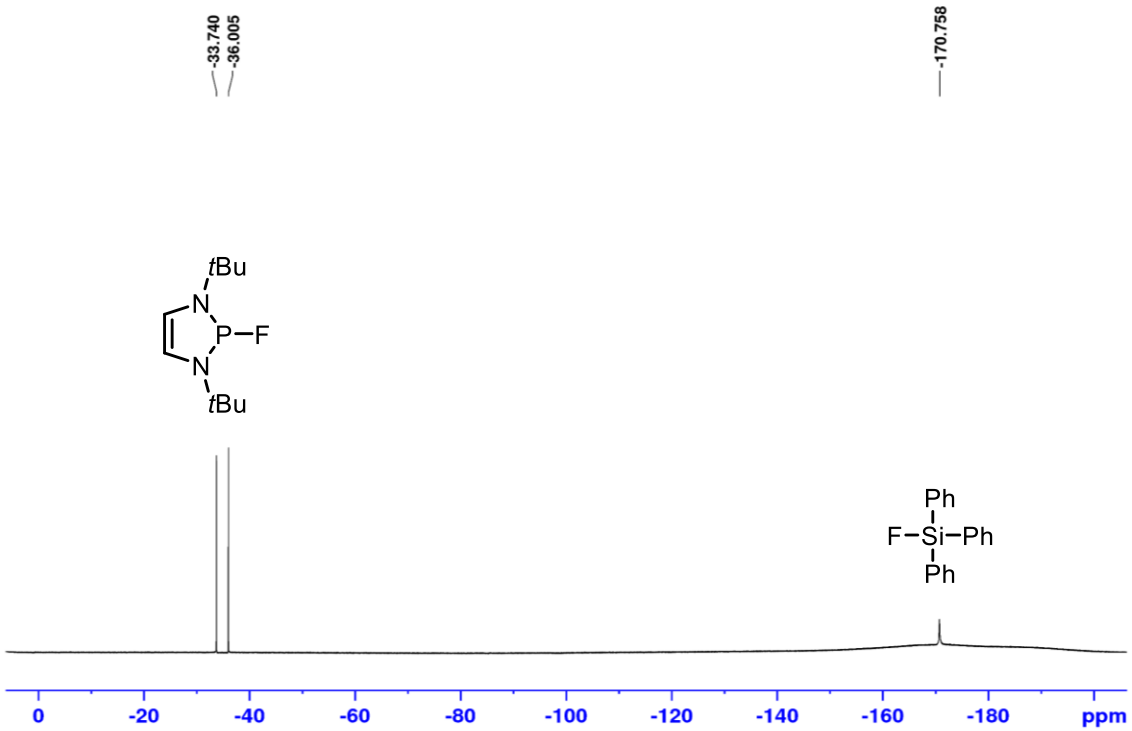


**Figure A180:** $^{19}F$ NMR spectrum (-100 center point) (282.4 MHz, THF/$C_6D_6$) of diazaphospholene fluoride **6-22** generation *in situ* from diazaphospholene bromide **6-51**.

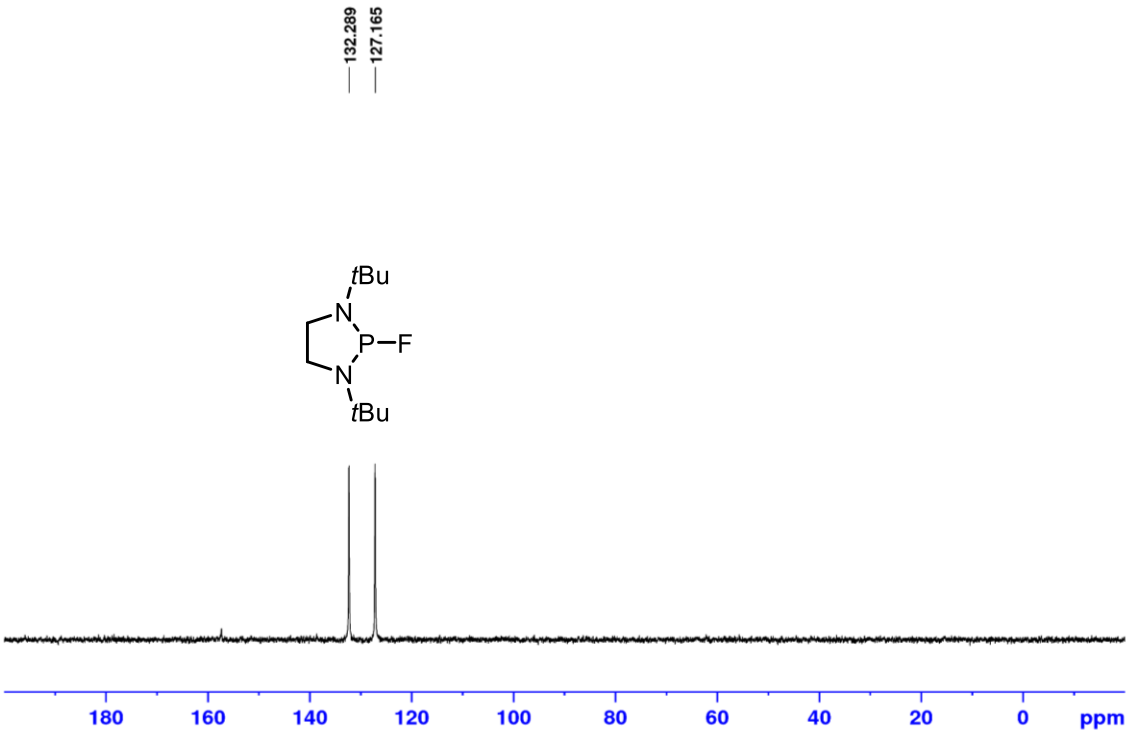


**Figure A181:** $^{31}P$ NMR spectrum (121.5 MHz, THF/$C_6D_6$) of saturated diazaphospholene fluoride generation *in situ* from saturated diazaphospholene chloride **6-63**.

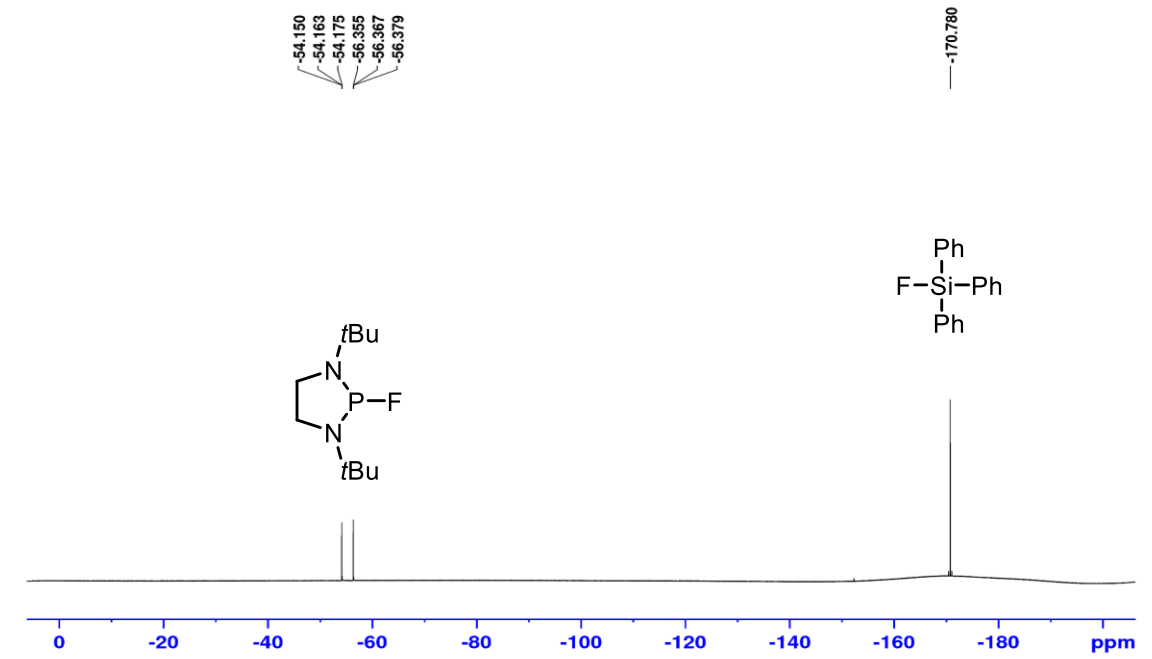


**Figure A182:** $^{19}F$ NMR spectrum (-100 center point) (282.4 MHz, THF/$C_6D_6$) of saturated diazaphospholene fluoride generation *in situ* from saturated diazaphospholene chloride **6-63.**

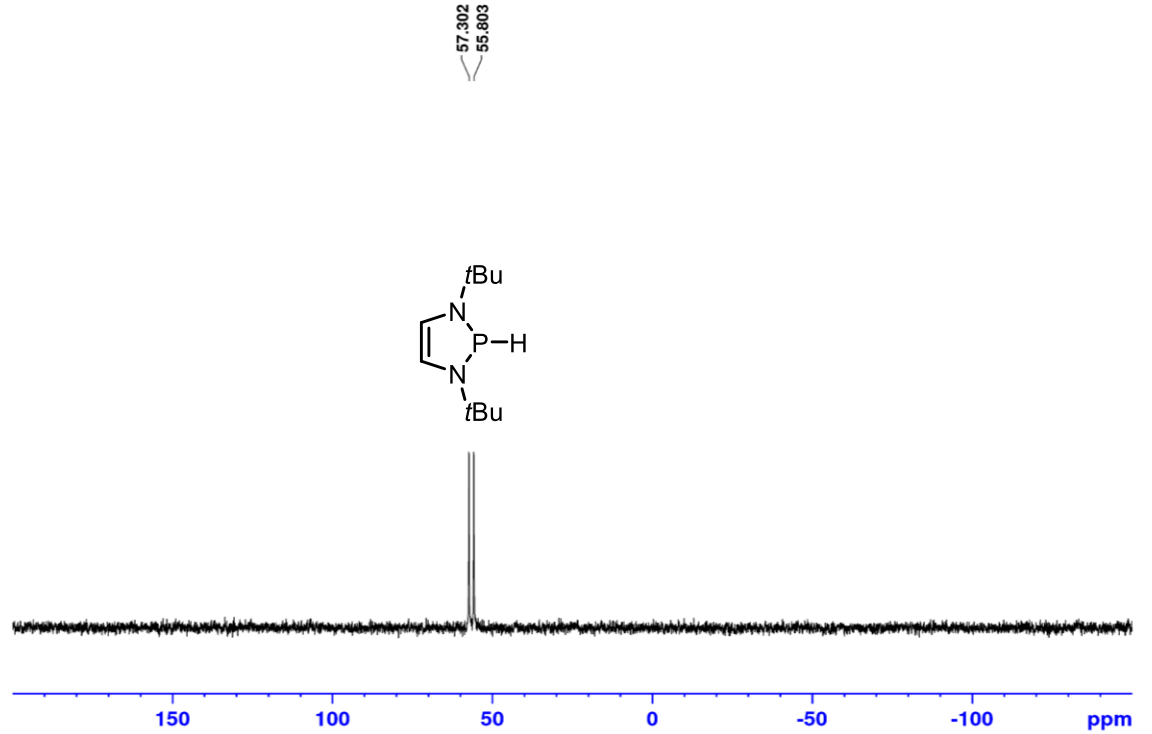


**Figure A183:** $^{31}P$ NMR spectrum (121.5 MHz, THF/$C_6D_6$) of diazaphospholene hydride **6-19** formation from fluoride **6-22** and $PhSiH_3$ with NMR acquisition after 15 min.

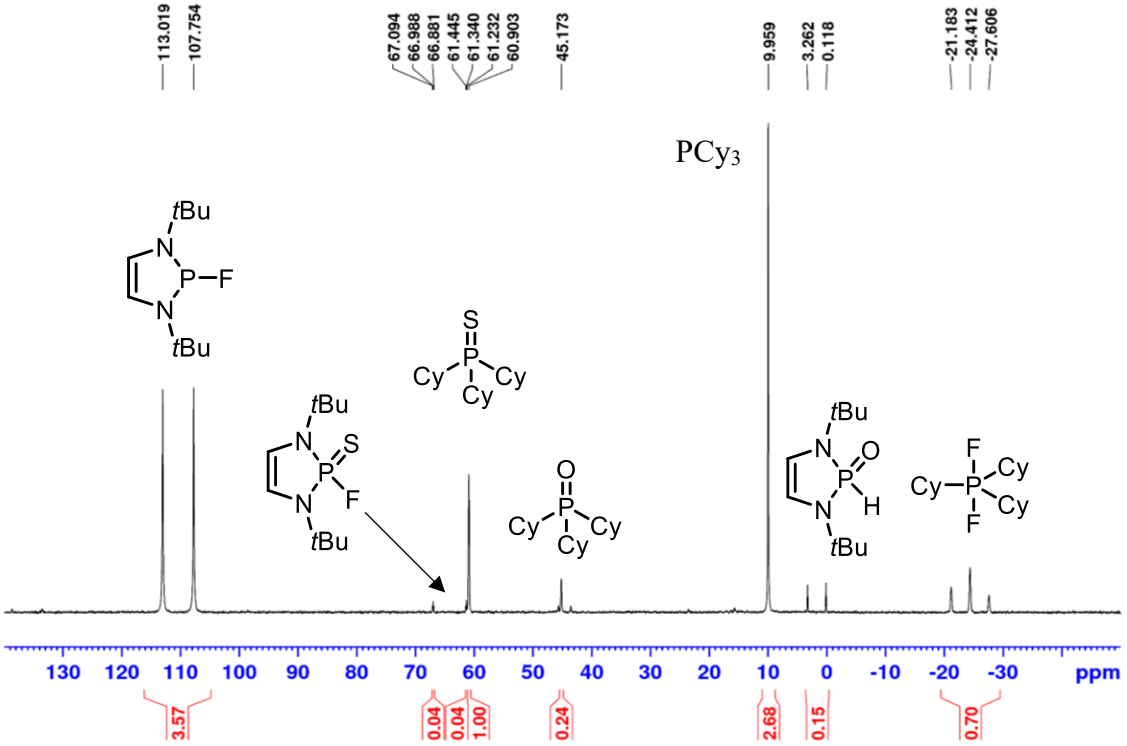


**Figure A184:** $^{31}$P NMR spectrum (121.5 MHz, THF/$C_6D_6$) of sulfur capture with $PCy_3$ **6-54** in the presence of diazaphospholene **6-21** after 30 min.

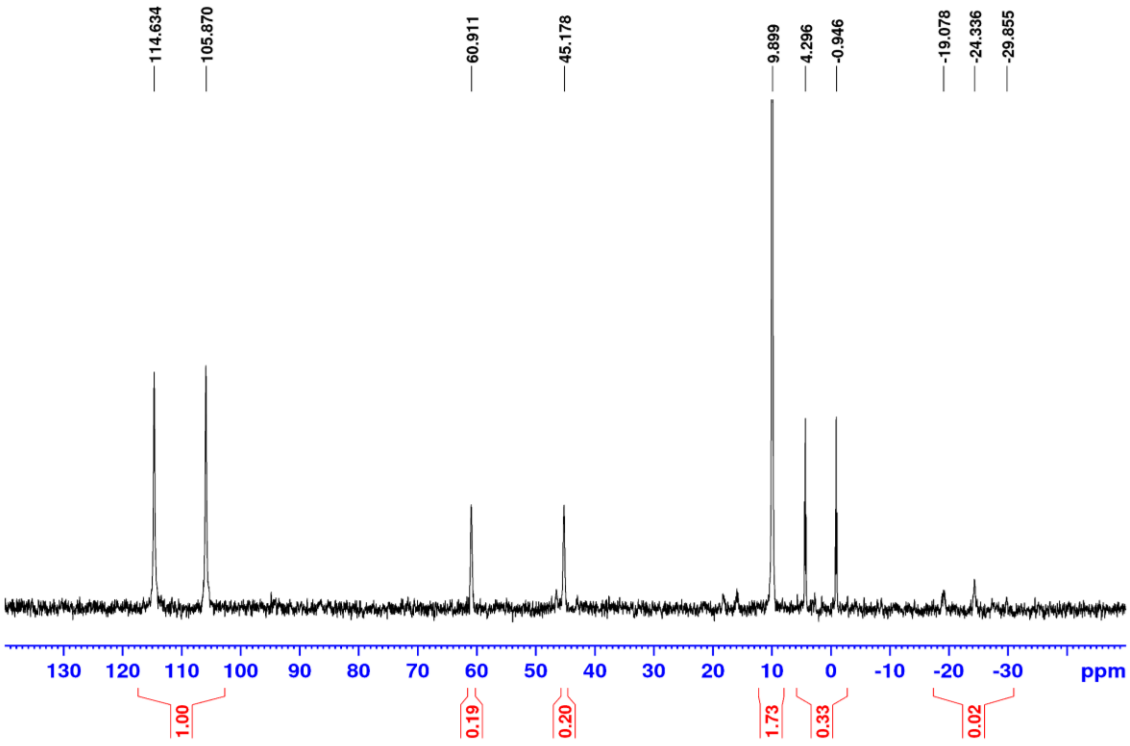


**Figure A185:** $^{31}$P NMR spectrum (121.5 MHz, THF/$C_6D_6$) of sulfur capture with $PCy_3$ **6-54** in the presence of diazaphospholene **6-19** after 6 h.

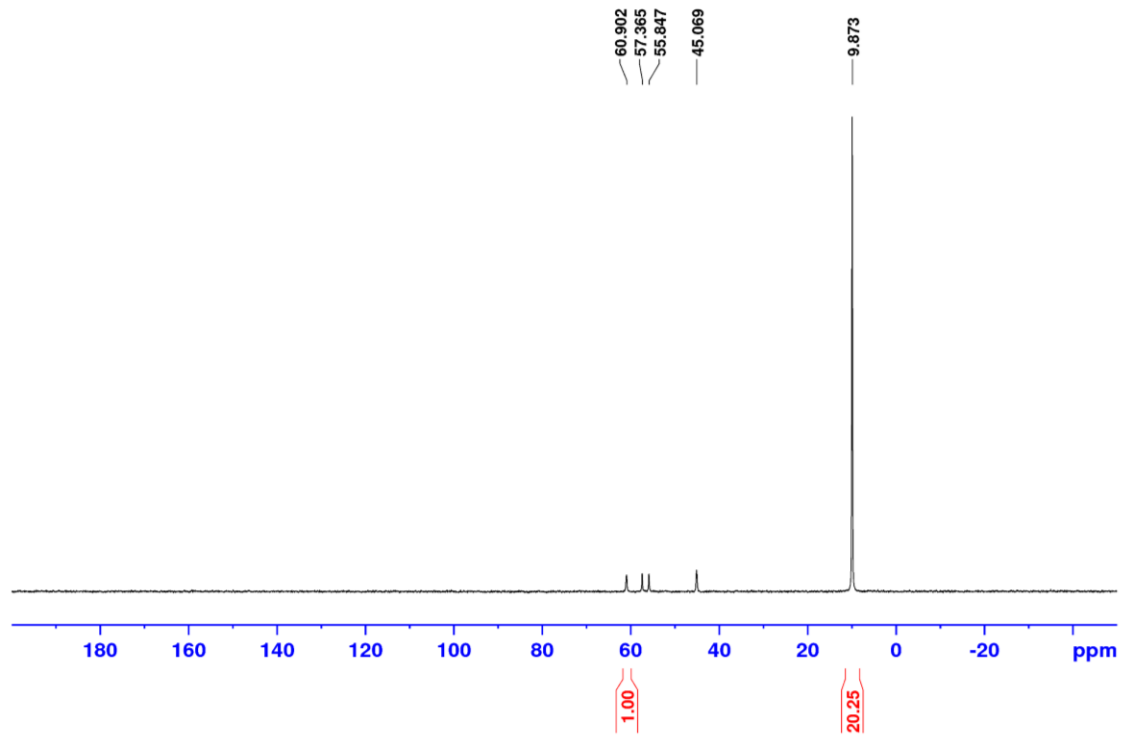


**Figure A186:** $^{31}P$ NMR spectrum (121.5 MHz, THF/$C_6D_6$) of early NMR scale catalytic tests no triethylamine **Entry 1, Table 6.2**.

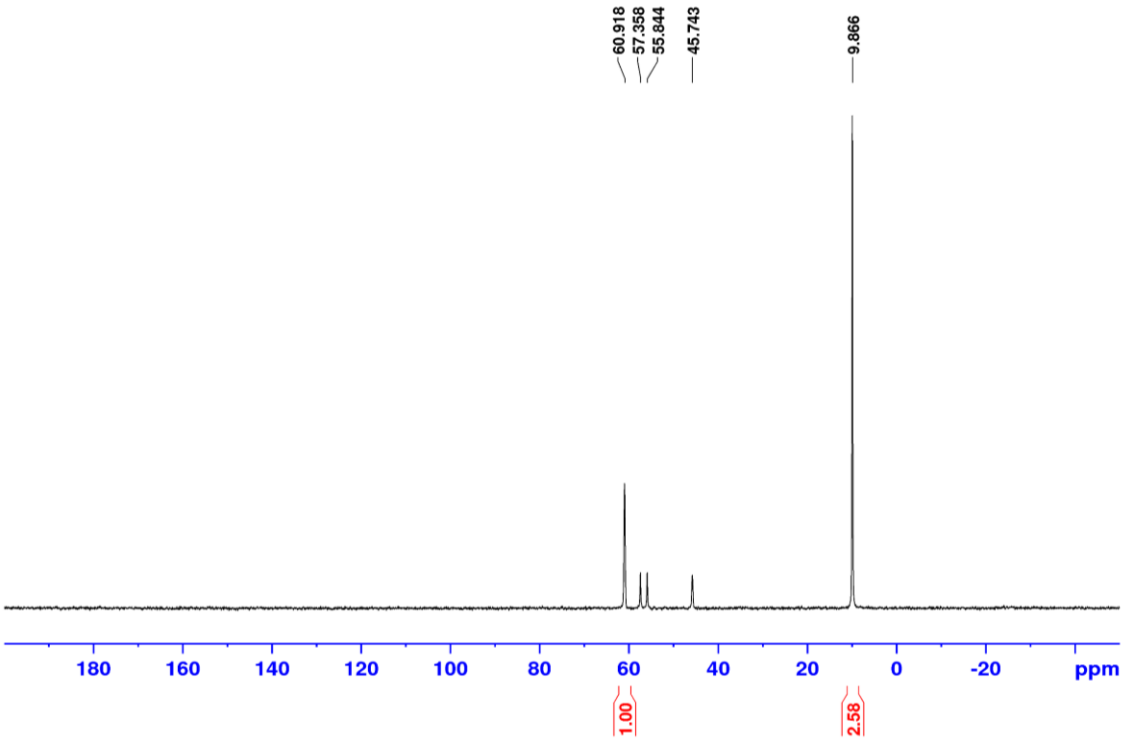


**Figure A187:** $^{31}P$ NMR spectrum (121.5 MHz, THF/$C_6D_6$) of early NMR scale catalytic tests **Entry 2, Table 6.2**.

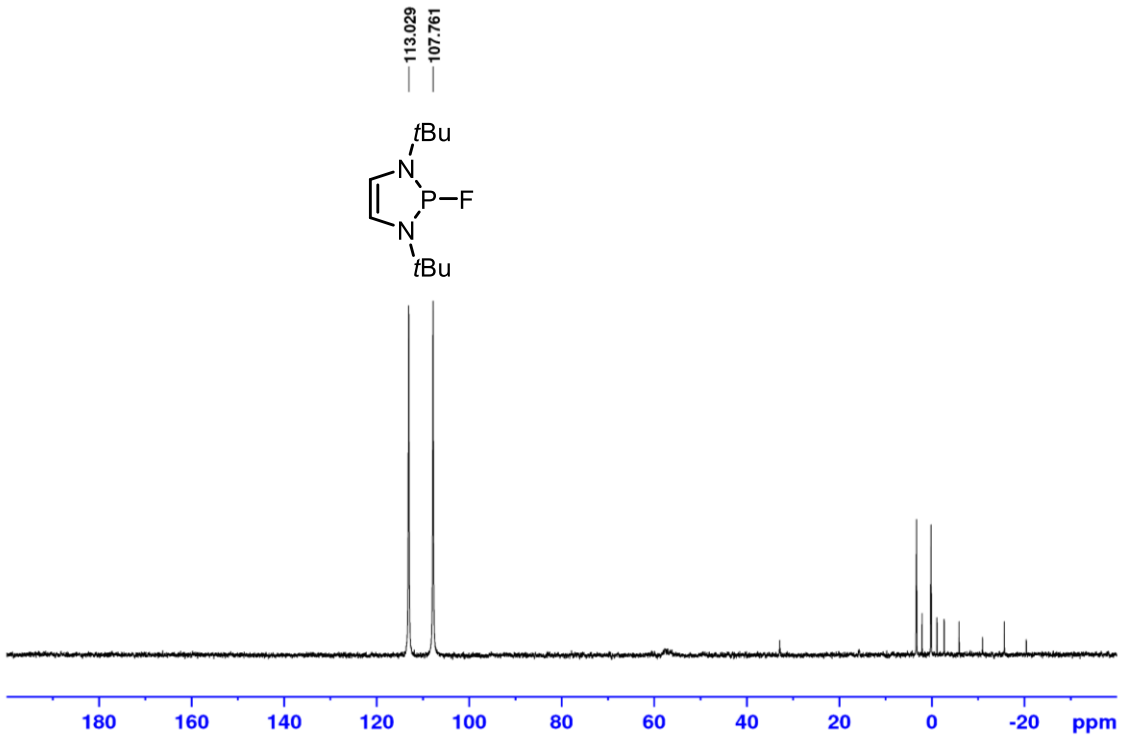


**Figure A188:** $^{31}P$ NMR spectrum (202.5 MHz, THF/$C_6D_6$) of detection of HF from combination of diazaphospholene hydride **6-19** and Fluolead.

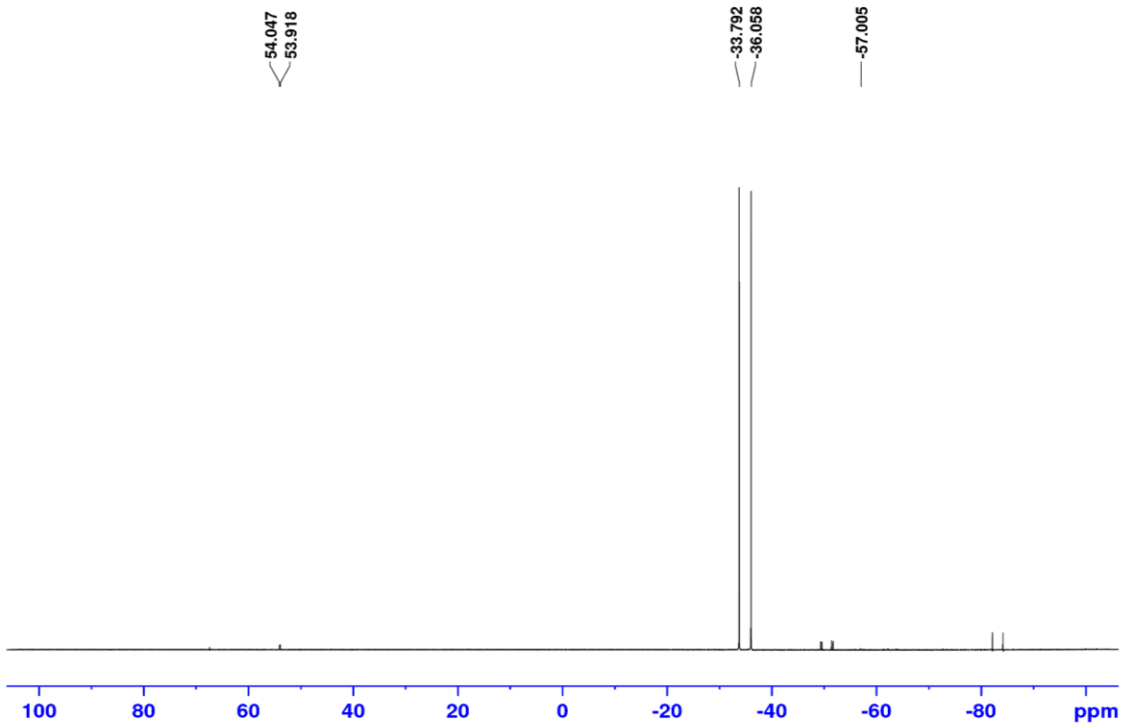


**Figure A189**: $^{19}F$ NMR spectrum (0 center point) (470.6 MHz, THF/$C_6D_6$) of detection of HF from combination of diazaphospholene hydride **6-19** and Fluolead.

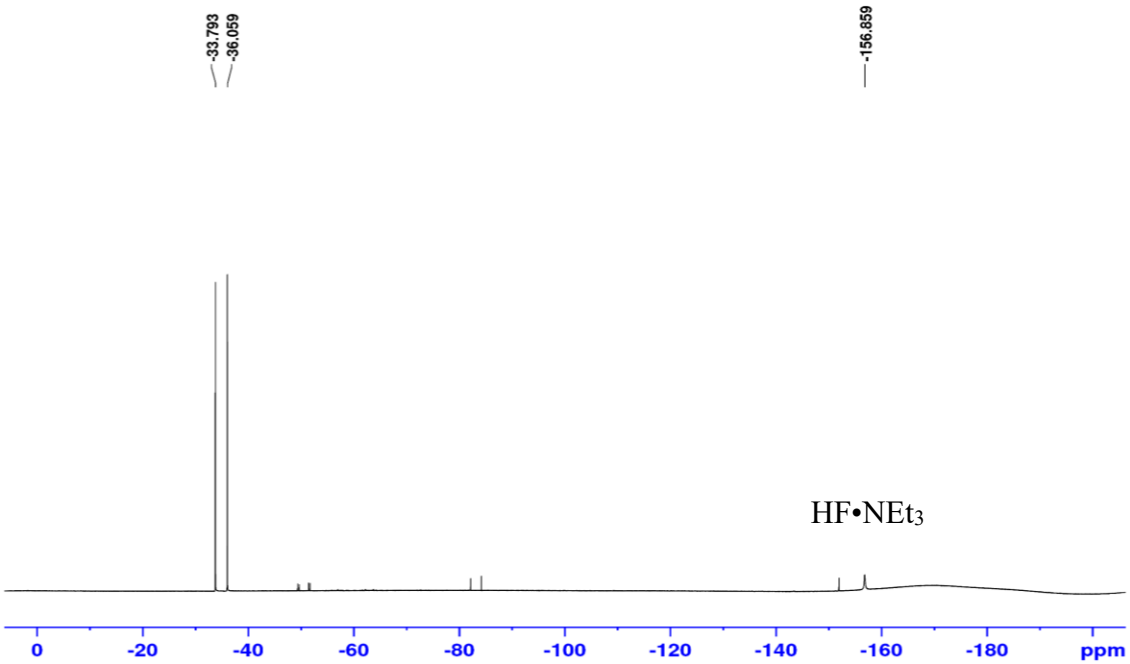


**Figure A190:** $^{19}F$ NMR spectrum (-100 center point) (470.6 MHz, THF/$C_6D_6$) of detection of HF from combination of diazaphospholene hydride **6-19** and Fluolead.

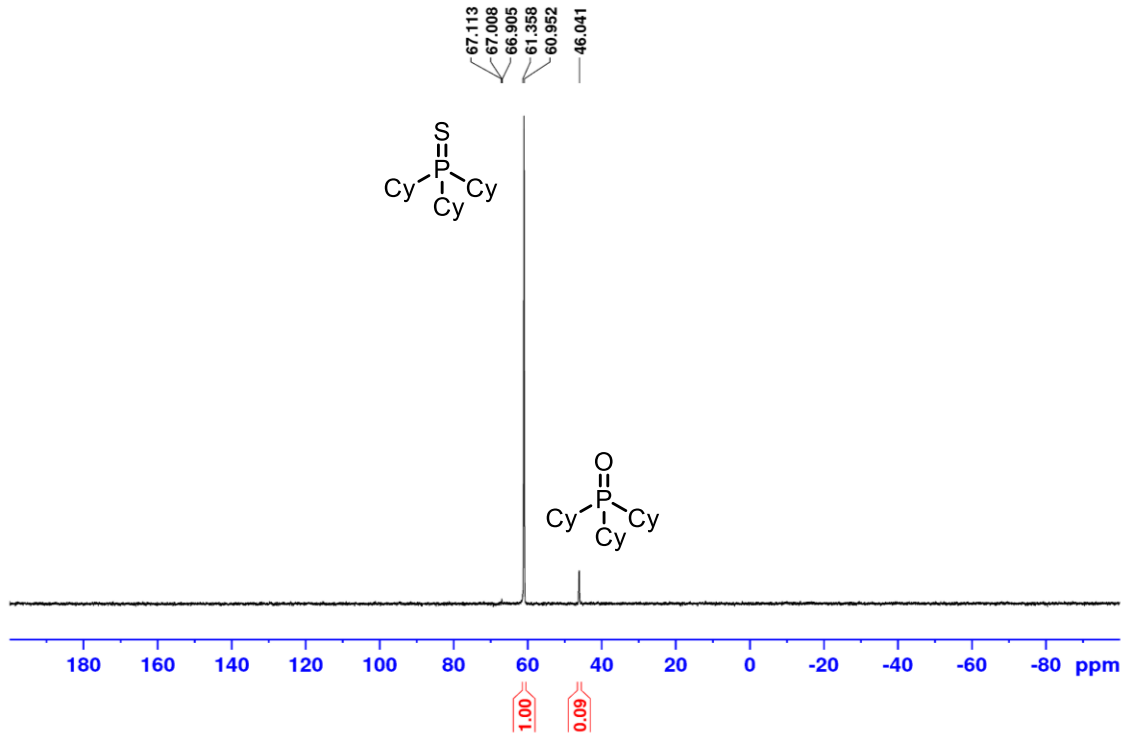


**Figure A 191:** $^{31}P$ NMR spectrum (202.5 MHz, THF/$C_6D_6$) of the decomposition of $SF_6$ catalyzed by diazaphospholene hydride **6-19** (5 mol%) **Entry 1, Table 6.7**.

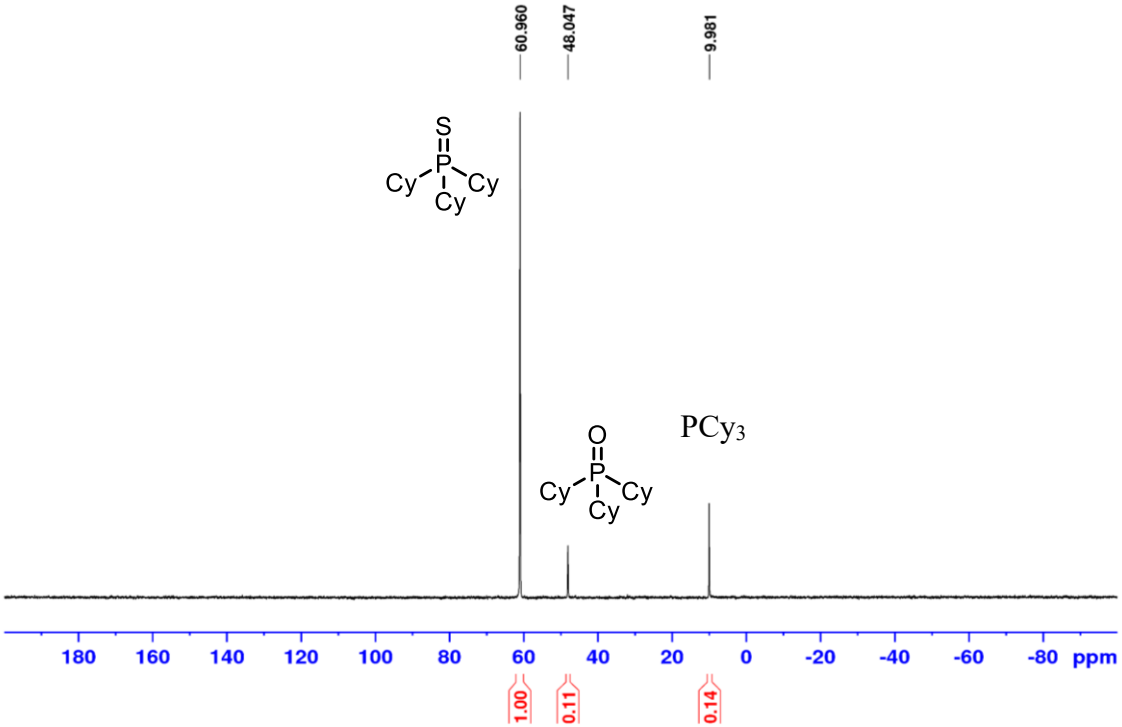


**Figure A192:** $^{31}$P NMR spectrum (202.5 MHz, THF/$C_6D_6$) of the decomposition of $SF_6$ catalyzed by diazaphospholene hydride **6-19** (5 mol%) **Entry 5, Table 6.7**.

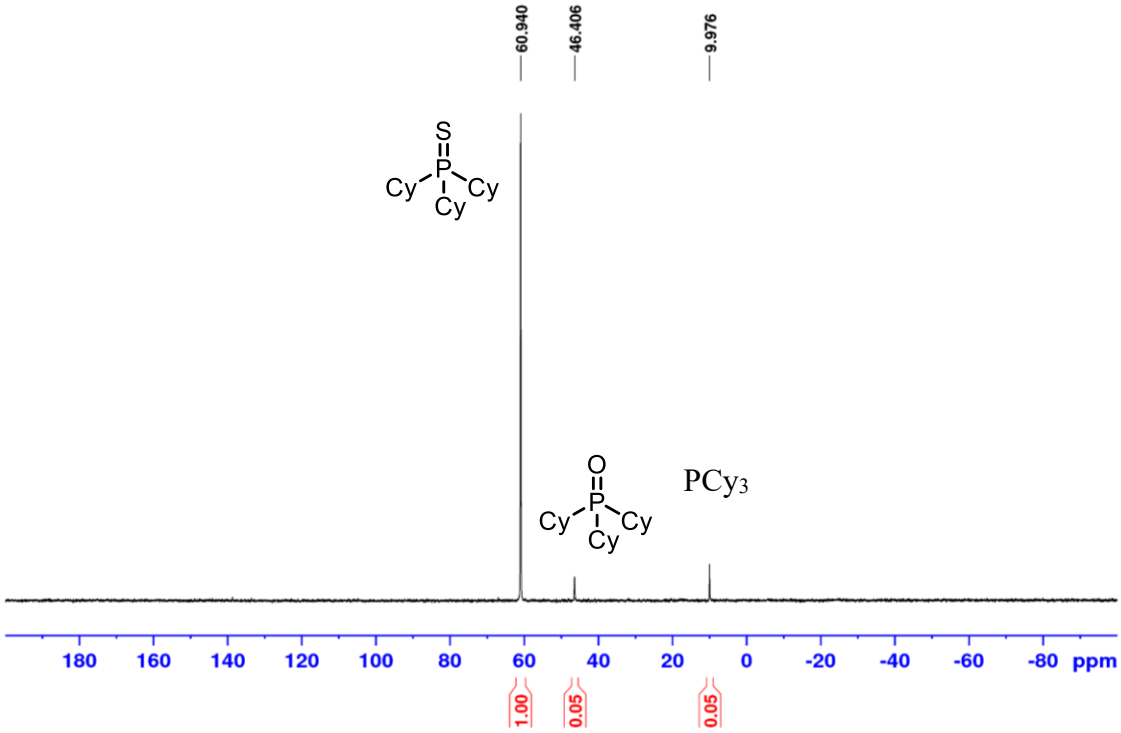


**Figure A193:** $^{31}$P NMR spectrum (202.5 MHz, THF/$C_6D_6$) of the decomposition of $SF_6$ catalyzed by diazaphospholene hydride **6-19** (2.5 mol%) **Entry 6, Table 6.7**.

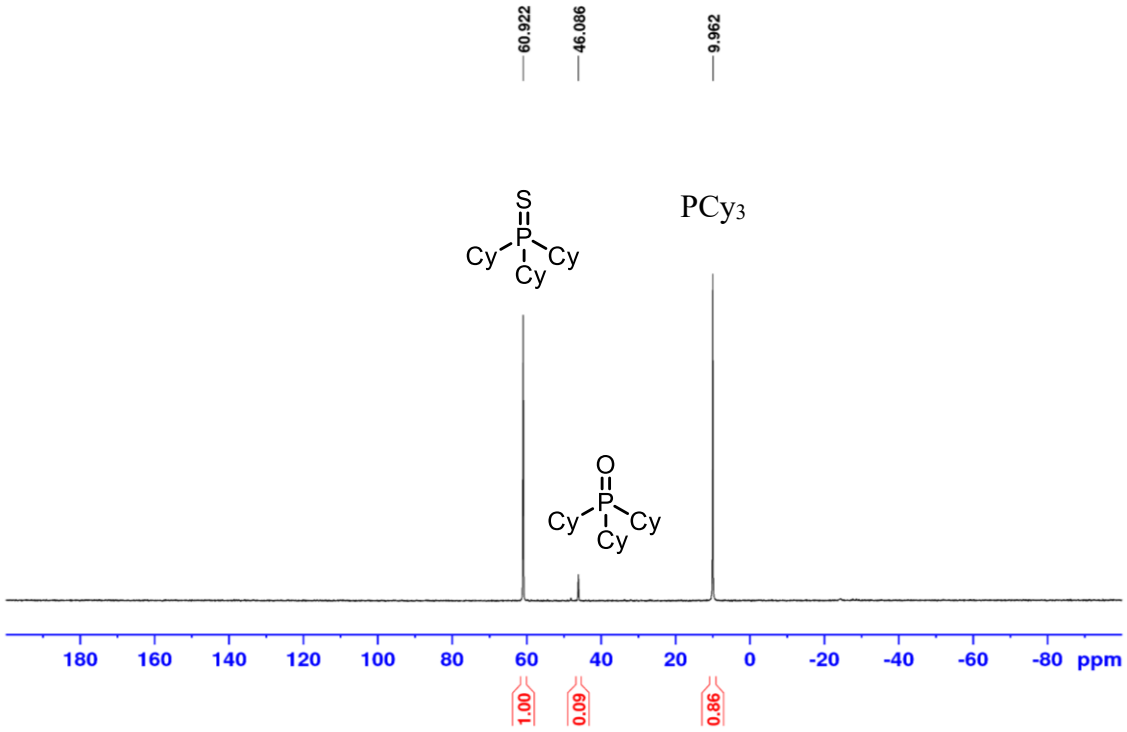


**Figure A194:** $^{31}$P NMR spectrum (202.5 MHz, THF/$C_6D_6$) of the decomposition of $SF_6$ catalyzed by diazaphospholene hydride **6-19** (1 mol%) **Entry 8, Table 6.7**.

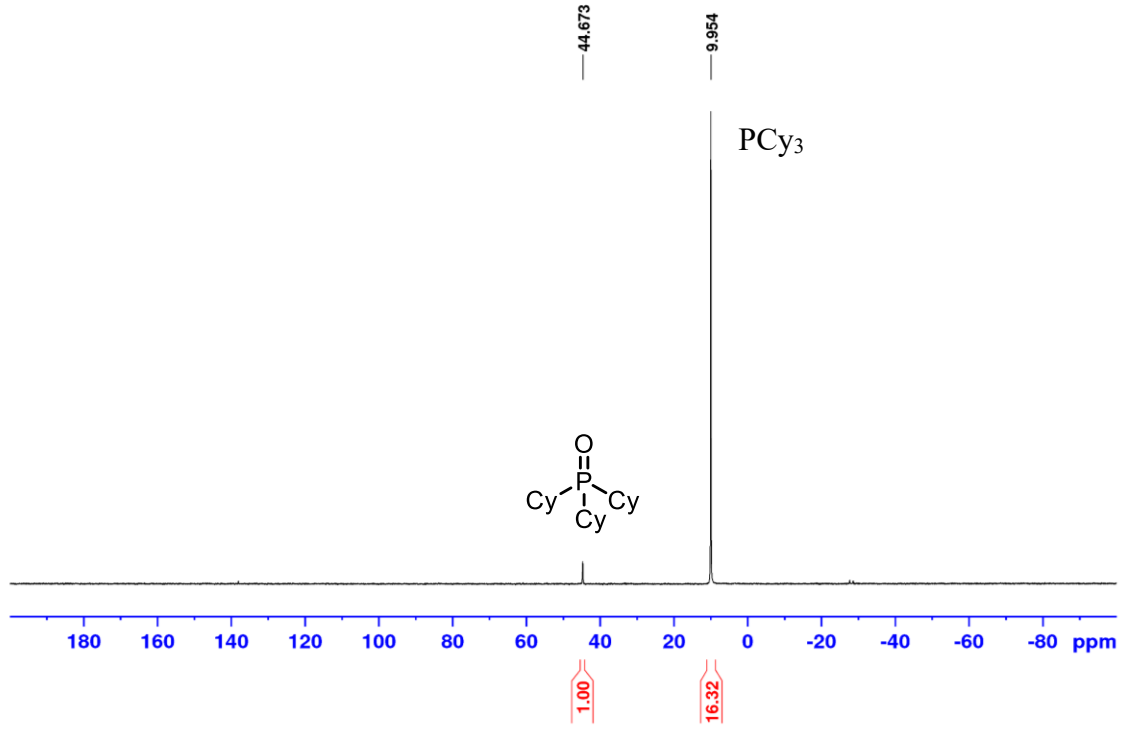


**Figure A195:** $^{31}$P NMR spectrum (202.5 MHz, THF/$C_6D_6$) of the decomposition of $SF_6$ control reaction with no catalyst **Entry 10, Table 6.7**.

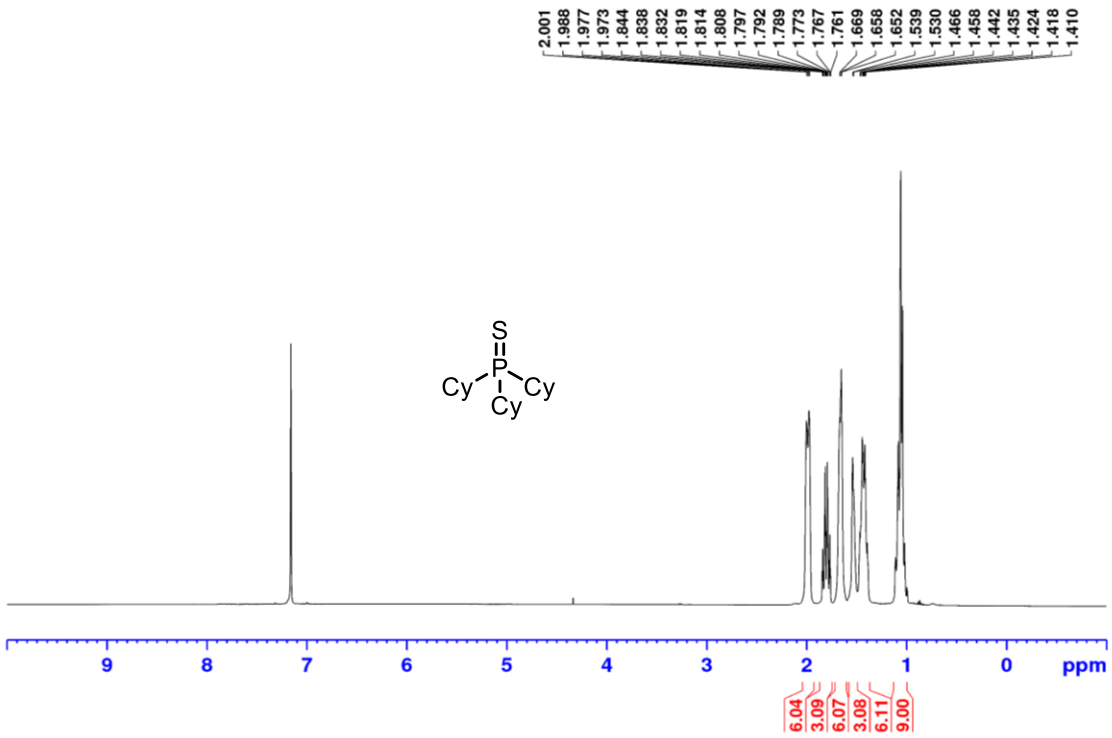


**Figure A196:** $^{1}$H NMR spectrum (500 MHz, $C_6D_6$) of isolated $SPCy_3$ **6-56** from **Entry 6, Table 6.7**.

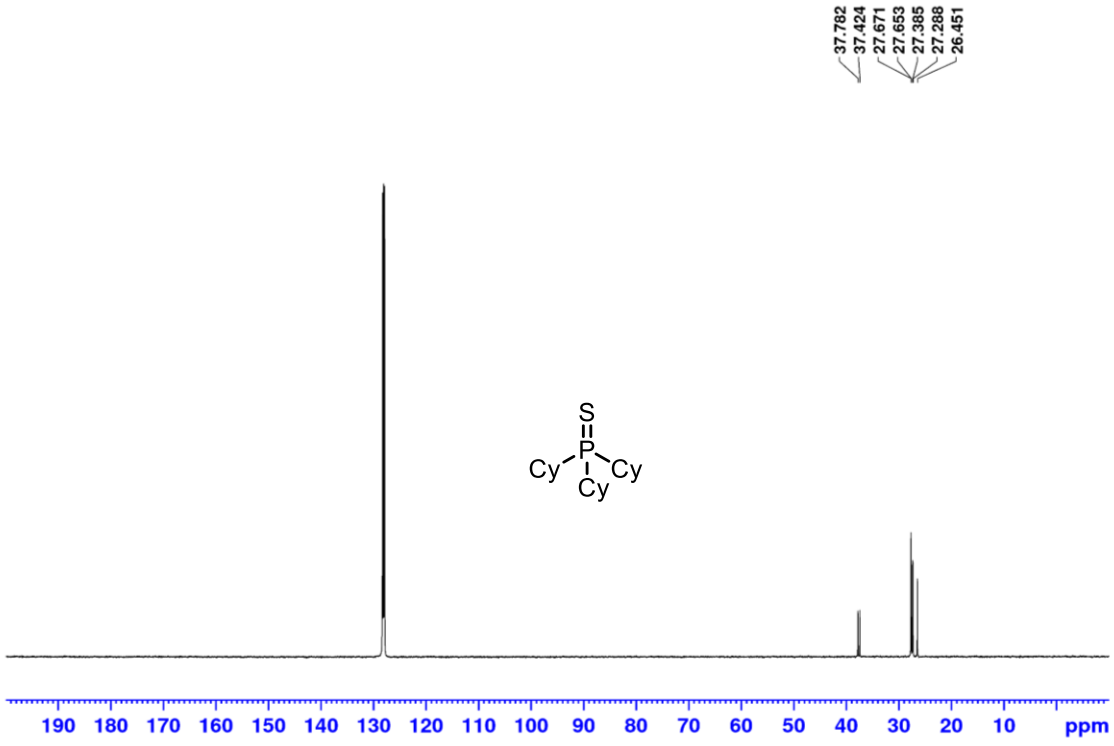


**Figure A197:** $^{13}$C {$^{1}$H} NMR spectrum (125.8 MHz, $C_6D_6$) of isolated $SPCy_3$ **6-56** from **Entry 6, Table 6.7**

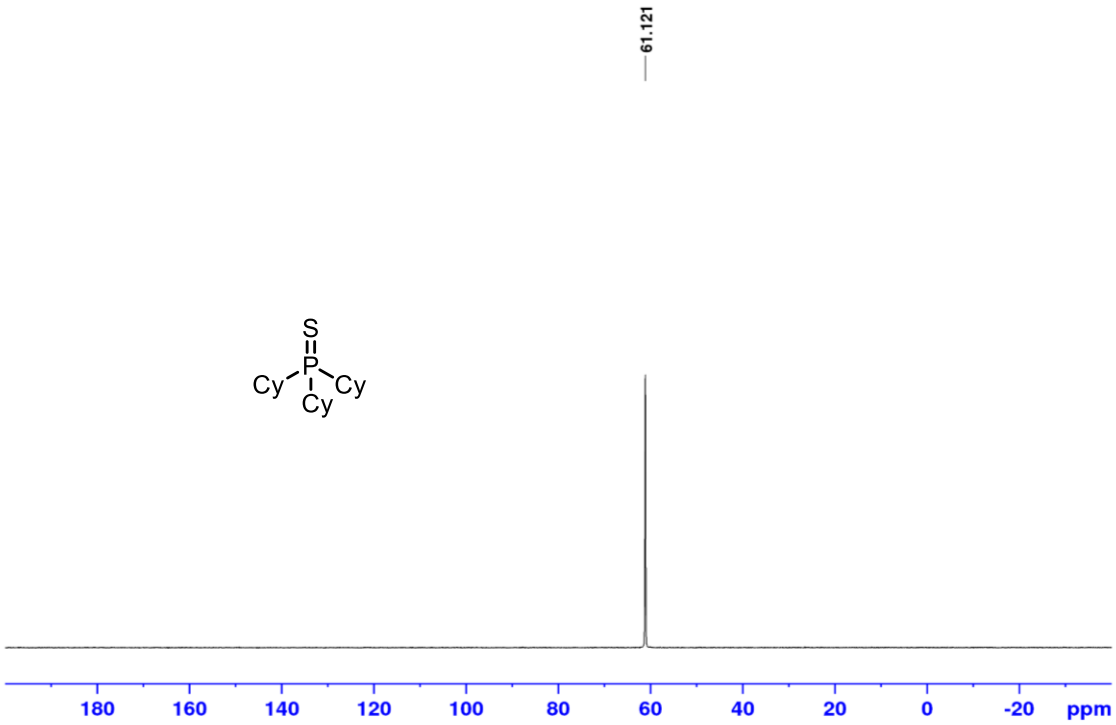


**Figure A198**: $^{31}P$ NMR spectrum (202.5 MHz, $C_6D_6$) of isolated $SPCy_3$ **6-56** from **Entry 6, Table 6.7**.

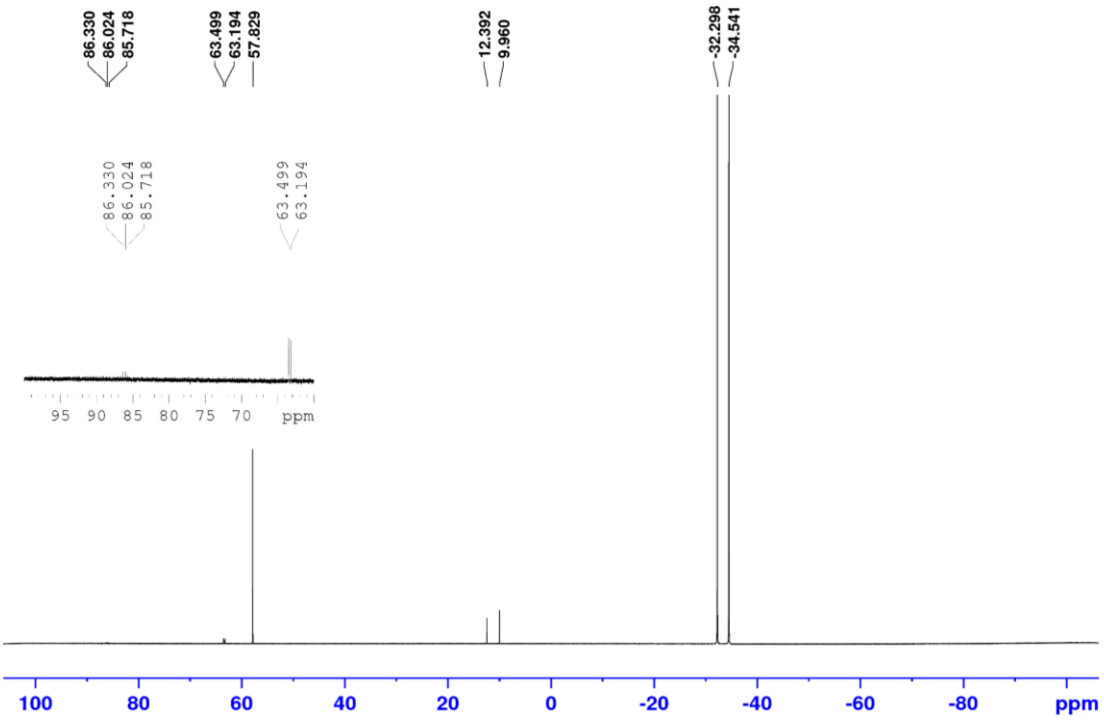


**Figure A199:** $^{19}F$ NMR spectrum (470.6 MHz, $C_6D_6$) of diazaphospholene hydride **6-19** in a mixture of 1-octene and $CH_3CN$ 1:1 post $SF_6$ addition. $CH_3CN$ layer.

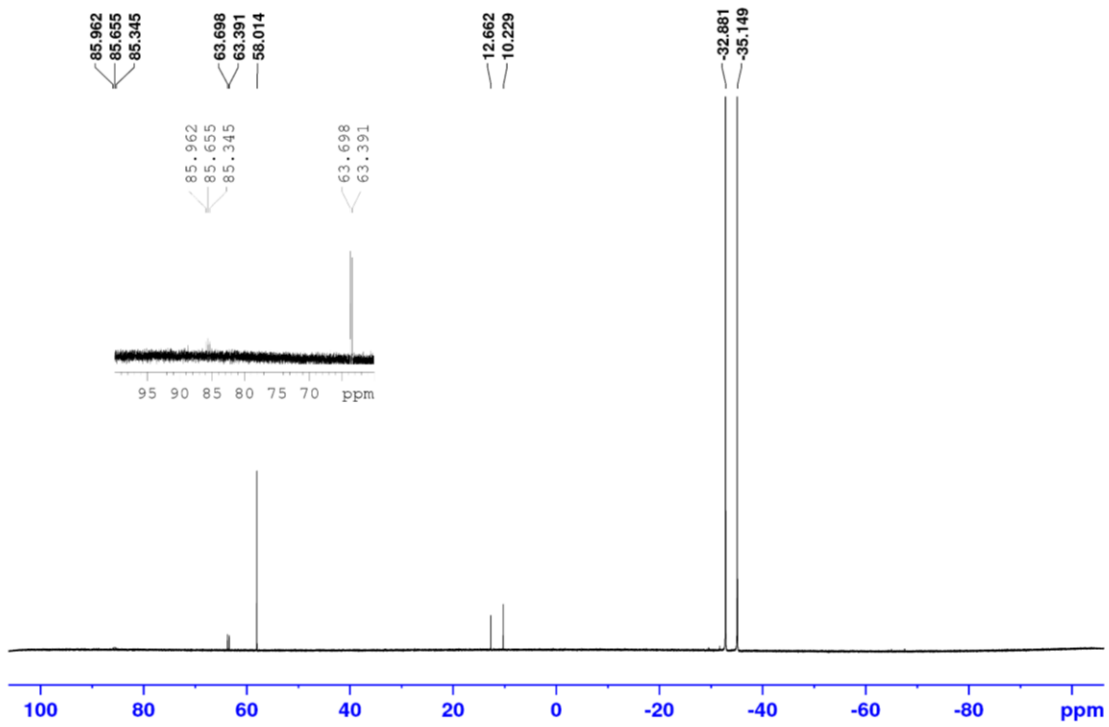


**Figure A200:** $^{19}F$ NMR spectrum (470.6 MHz, $C_6D_6$) of diazaphospholene hydride **6-19** in a mixture of 1-octene and $CH_3CN$ 1:1 post $SF_6$ addition. 1-octene layer.

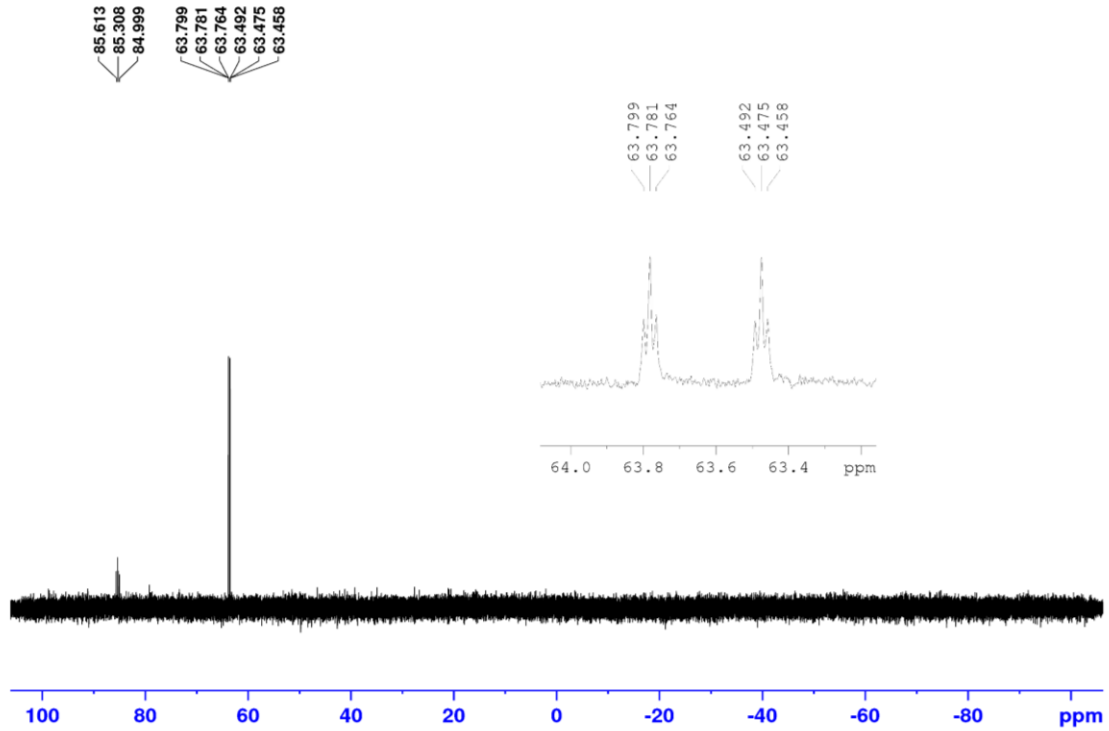


**Figure A201:** $^{19}F$ NMR spectrum (470.6 MHz, $C_6D_6$) of diazaphospholene hydride **6-19** in a mixture of 1-octene and $CH_3CN$ 1:1 post $SF_6$ addition. Isolated product.

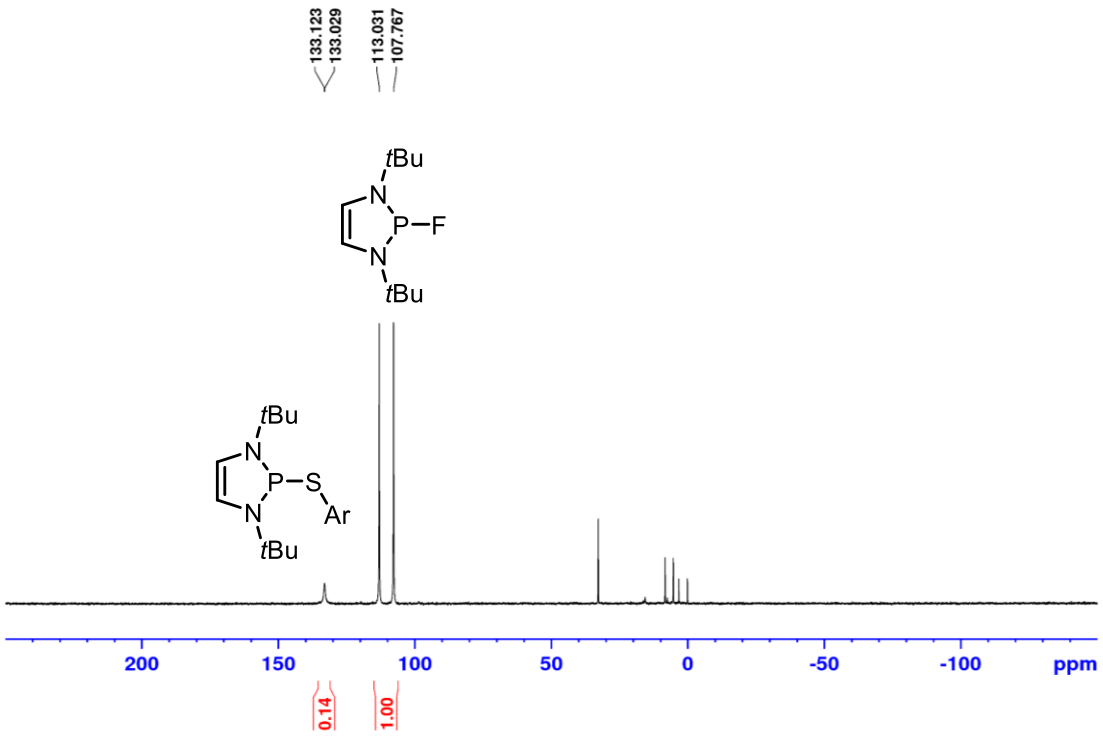


**Figure A202:** $^{31}$P NMR spectrum (202.5 MHz, THF/$C_6D_6$) of reaction of diazaphospholene dimer **6-21** with Fluolead. Ar = 2,6-(Me)-4-(*t*Bu)Ph.

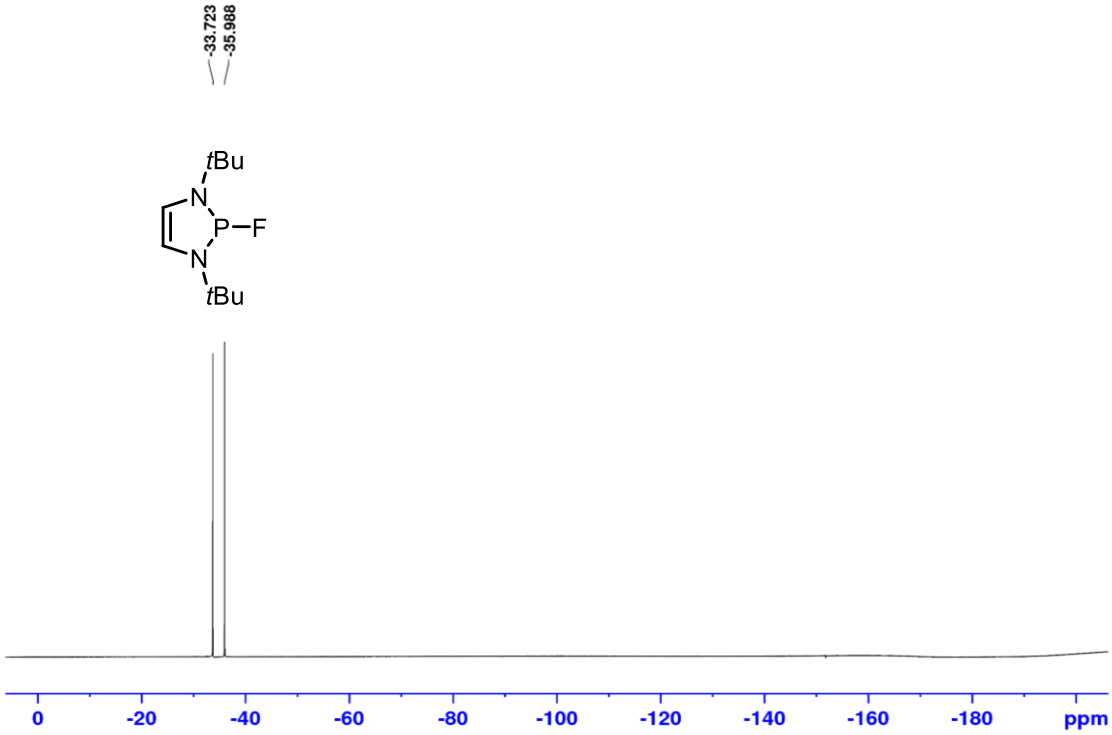


**Figure A203:** $^{19}$F NMR spectrum (-100 center point) (470.6 MHz, THF/$C_6D_6$) of reaction of diazaphospholene dimer **6-21** with Fluolead.

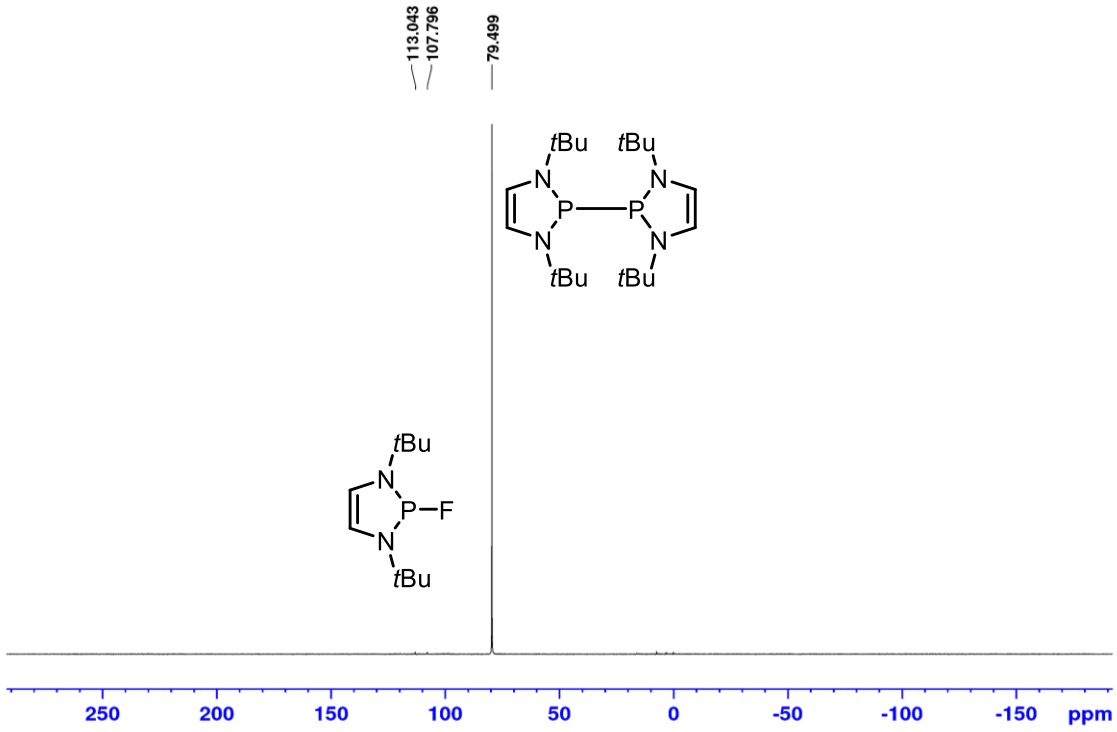


**Figure A204:** $^{31}$P NMR spectrum (202.5 MHz, THF/$C_6D_6$) of reaction of diazaphospholene dimer **6-21** with $PhSF_5$ 1 h no blue light.

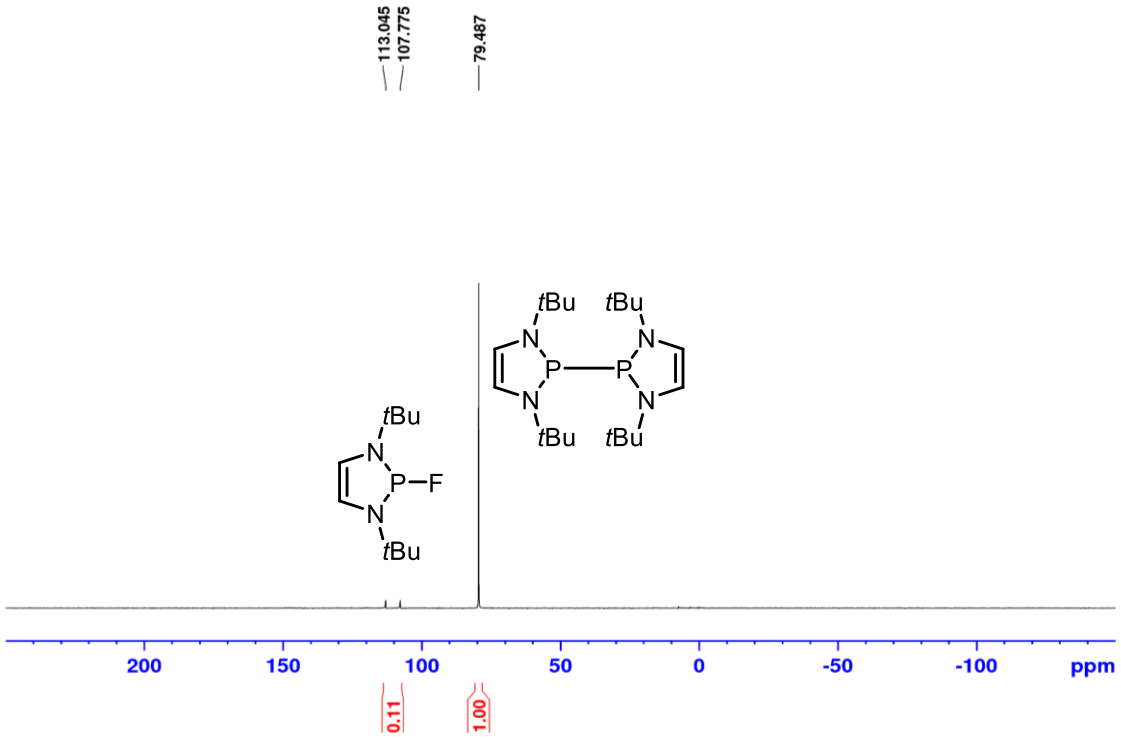


**Figure A205:** $^{31}$P NMR spectrum (202.5 MHz, THF/$C_6D_6$) of reaction of diazaphospholene dimer **6-21** with $PhSF_5$ 30 min blue light.

**E4: NMR Spectra for Section 6.4**

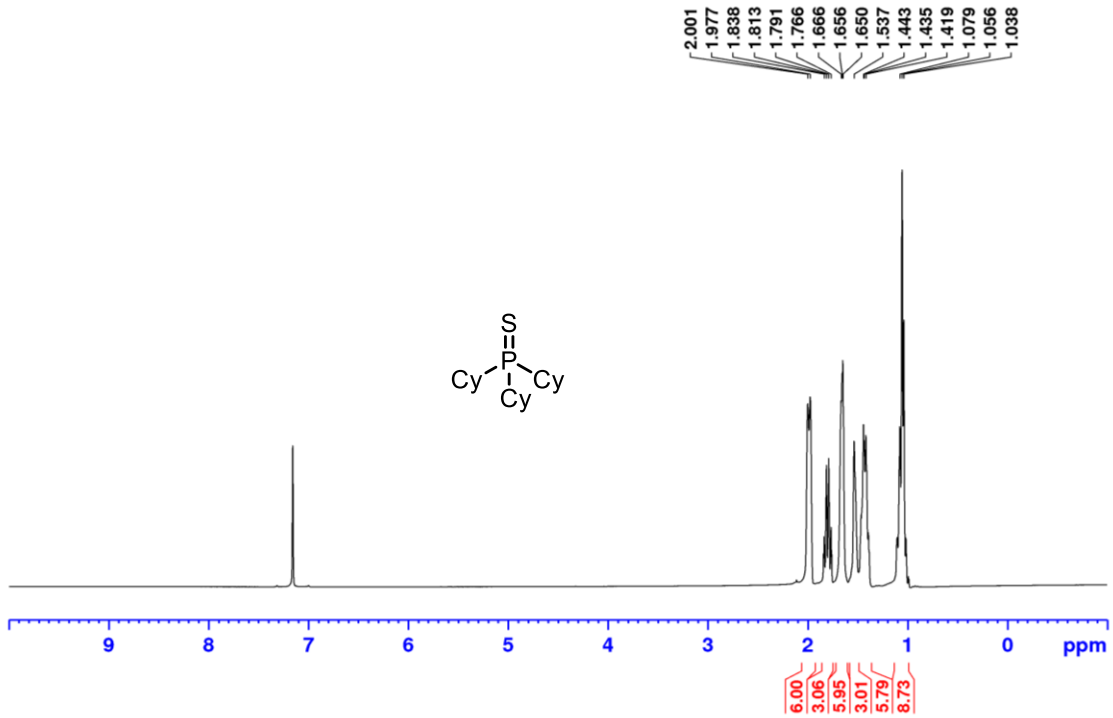


**Figure A206:** $^{1}$H NMR spectrum (500 MHz, $C_6D_6$) of isolated $SPCy_3$ **6-56** from $PCy_3$ and sulfur.

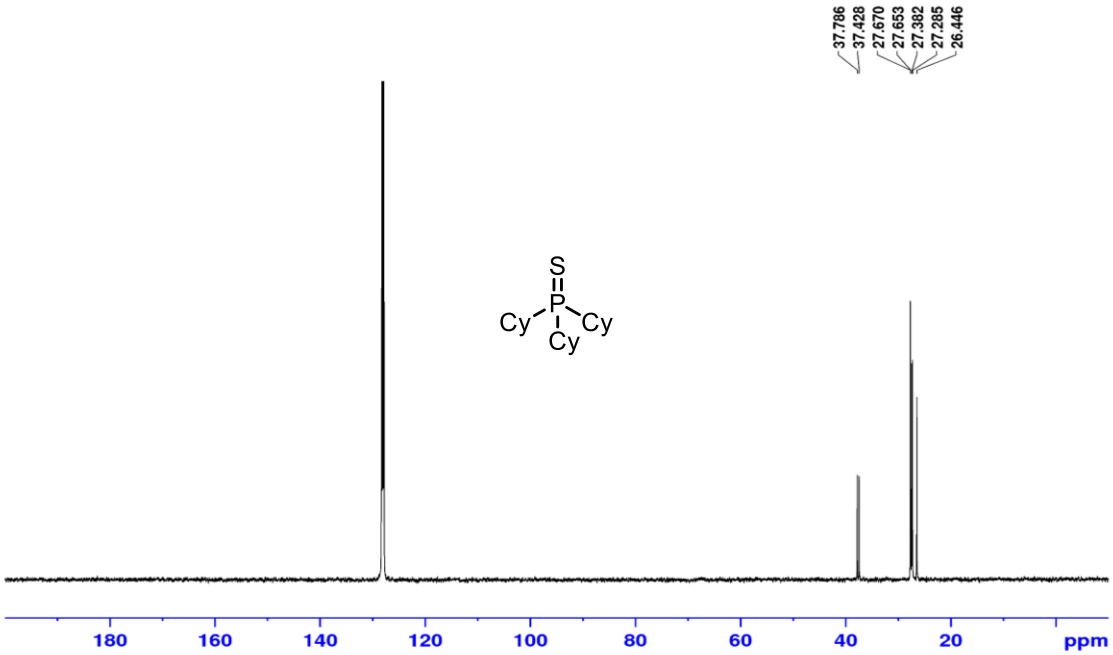


Figure A 207: $^{13}$C {$^{1}$H} NMR spectrum (125.8 MHz, $C_6D_6$) of isolated $SPCy_3$ **6-56** from $PCy_3$ and sulfur.

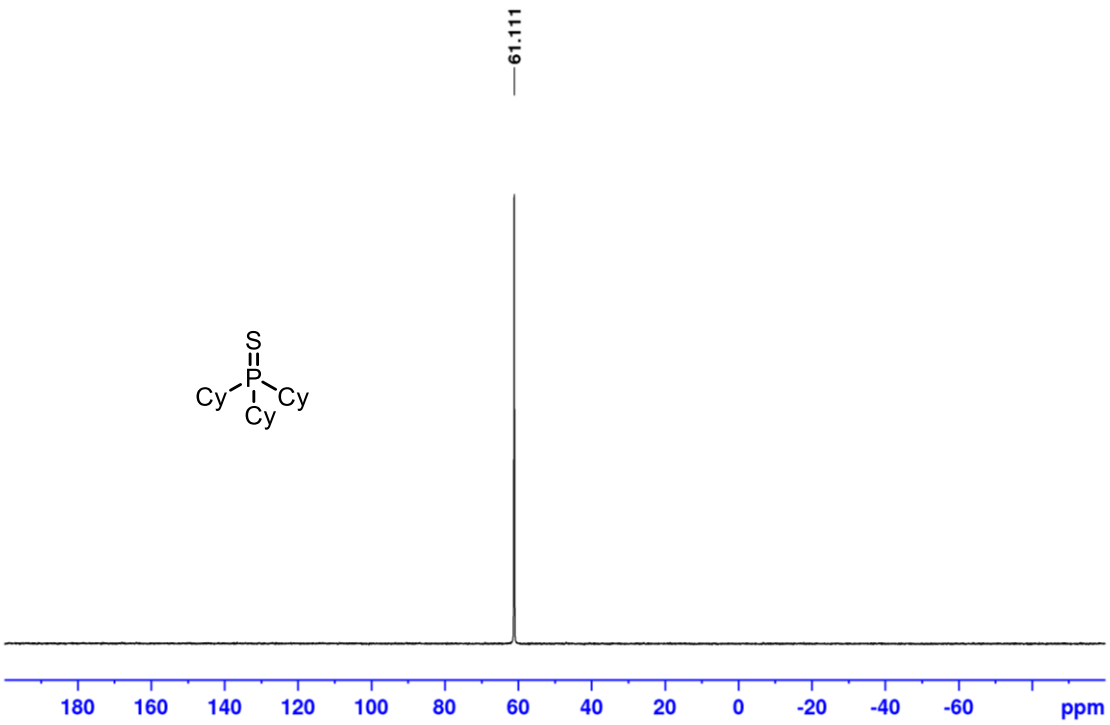


**Figure A 208:** $^{31}$P NMR spectrum (202.5 MHz, $C_6D_6$) of isolated $SPCy_3$ **6-56** from $PCy_3$ and sulfur.

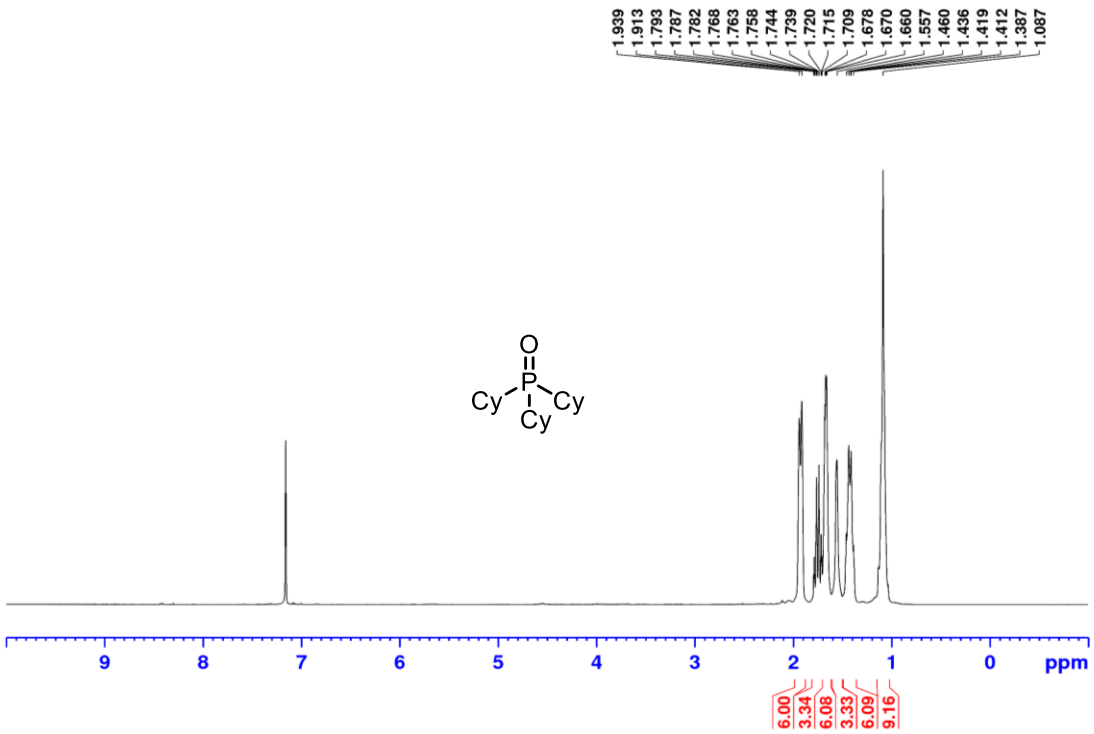


**Figure A209:** $^{1}$H NMR spectrum (500 MHz, $C_6D_6$) of isolated $OPCy_3$ **6-67** from $PCy_3$ and peroxide.

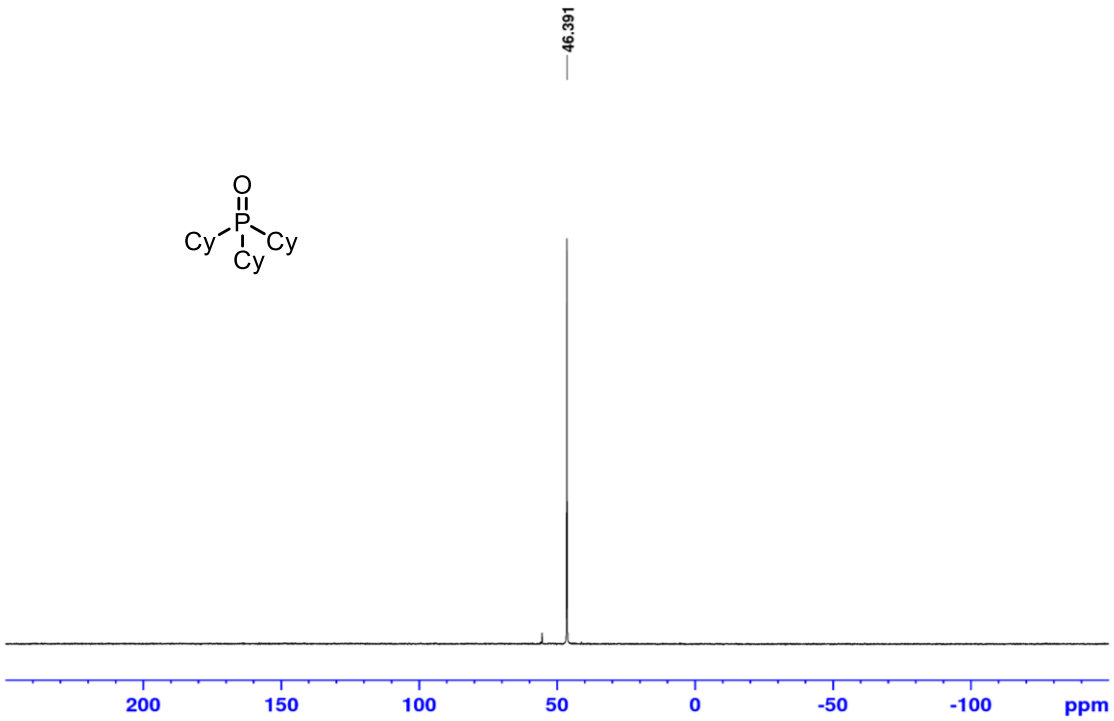


**Figure A210:** $^{31}P$ NMR spectrum (202.5 MHz, $C_6D_6$) of isolated $OPCy_3$ **6-67** from $PCy_3$ and peroxide.

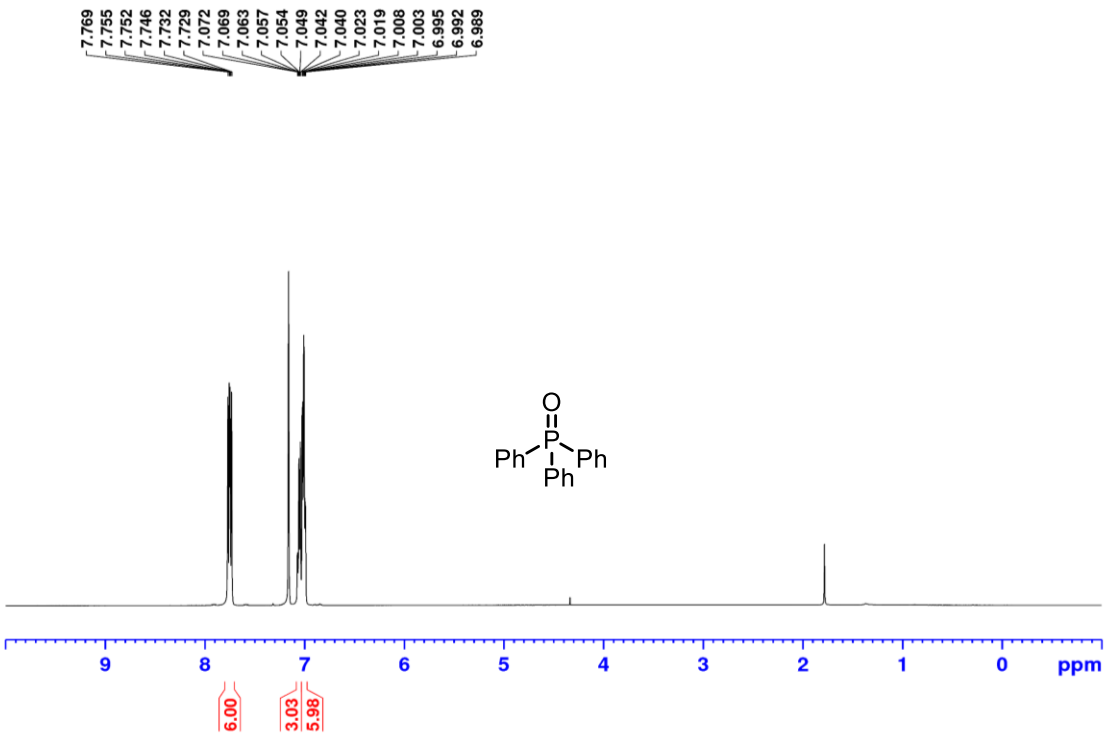


**Figure A211:** $^{1}H$ NMR spectrum (500 MHz, $C_6D_6$) of isolated $OPPh_3$ from $PPh_3$ and peroxide.

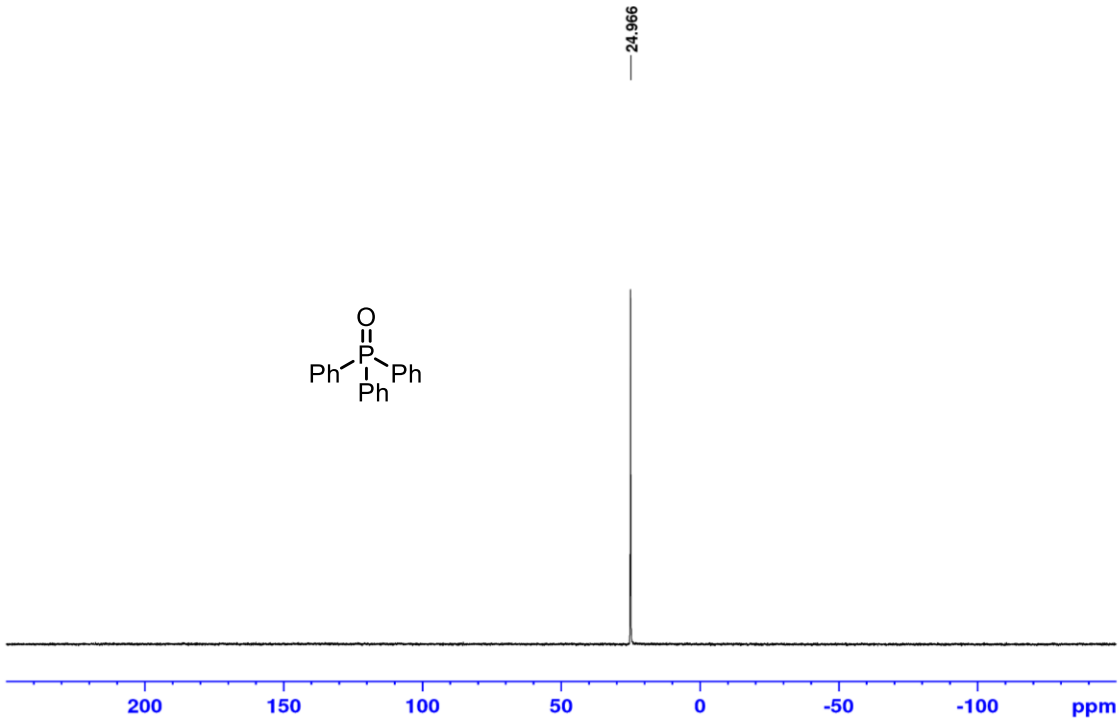


**Figure A212:** $^{31}P$ NMR spectrum (202.5 MHz, $C_6D_6$) of isolated $OPPh_3$ from $PPh_3$ and peroxide.

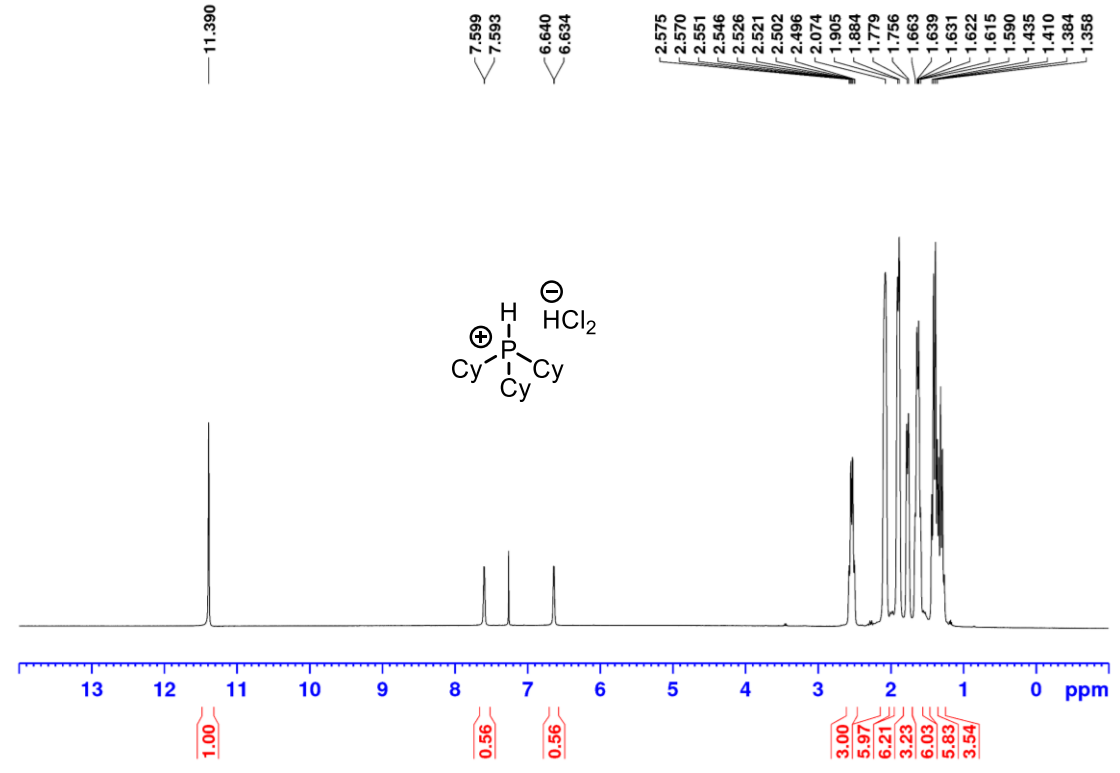


**Figure A213:** $^{1}H$ NMR spectrum (500 MHz, $C_6D_6$) of isolated $HCl_2$•$HPCy_3$ **6-69**.

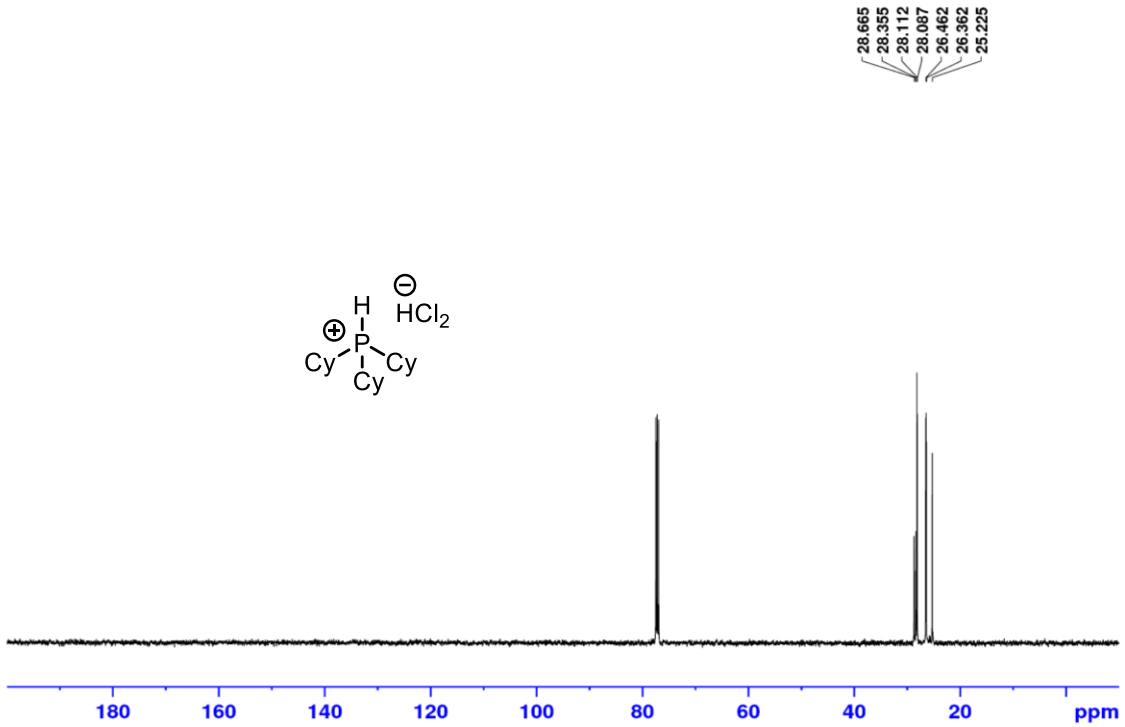


**Figure A214:** $^{13}C$ {$^{1}H$} NMR spectrum (125.8 MHz, $C_6D_6$) of isolated $HCl_2$•$HPCy_3$ **6-69**.

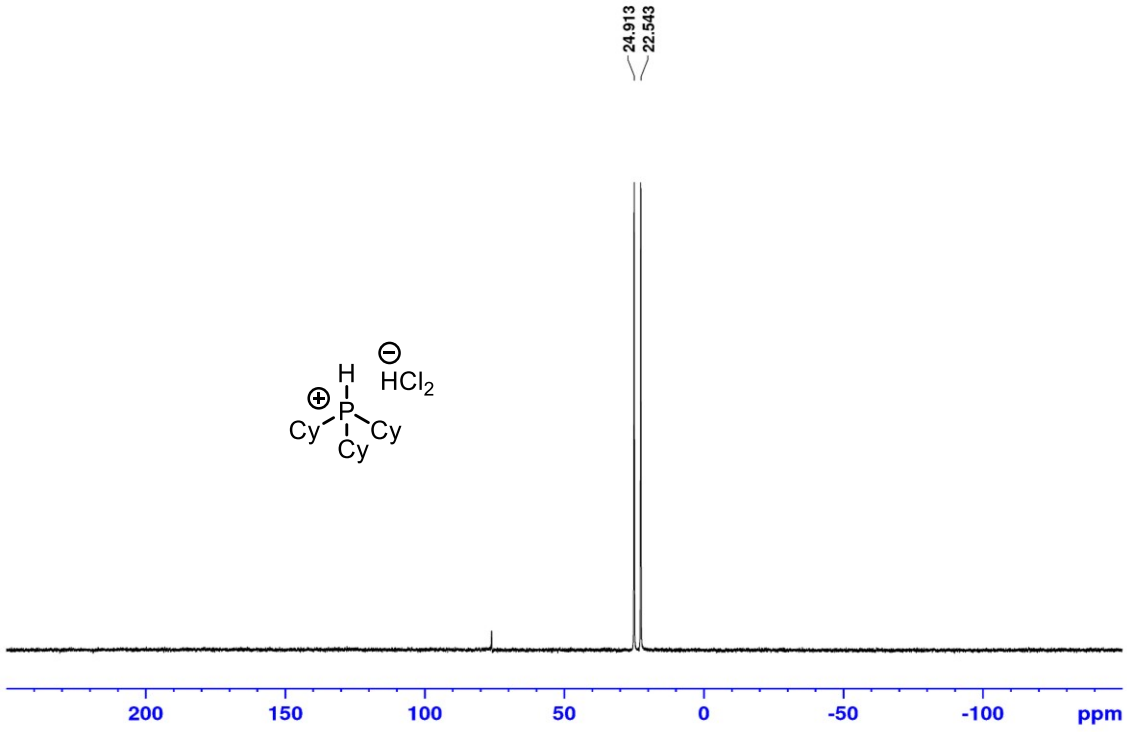


**Figure A215:** $^{31}P$ NMR spectrum (202.5 MHz, $C_6D_6$) of isolated $HCl_2$•$HPCy_3$ **6-69**.

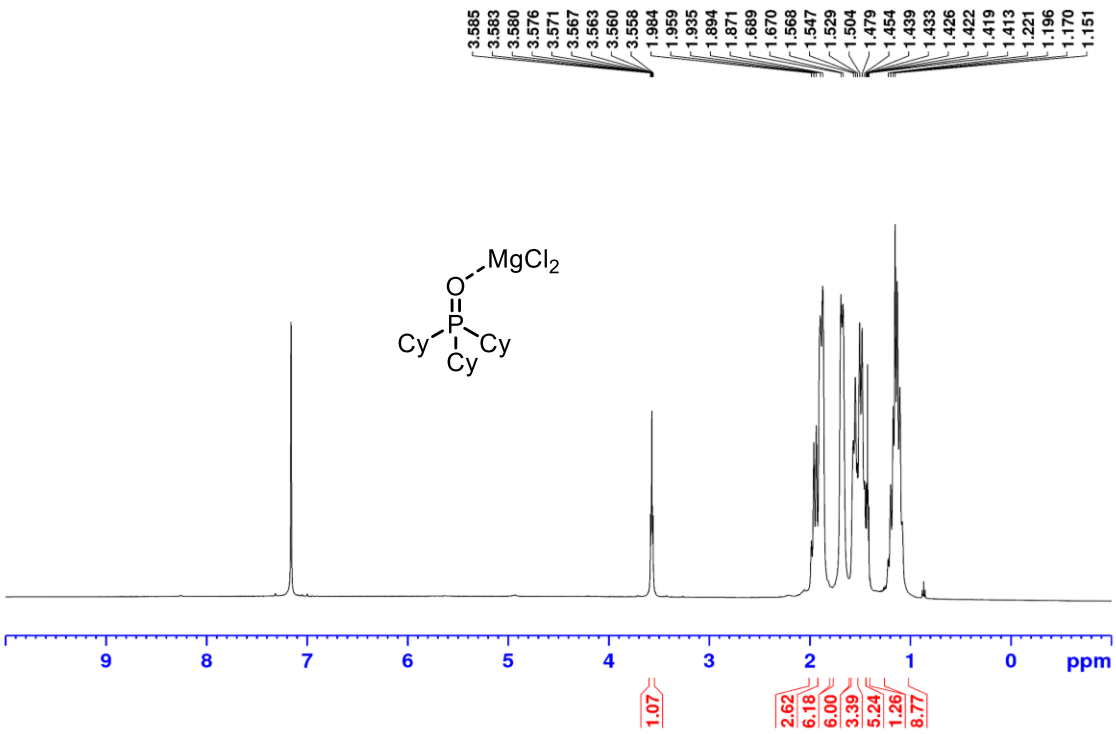


**Figure A216:** $^{1}$H NMR spectrum (500 MHz, $C_6D_6$) of impurity **6-68** at 58ppm.

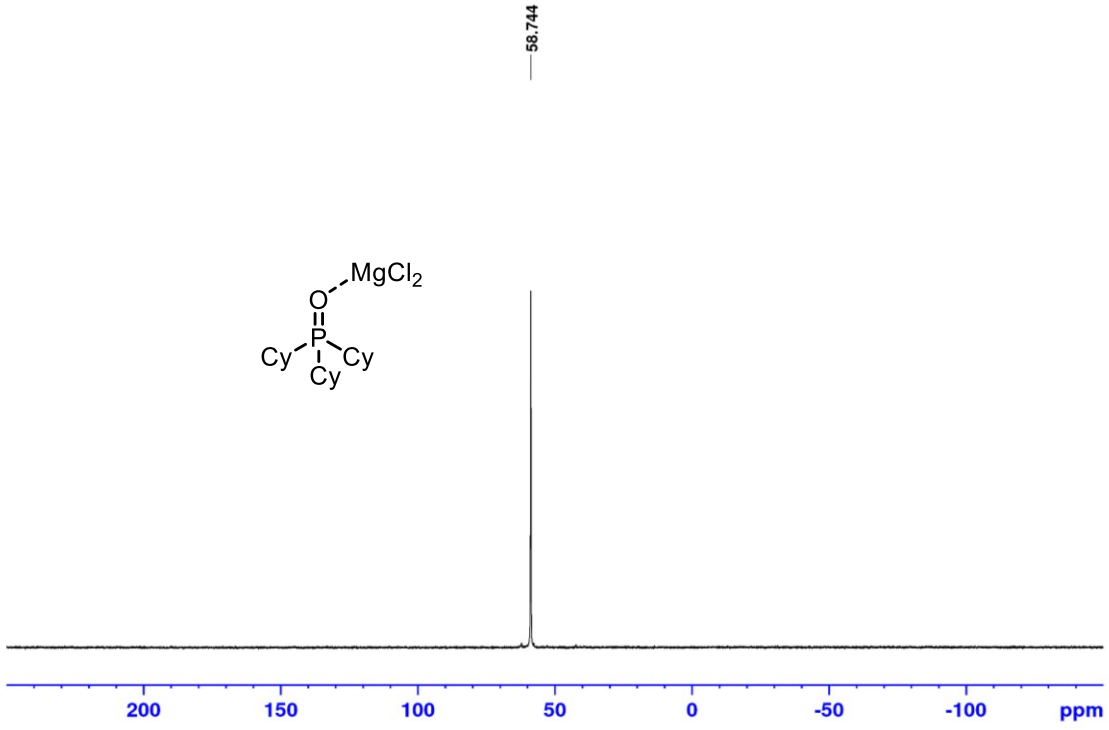


**Figure A217:** $^{31}$P NMR spectrum (202.5 MHz, $C_6D_6$) of impurity **6-68** at 58ppm.

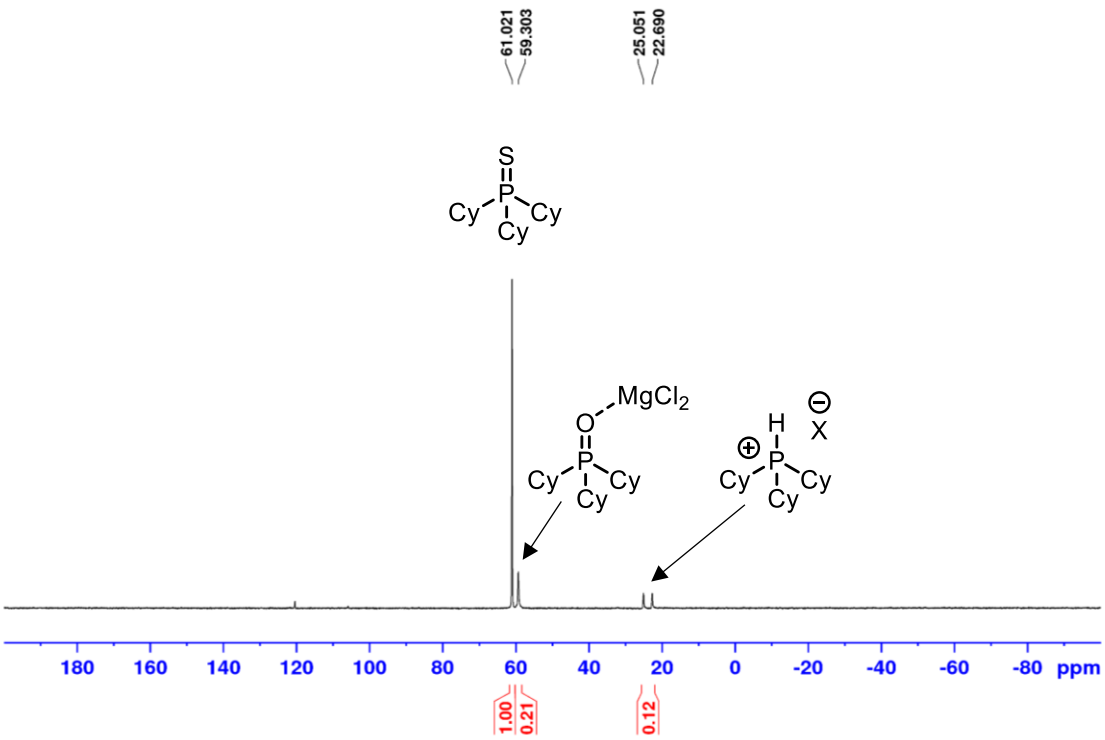


**Figure A218:** $^{31}$P NMR spectrum (202.5 MHz, $C_6D_6$) of **Entry 3, Table 6.8**.

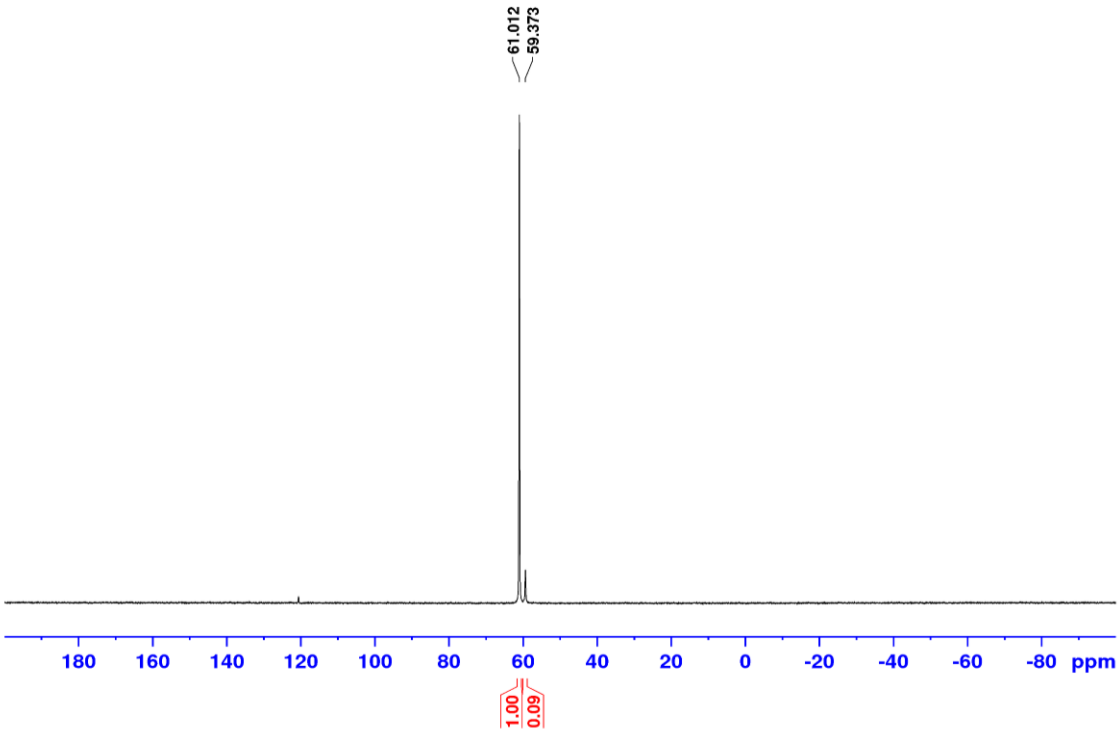


**Figure A219:** $^{31}$P NMR spectrum (202.5 MHz, $C_6D_6$) of **Entry 5, Table 6.8**.

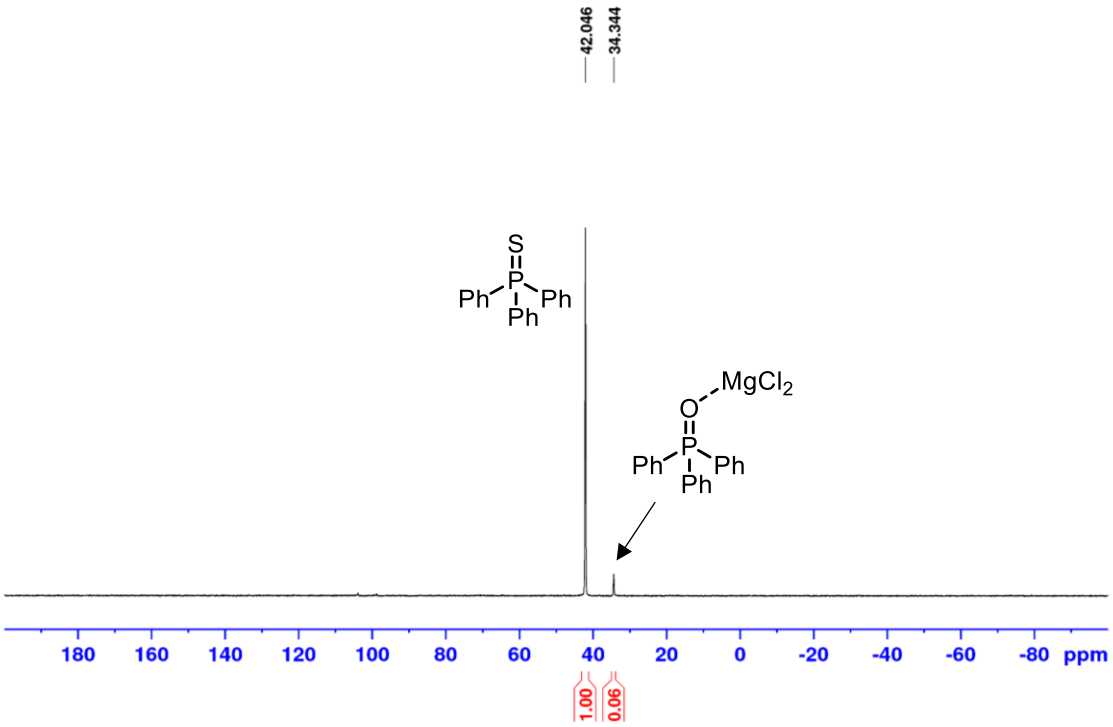


**Figure A220:** $^{31}$P NMR spectrum (202.5 MHz, $C_6D_6$) of **Entry 2, Table 6.10**.

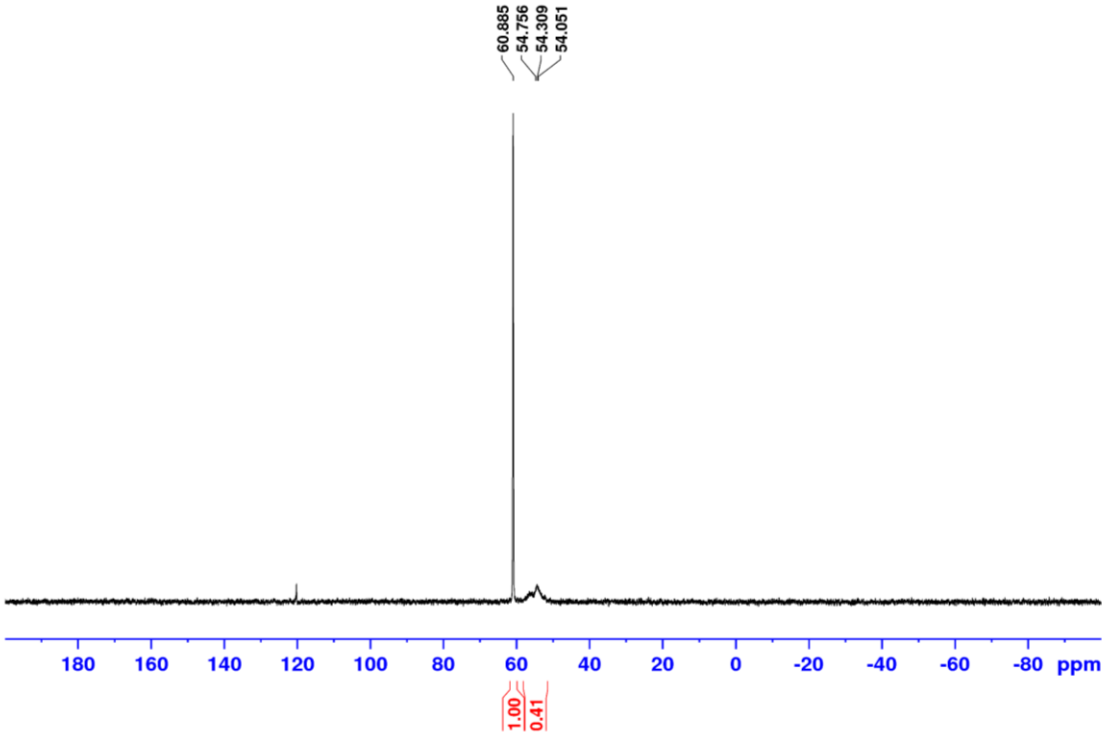


**Figure A221:** $^{31}$P NMR spectrum (202.5 MHz, $C_6D_6$) of **Entry 2, Table 6.11**.

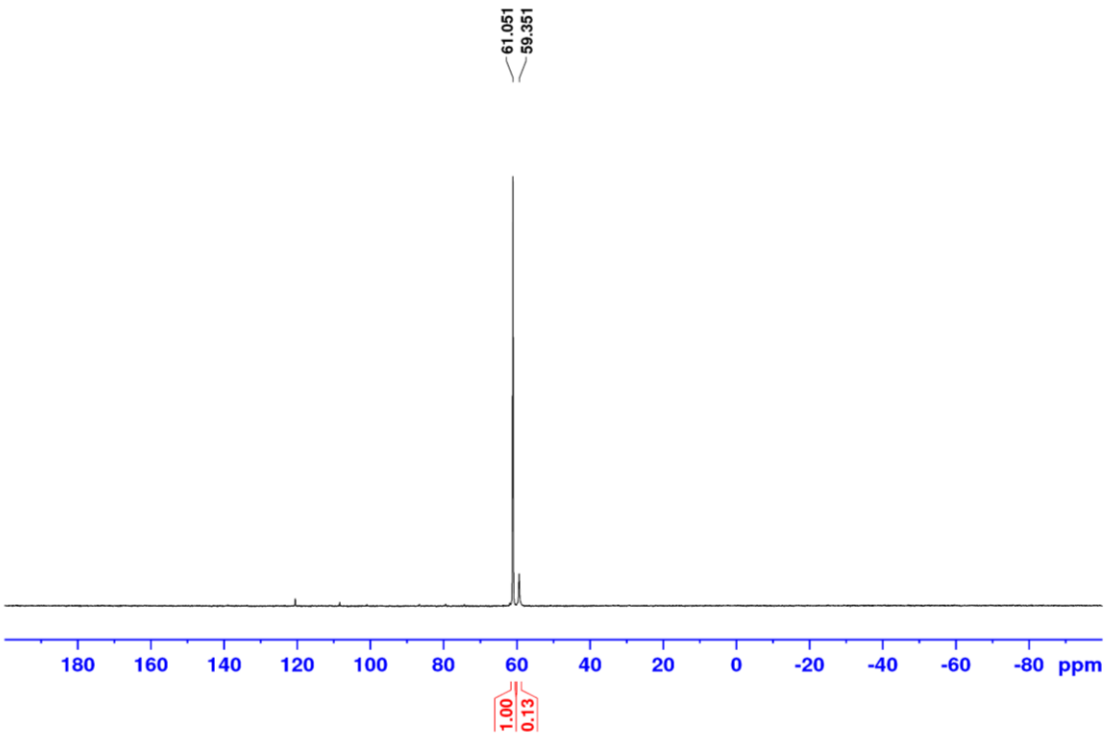


**Figure A222:** $^{31}P$ NMR spectrum (202.5 MHz, $C_6D_6$) of **Entry 5, Table 6.12**.

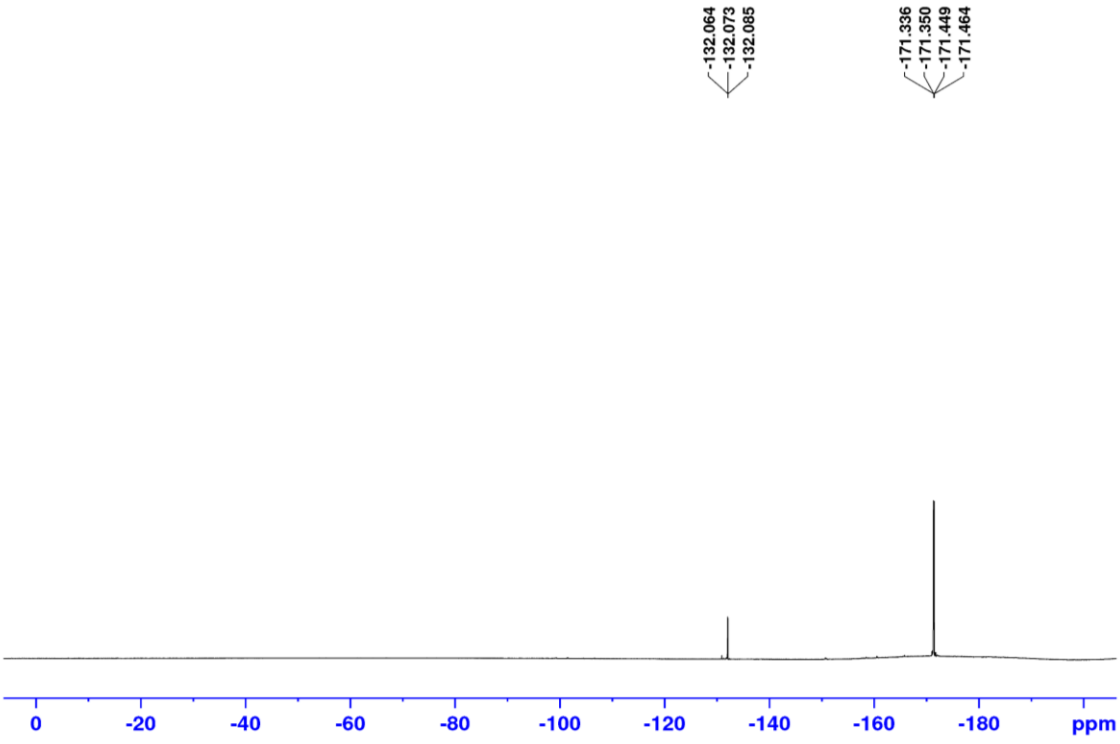


**Figure A223:** $^{19}F$ NMR spectrum (470.6 MHz, $C_6D_6$) of **Entry 5, Table 6.12**.

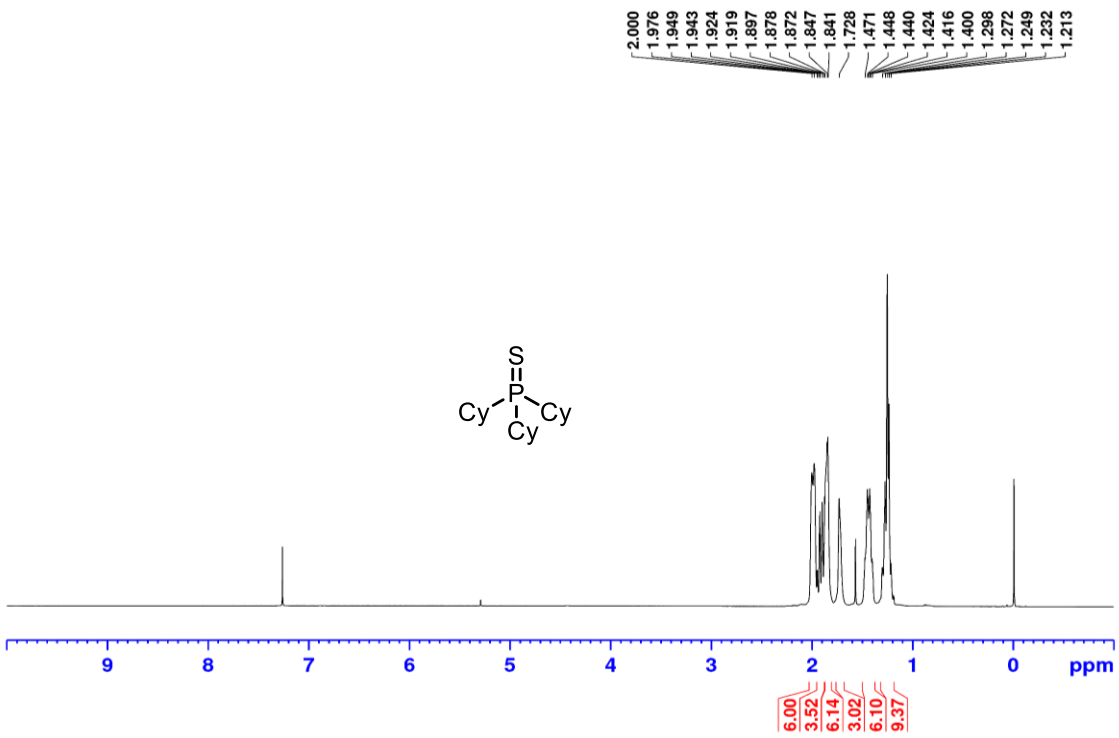


**Figure A224:** $^{1}$H NMR spectrum (500 MHz, $CDCl_3$) of isolated $SPCy_3$ **6-56** from **Entry 5, Table 6.12**.

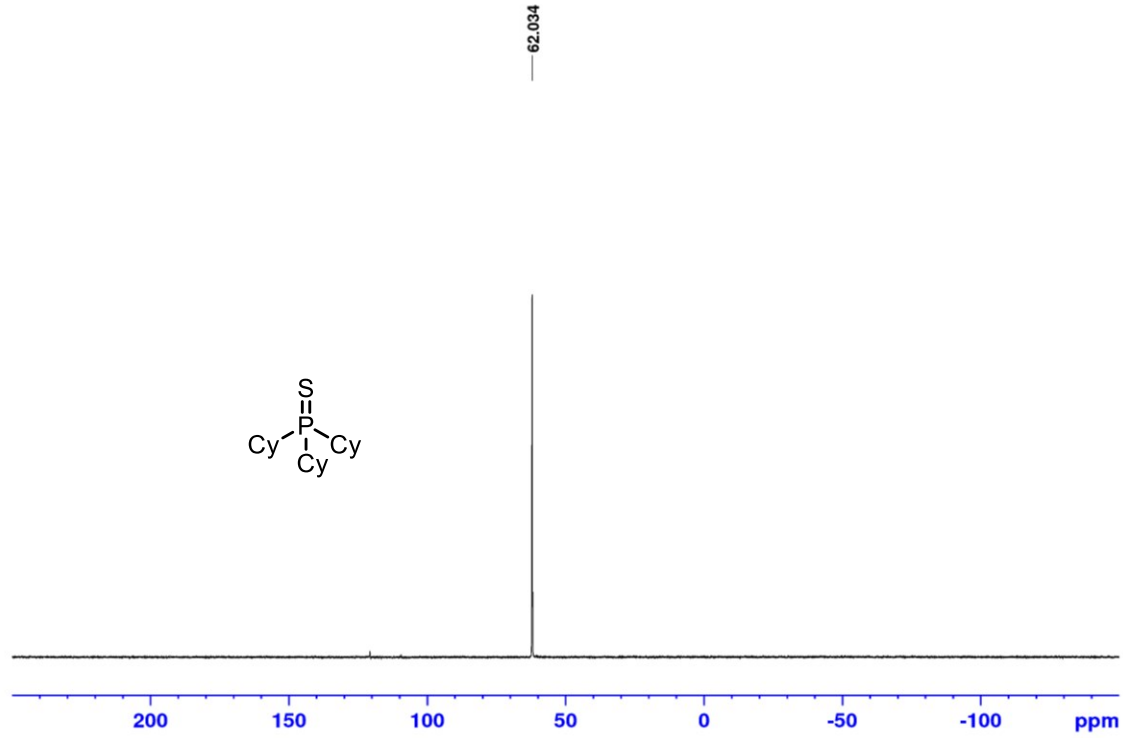


**Figure A225:** $^{31}$P NMR spectrum (202.5 MHz, $CDCl_3$) of isolated $SPCy_3$ **6-56** from **Entry 5, Table 6.12**.

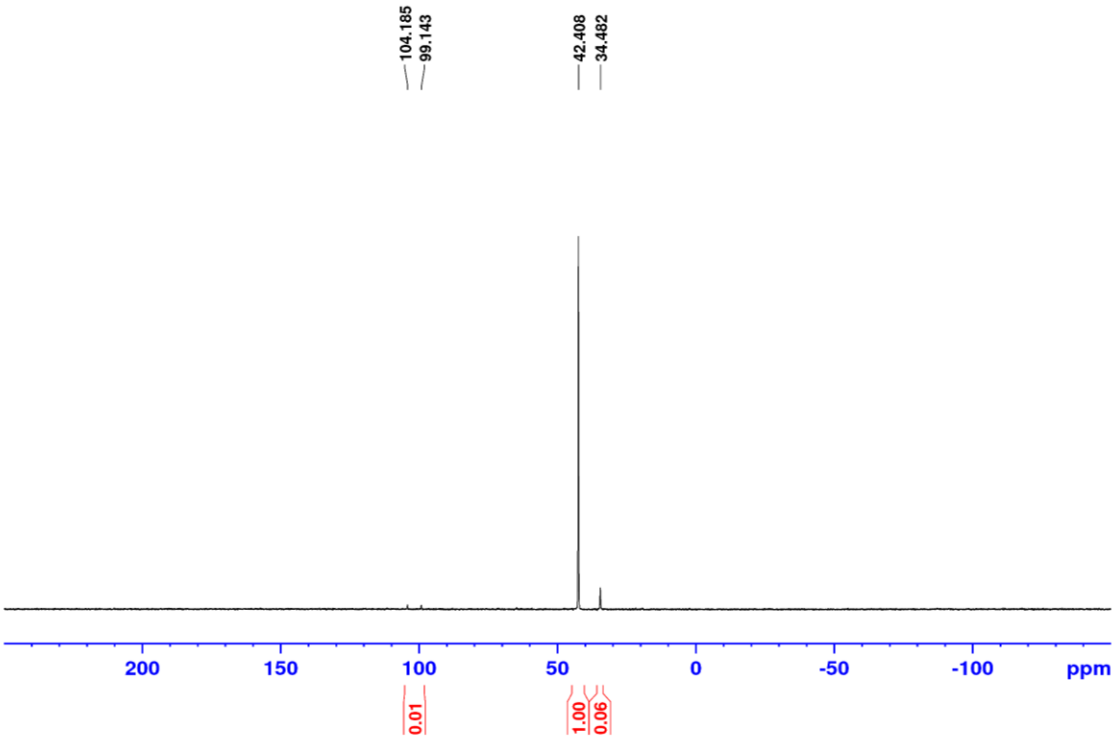


**Figure A226:** $^{31}$P NMR spectrum (202.5 MHz, $C_6D_6$) of **Entry 8, Table 6.12**.

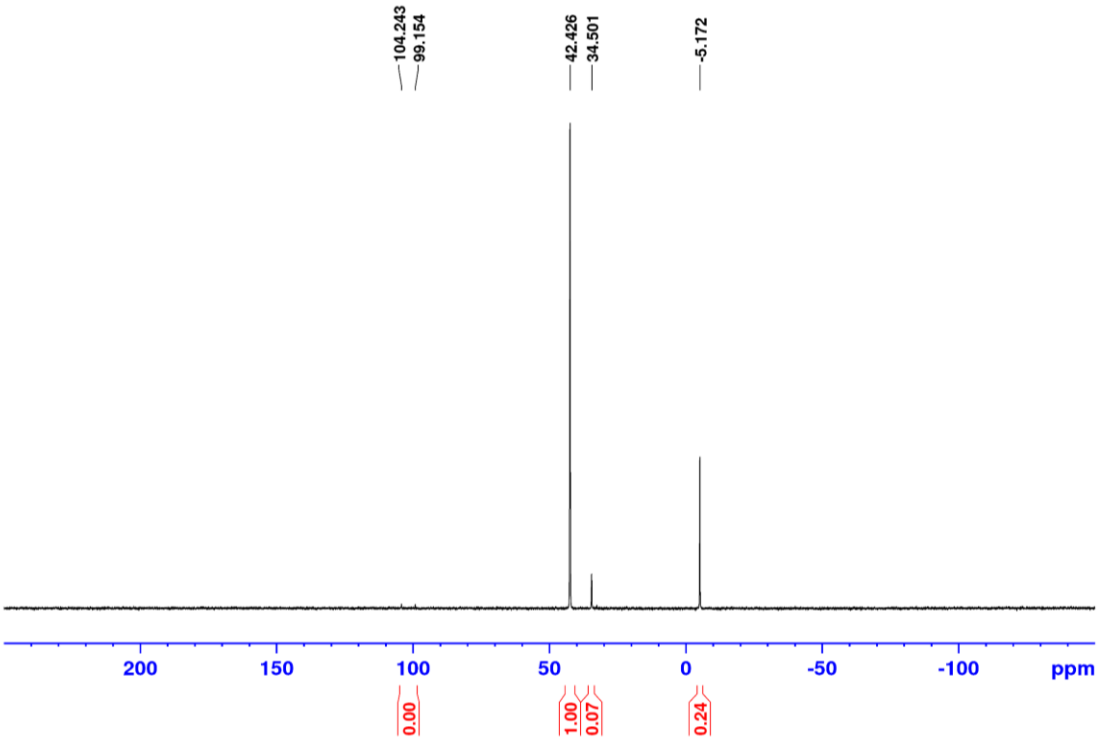


**Figure A227:** $^{31}$P NMR spectrum (202.5 MHz, $C_6D_6$) of **Entry 9, Table 6.12**.

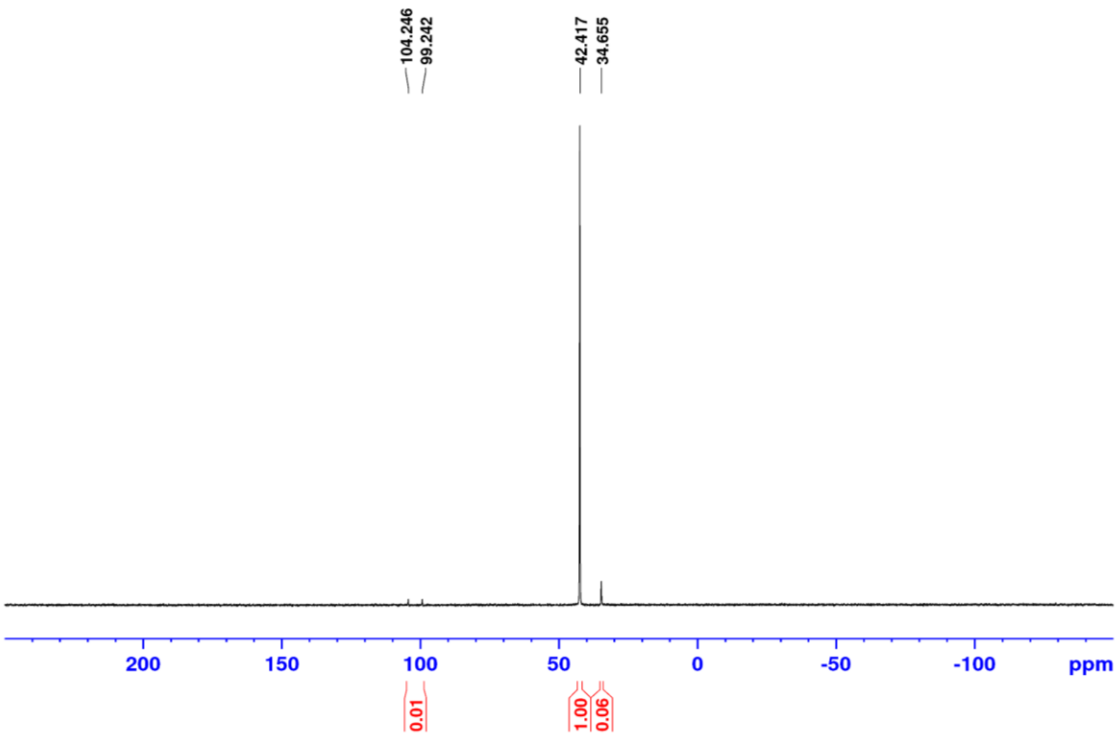


**Figure A228:** $^{31}P$ NMR spectrum (202.5 MHz, $C_6D_6$) of **Entry 10, Table 6.12**.

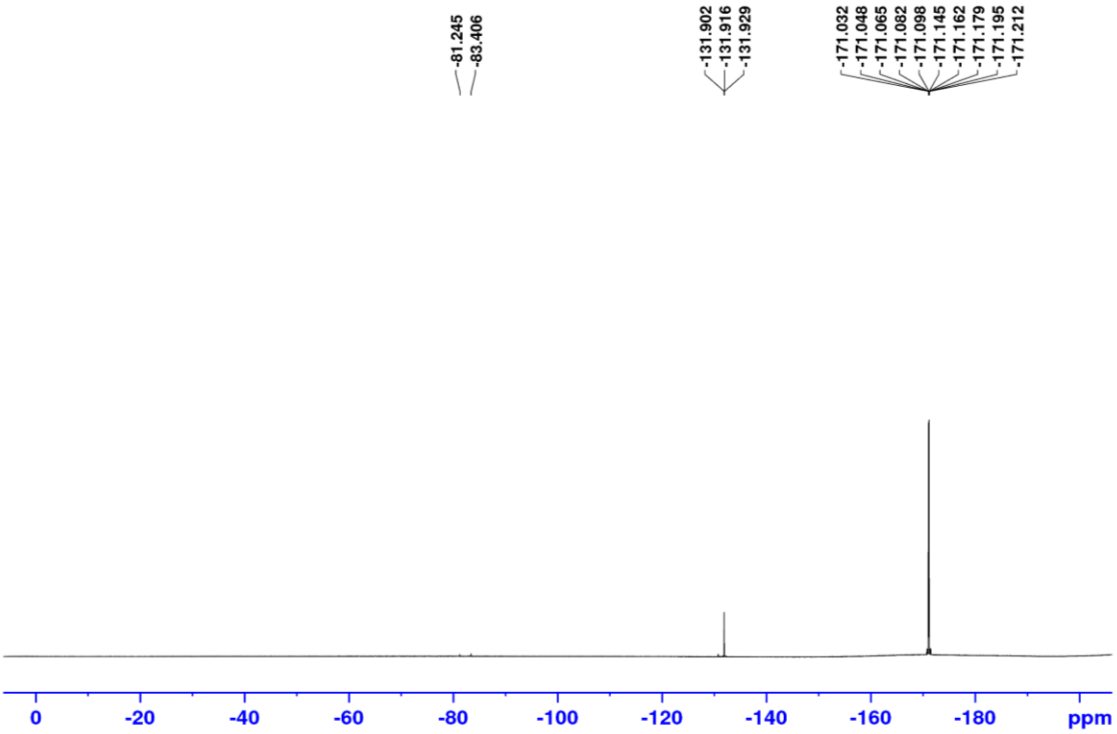


**Figure A229:** $^{19}F$ NMR spectrum (470.6 MHz, $C_6D_6$) of **Entry 10, Table 6.12**.

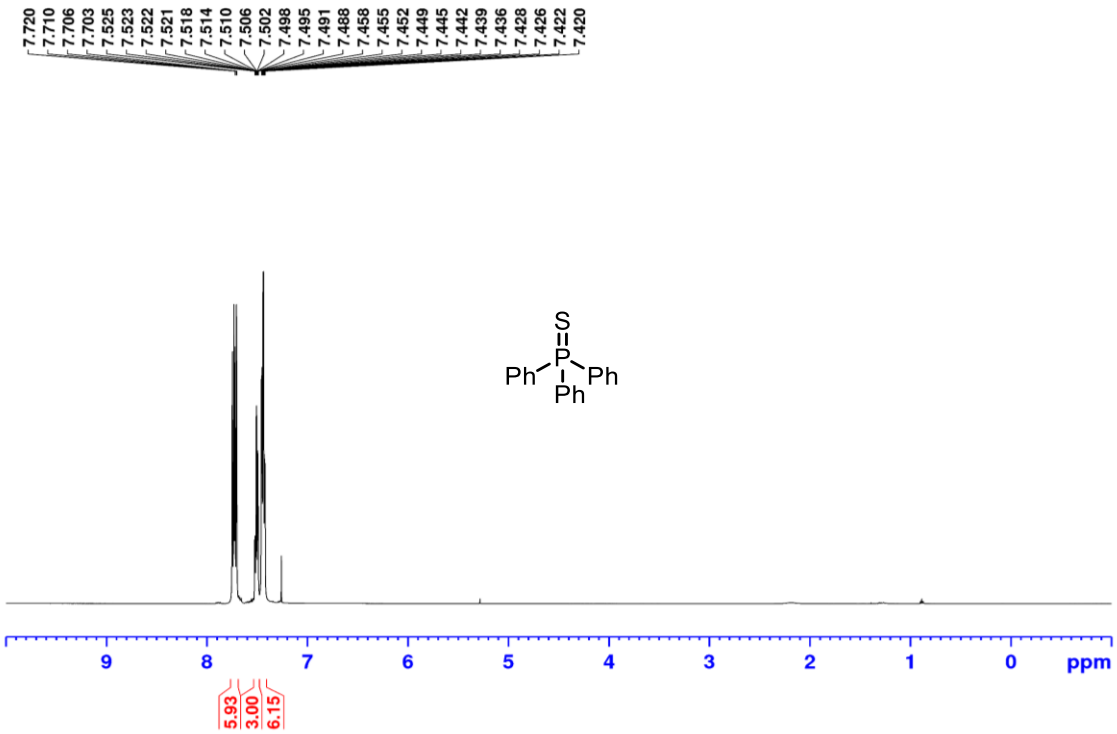


**Figure A230:** $^{1}$H NMR spectrum (500 MHz, $CDCl_3$) of isolated $SPPh_3$ **6-58** from **Entry 10, Table 6.12**.

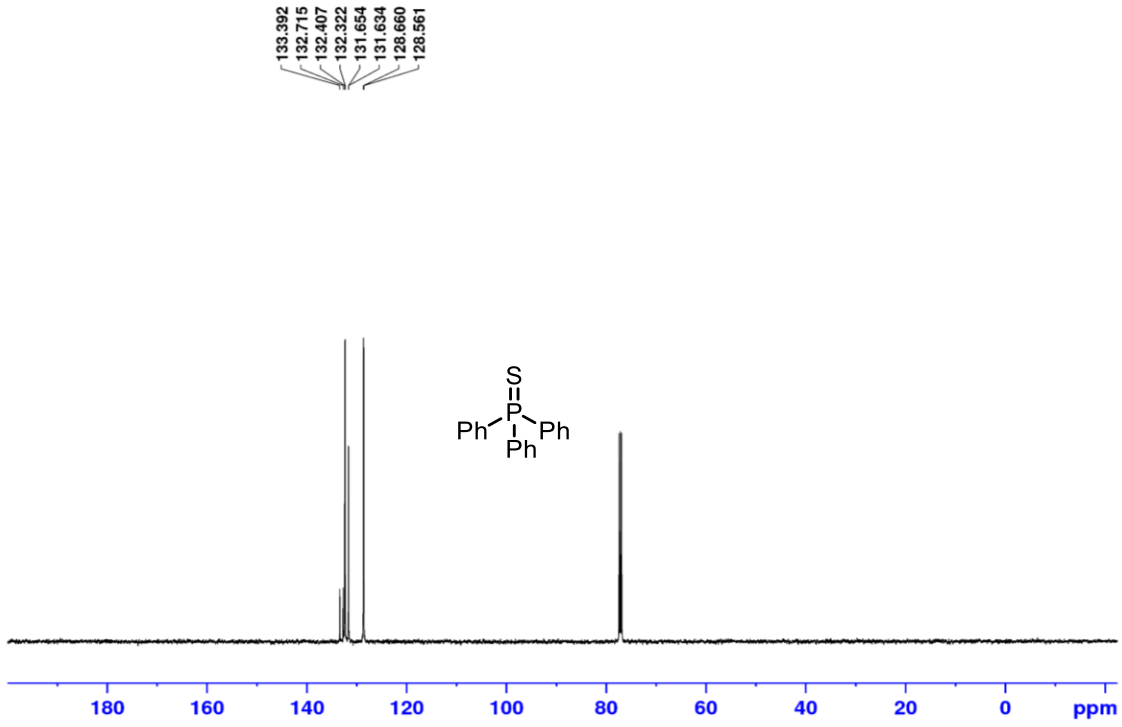


**Figure A231:** $^{13}$C $\{^{1}$H$\}$ NMR spectrum (125.8 MHz, $CDCl_3$) of isolated $SPPh_3$ **6-58** from **Entry 10, Table 6.12**.

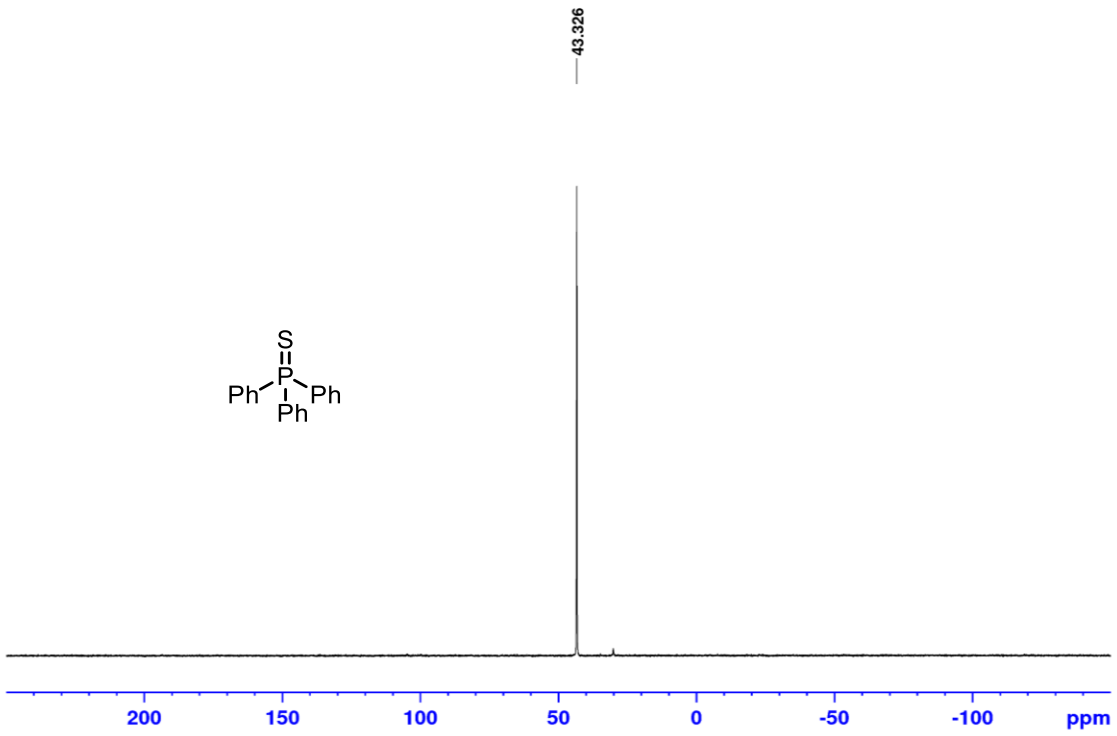


**Figure A232:** $^{31}$P NMR spectrum (202.5 MHz, $CDCl_3$) of isolated $SPPh_3$ **6-58** from **Entry 10, Table 6.12**.

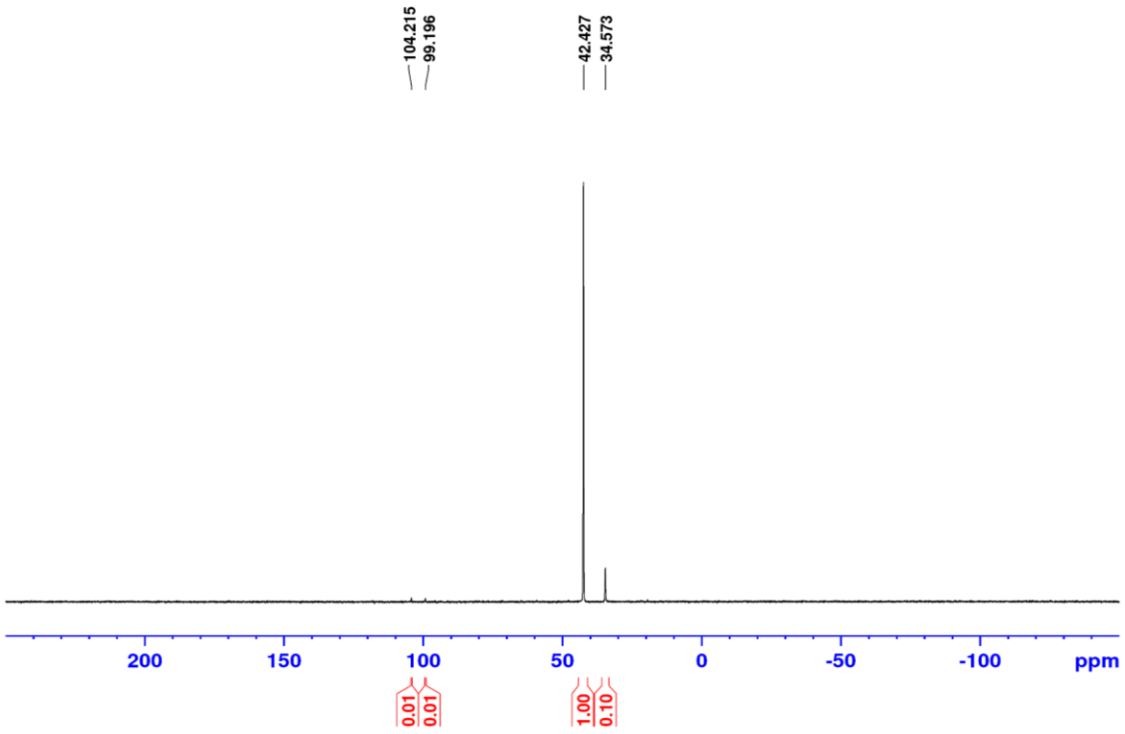


**Figure A233:** $^{31}$P NMR spectrum (202.5 MHz, $C_6D_6$) of **Entry 11, Table 6.12**.

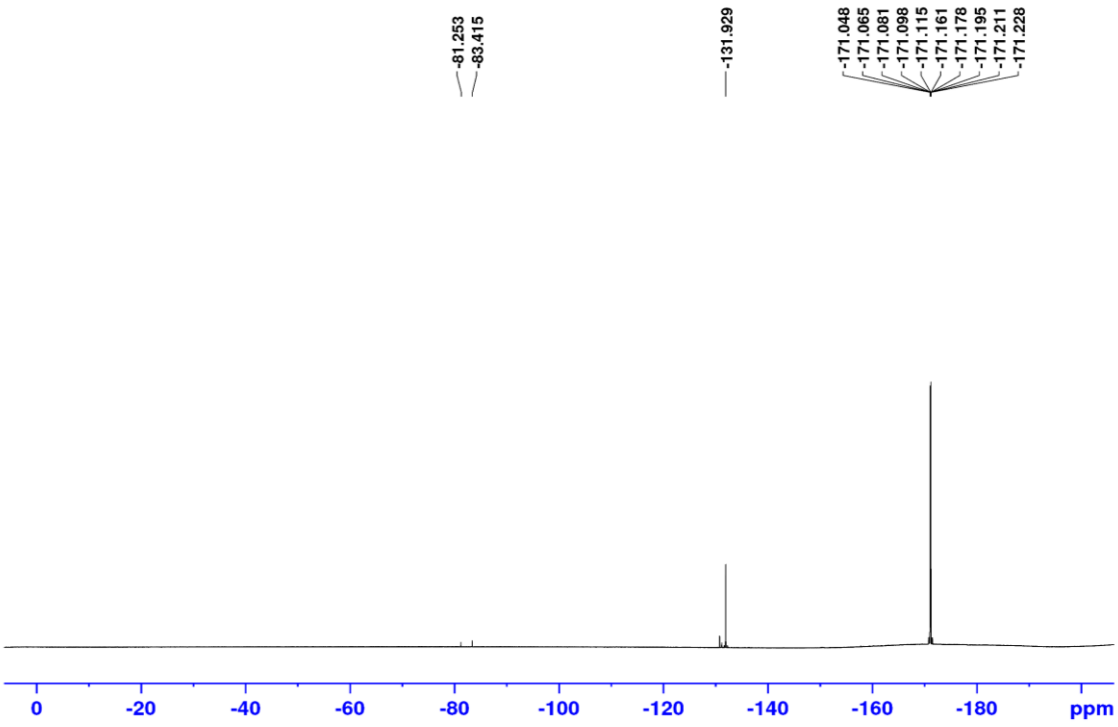


**Figure A234:** $^{19}F$ NMR spectrum (470.6 MHz, $C_6D_6$) of **Entry 11, Table 6.12**.

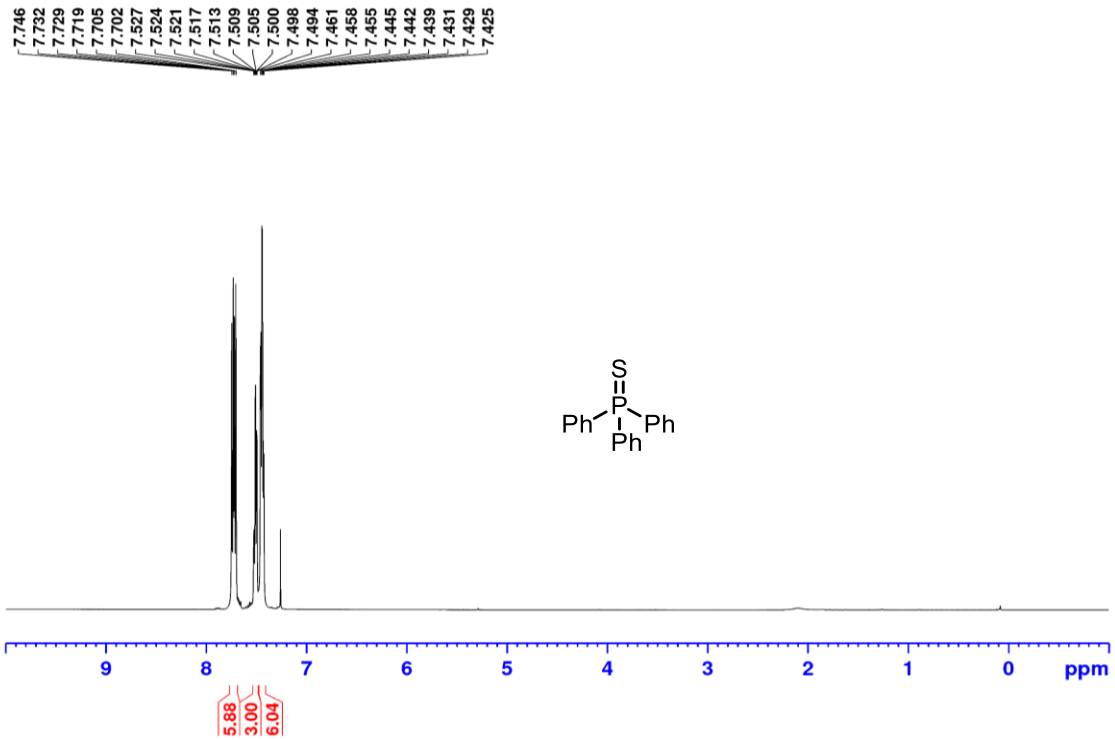


**Figure A235:** $^{1}H$ NMR spectrum (500 MHz, $CDCl_3$) of isolated $SPPh_3$ **6-58** from **Entry 11, Table 6.12**.

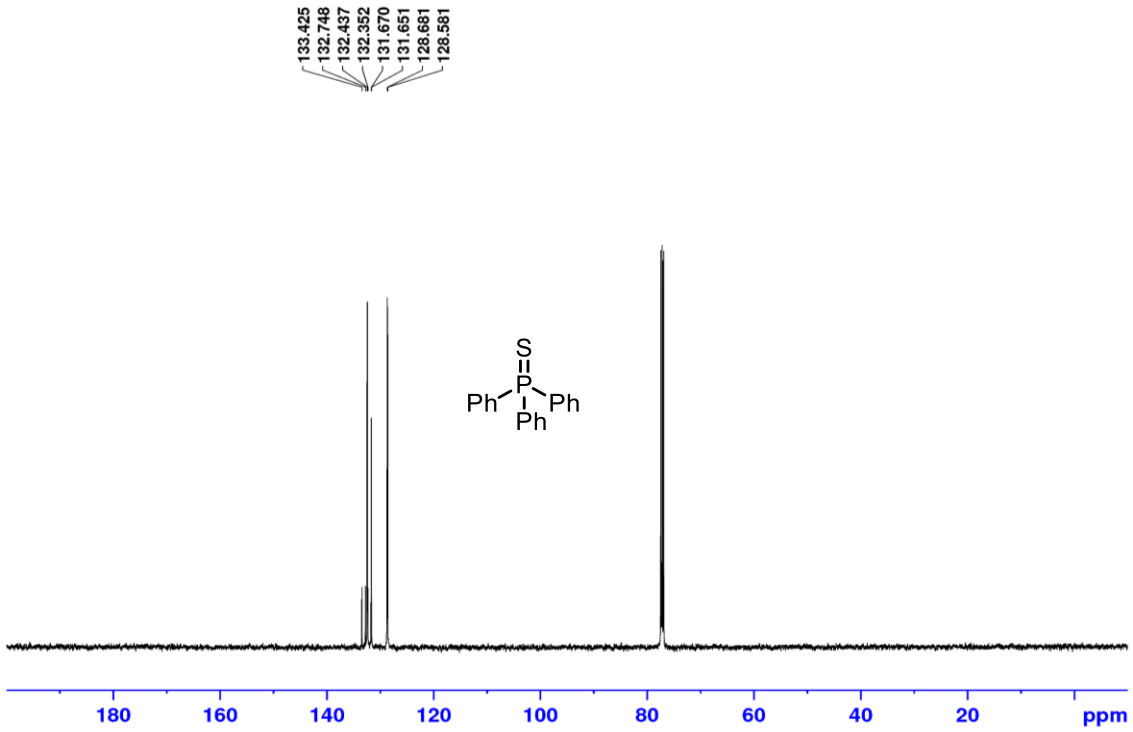


**Figure A236:** $^{13}C$ {$^{1}H$} NMR spectrum (125.8 MHz, $CDCl_3$) of isolated $SPPh_3$ **6-58** from **Entry 11, Table 6.12**.

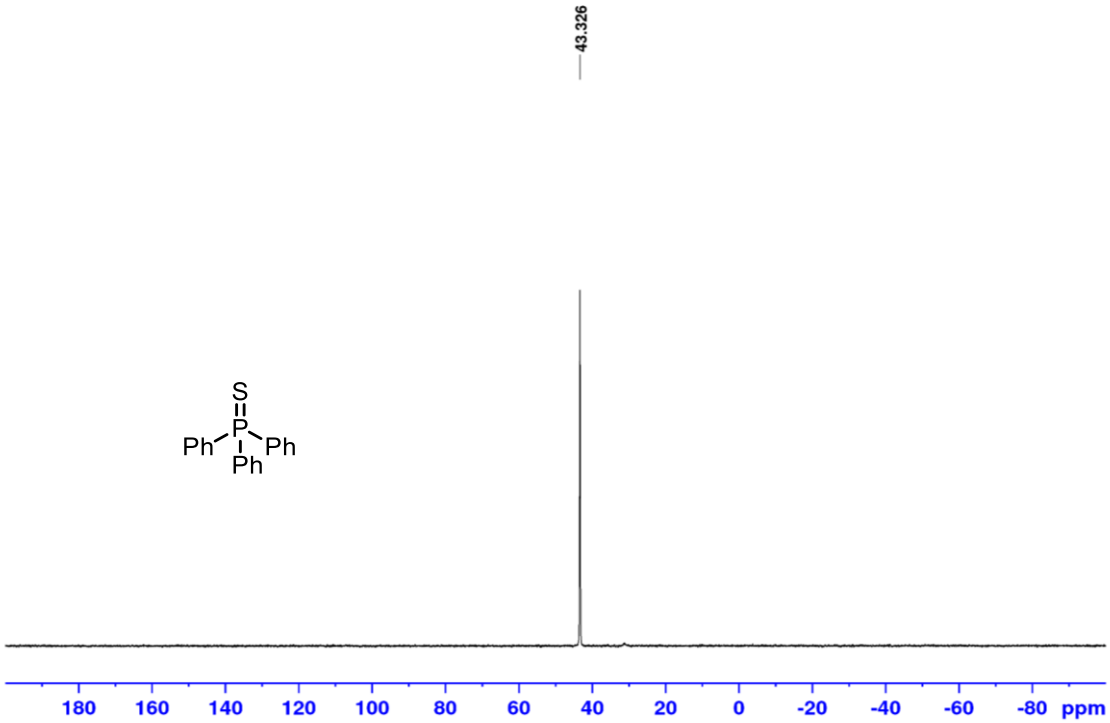


**Figure A237:** $^{31}P$ NMR spectrum (202.5 MHz, $CDCl_3$) of isolated $SPPh_3$ **6-58** from **Entry 11, Table 6.12**.

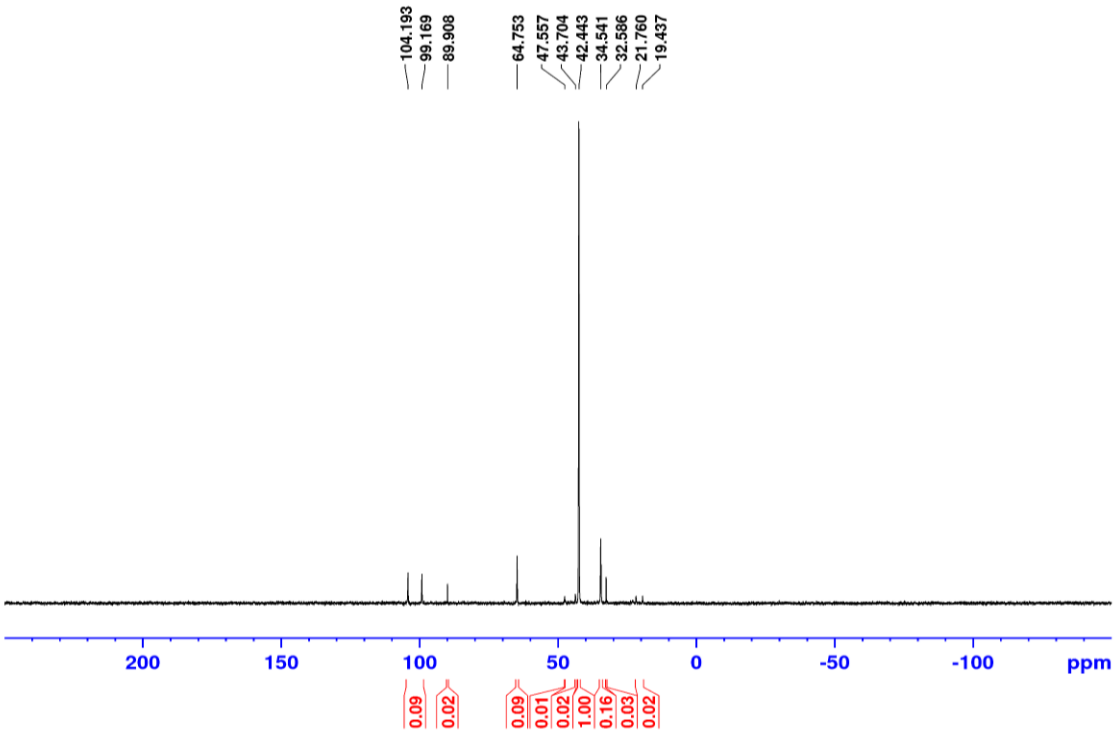


**Figure A238:** $^{31}$P NMR spectrum (202.5 MHz, $C_6D_6$) of **Entry 12, Table 6.12**.

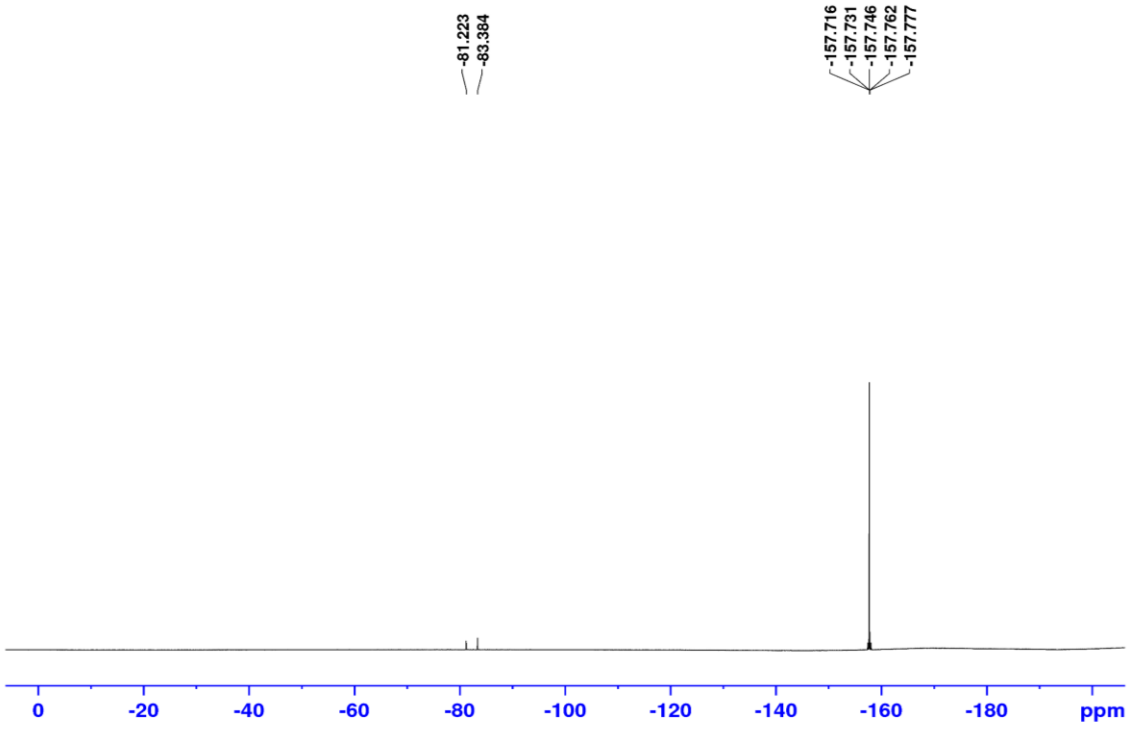


**Figure A239:** $^{19}$F NMR spectrum (470.6 MHz, $C_6D_6$) of **Entry 12, Table 6.12**.

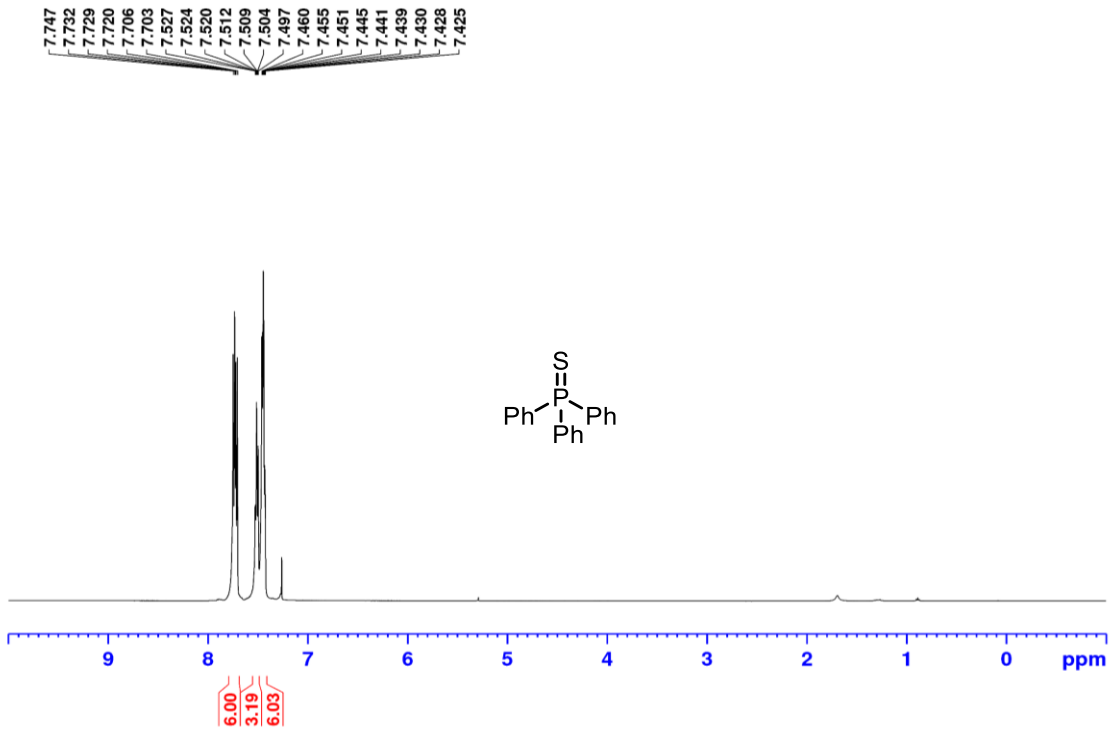


**Figure A240:** $^{1}$H NMR spectrum (500 MHz, $CDCl_3$) of isolated $SPPh_3$ **6-58** from **Entry 12, Table 6.12**.

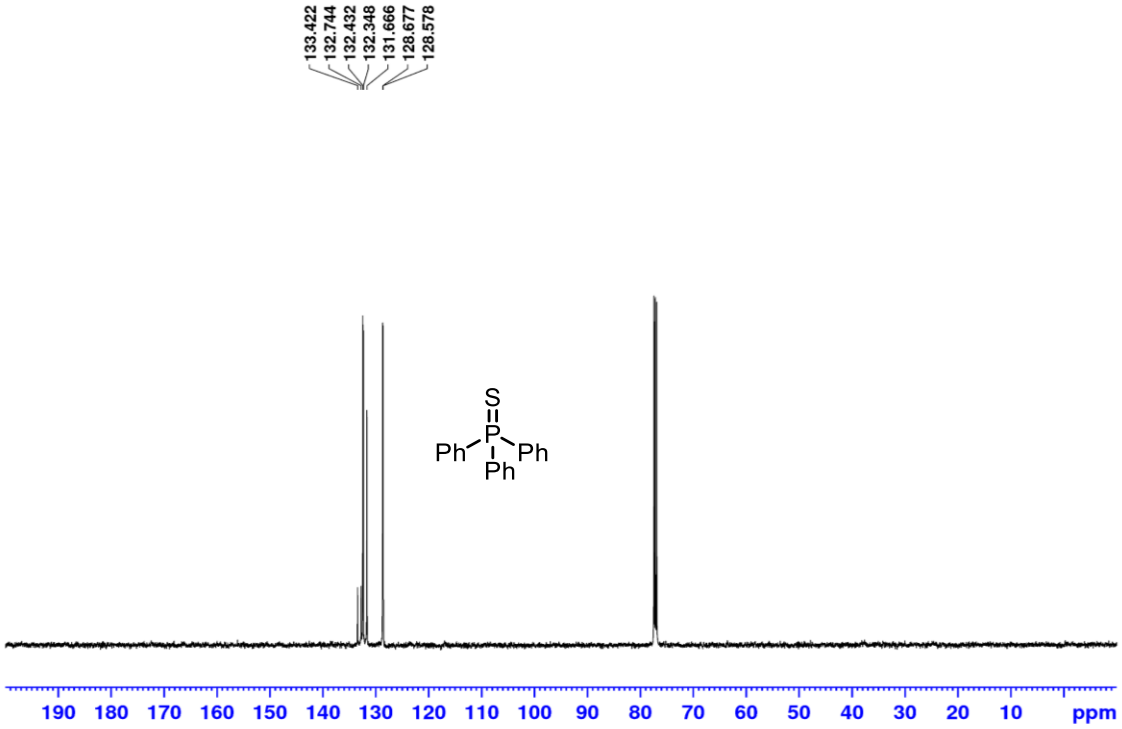


**Figure A241:** $^{13}$C $\{^{1}$H$\}$ NMR spectrum (125.8 MHz, $CDCl_3$) of isolated $SPPh_3$ **6-58** from **Entry 12, Table 6.12**.

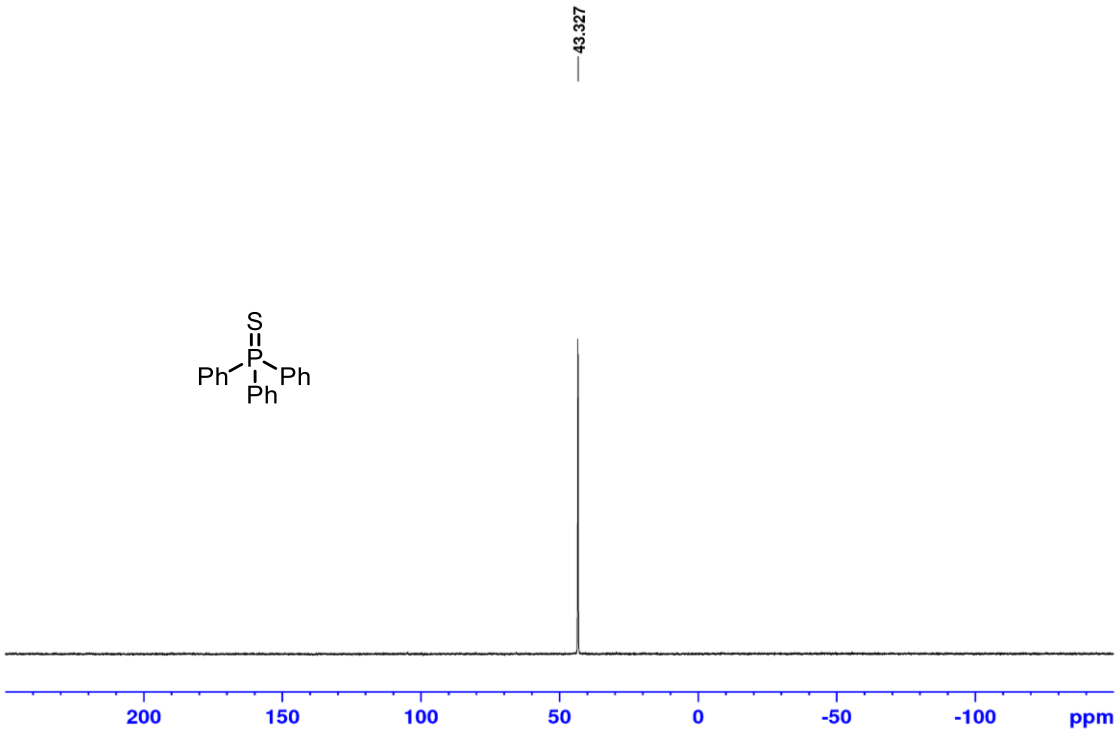


**Figure A242:** $^{31}P$ NMR spectrum (202.5 MHz, $CDCl_3$) of isolated $SPPh_3$ **6-58** from **Entry 12, Table 6.12**.

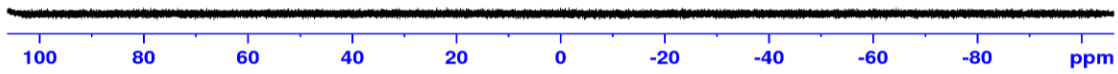


**Figure A243:** $^{19}F$ NMR spectrum (0 centre point) (470.6 MHz, $C_6D_6$) of thiophenol reaction with magnesium and dimethylchlorosilane.

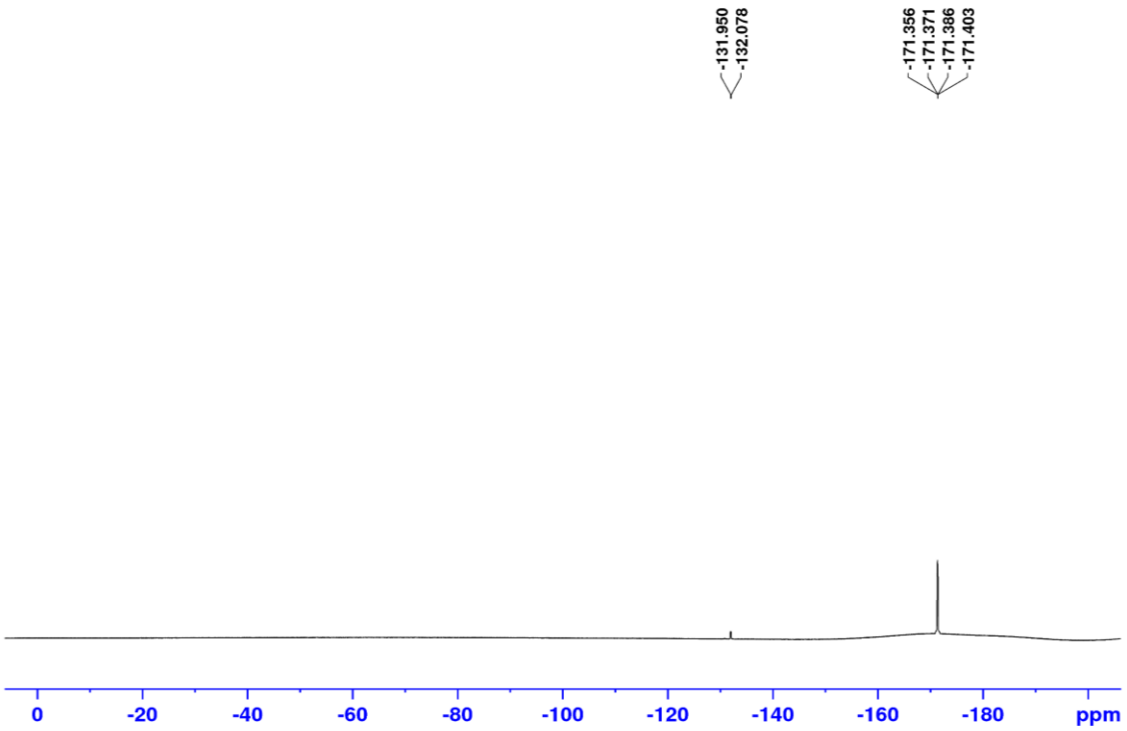


**Figure A244:** $^{19}F$ NMR spectrum (-100 centre point) (470.6 MHz, $C_6D_6$) of thiophenol reaction with magnesium and dimethylchlorosilane.

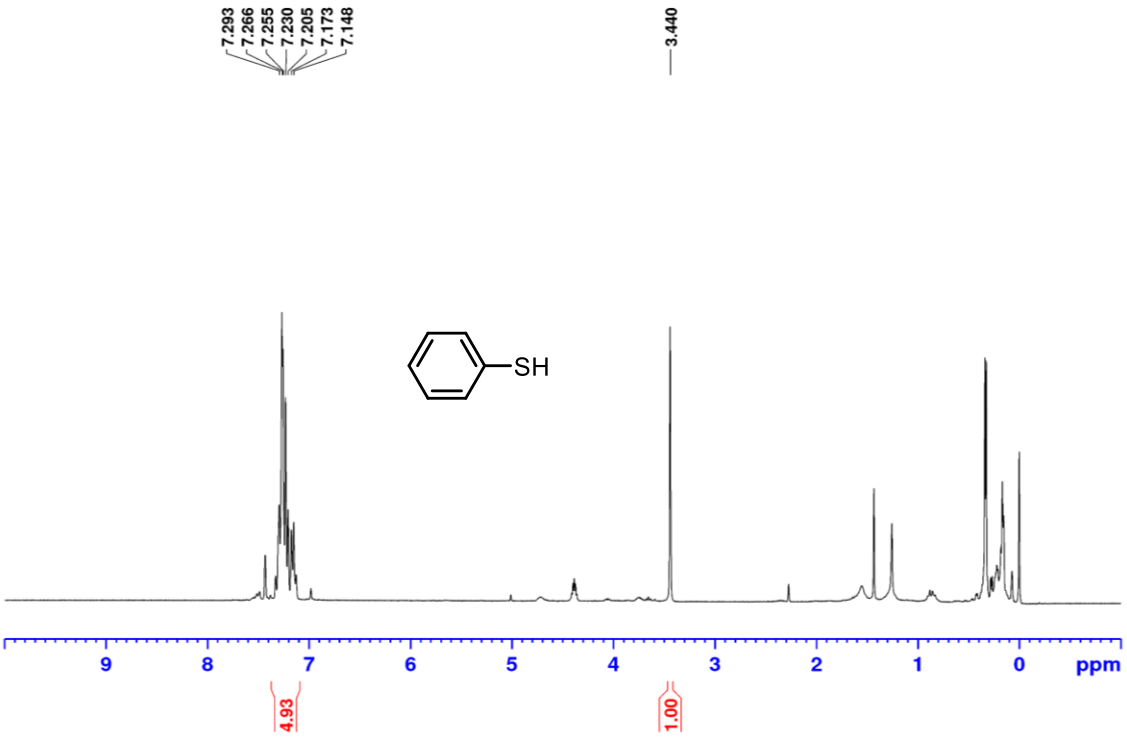


**Figure A245:** $^{1}H$ NMR spectrum (300 MHz, $CDCl_3$) of the extracted oil from the thiophenol reaction with magnesium and dimethylchlorosilane.

## Appendix F: Appendix for Chapter 7

### F1: Crystallographic Solution and Refinement Details

Crystallographic data for **7-13**. The crystal chosen was attached to the tip of a MicroLoop with Paratone-N oil. Measurements were made on a Bruker D8 VENTURE diffractometer equipped with a PHOTON III CMOS detector using monochromated Mo Kα radiation (λ = 0.71073 Å) from an Incoatec micro-focus sealed tube at 100 K [1]. The initial orientation and unit cell were indexed using a least-squares analysis of the reflections collected from a complete 360° phi-scan, 2 seconds per frame and 1° per frame. For data collection, a strategy was calculated to maximize data completeness and multiplicity, in a reasonable amount of time, and then implemented using the Bruker Apex 3 software suite [1]. The crystal to detector distance was set to 4.0 cm. Cell refinement and data reduction were performed with the Bruker SAINT [2] software, which corrects for beam inhomogeneity, possible crystal decay, Lorentz and polarisation effects. A multi-scan absorption correction was applied (SADABS [3]). The structure was solved using SHELXT-2014 [4] and was refined using a full-matrix least-squares method on $F^2$ with SHELXL-2018 [4]. The non-hydrogen atoms were refined anisotropically. The hydrogen atoms bonded to carbon were included at geometrically idealized positions and were not refined. The isotropic thermal parameters of these hydrogen atoms were fixed at $1.2U_{eq}$ of the parent carbon atom or $1.5U_{eq}$ for methyl hydrogens.

Crystallographic data for **7-15**. The crystal chosen was attached to the tip of a MicroLoop with Paratone-N oil. Measurements were made on a Bruker D8 VENTURE diffractometer equipped with a PHOTON III CMOS detector using monochromated Mo Kα radiation (λ = 0.71073 Å) from an Incoatec micro-focus sealed tube at 100 K [1]. The initial orientation and unit cell were indexed using a least-squares analysis of the reflections collected from a

complete 360° phi-scan, 1 second per frame and 1° per frame. For data collection, a strategy was calculated to maximize data completeness and multiplicity, in a reasonable amount of time, and then implemented using the Bruker Apex 3 software suite [1]. The crystal to detector distance was set to 4 cm. Cell refinement and data reduction were performed with the Bruker SAINT [2] software, which corrects for beam inhomogeneity, possible crystal decay, Lorentz and polarisation effects. A multi-scan absorption correction was applied (SADABS [3]). The structure was solved using SHELXT-2014 [4] and was refined using a full-matrix least-squares method on $F^2$ with SHELXL-2018 [4]. The refinement was unremarkable. The non-hydrogen atoms were refined anisotropically. The hydrogen atoms bonded to carbon were included at geometrically idealized positions and were not refined. The isotropic thermal parameters of these hydrogen atoms were fixed at $1.2U_{eq}$ of the parent carbon atom or $1.5U_{eq}$ for methyl hydrogens.

In the final refinement, five reflections below $\sin\theta/\lambda = 0.600$ were found to be missing. These strong reflections (1 0 0, 1 1 0, 0 2 0, -1 1 1, 0 1 1) must have saturated the detector during data collection or been partially obscured by the beam stop. They were measured but removed from the data set during processing.

Crystallographic data for **7-25**. The crystal chosen was attached to the tip of a MicroLoop with Paratone-N oil. Measurements were made on a Bruker D8 VENTURE diffractometer equipped with a PHOTON III CMOS detector using monochromated Mo Kα radiation (λ = 0.71073 Å) from an Incoatec micro-focus sealed tube at 100 K [1]. The initial orientation and unit cell were indexed using a least-squares analysis of the reflections collected from a complete 360° phi-scan, 5 seconds per frame and 1° per frame. For data collection, a strategy was calculated to maximize data completeness and multiplicity, in a reasonable

amount of time, and then implemented using the Bruker Apex 3 software suite [1]. The crystal to detector distance was set to 4.0 cm. Cell refinement and data reduction were performed with the Bruker SAINT [2] software, which corrects for beam inhomogeneity, possible crystal decay, Lorentz and polarisation effects. A multi-scan absorption correction was applied (SADABS [3]). The structure was solved using SHELXT-2014 [4] and was refined using a full-matrix least-squares method on $F^2$ with SHELXL-2018 [4]. The non-hydrogen atoms were refined anisotropically. The hydrogen atoms bonded to carbon were included at geometrically idealized positions and were not refined. The isotropic thermal parameters of these hydrogen atoms were fixed at $1.2U_{eq}$ of the parent carbon atom or $1.5U_{eq}$ for methyl hydrogens.

A total of 8 reflections were omitted from the final refinement because of poor agreement between $F^2_{obs}$ and $F^2_{calc}$ (1 -2 8;  -2 4 1; 2 -4 2; 3 -6 1; -3 6 0; 1 -3 7;  3 -6 9; 1 -3 8).

The crystals were provided in a vial still containing a small amount of the recrystallization solvent. After sitting overnight, all of the remaining solvent had evaporated and the formerly colourless crystals were taking on a purple tint. I wanted to run them before they deteriorated any further. Unfortunately, the bulb on the microscope had burned out and there was no replacement immediately available. So, I chose and mounted a crystal using only my normal vision. This required my using a crystal much larger than would usually have been chosen. Somewhat surprisingly, this large crystal was not twinned and its use seemed to result in no serious ill consequences in the final results obtained.


1) APEX 3 (Bruker, 2018) Bruker AXS Inc., Madison, Wisconsin, USA.
2) SAINT (Bruker, 2016)  Bruker AXS Inc., Madison, Wisconsin, USA.
3) SADABS (Bruker, 2016)  Bruker AXS Inc., Madison, Wisconsin, USA.

4) Sheldrick, G.M. (2015) *Acta Cryst*., A71, 3-8; Sheldrick, G.M. (2015) *Acta Cryst*., C71, 3-8.

**Table A11.** Crystal data and structure refinement for **7-13**.

| | | |
|---|---|---|
| Empirical formula | $C_{20}H_{29}FeN_2P$ | |
| Formula weight | 384.27 | |
| Temperature | 100(2) K | |
| Wavelength | 0.71073 Å | |
| Crystal system | Monoclinic | |
| Space group | $P2_1/c$ | |
| Unit cell dimensions | $a$ = 13.8500(6) Å | α = 90° |
| | $b$ = 7.8513(3) Å | β = 108.116(2)° |
| | $c$ = 18.7600(8) Å | γ = 90° |
| Volume | 1938.85(14) $Å^3$ | |
| $Z$ | 4 | |
| Density (calculated) | 1.316 $Mg/m^3$ | |
| Absorption coefficient | 0.864 $mm^{-1}$ | |
| F(000) | 816 | |
| Crystal size | 0.158 x 0.152 x 0.040 $mm^3$ | |
| Theta range for data collection | 2.284 to 35.735° | |
| Index ranges | -22<=h<=22, -12<=k<=12, -30<=l<=30 | |
| Reflections collected | 170095 | |
| Independent reflections | 8999 [R(int) = 0.0456] | |
| Completeness to theta = 25.242° | 99.8 % | |
| Absorption correction | Semi-empirical from equivalents | |
| Max. and min. transmission | 0.7470 and 0.6924 | |
| Refinement method | Full-matrix least-squares on $F^2$ | |
| Data / restraints / parameters | 8999 / 0 / 223 | |
| Goodness-of-fit on $F^2$ | 1.061 | |
| Final R indices [I>2sigma(I)] | R1 = 0.0256, wR2 = 0.0625 | |
| R indices (all data) | R1 = 0.0327, wR2 = 0.0667 | |
| Extinction coefficient | n/a | |
| Largest diff. peak and hole | 0.518 and -0.500 $e.Å^{-3}$ | |

**Table A12.** Crystal data and structure refinement for **7-15**.

| | |
|---|---|
| Empirical formula | $C_{20}H_{35}N_2P$ |

| | | |
|---|---|---|
| Formula weight | 334.47 | |
| Temperature | 100(2) K | |
| Wavelength | 0.71073 Å | |
| Crystal system | Monoclinic | |
| Space group | $P2_1/c$ | |
| Unit cell dimensions | $a$ = 17.1871(9) Å | α = 90° |
| | $b$ = 18.5294(9) Å | β = 110.507(2)° |
| | $c$ = 13.0007(7) Å | γ = 90° |
| Volume | 3877.9(4) $Å^3$ | |
| $Z$ | 8 | |
| Density (calculated) | 1.146 $Mg/m^3$ | |
| Absorption coefficient | 0.145 $mm^{-1}$ | |
| F(000) | 1472 | |
| Crystal size | 0.263 x 0.233 x 0.145 $mm^3$ | |
| Theta range for data collection | 2.530 to 40.248° | |
| Index ranges | -31<=h<=31, -33<=k<=33, -23<=l<=23 | |
| Reflections collected | 369918 | |
| Independent reflections | 24399 [R(int) = 0.0615] | |
| Completeness to theta = 25.242° | 99.9 % | |
| Absorption correction | Semi-empirical from equivalents | |
| Max. and min. transmission | 0.7484 and 0.7157 | |
| Refinement method | Full-matrix least-squares on $F^2$ | |
| Data / restraints / parameters | 24399 / 0 / 427 | |
| Goodness-of-fit on $F^2$ | 1.127 | |
| Final R indices [I>2sigma(I)] | R1 = 0.0384, wR2 = 0.0952 | |
| R indices (all data) | R1 = 0.0597, wR2 = 0.1125 | |
| Extinction coefficient | n/a | |
| Largest diff. peak and hole | 0.576 and -0.514 $e.Å^{-3}$ | |

**Table A13.** Crystal data and structure refinement for **7-25**.

| | |
|---|---|
| Empirical formula | $C_{22}H_{14}F_5N$ |
| Formula weight | 387.34 |
| Temperature | 100(2) K |
| Wavelength | 0.71073 Å |
| Crystal system | Triclinic |
| Space group | $P$-1 |

| | | |
|---|---|---|
| Unit cell dimensions | $a$ = 8.7335(7) Å | α = 115.290(3)° |
| | $b$ = 10.1713(9) Å | β = 96.232(3)° |
| | $c$ = 11.7438(10) Å | γ = 107.985(3)° |
| Volume | 861.36(13) $Å^3$ | |
| $Z$ | 2 | |
| Density (calculated) | 1.493 $Mg/m^3$ | |
| Absorption coefficient | 0.125 $mm^{-1}$ | |
| F(000) | 396 | |
| Crystal size | 0.500 x 0.330 x 0.135 $mm^3$ | |
| Theta range for data collection | 1.998 to 36.403° | |
| Index ranges | -14<=h<=14, -16<=k<=16, -19<=l<=19 | |
| Reflections collected | 97181 | |
| Independent reflections | 8377 [R(int) = 0.0549] | |
| Completeness to theta = 25.242° | 99.6 % | |
| Absorption correction | Semi-empirical from equivalents | |
| Max. and min. transmission | 0.7471 and 0.6711 | |
| Refinement method | Full-matrix least-squares on $F^2$ | |
| Data / restraints / parameters | 8377 / 0 / 253 | |
| Goodness-of-fit on $F^2$ | 1.036 | |
| Final R indices [I>2sigma(I)] | R1 = 0.0526, wR2 = 0.1373 | |
| R indices (all data) | R1 = 0.0819, wR2 = 0.1565 | |
| Extinction coefficient | n/a | |
| Largest diff. peak and hole | 0.476 and -0.339 $e.Å^{-3}$ | |

## F2: NMR Spectra for Chapter 7

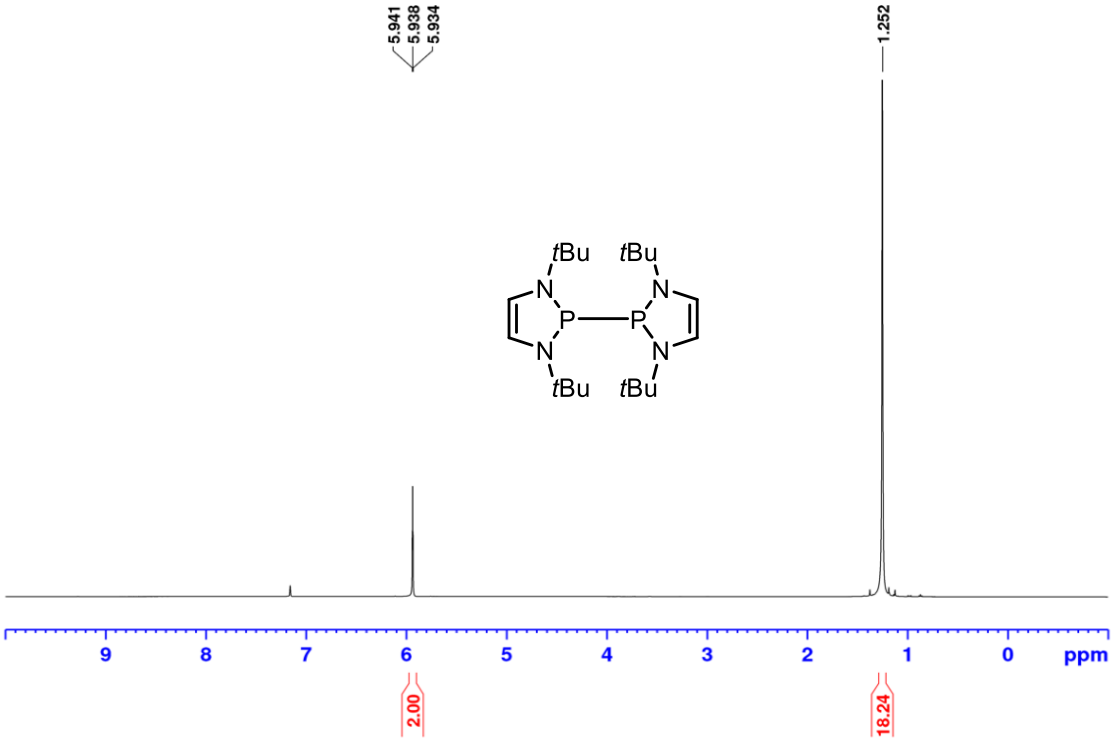


**Figure A246:** $^{1}$H NMR (500 MHz, $C_6D_6$) spectrum of diazaphospholene dimer **7-1**.

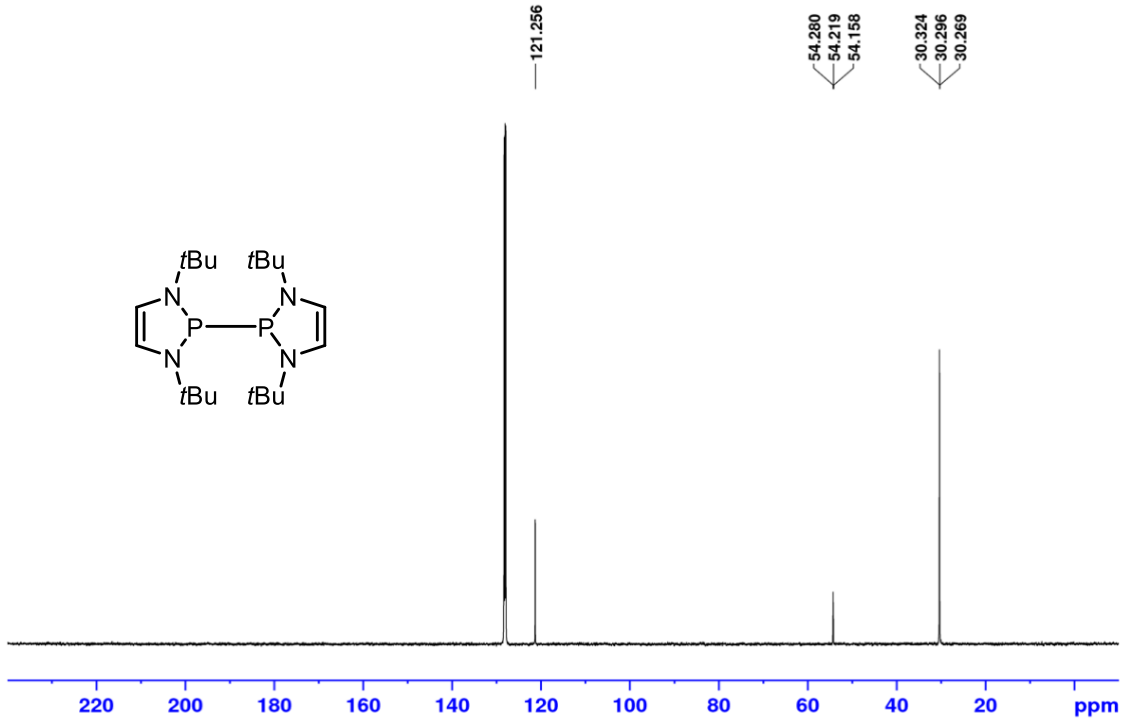


**Figure A247:** $^{13}$C {$^{1}$H} NMR (125.8 MHz, $C_6D_6$) spectrum of diazaphospholene dimer **7-1**.

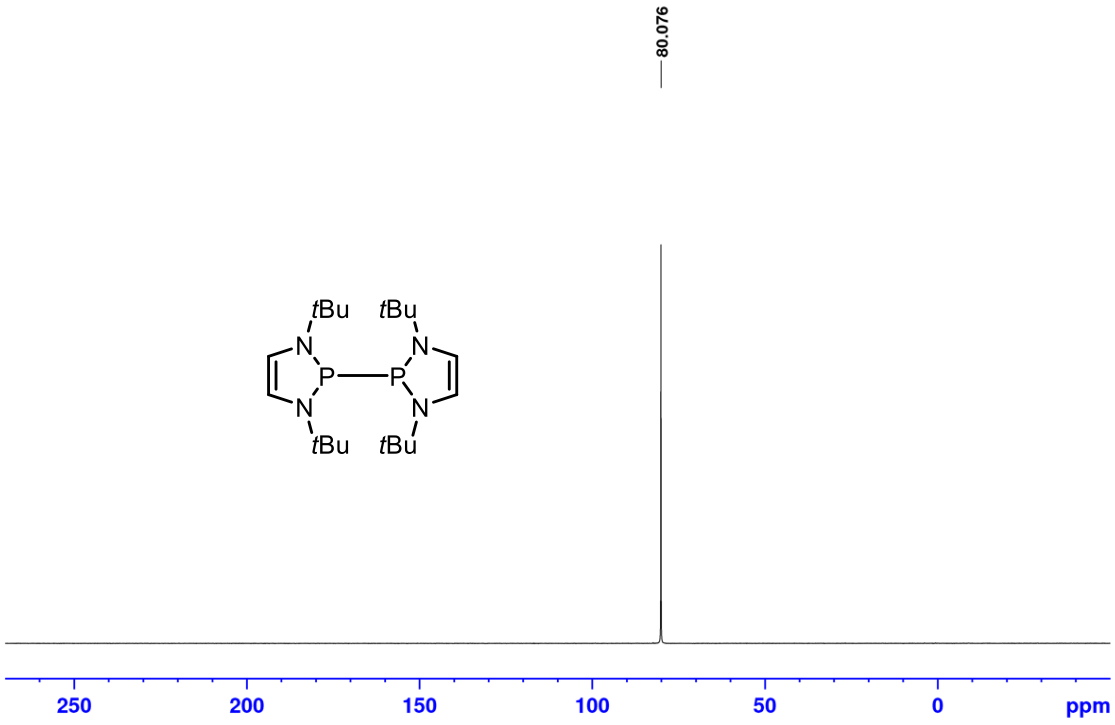


**Figure A248:** $^{31}$P NMR (202.5 MHz, $C_6D_6$) spectrum of diazaphospholene dimer **7-1**.

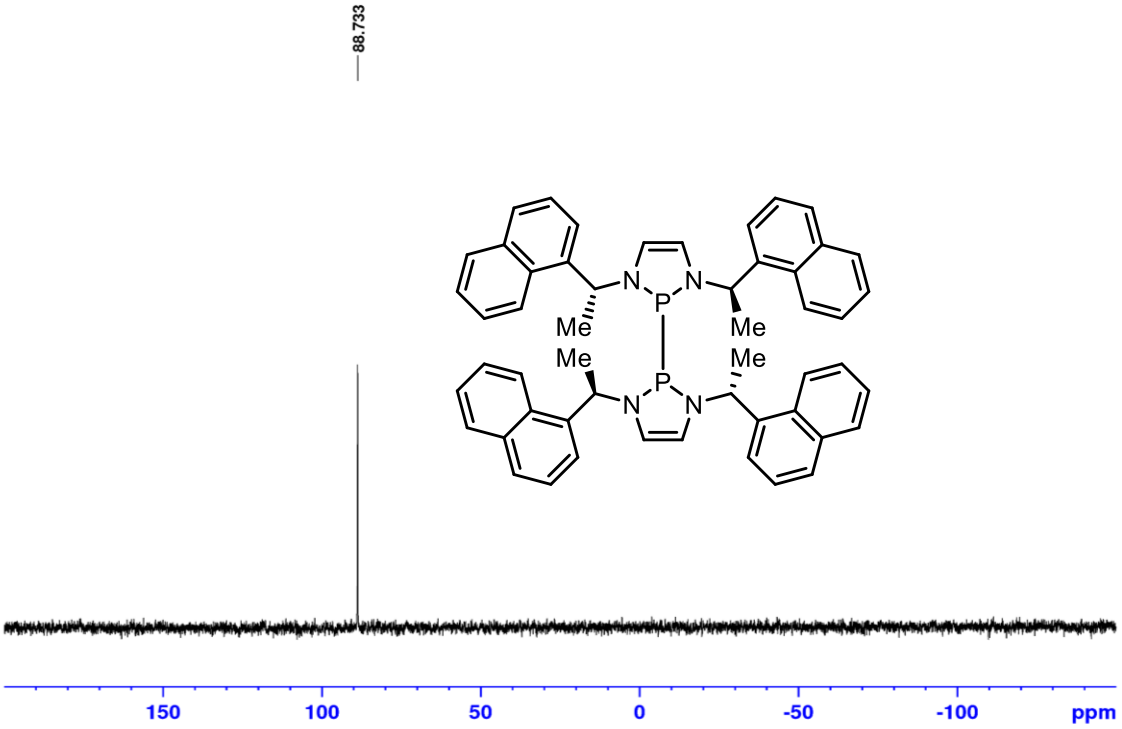


**Figure A249:** $^{31}$P NMR (202.5 MHz, $C_6D_6$) spectrum of diazaphospholene dimer **7-28**.

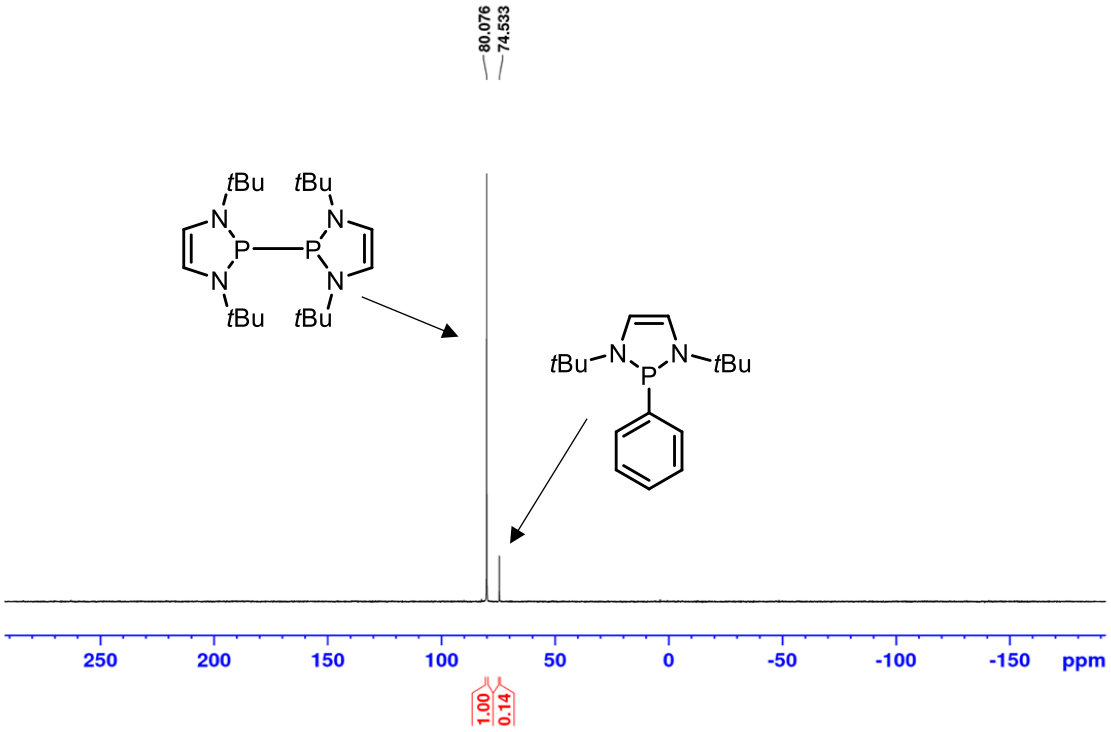


**Figure A250:** $^{31}P$ NMR (202.5 MHz, $C_6D_6$) spectrum of initial reaction of diazaphospholene dimer **7-1** with $Ph_2IPF_6$ after 10 min.

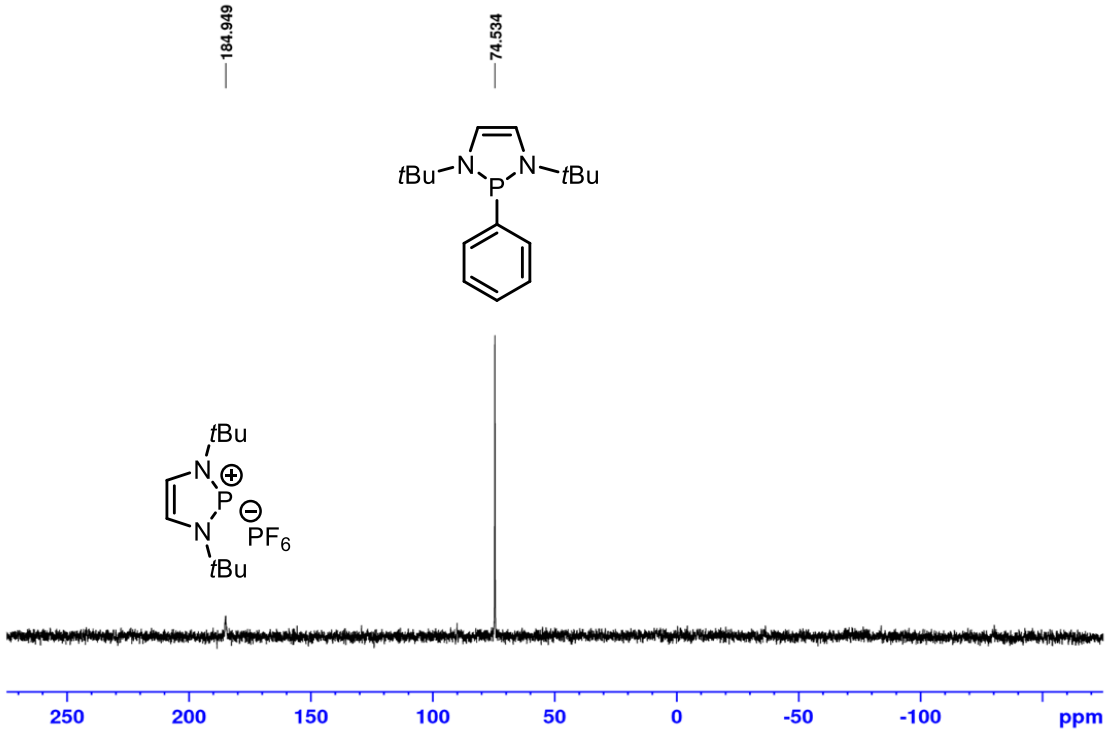


**Figure A251:** $^{31}P$ NMR (121.5 MHz, $C_6D_6$) spectrum of initial reaction of diazaphospholene dimer **7-1** with $Ph_2IPF_6$ after 4h.

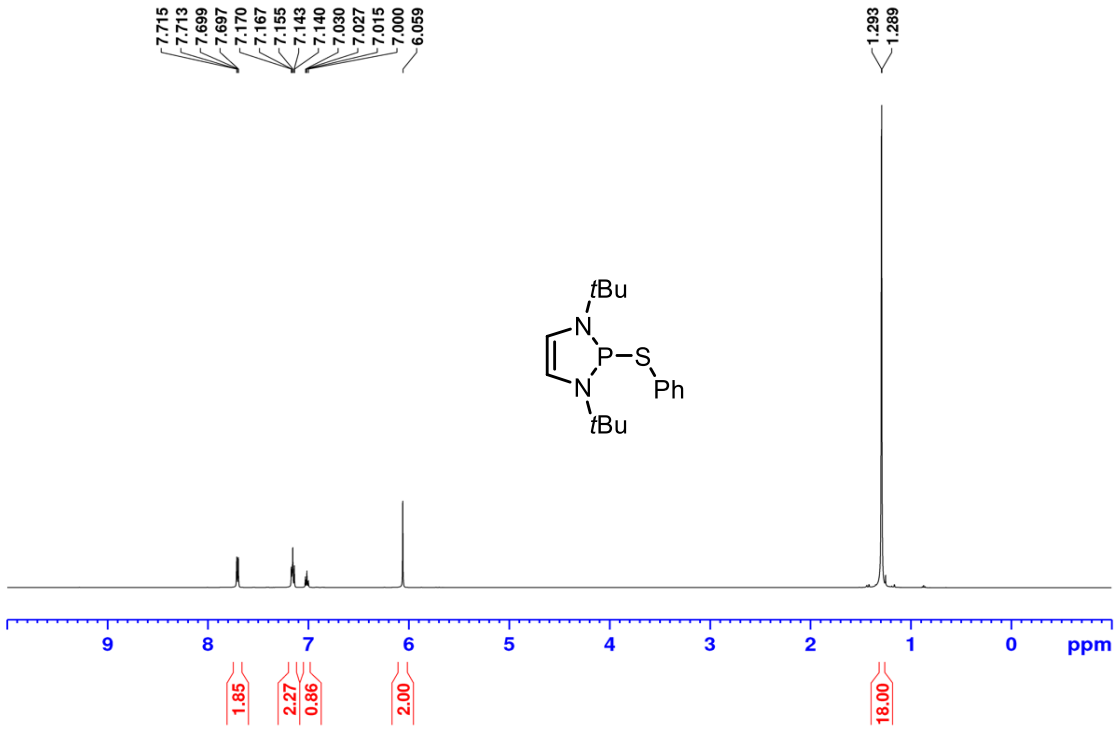


**Figure A252:** $^{1}$H NMR (500 MHz, $C_6D_6$) spectrum of *P*-thiophenylate diazaphospholene **7-23**.

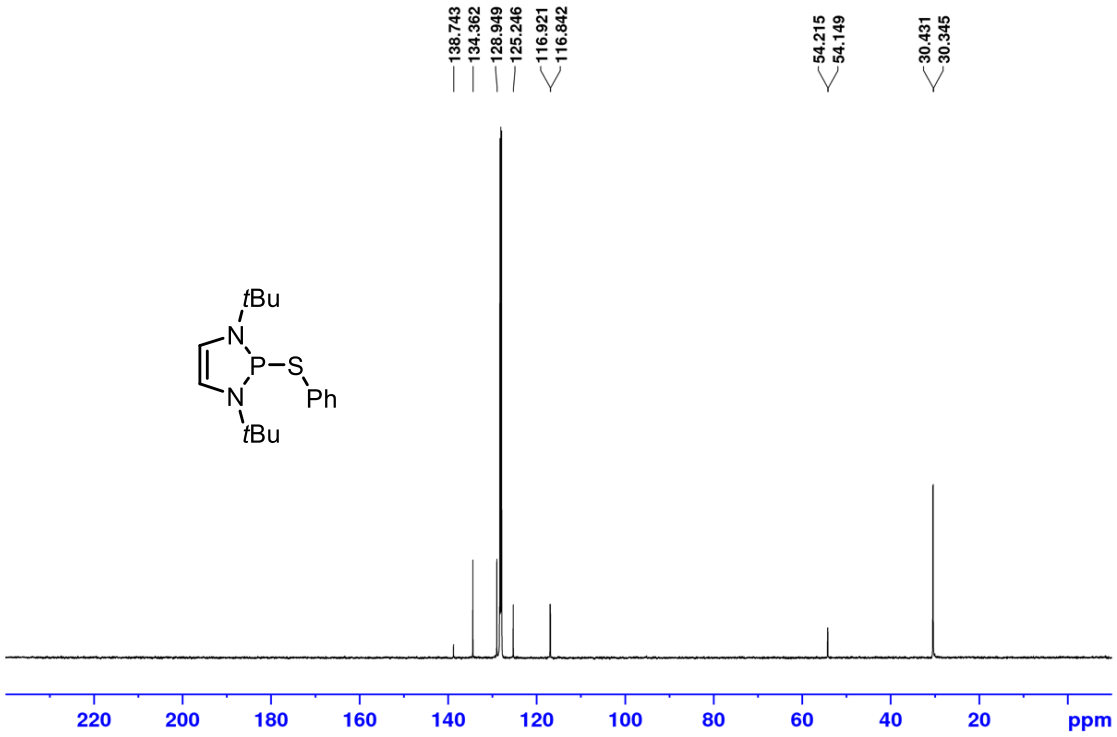


**Figure A253:** $^{13}$C {$^{1}$H} NMR (125.8 MHz, $C_6D_6$) spectrum of *P*-thiophenylate diazaphospholene **7-23**.

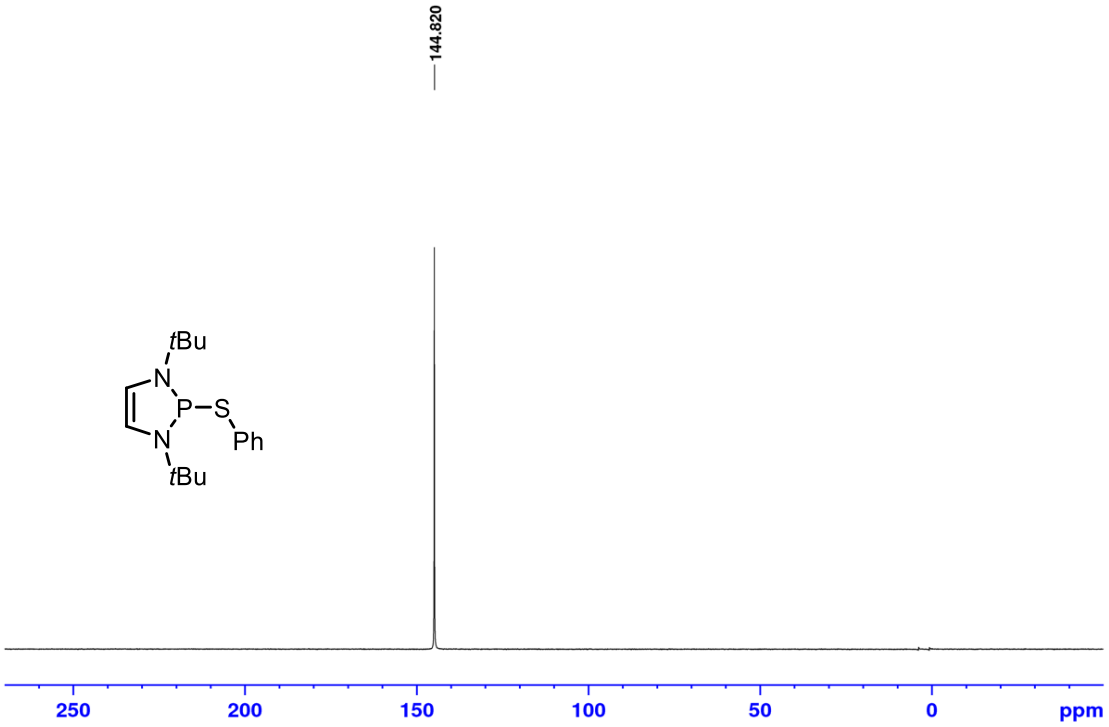


**Figure A254:** $^{31}$P NMR (202.5 MHz, $C_6D_6$) spectrum of *P*-thiophenylate diazaphospholene **7-23**.

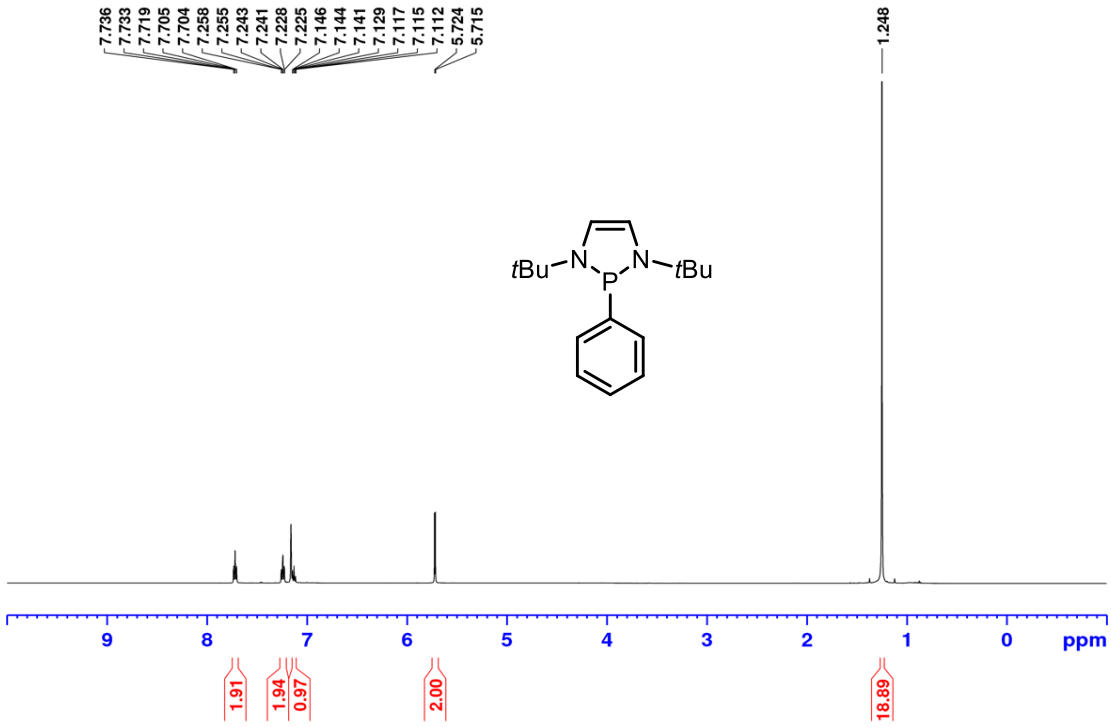


**Figure A255**: $^{1}$H NMR (500 MHz, $C_6D_6$) spectrum of *P*-phenyl diazaphospholene **7-3** from Grignard reagent.

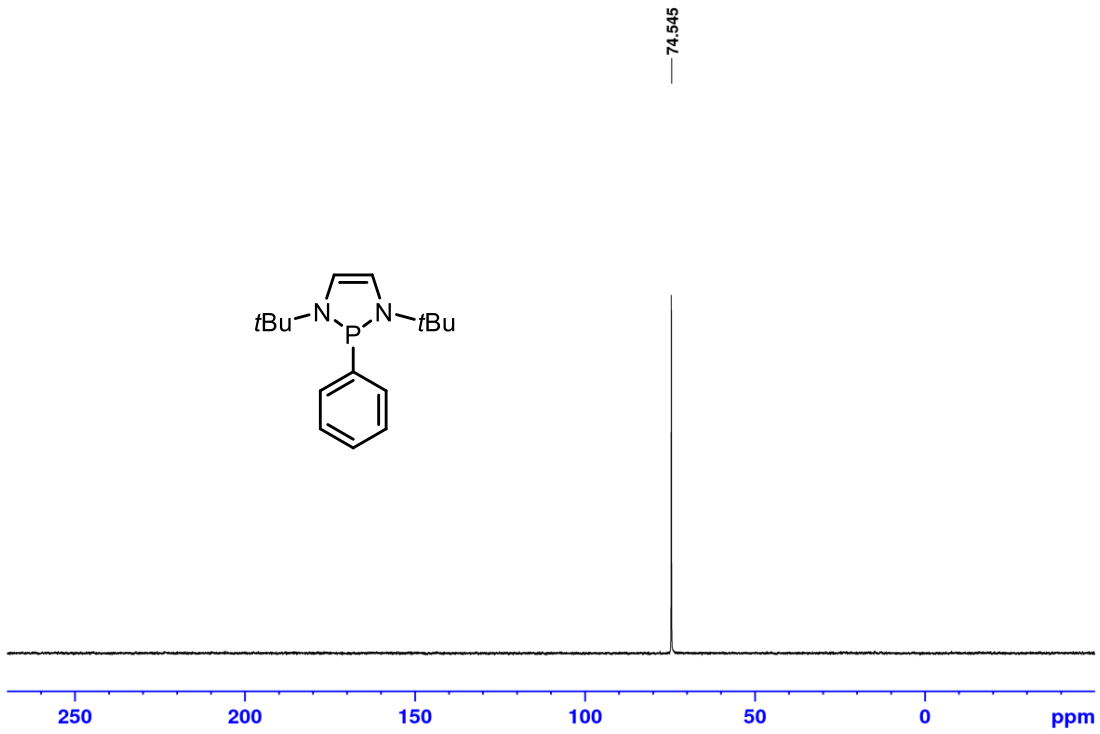


Figure A256: $^{31}$P NMR (202.5 MHz, $C_6D_6$) spectrum of *P*-phenyl diazaphospholene **7-3** from Grignard reagent.

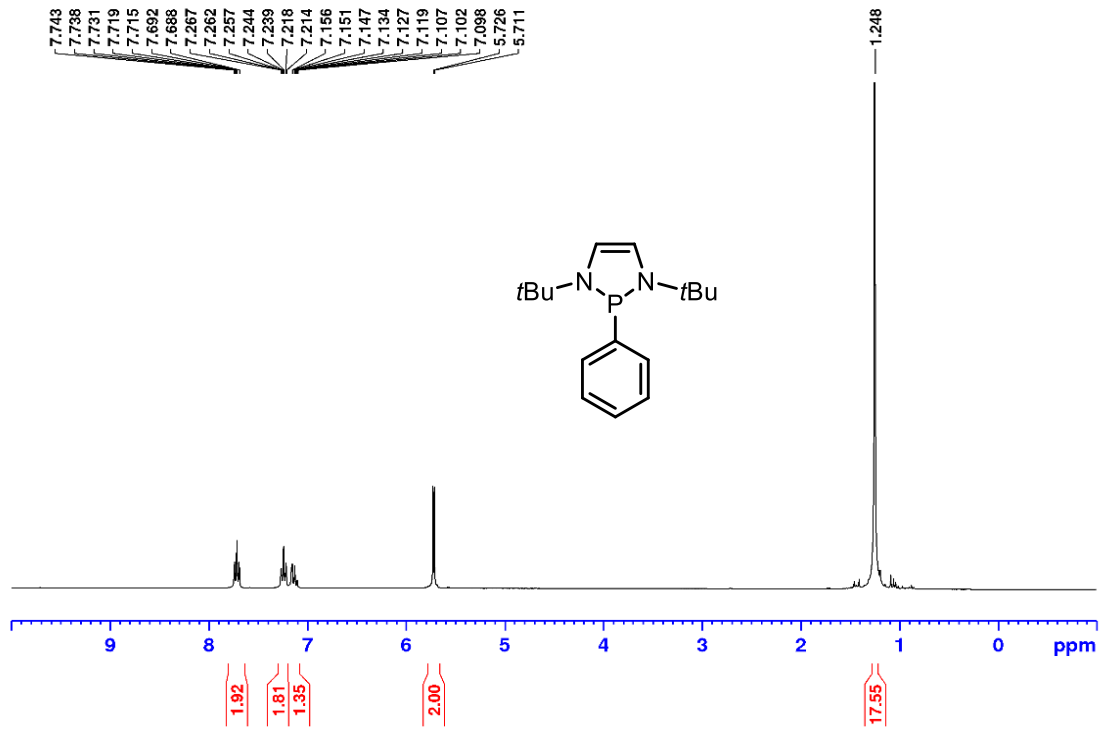


**Figure A257:** $^{1}$H NMR (300 MHz, $C_6D_6$) spectrum of *P*-phenyl diazaphospholene **7-3** from Iodobenzene.

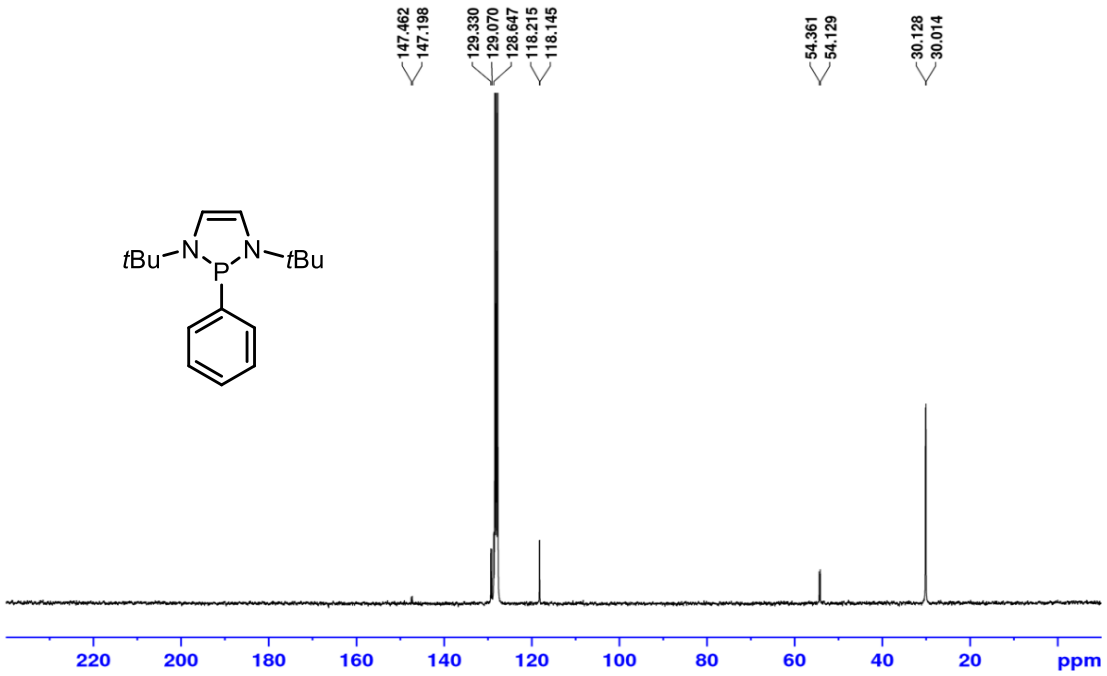


**Figure A258:** $^{13}C$ {$^{1}H$} NMR (75.5 MHz, $C_6D_6$) spectrum of *P*-phenyl diazaphospholene **7-3** from Iodobenzene.

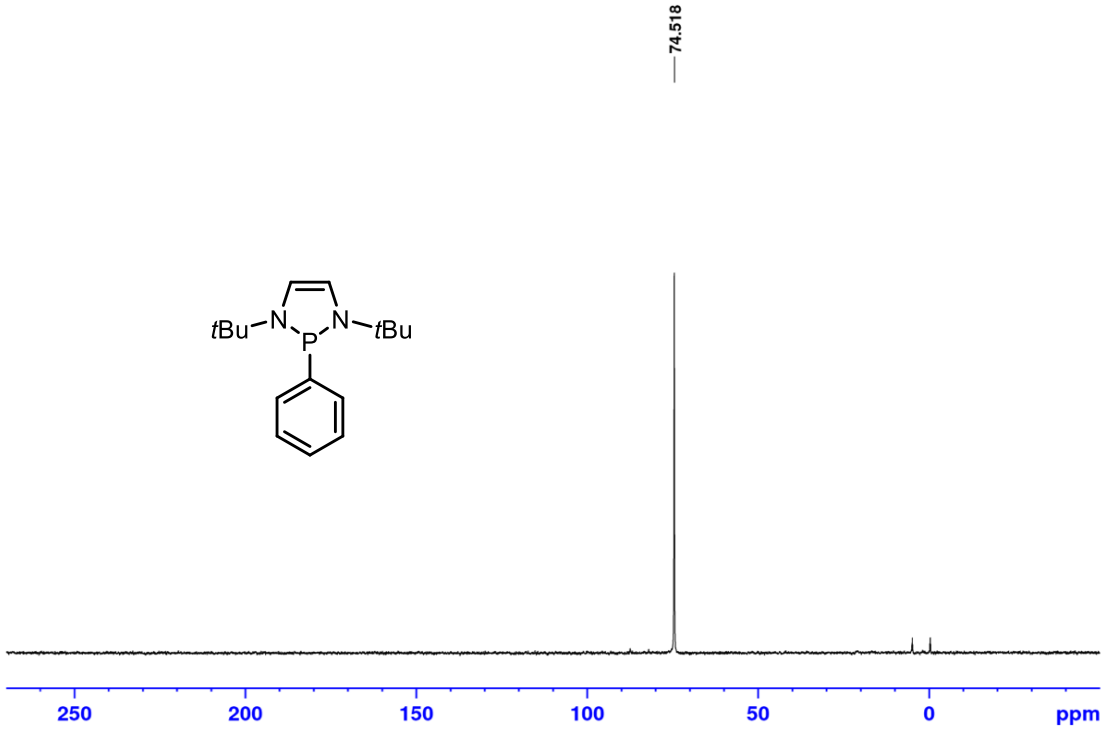


**Figure A259:** $^{31}P$ NMR (121.5 MHz, $C_6D_6$) spectrum of *P*-phenyl diazaphospholene **7-3** from Iodobenzene.

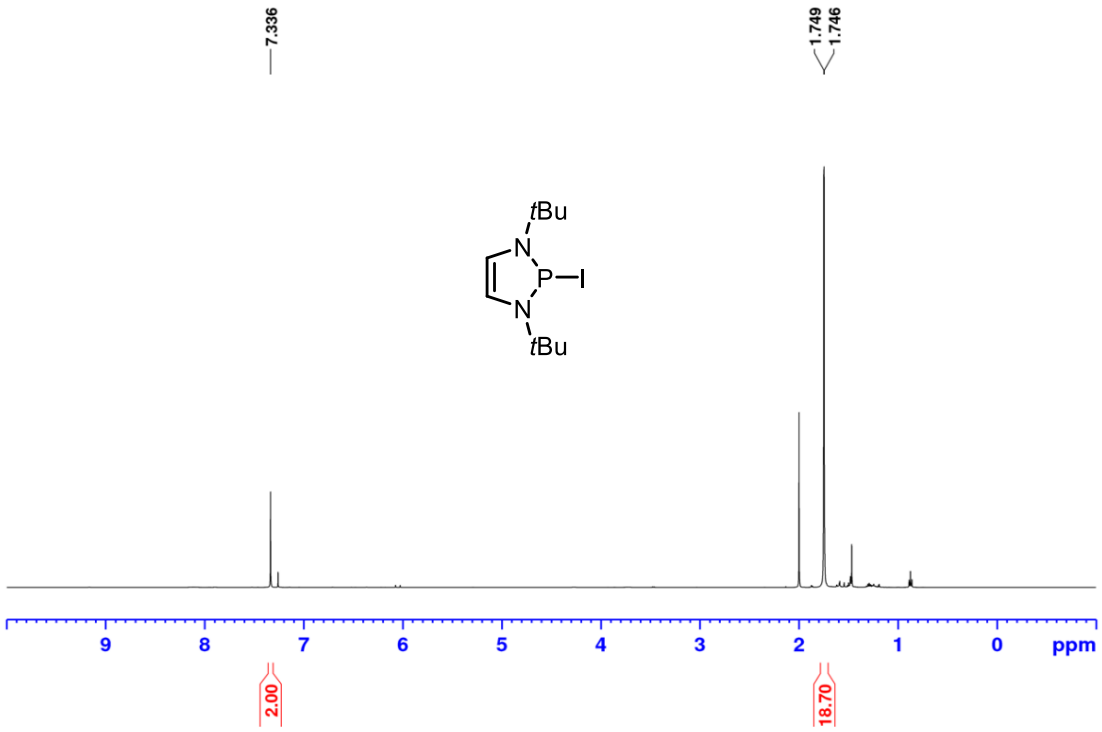


**Figure A260:** $^{1}$H NMR (500 MHz, $CDCl_3$) spectrum of diazaphospholene iodide **7-4** from Iodobenzene.

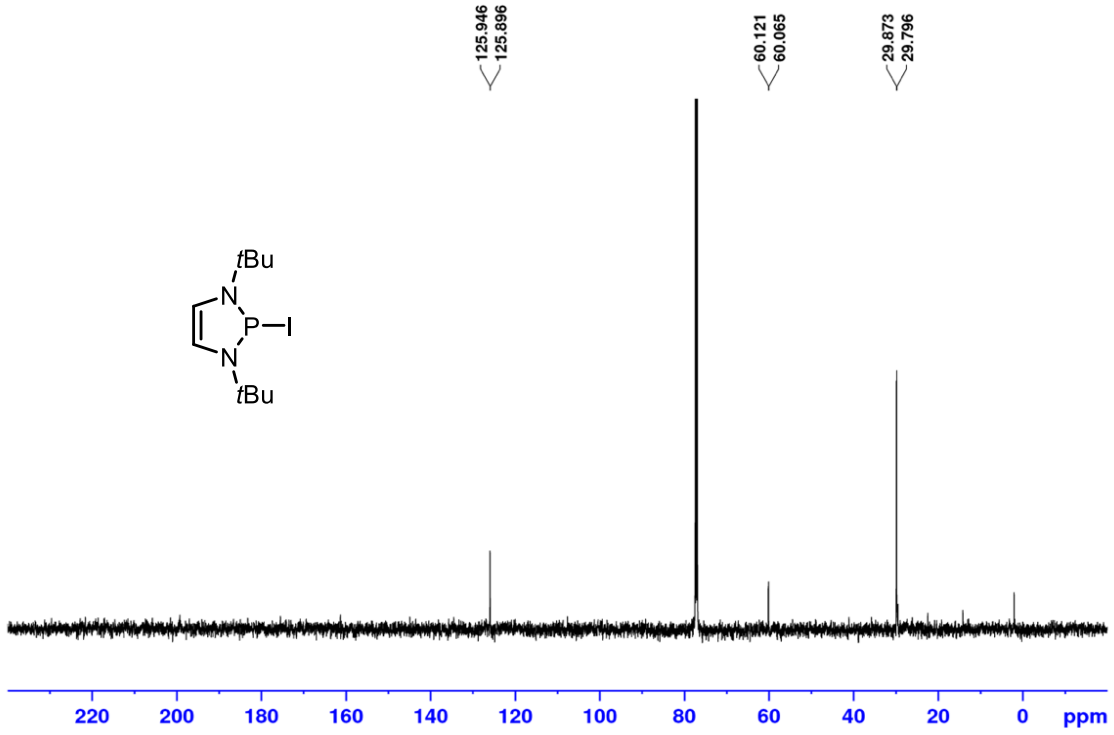


**Figure A261:** $^{13}$C {$^{1}$H} NMR (125.8 MHz, $CDCl_3$) spectrum of diazaphospholene iodide **7-4** from Iodobenzene.

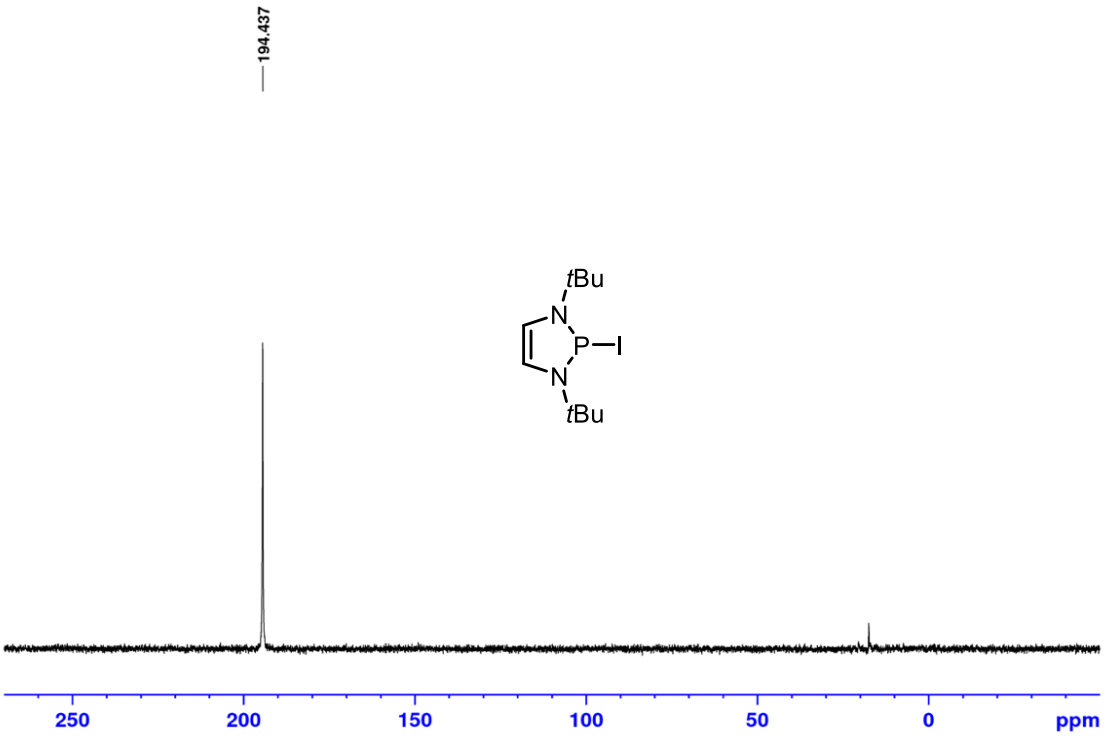


**Figure A262:** $^{31}P$ NMR (202.5 MHz, $CDCl_3$) spectrum of diazaphospholene iodide **7-4** from Iodobenzene.

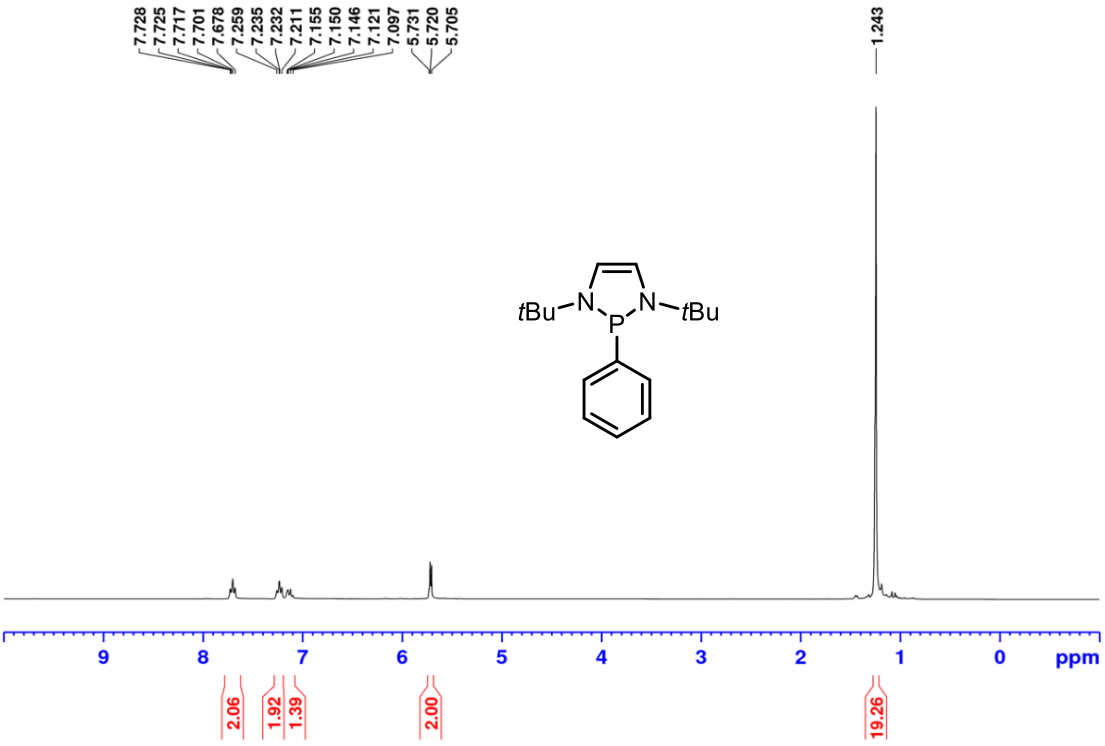


**Figure A263:** $^{1}H$ NMR (300 MHz, $C_6D_6$) spectrum of *P*-phenyl diazaphospholene **7-3** from bromobenzene.

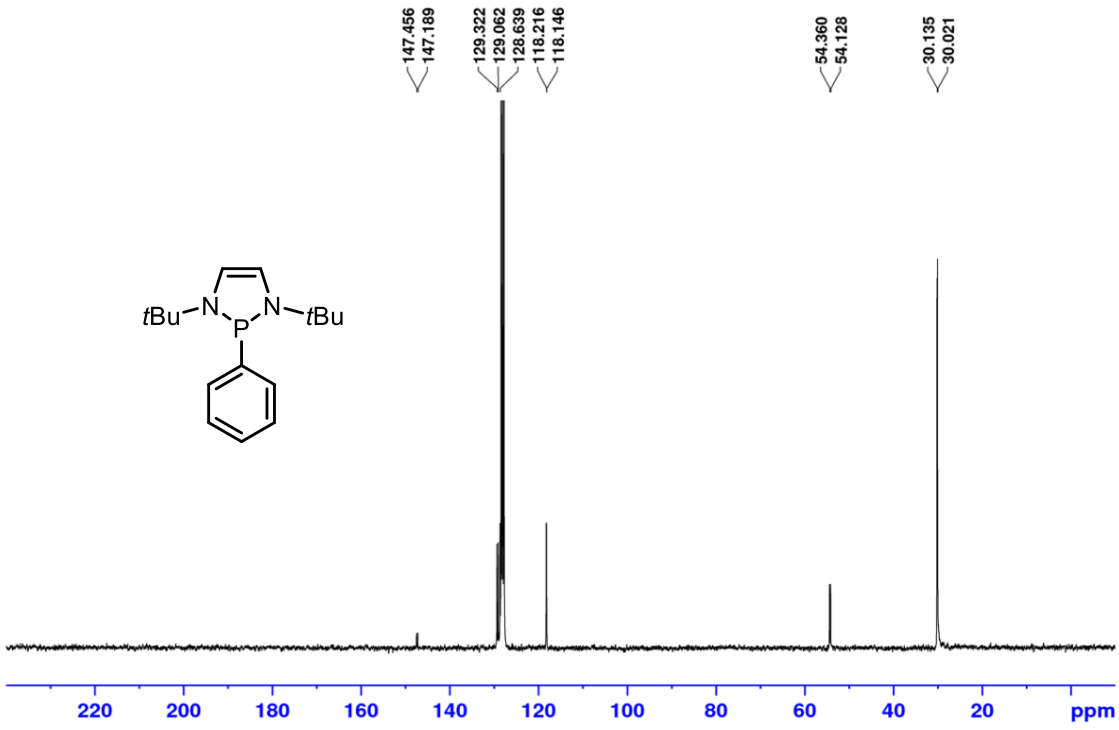


**Figure A264:** $^{13}C$ $\{^{1}H\}$ NMR (75.5 MHz, $C_6D_6$) spectrum of *P*-phenyl diazaphospholene **7-3** from bromobenzene.

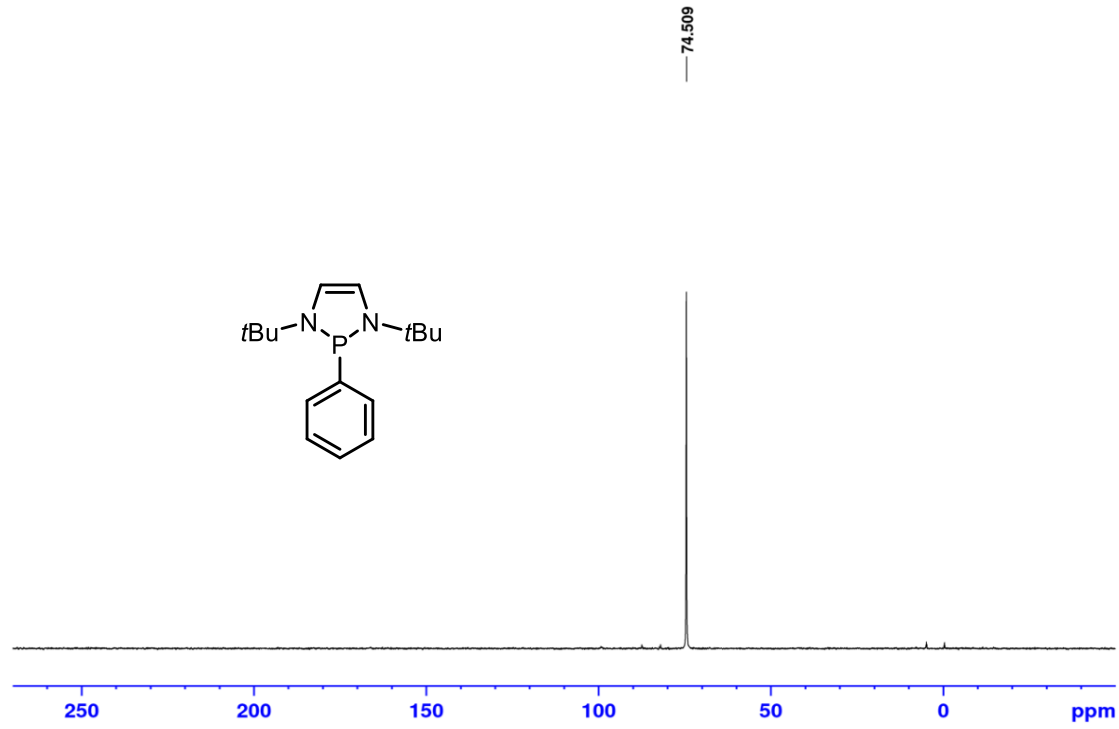


**Figure A265:** $^{31}P$ NMR (121.5 MHz, $C_6D_6$) spectrum of *P*-phenyl diazaphospholene **7-3** from bromobenzene.

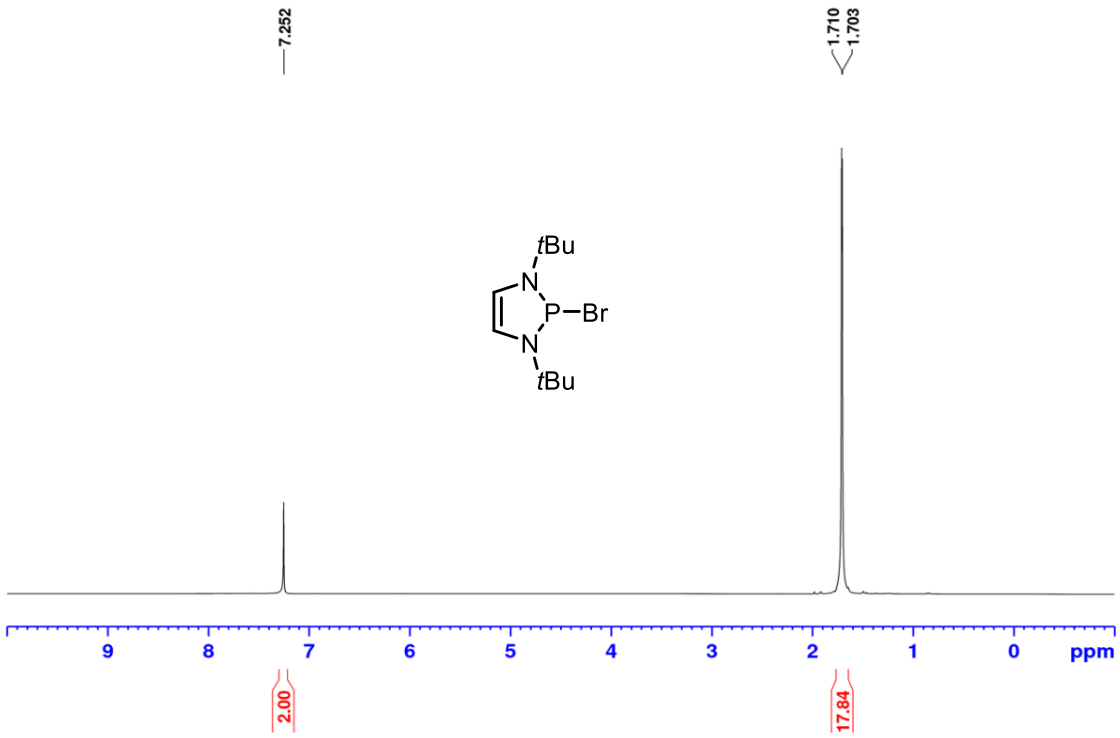


**Figure A266:** $^{1}$H NMR (300 MHz, $CDCl_3$) spectrum of diazaphospholene bromide **7-5** from bromobenzene.

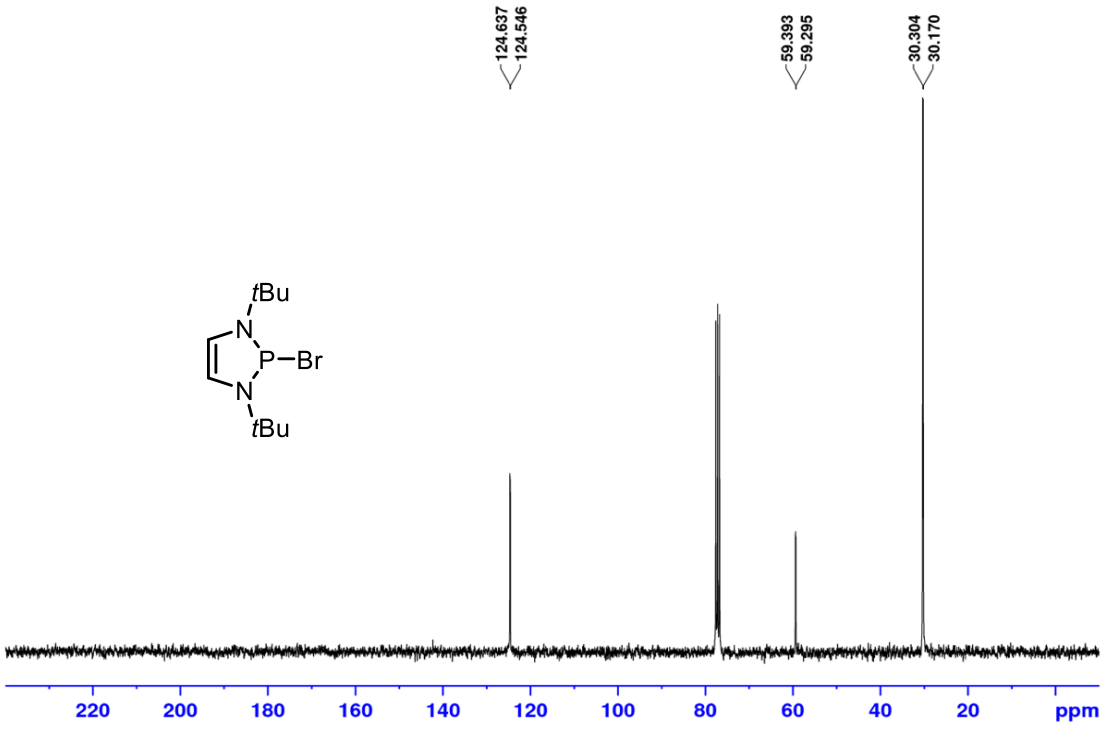


**Figure A267:** $^{13}$C {$^{1}$H} NMR (75.5 MHz, $CDCl_3$) spectrum of diazaphospholene bromide **7-5** from bromobenzene.

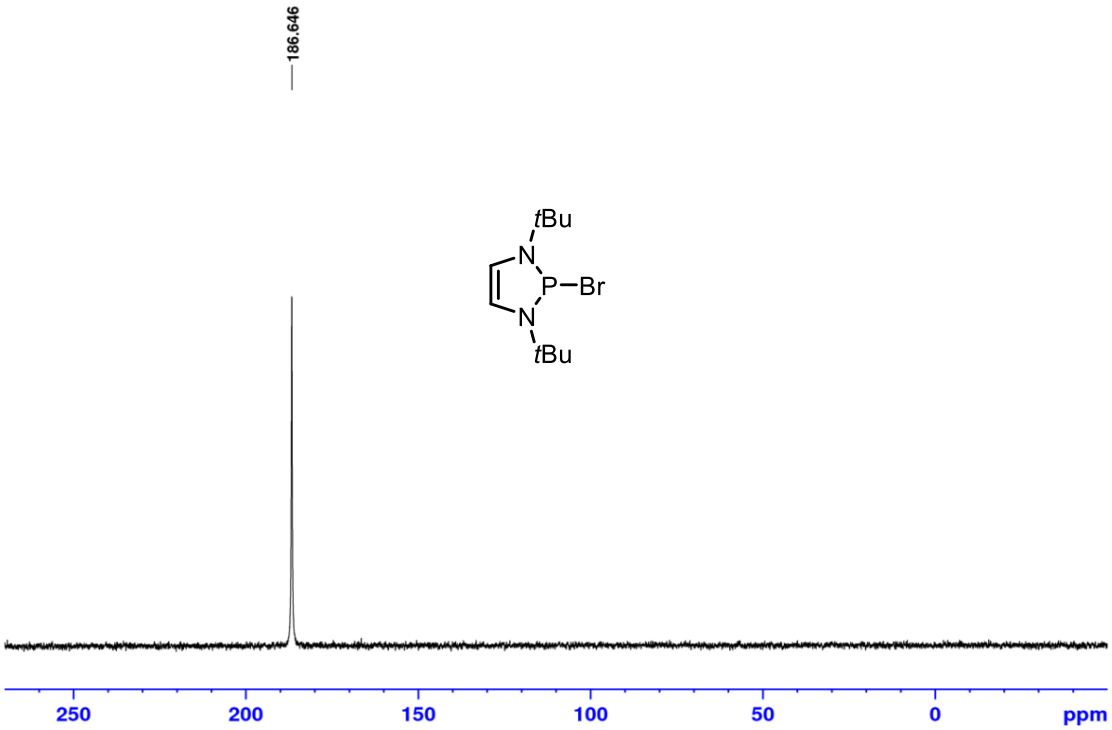


**Figure A268:** $^{31}P$ NMR (121.5 MHz, $CDCl_3$) spectrum of diazaphospholene bromide **7-5** from bromobenzene.

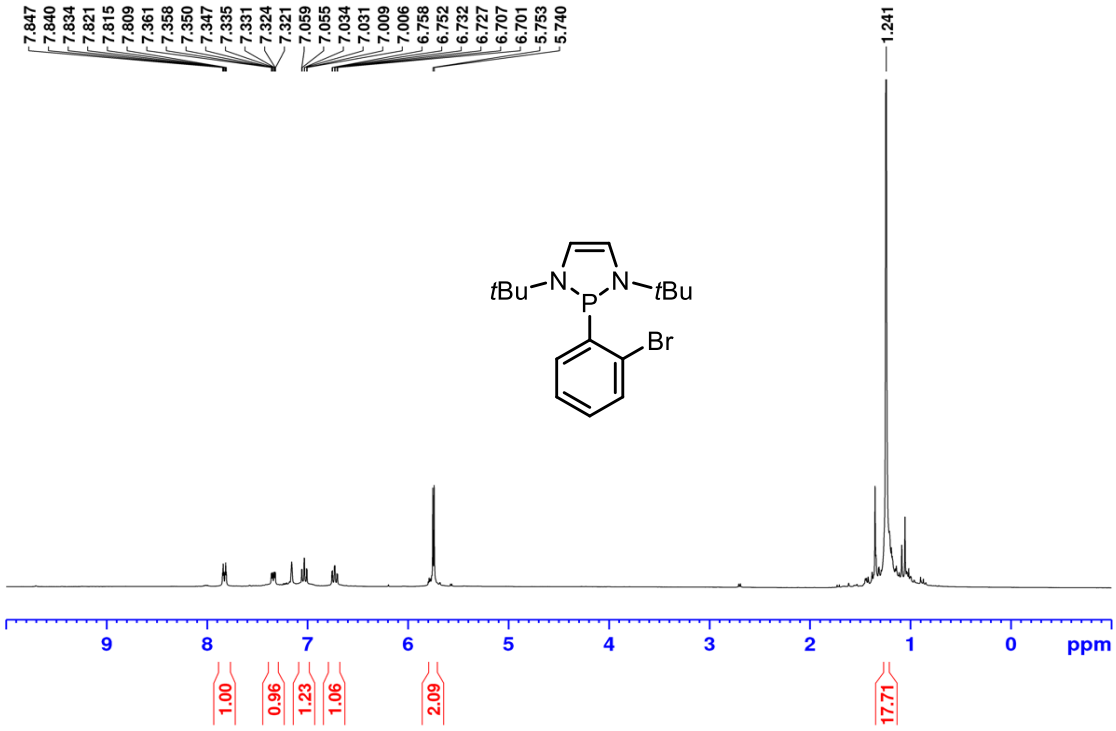


**Figure A 269:** $^{1}H$ NMR (300 MHz, $C_6D_6$) spectrum of *P*-(2-bromo-phenyl) diazaphospholene **7-12**.

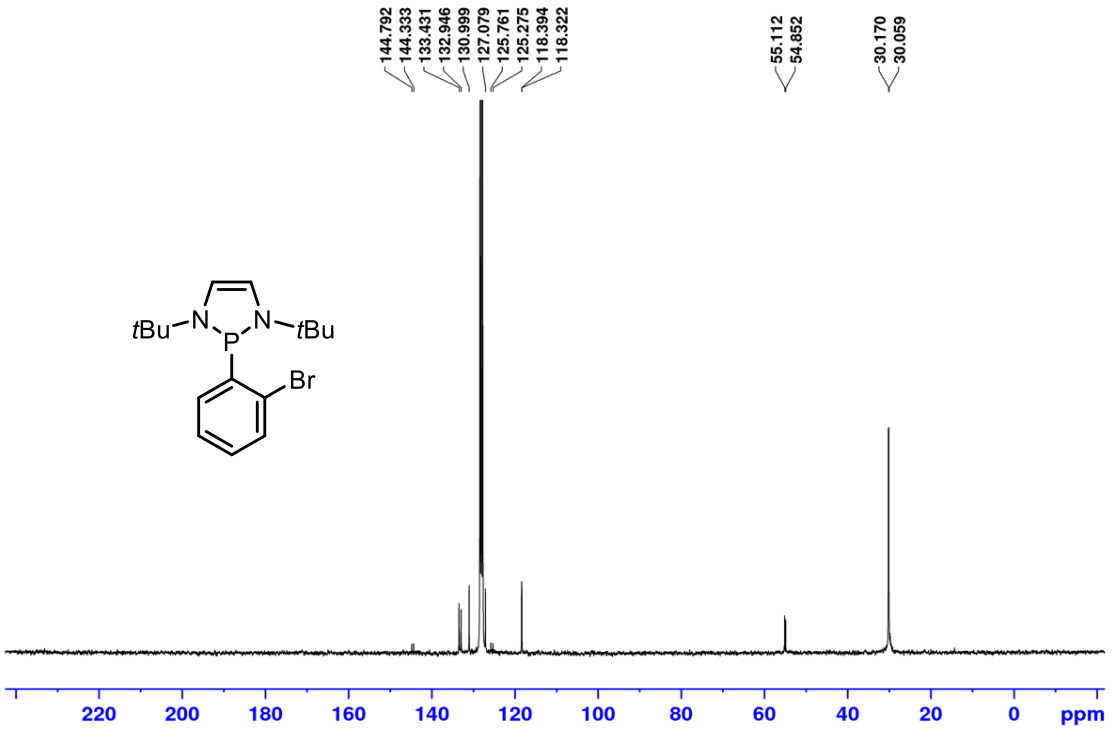


**Figure A270:** $^{13}C$ $\{^{1}H\}$ NMR (75.5 MHz, $C_6D_6$) spectrum of *P*-(2-bromo-phenyl) diazaphospholene **7-12**.

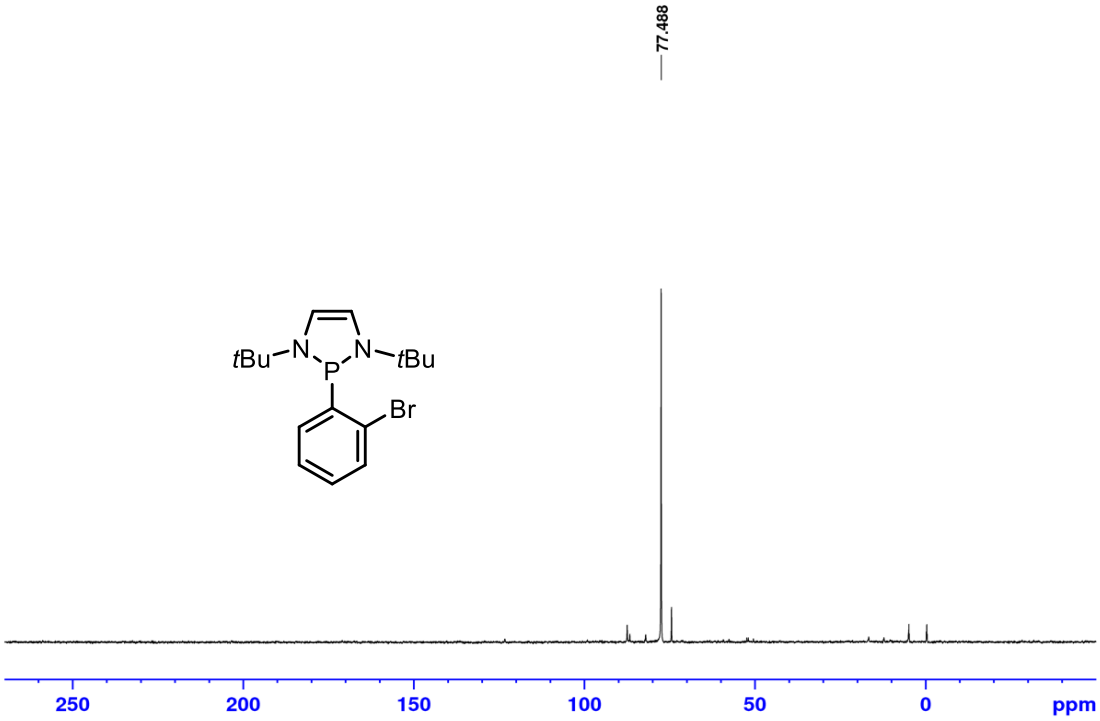


**Figure A271:** $^{31}P$ NMR (121.5 MHz, $C_6D_6$) spectrum of *P*-(2-bromo-phenyl) diazaphospholene **7-12**.

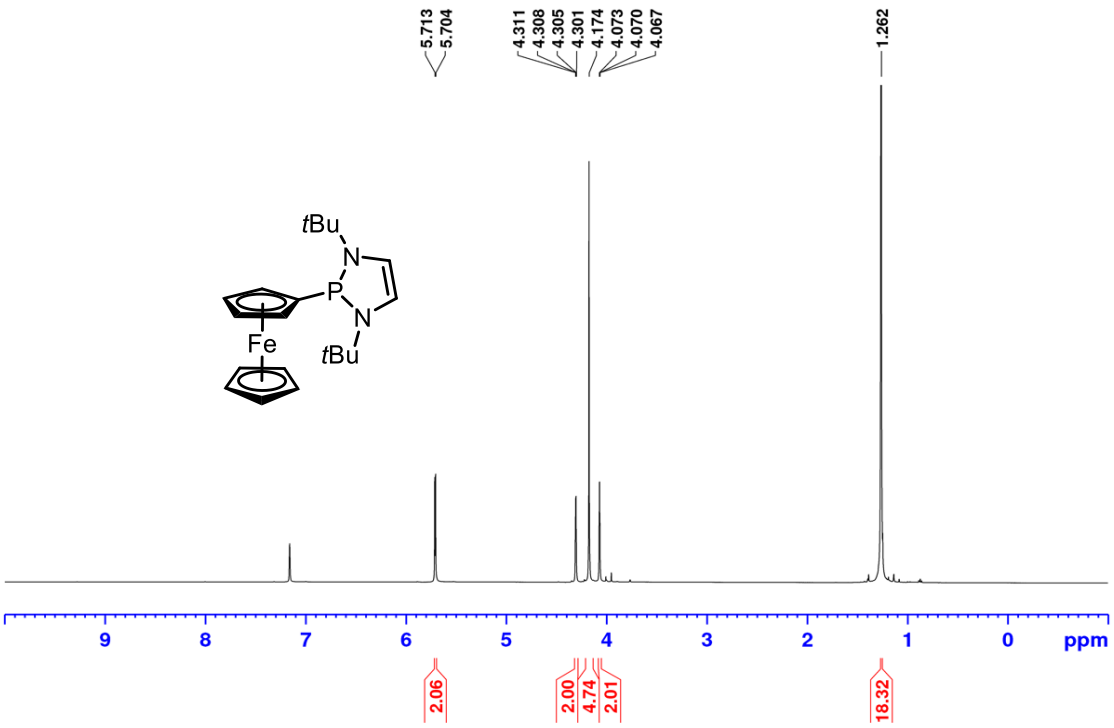


**Figure A272:** $^{1}$H NMR (500 MHz, $C_6D_6$) spectrum of *P*-ferrocenyl diazaphospholene **7-13**.

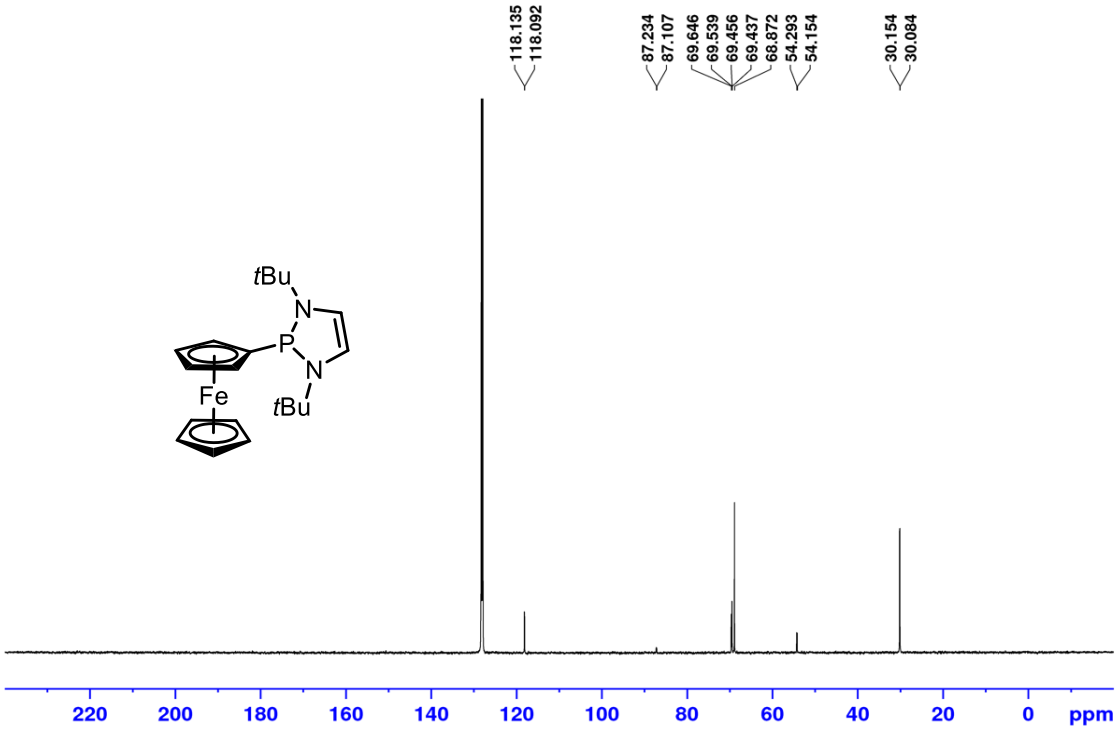


**Figure A273:** $^{13}$C {$^{1}$H} NMR (125.8 MHz, $C_6D_6$) spectrum of *P*-ferrocenyl diazaphospholene **7-13**.

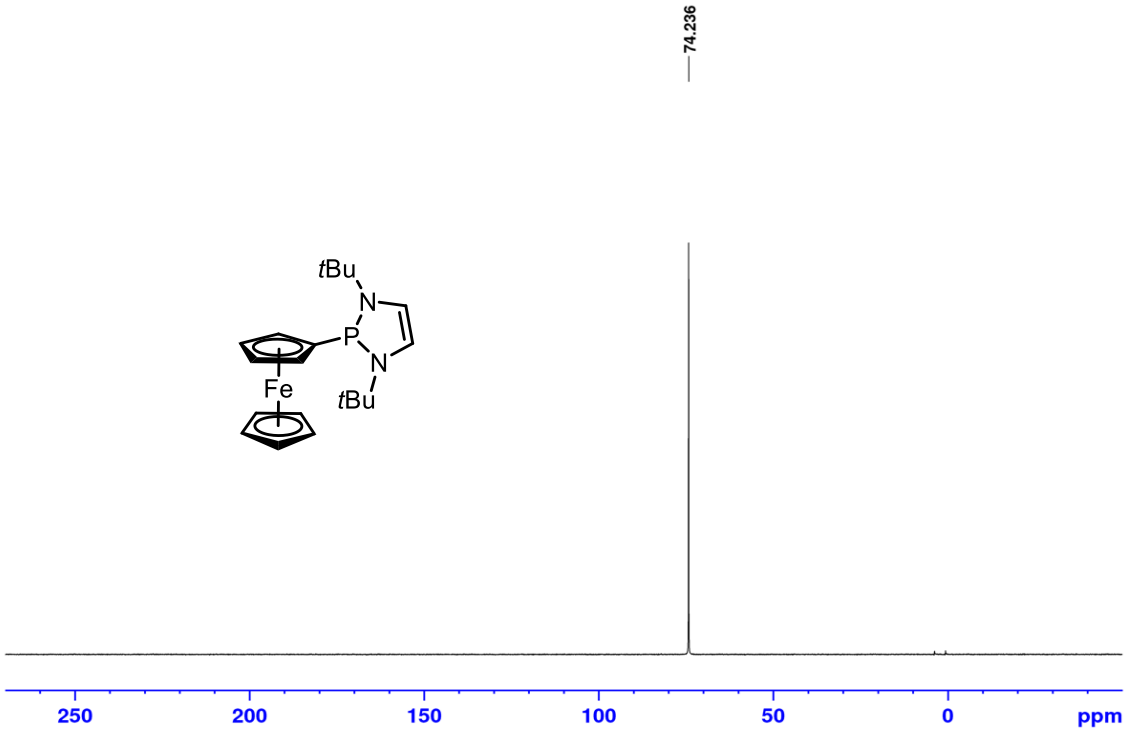


**Figure A274:** $^{31}$P NMR (202 MHz, $C_6D_6$) spectrum of *P*-ferrocenyl diazaphospholene **7-13**.

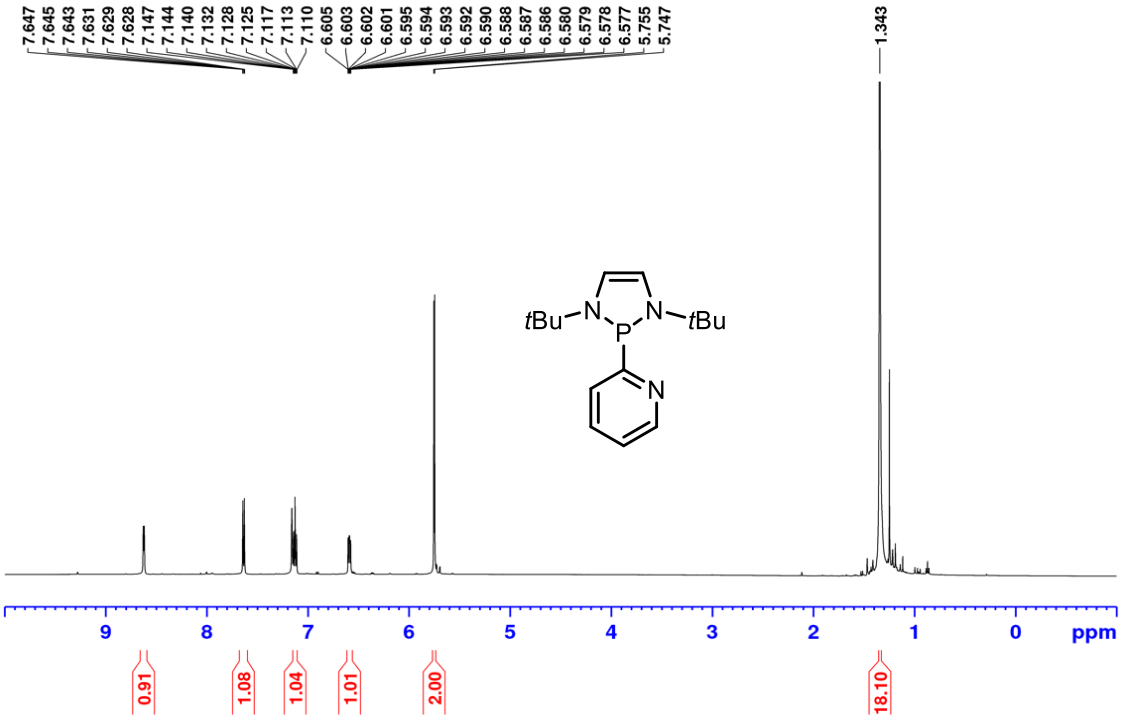


**Figure A275:** $^{1}$H NMR (500 MHz, $C_6D_6$) spectrum of *P*-(2-pyridyl) diazaphospholene **7-7**.

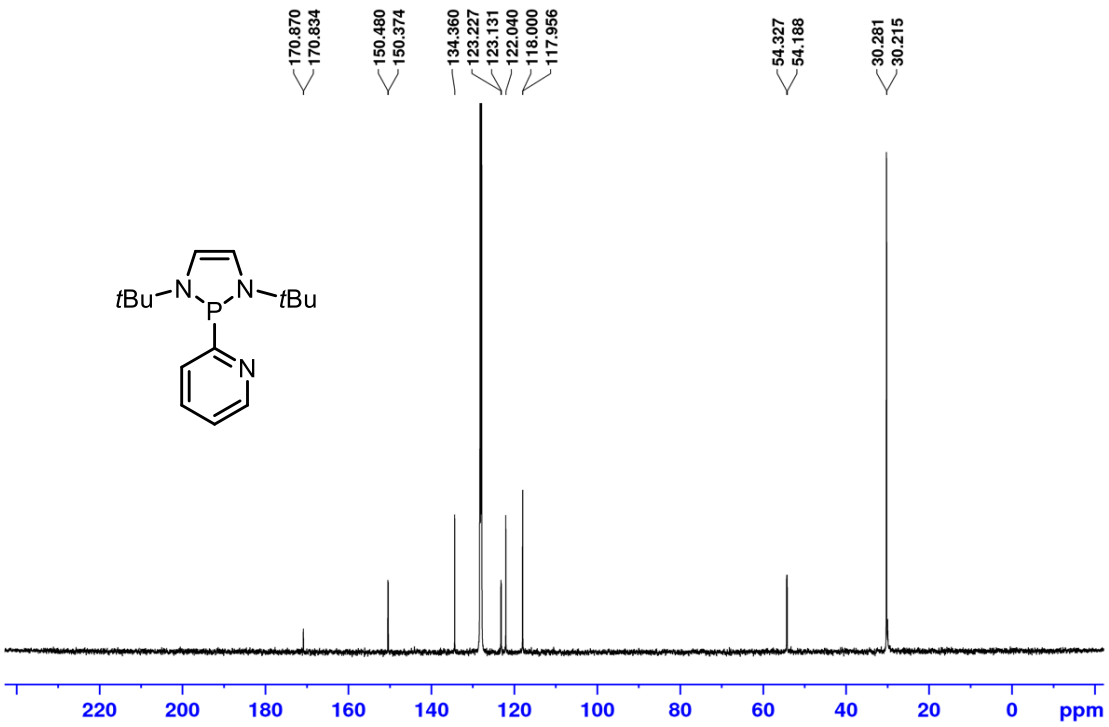


**Figure A276:** $^{13}C$ {$^{1}H$} NMR (125.8 MHz, $C_6D_6$) spectrum of *P*-(2-pyridyl) diazaphospholene **7-7**.

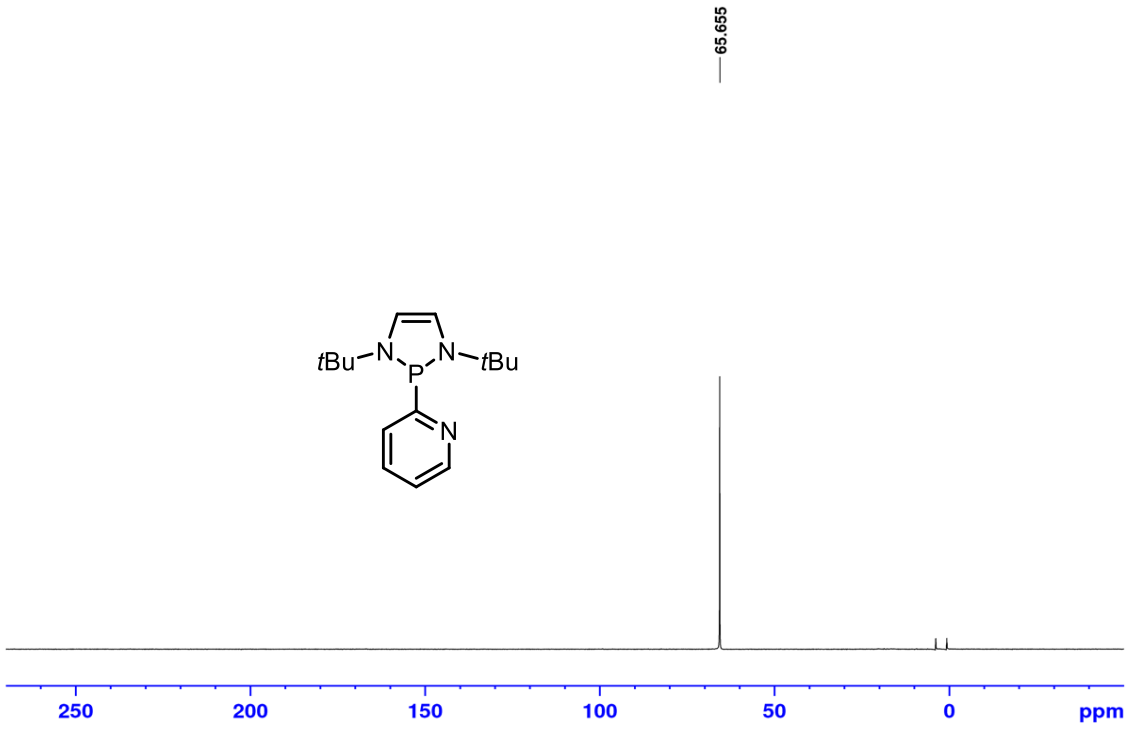


**Figure A277:** $^{31}P$ NMR (202 MHz, $C_6D_6$) spectrum of *P*-(2-pyridyl) diazaphospholene **7-7**.

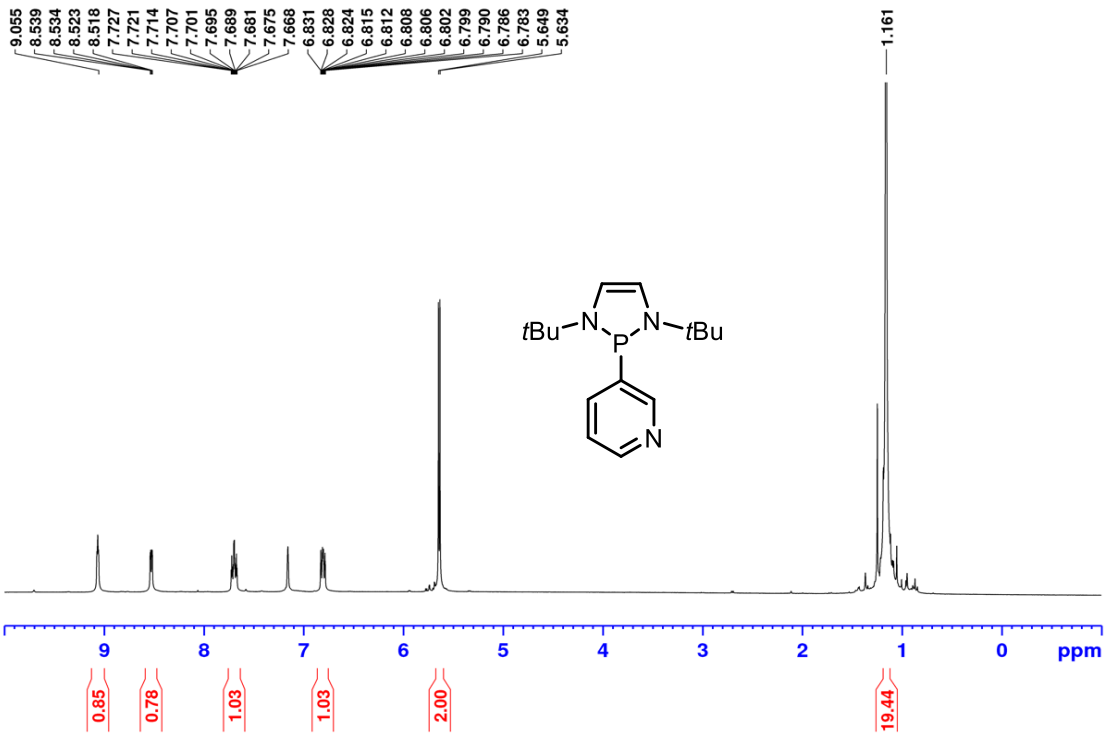


**Figure A278:** $^{1}$H NMR (300 MHz, $C_6D_6$) spectrum of *P*-(3-pyridyl) diazaphospholene **7-8**.

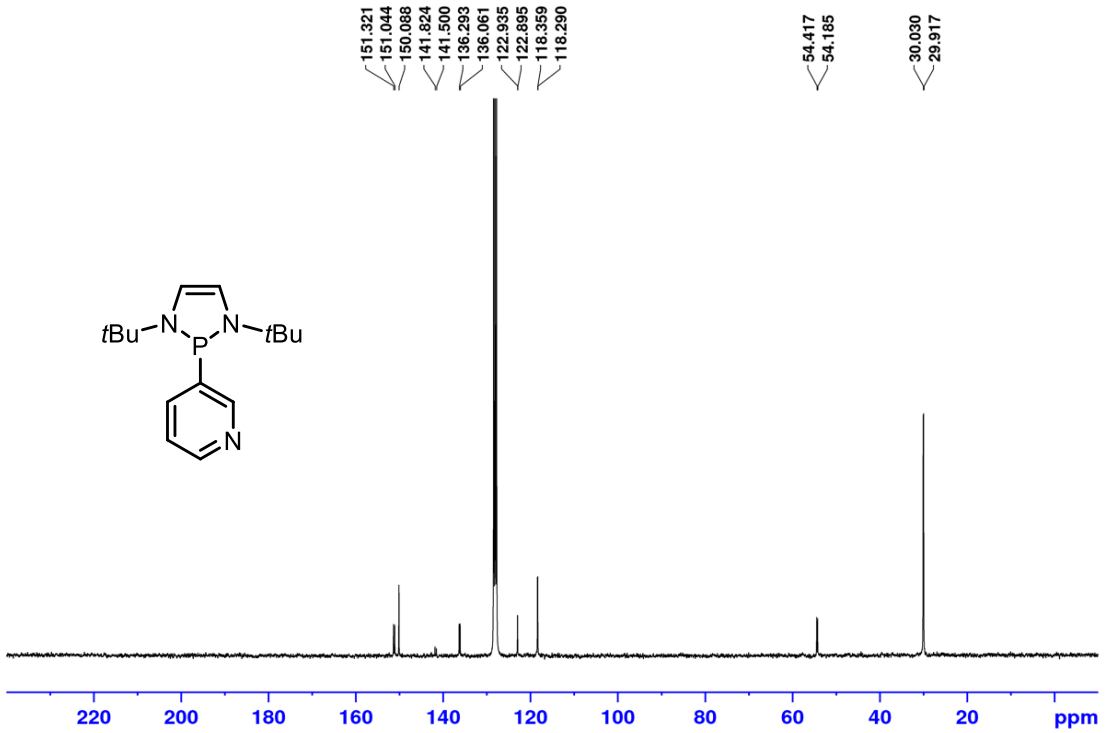


**Figure A279:** $^{13}$C {$^{1}$H} NMR (75.5 MHz, $C_6D_6$) spectrum of *P*-(3-pyridyl) diazaphospholene **7-8**.

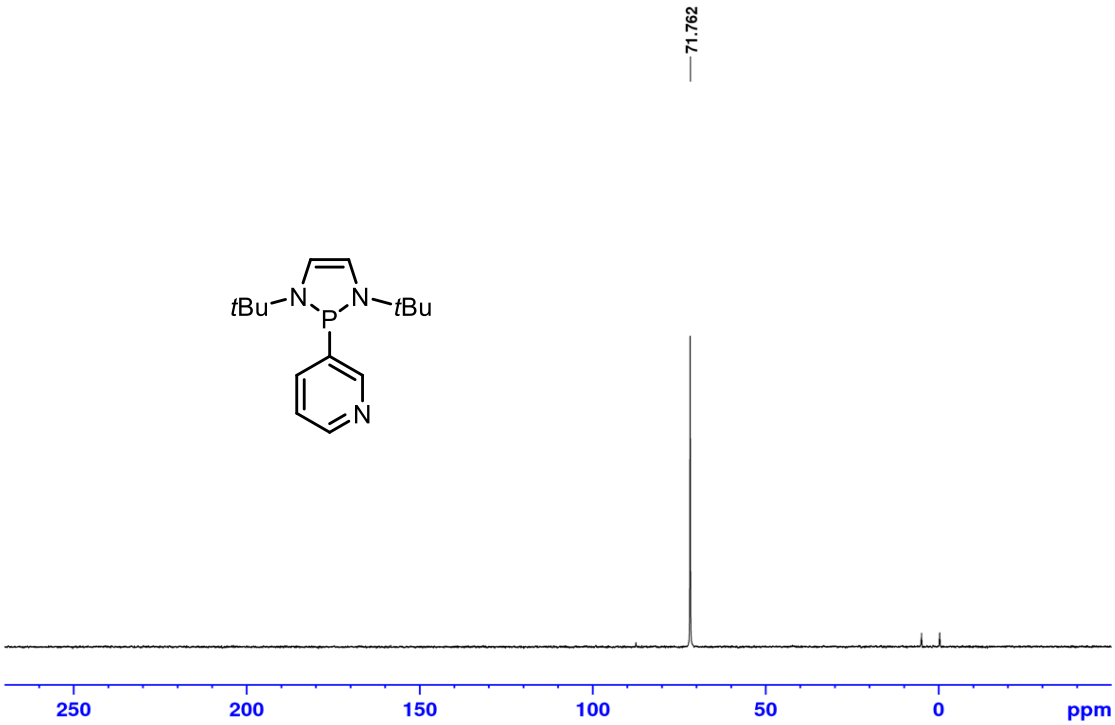


**Figure A280:** $^{31}$P NMR (121.5 MHz, $C_6D_6$) spectrum of *P*-(3-pyridyl) diazaphospholene **7-8**.

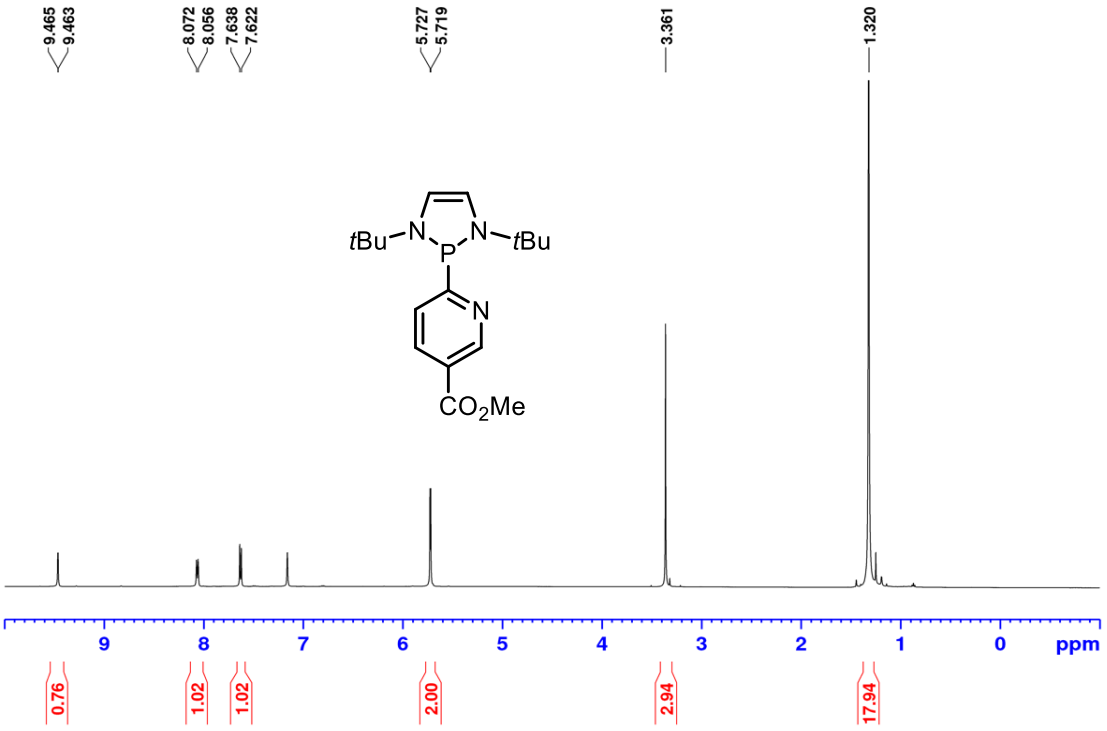


**Figure A281:** $^{1}$H NMR (500 MHz, $C_6D_6$) spectrum of *P*-(2-(6-methyl-nicotinyl)) diazaphospholene **7-9**.

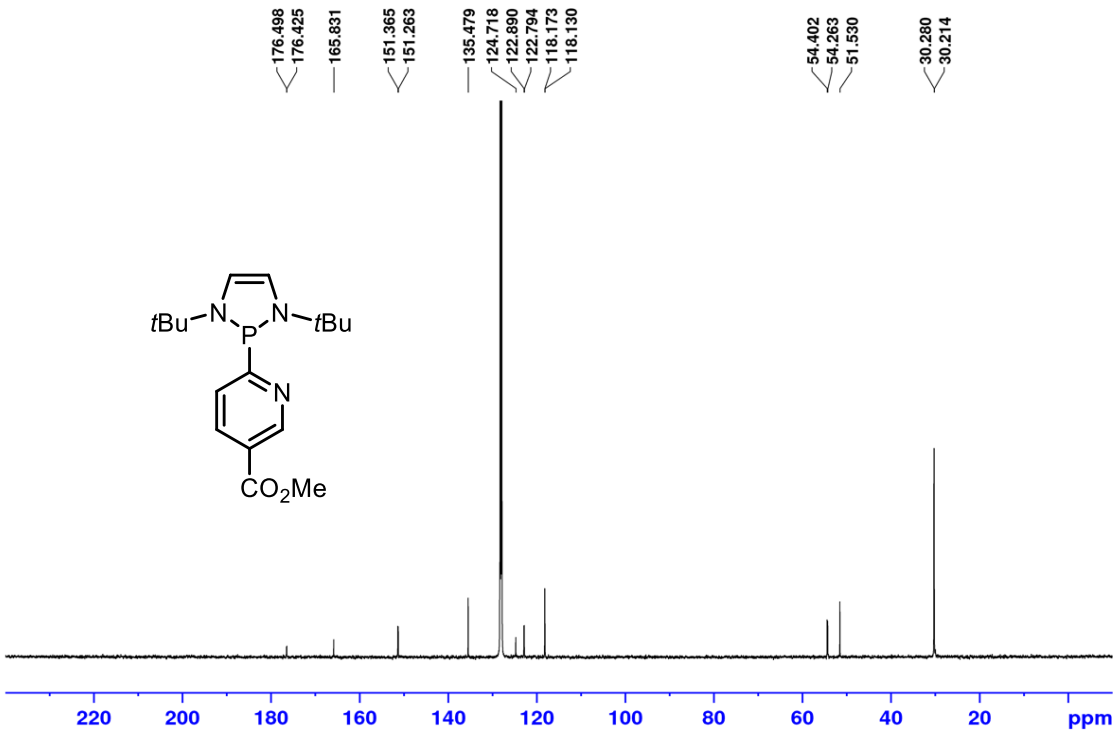


Figure A282: $^{13}C$ {$^{1}H$} NMR (125.8 MHz, $C_6D_6$) spectrum of *P*-(2-(6-methyl-nicotinyl)) diazaphospholene **7-9**.

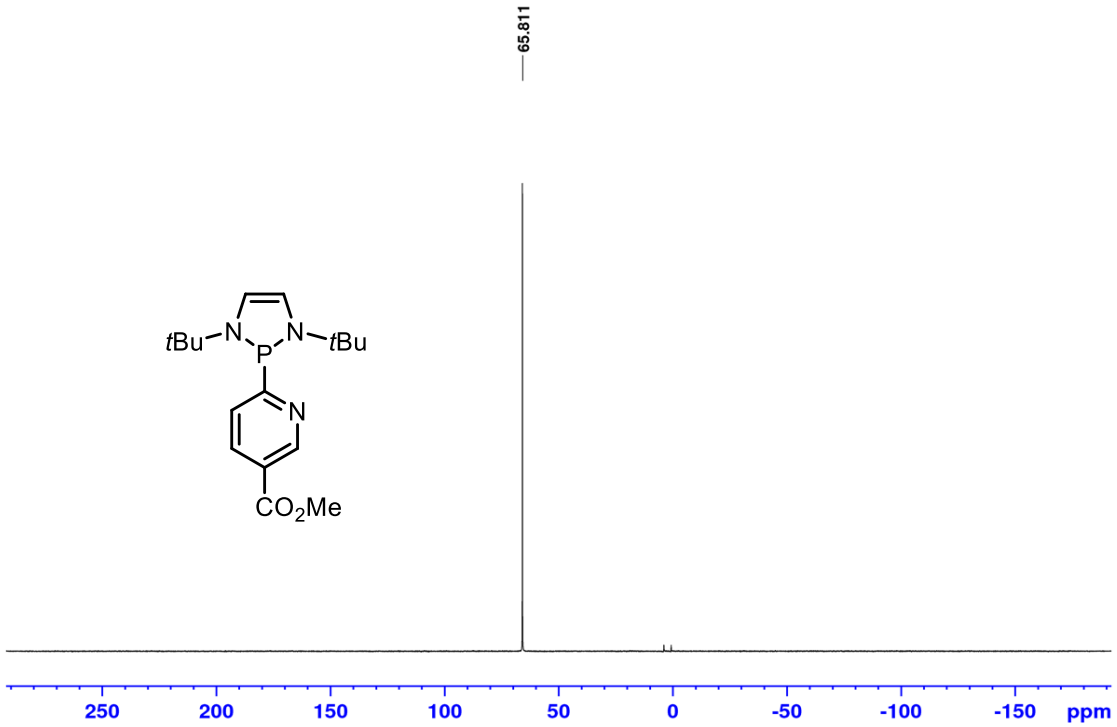


**Figure A283:** $^{31}P$ NMR (202.5 MHz, $C_6D_6$) spectrum of *P*-(2-(6-methyl-nicotinyl)) diazaphospholene **7-9**.

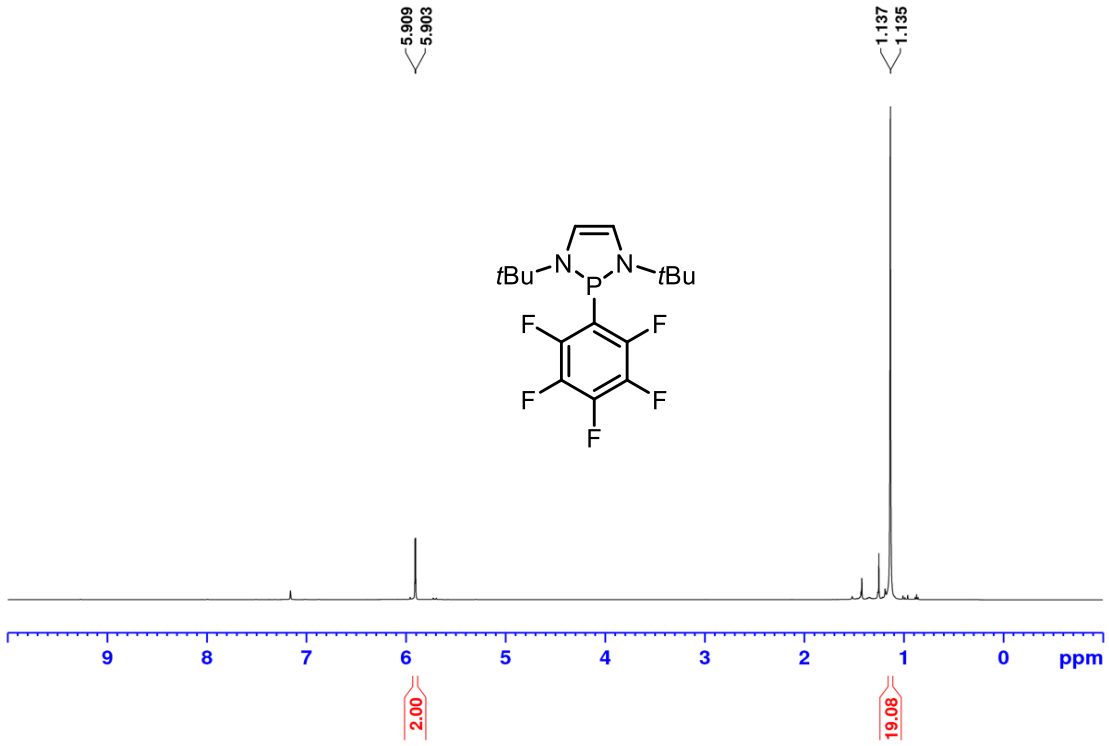


**Figure A284:** $^{1}$H NMR (500 MHz, $C_6D_6$) spectrum of *P*-pentafluorophenyl diazaphospholene **7-6**.

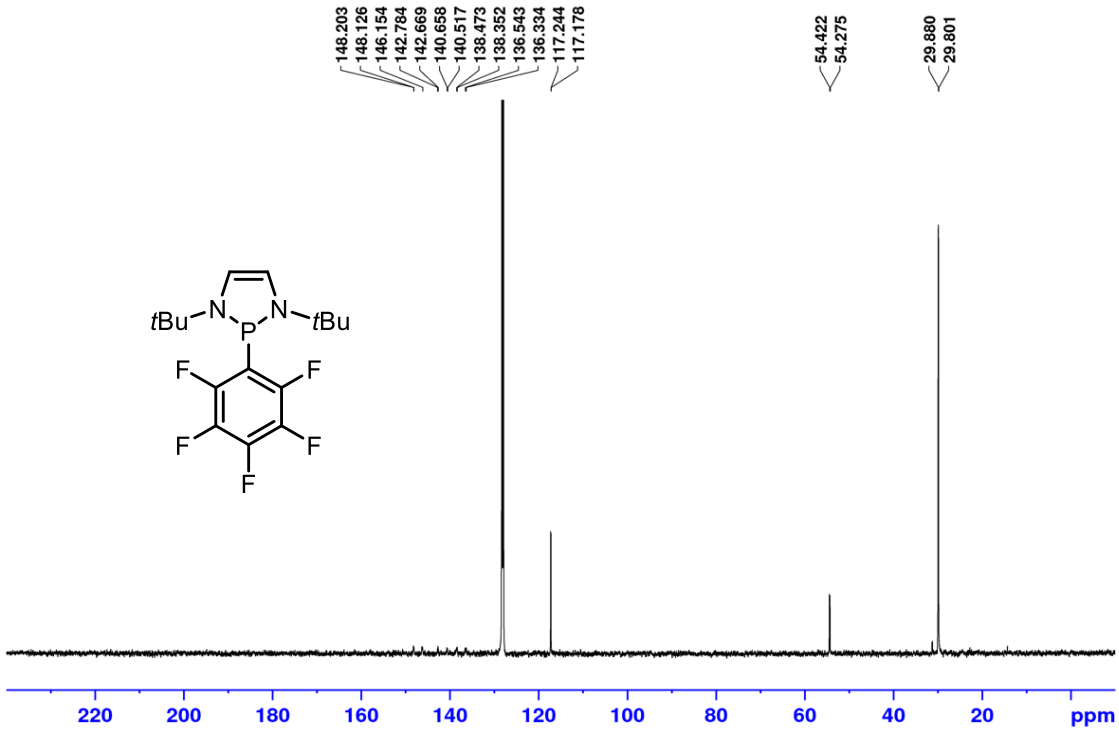


**Figure A285:** $^{13}$C {$^{1}$H} NMR (125.8 MHz, $C_6D_6$) spectrum of *P*-pentafluorophenyl diazaphospholene **7-6**.

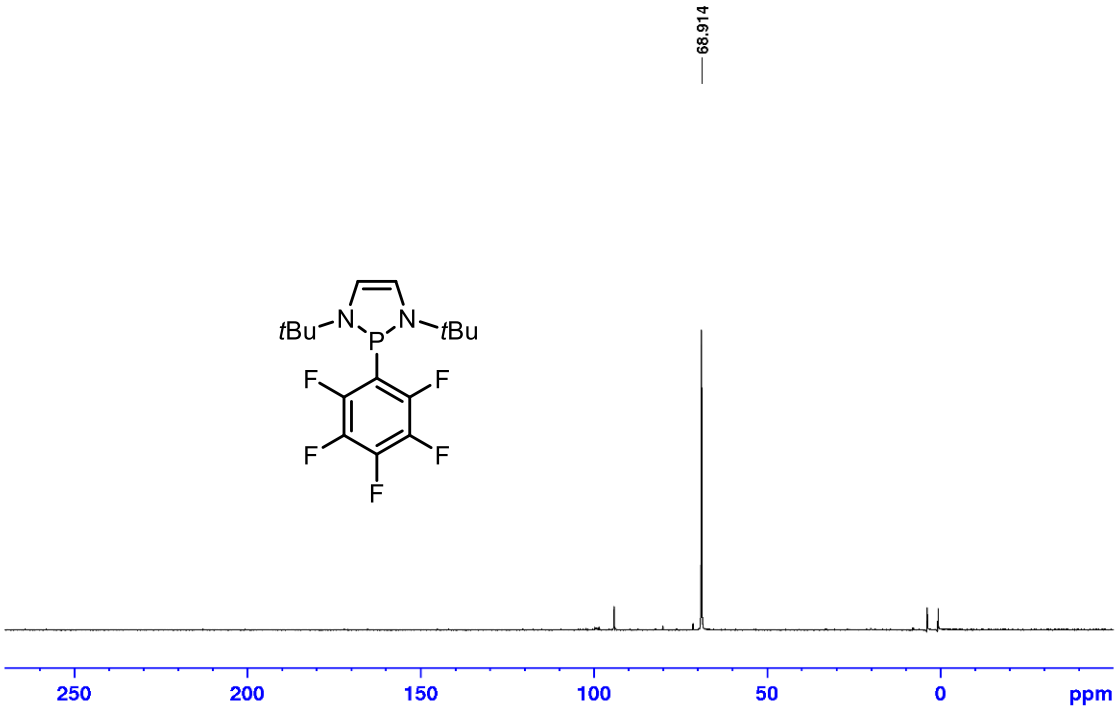


**Figure A286:** $^{31}P$ NMR (202.5 MHz, $C_6D_6$) spectrum of *P*-pentafluorophenyl diazaphospholene **7-6**.

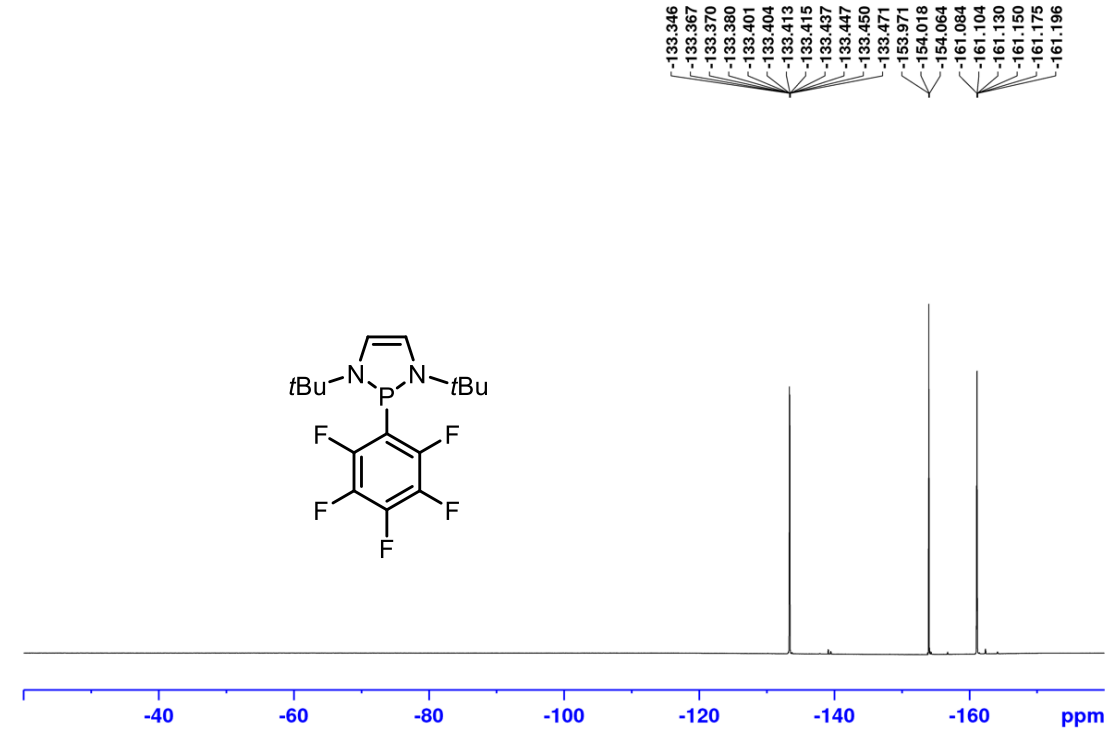


**Figure A287:** $^{19}F$ $\{^1H\}$ (470.6 MHz, $C_6D_6$) spectrum of *P*-pentafluorophenyl diazaphospholene **7-6**.

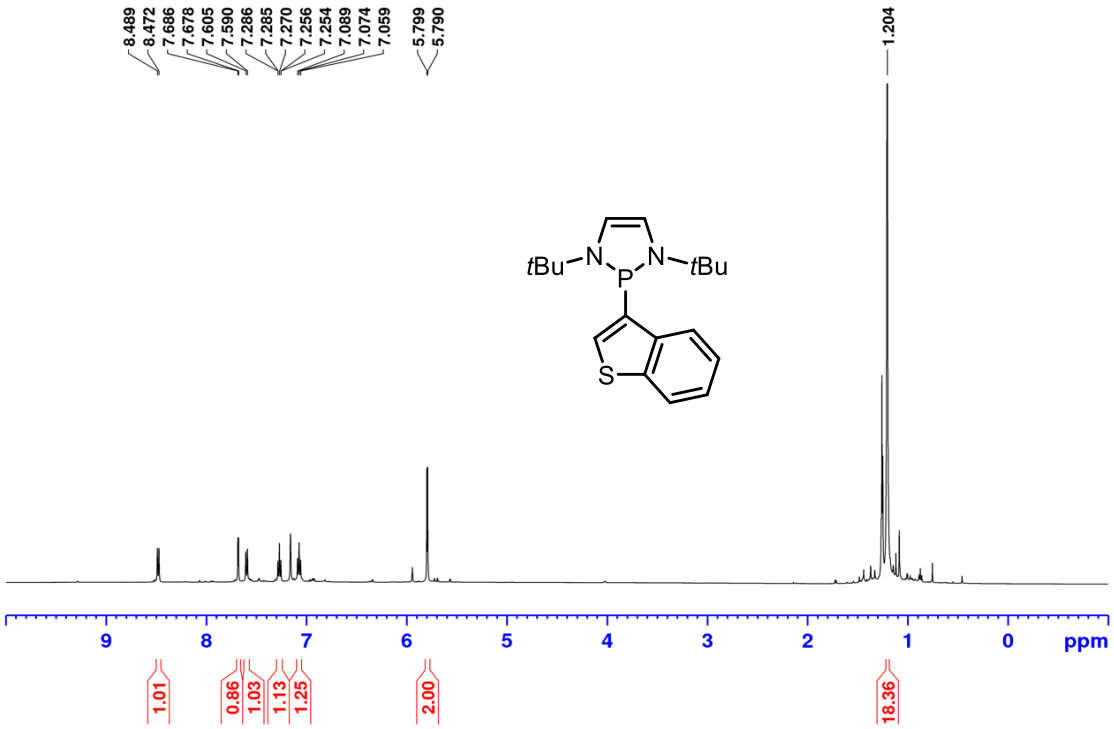


**Figure A288:** $^{1}$H NMR (500 MHz, $C_6D_6$) spectrum of *P*-(3-benzothienyl) diazaphospholene **7-10**.

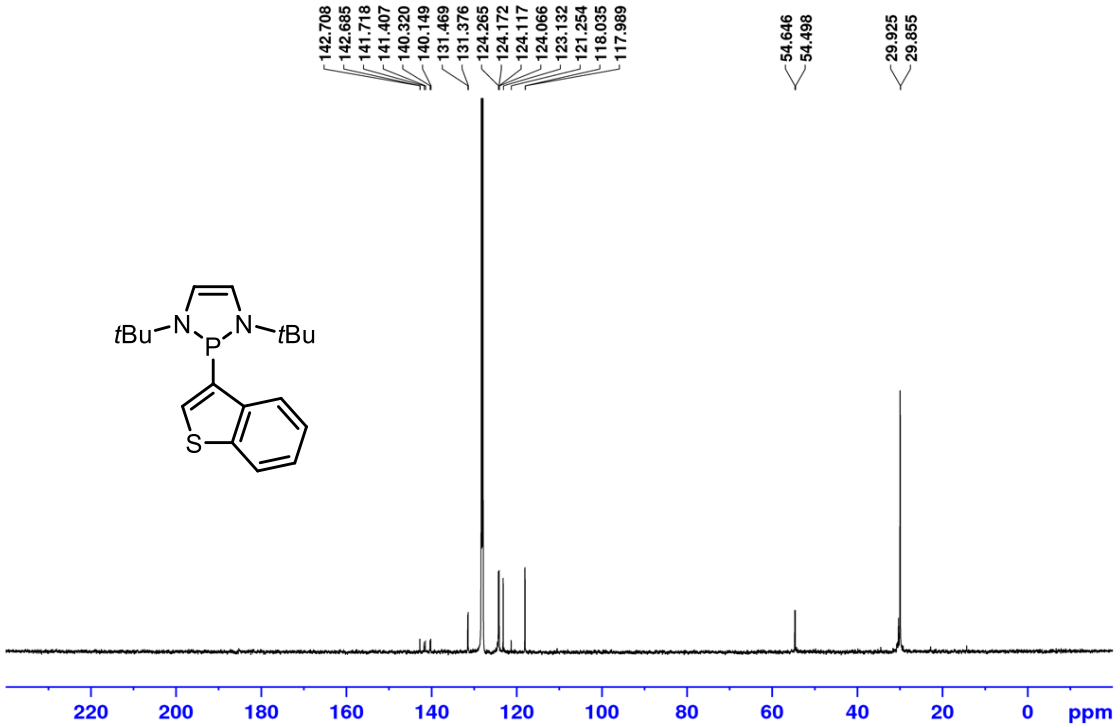


**Figure A289:** $^{13}$C {$^{1}$H} NMR (125.8 MHz, $C_6D_6$) spectrum of *P*-(3-benzothienyl) diazaphospholene **7-10**.

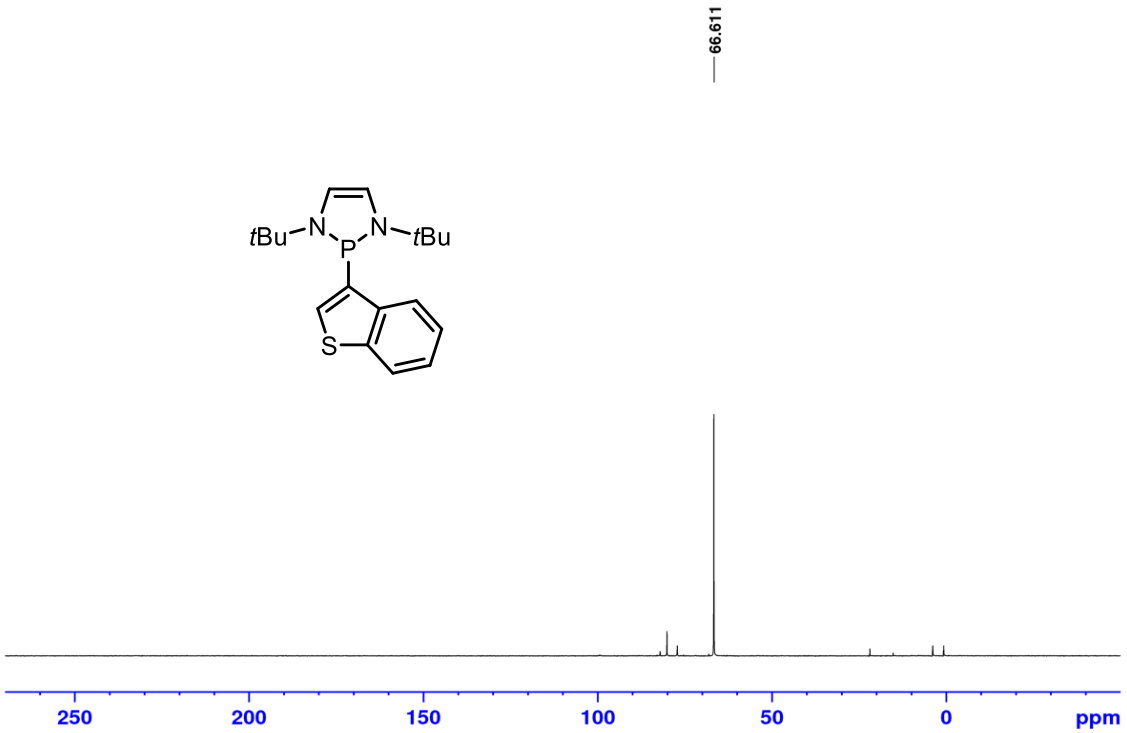


**Figure A290:** $^{31}$P NMR (202.5 MHz, $C_6D_6$) spectrum of *P*-(3-benzothienyl) diazaphospholene **7-10**.

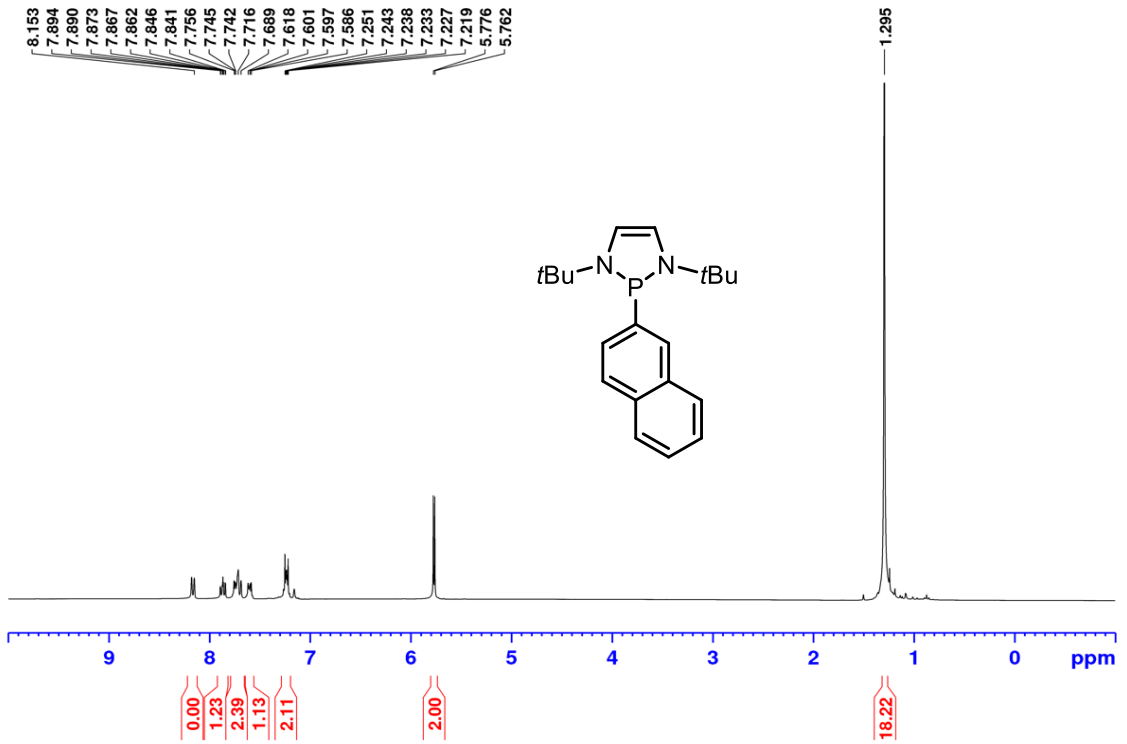


**Figure A291:** $^{1}$H NMR (300 MHz, $C_6D_6$) spectrum of *P*-(2-naphthyl) diazaphospholene **7-11**.

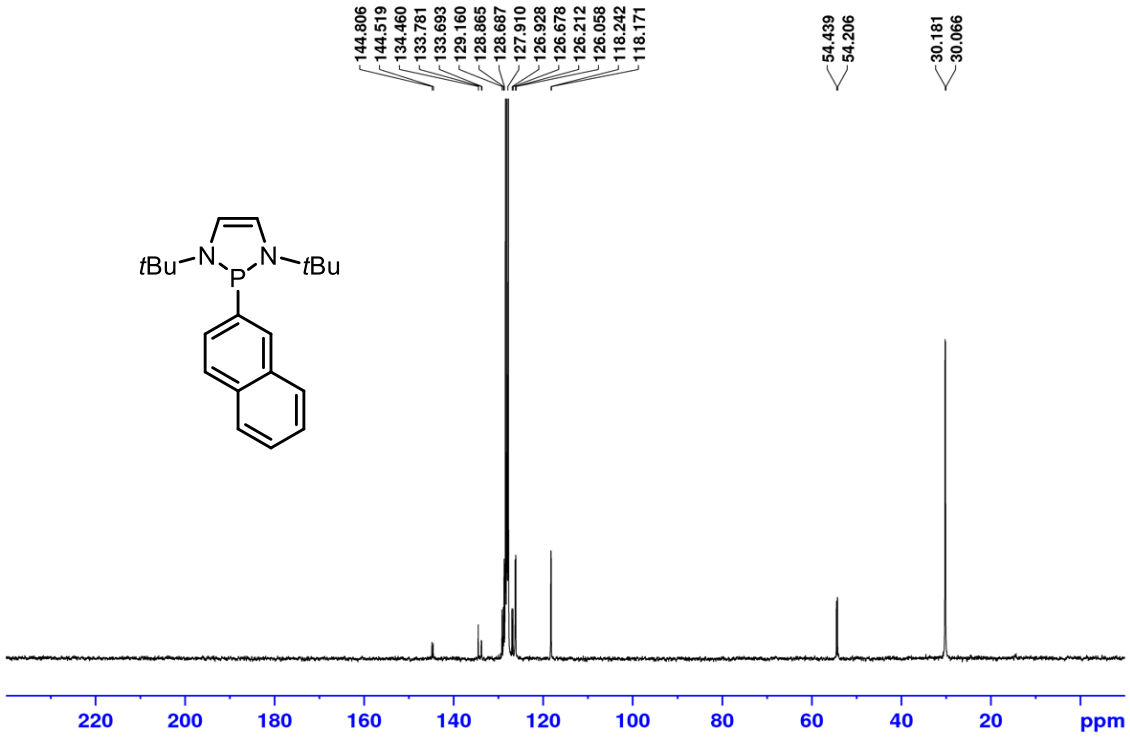


**Figure A292:** $^{13}C$ $\{^{1}H\}$ NMR (75.5 MHz, $C_6D_6$) spectrum of *P*-(2-naphthyl) diazaphospholene **7-11**.

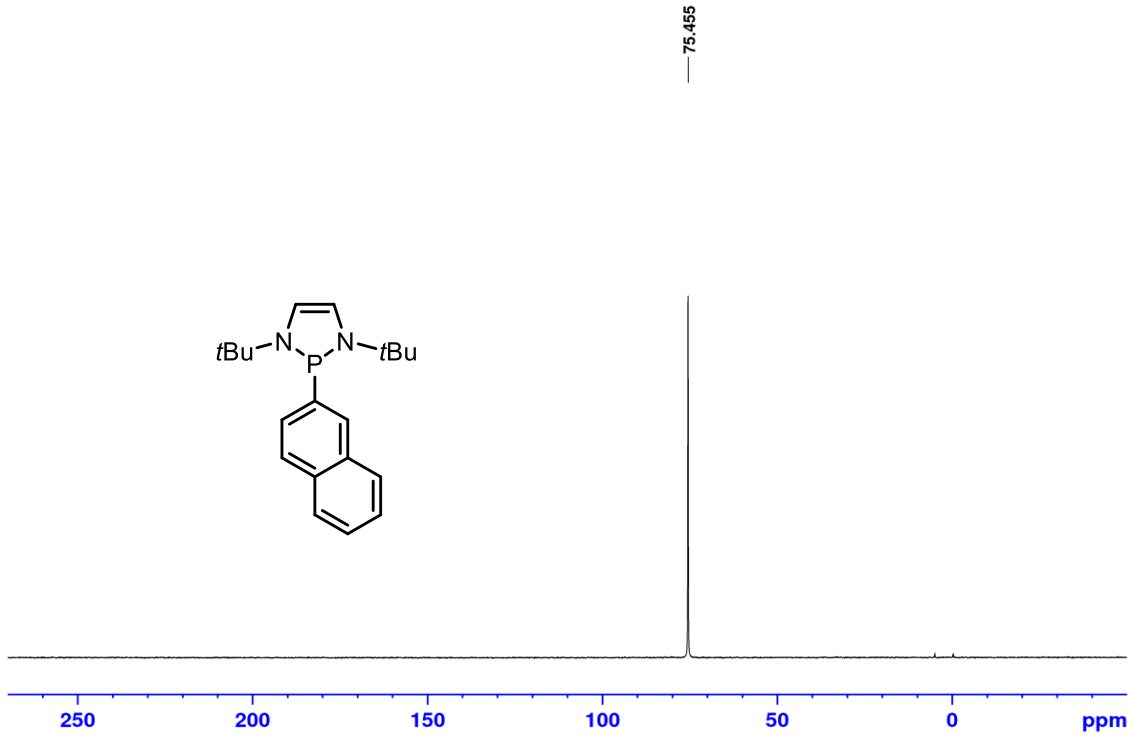


**Figure A293:** $^{31}P$ NMR (121.5 MHz, $C_6D_6$) spectrum of *P*-(2-naphthyl) diazaphospholene **7-11**.

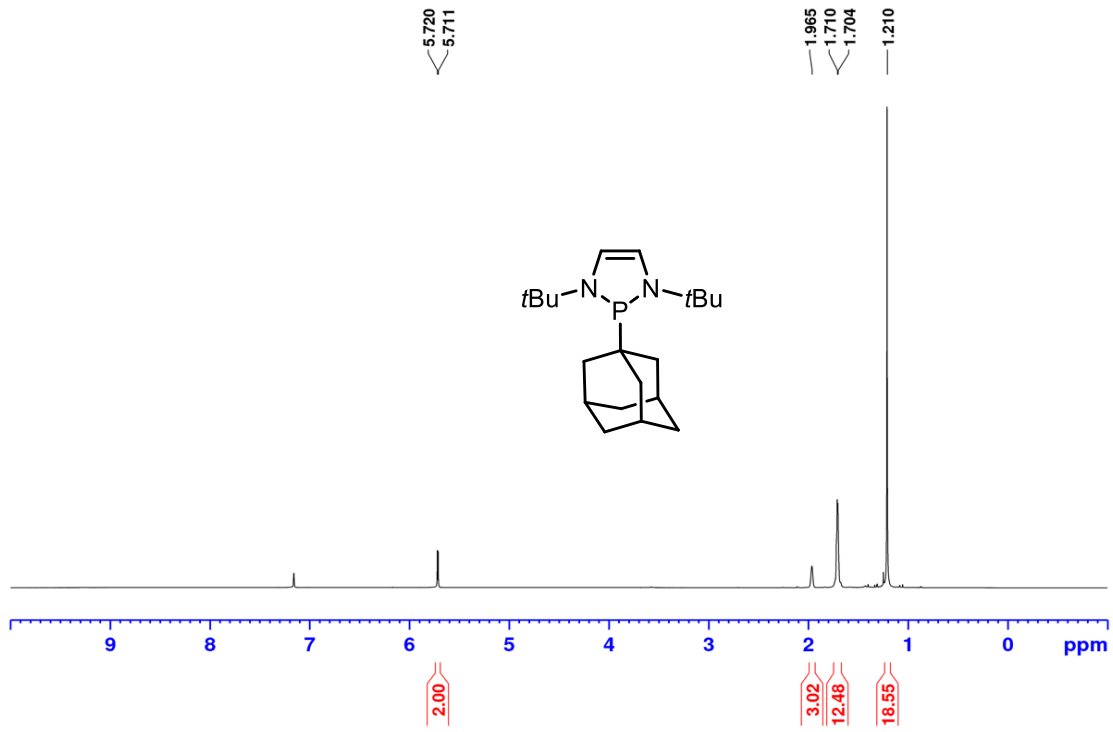


**Figure A294:** $^{1}$H NMR (500 MHz, $C_6D_6$) spectrum of *P*-adamantyl diazaphospholene **7-15**.

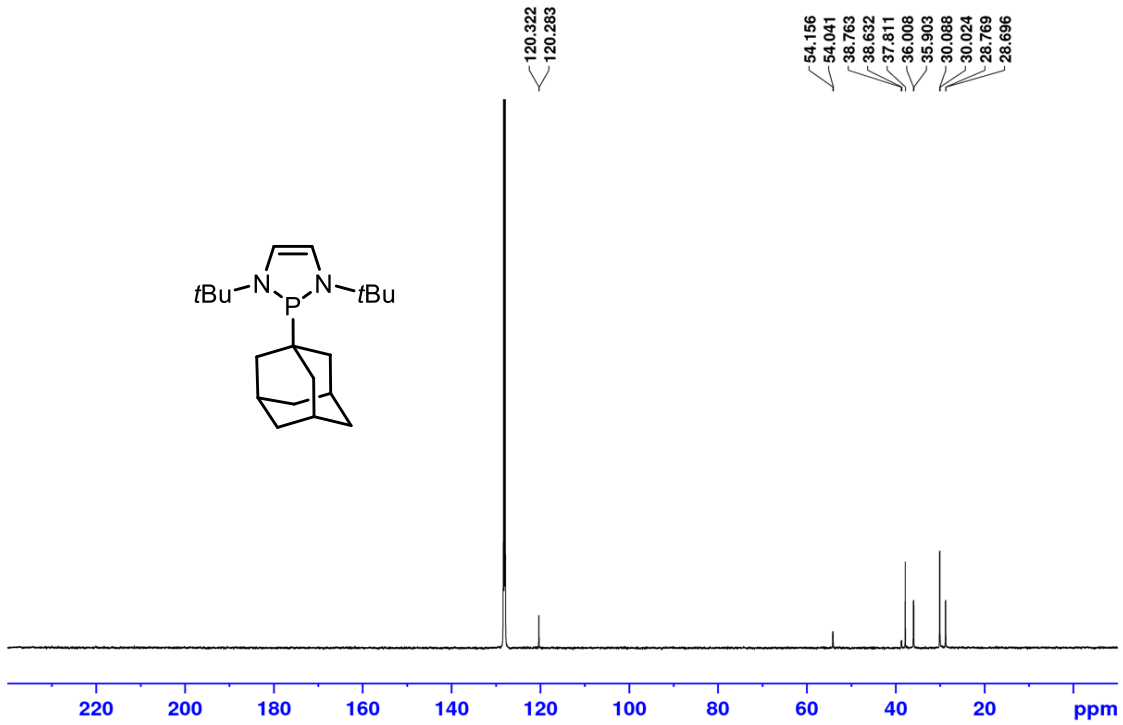


**Figure A295:** $^{13}$C {$^{1}$H} NMR (125.8 MHz, $C_6D_6$) spectrum of *P*-adamantyl diazaphospholene **7-15**.

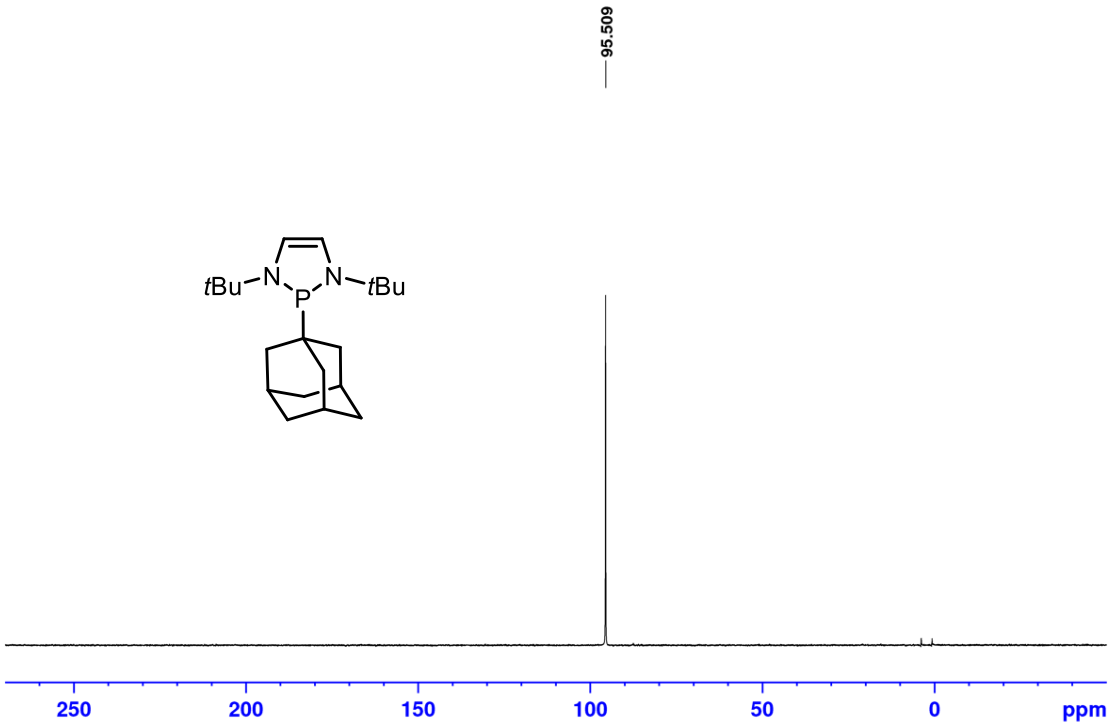


**Figure A296:** $^{31}$P NMR (202.5 MHz, $C_6D_6$) spectrum of *P*-adamantyl diazaphospholene **7-15**.

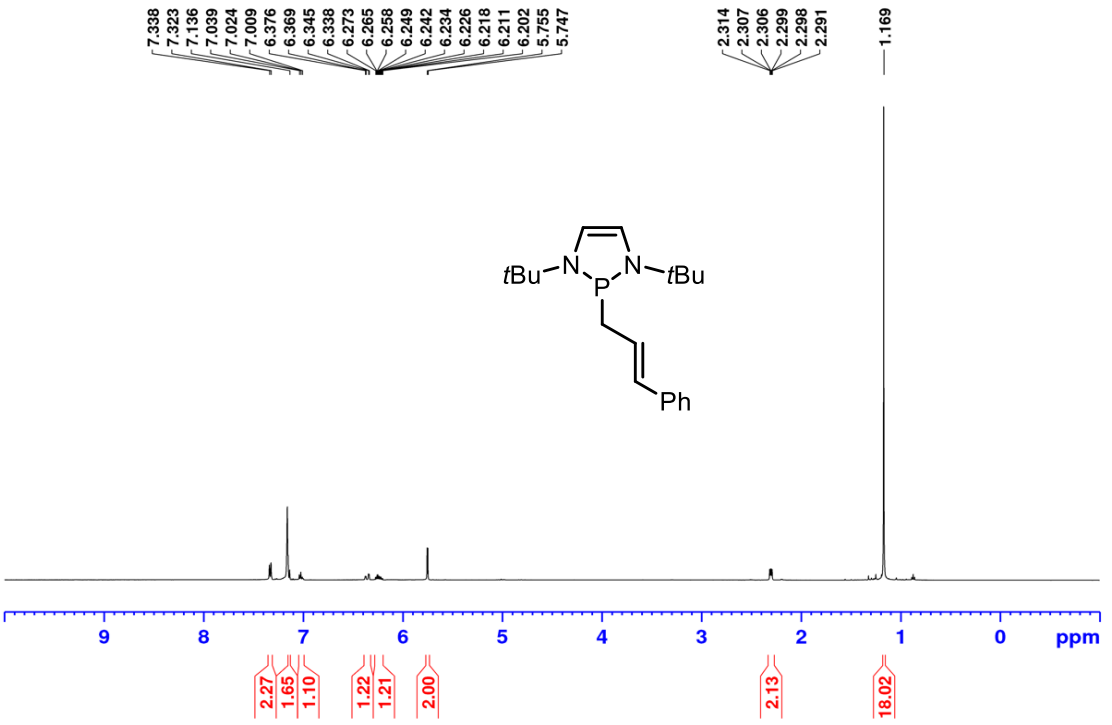


**Figure A297:** $^{1}$H NMR (500 MHz, $C_6D_6$) spectrum of *P*-cinnamyl diazaphospholene **7-16**.

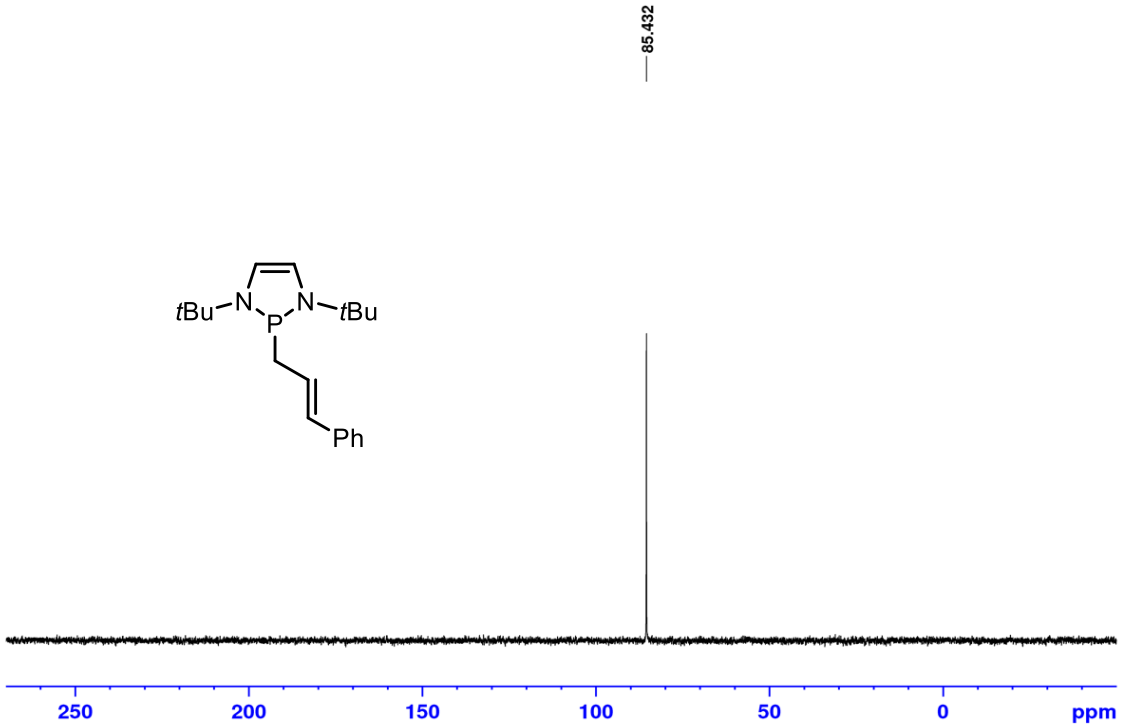


Figure A298: $^{31}$P NMR (202.5 MHz, $C_6D_6$) spectrum of *P*-cinnamyl diazaphospholene **7-16**.

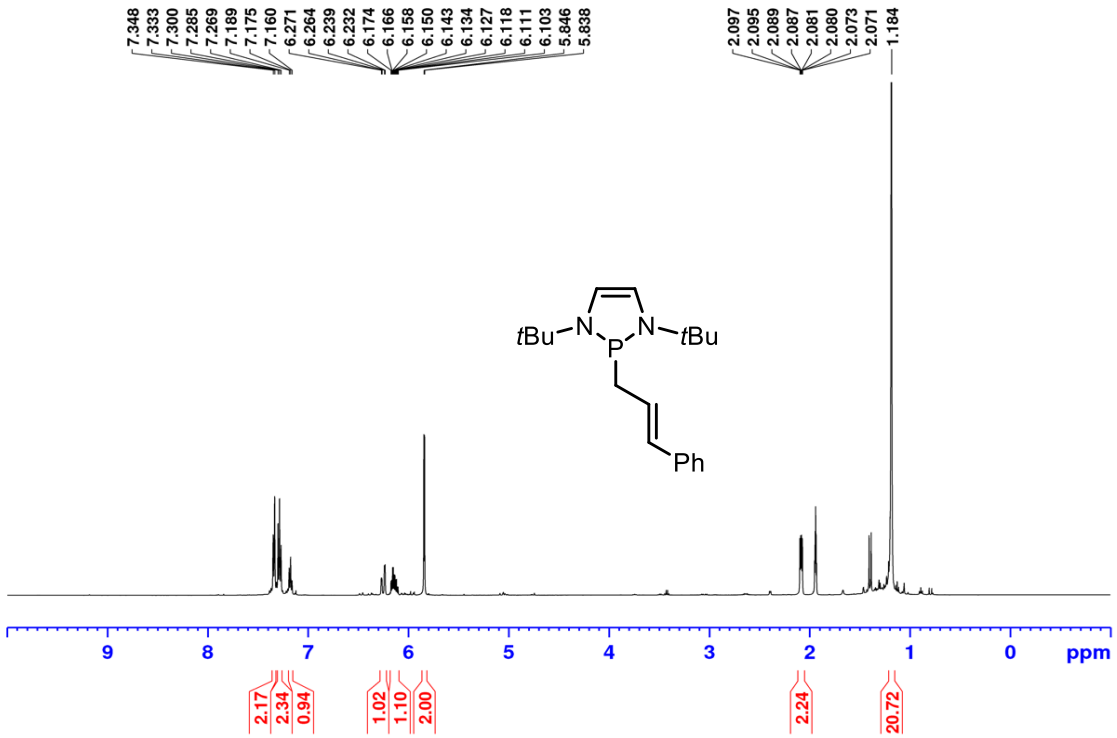


**Figure A299:** $^{1}$H NMR (500 MHz, $CD_3CN$) spectrum of *P*-cinnamyl diazaphospholene **7-16**.

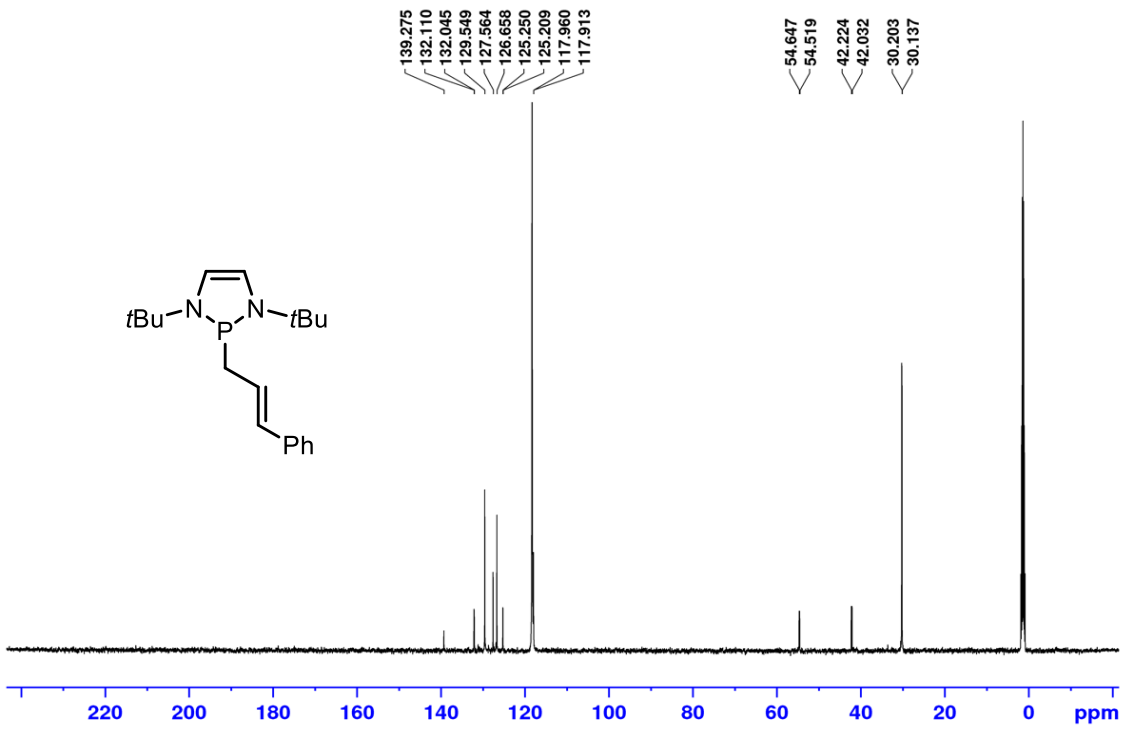


**Figure A300:** $^{13}C$ {$^{1}H$} NMR (125.8 MHz, $CD_3CN$) spectrum of *P*-cinnamyl diazaphospholene **7-16**.

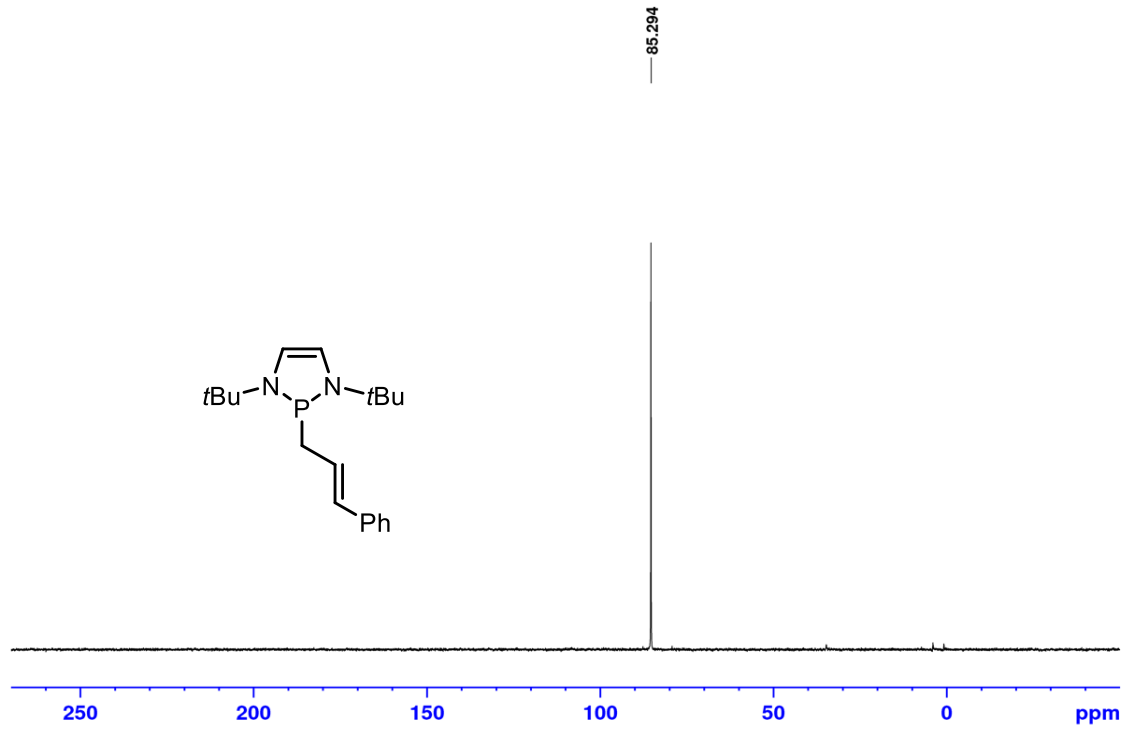


**Figure A301:** $^{31}P$ NMR (202.5 MHz, $CD_3CN$) spectrum of *P*-cinnamyl diazaphospholene **7-16**.

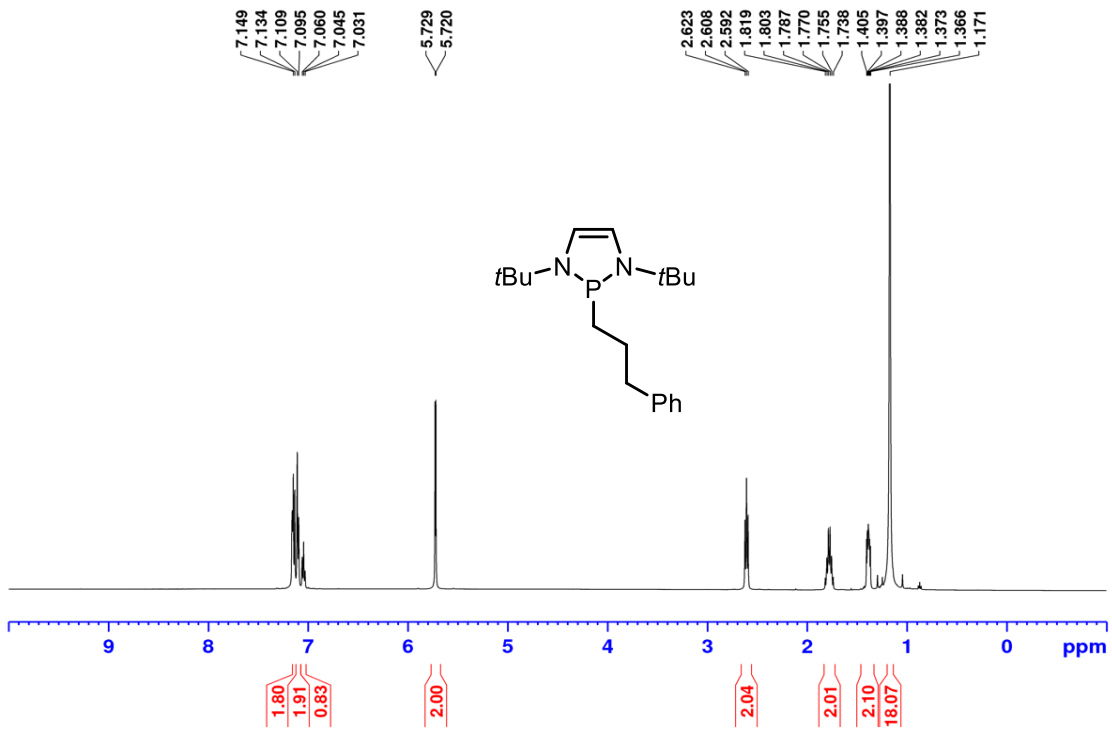


**Figure A302:** $^{1}$H NMR (500 MHz, $C_6D_6$) spectrum of *P*-(3-phenyl-1-propyl) diazaphospholene **7-17**.

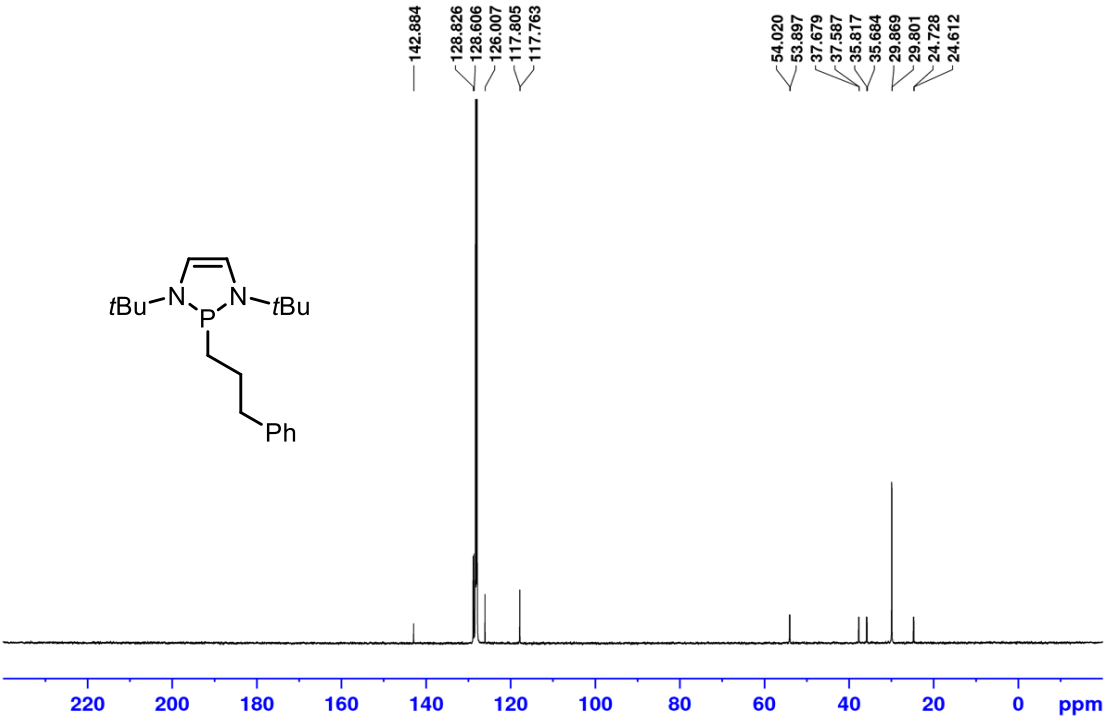


**Figure A303:** $^{13}$C {$^{1}$H} NMR (125.8 MHz, $C_6D_6$) spectrum of *P*-(3-phenyl-1-propyl) diazaphospholene **7-17**.

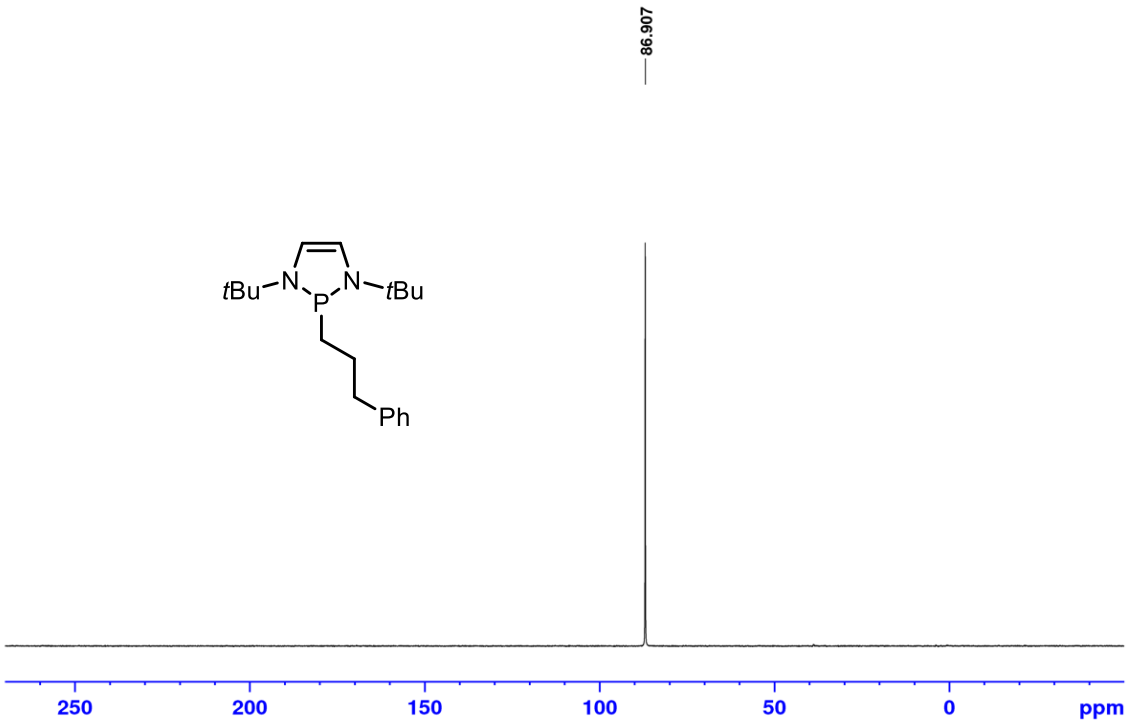


**Figure A304:** $^{31}$P NMR (202.5 MHz, $C_6D_6$) spectrum of *P*-(3-phenyl-1-propyl) diazaphospholene **7-17**.

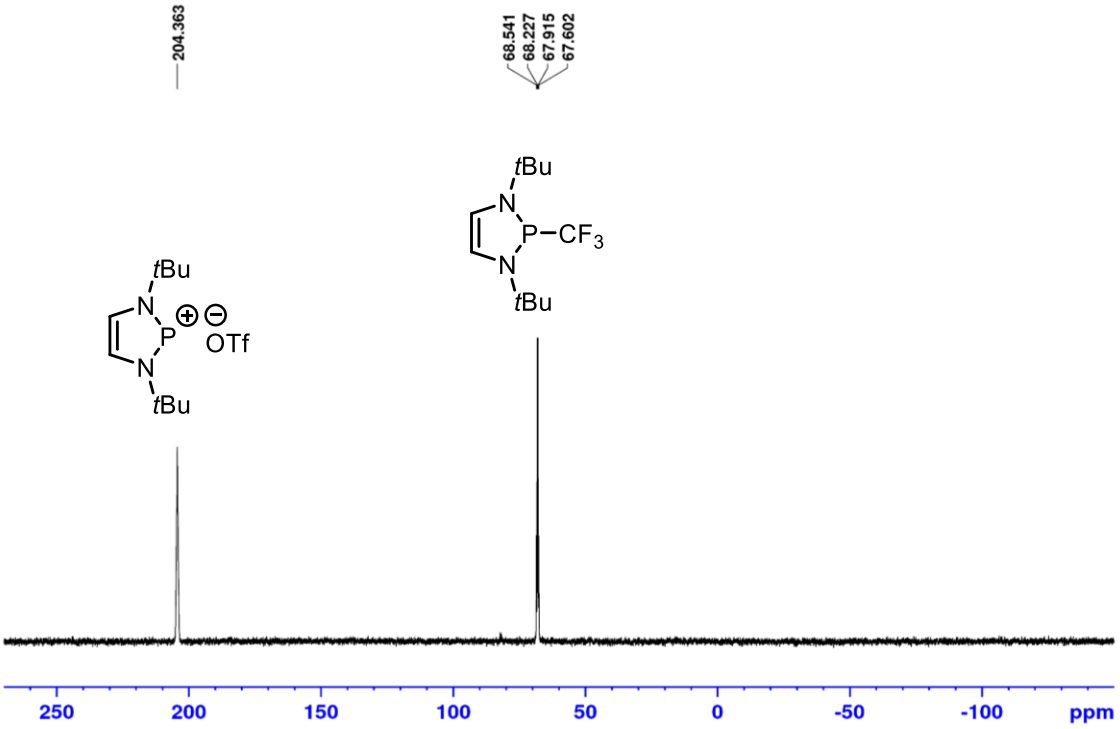


**Figure A305:** $^{31}$P NMR (202.5 MHz, $C_6D_6$) spectrum of reaction of diazaphospholene dimer **7-1** with Umemoto's reagent.

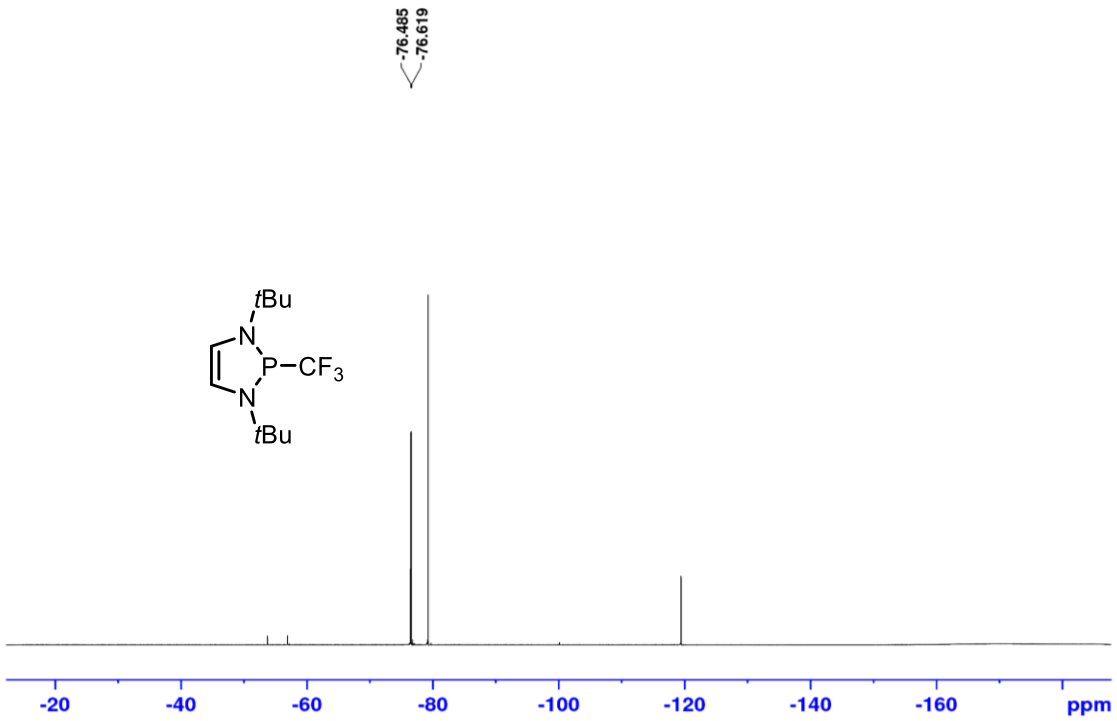


**Figure A306:** $^{19}F$ {$^{1}H$} (470.6 MHz, $C_6D_6$) spectrum of reaction of diazaphospholene dimer **7-1** with Umemoto's reagent**.**

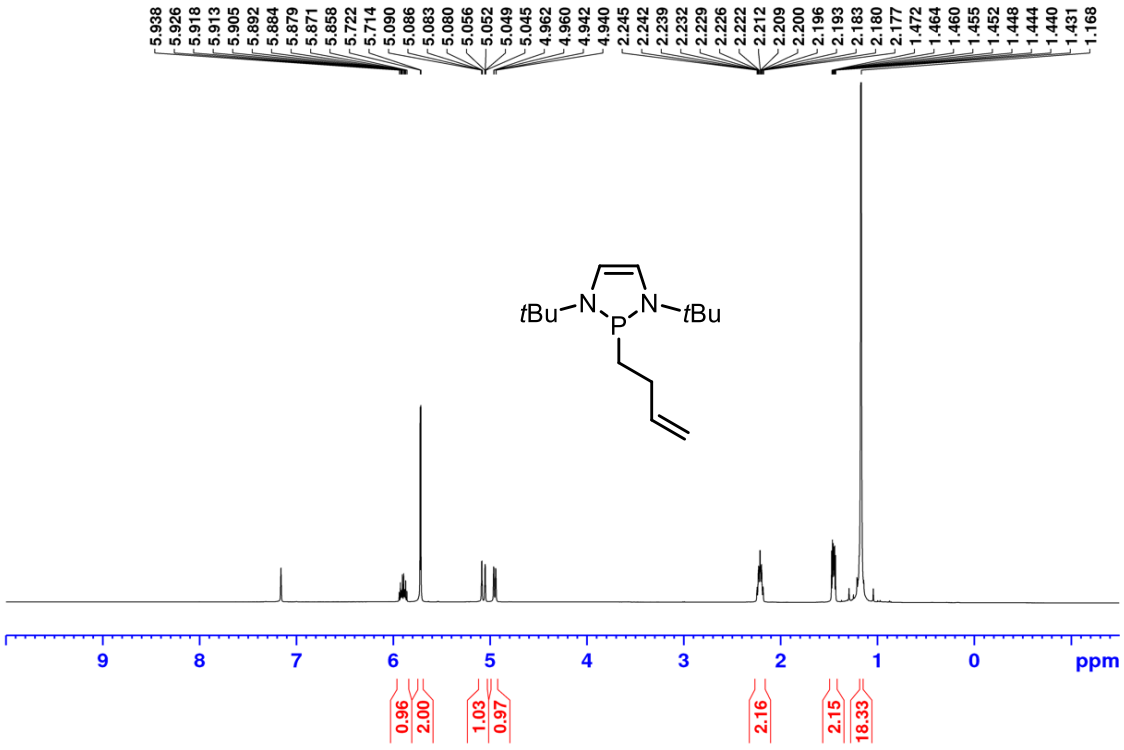


**Figure A307:** $^{1}H$ NMR (500 MHz, $C_6D_6$) spectrum of treatment of dimer **7-1** with cyclopropyl methyl bromide in toluene with blue light irradiation. *P*-(3-butenyl) diazaphospholene **7-18**.

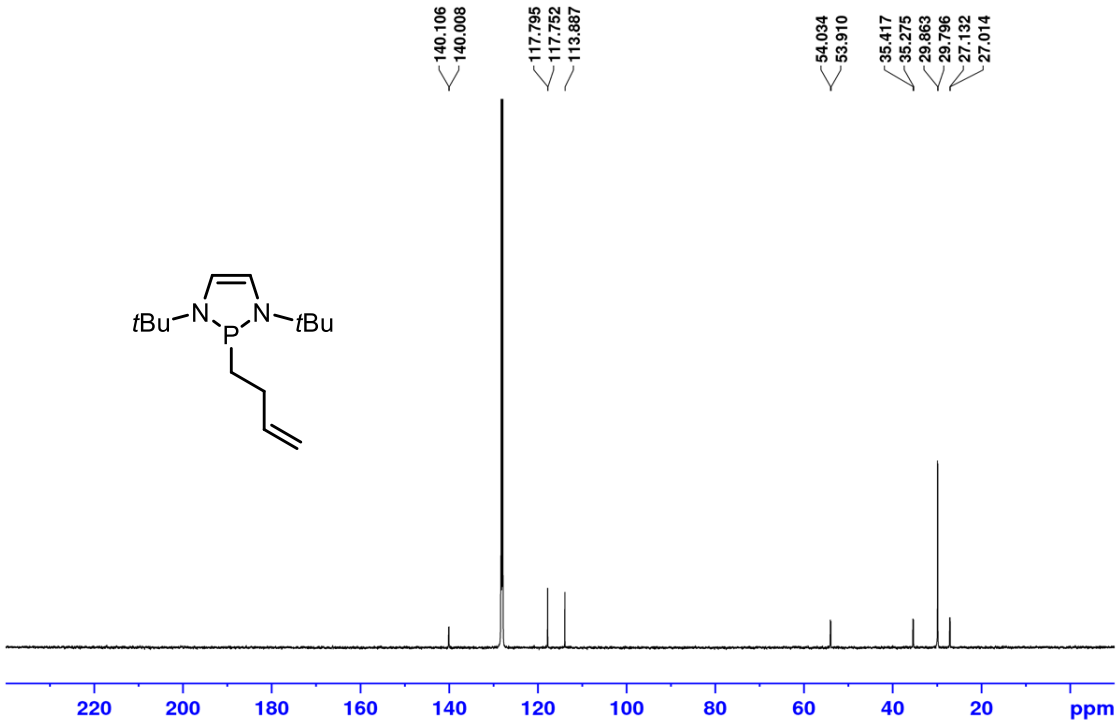


**Figure A308:** $^{13}C$ {$^{1}H$} NMR (125.8 MHz, $C_6D_6$) spectrum of treatment of dimer **7-1** with cyclopropyl methyl bromide in toluene with blue light irradiation. *P*-(3-butenyl) diazaphospholene **7-18**.

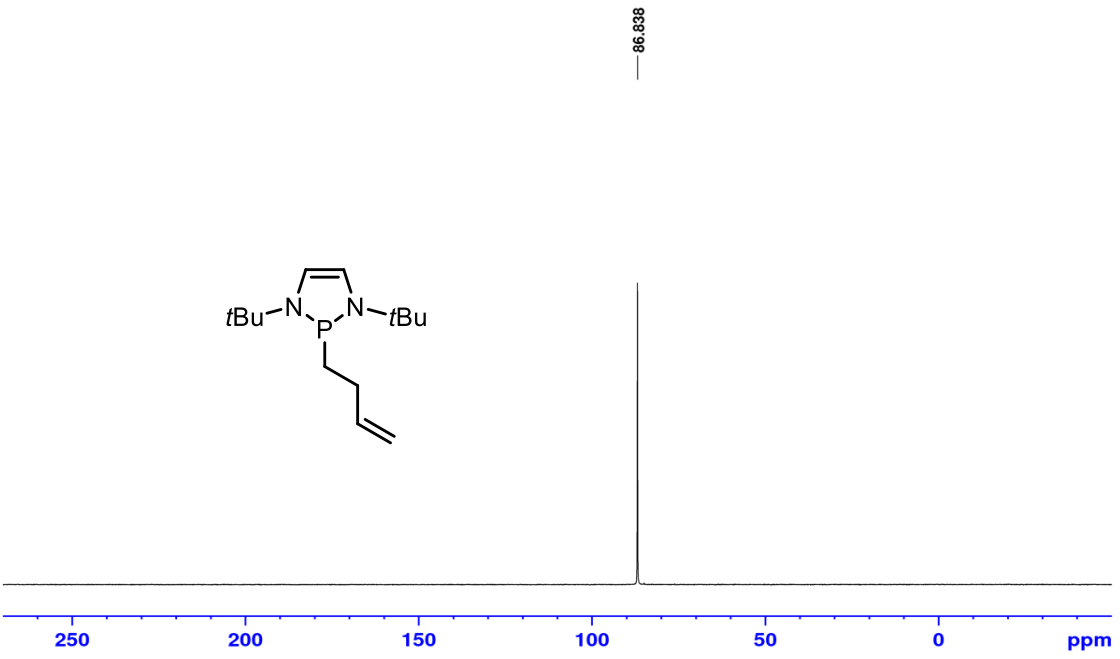


**Figure A309:** $^{31}P$ NMR (202.5 MHz, $C_6D_6$) spectrum of treatment of dimer **7-1** with cyclopropyl methyl bromide in toluene with blue light irradiation. *P*-(3-butenyl) diazaphospholene **7-18**.

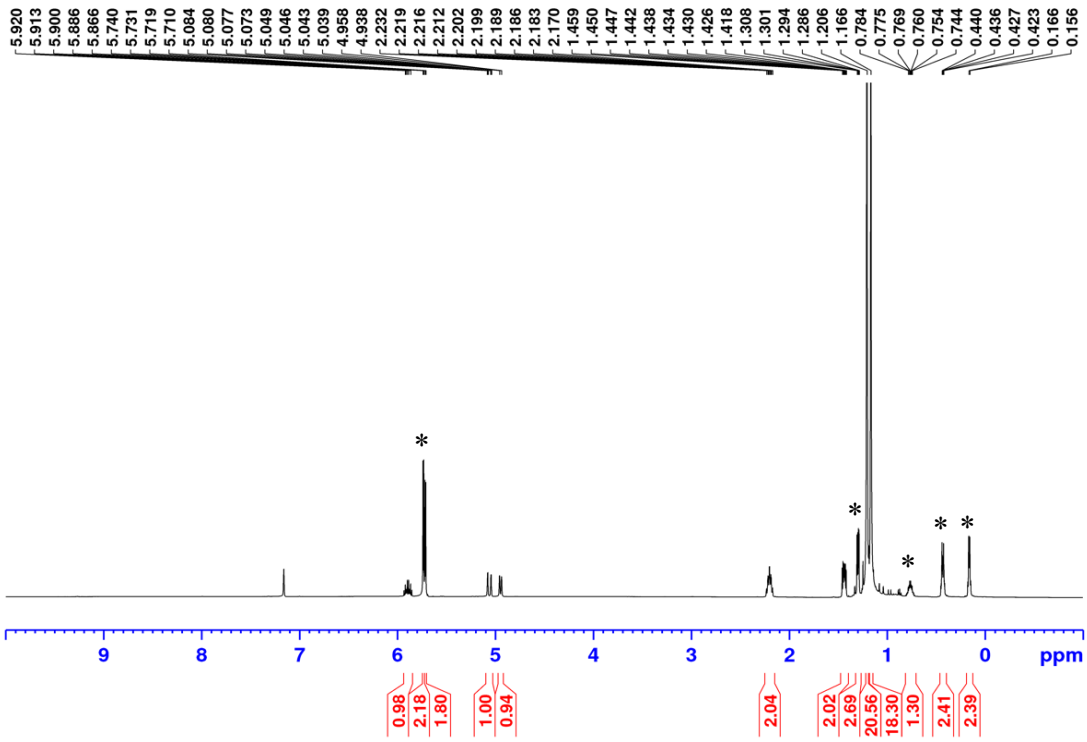


**Figure A310:** $^{1}$H NMR (300 MHz, $C_6D_6$) spectrum of treatment of dimer **7-1** with cyclopropyl methyl bromide in acetonitrile without blue light irradiation. *P*-(3-butenyl) diazaphospholene **7-18**. / *P*-(cyclopropylmethyl) diazaphospholene **7-19** (*).

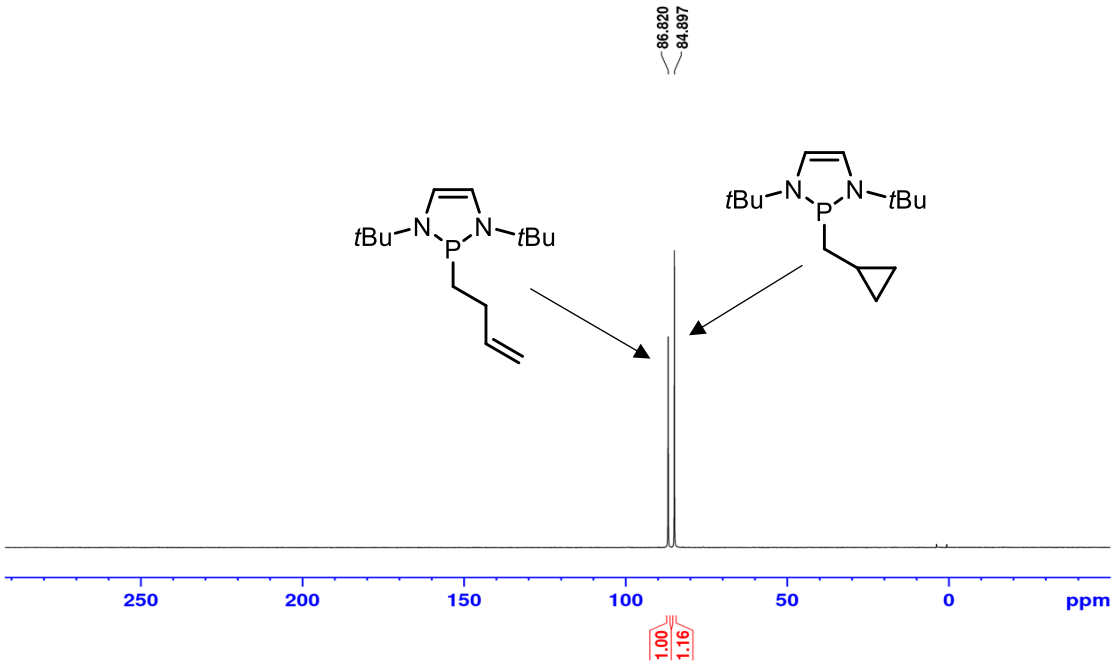


**Figure A311:** $^{31}$P NMR (121.5 MHz, $C_6D_6$) spectrum of spectrum of treatment of dimer **7-1** with cyclopropyl methyl bromide in acetonitrile without blue light irradiation. *P*-(3-butenyl) diazaphospholene **7-18**. / *P*-(cyclopropylmethyl) diazaphospholene **7-19**.

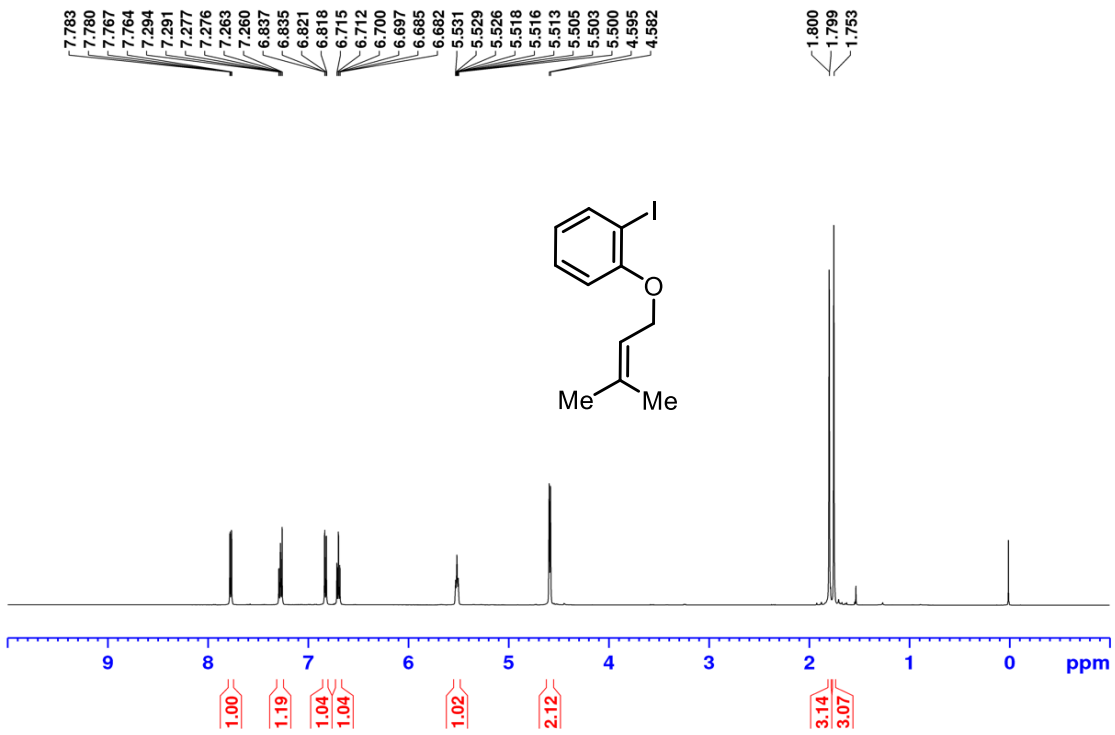


**Figure A312:** $^{1}$H NMR (500 MHz, $CDCl_3$) spectrum of 1-(2-Iodophenoxy)-3-methyl-2-butene.

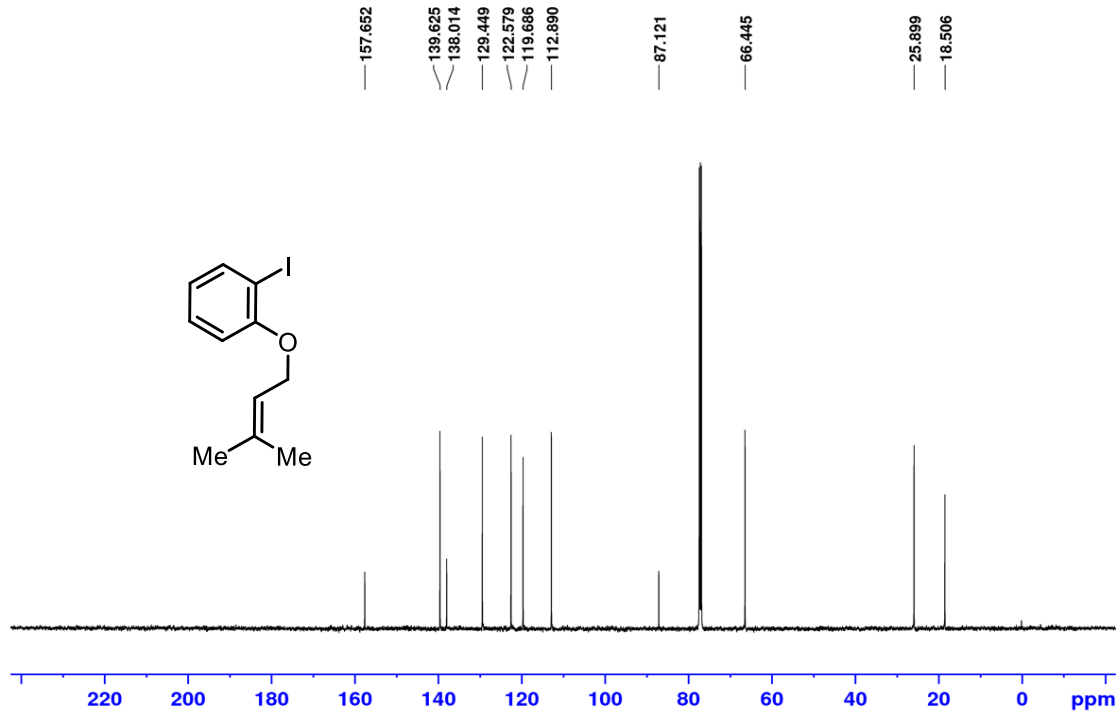


**Figure A313:** $^{13}$C {$^{1}$H} NMR (125.8 MHz, $CDCl_3$) spectrum of 1-(2-Iodophenoxy)-3-methyl-2-butene.

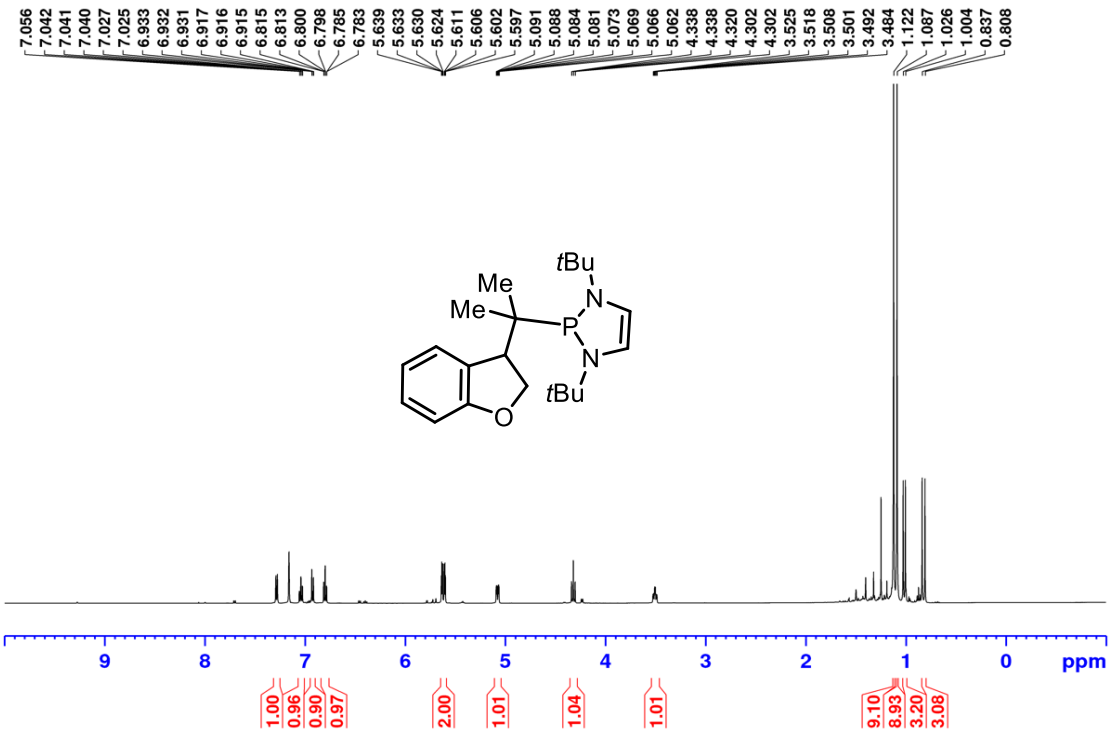


**Figure A314:** $^{1}$H NMR (500 MHz, $C_6D_6$) spectrum of compound **7-20**.

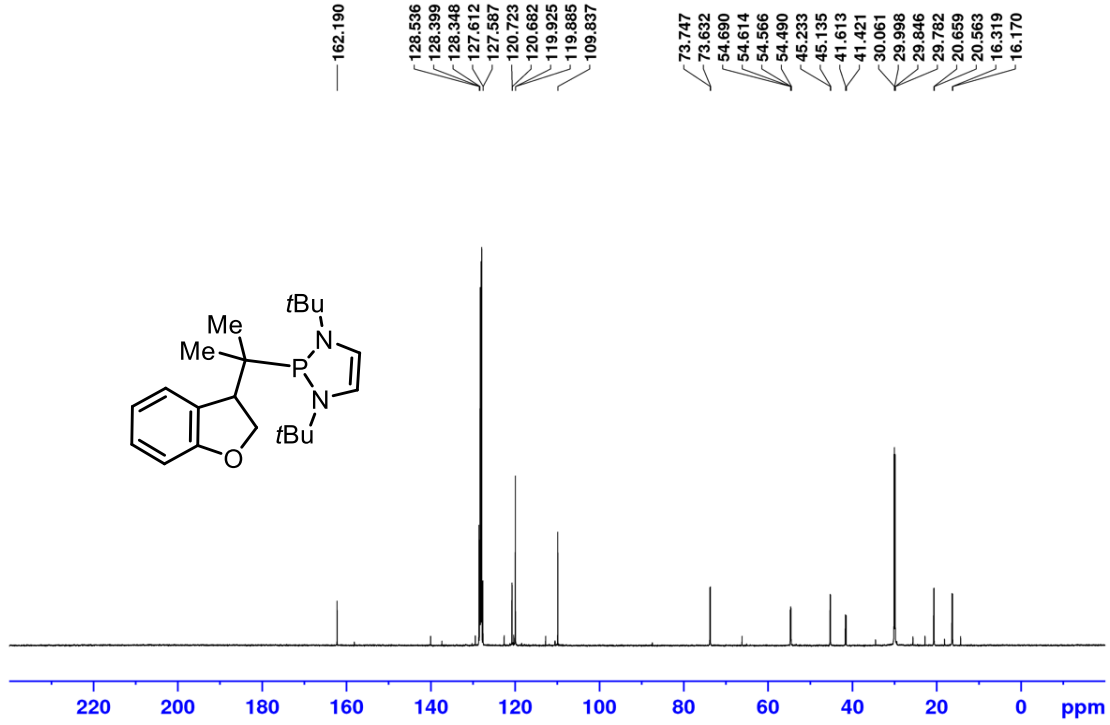


**Figure A315:** $^{13}$C {$^{1}$H} NMR (125.8 MHz, $C_6D_6$) spectrum of compound **7-20**.

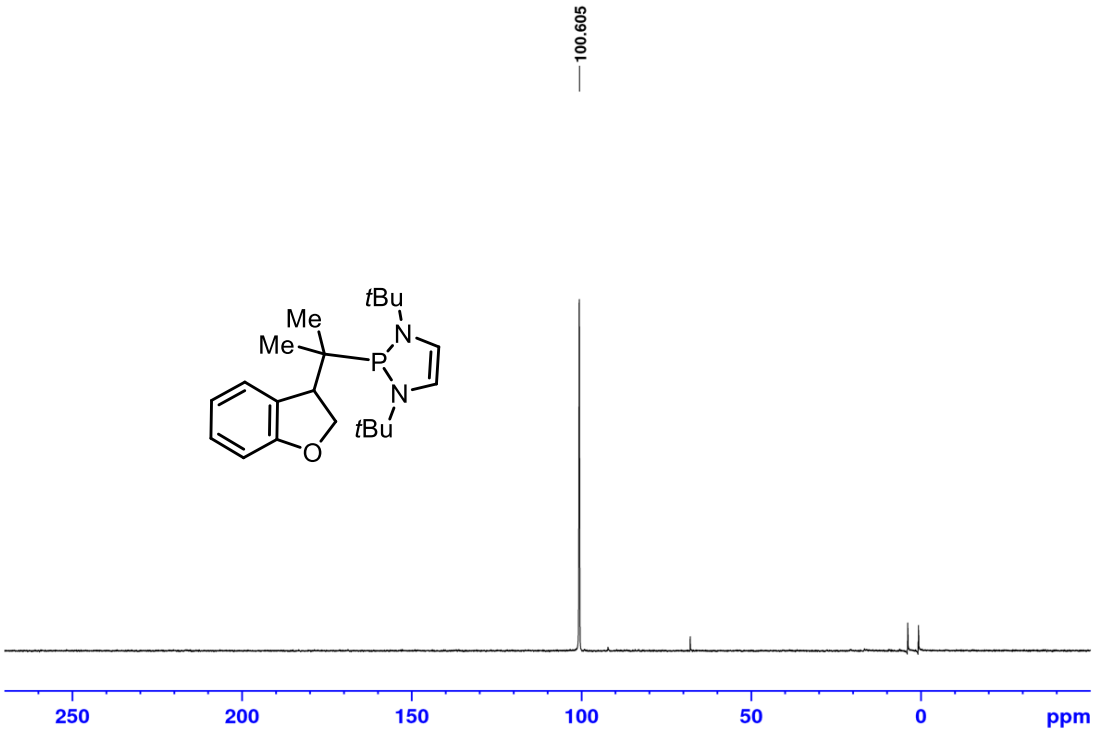


**Figure A316:** $^{31}$P NMR (202.5 MHz, $C_6D_6$) spectrum of compound **7-20**.

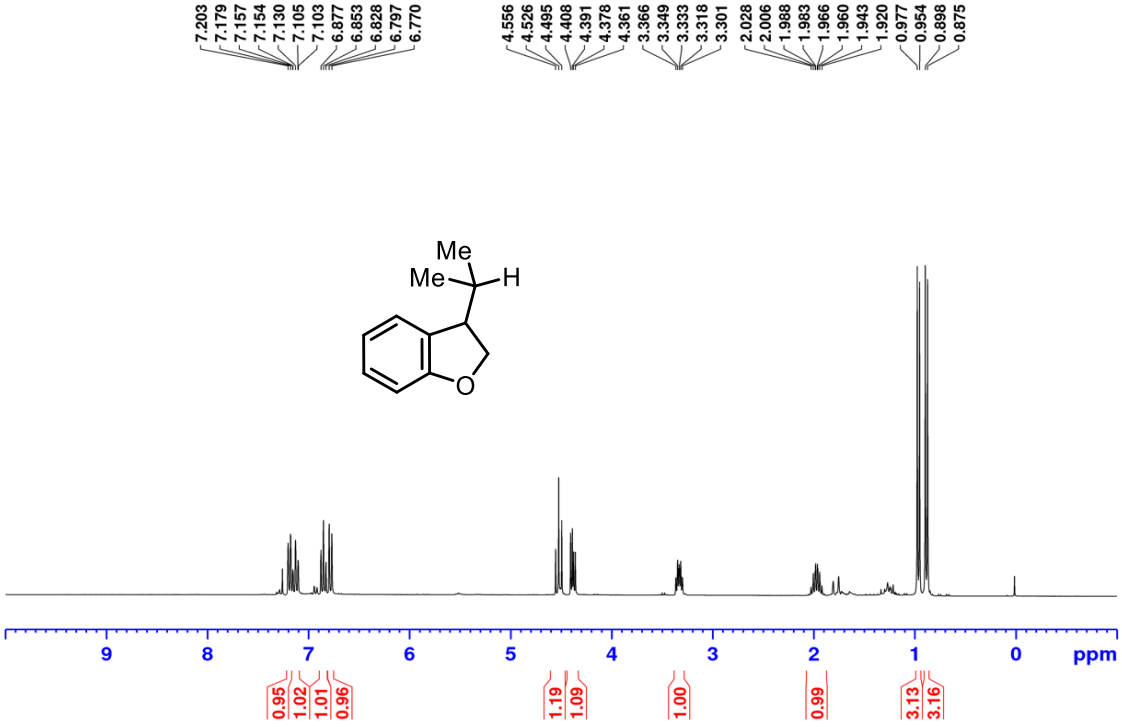


Figure A317: $^{1}$H NMR (500 MHz, $CDCl_3$) spectrum of compound **7-22**.

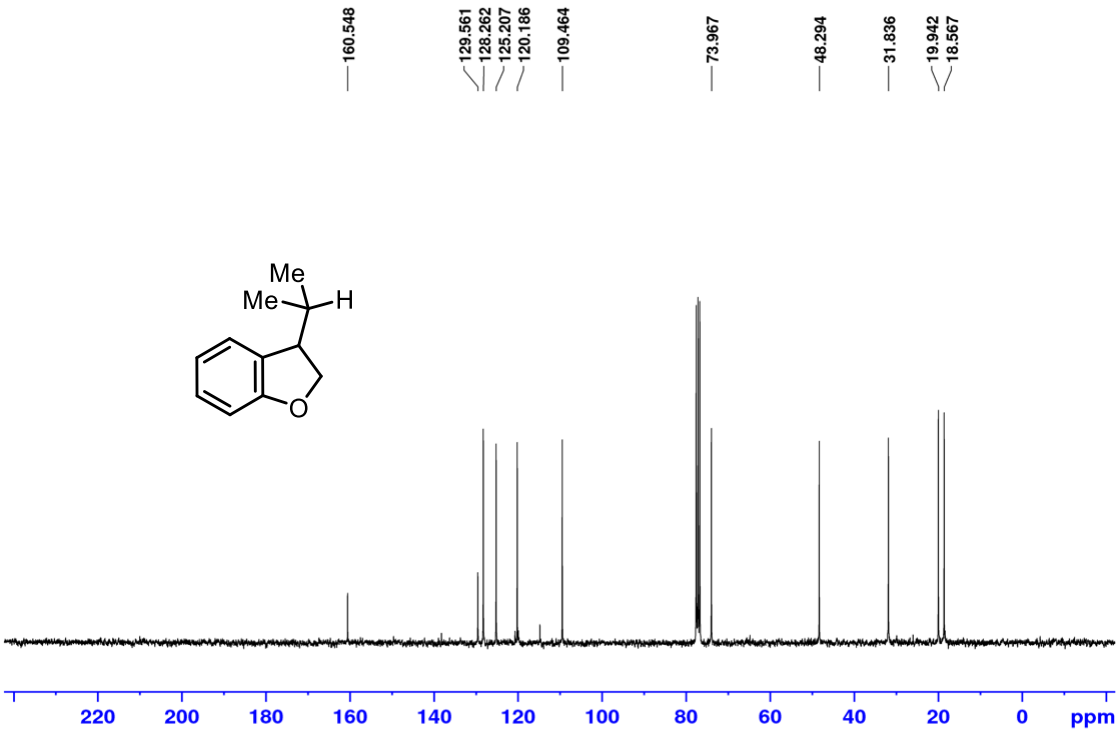


**Figure A318:** $^{13}C$ {$^{1}H$} NMR (125.8 MHz, $CDCl_3$) spectrum of compound **7-22**.

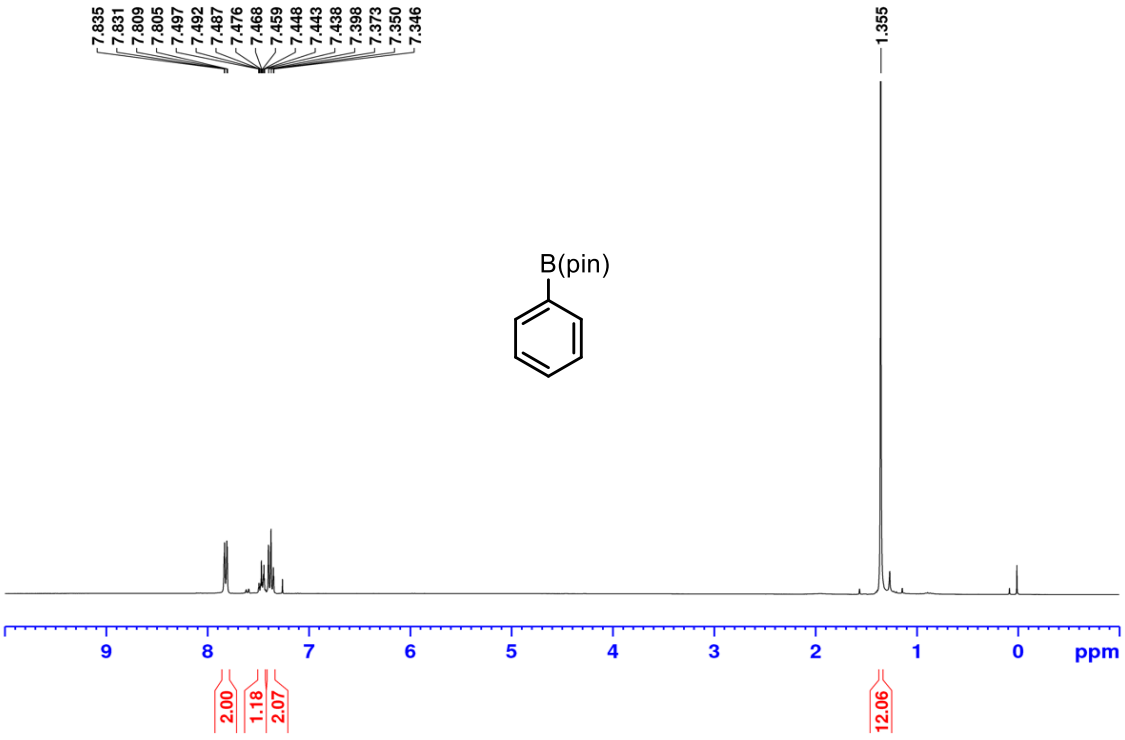


**Figure A319:** $^{1}H$ NMR (300 MHz, $CDCl_3$) spectrum of phenyl-Bpin **7-34**.

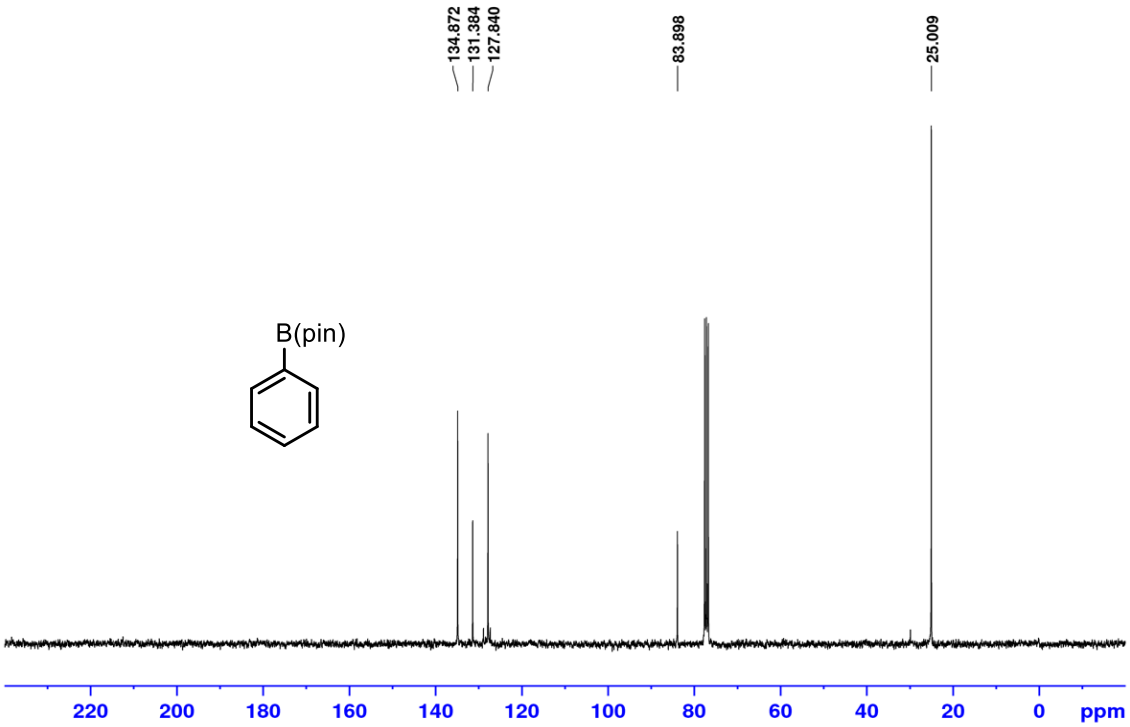


**Figure A320:** $^{13}C$ {$^{1}H$} NMR (75.5 MHz, $CDCl_3$) spectrum of phenyl-Bpin **7-34**.

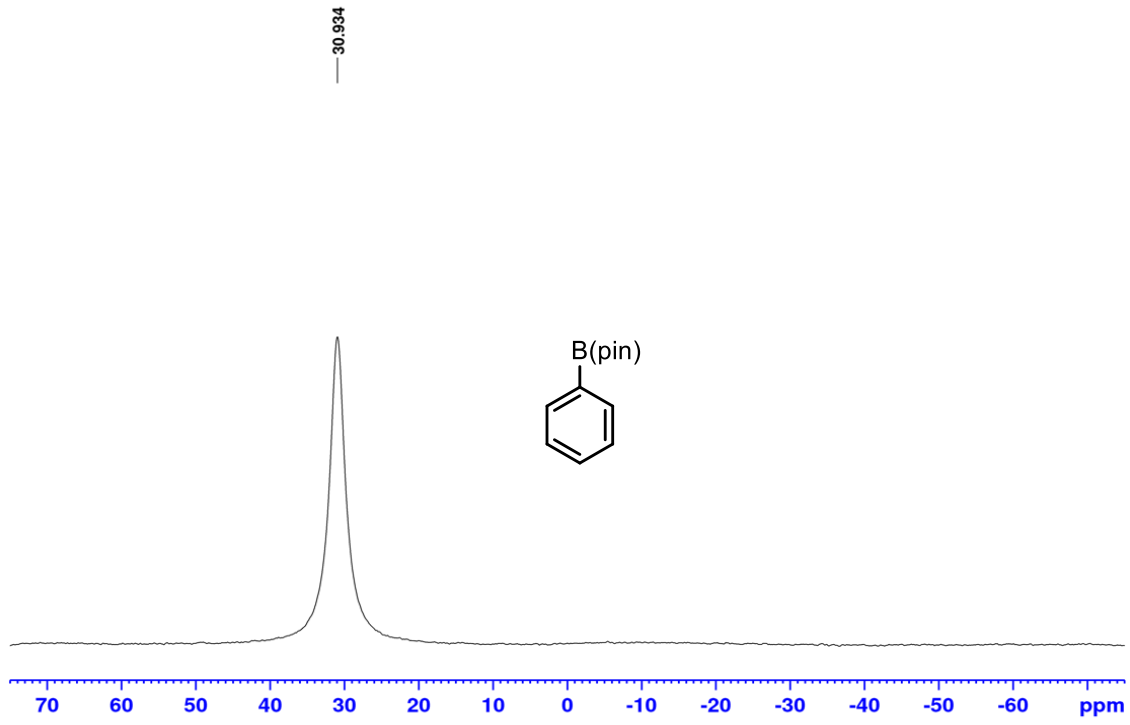


**Figure A321:** $^{11}B$ NMR (96.3 MHz, $C_6D_6$) spectrum of phenyl-Bpin **7-34**.

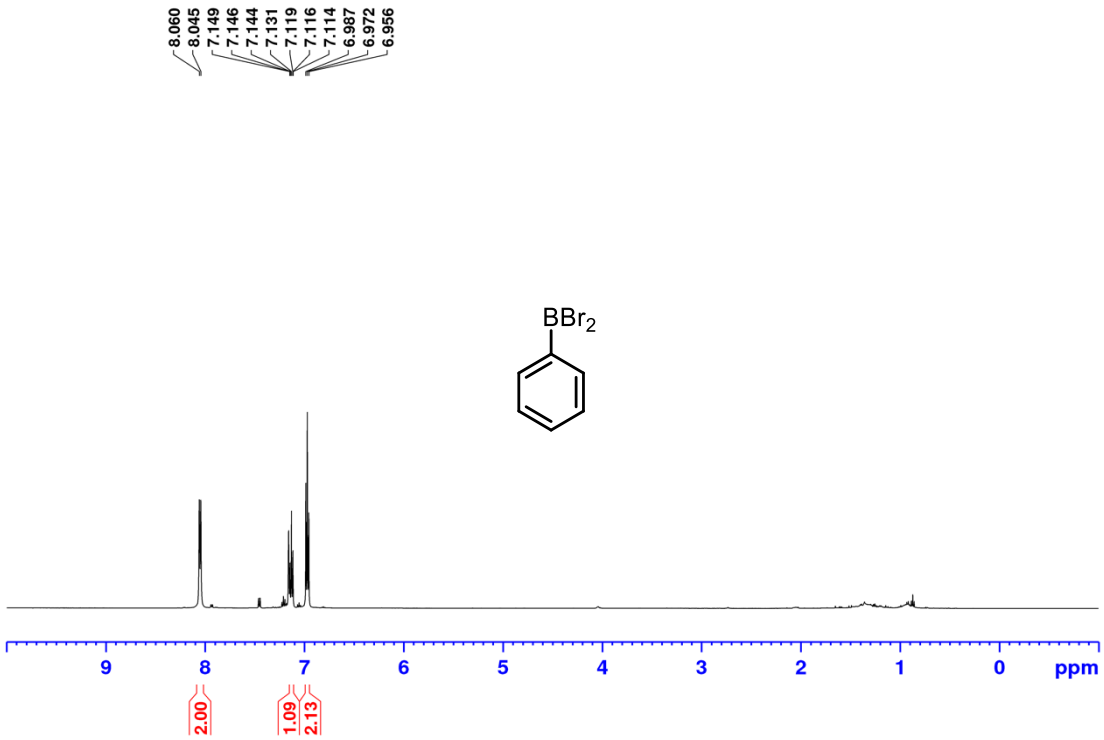


**Figure A322:** $^{1}$H NMR (500 MHz, $C_6D_6$) spectrum of phenyl-$BBr_2$ **7-32**.

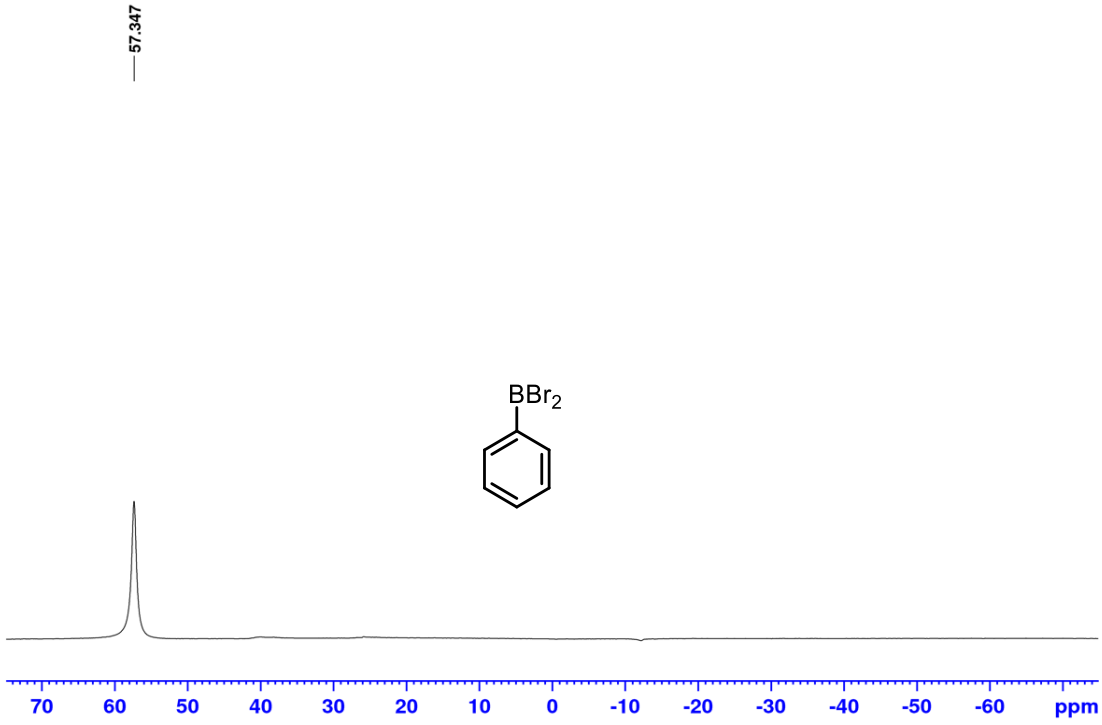


**Figure A323:** $^{11}$B NMR (160.5 MHz, $C_6D_6$) spectrum of phenyl-$BBr_2$ **7-32**.

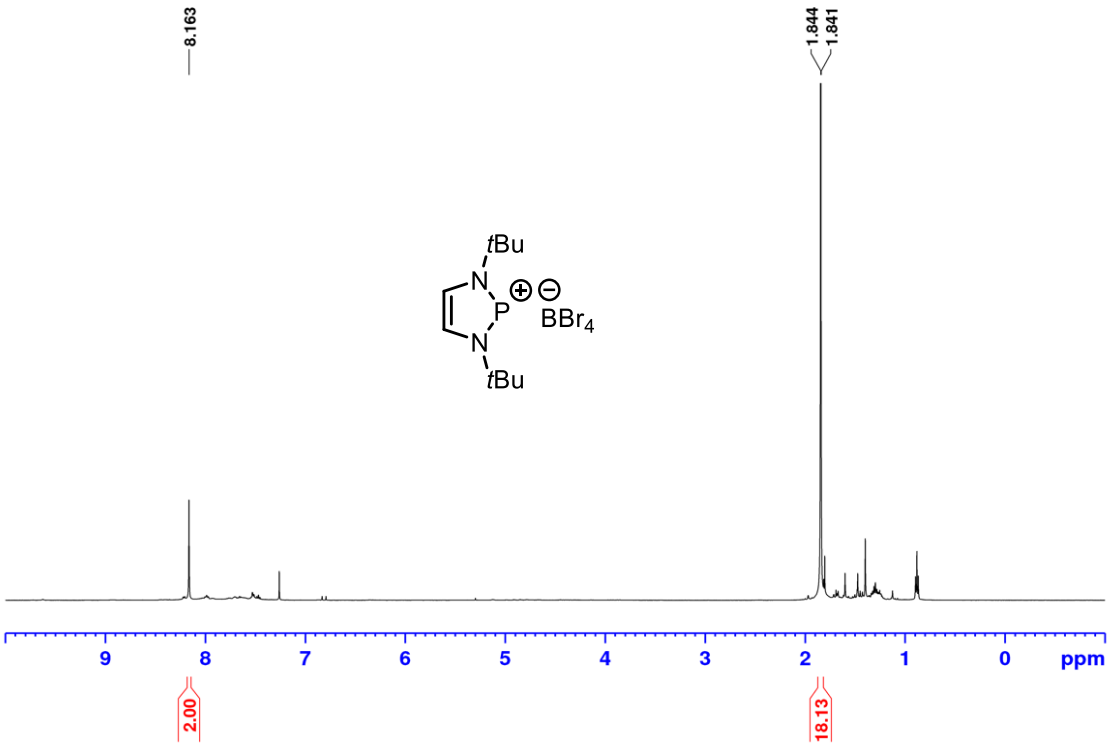


**Figure A324:** $^{1}$H NMR (500 MHz, $C_6D_6$) spectrum of compound **7-33**.

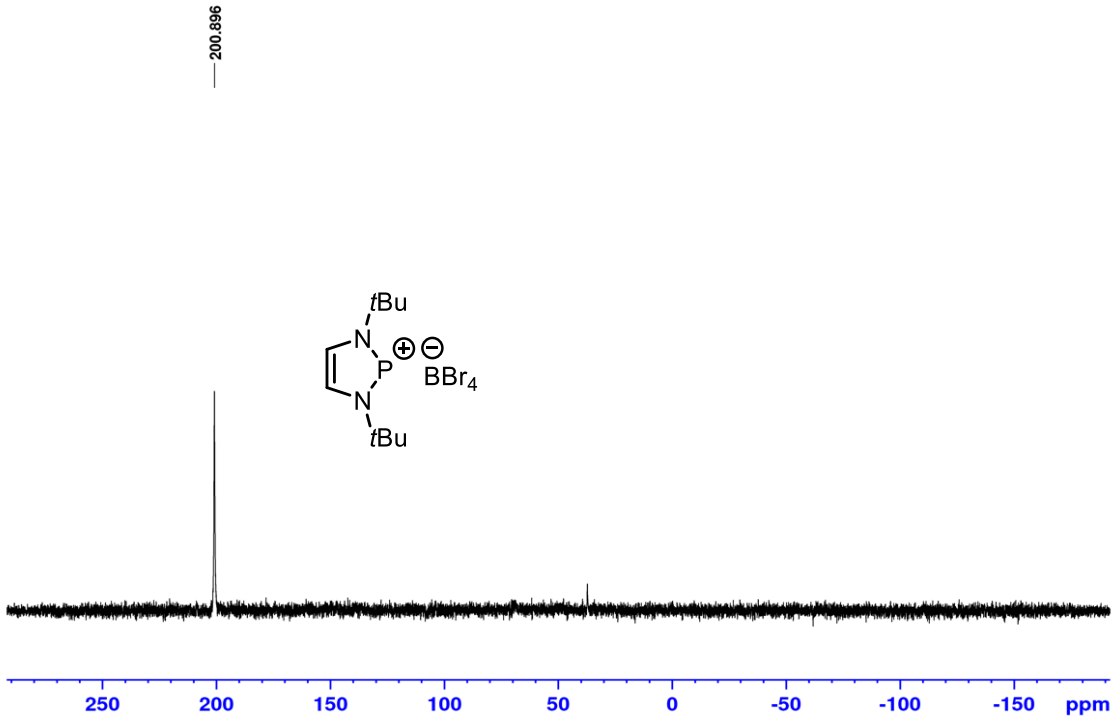


**Figure A325:** $^{31}$P NMR (202.5 MHz, $C_6D_6$) spectrum of compound **7-33**.

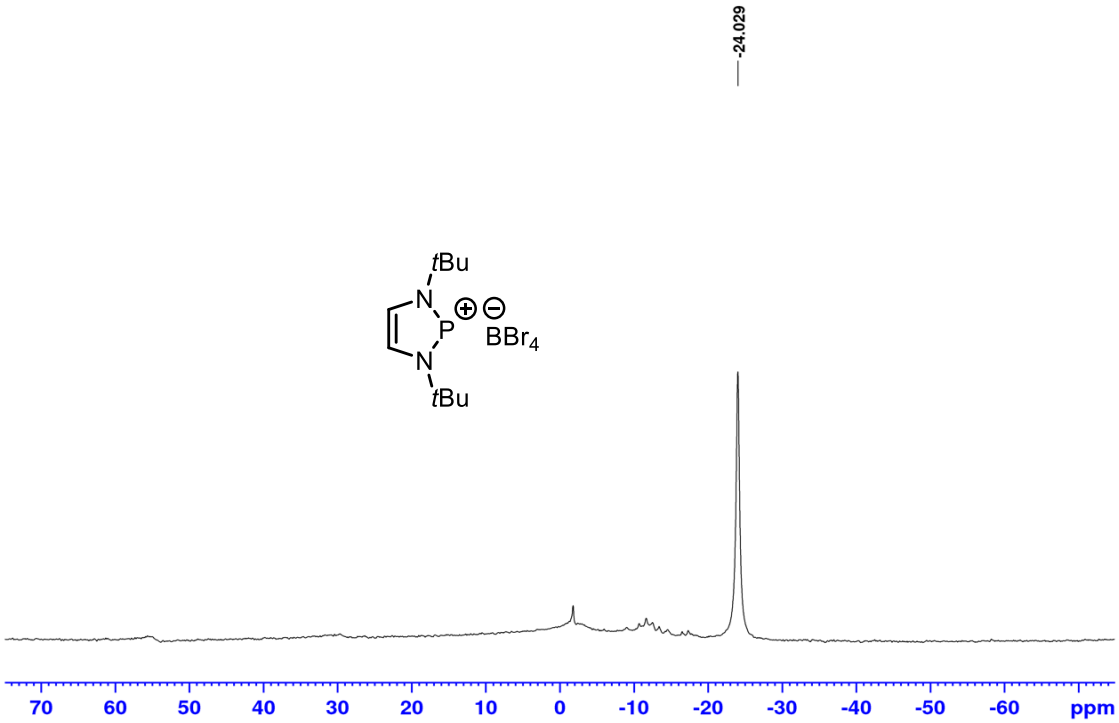


**Figure A326:** $^{11}$B NMR (160.5 MHz, $C_6D_6$) spectrum of compound **7-33**.

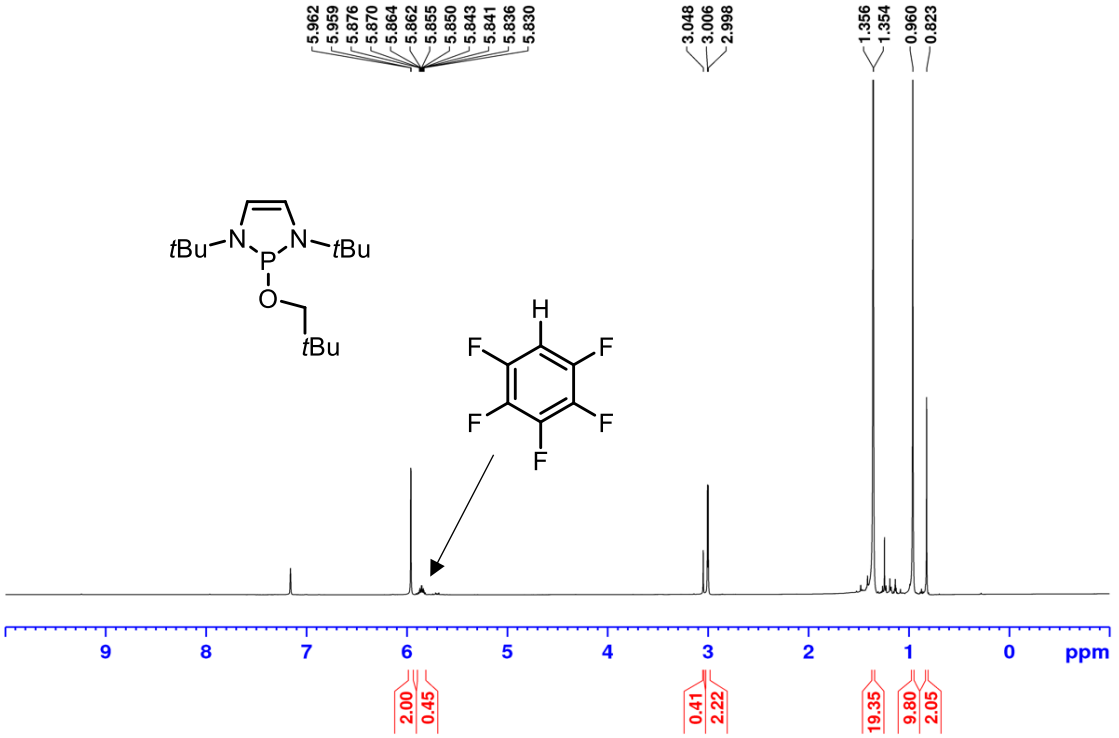


**Figure A327:** $^{1}$H NMR (500 MHz, $C_6D_6$) spectrum of reaction of *P*-pentafluorophenyl diazaphospholene **7-6** with neopentyl alcohol.

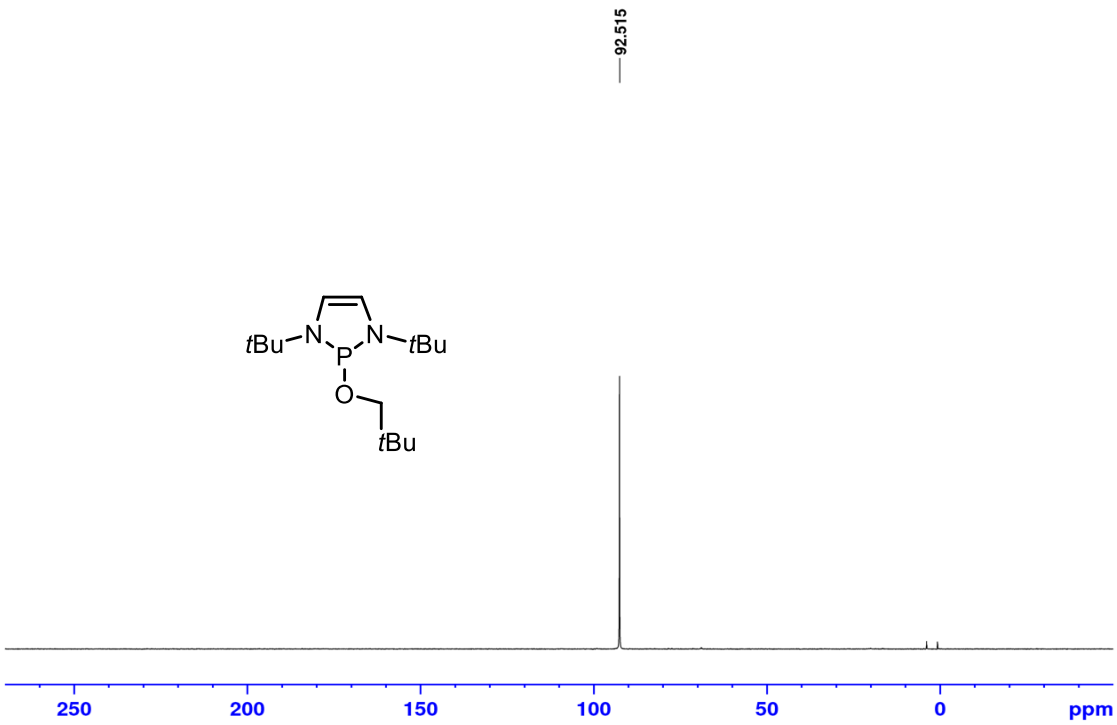


**Figure A328:** $^{31}P$ NMR (202.5 MHz, $C_6D_6$) spectrum of reaction of *P*-pentafluorophenyl diazaphospholene **7-6** with neopentyl alcohol.

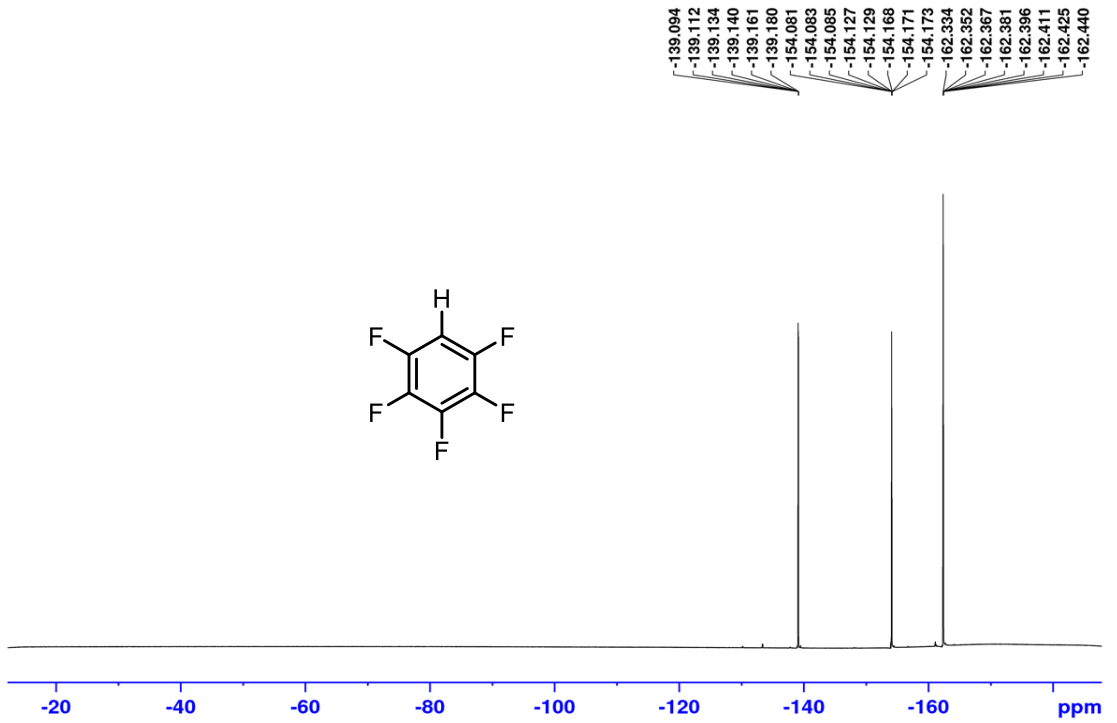


**Figure A329:** $^{19}F$ $\{^1H\}$ (470.6 MHz, $C_6D_6$) spectrum of reaction of *P*-pentafluorophenyl diazaphospholene **7-6** with neopentyl alcohol.

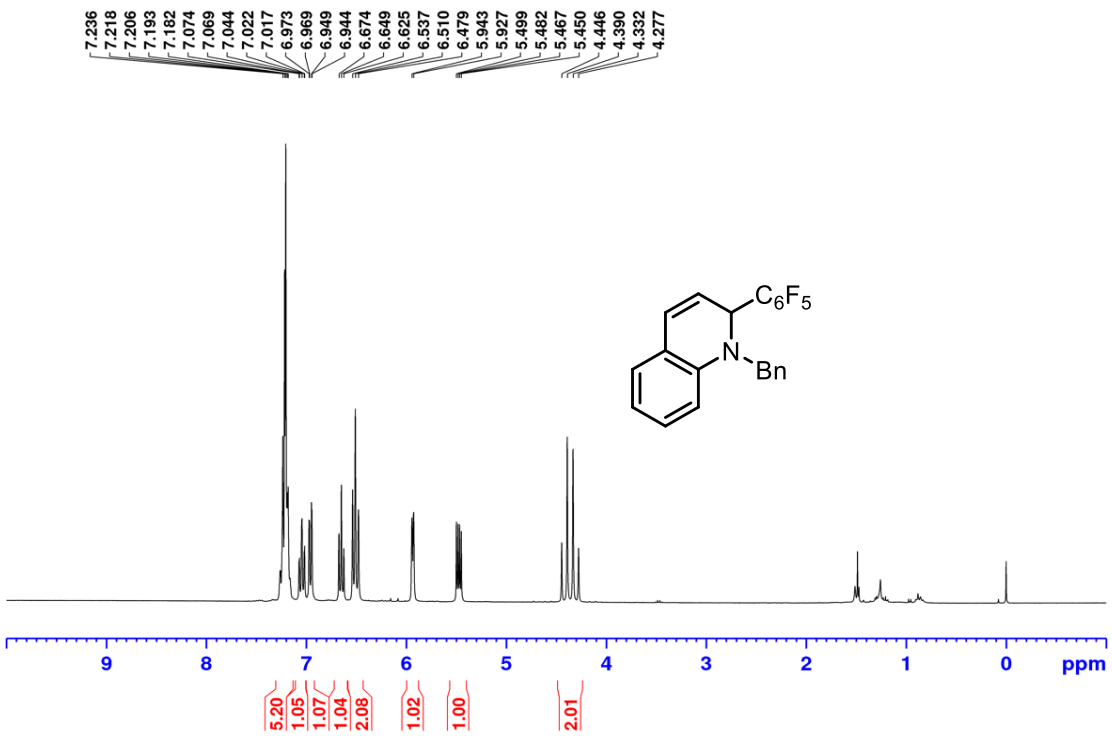


**Figure A330:** $^{1}$H NMR (500 MHz, $CDCl_3$) spectrum of compound **7-25**.

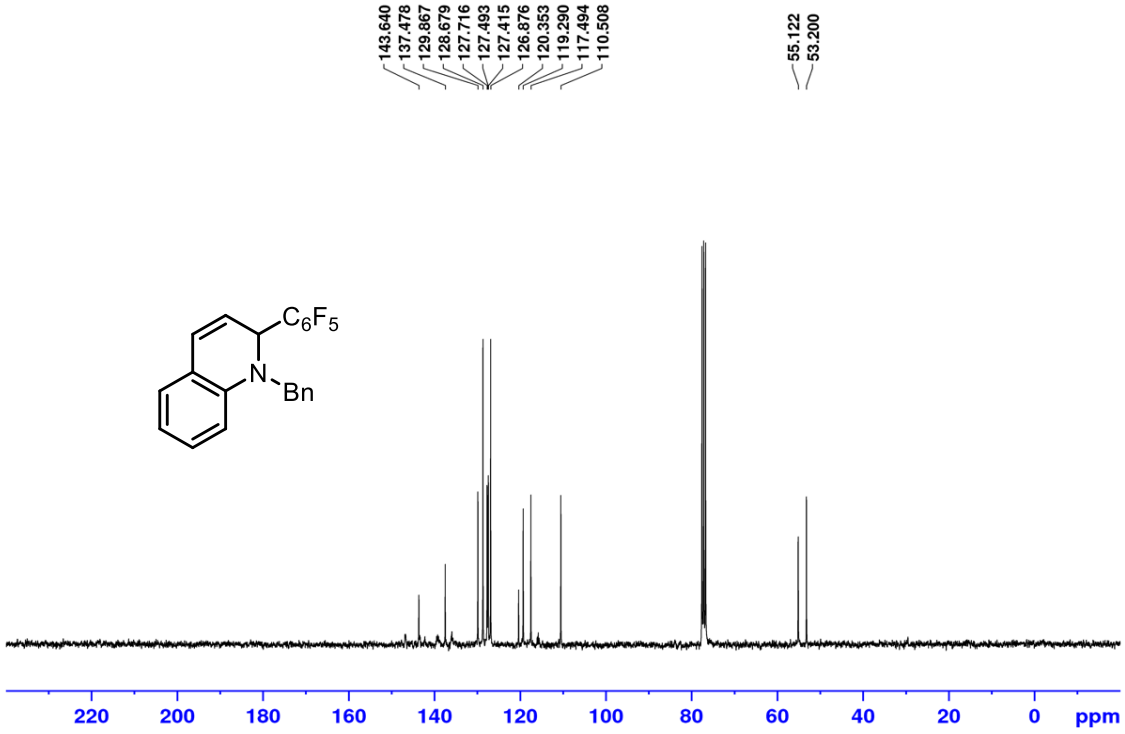


**Figure A331:** $^{13}$C {$^{1}$H} NMR (75.5 MHz, $CDCl_3$) spectrum of compound **7-25**.

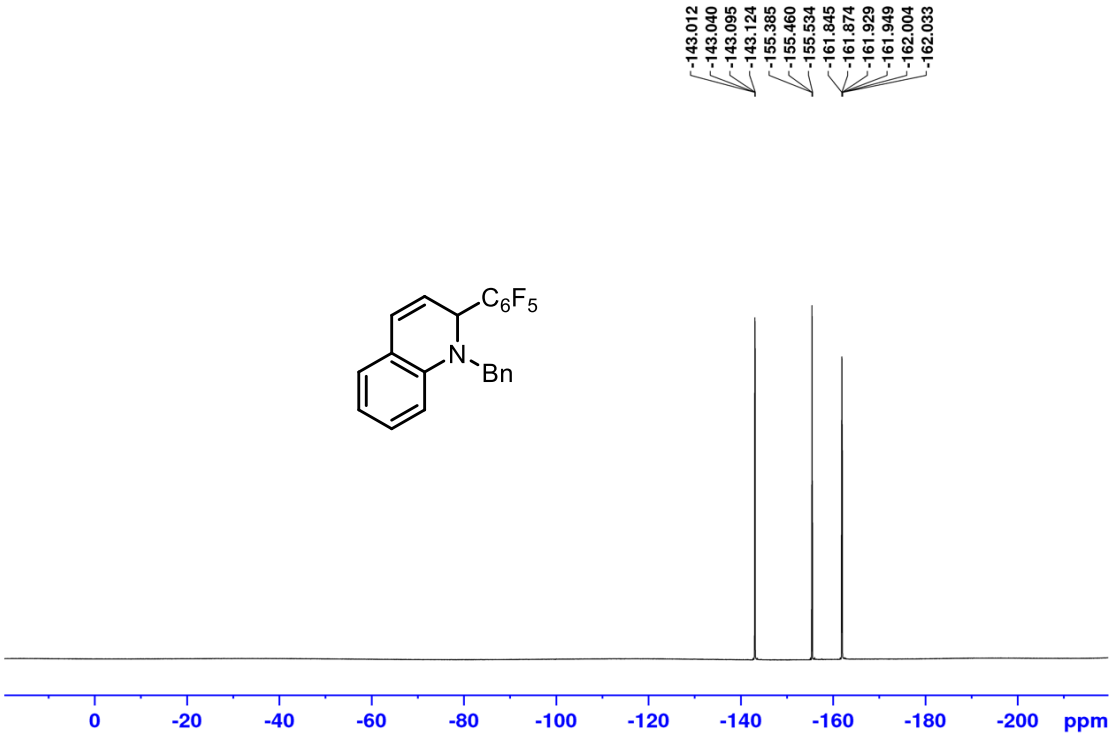


**Figure A332:** $^{19}F$ $\{^{1}H\}$ (470.6 MHz, $CDCl_3$) spectrum of compound **7-25**.

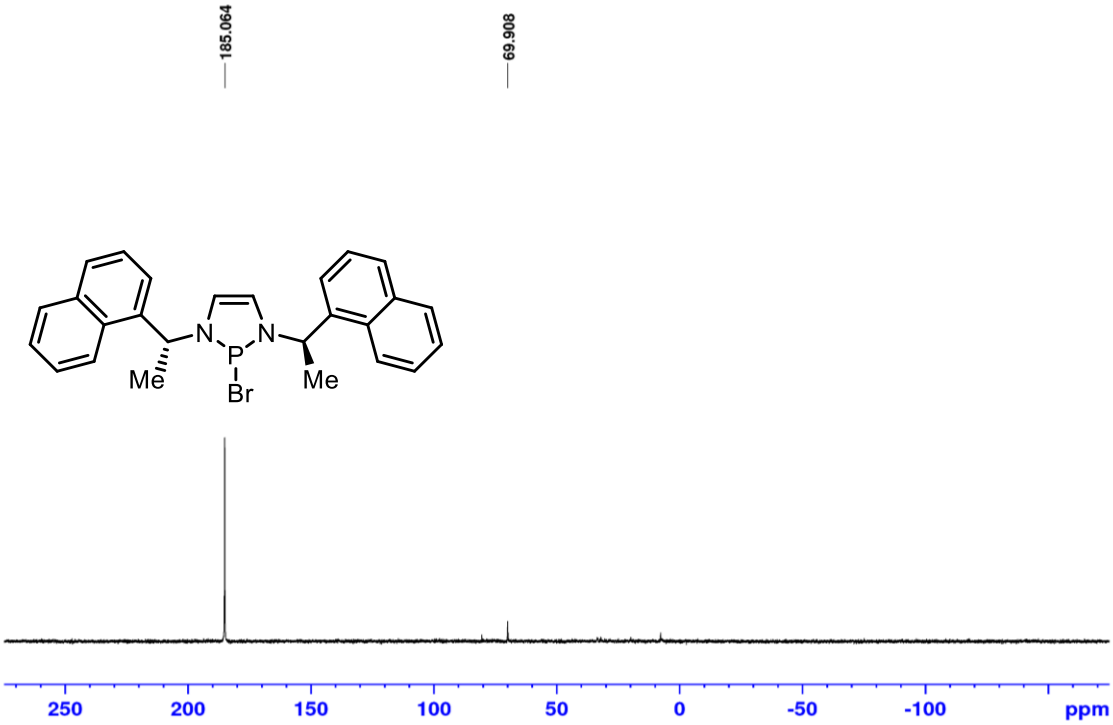


**Figure A333:** $^{31}P$ NMR (202.5 MHz, $CH_3CN$) spectrum of the formation of compound **7-25** from the addition of *P*-pentafluorophenyl *N*-(R)-napthylmethyl-diazaphospholene **7-29** (generated *in situ*) with *N*-benzyl quinolinium bromide.

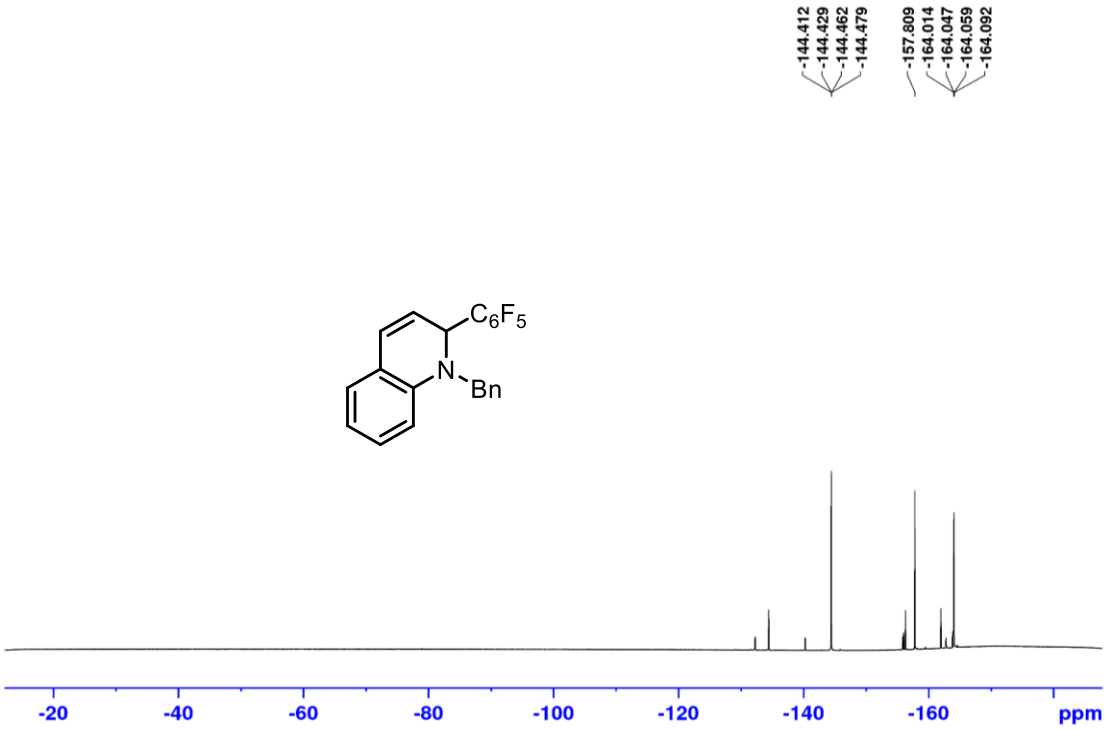


**Figure A334:** $^{19}F$ {$^{1}H$} (470.6 MHz, $CH_3CN$) spectrum of the formation of compound **7-25** from the addition of *P*-pentafluorophenyl *N*-(R)-napthylmethyl-diazaphospholene **7-29** (generated *in situ*) with *N*-benzyl quinolinium bromide.

## F3: HPLC Data for Chapter 7

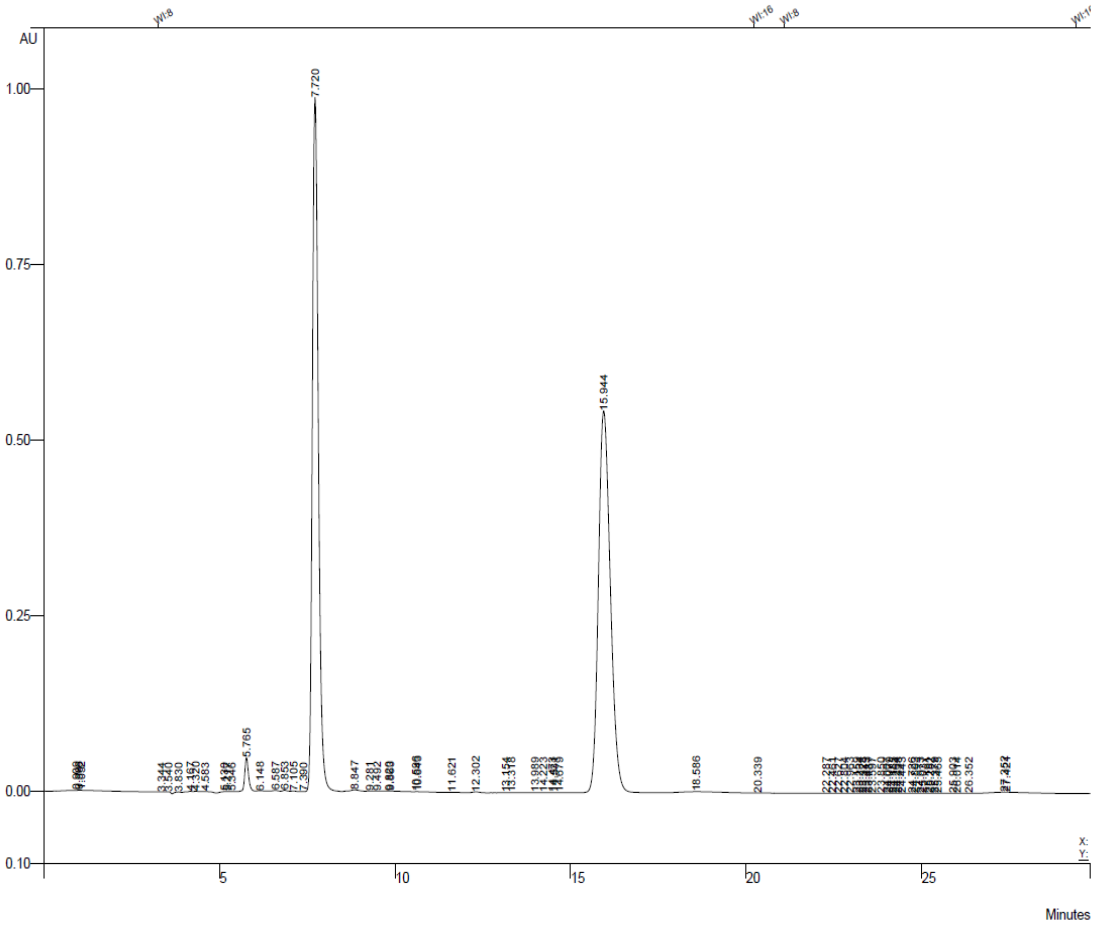


**Figure A335:** HPLC trace from the isolated compound **7-25** from the addition of *P*-pentafluorophenyl *N*-(R)-napthylmethyl-diazaphospholene **7-29** (generated *in situ*) with *N*-benzyl quinolinium bromide.

Print Date: Fri Feb 14 13:17:16 2020 Page 1 of 2

Title :
Run File : c:\star\data\brandon\matt adams\bh-xviii-33 acn sup2-14-202012;36;34 pm.run
Method File : C:\star\estelle.mth
Sample ID : BH-xviii-33 acn sup

Injection Date: 2/14/2020 12:36 PM Calculation Date: 2/14/2020 1:06 PM

Operator : matt Detector Type: 0325
Workstation: DALHOUSI-GZ0GPÿ□HÛè- Bus Address : 44
Instrument : Analytical System Sample Rate : 20.00 Hz
Channel : 1 = 254 nm Run Time : 29.817 min

** LC Workstation Version 6.41 ** 01907-64c0-ea4-04f1 **

Run Mode : Analysis
Peak Measurement: Peak Area
Calculation Type: Percent

| Peak No. | Peak Name | Result () | Ret. Time (min) | Time Offset (min) | Area (counts) | Sep. Code | Width 1/2 (sec) | Status Codes |
|---|---|---|---|---|---|---|---|---|
| 1 | | 0.1328 | 0.909 | 0.000 | 354563 | BV | 0.0 | |
| 2 | | 0.0336 | 0.986 | 0.000 | 89801 | VV | 0.0 | |
| 3 | | 0.2739 | 1.052 | 0.000 | 731136 | VP | 77.8 | |
| 4 | | 0.0633 | 3.344 | 0.000 | 169047 | BP | 4.2 | |
| 5 | | 0.0242 | 3.540 | 0.000 | 64659 | TS | 0.0 | |
| 6 | | 0.1107 | 3.830 | 0.000 | 295435 | PV | 0.0 | |
| 7 | | 0.1970 | 4.167 | 0.000 | 525883 | VV | 5.8 | |
| 8 | | 0.1942 | 4.320 | 0.000 | 518390 | VV | 10.5 | |
| 9 | | 0.2021 | 4.583 | 0.000 | 539519 | VV | 10.2 | |
| 10 | | 0.1056 | 5.130 | 0.000 | 281823 | VV | 5.8 | |
| 11 | | 0.0624 | 5.217 | 0.000 | 166462 | VV | 0.0 | |
| 12 | | 0.1600 | 5.346 | 0.000 | 427153 | VV | 0.0 | |
| 13 | | 2.6599 | 5.765 | 0.000 | 7099340 | VV | 6.7 | |
| 14 | | 0.0256 | 6.148 | 0.000 | 68205 | TS | 0.0 | |
| 15 | | 0.0454 | 6.587 | 0.000 | 121107 | TS | 0.0 | |
| 16 | | 0.0379 | 6.853 | 0.000 | 101068 | TS | 0.0 | |
| 17 | | 0.0149 | 7.105 | 0.000 | 39689 | TS | 0.0 | |
| 18 | | 0.0009 | 7.390 | 0.000 | 2499 | TS | 0.0 | |
| 19 | | 45.9233 | 7.720 | 0.000 | 122568048 | VV | 10.8 | |
| 20 | | 0.1681 | 8.847 | 0.000 | 448749 | TF | 0.0 | |
| 21 | | 0.0290 | 9.281 | 0.000 | 77305 | TF | 0.0 | |
| 22 | | 0.0603 | 9.492 | 0.000 | 160840 | TF | 0.0 | |
| 23 | | 0.0209 | 9.820 | 0.000 | 55738 | TF | 0.0 | |
| 24 | | 0.0536 | 9.863 | 0.000 | 143056 | TF | 0.0 | |
| 25 | | 0.0024 | 10.596 | 0.000 | 6366 | TF | 0.0 | |
| 26 | | 0.0250 | 10.643 | 0.000 | 66621 | TF | 0.0 | |
| 27 | | 0.0201 | 11.621 | 0.000 | 53778 | TS | 0.0 | |
| 28 | | 0.0612 | 12.302 | 0.000 | 163390 | TS | 0.0 | |
| 29 | | 0.0014 | 13.154 | 0.000 | 3834 | TF | 0.0 | |
| 30 | | 0.0008 | 13.318 | 0.000 | 2199 | TF | 0.0 | |
| 31 | | 0.0023 | 13.989 | 0.000 | 6256 | TF | 0.0 | |
| 32 | | 0.0016 | 14.223 | 0.000 | 4276 | TF | 0.0 | |
| 33 | | 0.0028 | 14.473 | 0.000 | 7385 | TF | 0.0 | |
| 34 | | 0.0013 | 14.531 | 0.000 | 3400 | TF | 0.0 | |
| 35 | | 0.0008 | 14.679 | 0.000 | 2154 | TF | 0.0 | |
| 36 | | 47.9974 | 15.944 | 0.000 | 128103880 | VB | 21.9 | |
| 37 | | 0.4155 | 18.586 | 0.000 | 1109005 | VB | 61.9 | |
| 38 | | 0.0071 | 20.339 | 0.000 | 18848 | BB | 1.5 | |
| 39 | | 0.0053 | 22.287 | 0.000 | 14263 | VV | 18.8 | |
| 40 | | 0.0057 | 22.461 | 0.000 | 15150 | VV | 0.0 | |
| 41 | | 0.0041 | 22.627 | 0.000 | 10914 | VV | 0.0 | |
| 42 | | 0.0100 | 22.804 | 0.000 | 26568 | VV | 0.0 | |
| 43 | | 0.0038 | 22.963 | 0.000 | 10228 | VV | 0.0 | |
| 44 | | 0.0110 | 23.159 | 0.000 | 29380 | VV | 0.0 | |
| 45 | | 0.0035 | 23.234 | 0.000 | 9368 | VV | 0.0 | |
| 46 | | 0.0054 | 23.328 | 0.000 | 14301 | VV | 0.0 | |
| 47 | | 0.0058 | 23.413 | 0.000 | 15501 | VV | 0.0 | |
| 48 | | 0.0045 | 23.487 | 0.000 | 12109 | VV | 0.0 | |
| 49 | | 0.0114 | 23.597 | 0.000 | 30382 | VV | 0.0 | |
| 50 | | 0.0106 | 23.850 | 0.000 | 28230 | VV | 0.0 | |
| 51 | | 0.0065 | 24.007 | 0.000 | 17255 | VV | 0.0 | |
| 52 | | 0.0067 | 24.079 | 0.000 | 17828 | VV | 0.0 | |
| 53 | | 0.0039 | 24.185 | 0.000 | 10508 | VV | 0.0 | |
| 54 | | 0.0066 | 24.264 | 0.000 | 17617 | VV | 0.0 | |
| 55 | | 0.0050 | 24.338 | 0.000 | 13410 | VV | 0.0 | |
| 56 | | 0.0084 | 24.443 | 0.000 | 22331 | VV | 0.0 | |
| 57 | | 0.0211 | 24.726 | 0.000 | 56197 | VV | 0.0 | |
| 58 | | 0.0078 | 24.803 | 0.000 | 20786 | VV | 0.0 | |
| 59 | | 0.0079 | 24.973 | 0.000 | 21054 | VV | 0.0 | |
| 60 | | 0.0110 | 25.037 | 0.000 | 29330 | VV | 0.0 | |
| 61 | | 0.0056 | 25.191 | 0.000 | 14830 | VV | 0.0 | |
| 62 | | 0.0073 | 25.252 | 0.000 | 19398 | VV | 0.0 | |
| 63 | | 0.0057 | 25.379 | 0.000 | 15203 | VV | 0.0 | |
| 64 | | 0.0075 | 25.465 | 0.000 | 19929 | VV | 0.0 | |
| 65 | | 0.0498 | 25.903 | 0.000 | 132854 | VV | 0.0 | |
| 66 | | 0.0333 | 26.014 | 0.000 | 88869 | VV | 0.0 | |
| 67 | | 0.0118 | 26.352 | 0.000 | 31406 | VV | 0.0 | |
| 68 | | 0.2221 | 27.352 | 0.000 | 592732 | VV | 0.0 | |
| 69 | | 0.3517 | 27.421 | 0.000 | 938697 | VB | 86.2 | |
| | Totals: | 100.0001 | | 0.000 | 266897535 | | | |

**Figure A336:** HPLC chart from the isolated compound **7-25** from the addition of *P*-pentafluorophenyl *N*-(R)-napthylmethyl-diazaphospholene **7-29** (generated in situ) with *N*-benzyl quinolinium bromide.

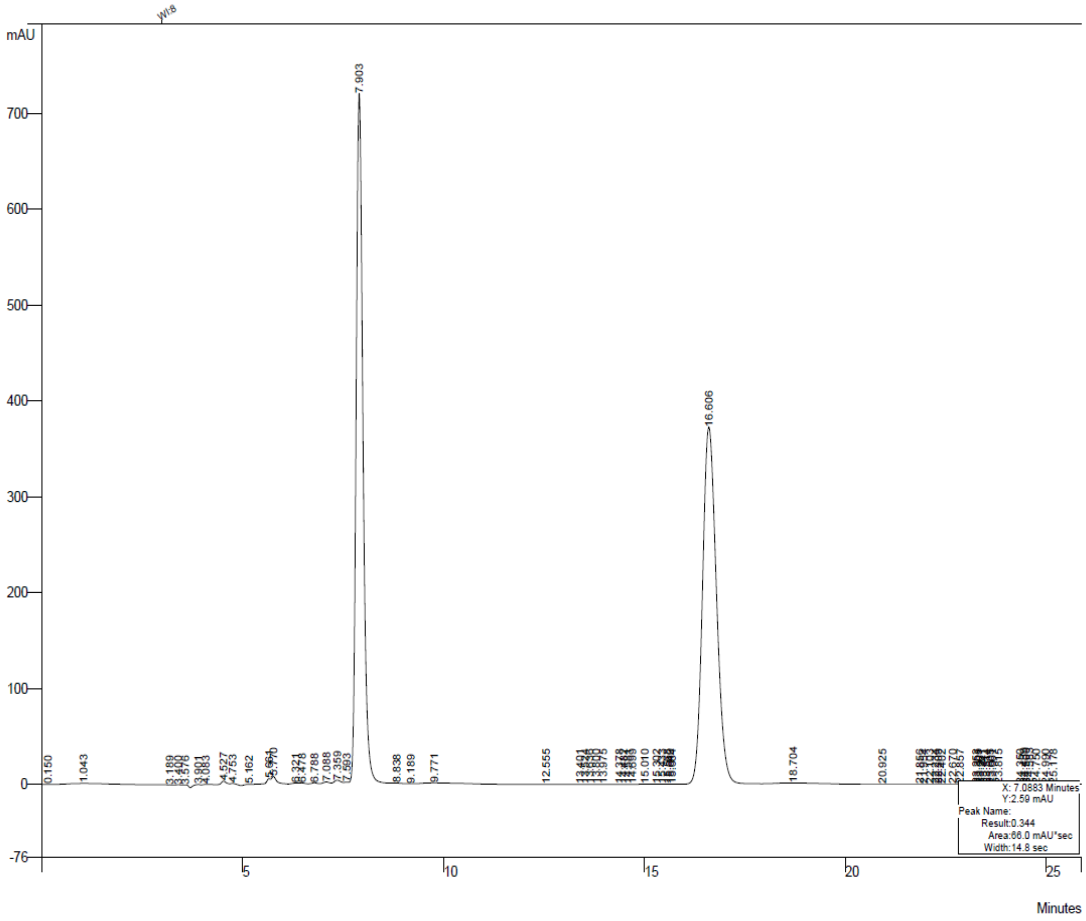


**Figure A337:** HPLC trace from the isolated racemate compound **7-25**.

Print Date: Tue Feb 11 15:17:17 2020 Page 1 of 2

Title :
Run File : c:\star\data\brandon\matt adams\bh-xviii-2 sup2-11-20202;51;04 pm.run
Method File : C:\star\estelle.mth
Sample ID : BH-xviii-2 sup

Injection Date: 2/11/2020 2:51 PM Calculation Date: 2/11/2020 3:16 PM

Operator : matt Detector Type: 0325
Workstation: DALHOUSI-GZ0GPy□HÛè- Bus Address : 44
Instrument : Analytical System Sample Rate : 20.00 Hz
Channel : 1 = 254 nm Run Time : 25.884 min

** LC Workstation Version 6.41 ** 01907-64c0-ea4-04f1 **

Run Mode : Analysis
Peak Measurement: Peak Area
Calculation Type: Percent

| Peak No. | Peak Name | Result () | Ret. Time (min) | Time Offset (min) | Area (counts) | Sep. Code | Width 1/2 (sec) | Status Codes |
|---|---|---|---|---|---|---|---|---|
| 1 | | 0.0017 | 0.150 | 0.000 | 3254 | BV | 6.7 | |
| 2 | | 0.4353 | 1.043 | 0.000 | 834671 | VB | 62.9 | |
| 3 | | 0.0267 | 3.189 | 0.000 | 51263 | BB | 2.6 | |
| 4 | | 0.1400 | 3.400 | 0.000 | 268437 | VP | 3.4 | |
| 5 | | 0.0491 | 3.576 | 0.000 | 94179 | TS | 0.0 | |
| 6 | | 0.1991 | 3.901 | 0.000 | 381725 | PV | 4.4 | |
| 7 | | 0.3509 | 4.083 | 0.000 | 672726 | VV | 7.6 | |
| 8 | | 0.4674 | 4.527 | 0.000 | 896051 | VV | 8.4 | |
| 9 | | 0.2728 | 4.753 | 0.000 | 523005 | VV | 10.9 | |
| 10 | | 0.2154 | 5.162 | 0.000 | 412939 | VV | 9.4 | |
| 11 | | 0.5960 | 5.661 | 0.000 | 1142639 | VV | 7.7 | |
| 12 | | 0.7738 | 5.770 | 0.000 | 1483612 | VV | 11.2 | |
| 13 | | 0.2662 | 6.321 | 0.000 | 510323 | VV | 19.7 | |
| 14 | | 0.2613 | 6.478 | 0.000 | 500893 | VV | 0.0 | |
| 15 | | 0.2930 | 6.788 | 0.000 | 561691 | VV | 0.0 | |
| 16 | | 0.3442 | 7.088 | 0.000 | 659927 | VV | 14.8 | |
| 17 | | 0.4768 | 7.359 | 0.000 | 914226 | VV | 12.5 | |
| 18 | | 0.1468 | 7.593 | 0.000 | 281423 | VV | 0.0 | |
| 19 | | 46.0952 | 7.903 | 0.000 | 88377168 | VB | 10.7 | |
| 20 | | 0.0108 | 8.838 | 0.000 | 20784 | TS | 0.0 | |
| 21 | | 0.0021 | 9.189 | 0.000 | 3967 | TF | 0.0 | |
| 22 | | 0.3821 | 9.771 | 0.000 | 732615 | TF | 0.0 | |
| 23 | | 0.0082 | 12.555 | 0.000 | 15671 | VV | 18.9 | |
| 24 | | 0.0315 | 13.401 | 0.000 | 60402 | VV | 0.0 | |
| 25 | | 0.0072 | 13.524 | 0.000 | 13805 | VV | 0.0 | |
| 26 | | 0.0072 | 13.636 | 0.000 | 13829 | VV | 0.0 | |
| 27 | | 0.0046 | 13.800 | 0.000 | 8853 | VV | 0.0 | |
| 28 | | 0.0130 | 13.975 | 0.000 | 24913 | VV | 0.0 | |
| 29 | | 0.0291 | 14.378 | 0.000 | 55709 | VV | 0.0 | |
| 30 | | 0.0099 | 14.482 | 0.000 | 19004 | VV | 0.0 | |
| 31 | | 0.0110 | 14.581 | 0.000 | 21058 | VV | 0.0 | |
| 32 | | 0.0083 | 14.699 | 0.000 | 15907 | VV | 0.0 | |
| 33 | | 0.0435 | 15.010 | 0.000 | 83423 | VV | 0.0 | |
| 34 | | 0.0133 | 15.302 | 0.000 | 25487 | VV | 0.0 | |
| 35 | | 0.0145 | 15.433 | 0.000 | 27708 | VV | 0.0 | |
| 36 | | 0.0114 | 15.568 | 0.000 | 21855 | VV | 0.0 | |
| 37 | | 0.0057 | 15.640 | 0.000 | 10997 | VV | 0.0 | |
| 38 | | 0.0125 | 15.684 | 0.000 | 24048 | VV | 0.0 | |
| 39 | | 47.4279 | 16.606 | 0.000 | 90932240 | VP | 22.3 | |
| 40 | | 0.3890 | 18.704 | 0.000 | 745855 | TS | 0.0 | |
| 41 | | 0.0012 | 20.925 | 0.000 | 2358 | TS | 0.0 | |
| 42 | | 0.0105 | 21.856 | 0.000 | 20212 | PV | 0.0 | |
| 43 | | 0.0069 | 21.954 | 0.000 | 13258 | VV | 0.0 | |
| 44 | | 0.0030 | 22.103 | 0.000 | 5758 | VV | 0.0 | |
| 45 | | 0.0031 | 22.234 | 0.000 | 5951 | VV | 0.0 | |
| 46 | | 0.0021 | 22.309 | 0.000 | 3948 | VV | 0.0 | |
| 47 | | 0.0021 | 22.402 | 0.000 | 4029 | VV | 0.0 | |
| 48 | | 0.0032 | 22.670 | 0.000 | 6169 | VV | 0.0 | |
| 49 | | 0.0039 | 22.857 | 0.000 | 7449 | VV | 0.0 | |
| 50 | | 0.0142 | 23.253 | 0.000 | 27201 | VV | 0.0 | |
| 51 | | 0.0019 | 23.305 | 0.000 | 3660 | VV | 0.0 | |
| 52 | | 0.0020 | 23.361 | 0.000 | 3898 | VV | 0.0 | |
| 53 | | 0.0038 | 23.441 | 0.000 | 7318 | VV | 0.0 | |
| 54 | | 0.0029 | 23.514 | 0.000 | 5518 | VV | 0.0 | |
| 55 | | 0.0031 | 23.605 | 0.000 | 5905 | VV | 0.0 | |
| 56 | | 0.0015 | 23.661 | 0.000 | 2918 | VV | 0.0 | |
| 57 | | 0.0066 | 23.815 | 0.000 | 12713 | VV | 0.0 | |
| 58 | | 0.0292 | 24.350 | 0.000 | 55944 | VV | 0.0 | |
| 59 | | 0.0075 | 24.439 | 0.000 | 14460 | VV | 0.0 | |
| 60 | | 0.0044 | 24.500 | 0.000 | 8444 | VV | 0.0 | |
| 61 | | 0.0115 | 24.583 | 0.000 | 21957 | VV | 0.0 | |
| 62 | | 0.0105 | 24.750 | 0.000 | 20046 | VV | 0.0 | |
| 63 | | 0.0068 | 24.990 | 0.000 | 12981 | VV | 0.0 | |

Print Date: Tue Feb 11 15:17:17 2020 Page 2 of 2

| | | | | | | | | |
|---|---|---|---|---|---|---|---|---|
| 64 | | 0.0037 | 25.178 | 0.000 | 7001 | VV | 0.0 | |
| | Totals: | 100.0001 | | 0.000 | 191727378 | | | |

**Figure A338:** HPLC chart from the isolated racemate compound **7-25**.

## Appendix G: Copyright Permissions

# Bis-aminocyclopropenylidene carbene borane catalyzed imine hydrogenation

B. S. N. Huchenski, C. J. Christopherson, K. N. Robertson and A. W. H. Speed, *Org. Biomol. Chem.*, 2019, **17**, 6158 **DOI:** 10.1039/C9OB01053J

# Protic additives or impurities promote imine reduction with pinacolborane

B. S. N. Huchenski and A. W. H. Speed, *Org. Biomol. Chem.*, 2019, **17**, 1999
**DOI:** 10.1039/C8OB02330A

# Room-temperature reduction of sulfur hexafluoride with metal phosphides

B. S. N. Huchenski and A. W. H. Speed, *Chem. Commun.*, 2021, Advance Article , **DOI:** 10.1039/D1CC01943K

JOHN WILEY AND SONS LICENSE
TERMS AND CONDITIONS

Jul 05, 2021

---

This Agreement between Mr. Blake Huchenski ("You") and John Wiley and Sons ("John Wiley and Sons") consists of your license details and the terms and conditions provided by John Wiley and Sons and Copyright Clearance Center.

| | |
|---|---|
| License Number | 5102671472652 |
| License date | Jul 05, 2021 |
| Licensed Content Publisher | John Wiley and Sons |
| Licensed Content Publication | European Journal of Organic Chemistry |
| Licensed Content Title | Functionalization of Bis-Diazaphospholene P–P Bonds with Diverse Electrophiles |
| Licensed Content Author | Blake S. N. Huchenski, Katherine N. Robertson, Alexander W. H. Speed |
| Licensed Content Date | Jul 23, 2020 |
| Licensed Content Volume | 2020 |
| Licensed Content Issue | 32 |
| Licensed Content Pages | 5 |
| Type of use | Dissertation/Thesis |

| | |
|---|---|
| Requestor type | Author of this Wiley article |
| Format | Print and electronic |
| Portion | Full article |
| Will you be translating? | No |
| Title | Small Molecule Activation Facilitated by Main Group Elements |
| Institution name | Dalhousie Univeristy |
| Expected presentation date | Aug 2021 |
| Requestor Location | Mr. Blake Huchenski<br>808 McLean st<br><br>Halifax, NS B3H 2T8<br>Canada<br>Attn: Mr. Blake Huchenski |
| Publisher Tax ID | EU826007151 |
| Total | 0.00 CAD |
| Terms and Conditions | |